# EMERGING INFECTIOUS DISEASES®

CDC
Centers for Disease Control and Prevention

## Waterborne Infections

January 2021

# EMERGING INFECTIOUS DISEASES®





Emerging Infectious Diseases is published monthly by the Centers for Disease Control and Prevention, 1600 Clifton Rd NE, Mailstop H16-2, Atlanta, GA 30329-4027, USA. Telephone 404-639-1960; email, eideditor@cdc.gov

# EMERGING INFECTIOUS DISEASES®

**Waterborne Infections** **January 2021**


**Joseph Mallord William Turner (1775–1851). *The Fighting Temeraire (Tugged to Her Last Berth to Be Broken Up), 1838* (1938).** Oil on canvas, 36 in × 48 in /91 cm × 122 cm. National Gallery, London, UK. Public Domain.

**About the Cover** p. 336

## Synopses



## Research

EMERGING INFECTIOUS DISEASES®
January 2021



## Historical Review



## Dispatches

## Research Letters



EMERGING INFECTIOUS DISEASES®
January 2021



## Comment Letters



## About the Cover



### Etymologia

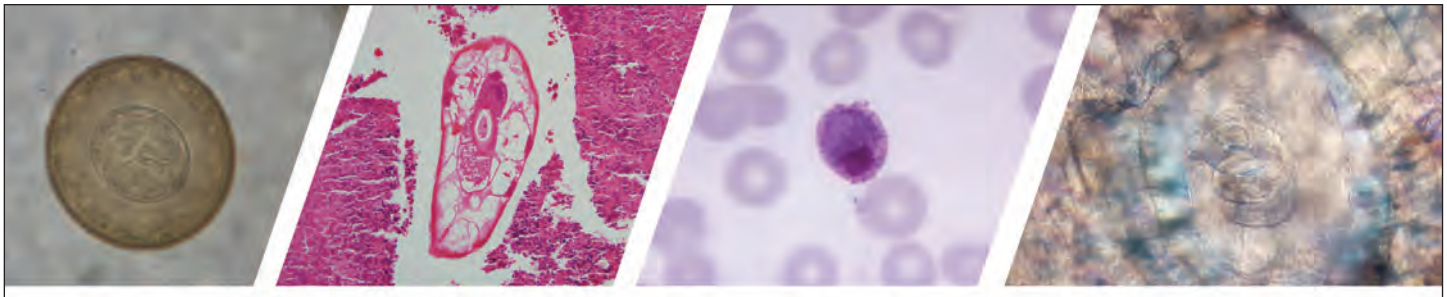

DPDx

# Diagnostic Assistance and Training in Laboratory Identification of Parasites

A free service of CDC available to laboratorians, pathologists, and other health professionals in the United States and abroad

- Diagnosis from photographs of worms, histological sections, fecal, blood, and other specimen types
- Expert diagnostic review
- Formal diagnostic laboratory report
- Submission of samples via secure file share

Visit the DPDx website for information on laboratory diagnosis, geographic distribution, clinical features, parasite life cycles, and training via Monthly Case Studies of parasitic diseases.

www.cdc.gov/dpdx
dpdx@cdc.gov

U.S. Department of Health and Human Services
Centers for Disease Control and Prevention

CS272346-DE

# Impact of Human Papillomavirus Vaccination, Rwanda and Bhutan

Iacopo Baussano, Felix Sayinzoga, Ugyen Tshomo, Vanessa Tenet, Alex Vorsters, Daniëlle A.M. Heideman, Tarik Gheit, Massimo Tommasino, Marie Chantal Umulisa, Silvia Franceschi, Gary M. Clifford

Rwanda and Bhutan, 2 low- and middle-income countries, implemented primarily school-based national human papillomavirus (HPV) vaccination in 2011 (Rwanda) and 2010 (Bhutan). We estimated vaccination effectiveness through urine-based HPV prevalence surveys in schools in 2013–2014 and 2017. In Rwanda, 912 participants from baseline surveys and 1,087 from repeat surveys were included, and in Bhutan, 973 participants from baseline surveys and 909 from repeat surveys were included. The overall effectiveness against vaccine-targeted HPV types (i.e., HPV-6/11/16/18) was 78% (95% CI 51%–90%) in Rwanda, and 88% (6%–99%) in Bhutan and against other α-9 types was 58% (21–78) in Rwanda and 63% (27–82) in Bhutan. No effect against other HPV types was detectable. Prevalence of vaccine-targeted HPV types decreased significantly, as well as that of other α-9 types, suggesting cross-protection. These findings provide direct evidence from low- and middle-income countries of the marked effectiveness of high-coverage school-based, national HPV vaccination programs.

Recent estimates suggest that, in the year 2018, ≈570,000 new cervical cancers cases occurred worldwide (*1*). Nearly half of the cases were diagnosed in women <50 years of age, and more than two thirds occurred in low- and middle-income countries (LMICs), particularly in southeastern Asia, Latin America, and sub-Saharan Africa. Human papillomavirus (HPV) types 16 and 18 are responsible for ≈70% of cervical cancers and HPV types 31/33/45/52/58 for another 20% (*2*).

Because cervical cancer is largely preventable, the Director-General of the World Health Organization recently made a global call for action toward the elimination of cervical cancer as a public health problem (*3*). Global implementation of vaccination against HPV with a high coverage underpins the global strategy devised to achieve this ambitious goal (*4*).

Licensed prophylactic HPV vaccines have demonstrated high safety (*5*) and efficacy against persistent HPV infections and precancerous lesions (*6*), and invasive cervical cancers (*7*), and HPV vaccination programs have been shown to be cost-effective in a wide range of settings worldwide (*8*). Furthermore, population-level impact against HPV prevalence and precancerous lesions has been consistently shown in high-income countries (HICs) with well-established HPV national vaccination programs (*9*). HPV vaccine has been disproportionately introduced in high-resource settings, and access to HPV vaccination in LMICs, particularly in Africa and Asia, remains limited (*10*).

Rwanda and Bhutan, both of which are LMICs, started national HPV vaccination programs in 2011 (Rwanda) and 2010 (Bhutan) (Figure 1). Both programs are primarily school-based, introduced a 3-dose schedule of quadrivalent vaccine targeting HPV-6/11/16/18, and switched to a 2-dose schedule in 2015 (Rwanda) and 2016 (Bhutan). In both countries, 12-year-old girls are the target age group for routine vaccination, but both countries had an initial expanded 3-dose catch-up campaign. In Rwanda, since 2011, the national vaccination program targeted all girls attending primary school grade 6 and, in years 2012 and 2013, also targeted girls attending secondary school grade 3, achieving reported coverage of 93% (*11*). In Bhutan, a 1-round catch-up campaign was conducted in 2010, targeting girls 13–18 years of age, achieving reported coverage of 89% (*12*).

The International Agency for Research on Cancer (IARC), in collaboration with the ministries of health of both countries, is conducting long-term studies, including a series of urine surveys, to provide direct evaluation of the population-level impact of HPV vaccination in LMICs (*13*). In 2016, we published the

Author affiliations: International Agency for Research on Cancer, Lyon, France (I. Baussano, V. Tenet, T. Gheit, M. Tommasino, M.C. Umulisa, G.M. Clifford); Ministry of Health, Kigali, Rwanda (F. Sayinzoga); Jigme Dorji Wangchuck National Referral Hospital, Thimphu, Bhutan (U. Tshomo); University of Antwerp, Antwerp, Belgium (A. Vorsters); Vrije Universiteit Amsterdam, Amsterdam, the Netherlands (D.A.M. Heideman); Centro di Riferimento Oncologico, Aviano, Italy (S. Franceschi)

DOI: https://doi.org/10.3201/eid2701.191364

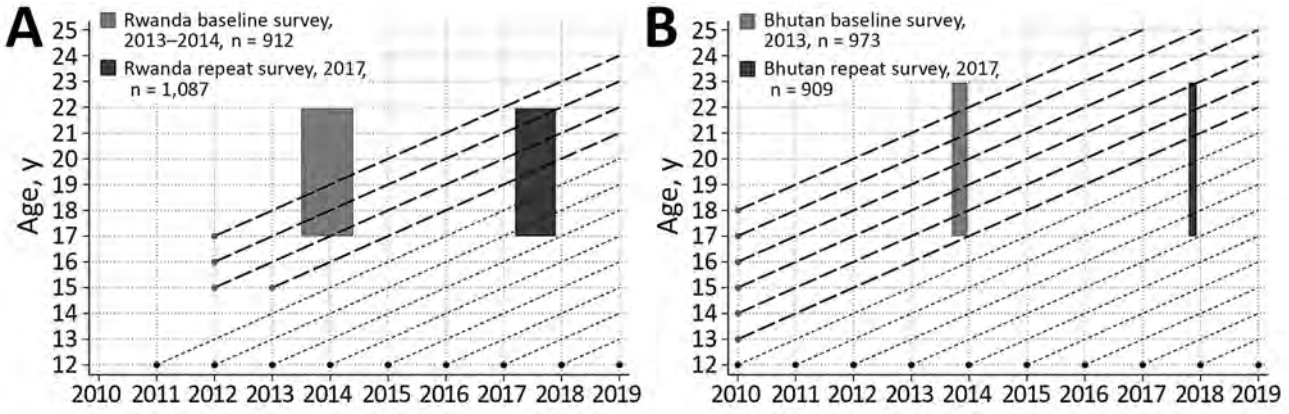


**Figure 1.** Timing of school-based human papillomavirus vaccination program and surveys in Rwanda (A) and Bhutan (B). Short dashed line represents routine vaccination. Long dashed line represents catch-up vaccination.

results of the baseline urine surveys among high-school female students (*13*). In this article, we quantify HPV prevalence in repeated surveys, comparing it with the baseline HPV prevalence to estimate population-level impact of HPV vaccination in both countries (*13*).

## Methods

To assess the impact of catch-up HPV vaccination programs in Rwanda and Bhutan, we compared HPV prevalence in women 17–22 years of age in successive urine-based surveys conducted in high schools during 2013–2014 (baseline survey) and 2017 (repeat survey) in both countries (Figure 1). In both countries, the nationwide HPV vaccination program had been launched before the implementation of the baseline surveys. The methods used in the baseline surveys to recruit the study population, collect the urine, extract DNA, and to test and genotype HPV are reported elsewhere (*13*). To ensure comparability of prevalence estimates over time, we used the same methods for the repeat surveys.

### Study Population

In the repeat surveys, we aimed at recruiting ≈1,000 female students 18–20 years of age in each country from the same high schools included in the baseline survey. In Rwanda, we included secondary schools in the Nyarugenge District of Kigali. Of the 22 schools (8 public and 14 private), all but 1 overlapped with the 21 schools included in the baseline survey. In Bhutan, we included high schools in the capital of the country, Thimphu (n = 7), and in the nearby town of Paro (n = 3). Of these 10 schools (3 public and 7 private), 6 overlapped with the 6 schools included in the baseline survey. School authorities gave full support to the conduct of the study, and no school refused participation. The repeat surveys were performed during March–November 2017 (Rwanda) and September–November 2017 (Bhutan). Students in the targeted age groups were invited by school staff to attend study information and recruitment meetings. The large majority of students present at information and recruitment meetings signed the informed consent form, but exact denominators of students by age in each school were not available. In Rwanda, 50 students 17 years of age and 24 students 21 years of age also attended recruitment meetings and were allowed to join the study. Similarly, in Bhutan, 10 students 17 years of age, 68 students 21 years of age, and 30 students 22 years of age also joined the study.

All students who signed an informed consent form received a device for self-collection of urine. Participants were asked to collect first-void urine from the first urination of the day and to return the urine sample on the same morning as collection. Urine samples were recovered at school entry the day after recruitment, and on this day, a short online questionnaire was filled in by a study interviewer (Rwanda) or directly by the student (Bhutan). The questionnaire included information on places of birth and living, history of sexual intercourse, and recalled HPV vaccination status. Urine samples and questionnaires could only be matched through an anonymized identification number.

### Urine Collection and DNA Extraction

Urine samples were self-collected by participants using a device (Colli PeeTM, Novosanis, https://novosanis.com) designed to collect the first 14 mL of first-void urine immediately into 7 mL of a urine-conservation medium to avoid DNA degradation (*14*) and to allow subsequent urine volume to exit the device into the toilet. Self-collected urine samples were

gathered and stored on ice at the school on the morning of sample taking; on the same day, the samples were transported to the central laboratory and stored at –20°C until shipment to IARC in cold boxes with ice packs. Subsequently, samples were shipped on dry ice to the Centre for the Evaluation of Vaccination, University of Antwerp, Belgium, where DNA extraction was performed as described elsewhere (*14*). DNA extracts were then shipped back to IARC on dry ice.

### HPV Testing and Genotyping

As in the baseline surveys, 2 methods of different analytical sensitivity were used for HPV testing to overcome the possible problem of the relative lack of sensitivity of HPV detection in urine. The primary HPV testing protocol was performed in the pathology department of Amsterdam University Medical Center, Vrije Universiteit Amsterdam, the Netherlands, where β-globin PCR analysis was first conducted to confirm the presence of human DNA in all specimens (*15*) and a general primer GP5+/6+-mediated PCR with enzyme immunoassay and subsequent genotyping readout was used to detect HPV DNA (*16*). A secondary type-specific E7 PCR bead-based multiplex genotyping assay (E7-MPG) with β-globin primers included was performed at IARC, Lyon, France, using a Luminex bead-based platform (*17*,*18*). This assay also detects DNA from *Chlamydia trachomatis*. Results were considered invalid when β-globin was undetectable by either 1 or both HPV assays.

### Statistical Analyses

For both countries, we compared the distribution of selected characteristics of female students in the baseline and repeat surveys by using $\chi^2$ tests and a p value of ≤0.05 for statistical significance. To estimate type-specific HPV prevalence among women recruited in the baseline and repeat surveys, HPV types were grouped as follows: HPV vaccine types (HPV-6, -11, -16, and -18), other α-9 types (HPV-31, -33, -35, -52, and -58), other α-7 types (HPV-39, -45, -59, and -68), and non–α 7/9 types detected by both genotyping tests (HPV-26, -51, -53, -56, -66, -70, -73, and -82). We adapted the framework proposed by Halloran et al. (*19*) to estimate the population-level impact of HPV vaccination in both countries by using different definitions of effectiveness on the basis of increasingly specific criteria to select comparison groups by reported vaccination status (Figure 2). Hence, we compared the type-specific HPV prevalence in all women, unvaccinated and vaccinated, recruited in the baseline and repeat surveys, to compute the overall effectiveness,

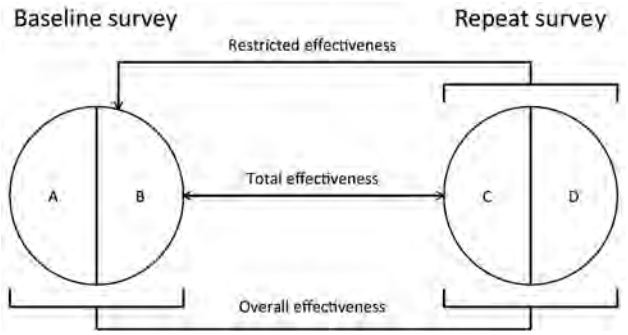


**Figure 2.** Analytical framework used to assess the impact of human papillomavirus (HPV) vaccination in Rwanda and Bhutan. A) Vaccinated participants in the baseline survey. B) Unvaccinated participants in the baseline survey. C) Vaccinated participants in the repeat survey. D) Unvaccinated participants in the repeat survey. Vaccine effectiveness (VE) was calculated as VE = (1 – PR)%, where PR is a prevalence ratio (PR). Each type of VE is defined according to specific criteria for selecting comparison groups on the basis of reported vaccination status. Overall effectiveness estimates, providing a measure of HPV prevalence reduction over time attributable to vaccination irrespective of the reported vaccination status of each person, were obtained by comparing the type-specific HPV prevalence in all women, unvaccinated and vaccinated, recruited in the baseline and repeat surveys. PR (C and D) / PR (A and B) = overall PR. Restricted effectiveness estimates, providing an approximate estimate of the impact of HPV vaccination versus an entirely unvaccinated population, were obtained by comparing the type-specific HPV prevalence in unvaccinated women in the baseline and all women in repeat surveys. PR (C and D) / PR (B) = restricted PR. Total effectiveness estimates, providing a vaccine efficacy estimate (similar to measures from clinical trials) from real-life settings, were obtained by comparing the type-specific HPV prevalence in unvaccinated women in the baseline and vaccinated women in repeat surveys. PR (C) / PR (B) = total PR, where PR (•) is the type-specific HPV prevalence in each participant group.

which provides a measure of HPV prevalence reduction over time attributable to vaccination, irrespective of the reported vaccination status of each person. We also compared the type-specific HPV prevalence in unvaccinated women in the baseline and all women in repeat surveys, to compute the restricted effectiveness to account for the fact that HPV vaccination had already been introduced in both countries when baseline surveys were conducted. Finally, we compared the type-specific HPV prevalence in unvaccinated women in the baseline and vaccinated women in repeat surveys, to compute the total effectiveness, which provides vaccine efficacy estimates from real-life settings (similar to measures from clinical trials).

We computed prevalence ratios (PR) for HPV detection and corresponding 95% CIs by using binomial regression models with a log link. Estimates for Rwanda were adjusted for age group, place of birth, and reported history of sexual intercourse (never vs.

ever or prefer not to answer). Estimates for Bhutan were adjusted only for reported history of sexual intercourse because of the small number of infections with HPV vaccine–targeted types observed. HPV vaccine effectiveness (VE) estimates and the corresponding 95% CIs were computed as (1 – PR)%. All statistical analyses were performed by using Stata SE 15.1 (StataCorp, https://www.stata.com).

### Ethics Approval

The research ethics boards of the ministries of health of Rwanda and Bhutan approved the studies in each country. The IARC Ethics Committee approved the studies in both countries.

## Results

In the repeat surveys, 1,198 students in Rwanda and 987 students in Bhutan signed the informed consent forms. Urine samples were not returned for 43 students in Rwanda and 4 students in Bhutan, results were invalid for 38 samples in Rwanda and 49 samples in Bhutan, and 2 additional exclusions were attributable to insufficient DNA for the second test (E7-MPG) in Rwanda. Other participants (28 from Rwanda, 25 from Bhutan) were excluded because of a lack of a questionnaire or because students could not recall their HPV vaccination status. Data from 1,087 students in Rwanda (median age 19 years; range 17–21 years) and 909 students in Bhutan (median age 19 years; range 17–22 years) were included in the final analyses (Table 1; Appendix Figure, https://wwwnc.cdc.gov/EID/article/27/1/19-1364-App1.pdf).

HPV vaccination was reported by 962 (89%) of study participants in Rwanda and 864 (95%) in Bhutan, and median age at vaccination was 14 years (range 10–18 years) in Rwanda and 12 years (range 10–19 years) in Bhutan. Among vaccinated girls in the studies, 94% in Rwanda and 90% in Bhutan reported

**Table 1.** Comparison of female students in HPV surveys, by selected characteristics, Rwanda baseline (2013–2014) and repeat (2017) surveys and Bhutan baseline (2013) and repeat (2017) surveys*

| | Rwanda | | Bhutan | |
|---|---|---|---|---|
| Characteristic | Baseline survey | Repeat survey | Baseline survey | Repeat survey |
| All | 912 | 1,087 | 973 | 909 |
| Age-group, y | | | | |
| 17–18 | 374 (41.0) | 536 (49.3) | 285 (29.3) | 347 (38.2) |
| 19 | 274 (30.0) | 326 (30.0) | 337 (34.6) | 303 (33.3) |
| 20–22 | 264 (29.0) | 225 (20.7) | 351 (36.1) | 259 (28.5) |
| $\chi^2$ | p<0.001 | | p<0.001 | |
| Place of birth | | | | |
| Capital | 497 (54.5) | 800 (73.6) | 309 (31.8) | 315 (34.7) |
| Outside capital | 415 (45.5) | 287 (26.4) | 663 (68.2) | 594 (65.3) |
| $\chi^2$ | p<0.001 | | p = 0.187 | |
| Place of living | | | | |
| With family or relative | 763 (83.7) | 936 (86.1) | 798 (82.0) | 765 (84.2) |
| Boarding school | 149 (16.3) | 151 (13.9) | 175 (18.0) | 144 (15.8) |
| $\chi^2$ | p = 0.127 | | p = 0.215 | |
| History of sexual intercourse | | | | |
| Never | 720 (79.0) | 729 (67.1) | 871 (89.5) | 760 (83.6) |
| Ever or prefer not to answer† | 192 (21.0) | 358 (32.9) | 102 (10.5) | 149 (16.4) |
| $\chi^2$ | p<0.001 | | p<0.001 | |
| *Chlamydia trachomatis*‡ | | | | |
| Negative | 892 (97.8) | 1047 (96.3) | 940 (96.6) | 872 (95.9) |
| Positive | 20 (2.2) | 40 (3.7) | 33 (3.4) | 37 (4.1) |
| $\chi^2$ | p = 0.052 | | p = 0.437 | |
| HPV vaccination | | | | |
| No | 519 (56.9) | 125 (11.5) | 77 (7.9) | 45 (5.0) |
| Yes | 393 (43.1) | 962 (88.5) | 896 (92.1) | 864 (95.0) |
| $\chi^2$ | p<0.001 | | p = 0.009 | |
| Age at vaccination§ | | | | |
| <14 | 12 (3.1) | 412 (46.5) | 12 (2.0) | 569 (87.4) |
| ≥14 | 378 (96.9) | 474 (53.5) | 591 (98.0) | 82 (12.6) |
| $\chi^2$ | p<0.001 | | p<0.001 | |
| No. doses§ | | | | |
| 1 | NA | 52 (5.5) | NA | 84 (9.9) |
| 2–3 | NA | 901 (94.5) | NA | 769 (90.2) |

*Values are no. (%) except as indicated. HPV, human papillomavirus; NA, not assessed.
†Includes 4 (Rwanda baseline), and 38 (Rwanda repeat), 43 (Bhutan baseline), and 20 (Bhutan repeat) students who preferred not to answer this question.
‡Detected by using E7 PCR bead-based multiplex genotyping assay.
§Does not add up to the total because of missing values.

being administered >1 dose of vaccine. In the baseline survey, 43% of participants in Rwanda and 92% of participants in Bhutan reported to be vaccinated. In both countries, the distribution of age at vaccination significantly shifted toward younger ages in the repeat surveys compared with baseline surveys. We compared the distribution of participants in the repeat survey by age group and other selected characteristics with the distribution of the same characteristics as observed in the 912 participants in Rwanda and 973 participants in Bhutan in the baseline surveys (Table 1). Students in the repeat surveys were younger than in the baseline surveys and more likely to report sexual intercourse history (33% vs. 21% [p<0.001] in Rwanda and 16% vs. 11% [p<0.001] in Bhutan). In Rwanda, participants enrolled in the repeat survey were also more likely to be born in the capital (Kigali) than in the baseline survey (74% vs. 55% [p<0.001]) and had a higher probability of *Chlamydia trachomatis* detection (4% vs. 2% [p = 0.052]). In both surveys and in both countries, detection of *C. trachomatis* was substantially higher in participants who reported a history of sexual activity (Appendix Table 1).

The distribution of participants' characteristics by vaccination history is detailed in Appendix Table 2. In the repeat surveys, the distribution of key characteristics was similar between vaccinated and unvaccinated participants in both countries.

We calculated prevalence and crude PR for groups of HPV types according to GP5+/6+ PCR, in both the baseline and repeat surveys in Rwanda (Figure 3, panel A) and Bhutan (Figure 3, panel B). In Rwanda, the prevalence of vaccine-targeted types decreased 2.5% to 0.7% (crude PR 0.29 [95% CI 0.13–0.65]) and prevalence of other α-9 types decreased from 2.9% to 1.5% (PR 0.52 [95% CI 0.28–0.96]), whereas the prevalence of other α-7 types was 2.1% in both surveys (PR 1.02 [95% CI 0.56–1.85]) and the prevalence of non–α 7/9 HPV types did not significantly change, increasing from 2.6% to 2.9% (PR 1.08 [95% CI 0.64–1.83]). In Bhutan, the prevalence of vaccine-targeted types decreased from 0.8% to 0.1% (PR 0.13 [95% CI 0.02–1.07]), prevalence of other α-9 types decreased from 2.8% to 1.2% (PR 0.44 [95% CI 0.22–0.87]), and prevalence of other α-7 types decreased from 2.7% to 1.7% (PR 0.62 [95% CI 0.33–1.16]), whereas the prevalence of the non–α 7/9 types did not significantly change, decreasing from 2.2% to 2.0% (PR 0.92 [95% CI 0.49–1.71]).

We calculated the adjusted vaccine impact on groups of HPV types in both Rwanda and Bhutan, as measured by estimates of overall, restricted, and total VE (Table 2). In both countries, the precision of statistically significant crude effectiveness estimates improved with adjustment (data not shown, but crude PRs and VE can be calculated from data in Table 2). Overall effectiveness against vaccine-targeted types was 78% (95% CI 51%–90%) in Rwanda and 88% (95% CI 6%–99%) in Bhutan, and increased moving through the scenarios of restricted effectiveness at 86% (95% CI 69%–94%) in Rwanda and 96% (95% CI 52%–100%) in Bhutan, up to a total effectiveness of 95% (95% CI 83%–99%) in Rwanda and 95% (95% CI 49%–100%) in Bhutan. The overall effectiveness against other α-9 types was 58% (95% CI 21%–78%) in Rwanda and 63% (95% CI 27%–82%) in Bhutan, the restricted effectiveness was 63% (95% CI 26%–81%) in Rwanda and 56% (95% CI –89%–90%) in Bhutan, and the total effectiveness was 60% (95% CI 19%–81%) in Rwanda and 58% (95% CI –81%–90%). In neither country were

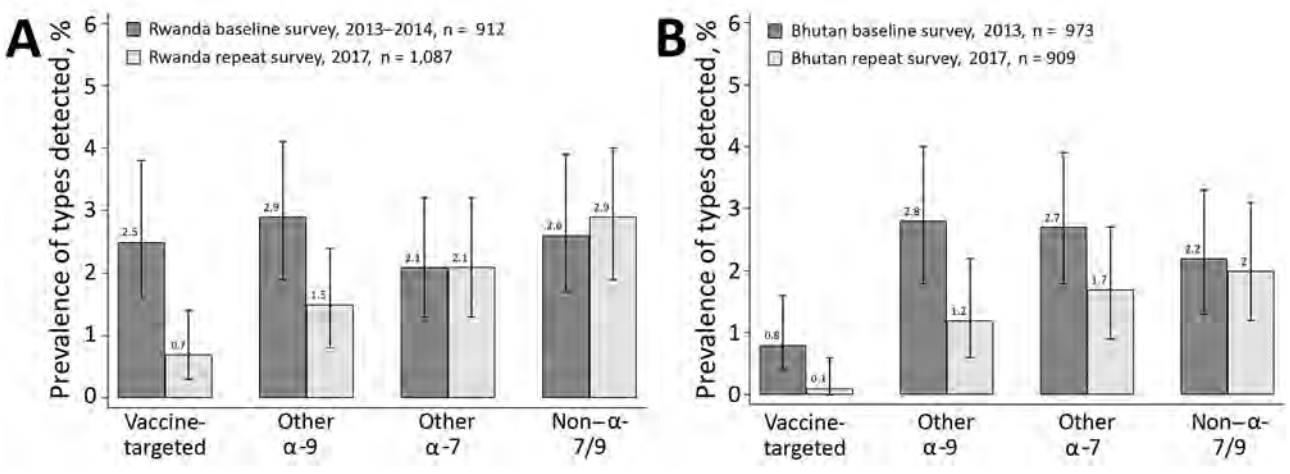


**Figure 3.** Overall crude human papillomavirus prevalence by general primer GP5+/6+-mediated PCR in baseline and repeat surveys in Rwanda (A) and Bhutan (B), with corresponding 95% CIs. Vaccine-targeted types (HPV-6, -11, -16, -18); other α-9 types (HPV-31, -33, -35, -52, -58); other α-7 types (HPV-39, -45, -59, -68); non–α 7/9 types (HPV-26, -51, -53, -56, -66, -70, -73, -82).

**Table 2.** PRs and VE for positivity for human papillomavirus by GP5+/6+ PCR, Rwanda and Bhutan*

| Country and type of effectiveness | HPV type† | No. (%) by vaccination status | | Adjusted PRs (95% CI)‡ | Adjusted VE, % (95% CI)‡ |
|---|---|---|---|---|---|
| | | Baseline survey | Repeat survey | | |
| Rwanda | | | | | |
| Overall§ | | All | All | | |
| | No. | 912 | 1,087 | | |
| | Vaccine-targeted | 23 (2.5) | 8 (0.7) | 0.22 (0.10 to 0.49) | 78 (51 to 90) |
| | Other α-9 | 26 (2.9) | 16 (1.5) | 0.42 (0.22 to 0.79) | 58 (21 to 78) |
| | Other α-7 | 19 (2.1) | 23 (2.1) | 0.82 (0.44 to 1.52) | 18 (–52 to 56) |
| | Non–α 7/9 | 24 (2.6) | 31 (2.9) | 0.85 (0.50 to 1.45) | 15 (–45 to 50) |
| Restricted¶ | | Unvaccinated | All | | |
| | No. | 519 | 1,087 | | |
| | Vaccine-targeted | 21 (4.0) | 8 (0.7) | 0.14 (0.06 to 0.31) | 86 (69 to 94) |
| | Other α-9 | 17 (3.3) | 16 (1.5) | 0.37 (0.19 to 0.74) | 63 (26 to 81) |
| | Other α-7 | 12 (2.3) | 23 (2.1) | 0.71 (0.35 to 1.43) | 29 (–43 to 65) |
| | Non–α 7/9 | 12 (2.3) | 31 (2.9) | 0.95 (0.49 to 1.85) | 5 (–85 to 51) |
| Total# | | Unvaccinated | Vaccinated | | |
| | No. | 519 | 962 | | |
| | Vaccine-targeted | 21 (4.0) | 3 (0.3) | 0.05 (0.01 to 0.17) | 95 (83 to 99) |
| | Other α-9 | 17 (3.3) | 15 (1.6) | 0.40 (0.19 to 0.81) | 60 (19 to 81) |
| | Other α-7 | 12 (2.3) | 19 (2.0) | 0.65 (0.31 to 1.37) | 35 (–37 to 69) |
| | Non–α 7/9 | 12 (2.3) | 25 (2.6) | 0.86 (0.43 to 1.71) | 14 (–71 to 57) |
| Bhutan | | | | | |
| Overall§ | | All | All | | |
| | No. | 973 | 909 | | |
| | Vaccine-targeted | 8 (0.8) | 1 (0.1) | 0.12 (0.01 to 0.94) | 88 (6 to 99) |
| | Other α-9 | 27 (2.8) | 11 (1.2) | 0.37 (0.18 to 0.73) | 63 (27 to 82) |
| | Other α-7 | 26 (2.7) | 15 (1.7) | 0.49 (0.26 to 0.92) | 51 (8 to 74) |
| | Non–α 7/9 | 21 (2.2) | 18 (2.0) | 0.77 (0.41 to 1.42) | 23 (–42 to 59) |
| Restricted¶ | | Unvaccinated | All | | |
| | No. | 77 | 909 | | |
| | Vaccine-targeted | 2 (2.6) | 1 (0.1) | 0.04 (0 to 0.48) | 96 (52 to 100) |
| | Other α-9 | 2 (2.6) | 11 (1.2) | 0.44 (0.10 to 1.89) | 56 (–89 to 90) |
| | Other α-7 | 1 (1.3) | 15 (1.7) | 1.08 (0.15 to 7.82) | –8 (–682 to 85) |
| | Non–α 7/9 | 3 (3.9) | 18 (2.0) | 0.47 (0.14 to 1.59) | 53 (–59 to 86) |
| Total# | | Unvaccinated | Vaccinated | | |
| | No. | 77 | 864 | | |
| | Vaccine-targeted | 2 (2.6) | 1 (0.1) | 0.05 (0 to 0.51) | 95 (49 to 100) |
| | Other α-9 | 2 (2.6) | 10 (1.2) | 0.42 (0.10 to 1.81) | 58 (–81 to 90) |
| | Other α-7 | 1 (1.3) | 15 (1.7) | 1.13 (0.16 to 8.21) | –13 (–721 to 84) |
| | Non–α 7/9 | 3 (3.9) | 17 (2.0) | 0.46 (0.15 to 1.48) | 54 (–48 to 85) |

*PR, prevalence ratio; VE, vaccine effectiveness.
†Vaccine-targeted types (HPV-6, -11, -16, -18); other α-9 types (HPV-31, -33, -35, -52, -58); other α-7 types (HPV-39, -45, -59, -68); non–α 7/9 types (HPV-26, -51, -53, -56, -66, -70, -73, -82).
‡Adjusted for age, ever had sexual intercourse, and place of birth in Rwanda, and for ever had sexual intercourse only in Bhutan.
§Entire baseline group compared with entire repeat group.
¶Unvaccinated baseline group compared with entire repeat group.
#Unvaccinated baseline group compared with vaccinated repeat group.

any effectiveness estimates against other HPV α-7 or non–α 7/9 types ever statistically significant.

According to testing with the more sensitive E7-MPG protocol, all HPV prevalence estimates were consistently higher, and corresponding HPV VE estimates consistently lower than the corresponding estimate shown for GP5+/6+. Also, in Bhutan, restricted and total effectiveness were not statistically significant in the E7-MPG PCR (Appendix Table 3).

## Discussion

By comparing type-specific HPV prevalence among young women in repeat surveys, we have assessed the early impact of HPV vaccination at the population-level in Rwanda and Bhutan, 2 LMICs implementing a national HPV vaccination program. In both countries, high-coverage in schools (≈90%) with quadrivalent vaccine has vastly decreased the prevalence of HPV types targeted by the vaccine (HPV-6, -11, -16, and -18), as well as significantly decreasing also that of other α-9 HPV types (HPV-31, -33, -35, -52, and -58), suggesting cross-protection (58% in Rwanda and 63% in Bhutan). On the other hand, no changes were observed in other HPV types during this period, suggesting that the prevalence reduction observed in both countries is entirely vaccine-driven and not attributable to changes over time in sexual behavior.

An important strength of our present study is the comparability of HPV prevalence estimates in the baseline and repeat surveys in both countries. To this

end, we adopted the same methods and procedures to recruit, interview, and test young women and used, as far as feasible, the same high-schools to recruit study participants. To account for behavioral changes that might have occurred in the source population, we adjusted our estimates for the reported history of sexual intercourse, which was more frequent in repeat surveys in both countries. The prevalence of non–α 7/9 HPV types (for which no prior evidence for cross-protection exists) did not significantly change over time. We also did not observe any indications of type replacement.

In both countries, HPV vaccination had been introduced before the implementation of the baseline surveys; 43% of study participants in Rwanda and 92% in Bhutan were vaccinated in the catch-up campaigns. Hence, our effectiveness estimates are underestimated because of vaccine-induced protection in the reference group. In particular, estimates of overall effectiveness are affected by both direct and indirect protection in the baseline group, whereas restricted and total effectiveness estimates are affected only by indirect protection. Furthermore, some baseline survey participants might have been sexually active and HPV-infected before being vaccinated. In Bhutan, because of the high vaccination coverage, the number of participants positive to vaccine-targeted HPV types in the reference group was tiny; therefore, effectiveness estimates are imprecise. Nevertheless, irrespective of the genotyping method considered, overall effectiveness was >80%. Restricted and total effectiveness were not statistically significant in tests using E7-MPG PCR. By contrast, in Rwanda where vaccination coverage in the reference group was much lower, estimates of effectiveness against vaccine-targeted and other α-9 types are more precise and consistently statistically significant.

We used 2 HPV testing methods of different analytical sensitivity (GP5+/6+ PCR and E7-MPG) to enable us to compare possibly different estimates of VE by assay and overcome the possible problem of the relative lack of sensitivity of HPV detection in urine. Significant overall effectiveness was shown with both methods used. However, we estimated stronger overall VE (78% in Rwanda and 88% in Bhutan) when HPV was measured by using GP5+/6+ PCR. The lower estimated VE might relate to the increased detection of low-level HPV DNA by E7-MPG that might have no clinical significance (*20*). In Bhutan, as mentioned previously, restricted and total effectiveness estimates were not statistically significant most likely because of few HPV vaccine-type positive women.

Population-level impact of HPV vaccination with both bivalent and quadrivalent vaccine, as well as cross-protection against other high-risk HPV types, have been repeatedly documented in HICs (*21*) The magnitude of the reduction in prevalence of cervical HPV types targeted by the quadrivalent vaccine impact estimated in Rwanda and Bhutan is similar to that recently recorded in repeat cross-sectional studies conducted in Australia (93% among women <25 years of age) (*22*) and the United States (86% among 14- to 19-year-olds and 71% among 20- to 24-year-olds) (*23*). The size of cross-protection of quadrivalent vaccine against α-9 HPV types estimated in our study is consistent with estimates reported in Australia (60% against HPV-31, -33, and -45) (*24*), the post-hoc analysis of trial data (22% against HPV-31, -33, -35, -52, and -58) (*25*), and findings of a metaanalysis summarizing data from HICs (17% against HPV-31, -33, -35, -45, -52, and -58) (*21*).

The most relevant limitation of our study is that baseline surveys could not be conducted in unvaccinated populations. As a result, overall effectiveness estimates are likely to be underestimated in both countries and the statistical power of the study, in particular in Bhutan, is reduced. For Bhutan, the overall effectiveness against vaccine-targeted HPV types reported in this article is the same as that estimated from surveys based on cervical cell samples (88% [95% CI 80%–92%]) (*26*). Furthermore, vaccination status was self-reported and could not be ascertained by using vaccination registries. This limitation might have particular impact on the estimations of restricted and total effectiveness, which use HPV prevalence among unvaccinated participants in baseline surveys as a reference category. To minimize the risk for recall bias, questions about HPV vaccination were accompanied by a detailed description of the vaccination process as implemented in each country. Furthermore, no other vaccine was given to age-groups targeted with HPV vaccination in the same period. Finally, our surveys were not designed, nor powered, to disentangle direct and indirect (herd) vaccine-induced protection, which has been repeatedly observed in studies conducted in HICs (*9*,*24*,*27*,*28*). However, the high overall effectiveness estimated in Bhutan (88%), despite very similar HPV vaccination coverage in the 2 surveys, suggests vaccine-induced indirect herd effect provided by older birth cohorts to younger ones. In the surveys based on cervical cell samples conducted in Bhutan, the indirect effectiveness was 78% (95% CI 61%–88%) (*26*). Such an intercohort protection mechanism has been observed in other community-randomized trials (*29*) and elucidated through modeling studies (*30*).

In summary, our study provides direct evidence from LMICs of the marked effectiveness of a high-coverage national catch-up HPV vaccination program.

The full impact of vaccination of the routine target cohorts, vaccinated before sexual debut, remains to be measured; continued monitoring will be necessary to assess the sustained impact of the 2-dose HPV vaccination schedule recently introduced in both countries. The reported findings will also be instrumental in supporting a long-term stakeholders' commitment to HPV vaccination, to inform future budget allocation exercises, and to adapt local cervical cancer screening programs to vaccinated populations. Furthermore, the repeat urine-based survey approach used in Rwanda and Bhutan to monitor the impact of HPV vaccination is well-accepted and remarkably adaptable to a wide range of settings and populations, making this approach particularly valuable to periodically assess the early impact of HPV vaccination.

### Acknowledgments

We are indebted to the technicians of the Molecular Pathology Unit of the Department of Pathology (Amsterdam University Medical Center, Vrije Universiteit Amsterdam, Cancer Center Amsterdam) for skillful laboratory work and to health-care workers in Rwanda and Bhutan for implementing fieldwork activities.

This work was supported by the Bill and Melinda Gates Foundation (http://www.gatesfoundation.org) (grant no. OPP1053353).

Where authors are identified as personnel of the International Agency for Research on Cancer or World Health Organization, the authors alone are responsible for the views expressed in this article and they do not necessarily represent the decisions, policy, or views of the International Agency for Research on Cancer or World Health Organization. D.A.M.H. is minority shareholder of Self-Screen B.V., a spin-off company of VU University Medical Center (currently known as Amsterdam University Medical Center, Vrije Universiteit Amsterdam) (*2*). Self-Screen B.V. holds patents related to the work and has developed and manufactured Conformité Européenne in vitro diagnostic assays, which are licensed to QIAGEN (QIAscreen HPV PCR Test and QIAsure Methylation Test) (*3*). D.A.M.H. has been on the speakers' bureau of QIAGEN and serves occasionally on the scientific advisory boards of Pfizer and Bristol-Myers Squibb. Outside the submitted work, A.V. is a co-founder and board member of Novosanis N.V., a spin-off of the University of Antwerp. Since January 2019, Novosanis N.V. is a wholly owned subsidiary of OraSure Technologies; in addition, A.V. has a patented liquid collection device (liquid sampler, kit of parts, and method for assembly [WO 2014/037152 A1 issued]); all rights and benefits are now owned by Orasure Technology Inc. The other authors declare that they have no conflicts of interest.

### About the Author

Dr. Baussano, an infectious diseases physician and epidemiologist, works at the International Agency for Research on Cancer, Lyon, France. His current research focuses on prevention and control of infection-related cancers both in high- and low or middle-income countries.

### References

1. Bray F, Ferlay J, Soerjomataram I, Siegel RL, Torre LA, Jemal A. Global cancer statistics 2018: GLOBOCAN estimates of incidence and mortality worldwide for 36 cancers in 185 countries. CA Cancer J Clin. 2018;68:394–424. https://doi.org/10.3322/caac.21492
2. de Martel C, Plummer M, Vignat J, Franceschi S. Worldwide burden of cancer attributable to HPV by site, country and HPV type. Int J Cancer. 2017;141:664–70. https://doi.org/10.1002/ijc.30716
3. World Health Organization. WHO Director-General calls for all countries to take action to help end the suffering caused by cervical cancer. 2018 [cited 2019 Mar 19]. http://www.who.int/reproductivehealth/call-to-action-elimination-cervical-cancer
4. Simms KT, Steinberg J, Caruana M, Smith MA, Lew JB, Soerjomataram I, et al. Impact of scaled up human papillomavirus vaccination and cervical screening and the potential for global elimination of cervical cancer in 181 countries, 2020-99: a modelling study. Lancet Oncol. 2019; 20:394–407. https://doi.org/10.1016/S1470-2045(18)30836-2
5. Arbyn M, Xu L, Simoens C, Martin-Hirsch PP. Prophylactic vaccination against human papillomaviruses to prevent cervical cancer and its precursors. Cochrane Database Syst Rev. 2018;5:CD009069. https://doi.org/10.1002/14651858.CD009069.pub3
6. Lehtinen M, Dillner J. Clinical trials of human papillomavirus vaccines and beyond. Nat Rev Clin Oncol. 2013;10:400–10. https://doi.org/10.1038/nrclinonc.2013.84
7. Lei J, Ploner A, Elfström KM, Wang J, Roth A, Fang F, et al. HPV Vaccination and the risk of invasive cervical cancer. N Engl J Med. 2020;383:1340–8. https://doi.org/10.1056/NEJMoa1917338
8. World Health Organization. Human papillomavirus vaccines: WHO position paper, May 2017. Wkly Epidemiol Rec. 2017;92:241–68.
9. Drolet M, Bénard É, Pérez N, Brisson M, Ali H, Boily M-C, et al.; HPV Vaccination Impact Study Group. Population-level impact and herd effects following the introduction of human papillomavirus vaccination programmes: updated systematic review and meta-analysis. Lancet. 2019;394:497–509. https://doi.org/10.1016/S0140-6736(19)30298-3
10. Bruni L, Diaz M, Barrionuevo-Rosas L, Herrero R, Bray F, Bosch FX, et al. Global estimates of human papillomavirus vaccination coverage by region and income level: a pooled analysis. Lancet Glob Health. 2016;4:e453–63. https://doi.org/10.1016/S2214-109X(16)30099-7
11. Binagwaho A, Wagner CM, Gatera M, Karema C, Nutt CT, Ngabo F. Achieving high coverage in Rwanda's national human papillomavirus vaccination programme. Bull World Health Organ. 2012;90:623–8. https://doi.org/10.2471/BLT.11.097253
12. Dorji T, Tshomo U, Phuntsho S, Tamang TD, Tshokey T, Baussano I, et al. Introduction of a National HPV vaccination program into Bhutan. Vaccine. 2015;33:3726–30. https://doi.org/10.1016/j.vaccine.2015.05.078

13. Franceschi S, Chantal Umulisa M, Tshomo U, Gheit T, Baussano I, Tenet V, et al. Urine testing to monitor the impact of HPV vaccination in Bhutan and Rwanda. Int J Cancer. 2016;139:518–26. https://doi.org/10.1002/ijc.30092
14. Vorsters A, Van den Bergh J, Micalessi I, Biesmans S, Bogers J, Hens A, et al. Optimization of HPV DNA detection in urine by improving collection, storage, and extraction. Eur J Clin Microbiol Infect Dis. 2014;33:2005–14. https://doi.org/10.1007/s10096-014-2147-2
15. de Roda Husman AM, Snijders PJ, Stel HV, van den Brule AJ, Meijer CJ, Walboomers JM. Processing of long-stored archival cervical smears for human papillomavirus detection by the polymerase chain reaction. Br J Cancer. 1995;72:412–7. https://doi.org/10.1038/bjc.1995.347
16. Jacobs MV, Walboomers JM, Snijders PJ, Voorhorst FJ, Verheijen RH, Fransen-Daalmeijer N, et al. Distribution of 37 mucosotropic HPV types in women with cytologically normal cervical smears: the age-related patterns for high-risk and low-risk types. Int J Cancer. 2000;87:221–7. https://doi.org/10.1002/1097-0215(20000715)87:2<221::AID-IJC11>3.0.CO;2-2
17. Schmitt M, Dondog B, Waterboer T, Pawlita M, Tommasino M, Gheit T. Abundance of multiple high-risk human papillomavirus (HPV) infections found in cervical cells analyzed by use of an ultrasensitive HPV genotyping assay. J Clin Microbiol. 2010;48:143–9. https://doi.org/10.1128/JCM.00991-09
18. Halec G, Schmitt M, Dondog B, Sharkhuu E, Wentzensen N, Gheit T, et al. Biological activity of probable/possible high-risk human papillomavirus types in cervical cancer. Int J Cancer. 2013;132:63–71. https://doi.org/10.1002/ijc.27605
19. Halloran ME, Struchiner CJ, Longini IM Jr. Study designs for evaluating different efficacy and effectiveness aspects of vaccines. Am J Epidemiol. 1997;146:789–803. https://doi.org/10.1093/oxfordjournals.aje.a009196
20. Clifford GM, Vaccarella S, Franceschi S, Tenet V, Umulisa MC, Tshomo U, et al. Comparison of two widely used human papillomavirus detection and genotyping methods, GP5+/6+-based PCR followed by reverse line blot hybridization and multiplex type-specific e7-based PCR. J Clin Microbiol. 2016;54:2031–8. https://doi.org/10.1128/JCM.00618-16
21. Drolet M, Bénard É, Boily MC, Ali H, Baandrup L, Bauer H, et al. Population-level impact and herd effects following human papillomavirus vaccination programmes: a systematic review and meta-analysis. Lancet Infect Dis. 2015;15:565–80. https://doi.org/10.1016/S1473-3099(14)71073-4
22. Machalek DA, Garland SM, Brotherton JML, Bateson D, McNamee K, Stewart M, et al. Very low prevalence of vaccine human papillomavirus types among 18- to 35-year old Australian women 9 years following implementation of vaccination. J Infect Dis. 2018;217:1590–600. https://doi.org/10.1093/infdis/jiy075
23. McClung NM, Lewis RM, Gargano JW, Querec T, Unger ER, Markowitz LE. Declines in vaccine-type human papillomavirus prevalence in females across racial/ethnic groups: data from a national survey. J Adolesc Health. 2019;65:715–22. https://doi.org/10.1016/j.jadohealth.2019.07.003
24. Tabrizi SN, Brotherton JM, Kaldor JM, Skinner SR, Liu B, Bateson D, et al. Assessment of herd immunity and cross-protection after a human papillomavirus vaccination programme in Australia: a repeat cross-sectional study. Lancet Infect Dis. 2014;14:958–66. https://doi.org/10.1016/S1473-3099(14)70841-2
25. Brown DR, Kjaer SK, Sigurdsson K, Iversen OE, Hernandez-Avila M, Wheeler CM, et al. The impact of quadrivalent human papillomavirus (HPV; types 6, 11, 16, and 18) L1 virus-like particle vaccine on infection and disease due to oncogenic nonvaccine HPV types in generally HPV-naive women aged 16-26 years. J Infect Dis. 2009;199:926–35. https://doi.org/10.1086/597307
26. Baussano I, Tshomo U, Tenet V, Heideman DAM, Wangden T, Franceschi S, et al. Prevalence of human papillomavirus and estimation of human papillomavirus vaccine effectiveness in Thimphu, Bhutan, in 2011–2012 and 2018: a cross-sectional study. Ann Intern Med. 2020 Sep 22 [Epub ahead of print]. https://doi.org/10.7326/M20-2849
27. Kavanagh K, Pollock KG, Cuschieri K, Palmer T, Cameron RL, Watt C, et al. Changes in the prevalence of human papillomavirus following a national bivalent human papillomavirus vaccination programme in Scotland: a 7-year cross-sectional study. Lancet Infect Dis. 2017;17:1293–302. https://doi.org/10.1016/S1473-3099(17)30468-1
28. Kahn JA, Widdice LE, Ding L, Huang B, Brown DR, Franco EL, et al. Substantial decline in vaccine-type human papillomavirus (HPV) among vaccinated young women during the first 8 years after HPV vaccine introduction in a community. Clin Infect Dis. 2016;63:1281–7. https://doi.org/10.1093/cid/ciw533
29. Lehtinen M, Luostarinen T, Vänskä S, Söderlund-Strand A, Eriksson T, Natunen K, et al. Gender-neutral vaccination provides improved control of human papillomavirus types 18/31/33/35 through herd immunity: Results of a community randomized trial (III). Int J Cancer. 2018;143:2299–310. https://doi.org/10.1002/ijc.31618
30. Baussano I, Garnett G, Segnan N, Ronco G, Vineis P. Modelling patterns of clearance of HPV-16 infection and vaccination efficacy. Vaccine. 2011;29:1270–7. https://doi.org/10.1016/j.vaccine.2010.11.082

Address for correspondence: Iacopo Baussano, International Agency for Research on Cancer, 150 cours Albert Thomas, 69372 Lyon CEDEX 08, France; email: baussanoi@iarc.fr

# Nosocomial Coronavirus Disease Outbreak Containment, Hanoi, Vietnam, March–April 2020

Cuong Duy Do, Vuong Minh Nong, An Van Ngo, Tra Thu Doan, Tuan Quang Nguyen, Phuong Thai Truong, Linus Olson, Mattias Larsson

We report on the public health response generated by an outbreak of coronavirus disease (COVID-19) that occurred during March 2020 at Bach Mai Hospital (BMH) in Hanoi, northern Vietnam's largest hospital complex. On March 18, a total of 3 distinct clusters of COVID-19 cases were identified at BMH. Diagnosis of the initial 3 COVID-19 cases led to contact tracing, symptom screening, and testing of 495 persons and limited quarantine of affected institutes or departments. When 27 staff members in the catering company tested positive for SARS-CoV-2, the entire BMH staff (7,664 persons) was put under quarantine. Contact tracing in the community resulted in an additional 52,239 persons being quarantined. After 3 weeks, the hospital outbreak was contained; no further spread occurred in the hospital. Rapid screening of cases, extensive testing, prompt quarantine, contact tracing, and social distancing contributed to prevent community transmission in Hanoi and northern Vietnam.

In Vietnam, as of September 19, 2020, there were 1,068 laboratory-defined cases of the coronavirus disease (COVID-19) and 35 deaths. The outbreak in Vietnam consisted of 2 waves: the first was during January 22–July 24 with imported cases from countries in the Asia–Pacific region and Europe (*1*–*3*), resulting in 417 cases and no deaths; the second wave began on July 25 in Da Nang, central Vietnam, with community transmission, resulting in 551 cases and 35 deaths (*4*).

Vietnam, a middle-income country in Southeast Asia with a population of ≈100 million and a long, porous border with China, had relatively few cases of COVID-19 and no deaths during the first wave of the outbreak. When the epidemic in China was first acknowledged in late December 2019, the government of Vietnam implemented rapid response and containment by investigation, contact tracing, and quarantine as well as broader community mitigation measures with substantial nonpharmacologic interventions (*5*). The government first strengthened border control measures on January 3; body temperature screening and health declarations by persons entering Vietnam were implemented on January 22. After a case of COVID-19 was detected in Vietnam on January 22 (*6*), the border with China was closed, and all persons entering Vietnam were placed in 14 days' quarantine at centralized facilities. Persons who were suspected of being infected and who had a travel history to Wuhan or Hubei Province in China before January 1, as well as their direct contacts, were also traced and placed in quarantine. Steering committees for COVID-19 prevention were established at each administrative division level, from province to district and commune, under the overall direction of a national committee headed by a deputy prime minister. Tracing was performed by local Center for Disease Control health workers and police forces using flight data and residence information. In addition, a health declaration system was developed on both web and mobile platforms for persons to report their symptoms and suspected cases in nearby living areas. The communication strategies were prepared in early January from various channels, including national and local TV programs, official press, and social media (*5*,*7*). All schools and universities remained closed after Tet (the lunar new year holiday) during January 23–May 4. At centralized facilities, quarantined persons were tested for severe acute respiratory syndrome coronavirus 2 (SARS-CoV-2) ≥2 times.

In January, the first 6 positive cases in Vietnam were diagnosed by the whole-genome sequencing

Author affiliations: Bach Mai Hospital, Hanoi, Vietnam (C.D. Do, V.M. Nong, A.V. Ngo, T.T. Doan, T.Q. Nguyen, P.T. Truong); Karolinska Institutet, Stockholm, Sweden (L. Olson, M. Larsson)

DOI: https://doi.org/10.3201/eid2701.202656

method, with an average of 3–4 days for returning the results. Nasopharyngeal samples were collected at the quarantine sites, then transferred to reference laboratories. Four national institutes act as reference laboratories for different regions of the country. Three of the 4 reference laboratories diagnosed the first 6 cases, including National Institute of Hygiene and Epidemiology (NIHE) in Hanoi, Pasteur Institute in Ho Chi Minh City, and Pasteur Institute in Nha Trang. From January 31 onward, the real-time reverse transcription PCR (RT-PCR) method was widely applied, which helped reduce the time for laboratory confirmation to 6 hours. The test kits were first donated by the World Health Organization (WHO), then provided by Viet-A Corporation (https://www.vietacorp.com).

During January 22–February 13, a total of 16 cases were detected in Vietnam during the first COVID-19 epidemic phase. Among these were 3 cases that were imported from Hubei Province in China to Vinh Phuc, a province near Hanoi; these 3 patients transmitted COVID-19 to 8 other persons, among them a 3-month-old infant (*8*). In response, an entire commune of 10,600 persons was placed in lockdown for 3 weeks. This early response and containment strategy was effective in preventing community transmission during the first phase of the pandemic, and all 16 patients have fully recovered from their illnesses (*9*).

Nosocomial transmission of SARS-CoV-2 has the potential to spark community transmission. In Italy, for example, the national outbreak was initiated by nosocomial transmission of SARS-CoV-2 from a patient in hospital in Codogno, Lombardy, whose delayed diagnosis (36 hours after admission) led to infection of many healthcare workers and other inpatients (*10*). Globally, healthcare workers were overrepresented among COVID-19 cases because they had a high level of exposure, especially those working in triage and COVID-19 screening and testing, along with healthcare workers who had direct patient contact in infectious disease and intensive care departments. In China, healthcare workers had 3.8% of all COVID-19 cases, and 14.8% of them had severe or critical illnesses (*11*).

On March 18 and March 19, the first 2 COVID-19 cases in healthcare workers at Bach Mai Hospital (BMH) in Hanoi were reported, leading to a widespread investigation and response effort at the hospital. We describe how a nosocomial COVID-19 outbreak in one of the largest hospitals in Vietnam was contained through rigorous testing, active case finding, contact tracing, and whole-hospital quarantine.

## Methods

### Setting

BMH is Hanoi's largest national tertiary general hospital, with nearly 3,000 inpatient beds and an average of 5,000 outpatients per day. The hospital has 34 clinical centers, institutes, and departments and 6 paraclinical departments, with >6,000 healthcare workers and nonclinical staff. Three affiliated national institutes are under BMH management: National Heart Institute (NHI), National Institute of Mental Health, and National Institute of Medical Expertise. The first branch of the National Hospital for Tropical Diseases (NHTD) is also located inside the BMH area, but has been a freestanding hospital since 2006. The NHTD has a second branch that was the designated hospital for COVID-19 patients in northern Vietnam, located in a suburban area of Hanoi. BMH has its own infectious disease facility, the Center for Tropical Diseases (CTD), separate from NHTD (Figure 1).

In early January 2020, BMH established 2 dedicated COVID-19 screening triage clinics for suspected cases. These clinics were located in separate areas from other departments of the hospital: the first was next to the main gate, and the second was set up near the CTD (Figure 1). Healthcare workers from the CTD operated both clinics, 1 doctor and 2 nurses working per shift. All patients were required to be screened at the clinics before they received any other services. Clinic staff performed general clinical examinations, gathered epidemiologic data, and classified whether each patient had a suspected case using general criteria issued by the Ministry of Health (MoH), including having ≥1 suspicious symptom (fever, cough, shortness of breath) and having a history of traveling through epidemic areas or having close contact with a patient with confirmed COVID-19 during the preceding 14 days. Before March 12, nasopharyngeal swab specimens from the suspected cases were transferred to the NIHE for SARS-CoV-2 confirmation. Beginning March 13, the specimens were processed and confirmed at BMH itself. Patients with suspected cases were transferred immediately, in dedicated vehicles, to the second branch of NHTD, even if test results had not yet been received.

### Study Design and Data Collection

We conducted a desk review of available documents, patient records, and public data collected during March 17–April 15, 2020. We retrieved demographic data from the official COVID-19 database provided by General Department of Preventive Medicine (https://ncov.vncdc.gov.vn). Symptoms and

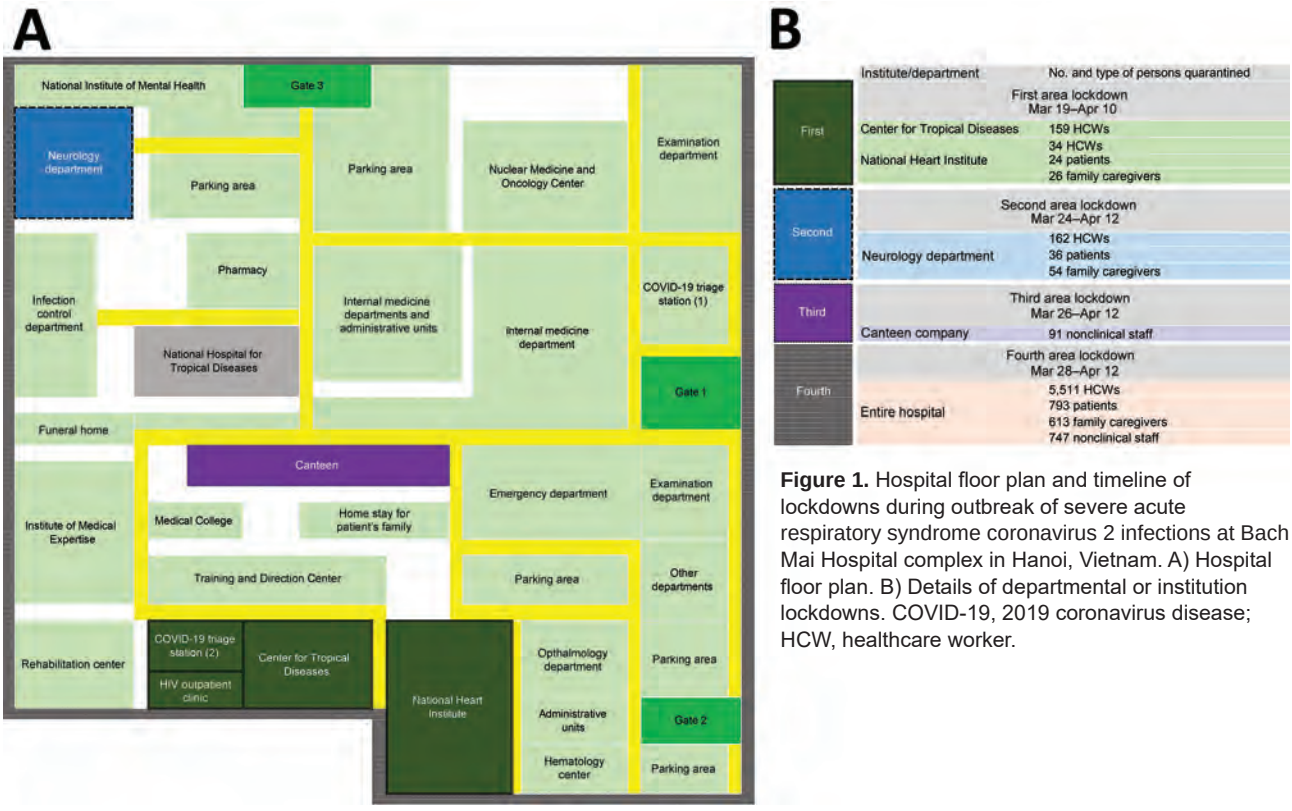


**Figure 1.** Hospital floor plan and timeline of lockdowns during outbreak of severe acute respiratory syndrome coronavirus 2 infections at Bach Mai Hospital complex in Hanoi, Vietnam. A) Hospital floor plan. B) Details of departmental or institution lockdowns. COVID-19, 2019 coronavirus disease; HCW, healthcare worker.

treatment data were systematically collected from the official MoH COVID-19 database (https://ncov.moh.gov.vn) and the MoH official press release website (https://suckhoedoisong.vn).

### Quarantine Measures

We established different definitions of suspected cases, as well as a hierarchy of contacts, between the BMH outbreak and standards management in Vietnam in general. The MoH's general guidelines defined a suspected case as illness in a person who had ≥1 suspicious symptom and had epidemiologic criteria such as travel abroad or direct contact with suspected cases. Patients with suspected cases were put in centralized quarantine for 14 days and tested for SARS-CoV-2. The contacts were categorized at 3 levels: F1 for close contacts of persons with laboratory-confirmed COVID-19 cases, F2 for close contacts of F1 persons, and F3 for close contacts of F2 persons. F1 persons were also placed in centralized quarantine and tested, whereas F2 and F3 persons were isolated and monitored at home. When a community had several confirmed cases and the index patients had multiple complicated contacts, the lockdown of a small administrative unit (usually at the commune level) was carried out.

In the outbreak at BMH, all persons who visited the hospital during March 10–March 20 were considered as the F1 group, regardless of their exposure to laboratory-confirmed cases. For contact tracing, 4 levels of contacts were followed up, from F1 to F4 (F4 comprised close contacts of F3), which is one level higher than the general guideline. F1 and F2 persons were quarantined at a centralized area, and F3 and F4 persons isolated at home (Table). Affected departments at the BMH area were isolated as soon as cases were detected, and lockdown of the entire hospital was implemented after the confirmation of 8 cases and 4 affected departments (Figure 1).

### SARS-COV-2 Testing Strategy

We tested all F1 persons quarantined at BMH for SARS-CoV-2 using RT-PCR in the microbiology department; persons at the CTD, NHI, and neurology department (ND) were tested 3 times to confirm the situations in these departments, and all others at BMH were tested once. Because of the requirement of ≥2 negative tests before a person was released from quarantine, Hanoi Center for Disease Control conducted an additional retest for all confirmed cases before the removal of lockdown. The test kits were either donated by the WHO or provided by Viet-A Corporation. In total, an estimated 15,000 tests were analyzed for quarantined persons at BMH. Each test cost ≈$30 USD.

F1 and F2 persons who were traced and quarantined in the community were provided ≥1 test by the local Center for Disease Control. The numbers of tests per person depended on the decision of the local steering committee, which considered the occurrence of symptoms and laboratory capacity.

The study was approved by the BMH ethics committee. We applied all ethics considerations needed according to MoH or by its designees.

## Results

### Timeline and Outbreak Management at BMH

During March 18–April 14, a total of 46 laboratory-confirmed COVID-19 cases were detected at BMH. The mean age of the patients was 44.9 years, and 80.4% were female. Ten (21.7%) patients were symptomatic; 91.3% had a history of admission to BMH or working or visiting an institute in the BMH complex, including healthcare workers (4.4%), nonclinical staff (58.7%), patients (13.0%), and family caregivers (15.2%) (Figure 2).

Case 86 was in a female nurse working at the HIV outpatient clinic of the CTD. On March 11, she had chest tightness and pain and was admitted to the NHI; her diagnosis was a clinical manifestation of preexisting hypertension illness. She had multiple contacts with CTD staff during lunch and break periods, including the patient with case 87, a 33-year-old female nurse working at the COVID-19 screening clinic who developed fever (38.5°C) and dry cough on March 18 and had a positive test for SARS-CoV-2 on the same day (Figure 2). Quarantine and mass testing were imposed for all of CTD on March 19, involving 159 healthcare workers. NHI was also put in quarantine on the same day; this quarantine included 84 persons (Figure 1).

Case 133 was in a 66-year-old woman who was admitted to Lai Chau General Hospital for stroke on February 29 and was transferred to the BMH neurology department (Figure 2). On March 22, she was transferred back to Lai Chau General Hospital because she developed fever and cough and tested positive for SARS-CoV-2. Quarantine was imposed at the neurology department on March 24 for a total of 252 persons: 162 healthcare workers, 36 patients, and 54 caregivers (Figure 1).

Of the 46 confirmed cases, 27 were from the hospital catering company (Figure 1). These persons provided food and drinks for staff and patients in the hospital and managed the hospital canteens and cleaning tasks. Thus, they moved throughout the hospital and worked close to one another. The reason for the transmission among the company staff might have been the close contact they had during their work without adequate protective equipment. Of the 91 catering company staff who worked at BMH, 28% were SARS-CoV-2 positive. Cases 174 and 184 were symptomatic, with fever and cough, but the others were asymptomatic.

On March 28, the quarantine was extended to all of BMH. A total of 7,664 persons were quarantined: 6,258 healthcare workers and other staff members, 793 inpatients, and 613 of the patients' related family caregivers (Figure 1).

BMH stopped new admissions on March 20, except for patients with severe and critical conditions. A total of 5,113 inpatients were transferred to local provincial hospitals or other specialized hospitals in Hanoi. These patients had non–COVID-19-related illnesses and were considered safe to transfer; they were managed as F1 persons and received preventive measures from the local government and Center for Disease Control. A total of 793 patients with non–COVID-19-related illnesses required treatment at BMH because of the severity of their illness. These patients were managed with a high level of infection control, including spacing beds ≥2 m apart, ensuring that all healthcare workers

**Table.** Definitions, risk assessment, mitigation strategy, and numbers of contacts traced in the COVID-19 outbreak at Bach Mai Hospital, Hanoi, Vietnam, March–April, 2020

| Group | Definition | Risk assessment | Strategy | No. tracings |
|---|---|---|---|---|
| F1 | All patients who visited the hospital, including discharged, transferred out, and outpatients<br>Family caregivers of patients<br>Healthcare workers<br>Medical students and visiting scholars<br>People who visited patients<br>People from catering company, including nonlocal staff<br>Private hired caregivers for patients | Highest | Quarantined at centralized centers for 14 d<br>Test for SARS-CoV-2<br>Daily health assessment by healthcare workers | 27,893 |
| F2 | Close contacts of F1 | High | | |
| F3 | Close contacts of F2 | Medium | Isolated at home for 14 d<br>Self-monitoring for at-risk symptoms<br>Remote health monitoring by local healthcare workers | 24,346 |
| F4 | Close contacts of F3 | Low | | |

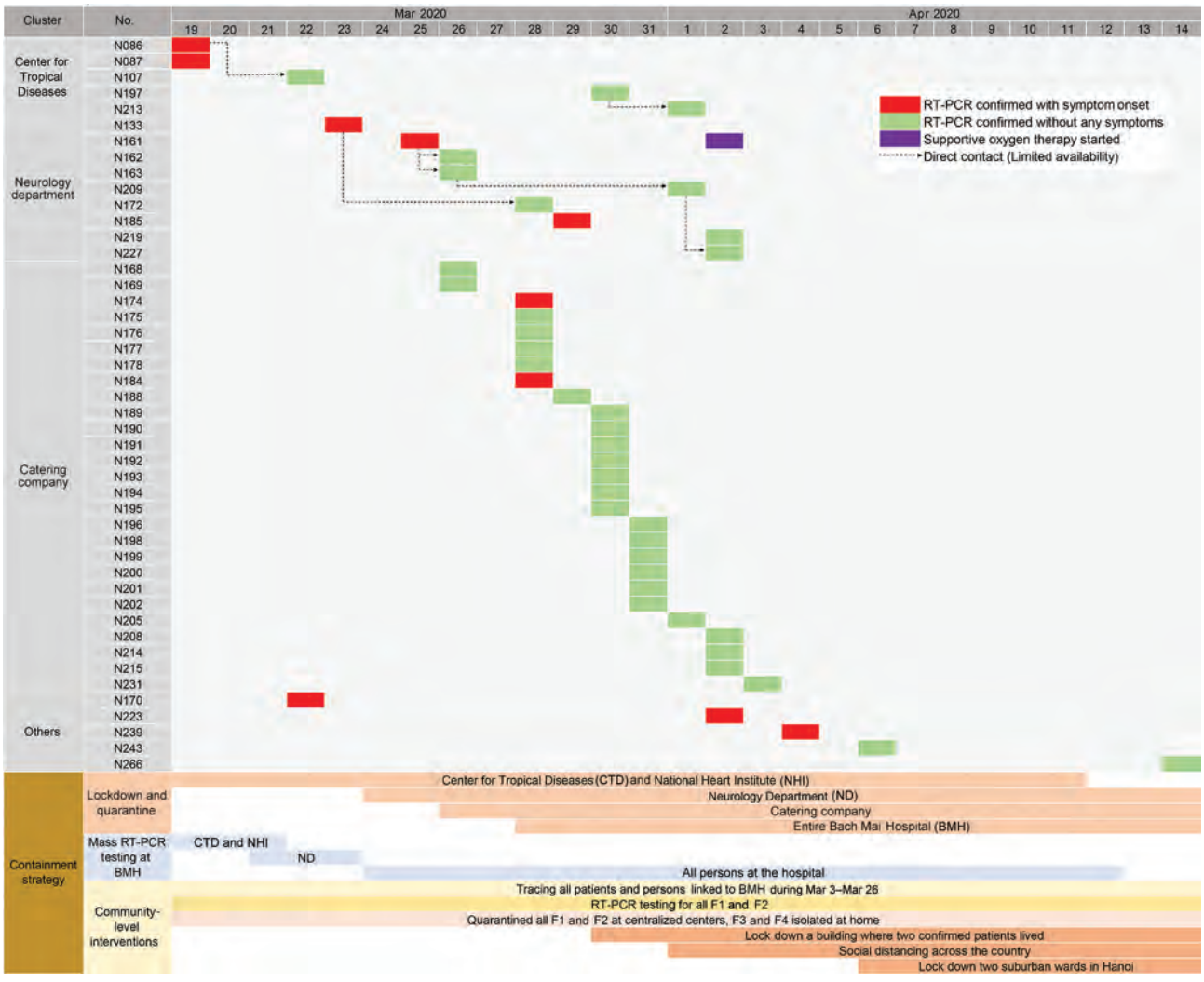


**Figure 2.** Details of severe acute respiratory syndrome coronavirus 2 infections positive cases and timeline of containment strategy for infections related to Bach Mai Hospital, Hanoi, Vietnam. RT-PCR, reverse transcription PCR.

used personal protective equipment, and having healthcare workers using N95 masks when performing aerosol-generating procedures associated with viral spread. In addition, only 1 healthcare worker at a time was allowed contact with a patient, except when a medical intervention required >1 person. Family caregivers were not permitted to have direct contact with patients. Body temperature measurement and mandatory medical reporting for all persons in and out of the hospital, enhanced room air flow, and retraining in infection prevention and control (IPC) were implemented for all the staff. Separate entryways for new emergency cases and routine dialysis patients were set. Other routine outpatients, such as patients with diabetes, hepatitis, or cardiovascular disease, were asked to delay their regular visits and go to local hospitals for care and treatment.

### Contact Tracing and Outbreak Containment in the Community

F1 persons were categorized into 7 groups. Four groups had registered information at BMH: healthcare workers, visiting scholars and students, nonclinical staff, and patients (both inpatients and outpatients). The other 3 groups, family, hired caregivers, and other persons who visited patients, could be found only by epidemiologic investigation, self-reported or reported in the local community. In addition, information on all cases was widely available on social media and media outlets, alerting members of the general community about potential exposure if they were at the hospital.

Healthcare workers, visiting scholars and students, severely or critically ill inpatients, and their family and hired caregivers were quarantined and

managed at BMH. All other BMH cases from March 10–20 (including 5,113 transferred patients) were traced and managed by the local Hanoi steering committee. A total of 52,239 persons were followed up in the community. Among those who were traced, 27,893 F1 and F2 persons were put in quarantine (Table). Nearly 30,000 RT-PCR tests were performed on F1 and F2 persons in the community.

## Discussion

We describe how nosocomial transmission in a large hospital was contained through extensive testing of all possibly exposed persons, even those without any symptoms; whole hospital quarantine for ≥2 weeks; contact tracing in the community; and quarantine of all contacts. From the beginning of the COVID-19 pandemic, testing strategy has been an essential intervention in preventing community spread of COVID-19 in Vietnam. As of May 13, 2020, >275,000 SARS-CoV-2 RNA tests had been conducted in Vietnam; the proportion of tests per confirmed case was ≈950 (*12*). These measures were put in place to prevent a generalized epidemic and a heavy burden on the healthcare system, which generally was overloaded, with only ≈9 doctors and 15 nurses per 10,000 population (*13*). One advantage during the outbreak at BMH was the laboratory capacity and available RT-PCR test kits provided by a local company. About 15,000 tests were done for persons quarantined at the hospital. More than half of these tests were analyzed at BMH itself, which helped to greatly reduce the waiting time for detecting cases. In addition, by March 21, there were 22 licensed laboratories, including 6 provincial Centers for Disease Control, able to perform RT-PCR tests for SARS-CoV-2 across the country, which increased the local case detection capacity.

All of BMH was quarantined after 8 cases of COVID-19 were detected in 4 departments. All persons linked to the hospital, including healthcare workers, inpatients, outpatients, visitors, and close contacts of these persons within 14 days before the lockdown (27,893 persons), were considered as having suspected cases, placed in centralized quarantine, and tested. Modeling suggested that active case tracing and early testing had a major effect on reducing the community transmission of COVID-19, up to 80% (*14*), and the outcomes from outbreak containment at BMH could provide good empirical evidence for this result. Active case tracing has been implemented in several other countries and has shown remarkable effectiveness (*15*–*18*).

Quarantine for all the contacts was the major factor for successful outbreak containment at BMH. However, quarantine was not always an acceptable solution for many other settings because of the lack of resources, facilities, or policy support (*19*,*20*). In the case of BMH, the decision on the whole-hospital quarantine was made by considering multiple criteria. The first advantage was the hospital's beds for transferred-out patients and the new 9-story building that could be used for the accommodation of quarantined persons. Second, the hospital contingency fund and support from the Hanoi city council were rapidly mobilized for food, drinks, and other necessities. In addition, the transmission from an unknown index case might have been the tip of an iceberg of undetected of community transmission in Hanoi that encouraged aggressive actions to prevent widespread community transmission.

Only 10 symptomatic cases were found among the 46 laboratory-confirmed COVID-19 cases in the outbreak (21.7%); 1 patient needed intensive care with mechanical ventilation (2.2%), and there were no deaths. Several large investigations with a similar approach to active case tracking efforts also showed a high rate of asymptomatic patients among persons who tested positive for SARS-CoV-2. For example, in a cohort of 829 employees who worked at Rutgers University and associated hospitals in New Jersey, USA, the prevalence of asymptomatic SARS-CoV-2 cases was 65.9% (E.S. Barrett et al., unpub. data, https://doi.org/10.1101/2020.04.20.20072470). A large population screening in Iceland showed that the positive rate among 13,080 nontargeted citizens was 0.8%, and 43% of SARS-CoV-2 positive cases were asymptomatic (*21*). In a homeless shelter in Boston, the asymptomatic rate among persons who tested positive for SARS-CoV-2 was 87.8% (*22*). These results emphasize the importance of detecting mild or asymptomatic COVID-19 cases because they may be vectors for transmission (*23*; D.C. Buitrago-Garcia et al., unpub. data, https://doi.org/10.1101/2020.04.25.20079103).

The relatively low rate of transmission to healthcare workers might be the result of use of personal protective equipment and masks, as well as other IPC activities. In addition, the outbreak occurred during a generally cool time of year, so opening windows and doors was still practiced in most of areas of the hospital, which could help to lower transmission risk, compared with having to use air conditioning during the warmer season (*24*). Most of the cases were in nonclinical staff members, which might be the result of high frequency of exposure with lack of protective equipment as well as work in crowded conditions in the kitchen and canteen. After the first cluster was detected at the CTD, a higher level of infection control was implemented, including retraining

in IPC measures for all staff. However, the compliance of nonmedical staff was inadequate, which might be the result of a lack of adequate information, training, and personal protective equipment, as well as management possibly underestimating the severity of the situation. This finding illustrates the importance for healthcare facilities to protect their nonclinical staff by providing appropriate training and adequate protective equipment, because these staff members may be both victims and vectors to other staff and patients (*25*,*26*).

The outbreak at BMH contributed to a decision to implement a social distancing campaign throughout Vietnam during April 1–April 14 and in Hanoi for an additional week after that. We found that the BMH outbreak uncovered both nosocomial and unexplained cases likely to have resulted from community transmission. The social distancing campaign might have contributed to reducing community transmission, as indicated in several other settings (*27*,*28*). In addition, experiences from the containment of the SARS outbreak in 2003 (*29*,*30*), which also occurred at BMH, helped hospital management make quarantine decisions faster. Many frontline healthcare workers who were present during the SARS outbreak 2003 were still working at BMH and contributed to the management, planning, and processing of the COVID-19 outbreak containment. Although containment in the BMH COVID-19 outbreak was successful, the index case was not found.

Our investigation is subject to several limitations. First, we could not estimate the coverage of contact tracing in the community because of the lack of information for some at-risk groups that did not register in the database (family/private caregivers and persons who visited patients). Second, because we did not interview all the patients who tested positive, the source and index cases were not fully interpreted. Finally, we did not perform a complete outbreak investigation, which reduced the validity of the containment outcomes and made it difficult to compare this study with other studies.

In conclusion, the COVID-19 outbreak containment at BMH is a noteworthy example in which a major university hospital was quarantined to prevent further community transmission. Containment of the outbreak in BMH could serve as an example for other settings that are experiencing new outbreaks of this highly transmissible disease.

We suggest several recommendations to prevent hospital COVID-19 nosocomial outbreaks. Strict triage stations should be established at all entrances; healthcare workers, nonclinical staff, and contract workers should be monitored and those with symptoms recommended to stay home if ill; and other key IPC measures should be instituted at the hospital according to the hierarchy of IPC controls. Protective equipment should be provided to all staff, both clinical and nonclinical, as well as training in how to use it correctly. In addition, cases of severe viral pneumonia should be monitored closely, with SARS-CoV-2 testing recommended when all other possible causes have been excluded. High-risk groups, such as patients with severe acute respiratory infections, healthcare workers, and elderly patients, should also be strictly monitored.

### Acknowledgments

We thank 2 infected nurses and all BMH staff for their contributions to this report. We also thank the government of Vietnam and everyone who followed the regulations.

### About the Author

Dr. Do is the director of the Center for Tropical Diseases, Bach Mai Hospital, Hanoi, Vietnam. He is a researcher in the field of infectious diseases and HIV.

### References

1. Hoang VM, Hoang HH, Khuong QL, La NQ, Tran TTH. Describing the pattern of the COVID-19 epidemic in Vietnam. Glob Health Action. 2020;13:1776526. https://doi.org/10.1080/16549716.2020.1776526
2. Ha BTT, Ngoc Quang L, Mirzoev T, Tai NT, Thai PQ, Dinh PC. Combating the COVID-19 epidemic: experiences from Vietnam. Int J Environ Res Public Health. 2020;17: 3125. https://doi.org/10.3390/ijerph17093125
3. Dinh L, Dinh P, Nguyen PDM, Nguyen DHN, Hoang T. Vietnam's response to COVID-19: prompt and proactive actions. J Travel Med. 2020;27:taaa047. https://doi.org/10.1093/jtm/taaa047
4. Vuong NM, Le Quyen NT, Tra DT, Do Van T, Tuan NQ, Co DX, et al. The second wave of COVID-19 in a tourist hotspot in Vietnam. J Travel Med. 2020;taaa174. https://doi.org/10.1093/jtm/taaa174
5. Pham QT, Rabaa MA, Duong HL, Dang QT, Tran DQ, Quach HL, et al.; OUCRU COVID-19 Research Group. The first 100 days of SARS-CoV-2 control in Vietnam. Clin Infect Dis. 2020;ciaa1130. https://doi.org/10.1093/cid/ciaa1130
6. Phan LT, Nguyen TV, Luong QC, Nguyen TV, Nguyen HT, Le HQ, et al. Importation and human-to-human transmission of a novel coronavirus in Vietnam. N Engl J Med. 2020;382:872–4. https://doi.org/10.1056/NEJMc2001272
7. Tran BX, Dang AK, Thai PK, Le HT, Le XTT, Do TTT, et al. Coverage of health information by different sources in communities: implication for COVID-19 epidemic response. Int J Environ Res Public Health. 2020;17:3577. https://doi.org/10.3390/ijerph17103577
8. Le HT, Nguyen LV, Tran DM, Do HT, Tran HT, Le YT, et al. The first infant case of COVID-19 acquired from a secondary transmission in Vietnam. Lancet Child Adolesc Health. 2020;4:405–6. https://doi.org/10.1016/S2352-4642(20)30091-2

9. Thanh HN, Van TN, Thu HNT, Van BN, Thanh BD, Thu HPT, et al. Outbreak investigation for COVID-19 in northern Vietnam. Lancet Infect Dis. 2020;20:535–6. https://doi.org/10.1016/S1473-3099(20)30159-6
10. Giuffrida A, Beaumont P. Coronavirus: inquiry opens into hospitals at centre of Italy outbreak. The Guardian. 2020 Feb 26 [cited 2020 Feb 28]. https://www.theguardian.com/world/2020/feb/26/coronavirus-inquiry-opens-into-hospitals-at-centre-of-italy-outbreak
11. Wu Z, McGoogan JM. Characteristics of and important lessons from the coronavirus disease 2019 (COVID-19) outbreak in China: summary of a report of 72 314 cases from the Chinese Center for Disease Control and Prevention. JAMA. 2020;323:1239–42. https://doi.org/10.1001/jama.2020.2648
12. Kennedy D, Vu V, Ritchie H, Bartlein R, Rothschild O, Bausch D, et al. COVID-19: Identifying countries with indicators of success in responding to the outbreak. Gates Open Res. 2020;4:62. https://doi.org/10.12688/gatesopenres.13140.1
13. Takashima K, Wada K, Tra TT, Smith DR. A review of Vietnam's healthcare reform through the Direction of Healthcare Activities (DOHA). Environ Health Prev Med. 2017;22:74. https://doi.org/10.1186/s12199-017-0682-z
14. Kretzschmar ME, Rozhnova G, Bootsma MCJ, van Boven M, van de Wijgert JHHM, Bonten MJM. Impact of delays on effectiveness of contact tracing strategies for COVID-19: a modelling study. Lancet Public Health. 2020;5:e452–9. https://doi.org/10.1016/S2468-2667(20)30157-2
15. Andrikopoulos S, Johnson G. The Australian response to the COVID-19 pandemic and diabetes—lessons learned. Diabetes Res Clin Pract. 2020;165:108246. https://doi.org/10.1016/j.diabres.2020.108246
16. Kucharski AJ, Klepac P, Conlan AJK, Kissler SM, Tang ML, Fry H, et al. Effectiveness of isolation, testing, contact tracing, and physical distancing on reducing transmission of SARS-CoV-2 in different settings: a mathematical modelling study. Lancet Infect Dis. 2020;20:1151–60. https://doi.org/10.1016/S1473-3099(20)30457-6
17. Lee SW, Yuh WT, Yang JM, Cho Y-S, Yoo IK, Koh HY, et al. Nationwide results of COVID-19 contact tracing in South Korea: individual participant data from an epidemiological survey. JMIR Med Inform. 2020;8:e20992. https://doi.org/10.2196/20992
18. Baker MG, Kvalsvig A, Verrall AJ. New Zealand's COVID-19 elimination strategy. Med J Aust. 2020;213:198. https://doi.org/10.5694/mja2.50735
19. Parmet WE, Sinha MS. Covid-19—the law and limits of quarantine. N Engl J Med. 2020;382:e28. https://doi.org/10.1056/NEJMp2004211
20. Peak CM, Kahn R, Grad YH, Childs LM, Li R, Lipsitch M, et al. Individual quarantine versus active monitoring of contacts for the mitigation of COVID-19: a modelling study. Lancet Infect Dis. 2020;20:1025–33. https://doi.org/10.1016/S1473-3099(20)30361-3
21. Gudbjartsson DF, Helgason A, Jonsson H, Magnusson OT, Melsted P, Norddahl GL, et al. Spread of SARS-CoV-2 in the Icelandic population. N Engl J Med. 2020;382:2302–15. https://doi.org/10.1056/NEJMoa2006100
22. Baggett TP, Keyes H, Sporn N, Gaeta JM. Prevalence of SARS-CoV-2 infection in residents of a large homeless shelter in Boston. JAMA. 2020;323:2191–2. https://doi.org/10.1001/jama.2020.6887
23. Al-Sadeq DW, Nasrallah GK. The incidence of the novel coronavirus SARS-CoV-2 among asymptomatic patients: a systematic review. Int J Infect Dis. 2020;98:372–80. https://doi.org/10.1016/j.ijid.2020.06.098
24. Dietz L, Horve PF, Coil DA, Fretz M, Eisen JA, Van Den Wymelenberg K. 2019 novel coronavirus (COVID-19) pandemic: built environment considerations to reduce transmission. mSystems. 2020;5:e00245-20. https://doi.org/10.1128/mSystems.00245-20
25. Wee LE, Sim XYJ, Conceicao EP, Aung MK, Goh JQ, Yeo DWT, et al. Construction of a container isolation ward: a rapidly scalable modular approach to expand isolation capacity during a COVID-19 pandemic. Infect Control Hosp Epidemiol. 2020 Sep 23 [Epub ahead of print]. https://doi.org/10.1017/ice.2020.1222
26. Hunter E, Price DA, Murphy E, van der Loeff IS, Baker KF, Lendrem D, et al. First experience of COVID-19 screening of health-care workers in England. Lancet. 2020;395:e77–8. https://doi.org/10.1016/S0140-6736(20)30970-3
27. Cheng H-Y, Jian S-W, Liu D-P, Ng T-C, Huang W-T, Lin H-H; Taiwan COVID-19 Outbreak Investigation Team. Contact tracing assessment of COVID-19 transmission dynamics in Taiwan and risk at different exposure periods before and after symptom onset. JAMA Intern Med. 2020;180:1156–63. https://doi.org/10.1001/jamainternmed.2020.2020
28. Matrajt L, Leung T. Evaluating the effectiveness of social distancing interventions to delay or flatten the epidemic curve of coronavirus disease. Emerg Infect Dis. 2020;26:1740–8. https://doi.org/10.3201/eid2608.201093
29. Le DH, Bloom SA, Nguyen QH, Maloney SA, Le QM, Leitmeyer KC, et al. Lack of SARS transmission among public hospital workers, Vietnam. Emerg Infect Dis. 2004;10:265–8. https://doi.org/10.3201/eid1002.030707
30. Tuan PA, Horby P, Dinh PN, Mai LTQ, Zambon M, Shah J, et al.; WHO SARS Investigation Team in Vietnam. SARS transmission in Vietnam outside of the health-care setting. Epidemiol Infect. 2007;135:392–401. https://doi.org/10.1017/S0950268806006996


Address for correspondence: Linus Olson, Department of Women's and Children's Health, Tomtebodavägen18 floor 8, Karolinska Institutet, SE-171 77 Stockholm, Sweden; email: linus.olson@ki.se

# Aspergillosis Complicating Severe Coronavirus Disease

Kieren A. Marr, Andrew Platt, Jeffrey A. Tornheim, Sean X. Zhang, Kausik Datta, Celia Cardozo, Carolina Garcia-Vidal

Aspergillosis complicating severe influenza infection has been increasingly detected worldwide. Recently, coronavirus disease–associated pulmonary aspergillosis (CAPA) has been detected through rapid reports, primarily from centers in Europe. We provide a case series of CAPA, adding 20 cases to the literature, with review of pathophysiology, diagnosis, and outcomes. The syndromes of pulmonary aspergillosis complicating severe viral infections are distinct from classic invasive aspergillosis, which is recognized most frequently in persons with neutropenia and in other immunocompromised persons. Combined with severe viral infection, aspergillosis comprises a constellation of airway-invasive and angio-invasive disease and results in risks associated with poor airway fungus clearance and killing, including virus- or inflammation-associated epithelial damage, systemic immunosuppression, and underlying lung disease. Radiologic abnormalities can vary, reflecting different pathologies. Prospective studies reporting poor outcomes in CAPA patients underscore the urgent need for strategies to improve diagnosis, prevention, and therapy.

Invasive aspergillosis is frequently recognized in persons who have severe immunosuppression, especially that associated with hematologic malignancies and transplantation. It is characterized by hyphal invasion through bronchial or lower airway tissues, with potential vascular invasion and hallmark radiographic findings reflective of hemorrhage and necrosis. However, *Aspergillus* species cause a broader constellation of pulmonary disease, pathologically characterized by inflammatory disease in the airway and acute and chronic invasion, largely depending on host risks (*1*). Much recent work has focused on describing epidemiology and significance of aspergillosis occurring after severe viral infections, especially influenza and coronavirus disease (COVID-19).

Aspergillosis associated with severe influenza virus infection (influenza-associated aspergillosis, IAA) was reported in 1951, when Abbott et al. described fatal infection in a woman with cavitary invasive pulmonary aspergillosis noted on autopsy (*2*). Scattered reports appeared in thereafter; Adalja et al. summarized 27 cases in the literature during 1952–2011, which reported predominance after influenza A infection, associated lymphopenia, and occurring in persons of a broad age range (14–89 years), but with little underlying lung disease (*3*). There were increased numbers of cases reported during and after the 2009 influenza A(H1N1) pandemic (*3*–*10*). In 2016, Crum-Cianflone summarized 57 cases from literature; most (70%) were associated with H1N1 influenza (*11*). Invasive aspergillosis was described, with complicating tracheobronchitis noted in 15.8%. Reported cases (68/128) during 1952–2018 were summarized by Vanderbeke et al. (*12*).

An increased understanding of IAA emerged from large cohort studies performed after 2015. One 7-year retrospective study in intensive care units (ICUs) in Belgium and the Netherlands reported rates varying from 14% in immunocompetent persons to 31% in immunocompromised persons (*13*). Within the influenza-infected cohort, male sex, hematologic malignancy, high acute physiological assessment and chronic health evaluation II (APACHE II) score, and corticosteroid use were associated with IAA, whereas underlying diabetes was associated with lower risks. Cohort studies conducted in Canada, China, and Taiwan reported similar risk profiles and that incidence of disease varied according to season and viral epidemiology (*14*–*17*). Despite these data, 2 recent survey studies reported that risk recognition is poor outside of countries in Europe (*18*,*19*). Only 63% of critical care physicians responding to an international survey were familiar with

Author affiliations: Johns Hopkins School of Medicine, Baltimore, Maryland, USA (K.A. Marr, J.A. Tornheim, S.X. Zhang, K. Datta); National Institutes of Health, Bethesda, Maryland, USA (A. Platt); Hospital Clinic of Barcelona, Barcelona, Spain (C. Cardozo, C. Garcia-Vidal)

DOI: https://doi.org/10.3201/eid2701.202896

IAA, and differences were notable between physicians in the United States (17%) and Europe (58%) (*19*). Similarly, a US Centers for Disease Control and Prevention–sponsored survey of infectious diseases practitioners reported that only 26% of 114 respondents were familiar with IAA (*18*).

An increased number of reports described a similar syndrome associated with severe COVID-19 (*20*–*45*). In this study, we add to this literature, report 20 additional cases from 2 centers in Spain and the United States and provide a review of literature describing the emerging entity of COVID-19–associated pulmonary aspergillosis (CAPA).

## Methods

### Case Series

Cases of CAPA were identified during March–June 2020 at Johns Hopkins University (Baltimore, MD, USA) and Hospital Clinic of Barcelona (Barcelona, Spain) by review of microbiologic and infectious diseases consult data, with approval of the institutional review boards of both institutions. Cases were defined as recovery of *Aspergillus* species from respiratory fluids (tracheobronchial secretions, sputum, bronchoalveolar lavage [BAL]) or positive (index ≥1) serum or BAL markers, identified with work-up for possible secondary pneumonia, typically clinically indicated with new fever or respiratory decompensation with new focal infiltrates on chest radiograph or computed tomography (CT) scan. Results for a Fungitell β-D Glucan Assay (https://www.fungitell.com) were reported when available but did not suffice to establish case diagnosis; 60 pg/mL was considered intermediate and ≥80 pg/mL was considered positive. Neither center used PCR-based testing for fungal infections during this period. Charts were reviewed to summarize demographic, clinical, and outcomes data, including day of hospitalization and ICU admission relative to reported onset of symptoms. World Health Organization (WHO) ordinal scale scores (0–8) at diagnosis of CAPA were estimated (*46*).

### Analyses

We calculated descriptive statistics for all data. These values are shown as frequencies, means (±SD), medians (with ranges), and proportions.

## Results

### Characteristics of Cases

Patient-level data were compiled in cases recognized before June 2020 at Johns Hopkins Medical Center and Hospital Clinic of Barcelona (Table, https://wwwnc.cdc.gov/EID/article/27/1/20-2896-T1.htm). Demographics mirrored those described for poor overall outcomes; advanced age and underlying diseases of hypertension and pulmonary disease predominated. Two patients had an underlying immunosuppressive disease. The most common immunosuppressing agents associated with CAPA included systemic or inhaled steroids, most frequently for adjunctive management of COVID-19 related inflammatory disease. CAPA was recognized a median of 11 days after symptom onset and 9 days after ICU admission. Most of these patients were hospitalized during stages characterized by inflammation or acute respiratory distress syndrome or afterwards, with lung injury, in the ICU and required respiratory support. Thus, WHO ordinal classifications at CAPA diagnoses were ≥5 (*46*).

In cases for which CT scans were performed, radiographic reports generally described a mixture of findings attributable to the virus (ground glass opacities and crazy-paving), findings consistent with airway inflammation and mucous plugging (bronchiectasis, airway wall thickening and irregularity, bronchiectasis), and radiographic findings consistent with airway-invasive disease (consolidations, tree-in-bud nodules) (Table; Figure 1). In some cases, larger nodules with necrosis and cavitation were noted. Although nodular necrosis with cavitation was described, no radiographic reports highlighted findings that are classically associated with angioinvasive disease (ground glass attenuation described as halos) (*47*).

Bronchoscopy was rare, and diagnosis was most frequently supported by tracheal aspirate culture; few patients had positive serum biomarkers. Seventeen (85%) cases were identified by positive culture; most (12/17, 71%) were identified by detection of *A. fumigatus*. Although rarely used, results of Fungitell β-D glucan assays were more frequently positive compared with serum galactomannan assays. All but 2 patients were given intravenous antifungal drugs, which included voriconazole, posaconazole, or liposomal amphotericin B. One patient (#2) was not treated for findings of a nodule and positive serum galactomannan result, was extubated, and survived. Another patient (#12) had diagnosis of CAPA established 1 day before death and never received antifungal therapy.

### Synopsis of Literature

Evidence of secondary aspergillosis developing in persons infected with severe acute respiratory

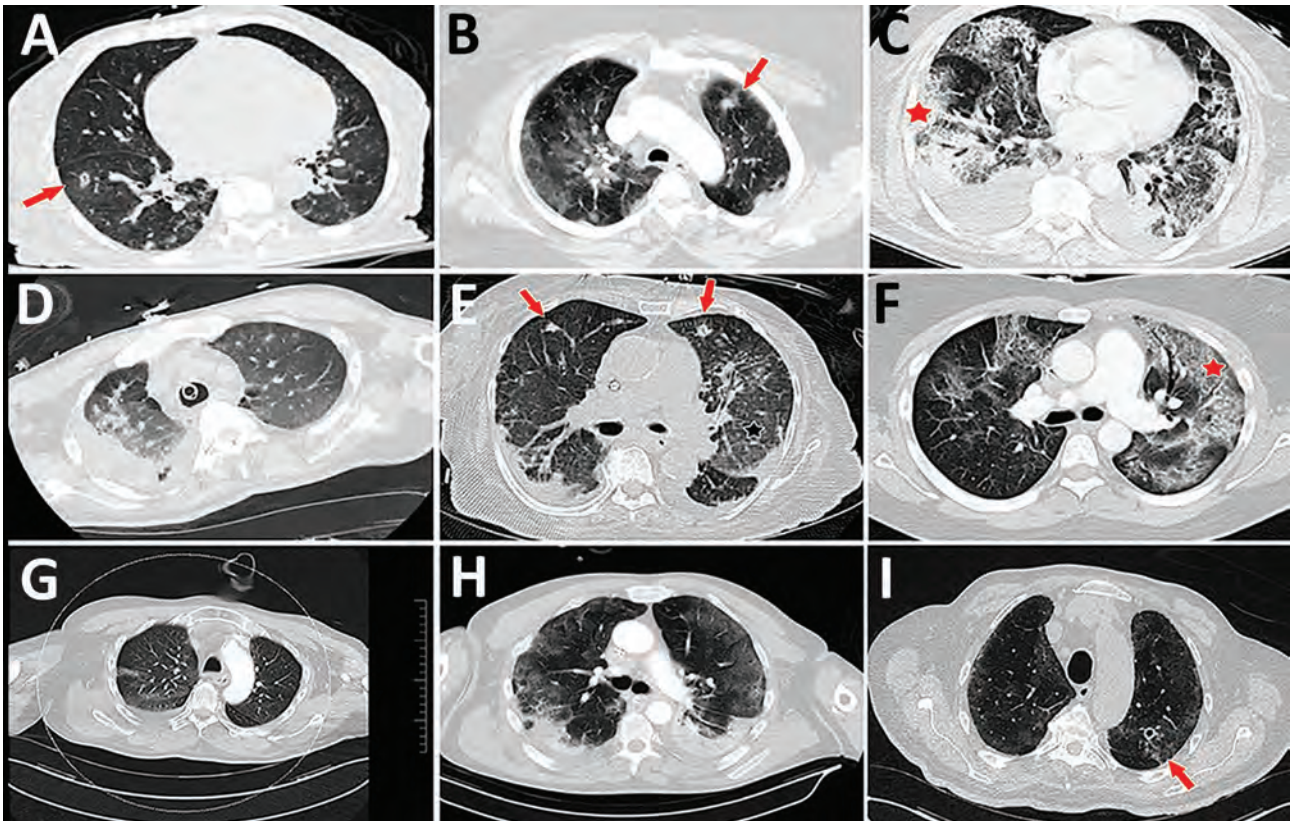


**Figure 1.** Representative computed tomography (CT) scans for 9 patients with aspergillosis complicating severe viral pneumonia in patients with coronavirus disease. Scans were obtained at or around diagnosis of coronavirus disease–associated pulmonary aspergillosis in this series of patients, described in the Table (https://wwwnc.cdc.gov/EID/article/27/1/20-2896-T1.htm). Corresponding case-patients are indicated with lettered superscripts in the radiology column of Table 1. Examples of nodules and cavitating nodules are indicated by red arrows, and prominent airway thickening and bronchiectasis in ground glass opacities are indicated by red stars.

syndrome coronavirus 2 was first evident in China but emphasized more clearly by case series from Europe. We provide a timeline of studies describing secondary aspergillosis occurring in persons with COVID-19, an entity that has become referred to CAPA (Figure 2) (*23*–*45*). Early reports from China noted frequent CT findings suggestive of invasive aspergillosis but provided few microbiologic or clinical details. Although without specific citation, a US Department of Defense document on COVID-19 noted that there were anecdotal communications of invasive aspergillosis documented in postmortem examinations in China (*23*). Use of empirical antifungal drugs was frequent; in a large study evaluating risk factors for death, ≈50% of persons had secondary infections, and antifungal therapy was administered in 22% (*21*,*22*). Radiographic descriptions were suggestive of invasive disease; in a study describing radiography in 51 patients, 11 (22%) had nodules with halos or reverse halos (*20*). Without manifestations of patient-specific data, these cohort studies nonetheless indicated that there were substantial issues with secondary fungal infections in persons who had WHO stage II–III disease. In a study from China that evaluated outcomes of persons who had increased levels of serum interleukin 6, mixed fungal infections occurred in 27.1% of 48 critically ill patients (*24*). In another study from China, *Aspergillus* species were recovered from respiratory fluids in 14% of COVID-19 patients (*24*).

Patient-level descriptions emerged quickly in small case series from Europe. In the first case series from Europe for COVID-19, a total of 1 of 5 patients had alveolar infiltrates on chest radiograph and *Aspergillus* spp. cultured from tracheal aspirate (*25*). Thereafter, rapid reports from centers in Austria, Belgium, France, Germany, the Netherlands, and Italy emerged (Figure 2). Differences in diagnostic methods and case definitions generated a wide degree of variability, and incidences ranged from 3.8% to 34% of persons admitted to ICUs (*24*–*45*). One center in China reported rates based on the denominator of persons hospitalized because of COVID-19 and that CAPA developed in 7% of 104 patients who had

CAPA (*33*). Bronchoscopy was variably and infrequently performed, but frequent positive results for lavage culture, galactomannan, and *Aspergillus* PCR were observed, and there was visual presence of thick mucoid secretions, sometimes with evidence of bronchial inflammation, such as ulcers (*33*). Using multivariable analysis, Wang et al. reported that advanced age, chronic lung disease, previous positive results for the β-D glucan assay, antimicrobial drug exposure, and mechanical ventilation to be risks for CAPA in persons who had COVID-19 (*33*). Histopathologic evidence of fungal invasion has been noted in some, but not all, patients who met CAPA definitions by airway culture or lavage galactomannan and underwent lung biopsy or autopsy (*32*,*38*,*42*). CAPA caused by an azole-resistant *A. fumigatus* isolate was first described in the Netherlands and then in the United Kingdom and France (*34*–*36*).

Results of 3 studies that used a prospective design provided the most accurate estimates of incidence, timing, and clinical usefulness. A prospective, multicenter study that used screening with serum biomarkers and bronchoscopy for 108 mechanically ventilated patients in Italy reported that 30 (27.7%) persons met CAPA criteria (median of 4 days after ICU admission and 14 days after COVID-19 diagnosis) (*38*). Higher mortality rates were noted for CAPA patients than for controls; there were trends to improved survival and decreased follow-up galactomannan levels after antifungal therapy. Another study from the Netherlands applied nondirected BAL by using a closed-circuit suction catheter at a median of 2 days (range 0–8 days) after mechanical ventilation and reported 9/42 (21.4%) patients met criteria for CAPA on the basis of culture or galactomannan BAL positivity; patients with CAPA had longer duration of ICU admission (*41*). Finally, another prospective study that used enhanced screening with blood and respiratory samples, antigen assays (galactomannan enzyme immunoassay [GM EIA] and β-D glucan assay), and an *Aspergillus* PCR reported that 19/135 patients met diagnostic criteria for CAPA when concurrent radiographic abnormalities were considered (*45*).

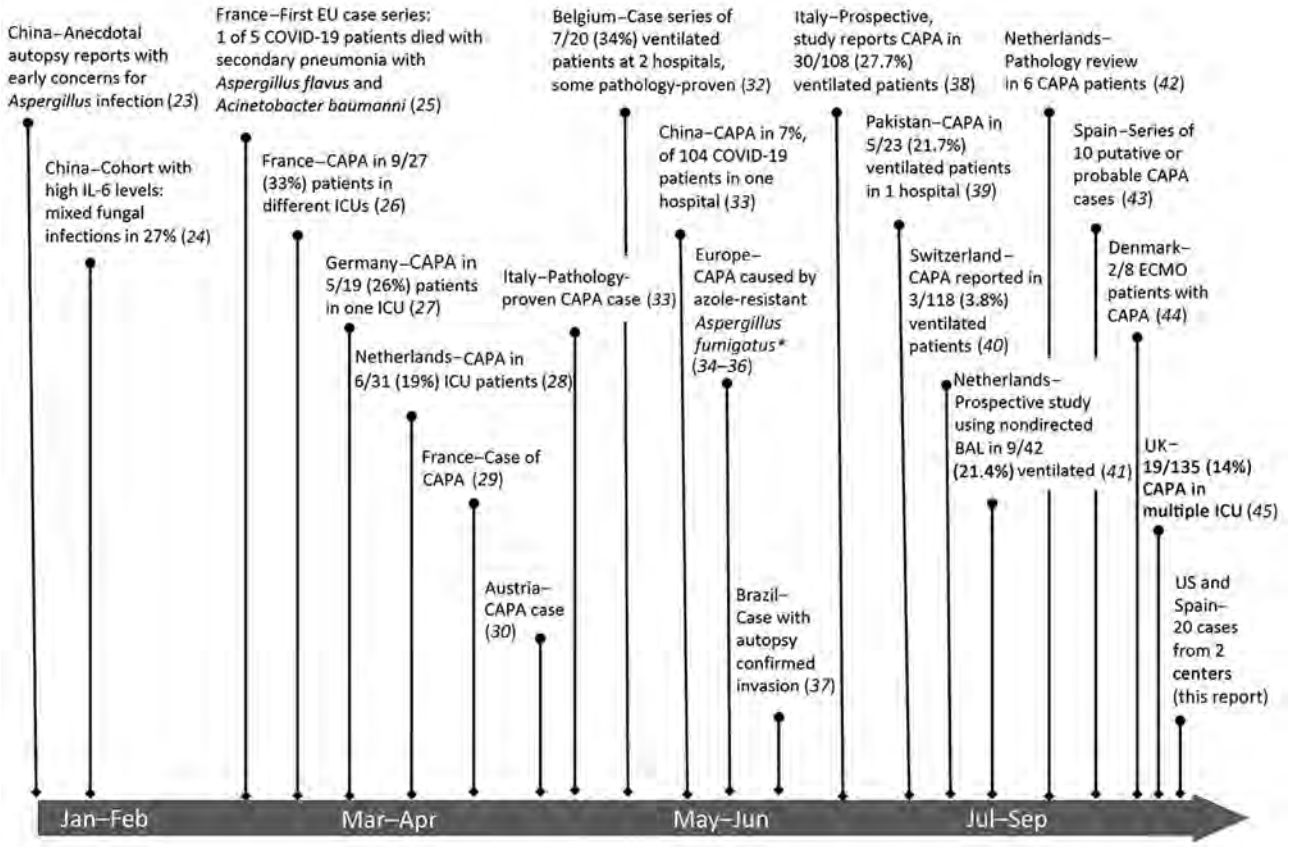


**Figure 2.** Timeline of cases, series, and cohort studies reported to describe emergence of coronavirus disease–associated pulmonary aspergillosis. Reports from China are indicated according to relative times that patients were given care; case series describing CAPA cases are depicted according to approximate time publication became available (preprint or publication), except as indicated (*). BAL, bronchioalveolar lavage; CAPA, coronavirus disease–associated pulmonary aspergillosis; ECMO, extracorporeal membrane oxygenation; EU, European Union; ICU, intensive care unit; IL-6, interleukin 6.

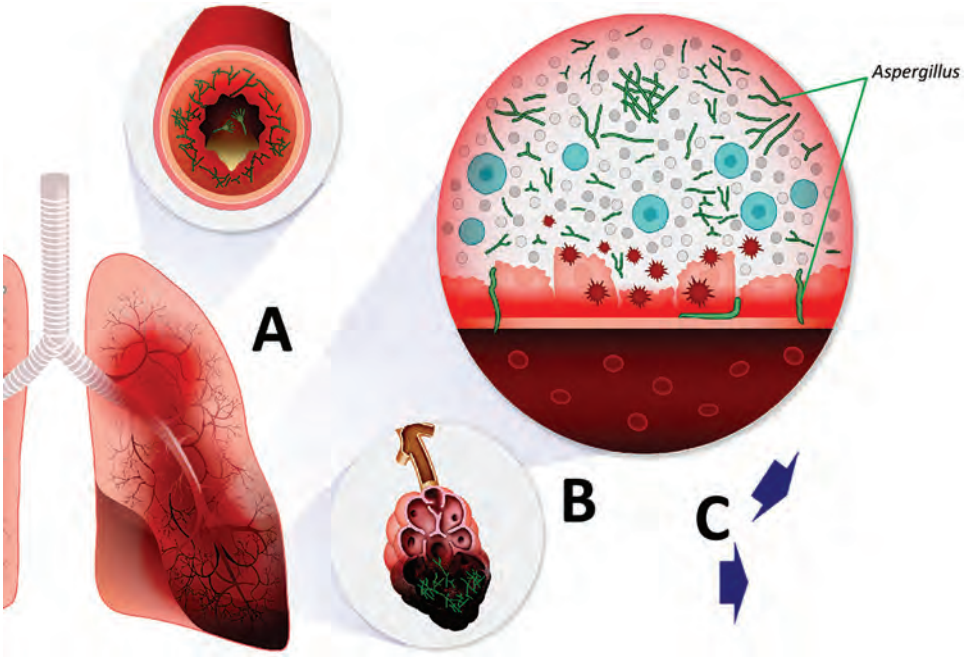


**Figure 3.** Schematic of coronavirus disease–associated pulmonary aspergillosis. *Aspergillus* conidia in airway are cleared poorly because of ≥1 defects in primary pulmonary immunity or secondary defenses, enabling conidial germination into hyphal morphotypes, which elicit increased inflammatory responses in the airway and potential invasion into the lungs. A mixed constellation of inflammatory to invasive airway disease, and invasive pulmonary aspergillosis leads to multiple manifestations, including tracheobronchitis and obstructive pneumonia, and complications of invasive fungal pneumonia (nodules, necrosis with cavities, pleural invasion). A) Airways. *Aspergillus* overgrowth causes pathologic airway inflammation and excess mucous production. B) Alveoli. Hyphal growth causes invasive pneumonia. C) Invasive aspergillosis tracheobronchitis postobstructive bacterial pneumonia.

## Discussion

Despite decades of case reporting and large cohort studies, many clinicians still fail to recognize that *Aspergillus* species can cause destructive inflammatory and invasive pathology in persons who have severe influenza, mistakenly ascribing culture results to benign airway colonization (*18*,*19*). With this in mind, the rapid recognition of CAPA, as described by reports from multiple centers (Figure 2), probably reflects previous learning and heightened awareness in centers in Europe and the clinical diligence that arises when encountering a new and unknown entity. We add 20 cases to the accumulating literature describing CAPA. Multiple pathophysiologic, clinical, and diagnostic considerations have emerged from observations reported to date.

First, pathophysiology of disease is distinct in this context, and not necessarily similar to invasive aspergillosis that occurs in classically immunosuppressed persons. Although it is broadly understood that *Aspergillus* species cause allergic manifestations, such as allergic bronchopulmonary aspergillosis, and a severe invasive pneumonia with potential angioinvasion, forms of chronic necrotizing or semiinvasive *Aspergillus* pulmonary disease are less well understood. These types of infections occur in persons who have more chronic immunosuppression, especially that related to prolonged steroids and chronic obstructive pulmonary disease. Common pathophysiology of these syndromes involves poor clearance of conidia, enabling bronchial inflammation and invasion, manifesting with distinct radiographic and clinical findings characteristic of airway invasion with slower development of necrosis, and exuberant and chronic tracheobronchitis, frequently with lack of angioinvasion, which limits its performance of serum-based diagnostics (*48*). Mounting evidence suggests that severe respiratory virus infections, especially influenza and infection with severe acute respiratory syndrome coronavirus 2, can be complicated by *Aspergillus* airway overgrowth with pulmonary infection similarly characterized by mixed airway inflammation and bronchial invasion (Figure 3).

Distinguishing between benign airway colonization and potential disease caused by *Aspergillus* spp. has always been difficult because conidia are common inhabitants of airways and do not always cause inflammatory or invasive disease. To improve the process of obtaining information about what constitutes disease, early efforts have been directed toward standardizing diagnostics and definitions by using a similar approach, as for IAA, which eliminates the classic immunocompromising host criteria and relies on BAL and serum antigen results to define certainty of disease (*49*–*51*). Cases reported in this study would be considered probable CAPA if tracheal aspirate or sputum cultures met microbiologic criteria. Although

more efforts are required to clarify definitions, clinicians should understand that definitions are not meant to provide clinical guidance, but to support a metric to compare epidemiology and clinical trial data. Three prospective cohort studies suggest that treatment with antifungal drugs might improve clinical outcomes (*38*,*41*,*45*), but definitive evidence of clinical usefulness necessitates larger comparative studies that use antifungal drugs for prevention or early therapy.

Most published studies suggest that CAPA occurs in ≈20%–30% of the most severely ill, mechanically ventilated COVID-19 patients (*24*–*45*). Perhaps the most accurate estimates of incidence emerged from 3 studies that deployed enhanced prospective screening and provided incidence estimates of 14%–20% and poor outcomes that might potentially be improved by use of antifungal therapy (*38*,*41*,*45*). Another study reported a particularly low rate of CAPA (3.8%) (*40*). Diagnostic differences probably contribute to variability in estimates.

Performance of diagnostic testing is variable depending on immunopathogenesis of disease. Persons who have extensive invasion into and beyond airways show positive serum GM EIA results more frequently than persons who had disease restricted to the endobronchial lumen. For this reason, sensitivity of the serum GM EIA assay is highest in hematology/oncology patients, ranging from 60% to 80%, but lower in ICU patients, estimated to be 30%–50% (*48*–*52*). In CAPA cases, serum GM EIAs have been infrequently positive. In our case series, results of β-D glucan assays were more frequently positive, but false-positive results would be anticipated because of to cross-reactivity (*52*). A prospective study reported a relatively large proportion of cases with positive results for β-D glucan assays for patients who had candidiasis (*38*). When applied to BAL, results for GM EIA appear positive more frequently, and some investigators reported potential utility of quantitative PCR or GM lateral flow tests in lavage (*24*–*45*). However, because none of these tests were developed and optimized for the nonhematology context, performance could be variable with different cutoff values.

Despite diagnostic limitations, several studies point to utility in routine use of fungal biomarkers and early screening in persons who have COVID-19, especially directed toward BAL. Lei et al. examined residual serum samples by using a β-D glucan assay and GM in 181 COVID-19 patients who had oxygen saturation <94% or respiratory rates >29 breaths/min, and reported positive results in the β-D glucan assay for 32 (17.7%) of 181 patients and positive results in the GM EIA for 14 (7.7%) of 181 patients sampled (*53*). In that study, most positive results occurred after 14 days of COVID-19 symptoms, which is consistent with the timing of recognized CAPA. Although their retrospective study was limited by lack of clinical and outcomes data, findings suggest that at least some cases might be identified by more aggressive use of a biomarker screening strategy. This suggestion was shown more definitively in prospective studies that evaluated BAL or lavage from a close-circuit system, with antifungal therapy applied for lavage GM EIA positivity potentially leading to improved outcomes (*38*,*41*,*45*). Deploying such a strategy might be limited in some centers by complexity of assays and difficulties in obtaining bronchoscopy because of viral infectivity.

Radiographic manifestations might be best understood when one considers that CAPA can be a constellation of mixed airway and invasive diseases. In our series and other reports, radiographic appearance varied from early evidence of airway inflammation and invasion (irregular airways to centrilobular nodules) to airway necrosis; this necrosis was most frequently characterized by cavitary nodules and progressive consolidation (*33*). Corresponding histopathology can be varied, including diffuse alveolar damage, with or without clear fungal invasion (*32*,*43*).

Although many questions linger, emerging evidence supports the conclusion that *Aspergillus* species cause mixed pathology in COVID-19 patients, ranging from airway inflammation to semiacute or acute bronchial invasion, similar, in most part, to that observed with severe influenza infections. Increased efforts are needed to determine the best ways to prevent, diagnose, and treat *Aspergillus* disease associated with COVID-19.

Creation of Figure 3 was supported by Cidara Therapeutics.

K.A.M. has received consultative income from Amplyx, Cidara, Merck, and Sfunga; licensing royalties from MycoMed Technologies; and research grant from Merck. C.G.-V. has received honoraria from Gilead Science, Merck, Novartis, Pfizer, Jannsen, and Lilly; and research grants from Gilead and Merck.

## About the Author

Dr. Marr is professor of medicine and vice chair of medicine for Innovation in Healthcare Implementation at Johns Hopkins School of Medicine, Baltimore, Maryland. Her primary research interests are fungal infections and diagnostics.

## References


1. Kosmidis C, Denning DW. The clinical spectrum of pulmonary aspergillosis. Thorax. 2015;70:270–7. https://doi.org/10.1136/thoraxjnl-2014-206291
2. Abbott JD, Fernando HV, Gurling K, Meade BW. Pulmonary aspergillosis following post-influenzal bronchopneumonia treated with antibiotics. BMJ. 1952;1:523–5. https://doi.org/10.1136/bmj.1.4757.523
3. Adalja AA, Sappington PL, Harris SP, Rimmele T, Kreit JW, Kellum JA, et al. Isolation of *Aspergillus* in three 2009 H1N1 influenza patients. Influenza Other Respir Viruses. 2011; 5:225–9. https://doi.org/10.1111/j.1750-2659.2011.00202.x
4. Alobaid K, Alfoudri H, Jeragh A. Influenza-associated pulmonary aspergillosis in a patient on ECMO. Med Mycol Case Rep. 2019;27:36–8. https://doi.org/10.1016/j.mmcr.2019.12.010
5. Kwon OK, Lee MG, Kim HS, Park MS, Kwak KM, Park SY. Invasive pulmonary aspergillosis after influenza a infection in an immunocompetent patient. Tuberc Respir Dis (Seoul). 2013;75:260–3. https://doi.org/10.4046/trd.2013.75.6.260
6. Lat A, Bhadelia N, Miko B, Furuya EY, Thompson GR III. Invasive aspergillosis after pandemic (H1N1) 2009. Emerg Infect Dis. 2010;16:971–3. https://doi.org/10.3201/eid1606.100165
7. Law P, Gelfand M, Nasser W, Shokouh-Amiri M, Boom A, Yataco J. Invasive aspergillosis in H1N1 influenza A pneumonia. Chest. 2011;140:103A. https://doi.org/10.1378/chest.1085959
8. Wauters J, Baar I, Meersseman P, Meersseman W, Dams K, De Paep R, et al. Invasive pulmonary aspergillosis is a frequent complication of critically ill H1N1 patients: a retrospective study. Intensive Care Med. 2012;38:1761–8. https://doi.org/10.1007/s00134-012-2673-2
9. Kim SH, Kim MN, Lee SO, Choi SH, Kim YS, Woo JH, et al. Fatal pandemic influenza A/H1N1 infection complicated by probable invasive pulmonary aspergillosis. Mycoses. 2012;55:189–92.
10. Lee JY, Joo EJ, Yeom JS, Song JU, Yim SH, Shin DS, et al. *Aspergillus* tracheobronchitis and influenza A co-infection in a patient with AIDS and neutropenia. Infect Chemother. 2014;46:209–15. https://doi.org/10.3947/ic.2014.46.3.209
11. Crum-Cianflone NF. Invasive aspergillosis associated with severe influenza infections. Open Forum Infect Dis. 2016;3:ofw171. https://doi.org/10.1093/ofid/ofw171
12. Vanderbeke L, Spriet I, Breynaert C, Rijnders BJ, Verweij PE, Wauters J. Invasive pulmonary aspergillosis complicating severe influenza: epidemiology, diagnosis and treatment. Curr Opin Infect Dis. 2018;31:471–80. https://doi.org/10.1097/QCO.0000000000000504
13. Schauwvlieghe AF, Rijnders BJ, Philips N, Verwijs R, Vanderbeke L, Van Tienen C, et al.; Dutch-Belgian Mycosis study group. Invasive aspergillosis in patients admitted to the intensive care unit with severe influenza: a retrospective cohort study. Lancet Respir Med. 2018;6:782–92. https://doi.org/10.1016/S2213-2600(18)30274-1
14. Huang L, Zhang N, Huang X, Xiong S, Feng Y, Zhang Y, et al. Invasive pulmonary aspergillosis in patients with influenza infection: a retrospective study and review of the literature. Clin Respir J. 2019;13:202–11. https://doi.org/10.1111/crj.12995
15. Schwartz IS, Friedman DZP, Zapernick L, Dingle TC, Lee N, Sligl W, et al. High rates of influenza-associated invasive pulmonary aspergillosis may not be universal: a retrospective cohort study from Alberta, Canada. Clin Infect Dis. 2020;Jan 6:ciaa007. https://doi.org/10.1093/cid/ciaa007
16. Zou P, Wang C, Zheng S, Guo F, Yang L, Zhang Y, et al. Invasive pulmonary aspergillosis in adults with avian influenza A (H7N9) pneumonia in China: a retrospective study. J Infect Dis. 2020;221(Suppl 2):S193–7. https://doi.org/10.1093/infdis/jiz682
17. Ku YH, Chan KS, Yang CC, Tan CK, Chuang YC, Yu WL. Higher mortality of severe influenza patients with probable aspergillosis than those with and without other coinfections. J Formos Med Assoc. 2017;116:660–70. https://doi.org/10.1016/j.jfma.2017.06.002
18. Toda M, Beekmann SE, Polgreen PM, Chiller TM, Jackson BR, Beer KD. Knowledge of infectious disease specialists regarding aspergillosis complicating influenza, United States. Emerg Infect Dis. 2020;26:809–11. https://doi.org/10.3201/eid2604.190953
19. Thevissen K, Jacobs C, Holtappels M, Toda M, Verweij P, Wauters J. International survey on influenza-associated pulmonary aspergillosis (IAPA) in intensive care units: responses suggest low awareness and potential underdiagnosis outside Europe. Crit Care. 2020;24:84. https://doi.org/10.1186/s13054-020-2808-8
20. Li Y, Xia L. Coronavirus disease 2019 (COVID-19): role of chest CT in diagnosis and management. AJR Am J Roentgenol. 2020;214:1280–6. https://doi.org/10.2214/AJR.20.22954
21. Yang X, Yu Y, Xu J, Shu H, Xia J, Liu H, et al. Clinical course and outcomes of critically ill patients with SARS-CoV-2 pneumonia in Wuhan, China: a single-centered, retrospective, observational study. Lancet Respir Med. 2020; 8:475–81. https://doi.org/10.1016/S2213-2600(20)30079-5
22. Chen R, Liang W, Jiang M, Guan W, Zhan C, Wang T, et al.; Medical Treatment Expert Group for COVID-19. Risk factors of fatal outcome in hospitalized subjects with coronavirus disease 2019 from a nationwide analysis in China. Chest. 2020;158:97–105. https://doi.org/10.1016/j.chest.2020.04.010
23. Matos RI, Chung KK, editors. DoD COVID-19 practice Management guide: clinical management of COVID-19. Washington (DC): Department of Health and Human Services; 2020 [cited 2020 Oct 1]. https://asprtracie.hhs.gov/technical-resources/resource/7899/dod-covid-19-practice-management-guide-clinical-management-of-covid-19
24. Chen X, Zhao B, Qu Y, Chen Y, Xiong J, Feng Y, et al. Detectable serum SARS-CoV-2 viral load (RNAaemia) is closely correlated with drastically elevated interleukin 6 (IL-6) level in critically ill COVID-19 patients. Clin Infect Dis. 2020;ciaa449. https://doi.org/10.1093/cid/ciaa449
25. Lescure FX, Bouadma L, Nguyen D, Parisey M, Wicky PH, Behillil S, et al. Clinical and virological data of the first cases of COVID-19 in Europe: a case series. Lancet Infect Dis. 2020;20:697–706. https://doi.org/10.1016/S1473-3099(20)30200-0
26. Alanio A, Dellière S, Fodil S, Bretagne S, Mégarbane B. Prevalence of putative invasive pulmonary aspergillosis in critically ill patients with COVID-19. Lancet Respir Med. 2020;8:e48–9. https://doi.org/10.1016/S2213-2600(20)30237-X
27. Koehler P, Cornely OA, Böttiger BW, Dusse F, Eichenauer DA, Fuchs F, et al. COVID-19 associated pulmonary aspergillosis. Mycoses. 2020;63:528–34. https://doi.org/10.1111/myc.13096
28. van Arkel AL, Rijpstra TA, Belderbos HN, van Wijngaarden P, Verweij PE, Bentvelsen RG. COVID-19-associated pulmonary aspergillosis. Am J Respir Crit Care Med. 2020;202:132–5. https://doi.org/10.1164/rccm.202004-1038LE
29. Blaize M, Mayaux J, Nabet C, Lampros A, Marcelin A-G, Thellier M, et al. Fatal invasive aspergillosis and coronavirus

disease in an immunocompetent patient. Emerg Infect Dis. 2020;26:1636–7. https://doi.org/10.3201/eid2607.201603
30. Prattes J, Valentin T, Hoenigl M, Talakic E, Reisinger AC, Eller P. Invasive pulmonary aspergillosis complicating COVID-19 in the ICU: a case report. Med Mycol Case Rep. 2020 May 11 [Epub ahead of print]. https://doi.org/10.1016/j.mmcr.2020.05.001
31. Antinori S, Rech R, Galimberti L, Castelli A, Angeli E, Fossali T, et al. Invasive pulmonary aspergillosis complicating SARS-CoV-2 pneumonia: a diagnostic challenge. Travel Med Infect Dis. 2020 May 26 [Epub ahead of print]. https://doi.org/10.1016/j.tmaid.2020.101752
32. Rutsaert L, Steinfort N, Van Hunsel T, Bomans P, Naesens R, Mertes H, et al. COVID-19-associated invasive pulmonary aspergillosis. Ann Intensive Care. 2020;10:71. https://doi.org/10.1186/s13613-020-00686-4
33. Wang J, Yang Q, Zhang P, Sheng J, Zhou J, Qu T. Clinical characteristics of invasive pulmonary aspergillosis in patients with COVID-19 in Zhejiang, China: a retrospective case series. Crit Care. 2020;24:299. https://doi.org/10.1186/s13054-020-03046-7
34. Meijer EF, Dofferhoff AS, Hoiting O, Buil JB, Meis JF. Buil, Meis JF. Azole-resistant COVID-19-associated pulmonary aspergillosis in an immunocompetent host: a case report. J Fungi (Basel). 2020;6:79. https://doi.org/10.3390/jof6020079
35. Mohamed A, Hassan T, Trzos-Grzbowska M, Thomas J, Quinn A, O'Sullivan M, et al. Med Mycol Case Rep. 2020 Jun 26 [Epub ahead of print]. https://10/1016/j.mmcr.2020.06.005
36. Ghelfenstein-Ferreira T, Saade A, Alanio A, Bretagne S, de Castro A, Hamane S, et al. Recovery of a triazole-resistant Aspergillus fumigatus in respiratory specimen of COVID-19 patient in ICU: a case report. Med Mycol Case Rep. 2020;Jul 2 [Epub ahead of print]. https://:doi:10.1016/j.mmcr.2020.06.006
37. Santana MF, Pivoto G, Alexandre MA, Baía-da-Silva DC, Borba MG, Val FA, et al. Confirmed invasive pulmonary aspergillosis and COVID-19: the value of postmortem findings to support antemortem management. Rev Soc Bras Med Trop. 2020;53:e20200401 [Epub ahead of print]. https://doi.org/10.1590/0037-8682-0401-2020
38. Bartoletti M, Pascale R, Cricca M, Rinaldi M, Maccaro A, Bussini L, et al.; PREDICO study group. Epidemiology of invasive pulmonary aspergillosis among COVID-19 intubated patients: a prospective study. Clin Infect Dis. 2020 Jul 28 [Epub ahead of print]. https://doi.org/10.1093/cid/ciaa1065
39. Nasir N, Farooqi J, Mahmood SF, Jabeen K. COVID-19-associated pulmonary aspergillosis (CAPA) in patients admitted with severe COVID-19 pneumonia: an observational study from Pakistan. Mycoses. 2020;63:766–70. https://doi.org/10.1111/myc.13135
40. Lamoth F, Glampedakis E, Boillat-Blanco N, Oddo M, Pagani JL. Incidence of invasive pulmonary aspergillosis among critically ill COVID-19 patients. Clin Microbiol Infect. 2020 Jul 10 [Epub ahead of print]. https://doi.org/10.1016/j.cmi.2020.07.010
41. Van Biesen S, Kwa D, Bosman RJ, Juffermans NP. Detection of invasive pulmonary aspergillosis in COVID-19 with non-directed bronchioalveolar lavage. Am J Respir Crit Car Med. 2020 Jul 15 [Epub ahead of print]. https://doi.org/10.1164/rccm.202005-2018LE
42. Flikweert AW, Grootenboers MJ, Yick DC, du Mée AW, van der Meer NJ, Rettig TC, et al. Late histopathologic characteristics of critically ill COVID-19 patients: different phenotypes without evidence of invasive aspergillosis, a case series. J Crit Care. 2020;59:149–55. https://doi.org/10.1016/j.jcrc.2020.07.002
43. Falces-Romero I, Ruiz-Bastián M, Díaz-Pollán B, Maseda E, García-Rodríguez J; SARS-CoV-2 Working Group. Isolation of *Aspergillus* spp. in respiratory samples of patients with COVID-19 in a Spanish tertiary care hospital. Mycoses. 2020 Aug 4 [Epub ahead of print]. https://doi.org/10.1111/myc.13155
44. Helleberg M, Steensen M, Arendrup MC. Invasive aspergillosis in patients with severe COVID-19 pneumonia. Clin Microbiol Infect. 2020 Aug 5 [Epub ahead of print]. https://doi.org/10.1016/j.cmi.2020.07.047
45. White PL, Dhillon R, Cordey A, Hughes H, Faggian F, Soni S, et al. A national strategy to diagnose COVID-19 associated invasive fungal disease in the ICU. Clin Infect Dis. 2020 Aug 29 [Epub ahead of print]. https://doi.org/10.1093/cid/ciaa1298
46. World Health Organization. COVID-19 therapeutic trial synopsis, draft document. In: R&D Blueprint; 2020 [cited 2020 Sep 25]. https://www.who.int/teams/blueprint/covid-19
47. Chabi ML, Goracci A, Roche N, Paugam A, Lupo A, Revel MP. Pulmonary aspergillosis. Diagn Interv Imaging. 2015;96:435–42. https://doi.org/10.1016/j.diii.2015.01.005
48. Teering S, Verreth A, Peeters A, Van Regenmortel N, De Laet I, Schoonheydt K, et al. Prognostic value of serum galactomannan in mixed ICU patients: a retrospective observational study. Anaesthesiol Intensive Ther. 2014;46:145–54. https://doi.org/10.5603/AIT.2014.0027
49. Blot SI, Taccone FS, Van den Abeele AM, Bulpa P, Meersseman W, Brusselaers N, et al. AspICU Study Investigators. A clinical algorithm to diagnose invasive pulmonary aspergillosis in critically ill patients. Am J Respir Crit Care Med. 2012;186:56–64. https://doi.org/10.1164/rccm.201111-1978OC
50. van de Groep K, Verboom DM, van de Veerdonk FL, Haas PA, van der Poll T, Schultz MJ, et al. Detection of invasive aspergillosis in critically ill patients with influenza: the role of plasma galactomannan. Am J Respir Crit Care Med. 2019;200:636–8. https://doi.org/10.1164/rccm.201903-0587LE
51. Bassetti M, Giacobbe DR, Grecchi C, Rebuffi C, Zuccaro V, Scudeller L, et al.; FUNDICU investigators. Performance of existing definitions and tests for the diagnosis of invasive aspergillosis in critically ill, adult patients: a systematic review with qualitative evidence synthesis. J Infect. 2020;81:131–46. https://doi.org/10.1016/j.jinf.2020.03.065
52. Lahmer T, Neuenhahn M, Held J, Rasch S, Schmid RM, Huber W. Comparison of 1,3-β-d-glucan with galactomannan in serum and bronchoalveolar fluid for the detection of *Aspergillus* species in immunosuppressed mechanical ventilated critically ill patients. J Crit Care. 2016;36:259–64. https://doi.org/10.1016/j.jcrc.2016.06.026
53. Lei Y, Song Y, Shu Y, Zhao Y, Huo X, Wang H, et al. Fungal antigenemia in patients with severe coronavirus disease 2019 (COVID-19): the facts and challenges. J Microbiol Immunol Infect. 2020;53:657–9. https://doi.org/10.1016/j.jmii.2020.05.010

Address for correspondence: Kieren A. Marr, Johns Hopkins School of Medicine, 720 Rutland Ave, Ross 1064, Baltimore, MD 21205, USA; email: kmarr4@jhmi.edu

# Invasive Fusariosis in Nonneutropenic Patients, Spain, 2000–2015

Elena Pérez-Nadales, Ana Alastruey-Izquierdo, María José Linares-Sicilia, Juan Carlos Soto-Debrán, Edson Abdala, Julio García-Rodríguez, Miguel Montejo, Patricia Muñoz, Miguel Salavert Lletí, Antonio Rezusta, Maite Ruiz Pérez de Pipaón, Lucrecia Yáñez, Esperanza Merino, María Isolina Campos-Herrero, José María Costa-Mateo, Jesús Fortún, Tomás García-Lozano, Carolina Garcia-Vidal, Mario Fernández-Ruiz, Ferrán Sánchez-Reus, Carmen Castro-Méndez, Inmaculada Guerrero-Lozano, Pere Soler-Palacín, José María Aguado, Luis Martínez-Martínez, Julian Torre-Cisneros,[1] Marcio Nucci,[1] the Spanish Fusariosis Study Group[2]

## Medscape EDUCATION ACTIVITY

In support of improving patient care, this activity has been planned and implemented by Medscape, LLC and Emerging Infectious Diseases. Medscape, LLC is jointly accredited by the Accreditation Council for Continuing Medical Education (ACCME), the Accreditation Council for Pharmacy Education (ACPE), and the American Nurses Credentialing Center (ANCC), to provide continuing education for the healthcare team.

Medscape, LLC designates this Journal-based CME activity for a maximum of 1.00 ***AMA PRA Category 1 Credit(s)™***. Physicians should claim only the credit commensurate with the extent of their participation in the activity.

Successful completion of this CME activity, which includes participation in the evaluation component, enables the participant to earn up to 1.0 MOC points in the American Board of Internal Medicine's (ABIM) Maintenance of Certification (MOC) program. Participants will earn MOC points equivalent to the amount of CME credits claimed for the activity. It is the CME activity provider's responsibility to submit participant completion information to ACCME for the purpose of granting ABIM MOC credit.

All other clinicians completing this activity will be issued a certificate of participation. To participate in this journal CME activity: (1) review the learning objectives and author disclosures; (2) study the education content; (3) take the post-test with a 75% minimum passing score and complete the evaluation at http://www.medscape.org/journal/eid; and (4) view/print certificate. For CME questions, see page 339.

**Release date: December 22, 2020; Expiration date: December 22, 2021**

**Learning Objectives**

Upon completion of this activity, participants will be able to:

- Describe the incidence of invasive fusariosis (IF) and fungal isolates from patients with IF in 18 Spanish hospitals during the 15-year period from 2000 to 2015, according to a retrospective observational study
- Determine the clinical features of patients with IF in 18 Spanish hospitals during the 15-year period from 2000 to 2015, according to a retrospective observational study
- Identify the treatment and outcomes of patients with IF in 18 Spanish hospitals during the 15-year period from 2000 to 2015, according to a retrospective observational study.

**CME Editor**

**Deanna Altomara, BA,** Copyeditor, Emerging Infectious Diseases. *Disclosure: Deanna Altomara, BA, has disclosed no relevant financial relationships.*

**CME Author**

**Laurie Barclay, MD,** freelance writer and reviewer, Medscape, LLC. *Disclosure: Laurie Barclay, MD, has disclosed no relevant financial relationships.*

**Authors**

*Disclosures:* ***Elena Pérez-Nadales, PhD; María José Linares-Sicilia, PhD; Juan Carlos Soto-Debrán, MS; Edson Abdala, PhD; Miguel Montejo, MD; Antonio Rezusta, PhD; Maite Ruiz Pérez de Pipaón, PhD; Lucrecia Yáñez, MD, PhD; Esperanza Merino, MD; María Isolina Campos-Herrero, PhD; José María Costa-Mateo, MD; Jesús Fortún, PhD; Tomás García-Lozano, MD; Mario Fernández-Ruiz, PhD; Ferrán Sánchez-Reus, PhD; Carmen Castro-Méndez, PhD; Inmaculada Guerrero-Lozano, PhD; Pere Soler-Palacín, MD, PhD, MSc; José María Aguado, PhD;*** *and* ***Luis Martínez-Martínez, MD, PhD,*** *have disclosed no relevant financial relationships.* ***Ana Alastruey-Izquierdo, PhD,*** *has disclosed the following relevant financial relationships: served as a speaker or a member of a speakers bureau for Gilead Sciences, Inc.; Merck Sharp & Dohme GmbH; Pfizer Inc.; received grants for clinical research from F2G Ltd.* ***Julio García-Rodríguez, PhD,*** *has disclosed the following relevant financial relationships: served as a speaker or a member of a speakers bureau for Gilead Sciences. Inc.; Pfizer Inc.* ***Patricia Muñoz, MD, PhD,*** *has disclosed the following relevant financial relationships: served as an advisor or consultant for Astellas Pharma, Inc.; Basilea Pharmaceutica Ltd.; Gilead Sciences, Inc.; Merck Sharp & Dohme GmbH; Nabriva Therapeutics plc; Pfizer Inc.; served as a speaker or a member of a speakers bureau for Angelini; Astellas Pharma, Inc.; Basilea Pharmaceutica Ltd.; Gilead Sciences, Inc.; Merck Sharp & Dohme GmbH; Pfizer Inc.; Roche; Werfen; received grants for clinical research from Astellas Pharma, Inc.; CIBERES; Fabbrica Italiana Sintetici S.P.A.; T2 Biosystems, Inc.* ***Miguel Salavert Lletí, PhD,*** *has disclosed the following relevant financial relationships: served as an advisor or consultant for: Gilead Sciences, Inc.; Merck Sharp & Dohme GmbH; Pfizer Inc.; served as a speaker or a member of a speakers bureau for: Gilead Sciences, Inc.; Janssen-Cilag; Merck Sharp & Dohme GmbH; Pfizer Inc.* ***Carolina Garcia-Vidal, PhD,*** *has disclosed the following relevant financial relationships: served as a speaker or a member of a speakers bureau for Gilead Sciences, Inc.; Janssen-Cilag; Merck Sharp & Dohme GmbH; Novartis Pharmaceuticals Corporation; Pfizer Inc.; received grants for clinical research from Gilead Sciences, Inc.; Merck Sharp & Dohme GmbH.* ***Julián Torre-Cisneros, MD, PhD,*** *has disclosed the following relevant financial relationships: served as an advisor or consultant for Merck Sharp & Dohme GmbH; Pfizer Inc.; Shionogi & Co., Ltd.; served as a speaker or a member of a speakers bureau for: Merck Sharp & Dohme GmbH; Pfizer Inc.; received grants for clinical research from Pfizer Inc.* ***Marcio Nucci, MD,*** *has disclosed the following relevant financial relationships: served as an advisor or consultant for Merck Sharp & Dohme GmbH; served as a speaker or a member of a speakers bureau for AbbVie Inc.; Astellas Pharma, Inc.; Basilea Pharmaceutica Ltd.; Gilead Sciences, Inc.; Merck Sharp & Dohme GmbH; Pfizer Inc.*

[1]These senior authors contributed equally to this article.

[2]Members are listed at the end of this article.

Invasive fusariosis (IF) is associated with severe neutropenia in patients with concurrent hematologic conditions. We conducted a retrospective observational study to characterize the epidemiology of IF in 18 Spanish hospitals during 2000–2015. In that time, the frequency of IF in nonneutropenic patients increased from 0.08 cases per 100,000 admissions in 2000–2009 to 0.22 cases per 100,000 admissions in 2010–2015. Nonneutropenic IF patients often had nonhematologic conditions, such as chronic cardiac or lung disease, rheumatoid arthritis, history of solid organ transplantation, or localized fusariosis. The 90-day death rate among nonneutropenic patients (28.6%) and patients with resolved neutropenia (38.1%) was similar. However, the death rate among patients with persistent neutropenia (91.3%) was significantly higher. We used a multivariate Cox regression analysis to characterize risk factors for death: persistent neutropenia was the only risk factor for death, regardless of antifungal therapy.

Invasive fusariosis (IF) is a fungal disease that mostly affects patients with hematologic malignancies or who have received hematopoietic cell transplants. These patients often have prolonged and profound neutropenia, low levels of T cells, or both (*1*,*2*). Despite advances in early diagnosis and treatment, IF remains associated with high morbidity and death rates (*3*,*4*).

Most studies on this fungal disease have occurred in North and South America (*4*–*9*). However, the epidemiology of IF in Europe has not been fully characterized; within Europe, most multicenter studies on IF have occurred in Italy and France (*8*,*10*–*12*). A multicenter study by the European Confederation of Medical Mycology reported 76 cases of IF during 2007–2012 (*13*). Most (60%) of these IF cases occurred in Italy but none in Spain. Previous single-center studies in Europe have reported regional differences in the distribution of *Fusarium* species and their susceptibilities to antimicrobial drugs, highlighting the importance of monitoring local epidemiologic data (*13*–*15*). We characterized the epidemiology of IF in Spain using a retrospective observational study that examined the effects of clinical and etiologic characteristics on outcomes in a cohort of 58 IF patients at hospitals in Spain.

## Methods

We conducted this study in 18 hospitals in Spain, 8 of which belong to the Spanish Network for Research in Infectious Diseases, Instituto de Salud Carlos III, in Madrid, Spain. The study was approved by Reina Sofía University Hospital Institutional Review Board (Córdoba, Spain), which waived the need to obtain written informed consent. During January 2000–December 2015, hospital staff reviewed microbiological and pathologic registries to identify cases of IF. Data were recorded in a password-protected, electronic clinical research file. We monitored the collected data for missing information, inconsistencies, and ambiguities; when necessary, we sent queries to the appropriate hospitals for clarification.

We conducted a blind review of reported cases of IF. In this study, we included only proven cases of IF according to the consensus definitions of invasive fungal diseases established by the European

Author affiliations: Spanish Network for Research in Infectious Diseases, Instituto de Salud Carlos III, Madrid, Spain (E. Pérez-Nadales, A. Alastruey-Izquierdo, M. Montejo, M. Ruiz Pérez de Pipaón, L. Yáñez, J. Fortún, C. Garcia-Vidal, M. Fernández-Ruiz, I. Guerrero-Lozano, P. Soler-Palacín, J.M. Aguado, L. Martínez-Martínez, J. Torre-Cisneros); Maimonides Biomedical Research Institute of Cordoba, Reina Sofia University Hospital, University of Cordoba, Cordoba, Spain (E. Perez-Nadales, M.J. Linares Sicilia, J. M. Costa-Mateo, L. Martínez-Martínez, J. Torre-Cisneros); Centro Nacional de Microbiología, Instituto de Salud Carlos III, Madrid, Spain (A. Alastruey-Izquierdo, J.C. Soto-Debrán); Hospital das Clinicas, Universidade de São Paulo, São Paulo, Brazil (E. Abdala); Hospital Universitario La Paz, Madrid (J. García-Rodríguez); Hospital Universitario Cruces, Baracaldo, Spain (M. Montejo); Hospital General Universitario Gregorio Marañón, Instituto de Investigación Sanitaria Hospital Gregorio Marañón, Universidad Complutense de Madrid, Madrid, Spain (P. Muñoz); Hospital Universitario "12 de Octubre," Instituto de Investigación Hospital "12 de Octubre," Universidad Complutense, Madrid, Spain (M. Fernández-Ruiz, J.M. Aguado); Hospital Universitario y Politécnico La Fe, Valencia, Spain (M. Salavert Lletí); Hospital Universitario Miguel Servet, Universidad de Zaragoza, Instituto de Investigación Sanitaria Aragón, Zaragoza, Spain (A. Rezusta); Hospital Universitario Virgen del Rocío, Seville, Spain (M. Ruiz Pérez de Pipaón); Hospital Universitario Marqués de Valdecilla, Instituto de Investigación Sanitaria Valdecilla, Santander, Spain (L. Yáñez); Hospital General Universitario de Alicante, Spain (E. Merino); Hospital Universitario de Gran Canaria Doctor Negrín, Las Palmas de Gran Canaria, Spain (M. I. Campos-Herrero); Hospital Ramón y Cajal, Madrid (J. Fortún); Fundación Instituto Valenciano de Oncología, Valencia, Spain (T. García-Lozano); Hospital Universitario de Bellvitge, Barcelona, Spain (C. Garcia-Vidal); Hospital de la Santa Creu i Sant Pau, Barcelona (F. Sánchez-Reus); Hospital Universitario Virgen de Valme, Seville (C. Castro-Méndez); Hospital Universitario Puerta del Mar, Cádiz, Spain (I. Guerrero-Lozano); Hospital Universitari Vall d'Hebron, Barcelona (P. Soler-Palacín); Universidade Federal do Rio de Janeiro, Rio de Janeiro, Brazil (M. Nucci)

DOI: https://doi.org/10.3201/eid2701.190782

Organization for Research and Treatment of Cancer and the Mycoses Study Group Education and Research Consortium (*16*,*17*). IF can be proven in 4 ways: microscopic examination of a specimen obtained by needle aspiration or biopsy that documents hyphae and isolates *Fusarium* spp. in the same tissue; blood culture yielding *Fusarium* spp. alongside signs consistent with an infectious disease process; isolation of *Fusarium* spp. in a normally sterile site (excluding bronchoalveolar lavage fluid, a paranasal or mastoid sinus cavity specimen, and urine) with accompanying signs of infection; or amplification and sequencing of *Fusarium* DNA in formalin-fixed paraffin-embedded tissue (*16*,*17*).

The participating hospitals identified *Fusarium* isolates using genetic sequencing, matrix-assisted laser desorption/ionization time-of-flight (MALDI-TOF) mass spectrometry, or morphologic characteristics. In addition, all biological samples available at the time of this retrospective study (i.e., *Fusarium* isolates and specimens for biopsies) were sent to the Mycology Reference Laboratory at the Instituto de Salud Carlos III for confirmatory genetic sequencing. The isolates were freeze-dried on potato agar slants on arrival and stored in distilled water. Molecular identification was based on the translation elongation factor 1α gene (*18*). Isolates were cultured in GYEP medium (0.3% yeast extract, 1.0% peptone; Francisco Soria Melguizo S.A., http://www.f-soria.es) with 2.0% glucose (Sigma-Aldrich Inc., https://www.sigmaaldrich.com) at 30°C for 24–48 h. Genomic DNA was isolated by using an extraction procedure described previously (*19*). Internal transcribed spacer region and a portion of the translation elongation factor 1α gene region were amplified as previously described (*20*). Alignment results were obtained and edited using Lasergene MegAlign Pro software from DNASTAR, Inc. (https://www.dnastar.com). All sequences were compared with reference sequences from GenBank and MycoBank (https://www.mycobank.org) databases by using InfoQuest FP version 4.50 software (Bio-Rad Laboratories, https://www.bio-rad.com). We also used an in-house database of the Mycology Reference Laboratory. When only biopsy specimens were available, we used real-time PCR specific for *Fusarium* species as previously described (*21*). When identified cases did not have available isolates or biologic material for PCR, we reported the specific *Fusarium* species only if obtained by MALDI-TOF mass spectrometry in conjunction with histopathology. We reported the remaining IF cases in patients with compatible clinical signs and symptoms as caused by *Fusarium* spp.

We defined survival as the time between the date of diagnosis and death or end of follow-up care (i.e., 90 days). We defined the date of diagnosis as the day of the first *Fusarium*-positive culture. We defined disseminated fusariosis as the involvement of >1 noncontiguous organ. We did not consider fungemia cases as disseminated disease unless >1 organ was involved (e.g., skin, lung, or sinuses) (*3*). We defined neutropenia as a blood neutrophil count <500 cells/mm$^3$ temporally related to the onset of fungal disease. We defined persistent neutropenia as cases with continued low neutrophil counts at the end of treatment or death. We defined resolution of neutropenia as a persistent recovery of blood neutrophil count >500/mm$^3$ as determined by available hospital records.

We calculated the incidence of IF using total admissions in the participating hospitals as the denominator; we expressed the incidence as the number of cases per 100,000 admissions. For statistical purposes, we arbitrarily defined 2 time periods: 2000–2009 and 2010–2015. We compared incidences between the different periods by $\chi^2$ test using WinPepi version 11.65 (Brixton Health, http://www.brixtonhealth.com). We considered $p \leq 0.05$ to be significant.

We collected variables describing patient demographic data, concurrent conditions, neutropenia, receipt of corticosteroids, clinical manifestations, diagnostic procedures, treatment, and outcome (i.e., 90-day survival). We compared categorical variables using $\chi^2$ or 2-tailed Fisher exact test, and we compared continuous variables using the Mann-Whitney U test. We conducted all statistical tests with SPSS Statistics 16.0 (IBM Inc., https://www.ibm.com) and R version 3.5.0 (R Foundation for Statistical Computing, https://www.r-project.org); we considered 2-sided p values <0.05 to be significant. We constructed unadjusted Kaplan–Meier curves and compared them using the log-rank test. In addition, we evaluated factors associated with 90-day survival. We evaluated the following variables by univariate and multivariable Cox regression analyses: age, sex, age-adjusted Charlson comorbidity index (*22*), underlying disease, receipt of antifungals and corticosteroids in the previous 30 days, neutropenia at diagnosis of fusariosis and at the end of follow-up, clinical manifestations, and primary treatment (monotherapy with a lipid formulation of amphotericin B, monotherapy with voriconazole, or combination treatment). We entered variables with $p<0.1$ by univariate analysis into the multivariate analysis; we included variables with $p<0.05$ by the multivariate analysis in the final model. We evaluated the prediction accuracy of the final Cox model using the area under the receiver operating characteristic curve.

## Results

### Incidence of IF

We identified 75 patients with *Fusarium* spp. isolated from clinical samples at 18 hospitals in Spain (Appendix Table 1, https://wwwnc.cdc.gov/EID/article/27/1/19-0782-App1.pdf) during 2000–2015. We excluded 10 patients with superficial infections and 7 with probable cases. In this study, the overall incidence of IF during 2000–2015 was 0.55 cases/100,000 admissions, corresponding to 0.42 neutropenic and 0.13 nonneutropenic patients/100,000 admissions (p<0.01). The overall incidence of IF was 0.40 cases/100,000 admissions during 2000–2009 and 0.79 cases/100,000 admissions during 2010–2015 (p<0.01). Among neutropenic patients, the incidence of IF increased from 0.32 to 0.57 cases/100,000 admissions (p = 0.06). Among nonneutropenic patients, the incidence of IF increased from 0.08 to 0.22 cases/100,000 admissions (p = 0.05). We also determined the annual cumulative incidence curves for the 2 groups of patients (Appendix Figure 1).

### Clinical Characteristics

We identified 58 cases of IF: 44 (75.9%) occurred in neutropenic patients and 14 (24.1%) in nonneutropenic patients (Table 1). Most (59%) patients were male. The median age was 67 years (interquartile range [IQR] 38–19 years) in neutropenic patients and 45 years (IQR 28–65 years) in nonneutropenic patients (p = 0.05). In total, 36.4% of neutropenic and 42.9% of nonneutropenic patients had received corticosteroid therapy in the previous 30 days (p = 0.66); 72.7% of neutropenic and 35.7% of nonneutropenic patients had received antifungal therapy in the previous 30 days (p = 0.66). At the end of follow-up (i.e., 90 days after diagnosis), 23 (52.3%) neutropenic patients had persistent neutropenia.

In total, 41 (93.2%) neutropenic and 5 (35.7%) nonneutropenic patients had hematologic malignancies (p<0.01). In the neutropenic patient group, the most common hematologic malignancies were acute myeloid leukemia (43.2%) and acute lymphoid leukemia (18.2%). The proportion of patients who had received hematopoietic stem cell transplants (HSCTs) was 25% (11/44; 8 allogeneic, 2 autologous, and 1 cord blood haploidentical) in neutropenic patients versus 21.4% (3/14; 1 allogeneic and 2 autologous) in nonneutropenic patients (p = 1.00). Four (9.7%) neutropenic patients and 1 (7.1%) nonneutropenic patient had graft-versus-host disease (p = 1.00). Overall, 21.4% of nonneutropenic patients and 2.3% of neutropenic patients had a history of solid organ transplantation (p = 0.04). Finally, 35.7% of nonneutropenic and 2.3% of neutropenic patients had other underlying conditions (p = 0.04). Five nonneutropenic patients had chronic cardiac disease, T-cell prolymphocytic leukemia, rheumatoid arthritis, chronic obstructive pulmonary disease, or infantile respiratory distress syndrome; 1 neutropenic patient had hemophagocytic lymphohistiocytosis.

Neutropenic patients were more likely than nonneutropenic patients to have a fever at the time of diagnosis (90.9% vs. 57.1%; p<0.01). Neutropenic patients also were more likely to have skin lesions (65.9% vs. 21.4%; p<0.01). We did not observe a difference in the proportion of patients with lung involvement in the IF infection (72.7% of neutropenic vs. 64.3% of nonneutropenic patients; p = 0.74). We also did not observe a difference in the rate of concurrent infections (56.8% of neutropenic vs. 42.9% of nonneutropenic patients; p = 0.36) (Appendix Table 2). Disseminated disease occurred more frequently among neutropenic patients (79.5%) than nonneutropenic patients (28.6%; p<0.01). In contrast, localized forms of IF, especially localized pneumonia (6.8% of neutropenic patients vs. 35.7% of nonneutropenic patients; p = 0.02) and fungemia (6.8% of neutropenic patients vs. 28.6% of nonneutropenic patients; p = 0.05), were more common among nonneutropenic patients. However, disseminated fungemia was more common among neutropenic than nonneutropenic patients (45.7% vs. 25%; p = 0.03). Among neutropenic patients, skin lesions were more common in persons with disseminated IF (77.1%) than localized IF (22.2%; p = 0.004); lung involvement also was more common among those with disseminated IF (82.9% vs. 33.3%; p = 0.007).

Nonneutropenic patients were more likely than neutropenic patients to have a diagnosis on the basis of positive culture alone (43.2% of neutropenic patients vs. 85.7% of nonneutropenic patients; p<0.01). Neutropenic patients were more likely to have a diagnosis on the basis of a positive culture and histopathology (52.3%) than nonneutropenic patients (14.3%; p = 0.01).

### Isolated *Fusarium* Species

Thirty-six patients (62.1%) received a species-level etiologic diagnosis using molecular methods: 26 (44.8%) by genetic sequencing and 10 (17.2%) by MALDI-TOF mass spectrometry (Table 2). Among these patients, *F. solani* species complex (SC) was the most common (18/58; 31.0%), along with *Gibberella fujikuroi* SC (10/58; 17.2%), and *F. oxysporum* SC (5/58; 8.6%). The remaining 22 (37.9%) cases were identified as caused by *Fusarium* spp. Among disseminated infections, most (74.4%) were reported to species level; the most

common were *F. solani* SC (15/39; 38.5%), *F. fukikuroi* SC (8/39; 20.5%), and *F. oxysporum* SC (3/39; 7.7%). In the cohort, disseminated IF also was caused by 2 *F. brachygibbosum* infections and 1 *F. dimerum* SC infection. Most (63.2%) localized infections were caused by *Fusarium* spp. *F. solani* SC (2/39; 5.1%), *F. fukikuroi* SC (2/39; 5.1%), and *F. oxysporum* SC (3/39; 7.7%) were the most common etiologic agents.

### Therapeutic Regimens

Overall, 62.1% of patients received monotherapy (29.3% azoles, 32.8% amphotericin B), 27.6% of

**Table 1.** Clinical characteristics of patients with invasive fusariosis, Spain, 2000–2015*

| Variables | Total | Nonneutropenic | Neutropenic | p value† |
|---|---|---|---|---|
| Total | 58 (100.0) | 14 (100.0) | 44 (100.0) | |
| Sex | | | | |
| M | 34 (58.6) | 8 (57.1) | 26 (59.1) | 0.9 |
| F | 24 (41.4) | 6 (42.9) | 18 (40.9) | 0.9 |
| Median age, y (IQR) | 51 (31–67) | 67 (38–79) | 45 (28–65) | 0.05‡ |
| Treatment history (previous 30 d) | | | | |
| Antifungal | 37 (63.8) | 5 (35.7) | 32 (72.7) | 0.01 |
| Corticosteroid | 22 (37.9) | 6 (42.9) | 16 (36.4) | 0.66 |
| Persistent neutropenia | 23 (39.7) | 0 | 23 (52.3) | |
| Concurrent conditions | | | | |
| Hematologic malignancy | 46 (79.3) | 5 (35.7) | 41 (93.2) | <0.01§ |
| Acute myeloid leukemia | 20 (34.5) | 1 (7.1) | 19 (43.2) | |
| Acute lymphoid leukemia | 8 (13.8) | 0 | 8 (18.2) | |
| Non-Hodgkin lymphoma | 5 (8.6) | 2 (14.3) | 3 (6.8) | |
| Aplastic anemia | 4 (6.9) | 0 | 4 (9.1) | |
| Multiple myeloma | 3 (5.2) | 2 (14.3) | 1 (2.3) | |
| Myelodysplasia | 2 (3.4) | 0 | 2 (4.5) | |
| Chronic lymphoid leukemia | 2 (3.4) | 0 | 2 (4.5) | |
| Chronic myeloid leukemia | 1 (1.7) | 0 | 1 (2.3) | |
| Hodgkin´s lymphoma | 1 (1.7) | 0 | 1 (2.3) | |
| History of hematopoietic stem cell transplant | 14 (24.1) | 3 (21.4) | 11 (25.0) | 1.00§ |
| Allogenic | 9 (15.5) | 1 (7.1) | 8 (18.2) | |
| Autologous | 4 (6.9) | 2 (14.3) | 2 (4.5) | |
| Cord blood haploidentical | 1 (1.7) | 0 | 1 (2.3) | |
| Graft-versus-host disease | 5 (8.6) | 1 (7.1) | 4 (9.1) | 1.00§ |
| Acute | 3 (5.2) | 0 | 3 (6.8) | |
| Chronic | 2 (3.4) | 1 (7.1) | 1 (2.3) | |
| Solid tumor | 2 (3.4) | 1 (7.1) | 1 (2.3) | 0.43§ |
| History of solid organ transplant | 4 (6.9) | 3 (21.4) | 1 (2.3) | 0.04§ |
| Other¶ | 10 (17.2) | 5 (35.7) | 1 (2.3) | <0.01§ |
| Clinical manifestations | | | | |
| Fever | 48 (82.8) | 8 (57.1) | 40 (90.9) | <0.01§ |
| Skin lesions | 32 (55.2) | 3 (21.4) | 29 (65.9) | <0.01 |
| Lung involvement | 41 (70.7) | 9 (64.3) | 32 (72.7) | 0.74§ |
| Sinusitis | 9 (15.5) | 1 (7.1) | 8 (18.2) | 0.43§ |
| Blindness | 4 (6.9) | 0 | 4 (9.1) | 0.56§ |
| Concurrent infection | 31 (53.4) | 6 (42.9) | 25 (56.8) | 0.36 |
| Bacterial | 17 (29.3) | 2 (14.3) | 15 (34.1) | 0.18§ |
| Fungal | 4 (6.9) | 1 (7.1) | 4 (9.1) | 0.56§ |
| Viral | 6 (10.3) | 3 (21.4) | 3 (6.8) | 0.15§ |
| Polymicrobial | 4 (6.9) | 1 (7.1) | 3 (6.8) | 1.00§ |
| Type of fusariosis | | | | |
| Localized | 19 (32.8) | 10 (71.4) | 9 (20.5) | <0.01§ |
| Cutaneous, localized | 3 (5.2) | 1 (7.1) | 2 (4.5) | 1.00§ |
| Pneumonia | 8 (13.8) | 5 (35.7) | 3 (6.8) | 0.02§ |
| Sinusitis | 1 (1.7) | 0 | 1 (2.3) | 1.00§ |
| Fungemia | 7 (12.1) | 4 (28.6) | 3 (6.8) | 0.05§ |
| Disseminated | 39 (67.2) | 4 (28.6) | 35 (79.5) | <0.01§ |
| Diagnosis | | | | |
| Culture | 31 (53.4) | 12 (85.7) | 19 (43.2) | <0.01 |
| Culture and histopathology | 25 (43.1) | 2 (14.3) | 23 (52.3) | 0.01 |
| Histopathology | 2 (3.4) | 0 | 2 (4.5) | 1.00 |

*Values are no. (%), except where indicated.
†p values obtained by $\chi^2$ test, except where indicated.
‡Determined by Mann-Whitney U test.
§Determined by Fisher exact test.
¶Other conditions reported include hemophagocytic lymphohistiocytosis, chronic cardiac disease, T-cell prolymphocytic leukemia, rheumatoid arthritis, chronic obstructive pulmonary disease, and infantile respiratory distress syndrome.

**Table 2.** Distribution of isolated *Fusarium* species, Spain, 2000–2015*

| Species | Total | Localized | Disseminated | p value† |
|---|---|---|---|---|
| Total | 58 (100.0) | 19 (100.0) | 39 (100.0) | |
| *F. solani* SC | 18 (31.0) | 3 (15.8) | 15 (38.5) | 0.08‡ |
| *Gibberella fujikuroi* SC | 10 (17.2) | 2 (10.5) | 8 (20.5) | 0.29 |
| *F. proliferatum* | 6 (10.3) | 0 | 6 (15.4) | 0.08 |
| *F. verticillioides* | 3 (5.2) | 2 (10.5) | 1 (2.6) | 0.25 |
| *F. fujikuroi* | 1 (1.7) | 0 | 1 (2.6) | 0.67 |
| *F. oxysporum* SC | 5 (8.6) | 2 (10.5) | 3 (7.7) | 0.53 |
| *F. brachygibbosum* | 2 (3.4) | 0 | 2 (5.1) | 0.45 |
| *F. dimerum* SC | 1 (1.7) | 0 | 1 (2.6) | 0.67 |
| *Fusarium* spp. | 22 (37.9) | 12 (63.2) | 10 (25.6) | <0.01 |

*Values are no. (%), except where indicated. All identifications (except undefined *Fusarium* spp.) obtained by genetic sequencing or matrix-assisted laser desorption/ionisation time-of-flight mass spectometry. SC, species complex.
†p values obtained by Fisher exact test, except where indicated.
‡Determined by $\chi^2$ test.

patients received combination therapy (e.g., azoles plus amphotericin B, mostly liposomal amphotericin B plus voriconazole), and 10.4% of patients did not receive an active treatment (3 patients were not treated, 2 received empirical caspofungin, and 1 received empirical micafungin) (Appendix Table 3). Nonneutropenic patients were more likely than neutropenic patients to receive voriconazole monotherapy (54.5% vs. 85.7%; p<0.01). We did not observe a difference in the proportions of patients who were treated with amphotericin B (36.4% of neutropenic patients vs. 21.4% of nonneutropenic patients; p = 0.35). Sixteen (36.4%) neutropenic patients received combination therapy: 14 received a lipid formulation of amphotericin B plus voriconazole and 2 received amphotericin B plus posoconazole. No nonneutropenic patients received combination therapy.

### Outcomes

By 90 days after diagnosis, 56.9% of all patients had died: 28.6% of nonneutropenic patients and 65.9% of patients with neutropenia at IF onset (p = 0.01). We analyzed these results using unadjusted Kaplan–Meier survival graphs (Appendix Figure 2; p = 0.03 by log-rank test). The death rate of nonneutropenic patients (28.6%) was similar to that of patients who had recovered from neutropenia (38.1%; p = 0.56) and both rates were significantly lower than among patients with persistent neutropenia (91.3%; p<0.01).

After 90 days, 66.7% of patients with localized and 36.8% with disseminated disease had died (p = 0.03). Overall, 66.7% (2/3) of patients with localized disease of the skin/soft tissue, 50% (4/8) with lung involvement, and 14.3% (1/7) with fungemia died.

In the assessment of prognostic factors, we analyzed 50 IF patients who received active antifungal therapy. In univariate analysis, 90-day death risk was associated with neutropenia at onset of IF and persistent neutropenia. Age, sex, age-adjusted Charlson comorbidity index, corticosteroid therapy in the previous 30 days, administration of antifungal in the previous 30 days, hematologic malignancy, history of HSCT, fungemia, disseminated disease, and the treatment type (i.e., monotherapy with a lipid formulation of amphotericin B, monotherapy with azoles or combined therapy) were not associated with 90-day survival. In multivariate analysis, persistent neutropenia (hazard ratio [HR] 7.08, 95% CI 1.91–26.17; p<0.01) was significantly associated with 90-day death risk (Table 3). We calculated adjusted Kaplan–Meier survival curves for the Cox regression model (Figure; area under the receiver operating characteristic curve = 0.83).

## Discussion

We described 58 cases of invasive *Fusarium* infections at 18 hospitals in Spain during a 15-year period (2000–2015). During this time, IF incidence increased from 0.40 (2000–2009) to 0.79 (2010–2015) cases per 100.000 admissions (p<0.01). Incidence of IF in neutropenic patients increased from 0.32 to 0.57 cases per 100,000 admissions (p = 0.06). We observed a 3-fold increase in the incidence of IF in nonneutropenic patients, from 0.08 to 0.22 cases per 100,000 admissions (p = 0.05). This increase might have been caused by an increase in the at-risk population, environmental exposure to *Fusarium* conidia, the increased use of antifungal prophylaxis, or a combination of these factors.

To date, the highest IF incidence rates worldwide are in healthcare centers in Brazil. A cohort of HSCT recipients at hospitals in Brazil during 1985–2001 had a 0.6% prevalence of IF (*1*). During 2007–2009, ≈10 years later, a prospective multicenter study by Nucci et al. reported a 3.7% IF prevalence among allogeneic HSCT patients and 3.4% among patients with acute myeloid leukemia (*7*). That study also found a 1-year cumulative incidence of 5.2% among those who had received an allogeneic HSCT and 3.8% among those with acute myeloid leukemia or myelodysplasia (*7*). A >10-fold increase,

**Table 3.** Univariate and multivariate Cox regression analyses for 90-day death rate in 50 patients treated for invasive fusariosis, Spain, 2000–2015*

| Characteristic | Unadjusted hazard ratio (95% CI) | p value | Adjusted hazard ratio (95% CI) | p value |
|---|---|---|---|---|
| Sex | | | | |
| M | 1.08 (0.52–2.25) | 0.84 | 0.87 (0.41–1.84) | 0.87 |
| F | 0.93 (0.45-1.93) | 0.84 | | |
| Median age, y (IQR) | 1.00 (0.99–1.01) | 0.94 | | |
| Charlson index | 1.01 (0.86–1.20) | 0.87 | 1.16 (0.96–1.40) | 0.12 |
| Treatment history (previous 30 d) | | | | |
| Antifungal | 1.83 (0.81–4.14) | 0.15 | | |
| Corticosteroid | 0.69 (0.33–1.45) | 0.33 | | |
| Neutropenia at onset | 3.16 (0.95–10.44) | 0.06 | | |
| Neutropenia at the end of follow-up | | | | |
| Nonneutropenia | Referent | | Referent | |
| Recovery from neutropenia | 1.47 (0.38–5.69) | 0.58 | 1.91 (0.48–7.64) | 0.35 |
| Persistent neutropenia | 5.62 (1.65–19.11) | 0.006 | 9.27 (2.43–35.42) | 0.001 |
| Hematologic malignancy | 2.44 (0.74–8.06) | 0.14 | | |
| History of hematopoietic stem cell transplant | 1.39 (0.65–2.99) | 0.4 | | |
| Fungemia | 0.21 (0.03–1.54) | 0.13 | | |
| Disseminated disease | 1.90 (0.77–4.67) | 0.16 | | |
| Antifungal therapy | | | | |
| Monotherapy with lipid formulation of amphotericin B | 1.95 (0.92–4.12) | 0.08 | | |
| Monotherapy with azoles | 0.47 (0.19–1.15) | 0.10 | | |
| Combined therapy | 1.08 (0.50–2.33) | 0.84 | | |

*Area under the receiver operating characteristic curve for this model was 0.82.

from 86 to 1,023 IF cases per 100,000 admissions, occurred among patients with hematologic malignancies at a healthcare center in Brazil from 2000–2005 to 2006–2010 (*5*). In the United States, a prospective multicenter study conducted by the Transplant-Associated Infection Surveillance Network during 2001–2006 reported a 1-year cumulative incidence of up to 0.3% of non-*Aspergillus* mold infections (*23*). In Italy, a multicenter retrospective study reported a 0.2% incidence of IF among patients who had received an allogenic HSCT during 1999–2003 (*24*).

In this cohort in Spain, IF occurred frequently in patients with hematologic conditions and in HSCT recipients. IF occurs almost entirely in markedly immunosuppressed patients who usually are neutropenic; we identified IF in nonneutropenic patients, including patients with a history of solid organ transplants, chronic cardiac or lung disease, or rheumatoid arthritis. These findings are in agreement with Park et al. (*9*), who studied 37 patients with IF and noted that 54.1% of IF patients were nonneutropenic, 83.8% had hematologic malignancies, and 16.2% had history of solid organ transplantation (*9*). Thus, nonneutropenia and certain nonhematologic conditions might not be uncommon among IF patients.

Lungs, the bloodstream, and the skin were the organs most frequently affected by IF. *Fusarium* species produce aleuroconidia, yeastlike structures that can invade the bloodstream and might cause fungemia and metastatic skin lesions (*25*).

IF is associated with high death rates. This cohort had a 90-day death rate of 56.9%, similar to rates

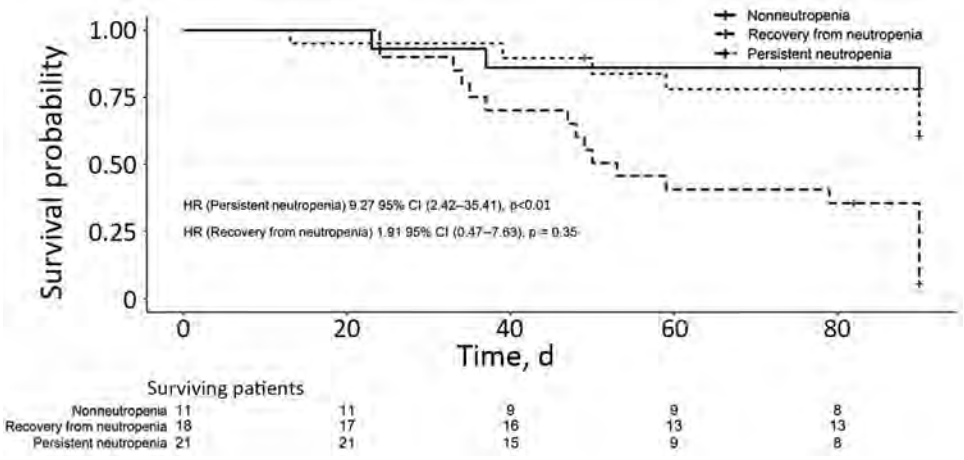


**Figure.** Adjusted Kaplan-Meier curves obtained from the stratified Cox regression model for 90-day survival in 50 patients treated for invasive fusariosis, Spain, 2000–2015. HR, hazard ratio.

noted in other studies (*3*,*4*,*12*,*26*). The death rates of nonneutropenic and neutropenic patients who recovered from neutropenia were similar (28.6% of nonneutropenic patients vs. 38.1% of neutropenic patients; p = 0.56), consistent with previous reports that 70% of IF cases resolve when patients recover from neutropenia (*27*). In this cohort, patients with persistent neutropenia had a 91.3% death rate despite antifungal therapy. Persistent neutropenia was the single most predictive prognostic factor in IF, consistent with previous reports (*2*).

Researchers must identify effective therapeutic strategies to improve the prognosis of IF patients with persistent neutropenia. The treatment practices observed in our study align with guidelines from the European Society of Clinical Microbiology and Infectious Diseases Fungal Infection Study Group and European Confederation of Medical Mycology (*13*). We examined the effects of different therapeutic regimens on 90-day death rate. We found no differences in the outcome of patients treated with voriconazole and those receiving a lipid formulation of amphotericin B. Combination therapy also was not associated with outcome, consistent with results from the largest study series conducted so far (*3*,*12*). However, these results must be interpreted with caution. Nucci et al. (*3*) found that patients receiving combination therapy had more severe disease (*3*), possibly influencing the clinician's decision to administer 2 drugs. In our study, no nonneutropenic patients received combination therapy; further studies should examine the potential benefits of combination therapy in nonneutropenic patients. Finally, because we observed similar clinical responses in patients treated with a lipid formulation of amphotericin B or voriconazole as monotherapies, clinicians might not need to rely on antifungal susceptibility tests to guide treatment. Most clinically relevant *Fusarium* isolates exhibit high minimal inhibitory concentrations to most antifungals, including azoles, echinocandins, and polyenes (*28*–*30*).

Our study is subject to the limitations of retrospective observational studies. For example, the sample size was limited to the cases with available data. Despite being a multicenter study during a 15-year period, the sample size might be insufficient to detect significant differences in some groups. Furthermore, clinicians might prescribe a more potent treatment regimen for patients with severe disease, possibly skewing our analysis of treatment outcomes. Although all IF cases in this retrospective study met standard criteria (*16*,*17*), we could not determine the causative species in every case. Thus, the *Fusarium* species was only reported when determined by genomic sequencing or MALDI-TOF mass spectrometry, because these techniques have high agreement rates (89.8%–97.0%) (*31*–*33*). All remaining IF cases in our series were reported as *Fusarium* spp. We also were not able to culture all *Fusarium* isolates because of a lack of specimens, especially for cases occurring before 2010 in hospitals in which *Fusarium* isolates were not collected as part of routine procedures

In conclusion, our data show that IF is an emerging infection in Spain. We report an increase in the incidence of IF among nonneutropenic patients, including those with hematologic conditions and other concurrent conditions, such as chronic cardiac or lung diseases, rheumatoid arthritis, or history of solid organ transplants. Our results support previous studies reporting that IF survival is critically dependent on resolution of neutropenia.

Members of the Spanish Fusariosis Study Group include: Cesar Vargas Ayala, Paula Pescador Martin, and Laura Alonso Acero (Hospital Universitario La Paz, Madrid, Spain); Leire López-Soria, Laura Guio-Carrión, and Roberto Céspedes (Hospital Universitario Cruces, Bilbao, Spain); M. Carmen Martínez Jiménez, Maricela Valerio, and Jesús Guinea (Hospital General Universitario Gregorio Marañón, Madrid, Spain); Elisa Ibáñez Martínez, Sandra Cuellar-Tovar, and Jaime Sanz-Caballer (Hospital Universitario y Politécnico La Fe, Valencia, Spain); Lissette Costilla (Hospital Universitario Miguel Servet, Zaragoza, Spain); Maria Pía Roiz-Mesones (Hospital Universitario Marqués de Valdecilla, Santander, Spain); Cristina Gil-Cortés and Carmen Botella-Prieto (Hospital General Universitario de Alicante, Alicante, Spain); Iballa Horcajada-Herrera (Hospital Universitario de Gran Canaria Doctor Negrín, Las Palmas de Gran Canaria, Spain); Juan José Castón, Alejandra M. Natera, and Ipek Guler (Maimonides Biomedical Research Institute of Cordoba, Reina Sofia University Hospital, University of Cordoba, Cordoba, Spain); Pilar Martín-Dávila and Elia Gómez-García de la Pedrosa (Hospital Universitario Ramón y Cajal, Madrid); Eduardo Aznar-Oroval and Agustín Iranzo (Fundación Instituto Valenciano de Oncología, Valencia); Josefina Ayats and Carlota Gudiol (Hospital Universitario de Bellvitge, Barcelona, Spain); Ana Pérez-Ayala (Hospital Universitario 12 de Octubre, Madrid); Cristina Lopez-Querol and Alicia Mulero Serralta (Hospital de la Santa Creu i Sant Pau de Barcelona, Barcelona); Estrella Martin-Mazuelos (Hospital Universitario Virgen de Valme, Seville, Spain); Manuel Rodríguez-Iglesias (Hospital Universitario Puerta del Mar, Cádiz, Spain); and M. Teresa Martin-Gómez (Hospital Universitari Vall d'Hebrón, Barcelona).

This work was supported by Plan Nacional de I+D+I 2013–2016 and Instituto de Salud Carlos III, Subdirección General de Redes y Centros de Investigación Cooperativa, Ministerio de Ciencia, Innovación y Universidades, Spanish Network for Research in Infectious Diseases (REIPI RD16/0016/0008; RD16/CIII/0004/0003), cofinanced by European Development Regional Fund "A way to achieve Europe," Operative Program Intelligent Growth 2014–2020. M.F.R. holds a "Miguel Servet" research contract (CP18/00073) from Instituto de Salud Carlos III, Madrid.

## About the Author

Dr. Pérez-Nadales is a research fellow at the Infectious Diseases Group at Maimonides Biomedical Research Institute of Córdoba, Spain. Her research interests include clinical and molecular epidemiology of invasive fungal infections and infections caused by multidrug-resistant bacteria.

## References

1. Nucci M, Marr KA, Queiroz-Telles F, Martins CA, Trabasso P, Costa S, et al. *Fusarium* infection in hematopoietic stem cell transplant recipients. Clin Infect Dis. 2004;38:1237–42. https://doi.org/10.1086/383319
2. Nucci M, Anaissie EJ, Queiroz-Telles F, Martins CA, Trabasso P, Solza C, et al. Outcome predictors of 84 patients with hematologic malignancies and *Fusarium* infection. Cancer. 2003;98:315–9. https://doi.org/10.1002/cncr.11510
3. Nucci M, Marr KA, Vehreschild MJGT, de Souza CA, Velasco E, Cappellano P, et al. Improvement in the outcome of invasive fusariosis in the last decade. Clin Microbiol Infect. 2014;20:580–5. https://doi.org/10.1111/1469-0691.12409
4. Horn DL, Freifeld AG, Schuster MG, Azie NE, Franks B, Kauffman CA. Treatment and outcomes of invasive fusariosis: review of 65 cases from the PATH Alliance registry. Mycoses. 2014;57:652–8. https://doi.org/10.1111/myc.12212
5. Nucci M, Varon AG, Garnica M, Akiti T, Barreiros G, Trope BM, et al. Increased incidence of invasive fusariosis with cutaneous portal of entry, Brazil. Emerg Infect Dis. 2013;19:1567–72. https://doi.org/10.3201/eid1910.120847
6. Nucci M, Anaissie E. Cutaneous infection by *Fusarium* species in healthy and immunocompromised hosts: implications for diagnosis and management. Clin Infect Dis. 2002;35:909–20. https://doi.org/10.1086/342328
7. Nucci M, Garnica M, Gloria AB, Lehugeur DS, Dias VCH, Palma LC, et al. Invasive fungal diseases in haematopoietic cell transplant recipients and in patients with acute myeloid leukaemia or myelodysplasia in Brazil. Clin Microbiol Infect. 2013;19:745–51. https://doi.org/10.1111/1469-0691.12002
8. Girmenia C, Pagano L, Corvatta L, Mele L, del Favero A, Martino P. The epidemiology of fusariosis in patients with haematological diseases. Gimema Infection Programme. Br J Haematol. 2000;111:272–6.
9. Park BJ, Pappas PG, Wannemuehler KA, Alexander BD, Anaissie EJ, Andes DR, et al. Invasive non-*Aspergillus* mold infections in transplant recipients, United States, 2001-2006. Emerg Infect Dis. 2011;17:1855–64. https://doi.org/10.3201/eid1710.110087
10. Hennequin C, Lavarde V, Poirot JL, Rabodonirina M, Datry A, Aractingi S, et al. Invasive *Fusarium* infections: a retrospective survey of 31 cases. J Med Vet Mycol. 1997;35:107–14. https://doi.org/10.1080/02681219780000991
11. Pagano L, Caira M, Candoni A, Offidani M, Fianchi L, Martino B, et al. The epidemiology of fungal infections in patients with hematologic malignancies: the SEIFEM-2004 study. Haematologica. 2006;91:1068–75.
12. Lortholary O, Obenga G, Biswas P, Caillot D, Chachaty E, Bienvenu A-L, et al.; French Mycoses Study Group. International retrospective analysis of 73 cases of invasive fusariosis treated with voriconazole. Antimicrob Agents Chemother. 2010;54:4446–50. https://doi.org/10.1128/AAC.00286-10
13. Tortorano AM, Prigitano A, Esposto MC, Arsic Arsenijevic V, Kolarovic J, Ivanovic D, et al.; ECMM Working Group. European Confederation of Medical Mycology (ECMM) epidemiological survey on invasive infections due to Fusarium species in Europe. Eur J Clin Microbiol Infect Dis. 2014;33:1623–30. https://doi.org/10.1007/s10096-014-2111-1
14. Tortorano AM, Prigitano A, Dho G, Esposto MC, Gianni C, Grancini A, et al. Species distribution and in vitro antifungal susceptibility patterns of 75 clinical isolates of *Fusarium* spp. from northern Italy. Antimicrob Agents Chemother. 2008;52:2683–5. https://doi.org/10.1128/AAC.00272-08
15. Dalyan Cilo B, Al-Hatmi AMS, Seyedmousavi S, Rijs AJMM, Verweij PE, Ener B, et al. Emergence of fusarioses in a university hospital in Turkey during a 20-year period. Eur J Clin Microbiol Infect Dis. 2015;34:1683–91. https://doi.org/10.1007/s10096-015-2405-y
16. Donnelly JP, Chen SC, Kauffman CA, Steinbach WJ, Baddley JW, Verweij PE, et al. Revision and Update of the Consensus Definitions of Invasive Fungal Disease From the European Organization for Research and Treatment of Cancer and the Mycoses Study Group Education and Research Consortium. Clin Infect Dis. 2020;71:1367–76. https://doi.org/10.1093/cid/ciz1008
17. De Pauw B, Walsh TJ, Donnelly JP, Stevens DA, Edwards JE, Calandra T, et al.; European Organization for Research and Treatment of Cancer/Invasive Fungal Infections Cooperative Group; National Institute of Allergy and Infectious Diseases Mycoses Study Group (EORTC/MSG) Consensus Group. Revised definitions of invasive fungal disease from the European Organization for Research and Treatment of Cancer/Invasive Fungal Infections Cooperative Group and the National Institute of Allergy and Infectious Diseases Mycoses Study Group (EORTC/MSG) Consensus Group. Clin Infect Dis. 2008;46:1813–21. https://doi.org/10.1086/588660
18. Geiser DM, del Mar Jiménez-Gasco M, Kang S, Makalowska I, Veeraraghavan N, Ward TJ, et al. FUSARIUM-ID v. 1.0: A DNA sequence database for identifying Fusarium. Eur J Plant Pathol. 2004;110:473–9. https://doi.org/10.1023/B:EJPP.0000032386.75915.a0
19. Holden D. DNA mini prep method for *Aspergillus fumigatus* (and other filamentous fungi). In: Maresca B, Kobayashi G, editors. Molecular biology of pathogenic fungi, a laboratory manual. New York: Telos Press; 1994. p. 3–4.
20. Alastruey-Izquierdo A, Alcazar-Fuoli L, Rivero-Menéndez O, Ayats J, Castro C, García-Rodríguez J, et al. Molecular identification and susceptibility testing of molds isolated in a prospective surveillance of triazole resistance in Spain (FILPOP2 Study). Antimicrob Agents Chemother. 2018;62. AAC.00358-18.
21. Bernal-Martínez L, Buitrago MJ, Castelli MV, Rodríguez-Tudela JL, Cuenca-Estrella M. Detection of invasive infection caused by *Fusarium solani* and non-*Fusarium solani* species using a duplex quantitative PCR-

based assay in a murine model of fusariosis. Med Mycol. 2012;50:270–5. https://doi.org/10.3109/13693786.2011.604047
22. Charlson M, Szatrowski TP, Peterson J, Gold J. Validation of a combined comorbidity index. J Clin Epidemiol. 1994; 47:1245–51. https://doi.org/10.1016/0895-4356(94)90129-5
23. Kontoyiannis DP, Marr KA, Park BJ, Alexander BD, Anaissie EJ, Walsh TJ, et al. Prospective surveillance for invasive fungal infections in hematopoietic stem cell transplant recipients, 2001-2006: overview of the Transplant-Associated Infection Surveillance Network (TRANSNET) Database. Clin Infect Dis. 2010;50:1091–100. https://doi.org/10.1086/651263
24. Pagano L, Caira M, Nosari A, Van Lint MT, Candoni A, Offidani M, et al. Fungal infections in recipients of hematopoietic stem cell transplants: results of the SEIFEM B-2004 study—Sorveglianza Epidemiologica Infezioni Fungine Nelle Emopatie Maligne. Clin Infect Dis. 2007;45:1161–70. https://doi.org/10.1086/522189
25. Anaissie E, Grazziutti M, Nucci M. Invasive fungal infections in cancer patients. In: Anaissie E, McGinnis M, Pfaller M, editors. Clinical mycology. 2nd ed. Amsterdam: Elsevier; 2009. p. 431–71.
26. Campo M, Lewis RE, Kontoyiannis DP. Invasive fusariosis in patients with hematologic malignancies at a cancer center: 1998-2009. J Infect. 2010;60:331–7. https://doi.org/10.1016/j.jinf.2010.01.010
27. Lionakis MS, Kontoyiannis DP. *Fusarium* infections in critically ill patients. Semin Respir Crit Care Med. 2004;25:159–69. https://doi.org/10.1055/s-2004-824900
28. Al-Hatmi AMS, van Diepeningen AD, Curfs-Breuker I, de Hoog GS, Meis JF. Specific antifungal susceptibility profiles of opportunists in the *Fusarium fujikuroi* complex. J Antimicrob Chemother. 2015;70:1068–71. bMed
29. Alastruey-Izquierdo A, Cuenca-Estrella M, Monzón A, Mellado E, Rodríguez-Tudela JL. Antifungal susceptibility profile of clinical *Fusarium* spp. isolates identified by molecular methods. J Antimicrob Chemother. 2008;61:805–9. https://doi.org/10.1093/jac/dkn022
30. Al-Hatmi AMS, Normand A-C, Ranque S, Piarroux R, de Hoog GS, Meletiadis J, et al. Comparative evaluation of Etest, EUCAST, and CLSI Methods for amphotericin B, voriconazole, and posaconazole against clinically relevant *Fusarium* species. Antimicrob Agents Chemother. 2016;61:e01671–16.
31. Marinach-Patrice C, Lethuillier A, Marly A, Brossas JY, Gené J, Symoens F, et al. Use of mass spectrometry to identify clinical *Fusarium* isolates. Clin Microbiol Infect. 2009; 15:634–42. https://doi.org/10.1111/j.1469-0691.2009.02758.x
32. Triest D, Stubbe D, De Cremer K, Piérard D, Normand AC, Piarroux R, et al. Use of matrix-assisted laser desorption ionization-time of flight mass spectrometry for identification of molds of the *Fusarium* genus. J Clin Microbiol. 2015;53:465–76. https://doi.org/10.1128/JCM.02213-14
33. Paziani MH, Tonani Carvalho L, Melhem MSC, Almeida MTG, Nadaletto Bonifácio da Silva ME, Martinez R, et al. First comprehensive report of clinical *Fusarium* strains isolated in the state of Sao Paulo (Brazil) and identified by MALDI-TOF MS and molecular biology. Microorganisms. 2019;8:66. https://doi.org/10.3390/microorganisms8010066

Address for correspondence: Julián Torre-Cisneros, Clinical Unit of Infectious Diseases, Reina Sofía University Hospital, Maimonides Biomedical Research Institute of Córdoba (IMIBIC), University of Córdoba, Córdoba, Spain; e-mail: julian.torre.sspa@juntadeandalucia.es

# Rising Ethnic Inequalities in Acute Rheumatic Fever and Rheumatic Heart Disease, New Zealand, 2000–2018

Julie Bennett, Jane Zhang, William Leung, Susan Jack, Jane Oliver, Rachel Webb, Nigel Wilson, Dianne Sika-Paotonu, Matire Harwood, Michael G. Baker

## Medscape EDUCATION ACTIVITY

In support of improving patient care, this activity has been planned and implemented by Medscape, LLC and Emerging Infectious Diseases. Medscape, LLC is jointly accredited by the Accreditation Council for Continuing Medical Education (ACCME), the Accreditation Council for Pharmacy Education (ACPE), and the American Nurses Credentialing Center (ANCC), to provide continuing education for the healthcare team.

Medscape, LLC designates this Journal-based CME activity for a maximum of 1.00 ***AMA PRA Category 1 Credit(s)™***. Physicians should claim only the credit commensurate with the extent of their participation in the activity.

Successful completion of this CME activity, which includes participation in the evaluation component, enables the participant to earn up to 1.0 MOC points in the American Board of Internal Medicine's (ABIM) Maintenance of Certification (MOC) program. Participants will earn MOC points equivalent to the amount of CME credits claimed for the activity. It is the CME activity provider's responsibility to submit participant completion information to ACCME for the purpose of granting ABIM MOC credit.

All other clinicians completing this activity will be issued a certificate of participation. To participate in this journal CME activity: (1) review the learning objectives and author disclosures; (2) study the education content; (3) take the post-test with a 75% minimum passing score and complete the evaluation at http://www.medscape.org/journal/eid; and (4) view/print certificate. For CME questions, see page 340.

**Release date: December 22, 2020; Expiration date: December 22, 2021**

**Learning Objectives**

Upon completion of this activity, participants will be able to:

- Analyze the global epidemiology of ARF and RHD
- Distinguish risk factors for ARF in the current study
- Evaluate trends in the epidemiology of ARF in the current study
- Evaluate trends in the epidemiology of RHD in the current study.

**CME Editor**

**Amy J. Guinn, BA, MA,** Copyeditor, Emerging Infectious Diseases. *Disclosure: Amy J. Guinn, BA, MA, has disclosed no relevant financial relationships.*

**CME Author**

**Charles P. Vega, MD,** Health Sciences Clinical Professor of Family Medicine, University of California, Irvine School of Medicine, Irvine, California. *Disclosure: Charles P. Vega, MD, has disclosed the following relevant financial relationships: served as an advisor or consultant for GlaxoSmithKline.*

**Authors**

*Disclosures:* ***Julie Bennett, PhD; Jane Zhang, MSc; William Leung, MSc; Susan Jack, PhD; Jane Oliver, PhD; Rachel Webb, MBChB, FRACP; Nigel Wilson, MBChB; Michael G. Baker, MBChB;*** *and* ***Dianne Sika-Paotonu, PhD*** *have disclosed no relevant financial relationships.* ***Matire Harwood, PhD,*** *has disclosed the following relevant financial relationships: received grants for clinical research from Health Research Council NZ, Heart Foundation NZ.*

Author affiliations: University of Otago, Wellington (J. Bennett, J. Zhang, W. Leung, D. Sika-Paotonu, M.G. Baker); Southern District Health Board, Dunedin, New Zealand (S. Jack); University of Melbourne, Melbourne, Victoria, Australia (J. Oliver); Murdoch Children's Research Institute, Melbourne (J. Oliver); Auckland District Health Board, Auckland, New Zealand (R. Webb, N. Wilson); University of Auckland, Auckland (D. Sika-Paotonu, M. Harwood)

DOI: https://doi.org/10.3201/eid2701.191791

We describe trends in acute rheumatic fever (ARF), rheumatic heart disease (RHD), and RHD deaths among population groups in New Zealand. We analyzed initial primary ARF and RHD hospitalizations during 2000–2018 and RHD mortality rates during 2000–2016. We found elevated rates of initial ARF hospitalizations for persons of Māori (adjusted rate ratio [aRR] 11.8, 95% CI 10.0–14.0) and Pacific Island (aRR 23.6, 95% CI 19.9–27.9) ethnicity compared with persons of European/other ethnicity. We also noted higher rates of initial RHD hospitalization for Māori (aRR 3.2, 95% CI 2.9–3.5) and Pacific Island (aRR 4.6, 95% CI 4.2–5.1) groups and RHD deaths among these groups (Māori aRR 12.3, 95% CI 10.3–14.6, and Pacific Island aRR 11.2, 95% CI 9.1–13.8). Rates also were higher in socioeconomically disadvantaged neighborhoods. To curb high rates of ARF and RHD, New Zealand must address increasing social and ethnic inequalities.

Acute rheumatic fever (ARF) is a preventable multisystem inflammatory disease that develops in <3% of persons with untreated group A *Streptococcus* (GAS) pharyngitis (*1*,*2*). Recently, GAS skin infections have been proposed to cause ARF, either directly or in combination with GAS pharyngitis (*3*). The severe sequela of ARF is rheumatic heart disease (RHD) with regurgitation from the mitral valve, aortic valve, or both. RHD is a serious condition that can lead to cardiac failure, stroke, and early death (*4*).

ARF and RHD remain major causes of illness and death (*5*). In 2015, global prevalence of RHD was ≈34 million cases and ≈320,000 RHD-associated deaths occurred (*6*). During the 20th century, improved living conditions resulted in dramatic declines in ARF (*7*). The introduction of antimicrobial drugs in the 1950s and 1960s further reduced the burden of disease and ushered in an effective treatment for GAS pharyngitis (*8*,*9*). Although now rare in high-income countries, ARF and RHD continue to affect populations in economically disadvantaged areas (*10*) and epidemic outbreaks occur in populations that are separated geographically (*11*,*12*).

The incidence of RHD is highest in Oceania, South Asia, and central sub-Saharan Africa (*6*). However, some of the highest reported ARF rates are among indigenous and Pacific Islander populations in Australia and New Zealand (*13*). The incidence rate among indigenous children in Australia in the peak age group, 5–14 years, is 245–351 cases/100,000 population (*14*), but in New Zealand, ARF almost exclusively affects indigenous Māori and Pacific Island children living in socioeconomically deprived areas of the North Island (*15*,*16*). During 2017–2018, the rate of initial ARF hospitalizations among Māori children 5–14 years of age was 25 cases/100,000 population; among Pacific Island children, the rate was 81 cases/100,000 population (*17*).

Population-level burden estimates rarely are reported in international literature, partially because of challenges with diagnosing both ARF and RHD and a lack of high-quality surveillance systems for monitoring these conditions. ARF is notifiable to public health authorities in New Zealand, but RHD is not. In addition, historically there has been national undernotification of ARF cases (*18*). Consequently, coded hospitalization data, which are based on the coding system of the International Classification of Diseases (ICD), 9th Revision (ICD-9) and 10th Revision (ICD-10), provide the most comprehensive base for describing ARF and RHD incidence and distribution.

We assessed trends in the incidence of ARF, the frequency of initial hospitalizations for RHD, and RHD mortality rates in New Zealand during 2000–2018. In addition, we assessed the extent to which these conditions are concentrated in specific population groups, based on age, ethnicity, sex, socioeconomic deprivation, and geographic location.

## Methods

### Data Sources

In New Zealand, we can use National Health Index (NHI) numbers (*19*) to identify cases in health data and link information across datasets. We conducted a descriptive epidemiologic study that linked encrypted NHI numbers to ARF and RHD hospital discharge data in New Zealand from 2000 through 2018. To identify cases of initial ARF and recurrent ARF, we used hospital discharge data coded with the ICD in the National Minimum Dataset (*20*), which includes information on all publicly funded hospitalizations in New Zealand.

We defined initial cases as a patient's first known hospitalization for ARF, which had ICD-10 codes I00, I01, or I02 recorded as their principal diagnosis. We excluded cases in persons who had a previous admission for ARF (ICD-9 codes 390–392) or RHD (ICD-9 codes 393–398) as principal or additional diagnoses since 1988 when the records began. We defined recurrences as all readmissions with ARF as principal diagnosis that occurred ≥180 days after a previous ARF discharge.

We defined initial RHD cases as a patient's first hospitalization with a principal diagnosis of RHD (ICD-10 codes I05, I06, I07, I09, or I09) and no previous admission for RHD as principal or additional diagnoses since 1988. We defined RHD death as the underlying cause of death (ICD-10 codes I05, I06,

I07, I08, or I09) as recorded in the National Mortality Collection (*21*).

We excluded all non–New Zealand residents from these analyses because they are not part of the usual New Zealand population. We used the New Zealand Deprivation Index (NZDep13) to assess socioeconomic deprivation (*22*). NZDep13 is an area-based measure of socioeconomic deprivation based on 9 variables from the 2013 census. Decile 10 represents areas considered the most socioeconomically deprived, and decile 1 represents areas with the least deprivation scores. In this article, when we describe the epidemiology of ARF and RHD, we generally are referring to initial ARF or RHD hospitalizations.

### Statistical Analysis

ARF and RHD data were used to calculate the frequencies, rates, rate ratios (RRs), adjusted rate ratios (aRRs), and 95% CIs across selected population groups. To look for time trends, we split the observation into 2 periods: 2000–2009 and 2010–2018 or 2010–2016 for RHD deaths, the timeframe for which mortality data are available. We examined rates of ARF and RHD in relation to characteristics including age, sex, ethnicity, and the district health board (DHB) in which cases occurred. We used DHBs for geographic analysis because they represent the patient's place of residence. We calculated rates and RRs for ARF for persons <30 years of age because this group accounts for 93.4% of the disease burden. For RHD and RHD mortality, we restricted rates and RRs to persons <70 years of age because the ICD codes are considered to be less specific for RHD in older populations; for example, ICD-10 code I08 includes nonrheumatic heart disease, such as age-related degenerative valvular heart disease that can result in nonrheumatic aortic and mitral valve dysfunction.

We used Poisson regression to calculate RR and 95% CI adjusting for age, sex, ethnicity, and socioeconomic deprivation. We also reported RR by using a defined reference rate from 2000–2009. We used linear regression to examine trends in initial ARF and RHD primary hospitalization rates across most variables. We used the test for trend to evaluate trends over time and considered $p<0.05$ statistically significant. We performed data analysis by using Excel (Microsoft, https://www.microsoft.com) and SAS 9.4 (SAS Institute, Inc., https://www.sas.com).

Denominator population data were population estimates, calculated from linear interpolation of national census data (*23*). The population of New Zealand at the start of the study was 3.9 million and increased to 4.9 million in 2018. The analysis used the prioritized ethnicity categorizations, which is consistent with national Ministry of Health ethnicity data protocols (*24*). Ethnic groups included in the analysis were Māori, who make up 16.5% of New Zealand's total population; Pacific Islander (8.1%); Asian (15.1%); and European/other (70.2%). The major Pacific groups in New Zealand are Samoan, Tongan, Cook Island Māori, and Niuean. The major Asian groups are Chinese, Indian, Filipino, and Korean.

### Ethics

The University of Otago Human Research Ethics Committee granted ethical approval for this study (approval no. HD19/033). The Ngāi Tahu Research Consultation Committee also consulted on the study.

## Results

### ARF Incidence Trends and Distribution

During 2000–2018, we noted 2,752 initial hospitalizations with ARF as the principal diagnosis, an average of 145 initial ARF hospitalizations per year. Over the same period, 288 persons were rehospitalized with ARF as their principal diagnosis, an average of 15 recurrent cases per year and 9.5% of the total ARF hospitalizations. Most (47.8%) recurrent cases were among children 10–14 years of age. During 2000–2016, only 3 ARF deaths were recorded, so we did not analyze this outcome further.

During 2000–2018, annual national initial ARF hospitalization rates ranged from 2.2 to 4.5 cases/100,000 population, an average rate of 3.4 cases/100,000 population (Figure 1). Annual rates of initial ARF hospitalization increased slightly over the study period, but the increase was not statistically significant ($p = 0.58$). Annual rates of recurrent ARF hospitalizations ranged from 0.1 to 0.8 cases/100,000 population, an average rate of 0.4 cases/100,000 population. Annual rates of recurrent ARF hospitalizations remained stable over time ($p = 0.93$ by test for trend).

During 2000–2018, most (93.4%) ARF cases occurred in persons <30 years of age, among whom most (43.0%) children hospitalized with initial ARF were 10–14 years of age, a rate of 20.6 cases/100,000 population (Figure 2). However, 92.6% of initial ARF cases among persons <30 years of age were among Māori or Pacific Islanders; Māori accounted for 48.9% of cases and Pacific Islanders for 43.7%. Pacific Islanders had the highest average initial ARF hospitalization rates among persons <30 years of age, 38.1 cases/100,000 population, and rates


**Figure 1**. Annual rates of initial and recurrent acute rheumatic fever hospitalizations, New Zealand, 2000–2018. ARF, acute rheumatic fever.

among Māori were 16.8 cases/100,000 population (Figure 3).

Initial ARF hospitalization rates peaked at 35.9 cases/100,000 population among Māori children 5–14 years of age and at 79.6 cases/100,000 population for Pacific Island children. By comparison, rates for European/other ethnicities were 1.6 cases/100,000 population. The net effect of the elevated rates among Māori and Pacific Island children means that by age 20, the cumulative risk for hospitalized ARF is 1.2% for Pacific Islanders, 0.5% of Māori, and 0.01% for other ethnicities.

Patients with initial ARF hospitalizations were more likely (aRR 5.2, 95% CI 4.0–6.8) to come from the most socioeconomically deprived areas of the country (NZDep 9–10). The most socioeconomically disadvantaged neighborhoods had greater increases in ARF hospitalizations over time. Independent of socioeconomic deprivation, Pacific Islanders and Māori <30 years of age had markedly higher rates of initial ARF hospitalization than persons in other ethnic groups (Table 1) and rates for Pacific Islanders increased greatly over time (RR 1.3, 95% CI 1.2–1.5).

Rates of initial ARF hospitalizations increased for persons <30 years of age from the 2000–2009 period to the 2010–2018. Increases were statistically significant for persons 15–19 and 20–29 years of age ($p<0.05$).

Rates of ARF vary throughout regions of New Zealand. Counties Manukau, in South Auckland, had the highest rate for initial ARF hospitalization among persons <30 years of age (21.7 cases/100,000 population), but rates also were high in Northland (17.4 cases/100,000 population). Over the study period, the DHBs of Counties Manukau and the Hutt Valley had statistically significant increases in rates of initial ARF hospitalization ($p<0.01$) (Appendix Table 1, https://wwwnc.cdc.gov/EID/article/27/1/19-1791-App1.pdf).

### RHD Incidence Trends and Distribution

During 2000–2018, a total of 12,094 hospitalizations with a principal diagnosis of RHD were reported, an average of 636 admissions per year. Of these, 5,109 persons were hospitalized with an initial RHD diagnosis, an annual average of 269 persons. During the study period, national initial RHD hospitalization rates ranged from 4.1 to 10.0 cases/100,000 population, an average incidence rate of 6.2 cases/100,000 population (Figure 4). Total rates of RHD hospitalizations as principal diagnosis, including initial and repeat admissions, ranged 11.5 to 17.9 cases/100,000 population, an annual rate of 14.3 cases/100,000 population. The mean age of initial RHD hospitalization was 60 years, with a median age of 67 years.

We analyzed RHD cases according to sociodemographic characteristics for patients aged <70 years (Table 2). We noted that initial RHD primary hospitalization rates increased over time at a statistically significant level (RR 1.09, 95% CI 1.01–1.17; $p = 0.03$).

We found that risk for RHD is associated with increasing age, Māori and Pacific Islander ethnicity, and socioeconomic deprivation. We also noted a weak association for male over female sex. Rates are markedly higher in some geographic areas (DHBs), but most disappear after adjustment for other sociodemographic factors. Māori and Pacific Islanders RHD rates rose markedly over the observation period but RHD rates rose markedly over the observation period for children 0–9 years of age ($p = 0.01$) and 10–19 years of age ($p<0.01$) than for any other age groups.

The initial RHD primary hospitalization rate for Pacific Islanders <70 years of age was 11.6 cases/100,000 population, and this group was 4.6 times more likely to be hospitalized for RHD than persons in the European/other group; Māori were 3.2 times more likely to be hospitalized for RHD (Table 2). Over the study period, rates of RHD rose at statistically

significant levels among persons <70 years of age in both Māori (p = 0.01) and Pacific Islander (p = 0.01) populations. Geographically, Counties Manukau DHB had the most cases of RHD and Tairawhiti DHB had the highest rate for initial RHD hospitalizations (Table 2; Appendix Table 1).

Over the study period, persons living in the most socioeconomically deprived areas (NZDep 9–10) had the highest rates of initial hospitalization with a principal diagnosis of RHD, 7.6 cases/100,000 population. The most socioeconomically deprived areas (NZDep 9–10) experienced major increases in initial RHD hospitalizations over the study period (Table 2). Māori and Pacific Islanders living in the most socioeconomically-deprived areas were much more likely to be hospitalized with RHD (Māori aRR 10.58, 95% CI 8.88–12.61; Pacific Islander aRR 13.80, 95% CI 11.48–16.58) than European/other (aRR 3.33, 95% CI 2.76–4.01) or Asian (aRR 1.82, 95% CI 1.25–2.64) populations living in the most socioeconomically deprived areas.

### RHD Mortality Rates and Distribution

During 2000–2016, a total of 2,435 deaths were attributed to RHD, with an average of 143 deaths per year and a rate of 3.4 deaths/100,000 population. The highest rates for RHD coded as the underlying cause of death occurred among persons 60–69 years of age. We noted a 42.6% decline in RHD mortality rates among persons <70 years of age from the 2000–2009 period to the 2010–2016 period.

RHD mortality rates for people <70 years varied according to sociodemographic characteristics (Table 3). The risk for RHD death was most strongly associated with increasing age, Māori and Pacific Islander ethnicity, and socioeconomic deprivation. Pacific Islanders <70 years of age had an average RHD mortality rate of 4.4 deaths/100,000 population and were more likely to die from RHD than persons of European/other ethnicity (aRR 11.2, 95% CI 9.1–13.8); Māori had an RHD mortality rate of 4.3 deaths/100,000 population and were also more likely than European/other to die from RHD (aRR 12.3, 95% CI 10.3–14.6). Among RHD deaths, 73.8% were persons of Māori and Pacific Islander ethnicity.

Although a decline in RHD mortality rates has occurred across all sociodemographic groups, it has been least apparent among Pacific Islanders. The mean age at RHD death for Māori was 59.2 years, for Pacific Islanders 55.2 years, for Asians 66.0 years, and for European/other ethnicities 80.0 years. RHD death was associated with socioeconomic deprivation; persons living in the most socioeconomically deprived areas were more likely to die from RHD (aRR 3.3, 95% CI 2.3–4.3) than those in the least socioeconomically deprived areas. In addition, Māori living in high deprivation areas (NZDep9–10) were much more likely to die from RHD (aRR 47.52, 95% CI 30.71–73.55), as were Pacific Islanders (aRR 37.46, 95% CI 23.63–59.39). More female (496) than male (394) persons died from RHD over the study period, although this difference was not statistically significant.

### Trends in ARF and RHD by Age and Ethnicity

We assessed ARF and RHD hospitalizations and RHD deaths by age and ethnic group during 2000–2018 (Figure 5). Māori and Pacific Islander populations suffered the highest rates across all outcomes. In addition, Māori and Pacific Islanders had higher rates

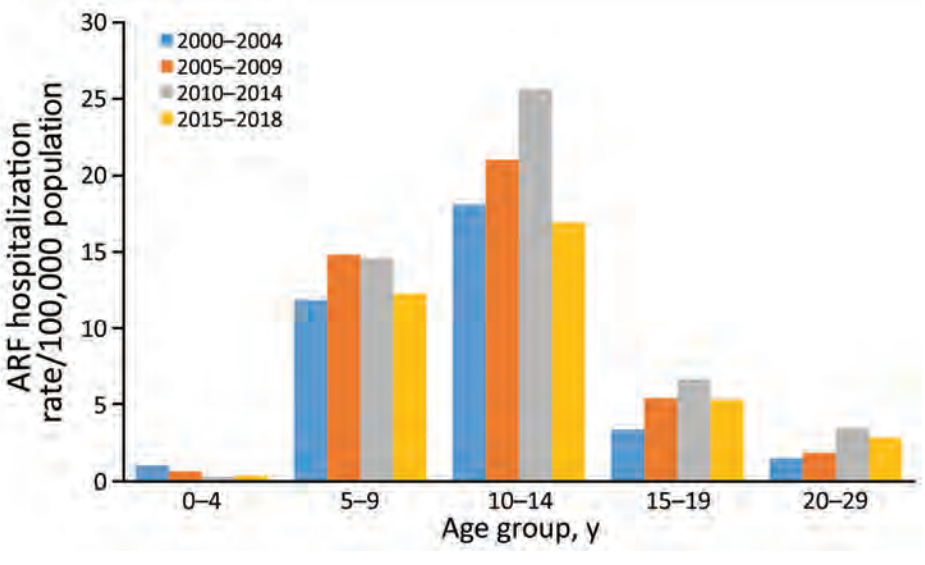


**Figure 2.** Incidence of initial acute rheumatic fever hospitalizations by age group and time period, New Zealand, 2000–2018. ARF, acute rheumatic fever.

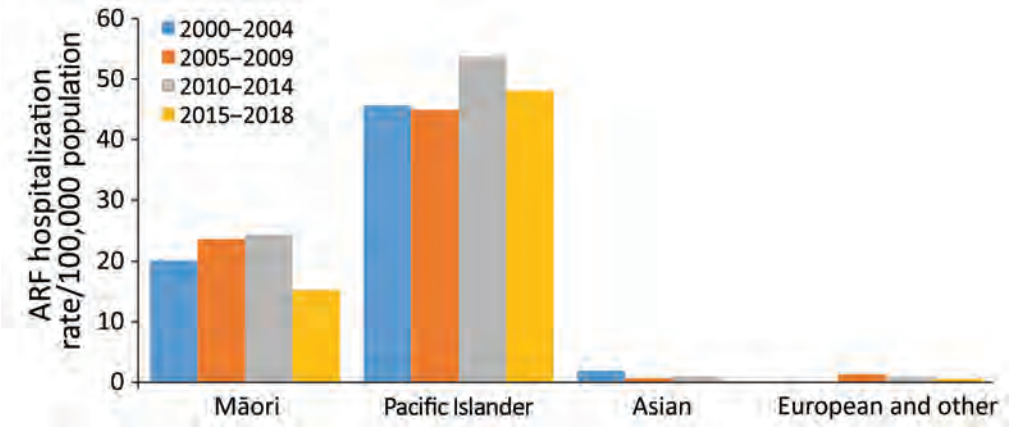


**Figure 3.** Incidence of initial acute rheumatic fever hospitalizations by major ethnic group and time period among persons <30 years of age, New Zealand, 2000–2018. ARF, acute rheumatic fever.

of outcomes in younger age groups than European/other or Asian populations.

## Discussion

We provide a comprehensive overview of the epidemiology of ARF, RHD, and death from RHD in New Zealand. Our study builds on previous reports (*15*,*25*–*28*) that examine how the disease burden is shifting and becoming more concentrated in specific population groups.

The overall rate of ARF remained relatively constant during 2000–2018. A marked shift in the distribution demonstrated a major decrease in initial ARF hospitalization rates in persons of European/other ethnicity, but rates have not declined for Māori and have continued to rise for Pacific Islanders. Most

**Table 1.** Acute rheumatic fever initial hospitalizations and adjusted rate ratios for patients <30 years of age, according to key sociodemographic characteristics, New Zealand, 2000–2018*

| Category | No. cases | Crude rate of ARF at initial hospitalization/100,000 population | aRR (95% CI) | RR in 2010–2018 vs. 2000–2009 (95% CI) |
|---|---|---|---|---|
| Age† | | | | |
| <5 | 35 | 0.62 | 0.18 (0.13–0.25) | 0.42 (0.20–0.88) |
| 5–9 | 768 | 13.45 | 4.10 (3.57–4.70) | 1.01 (0.88–1.17) |
| 10–14 | 1,184 | 20.55 | 6.58 (5.77–7.51) | 1.08 (0.96–1.21) |
| 15–19 | 308 | 5.27 | 1.81 (1.54–2.13) | 1.29 (1.03–1.62) |
| 20–29 | 276 | 2.27 | Referent | 1.86 (1.45–2.38) |
| Sex‡ | | | | |
| M | 1,493 | 8.60 | 1.34 (1.24–1.45) | 1.09 (0.99–1.21) |
| F | 1,078 | 6.42 | Referent | 1.18 (1.05–1.33) |
| Ethnicity (prioritized)§ | | | | |
| Māori | 1,257 | 16.77 | 11.84 (10.02–13.98) | 1.09 (0.98–1.22) |
| Pacific Islander | 1,124 | 38.12 | 23.57 (19.88–27.94) | 1.30 (1.16–1.47) |
| Asian | 23 | 0.55 | 0.64 (0.41–0.99) | 0.41 (0.18–0.98) |
| European and other | 167 | 0.86 | Referent | 0.61 (0.44–0.84) |
| Socioeconomic deprivation level¶ | | | | |
| 1–2 | 61 | 1.06 | Referent | 0.63 (0.38–1.05) |
| 3–4 | 128 | 2.16 | 1.65 (1.21–2.23) | 0.85 (0.60–1.20) |
| 5–6 | 160 | 2.51 | 1.60 (1.19–2.25) | 0.91 (0.67–1.24) |
| 7–8 | 405 | 5.57 | 2.58 (1.96–3.38) | 1.31 (1.08–1.59) |
| 9–10 | 1,817 | 20.58 | 5.21 (4.01–6.75) | 1.16 (1.06–1.27) |
| District health board# | | | | |
| Northland | 206 | 17.36 | 7.56 (4.39–13.02) | 1.10 (0.84–1.45) |
| Counties Manukau, South Auckland | 909 | 21.67 | 7.37 (4.32–12.53) | 1.23 (1.08–1.41) |
| Tairawhiti, Gisborne | 63 | 16.01 | 5.47(3.06–9.80) | 1.45 (0.88–2.39) |
| South Island, 5 DHBs | 67 | 0.91 | Referent | 1.21 (0.71–1.88) |
| Total | 2,571 | 7.53 | | 1.13 (1.04–1.22) |

*An additional 181 (6.6% of total) cases occurred among persons ≥30 years of age during 2000–2018. aRR, adjusted rate ratio; DHB, district health board; RR, rate ratio.
†RR adjusted for sex, ethnicity, and socioeconomic deprivation.
‡RR adjusted for age, ethnicity, and socioeconomic deprivation.
§RR adjusted for age, sex, and socioeconomic deprivation.
¶RR adjusted for age, sex, and ethnicity.
#RR adjusted for age, sex, ethnicity, and socioeconomic deprivation; 3 DHBs highest incidence and 1 DHB with lowest incidence shown. A full list of DHBs is provided in Appendix Table 1 (https://wwwnc.cdc.gov/EID/article/27/1/19-1791-App1.pdf).

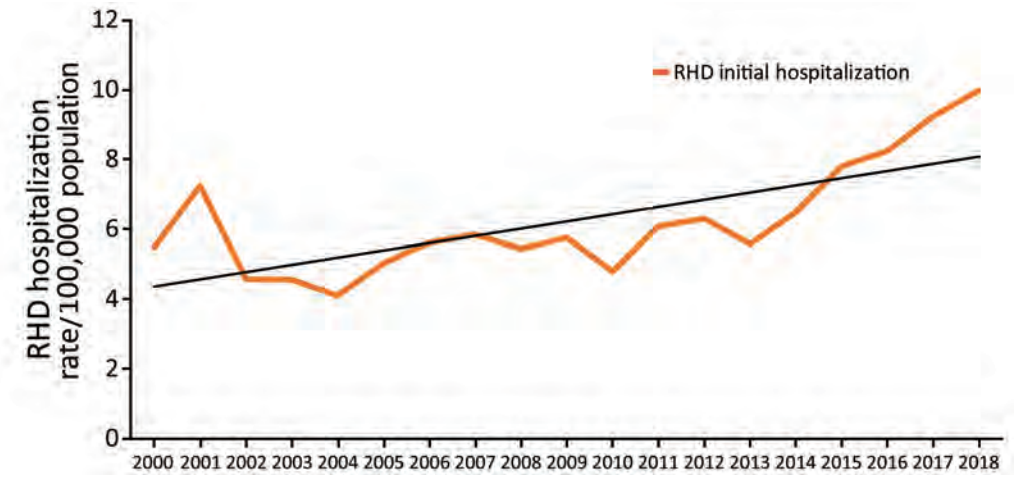


**Figure 4.** New Zealand annual incidence rates of initial RHD hospitalizations, all ages, 2000–2018. RHD, rheumatic heart disease.

(93.4%) initial ARF cases are among persons <30 years of age, and most (92.6%) occur in Māori and Pacific Islanders. Rates of ARF in some population subgroups remain among the highest reported in a high-income country, showing stark ethnic inequalities. For children 5–14 years of age, the rates for Māori (35.9 cases/100,000 population) and Pacific Islanders (79.6 cases/100,000 population) are similar to rates in many

**Table 2.** Rheumatic heart disease initial hospitalization rates and adjusted rate ratios for patients <70 years of age according to key sociodemographic characteristics, New Zealand, 2000–2018*

| Characteristics | No. cases | Crude rate of RHD at initial hospitalization/100,000 population | aRR (95% CI) | RR in 2010–2018 vs. 2000–2009 (95% CI) |
|---|---|---|---|---|
| Age, y† | | | | |
| 0–9 | 154 | 1.35 | Referent | 1.53 (1.11–2.11) |
| 10–19 | 322 | 2.77 | 2.21 (1.82–2.68) | 1.51 (1.21–1.88) |
| 20–29 | 164 | 1.47 | 1.30 (1.04–1.62) | 0.95 (0.69–1.29) |
| 30–39 | 208 | 1.87 | 1.83 (1.49–2.26) | 0.81 (0.62–1.07) |
| 40–49 | 420 | 3.60 | 3.84 (3.19–4.62) | 1.07 (0.88–1.30) |
| 50–59 | 678 | 6.69 | 7.66 (6.43–9.14) | 0.93 (0.80–1.08) |
| 60–69 | 957 | 12.87 | 15.66 (13.18–18.61) | 1.13 (1.00–1.29) |
| Sex‡ | | | | |
| M | 1,405 | 3.74 | 1.12 (1.04–1.21) | 1.14 (1.03–1.26) |
| F | 1,498 | 4.06 | Referent | 1.04 (0.93–1.15) |
| Ethnicity§ | | | | |
| Māori | 892 | 7.30 | 3.21 (2.93–3.52) | 1.24 (1.09–1.42) |
| Pacific Islander | 574 | 11.60 | 4.62 (4.16–5.15) | 1.28 (1.08–1.51) |
| Asian | 123 | 1.47 | 0.71 (0.59–0.86) | 0.80 (0.56–1.14) |
| European and other | 1,314 | 2.68 | Referent | 0.95 (0.86–1.10) |
| Socioeconomic deprivation level¶ | | | | |
| 1–2 | 222 | 1.60 | Referent | 0.79 (0.60–1.02) |
| 3–4 | 324 | 2.34 | 1.42 (1.20–1.68) | 0.85 (0.68–1.05) |
| 5–6 | 441 | 3.05 | 1.76 (1.49–2.06) | 1.07 (0.89–1.29) |
| 7–8 | 642 | 4.15 | 2.19 (1.88–2.55) | 1.12 (0.56–1.31) |
| 9–10 | 1,274 | 7.58 | 3.10 (2.67–3.60) | 1.21 (1.09–1.36) |
| District health board# | | | | |
| Northland | 150 | 5.57 | 1.32 (1.03–1.69) | 0.94 (0.68–1.29) |
| Counties Manukau, South Auckland | 478 | 5.70 | 1.44 (1.16–1.78) | 1.05 (0.88–1.26) |
| Tairawhiti, Gisborne | 90 | 11.13 | 2.38 (1.79–3.16) | 1.73 (1.12–2.66) |
| Hutt Valley, Wellington | 107 | 4.33 | 1.51 (1.15–1.97) | 1.38 (0.94–2.03) |
| Southern, South Island | 110 | 2.14 | Referent | 1.11 (0.76–1.61) |
| Total | 2,903 | 3.90 | | 1.09 (1.01–1.17) |

*An additional 2,212 cases (43.2% of total) occurred among persons ≥70 years of age during 2000–2018. aRR, adjusted rate ratio; DHB, district health board; RHD, rheumatic heart disease; RR, rate ratio.
†RR adjusted for sex, ethnicity, and socioeconomic deprivation.
‡RR adjusted for age, ethnicity, and socioeconomic deprivation.
§RR adjusted for age, sex, and socioeconomic deprivation.
¶RR adjusted for age, sex, and ethnicity.
#RR adjusted for age, sex, ethnicity, and socioeconomic deprivation; 4 highest incidence DHBs, and the 1 lowest DHB shown. A full list of DHBs is provided in Appendix Table 1 (https://wwwnc.cdc.gov/EID/article/27/1/19-1791-App1.pdf).

**Table 3.** Mortality rates of rheumatic heart disease and adjusted rate ratios for people aged <70 y, according to key sociodemographic characteristics, New Zealand, 2000–2016*

| Category | No. deaths | Crude rate of RHD deaths/100,000 population | aRR (95% CI) | RR during 2010–2016 vs. 2000–2009 (95% CI) |
|---|---|---|---|---|
| Age† | | | | |
| <40 | 126 | 0.31 | Referent | 0.66 (0.45–0.96) |
| 40–49 | 163 | 1.56 | 7.27 (5.76–9.18) | 0.68 (0.49–0.94) |
| 50–59 | 249 | 2.80 | 15.09 (12.17–18.72) | 0.53 (0.41–0.70) |
| 60–69 | 352 | 5.48 | 34.15 (27.80–41.95) | 0.56 (0.45–0.69) |
| Sex‡ | | | | |
| M | 394 | 1.21 | 0.88 (0.75–0.98) | 0.56 (0.45–0.69) |
| F | 496 | 1.49 | Referent | 0.61 (0.51–0.73) |
| Ethnicity§ | | | | |
| Māori | 467 | 4.34 | 12.27 (10.32–14.58) | 0.53 (0.44–0.65) |
| Pacific Islander | 190 | 4.37 | 11.16 (9.05–13.76) | 0.77 (0.57–1.02) |
| Asian | 20 | 0.29 | 0.8 7(0.55–1.38) | 0.09 (0.02–0.40) |
| European and other | 213 | 0.49 | Referent | 0.63 (0.47–0.84) |
| Socioeconomic deprivation level¶ | | | | |
| 1–2 | 48 | 0.39 | Referent | 0.23 (0.11–0.46) |
| 3–4 | 67 | 0.55 | 1.23 (0.85–1.78) | 0.51 (0.30–0.84) |
| 5–6 | 113 | 0.88 | 1.72 (1.23–2.42) | 1.01 (0.70–1.46) |
| 7–8 | 188 | 1.37 | 2.17 (1.57–2.99) | 0.54 (0.40–0.73) |
| 9–10 | 474 | 3.18 | 3.18 (2.34–4.33) | 0.58 (0.48–0.71) |
| District health board# | | | | |
| Northland | 52 | 2.18 | 1.13 (0.76–1.69) | 0.48 (0.24–0.94) |
| Counties Manukau, South Auckland | 168 | 2.28 | 1.65 (1.21–2.24) | 0.75 (0.53–1.05) |
| Tairawhiti, Gisborne | 33 | 4.56 | 2.22 (1.42–3.48) | 0.35 (0.15–0.83) |
| South Island, 5 DHBs | 81 | 0.53 | Referent | 0.50 (0.31–0.82) |
| Total | 890 | 1.35 | | 0.58 (0.51–0.67) |

*An additional 1,545 (63.4% of total) deaths occurred among persons ≥70 years of age during 2000–2016. aRR, adjusted rate ratio; DHB, district health board; RHD, rheumatic heart disease; RR, rate ratio.
†RR adjusted for sex, ethnicity, and socioeconomic deprivation.
‡RR adjusted for age, ethnicity, and socioeconomic deprivation.
§RR adjusted for age, sex, and socioeconomic deprivation.
¶RR adjusted for age, sex, and ethnicity.
#RR adjusted for age, sex, ethnicity, and socioeconomic deprivation; 3 highest incidence DHBs and the DHB with lowest incidence shown. A full list of DHBs is provided in Appendix Table 1 (https://wwwnc.cdc.gov/EID/article/27/1/19-1791-App1.pdf).

low-income countries (*5*,*29*,*30*) and to the high rates previously reported in New Zealand (*25*,*26*). The net effect of these high rates means that, by age 20, the cumulative risk for ARF is 1.2% for Pacific Islanders and 0.5% for Māori, compared with 0.01% for European/other ethnicities. This iniquitous distribution of ARF drives elevated rates of RHD and premature death from RHD across the lifespan for Māori and Pacific Islanders.

Analysis of the sociodemographic characteristics showed ARF almost exclusively affects Māori and Pacific Island children and young adults. Disaggregating these characteristics shows independent contributions from ethnicity, socioeconomic deprivation, and geographic location (Appendix Table 2). Among persons <30 years of age, Māori had a markedly increased (unadjusted) risk for ARF (RR 19.6, 95% CI 16.7–23.0) as did Pacific Islanders (RR 44.5, 95% CI 37.9–52.4) compared with the risk for the European/other group. This elevated risk was reduced after adjustment for socioeconomic deprivation and further reduced after adjustment for geographic location. However, a residual increased risk persisted (RR 9.0, 95% CI 8.2–9.8 for Māori and RR 16.6, 95% CI 14.8–18.6 for Pacific Islanders). A positive finding was that ARF recurrence rates have remained stable over time, with a rate of 0.4 cases/100,000 population. In addition, these cases represent ≈9.5% of total ARF hospitalizations, suggesting successful operation of secondary prevention programs.

RHD hospitalization rates rose greatly over the study period. RHD is concentrated in older age groups and 43.3% of RHD hospitalizations occur among persons >70 years of age. Current trends reflect patterns of ARF that have occurred over the past few decades (cohort effects) and changes in clinical awareness and diagnostic practices. However, Māori and Pacific Islanders again suffer the greatest burden of disease, 50.5% of cases among persons <70 years of age. Ethnic inequalities are less marked for RHD than for ARF, probably reflecting cohort effects from previous decades when ARF inequalities were less marked (*25*). As is the case for ARF, the increased risk for RHD among Māori and Pacific Islanders is

associated with deprivation and region in addition to an independent association with ethnicity.

We noted steep declines in RHD mortality rates during 2000–2016. Nonetheless, Māori and Pacific Islanders once more bear the greatest burden of disease, accounting for 73.8% of deaths among persons <70 years of age. As with ARF and RHD hospitalizations, the increased risk for Māori and Pacific Islanders is associated with socioeconomic deprivation and region in addition to an independent association with ethnicity.

A strength of this study is the comprehensive nature of the outcome data used. However, the administrative data used has some limitations, both in identifying and reporting cases of ARF and RHD. A case can be missed if a person did not seek medical attention, did not have symptoms recognized as ARF or RHD by a medical professional, or was not hospitalizeddespite a diagnosis. Consequently, the ARF findings likely underestimate the true incidence of disease. In comparison, RHD hospitalizations might be overestimated due to ICD-10 directives for RHD. Further clinical validation of ICD codes is needed to improve identification of RHD in administrative data in New Zealand and globally. One approach that would greatly help validation would be implementation of a national patient registry, which would enable improved uptake of prophylaxis by patients, better clinical service coordination, and improved healthcare sector performance monitoring. RHD mortality data have similar coding limitations to those seen for RHD hospitalizations. In addition, many RHD deaths are undercounted because they manifest as other circulatory diseases, such as heart failure and strokes (*31*).

Despite those limitations, this study provides a comprehensive overview of the incidence and distribution of ARF, RHD, and RHD deaths in New Zealand. A particularly stark finding is the marked ethnic inequalities in disease burden with ARF disproportionally affecting Māori and Pacific Island

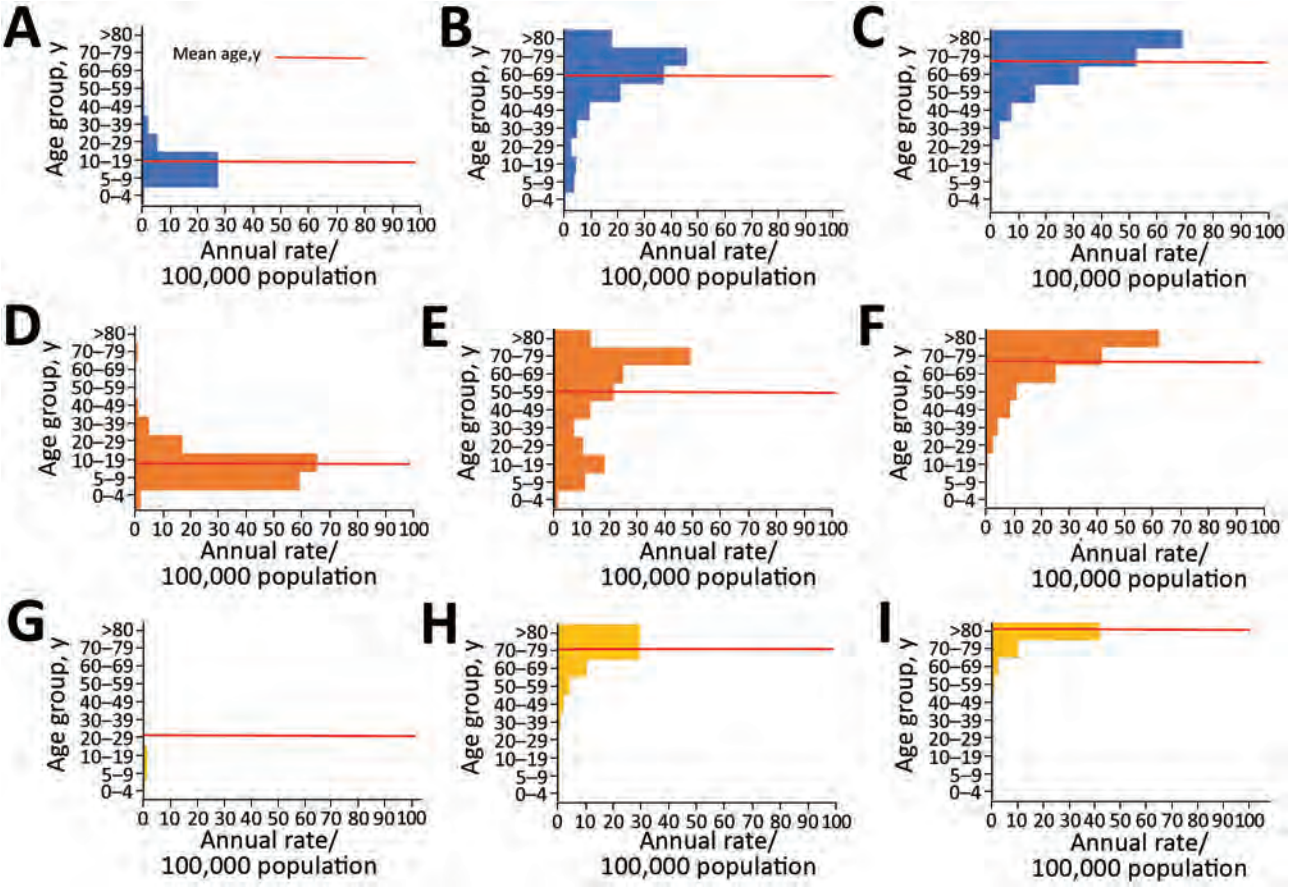


**Figure 5.** Age distribution of ARF, RHD, and RHD mortality rates across major ethnic groups, New Zealand, 2000–2018. A) ARF incidence among Māori; B) RHD incidence among Māori; C) RHD mortality rates among Māori; D) ARF incidence among Pacific Islanders; E) RHD incidence among Pacific Islanders; F) RHD mortality rates among Pacific Islanders; G) ARF incidence among European or other persons; H) RHD incidence among European or other persons; I) RHD mortality rates among European or other persons. ARF, acute rheumatic fever; RHD, rheumatic heart disease.

children, and RHD, and RHD deaths disproportionately affecting Māori and Pacific Islander adults, particularly those living in high socioeconomic deprivation. We saw evidence of a cohort effect; new cases of ARF were becoming rare in European/other children, RHD was declining among European/other adults, and RHD deaths were becoming uncommon in European/other persons <70 years of age. However, rates of initial ARF in Māori children remain high and are not decreasing, and rates appear to be rising in Pacific Island children, condemning these groups to a lifetime living with the effects of RHD. To help curb the continuing high rates of ARF and RHD, New Zealand and other countries must address the large and increasing social and ethnic inequalities.

The Health Research Council (HRC) of New Zealand provided funding for the study.

## About the Author

Dr. Bennett is a senior research fellow in the Department of Public Health, at the University of Otago, Wellington. She has a wide range of public health research interests, with a particular focus on infectious diseases (rheumatic fever, rheumatic heart disease) air pollution and housing.

## References

1. McDonald M, Currie BJ, Carapetis JR. Acute rheumatic fever: a chink in the chain that links the heart to the throat? Lancet Infect Dis. 2004;4:240–5. https://doi.org/10.1016/S1473-3099(04)00975-2
2. Cunningham MW. Rheumatic fever revisited. Nat Rev Cardiol. 2014;11:123. https://doi.org/10.1038/nrcardio.2012.197-c1
3. McDonald M, Currie BJ, Carapetis JR. Acute rheumatic fever: a chink in the chain that links the heart to the throat? Lancet Infect Dis. 2004;4:240–5
4. Heart Foundation of New Zealand. New Zealand guidelines for rheumatic fever: diagnosis, management and secondary prevention of acute rheumatic fever and rheumatic heart disease: 2014 update [cited 2019 Dec 1]. https://www.heartfoundation.org.nz/resources/acute-rheumatic-fever-and-rheumatic-heart-disease-guideline
5. Carapetis JR. Rheumatic heart disease in developing countries. N Engl J Med. 2007;357:439–41. https://doi.org/10.1056/NEJMp078039
6. Watkins DA, Johnson CO, Colquhoun SM, Karthikeyan G, Beaton A, Bukhman G, et al. Global, regional, and national burden of rheumatic heart disease, 1990–2015. N Engl J Med. 2017;377:713–22. https://doi.org/10.1056/NEJMoa1603693
7. Gordis L. The virtual disappearance of rheumatic fever in the United States: lessons in the rise and fall of disease. T. Duckett Jones memorial lecture. Circulation. 1985;72:1155–62. https://doi.org/10.1161/01.CIR.72.6.1155
8. Clemmesen S. Rheumatic fever statistics in Denmark from 1878 to 1946 and their significance in profylaxis. Acta Med Scand. 1949;135(S234):109–17. https://doi.org/10.1111/j.0954-6820.1949.tb05601.x
9. Quinn RW. Comprehensive review of morbidity and mortality trends for rheumatic fever, streptococcal disease, and scarlet fever: the decline of rheumatic fever. Rev Infect Dis. 1989;11:928–53. https://doi.org/10.1093/clinids/11.6.928
10. Jaine R, Baker M, Venugopal K. Acute rheumatic fever associated with household crowding in a developed country. Pediatr Infect Dis J. 2011;30:315–9. https://doi.org/10.1097/INF.0b013e3181fbd85b
11. Veasy LG, Tani LY, Hill HR. Persistence of acute rheumatic fever in the intermountain area of the United States. J Pediatr. 1994;124:9–16. https://doi.org/10.1016/S0022-3476(94)70247-0
12. Veasy LG, Wiedmeier SE, Orsmond GS, Ruttenberg HD, Boucek MM, Roth SJ, et al. Resurgence of acute rheumatic fever in the intermountain area of the United States. N Engl J Med. 1987;316:421–7. https://doi.org/10.1056/NEJM198702193160801
13. Carapetis JR, McDonald M, Wilson NJ. Acute rheumatic fever. Lancet. 2005;366:155–68. https://doi.org/10.1016/S0140-6736(05)66874-2
14. Australian Institute of Health and Welfare. Field B. Rheumatic heart disease: all but forgotten in Australia except among Aboriginal and Torres Strait Islander peoples. Canberra, ACT, AUS: The Institute; 2004 [cited 2019 Nov 5]. https://www.aihw.gov.au/getmedia/00df75e1-701f-4081-9079-bae3a05ccd80/bulletin16.pdf
15. Milne RJ, Lennon DR, Stewart JM, Vander Hoorn S, Scuffham PA. Incidence of acute rheumatic fever in New Zealand children and youth. J Paediatr Child Health. 2012;48:685–91. https://doi.org/10.1111/j.1440-1754.2012.02447.x
16. Webb R, Wilson N. Rheumatic fever in New Zealand. J Paediatr Child Health. 2013;49:179–84. https://doi.org/10.1111/j.1440-1754.2011.02218.x
17. Ministry of Health, Institute of Environmental Science and Research Limited. Rheumatic fever bi-annual report July 2017–June 2018 [cited 2019 Nov 10]. https://surv.esr.cri.nz/surveillance/RheumaticFever.php
18. Oliver J, Pierse N, Baker MG. Estimating rheumatic fever incidence in New Zealand using multiple data sources. Epidemiol Infect. 2015;143:167–77. https://doi.org/10.1017/S0950268814000296
19. New Zealand Ministry of Health. National Health Index [cited 2019 May 5]. https://www.health.govt.nz/our-work/health-identity/national-health-index
20. New Zealand Ministry of Health. National Minimum Dataset (hospital events) [cited 2019 Jun 2]. http://www.health.govt.nz/nz-health-statistics/national-collections-and-surveys/collections/national-minimum-dataset-hospital-events
21. New Zealand Ministry of Health. Mortality Collection [cited 2019 Jun 20]. https://www.health.govt.nz/nz-health-statistics/national-collections-and-surveys/collections/mortality-collection
22. Salmond CE, Crampton P. Development of New Zealand's deprivation index (NZDep) and its uptake as a national policy tool. Can J Public Health. 2012;103(Suppl 2):S7–11.
23. Stats NZ. Age, sex and ethnic group projections, 2013 [cited 2019 Jun 1]. https://www.stats.govt.nz/tools/nz-dot-stat
24. New Zealand Ministry of Health. HISO 10001 ethnicity data protocols for the health and disability sector 2016: consultation document [cited 2019 May 20]. https://www.health.govt.nz/publication/hiso-10001-ethnicity-data-protocols-health-and-disability-sector-2016-consultation-document

25. Jaine R, Baker M, Venugopal K. Epidemiology of acute rheumatic fever in New Zealand 1996–2005. J Paediatr Child Health. 2008;44:564–71. https://doi.org/10.1111/j.1440-1754.2008.01384.x
26. Milne RJ, Lennon D, Stewart JM, Vander Hoorn S, Scuffham PA. Mortality and hospitalisation costs of rheumatic fever and rheumatic heart disease in New Zealand. J Paediatr Child Health. 2012;48:692–7. https://doi.org/10.1111/j.1440-1754.2012.02446.x
27. Gurney JK, Stanley J, Baker MG, Wilson NJ, Sarfati D. Estimating the risk of acute rheumatic fever in New Zealand by age, ethnicity and deprivation. Epidemiology & Infection. 2016;144:3058–67
28. Baker MG, Gurney J, Oliver J, Moreland NJ, Williamson DA, Pierse N, et al. Risk factors for acute rheumatic fever: literature review and protocol for a case-control study in New Zealand. Int J Environ Res Public Health. 2019;16:E4515. https://doi.org/10.3390/ijerph16224515
29. Seckeler MD, Hoke TR. The worldwide epidemiology of acute rheumatic fever and rheumatic heart disease. Clin Epidemiol. 2011;3:67–84. https://doi.org/10.2147/CLEP.S12977
30. Jaine R. Acute rheumatic fever in New Zealand: epidemiology and the role of household crowding. Dissertation. University of Otago; 2007.
31. Wilson N, Mitchelson B, Peat B, Webb R, Anderson A, Jack S, et al. The New Zealand rheumatic heart disease registry. Heart Lung Circ. 2018;27:S19. https://doi.org/10.1016/j.hlc.2018.05.141

Address for correspondence: Julie Bennett, Department of Public Health, University of Otago, Wellington, 23A Mein St, Newtown, Wellington 6021, New Zealand; email: julie.bennett@otago.ac.nz

# Differential Yellow Fever Susceptibility in New World Nonhuman Primates, Comparison with Humans, and Implications for Surveillance

Natália C.C. de Azevedo Fernandes, Juliana M. Guerra, Josué Díaz-Delgado, Mariana S. Cunha, Leila del C. Saad, Silvia D. Iglezias, Rodrigo A. Ressio, Cinthya dos Santos Cirqueira, Cristina T. Kanamura, Isis P. Jesus, Adriana Y. Maeda, Fernanda G.S. Vasami, Júlia de Carvalho, Leonardo J.T. de Araújo, Renato Pereira de Souza, Juliana S. Nogueira, Roberta M.F. Spinola, José L. Catão-Dias

A major outbreak of yellow fever (YF) occurred in Brazil during 2016–2018. Epizootics in New World nonhuman primates are sentinel events for YF virus circulation. However, genus-specific susceptibilities and suitability for YF surveillance remain poorly understood. We obtained and compared epidemiologic, histopathologic, immunohistochemical, and molecular results from 93 human and 1,752 primate cases submitted during the recent YF outbreak in Brazil (2017), with the support of the Brazilian National YF Surveillance Program. We detected heterogeneous YF-associated profiles among the various genera of primates we analyzed. *Alouatta* primates were the most reliable sentinel; *Sapajus* and *Callicebus* primates had higher viral loads but lower proportional mortality rates. *Callithrix* primates were the least sensitive, showing lower viral loads, lower proportional mortality rates, and no demonstrable YF virus antigen or extensive lesions in liver, despite detectable viral RNA. These differences in susceptibility, viral load, and mortality rates should be considered in strategic surveillance of epizootics and control measures for YF.

Author affilations: Instituto Adolfo Lutz, São Paulo, Brazil (N.C.C. de Azevedo Fernandes, J.M. Guerra, J. Díaz-Delgado, M.S. Cunha, S.D. Iglezias, R.A. Ressio, C. dos Santos Cirqueira, C.T. Kanamura, I.P. Jesus, A.Y. Maeda, F.G.S. Vasami, J. de Carvalho, L.T. de Araújo, R. Pereira de Souza, J.S. Nogueira); Universidade de São Paulo, São Paulo (N.C.C. de Azevedo Fernandes, J.M. Guerra, J. Díaz-Delgado, J.L. Catão-Dias); Texas A&M Veterinary Medical Diagnostic Laboratory, College Station, Texas, USA (J. Díaz-Delgado); Centro de Vigilância Epidemiológica Prof. Alexandre Vranjac, São Paulo (L.D.C. Saad, R.M.F. Spinola)

DOI: https://doi.org/10.3201/eid2701.191220

Yellow fever (YF) is a zoonosis caused by YF virus (YFV; family *Flaviviridae*, genus *Flavivirus*) that has 2 established cycles in South America: urban and sylvatic. The sylvatic cycle is maintained by forest canopy mosquitoes (*Sabethes* spp. and *Haemagogus* spp.) and New World primates (NWPs); humans are accidental hosts (*1*,*2*). During 2016–2018, YF reemerged in Brazil, posing new threats with major epidemic waves in areas with low viral circulation, although without evidence of the urban cycle (*3*). The national surveillance program in Brazil for YF primarily relies on YF investigation in deceased free-ranging NWPs (*4*). Surveillance of epizootics in NWPs plays a pivotal role for deployment of prevention actions, emphasizing immediate vaccination of susceptible human populations (*5*).

Brazil has broad and heterogeneous NWP (suborder Platyrrhini) diversity: 5 families, 21 genera, and 176 species (*6*). Nevertheless, knowledge of YF in NWP species is limited; most efforts have focused on serologic testing of the species *Leontopithecus chrysomelas* (*7*), *Alouatta* spp. (*8*,*9*), *Cebus* spp.(*10*), and *Saguinus* spp. and *Saimiri* spp. (*10*). Only howler monkeys (*Alouatta* sp.) have well-documented liver involvement in consequence of natural YF infection (*11*) and are considered reliable sentinels of YFV circulation, because they show higher susceptibility to YF than humans and develop a fatal hepatic failure with massive cellular death (*1*,*4*,*12*). Howler monkeys and laboratory NWP models usually have hepatic changes similar to those found in humans (*3*,*11*): massive necrosis/apoptosis associated with Councilman–Rocha Lima bodies, steatosis, and mild inflammatory

infiltrates (*13*,*14*), although diverging pathologic features might also be seen (*3*). Further knowledge of YF pathogenic aspects is needed to guarantee that samples from various species of NWPs would be adequately used for YF surveillance purposes to ensure appropriate diagnoses and subsequent public health responses. In addition, this knowledge will clarify the effect of YF in the wide range of NWPs in Brazil.

During the last YF outbreak in Brazil (2016–2018), we observed differences among genera not only in YF prevalence but also in YF viral load, as reported (*15*). These differences might have implications for NWP as amplifying hosts or as reservoirs in YF cycle. The term reservoir refers to an animal with persistent infection, sometimes without clinical signs, and sufficient amount of pathogen to act as source of infection. Amplifier, although used as a synonym, is a broad term referring to a host with high viral load and source of infection (*16*). Thus, we hypothesized that there are different genus-specific susceptibilities among NWPs that could affect YF surveillance/monitoring. To reduce this knowledge gap, we characterized and compared the histopathologic signature of YF-associated liver disease, viral antigen detection by immunohistochemical analysis (IHC), and molecular findings in samples from humans and NWPs infected by YFV that were received during 2017 at Adolfo Lutz Institute (São Paulo, Brazil).

## Methods

### Data and Sample Collection

We obtained formalin-fixed, paraffin-embedded and fresh frozen (−70°C) liver samples from NWPs and humans from São Paulo state, Brazil, that were submitted for YF diagnosis to the Adolfo Lutz Institute during 2017, according to the Brazilian National Surveillance Program of YF by the Ministry of Health of Brazil (*4*). The Adolfo Lutz Institute is an official laboratory for the diagnosis of YFV in humans and primates. NWP samples came from standardized necropsies performed by local surveillance agents. Epidemiologic (carcass location and date) and biological (genera, sex, age) data were obtained from notification files (Sistema Nacional de Agravos de Notificação) sent with the samples. Cases designated as *Cebus* spp. were reclassified as *Sapajus* spp., according to Alfaro et al. (*17*). Only NWP cases with genera identified and formalin-fixed, paraffin-embedded liver tissue were included in this study. For humans, samples from patients with suspected or confirmed YF who died were obtained; only cases with quantitative reverse transcription PCR (qRT-PCR) results from fresh liver samples were included. Adverse vaccine effects and transplant cases were excluded. All procedures were approved by the Animal Use and Research Ethical Committees of the Adolfo Lutz Institute (CEUA-IAL no. 11/2016 and CEP-IAL no. 3.121.328–caaee 96138818.0.0000.0059) and the Instituto Chico Mendes de Conservação da Biodiversidade protocol 50551–3.

### Spatial Analysis

Cases positive by IHC or qRT-PCR were tabulated and plotted. Plots were made by using a map of São Paulo state and QGis software (https://qgis.org).

### Histopathologic and Immunohistochemical Analyses

Protocols and procedures were conducted in the enhanced laboratory Biosafety Level 2 facility of the Adolfo Lutz Institute. All formalin-fixed, paraffin-embedded liver tissue samples were processed and stained with hematoxylin and eosin for histopathologic examination. IHC was performed according to our laboratory protocols. Liver tissue sections were subjected to antigen retrieval in a pressure cooker in citrate buffer for 3 min (120°C, pH 6.0) and then incubated overnight with polyclonal anti-YF (mouse hyperimmune antiserum against wild strain; Núcleo de Doença de Transmissão Vetorial, Virology Center, Adolfo Lutz Institute) (*3*,*12*). Signal amplification was performed by using the Horseradish Peroxidase–Conjugated Polymer Detection System (REVEAL Biotin-Free Polyvalent; Spring Bioscience Corp., https://www.cmocro.com) and visualized by using diaminobenzidine (D-5637; Sigma-Aldrich, https://www.sigmaaldrich.com) and counterstaining with Harris hematoxylin. In selected instances, amplification was performed by using AP conjugated polymer (MACH4 Universal AP Polymer Kit; Biocare Medical, https://biocare.net) and visualized by using fast red chromogen (WARP RED chromogen kit; Biocare Medical). Known NWPs and human positive and negative control tissues with omitted first-layer antibody were included.

NWP cases were classified according to the distribution, extent, and nature of microscopic findings after staining with hematoxylin and eosin as described (Appendix Table 1, https://wwwnc.cdc.gov/EID/article/27/1/19-1220-App1.pdf). For IHC, cases were classified as positive, negative, or inadequate on the basis of YFV antigen detection and varying degrees of typical YF-associated lesions. Inadequate classification refers to highly autolyzed/decomposed cases with lack of immunolabeling. Human cases were classified as full spectrum of YF-associated hepatic lesions or other histologic patterns. We provide a detailed description of other histologic patterns.

### Molecular Analysis by Using qRT-PCR

Total RNA was extracted from fresh frozen liver by using the QIAamp RNA Blood Mini Kit (QIAGEN, https://www.qiagen.com), according to the manufacturer's instructions. Amplification of YFV fragments were performed by using a described protocol (*18*) that targets the highly conserved 5′ noncoding region of the genome (112 bp) and is based on a TaqMan qRT-PCR protocol. Quantification cycle (Cq) was used as a reference for viral load (in a standard curve with YFV vaccine 17D, a titer of $10^5$ PFU/mL had a mean Cq = 16, and 1 PFU/mL had a mean Cq = 35.6).

### Statistical Analysis

Data were tabulated and analyzed by using Portal Action (http://www.portalaction.com.br) and R software (https://www.r-project.org). For categorical data, we used $\chi^2$ or Fisher exact test (2-tailed) tests. For continuous data, after using the Shapiro-Wilk normality test, we applied the Kruskal-Wallis test. Agreement between IHC and qRT-PCR was calculated by using the Cohen kappa contingency coefficient. Sensitivity, specificity, positive predictive value, negative predictive value, and accuracy of histologic analysis were calculated; inadequate cases obtained by IHC were excluded. The IHC detection limit (qRT-PCR Cq value) was obtained by using receiver operating characteristic curve analysis. Correlation of nonparametric data was calculated by using the Spearman test, and a standard curve was created. Statistical difference was defined as $p<0.05$.

## Results

### NWPs

We analyzed 1,752 NWPs: 413 (23.6%) were female, 638 (36.4%) were male, and 701 (40%) did not have sex identified. Distribution by genus was 921 (52.6%) *Callithrix* spp., 708 (40.4%) *Alouatta* spp., 95 (5.4%) *Sapajus* spp., and 28 (1.6%) *Callicebus* spp. *Alouatta* and *Sapajus* species had higher proportions of males than did *Callithrix* and *Callicebus* spp. ($p<0.01$). We compiled a population profile, including sex and age distribution by genus (Appendix Table 2), and a spatial distribution of positive NWPs, all from São Paulo state, by IHC, qRT-PCR, or both (Appendix Figure 1).

All cases had IHC results. Of 1,752 cases, 468 (26.7%) were positive for YF: 437 (61.7%) of 708 *Alouatta* spp., 8 (28.6%) of 28 *Callicebus* spp., 13 (13.7%) of 95 *Sapajus* spp., and 10 (1.1%) of 921 *Callithrix* spp. Of the remaining cases, 1,171 (66.8%) were negative and 113 (6.4%) had inadequate results because of autolysis or absence of liver samples. No age ($p = 0.55$) or sex ($p = 0.72$) difference between positive and negative groups was detected.

Microscopic evaluation of IHC-positive cases identified 432 (92.3%) of 468 cases that had a full spectrum of YF hepatic lesions (Figure 1). Three had other histologic patterns: 2 (0.4%) had apoptotic hepatocytes, and 1 (0.2%) had mild degenerative and reaction findings. These 3 cases were *Alouatta* spp. (Appendix Figure 2). Among all positive cases, 33 (7.1%) had autolysis that impaired histologic classification; these cases were excluded from further analysis.

Of all cases evaluated, 1,193 (68.1%) of 1,752 had qRT-PCR results, and 277 (23.2%) of those had detectable YFV: 243 (64.5%) of 374 *Alouatta* spp., 5 (31.2%) of 16 *Callicebus* spp., 5 (7.5%) of 67 *Sapajus* spp., and 24 (3.3%) of 736 *Callithrix* spp. Some cases had inadequate IHC results because of autolysis/decomposition: 2 *Callithrix* spp. and 12 *Alouatta* spp. We found that 24 (8.7%) of 277 (8.7%) qRT-PCR–positive cases had negative results by IHC: 15/24 *Callithrix* spp. (62.5%), 8/243 *Alouatta* spp. (3.3%) and 1/5 *Callicebus* spp. (20%). These cases were called discordant cases, and the remaining cases were called concordant cases.

The discordant group represented, excluding autolyzed tissues, 15 (68.2%) of 22 positive *Callithrix* spp. by qRT-PCR, and 8 (3.5%) of 231 positive *Alouatta* spp. This group included 15 cases with mild degenerative and reactional findings, 4 with steatosis, 1 with non–YF-associated hepatitis, 2 with apoptotic hepatocytes, 1 with multinucleation of hepatocytes, and 1 with no lesions. One case in a *Sapajus* spp. that had a positive IHC result and a negative qRT-PCR result was not considered for statistical analysis because of intense autolysis that impaired morphologic analysis.

Regarding viral load, *Callithrix* spp. had a higher Cq (median 34, range 9–37) than other genera ($p<0.001$). There was no significant difference in Cq for *Alouatta*, *Callicebus*, and *Sapajus* spp. The discordant group had a higher Cq (median 34, range 12–37) than the concordant group (median 12, range 5–35) ($p<0.001$). When we compared viral load in the concordant group, we observed no difference for NWP genera. We compared Cq values for the concordant and discordant groups (Figure 2) and the distribution of Cq values for *Alouatta* and *Callithrix* spp. and humans (Appendix Figures 3–5).

We calculated YF-associated proportional mortality rates on the basis of cases with liver antigen detected by IHC divided by all cases and YF proportional infections as number of cases with detectable YF virus by qRT-PCR divided by all cases. *Callithrix* sp. was the only genus with difference between proportional YF-related mortality rates and infection

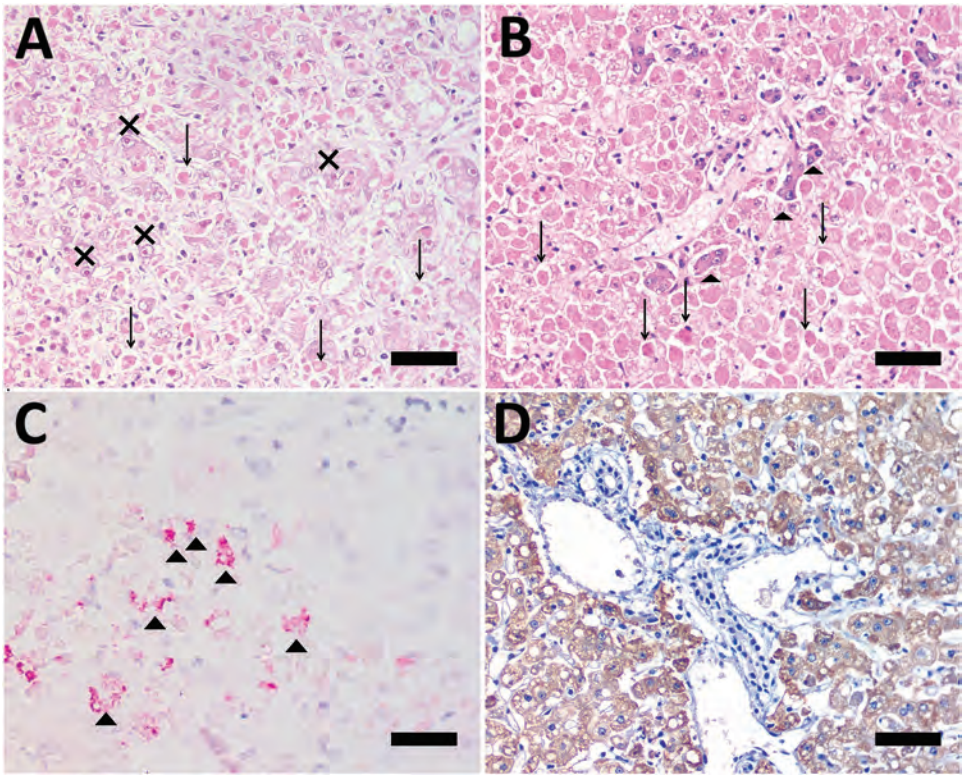


**Figure 1.** Photomicrographs of liver from human patient (A, C) and *Callicebus* spp. monkey (B, D) with full spectrum of yellow fever (YF)–associated lesions, Brazil. Midzonal necrosis with multiple Councilman-Rocha Lima bodies (arrows), mild steatosis, and hepatocytes with eosinophilic nucleoli (Torres body [Xs]) (hematoxylin and eosin stained). B) Necrosis/apoptosis (diffuse and panlobular), associated with multiple Councilman-Rocha Lima bodies (arrows) and a few remaining viable hepatocytes (arrowheads) in periportal area (hematoxylin and eosin stained). C) Positive, multifocal immunolabeling for YF antigen (arrowheads) (anti-YF, Warp red, counterstained with hematoxylin). D) Intense and diffuse immunolabeling for YF antigen (anti-YF, 3,3'-diaminobenzidine counterstaining with hematoxylin). Scale bars indicate 50 µm.

(p = 0.01), and proportional YF-related mortality rates and infection were different for NWP genera (p<0.01) (Table 1).

### Humans

We received 93 specimens from human case-patients who had suspected YF, 68 (73.1%) men and 25 (26.9%) women. Of these, 48 (51.6%) had detectable YFV by qRT-PCR, 40 (83.3%) men and 8 (16.7%) women. Of these 48 patients, 46 (95.8%) were IHC positive (concordant) and 2 (4.7%) were IHC negative (discordant). The mean ± SD age for positive case-patients by qRT-PCR (48.8 ± 14.9 years) was higher than for negative case-patients (41.5 ± 18.8 years) (p = 0.04), and a higher prevalence was found in men (p = 0.03). The mean ± SD time in days between onset of clinical signs and time of death (TOD) was 10.7 ± 4.8 (minimum 2 days, maximum 26 days). There was a direct correlation between TOD and Cq (ρ = 0.37; p = 0.007), indicating an inverse correlation between TOD and viral load (Appendix Figure 6).

All IHC-positive cases showed a full spectrum of YF-associated lesions; 2 discordant cases had other histologic patterns (Appendix Table 3, Figure 7). Regarding viral load, humans had a median Cq of 20 (range 12–38). Human patients had significantly higher Cq values than NWPs in general (p<0.001), except when compared with *Callithrix* spp. When we compared human concordant and NWP concordant cases, humans had a higher Cq than all genera of NWP. We compiled the distribution of Cq values for different NWP genera and humans (Figure 3) and the main characteristics of positive cases among humans and NWPs (Table 2).

### Comparison of Methods

Histopathologic examination showed high sensitivity and specificity for most genera of NWPs and for human specimens if one considers the full spectrum of YF-associated lesions as positive results (Table 3). Agreement between qRT-PCR and IHC for detection of YFV was good for NWPs (κ = 0.936, 95% CI 0.911–0.961) and humans (κ = 0.957, 95% CI 0.898–1.000). Analysis of NWPs by genera showed that *Callithrix* spp. had lower agreement (κ = 0.475, 95% CI 0.251–0.698) than other genera.

The detection limit for IHC was calculated by using receiver operating characteristic curve analysis and considered the Cq value for liver samples. For NWPs in general, the cutoff value was 21 (sensitivity 99.2%, specificity 95.6%). For *Alouatta* spp., the cutoff value was 21 (sensitivity 99.1%, specificity 87.5%); for *Callithrix* spp., the cutoff value was 12 (specificity and sensitivity 100%) (p<0.0001).

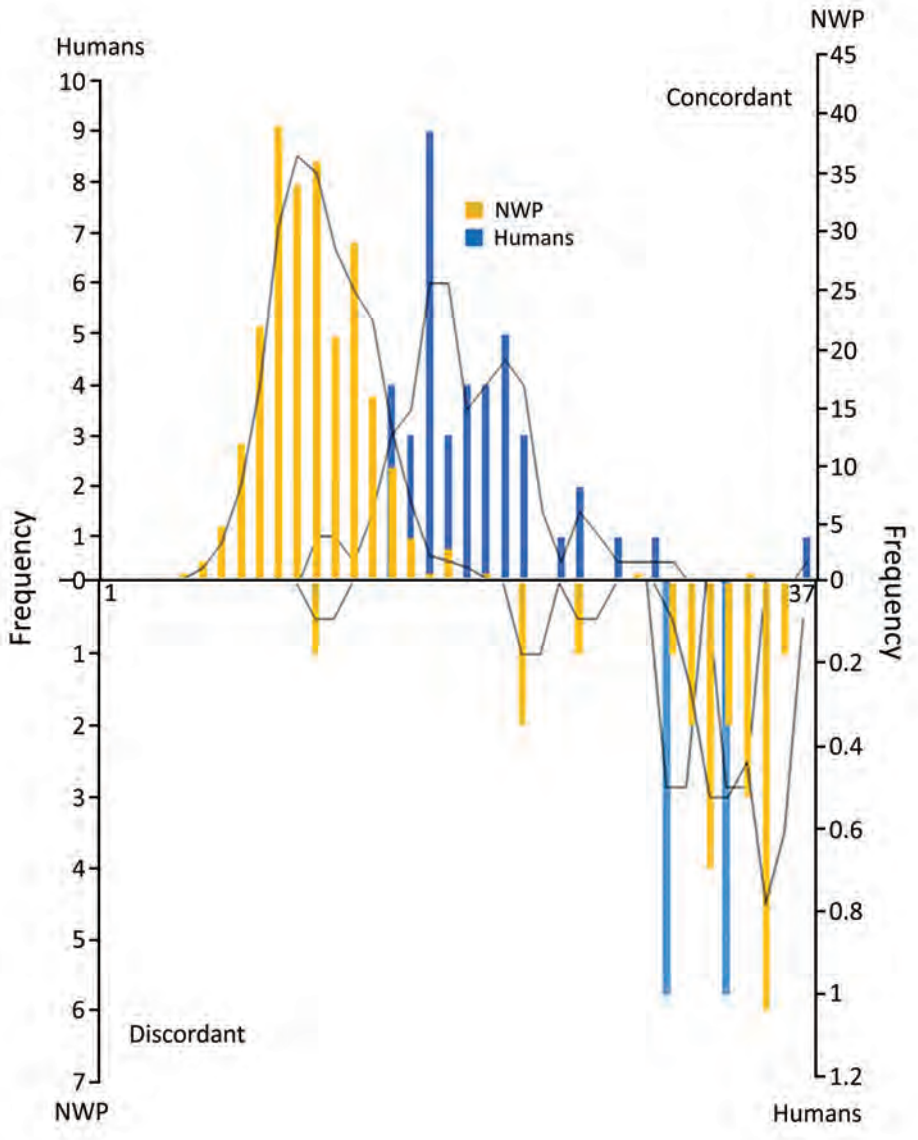


**Figure 2.** Distribution of Cq values for yellow fever in humans and NWP for concordant and discordant groups, Brazil. Discordant cases had higher Cq values, indicated on right side of the lower histogram, and concordant cases had lower Cq values (higher in humans than in NWP) in the upper histogram. Concordance was determined by using immunohistochemical analysis. The y-axes indicate number of persons and the x-axes indicate Cq value. Cq, quantification cycle; NWP, New World primate.

## Discussion

A major epidemic of YF occurred in Brazil during 2016–2018. This epidemic had a dramatic progression in São Paulo state, and virus circulated in areas without vaccination coverage (*15*,*19*). Wildlife surveillance is a pivotal tool for understanding arbovirus dynamics, despite difficulties in obtaining high-quality samples for analysis (*20*). A nonhuman primate (NHP) (rhesus monkey) is a useful model for YF (*21*) because it shows lesions similar to those in humans, although comparative studies among animals and humans, especially in an epidemic context, have not been conducted.

We analyzed a specific set of human samples that had a profile compatible with a sylvatic cycle: predominance of middle-age men, as proposed elsewhere (*19*). During 2012–2014, a YF outbreak occurred in the South Omo Zone in Ethiopia, which also had a higher mortality rate for adult men (*22*).

**Table 1.** Yellow fever–related mortality and infections rates for different genera of NWPs, Brazil*

| Genus | Mortality rate, no. IHC positive/no. tested (%) | Infection rate, no. IHC or qRT-PCR positive/no. tested (%) | p value |
|---|---|---|---|
| *Alouatta* | 437/708 (61.72) | 445/708 (62.85) | 0.8 |
| *Callicebus* | 8/28 (28.57) | 9/28 (32.14) | 1 |
| *Callithrix* | 10/921 (1.09) | 25/921 (2.71) | 0.015 |
| *Sapajus* | 13/95 (13.68) | 13/95 (13.68) | 1 |

*IHC, immunohistochemical analysis; NWPs, New Word primates; qRT-PCR, quantitative reverse transcription PCR.

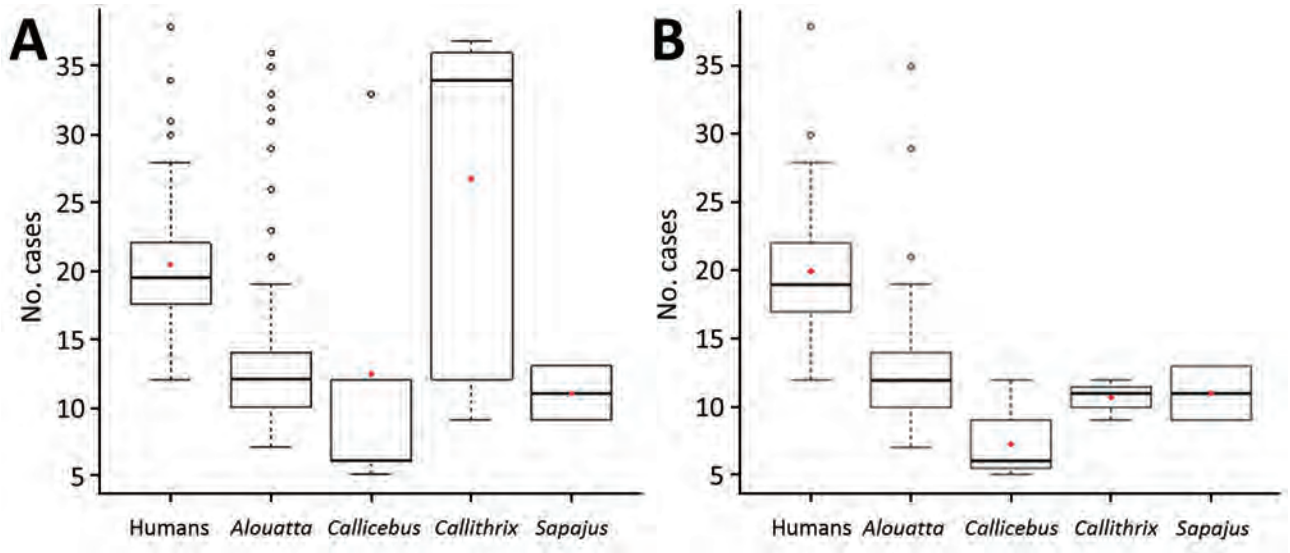


**Figure 3.** Distribution of Cq values for yellow fever for concordant and discordant cases (A) and cases in different New World primates and in humans (B), Brazil. Box plots indicate Cq values among the groups, indicated by the y-axes, minimum, first quartile, third quartile, and maximum Cq values. Horizontal bars indicate medians. Circles indicate outlier Cq values, and red diamonds indicate mean Cq values. Concordance was determined by using immunohistochemical analysis (lesions and viral antigen in hepatocytes).

However, other urban arboviral disease outbreaks, such as dengue, show similar proportions in both sexes and a lower median age (*23*).

In NWPs, there was no difference in sex and age group distribution between positive and negative cases for YF, although adult males, especially from the genus *Alouatta*, were the most affected. Moreno et al. (*24*) observed the same profile in an outbreak among NWPs in Argentina, which highlighted the impact of conservation and reduction of population growth and mortality rates once adults have an effect on population reproductive capacity and provide care of young animals.

Most human samples had a traditional histologic pattern (positive results for IHC) consistent with YF (*1*,*13*,*14*). Similarly to NWPs, we found discordant results for human case-patients who had lower viral loads, 1 of them limited by histologic over-fixation. Fixation periods >1 week might reduce immunoreactivity in tissues, even for robust antigens, such Ki-67 (*25*). In case-patients who had low viral loads and probably low amounts of antigen, these factors might have a higher negative effect. A direct correlation between TOD and Cq was observed for humans. This finding could explain the higher Cq values for humans than for NWPs because animals were mostly free living and were found dead without having any previous veterinary assistance. Also, the higher viral load among NWPs might indicate the higher potential of them as a group to act as amplifiers compared with humans.

*Alouatta* spp. accounted for >90% of IHC-positive cases; this genus also had the highest proportional mortality rate attributable to YF and was the most affected animal group. *Alouatta* spp. are reported as being highly sensitive to YFV and the major sentinel in YF epidemics; epizootics have been reported in Venezuela (*12*) and Argentina (*24*), which affected howler monkeys and humans. In Brazil during the outbreak of 2008–2009, thousands of howler monkeys died in the southern region (*26*). There was also a major reduction in populations of these animals. In São Paulo state (*8*), both situations led to expansion of the YF vaccine coverage area.

*Callicebus* spp. is one of the most diverse genera of NWP and widely distributed in South America (*27*). Although these monkeys have been described as being resistant to YF (*26*), there are a few reports of YFV, including a genomic sequence extracted from a virus isolated from a monkey of this genus (*28*). We found no information regarding mortality rates or histologic pattern of lesions in the literature. In our study, *Callicebus* spp. monkeys were sensitive to YFV and developed a full spectrum of liver lesions, similar to those in humans, and a high viral load. These manifestations also occurred for *Sapajus* spp. monkeys.

*Callithrix* spp. overrepresented the analyzed animals, although only 1.1% of them died from YF. *Callithrix* is a genus widely distributed in São Paulo state and contains a vulnerable native species, *C. aurita*, a species introduced from northeastern Brazil; *C. jacchus* and *C. penicillata*, which were reeintroduced

**Table 2.** Summary of main findings of human and NWP cases of yellow fever, Brazil*

| Category | Human | NWP genus | | | |
|---|---|---|---|---|---|
| | | *Alouatta* spp., n = 445 | *Sapajus* spp., n = 13 | *Callithrix* spp., n = 25 | *Callicebus* spp., n = 9 |
| Sex | | | | | |
| M | 40 | 208 | 5 | 9 | 3 |
| F | 8 | 79 | 5 | 5 | 5 |
| Age | | | | | |
| Humans, y | | | | | |
| 0–19 | 0 | | | | |
| 20–30 | 5 | | | | |
| 31–45 | 13 | | | | |
| 46–65 | 24 | | | | |
| >65 | 7 | | | | |
| NWP, category | | | | | |
| Cub | | 18 | 0 | 1 | 0 |
| Young | | 39 | 4 | 0 | 3 |
| Adult | | 165 | 5 | 11 | 4 |
| Hepatic histology† | | | | | |
| Full spectrum of YF-associated lesions | 45 | 403 | 12 | 9 | 8 |
| Incomplete spectrum of YF-associated lesions | 3 | 11 | 0 | 15 | 1 |
| IHC and RT-qPCR profile | | | | | |
| Concordant | 46 | 223 | 5 | 7 | 4 |
| Discordant | 2 | 7 | 0 | 14 | 1 |
| Quantification cycle | | | | | |
| <10 | 0 | 73 | 2 | 3 | 3 |
| 11–20 | 28 | 147 | 3 | 4 | 1 |
| 21–30 | 17 | 5 | 0 | 0 | 0 |
| >30 | 3 | 5 | 0 | 14 | 1 |

*IHC, immunohistochemical analysis; NA, not applicable; NWPs, New Word primates; RT-qPCR, reverse transcription quantitative PCR.
†Cases with marked autolysis were excluded.

from the savannah; and natural hybrids (*29*). Regarding YF, most experimental studies date from the 1930s and 1940s in which YFV was transmitted from inoculated *C. penicillata* monkeys to rhesus monkeys through mosquitos. Although some of the experimented animals had fevers and died, none of them had typical hepatic lesions of YF (*30*).

Knowledge about NWP hosts and their susceptibility to YFV could help clarify the potential of maintenance of virus in interepidemic periods among these different genera and anticipate new spillovers or establishment of enzootic cycles. It is useful to consider behavioral changes in human and NWP populations, such as anthropic invasion in natural areas, frequently in forest areas; intensification of agricultural activities; and presence of some genera of NWPs in urban areas. Santos et al. (*31*) reported that *C. penicillata* monkeys are capable of adapting to urban environments; can keep natural behavior and group sizes; and adapt to food sources normally found in these areas. In our study, we found positive callitrichids in urban or periurban areas, as well as *Alouatta* spp. monkeys in parks within urban areas, such as São Paulo. Therefore, the traditional division into 2 YF cycles (sylvatic and urban) might be insufficient or inaccurate to describe the complexity seen in this recent outbreak, and the coexistence of humans, NWPs, and vectors adapted to both groups in the same environment must be considered.

Valentine et al. discussed sylvatic cycles of arboviruses and highlighted the role of NHPs as hosts for chickungunya and Mayaro fever, although the possibility of other NHP reservoirs for both diseases is debated (*32*). The distinction among amplifiers and reservoirs in arbovirus cycles is complex, especially because of the acute nature of infection;

**Table 3.** Performance of histopathologic analysis in diagnosing yellow fever in NWPs and humans, Brazil*

| Category | Sensitivity | Specificity | PPV | NPV | IHC and qRT-PCR agreement, κ |
|---|---|---|---|---|---|
| NWPs | | | | | |
| All genera | 94.1 (91.6–96.1) | 99.5 (98.8–99.8) | 98.6 (97–99.4) | 97.6 (96.6–98.3) | 0.97 (0.91–0.96) |
| *Alouatta* | 97.3 (95.3–98.7) | 98.2 (95.6–99.5) | 99 (97–99.4) | 95.3 (91.9–97.3) | 0.95 (0.92–0.98) |
| *Callithrix* | 37.5 (18.8–59.4) | 99.9 (99.3–100.0) | 90.0 (54.3–98.6) | 98.2 (97.5–98.7) | 0.47 (0.25–0.70) |
| *Sapajus* | 100 (73.5–100.0) | 100 (94.4–100.0) | 100 (94.4–100.0) | 100.0 (94.4–100.0) | 0.90 (0.70–1.00) |
| *Callicebus* | 88.9 (51.7–99.7) | 94.7 (74.0–99.9) | 88.9 (53.9–98.2) | 94.7 (73.9–99.1) | 0.85 (0.56–1.00) |
| Humans | 97.9 (88.7–99.9) | 97.8 (88.5–99.9) | 97.9 (86.9–99.7) | 97.8 (86.6–99.7) | 0.96 (0.90–1.00) |

*Values are % (95% CI). IHC, immunohistochemical analysis; NPV, negative predictive value; NWPs, New Word primates; PPV, positive predictive value; RT-qPCR, reverse transcription quantitative PCR.

short time for viremia and high mortality rates are characteristics not compatible with the classical reservoir definition (*16*).

Viral persistence in a host must not cause death or serious disease, and in short-term infections, such as YFV, the virus must find a new susceptible host within a host population to keep permanent circulation (*33*). Thus, arthropod vectors are considered the most suitable reservoir for arbovirus, and NHPs are commonly described as amplifiers (*16*). The profile exhibited by callitrichids in our study differed from those of other genera, and similar to our findings in dead animals, living animals might have low viremia with no clinical hepatitis. Consequently, the role of callitrichids as amplifiers must be questioned, and their potential as a reservoir population warrants further research.

São Paulo state has a strict range of callitrichid species: *C. penicillata*, *C. jacchus*, *C. aurita*, and hybrid *Callithrix*. These taxonomic variations might be related to differential patterns. A group of animals with high viral loads (similar to the other studied genera) and hepatic lesions could affect general susceptibility in a population. In a surveillance context, callitrichids have a minor role as sentinels because of their low prevalence, although they could be relevant in urban areas, if one considers how adapted they are to these environments and different they are from the other genera analyzed. Discordant cases represent a diagnostic and medical challenge that has clinical and epidemiologic implications, especially in NWPs, because there is usually no available clinical information, such as clinical signs and other laboratory findings (liver markers, blood count). We did not observe any specific liver lesion in these cases.

In our study, callitrichids represented most samples but showed the lowest positivity rates, which was consistent with results of laboratory methods. Better selection of animals for analysis based on geographic locations and host populations from other genera could guide economic and personnel resources and optimize surveillance.

The histologic pattern for YF, especially Councilman-Rocha Lima bodies, was described more than a century ago (*34*), and its role as a diagnostic tool has been reinforced in other reports (*13*,*14*). In our study, histology was a sensitive tool for use with human and NWP samples; callitrichids were the exception. IHC for YF provided etiologic confirmation and high agreement with qRT-PCR results, even for autolyzed cases (*3*).

IHC and qRT-PCR had similar usefulness in diagnosing YF in an epidemic context. Furthermore, an inexpensive analysis, such as histopathologic analysis, could provide useful information, such as excluding negative cases, increasing laboratory response, and detecting other infectious diseases, some of them zoonoses. Moreover, histopathologic analysis, especially IHC, might be a useful screening examination because of its high sensitivity, low cost, and limited human resource requirements. The cases we report as discordant and positive cases with minimal histological lesions illustrate the usefulness of submission of complete epidemiologic and clinical information and samples from different organs for histologic analysis. In addition, a well-trained pathologist with experience in YF diagnosis in NWPs is needed to ensure a sensitive and specific diagnosis on the basis of histologic criteria.

Our study had some limitations. We could not identify species of NWPs, and differential susceptibility among members of the same genus is still unknown. We might have had bias related to sample representation because collection of carcasses was limited to areas near trails or roads. Also, this study was restricted to São Paulo state landscapes and its NWP diversity. Although the genera analyzed are distributed in other geographic areas, more studies with different neotropical primates are needed to ensure ideal surveillance.

In conclusion, NWPs are not a homogenous group and show differences regarding susceptibility, viral load, and proportional YF-associated mortality rates. Clarification of the differences within NWP genera and between NWPs and humans might help to improve and optimize strategic surveillance by directing laboratory resources to most susceptible genera and applying diagnostic tests in a more rational way.

**Acknowledgments**

We thank all professionals directly or indirectly involved in YF surveillance in São Paulo state; field and surveillance agents and laboratorial staff, especially those from the Centro de Vigilância Epidemiológica Prof. Alexandre Vranjac and the Pathology and Virology Center, Instituto Adolfo Lutz; Andreia Latorre for critically reviewing the manuscript, and Chris Gardiner for reviewing the English version of the manuscript.

The Yellow Fever Surveillance Program was supported by the Ministry of Health, Secretaria de Estado da Saúde, Coordenadoria de Controle de Doenças, the Adolfo Lutz Institute, and other public institutions. The postgraduate program was supported by Coordenação de Aperfeiçoamento de Pessoal de Nível Superior and the

National Council for Scientific and Technological Development. J.D.-D. is a recipient of a postdoctoral fellowship from Fundação de Amparo à Pesquisa do Estado de São Paulo (grant 2017/02223-8).

N.C.C.A.F performed the literature search, evaluated IHC results and histopathology, analyzed data, and wrote the manuscript, J.M.G. evaluated IHC results and histopathology and reviewed the manuscript; J.D.-D. evaluated IHC results and histopathology; M.S.C. performed qRT-PCR and analyzed data; L.C.S. performed spatial analysis and tabulated results; S.D'A.I. evaluated IHC results and histopathology of human cases; R.A.R., C.S.C., and C.T.K. conducted IHC reactions; I.P.J. reviewed files and tabulated data, A.Y.M. and F.G.S.V. performed qRT-PCR; J.C. processed samples, reviewed files and tabulated data; L.J.T.A. analyzed IHC data; R.P.S. analyzed qRT-PCR data; J.S.N. analyzed human data; R.M.F.S. interpreted data; and J.L.C.D. mentored the work. All authors critically read the manuscript and agreed with the final version.

## About the Author

Dr. Fernandes is a PhD student at the School of Veterinary Medicine and Animal Science, University of São Paulo, São Paulo, Brazil, and the lead veterinary pathologist responsible for yellow fever in NHPs at the Adolfo Lutz Institute, São Paulo, Brazil. Her primary research interests are comparative pathology of human and NHP yellow fever–associated disease, and characterizing species-specific pathogenic mechanisms and factors modulating yellow fever–endemic cycles and triggering outbreaks among humans and NHPs in the Americas.

## References

1. Monath TP, Vasconcelos PF. Yellow fever. J Clin Virol. 2015;64:160–73. https://doi.org/10.1016/j.jcv.2014.08.030
2. Possas C, Lourenço-de-Oliveira R, Tauil PL, Pinheiro FP, Pissinatti A, Cunha RV, et al. Yellow fever outbreak in Brazil: the puzzle of rapid viral spread and challenges for immunisation. Mem Inst Oswaldo Cruz. 2018;113:e180278. https://doi.org/10.1590/0074-02760180278
3. Fernandes NC, Cunha MS, Guerra JM, Réssio RA, Cirqueira CD, Iglezias SD, et al. Outbreak of yellow fever among nonhuman primates, Espirito Santo, Brazil, 2017. Emerg Infect Dis. 2017;23:2038–41. https://doi.org/10.3201/eid2312.170685
4. Brazil Ministry of Health, Secretaria de Vigilância em Saúde, Departamento de Vigilância de Doenças Tranmissíveis. Guide to epizootics surveillance in non-human primates and entomology applied to the yellow fever surveillance [in Portuguese]. 2nd ed. Brasília: The Ministry; 2017.
5. Callender DM. Management and control of yellow fever virus: Brazilian outbreak January–April, 2018. Glob Public Health. 2019;14:445–55. https://doi.org/10.1080/17441692.2018.1512144
6. Rylands AB, Mittermeier RA. Taxonomic listing of the new world primates. IUCN Species Survival Commission, Primate Specialist Group. Austin, TX; 2019 [cited 2020 Oct 7]. http://www.primate-sg.org/taxonomy
7. Catenacci LS, Ferreira M, Martins LC, De Vleeschouwer KM, Cassano CR, Oliveira LC, et al. Surveillance of arboviruses in primates and sloths in the Atlantic forest, Bahia, Brazil. EcoHealth. 2018;15:777–91. https://doi.org/10.1007/s10393-018-1361-2
8. Moreno ES, Spinola R, Tengan CH, Brasil RA, Siciliano MM, Coimbra TL, et al. Yellow fever epizootics in non-human primates, São Paulo state, Brazil, 2008–2009. Rev Inst Med Trop São Paulo. 2013;55:45–50. https://doi.org/10.1590/S0036-46652013000100008
9. Rifakis PM, Benitez JA, De-la-Paz-Pineda J, Rodriguez-Morales AJ. Epizootics of yellow fever in Venezuela (2004–2005): an emerging zoonotic disease. Ann N Y Acad Sci. 2006;1081:57–60. https://doi.org/10.1196/annals.1373.005
10. Bensabath DG, Shope RE, Andrade AH, Souza AP. Recovery of Amarilico virus, coning from a single centinella, in the surroundings of Belem, Brazil [in Portuguese]. Bol. OPAS. 1966;60:187–92.
11. Leal SG, Romano AP, Monteiro RV, Melo CB, Vasconcelos PF, Castro MB. Frequency of histopathological changes in Howler monkeys (*Alouatta* sp.) naturally infected with yellow fever virus in Brazil. Rev Soc Bras Med Trop. 2016;49:29–33. https://doi.org/10.1590/0037-8682-0363-2015
12. de Almeida MA, Dos Santos E, da Cruz Cardoso J, da Fonseca DF, Noll CA, Silveira VR, et al. Yellow fever outbreak affecting *Alouatta* populations in southern Brazil (Rio Grande do Sul State), 2008-2009. Am J Primatol. 2012;74:68–76. https://doi.org/10.1002/ajp.21010
13. Vieira WT, Gayotto LC, de Lima CP, de Brito T. Histopathology of the human liver in yellow fever with special emphasis on the diagnostic role of the Councilman body. Histopathology. 1983;7:195–208. https://doi.org/10.1111/j.1365-2559.1983.tb02235.x
14. Quaresma JA, Barros VL, Pagliari C, Fernandes ER, Guedes F, Takakura CF, et al. Revisiting the liver in human yellow fever: virus-induced apoptosis in hepatocytes associated with TGF-β, TNF-α and NK cells activity. Virology. 2006;345:22–30. https://doi.org/10.1016/j.virol.2005.09.058
15. Cunha MS, da Costa AC, de Azevedo Fernandes NC, Guerra JM, Dos Santos FC, Nogueira JS, et al. Epizootics due to yellow fever virus in São Paulo State, Brazil: viral dissemination to new areas (2016–2017). Sci Rep. 2019;9:5474. https://doi.org/10.1038/s41598-019-41950-3
16. Kuno G, Mackenzie JS, Junglen S, Hubálek Z, Plyusnin A, Gubler DJ. Vertebrate reservoirs of arboviruses: myth, synonym of amplifier, or reality? Viruses. 2017;9:1–28. https://doi.org/10.3390/v9070185
17. Alfaro JW, Silva JD Jr, Rylands AB. How different are robust and gracile capuchin monkeys? An argument for the use of *Sapajus* and *Cebus*. Am J Primatol. 2012;74:273–86. https://doi.org/10.1002/ajp.22007
18. Domingo C, Patel P, Yillah J, Weidmann M, Méndez JA, Nakouné ER, et al. Advanced yellow fever virus genome detection in point-of-care facilities and reference laboratories. J Clin Microbiol. 2012;50:4054–60. https://doi.org/10.1128/JCM.01799-12
19. Faria NR, Kraemer MU, Hill SC, Goes de Jesus J, Aguiar RS, Iani FC, et al. Genomic and epidemiological monitoring of yellow fever virus transmission potential. Science. 2018;361:894–9. https://doi.org/10.1126/science.aat7115

20. Pandit PS, Doyle MM, Smart KM, Young CC, Drape GW, Johnson CK. Predicting wildlife reservoirs and global vulnerability to zoonotic Flaviviruses. Nat Commun. 2018;9:5425. https://doi.org/10.1038/s41467-018-07896-2
21. Engelmann F, Josset L, Girke T, Park B, Barron A, Dewane J, et al. Pathophysiologic and transcriptomic analyses of viscerotropic yellow fever in a rhesus macaque model. PLoS Negl Trop Dis. 2014;8:e3295. https://doi.org/10.1371/journal.pntd.0003295
22. Mulchandani R, Massebo F, Bocho F, Jeffries CL, Walker T, Messenger LA. A community-level investigation following a yellow fever virus outbreak in South Omo Zone, South-West Ethiopia. PeerJ. 2019;7:e6466. https://doi.org/10.7717/peerj.6466
23. Miagostovich MP, Nogueira RM, Cavalcanti SM, Marzochi KB, Schatzmayr HG. Dengue epidemic in the state of Rio de Janeiro, Brazil: virological and epidemiological aspects. Rev Inst Med Trop São Paulo. 1993;35:149–54. https://doi.org/10.1590/S0036-46651993000200006
24. Moreno ES, Agostini I, Holzmann I, Di Bitetti MS, Oklander LI, Kowalewski MM, et al. Yellow fever impact on brown howler monkeys (*Alouatta guariba clamitans*) in Argentina: a metamodelling approach based on population viability analysis and epidemiological dynamics. Mem Inst Oswaldo Cruz. 2015;110:865–76. https://doi.org/Z10.1590/0074-02760150075
25. Sato M, Kojima M, Nagatsuma AK, Nakamura Y, Saito N, Ochiai A. Optimal fixation for total preanalytic phase evaluation in pathology laboratories: a comprehensive study including immunohistochemistry, DNA, and mRNA assays. Pathol Int. 2014;64:209–16. https://doi.org/10.1111/pin.12164
26. Bicca-Marques JC, Freitas DS. Conservation letter: the role of monkeys, mosquitoes, and humans in the occurrence of a yellow fever outbreak in a fragmented landscape in south Brazil : protecting howler monkeys is a matter of public health. Access. 2010;3:78–89.
27. Hoyos M, Bloor P, Defler T, Vermeer J, Röhe F, Farias I. Phylogenetic relationships within the *Callicebus cupreus* species group (Pitheciidae: Primates): biogeographic and taxonomic implications. Mol Phylogenet Evol. 2016;102:208–19. https://doi.org/10.1016/j.ympev.2016.05.031
28. Rezende IM, Sacchetto L, Munhoz de Mello É, Alves PA, Iani FC, Adelino TÉ, et al. Persistence of yellow fever virus outside the Amazon Basin, causing epidemics in southeast Brazil, from 2016 to 2018. PLoS Negl TropDis. 2018;12:e0006538. https://doi.org/10.1371/journal.pntd.0006538
29. Nogueira DM, Ferreira AM, Goldschmidt B, Pissinatti A, Carelli JB, Verona CE. Cytogenetic study in natural hybrids of *Callithrix* (Callitrichidae: Primates) in the Atlantic forest of the state of Rio de Janeiro, Brazil. Iheringia Ser Zool. 2017;101:156–60. https://doi.org/10.1590/S0073-47212011000200002
30. Davis NC. The susceptibility of marmosets to yellow fever virus. J Exp Med. 1930;52:405–16. https://doi.org/10.1084/jem.52.3.405
31. Santos M, Duarte M, Young R. Behavioural and ecological aspects of black tuftedear marmosets, *Callithrix penicillata* (Geoffroy, 1812) (Primates: Callitrichidae) in a semiurban environment. Revista de Etologis. 2014;13:37–46.
32. Valentine MJ, Murdock CC, Kelly PJ. Sylvatic cycles of arboviruses in non-human primates. Parasit Vectors. 2019;12:463. https://doi.org/10.1186/s13071-019-3732-0
33. Mims CA. The meaning of persistent infections in nature. Bull World Health Organ. 1975;52:747–51.
34. Klion FM, Schaffner F. The ultrastructure of acidophilic "Councilman-like" bodies in the liver. Am J Pathol. 1966;48:755–67.

Address for correspondence: Natália C.C. de Azevedo Fernandes, Instituto Adolfo Lutz, Centro de Patologia, Av. Dr. Arnaldo, 355, CEP 01296000, Pacaembú, São Paulo, SP, Brazil; email: nccafernandes@yahoo.com.br

# Comparative Omics Analysis of Historic and Recent Isolates of Bordetella pertussis and Effects of Genome Rearrangements on Evolution

Ana Dienstbier, Fabian Amman, Denisa Petráčková, Daniel Štipl, Jan Čapek, Jana Zavadilová, Kateřina Fabiánová, Jakub Držmíšek, Dilip Kumar, Mark Wildung, Derek Pouchnik, Branislav Večerek

Despite high vaccination coverage, pertussis is increasing in many industrialized countries, including the Czech Republic. To better understand *Bordetella pertussis* resurgence, we analyzed historic strains and recent clinical isolates by using a comparative omics approach. Whole-genome sequencing showed that historic and recent isolates of *B. pertussis* have substantial variation in genome organization and form separate phylogenetic clusters. Subsequent RNA sequence analysis and liquid chromatography with mass tandem spectrometry analyses showed that these variations translated into discretely separated transcriptomic and proteomic profiles. When compared with historic strains, recent isolates showed increased expression of flagellar genes and genes involved in lipopolysaccharide biosynthesis and decreased expression of polysaccharide capsule genes. Compared with reference strain Tohama I, all strains had increased expression and production of the type III secretion system apparatus. We detected the potential link between observed effects and insertion sequence element–induced changes in gene context only for a few genes.

*Bordetella pertussis* is a gram-negative, strictly human pathogen of the respiratory tract and the major causative agent of whooping cough. This highly contagious disease is especially severe in infants and remains a major cause of infant illness and death worldwide, predominantly in industrialized countries (*1*). Although pertussis is a vaccine-preventable disease, increased incidence is being observed in some countries that have highly vaccinated populations, including the Czech Republic (*2*–*4*). Although several factors are contributing to pertussis resurgence in these countries (*5*–*7*), the 2 prominent factors are incomplete and short-lived immunity induced by current acellular vaccines (*8*–*10*) and genetic variation, leading to escape from immunity by antigenic variation (*11*–*13*).

*B. pertussis* has an efficient mechanism of genome structure diversification because it contains >200 copies of insertion sequence 481 (IS481) in its genome (*14*). IS element–mediated homologous recombination results in excision or insertion of flanking genome regions and leads to genome reduction and decay (*14*–*16*), as well as genome rearrangements (*17,18*) and large duplications (*19*). Furthermore, a previous study indicated that gene order rearrangements associated with IS elements can alter gene expression profiles in *B. pertussis* (*20*). Recently, we have shown that, besides their effect on genome structure and stability, ISs can affect expression profiles of neighboring genes by IS element–specific promoters (*21*).

On the basis of these observations, we hypothesized that strains with different genomic organization should display altered global transcriptomic and, consequently, proteomic profiles, and thereby genome rearrangements might contribute to strain variation and adaptation. To validate this assumption, we have performed genomic, transcriptomic, and proteomic analyses of recent clinical isolates from the Czech

Author affiliations: Institute of Microbiology of the Czech Academy of Sciences, Prague, Czech Republic (A. Dienstbier, D. Petráčková, D. Štipl, J. Čapek, J. Držmíšek, D. Kumar, B. Večerek); Institute for Theoretical Chemistry of the University of Vienna, Vienna, Austria (F. Amman); National Institute of Public Health, Prague (J. Zavadilová, K. Fabiánová); Washington State University, Pullman, Washington, USA (M. Wildung, D. Pouchnik)

DOI: https://doi.org/10.3201/eid2701.191541

Republic obtained during 2008–2015, previously characterized vaccine strains isolated during 1954–1965 (*22*) (hereafter referred to as historic strains), and the reference strain Tohama I.

## Materials and Methods

### Bacterial Strains and Growth Conditions

Recent isolates of *B. pertussis* from the Czech Republic were obtained from the National Institute of Public Health in Prague (Table 1). Historic strains from the Czech Republic (*22*) and reference strain Tohama I (*23*) have been described. All strains were cultivated on Bordet-Gengou agar plates supplemented with 15% sheep blood for 3–4 days at 37°C. For liquid cultures, bacteria were grown in Stainer-Scholte medium (*24*) supplemented with 0.1% cyclodextrin and 0.5% casamino acids (Difco, https://www.fishersci.com) at 37°C. To harvest samples for DNA, RNA, and protein isolation, *B. pertussis* cells were grown overnight in Stainer-Scholte medium to mid-exponential phase of growth (optical density ≈1.0). Three independent cultivations were performed to collect 3 biologic replicates of each of the strains for RNA and protein isolation.

### Genomic Analyses

For the genome organization analysis, genomic sequences were aligned by using the progressive Mauve algorithm (*25*) and clustered on the basis of their genome organization similarity by using the maximum-likelihood for the gene order pipeline (*26*). For single-nucleotide polymorphism (SNP) analysis, IS elements within the genomes were masked with Ns, and resulting sequences were aligned by using Mugsy software (*27*). SNPs were extracted by using custom scripts (https://genohub.com). Maximum-parsimony phylogenetic analysis was performed on sequences with masked IS elements by using the kSNP3 program with a k number of 23 (*28*). The unrooted phylogenetic tree was visualized by using iTOL (*29*).

### RNA Isolation, Sequencing, and Data Analysis

We provide information on RNA isolation, sequencing, and data analysis (Appendix 1, https://wwwnc.cdc.gov/EID/article/27/1/19-1541-App1.pdf). RNA sequencing data from sequencing runs were deposited in the European Nucleotide Archive under project accession no. PRJEB34096. We defined significance as a q value <0.05 (p value adjusted for multiple testing correction [Appendix 1]).

### Protein Sample Preparation and Proteomic Analysis

We compiled information on protein sample preparation and label-free proteomic analysis, which used liquid chromatography with mass tandem spectrometry analyses (Appendix 1). Proteomics data were deposited in the ProteomeXchange Consortium by using the PRIDE partner repository with the dataset identifier PXD015184.

## Results

### Genome Organization and Content of Recent Isolates

We determined complete de novo genome assemblies of 9 recent isolates of *B. pertussis* strains collected in the Czech Republic during 2008–2015 from patients representing different age groups and vaccination status (Table 1). Genotyping of recent strains showed that they belonged to *ptxP3* lineage. SNP-based phylogenetic analysis of these strains and >350 complete *B. pertussis* genome sequences currently deposited in GenBank (Appendix 2 Table 1, https://wwwnc.cdc.gov/EID/article/27/1/19-1541-App2.xlsx) showed that recent *B. pertussis* isolates cluster with *ptxP3* isolates from other countries, demonstrating worldwide spread and lack of geographic signature (Figure 1). The genome alignment of recent isolates and previously characterized historic strains belonging to the *ptxP1* lineage (*22*) showed that all genomes contain large-scale structural rearrangements (Figure 2, panel A). According to their genome organization, sequenced strains could be classified into 8 groups. None of the historic strains clustered with any of the

**Table 1.** Characteristics of recent isolates of *Bordetella pertussis* and 9 infected patients, Czech Republic*

| | Strain information | | Patient information | |
|---|---|---|---|---|
| Year | Name | Genotype | Age, y/sex | Vaccination status |
| 2008 | Bp155 | *ptxP3, fim2–1, fim3B, prn2* | <1/M | Not vaccinated |
| 2008 | Bp312 | *ptxP3, fim2–1, fim3B, prn2* | 45/F | wP |
| 2012 | Bp6260 | *ptxP3, fim2–1, fim3A, prn2* | <1/F | Not vaccinated |
| 2012 | Bp6242 | *ptxP3, fim2–1, fim3B, prn2* | 67/F | Not vaccinated |
| 2012 | Bp6384 | *ptxP3, fim2–1, fim3A, prn2* | 69/M | Not vaccinated |
| 2012 | K10 | *ptxP3, fim2–1, fim3B, prn3* | 8/F | aP |
| 2014 | Bp82 | *ptxP3, fim2–1, fim3A, prn2* | 14/F | wP plus aP |
| 2014 | Bp46 | *ptxP3, fim2–1, fim3A, prn2* | 15/M | wP plus aP |
| 2015 | Bp318 | *ptxP3, fim2–1, fim3A, prn2* | 7/F | aP |

*aP, acellular vaccine; wP, whole-cell vaccine.

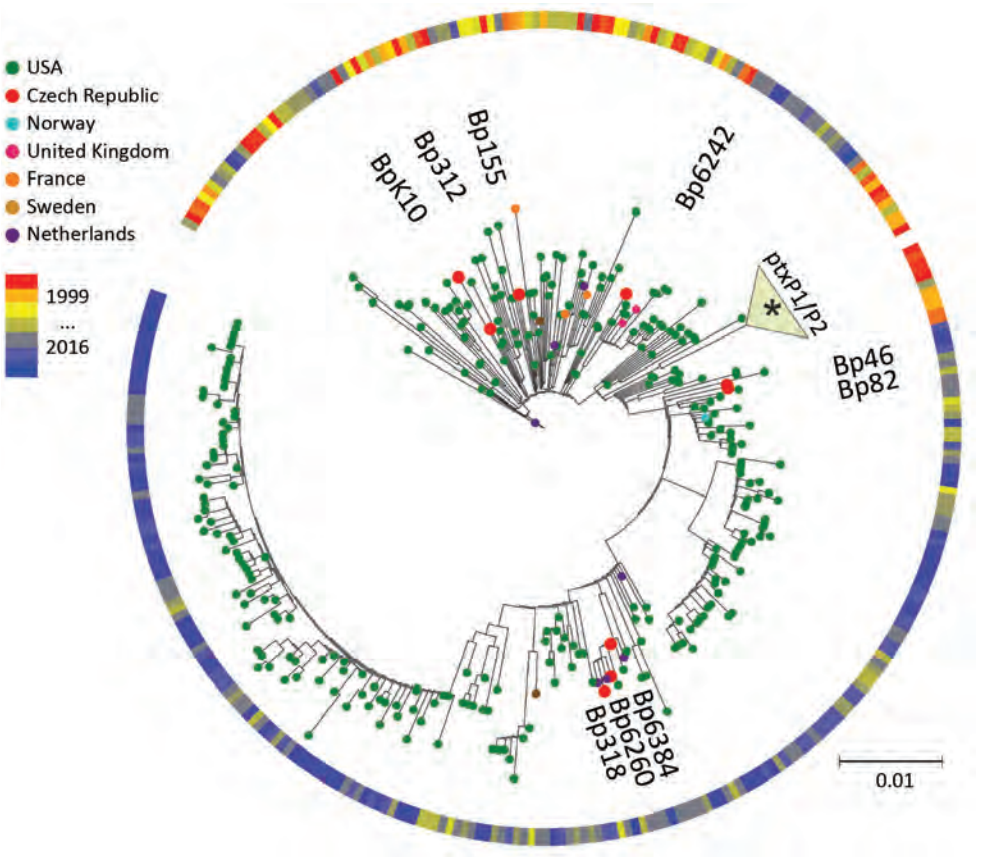


**Figure 1.** Maximum-parsimony, unrooted phylogenetic tree based on single-nucleotide polymorphism analysis of available genome sequences of *Bordetella pertussis*. Red dots indicate recent isolates from the Czech Republic. Year and country of isolation are color-coded. The 3 black dots indicate time span between 1999 and 2016. Asterisk (*) indicates association of historic strains from the Czech Republic with the *ptxP1*/*ptxP2* clade. Scale bar indicates nucleotide substitutions per site.

recent isolates. The separation of these 2 groups was verified by using a maximum-likelihood phylogenetic tree, which was constructed on the basis of the genome organization of all sequenced strains from the Czech Republic (Figure 2, panel B).

To check whether there are also sequence signatures differentiating these 2 groups of strains, we performed SNP analysis, which yielded 35 SNPs (15 synonymous, 13 nonsynonymous, and 7 intergenic) (Appendix 2 Table 2) and distinguished historic and recent isolates. Variants found in historic strains were also present in Tohama I. One of the new SNPs specific for recent isolates was identified in the promoter region of the *bteA* gene, which encodes the type III secretion system (T3SS) effector. Approximately one third of the SNPs have been reported to be specific for the *ptxP3* lineage isolates from other countries (*30*). When compared with those of historic strains, the genome size of recent isolates was substantially reduced, thereby confirming ongoing gene loss within the global population of *B. pertussis* (Appendix 2 Table 3). Analysis of genome alignments showed 2 regions of difference (RD) between the 2 groups of strains from the Czech Republic, which corresponded to previously identified regions RD3 and RD10 (*20*). Although RD3 (28.7 kb, spans genes *BP0910A–BP0937*) is absent in all recent isolates, the RD10 (25.1 kb, spans genes *BP1948–BP1968*) is absent in all recent isolates and historic strain V67.

### Transcriptomic Profiles and Genomic Structure Alterations

Total RNA was isolated from biologic triplicates of *B. pertussis* Tohama I strain; historic strains VS393, VS67, and VS401; and recent isolates Bp318, Bp155, Bp46, Bp6242, and BpK10 and analyzed by using RNA sequencing. These strains were selected on the basis of genome organization and phylogenetic distances to encompass the highest variability among the studied strains (Figure 2, panel B). Hierarchical clustering of RNA sequence data showed that samples from both groups of strains from the Czech Republic clustered separately from each other and from Tohama I (Figure 3). Consistent with phylogenetic analysis (Figure 2, panel B), we found that samples of strain VS67 formed a separate cluster. These analyses suggested that among historic strains, the VS67 strain displays closest distance to recent strains, which is consistent with our

previous observation that the VS67 strain clusters together with a recent U.S. isolate (22).

Differential expression (DE) analysis identified 78, 124, and 115 significantly ($q<0.05$ for all comparisons) modulated *B. pertussis* genes ($-1 \geq \log_2 FC \geq 1$) between recent isolates and historic strains, recent isolates and Tohama I, and historic strains and Tohama I, respectively (Appendix 2 Table 4). Among the DE genes, 30 were up-regulated in recent isolates compared with historic strains, including those encoding the flagella apparatus (*flgB-J*), LuxR (*BP1969*), and ArsR (*BP2946*) families of transcriptional regulators, phosphoglucomutase (*pgm*), phosphoglucose isomerase (*pgi*), and nicotinate-nucleotide diphosphorylase (*nadC*). Conversely, among the 48 DE genes down-regulated in recent isolates were genes encoding the polysaccharide capsule proteins (*kpsEMT*), several ABC transporters, and central metabolism enzymes, including those involved in tryptophan synthesis (*trpDEG*). Expression of several virulence

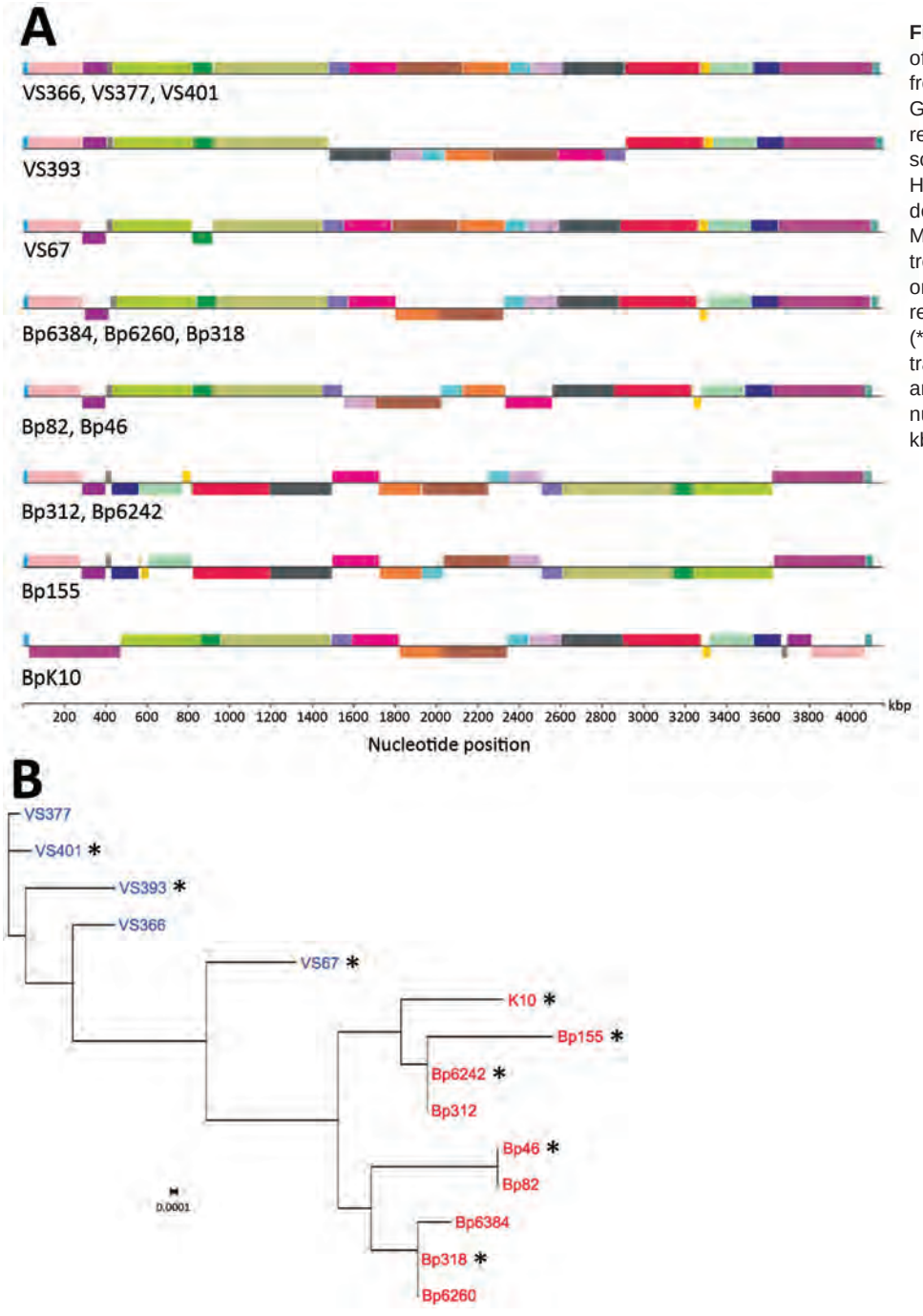


**Figure 2.** Genomic analyses of *Bordetella pertussis* isolates from the Czech Republic. A) Genome alignment of historic and recent isolates showing large-scale genome rearrangements. Homologous gene blocks are denoted by the same color. B) Maximum-likelihood phylogenetic tree based on genomic organization of historic (blue) and recent (red) isolates. Asterisk (*) indicates strains selected for transcriptomic and proteomic analyses. Scale bar indicates nucleotide substitutions per site. kbp, kilobasepairs.

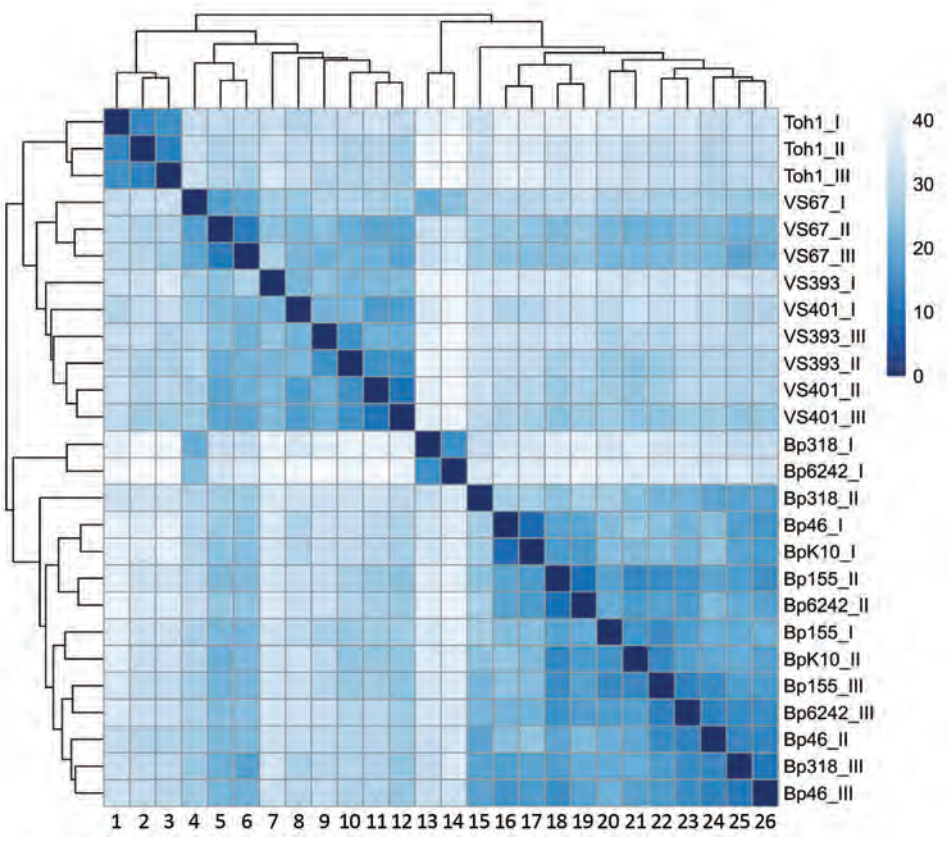


**Figure 3.** Heat map of sample-to-sample distances showing the hierarchical clustering of historic and recent isolates of *Bordetella pertussis* from the Czech Republic and the Tohama I strain. Colored scale bar and numbers on the right indicate Euclidian distances between samples calculated by using rlog-normalized RNA sequence data. 1, Toh1_1; 2, Toh1_II; 3, Toh1_III; 4, VS67_1; 5, VS67_II; 6, VS67_III; 7, VS93_I; 8,VS401_I; 9,VS393_III; 10, VS393_II; 11, VS401_II; 12,VS401_III; 13, Bp318_I; 14, Bp6242_I; 15, Bp318_II; 16, Bp46_I; 17, BpK10_I; 18, Bp155_II; 19, Bp6242_II; 20, Bp155_I; 21, BpK10_II; 22, Bp155_III; 23, Bp6242_III; 24, Bp46_II; 25, Bp318_III; 26, Bp46_III.

factors, including pertactin, tracheal colonization factor, filamentous hemagglutinin, and pertussis toxin subunit S3, was significantly up-regulated in recent isolates. However, the increase did not reach the 2-fold threshold. A recent isolate-specific SNP, which was identified in the promoter region of the *bteA* gene, did not result in a significant change of gene expression (Appendix 2 Table 4). Among the DE genes that showed increased expression in both groups of strains from the Czech Republic compared with Tohama I, we identified numerous genes within the T3SS *bcs*/*btr* locus, including *bsp22*, *bopN*, *bopB*, and *bopD* and several genes involved in sulfate metabolism (*cysADITW*).

Gene ontology enrichment (Figure 4, panel A) showed that within the set of genes, which were significantly modulated between recent and historic isolates, categories such as bacterial type flagellum-dependent cell motility, polysaccharide biosynthesis, and tryptophan biosynthesis were highly enriched. Conversely, when we compared both groups of isolates from the Czech Republic to Tohama I (Figure 4, panel C), genes associated with sulfate transmembrane transport, pathogenesis, and protein secretion by the type III secretion system terms were enriched among the DE genes.

### Clustering of Proteomic Profiles of Recent Isolates, Historic Strains, and Tohama I Strain

The cell-associated (bacterial pellets) and cell-free (culture supernatants) fractions of selected *B. pertussis* strain cultures were analyzed by using liquid chromatography with mass tandem mass spectrometry. First, hierarchical clustering of the cell-associated protein profiles showed that consistent with RNA sequencing data, strains from the Czech Republic cluster separately from Tohama I and despite high variability among biologic replicates, separation of historic and recent strains was still apparent (Figure 5, panel A). Similarly, hierarchical clustering of secreted proteins indicated that recent isolates cluster apart from historic strains and Tohama I (Figure 5, panel B).

Label-free quantification of cell-associated protein intensities identified 33, 132, and 87 proteins showing significantly changed abundance between recent and historic strains, recent strains and Tohama I, and historic strains and Tohama I, respectively (Appendix 2 Table 5). In good correlation with transcriptomic data, we found that protein levels of hydroxymethyglutaryl-CoA lyase (BP3695), ArsR family transcriptional factor BP2946, small lipoprotein BP2782, and nicotinate-nucleotide diphosphorylase NadC were increased, but levels of several central metabolism

enzymes (BP0624–BP0629), tryptophan synthesis genes, and polysaccharide capsule proteins were decreased in recent isolates compared with historic strains (Table 2). Also in support of RNA sequencing data, we determined that various components of the T3SS apparatus and several proteins involved in metabolism of sulfate showed increased abundance compared with Tohama I (Table 3). All strains from the Czech Republic produced pertactin, but flagellar proteins were not detected in any of the studied strains.

Label-free quantification analysis of secreted proteins showed that 121, 130, and 43 proteins displayed significant changes in abundance between recent and historic strains, recent strains and Tohama I, and historic strains and Tohama I, respectively (Appendix 2 Table 6). Levels of several secreted proteins were in good agreement with transcriptomic data (e.g., strains from the Czech Republic and in particular recent isolates secreted increased amounts of several T3SS proteins compared with Tohama I) (Table 3). Abundance of all pertussis toxin subunits and associated transport protein PtlE was higher in recent isolates than in historic strains, which suggests that some of the differences between the *ptxP1* and *ptxp3* strains are also manifested at the level of protein secretion.

### Changes in Genome Structure and Alterations in Gene Expression

Considering the observed differences between historic and recent strains, we attempted to track back the modulated gene expression profiles to alterations in the genome sequence and structure. Because our SNP analysis (Table 2) suggested that there were no SNPs that could explain the altered expression of the DE genes, we have additionally inspected the upstream regions of all DE genes for larger sequence variations. We identified such variations in 4 genes. The gene toh_02779 (*BP2827*) was preceded by an *IS481* element in Bp155, Bp6242, and BpK10, but not in other strains. In addition, 3 DE genes with an upstream *IS481* element had varying gene context further upstream of the transposase in the studied strains (Table 4). Apparently, the observed differences in expression of these genes could be potentially linked to the upstream IS elements.

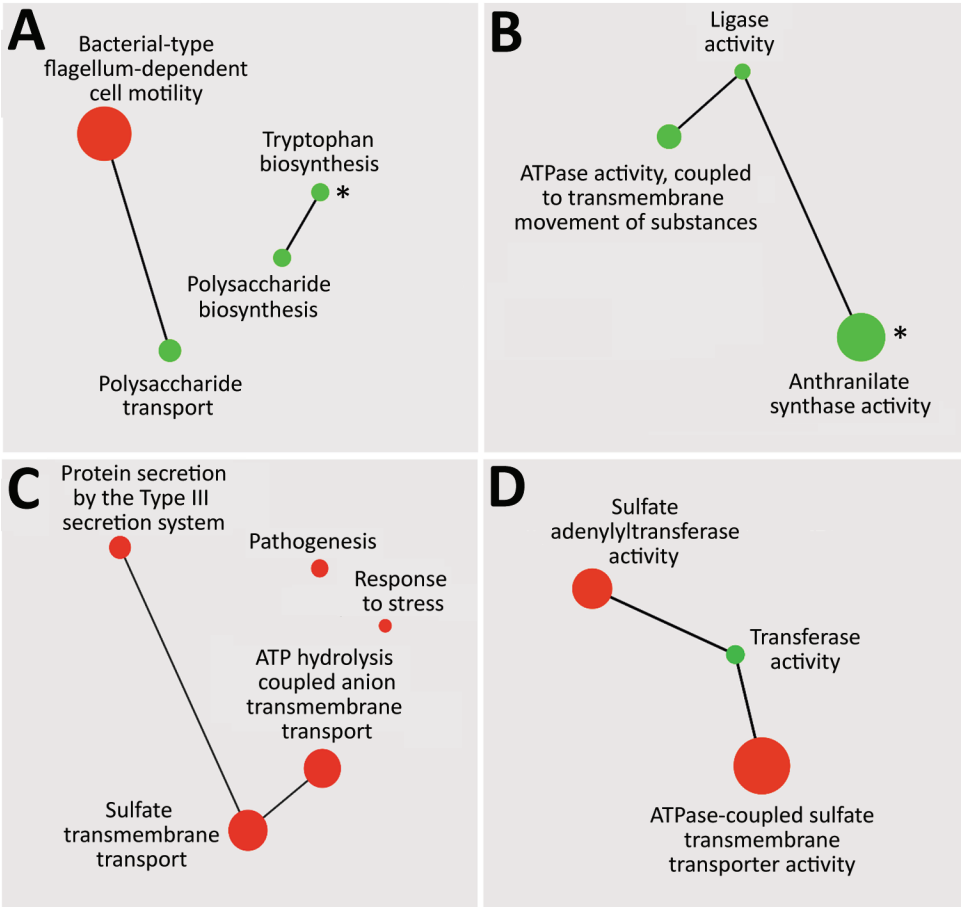


**Figure 4.** Gene ontology enrichment analysis of genes down-regulated or up-regulated between recent and historic strains of *Bordetella pertussis* from the Czech Republic (A, B) or between both groups of strains from the Czech Republic and Tohama I (C, D). Enriched terms from the domains' biological process (A, C) and molecular function (B, D) and their catenations, shown as green circles (down-regulated genes) and red circles (up-regulated genes), were summarized by using Revigo (http://revigo.irb.hr) and visualized by using Cytoscape (https://cytoscape.org) as interactive scatter plots. Circle size indicates level of enrichment. Asterisks (*) in panels A and B indicate gene ontology terms that were enriched also for genes down-regulated in recent isolates compared with Tohama I.

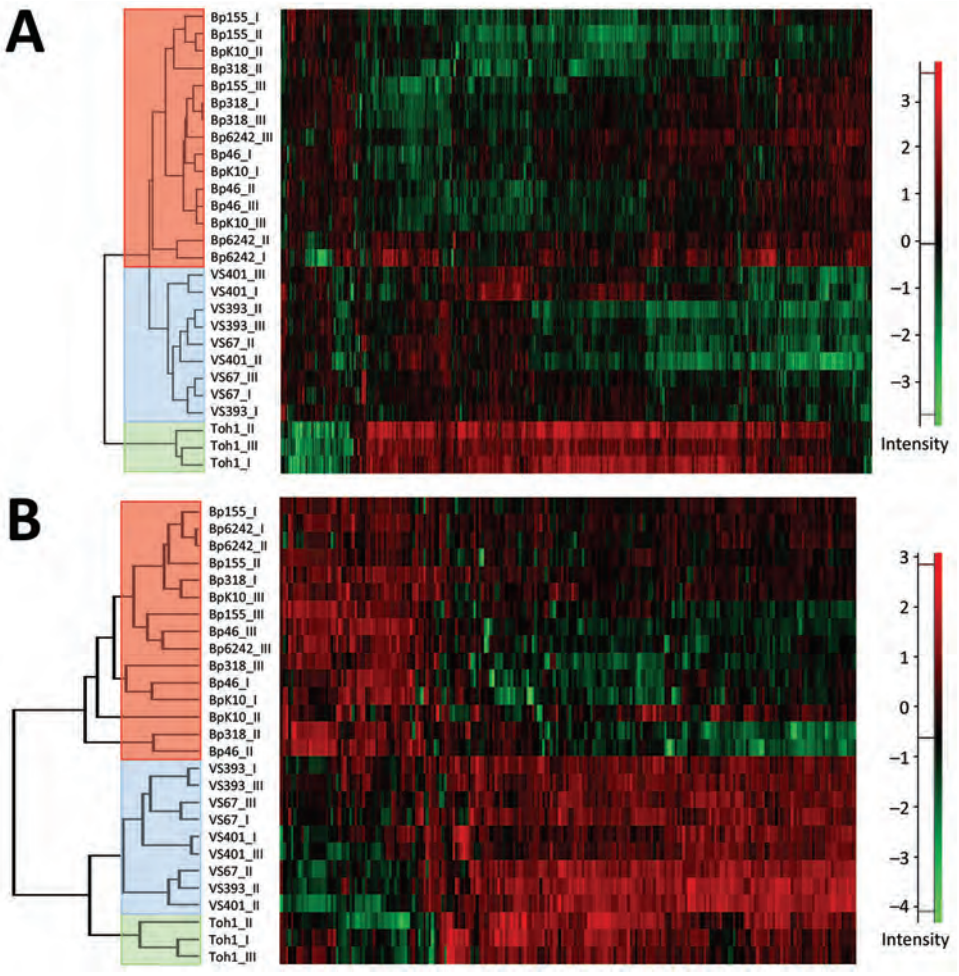


**Figure 5.** Heatmaps showing hierarchical clustering performed on Z-score normalized $\log_2$-transformed label-free intensity values of cell-associated (A) or secreted (B) protein fractions of historic and recent isolates of *Bordetella pertussis* from the Czech Republic and the Tohama I strain. Clustering of recent, historic, and Tohama I strains is indicated by red, blue, and green, respectively. Scale bars indicate intensity of proteins normalized by Z-score.

We then tested the possible effect of genome rearrangements on the distance of the DE genes from the origin of replication (*oriC*), a parameter that can greatly affect gene expression (*31*). We determined the distance from *oriC* to all the genes significantly deregulated between recent and historic strains, and although expression of some of the genes inversely correlated with the distance from *oriC*, the differences were not significant.

## Discussion

We conducted a comparative study analyzing the link between genomic organization, gene expression profiles, and protein production/secretion in historic and recent strains of *B. pertussis*. Our results indicate that global changes in genomic structures observed between historic and recent isolates of *B. pertussis* from the Czech Republic translated into different gene expression and protein production profiles. Similarly to other countries, the IS element–driven recombination led to large changes in genomic structures and to considerable gene loss in the isolates from the Czech Republic over the past 50–60 years. Results of our integrated omics analysis support our assumption that genomic rearrangements might affect global expression profiles and phenotypic diversity in *B. pertussis*. Hierarchical clustering of our omics data indicates that strains, which cluster apart at genomic structure level, also have distinct transcriptomic and proteomic profiles.

Given the extent of genome structural variability among both groups of strains, the number of differentially expressed genes was rather low (≈2% of all coding genes). Earlier DNA microarray studies suggested that gene expression profiles between *ptxP1* strains and recent resurgence-associated *ptxP3* lineage differ only subtly (*32*,*33*). Although we have identified an increased number of significantly modulated genes, our data on historic (*ptxP1*) and recent (*ptxP3*) isolates are consistent with these reports. None of the gene expression alterations could be shown to result from nucleotide polymorphism, and only a few could be

**Table 2.** Genes expressing consistently changed RNA and protein levels between recent and historic isolates of *Bordetella pertussis*, Czech Republic*

| Gene in Tohama I | Gene group | Gene name | Transcriptome | Proteome | Annotation |
|---|---|---|---|---|---|
| toh_00606 | Group_2206 | BP0624 | −2.2 | −2.5 | Substrate-CoA ligase |
| toh_00607 | Group_2604 | BP0625 | −2.3 | −3.3 | Acyl-CoA dehydrogenase |
| toh_00609 | Group_2725 | BP0627 | −2.0 | −3.3 | Enoyl-CoA hydratase/isomerase |
| toh_00610 | Group_895 | BP0628 | −2.4 | −2.8 | Pyruvate dehydrogenase component |
| toh_00611 | *pdhA* | BP0629 | −2.3 | −2.8 | Pyruvate dehydrogenase component |
| toh_01576 | Group_23 | WP_003811211.1 | −6.8 | −3.3 | Capsular biosynthesis protein |
| toh_01584 | *wza* | BP1628 | −6.8 | −2.2 | Capsular polysaccharide export protein |
| toh_02732 | Group_1068 | BP2782 | −3.9 | −3.0 | Lipoprotein |
| toh_02896 | Group_128 | BP2946 | 3.6 | 2.3 | *ArsR* family transcriptional regulator |
| toh_03214 | *trpD* | BP3262 | −2.1 | **−1.4** | Anthranilate phosphoribosyltransferase |
| toh_03215 | *trpG* | BP3263 | −2.4 | **−1.5** | Anthranilate synthase component II |
| toh_03216 | *trpE* | BP3264 | −2.4 | **−1.4** | Anthranilate synthase component I |
| toh_03637 | Group_1064 | BP3695 | 3.3 | 5.5 | Hydroxymethylglutaryl-CoA lyase |
| toh_03667 | *nadC* | BP3725 | 2.5 | 11.8 | Nicotinate-nucleotide diphosphorylase |

*Fold change values for recent isolates/historic strains comparison are shown for RNA sequencing and proteomic analyses. Values that did not indicate statistical significance (FC≥2; adjusted p<0.05) are shown in bold. toh, Tohama

linked to IS element–induced changes in the local gene context. Upstream of the *IS481* element adjacent to the *BP1492* gene, we identified the *BPt20* tRNA gene in most historic strains and Tohama I, which is, however, missing in recent isolates and historic strain VS67. Thus, it is possible that the activity of the strong tRNA promoter is responsible for increased expression of the *BP1492* gene in historic strains. Also, the presence of an *IS481* element in front of the *BP2827* gene in Bp155, Bp6242, and BpK10 strains might explain the increased expression of this gene in recent isolates. In support of this possibility, when compared with all other strains lacking this IS element, these 3 recent isolates showed highly increased expression of this gene. It is also possible that the observed differences in gene expression between historic and recent strains result from changes in genome organization or gene loss. Bacterial chromosome organization appears to favor a conserved gene order (*34*), and changes in genome architecture and topology can affect gene expression (*35,36*). Therefore, it is conceivable that genome rearrangements, resulting in changes in gene order and orientation or in large deletions, might affect transcriptomic profiles in *B. pertussis*.

We have identified 2 previously characterized regions of difference between historic and recent strains, which might offer alternative explanation for the observed differences in gene expression (*20,37*). Consistent with these reports, our reports found that genes within RD3 and RD10 are missing in all recent isolates. RD3 contains 2 putative transcriptional regulators (*BP0924* and *BP0928*) of unknown function. Thus, it is probable that absence of these regulators in recent isolates might be accountable for some of the identified alterations in gene expression.

Furthermore, RNA sequencing analysis identified 2 transcriptional regulator genes that are expressed at higher levels in recent isolates, and suggested that some of the observed differences between historic and recent strains might also result from altered expression of regulatory genes. *BP1969*, which encodes a LuxR family transcriptional factor, lies upstream of the *BP1970* and *BP1971* genes, which encode phosphoglucomutase Pgm and phosphoglucose isomerase Pgi. Similarly to *BP1969*, *pgm* and *pgi* genes were significantly up-regulated in recent strains. Therefore, we assume that the *BP1969* gene probably represents a cognate regulator for these glycolytic genes. Besides its role in glycolysis, Pgm catalyzes the generation of sugar nucleotides needed for biosynthesis of lipopolysaccharide and cell wall and was shown to be required for virulence of *B. bronchiseptica* (*38*) and several other pathogens (*39,40*). Strains lacking the *pgm* gene showed increased susceptibility to antimicrobial peptides and were attenuated in in vivo models of infection (*38–40*). Pgi catalyzes the second step in glycolysis and was shown to be required for virulence of *Xanthomonas campestris* (*41*). Thus, we presume that

**Table 3.** Genes expressing consistently increased RNA and protein levels in historic and recent isolates of *Bordetella pertussis*, Czech Republic, compared with Tohama I*

| Gene in Tohama I | Gene group | Gene name | Transcriptome | | Proteome | | Secretome | | Annotation |
|---|---|---|---|---|---|---|---|---|---|
| | | | Cz/Toh | VS/Toh | Cz/Toh | VS/Toh | Cz/Toh | VS/Toh | |
| toh_00485 | Group_1902 | BP0500 | 2.1 | 2.8 | **1.5** | **1.3** | 6.0 | 5.1 | T3SS effector BopC |
| toh_00936 | *Sbp* | BP0966 | 14.7 | 13.0 | 5.6 | 4.6 | ND | ND | Sulfate-binding protein |
| toh_02200 | *bscI* | BP2249 | 2.1 | 3.1 | **1.2** | ND | 2.8 | 6.2 | T3SS protein BscI |
| toh_02203 | *bopB* | BP2252 | 2.1 | 3.0 | 3.1 | 2.8 | 2.1 | 1.8 | T3SS protein BopB |
| toh_02204 | *bopD* | BP2253 | **1.8** | 2.5 | 2.0 | 1.5 | 3.7 | 2.3 | T3SS protein BopD |
| toh_02205 | *bcrH1* | BP2254 | 2.3 | 4.0 | 2.5 | 2.1 | **1.6** | **3.1** | T3SS protein |
| toh_02206 | Group_1710 | BP2255 | 2.4 | 3.8 | 3.9 | 4.0 | 4.8 | **1.7** | Hypothetical protein |
| toh_02207 | *bsp22* | BP2256 | 2.4 | 3.6 | **1.6** | **1.5** | 3.6 | **1.8** | T3SS protein Bsp22 |
| toh_02208 | *bopN* | BP2257 | 2.5 | 2.9 | **1.3** | **1.0** | 3.1 | **1.5** | T3SS protein BopN |
| toh_02210 | Group_2630 | BP2259 | 2.0 | 2.4 | **1.4** | **1.9** | 5.1 | **2.4** | Putative T3SS protein |
| toh_02214 | *bscE* | BP2263 | 2.3 | **1.5** | 5.2 | 4.5 | 2.0 | **2.3** | T3SS protein BscE |
| toh_03375 | Group_1130 | BP3434 | 6.1 | 4.4 | 3.3 | 1.9 | 2.6 | **1.8** | Exported protein |

*Fold change values resulting from comparison of either recent isolates (Cz) or historic strains (VS) with Tohama I strain (Toh) are shown for RNA sequencing and proteomic analyses. Values that did not indicate statistical significance (FC≥2; adjusted p<0.05) are shown in bold. ND, not determined; toh, Tohama.

increased expression and production of both enzymes might contribute to increased virulence and fitness of the *ptxP3* lineage.

Among other modulated genes, expression of numerous genes within the operon encoding the flagellar apparatus was significantly increased in recent isolates. However, we could not corroborate this finding because we did not detect any flagellar proteins in our samples. Recent observations suggest that *B. pertussis* is motile under modulatory Bvg-conditions (*42*) and that motility genes are up-regulated during adaptation to the mouse respiratory tract (*43*). Apparently, in vivo conditions, prevailing during *B. pertussis* infections in mice, cannot be completely reproduced under standard laboratory growth conditions, as documented (*43*,*44*), and further experiments are required to determine whether the increased expression translates into higher motility of recent isolates and contributes to improved ability of *ptxP3* strains to colonize the respiratory tract (*33*).

Conversely, expression of an almost complete operon that encodes genes involved in polysaccharide capsule synthesis was substantially down-regulated in recent isolates. This observation is consistent with that of a previous report (*45*) and demonstrates that capsule proteins are produced by *B. pertussis*. This finding also involves the protein responsible for polysaccharide biosynthesis TviD (*BP1618*), which has been reported to be encoded by a pseudogene (*14*).

Data on the role of the capsule in the virulence and physiologic fitness of *B. pertussis* are contradictory. Hoo et al. (*46*) showed that the capsule proteins are expressed during the infection and are required for an efficient colonization of mouse lungs. In contrast, in vitro assays showed that the capsule did

**Table 4**. Proteins encoded in regions upstream of an *IS481* element adjacent to differentially expressed genes in recent and historic strains of *Bordetella pertussis*, Czech Republic*

| Strain | Protein | | |
|---|---|---|---|
| | toh_01451 (BP1492) | toh_01915 (BP1969) | toh_02005 (BP2055) |
| Tohama I | tRNA | Partial phosphonate monoester hydrolase | Partial cyclopropane-fatty-acyl-phospholipid synthase |
| VS393 | tRNA | Partial phosphonate monoester hydrolase | Partial cyclopropane-fatty-acyl-phospholipid synthase |
| VS401 | tRNA | Partial phosphonate monoester hydrolase | IS481 element |
| VS67 | Partial FUSC family protein | Partial phosphonate monoester hydrolase | Partial cyclopropane-fatty-acyl-phospholipid synthase |
| Bp318 | Partial FUSC family protein | MarR family transcriptional regulator | Partial cyclopropane-fatty-acyl-phospholipid synthase |
| Bp155 | Partial FUSC family protein | MarR family transcriptional regulator | Partial cyclopropane-fatty-acyl-phospholipid synthase |
| Bp46 | Partial FUSC family protein | MarR family transcriptional regulator | Partial cyclopropane-fatty-acyl-phospholipid synthase |
| Bp6242 | Partial FUSC family protein | MarR family transcriptional regulator | Partial cyclopropane-fatty-acyl-phospholipid synthase |
| BpK10 | Partial FUSC family protein | MarR family transcriptional regulator | Partial cyclopropane-fatty-acyl-phospholipid synthase |

*IS481, insertion sequence 481.

not protect *B. pertussis* cells from phagocytosis and serum killing (*45*) and that the capsule locus was not expressed during infection of mouse respiratory tract (*43*). Therefore, it is difficult to assess whether reduced production of capsule proteins provides recent strains with any selective advantage. Nevertheless, the capsular polysaccharides of several gram-negative bacteria are highly immunogenic and were used to formulate carbohydrate–protein conjugate vaccines (*47*). Therefore, it is possible that in circulating isolates of *B. pertussis*, reduced production of the capsule synthesis apparatus contributes to evasion from the host immune response.

Our omics data manifest that, in spite of being isolated at the similar period of time, historic strains are substantially distinct from the reference strain Tohama I. Previous genomic analyses documented that several different clusters of *B. pertussis* circulated in Europe and the United States already in prevaccine and early vaccine eras and that their genomes were different from Tohama I (*20*,*37*). Our results with strains from the Czech Republic are consistent with these observations and also confirm this distinction at the transcriptomic and proteomic levels. For example, expression and production of various sulfate metabolism factors (*sbp*, *cysT*, *cysA*) were strongly reduced in Tohama I compared with strains from the Czech Republic. Likewise, we demonstrated that recent and historic strains had significantly increased expression, production, and secretion of several T3SS components. This observation is consistent with previous reports (*48*,*49*) and confirms that not only recent isolates but also low-passage historic strains of *B. pertussis* are T3SS proficient (*48*,*49*). We conclude that, in agreement with previous reports (*37*,*50*), the Tohama I strain is not a good representative of the circulating *B. pertussis* population.

Collectively, our data suggest that, besides shaping the evolution of *B. pertussis* on a genomic scale, the genome rearrangement and genome reduction processes also affect global transcriptomic and proteomic profiles. In agreement with results of a previous report (*20*), we assume that these mechanisms counterbalance the low level of genetic variability observed in this pathogen and strongly contribute to adaptation of the global population of *B. pertussis*.

### Acknowledgments

We thank Richard Neuboeck helping to setup software for some of the analyses, Michael Weigand for providing the sequence of the *oriC* region, and Karel Harant and Pavel Talacko for performing the liquid chromatography with mass tandem spectrometry analyses runs.

This study was supported by Czech Health Research Council (http://www.azvcr.cz) grant 16-30782A to B.V., Czech Research Foundation (http://www.qacr.cz) grant 19-12338S to B.V., institutional funding RVO61388971, and a mobility grant from the Czech Academy of Sciences (MSM200201702) to A.D. This study was also supported by the project "BIOCEV—Biotechnology and Biomedicine Centre of the Academy of Sciences and Charles University" (CZ.1.05/1.1.00/02.0109) from the European Regional Development Fund.

### About the Author

Dr. Dienstbier is a postdoctoral fellow in the Laboratory of Post-transcriptional Control of Gene Expression, Institute of Microbiology, Czech Academy of Sciences, Prague, Czech Republic. Her research interests are genomics and transcriptomics of *B. pertussis* strains and molecular mechanisms underlying the pathogenesis of pertussis.

### References

1. Centers for Disease Control and Prevention. Vaccine preventable deaths and the Global Immunization Vision and Strategy, 2006–2015. MMWR Morb Mortal Wkly Rep. 2006;55:511–5.
2. Raguckas SE, VandenBussche HL, Jacobs C, Klepser ME. Pertussis resurgence: diagnosis, treatment, prevention, and beyond. Pharmacotherapy. 2007;27:41–52. https://doi.org/10.1592/phco.27.1.41
3. van Gent M, Heuvelman CJ, van der Heide HG, Hallander HO, Advani A, Guiso N, et al. Analysis of *Bordetella pertussis* clinical isolates circulating in European countries during the period 1998–2012. Eur J Clin Microbiol Infect Dis. 2015;34:821–30. https://doi.org/10.1007/s10096-014-2297-2
4. Fabiánová K, Benes C, Kríz B. A steady rise in incidence of pertussis since nineties in the Czech Republic. Epidemiol Mikrobiol Imunol. 2010;59:25–33.
5. Sealey KL, Belcher T, Preston A. *Bordetella pertussis* epidemiology and evolution in the light of pertussis resurgence. Infect Genet Evol. 2016;40:136–43. https://doi.org/10.1016/j.meegid.2016.02.032
6. Esposito S, Stefanelli P, Fry NK, Fedele G, He Q, Paterson P, et al.; World Association of Infectious Diseases and Immunological Disorders (WAidid) and the Vaccine Study Group of the European Society of Clinical Microbiology and Infectious Diseases (EVASG). Pertussis prevention: reasons for resurgence, and differences in the current acellular pertussis vaccines. Front Immunol. 2019;10:1344. https://doi.org/10.3389/fimmu.2019.01344
7. Cherry JD. Epidemic pertussis and acellular pertussis vaccine failure in the 21st century. Pediatrics. 2015;135:1130–2. https://doi.org/10.1542/peds.2014-4118
8. Klein NP, Bartlett J, Rowhani-Rahbar A, Fireman B, Baxter R. Waning protection after fifth dose of acellular pertussis vaccine in children. N Engl J Med. 2012;367:1012–9. https://doi.org/10.1056/NEJMoa1200850
9. Liko J, Robison SG, Cieslak PR. Priming with whole-cell versus acellular pertussis vaccine. N Engl J Med. 2013;368:581–2. https://doi.org/10.1056/NEJMc1212006
10. Burdin N, Handy LK, Plotkin SA. What is wrong with pertussis Vvccine immunity? The problem of waning effectiveness of

pertussis vaccines. Cold Spring Harb Perspect Biol. 2017;9:a029454. https://doi.org/10.1101/cshperspect.a029454
11. Bart MJ, Harris SR, Advani A, Arakawa Y, Bottero D, Bouchez V, et al. Global population structure and evolution of *Bordetella pertussis* and their relationship with vaccination. MBiol. 2014;5:e01074. https://doi.org/10.1128/mBio.01074-14
12. Mooi FR, Van Der Maas NA, De Melker HE. Pertussis resurgence: waning immunity and pathogen adaptation: two sides of the same coin. Epidemiol Infect. 2014;142:685–94. https://doi.org/10.1017/S0950268813000071
13. Bouchez V, Hegerle N, Strati F, Njamkepo E, Guiso N. New data on vaccine antigen deficient *Bordetella pertussis* isolates. Vaccines (Basel). 2015;3:751–70. https://doi.org/10.3390/vaccines3030751
14. Parkhill J, Sebaihia M, Preston A, Murphy LD, Thomson N, Harris DE, et al. Comparative analysis of the genome sequences of *Bordetella pertussis*, *Bordetella parapertussis* and *Bordetella bronchiseptica*. Nat Genet. 2003;35:32–40. https://doi.org/10.1038/ng1227
15. Cummings CA, Brinig MM, Lepp PW, van de Pas S, Relman DA. *Bordetella* species are distinguished by patterns of substantial gene loss and host adaptation. J Bacteriol. 2004;186:1484–92. https://doi.org/10.1128/JB.186.5.1484-1492.2004
16. Linz B, Ivanov YV, Preston A, Brinkac L, Parkhill J, Kim M, et al. Acquisition and loss of virulence-associated factors during genome evolution and speciation in three clades of *Bordetella* species. BMC Genomics. 2016;17:767. https://doi.org/10.1186/s12864-016-3112-5
17. Bowden KE, Weigand MR, Peng Y, Cassiday PK, Sammons S, Knipe K, et al. Genome structural diversity among 31 *Bordetella pertussis* isolates from two recent U.S. whooping cough statewide epidemics. MSphere. 2016; 1:e00036–16. https://doi.org/10.1128/mSphere.00036-16
18. Weigand MR, Peng Y, Loparev V, Batra D, Bowden KE, Burroughs M, et al. The history of *Bordetella pertussis* genome evolution includes structural rearrangement. J Bacteriol. 2017;199:e00806–16. https://doi.org/10.1128/JB.00806-16
19. Ring N, Abrahams JS, Jain M, Olsen H, Preston A, Bagby S. Resolving the complex *Bordetella pertussis* genome using barcoded nanopore sequencing. Microb Genom. 2018;4. https://doi.org/10.1099/mgen.0.000234
20. Brinig MM, Cummings CA, Sanden GN, Stefanelli P, Lawrence A, Relman DA. Significant gene order and expression differences in *Bordetella pertussis* despite limited gene content variation. J Bacteriol. 2006;188:2375–82. https://doi.org/10.1128/JB.188.7.2375-2382.2006
21. Amman F, D'Halluin A, Antoine R, Huot L, Bibova I, Keidel K, et al. Primary transcriptome analysis reveals importance of IS elements for the shaping of the transcriptional landscape of *Bordetella pertussis*. RNA Biol. 2018; 15:967–75. https://doi.org/10.1080/15476286.2018.1462655
22. Dienstbier A, Pouchnik D, Wildung M, Amman F, Hofacker IL, Parkhill J, et al. Comparative genomics of Czech vaccine strains of *Bordetella pertussis*. Pathog Dis. 2018;76. https://doi.org/10.1093/femspd/fty071
23. Kasuga T, Nakase Y, Ukishima K, Takatsu K. Studies on *Haemophilis pertussis*. III. Some properties of each phase of *H. pertussis*. Kitasato Arch Exp Med. 1954;27:37–47.
24. Stainer DW, Scholte MJ. A simple chemically defined medium for the production of phase I *Bordetella pertussis*. J Gen Microbiol. 1970;63:211–20. https://doi.org/10.1099/00221287-63-2-211
25. Darling AE, Mau B, Perna NT. progressiveMauve: multiple genome alignment with gene gain, loss and rearrangement. PLoS One. 2010;5:e11147. https://doi.org/10.1371/journal.pone.0011147
26. Hu F, Lin Y, Tang J. MLGO: phylogeny reconstruction and ancestral inference from gene-order data. BMC Bioinformatics. 2014;15:354. https://doi.org/10.1186/s12859-014-0354-6
27. Angiuoli SV, Salzberg SL. Mugsy: fast multiple alignment of closely related whole genomes. Bioinformatics. 2011;27:334–42. https://doi.org/10.1093/bioinformatics/btq665
28. Gardner SN, Slezak T, Hall BG. kSNP3.0: SNP detection and phylogenetic analysis of genomes without genome alignment or reference genome. Bioinformatics. 2015; 31:2877–8. https://doi.org/10.1093/bioinformatics/btv271
29. Letunic I, Bork P. Interactive tree of life (iTOL) v3: an online tool for the display and annotation of phylogenetic and other trees. Nucleic Acids Res. 2016;44(W1):W242–5. https://doi.org/10.1093/nar/gkw290
30. Sealey KL, Harris SR, Fry NK, Hurst LD, Gorringe AR, Parkhill J, et al. Genomic analysis of isolates from the United Kingdom 2012 pertussis outbreak reveals that vaccine antigen genes are unusually fast evolving. J Infect Dis. 2015;212:294–301. https://doi.org/10.1093/infdis/jiu665
31. Block DH, Hussein R, Liang LW, Lim HN. Regulatory consequences of gene translocation in bacteria. Nucleic Acids Res. 2012;40:8979–92. https://doi.org/10.1093/nar/gks694
32. de Gouw D, Hermans PW, Bootsma HJ, Zomer A, Heuvelman K, Diavatopoulos DA, et al. Differentially expressed genes in *Bordetella pertussis* strains belonging to a lineage which recently spread globally. PLoS One. 2014; 9:e84523. https://doi.org/10.1371/journal.pone.0084523
33. King AJ, van der Lee S, Mohangoo A, van Gent M, van der Ark A, van de Waterbeemd B. Genome-wide gene expression analysis of *Bordetella pertussis* isolates associated with a resurgence in pertussis: elucidation of factors involved in the increased fitness of epidemic strains. PLoS One. 2013;8:e66150. https://doi.org/10.1371/journal.pone.0066150
34. Kang Y, Gu C, Yuan L, Wang Y, Zhu Y, Li X, et al. Flexibility and symmetry of prokaryotic genome rearrangement reveal lineage-associated core-gene-defined genome organizational frameworks. MBiol. 2014;5:e01867. https://doi.org/10.1128/mBio.01867-14
35. Dorman CJ. Genome architecture and global gene regulation in bacteria: making progress towards a unified model? Nat Rev Microbiol. 2013;11:349–55. https://doi.org/10.1038/nrmicro3007
36. Bryant JA, Sellars LE, Busby SJ, Lee DJ. Chromosome position effects on gene expression in *Escherichia coli* K-12. Nucleic Acids Res. 2014;42:11383–92. https://doi.org/10.1093/nar/gku828
37. Kallonen T, Gröndahl-Yli-Hannuksela K, Elomaa A, Lutyńska A, Fry NK, Mertsola J, et al. Differences in the genomic content of *Bordetella pertussis* isolates before and after introduction of pertussis vaccines in four European countries. Infect Genet Evol. 2011;11:2034–42. https://doi.org/10.1016/j.meegid.2011.09.012
38. West NP, Jungnitz H, Fitter JT, McArthur JD, Guzmán CA, Walker MJ. Role of phosphoglucomutase of *Bordetella bronchiseptica* in lipopolysaccharide biosynthesis and virulence. Infect Immun. 2000;68:4673–80. https://doi.org/10.1128/IAI.68.8.4673-4680.2000
39. Ugalde JE, Czibener C, Feldman MF, Ugalde RA. Identification and characterization of the *Brucella abortus* phosphoglucomutase gene: role of lipopolysaccharide in virulence and intracellular multiplication. Infect Immun. 2000;68:5716–23. https://doi.org/10.1128/IAI.68.10.5716-5723.2000

40. Hardy GG, Magee AD, Ventura CL, Caimano MJ, Yother J. Essential role for cellular phosphoglucomutase in virulence of type 3 *Streptococcus pneumoniae*. Infect Immun. 2001;69:2309–17. https://doi.org/10.1128/IAI.69.4.2309-2317.2001
41. Tung SY, Kuo TT. Requirement for phosphoglucose isomerase of *Xanthomonas campestris* in pathogenesis of citrus canker. Appl Environ Microbiol. 1999;65:5564–70. https://doi.org/10.1128/AEM.65.12.5564-5573.1999
42. Hoffman CL, Gonyar LA, Zacca F, Sisti F, Fernandez J, Wong T, et al. *Bordetella pertussis* can be motile and express flagellum-like structures. MBiol. 2019;10:e00787–19. https://doi.org/10.1128/mBio.00787-19
43. van Beek LF, de Gouw D, Eleveld MJ, Bootsma HJ, de Jonge MI, Mooi FR, et al. Adaptation of *Bordetella pertussis* to the respiratory tract. J Infect Dis. 2018;217:1987–96. https://doi.org/10.1093/infdis/jiy125
44. Wong TY, Hall JM, Nowak ES, Boehm DT, Gonyar LA, Hewlett EL, et al. Analysis of the *in vivo* transcriptome of *Bordetella pertussis* during infection of mice. MSphere. 2019; 4:e00154–19. https://doi.org/10.1128/mSphereDirect.00154-19
45. Neo Y, Li R, Howe J, Hoo R, Pant A, Ho S, et al. Evidence for an intact polysaccharide capsule in *Bordetella pertussis*. Microbes Infect. 2010;12:238–45. https://doi.org/10.1016/j.micinf.2009.12.002
46. Hoo R, Lam JH, Huot L, Pant A, Li R, Hot D, et al. Evidence for a role of the polysaccharide capsule transport proteins in pertussis pathogenesis. PLoS One. 2014;9:e115243. https://doi.org/10.1371/journal.pone.0115243
47. Ada G, Isaacs D. Carbohydrate-protein conjugate vaccines. Clin Microbiol Infect. 2003;9:79–85. https://doi.org/10.1046/j.1469-0691.2003.00530.x
48. Fennelly NK, Sisti F, Higgins SC, Ross PJ, van der Heide H, Mooi FR, et al. *Bordetella pertussis* expresses a functional type III secretion system that subverts protective innate and adaptive immune responses. Infect Immun. 2008;76:1257–66. https://doi.org/10.1128/IAI.00836-07
49. Gaillard ME, Bottero D, Castuma CE, Basile LA, Hozbor D. Laboratory adaptation of *Bordetella pertussis* is associated with the loss of type three secretion system functionality. Infect Immun. 2011;79:3677–82. https://doi.org/10.1128/IAI.00136-11
50. Caro V, Bouchez V, Guiso N. Is the sequenced *Bordetella pertussis* strain Tohama I representative of the species? J Clin Microbiol. 2008;46:2125–8. https://doi.org/10.1128/JCM.02484-07

Address for correspondence: Branislav Večerek, Institute of Microbiology, Czech Academy of Sciences, Videnska 1083, 14220 Prague 4, Czech Republic; email: vecerek@biomed.cas.cz

# Hospitalization for Invasive Pneumococcal Diseases in Young Children before Use of 13-Valent Pneumococcal Conjugate Vaccine, Suzhou, China

Kaile Chen, Xiyan Zhang, Yunzhen Tao, Yunzhong Wang, Jian Xue, Changpeng Liu, Shuang Feng, Yongdong Yan, Qinghui Chen, Jianmei Tian, Genming Zhao, Xuejun Shao, Tao Zhang

A 13-valent pneumococcal conjugate vaccine against invasive pneumococcal disease (IPD) was introduced in China in April 2017. We describe 105 children <5 years of age who were hospitalized for IPD at Soochow University Affiliated Children's Hospital in Suzhou, China, during January 2010–December 2017. We calculated the incidence of hospitalization for IPD as 14.55/100,000 children in Suzhou. We identified 8 different capsular serotypes: 6B (28.4% of cases), 14 (18.9% of cases), 19A (18.9% of cases), 19F (12.2% of cases), 23F (10.8% of cases), 20 (4.1% of cases), 9V (4.1% of cases), and 15B/C (2.7% of cases). These results provide baseline data of IPD before the introduction of this vaccine in China, enabling researchers to better understand its effects on IPD incidence.

*Streptococcus pneumoniae* infections are a major cause of illness and death in infants and children worldwide, especially in developing countries (*1*). The World Health Organization estimates that pneumococcal diseases cause ≈1.6 million deaths every year, of which ≈1.0 million occur in children <5 years of age (*2*). Invasive pneumococcal diseases (IPDs) such as bacteremic pneumonia, febrile bacteremia, and meningitis often are fatal, and ≈25%–50% of survivors have serious neurological sequelae (*3*). IPD incidence varies among countries and populations (*4*,*5*). Very young or old age, concurrent conditions, malnutrition, poor healthcare, and low socioeconomic status are risk factors for IPD.

The growing resistance of *S. pneumoniae* to common antimicrobial drugs highlights the importance of vaccines in preventing pneumococcal disease (*6*,*7*). In China, vaccines fall under 2 categories: category I vaccines, which guard against diseases such as hepatitis B, polio, and measles, are mandatory, and are provided by the government; and category II vaccines, which are optional and commercially available. The 7-valent pneumococcal conjugate vaccine (PCV7) was licensed as a category II vaccine in mainland China in 2008; the estimated uptake rate was 2%–7% (*8*,*9*). The 13-valent pneumococcal conjugate vaccine (PCV13) was introduced in mainland China in November 2016 as a category II vaccine. To evaluate the effect of PCV13 on IPD incidence, we describe baseline epidemiologic characteristics of illness, hospitalization, and death associated with the disease. Li et al. evaluated surveillance data from 4 prefecture cities (Jinan, Yichang, Shijiazhuang, and Guigang) and reported that *S. pneumoniae* was the most common cause of bacterial meningitis in children <5 years of age during 2006–2009 (*10*). However, few data exist on the incidence of pneumococcal pneumonia, sepsis, and other manifestations of IPD in different regions of mainland China.

We describe IPD among patients <5 years of age who were treated at Soochow University Affiliated Children Hospital (SCH) in Suzhou, China, during 2010–2017. We used a rapid method of the World Health Organization to estimate the baseline incidence of IPD hospitalization (*11*) among this age group.

Author affiliations: Fudan University, Shanghai, China (K. Chen, X. Zhang, C. Liu, S. Feng, G. Zhao, T. Zhang); Key Laboratory of Public Health Safety, Ministry of Education, Shanghai (K. Chen, X. Zhang, C. Liu, S. Feng, G. Zhao, T. Zhang); Soochow University Affiliated Children's Hospital, Suzhou, China (Y. Tao, Y. Wang, J. Xue, Y. Yan, Q. Chen, J. Tian, X. Shao)

DOI: https://doi.org/10.3201/eid2701.181415

## Methods

### Study Site and Catchment Area

The study was conducted in Suzhou, a major city with a population of ≈12 million persons in the southeast area of Jiangsu Province in eastern China. Suzhou consists of 5 municipal districts (Gusu, New and High-Tech, Wuzhong, Xiangcheng, and Industrial Park) and 5 county-level cities. SCH, which is in Gusu, is the only tertiary children's hospital in Suzhou. In 2016, the hospital recorded ≈1.9 million outpatient and emergency visits and 45,000 hospitalizations. Hospital records indicate that, during 2011–2014, a total of 84.9% of patients <5 years of age with influenza-like illness and 63.3% of patients <5 years of age with meningitis or encephalitis resided in the 5 municipal districts of Suzhou *(12)*. According to a 2011 healthcare utilization survey (*13*,*14*), SCH patients accounted for 67.7% of total discharges of children <5 years of age from all 96 hospitals in downtown Suzhou. We defined the catchment area of SCH as the 5 municipal districts of Suzhou; we assumed that 67.7% of children <5 years of age who resided in the catchment areas would be treated at SCH. The study was conducted in accordance with internationally recognized standards for ethical research and was approved by the institutional review boards of the School of Public Health, Fudan University (approval no. 2015-04-0545) and SCH.

### Case Definition, Identification, and Serotyping

We defined IPD patients as those from whom *S. pneumoniae* was isolated from a normally sterile body site such as cerebrospinal fluid (CSF), blood, or pleural fluid. Within 24 hours after admission, the hospital collects CSF specimens from patients with suspected meningitis, defined as acute onset of fever with change in mental status, meningeal signs (e.g., neck stiffness, headache), or both; blood cultures from patients with a temperature of >39.0°C; and pleural fluid from patients with suspected effusion detected in chest radiography or computed tomography scan. The specimens were sent to the laboratory at SCH for bacterial culture ≤2 hours after collection according to the standard methods of collection, transport, and culturing (*7*). Laboratory physicians identified isolates as *S. pneumoniae* by morphologic features, α-hemolysis, Gram staining, and bile solubility or optochin susceptibility using Oxoid Optochin Discs (Thermo Fisher Scientific, https://www.thermofisher.com).

We collected the *S. pneumoniae*–positive isolates from SCH and sent them to the Key Laboratory of Public Health Safety at Fudan University, Shanghai, for serotyping. We identified the serotypes of pneumococcal isolates using the Quellung reaction with antisera (Statens Serum Institute, https://en.ssi.dk), a multiplex PCR described previously (*15*), or both.

### Demographic Information

We obtained information on the annual population of children <5 years of age in the catchment area during 2010–2017 from the immunization program database at the Suzhou Center for Disease Control and Prevention, which serves all residents and >95% of the migrant population in this age group in Suzhou. Almost all newborn children in Suzhou, regardless of residence, are immunized; all immunizations are logged in the program database.

### Estimating Incidence of Hospitalization for IPD

We used a rapid method from the World Health Organization to calculate the incidence of hospitalization for IPD (*11*). This method uses the sentinel hospital's meningitis surveillance system to identify the numerator as potential bacterial meningitis cases and the denominator as the estimated number of children at risk for meningitis in the catchment area. China does not have a nationwide meningitis surveillance system, but SCH collects routine CSF, blood, and pleural fluid cultures from children with suspected IPD. We estimated the denominator (i.e., children at risk for IPD in the area) by multiplying the population <5 years of age in the catchment area by the percentage of children in that age group who are treated at SCH (67.7%). Thus, we calculated the incidence of hospitalization for IPD in the catchment area of SCH (Y) as

$$Y = \frac{\text{IPD cases in SCH}}{\text{Children <5 years of age in catchment area} \times 67.7\%}$$

We used the Wilson method for binominal distribution to estimate 95% CIs of IPD hospitalizations. We used the $\chi^2$ test to compare the incidence of hospitalization across different age groups. We conducted all statistical analyses using SAS version 9.4 (SAS Institute, https://www.sas.com).

## Results

### Characteristics of IPD Patients

During January 2010–December 2017, SCH collected 20,260 CSF specimens from children <5 years of age. Among the specimens, 283 tested positive for bacterial infections, including 46 (16.3%) positive for *S. pneumoniae* and 51 (18.0%) positive for *Staphylococcus epidermidis*. SCH also collected 62,858 blood and

138 pleural effusion specimens for bacterial detection from children <5 years of age. Of these samples, 2,432 blood and 29 pleural effusion cultures tested positive for bacterial infection. *S. pneumoniae* was the sixth most common bacteria in the positive blood cultures (110/2,432; 4.5%) and the most common bacteria in the positive pleural effusion cultures (16/29; 55.2%). The proportion of samples that tested positive for *S. pneumoniae* from children <5 years of age were 0.2% (46/20,260) in CSF, 0.2% (110/ 62,858) in blood, and 11.6% (16/138) in pleural effusion samples. After accounting for duplicate specimens, SCH identified 105 patients <5 years of age with IPD during 2010–2017. The male:female ratio was 1.3; 54.3% were 2–<5 years of age. Common diagnoses included meningitis (31.4%), pneumonia (28.6%), and sepsis (21.0%) (Table 1).

### Incidence of Hospitalization for Children with IPD

The population of children <5 years of age in the catchment area increased from 90,756 in 2010 to 171,676 in 2017. During January 2010–December 2017, the estimated annual incidence of hospitalization for IPD among children in this age group in Suzhou ranged from 8.16 to 17.86 per 100,000 children, peaking in 2015 (Table 2). The incidence of hospitalization for IPD fluctuated without significance ($\chi^2$ = 1.51; p>0.05) (Figure 1). The IPD hospitalization incidence differed among age groups and was highest among children <1 year of age ($\chi^2$ = 6.73; p<0.05). The incidence of hospitalization among children <5 years of age was 4.57 (95% CI 3.26–6.42)/100,000 children for meningitis, 4.16 (95% CI 2.91–5.93)/100,000 children for bacteremic pneumonia, and 3.05 (95% CI 2.01–4.62)/100,000 children for sepsis.

### Serotype Distribution and Incidence of IPD Hospitalizations by Serotype

SCH sent 74 (70.5%) pneumococcal isolates from patients with IPD to the laboratory for serotyping. We identified 8 different capsular serotypes: 6B (21/74; 28.4%), 14 (14/74; 18.9%), 19A (14/74; 18.9%), 19F (9/74; 12.2%), 23F (8/74; 10.8%), 20 (3/74; 4.1%), 9V (3/74; 4.1%), and 15B/C (2/74; 2.7%). Thus, the serotype coverage rate, or the percentage of cases caused by serotypes preventable by vaccination, of PCV10 was 74.4% and PCV13 was 93.2%.

Among patients with meningitis, serotypes 6B (10/25; 40.0%) and 14 (6/25; 24.0%) were most common. Of patients with sepsis, the most common serotypes were 23F (5/14; 35.7%) and 19A (3/14; 21.4%) (Figure 2). However, these findings were not significant. We calculated the estimated serotype-specific IPD hospitalization incidences to be 4.13 (95% CI 2.89–5.90)/100,000 children for 6B, 2.75 (95% CI 1.78–4.26)/100,000 children for 14, 2.75 (95% CI 1.78–4.26)/100,000 children for 19A, 1.77 (95% CI 1.03–3.04)/100,000 children for 19F, 1.57 (95% CI 0.89–2.89)/100,000 children for 23F, 0.59 (95% CI 0.24–1.48)/100,000 children for 20 and 9V, and 0.39 (95% CI 0.13–1.19)/100,000 children for 15B/C (Figure 2).

## Discussion

We describe children hospitalized for IPD at SCH during January 2010–December 2017. We used

**Table 1.** Characteristics of children with invasive pneumococcal diseases, Suzhou, China, 2010–2017

| Characteristic | Age group, no. (%) | | | |
|---|---|---|---|---|
| | <1 y | 1–<2 y | 2–<5 y | Total |
| Total | 31 (100.0) | 17 (100.0) | 57 (100.0) | 105 (100.0) |
| Sex | | | | |
| M | 17 (54.8) | 10 (58.8) | 33 (57.9) | 60 (57.1) |
| F | 14 (45.2) | 7 (41.2) | 24 (42.1) | 45 (42.9) |
| Year | | | | |
| 2010 | 5 (16.1) | 1 (5.9) | 4 (7.0) | 10 (9.5) |
| 2011 | 4 (12.9) | 4 (23.5) | 3 (5.3) | 11 (10.5) |
| 2012 | 4 (12.9) | 1 (5.9) | 5 (8.8) | 10 (9.5) |
| 2013 | 5 (16.1) | 4 (23.5) | 4 (7.0) | 13 (12.4) |
| 2014 | 4 (12.9) | 4 (23.5) | 9 (15.8) | 17 (16.2) |
| 2015 | 5 (16.1) | 1 (5.9) | 12 (21.1) | 18 (17.1) |
| 2016 | 2 (6.5) | 1 (5.9) | 6 (10.5) | 9 (8.6) |
| 2017 | 2 (6.5) | 1 (5.9) | 14 (24.6) | 17 (16.2) |
| Primary discharge diagnosis | | | | |
| Meningitis | 16 (51.6) | 4 (23.5) | 13 (22.8) | 33 (31.4) |
| Pneumonia | 7 (22.6) | 3 (17.6) | 20 (35.1) | 30 (28.6) |
| Sepsis | 6 (19.4) | 6 (35.3) | 10 (17.5) | 22 (21.0) |
| Upper respiratory infection | 1 (3.2) | 1 (5.9) | 1 (1.8) | 3 (2.9) |
| Bronchitis | 0 | 1 (5.9) | 1 (1.8) | 2 (1.9) |
| Other* | 1 (3.2) | 2 (11.8) | 12 (21.1) | 15 (14.3) |

*Other conditions: leukemia (6 cases), anemia (1 case), endocarditis (2 cases), arrhythmia (2 cases), acute otitis media (1 case), jaundice (1 case), acute gastritis (1 case), and psoas abscess (1 case).

**Table 2.** Estimated IPD hospitalization incidence among children <5 years of age, Suzhou, China, 2010–2017*

| | Children <1 y of age | | | Children 1–<2 y of age | | | Children 2–<5 y of age | | |
|---|---|---|---|---|---|---|---|---|---|
| Year | IPD cases at SCH | Pop.† | HI‡ (95% CI) | IPD cases at SCH | Pop.† | HI‡ (95% CI) | IPD cases at SCH | Pop.† | HI‡ (95% CI) |
| 2010 | 5 | 21,510 | 34.33 (14.67–80.35) | 1 | 19,433 | 7.60 (1.34–43.02) | 4 | 49,813 | 11.86 (4.61–30.51) |
| 2011 | 4 | 22,731 | 25.99 (10.11–66.81) | 4 | 20,136 | 29.34 (11.41–75.43) | 3 | 50,527 | 8.77 (2.98–25.79) |
| 2012 | 4 | 26,452 | 22.35 (8.69–57.46) | 1 | 25,483 | 5.80 (1.02–32.83) | 5 | 70,423 | 10.49 (4.48–25.54) |
| 2013 | 5 | 23,893 | 30.91 (13.20–72.35) | 4 | 31,228 | 18.92 (7.36–48.65) | 4 | 76,041 | 7.77 (3.02–19.98) |
| 2014 | 4 | 29,110 | 20.30 (7.89–52.18) | 4 | 28,006 | 21.10 (8.21–54.26) | 9 | 87,752 | 15.15 (7.97–28.79) |
| 2015 | 5 | 22,745 | 32.48 (13.87–76.02) | 1 | 34,119 | 4.33 (0.76–24.53) | 12 | 92,038 | 19.26 (11.02–33.66) |
| 2016 | 2 | 32,360 | 9.13 (2.5–33.28) | 1 | 27,768 | 5.32 (0.94–30.13) | 6 | 102,818 | 8.62 (3.95–18.80) |
| 2017 | 2 | 31,415 | 9.40 (2.58–34.28) | 1 | 38,255 | 3.86 (0.68–21.88) | 14 | 102,006 | 20.27 (12.07–34.02) |
| Total | 31 | 210,216 | 21.78 (15.34–30.91) | 17 | 224,428 | 11.19 (6.99–17.92) | 57 | 631,418 | 13.33 (10.29–17.27) |

*Incidence is cases/100,000 children. HI, hospitalization incidence; IPD, invasive pneumococcal disease; pop., population; SCH, Suzhou University Affiliated Children Hospital.
†Population <5 years of age in Suzhou (5 municipal districts).
‡Hi calculated by dividing no. IPD cases at SCH by 67.7% of population <5 years of age in Suzhou.

previous studies (*12*–*14*) to estimate the incidence of hospitalization for IPD among children <5 years of age in Suzhou. During January 2010–December 2017, the annual incidence of hospitalization for IPD in Suzhou ranged from 8.16 to 17.86/100,000 children and the average incidence was 14.55/100,000 children. The annual incidence of IPD did not significantly change during the 8-year period, peaking at 17.86/100,000 children in 2015. The IPD hospitalization incidence was highest (21.78 hospitalizations/100,000 children) among those <1 year of age and lowest (13.33 hospitalizations/100,000 children) among those 2–<5 years of age.

We estimated the incidence of hospitalization for pneumococcal meningitis as 4.57/100,000 children. A systematic review in China estimated the mean incidence of pneumococcal meningitis in children 1–23 months of age as 5.1 cases/100,000 children during 1999–2003 (*16*). Another study in China estimated the incidence of bacterial meningitis as 6.95–22.30 cases/100,000 children <5 years of age during 2006–2009; *S. pneumoniae* caused 53% of these cases (*10*), indicating a pneumococcal meningitis incidence of ≈3.7–11.8/100,000 children. This incidence is comparable to our estimates. A study in Beijing estimated the incidence of sepsis in adults as 461 cases/100,000 persons (*17*), but that study did not classify patients on the basis of bacterial infection. Many studies around the world indicate similar incidences of IPD before the use of PCVs (*18*–*20*). A 20-year study in Atlanta, Georgia, USA, showed that during 2003–2013, the overall IPD rate was 8.03–14.02 cases/100,000 persons; incidence was also estimated by using *S. pneumoniae* isolates collected from normally sterile sites (*4*). The IPD incidence of children <5 years of age

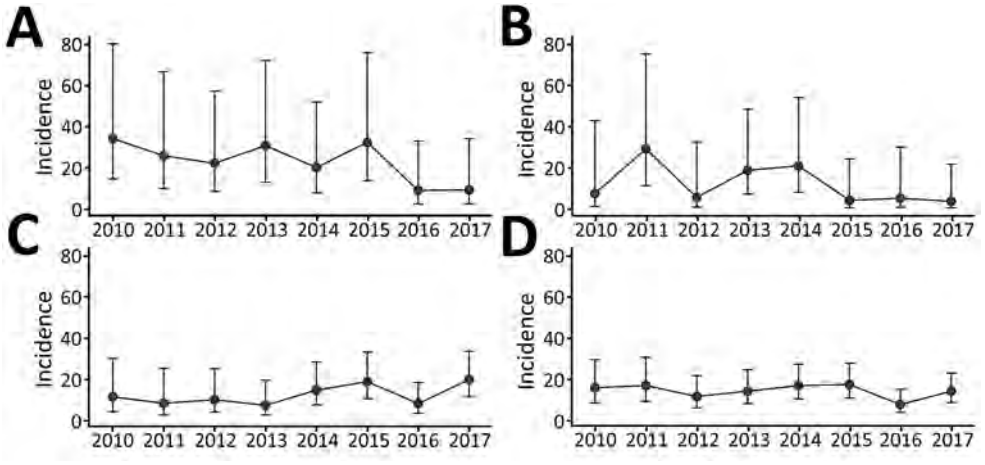


**Figure 1.** Estimated invasive pneumococcal diseases hospitalization incidence per 100,000 children among children <5 years of age, by age and year, Suzhou, China, 2010–2017. A) Children <1 year of age; B) children 1–<2 years of age; C) children 2–<5 years of age; D) children <5 years of age. Error bars indicate 95% CIs.

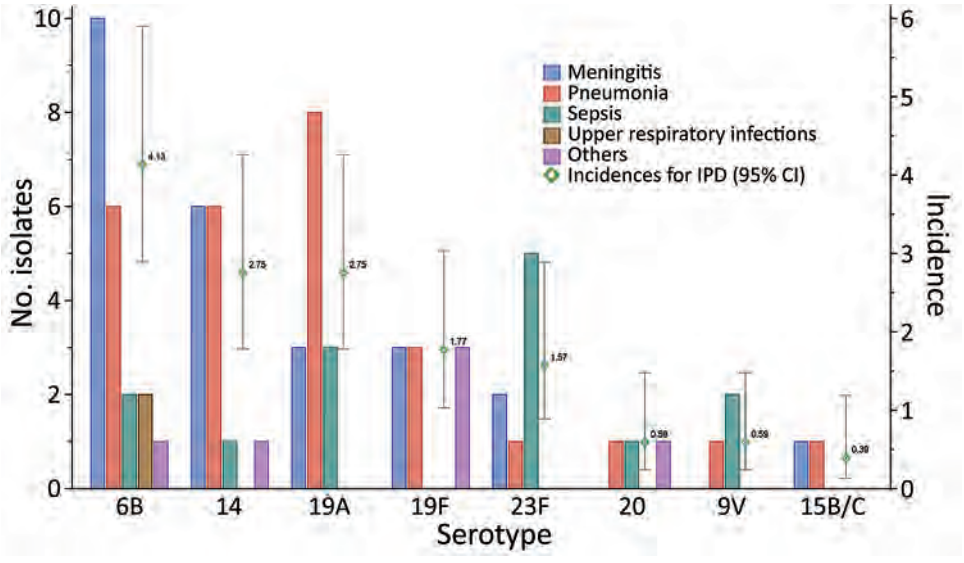


**Figure 2.** Association of serotype of *Streptococcus pneumoniae* with primary discharge diagnosis (data bars) and serotype-specific hospitalization incidence (data points, cases per 100,000 children) of children <5 years of age, Suzhou, China, 2010–2017. Error bars indicate 95% CIs.

in India in 2006 was 1,500 cases/100,000 persons (*5*), much higher than in China and other countries.

The proportion of CSF, blood, and pleural effusion samples that tested positive for *S. pneumoniae* were lower than those found in studies in India and Turkey (*21*,*22*). Possible reasons for the lower proportion of *S. pneumoniae*–positive samples included the common use of antimicrobial drugs before hospital admission (*7*,*10*) and the use of only traditional bacterial cultures, which are less sensitive than immunochromatography and PCR, for identification of *S. pneumoniae*. We did not collect data on antimicrobial drug usage, but our previous study in the same hospital during 2006–2007 found that ≈86% of children with lower respiratory tract infections used antimicrobial drugs, not all of which were prescribed, before admission (*23*). Li et al. showed that, in China's general hospitals, the percentage of outpatients treated with prescribed antimicrobial drugs declined from 20.17% in 2012 to 12.94% in 2016 (*24*). Since 2012, China has improved the judicious use of antimicrobial drugs; however, the inappropriate use of antimicrobial drugs in children remains a serious problem (*25*,*26*). We might underestimate the incidence of hospitalization for IPD because pretreating with antimicrobial drugs at home might reduce the proportion of IPD patients who test positive for *S. pneumoniae*.

In this study, we found that serotypes 6B, 14, and 19A caused 66.2% of all IPD infections. These results differ from those of our recent systematic review (*27*), which found 19F and 19A to be the most common serotypes among invasive strains isolated from children in mainland China during 2000–2016. Furthermore, a study in England and Wales found serotype 18C to be the most common serotype among children <5 years of age with meningitis (*28*). Therefore, we believe the distribution of pneumococcal serotypes varies with geographic location.

PCVs have been introduced in >100 countries, possibly contributing to a major reduction in the incidence of IPD (*29*). During most of the study period, PCV7 was the only PCV available in mainland China; whether this vaccination decreased the incidence of IPD in China is unknown. PCV7 uptake in China was very low, an estimated 2%–7% (*8*,*9*). Our previous study showed that 87.4% of IPD cases among children in mainland China (*27*) were caused by pneumococcal serotypes preventable by PCV13; in the study we report here, that proportion increased to 93.2%. Therefore, if the vaccine uptake of PCV13 in China is sufficiently high, we expect similar reductions in the incidence of IPD in children in China, as has been observed in other countries (*29*).

The major limitation of this study is that common antimicrobial drug use might have reduced the proportion of specimens that tested positive for *S. pneumoniae*, causing us to underestimate the IPD hospitalization incidence. In addition, SCH only took blood cultures of patients with a temperature >39.0°C; this policy might overlook IPD patients without fever. Furthermore, we did not have data on IPD patients in Suzhou who were not treated at SCH. Because SCH treated 67.7% of children <5 years of age who were discharged from hospitals in downtown Suzhou in 2011 (*13*), we used this proportion to estimate the number of children at risk for IPD in Suzhou; we might have overestimated or underestimated the incidence of IPD. Our previous study found that ≈50% of children with influenza-like illness in the catchment area are treated at SCH (*12*). Because SCH is the only pediatric tertiary hospital in Suzhou and IPDs are more severe than influenza-like illnesses, we assumed that the

proportion of children with IPD in the catchment area who were treated at SCH would be >50%. Finally, the small number of identified IPD cases might skew our estimates.

In conclusion, we found that the incidence of hospitalization for IPD in Suzhou was similar to that of populations in China and other countries before the use of PCVs. In addition, the IPD hospitalization incidence did not significantly change during 2010–2017. In China, a high proportion of pneumococcal serotypes are preventable with PCV13. These results provide baseline data of IPD incidence before PCV13 use in China.

### Acknowledgements

We thank the physicians and the laboratory staff at Soochow University Affiliated Children Hospital who contributed to this study. We also thank Zhang Fangmin for assistance with data collection.

This study was supported by the National Natural Science Foundation of China (grant no. 81102166), the Shanghai Municipal Health and Family Planning (grant nos. GWTD2015S05 and 15GWZK0101), the National Key Research and Development Program of China (grant no. 2017YFC0211700), the SINO-US collaborative program on Emerging and Re-Emerging Infectious Diseases (grant no. 5U2GGH000018), and the Application Research on Key Technologies of People's Livelihood Science and Technology in Suzhou (grant no. SS201867).

## About the Author

Ms. Chen has an MPH from Fudan University. Her research interests include the epidemiology of infectious diseases and pneumococcal diseases.

### References

1. Weinberger DM, Harboe ZB, Sanders EAM, Ndiritu M, Klugman KP, Rückinger S, et al. Association of serotype with risk of death due to pneumococcal pneumonia: a meta-analysis. Clin Infect Dis. 2010;51:692–9. https://doi.org/10.1086/655828
2. World Health Organization. Pneumococcal conjugate vaccine for childhood immunization. 2007 [cited 2018 Jun 30]. https://apps.who.int/iris/handle/10665/240901
3. O'Brien KL, Wolfson LJ, Watt JP, Henkle E, Deloria-Knoll M, McCall N, et al.; Hib and Pneumococcal Global Burden of Disease Study Team. Burden of disease caused by *Streptococcus pneumoniae* in children younger than 5 years: global estimates. Lancet. 2009;374:893–902. https://doi.org/10.1016/S0140-6736(09)61204-6
4. Schroeder MR, Chancey ST, Thomas S, Kuo WH, Satola SW, Farley MM, et al. A population-based assessment of the impact of 7- and 13-valent pneumococcal conjugate vaccines on macrolide-resistant invasive pneumococcal disease: emergence and decline of *Streptococcus pneumoniae* serotype 19A (CC320) with dual macrolide resistance mechanisms. Clin Infect Dis. 2017;65:990–8. https://doi.org/10.1093/cid/cix446
5. Shah AS, Nisarga R, Ravi Kumar KL, Hubler R, Herrera G, Kilgore PE. Establishment of population-based surveillance for invasive pneumococcal disease in Bangalore, India. Indian J Med Sci. 2009;63:498–507. https://doi.org/10.4103/0019-5359.58879
6. Kang CI, Song JH. Antimicrobial resistance in Asia: current epidemiology and clinical implications. Infect Chemother. 2013;45:22–31. https://doi.org/10.3947/ic.2013.45.1.22
7. Zhang X, Tian J, Shan W, Xue J, Tao Y, Geng Q, et al. Characteristics of pediatric invasive pneumococcal diseases and the pneumococcal isolates in Suzhou, China before introduction of PCV13. Vaccine. 2017;35:4119–25. https://doi.org/10.1016/j.vaccine.2017.06.046
8. Mo X, Tobe RG, Liu X, Mori R. Cost-effectiveness and health benefits of pediatric 23-valent pneumococcal polysaccharide vaccine, 7-valent pneumococcal conjugate vaccine and forecasting 13-valent pneumococcal conjugate vaccine in China. Pediatr Infect Dis J. 2016;35:e353–61. https://doi.org/10.1097/INF.0000000000001288
9. Boulton ML, Ravi NS, Sun X, Huang Z, Wagner AL. Trends in childhood pneumococcal vaccine coverage in Shanghai, China, 2005–2011: a retrospective cohort study. BMC Public Health. 2016;16:109. https://doi.org/10.1186/s12889-016-2785-7
10. Li Y, Yin Z, Shao Z, Li M, Liang X, Sandhu HS, et al.; Acute Meningitis and Encephalitis Syndrome Study Group. Population-based surveillance for bacterial meningitis in China, September 2006–December 2009. Emerg Infect Dis. 2014;20:61–9. https://doi.org/10.3201/eid2001.120375
11. Home C; Centers for Disease Control and Prevention (CDC). Estimating meningitis hospitalization rates for sentinel hospitals conducting invasive bacterial vaccine-preventable diseases surveillance. MMWR Morb Mortal Wkly Rep. 2013;62:810–2.
12. Zhang T, Zhang J, Hua J, Wang D, Chen L, Ding Y, et al. Influenza-associated outpatient visits among children less than 5 years of age in eastern China, 2011–2014. BMC Infect Dis. 2016;16:267. https://doi.org/10.1186/s12879-016-1614-z
13. Zhang X, Zhang J, Chen L, Feng L, Yu H, Zhao G, et al. Pneumonia and influenza hospitalizations among children under 5 years of age in Suzhou, China, 2005–2011. Influenza Other Respir Viruses. 2017;11:15–22. https://doi.org/10.1111/irv.12405
14. Shan W, Shi T, Zhang X, Xue J, Wang Y, Yu J, et al. Hospitalization rate and population-based incidence of hospitalization for community-acquired pneumonia among children in Suzhou, China. Pediatr Infect Dis J. 2018;37:1242–7.
15. Geng Q, Zhang T, Ding Y, Tao Y, Lin Y, Wang Y, et al. Molecular characterization and antimicrobial susceptibility of *Streptococcus pneumoniae* isolated from children hospitalized with respiratory infections in Suzhou, China. PLoS One. 2014;9:e93752. https://doi.org/10.1371/journal.pone.0093752
16. Lin TY, Shah NK, Brooks D, Garcia CS. Summary of invasive pneumococcal disease burden among children in the Asia-Pacific region. Vaccine. 2010;28:7589–605. https://doi.org/10.1016/j.vaccine.2010.07.053
17. Zhou J, Tian H, Du X, Xi X, An Y, Duan M, et al.; for China Critical Care Clinical Trials Group (CCCCTG). Population-based epidemiology of sepsis in a subdistrict of Beijing. Crit Care Med. 2017;45:1168–76. https://doi.org/10.1097/CCM.0000000000002414

18. Rendi-Wagner P, Georgopoulos A, Kundi M, Mutz I, Mattauch M, Nowak J, et al. Prospective surveillance of incidence, serotypes and antimicrobial susceptibility of invasive *Streptococcus pneumoniae* among hospitalized children in Austria. J Antimicrob Chemother. 2004;53:826–31. https://doi.org/10.1093/jac/dkh211
19. von Kries R, Hermann M, Hachmeister A, Siedler A, Schmitt HJ, Al-Lahham A, et al. Prediction of the potential benefit of different pneumococcal conjugate vaccines on invasive pneumococcal disease in German children. Pediatr Infect Dis J. 2002;21:1017–23. https://doi.org/10.1097/00006454-200211000-00008
20. von Kries, Siedler A, Schmitt HJ, Reinert RR. Proportion of invasive pneumococcal infections in German children preventable by pneumococcal conjugate vaccines. Clin Infect Dis. 2000;31:482–7.
21. Manoharan A, Manchanda V, Balasubramanian S, Lalwani S, Modak M, Bai S, et al.; Alliance for Surveillance of Invasive Pneumococci Study Group. Invasive pneumococcal disease in children aged younger than 5 years in India: a surveillance study. Lancet Infect Dis. 2017;17:305–12. https://doi.org/10.1016/S1473-3099(16)30466-2
22. Ceyhan M, Yildirim I, Balmer P, Borrow R, Dikici B, Turgut M, et al. A prospective study of etiology of childhood acute bacterial meningitis, Turkey. Emerg Infect Dis. 2008;14:1089–96. https://doi.org/10.3201/eid1407.070938
23. Zhang T, Black S, Hao C, Ding Y, Ji W, Chen R, et al. The blind nasotracheal aspiration method is not a useful tool for pathogen detection of pneumonia in children. PLoS One. 2010;5:e15885. https://doi.org/10.1371/journal.pone.0015885
24. Li D. Trend analysis of antibiotic use in China's general hospitals during 2012–2016 [master's thesis]. CNKI.net. 2019 [cited 2019 Jul 1]. https://tinyurl.com/trendanalysisli2019
25. Chang J, Xu S, Zhu S, Li Z, Yu J, Zhang Y, et al. Assessment of non-prescription antibiotic dispensing at community pharmacies in China with simulated clients: a mixed cross-sectional and longitudinal study. Lancet Infect Dis. 2019;19:1345–54. https://doi.org/10.1016/S1473-3099(19)30324-X
26. Measures for the administration of clinical application of antibiotics (Order No. 84 of the Ministry of Health) [in Chinese]. 2012 [cited 2018 Jun 10]. http://www.nhc.gov.cn/fzs/s3576/201205/2f773c2ddbd84e19aab0b4b2d9741900.shtml
27. Chen K, Zhang X, Shan W, Zhao G, Zhang T. Serotype distribution of *Streptococcus pneumoniae* and potential impact of pneumococcal conjugate vaccines in China: A systematic review and meta-analysis. Hum Vaccin Immunother. 2018;14:453–463.
28. van Hoek AJ, Andrews N, Waight PA, George R, Miller E. Effect of serotype on focus and mortality of invasive pneumococcal disease: coverage of different vaccines and insight into non-vaccine serotypes. PLoS One. 2012;7:e39150. https://doi.org/10.1371/journal.pone.0039150
29. Rodgers GL, Klugman KP. The future of pneumococcal disease prevention. Vaccine. 2011;29:C43–8. https://doi.org/10.1016/j.vaccine.2011.07.047


Address for correspondence: Tao Zhang, Department of Epidemiology, School of Public Health, Fudan University, PO Box 289, 138 Yi Xue Yuan Rd, Shanghai 200032, China; email: tzhang@shmu.edu.cn; Xuejun Shao, Soochow University Affiliated Children's Hospital, Suzhou 215008, China; email: xjshao@suda.edu.cn

# Human Diversity of Killer Cell Immunoglobulin-Like Receptors and Human Leukocyte Antigen Class I Alleles and Ebola Virus Disease Outcomes

Tony Wawina-Bokalanga, Bert Vanmechelen, Valentine Lhermitte, Joan Martí-Carreras, Valentijn Vergote, Fara Raymond Koundouno, Joseph Akoi-Boré, Ruth Thom, Tom Tipton, Kimberley Steeds, Kéita Balla Moussa, Ablam Amento, Lies Laenen, Sophie Duraffour, Martin Gabriel, Paula Ruibal, Yper Hall, Mandy Kader-Kondé, Stephan Günther, Guy Baele, Cesar Muñoz-Fontela, Johan Van Weyenbergh, Miles W. Carroll, Piet Maes

We investigated the genetic profiles of killer cell immunoglobulin-like receptors (KIRs) in Ebola virus–infected patients. We studied the relationship between KIR–human leukocyte antigen (HLA) combinations and the clinical outcomes of patients with Ebola virus disease (EVD). We genotyped KIRs and HLA class I alleles using DNA from uninfected controls, EVD survivors, and persons who died of EVD. The activating *2DS4–003* and inhibitory *2DL5* genes were significantly more common among persons who died of EVD; *2DL2* was more common among survivors. We used logistic regression analysis and Bayesian modeling to identify *2DL2*, *2DL5*, *2DS4–003*, *HLA-B-Bw4-Thr*, and *HLA-B-Bw4-Ile* as probably having a significant relationship with disease outcome. Our findings highlight the importance of innate immune response against Ebola virus and show the association between KIRs and the clinical outcome of EVD.

Author affiliations: KU Leuven, Leuven, Belgium (T. Wawina-Bokalanga, B. Vanmechelen, V. Lhermitte, J. Martí-Carreras, V. Vergote, L. Laenen, G. Baele, J. Van Weyenbergh, P. Maes); University Julius Nyerere of Kankan, Conakry, Guinea (F.R. Koudouno); Institut National de Santé Publique, Conakry (J. Akoi-Boré); Public Health England, Salisbury, UK (R. Thom, T. Tipton, K. Steeds, Y. Hall, M.W. Carroll); Centre d'Excellence de Formation et Recherche sur les Maladies Prioritaires en Guinée, Conakry (K.B. Moussa, A. Amento, M. Kader-Kondé); German Center for Infection Research, Hamburg-Lübeck-Borstel-Riems, Germany (S. Duraffour, M. Gabriel); Bernhard Nocht Institute for Tropical Medicine, Hamburg, Germany (S. Duraffour, M. Gabriel, P. Ruibal, S. Günther, C. Muñoz-Fontela)

DOI: https://doi.org/10.3201/eid2701.202177

Ebola virus (EBOV) is an enveloped, nonsegmented, negative-sense, single-stranded RNA virus that belongs to the genus *Ebolavirus* in the family *Filoviridae*. This genus comprises 6 species recognized by the International Committee on Taxonomy of Viruses: *Zaire ebolavirus*, *Sudan ebolavirus*, *Bundibugyo ebolavirus*, *Tai Forest ebolavirus*, *Reston ebolavirus*, and the recently discovered *Bombali ebolavirus* (*1*).

Since the first recorded Ebola virus outbreaks in 1976 in Zaire (now the Democratic Republic of the Congo [DRC]) and southern Sudan, other outbreaks of Ebola virus disease (EVD) have been reported in Africa. The West Africa Ebola virus outbreak in 2013–2016, which mainly affected Guinea, Liberia, and Sierra Leone, was the largest and most widespread EVD outbreak. According to the World Health Organization, this outbreak comprised 28,646 confirmed, probable, and suspected EVD cases and caused 11,323 reported deaths (*2*).

On June 25, 2020, the DRC's Ministry of Health declared the second largest EVD outbreak to be over (*3*). According to the DRC's Ministry of Health, this outbreak caused 3,470 confirmed and probable EVD cases. A total of 2,299 infected persons died, and 1,171 persons survived.

EBOV quickly overwhelms the host's innate immune response and causes an acute febrile illness along with headache, vomiting, abdominal pain, diarrhea, severe fatigue, coagulation disorders, hypotension, lymphopenia, and thrombocytopenia (*4*,*5*). Some EBOV infections generate a cytokine storm, which hinders peripheral natural killer

cells (NK) and T and B lymphocytes. This response can induce multiorgan failure, hypovolemic shock, and death (*6*).

NK cells, among other cells, are key effector cells of the innate immune system and play a crucial role in the antiviral response. The effector capability of NK cells has been described in a wide range of viral infections, such as hepatitis B, hepatitis C (HCV), HIV, and human cytomegalovirus infection (*7*). Few studies have examined NK cell levels and function in EVD patients; those studies documented lower NK cell levels among persons who died of EVD compared with survivors (*8*–*10*). One study also observed an increase in inhibitory receptor KIR2DL1 in NK cells during EVD (*8*). In addition, researchers have demonstrated the cytotoxic effect of NK cells during experimentally induced EBOV infection in nonhuman primates and its protective and deleterious effects in NK-depleted mice (*11*–*14*). Activated NK cells respond to EBOV-infected cells by releasing perforin and granzyme, which mediate the cytolysis of EBOV-infected cells. Furthermore, the ability of NK cells to secrete cytokines such as interferon-γ, interferon-α/β, and tumor necrosis factor-α is essential to the immune response (*5*). Reed et al. demonstrated that lethal EBOV infection is associated with loss and decreased activity of NK cells (*11*). In addition, Cimini et al. observed that patients who died of EVD had lower NK cell frequencies than patients who survived (*8*). The mechanism behind this association is still unknown; however, the degree of loss is highly correlated with fatal disease outcome.

The cytotoxic and secretory functions of NK cells are regulated through the interaction between human leukocyte antigens (HLA) class I molecules on target cells and receptors, such as the killer cell immunoglobulin-like receptors (KIRs), on NK cells (*15*). KIRs are members of the immunoglobulin superfamily type I receptors, and they are encoded by a family of highly polymorphic genes located on human chromosome 19q13.4 within the leukocyte receptor complex (*16*). They are expressed on the surface of NK cells and certain T lymphocytes and regulate the function and development of these cells. NK cells recognize HLA class I molecules on the surface of host cells, enabling them to distinguish between self and nonself and to target infected or malignant cells for lysis (*17*).

Researchers have identified 16 KIR genes, of which 8 are inhibitory (*2DL1–5*, *3DL1–3*), 6 are activating (*2DS1–5*, *3DS1*), and 2 are pseudogenes (*2DP1* and *3DP1*). Some KIRs, such as *2DL4*, *3DL2*, and *3DL3*, contain sequences for activating and inhibitory receptors (*18*). Inhibitory KIRs interact with specific motifs of HLA class I molecules. One such motif is the amino acid at position 80 of HLA: lysine or asparagine for HLA-C alleles and threonine or isoleucine for HLA-B-Bw4 and HLA-A-Bw4 alleles (*19*).

The number and types of KIRs vary considerably among individual persons, who might exhibit 7–12 KIRs for each haplotype. A person might have haplotype A, which exhibits more inhibitory KIRs, or haplotype B, which exhibits more activating KIRs (*19*). The AB or BB haplotype is characterized by the presence of the *2DL2*, *2DL5*, *3DS1*, *2DS1*, *2DS2*, *2DS3*, or *2DS5* genes. None of these genes are present in the AA haplotype, which contains only a single activating KIR gene, *2DS4* (with a deleted variant of 22 bp in exon 5, *2DS4–003*) (*20*). Because these genes are so variable and the KIR/HLA combinations play a key role in immune response, understanding this variability is important for genotyping studies (*21*). Genetic studies have shown that the distribution of KIR genes and KIR/HLA combinations vary widely; furthermore, these variations can predict disease outcomes in persons with hepatitis B, HCV, human T-lymphotropic virus type 1 (HTLV-1), or HIV-1 infections (*22*,*23*). During HIV-1, HCV, or HTLV-1 infection, CD8+ cells mediate much of the protective effect of inhibitory KIRs (*24*).

We determined the genetic profiles of KIR genes and HLA class I alleles in DNA samples from persons infected with EBOV Makona variant in Guinea. We also assessed the distribution of HLA class I genotypes during an EVD outbreak and the relationship between specific KIR/HLA combinations and the clinical outcomes of persons with EVD.

## Materials and Methods

### Study Samples

We studied samples from patients in whom EVD was diagnosed during the 2013–2016 outbreak. We collected serum samples from 77 uninfected controls and 101 EVD survivors in Guéckédou, Guinea, during May 2015–September 2017. In addition, the European Mobile Laboratory provided DNA isolated from whole blood samples of 119 persons who had died of EVD.

We defined EVD survivors as EBOV-infected patients who had survived the acute phase of EVD and were discharged from the Ebola treatment center in Guéckédou after testing negative for Ebola 4 times by reverse transcription PCR. The survivors in our study included only persons with an original certificate of

survivorship issued by the Guinean government. Controls tested negative for EBOV-specific antibodies and EBOV neutralizing antibodies in plasma.

We collected blood samples in EDTA tubes for routine blood tests, serologic assays for EBOV antigen, and nucleic acid detection of EBOV RNA by reverse transcription PCR. Afterward, we isolated peripheral blood mononuclear cells (PBMCs) from whole blood samples using Ficoll-Paque density gradient centrifugation (Sigma-Aldrich Inc., https://www.sigmaaldrich.com) according to the manufacturer's instructions. To store PBMCs at room temperature, we used DNAgard Blood (Sigma-Aldrich Inc.) according to the manufacturer's instructions.

### Genomic DNA Extraction

We extracted genomic DNA from PBMCs from EVD survivors and controls. We used the QIAamp DNA Mini kit (QIAGEN, https://www.qiagen.com) for DNA extraction according to the manufacturer's instructions. We eluted the purified DNA in 100 µL buffer AE and quantified it using a NanoDrop spectrophotometer (ThermoFisher Scientific, https://www.thermofisher.com).

### Whole-Genome Amplification

We conducted whole-genome amplification of DNA samples using the multiple displacement amplification Repli-g mini kit (QIAGEN) according to the manufacturer's instructions. We then purified DNA with a rapid in-house method using ethanol precipitation. For this procedure, we first mixed 1:10 volume sodium acetate (3 M, pH 5.5) with 2 volumes absolute ethanol in a 1.5 mL Eppendorf tube. After inverting the tube, we incubated the reaction mixture at −80°C for 2 h and then centrifuged at 20,000 × *g* for 30 min. We withdrew the supernatant and washed the pellet with 70% ethanol, then centrifuged the mixture at maximum speed for 15 min. After removing the supernatant, we air-dried the pellet at 50°C and then resuspended in 50 µL buffer AE. We stored the extracted DNA products at −20°C.

### KIR and HLA Class I Genotyping

We established the presence or absence of 14 KIR genes and 2 pseudogenes (*2DP1* and *3DP1*) by PCR using primers, as published in previous studies (*25*–*27*). We used Primer3 version 0.4.0 software (https://bioinfo.ut.ee/primer3-0.4.0) to design specific primers targeting *2DL5* and *2DS4–001*. We conducted HLA genotyping for 5 HLA class I alleles known to be KIR ligands: *HLA-C1-Asn80* (*2DL2*, *2DL3*, and *2DS2*), *HLA-C2-Lys80* (*2DL1* and *2DS1*), *HLA-B-Bw4-Thr80* (*3DL1*), *HLA-B-Bw4-Ile80* (*3DS1* and *3DL1*), and *HLA-A-Bw4* (*3DL1* and *3DL2*) (*28*) (Appendix Table 1, https://wwwnc.cdc.gov/EID/article/27/1/20-2177-App1.pdf).

We conducted PCR on amplified genomic DNA from uninfected controls, EVD survivors, and persons who died of EVD. We conducted amplifications using a Biometra TRIO-Analytik Jena Thermocycler (Westburg, https://www.westburg.eu). For each PCR, we used a 30 µL mixture containing ≥10 ng of DNA sample, 6 µL 5× QIAGEN OneStep reverse transcription PCR buffer, 1 µL dNTP mix with 10 mM of each dNTP, 1 µL QIAGEN OneStep reverse transcription PCR enzyme mix, 0.6 µM of each primer, and RNase-free water. In negative samples, we also added 0.6 µM of an internal control primer set to verify the true absence of KIR genes and HLA class I alleles. We ran each PCR in triplicate (Appendix Tables 2, 3). We ran the amplified DNA on 6% polyacrylamide gels and electrophoresed it in 1× Tris-borate-EDTA buffer. We stained gels with Midori green direct and visualized them under UV light using a gel imager camera.

### Statistical Data Analysis

We tested the difference in frequency of KIR/HLA haplotypes using the Fisher exact test. To avoid type I error, we calculated an adjusted p value with Bonferroni correction and used the resulting p value ($p<0.02$) to determine significance. We conducted binary logistic regression to assess the effect of HLA and KIR genotypes on the clinical outcome of patients with EVD. We selected any variable with a significant univariate test at a relaxed p value of 0.25 as a candidate for the multivariate analysis. This criterion enabled us to reduce the initial number of variables (i.e., genes) in the model, while simultaneously reducing the risk of missing important variables (*29*,*30*). After preselection, we built a binomial logistic regression model that comprised all remaining explanatory variables and performed backward elimination. The model simultaneously used Bayesian information criterion (*31*) and Fisher exact tests at the 5% significance level.

As an extension to the binomial analysis, we conducted multinomial logistic regression. This model assessed the effect of HLA and KIR genotypes on the clinical outcome of patients with EVD and determined the KIR gene profile associated with these outcomes. We conducted Bayesian model averaging (BMA) using the R packages BMA and mlogitBMA (*32*,*33*). These packages enabled us to account for uncertainty about the explanatory variables using a Bayesian information criterion approximation to the

posterior model probabilities. After removing variables that generated collinearity issues, we searched the model space using the fast leaps and bounds algorithm (*34*). As the first step in applying BMA to solve the variable selection problem for multinomial logit data, mlogitBMA uses the approach of Begg and Gray (*35*), which approximates large-scale multinomial logistic regressions as a series of binary logistic regressions (*36*).

### Ethics Approval

The National Committee of Ethics in Medical Research of Guinea approved the use of diagnostic leftover samples and corresponding patient data for this study (approval no. 11/CNERS/14). Samples from EVD survivors and controls were collected under ethics protocols approved by the Guinean National Ethics Committee for Research and Health (approval no. 33/CNERS/15). We obtained written and informed consent from controls and EVD survivors. Ethical permission for the work conducted at KU Leuven on the DNA samples was reviewed and approved by the KU Leuven ethics committee under reference no. S58836.

## Results

### KIR Haplotypes Associated with EVD Outcome

Of 77 controls, 101 survivors, and 119 persons who died of EVD, an average of 78% of each category had 11 shared haplotypes, which differed from each other by the presence or absence of 9 KIR genes (Figure 1). The remaining participants (20 controls, 14 survivors, and 31 persons who died of EVD) had a rare KIR haplotype that lacked ≥3 KIR genes (data not shown). The frequency of the KIR AA haplotype was significantly higher for persons who died of EVD (6.7%) than for survivors (0.99%; p = 0.04). One KIR BB haplotype was significantly more common among the survivors (37.6%) than among persons who died of EVD (17.6%; p<0.01). All participants had the *2DL1*, *3DL1*, *3DL2*, *3DL3*, *2DP1*, and *3DP1–004* genes.

### Frequency of KIR Genotypes

We found the *2DL2* gene in 98% of survivors and 83.2% of persons who died of EVD. Likewise, we found the *2DL5* gene in 46.5% of survivors and 63% of persons who died of EVD (Table 1). These results

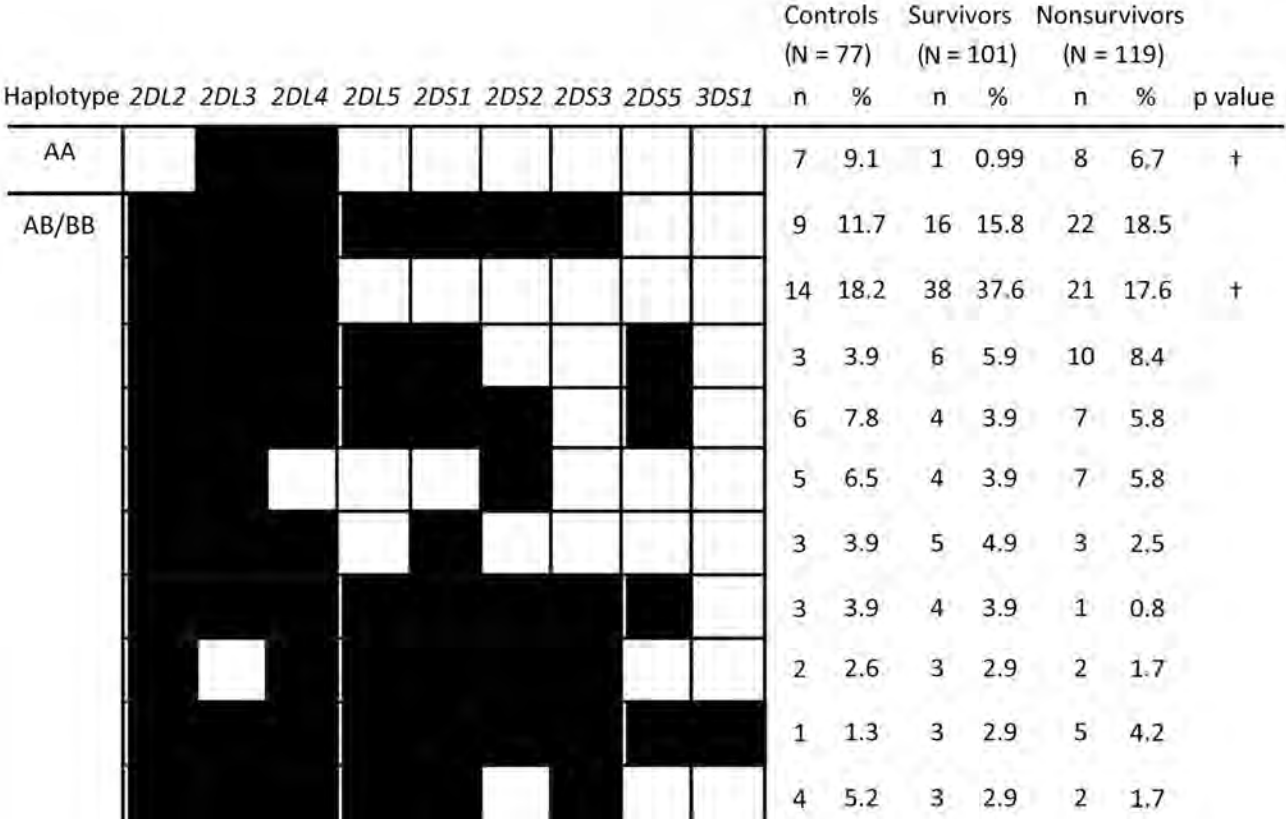


**Figure 1.** Killer cell immunoglobulin-like receptor haplotypes among the control group, Ebola survivors, and persons who died of Ebola virus disease in Guinea, 2015–2017. Percentage of each haplotype was calculated and defined as the number of persons with the killer cell immunoglobulin-like receptor haplotype (n) divided by the number of persons (N) in the studied group. Black boxes indicate presence of genes; white boxes indicate absence of genes. †p<*Pc* (survivors vs. fatalities). *Pc*, corrected p value.

**Table 1.** Frequency of KIR genes and HLA class I alleles among control group, Ebola survivors, and persons who died of Ebola virus disease, Guinea, 2015–2017*

| Gene | Controls, no. (%) | Survivors, no. (%) | Persons who died, no. (%) | p value |
|---|---|---|---|---|
| Inhibitory KIRs | | | | |
| *2DL1* | 77 (100.0) | 101 (100.0) | 119 (100.0) | |
| *2DL2* | 67 (87.0) | 99 (98.0) | 99 (83.2) | †‡ |
| *2DL3* | 71 (92.2) | 94 (93.1) | 112 (94.1) | |
| *2DL4* | 77 (100.0) | 100 (99.0) | 118 (99.1) | |
| *2DL5* | 42 (54.5) | 47 (46.5) | 75 (63.0) | † |
| *3DL1* | 77 (100.0) | 101 (100.0) | 118 (99.1) | |
| *3DL2* | 76 (98.7) | 101 (100.0) | 119 (100.0) | |
| *3DL3* | 77 (100.0) | 101 (100.0) | 119 (100.0) | |
| Activating KIRs | | | | |
| *2DS1* | 46 (59.7) | 55 (54.4) | 74 (62.2) | |
| *2DS2* | 37 (48.0) | 46 (45.5) | 55 (46.2) | |
| *2DS3* | 23 (29.8) | 30 (29.7) | 40 (33.6) | |
| *2DS4–001* | 70 (90.9) | 94 (93.1) | 103 (86.6) | |
| *2DS4–003* | 40 (51.9) | 41 (40.6) | 67 (56.3) | † |
| *2DS5* | 23 (29.8) | 26 (25.7) | 40 (33.6) | |
| *3DS1* | 5 (6.5) | 4 (3.9) | 13 (10.9) | |
| Pseudogenes | | | | |
| *2DP1* | 77 (100.0) | 100 (99.0) | 116 (97.5) | |
| *3DP1–001* | 6 (7.8) | 4 (3.9) | 8 (6.7) | |
| *3DP1–004* | 76 (98.7) | 99 (98.0) | 117 (98.3) | |
| HLA class I alleles | | | | |
| HLA-C1$^{Asn80}$ | 55 (71.4) | 78 (77.2) | 85 (71.4) | |
| HLA-C2$^{Lys80}$ | 58 (75.3) | 74 (73.3) | 88 (73.9) | |
| HLA-B-Bw4$^{Thr80}$ | 8 (10.4) | 9 (8.9) | 22 (18.5) | |
| HLA-B-Bw4$^{Ile80}$ | 33 (42.8) | 48 (47.5) | 38 (31.9) | |
| HLA-A-Bw4 | 23 (29.8) | 26 (25.7) | 37 (31.1) | |

*Frequency (%) of each KIR gene or HLA class I allele was calculated and defined as the number of individuals having the gene or allele divided by the number of persons in the studied group. HLA, human leukocyte antigen; KIR, killer cell immunoglobulin-like receptor; *Pc*, corrected p value.
†p value <*Pc* (survivors vs. persons who died).
‡p value <*Pc* (controls vs. survivors).

suggest that inhibitory *2DL2* and *2DL5* might be associated with the outcome of persons with EVD.

### Relevant KIR Genes and HLA Class I Alleles in Survivors and Persons Who Died of EVD

The binomial logistic regression model (Table 2) retained 4 KIR genes and 2 HLA class I alleles as covariates in our final model, implying that these genes exhibit a significant relationship with disease outcome. Because of the relatively small number of participants, we validated these findings through BMA. The KIR genes *2DL2*, *2DL5*, and *2DS4–0003* and the HLA class I alleles *HLA-B-Bw4-Thr* and *HLA-B-Bw4-Ile* were present in >15% of the models explored during our BMA analysis (Table 3; Appendix Figure 1). These 5 covariates are almost identical to those identified in the binary regression models (Tables 2, 3).

### HLA Haplotypes

We identified 23 HLA class I haplotypes. These haplotypes differed by the presence or absence of 2 HLA-C, 2 HLA-B, or 1 HLA-A alleles (Figure 2). The HLA haplotype characterized by the presence of *HLA-C1$^{Asn80}$*, *HLA-C2 $^{Lys80}$*, and *HLA-A-Bw4* was significantly more common among persons who died (11.7%) than survivors (4.95%; p<0.01).

### Functional Analysis of HLA and KIR Gene Combinations

To further evaluate whether biologically relevant KIR/HLA combinations affect the outcome of patients with EVD, we conducted a functional analysis of 5 HLA class I alleles and their respective inhibitory and activating KIRs (Appendix Table 1); we compared the results of uninfected controls, persons who died of EVD, and survivors. We used previously

**Table 2.** Results from multivariate logistic regression model of human leukocyte antigen class I and killer cell immunoglobulin-like receptor genes in controls and Ebola virus–infected patients, Guinea, 2015–2017

| Term | β estimate | SE | p value |
|---|---|---|---|
| Intercept (β0) | −2.27 | 0.84 | <0.01 |
| *2DL2* (β1) | 2.73 | 0.82 | <0.01 |
| *2DL5* (β2) | −1.94 | 0.67 | <0.01 |
| *2DS1* (β3) | 1.35 | 0.67 | <0.05 |
| *2DS4–0003* (β4) | −0.63 | 0.31 | <0.05 |
| *HLA-B-Bw4-Thr* (β5) | −1.20 | 0.48 | <0.05 |
| *HLA-B-Bw4-Ile* (β6) | 0.76 | 0.31 | <0.05 |

**Table 3.** Results from the multinomial logistic regression of human leukocyte antigen class I and killer cell immunoglobulin-like receptor genes in Ebola virus–infected patients, Guinea, 2015–2017*

| Term | p ≠ 0 | β estimate | SE | Best model |
|---|---|---|---|---|
| *2DL2* | 88.1 | 1.02 | 0.54 | 1.18 |
| *2DL5* | 59.1 | −0.43 | 0.46 | −0.65 |
| *KIR2DS4.0003* | 16.6 | −0.08 | 0.20 | (...) |
| *HLA-B-Bw4-Thr* | 45.8 | −0.38 | 0.48 | (...) |
| *HLA-B-Bw4-Ile* | 45.1 | 0.27 | 0.34 | (...) |

*Intercepts have been omitted for interpretation purposes. p ≠ 0 indicates the probability that the coefficient for a given predictor is not zero. Ellipses (...) represent predictors that were not present in the best model.

validated functional KIR/HLA pairs (*28*) to stratify each group of participants into inhibitory and activating KIR/HLA ligands and scored each KIR/HLA combination: 0, absence of both KIR and HLA ligand; 1, presence of either KIR or HLA ligand; 2, weak affinity between KIR and HLA; or 3, strong affinity between KIR and HLA. Survivors had a total inhibitory KIR/HLA score that was significantly higher than in persons who died of EVD (p<0.01 by Kruskall-Wallis test with false discovery rate correction), whereas no significant difference was observed in the total activating KIR/HLA score Figure 3.

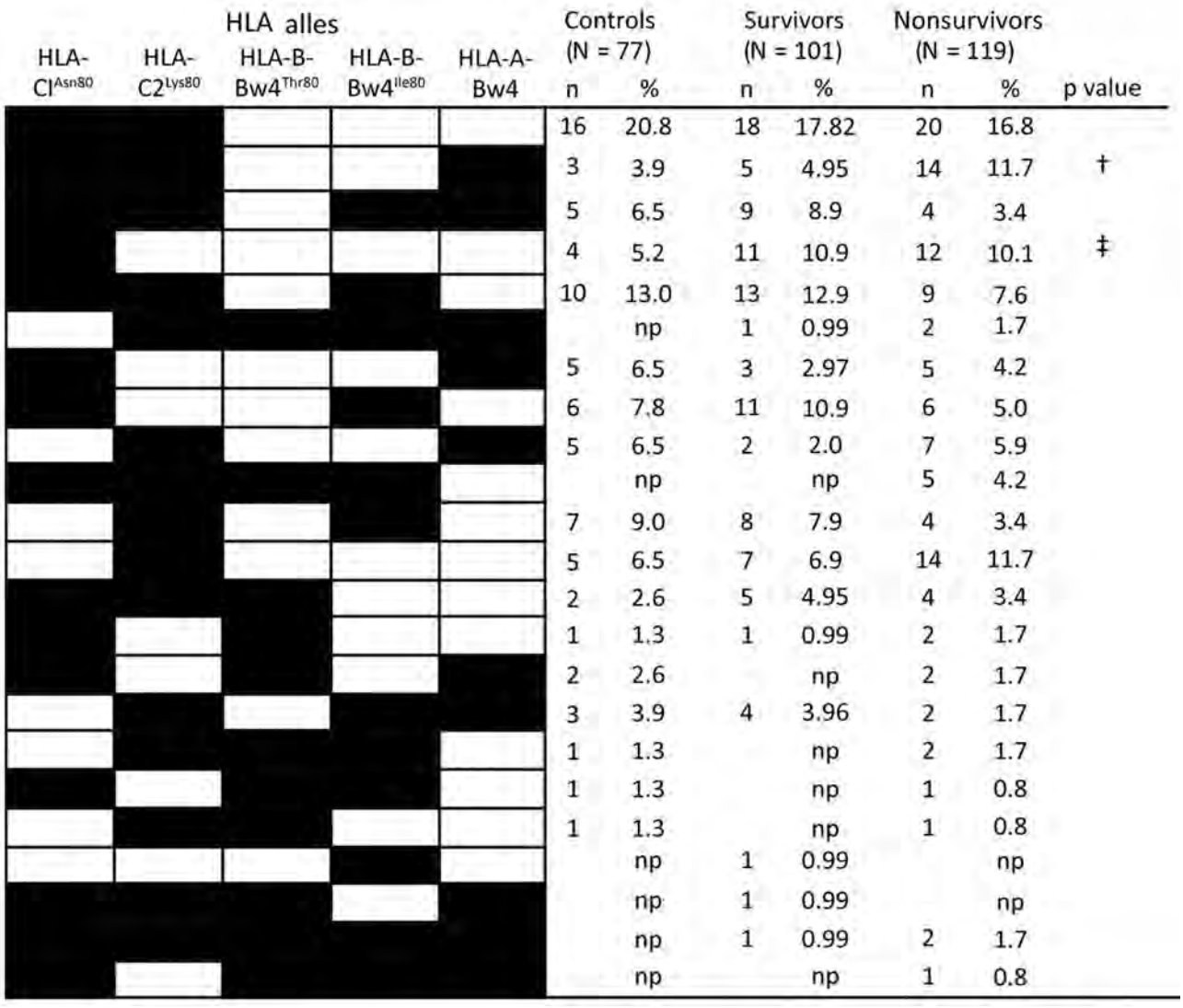


**Figure 2.** HLA haplotypes identified among the control group, Ebola survivors, and persons who died of Ebola virus disease in Guinea, 2015–2017. Percentage of each haplotype was calculated and defined as the number of persons with the HLA haplotype (n) divided by the number of individuals (N) in the studied group. Black boxes indicate presence of genes; white boxes indicate absence of genes. †p<*Pc* (survivors vs fatalities); ‡p<*Pc* (controls vs infected cases). HLA, human leukocyte antigen; NP, not present; *Pc*, corrected p value.

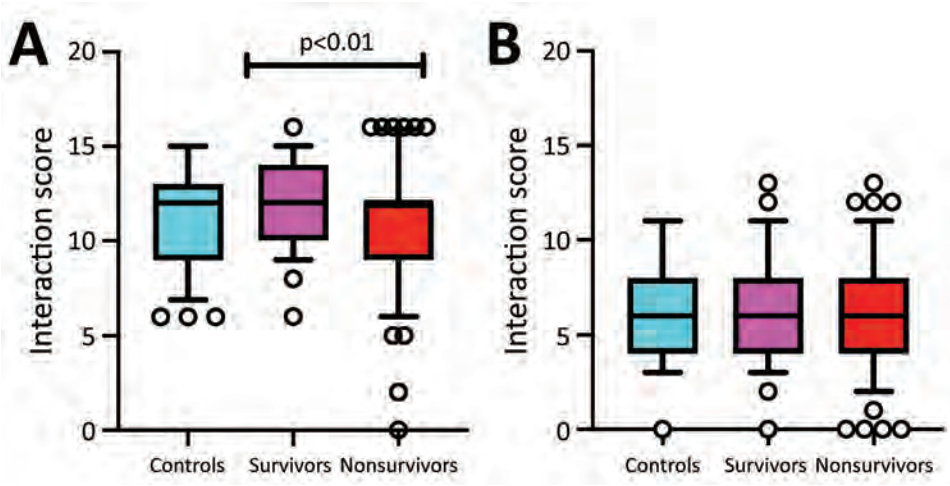


**Figure 3**. Statistical comparison of all inhibitory and activating killer cell immunoglobulin receptors (KIRs) between controls, survivors, and persons who died of Ebola virus disease in Guinea, 2015–2017. A) All inhibitory KIRs with their specific HLA ligands are compared between studied groups. Persons who did and did not survive differed significantly. B) Comparison of activating KIRs with their specific HLA ligands between studied groups. HLA, human leukocyte antigen.

## Discussion

Despite the presumed protective role played by NK cells against EBOV, few studies have been conducted on KIRs and their specific HLA ligands during EVD (*6*,*37*). Our study shows that EBOV-infected patients have diverse HLA and KIR genotypes. The KIR haplotype lacking the *2DL2*, *2DL5*, *2DS1*, *2DS2*, *2DS3*, *2DS5*, and *3DS1* genes was significantly more common among persons who died of EVD (6.7%) than survivors (0.99%; p = 0.04) (Figure 1). We used BMA analysis to identify the KIR genes *2DL2*, *2DL5*, and *2DS4–003* as possibly associated with disease outcomes. Contrary to findings by Wauquier et al. (*37*), we found that frequencies of activating *2DS1* and *2DS3* were not significantly correlated with disease outcomes. In addition, the KIR *2DS4–003* and *2DL5* genes were significantly more common among persons who died of EVD than among survivors. This discrepancy might be caused by differences in sample size or genetic makeup of the study populations.

Using the KIR Allele Frequency Net Database (http://www.allelefrequencies.net), we compared the frequency of inhibitory and activating KIR genes from this study with different populations. These populations were from countries in West Africa (i.e., Côte d'Ivoire, Nigeria, Ghana, Equatorial Guinea, and Senegal), Central Africa (i.e., DRC, Gabon, and Uganda), South Africa (i.e., South Africa and Zimbabwe), and a group of mixed population from Reunion, Comoros, and South Africa. Inhibitory *2DL2* and activating *2DS1* frequencies were higher for our study group than for all other studied populations from West Africa (p<0.01), Central Africa (p<0.01), and South Africa (p<0.01) (Appendix Figure 2). The apparent discrepancy between our study and that of Wauquier et al. (*37*) might be largely explained by differences in population genetics between Guinea and Gabon, where Wauquier et al. recruited participants. These differences might be promulgated by the rapid evolution of human KIR genes, partly in response to viral diversity (*38*).

Another study found increased levels of inhibitory KIR *2DL1* at the cell surface of NK cells in EVD patients from Guinea (*8*) during the same outbreak. However, that study's small sample size did not enable the detection of differences between the 8 survivors and 6 persons who died of EVD. Our data suggests that KIR *2DL2* has a protective role in EVD; similarly, this gene is protective against HIV-1 and HCV infection because it enhances the protective effect of HLA-B57 on viral load, slows the reduction in CD4 count, and enables spontaneous clearance of HCV (*23*). On the other hand, KIR *2DL2* strongly enhanced the protective effect of HLA-C8 and the detrimental effect of HLA-B54 on disease outcome in HTLV-1 infection (*24*). It will be important to further investigate whether the proposed protective effect of KIR *2DL2* in EVD might be mediated by the patient's viral load.

All participants in our study had the KIR *3DL3* gene. Existing data show that *3DL3* transcripts are overexpressed in persons who died of EVD compared with survivors in recovery (p<0.01) and in the viremic phase (p = 0.17; data not shown) (*39*). Our findings support the hypothesis that genomic and transcriptomic mechanisms of KIR regulation play a role in EVD outcomes.

Although persons from all groups had the inhibitory *3DL1* gene, the frequency of its low-affinity ligand HLA-B-Bw4$^{Thr80}$ was significantly higher among persons who died (18.5%) than among survivors (8.9%). In contrast, its high-affinity ligand HLA-B-Bw4$^{Ile80}$ allele was more common among survivors (47.5%) than among persons who died of EVD (31.9%).

In conclusion, EVD survivors express less activating and more inhibitory KIRs (Table 2) and more functional inhibitory KIR/HLA pairs (Figure 3) through genomic and transcriptomic (*39*) mechanisms, than persons who died of EVD. We hypothesize that these genetic differences contribute to the uncontrolled innate immune response observed in EVD (*6*). This response is mediated mostly by NK cells, although KIRs might also participate (*24*).

Although researchers have made substantial advances in drug and vaccine development for EVD in the last 5 years, researchers should also investigate the potential effects of blocking KIR receptors on disease outcome. These biomarkers could lead to new therapeutic approaches, preferentially targeting the innate immune system, for future EVD outbreaks. Our study had a reasonable sample size, but further investigations should examine a larger cohort.

### Acknowledgments

We thank the authorities of Conakry, especially the Ministry of Health and Public Hygiene, for supporting the study. We thank the staff members of the Centre d'Excellence de Formation et Recherche sur les Maladies Prioritaires en Guinée in Conakry for their collaboration. We extend our thanks to John L. Mokili for proofreading the manuscript. We thank Thierry Matonda-Ma-Nzuzi for great support on data analysis. Finally, we gratefully acknowledge all members of the Association des Survivants d'Ebola from Guéckédou and Coyah for being involved in this study.

B.V. is supported by a grant for strategic basic research from Fonds Wetenschappelijk Onderzoek/Research Foundation—Flanders (grant no. 1S28617N). J.M.C. was supported by HONOURs Marie-Sklodowska-Curie training network (grant no. 721367). G.B. acknowledges support from the KU Leuven Internal Funds under grant agreement C14/18/094. This work was supported by the Special Research Fund, KU Leuven Bijzonder Onderzoeksfonds (grant no. C14/17/100), the European Union's Horizon 2020 research and innovation program under grant agreement no. 666100 (EVIDENT) and service contract no. IFS/2011/272-372 funded by European Commission Directorate-General for International Cooperation and Development.

## About the Author

Dr. Wawina-Bokalanga is a doctoral student at KU Leuven-Rega Institute for Medical Research. His research interests include emerging and reemerging viral diseases with a focus on genome sequencing, immunogenetics and public health interventions.

## References

1. Goldstein T, Anthony SJ, Gbakima A, Bird BH, Bangura J, Tremeau-Bravard A, et al. The discovery of Bombali virus adds further support for bats as hosts of ebolaviruses. [Erratum in: Nat Microbiol. 2018;3:1486]. Nat Microbiol. 2018;3:1084–9. https://doi.org/10.1038/s41564-018-0227-2
2. World Health Organization. Ebola situation reports: archive. 2016 Jun [cited 2019 May 14]. http://www.who.int/csr/disease/ebola/situation-reports/archive
3. World Health Organization. Ebola in the Democratic Republic of the Congo: North Kivu, Ituri 2018–2020. 2020 Jul [cited 2020 Aug 15]. https://www.who.int/emergencies/diseases/ebola/drc-2019
4. Ansari AA. Clinical features and pathobiology of ebolavirus infection. J Autoimmun. 2014;55:1–9. https://doi.org/10.1016/j.jaut.2014.09.001
5. Falasca L, Agrati C, Petrosillo N, Di Caro A, Capobianchi MR, Ippolito G, et al. Molecular mechanisms of Ebola virus pathogenesis: focus on cell death. Cell Death Differ. 2015;22:1250–9. https://doi.org/10.1038/cdd.2015.67
6. Wauquier N, Becquart P, Padilla C, Baize S, Leroy EM. Human fatal zaire ebola virus infection is associated with an aberrant innate immunity and with massive lymphocyte apoptosis. PLoS Negl Trop Dis. 2010;4:e837. https://doi.org/10.1371/journal.pntd.0000837
7. Boeijen LL, Hou J, de Groen RA, Verbon A, Boonstra A. Persistent replication of HIV, Hepatitis C virus (HCV), and HBV results in distinct gene expression profiles by human NK cells. J Virol. 2019;93:e00575–18.
8. Cimini E, Viola D, Cabeza-Cabrerizo M, Romanelli A, Tumino N, Sacchi A, et al. Different features of Vδ2 T and NK cells in fatal and non-fatal human Ebola infections. PLoS Negl Trop Dis. 2017;11:e0005645. https://doi.org/10.1371/journal.pntd.0005645
9. McElroy AK, Akondy RS, Mcllwain DR, Chen H, Bjornson-Hooper Z, Mukherjee N, et al. Immunologic timeline of Ebola virus disease and recovery in humans. JCI Insight. 2020;5:e137260. https://doi.org/10.1172/jci.insight.137260
10. Sanchez A, Lukwiya M, Bausch D, Mahanty S, Sanchez AJ, Wagoner KD, et al. Analysis of human peripheral blood samples from fatal and nonfatal cases of Ebola (Sudan) hemorrhagic fever: cellular responses, virus load, and nitric oxide levels. J Virol. 2004;78:10370–7. https://doi.org/10.1128/JVI.78.19.10370-10377.2004
11. Reed DS, Hensley LE, Geisbert JB, Jahrling PB, Geisbert TW. Depletion of peripheral blood T lymphocytes and NK cells during the course of Ebola hemorrhagic fever in cynomolgus macaques. Viral Immunol. 2004;17:390–400. https://doi.org/10.1089/vim.2004.17.390
12. Geisbert TW, Hensley LE, Larsen T, Young HA, Reed DS, Geisbert JB, et al. Pathogenesis of Ebola hemorrhagic fever in cynomolgus macaques: evidence that dendritic cells are early and sustained targets of infection. Am J Pathol. 2003;163:2347–70. https://doi.org/10.1016/S0002-9440(10)63591-2
13. Warfield KL, Perkins JG, Swenson DL, Deal EM, Bosio CM, Aman MJ, et al. Role of natural killer cells in innate protection against lethal Ebola virus infection. J Exp Med. 2004;200:169–79. https://doi.org/10.1084/jem.20032141
14. Fausther-Bovendo H, Qiu X, He S, Bello A, Audet J, Ippolito G, et al. NK cells accumulate in infected tissues and

contribute to pathogenicity of Ebola virus in mice. J Virol. 2019;93:e01703–18. https://doi.org/10.1128/JVI.01703-18
15. Marcenaro E, Carlomagno S, Pesce S, Della Chiesa M, Parolini S, Moretta A, et al. NK cells and their receptors during viral infections. Immunotherapy. 2011;3:1075–86. https://doi.org/10.2217/imt.11.99
16. Hsu KC, Chida S, Geraghty DE, Dupont B. The killer cell immunoglobulin-like receptor (KIR) genomic region: gene-order, haplotypes and allelic polymorphism. Immunol Rev. 2002;190:40–52. https://doi.org/10.1034/j.1600-065X.2002.19004.x
17. Parham P. MHC class I molecules and KIRs in human history, health and survival. Nat Rev Immunol. 2005;5:201–14. https://doi.org/10.1038/nri1570
18. Pegram HJ, Andrews DM, Smyth MJ, Darcy PK, Kershaw MH. Activating and inhibitory receptors of natural killer cells. Immunol Cell Biol. 2011;89:216–24. https://doi.org/10.1038/icb.2010.78
19. Middleton D, Curran M, Maxwell L. Natural killer cells and their receptors. Transpl Immunol. 2002;10:147–64. https://doi.org/10.1016/S0966-3274(02)00062-X
20. González-Galarza FF, Takeshita LY, Santos EJ, Kempson F, Maia MH, da Silva AL, et al. Allele frequency net 2015 update: new features for HLA epitopes, KIR and disease and HLA adverse drug reaction associations. Nucleic Acids Res. 2015;43(D1):D784–8. https://doi.org/10.1093/nar/gku1166
21. Passweg JR, Huard B, Tiercy JM, Roosnek E. HLA and KIR polymorphisms affect NK-cell anti-tumor activity. Trends Immunol. 2007;28:437–41. https://doi.org/10.1016/j.it.2007.07.008
22. Podhorzer A, Dirchwolf M, Machicote A, Belen S, Montal S, Paz S, et al. The clinical features of patients with chronic hepatitis C virus infections are associated with killer cell immunoglobulin-like receptor genes and their expression on the surface of natural killer cells. Front Immunol. 2018;8:1912. https://doi.org/10.3389/fimmu.2017.01912
23. Martin MP, Naranbhai V, Shea PR, Qi Y, Ramsuran V, Vince N, et al. Killer cell immunoglobulin-like receptor 3DL1 variation modifies HLA-B*57 protection against HIV-1. J Clin Invest. 2018;128:1903–12. https://doi.org/10.1172/JCI98463
24. Boelen L, Debebe B, Silveira M, Salam A, Makinde J, Roberts CH, et al. Inhibitory killer cell immunoglobulin-like receptors strengthen $CD8^+$ T cell-mediated control of HIV-1, HCV, and HTLV-1. Sci Immunol. 2018;3:3. https://doi.org/10.1126/sciimmunol.aao2892
25. Gagne K, Brizard G, Gueglio B, Milpied N, Herry P, Bonneville F, et al. Relevance of KIR gene polymorphisms in bone marrow transplantation outcome. Hum Immunol. 2002;63:271–80. https://doi.org/10.1016/S0198-8859(02)00373-7
26. Vilches C, Castaño J, Gómez-Lozano N, Estefanía E. Facilitation of KIR genotyping by a PCR-SSP method that amplifies short DNA fragments. Tissue Antigens. 2007;70:415–22. https://doi.org/10.1111/j.1399-0039.2007.00923.x
27. Tajik N, Shahsavar F, Nasiri M, Radjabzadeh MF. Compound KIR-HLA genotype analyses in the Iranian population by a novel PCR-SSP assay. Int J Immunogenet. 2010;37:159–68. https://doi.org/10.1111/j.1744-313X.2010.00906.x
28. Kulkarni S, Martin MP, Carrington M. The yin and yang of HLA and KIR in human disease. Semin Immunol. 2008;20:343–52. https://doi.org/10.1016/j.smim.2008.06.003
29. Bendel RB, Afifi AA. Comparison of stopping rules in forward stepwise regression. J Am Stat Assoc. 1977;72:46–53.
30. Costanza MC, Afifi AA. Comparison of stopping rules in forward stepwise discriminant-analysis. J Am Stat Assoc. 1979;74:777–85. https://doi.org/10.1080/01621459.1979.10481030
31. Schwarz G. Estimating the dimension of a model. Ann Stat. 1978;6:461–4. https://doi.org/10.1214/aos/1176344136
32. Raftery AE, Painter IS, Volinsky CT. BMA: an R package for Bayesian model averaging. 2005 [cited 2018 Sep 11]. https://www.r-project.org/doc/Rnews/Rnews_2005-2.pdf
33. Sevcikova H, Raftery A. mlogitBMA: Bayesian model averaging for multinomial logit model. 2013. [cited 2018 Sep 22] http://cran.r-project.org/web/packages/mlogitBMA/index.html
34. Raftery AE. Bayesian model selection in social research. Sociol Methodol. 1995;25:111–63. https://doi.org/10.2307/271063
35. Begg CB, Gray R. Calculation of polychotomous logistic regression parameters using individualized regressions. Biometrika. 1984;71:11–8. https://doi.org/10.2307/2336391
36. Yeung KY, Bumgarner RE, Raftery AE. Bayesian model averaging: development of an improved multi-class, gene selection and classification tool for microarray data. Bioinformatics. 2005;21:2394–402. https://doi.org/10.1093/bioinformatics/bti319
37. Wauquier N, Padilla C, Becquart P, Leroy E, Vieillard V. Association of KIR2DS1 and KIR2DS3 with fatal outcome in Ebola virus infection. Immunogenetics. 2010;62:767–71. https://doi.org/10.1007/s00251-010-0480-x
38. Augusto DG, Norman PJ, Dandekar R, Hollenbach JA. Fluctuating and geographically specific selection characterize rapid evolution of the human KIR region. Front Immunol. 2019;10:989. https://doi.org/10.3389/fimmu.2019.00989
39. Reynard S, Journeaux A, Gloaguen E, Schaeffer J, Varet H, Pietrosemoli N, et al. Immune parameters and outcomes during Ebola virus disease. JCI Insight. 2019;4:e125106. https://doi.org/10.1172/jci.insight.125106

Address for correspondence: Piet Maes, Department of Microbiology, Immunology and Transplantation, Division of Clinical and Epidemiological Virology, KU Leuven—Rega Institute for Medical Research, Herestraat 49, BE-3000 Leuven, Belgium; email: piet.maes@kuleuven.be

# IgG Seroconversion and Pathophysiology in Severe Acute Respiratory Syndrome Coronavirus 2 Infection

Henry M. Staines,[1] Daniela E. Kirwan,[1] David J. Clark,[1] Emily R. Adams, Yolanda Augustin, Rachel L. Byrne, Michael Cocozza, Ana I. Cubas-Atienzar, Luis E. Cuevas, Martina Cusinato, Benedict M.O. Davies, Mark Davis, Paul Davis, Annelyse Duvoix, Nicholas M. Eckersley, Daniel Forton, Alice J. Fraser, Gala Garrod, Linda Hadcocks, Qinxue Hu, Michael Johnson, Grant A. Kay, Kesja Klekotko, Zawditu Lewis, Derek C. Macallan, Josephine Mensah-Kane, Stefanie Menzies, Irene Monahan, Catherine M. Moore, Gerhard Nebe-von-Caron, Sophie I. Owen, Chris Sainter, Amadou A. Sall, James Schouten, Christopher T. Williams, John Wilkins, Kevin Woolston, Joseph R.A. Fitchett, Sanjeev Krishna,[2] Tim Planche[2]

We investigated the dynamics of seroconversion in severe acute respiratory syndrome coronavirus 2 (SARS-CoV-2) infection. During March 29–May 22, 2020, we collected serum samples and associated clinical data from 177 persons in London, UK, who had SARS-CoV-2 infection. We measured IgG against SARS-CoV-2 and compared antibody levels with patient outcomes, demographic information, and laboratory characteristics. We found that 2.0%–8.5% of persons did not seroconvert 3–6 weeks after infection. Persons who seroconverted were older, were more likely to have concurrent conditions, and had higher levels of inflammatory markers. Non-White persons had higher antibody concentrations than those who identified as White; these concentrations did not decline during follow-up. Serologic assay results correlated with disease outcome, race, and other risk factors for severe SARS-CoV-2 infection. Serologic assays can be used in surveillance to clarify the duration and protective nature of humoral responses to SARS-CoV-2 infection.

Severe acute respiratory syndrome coronavirus 2 (SARS-CoV-2) is a betacoronavirus that causes coronavirus disease (COVID-19), a respiratory infection with systemic involvement and an estimated 1% death rate (*1*). COVID-19 was first documented in Wuhan, China (*2*), at the end of 2019. The outbreak quickly transformed into a pandemic. Countries have tried to manage the pandemic by implementing different strategic interventions with varying levels of success (*3*). Experts agree that diagnostic tests, and the subsequent interventions they generate, are essential to controlling SARS-CoV-2 transmission.

Reverse transcription PCR (RT-PCR) relies on RNA sequencing rather than viral proteins, enabling researchers to develop assays shortly after the viral sequence is identified. Because of this advantage, RT-PCR quickly became a common testing method for COVID-19 (*4*). However, the urgent global scale-up of nucleic acid amplification testing, including PCR, exposed supply chain vulnerabilities, such as shortages of swabs and reagents. Diagnostic tests remain unaffordable in many developing countries, limiting national containment strategies.

Serologic assays for viral infections can contribute to vaccine development, diagnostic deployment, and prescription of new therapeutics. They

Author affiliations: St. George's, University of London, London, UK (H.M. Staines, D.E. Kirwan, D.J. Clark, Y. Augustin, M. Cuisinato, B.M.O. Davies, N.M. Eckersley, D. Forton, L. Hadcocks, Q. Hu, D.C. Macallan, I. Monahan, C.M. Moore, S. Krishna, T. Planche); Liverpool School of Tropical Medicine, Liverpool, UK (E.R. Adams, R.L. Byrne, A.I. Cubas-Atienzar, L.E. Cuevas, A.J. Fraser, G. Garrod, G.A. Kay, S. Menzies, S.I. Owen, C.T. Williams); Mologic, Thurleigh, UK (M. Cocozza, M. Davis, P. Davis, A. Duvoix, M. Johnson, K. Klekotko, Z. Lewis, J. Mensah-Kane, G. Nebe-von-Caron, C. Sainter, J. Schouten, J. Wilkins, K. Woolston, J.R.A. Fitchett); St. George's University Hospitals National Health Services Foundation Trust, London (D. Forton, S. Krishna, T. Planche); Institut Pasteur, Dakar, Senegal (A.A. Sall); Universitätsklinikum Tübingen, Tübingen, Germany (S. Krishna); Centre de Recherches Médicales de Lambaréné, Lambaréné, Gabon (S. Krishna)

DOI: https://doi.org/10.3201/eid2701.203074

[1]These first authors contributed equally to this article.

[2]These senior authors contributed equally to this article.

might also offer insight into pathophysiological aspects of COVID-19. We used ELISA (Mologic Ltd., https://mologic.co.uk) for COVID-19 to characterize the serologic response in SARS-CoV-2 infection. These tests were designed for affordability and accuracy, enabling access and manufacture in low- and middle-income countries. We used these tests on serum samples from persons with confirmed SARS-CoV-2 infection in London, UK, to identify demographic and clinical variables that might influence antibody responses.

## Methods

### Ethics

Development of the SARS-CoV-2 IgG ELISA is available elsewhere (E.R. Adams, unpub. data, https://www.medrxiv.org/content/10.1101/2020.04.29.20082099v1). We analyzed antibody dynamics using anonymized excess diagnostic material from patients with PCR-confirmed SARS-CoV-2 infection. The study was sponsored by St. George's Hospital National Health Services Foundation Trust (London) and has Institutional Review Board ethics approval (Development and Assessment of Rapid Testing for SARS-CoV-2 outbreak study; Integrated Research Application System project ID: 282104; Research Ethics Committee reference: 20/SC/0171). The trial is registered at ClinicalTrials.gov under NCT04351646.

### Reference RT-PCR

Staff at St. George's Hospital used Sigma Virocult (MWE, https://www.mwe.co.uk) to collect nose and throat swab samples from patients with SARS-CoV-2 infection; we prepared the samples with RNA extraction kits (Roche Molecular Systems Inc., https://www.lifescience.roche.com). We confirmed infection with the RealStar SARS-CoV-2 RT-PCR Kit selective for the S and E genes (Altona Diagnostics GmbH, https://www.altona-diagnostics.com) or cobas SARS-CoV-2 Test selective for the E gene and open reading frames 1ab (Roche Molecular Systems, Inc.).

### Clinical Samples

South West London Pathology (London) provides microbial diagnostic testing for the region, including St. George's Hospital, a tertiary teaching hospital. We obtained excess diagnostic material from South West London Pathology in the form of serum samples from patients with RT-PCR confirmed SARS-CoV-2 infection. The serum samples were anonymized and stored at 4°C for ≤2 weeks. Patients were sampled longitudinally to assess antibody dynamics; the data comprised ≥30 samples per day. If samples became unavailable from 1 patient (i.e., the patient was discharged or died), we added a new patient to the cohort. Excess diagnostic material was collected from 177 persons during March 29–May 22, 2020. The study population consisted of 9.9% (177/1,785) of persons (patients and staff) who tested positive for SARS-CoV-2 infection at South West London Pathology during this period.

### Participants and Clinical Data

We obtained data from patients' electronic medical records. We coded outcomes (as of May 22) as hospital admission, intensive care unit stay, death, or discharge. We recorded the length of hospital stay of patients who were discharged or died. We considered peaks of inflammatory markers (e.g., C-reactive protein [CRP]) to be the highest values recorded from 5 days before the first positive swab sample through the end of the study. We obtained blood values at the time of diagnosis (within 3 days after the first positive swab sample was taken).

### ELISA for SARS-CoV-2 IgG

We used the COVID-19 IgG ELISA developed by Mologic Ltd. and manufactured by Omega (Omega Diagnostics Group PLC, http://www.omega-diagnostics.com), according to the manufacturer's instructions (Appendix 1, https://wwwnc.cdc.gov/EID/article/27/1/20-3074-App1.pdf). The assay contained the spike and nucleoprotein antigens of SARS-CoV-2. Between plate coefficients of variation were 21.0% (lower cutoff) and 16.5% (positive control; n = 16). Higher ambient temperatures in the laboratory resulted in higher optical density readings (Appendix 2, https://wwwnc.cdc.gov/EID/article/27/1/20-3074- App2.xlsx).

### Statistical Analyses

We cross-checked and normalized raw ELISA data to enable comparison (Appendix 1; Figure 1). We also resolved manual handling errors (Appendix 1). We applied 2-tailed parametric and nonparametric tests as appropriate, using PRISM version 8.0 (https://www.graphpad.com) for data analysis and display. We conducted a 1-way analysis of variance to compare the effects of race and demographic information on patient outcomes. We used multivariate linear regression to determine the relationship between mean normalized optical density (NOD) and age, sex, peak CRP, number of concurrent conditions, respiratory symptoms, and race.

### Patient and Public Involvement

We acknowledge the importance of patient and public involvement in clinical studies. However, because of the rapid progression of COVID-19 and the challenges of lockdown in the United Kingdom, we did not have sufficient time to involve patients and members of the public in the development, implementation, or interpretation of this study.

## Results

We studied 177 patients who provided 645 distinct excess diagnostic material samples (Table 1). Patients were from diverse ethnic backgrounds (34% White, 35% non-White, 31% unreported; Appendix 1 Table 1), the a median age was 64 years (interquartile range [IQR] 52–77 years). Fifty-seven percent were male, and 73% had ≥1 concurrent condition. Nineteen percent were asymptomatic and did not report respiratory symptoms at admission; these patients tested positive for SARS-CoV-2 infection while receiving treatment for other conditions. Among the 143 symptomatic patients, the median time from symptom onset to testing was 6 days (IQR 3–9 days). Of the 177 patients, 166 (94%) were hospitalized, 7 (4%) were staff, and 4 (2%) were outpatients. Of the hospitalized patients, 44 (27%) died (median time to death was 19.1 days [IQR 14.8–24.8 days]), 108 (65%) were discharged (median length of stay was 19.3 days [IQR 10.6–31.1 days]), and 14 (8%) remained hospitalized at the end of the study. Sixty-three (38%) patients were admitted to intensive care during the study.

**Table 1.** Demographic and clinical characteristics of patients with severe acute respiratory syndrome coronavirus 2 infection, United Kingdom, 2020*

| Characteristics | Results |
|---|---|
| Median age, y (IQR) | 64 (52–77) |
| Median body mass index (IQR)† | 25.4 (21.9–30.5) |
| Sex | |
| M | 100 (56.5) |
| F | 77 (43.5) |
| Race | |
| White | 60 (33.9) |
| Non-White | 61 (34.5) |
| Other/not known | 56 (31.6) |
| Concurrent conditions | |
| 0 | 47 (26.6) |
| 1 | 52 (29.4) |
| 2 | 50 (28.2) |
| ≥3 | 28 (15.8) |
| Symptoms | |
| Symptomatic | 143 (80.8) |
| Median days from symptom onset to PCR (IQR) | 6 (3–9) |
| Diagnostic site | |
| Emergency department | 90 (50.8) |
| Outpatient | 12 (6.8) |
| Ward | 54 (30.5) |
| Intensive care unit | 14 (7.9) |
| Occupational health staff | 7 (4.0) |
| Treatment location | |
| Occupational health staff | 7 (4.0) |
| Outpatient | 4 (2.3) |
| Hospital | 166 (93.8) |
| Admitted to intensive care unit | 63 (38.0) |
| Outcomes | |
| Never hospitalized | 11 (6.2) |
| Discharged | 108 (61.0) |
| Median length of stay, d (IQR) | 19.3 (10.6–31.1) |
| Death | 44 (24.9) |
| Median length of stay, d (IQR) | 19.1 (14.8–24.8) |
| Death and/or ICU admission | 80 (45.2) |
| Still in hospital‡ | 14 (7.9) |

*Values are no. (%) except as indicated. ICU, intensive care unit; IQR, interquartile range.
†Height unavailable for 13 patients.
‡As of May 22, 2020.

We normalized optical densities proportional to levels of SARS-CoV-2 IgG (Figure 1, panel A). Of the 177 patients, 149 (84% [95% CI 78%–89%]) had already seroconverted at the time of the first serologic test, 13 (7.3% [95% CI 4.3%–12.1%]) seroconverted after the first serologic test, and 15 (8.5 % [95% CI 5.2–13.5%]) did not seroconvert during the entire follow-up period (Appendix 1 Figure 2). Of the 15 patients who did not seroconvert, samples from beyond day 20 were available for 4 patients (26%); we did not detect IgG in these samples. This finding suggests that 2.0%–8.5% of patients might not develop detectable IgG against SARS-CoV-2.

We plotted NODs by time after a patient's first positive swab sample (Figure 1, panel B) and after symptom onset (Figure 1, panel C). NODs plateaued ≈12 days after PCR and ≈19 days after symptom onset; this time difference is consistent with the median time of 6 days between symptom onset and PCR. After seroconversion, mean NODs remained stable over the course of the study (up to ≈60 days after symptom onset).

We assessed whether the rate of seroconversion was associated with patient age (≤70 or >70 years), sex, or respiratory symptoms. None of these variables were discernably associated with seroconversion rates (Appendix 1 Figure 3, panels A–C). NOD IgG levels were not associated with sex or the presence of respiratory symptoms. (Appendix 1 Figure 4, panels A, B).

Patients of non-White race had higher mean NODs than those of White race (1.06 vs. 0.85; $F = 1.61$, df = 119; p = 0.04 by unpaired Student *t*-test) (Appendix 1 Figure 4, panel C). No other differences were associated with race. We used a multivariate analysis to identify variables independently associated with NODs; the mean NOD was associated only with age, peak CRP, and race. Although age, sex, peak CRP, number of concurrent conditions, respiratory

symptoms, and race were associated with patient outcome in the univariate analysis, only peak CRP was associated with poor outcome in the multivariate analysis (Appendix 1).

Persons who seroconverted were older than those who did not (median age 65.5 vs. 41.0 years; p<0.01 by Mann-Whitney test) and more likely to have ≥1 concurrent condition (124/130 vs. 38/47; p<0.01 by Fisher exact test). History of hypertension was associated with a higher probability of seroconversion (74/75 persons with hypertension vs. 88/102 persons without hypertension; p<0.01 by Fisher exact test). Body mass index was higher among the group who seroconverted (25.7 vs. 21.2; p = 0.03 by Mann-Whitney test).

Unlike other markers of inflammation, CRP is routinely measured in patients with COVID-19. Rising CRP levels are indicators of a poor prognosis (if other causes are excluded), and are associated with cytokine release syndrome (*5*; Y. Woo, unpub. data, https://osf.io/mxsvw). CRP levels were significantly higher in patients with respiratory symptoms at diagnosis than in those without symptoms (Figure 2, panel A). Patients who died or required intensive care during the study period had higher CRP levels than patients who did not die or require intensive care (Figure 2, panel B). Patients who did not seroconvert had lower CRP levels than those who did (Figure 2, panel C). Peak CRP levels had more pronounced associations with outcomes and seroconversion than did CRP levels at the time of the first positive swab sample result (Figure 2, panels D–F). CRP levels peaked a median of 12 days (IQR 8–17 days) after symptom onset and 4 days (IQR 1–11 days) after the first positive PCR result. Other inflammatory markers, such as peak D-dimer, fibrinogen, and ferritin, were also higher in patients with respiratory symptoms at diagnosis. However, these data were available for fewer patients (Table 2; Appendix 1 Table 3).

## Discussion

Our results illustrate serologic responses over the course of SARS-CoV-2 infection. Serologic tests can enhance diagnostic capability, especially during later infection (*4*,*6*,*7*), when viral loads might decrease. Serologic testing might also inform surveillance, seroepidemiologic studies, and contact tracing. Our study shows that a substantial proportion of COVID-19 patients require 3–6 weeks to generate antibodies. Furthermore, 2.0%–8.5% of patients do not have detectable antibodies within 60 days after infection. Most research on antibody dynamics came from China during the early stages of the pandemic (*4*,*6*,*8*). Here, we describe variables that influence IgG dynamics in SARS-CoV-2 infections in diverse populations.

The performance metrics of this ELISA (Figure 1; Appendix 2) are comparable to other validated assays. This first-generation ELISA might confirm infection in patients without a virologic diagnosis. We applied this test to study an ethnically and clinically diverse population. In most persons who seroconverted, the conversion

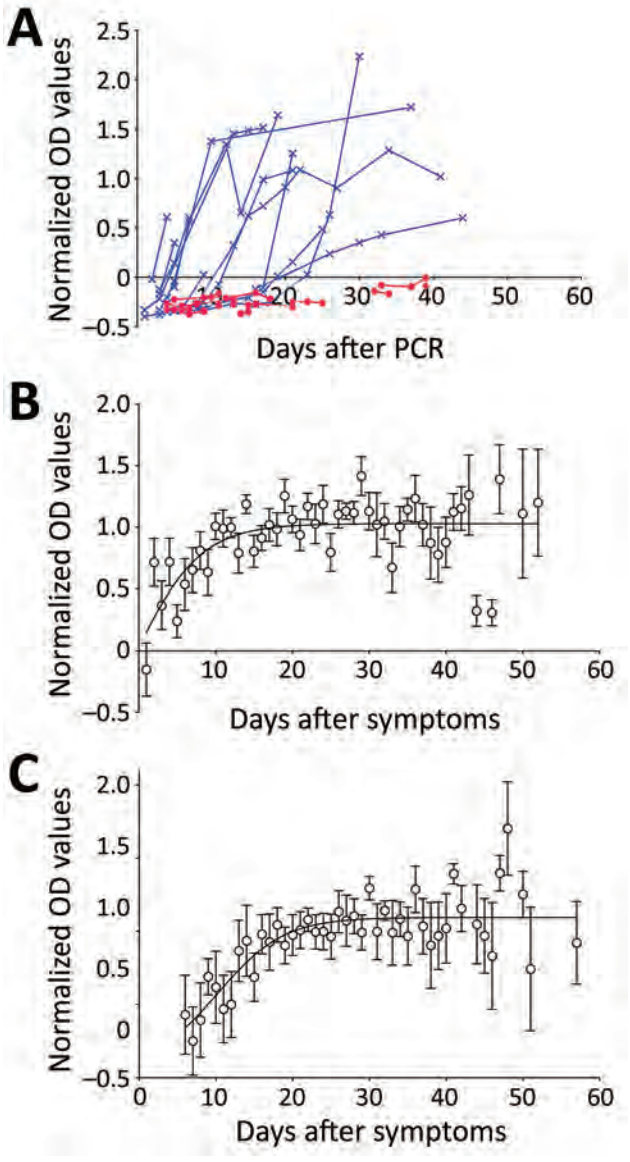


**Figure 1.** Antibody dynamics in patients with severe acute respiratory syndrome coronavirus 2, United Kingdom, 2020. A) NOD by days after first positive PCR result. Blue indicates seroconverting patients; red indicates nonseroconverting patients. B) Mean (± SEM) NODs (≥3 samples per time point; n = 48) by days after first positive PCR result for those who seroconverted. A 4-parameter sigmoidal unconstrained model is shown ($r^2$ = 0.45). C) Mean (± SEM) NODs (≥3 per time point; n = 45) by days after symptom onset for patients who seroconverted. A 4-parameter sigmoidal unconstrained model is shown ($r^2$ = 0.63). NOD, normalized optical density.

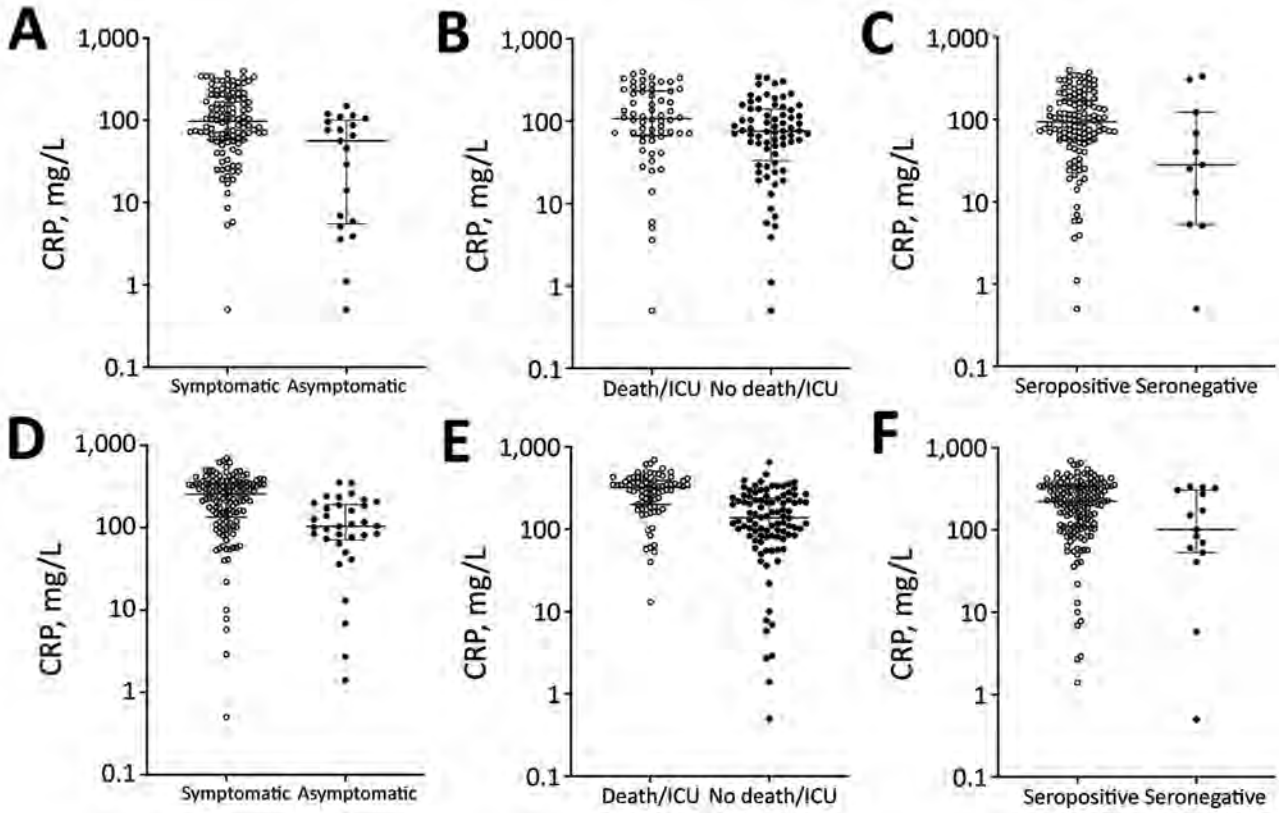


**Figure 2.** Relationships between CRP levels, symptoms, outcomes, and NODs of patients with severe acute respiratory syndrome coronavirus 2, United Kingdom, 2020. A–C) CRPs at diagnosis for A) 113 symptomatic (open circles) and 21 asymptomatic (closed circles) patients (CRP 97 vs. 56; p<0.01); B) 62 patients admitted to intensive care and/or who died (open circles) and 72 who were not admitted to intensive care (closed circles) (CRP 107 vs. 75.5; p = 0.01); C) 123 patients who seroconverted (open circles) and 11 who did not (closed circles) (CRP 93 vs. 28; p = 0.04). D–F) Peak CRPs corresponding to the populations in A–C: D) 255 (n = 142) vs. 104 (n = 34) (p<0.01); E) 322 (n = 80) vs. 137.5 (n = 96) (p<0.01); F) 224 (n = 161) vs. 101 (n = 15) (p = 0.03). Statistical significance calculated using Mann-Whitney test for CRPs (mg/L). CRP, C-reactive protein; NOD, normalized optical density.

was relatively rapid; NODs remained stable for weeks after infection (Figure 1). The probability of seroconversion was associated with increased age and concurrent conditions such as hypertension and increased body mass index. Higher NODs were associated with non-White race, admission to hospital, and higher peaks for inflammatory markers, such as CRP. Higher antibody titers are associated with clinical severity (i.e., death or admission to intensive care during study) in our cohort, in agreement with findings from other studies (*4*).

CRP is a sensitive marker of elevated proinflammatory cytokines, including interleukin 6. These cytokines might play a central role in cytokine release syndrome, which is associated with increased risk for death (Y. Woo, unpub. data, https://osf.io/mxsvw). Interventions such as tocilizumab, an interleukin-6 receptor antibody, interrupt the proinflammatory cascade. Such interventions might limit disease progression and reduce risk for death (*9*; E. Baker, unpub. data, https://osf.io/d2nh8); they are being studied in several randomized clinical trials. In our study, a small proportion of patients did not seroconvert within 20 days after testing positive for SARS-CoV-2 infection. Several mechanisms might explain this finding. First, these patients might never seroconvert. Second, their immune responses might be confined to other antigens or mediated through T cells. Another probable explanation is that some relatively mild infections might be restricted to the mucosal cells of the respiratory tract, where antibody responses are dominated by the secretory immune system. In this scenario, the systemic immune system might produce little or no IgG.

The association of higher NODs with elevated CRPs could indicate several potential pathways. For example, antibody responses might be closely related to cytokine response syndrome, which in turn is associated with more severe disease and death. Alternatively, elevated CRPs might indicate a more pronounced innate immune response in persons already

**Table 2.** Selected laboratory values of patients with severe acute respiratory syndrome coronavirus 2 infection, United Kingdom, 2020*

| Variable (reference range) | At diagnosis | | Peak | |
|---|---|---|---|---|
| | No. | Median (IQR) | No. | Median (IQR) |
| C-reactive protein (0–5 mg/L) | 134 | 86 (52.5–164) | 176 | 215.5 (103–334) |
| Nadir lymphocytes count (1.1–4.0 × $10^9$/L) | 134 | 0.9 (0.6–1.4) | 177 | 0.6 (0.4–0.8) |
| Ferritin (30–400 μg/L) | 42 | 1,084 (630–1,721) | 89 | 1,335 (846–2,758) |
| Fibrinogen (1.6–4.8 g/L) | 133 | 5.5 (4.2–6.7) | 166 | 7.0 (5.5–9.15) |
| D-dimer (21–300 ng/mL) | 64 | 704 (395–1,079) | 111 | 1,905 (498–4,095) |
| Lactate dehydrogenase (0–250 U/L) | 47 | 475 (280–597.5) | 87 | 490 (344.5–704) |

*IQR, interquartile range.

at risk for severe disease and death. This heightened innate response might be associated with a higher viral load (potentially caused by enhanced viral replication mechanisms) and genetic interactions that influence innate inflammatory pathways. Therefore, a higher viral load might lead to higher NODs for antibodies in the acquired immune response pathways. Small trials on the potential therapeutic benefits of interventions using passive antibody transfer (*10*) suggest that the heightened innate response hypothesis is more probable (*11*). Higher antibody responses are also associated with higher doses of a nonreplicating Ad5-vectored vaccine for SARS-CoV-2 (*12*).

Limitations of PCR include difficulties with sampling; different sample types and techniques yield varying results. Furthermore, PCR demonstrates diminishing diagnostic yield for COVID-19 as respiratory viral loads fall and symptoms subside (*8*,*13*). It might also produce false positives caused by lingering viral nucleic acid, which is not infective yet can persist for weeks after infection. Contamination could also occur during sample handling; because PCR requires amplification steps, this assay has heightened risk for contamination. Serologic testing, and the ability to detect viral antigens, may increase diagnostic accuracy for COVID-19. Our findings support early studies suggesting that physicians should consider these diagnostic modalities in conjunction, especially when a patient has negative PCR results but has symptoms of COVID-19 (*6*). Many COVID-19 patients experience a delay in care, a trend that emphasizes the importance of containment strategies that encourage isolation.

One limitation of our study is that it is based mainly on hospitalized patients, of whom 1 in 5 did not have COVID-19 symptoms. Further studies should document antibody dynamics of patients with less severe infections, such as healthcare workers (*14*), and patients with low viral loads at the time of consultation. Our findings will complement the large cross-sectional and longitudinal serologic surveys, especially as high-quality tests become more widely available. NODs were within a limited dynamic range (we could not conduct dilution studies because of small sample volumes) but nevertheless associated with clinically relevant features of COVID-19. Prospective studies are assessing the relationships between viral loads and serologic responses in patients. Regular and long-term serologic assays will be essential to monitoring the duration of the humoral response and its protective role against SARS-CoV-2.

When interpreting serologic assays of COVID-19 patients, physicians should consider factors that can influence the probability of seroconversion. Our study elucidates some of these factors. We found that less severe infections and younger age were associated with reduced probability of seroconversion. Risk factors for more severe disease, such as non-White race, increased age, and hypertension, are also associated with increased inflammatory responses, higher normalized antibody titers, and probability of seroconversion.

This article was preprinted at https://www.medrxiv.org/content/10.1101/2020.06.07.20124636v2.

**Acknowledgments**

We are greatly indebted to the National Association of Blood Bikes for their unwavering assistance in transporting samples, prototypes, and validated devices between Liverpool, Bedford, and London. Without their help, we could not have delivered 2 Conformité Européenne–marked products in 8 weeks from project launch. We also thank the tireless laboratory staff and informatics team, especially James Lawrence, of South West London Pathology.

This study was supported by a UK Department for International Development/Wellcome Trust Epidemic Preparedness coronavirus grant (grant no. 220764/Z/20/Z) to J.R.A.F., S.K., H.M.S., E.R.A., L.E.C., A.A.S. and by the Rosetrees Trust and the John Black Charitable Foundation (grant no. M959) to H.M.S., D.J.C., T.P., S.K., and J.R.A.F. In addition, D.E.K. is supported by Medical Research Council, UK, under fellowship no. MR/P019978/2. H.M.S. is supported by the Wellcome Trust Institutional Strategic Support Fund (204809/Z/16/Z) awarded to St George's, University of London, London.

## About the Author

Dr. Staines leads a research group at St George's, University of London, London. His main research interests are infectious diseases and diagnostics.

## References


1. Yang X, Yu Y, Xu J, Shu H, Xia J, Liu H, et al. Clinical course and outcomes of critically ill patients with SARS-CoV-2 pneumonia in Wuhan, China: a single-centered, retrospective, observational study. [Erratum in: Lancet Respir Med. 2020;8:e26]. Lancet Respir Med. 2020;8:475–81. https://doi.org/10.1016/S2213-2600(20)30079-5
2. Chan JF, Yuan S, Kok KH, To KK, Chu H, Yang J, et al. A familial cluster of pneumonia associated with the 2019 novel coronavirus indicating person-to-person transmission: a study of a family cluster. Lancet. 2020;395:514–23. https://doi.org/10.1016/S0140-6736(20)30154-9
3. Our World in Data. Coronavirus pandemic (COVID-19). 2020 [cited 2020 Jun 5]. https://ourworldindata.org/coronavirus
4. Zhao J, Yuan Q, Wang H, Liu W, Liao X, Su Y, et al. Antibody responses to SARS-CoV-2 in patients of novel coronavirus disease 2019. Clin Infect Dis. 2020 Mar 28 [Epub ahead of print]. https://doi.org/10.1093/cid/ciaa344
5. Ruan Q, Yang K, Wang W, Jiang L, Song J. Clinical predictors of mortality due to COVID-19 based on an analysis of data of 150 patients from Wuhan, China. [Erratum in: Intensive Care Med. 2020;46:1294–7]. Intensive Care Med. 2020;46:846–8. https://doi.org/10.1007/s00134-020-05991-x
6. Guo L, Ren L, Yang S, Xiao M, Chang D, Yang F, et al. Profiling early humoral response to diagnose novel coronavirus disease (COVID-19). Clin Infect Dis. 2020;71:778–85. https://doi.org/10.1093/cid/ciaa310
7. Kucirka LM, Lauer SA, Laeyendecker O, Boon D, Lessler J. Variation in false-negative rate of reverse transcriptase polymerase chain reaction-based SARS-CoV-2 tests by time since exposure. Ann Intern Med. 2020;173:262–7. https://doi.org/10.7326/M20-1495
8. Long QX, Liu BZ, Deng HJ, Wu GC, Deng K, Chen YK, et al. Antibody responses to SARS-CoV-2 in patients with COVID-19. Nat Med. 2020;26:845–8. https://doi.org/10.1038/s41591-020-0897-1
9. Xu X, Han M, Li T, Sun W, Wang D, Fu B, et al. Effective treatment of severe COVID-19 patients with tocilizumab. Proc Natl Acad Sci U S A. 2020;117:10970–5. https://doi.org/10.1073/pnas.2005615117
10. Salazar E, Perez KK, Ashraf M, Chen J, Castillo B, Christensen PA, et al. Treatment of coronavirus disease (COVID-19) patients with convalescent plasma. Am J Pathol. 2020;190:1680–90. https://doi.org/10.1016/j.ajpath.2020.05.014
11. Jiang S, Hillyer C, Du L. Neutralizing antibodies against SARS-CoV-2 and other human coronaviruses. [Erratum in: Trends Immunol. 2020;41:545]. Trends Immunol. 2020;41:355–9. https://doi.org/10.1016/j.it.2020.03.007
12. Zhu FC, Li YH, Guan XH, Hou LH, Wang WJ, Li JX, et al. Safety, tolerability, and immunogenicity of a recombinant adenovirus type-5 vectored COVID-19 vaccine: a dose-escalation, open-label, non-randomised, first-in-human trial. Lancet. 2020;395:1845–54. https://doi.org/10.1016/S0140-6736(20)31208-3
13. Xie C, Jiang L, Huang G, Pu H, Gong B, Lin H, et al. Comparison of different samples for 2019 novel coronavirus detection by nucleic acid amplification tests. Int J Infect Dis. 2020;93:264–7. https://doi.org/10.1016/j.ijid.2020.02.050
14. Fafi-Kremer S, Bruel T, Madec Y, Grant R, Tondeur L, Grzelak L, et al. Serologic responses to SARS-CoV-2 infection among hospital staff with mild disease in eastern France. EBioMedicine. 2020;59:102915. https://doi.org/10.1016/j.ebiom.2020.102915


Address for correspondence: Sanjeev Krishna, Institute for Infection & Immunity, St. George's, University of London, Cranmer Terrace London, SW17 0RE, UK; email: s.krishna@sgul.ac.uk; Tim Planche, Department of Medical Microbiology, St. George's University Hospitals NHS Foundation Trust, Blackshaw Rd, London, SW17 0QT, UK; email: tplanche@sgul.ac.uk

# Performance of Nucleic Acid Amplification Tests for Detection of Severe Acute Respiratory Syndrome Coronavirus 2 in Prospectively Pooled Specimens

Hannah Wang, Catherine A. Hogan, Jacob A. Miller, Malaya K. Sahoo, ChunHong Huang, Kenji O. Mfuh, Mamdouh Sibai, James Zehnder, Brendan Hickey, Nasa Sinnott-Armstrong, Benjamin A. Pinsky

Pooled nucleic acid amplification tests for severe acute respiratory syndrome coronavirus 2 could increase availability of testing at decreased cost. However, the effect of dilution on analytical sensitivity through sample pooling has not been well characterized. We tested 1,648 prospectively pooled specimens by using 3 nucleic acid amplification tests for severe acute respiratory syndrome coronavirus 2: a laboratory-developed real-time reverse transcription PCR targeting the envelope gene, and 2 commercially available Panther System assays targeting open reading frame 1ab. Positive percent agreement (PPA) of pooled versus individual testing ranged from 71.7% to 82.6% for pools of 8 and from 82.9% to 100.0% for pools of 4. We developed and validated an independent stochastic simulation model to estimate effects of dilution on PPA and efficiency of a 2-stage pooled real-time reverse transcription PCR testing algorithm. PPA was dependent on the proportion of tests with positive results, cycle threshold distribution, and assay limit of detection.

The ability of clinical laboratories to meet the demand for severe acute respiratory syndrome coronavirus 2 (SARS-CoV-2) testing is critical for reducing coronavirus disease (COVID-19)–related illness, death, and economic impact. Pooled testing has the potential to decrease resources required for population-level screening and can provide valuable data to inform public health policies (*1*,*2*). Several previous experimental and modeling studies have demonstrated the feasibility of pooled SARS-CoV-2 nucleic acid amplification testing (NAAT), in pools of ≤32 individual samples (*3*–*9*). However, the potential increase in efficiency gained by pooled testing is offset by a theoretical dilution-related decrease in analytical sensitivity (*8*,*10*).

Despite this decrease in sensitivity, pooled testing of blood donors for transfusion-transmitted infections, such as those with HIV-1 and hepatitis C virus, has proven to be safe and effective (*11*). This efficacy varies depending on the performance characteristics of the assay, the prevalence of infection, viral load kinetics, and pooling size, and strategy. For agents with variable seasonal or geographic prevalence, such as West Nile virus, many blood banks use adaptive risk-based pooling strategies, switching from pooled to individual testing when there is an increase in regional prevalence (*12*). Adapting a similar risk-based pooling strategy for SARS-CoV-2 has the potential to enable more widespread testing of high-risk populations and asymptomatic critical infrastructure workers, guide aggressive contact-tracing measures, and help direct public health interventions to where they are most needed. However, there are limited prospective data on assay-specific performance characteristics of pooled testing to guide implementation of such a strategy. Furthermore, there is little evidence on parallel test performance of different assays on pooled samples to direct choice of method.

In this study, we aimed to evaluate the test performance characteristics of 1 laboratory-developed and 2 commercially available SARS-CoV-2 NAATs for 1,648 individual respiratory specimens prospectively grouped in pools of 8 and 4. We used these data to

Author affiliations: Stanford University School of Medicine, Stanford, California, USA (H. Wang, C.A. Hogan, J.A. Miller, M.K. Sahoo, C. Huang, J. Zehnder, N. Sinnott-Armstrong, B.A. Pinsky); Stanford Health Care, Stanford (K.O. Mfuh, M. Sibai, B.A. Pinsky); Stanford University, Stanford (N. Sinnott-Armstrong)

DOI: https://doi.org/10.3201/eid2701.203379

validate a stochastic model to estimate optimal pool size, efficiency, and expected positive percent agreement (PPA) of a 2-stage pooled testing algorithm that takes into account prevalence, viral load distribution, and assay analytical sensitivity.

## Methods

### Clinical Specimens

The Stanford Clinical Virology Laboratory receives samples from tertiary-care academic hospitals and affiliated outpatient facilities in the San Francisco Bay Area of California. Prospective pooling of consecutive nasopharyngeal or oropharyngeal swab specimens submitted for SARS-CoV-2 testing during the morning shift was conducted during June 10–19, 2020, for evaluation of a pool size of 8 and during July 6–July 23, 2020, for evaluation of a pool size of 4. Samples submitted for testing were collected from symptomatic and asymptomatic inpatients and outpatients, either for clinical care or in the context of COVID-related epidemiologic surveillance studies and drug trials at our institution. As samples from persons enrolled in these studies and trials were received daily in batches, they were randomly evenly distributed among pools on a daily basis. This distribution was conducted to preserve the independence between samples in the same pool; these samples had not been tested before receipt in our laboratory and were otherwise treated identically to nonresearch samples. Nonresearch samples were otherwise assigned to pools consecutively. Additional laboratorywide data on proportion of tests positive and cycle threshold ($C_t$) value distribution were obtained from all specimens (n = 74,162) tested during March 1–June 24, 2020. This study was conducted with Stanford institutional review board approval (protocol no. 48973), and individual consent was waived.

### Pool Size Determination

In this study, an initial pool size of 8 was selected on the basis of pilot experiments with pool sizes ranging from 4 to 10 (B.A. Pinsky, unpub. data), and the logistical consideration that pooling in multiples of 4 would be more efficient for the robotic liquid handlers in our laboratory. After review of the test performance characteristics of 8-sample pooling in conjunction with the results of an independent stochastic simulation model, additional testing was performed to evaluate a pool size of 4 to generate empiric data for further model validation. Subset analyses of first tests versus follow-up tests were conducted by retrospectively assigning pools to 1 of the 2 groups on the basis of the status of the positive sample(s) in that pool. Pools containing positive samples belonging to both groups were excluded from this analysis. To validate the performance of the model for additional pool sizes, an external in silico dataset was obtained on the basis of pool sizes of 3 and 5. The in silico analysis was performed according to US Food and Drug Administration recommendations (Appendix, https://wwwnc.cdc.gov/EID/article/27/1/20-3379-App1.pdf) (*13*).

### Sample Pooling, Extraction, and NAAT

Pools were constructed before nucleic acid extraction by combining 500 µL from each of the individual samples. For a pool size of 8, this resulted in a total volume of 4 mL and a dilution factor of 1:8. For a pool size of 4, this resulted in a total volume of 2 mL and a dilution factor of 1:4.

Subsequently, total nucleic acids were extracted from 500 µL taken from each pool and each individual specimen by using QIAsymphony and the QIAsymphony DSP Virus/Pathogen Midi Kit (QIAGEN, https://www.qiagen.com) and eluted into 60 µL of AVE buffer according to manufacturer's instructions. Real-time reverse transcription PCR (rRT-PCR) was performed by using an emergency use authorization laboratory-developed test (LDT) targeting the envelope gene with the Rotor-Gene Q Instrument (QIAGEN) as described (*14*–*16*), with pooled samples tested on the same run as component individual samples. A $C_t$ result of 40–45 was considered an indeterminate result, which was adjudicated by repeat testing and resulted as positive if reproducible with an acceptable amplification curve. Specimens were only reported as negative if the internal control human RNase P gene was detected at a $C_t$<35.

On the same day as QIAsymphony extraction, another 500 µL from each pool was transferred to a Hologic Panther Specimen Lysis Tube (Hologic, https://www.hologic.com) and tested by using the Panther Fusion SARS-CoV-2 Assay (Hologic) and Panther Aptima SARS-CoV-2 assay (Hologic) per the manufacturer's recommendations (*17*,*18*). In addition to the manufacturer-set cutoff value, receiver operating characteristic (ROC) curve analysis of pooled relative light unit (RLU) values, with individual test results as the reference method, was used to determine the optimal RLU discrimination threshold. A focused electronic medical record review was conducted for all samples.

### Statistical Analysis

ROC curve analysis was conducted by using R package pROC (*19*). PPA and negative percent agreement

(NPA) were calculated by using individual testing as the reference method and were reported with exact (Clopper-Pearson) 95% CIs (*20*). Passing-Bablok regression was used to compare $C_t$ values of the individual LDT, pooled LDTs, and pooled Panther Fusion assays. The 95% CIs of slope, intercept, and bias were calculated by using an ordinary nonparametric bootstrap resampling method with default parameters in R package mcr. Paired *t*-tests were used to compare the mean differences between paired $C_t$ values among different assays. A Student *t*-test was used to compare the mean difference between internal control RNase P $C_t$ values in false-negative and true-negative pools. All comparisons were 2-sided with type I error set at 0.05. We used the laboratory-wide $C_t$ value distribution and a separate limit of detection (LoD) experiment to develop a stochastic simulation model to estimate PPA and efficiency for a 2-stage pooled testing algorithm, which was subsequently validated by using the independent empiric pools of 8 and pools of 4 data, as well as in silico pools of 5 and pools of 3 data. We provide the methods used to develop this model (Appendix).

## Results

### Assay Comparisons for Pools of 8

To evaluate a pool size of 8, a total of 112 pools from 896 samples were each tested on 3 different NAAT platforms (Table 1). Two pools were invalid, 1 by the Panther Fusion assay (0.9%), and 1 by the Panther Aptima assay (0.9%), and were excluded from subsequent analysis. All 16 individual samples in these 2 pools showed negative results. The remaining 110 pools contained 880 individual samples. Four samples were tested in duplicate in 2 different pools and showed identical results. Among the 880 individual samples, 58 (6.6%) showed positive results and a median $C_t$ value of 31.4 (interquartile range 22.1–35.5). First-time diagnostic specimens had a higher median $C_t$ value than specimens that underwent follow-up tests (Table 2). ROC curve analysis for the Panther Aptima showed optimal cutoff values between 343 and 393 RLUs; a cutoff value of 350 was chosen as the nearest round number (Panther Aptima-350) (Appendix Table 1, Figure 1).

Among the tested pools of 8, a total of 41.8% (46/110) contained ≥1 positive sample. The positive pools comprised 36 pools with 1 positive sample, 9 pools with 2 positive samples, and 1 pool with 4 positive samples (Table 3). There were 3 false-positive pools, 1 on each platform, in which each of the individual samples showed negative results. The overall PPA of pooled testing ranged from 71.7% to 82.6%, and NPA ranged from 98.4% to 100.0% (Table 4). The 14 pools containing positive first-time diagnostic samples had higher PPAs than the 28 pools containing positive follow-up test samples in an LDT (Appendix Table 3).

There were 16 total pools for which ≥1 method showed false-negative results. Except for the 1 pool containing 4 positive specimens, which was not detected by Panther Aptima using the manufacturer's cutoff value (Panther Aptima-M), the remaining 15 false-negative pools each contained only 1 positive specimen. For all missed pools, the $C_t$ value of the individual positive sample was >34 (median 36.6, interquartile range 35.5–37.7) (Figure 1). Among individual positive specimens in the dataset for pools of 8, a total of 22 (37.9%) had $C_t$ values >34. A total of 13/22 (59.1%) were false negative for the LDT, 11/22 (50.0%) for the LDT Panther Fusion, 15/22 (68%) for the LDT Panther Aptima-M, and 8/22 (36.4%)for the LDT Panther Aptima-350. Each of these false-negative samples was collected from known symptomatic or convalescent-phase patients being monitored for viral clearance; none of these samples were initial diagnostic specimens. The pooled LDT RNase P internal control $C_t$ values were similar in false-negative (mean 23.5, 95% CI 22.7–24.3) and true-negative (mean 23.4, 95% CI 22.7–24.1; p = 0.7) pools.

**Table 1.** Performance of nucleic acid amplification tests for detection of severe acute respiratory syndrome coronavirus 2 in prospectively pooled specimens, by testing platform*

| Test name | Gene target(s) | Internal control | Method | Strategy | Reference |
|---|---|---|---|---|---|
| LDT | Envelope | RNase P | rRT-PCR | Pools of 8†, pools of 4† | (*1*,*14*–*16*) |
| Panther Fusion | ORF1ab | Reagent spike-in | rRT-PCR | Pools of 8†, pools of 5†, pools of 3‡ | (*17*) |
| Panther Aptima-M | ORF1ab | Reagent spike-in | TMA | Pools of 8 with manufacturer-set RLU cutoff† | (*18*) |
| Panther Aptima-350 | ORF1ab | Reagent spike-in | TMA | Pools of 8 with RLU cutoff of >350†§ | (*18*) |

*Panther Aptima-M, Panther Aptima with manufacturer-set relative light unit cutoff value; Panther Aptima-350, Panther Aptima with relative light unit cutoff value >350 considered positive. Both products were from Hologic (https://www.hologic.com). LDT, laboratory-developed test; ORF1ab, open reading frame 1ab; rRT-PCR, real-time reverse transcription PCR; RLU, relative light unit; TMA, transcription-mediated amplification.
†Pooled testing strategy was assessed empirically at Stanford Clinical Virology Laboratory, with individual samples evaluated by LDT.
‡Pooled testing strategy assessed by in silico sensitivity analysis, with individual samples evaluated by Panther Fusion.
§Panther Aptima RLU cutoff of 350 selected based on receiver operating characteristic curve (Appendix Figure 1, https://wwwnc.cdc.gov/EID/article/27/1/20-3379-App1.pdf).

**Table 2.** Proportion of tests positive for severe acute respiratory syndrome coronavirus 2 with median $C_t$ values in pooled testing and laboratorywide clinical testing datasets, subset by testing indication*

| Dataset | No. positive samples/no. total samples (%) | | | Median $C_t$ value (IQR) | | |
|---|---|---|---|---|---|---|
| | All | First | Follow-up | All | First | Follow-up |
| Pools of 8† | 58/880 (6.6) | 24/657 (3.7) | 34/223 (15.2) | 31.4 (22.1–35.5) | 24.4 (18.4–33.1) | 34.1 (29.0–36.8) |
| Pools of 4‡ | 38/768 (4.9) | 28/491 (5.7) | 10/277 (3.6) | 29.3 (20.3–33.9) | 27.5 (19.4–32.6) | 32.2 (24.9–34.5) |
| Hologic§ | 10,000/52,272 (19.1) | NA | NA | 26.2 (20.7–32.6) | NA | NA |
| Laboratory-wide¶ | 1,358/74,162 (1.8) | 1,109/66,070 (1.7) | 249/8,092 (3.1) | 28.5 (23.0–34.3) | 27.2 (22.2–32.4) | 34.2 (29.0–37.4) |
| March | 555/8,896 (6.2) | 489/8,557 (5.7) | 66/339 (19.5) | 26.7 (21.9–31.5) | 26.4 (21.8–31.2) | 28.6 (22.6–35.2) |
| April | 518/22,671 (2.3) | 404/21,167 (1.9) | 114/1,504 (7.5) | 30.6 (24.8–36.0) | 28.8 (22.7–34.6) | 35.4 (32.9–38.0) |
| May | 172/21,833 (0.8) | 136/19,505 (0.7) | 36/2,328 (1.5) | 27.5 (23.3–34.7) | 26.1 (22.5–31.3) | 35.4 (30.4–37.3) |
| June | 113/20,762 (0.5) | 80/16,841 (0.5) | 33/3,921 (0.84) | 28.2 (21.2–33.6) | 27.4 (21.3–32.7) | 30.6 (20.2–34.4) |

*$C_t$, cycle threshold; IQR, interquartile range; NA, not available.
†Pools of 8 specimens were tested in our clinical laboratory during June 10–19, 2020.
‡Pools of 4 specimens were tested in our clinical laboratory during July 6–23, 2020.
§Hologic dataset comprises specimens tested clinically by Panther Fusion (https://www.hologic.com) during March 1–July 31, 2020 at 2 different external sites. These data were used to perform in silico sensitivity analysis to evaluate pool sizes of 3 and 5.
¶Composed of clinical specimens obtained during March 1–June 24, 2020.

### Linearity Studies for Pools of 8

For pools containing only 1 positive sample, the pooled rRT-PCRs showed positive systematic bias when compared with the individual LDT assay, as shown by the Passing-Bablok regression intercept value being >0. Mean bias between pooled and individual $C_t$ values was 3.4 cycles (95% limits of agreement 1.2–5.6; p<0.001) by LDT and 4.0 cycles (95% limits of agreement 0.0–8.0; p<0.001) by Panther Fusion (Figure 2). Panther Fusion showed negative proportional bias when compared with individual and pooled LDTs, as shown by Passing-Bablok regression slopes with 95% CIs that do not contain 1. This result is additionally highlighted in the Bland-Altman plots, which demonstrate that at higher $C_t$ values, Panther Fusion outperforms the LDT.

### Model Estimates

The modeled PPA estimate is sensitive to the input parameters of proportion of positive tests, assay analytical sensitivity, and viral load distribution. The analytical sensitivity of the assay is approximated in this model by the $C_t$ value corresponding to the probability of detecting 95% of true-positive samples, otherwise known as the 95% LoD. Specimens with $C_t$ beyond the LoD are assigned a decreasing probability of detection on the basis of a probit regression curve, the shape of which was determined in the initial validation of the LDT (Appendix Figure 5). The viral load distribution of the tested population is approximated in this model by the proportion of samples with $C_t$ greater than the LoD. This makes the model output independent of the actual LoD $C_t$ value itself, enabling the model to be used across different rRT-PCRs.

**Table 3.** Results of 8-sample pooled testing, by testing platform and number of positive specimens per pool (n = 110) for detection of severe acute respiratory syndrome coronavirus 2*

| Pool no. | Pooled testing | | | | Individual testing | | |
|---|---|---|---|---|---|---|---|
| | LDT | Panther Fusion | Panther Aptima-M | Panther Aptima-350 | Positive, (no. 1 PP, no. >1 PP) | Negative | Total no. pools |
| 1 | + | + | + | + | 30 (21, 9) | 0 | 30 |
| 2 | + | + | – | + | 2 (1, 1) | 0 | 2 |
| 3 | + | + | – | – | 0 (0, 0) | 0 | 0 |
| 4 | + | – | + | + | 0 (0, 0) | 0 | 0 |
| 5 | + | – | – | + | 0 (0, 0) | 0 | 0 |
| 6 | + | – | – | – | 1 (1, 0) | 1† | 2 |
| 7 | – | + | + | + | 2 (2, 0) | 0 | 2 |
| 8 | – | + | – | + | 1 (1, 0) | 0 | 1 |
| 9 | – | + | – | – | 0 (0, 0) | 1‡ | 1 |
| 10 | – | – | + | + | 2 (2, 0) | 0 | 2 |
| 11 | – | – | – | + | 1 (1, 0) | 1§ | 2 |
| 12 | – | – | – | – | 7 (7, 0) | 61 | 68 |
| No. positive pools | 34 | 36 | 34 | 39 | 46 (36, 10) | – | – |
| No. negative pools | 76 | 74 | 76 | 71 | – | 64 | – |
| Total no. pools | 110 | 110 | 110 | 110 | – | – | 110 |

*Panther Aptima with manufacturer-set relative light unit cutoff. Panther Aptima-350, Panther Aptima with relative light unit cutoff value >350 was considered positive; $C_t$, cycle threshold; LDT, laboratory-developed test; Pos, positive; RLU, relative light unit; 1 PP, 1 positive specimen in pool; >1 PP, >2 positive specimens in pool; –, negative; +, positive.
†False-positive LDT $C_t$ value was 37.5.
‡False-positive Panther Fusion $C_t$ value was 38.8.
§False-positive Panther Aptima-350 RLU value was 434.

**Table 4.** Performance characteristics and efficiency of 8-sample and 4-sample pooled testing, by testing platform (n = 302), for detection of severe acute respiratory syndrome coronavirus 2 in prospectively pooled specimens*

| Testing platform | Pool size | PPA, % (95% CI) | NPA,% (95% CI) | Pools positive, % | Average test run/sample |
|---|---|---|---|---|---|
| LDT | 8 | 71.7 (56.5–84.0) | 98.4 (91.5–100.0) | 30.9 | 0.434 |
| Panther Fusion | 8 | 76.1 (61.2–87.4) | 98.4 (91.5–100.0) | 32.7 | 0.452 |
| Panther Aptima-M | 8 | 73.9 (58.9–85.7) | 100.0 (94.3–100.0) | 30.9 | 0.434 |
| Panther Aptima-350 | 8 | 82.6 (68.6–92.2) | 98.4 (91.5–100.0) | 34.5 | 0.470 |
| LDT | 4 | 94.3 (80.8–99.3)† | 100 (97.7–100.0) | 17.2 | 0.422 |
| Panther Fusion‡ | 4 | 100.0 (85.8–100.0) | 100 (96.7–100.0) | 17.6 | 0.426 |
| Panther Aptima-M | 4 | 82.9 (66.2–93.4)† | 100 (97.7–100.0) | 15.1 | 0.401 |
| Panther Aptima-350 | 4 | 88.6 (73.3–96.8)† | 100 (97.7–100.0) | 16.2 | 0.411 |

*Panther Aptima-M, Panther Aptima with manufacturer-set RLU cutoff value. Panther Aptima-350, Panther Aptima with RLU cutoff value >350 was considered positive. Both products from Hologic (https://www.hologic.com). LDT, laboratory-developed test; NPA, negative percent agreement; PPA, positive percent agreement; RLU, relative light unit.
†Restricting the performance characteristics comparison to only the 136 pools tested by Panther Fusion resulted in a PPA as follows: LDT 100% (95% CI 85.8%–100.0%), Aptima-M 91.7% (95% CI 73.0%–99.0%), and Aptima-350 95.8% (95% CI 78.9%–99.9%).
‡A total of 56 of the 192 pools tested on the other platforms were not tested by Panther Fusion.

If the assay analytical sensitivity is kept constant, but the tested population changes such that a greater proportion have a $C_t$ value beyond the 95% LoD, PPA decreases (Figure 3, panel A). Conversely, if the patient population is kept constant, but assay analytical sensitivity increases (i.e., from lower $C_t$ LoD to higher $C_t$ LoD), PPA increases (Figure 4, panel A). However, if assay analytical sensitivity changes and the tested population shifts accordingly such that it retains the same proportion $C_t$ >LoD, then the PPA stays constant (Appendix Figure 6). In contrast, the average expected tests per sample is almost entirely determined by pool size and prevalence, whereas analytical sensitivity (LoD $C_t$) and the underlying $C_t$ distribution minimally affect efficiency because of small absolute numbers of false-positive pools (Figure 3, panel B; Figure 4, panel B). To achieve a 5% absolute difference in efficiency with an increase in LoD $C_t$ from 32 to 40, a prevalence of 25% would be required.

Both PPA and tests per sample are highly dependent on pool size and prevalence of infection. As prevalence increases, PPA can counterintuitively increase with larger pool sizes because there is a greater likelihood of having more than 1 positive sample in a given pool, which would be expected to increase PPA. Similarly, test efficiency can decrease with larger pool sizes because the likelihood of deconvoluting a positive pool increases. Estimated PPA and average tests per sample for inputs of percentage of positive tests 0.1%–15.0% and proportion of samples with Ct value above the LoD ranging from 5% to 30% are available (Appendix Table 4).

### Model Sensitivity Analyses and Validation

One-way deterministic and probabilistic sensitivity analyses incorporating uncertainty in the underlying model assumptions of dilutional effect and probit regression shape demonstrate a moderate (±2% to ±7%) effect on PPA, which is more pronounced with larger pool sizes and proportion of $C_t$ values above the LoD (Appendix Figure 7). In contrast, these parameters have a much smaller effect on testing efficiency

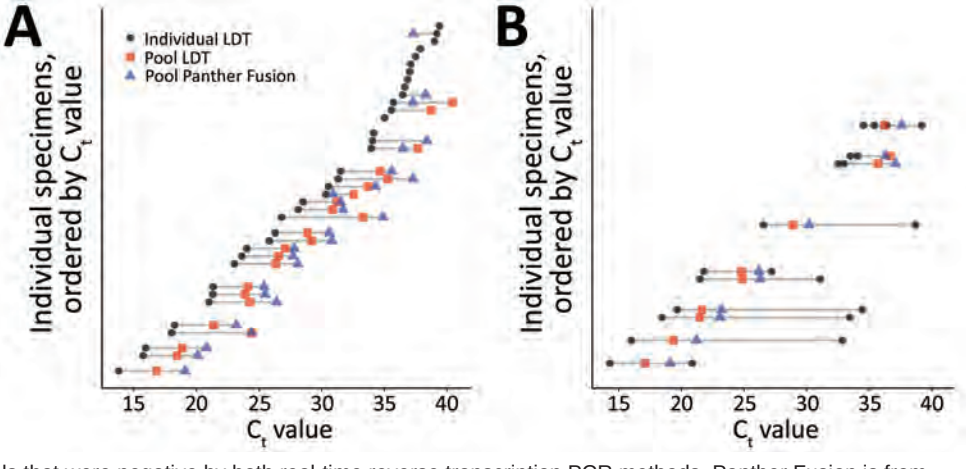


**Figure 1.** Performance of nucleic acid amplification tests for detection of severe acute respiratory syndrome coronavirus 2 in prospectively pooled specimens. For a pool size of 8, paired individual and pooled $C_t$ values for each individually positive sample (n = 58), in order of increasing individual $C_t$ value. A) Pools comprising only 1 positive sample/pool. B) Pools comprising ≥2 positive samples/pool. The gray lines span the range of $C_t$ values associated with a given pool. Rows without gray lines indicate individually positive samples belonging to pools that were negative by both real-time reverse transcription PCR methods. Panther Fusion is from Hologic (https://www.hologic.com). $C_t$, cycle threshold; LDT, laboratory-developed test.

(Appendix Figure 8). The 95% CIs for the empirically determined and modeled PPAs overlapped for most of the evaluated empiric datasets, although these values overestimated PPA for the LDT follow-up tests only subset (Figure 5). For the in silico validation data, the modeled PPA was similar for pool sizes of 5 and 3, despite in silico data analysis predicting a higher PPA for pools of 3. Modeled testing efficiency was actually slightly higher for pools of 3 than pools of 5, which was probably caused by the high prevalence of 19.1% in this dataset (Appendix Table 3).

## Discussion

In this study, >1,600 samples were tested in pool sizes of 8 and 4 by using 3 different SARS-CoV-2 platforms, and pooled testing showed decreased PPA relative to

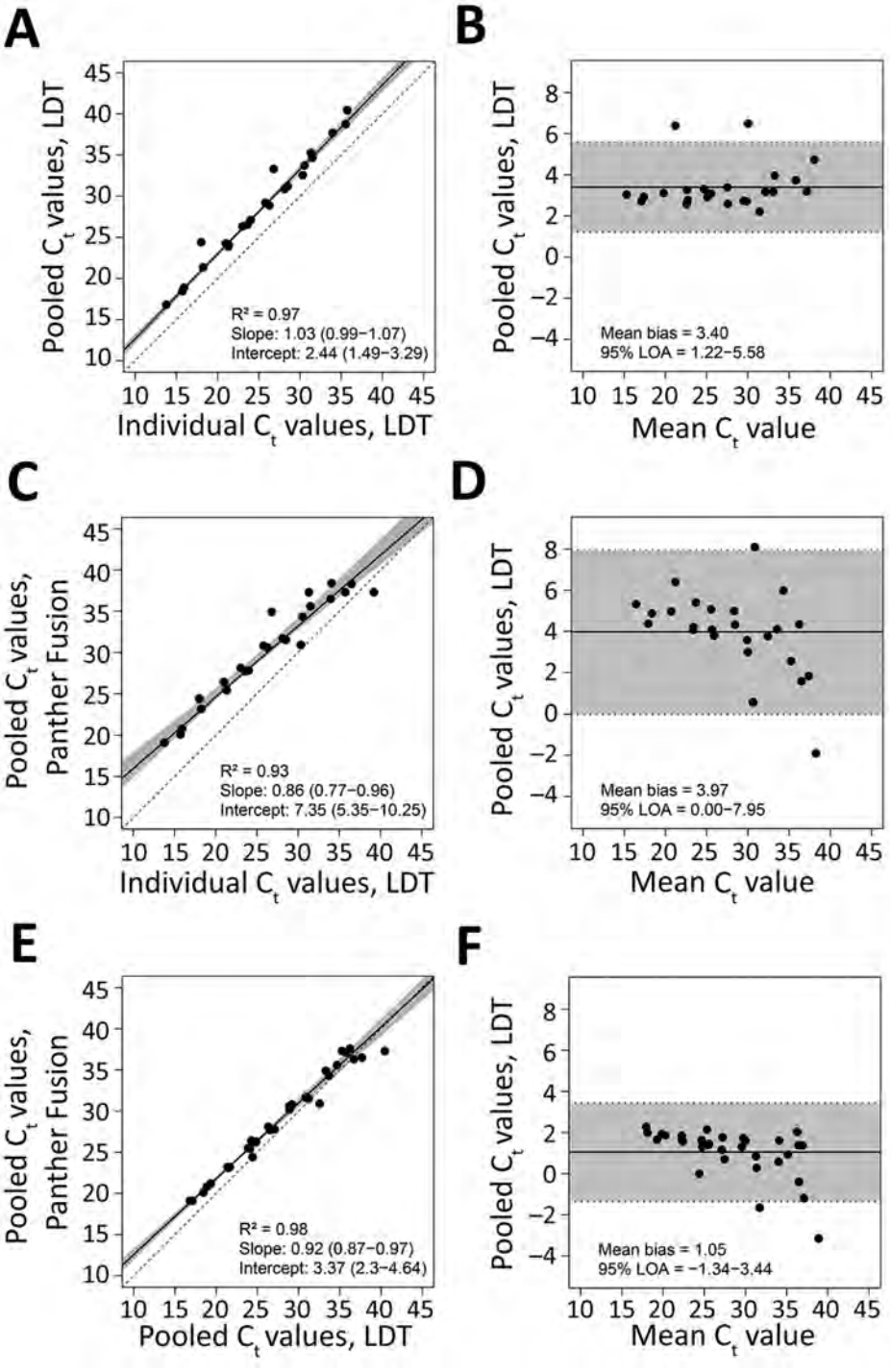


**Figure 2.** Performance of nucleic acid amplification tests for detection of severe acute respiratory syndrome coronavirus 2 in prospectively pooled specimens. Passing-Bablok regression and Bland-Altman plots for pools of 8 containing only 1 positive sample, tested by A and B) pooled LDT versus individual LDT (n = 23) (A, B); pooled Panther Fusion versus individual LDT (n = 25) (C, D); and pooled Panther Fusion versus pooled LDT (n = 32) (E, F). For the Passing-Bablok regression plots (A, C, and E), the solid line indicates the line of regression. 95% CIs are shaded in gray. The dashed line indicates the line of identity. The slope and intercept of the regression line are reported with 95% CIs in parentheses. For the Bland-Altman plots (B, D, and F), the solid line represents the mean difference in $C_t$ value. 95% limits of agreement are shaded in gray. Panther Fusion is from Hologic (https://www.hologic.com). $C_t$, cycle threshold; LDT, laboratory-developed test; LOA, limits of agreement.

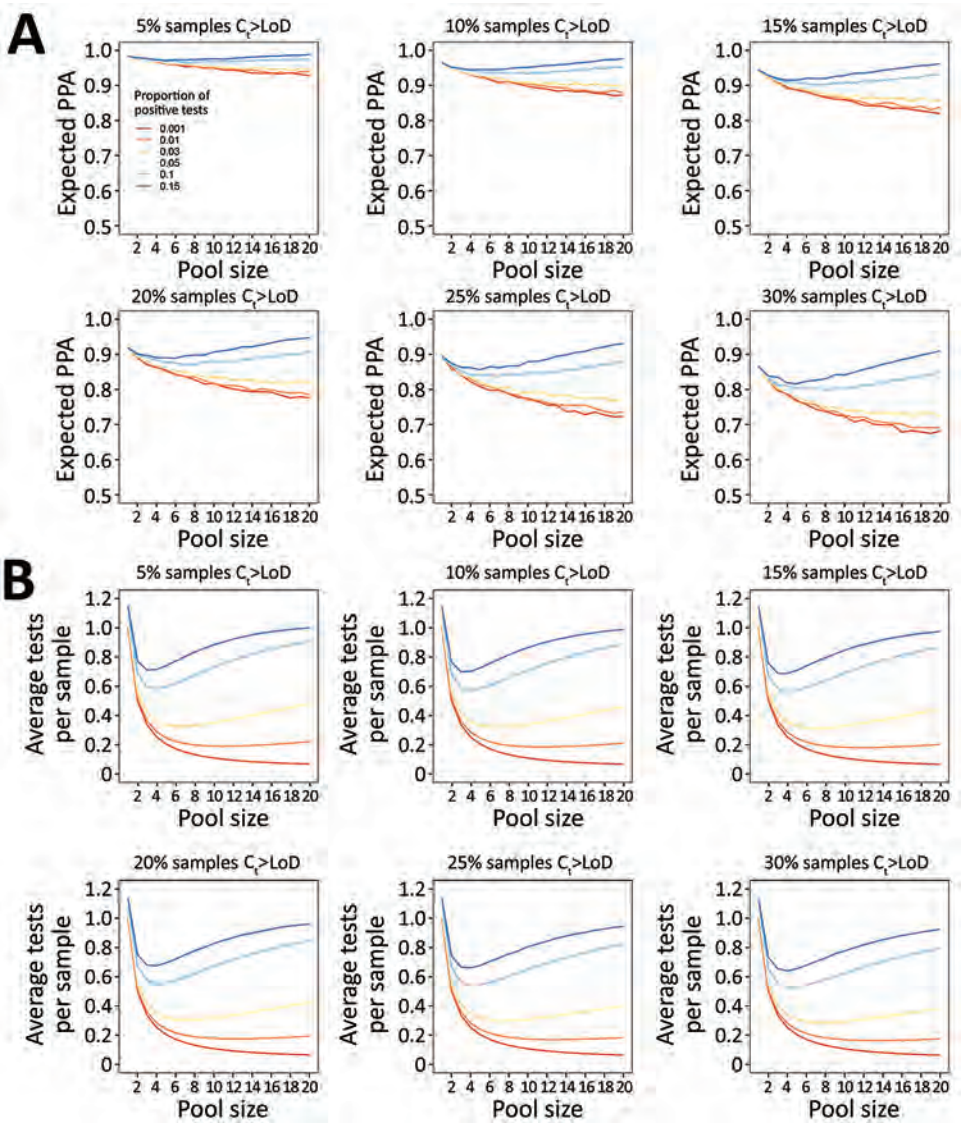


**Figure 3.** Performance of nucleic acid amplification tests for detection of severe acute respiratory syndrome coronavirus 2 in prospectively pooled specimens. Model-estimated PPA and testing efficiency, by pool size, proportion of tests positive, and proportion of samples with $C_t$ above the 95% LoD. For these estimates, LoD has been held constant at the experimentally-derived $C_t$ of 35.9, although results are independent of specific LoD value. A) Expected PPA between pooled and individual testing at pool sizes of 1–20. PPA decreases with decreasing proportion of test results positive (indicated by colored lines in each plot), and with increasing proportion of samples with $C_t$ values beyond the 95% LoD (each panel). At >5% test positivity, expected PPA starts to increase at larger pool sizes because there is a greater likelihood of 2 positive samples being in the same pool. The baseline PPA (pool size of 1) reflects the likelihood of obtaining the same individual result with repeat (nonpooled) testing. B) Estimated average tests per sample that would be performed at each pool size, with a lower number of average tests per sample corresponding to higher testing efficiency. Efficiency increases with decreasing proportion of test results positive, and slightly increases with increasing samples with $C_t$ above the LoD. Each missed pool results in fewer deconvolutions, and thus fewer total tests performed. $C_t$, cycle threshold; LoD, limit of detection; PPA, positive percent agreement.

individual samples. False-negative results occurred exclusively in pools containing samples with low estimated viral load ($C_t$ >34). Overlapping CIS in PPA and NPA at each pool size suggest that the lower test performance is inherent to the pooling process itself, rather than the assay. Although Panther Fusion $C_t$ values were on average higher than those of the LDT, the negative proportional bias suggests that at low estimated viral loads ($C_t$ >36), the Panther Fusion outperformed the LDT. This finding might be caused by the different targets of amplification (envelope gene versus open reading frame 1ab) or PCR efficiency. These subtle differences between the 2 assays highlight the method-dependent nature of test performance, a variable that cannot be anticipated, and therefore is not explicitly accounted for in most statistical models of pooled testing. Thus, method comparison studies should be performed before large-scale implementation of any pooled testing strategies, especially those that use different platforms for the pooled and individual stages of testing.

The findings of our study contrast with those of a recent study=, which concluded that pooling in groups of 8 did not compromise test performance (*5*). This finding might be explained by differences in patient population, higher proportion of positive pools

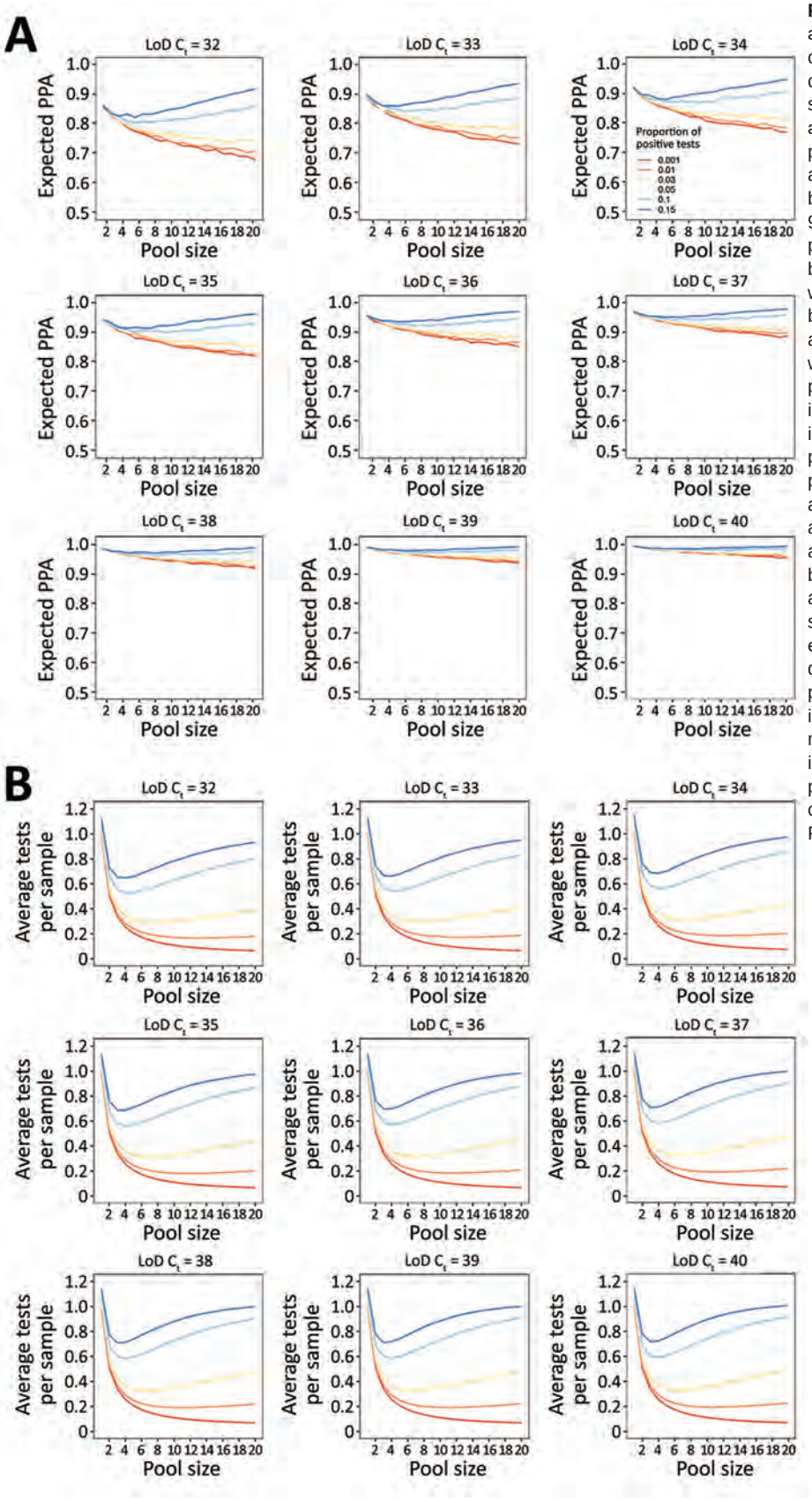


**Figure 4.** Performance of nucleic acid amplification tests for detection of severe acute respiratory syndrome coronavirus 2 in prospectively pooled specimens. Model-estimated PPA and testing efficiency, by pool size, proportion of tests positive, and assay analytical sensitivity as approximated by the $C_t$ corresponding to the 95% LoD. For these estimates, the population viral load distribution has been held constant at 15% of samples with $C_t$ values >35. A) Expected PPA between pooled and individual testing at pool sizes of 1–20. PPA decreases with decreasing proportion of tests positive (indicated by colored lines in each plot) and increases with increased analytical sensitivity (each panel). This result occurs because the proportion of individual samples with a $C_t$ value above each LoD decreases as the $C_t$ LoD increases. B) Estimated average tests per sample that would be performed at each pool size, with a lower number of average tests per sample corresponding to higher testing efficiency. Efficiency increases with decreasing proportion of test results positive, and slightly decreases with increased analytical sensitivity because more pools detected results in an increased number of individual tests performed at the deconvolution step. $C_t$, cycle threshold; LoD, limit of detection; PPA, positive percent agreement.

and rRT-PCR result interpretation. Another recent study of artificially constructed pools reported no major decrease in sensitivity in pools of ≤32 samples (*3*). This finding is probably explained by the relatively low starting $C_t$ values of individual positive samples in this study; none exceeded a $C_t$ of 30. However, this study and other experimental studies have shown empirical increases in pooled $C_t$ values directly proportional to dilution factor, a relationship that was also observed in our study (*3*,*4*,*9*).

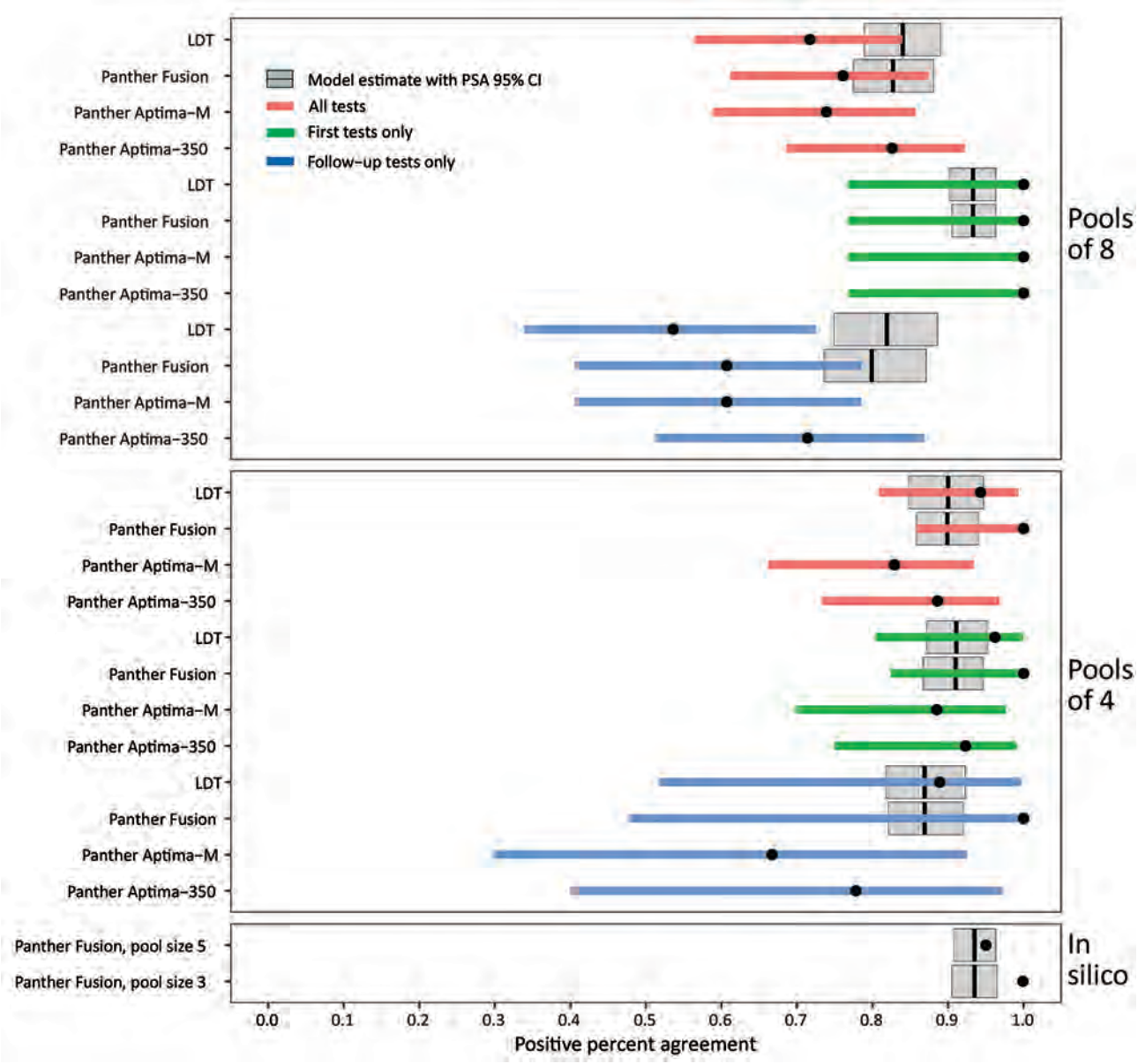


**Figure 5.** Performance of nucleic acid amplification tests for detection of severe acute respiratory syndrome coronavirus 2 in prospectively pooled specimens. Empiric and modeled estimates of positive percent agreement (PPA) with 95% CIs for each pool size, testing platform, and sample type (all versus first initial diagnostic versus follow-up). Black circles indicate empiric PPA point estimates, and colored horizontal bars indicate 95% CI. The 95% CI for the in silico data are too narrow to be visible in this plot. Gray boxplots indicate the modeled estimate of PPA, vertical black lines indicate the modeled PPA point estimate, and gray box indicates the 95% CI of the probabilistic sensitivity analysis. No modeled estimates are available for Panther Aptima because this is a transcription-mediated amplification assay, and the model is based on dilutional effects inherent to real-time PCR only. The empiric 95% CIs contain the modeled PPA point estimates for all conditions except for pools of 8 follow-up tests only and the in silico data. Data used to generate this figure are provided in Appendix Table 3 (https://wwwnc.cdc.gov/EID/article/27/1/20-3379-App1.pdf). Panther Fusion and Panther Aptima are from Hologic (https://www.hologic.com). LDT, laboratory-developed test; PSA, probabilistic sensitivity analysis.

These differences highlight the effect of viral load distribution and assay analytical sensitivity on pooled test performance, both of which should be taken into account when choosing pool size and diagnostic assay. Although samples with $C_t$ values >33 have not been reported to produce cultivable virus in convalescent phase COVID-19 patients (*21*), >15% of first-time diagnostic specimens in our laboratory were detected at a $C_t$ ≥35. A similar proportion of weakly positive samples that had high $C_t$ values at a public health department virology laboratory in New York has been described (S.B. Griesemer, unpub. data). Assays with lower analytical sensitivity may miss specimens with late $C_t$ values, for which the potential associated burden of onward transmission is currently unclear.

The stochastic model in this study demonstrated that expected PPA between pooled and individual rRT-PCRs was highly dependent on assay analytical sensitivity (represented by 95% LoD), viral load distribution of test-positive patients (represented by proportion $C_t$ >LoD), pool size, and disease prevalence (represented by proportion of tests positive). The model outputs were not always intuitive; larger pool sizes were not always less sensitive or more efficient. With increased prevalence, larger pool sizes were more sensitive because they were more likely to contain >1 positive sample/pool. They were also less efficient because a larger proportion were positive and required deconvolution.

The model output was largely independent of the actual LoD and viral load-to-$C_t$ value relationship of a given assay, making it generalizable across different rRT-PCRs. The only input parameters it requires are the proportion of positive test results and the proportion of samples with $C_t$ >LoD, both of which should be readily available to any laboratories conducting clinical testing. Future studies on the sensitivity of pooled testing strategies should report these parameters.

Previous models of pooled testing strategies for SARS-CoV-2 have primarily examined the effect of pool size and prevalence on testing efficiency but have not addressed the expected decrement in assay sensitivity that accompanies a putative increase in efficiency (*6*,*22*). Those studies that have examined sensitivity did not explicitly model the effect of variable viral load distribution of test-positive patients, a parameter that can vary based on the underlying patient population (asymptomatic versus symptomatic and severe versus nonsevere), purpose of testing (diagnostic versus follow-up), and specimen type (*8*,*23*–*27*). In addition, previous modeling studies and in silico analyses have mostly used the $C_t$ cutoff value of the assay, assuming 100% detection below the cutoff value, and 0% detection above it. In contrast, our model incorporates the probabilistic nature of detection at and above the LoD, which better approximates reality.

Our approach is limited by the generalizability of the probit regression shape and the equation estimating dilutional effect, as demonstrated by the variability seen on probabilistic and deterministic sensitivity analysis. Furthermore, the model assumes that the PCR is 100% efficient and that it is devoid of any proportional bias between individual and pooled tests. In addition, the model might underestimate PPA and efficiency of pooled testing if samples in each pool are not independent; placing samples with higher pretest probability in the same pool would decrease the total number of positive pools and increase the likelihood of detection. This feature could be leveraged by pooling specimens from persons in the same household or social distancing pod, such as coworkers on the same shift or students sharing a classroom. These factors, among others, might be the reasons for which the probabilistic sensitivity analysis CIs often did not contain the empiric point estimate in our validation data. These unaccounted-for factors might limit the ability of the model to provide a reliable point estimate.

The strengths of our study include its relatively large sample size, prospective rather than experimental construction of pools, and assessment of 2 different pool sizes. It also compared 3 different SARS-CoV-2 assays, 2 of which are commercially available on highly automated platforms suitable for large-scale testing. Our study was limited by its assessment of only a 2-stage pooling strategy. An additional limitation includes selection bias because the proportion of positive test results in the study specimens was higher because of the inclusion of follow-up samples from known COVID-19 patients enrolled in clinical research studies. Finally, test performance might vary depending on specimen collection medium, which we did not assess in this study (S.B. Griesemer, unpub. data).

In conclusion, a 2-stage pooled testing strategy for detection of SARS-CoV-2 by nucleic acid amplification is feasible and has the potential to strongly increase testing capacity. However, increased pool size and efficiency can compromise PPA. More studies examining early viral load kinetics and infectiousness are needed to fully evaluate the risks versus benefits of pooled testing. We provide a model to predict optimal pool size and associated expected PPA based on limit of detection, $C_t$ value distribution, and proportion

of positive test results. If this model can be externally validated, it might be useful in guiding SARS-CoV-2 pooled testing in other laboratories and as part of an adaptive risk-based strategy.

### Acknowledgments

We thank the Stanford Clinical Virology Laboratory staff for their dedication and commitment to patient care in the face of unprecedented challenges presented by the COVID-19 pandemic, and Hologic, Inc. for graciously providing in silico data from their pooling evaluations.

N.S.-A. is supported by a Stanford Graduate Fellowship.

Work was performed by B.H. during his personal time. B.H. is an employee of Google LLC.

## About the Author

Dr. Wang is a resident physician in the Department of Anatomic and Clinical Pathology at Stanford Hospital, Palo Alto, CA. Her primary research interests focus on infectious disease molecular diagnostics and the application of machine-learning algorithms and other computational methods to effectively leverage those diagnostics for patient care.

### References

1. Hogan CA, Sahoo MK, Pinsky BA. Sample pooling as a strategy to detect community transmission of SARS-CoV-2. JAMA. 2020;323:1967–9. https://doi.org/10.1001/jama.2020.5445
2. Wacharapluesadee S, Kaewpom T, Ampoot W, Ghai S, Khamhang W, Worachotsueptrakun K, et al. Evaluating the efficiency of specimen pooling for PCR-based detection of COVID-19. J Med Virol. 2020;May 13:2193–9. https://doi.org/10.1002/jmv.26005
3. Yelin I, Aharony N, Shaer Tamar E, Argoetti A, Messer E, Berenbaum D, et al. Evaluation of COVID-19 RT-qPCR test in multi-sample pools. Clin Infect Dis. 2020;May 2:ciaa531. https://doi.org/10.1093/cid/ciaa531
4. Abdalhamid B, Bilder CR, McCutchen EL, Hinrichs SH, Koepsell SA, Iwen PC. Assessment of specimen pooling to conserve SARS CoV-2 testing resources. Am J Clin Pathol. 2020;153:715–8. https://doi.org/10.1093/ajcp/aqaa064
5. Ben-Ami R, Klochendler A, Seidel M, Sido T, Gurel-Gurevich O, Yassour M, et al.; Hebrew University-Hadassah COVID-19 Diagnosis Team. Large-scale implementation of pooled RNA extraction and RT-PCR for SARS-CoV-2 detection. Clin Microbiol Infect. 2020;26:1248–53. https://doi.org/10.1016/j.cmi.2020.06.009
6. Eberhardt JN, Breuckmann NP, Eberhardt CS. Multi-stage group testing improves efficiency of large-scale COVID-19 screening. J Clin Virol. 2020;128:104382. https://doi.org/10.1016/j.jcv.2020.104382
7. Lohse S, Pfuhl T, Berkó-Göttel B, Rissland J, Geißler T, Gärtner B, et al. Pooling of samples for testing for SARS-CoV-2 in asymptomatic people. Lancet Infect Dis. 2020;3099:2019–20. https://doi.org/10.1016/S1473-3099(20)30362-5
8. Pilcher CD, Westreich D, Hudgens MG. Group testing for SARS-CoV-2 to enable rapid scale-up of testing and real-time surveillance of incidence. J Infect Dis. 2020;222:903–9. https://doi.org/10.1093/infdis/jiaa378
9. Eis-Hübinger AM, Hönemann M, Wenzel JJ, Berger A, Widera M, Schmidt B, et al. Ad hoc laboratory-based surveillance of SARS-CoV-2 by real-time RT-PCR using minipools of RNA prepared from routine respiratory samples. J Clin Virol. 2020;127:104381. https://doi.org/10.1016/j.jcv.2020.104381
10. Perchetti GA, Sullivan K-W, Pepper G, Huang M-L, Breit N, Mathias P, et al. Pooling of SARS-CoV-2 samples to increase molecular testing throughput. J Clin Virol. 2020;131:104570. https://doi.org/10.1016/j.jcv.2020.104570
11. Busch MP, Kleinman SH, Jackson B, Stramer SL, Hewlett I, Preston S. Committee report: nucleic acid amplification testing of blood donors for transfusion-transmitted infectious diseases: report of the Interorganizational Task Force on Nucleic Acid Amplification Testing of Blood Donors. Transfusion. 2000;40:143–59. https://doi.org/10.1046/j.1537-2995.2000.40020143.x
12. Custer B, Tomasulo PA, Murphy EL, Caglioti S, Harpool D, McEvoy P, et al. Triggers for switching from minipool testing by nucleic acid technology to individual-donation nucleic acid testing for West Nile virus: analysis of 2003 data to inform 2004 decision making. Transfusion. 2004;44:1547–54. https://doi.org/10.1111/j.0041-1132.2004.04227.x
13. Food and Drug Administration. Molecular diagnostic template for laboratories, July 28, 2020 [cited 2020 Sep 18]. https://www.fda.gov/media/135658/download
14. Food and Drug Administration. EUA summary: SARS-CoV-2 RT-PCR assay (Stanford Health Care Clinical Virology Laboratory). April 8, 2020 [cited 2020 Jul 11]. https://www.fda.gov/media/136818/download
15. Bulterys PL, Garamani N, Stevens B, Sahoo MK, Huang C, Hogan CA, et al. Comparison of a laboratory-developed test targeting the envelope gene with three nucleic acid amplification tests for detection of SARS-CoV-2. J Clin Virol. 2020;129:104427. https://doi.org/10.1016/j.jcv.2020.104427
16. Corman VM, Landt O, Kaiser M, Molenkamp R, Meijer A, Chu DKW, et al. Detection of 2019 novel coronavirus (2019-nCoV) by real-time RT-PCR. Euro Surveill. 2020;25:1–8. https://doi.org/10.2807/1560-7917.ES.2020.25.3.2000045
17. Food and Drug Administration. EUA summary: SARS-CoV-2 assay (Panther Fusion System), April 24, 2020 [cited 2020 Jul 11]. https://www.fda.gov/media/136156/download
18. Food and Drug Administration. EUA Summary: Aptima SARS-CoV-2, May 14, 2020 [cited 2020 Jul 11]. https://www.fda.gov/media/138096/download
19. Robin X, Turck N, Hainard A, Tiberti N, Lisacek F, Sanchez JC, et al. pROC: an open-source package for R and S+ to analyze and compare ROC curves. BMC Bioinformatics. 2011;12:77. https://doi.org/10.1186/1471-2105-12-77
20. Altman D, Machin D, Bryant T, Gardner M, editors. Statistics with confidence. 2nd ed. London: British Medical Journal Books; 2000.
21. La Scola B, Le Bideau M, Andreani J, Hoang VT, Grimaldier C, Colson P, et al. Viral RNA load as determined by cell culture as a management tool for discharge of SARS-CoV-2 patients from infectious disease wards. Eur J Clin Microbiol Infect Dis. 2020;39:1059–61. https://doi.org/10.1007/s10096-020-03913-9
22. Aragón-Caqueo D, Fernández-Salinas J, Laroze D. Optimization of group size in pool testing strategy for SARS-CoV-2: a simple mathematical model. J Med Virol. 2020;Apr 24:1988–94. https://doi.org/10.1002/jmv.25929

23. Cherif A, Grobe N, Wang X, Kotanko P. Simulation of pool testing to identify patients with coronavirus disease 2019 under conditions of limited test availability. JAMA Netw Open. 2020;3:e2013075. https://doi.org/10.1001/jamanetworkopen.2020.13075
24. Pan Y, Zhang D, Yang P, Poon LLM, Wang Q. Viral load of SARS-CoV-2 in clinical samples. Lancet Infect Dis. 2020;20:411–2. https://doi.org/10.1016/S1473-3099(20)30113-4
25. Xu T, Chen C, Zhu Z, Cui M, Chen C, Dai H, et al. Clinical features and dynamics of viral load in imported and non-imported patients with COVID-19. Int J Infect Dis. 2020;94:68–71. https://doi.org/10.1016/j.ijid.2020.03.022
26. To KK, Tsang OT, Leung WS, Tam AR, Wu TC, Lung DC, et al. Temporal profiles of viral load in posterior oropharyngeal saliva samples and serum antibody responses during infection by SARS-CoV-2: an observational cohort study. Lancet Infect Dis. 2020;20:565–74. https://doi.org/10.1016/S1473-3099(20)30196-1
27. Wölfel R, Corman VM, Guggemos W, Seilmaier M, Zange S, Müller MA, et al. Virological assessment of hospitalized patients with COVID-2019. Nature. 2020;581:465–9. https://doi.org/10.1038/s41586-020-2196-x

Address for correspondence: Benjamin A. Pinsky, Stanford University School of Medicine, 3375 Hillview, Rm 2913, Palo Alto, CA 94304, USA; email: bpinsky@stanford.edu

# Susceptibility of Domestic Swine to Experimental Infection with Severe Acute Respiratory Syndrome Coronavirus 2

Brad S. Pickering, Greg Smith, Mathieu M. Pinette, Carissa Embury-Hyatt, Estella Moffat, Peter Marszal, Charles E. Lewis

Severe acute respiratory syndrome coronavirus 2 (SARS-CoV-2), the agent that causes coronavirus disease, has been shown to infect several species. The role of domestic livestock and associated risks for humans in close contact with food production animals remains unknown for many species. Determining the susceptibility of pigs to SARS-CoV-2 is critical to a One Health approach to manage potential risk for zoonotic transmission. We found that pigs are susceptible to SARS-CoV-2 after oronasal inoculation. Among 16 animals, we detected viral RNA in group oral fluids and in nasal wash from 2 pigs, but live virus was isolated from only 1 pig. Antibodies also were detected in only 2 animals at 11 and 13 days postinoculation but were detected in oral fluid samples at 6 days postinoculation, indicating antibody secretion. These data highlight the need for additional livestock assessment to determine the potential role of domestic animals in the SARS-CoV-2 pandemic.

Severe acute respiratory syndrome coronavirus 2 (SARS-CoV-2) causes coronavirus disease (COVID-19) in humans; symptoms can range from asymptomatic to mild or severe, including severe respiratory distress and sometimes death (*1*). Rapidly spreading, the novel SARS-CoV-2 virus emerged in China in late 2019, and on March 11, 2020, the World Health Organization declared a pandemic (*2*). SARS-CoV-2 is believed to have originated in bats, but its origins are still under intense investigation, and reports continue to identify the ability of the virus to infect additional animal species (*3*–*8*).

Author affiliations: University of Manitoba, Winnipeg, Manitoba, Canada (B.S. Pickering); Canadian Food Inspection Agency, Winnipeg (B.S. Pickering, G. Smith, M.M. Pinette, C. Embury-Hyatt, E. Moffat, P. Marszal); Iowa State University, Ames, Iowa, USA (B.S. Pickering, C.E. Lewis)

DOI: https://doi.org/10.3201/eid2701.203399

Detection of natural infections sheds light on knowledge gaps in SARS-CoV-2 transmission and raised concerns of amplifying or reservoir hosts. In turn, clarification of wild and domestic animal susceptibility can help us assess their potential roles in and risks for transmission to prevent future disease spread. Domestic swine, one of the most highly produced agricultural species, previously have impacted public health (*9*–*12*). Backyard, small stakeholder animal production has increased in both rural and urban environments and provides a source of high-quality protein and income in these areas, but the practice also can serve as a source for zoonotic disease; therefore, the potential role of pigs in the spread of SARS-CoV-2 should be investigated (*13*). Recent evidence for involvement of production animals in SARS-CoV-2 transmission was highlighted in the Netherlands, where anthroponotic transmission from humans to farmed mink was proposed with subsequent zoonotic transmission to ≥2 humans from mink (*14*). That case further exemplifies the need to identify the potential role of production animals in disease transmission.

Angiotensin-converting enzyme 2 (ACE2) has been identified as the receptor for SARS-CoV-2 in human cells (*15*). A BLAST (https://blast.ncbi.nlm.nih.gov) query of the protein database by using translated nucleotide (BLASTx) from the human ACE2 coding sequence predicts 98% coverage and 81% identity for the homologous receptor in swine. Of note, using the same search, mink (*Mustela lutreola*) show 82% similar identity and domestic felines (*Felis catus*) show 85% similar identity to the human ACE2 for their cognate receptors. Moreover, mink and cats both have been reported to be susceptible to SARS-CoV-2 and have shown transmission to other animals (*5*,*16*). Zhou et al. (*17*) used in vitro infectivity studies testing ACE2

receptors from laboratory mice, horseshoe bats (*Rhinolophus sinicus*), civets, and the domestic pig, and found all receptors except those from mice entered HeLa cells, indicating a functional target for SARS-CoV-2. Moreover, the authors used additional known coronavirus receptors, including both aminopeptidase N and dipeptidyl peptidase 4, and found neither are used for cell entry (*17*), underlining the specificity for the ACE2 receptor.

We aimed to determine whether domestic swine are susceptible to SARS-CoV-2 infection by testing for live SARS-CoV-2 virus after experimental inoculation. After oronasal inoculation, we assessed swine for clinical signs and pathology, evidence of virus shedding, viral dissemination within tissues, and seroconversion.

## Methods

Experimental design, including housing conditions, sampling regimens, and humane endpoints, were approved by the Animal Care Committee of the Canadian Science Centre for Human and Animal Health (no. AUD #C-20-005). All procedures and housing conditions were in strict accordance with the Canadian Council on Animal Care guidelines. Group housing was in Biosecurity Level 3 (BSL-3) zoonotic large animal cubicles. Animals were provided commercial toys for enrichment and access to food and water ad libitum. All invasive procedures, including experimental inoculation and sample collection (nasal washes, rectal swabs, and blood collection), were performed under isoflurane gas anesthesia, and animals were euthanized by intravenous administration of a commercial sodium pentobarbital solution.

### Study Design

We obtained 19 domestic, 8-week-old American Yorkshire crossbred pigs (*Sus scrufa domesticus*), 6 castrated males and 13 females, locally sourced from a high health status farm in Manitoba, Canada. We obtained animals locally, rather than from a specific pathogen–free colony, to determine the risk to farmed pigs in Canada. We oronasally challenged 16 pigs with $1 \times 10^6$ PFU/animal in a total of 3 mL Dulbecco's Modified Eagle's Medium (DMEM; Wisent, http://www.wisentbioproducts.com) under sedation with isoflurane. We distributed 1 mL per nostril and placed 1 mL in the distal pharynx by using a sterile, tomcat-style catheter. We confirmed the challenge dose by back-titration of the inoculum on Vero E6 cells.

We divided the 16 inoculated pigs into 2 groups of 8, and each group was housed in a separate BSL-3 cubicle. At day 10, we introduced 2 naive pigs, 1 into each cubicle with the inoculated pigs, to serve as in-room transmission controls. Animal numbers were not based on power analysis but on limitations of the containment animal room size and requirements of Canadian Council on Animal Care guidelines. Group assignments for day of euthanasia and necropsy were based on randomization at the time of permanent animal identification via ear tags.

At the time of inoculation (day 0) and every other day beginning at 3 days postinoculation (dpi) until day 15, we performed a physical examination, including collection of blood; rectal, oral, and nasal swabs; and nasal wash with sterile Delbecco's phosphate-buffered saline (D-PBS). We began performing necropsies and post-mortem sampling starting at 3 dpi (Table 1). We sampled and necropsied 1 additional uninoculated pig to serve as a farm control providing negative control tissues. We sampled the remaining pigs at 22 dpi and 29 dpi. We collected group oral fluids from rope chews daily.

### Animal Sampling

Oral, rectal, and nasal swab specimens were taken from each pig under general anesthesia by using isoflurane. Samples were placed into sterile D-PBS containing streptomycin, vancomycin, nystatin, and gentamycin. Fluid was collected from a bilateral nasal wash by using sterile D-PBS. Blood was collected in serum, sodium citrate, sodium heparin, and K3 EDTA collection tubes via jugular venipuncture.

### Hematology, Chemistry, and Blood Gas Analyses

Hematology was performed on an HM5 analyzer (Abaxis, https://www.abaxis.com) by using K3 EDTA-treated whole blood. We evaluated erythrocytes, hemoglobin, hematocrit, mean corpuscular volume, mean corpuscular hemoglobin, mean corpuscular hemoglobin concentration, red cell distribution weight, platelets, mean platelet volume, leukocytes, and absolute and percent neutrophil count, lymphocyte count, monocyte count, eosinophil count, and basophil count. Blood chemistries were evaluated on a VetScan 2 (Abaxis) with Comprehensive Diagnostic Profile rotors (Abaxis) by using serum stored at −80°C until tested. We evaluated glucose, blood urea nitrogen, creatinine, calcium, albumin, total protein, alanine aminotransferase, aspartate aminotransferase, alkaline phosphatase, amylase, potassium, sodium, phosphate, chloride, globulin, and total bilirubin. We used sodium heparin-treated blood to analyze venous blood gases by using an iSTAT Alinity V (Abaxis) instrument with a

CG4+ cartridge (Abaxis) to measure lactate, pH, total carbon dioxide, partial pressure carbon dioxide, partial pressure oxygen, soluble oxygen, bicarbonate, and base excess. We used age-specific values and the instrument reference intervals to establish normal ranges (*18*–*20*).

### Necropsy

Necropsy was performed after euthanasia via sodium pentobarbital overdose, confirmation of death, and exsanguination by femoral artery laceration. We collected tissue samples from skeletal muscle, abdominal fat, liver, spleen, pancreas, duodenum, jejunum, ileum, spiral colon, kidney, gastrohepatic and mesenteric lymph nodes, right cranial lung lobe, right middle lung lobe, right caudal lung lobe, left cranial lung lobe, left caudal lung lobe, trachea, heart, tracheobronchial lymph nodes, cervical spinal cord, meninges, cerebrum, cerebellum, brainstem, olfactory bulb, nasal turbinates, submandibular lymph nodes, tonsils, trigeminal ganglion, and the entire eye. From female animals, we collected the uterus and ovaries of the reproductive tract en bloc. We collected epiglottis and laryngeal folds from some animals. We split tissue samples between 10% neutral-buffered formalin and fresh tissue. We also collected cerebrospinal fluid, urine (when possible), vitreous, and bronchoalveolar lavage by using DMEM.

We fixed tissues in 10% neutral phosphate-buffered formalin. We routinely processed and sectioned tissue at 5 μm and stained with hematoxylin and eosin (HE) for histopathologic examination. We performed in situ hybridization on 5 μm paraffin-embedded formalin-fixed tissue sections by using RNAscope 2.5HD Detection Reagent Red kit and V-nCoV2019-S probe (Advanced Cell Diagnostics, http://rna.acdbio.com). Then, we counterstained sections with Gill's 1 hematoxylin (Leica Biosystems, https://www.leicabio-systems.com), dried, and coverslipped.

We propagated SARS-CoV-2 isolate hCoV-19/Canada/ON-VIDO-01/2020 (GISAID accession no. EPI_ISL_425177), on Vero E6 cells in DMEM supplemented with 1% fetal bovine serum. We titrated virus by plaque assay and performed viral isolation as previously described (*21*,*22*).

### Tissue Homogenization and Virus Isolation

Weighed, frozen tissue sections in Precellys bead mill tubes (Bertin, https://en.esbe.com) were thawed, and we added D-PBS to make 10% (w/v) tissue homogenates. We processed tubes by using a Minilys personal tissue homogenizer (Bertin, https://www.bertin-instruments.com) and clarified by centrifugation at 2,000 × *g*. We used TriPure Reagent (Roche, https://www.roche.com) to inactivate clarified homogenates, swab specimens, and fluids collected from experimental animals and extracted RNA in duplicate. Samples positive by semiquantitative real-time RT-PCR (qRT-PCR) samples were tested for virus isolation through standard plaque assay on Vero E6 cells by using freshly prepared homogenates of frozen tissue.

**Table 1.** Sampling and necropsy schedule for pigs experimentally inoculated with SARS-CoV-2*

| | Days post inoculation | | | | | | | | | |
|---|---|---|---|---|---|---|---|---|---|---|
| Pig ID | 0 | 3 | 5 | 7 | 9 | 11 | 13 | 15 | 22 | 29 |
| Cubicle 1 | | | | | | | | | | |
| 20–01 | S | **S** | – | – | – | – | – | – | – | – |
| 20–02 | S | S | **S** | – | – | – | – | – | – | – |
| 20–03 | S | S | S | **S** | – | – | – | – | – | – |
| 20–04 | S | S | S | S | **S** | – | – | – | – | – |
| 20–05 | S | S | S | S | S | **S** | – | – | – | – |
| 20–06 | S | S | S | S | S | S | **S** | – | – | – |
| 20–07 | S | S | S | S | S | S | S | **S** | – | – |
| 20–08 | S | S | S | S | S | S | S | S | **S** | – |
| Cubicle 2 | | | | | | | | | | |
| 20–09 | S | **S** | – | – | – | – | – | – | – | – |
| 20–10 | S | S | **S** | – | – | – | – | – | – | – |
| 20–11 | S | S | S | **S** | – | – | – | – | – | – |
| 20–12 | S | S | S | S | **S** | – | – | – | – | – |
| 20–13 | S | S | S | S | S | **S** | – | – | – | – |
| 20–14 | S | S | S | S | S | S | **S** | – | – | – |
| 20–15 | S | S | S | S | S | S | S | **S** | – | – |
| 20–16 | S | S | S | S | S | S | S | S | **S** | **S** |
| Contact animals | | | | | | | | | | |
| 20–17 | S | S | S | S | S | S | S | S | S | **S** |
| 20–18 | S | S | S | S | S | S | S | S | **S** | – |
| 20–19 | S | S | S | S | **S** | – | – | – | – | – |

*Bold indicates necropsy. Underline indicates introduction of contact animal to cubicle 1 or 2. ID, identification; S, sample collected; SARS-CoV-2, severe acute respiratory syndrome coronavirus 2; –, no sample collected.

### RNA Extraction

We extracted total RNA from cell culture and experimental samples, including nasal, oral, and rectal swab specimens; nasal washes; oral fluids; whole blood in sodium citrate; and tissues by using MagMax CORE Nucleic Acid Purification Kits (ThermoFisher Scientific, https://www.thermofisher.com) per manufacturer's recommendation with the following modifications. In brief, we diluted samples in TriPure Reagent (Sigma-Aldrich, https://www.sigmaaldrich.com) at a 1:9 ratio and used this in place of the manufacturer's lysis buffer for inactivation. We used 650 µL of TriPure-inactivated sample, 30 µL of binding beads, and 350 µL of kit-provided CORE binding buffer spiked with ARM-ENTERO (Asuragen, https://asuragen.com) enteroviral armored RNA, then single washes in both wash 1 and wash 2 buffers, and a final elution volume of 30 µL of kit-supplied elution buffer by using the automated MagMax Express 96 system running the KingFisher-96 Heated Script MaxMAX_CORE_KF-96 (ThermoFisher Scientific). The spiked enteroviral armored RNA was used as an exogenous extraction and reaction control.

### Detection of SARS-CoV-2

We performed qRT-PCR on all extracted samples by using primers and a probe specific for SARS-CoV-2 envelope (E) gene (*23*), including forward primer E_SARBECO_F1 (5′-ACAGGTACGTTAATAGTTAATAGCGT-3′); reverse primer E_SARBECO_R2 (5′-ATATTGCAGCAGTACGCACACA-3′); and probe E_SARBECO-P1 (5′-ACACTAGCCATCCTTACTGCGCTzTCG-3′) We prepared master mix for qRT-PCR by using TaqMan Fast Virus 1-step Master Mix (ThermoFisher Scientific) according to manufacturer's specifications by using 0.4 µmol of each E gene primer and 0.2 µmol of probe per reaction. Reaction conditions were 50°C for 5 min, 95°C for 20 s, and 40 cycles of 95°C for 3 s then 60°C for 30 s. Runs were performed by using a 7500 Fast Real-Time PCR System (Thermofisher, ABI), and semiquantitative results were calculated based on a gBlock (Integrated DNA Technologies, https://www.idtdna.com) standard curve for SARS-CoV-2 E gene. For confirmation, we used SARS-CoV-2–specific primers targeting the spike (S) gene and the RNA-dependent RNA polymerase (RdRp) gene. For S, we used the forward primer SARS2_Spike_FOR (5′-TGATTGCCTTGGTGATATTGCT-3′); the reverse primer SARS2_Spike_REV (5′-CGCTAACAGTGCAGAAGTGTATTGA-3′); and the probe SARS2_Spike_Probe (5′-TGCCACCTTTGCTCACAGATGAAATGA-3′). For RdRp, we used forward primer RdRp_SARSr-F (5′-GTGARATGGTCATGTGTGGCGG-3′); reverse primer RdRp_SARSr-R (5′-CARATGTTAAASACACTATTAGCATA-3′); and probe RdRp_SARSr-P2 (5′-CAGGTGGAACCTCATCAGGAGATGC-3′). We tested all samples in duplicate and considered cycle threshold ($C_t$) <36 positive.

### Genome Sequencing

We were able to extract SARS-CoV-2 RNA from the submandibular lymph node of 1 pig (20–06), which was processed for high-throughput sequencing by CFIA National Centre for Foreign Animal Disease (NCFAD) Genomics Unit with enrichment for sequences for vertebrate viruses according to previously published method (*24*,*25*) and sequenced on a MiSeq (Illumina, https://www.illumina.com) using MiSeq Reagent Kit v3 (600-cycle; Illumina). Data analysis also were performed by the CFIA NCFAD Genomics Unit using nf-villumina version 2.0.0 (https://github.com/peterk87/nf-villumina), an in-house workflow developed by using Nextflow (*26*), which performed read quality filtering with fastp (*27*); Centrifuge version 1.0.4-beta (*28*) and Kraken2 version 2.0.8 (*29*) read taxonomic classification using an index of the National Center for Biotechnology Information (NCBI) nucleotide database (downloaded 2020 Feb 4); a Kraken2 index of NCBI RefSeq (https://www.ncbi.nlm.nih.gov/refseq) sequences of archaea, bacterial, viral, and human genomes GRCh38 (downloaded and built on 2019 Mar 22); removal of nonviral reads (i.e., not classified as belonging to superkingdom "Viruses" (NCBI taxonomic identification 10239) by using Kraken2 and Centrifuge taxonomic classification results; de novo metagenomics assembly of taxonomically filtered reads by Shovill version 1.0.9 (*30*), Unicycler version 1.0.9 (*31*), and Megahit version 1.2.9 (*32*); and nucleotide BLAST+ version 2.9.0 (*33*,*34*) search of all assembled contigs against the NCBI nucleotide BLAST database (downloaded 2020 April 10) using the "update_blastb.pl" script as part of the blast Bioconda package (*35*). We mapped nf-villumina taxonomically filtered reads against the top viral nucleotide BLAST match, SARS-CoV-2 isolate 2019-nCoV/USA-CA3/2020, MT027062.1, to generate a majority consensus sequence.

### Serum Neutralization Assays

We determined neutralizing antibody titers in serum samples by using a plaque reduction neutralization test (PRNT) against SARS-CoV-2. Serial 5-fold dilutions of heat inactivated (30 min at 56°C) serum samples were incubated with virus for 1 h at 37°C. Each virus–serum mixture was then added to duplicate wells of Vero E6 cells in a 48-well format, incubated for 1 h at 37°C, and overlaid with 500 µL

**Table 2.** Detection of SARS-CoV-2 by real-time reverse transcription PCR of samples from experimentally inoculated pigs*

| Samples | Days postinoculation | | | | | | | | | |
|---|---|---|---|---|---|---|---|---|---|---|
| | 0 | 3 | 5 | 7 | 9 | 11 | 13 | 15 | 22 | 29 |
| Swab specimens | 0/57 | 0/57 | 0/51 | 0/45 | 0/39 | 0/30 | 0/24 | 0/18 | 0/12 | 0/6 |
| Nasal wash | 0/16 | **2/16** | 0/14 | 0/12 | 0/12 | 0/10 | 0/8 | 0/6 | 0/4 | 0/2 |
| Blood | 0/16 | 0/16 | 0/14 | 0/12 | 0/12 | 0/10 | 0/8 | 0/6 | 0/4 | 0/2 |

*Results are reported as number positive/number of samples collected. Bold text indicates clinically significant findings. SARS-CoV-2, severe acute respiratory syndrome coronavirus 2.

of 2.0% carboxymethylcellulose in DMEM per well. Plates were then incubated at 37°C for 72 h, fixed with 10% buffered formalin, and stained with 0.5% crystal violet. Serum dilutions with >70% reduction of plaque counts compared with virus controls were considered positive for virus neutralization. We used negative serum samples plus virus controls to estimate the percent reduction.

### Surrogate Virus Neutralization Test

Detection and semiquantitation of neutralizing antibodies were determined by using SARS-CoV-2 Surrogate Virus Neutralization Test Kit (Genscript, https://www.genscript.com) according to the manufacturer's instructions. All samples from 7–29 dpi were assessed, including archived negative serum samples and kit-supplied negative controls. We considered values above the manufacturer's recommended cutoff of 20% positive for neutralization.

## Results

Starting at 1 dpi, a mild, bilateral ocular discharge developed in the 16 experimentally inoculated pigs; in some cases, this discharge was accompanied by serous nasal secretion. Discharge was observed for only the first 3 dpi. Temperatures among pigs remained normal throughout the study (Appendix Table 1, https://wwwnc.cdc.gov/EID/article/27/1/20-3399-App1.xlsx). Overall, animals did not develop clinically observable respiratory distress; however, 1 animal (pig 20–06) had mild depression with a cough at 1 dpi, which continued through 4 dpi. This animal did not display additional clinical signs over the course of the study.

Viral shedding can occur through droplets from coughing, sneezing, oral fluids, or gastrointestinal involvement. Thus, we developed a sampling schedule to determine the incidence of viral shedding (Table 1). Starting at 3 dpi, we sampled oral, nasal, and rectal swabs every other day up to 15 dpi, in case of delayed onset (*1*). We extracted nucleic acid from swabs and performed qRT-PCR to identify SARS-CoV-2 by targeting the E gene, but we did not detect viral RNA in swabs from any animals over the course of the study (Table 2).

Nasal washes are a sensitive method for detection of pathogens in swine, and we routinely sampled nasal washes by using sterile D-PBS to rinse nasal passages. Two pigs (20–10 and 20–11) displayed low levels of viral RNA by qRT-PCR at 3 dpi (Table 2). We attempted recovery of live virus from PCR-positive nasal wash samples, but neither produced cytopathic effect or increased RNA detection via qRT-PCR of the cell culture supernatant.

We also used a noninvasive, group sampling method to evaluate viral shedding. A cotton rope was hung in animal pens before feeding; when pigs chewed on the rope, they deposited oral fluids. We processed fluids from ropes daily and samples from cubicle 1 had a weak positive signal for viral RNA at 3 dpi by qRT-PCR (Tables 1, 3). We attempted virus isolation from this sample but were not able to isolate

**Table 3.** Detection of SARS-CoV-2 by real-time reverse transcription PCR of oral fluid samples from experimentally inoculated pigs*

| dpi | No. samples tested | No. samples positive |
|---|---|---|
| 0 | 2 | 0 |
| 1 | 2 | 0 |
| 2 | 2 | 0 |
| 3 | 2 | **1** |
| 4 | 2 | 0 |
| 5 | 2 | 0 |
| 6 | 2 | 0 |
| 7 | 2 | 0 |
| 8 | 2 | 0 |
| 9 | 2 | 0 |
| 10 | 2 | 0 |
| 11 | 2 | 0 |
| 12 | 2 | 0 |
| 13 | 2 | 0 |
| 14 | 2 | 0 |
| 15 | 2 | 0 |
| 16 | 2 | 0 |
| 17 | 2 | 0 |
| 18 | 2 | 0 |
| 19 | 2 | 0 |
| 20 | 2 | 0 |
| 21 | 2 | 0 |
| 22 | 1 | 0 |
| 23 | 1 | 0 |
| 24 | 1 | 0 |
| 25 | 1 | 0 |
| 26 | 1 | 0 |
| 27 | 1 | 0 |
| 28 | 1 | 0 |
| 29 | 1 | 0 |

*Oral fluid samples were collected from shared chew toys placed in enclosures for animal enrichment. Bold text indicates clinically significant results. dpi, days post inoculation; SARS-CoV-2, severe acute respiratory syndrome coronavirus 2.

the virus. Of note, the positive oral fluid did not come from the same room as the 2 positive nasal washes from pig 20–10 and pig 20–11, which were housed in cubicle 2. Therefore, at least 3 animals provide evidence of viral nucleic acid in oronasal secretions from 2 independent animal rooms. In addition, we did not detect viral infection at any point from the 2 naive transmission contact pigs introduced to the infected pigs at 10 dpi.

After collecting samples, we attempted SARS-CoV-2 detection from whole blood by qRT-PCR (Table 1). Viremia, as indicated by the presence of viral RNA in the blood, was not detected in any animal during the study (Table 2). We measured blood cell counts by using the VetScan HM5 (Abaxis), blood chemistries by using VetScan 2 (Abaxis), and blood gases by using i-STAT (Abbott, https://www.abbott.com). Although some laboratory variation was observed during the study, changes were minimal and inconclusive, and profiles consistent with acute viral infection or subsequent organ damage were not observed.

To identify potential target tissues or gross lesions consistent with SARS-CoV-2, we performed necropsy on 2 animals every other day from 3 dpi through 15 dpi and necropsied an additional 2 pigs at both 22 dpi and 29 dpi (Table 1). No clinically significant pathology was observed that could be attributed directly to a viral infection. We performed qRT-PCR across all tissues and samples collected at necropsy targeting the E gene of SARS-CoV-2 (Table 4). One tissue sample, the submandibular lymph node from pig 20–06, necropsied at 13 dpi, was positive by qRT-PCR ($C_t$ = 32) for viral RNA. The tissue sample testing was repeated in triplicate, on independent days, and generated consistent results. Further, RNA was extracted from homogenized tissue, and we recovered the full genome sequence of SARS-CoV-2 from pig 20–06.

**Table 4.** Detection of SARS-CoV-2 by real-time reverse transcription PCR of tissue samples from experimentally inoculated pigs*

| Pig ID | dpi | No. samples tested | No. samples positive |
|---|---|---|---|
| 20–01 | 3 | 35 | 0 |
| 20–09 | 3 | 35 | 0 |
| 20–02 | 5 | 36 | 0 |
| 20–10 | 5 | 35 | 0 |
| 20–03 | 7 | 35 | 0 |
| 20–11 | 7 | 35 | 0 |
| 20–04 | 9 | 35 | 0 |
| 20–12 | 9 | 34 | 0 |
| 20–05 | 11 | 35 | 0 |
| 20–13 | 11 | 36 | 0 |
| 20–06 | 13 | 35 | **1** |
| 20–14 | 13 | 35 | 0 |
| 20–07 | 15 | 36 | 0 |
| 20–15 | 15 | 35 | 0 |
| 20–08 | 22 | 35 | 0 |
| 20–18 | 22 | 35 | 0 |
| 20–16 | 29 | 35 | 0 |
| 20–17 | 29 | 35 | 0 |

*Tissue samples were collected from pigs during necropsy from skeletal muscle, abdominal fat, liver, spleen, pancreas, duodenum, jejunum, ileum, spiral colon, kidney, gastrohepatic and mesenteric lymph nodes, right cranial lung lobe, right middle lung lobe, right caudal lung lobe, left cranial lung lobe, left caudal lung lobe, trachea, heart, tracheobronchial lymph nodes, cervical spinal cord, meninges, cerebrum, cerebellum, brainstem, olfactory bulb, nasal turbinates, submandibular lymph nodes, tonsils, trigeminal ganglion, and the entire eye. Bold text indicates clinically significant results. dpi, days postinoculation; ID, identification; SARS-CoV-2, severe acute respiratory syndrome coronavirus 2.

We generated a 10% homogenate from the submandibular lymph node of pig 20–06 and used it to infect Vero E6 cells. We took aliquots from the cell culture on days 2 and 3 postinfection to monitor viral replication as indicated by an increasing quantity of RNA. On day 3, we observed mild cytopathogenic effect in the first passage with an increase in viral RNA measured by qRT-PCR targeting the E, S, and RdRp genes. The first passage supernatant was clarified by centrifugation and a second passage performed in Vero E6 cells. At day 2 postinfection of the second passage, we observed substantial cytopathogenic effect and increasing copies of SARS-CoV-2 viral RNA, confirmed by qRT-PCR. Together, these findings demonstrated the presence of live, replication-competent SARS-CoV-2 virus isolated from the submandibular lymph node of pig 20–06 (Table 2).

We monitored development of SARS-CoV-2 neutralizing antibodies over the course of study. Starting at 7 dpi, we obtained serum from individual animals for both virus neutralization test (VNT) and a surrogate VNT (sVNT) using cPass Neutralization Antibody Detection kit (Genscript, https://www.genscript.com). Serum samples first were tested by using a traditional VNT; 1 pig (20–07) generated neutralizing antibody titers, albeit weak, at a 1:5 dilution with a 70% reduction of plaques at both 13 dpi and 15 dpi (Table 5). Consequently, the sVNT assay identified the same animal, pig 20–07, as antibody-positive with 0.188 μg/mL antibody at 15 dpi. A second pig (20–14) generated antibodies at 11 dpi (0.113 μg/mL) and 13 dpi (0.224 μg/mL). We also used sVNT to identify secreted antibody in oral fluids. Of note, at 6 dpi we detected positive antibody (0.133 μg/mL) from group oral fluid collected from cubicle 1 (Table 5).

## Discussion

Our study found that domestic swine are susceptible to low levels of SARS-CoV-2 viral infection. Among

**Table 5.** Neutralizing antibody development in serum and oral fluids from pigs experimentally inoculated with SARS-CoV-2*

| Pig ID | Serum samples, dpi, VNT/sVNT | | | | | | |
|---|---|---|---|---|---|---|---|
| | 0 | 7 | 9 | 11 | 13 | 15 | 22 | 29 |
| 20–01 | –/– | –/– | –/– | –/– | –/– | –/– | –/– | –/– |
| 20–02 | –/– | –/– | –/– | –/– | –/– | –/– | –/– | –/– |
| 20–03 | –/– | –/– | –/– | –/– | –/– | –/– | –/– | –/– |
| 20–04 | –/– | –/– | –/– | –/– | –/– | –/– | –/– | –/– |
| 20–05 | –/– | –/– | –/– | –/– | –/– | –/– | –/– | –/– |
| 20–06 | –/– | –/– | –/– | –/– | –/– | –/– | –/– | –/– |
| 20–07 | –/– | –/– | –/– | –/– | **+/–** | **+/0.188** | –/– | –/– |
| 20–08 | –/– | –/– | –/– | –/– | –/– | –/– | –/– | –/– |
| 20–09 | –/– | –/– | –/– | –/– | –/– | –/– | –/– | –/– |
| 20–10 | –/– | –/– | –/– | –/– | –/– | –/– | –/– | –/– |
| 20–11 | –/– | –/– | –/– | –/– | –/– | –/– | –/– | –/– |
| 20–12 | –/– | –/– | –/– | –/– | –/– | –/– | –/– | –/– |
| 20–13 | –/– | –/– | –/– | –/– | –/– | –/– | –/– | –/– |
| 20–14 | –/– | –/– | –/– | **–/0.113** | **–/0.224** | –/– | –/– | –/– |
| 20–15 | –/– | –/– | –/– | –/– | –/– | –/– | –/– | –/– |
| 20–16 | –/– | –/– | –/– | –/– | –/– | –/– | –/– | –/– |
| 20–17 | –/– | –/– | –/– | –/– | –/– | –/– | –/– | –/– |
| 20–18 | –/– | –/– | –/– | –/– | –/– | –/– | –/– | –/– |
| 20–19 | –/– | –/– | –/– | –/– | –/– | –/– | –/– | –/– |

| | Oral sample collection, dpi† | | | | | | | | | | | | | | | |
|---|---|---|---|---|---|---|---|---|---|---|---|---|---|---|---|---|
| | 0 | 1 | 2 | 3 | 4 | 5 | 6 | 7 | 8 | 9 | 10 | 11 | 12 | 13 | 14 | 15 |
| All | – | – | – | – | – | – | **0.113** | – | – | – | – | – | – | – | – | – |

*Individual serum samples were collected from pigs; oral fluid samples were collected from shared rope chews placed in enclosures. VNT is measured 1:5; sVNT is measured µg/mL. Bold text indicates results with clinical significance. dpi, days post inoculation; sVNT, surrogate virus neutralization test; VNT, virus neutralization test; –, no detectable neutralizing antibodies; +, neutralizing antibodies detected.
†sVNT only.

16 experimentally inoculated animals, 5 (31.3%) displayed some level of exposure or elicited an immune response to the virus. Only 1 pig in our study retained live virus, but 2 other animals had detectible RNA measured in nasal wash, and another 2 developed antibodies. One pig (20–06) displayed mild, nonspecific clinical signs, including coughing and depression. Then, over the 9 days between cessation of clinical signs and postmortem evaluation, we found this pig maintained the virus in the submandibular lymph node, but virus was undetected in other samples from this animal. In addition, multiple pigs demonstrated mild ocular and nasal discharge that appeared during the immediate, postinfection period. Of note, among 5 animals with potential infection, we detected only low levels of viral RNA; no live viral shedding was identified.

After detection of viral RNA in group oral fluids collected by rope chews at 3 dpi, we detected secreted antibody by using sVNT; we detected viral RNA in the same sample type at 6 dpi. The amount of antibody measured in oral fluids from swine would be considered below a protective cutoff based on comparisons to classical neutralizing titers, however the discovery of secreted antibody in oral fluids might be useful for surveillance efforts. This finding also demonstrates the possibility that human saliva should be evaluated as a less invasive method to provide accompanying evidence with serosurveillance studies for exposure to SARS-CoV-2.

The results of this study contradict previous reports indicating swine are not susceptible to SARS-CoV-2 infection (*4*,*36*). Previous studies did not detect RNA in swabs or organ samples, and no seroconversion was measured. Infectious dose, viral isolate, age, and breed or colony of swine could affect study outcomes. Of note, we used a 10-fold higher viral dose for experimental infection than was used in previous studies. Moreover, we obtained animals from a high health status farm in Manitoba, rather than a specific pathogen–free colony, to determine the risk to farmed pigs in Canada. Altogether, these findings indicate that further investigations into the susceptibility of additional domestic livestock species should be conducted to assess their risk for infection and zoonoses. Finally, we emphasize that to date no SARS-CoV-2 cases among domestic livestock have been documented by natural infection; however, the results of this study support further investigations into the role that animals might play in the maintenance and spread of SARS-CoV-2.

This article was preprinted at https://biorxiv.org/cgi/content/short/2020.09.10.288548v1.

## Acknowledgments

We thank the Public Health Agency of Canada and Drs. Mubareka and Kozak at the Sunnybrook Health Sciences Centre, University of Toronto, and VIDO-Intervac at the University of Saskatchewan for SARS-CoV-2 isolate for this study. We also think the Animal Care and

Genomics units for their support during this project and Claire Andreasen for her review of the clinical pathology findings.

Funding for this project was provided by the Canadian Food Inspection Agency and the Canadian Institutes of Health Research. C.L. is funded through the United States Department of Agriculture Animal Plant Health Inspection Service's National Bio- and Agro-defense Facility Scientist Training Program.

Author contributions: B.P. conceived the research. B.P, G.S., M.M.P., E.M, P.M., and C.E.L. performed the experiments. B.P, G.S., M.M.P., C.E.H., and C.E.L. analyzed the data. B.P. wrote the manuscript with input from B.P, G.S., M.M.P., E.M., and C.E.L. All authors discussed the results and reviewed the manuscript.

## About the Author

Dr. Pickering is the head of the Special Pathogens Unit at the National Centre for Foreign Animal Disease with the Canadian Food Inspection Agency. His research focuses on high consequence pathogens including both emerging and reemerging zoonotic diseases of veterinary importance.

## References

1. Li Q, Guan X, Wu P, Wang X, Zhou L, Tong Y, et al. Early transmission dynamics in Wuhan, China, of novel coronavirus–infected pneumonia. N Engl J Med. 2020;382:1199–207. https://doi.org/10.1056/NEJMoa2001316
2. World Health Organization. WHO Director-General's opening remarks at the media briefing on COVID19, March 11, 2020 [cited 2020 Jun 14]. https://www.who.int/dg/speeches/detail/who-director-general-s-opening-remarks-at-the-media-briefing-on-covid-19---11-march-2020
3. Sia SF, Yan LM, Chin AWH, Fung K, Choy KT, Wong AYL, et al. Pathogenesis and transmission of SARS-CoV-2 in golden hamsters. Nature. 2020;583:834–8. https://doi.org/10.1038/s41586-020-2342-5
4. Shi J, Wen Z, Zhong G, Yang H, Wang C, Huang B, et al. Susceptibility of ferrets, cats, dogs, and other domesticated animals to SARS-coronavirus 2. Science. 2020;368:1016–20. https://doi.org/10.1126/science.abb7015
5. Oreshkova N, Molenaar R-J, Vreman S, Harders F, Oude Munnink BB, Hakze-van der Honing RW, et al. SARS-CoV-2 infection in farmed minks, the Netherlands, April and May 2020. Euro Surveill. 2020;25:2001005. https://doi.org/10.2807/1560-7917.ES.2020.25.23.2001005
6. Lam TT, Jia N, Zhang YW, Shum MH, Jiang JF, Zhu HC, et al. Identifying SARS-CoV-2-related coronaviruses in Malayan pangolins. Nature. 2020;583:282–5. https://doi.org/10.1038/s41586-020-2169-0
7. Andersen KG, Rambaut A, Lipkin WI, Holmes EC, Garry RF. The proximal origin of SARS-CoV-2. Nat Med. 2020;26:450–2. https://doi.org/10.1038/s41591-020-0820-9
8. Abdel-Moneim AS, Abdelwhab EM. Evidence for SARS-CoV-2 infection of animal hosts. Pathogens. 2020;9:E529. https://doi.org/10.3390/pathogens9070529
9. Smith TC, Harper AL, Nair R, Wardyn SE, Hanson BM, Ferguson DD, et al. Emerging swine zoonoses. Vector Borne Zoonotic Dis. 2011;11:1225–34. https://doi.org/10.1089/vbz.2010.0182
10. Chua KB, Bellini WJ, Rota PA, Harcourt BH, Tamin A, Lam SK, et al. Nipah virus: a recently emergent deadly paramyxovirus. Science. 2000;288:1432–5. https://doi.org/10.1126/science.288.5470.1432
11. Chua KB, Goh KJ, Wong KT, Kamarulzaman A, Tan PS, Ksiazek TG, et al. Fatal encephalitis due to Nipah virus among pig-farmers in Malaysia. Lancet. 1999;354:1257–9. https://doi.org/10.1016/S0140-6736(99)04299-3
12. Mansfield KL, Hernández-Triana LM, Banyard AC, Fooks AR, Johnson N. Japanese encephalitis virus infection, diagnosis and control in domestic animals. Vet Microbiol. 2017;201:85–92. https://doi.org/10.1016/j.vetmic.2017.01.014
13. Roth JA. Veterinary vaccines and their importance to animal health and public health. Procedia Vaccinol. 2011;5:127–36. https://doi.org/10.1016/j.provac.2011.10.009
14. Enserink M. Coronavirus rips through Dutch mink farms, triggering culls. Science. 2020;368:1169. https://doi.org/10.1126/science.368.6496.1169
15. Letko M, Marzi A, Munster V. Functional assessment of cell entry and receptor usage for SARS-CoV-2 and other lineage B betacoronaviruses. Nat Microbiol. 2020;5:562–9. https://doi.org/10.1038/s41564-020-0688-y
16. Halfmann PJ, Hatta M, Chiba S, Maemura T, Fan S, Takeda M, et al. Transmission of SARS-CoV-2 in domestic cats. N Engl J Med. 2020;383:592–4. https://doi.org/10.1056/NEJMc2013400
17. Zhou P, Yang XL, Wang XG, Hu B, Zhang L, Zhang W, et al. A pneumonia outbreak associated with a new coronavirus of probable bat origin. Nature. 2020;579:270–3. https://doi.org/10.1038/s41586-020-2012-7
18. Friendship RM, Lumsden JH, McMillan I, Wilson MR. Hematology and biochemistry reference values for Ontario swine. Can J Comp Med. 1984;48:390–3.
19. Perri AM, O'Sullivan TL, Harding JCS, Wood RD, Friendship RM. Hematology and biochemistry reference intervals for Ontario commercial nursing pigs close to the time of weaning. Can Vet J. 2017;58:371–6.
20. Ventrella D, Dondi F, Barone F, Serafini F, Elmi A, Giunti M, et al. The biomedical piglet: establishing reference intervals for haematology and clinical chemistry parameters of two age groups with and without iron supplementation. BMC Vet Res. 2017;13:23. https://doi.org/10.1186/s12917-017-0946-2
21. Weingartl HM, Berhane Y, Caswell JL, Loosmore S, Audonnet JC, Roth JA, et al. Recombinant nipah virus vaccines protect pigs against challenge. J Virol. 2006;80:7929–38. https://doi.org/10.1128/JVI.00263-06
22. Li M, Embury-Hyatt C, Weingartl HM. Experimental inoculation study indicates swine as a potential host for Hendra virus. Vet Res. 2010;41:33. https://doi.org/10.1051/vetres/2010005
23. Corman VM, Landt O, Kaiser M, Molenkamp R, Meijer A, Chu DK, et al. Detection of 2019 novel coronavirus (2019-nCoV) by real-time RT-PCR. Euro Surveill. 2020;25:2000045. https://doi.org/10.2807/1560-7917.ES.2020.25.3.2000045
24. Papineau A, Berhane Y, Wylie TN, Wylie KM, Sharpe S, Lung O. Genome Organization of Canada Goose Coronavirus, A Novel Species Identified in a Mass Die-off of Canada Geese. Sci Rep. 2019;9:5954. https://doi.org/10.1038/s41598-019-42355-y
25. Lung O, Nebroski M, Gupta S, Goater C. Genome Sequences of Ambystoma Tigrinum Virus Recovered during a Mass

Die-off of Western Tiger Salamanders in Alberta, Canada. Microbiol Resour Announc. 2019;8:e00265–19. https://doi.org/10.1128/MRA.00265-19
26. Di Tommaso P, Chatzou M, Floden EW, Barja PP, Palumbo E, Notredame C. Nextflow enables reproducible computational workflows. Nat Biotechnol. 2017;35:316–9. https://doi.org/10.1038/nbt.3820
27. Chen S, Zhou Y, Chen Y, Gu J. fastp: an ultra-fast all-in-one FASTQ preprocessor. Bioinformatics. 2018;34:i884–90. https://doi.org/10.1093/bioinformatics/bty560
28. Kim D, Song L, Breitwieser FP, Salzberg SL. Centrifuge: rapid and sensitive classification of metagenomic sequences. Genome Res. 2016;26:1721–9. https://doi.org/10.1101/gr.210641.116
29. Wood DE, Lu J, Langmead B. Improved metagenomic analysis with Kraken 2. Genome Biol. 2019;20:257. https://doi.org/10.1186/s13059-019-1891-0
30. Seemann T. tseemann/shovill [cited 2020 Jun 29]. https://github.com/tseemann/shovill
31. Wick RR, Judd LM, Gorrie CL, Holt KE. Unicycler: resolving bacterial genome assemblies from short and long sequencing reads. PLOS Comput Biol. 2017;13:e1005595. https://doi.org/10.1371/journal.pcbi.1005595
32. Li D, Luo R, Liu CM, Leung CM, Ting HF, Sadakane K, et al. MEGAHIT v1.0: A fast and scalable metagenome assembler driven by advanced methodologies and community practices. Methods. 2016;102:3–11. https://doi.org/10.1016/j.ymeth.2016.02.020
33. Camacho C, Coulouris G, Avagyan V, Ma N, Papadopoulos J, Bealer K, et al. BLAST+: architecture and applications. BMC Bioinformatics. 2009;10:421. https://doi.org/10.1186/1471-2105-10-421
34. Altschul SF, Gish W, Miller W, Myers EW, Lipman DJ. Basic local alignment search tool. J Mol Biol. 1990;215:403–10. https://doi.org/10.1016/S0022-2836(05)80360-2
35. Grüning B, Dale R, Sjödin A, Chapman BA, Rowe J, Tomkins-Tinch CH, et al.; Bioconda Team. Bioconda: sustainable and comprehensive software distribution for the life sciences. Nat Methods. 2018;15:475–6. https://doi.org/10.1038/s41592-018-0046-7
36. Schlottau K, Rissmann M, Graaf A, Schön J, Sehl J, Wylezich C, et al. SARS-CoV-2 in fruit bats, ferrets, pigs, and chickens: an experimental transmission study. Lancet Microbe. 2020;1:e218–25. https://doi.org/10.1016/S2666-5247(20)30089-6

Address for correspondence: Brad Pickering, Canadian Food Inspection Agency, 1015 Arlington St, Winnipeg, MB R3E 3M4, , Canada; email: bradley.pickering@canada.ca

# Intrafamilial Exposure to SARS-CoV-2 Associated with Cellular Immune Response without Seroconversion, France

Floriane Gallais, Aurélie Velay, Charlotte Nazon, Marie-Josée Wendling, Marialuisa Partisani, Jean Sibilia, Sophie Candon, Samira Fafi-Kremer

We investigated severe acute respiratory syndrome coronavirus 2 (SARS-CoV-2)–specific antibodies and T-cell responses against SARS-CoV-2 and human coronavirus (HCoV) 229E and OC43 in 11 SARS-CoV-2 serodiscordant couples in Strasbourg, France, in which 1 partner had evidence of mild coronavirus disease (COVID-19) and in 10 unexposed healthy controls. Patients with confirmed COVID-19 were considered index patients and their partners close contacts. All index patients displayed positive SARS-CoV-2–specific antibody and T-cell responses that lasted up to 102 days after symptom onset. All contacts remained seronegative for SARS-CoV-2; however, 6 reported COVID-19 symptoms within a median of 7 days after their partners, and 4 of those showed a positive SARS-CoV-2–specific T-cell response against 3 or 4 SARS-CoV-2 antigens that lasted up to 93 days after symptom onset. The 11 couples and controls displayed positive T-cell responses against HCoV-229E or HCoV-OC43. These data suggest that exposure to SARS-CoV-2 can induce virus-specific T-cell responses without seroconversion.

Coronavirus disease (COVID-19), caused by infection with severe acute respiratory syndrome coronavirus 2 (SARS-CoV-2), is a pandemic that raises a major concern all around the world (*1*). To contain the spread of the virus, several countries have imposed population lockdowns (*2*). In France, the first cases of COVID-19 were recorded at the end of January 2020 (*3*). Due to the rapid increase of new cases and death, a lockdown was imposed during March 17–May 11, 2020. After the lifting of the lockdown, the number of new cases of SARS-CoV-2 decreased substantially. However, we cannot exclude the possibility that a second pandemic wave could occur; an increase in new cases had already been observed in the first week of August 2020 in several regions (*4*).

Estimating infections with immunizing effects is crucial in helping to predict the postpandemic dynamics of the virus (*4*). Serologic tests for SARS-CoV-2 have been developed to determine the extent of immunity to the virus (*4*), and immunity certifications based on the results of these tests have been considered by some countries in Europe and by the US government. Several persons belonging to households with an index COVID-19 patient reported symptoms of COVID-19 but remained seronegative even though the index patient practiced no quarantine measures. The absence of antiviral antibodies after exposure has been previously reported for other viral infections. In these cases, the presence of virus-specific T-cell responses provided proof of viral transmission (*5*). In this study, we investigated humoral and cellular responses to SARS-CoV-2 in 11 serodiscordant couples in whom 1 partner had evidence of mild COVID-19 and in 10 unexposed healthy blood donors (controls). We also explored the T-cell response against 2 human coronaviruses (HCoV) that cause common colds, given the potential cross-reactive immunity between SARS-CoV-2 and common cold HCoVs.

## Materials and Methods

### Study Participants

We included in the study 11 couples in whom 1 of the 2 partners met clinical, epidemiologic, and laboratory criteria for a mildly symptomatic confirmed COVID-19 case. We collected blood samples from both

Author affiliations: Strasbourg University Hospital, Strasbourg, France (F. Gallais, A. Velay, C. Nazon, M.-J. Wendling, M. Partisani, J. Sibilia, S. Fafi-Kremer); Strasbourg University, Strasbourg (F. Gallais, A. Velay, C. Nazon, M.-J. Wendling, J. Sibilia, S. Fafi-Kremer); Rouen University Hospital, Rouen, France (S. Candon)

DOI: https://doi.org/10.3201/eid2701.203611

partners of each couple during May 7–June 26, 2020. Ten healthy blood donors who had not been exposed to COVID-19 patients and who had tested negative for SARS-CoV-2 antibodies were enrolled as controls. All participants gave written informed consent for research according to protocols approved by the institutional review board of Strasbourg University Hospitals (ClinicalTrials.gov NCT 04405726).

### SARS-CoV-2 Reverse Transcription PCR

We performed in-house real-time reverse transcription PCR (rRT-PCR) tests for SARS-CoV-2 nucleic acid on samples from nasopharyngeal swab specimens collected during the symptomatic phase from 8 index patients and 3 contacts. Primer and probe sequences target 2 regions of the RdRp gene and are specific to SARS-CoV-2. Assay sensitivity is ≈10 copies/reaction (https://www.who.int/docs/default-source/coronaviruse/real-time-rt-pcr-assays-for-the-detection-of-sars-cov-2-institut-pasteur-paris.pdf).

### Serologic Tests

We used 3 serologic assays to detect the presence of SARS-CoV-2 antibodies. The Abbott Architect SARS-CoV-2IgGassay(Abbott,https://www.corelaboratory.abbott) is a chemiluminescent microparticle immunoassay for detecting IgG against the SARS-CoV-2 nucleoprotein and has sensitivity and specificity close to 100% (*6*,*7*). The EUROIMMUN SARS-CoV-2 assay (EUROIMMUN, https://www.euroimmun.com) is an ELISA for detecting IgG and IgA against the SARS-CoV-2 S1 domain of the spike glycoprotein, including the immunologically relevant receptor-binding domain. This assay was reported to have a clinical specificity of 98% for IgG and 91% for IgA detection, with a maximal sensitivity reached after 28 days after symptom onset (IgG 98% and IgA 95%) (*7*). The Biosynex COVID-19 BSS assay (Biosynex, https://www.biosynex.com) is a lateral flow assay for detecting IgM and IgG directed against the SARS-CoV-2 receptor-binding domain of the spike glycoprotein and has a sensitivity of 95.6% and a specificity of 99.4% (*8*). All 3 assays were approved by the French National Agency of Medicine and Health Products Safety for their excellent analytical performances. All tests were performed according to manufacturer instructions.

### Interferon-Gamma Enzyme-Linked Immunospot Assay

We investigated T-cell immune response against SARS-CoV-2 by performing an interferon-gamma (IFN-γ) enzyme-linked ImmunoSpot ELISPOT assay (ImmunoSpot, http://www.immunospot.com) in duplicate on fresh peripheral blood mononuclear cells (PBMC) isolated from heparin-anticoagulated blood. PBMCs were seeded at 200,000 CD3+ cells/well after dilution according to measurement of CD3+ cell frequencies by flow cytometry. They were stimulated for 20 ±4 h with overlapping 15-mer peptide pools used at a final concentration of 1 μg/mL and spanning the sequences of the N-terminal portion of the SARS-CoV-2 spike glycoprotein (pool S1, amino acid residues 1–643) and the C-terminal part of the same protein (pool S2, amino acid residues 633–1273), the nucleoprotein (N), the membrane protein (M), the envelope small membrane protein (E), and the accessory proteins 3A, 7A, 8 and 9B (PepMix; JPT Peptide Technologies, https://www.jpt.com).

To investigate the possibility of preexisting cross-reactive coronavirus-specific T cells, PBMCs were stimulated in parallel with peptide pools spanning the spike glycoprotein sequences of HCoV-229E (ES1 and ES2) and HCoV-OC43 (OS1 and OS2). Phytohemagglutinin (PHA) was used in duplicate as a positive control and culture medium in quadruplicate as a negative control. After colorimetric revelation of IFN-γ capture (UCytech, https://ucytech.com), spots were counted using an ELISPOT reader (AID, https://www.aid-diagnostika.com). For each condition, the mean number of spot-forming cells per million CD3+ cells was calculated from duplicates after subtraction of the background value obtained from negative controls to determine the frequency of antigen-specific T cells. The threshold defining T-cell reactivity for 1 antigen was set at >3 SD of the negative control background. The SARS-CoV-2-specific T-cell response was considered positive if analysis showed reactivity for ≥3 SARS-CoV-2 antigens.

## Results

The median age of the 11 couples was 49 years (range 38–65 years); 11 (50%) were male (Table 1). Partners who met the confirmed case definition of COVID-19 (positive for SARS-CoV-2 by RT-PCR or serology or both) were the first to report symptoms in each couple and were considered index patients (P). Because of the lockdown from March 17 to May 11, 2020, each couple stayed in the same household during this period. Therefore, the partner of each index patient was considered a close contact (C) as defined by the US Centers for Disease Control and Prevention (CDC).

During March 2–April 9, all index patients reported histories of ≥1 symptoms: 8 had fever, 6 had cough, 4 had fatigue, 8 had headache, 8 had anosmia, 7 had ageusia, 3 had dyspnea, and 3 had myalgia (Table 1). We tested 8 of these patients for SARS-CoV-2 using RT-PCR on nasopharyngeal samples; results for 7 were positive

**Table 1.** Clinical and virological characteristics of COVID-19 patients and their contacts at symptom onset, Strasbourg, France, March 10–26, 2020*

| ID | Age, y/sex | RT-PCR† | Symptoms | | | | | | | | Duration of symptoms, d | Symptom onset delay, d‡ |
|---|---|---|---|---|---|---|---|---|---|---|---|---|
| | | | Fever | Cough | Fatigue | Headache | Anosmia | Agueusia | Dyspnea | Myalgia | | |
| Couples with symptomatic contacts | | | | | | | | | | | | |
| P1 | 47/F | ND | Y | N | Y | Y | Y | Y | N | Y | 15 | 5 |
| C1 | 50/M | ND | Y | N | N | N | N | N | N | N | 3 | |
| P2 | 54/F | ND | Y | Y | Y | Y | Y | | Y | N | 13 | 7 |
| C2 | 57/M | ND | Y | N | Y | Y | N | N | Y | N | 6 | |
| P4§ | 45/M | Pos (8.39) | Y | Y | N | Y | Y | Y | N | N | 12 | 6 |
| C4 | 48/F | Neg | Y | Y | N | Y | N | N | N | N | 10 | |
| P5 | 38/M | Pos (7.65) | Y | N | N | Y | Y | Y | N | N | 2 | 10 |
| C5 | 40/F | Neg | N | Y | N | Y | N | N | N | N | 7 | |
| P7 | 45/M | Pos | Y | Y | N | N | Y | Y | N | Y | 4 | 1 |
| C7 | 45/F | Neg | N | N | N | N | N | Y | N | N | 1 | |
| P8 | 63/M | Pos | Y | N | Y | Y | Y | Y | N | N | 10 | 10 |
| C8 | 57/F | ND | N | N | Y | N | N | N | N | Y | 10 | |
| Couples with asymptomatic contacts | | | | | | | | | | | | |
| P3 | 65/F | ND | N | Y | N | Y | N | N | N | N | 9 | NA |
| C3 | 61/M | ND | Asymptomatic | | | | | | | | NA | |
| P6# | 43/F | Pos (3.99) | N | Y | N | N | Y | Y | Y | N | 7 | NA |
| C6 | 45/M | ND | Asymptomatic | | | | | | | | NA | |
| P9 | 57/M | Pos (6.20) | Y | Y | N | N | N | N | Y | Y | 14 | NA |
| C9 | 58/F | ND | Asymptomatic | | | | | | | | NA | |
| P10 | 39/F | Neg | N | N | N | Y | Y | Y | N | N | 10 | NA |
| C10 | 39/M | ND | Asymptomatic | | | | | | | | NA | |
| P11 | 58/F | Pos (8.46) | Y | N | Y | Y | N | N | N | N | 21 | NA |
| C11 | 57/M | ND | Asymptomatic | | | | | | | | NA | |

*In ID column, same number indicates partners in 1 couple. C, contact; d, days; ID, identification; ND, not done; NA, not applicable; neg, negative; P, index patient; pos, positive; RT-PCR, reverse-transcription PCR; SARS-CoV-2, severe acute respiratory syndrome coronavirus 2.
†SARS-CoV-2 RT-PCR was performed in nasopharyngeal specimens during the symptomatic phase. When available, viral load (log copies/reaction) is indicated in parentheses below the result.
‡Days from symptom onset in index patient to onset in contact.
§This index patient quarantined himself by dining separately and wearing a mask after positive SARS-CoV-2 PCR testing 1 day after symptom onset.
#This index patient wore a mask after positive SARS-CoV-2 PCR testing 3 days after symptom onset.

(Table 1). The duration of symptoms varied (2–21 days, median 10 days). During this symptomatic phase, all couples rigorously washed their hands, and each avoided hugs and kisses with his or her partner except couple 2. Nine of the 11 couples slept in the same bed. Only 2 index patients, P4 and P6 (i.e., the index partners from couples 4 and 6), quarantined themselves by eating and sleeping separately or wearing a mask or both for 1 day (P4) and 3 days (P6) after symptom onset.

We performed serologic testing for SARS-CoV-2 antibodies in index patients at a median of 68 days (range 49–102 days) after symptom onset. All displayed IgG against the SARS-CoV-2 N protein, the spike glycoprotein, or both, as indicated by the 3 serologic assays (Table 2), confirming the persistence of the SARS-CoV-2 antibodies for up to 102 days after symptom onset. Results of tests for SARS-CoV-2 IgA were positive for 7 of the 11 index patients (Table 2).

Six of the 11 contacts (C1, C2, C4, C5, C7, and C8) experienced symptoms 1–10 days after symptom onset in their partners (Table 1). We tested 3 of them for SARS-CoV-2 RNA by RT-PCR on samples from nasopharyngeal swab specimens during the symptomatic phase; results for all were negative (Table 1). Three had fever, 2 had cough, 2 had fatigue, 3 had headache, 1 had ageusia, 1 had dyspnea, and 1 had myalgia. The duration of symptoms varied (1–10 days, median 7 days) (Table 1). We performed serologic testing for SARS-CoV-2 at a median of 59 days (range 44–93 days) after symptom onset in symptomatic contacts and at the same time as their partners for asymptomatic contacts. All the contacts, including the symptomatic ones, were SARS-CoV-2 seronegative for IgM, IgA (except 1 equivocal result), and IgG (Table 2).

To investigate the SARS-CoV-2–specific T-cell response in the 11 couples, we collected fresh PBMC samples on the same day as the serum collections. We then stimulated the samples with 4 structural and 4 accessory SARS-CoV-2 proteins followed by IFN-γ ELISPOT analysis. All index and contact patients had

normal lymphocyte counts (Table 2). All index patients showed SARS-CoV-2–specific IFN-γ responses against 4–8 SARS-CoV-2 antigens (Table 2; Figure 1). All of their immune systems recognized the structural proteins S1, S2, N, and M, and 9 of them recognized ≥1 accessory protein (3A, 7A, 8, or 9B), showing that SARS-CoV-2–specific T-cell responses had developed (Figures 1, 2; Appendix Figure 1, https://wwwnc.cdc.gov/EID/article/27/1/20-3611-App1.pdf). Blood samples were collected 49–102 days after symptom onset, which suggests that antiviral T cells are maintained for up to 102 days in patients having recovered from mild COVID-19.

We evaluated SARS-CoV-2–specific T-cell response in contacts at a median time of 59 days (range 44–93 days) after symptom onset in symptomatic contacts and at the same time as their partner for asymptomatic contacts. Among the 6 symptomatic contacts, 4 (C1, C4, C5, and C8) displayed a positive SARS-CoV-2–specific T-cell response with a reactivity to ≥3 SARS-CoV-2 antigens (Figure 1, row A; Appendix Figure 1). Contact C1 exhibited T-cell reactivity against 4 SARS-CoV-2 antigens, including 1 structural protein (S1) and 3 accessory proteins; contact C5 exhibited T-cell reactivity against 2 and C8 against 3 structural proteins (N, E, and S2 for C8) and the accessory protein 9B. Contact C4 exhibited T-cell reactivity against 1 structural protein (S2) and 2 accessory proteins. Although symptomatic contact C7 exhibited T-cell SARS-CoV-2–specific response against a single antigen (structural protein S1), the frequency of IFN-γ–producing T cells was higher than that observed in his partner (mean 353 ± 53 vs. 126 ± 25 spot-forming units/1 million cells). Symptomatic contact C2 and asymptomatic contacts C6, C9, and C10 exhibited a low

**Table 2.** Humoral and cellular immune response to SARS-CoV-2 of COVID-19 patients and their contacts 44–102 days after symptom onset, Strasbourg, France, 2020*

| ID† | Lymphocyte count, × $10^9$/L | Days from symptom onset to sample collection | SARS-CoV-2 serologic test result | Assay results: Biosynex Antigen: RBD of protein S IgM | Assay results: Biosynex Antigen: RBD of protein S IgG | Assay results: Abbott Architect Antigen: protein N (index value) IgG | Assay results: Euroimmun Antigen: protein S (index value) IgG/IgA | SARS-CoV-2–specific T-cell response (no. antigens) |
|---|---|---|---|---|---|---|---|---|
| Couples with symptomatic contacts | | | | | | | | |
| P1 | 1.3 | 58 | Pos | Neg | Pos | Pos (3.36) | Pos (2.28)/neg | Pos (5)† |
| C1 | 1.8 | 53 | Neg | Neg | Neg | Neg | Neg/neg | Pos (4)† |
| P2 | 2.0 | 51 | Pos | Neg | Pos | Pos (4.3) | Pos (2.3)/neg | Pos (7)† |
| C2 | 1.5 | 44 | Neg | Neg | Neg | Neg | Neg/neg | Neg (1) |
| P4 | 1.6 | 57 | Pos | Pos | Pos | Pos (6.48) | Pos (4.24)/pos (4.16) | Pos (4)† |
| C4 | 1.7 | 51 | Neg | Neg | Neg | Neg | Neg/neg | Pos (3)† |
| P5 | 1.6 | 68 | Pos | Pos | Pos | Pos (3.97) | Pos (4.86)/pos (2.38) | Pos (7)† |
| C5 | 2.0 | 80 | Neg | Neg | Neg | Neg | Neg/neg | Pos (3)† |
| P7 | 1.3 | 64 | Pos | Pos | Neg | Pos (4.18) | Pos (3.43)/doubtful (0.94) | Pos (4)† |
| C7 | 2.2 | 64 | Neg | Neg | Neg | Neg | Neg/neg | Neg (1) |
| P8 | 1.9 | 102 | Pos | Pos | Pos | Pos (7.55) | Pos (5.39)/pos (9.23) | Pos (5)† |
| C8 | 1.9 | 93 | Neg | Neg | Neg | Neg | Neg/neg | Pos (4)† |
| Couples with asymptomatic contacts | | | | | | | | |
| P3 | 1.7 | 49 | Pos | Pos | Pos | Pos (8.4) | Pos (7.23)/pos (3.83) | Pos (8)† |
| C3 | 1.5 | NA | Neg | Neg | Neg | Neg | Neg/Neg | Neg (0) |
| P6 | 2.1 | 69 | Pos | Pos | Pos | Pos (6.37) | Pos (5.73)/pos (2.49) | Pos (6)† |
| C6 | 2.2 | NA | Neg | Neg | Neg | Neg | Neg/doubtful (0.85) | Neg (1) |
| P9 | 2.4 | 88 | Pos | Pos | Pos | Pos (7.48) | Pos (7.02)/pos (5.98) | Pos (6)† |
| C9 | 3.0 | NA | Neg | Neg | Neg | Neg | Neg/neg | Neg (1) |
| P10 | 1.9 | 99 | Pos | Pos | Neg | Pos (2.46) | Pos (1.75)/doubtful (0.95) | Pos (5)† |
| C10 | 1.1 | NA | Neg | Neg | Neg | Neg | Neg/neg | Neg (1) |
| P11 | 1.7 | 100 | Pos | Neg | Pos | Neg | Pos (4.01)/pos (1.72) | Pos (6)† |
| C11 | 1.9 | NA | Neg | Neg | Neg | Neg | Neg/neg | Neg (0) |

*In ID column, same number indicates P and C are partners in 1 couple. C, contact; ID, identification; neg, negative; P, index patient; pos, positive; PBMC, peripheral blood mononuclear cells; NA, not applicable; RBD, receptor-binding domain; SARS-CoV-2, severe acute respiratory syndrome coronavirus 2.

frequency of T-cell reactivity against a single antigen (S2 = 2, E = 1, 9B = 1) that was not considered here as a positive specific T-cell response to SARS-CoV-2 (Figure 1, row A and B; Figure 2; Appendix Figure 1). The asymptomatic contacts C3 and C11 showed no T-cell response against any of the SARS-CoV-2 antigens (Figure 1, row B; Appendix Figure 1).

We included 10 unexposed HD as controls, with a mean age of 46 years (range 29–60 years). We confirmed their SARS-CoV-2 seronegative status with the 3 serologic assays. Five of them displayed low T-cell reactivity to SARS-CoV-2 against 1 or 2 antigens (S1, S2, M, 9B) (Figure 1, row C; Appendix Figure 1).

A recent study demonstrated that several CD4 T cells reacting to SARS-CoV-2 epitopes were a result of a cross-reaction with corresponding homologous sequences from commonly circulating HCoVs including OC43 and 229E, which can cause common colds

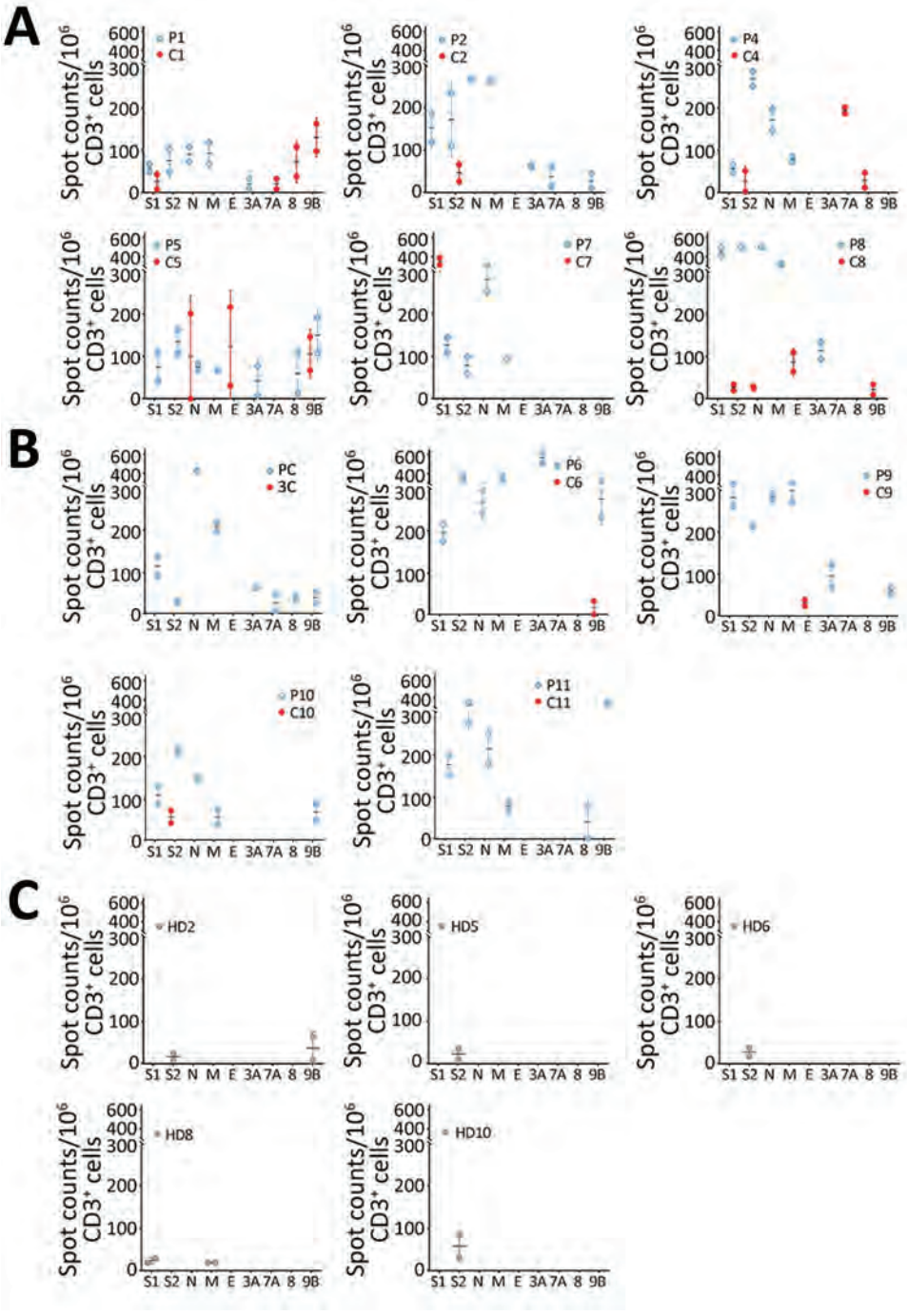


**Figure 1.** SARS-CoV-2–specific T-cell response patterns in index patients, contacts, and unexposed healthy donors in study of intrafamilial exposure to SARS-CoV-2, France. A, B) Spot counts of SARS-CoV-2–specific T cells measured by interferon-gamma (IFN-γ) ELISPOT assay are shown for 11 couples, each including 1 confirmed coronavirus disease case (P) and 1 SARS-CoV-2 seronegative symptomatic (A) or asymptomatic (B) contact (C). C) Spot counts of IFN-γ–producing T cells in response to SARS-CoV-2 antigens are shown for the 5 out of the 10 controls (HD) tested who displayed detectable T-cell responses. All experiments were performed in duplicate. Data are shown as means and standard deviations of spots counts of IFN-γ–producing T cells per 1 million CD3+ cells. Each dot represents a single measured value. Blue dots correspond to T-cell responses detected in index patients, red dots correspond to those detected in contacts and gray dots to those found in healthy donors. The x-axis represents the SARS-CoV-2 antigens spanned by the peptide pools used in ELISPOT assays: the N-terminal and C-terminal regions of SARS-CoV-2 spike glycoprotein (S1 and S2, respectively); the N, M, and E proteins; and the accessory proteins 3A, 7A, 8, and 9B. C, contact; E, envelope small membrane protein; HD, healthy blood donor (control); M, membrane protein; N, nucleoprotein; P, index patient; SARS-CoV-2, severe acute respiratory syndrome coronavirus 2.

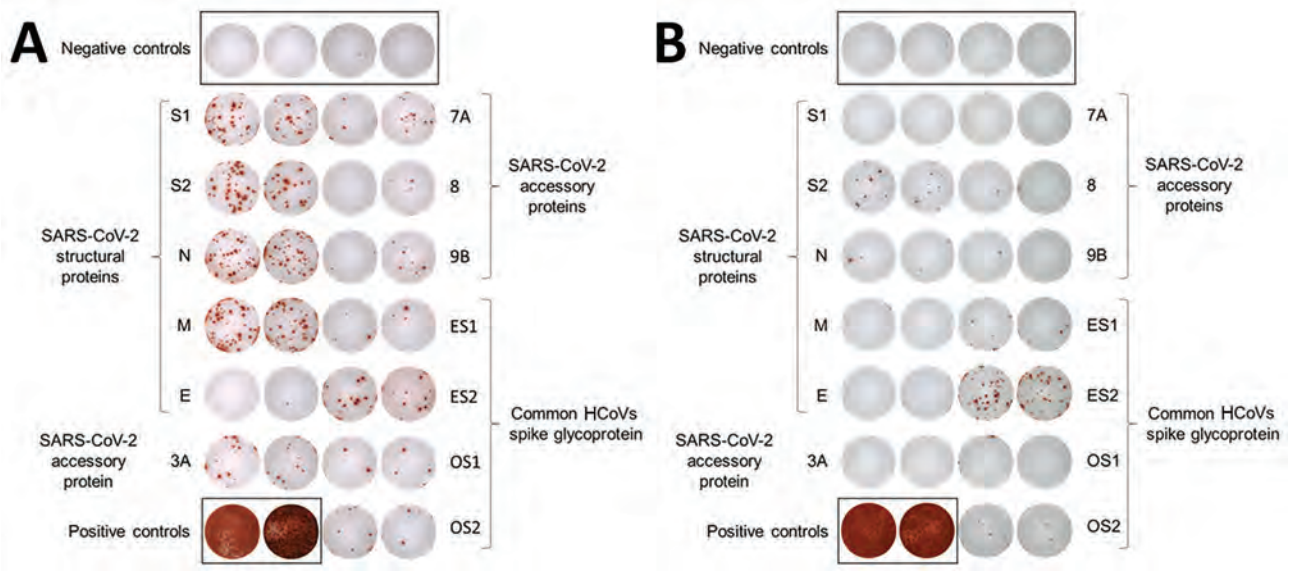


**Figure 2.** Example of IFNγ ELISPOT images corresponding to couple 2 (P2 and C2) in a study of intrafamilial exposure to SARS-CoV-2, France. T-cell–specific response was evaluated using peptide pools spanning SARS-CoV-2 structural protein (spike glycoprotein: N-terminal region = S1, C-terminal region = S2, N, M, and E proteins); SARS-CoV-2 accessory proteins (3A, 7A, 8, and 9B); and the N-terminal and C-terminal regions of the spike glycoprotein of common cold human coronaviruses 229 (ES1 and ES2) and OC43 (OS1 and OS2). All experiments were performed in duplicates with 4 wells of negative controls (cells with culture medium only) and 2 wells of positive controls (phytohemagglutinin) for each individual. P2 was reactive to all antigens tested except for SARS-CoV-2 proteins E and 8, whereas C2 was reactive to 1 SARS-CoV-2 protein only (S2) and to ES1, ES2, and OS2. C, contact; E, envelope small membrane protein; HCoV, human coronavirus; M, membrane protein; N, nucleoprotein; P, index patient; SARS-CoV-2, severe acute respiratory syndrome coronavirus 2.

(*9*). To investigate if there was a correlation between T-cell responses against SARS-CoV-2 and common cold HCoVs, we tested the 11 couples and the 10 unexposed controls for reactivity against the spike glycoprotein (S1 and S2 regions) of HCoV-229E and HCoV-OC43. All but 1 HD (HD9) showed IFN-γ–producing T cells directed against these antigens (Figure 3; Appendix Figure 2). Eight index patients (P2, P3, P4, P5, P6, P7, P10, and P11), 7 contacts (C1, C2, C4, C8, C9, C10, and C11), and 7 controls displayed a positive T-cell response against both HCoV-229E and HCoV-OC43. Three index patients (P1, P8, and P9), 4 contacts (C3, C5, C6, and C7), and 2 controls displayed positive T-cell responses only against HCoV-229E. We found no correlation between the responses to S1 and S2 peptide pools of SARS-CoV-2 and HCoVs (Figure 4).

## Discussion

In this study, we demonstrate that intrafamilial contacts can display a SARS-CoV-2–specific T-cell response in the absence of seroconversion, especially when they have been symptomatic. This T-cell response provides evidence that transient or anatomically contained SARS-CoV-2 infection, or both, may have occurred and that T-cell responses would be more sensitive indicators of SARS-Co-V-2 exposure than antibodies.

Each couple stayed in the same household during the COVID-19 episode and the partners were in close contact for a long time due to the lockdown. Although 5 contacts were asymptomatic, 6 exhibited symptoms a median of 7 days after symptom onset in their partners, suggesting that at least those 6 were infected. However, results from neither RT-PCR nor serology testing using 3 different assays and targeting 2 different SARS-CoV-2 structural proteins were positive in contacts. In contrast, analysis of SARS-CoV-2–specific T-cell response showed a positive response against ≥3 antigens, including structural proteins in 4 symptomatic contacts, strongly suggesting that they were infected with SARS-CoV-2.

Five unexposed controls and 1 symptomatic and 3 asymptomatic contacts exhibited low frequencies of SARS-CoV-2 IFN-γ–producing T cells. Because these 4 contacts were exposed to COVID-19 patients and the unexposed controls donated blood in April and May 2020, it is unclear whether the detectable T-cell responses were the result of cross-reactivity with common cold HCoV antigens, as previously reported (*10*–*12*) or of SARS-CoV-2 infection. Al-

though recent research provided direct evidence of cross-reactivity between SARS-CoV-2 epitopes and common cold HCoVs (*9*), we observed no obvious relationship between the magnitude of T-cell responses against spike glycoproteins of common cold HCoVs and SARS-CoV-2 in index patients, contacts, and unexposed HD. In parallel with our findings, another recent study (*13*) reported finding memory T-cell response against SARS-CoV-2 structural proteins in exposed family members and healthy persons lacking detectable circulating antibodies who donated blood during the pandemic.

There are multiple explanations for virus-specific T cells developing without any antibody response. A study in a small cohort of patients (*14*) reported that 40% of asymptomatic and 12.9% of patients with mild COVID-19 no longer had antibodies 56 days after being discharged from the hospital. In our study, the serum samples were collected between 49 to 102 days after symptom onset, so it is possible that the contacts had lost their antibodies during this period. It is also possible that very low levels of antibodies that might have developed in contacts were not detected by the serologic assays we used. The lack of specific antibodies might also be because of exposure to low doses of the virus with brief and transient viral replication, to a downstream event of protective innate immune response, or to abortive replication of defective viral genomes (*5*).

Eventually, the presence of SARS-CoV-2-specific T-cell response, whether because of infection with SARS-CoV-2 or a cross-reaction, might explain the mild and rapidly resolved symptoms in index patients and symptomatic contacts and the resistance of other contacts to symptomatic SARS-CoV-2 infection. However, this possible explanation needs to be investigated further in a large cohort.

Our study is subject to several limitations. First, our findings suffer from a limited sample size, although this is a unique cohort, and it was not possible to increase

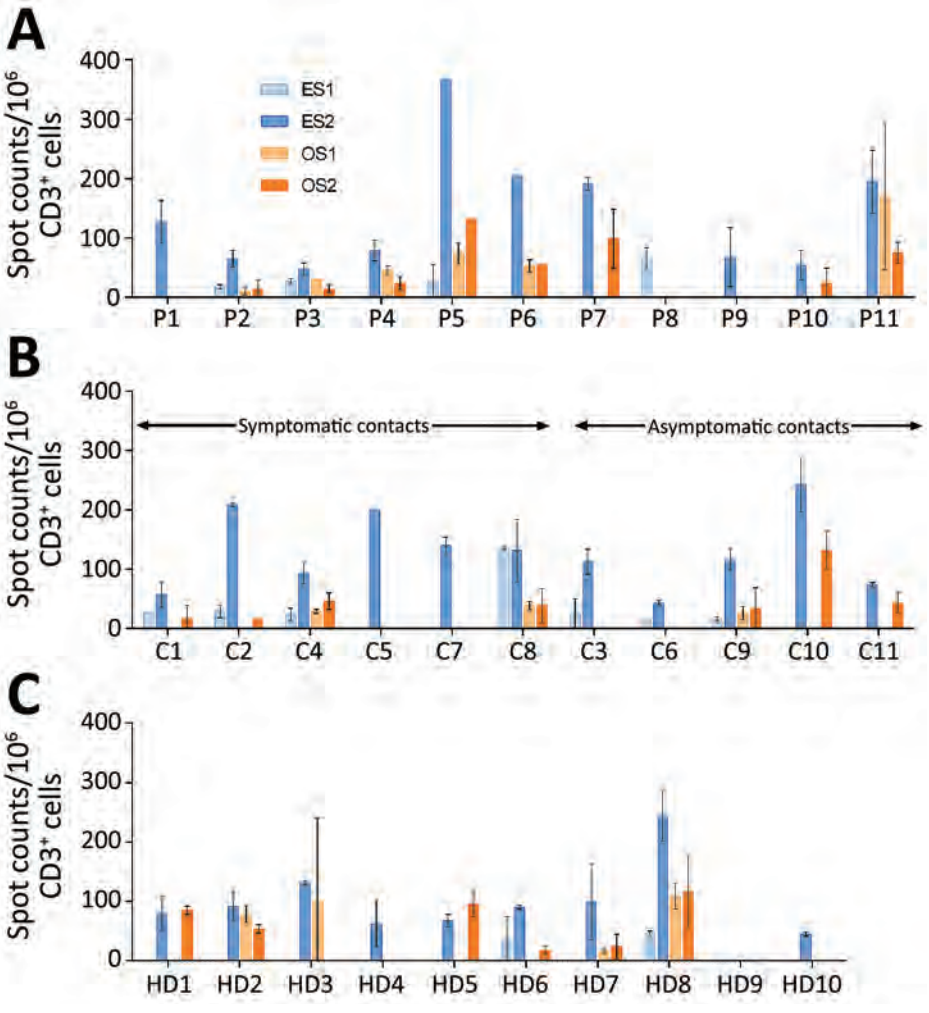


**Figure 3.** Frequency of specific T cells directed against spike glycoprotein antigens of the 2 common cold HCoVs 229E and OC43 in study of intrafamilial exposure to SARS-CoV-2, France. A) Index patients (n = 11); B) seronegative partners of index patients (n = 11); C) unexposed healthy controls (n = 10). Spot counts of common cold human coronaviruses-specific T cells were measured by interferon-gamma ELISPOT assay. All experiments were performed in duplicate. Data are shown as means and standard deviations of spot counts of interferon-gamma–producing T cells per 1 million CD3+ cells. T-cell secretion of IFN-γ was determined in response to peptide pools spanning the N-terminal and the C-terminal regions of the spike glycoprotein of HCoV 229E (ES1 and ES2 subpools) and HCoV OC43 (OS1 and OS2 subpools). Each color corresponds to 1 antigen subpool. C, contact; HCoV, human coronavirus; HD, healthy blood donor (control); P, index patient; SARS-CoV-2, severe acute respiratory syndrome coronavirus 2.

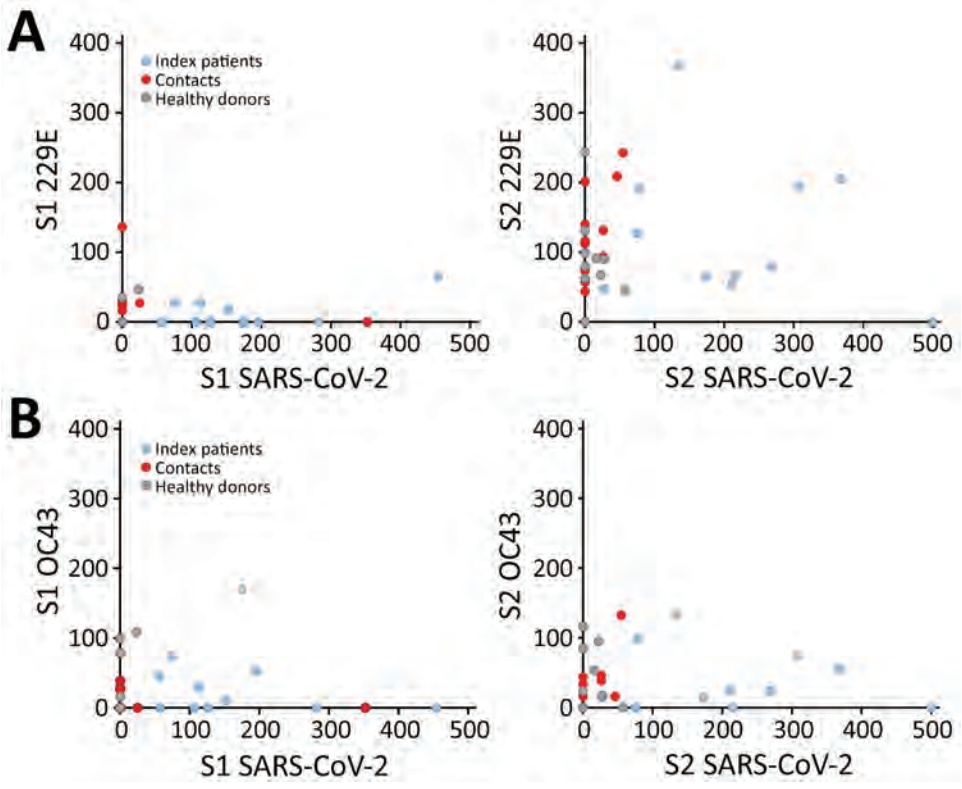


**Figure 4.** Correlation of the T-cell responses against spike glycoprotein antigens of SARS-CoV-2 and HCoVs 229E and OC43 in study of intrafamilial exposure to SARS-CoV-2, France. Means of spot counts of interferon gamma–producing T cells per 1 million CD3+ cells in response to peptide pools spanning the N terminal (S1) and the C-terminal (S2) regions of spike glycoproteins of SARS-CoV-2 compared with HCoV-229E (A) and HCoV-OC43 (B) in 11 confirmed coronavirus disease cases (index patients), their seronegative partners (contacts), and 10 healthy blood donor controls. HCoV, human coronavirus; SARS-CoV-2, severe acute respiratory syndrome coronavirus 2.

the sample size. Second, because of the unavailability of PBMCs collected before the pandemic, we recruited unexposed HD who donated their blood during the pandemic as controls, so we cannot exclude a potential infection by SARS-CoV-2 before the enrollment in the study. Third, although we detected high frequencies of T-cell response against diverse SARS-CoV-2 proteins in symptomatic contacts lacking circulating antibodies, it remains possible that a part of this response may be a result of cross-reaction with common cold HCoVs.

Overall, our results indicate that persons exposed to SARS-CoV-2 may develop virus-specific T-cell responses without detectable circulating antibodies. This aspect of the immune response against SARS-CoV-2 contributes substantially to the understanding of the natural history of COVID-19. Furthermore, our data indicate that epidemiologic data relying solely on the detection of SARS-CoV-2 antibodies may lead to a substantial underestimation of prior exposure to the virus. Our data may also have implications for vaccine development and tracking the future evolution of the SARS-CoV-2 pandemic.

### Acknowledgments

We thank all the participants in this study.

This study was supported by the Strasbourg University Hospital (COVID-HUS study, HUS N°7760), the Agence Nationale de la Recherche (ANR), Laboratoire d'Excellence TRANSPLANTEX (ANR-11-LABX-0070_TRANSPLANTEX), and Institut National de la Santé et de la Recherche Médicale (UMR_S 1109).

### About the Author

Ms. Gallais is a PhD student under the supervision of Prof. S. Fafi-Kremer at the virology laboratory of Strasbourg University Hospital, INSERM unit 1109. She is working on understanding the mechanisms of viral infection control by the host's immune response. Her current research is focused on the cellular immune response against SARS-CoV-2 in the context of the COVID-19 pandemic.

### References

1. Li Q, Guan X, Wu P, Wang X, Zhou L, Tong Y, et al. Early transmission dynamics in Wuhan, China, of novel coronavirus-infected pneumonia. N Engl J Med. 2020;382:1199–207. https://doi.org/10.1056/NEJMoa2001316
2. Studdert DM, Hall MA. Disease control, civil liberties, and mass testing—calibrating restrictions during the Covid-19 pandemic. N Engl J Med. 2020;383:102–4. https://doi.org/10.1056/NEJMp2007637
3. Lescure FX, Bouadma L, Nguyen D, Parisey M, Wicky PH, Behillil S, et al. Clinical and virological data of the first cases of COVID-19 in Europe: a case series. Lancet Infect Dis. 2020;20:697–706. https://doi.org/10.1016/S1473-3099(20)30200-0
4. Kissler SM, Tedijanto C, Goldstein E, Grad YH, Lipsitch M. Projecting the transmission dynamics of SARS-CoV-2

through the postpandemic period. Science. 2020;368:860–8. https://doi.org/10.1126/science.abb5793
5. Heller T, Werner JM, Rahman F, Mizukoshi E, Sobao Y, Gordon AM, et al. Occupational exposure to hepatitis C virus: early T-cell responses in the absence of seroconversion in a longitudinal cohort study. J Infect Dis. 2013;208:1020–5. https://doi.org/10.1093/infdis/jit270
6. Bryan A, Pepper G, Wener MH, Fink SL, Morishima C, Chaudhary A, et al. Performance characteristics of the Abbott Architect SARS-CoV-2 IgG assay and seroprevalence in Boise, Idaho. J Clin Microbiol. 2020;58:e00941-20. https://doi.org/10.1128/JCM.00941-20
7. Velay A, Gallais F, Benotmane I, Wendling MJ, Danion F, Collange O, et al. Evaluation of the performance of SARS-CoV-2 serological tools and their positioning in COVID-19 diagnostic strategies. Diagnostic microbiology and infectious disease. 2020;98:115181. https://doi.org/10.1016/j.diagmicrobio.2020.115181
8. Fafi-Kremer S, Bruel T, Madec Y, Grant R, Tondeur L, Grzelak L, et al. Serologic responses to SARS-CoV-2 infection among hospital staff with mild disease in eastern France. EBioMedicine. 2020;59:102915. https://doi.org/10.1016/j.ebiom.2020.102915
9. Mateus J, Grifoni A, Tarke A, Sidney J, Ramirez SI, Dan JM, et al. Selective and cross-reactive SARS-CoV-2 T cell epitopes in unexposed humans. Science. 2020;370:eabd3871. https://doi.org/10.1126/science.abd3871
10. Braun J, Loyal L, Frentsch M, Wendisch D, Georg P, Kurth F, et al. SARS-CoV-2-reactive T cells in healthy donors and patients with COVID-19. Nature. 2020. https://doi.org/10.1038/s41586-020-2598-9
11. Grifoni A, Weiskopf D, Ramirez SI, Mateus J, Dan JM, Moderbacher CR, et al. Targets of T cell responses to SARS-CoV-2 coronavirus in humans with COVID-19 disease and unexposed individuals. Cell. 2020;181:1489–1501.e15. https://doi.org/10.1016/j.cell.2020.05.015
12. Le Bert N, Tan AT, Kunasegaran K, Tham CYL, Hafezi M, Chia A, et al. SARS-CoV-2-specific T cell immunity in cases of COVID-19 and SARS, and uninfected controls. Nature. 2020;584:457–62. https://doi.org/10.1038/s41586-020-2550-z
13. Sekine T, Perez-Potti A, Rivera-Ballesteros O, Strålin K, Gorin J-B, Olsson A, et al.; Karolinska COVID-19 Study Group. Robust T cell immunity in convalescent individuals with asymptomatic or mild COVID-19. Cell. 2020;183:158–68.e14. https://doi.org/10.1016/j.cell.2020.08.017
14. Long QX, Tang XJ, Shi QL, Li Q, Deng HJ, Yuan J, et al. Clinical and immunological assessment of asymptomatic SARS-CoV-2 infections. Nat Med. 2020;26:1200–4. https://doi.org/10.1038/s41591-020-0965-6

Address for correspondence: Samira Fafi-Kremer, Virology Laboratory and INSERM UMR_S 1109, Strasbourg University Hospitals, 3 rue Koeberlé, F-67000 Strasbourg, France; email: samira.fafi-kremer@unistra.fr

# Cellular Immunity in COVID-19 Convalescents with PCR-Confirmed Infection but with Undetectable SARS-CoV-2–Specific IgG

Sina Schwarzkopf, Adalbert Krawczyk, Dietmar Knop, Hannes Klump, Andreas Heinold, Falko M. Heinemann, Laura Thümmler, Christian Temme, Marianne Breyer, Oliver Witzke, Ulf Dittmer, Veronika Lenz, Peter A. Horn, Monika Lindemann

We investigated immune responses against severe acute respiratory syndrome coronavirus 2 (SARS-CoV-2) among a group of convalescent, potential blood donors in Germany who had PCR-confirmed SARS-CoV-2 infection. Sixty days after onset of symptoms, 13/78 (17%) study participants had borderline or negative results to an ELISA detecting IgG against the S1 protein of SARS-CoV-2. We analyzed participants with PCR-confirmed infection who had strong antibody responses (ratio >3) as positive controls and participants without symptoms of SARS-CoV-2 infection and without household contact with infected patients as negative controls. Using interferon-γ ELISpot, we observed that 78% of PCR-positive volunteers with undetectable antibodies showed T-cell immunity against SARS-CoV-2. We observed a similar frequency (80%) of T-cell immunity in convalescent donors with strong antibody responses but did not detect immunity in negative controls. We concluded that, in convalescent patients with undetectable SARS-CoV-2 IgG, immunity may be mediated through T cells.

One promising therapeutic option to treat severely ill patients with coronavirus disease (COVID-19) is the use of convalescent plasma (CP) of donors who recovered from severe acute respiratory syndrome coronavirus 2 (SARS-CoV-2) infection (*1*–*3*). When searching for potential CP donors with PCR-confirmed SARS-CoV-2 infection, we observed that 17% of those who volunteered had either borderline or negative results (ratio <1.1) to a SARS-CoV-2 IgG ELISA. We decided to follow up with these volunteers by repeating antibody tests and by assessing T-cell immunity by enzyme-linked immunospot (ELISpot) assay for interferon-γ (IFN-γ).

Zhao et al. described the importance of T cells for the recovery from a structurally related coronavirus, the Middle East respiratory syndrome (MERS) virus, in 2017 (*4*); Braun et al. speculated that T-cell immunity could also be protective against infection with SARS-CoV-2 (*5*). Recently, SARS-CoV-2–specific T cells were detected in persons with a history of mild COVID-19 infection and in antibody-seronegative family members of COVID-19 patients (*6*; F. Gallais et al., unpub. data. https://doi.org/10.1101/2020.06.21.20132449). However, the seronegative persons in these 2 previous studies either tested negative or were not tested by SARS-CoV-2 PCR. It remains unclear if the T-cell responses detected in SARS-CoV-2 IgG–negative persons without PCR-confirmed infection were induced by SARS-CoV-2 or prior infection with a different coronavirus. In our study, we focused on a cohort with mild PCR-confirmed SARS-CoV-2 infection and undetectable SARS-CoV-2 IgG. This group is unique because it is biased toward male volunteers who felt healthy enough to donate blood.

In this study we established a SARS-CoV-2–specific ELISpot assay and analyzed the T-cell responses in distinct groups of potential blood donors; donors with a previously PCR-confirmed SARS-CoV-2 infection and undetectable or strong spike S1 IgG response; and SARS-CoV-2–negative controls without a history of COVID-19–related symptoms or household contact with infected patients. We furthermore conducted follow-up testing for immunity to

Author affiliations: Institute for Transfusion Medicine, University Hospital Essen, University of Duisburg-Essen, Essen, Germany (S. Schwarzkopf, D. Knop, H. Klump, A. Heinold, F.M. Heinemann, L. Thümmler, C. Temme, M. Breyer, V. Lenz, P.A. Horn, M. Lindemann); Department of Infectious Diseases, West German Centre of Infectious Diseases, Universitätsmedizin Essen, University of Duisburg-Essen, Essen (A. Krawczyk, O. Witzke); Institute for Virology, University Hospital Essen, University of Duisburg-Essen, Essen (U. Dittmer)

DOI: https://doi.org/10.3201/eid2701.203772

SARS-CoV-2 until a median of 75 days (range 24–154) after the onset of symptoms and correlated results of SARS-CoV-2–specific T- and B-cell immunity.

The study was approved by the local ethics committee (approval no. 20-9225-BO). All volunteers provided informed consent to participate in the study, which has been performed in accordance with the ethics standards noted in the 1964 Declaration of Helsinki and its later amendments or comparable ethics standards.

## Materials and Methods

### Study Participants

We used a questionnaire to look for potential plasma donors who recovered from SARS-CoV-2 infection. The questionnaire addressed characteristics and additional parameters determining suitability as blood donor (Table). We received >550 questionnaires; 310 volunteers had had PCR-confirmed SARS-CoV-2 infection. We selected 78 volunteers (54 male, 24 female) who had PCR-confirmed SARS-CoV-2 infection as participants. Their median age was 47 years (19–66) years. We preferred donors who tested negative by a second SARS-CoV-2 PCR and had experience donating blood; we especially sought donors with the blood type AB (because they are universal plasma donors) and donors with a body weight >60 kg (because they can donate 3 units of convalescent plasma). We preferentially recruited those living in close vicinity to University Hospital Essen. Because we observed antibodies against human leukocyte antigens and human neutrophil antigens, which prohibited blood donation, mainly in female patients (n = 4), we preferred male donors, of whom 1 had these leukocyte antibodies. Only 4 of the participants received oxygen supplementation and none ventilator treatment. Of note, 39/78 participants were infected during skiing holidays. Unfortunately, radiograph and computed tomography data were not available; they are usually performed only for critically ill patients in Germany. Thus, our cohort is unique because it is biased toward especially healthy male blood donors with mild courses of COVID-19. We tested donor serum samples for IgG against the S1 protein of SARS-CoV-2 by ELISA. Furthermore, results of a standard neutralization assay were available in donors with negative or borderline antibody ratios.

In the negative control group we included 22 healthy participants (6 male, 16 female) who had no symptoms of SARS-CoV-2 infection and no household

**Table**. Clinical characteristics of 78 potential convalescent-plasma donors with PCR-confirmed severe acute respiratory syndrome coronavirus 2 infection, grouped by antibody ratio, Germany*

| Parameter | Ratio <1.1 | Ratio 1.1–3.0 | Ratio >3.0 |
|---|---|---|---|
| All donors | 13 (16.7) | 24 (30.8) | 41 (52.6) |
| Age, y | 45 (19–55) | 51 (28–65) | 47 (20–66) |
| Sex, M/F | 6/7 | 19/5 | 29/12 |
| Body mass index | 25.2 (22.3–30.1) | 24.9 (22.8–28.1) | 26.7 (22.2–36.8) |
| Interval to onset of symptoms, d | 52 (32–100) | 60 (24–98) | 64 (22–112) |
| Stay in risk area/risk contact | 6 | 17 | 20 |
| Symptoms of COVID-19 infection | | | |
| Cough | 7 | 19 | 30 |
| Fever | 9 | 13 | 24 |
| Shortage of air | 3 | 4 | 15 |
| Rhinitis | 7 | 7 | 16 |
| Sore throat | 6 | 8 | 15 |
| Limb pain | 7 | 15 | 19 |
| Shivering | 6 | 8 | 15 |
| Diarrhea | 5 | 6 | 15 |
| Weight loss | 3 | 2 | 9 |
| Nausea | 0 | 0 | 4 |
| Loss of appetite | 5 | 3 | 12 |
| Headaches | 7 | 16 | 26 |
| Skin rash | 1 | 1 | 1 |
| Swelling of lymph nodes | 3 | 0 | 2 |
| Loss of sense of smell and taste | 8 | 16 | 18 |
| Necessity of oxygen supply | 0 | 1 | 3 |
| Antimicrobial treatment | 1 | 3 | 7 |
| Blood group | | | |
| O | 5 | 12 | 16 |
| A | 6 | 8 | 16 |
| B | 0 | 0 | 6 |
| AB | 1 | 3 | 3 |
| ND | 1 | 1 | 0 |

*Values are no. donors or median (range). Ratio is IgG against the S1 protein. ND, not determined.

contact with infected patients since January 2020. Their median age was 48 years (range 28–60 years).

### Antibody ELISA

We determined IgG antibodies by a CE-marked Anti-SARS-CoV-2 IgG semiquantitative ELISA (Euroimmun, https://www.euroimmun.com), according to the manufacturer's instructions. The ELISA plates were coated with recombinant SARS-CoV-2 spike protein (S1 domain). Serum samples were analyzed automatically at 1:100 dilution, using the Immunomat (Virion\Serion, https://www.virion-serion.de). Results are given as the ratio of patient sample/control sample). An antibody ratio of ≥1.1 was considered positive, of ≥0.8 to <1.1 borderline, and of <0.8 negative.

### Virus Neutralization Assay

Vero E6 cells (ATCC CRL-1586, https://www.atcc.org) and SARS-CoV-2 virus were cultured as described by Heilingloh et al. (*7*). Neutralization capacity of serum samples was determined by endpoint dilution assay, expressed as 50% tissue culture infective dose ($TCID_{50}$)/mL. Serial dilutions (1:20–1:2560) of serum samples were incubated with 100 $TCID_{50}$ of SARS-CoV-2 for 1 h at 37°C and added afterwards to confluent Vero E6 cells cultured in 96-well microtiter plates. On day 3 after infection, the cells were stained with crystal violet (Roth, https://www.carlroth.com) and dissolved in 20% methanol (Merck, https://www.merck.com); we analyzed the appearance of cytopathic effects (CPE) by light microscopy. The neutralizing titer was defined as the reciprocal of the highest serum dilution at which no CPE breakthrough in any of the triplicate cultures was observed.

### ELISpot Assay

ELISpot stripes containing PVDF membranes (MilliporeSigma MultiScreen HTS; Fisher Scientific, https://www.fishersci.com) were activated with 50 μL of 35% ethanol for 10 s and washed with distilled water. Plates were then coated for 3 h with 60 μL of monoclonal antibodies against IFN-γ (10 μg/mL of clone 1-D1K; Mabtech, https://www.mabtech.com). Thereafter, ELISpot plates were washed and then blocked with 150 μL AIM-V (Thermo Fisher Scientific, https://www.thermofisher.com). After 30 min at 37°C, AIM-V was discarded and duplicates of 250,000 peripheral blood mononuclear cells (PBMC) were grown in the presence or absence of either PepTivator SARS-CoV-2 protein S1/S2 or membrane (M) protein (600 pmol/mL of each peptide; Miltenyi Biotec, https://www.miltenyibiotec.com) or an S1 protein (4 μg/mL; Sino Biologic, https://www.sinobiological.com) in 150 μL of AIM-V. The peptide mix (PepTivator) of the S1/S2 protein covered the immunodominant domains, the peptide mix of the M protein, and the complete sequence of the glycoprotein. The S1 protein was a recombinant protein expressed in (human) HEK293 cells (Appendix Figure 1, https://wwwnc.cdc.gov/EID/article/27/1/20-3772- App1.pdf). After 19 h incubation at 37°C, the ELISpot plates were washed and captured IFN-γ was detected by incubation for 1 h with 50 μL of the alkaline phosphatase-conjugated monoclonal antibody against IFN-γ (clone 7-B6–1, Mabtech), diluted 1:200 with phosphate-buffered saline plus 0.5% bovine serum album. After further washing, 50 μL of nitro blue tetrazolium/5-bromo-4-chloro-3-indolylphosphate was added; purple spots appeared within 7 min. Spot numbers were analyzed by an ELISpot reader (AID Fluorospot, Autoimmun Diagnostika GmbH, https://www.aid-diagnostika.com). Mean values of duplicate cell cultures were considered. We determined SARS-CoV-2–specific spots by spot increment, defined as stimulated minus nonstimulated values. Stimulated spot numbers ≥3-fold higher than negative (unstimulated) controls combined with an increment value of ≥3 to any of the 3 antigens were considered positive. Of note, the negative controls reached a mean value of 0.27 spots and an SD of 0.48 (Appendix).

### Statistical Analysis

We performed statistical analysis using GraphPad Prism version 8.0.1 (https://www.graphpad.com) and IBM SPSS Statistics 23 (https://www.ibm.com/spss/statistics) software. We used linear regression analysis for numerical variables. The analysis of categorical variables was performed by Mann-Whitney test or 1-way analysis of variance (Kruskal-Wallis test) with Dunn's correction for multiple comparisons, as appropriate. Two-sided p values <0.05 were considered significant.

## Results

In 78 potential convalescent plasma donors with PCR-confirmed SARS-CoV-2 infection, the median interval between onset of symptoms and first blood sampling was 60 days (range 22–112 days) (Figure 1). Thirteen out of 78 (17%) donors had either borderline or negative results (ratio <1.1) to the Anti-SARS-CoV-2 IgG ELISA (Euroimmun). Altogether, 28 CP donors were tested again at later time points, a median of 75 days (24–154 days) after onset of symptoms. Retesting in 10 participants with a ratio of <1.1 showed that most antibody results (9/10) remained similar. The median interval between both

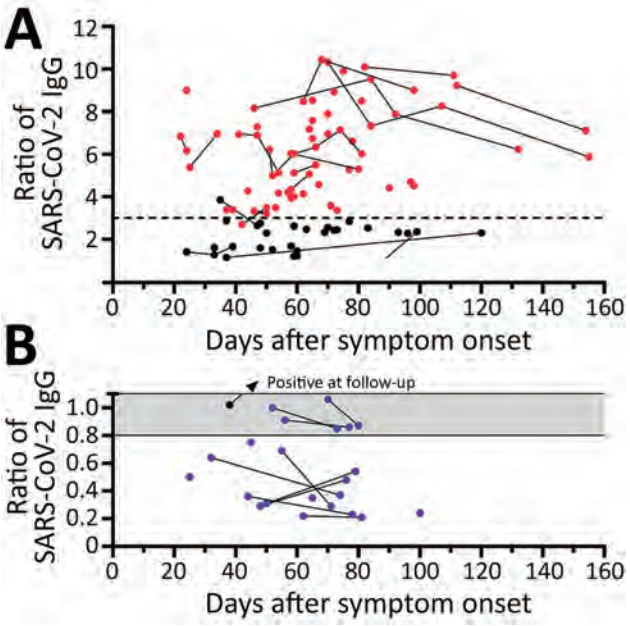


**Figure 1.** Distribution of SARS-CoV-2 IgG in 78 potential convalescent-plasma donors with PCR-confirmed infection, Germany. Red dots represent study participants with antibody ratio >3; black dots, participants with a ratio of 1.1–3; blue dots, participants with ratio <1.1. Sequential data are connected. Horizontal dashed line indicates a ratio of 3. A) Antibody ratios in the positive or intermediate range. B) Antibody ratios in the borderline or negative range. Gray shading indicates borderline values (ratio of 0.8–1.1); scale is adjusted to enhance data visualization. SARS-CoV-2, severe acute respiratory syndrome coronavirus 2.

blood samplings in this group was 25 days (range 10–61 days). In 1 volunteer with a borderline ratio, the value increased over time and became positive. In donors with higher antibody ratios, the values also remained at a similar level. In all participants with an antibody ratio <0.8, no neutralizing antibodies could be found; in those with a ratio of 0.8–1.1, the titer was 1:20–1:40.

We compared the characteristics of participants with undetectable antibodies to those with intermediate (1.1–3.0) or high antibody ratio (>3) (Table). Of note, in the total cohort of 78 potential blood donors, the median antibody ratio was 3.37; we chose a ratio of 3 as our internal cutoff for convalescent plasma donations. None of the parameters, including age, sex, body mass index, interval to onset of symptoms, risk exposure, symptoms of SARS-CoV-2 infection, need for oxygen or antibiotic treatment, or blood group, differed significantly. However, female participants tended to be overrepresented in the group with undetectable antibodies (p = 0.1 by Kruskal-Wallis test). One of the 78 potential CP donors did not report any symptoms of SARS-CoV-2 infection in the questionnaire. This participant showed an antibody ratio of 3.9.

Cellular immunity was determined from day 24 to day 154 after the onset of COVID-19 symptoms, parallel to antibody testing (Appendix Figure 2). Immunity was followed up as a control in participants with undetectable or low antibodies (irrespective of a triggering event) or when plasma was donated. We established an IFN-γ ELISpot assay separately for each of various stimuli, peptide pools of the S1/S2 and the M protein, and an S1 protein antigen of SARS-CoV-2 (Figures 2, 3). None of the ELISpot responses differed significantly between 9 participants with undetectable antibody responses (ratio <1.1) and 15 with high antibody responses (ratio >3) (Figure 2). However, ELISpot responses to all stimuli were substantially higher than in the negative controls. Nevertheless, the strength of responses toward the S1 protein tended to be higher in the group with a ratio of >3 versus <1.1 (Figure 2, panel A); whereas it was only marginally higher toward the S1/S2 peptides (Figure 2 panel B) and similar toward M peptides (Figure 2, panel C). The strength of responses toward S1/S2 peptides tended to be higher overall than the S1 protein alone. CP donors with an antibody ratio <1.1 showed a median frequency of 3 spots per 250,000 PBMC for stimulation with S1 protein, 6 with S1/S2 peptides, and 11 with M peptides. CP donors with an antibody ratio >3 showed a median frequency of 7 spots per 250,000 PBMC with S1 protein, 10 with S1/S2 peptides, and 13 with M peptides.

To analyze a possible interrelationship between T cell responses against different SARS-CoV-2 antigens and between T- and B-cell responses, we plotted results of various assays (Figure 3; Appendix Figure 3). We observed that patients whose antibody ratio was <1.1 showed robust ELISpot responses mainly directed against the M protein, whereas patients who had a ratio >3 had responses similarly directed against S1/S2 or S1 protein and M protein (Figure 3). We furthermore found that cellular responses against S1/S2 or S1 protein were all low (maximum of 13 spots increment against S1/S2 and 5 against S1 protein) in participants with an antibody ratio <1.1. In contrast, participants with a ratio >3 reached maximum values of 85 (S1/S2 protein) and 32 (S1 protein) spots increment. Maximum responses toward M peptides were more similar: 39 spots increment in CP donors with a ratio of <1.1 or 57 in those with ratio >3.

Cellular immunity toward any of the SARS-CoV-2 antigens was detectable in 7/9 (78%) participants who had an antibody ratio <1.1. In comparison, 12/15 (80%) donors with an antibody ratio of >3 had

detectable cellular immunity. Considering all potential CP donors with PCR-confirmed SARS-CoV-2 infection (also those with a ratio of 1.1–3), 22/28 (79%) were classified as positive by ELISpot.

In summary, we could detect T-cell immunity against SARS-CoV-2 in most of the SARS-CoV-2 PCR-positive healthy participants with undetectable IgG antibodies against the S1 protein. In this group, T-cell immunity was more strongly directed against the M than the S1 protein.

## Discussion

We focused on a cohort of volunteer study participants with PCR-confirmed SARS-CoV-2 infection who did not react positive to an S1-specific SARS-CoV-2 IgG ELISA. We observed undetectable humoral response in 17% of our potential blood donors. Similar to our data, other groups reported a lack of antibody response in a subset of patients infected with SARS-CoV-2. For example, a study in China reported absence of antibodies in 10%–20% of participants (W. Tan et al., unpub. data, https://doi.org/10.1101/2020.03.24.20042382). Moreover, Cervia et al. described that, in 15%–20% of S protein–seronegative patients (IgG in the serum), S protein–specific IgA was detectable at several mucosal sites (C. Cervia et al., unpub. data, https://doi.org/10.1101/2020.05.21.108308). Previous publications demonstrated that the magnitude of the humoral response toward SARS-CoV-2 was dependent on the duration and magnitude of viral antigen exposure (*8*,*9*; C. Cervia et al.). The absence of durable systemic IgG responses may indicate mild and transient SARS-CoV-2 infection that was cleared effectively (e.g., by the innate immune system) (*10*). However, whether this transient immune response had led to protective immunity needs to be clarified. The detection of SARS-CoV-2–specific IgG is not considered consistently to be a correlate of virus control (*11*–*13*).

Protection of humans against reinfection can be proven definitively only by rechallenge. However, the assessment of cellular immunity can supplement the data on humoral response. The specificity of T-cell assays critically depends on the antigen used for stimulation. In this study, we chose the S protein as stimulus because of its importance as a target for neutralizing antibodies and because it contains major immunodominant epitopes. It mediates the entry of the SARS-CoV-2 virus into the host cell (*14*,*15*). The S1 subunit of the S protein acts on the cell binding, and the S2 subunit acts on the fusion of the viral membrane to the cell membrane (*16*; H. Wang et al., unpub. data, https://doi.org/10.1101/2020.03.26.994756). Data by Okba et al. (*17*) indicate that S1 is the most specific antigen for the diagnosis of COVID-19. The S2 subunit is the more conserved one, and could cross-react with the S protein of severe acute respiratory syndrome coronavirus (SARS-CoV-1) or MERS-CoV (*17*,*18*). However, the infection rate with SARS-CoV-1 or MERS-CoV appears low in Caucasian populations. We selected the M protein, another surface protein of SARS-CoV-2, as a second stimulus because it has been observed to also contain dominant T-cell epitopes (*19*). It plays a central role in virus assembly (*20*)

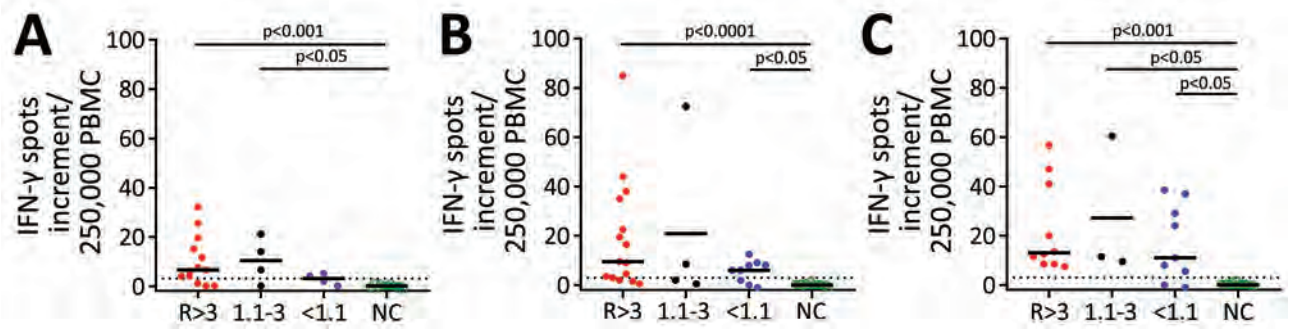


**Figure 2.** Cellular immunity against severe acute respiratory syndrome coronavirus 2 (SARS-CoV-2) as determined by ELISpot assay in potential convalescent-plasma donors with PCR-confirmed infection, Germany. Peripheral blood mononuclear cells of volunteers were stimulated by an S1 protein antigen of SARS-CoV-2 (A) and by peptide pools of the S1/S2 (B) and the M protein (C). If volunteers were tested sequentially, we only included the first dataset. The 3 left groups represent potential convalescent-plasma donors with PCR-confirmed SARS-CoV-2 infection. They either had a strong positive antibody response to the SARS-CoV-2 IgG ELISA as defined by an antibody ratio (R) of >3 (n = 15), an intermediate response (ratio of 1.1–3, n = 4) or borderline or negative results (ratio of <1.1, n = 9). The right group displays data in healthy controls without symptoms of respiratory or gastrointestinal infections and without household contact with SARS-CoV-2 infected patients since January 2020 (n = 22). The group has tested negative or has not been tested by SARS-CoV-2 PCR. Responses in the 4 groups of volunteers were compared by Kruskal-Wallis test with Dunn's correction. Dotted lines represent 3 spots increment. Horizontal lines indicate median values. Stimulation by S1 protein could not be performed in 7 volunteers; stimulation by the M peptide pool could not be performed in 6. Red dots represent volunteers with an antibody ratio >3; black dots, volunteers with a ratio of 1.1–3; blue dots, volunteers with ratio <1.1; green, NC. IFN-γ, interferon-γ; NC, negative controls.

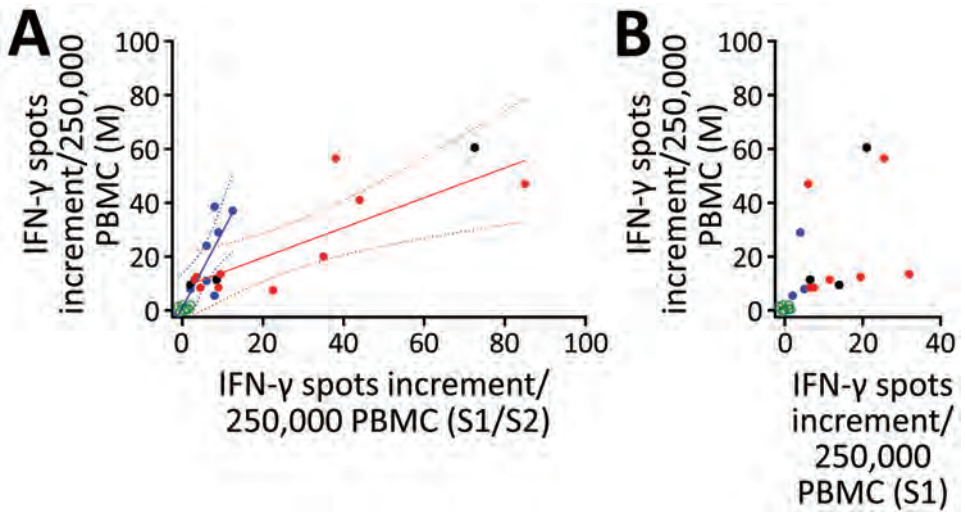


**Figure 3.** Interrelationship between results of various severe acute respiratory syndrome coronavirus 2 (SARS-CoV-2)–specific cellular assays in potential convalescent-plasma donors with PCR-confirmed infection, Germany. The plots include the first dataset in potential convalescent plasma donors and in negative controls. Red dots represent volunteers with an antibody ratio >3; black dots, volunteers with a ratio of 1.1–3; blue dots, volunteers with ratio <1.1; green dots, NC. PBMCs of volunteers were stimulated by peptide pools of the S1/S2 and the M protein and by an S1 protein antigen of SARS-CoV-2. A) Analysis of ELISpot assay with S1/S2 peptides versus M peptides. We performed 2 linear regression analyses separately for potential plasma donors with an IgG ratio >3 and <1.1. Solid lines show regression lines and dotted lines 95% CI. B) Analysis of ELISpot assay with S1 protein versus M peptides. ELISpot, enzyme-linked immunospot; IFN-γ, interferon-γ; PBMC, peripheral blood mononuclear cells.

and is more likely a target of cross-reactive T cells. Structural comparisons of SARS-CoV-1 and SARS-CoV-2 proteins showed 76% identity for the S protein and more for other structural proteins: 91% for the envelope protein, 90% for the M protein, and 95% for nucleocapsid (*19*). We observed that potential CP donors with undetectable antibodies against the S1 protein of SARS-CoV-2 had T-cell responses more strongly directed against the M than the S1 protein. Thus, we speculated that their T cells may preferentially target viral peptides involved in virus assembly rather than cell binding; this hypothesis needs confirmation. Responses toward the S1/S2 peptides were stronger than to the S1 protein, possibly because additional immunodominant T-cell epitopes in the S2 antigen caused the stronger response. The finding that the T-cell responses to the S1 protein, which is most specific to SARS-CoV-2, were relatively low raises the issue of potential cross-reactivity after stimulation with the S1/S2 or M peptides. Cross-reactivity has been shown for antibodies directed against SARS-CoV-1 and SARS-CoV-2 (*13*).

Similarly, SARS-CoV-2 cross-reactive T cells due to contact to common coronaviruses may occur (*5*,*21*) that could interfere with the specificity of our ELISpot assays. Nevertheless, recent PCR-confirmed SARS-CoV-2 infection could have caused the frequency of reactive T cells toward SARS-CoV-2 to be higher in the current cohort of potential CP donors than those reactive toward other common coronaviruses. Furthermore, cross-reactive T cells could be protective against SARS-CoV-2 infection, especially in children and young adults with frequent social contacts (*5*). Using flow cytometry, Braun et al. (*5*) detected pre-existing SARS-CoV-2 S-cross-reactive CD4+ T cells in 34% of healthy donors, and Grifoni et al. (*25*) in ≈40%–60% of unexposed persons. However, arguing against cross-reactivity interfering with our ELISpot assays, we observed negative T-cell responses in the negative control group.

Of interest, differences between participants with a ratio of <1.1 and of >3 seem to be more pronounced after stimulation with the S1 protein than the S1/S2 peptides. Thus, apart from the M protein, the S2 protein may be an additional target of T-cell responses, especially in participants with undetectable T- and B-cell responses against the S1 protein.

Chandrashekar et al. observed near-complete protection in 9 rhesus macaques after SARS-CoV-2 infection (*22*). After initial viral clearance, upon re-challenge, the animals showed a 5 $\log_{10}$ reduction in median viral loads compared with primary infection and an anamnestic humoral and cellular immune response. Moreover, Deng et al. reported that viral load remained negative in 4 rhesus macaques upon rechallenge with SARS-CoV-2 but showed a transient increase in body temperature (*23*). Similarly, Kirkcaldy et al. reported limited evidence of reinfection in humans with previously documented COVID-19 (*24*). Other studies demonstrated that SARS-CoV-2–specific T cells were detectable in the majority of recovered patients (*21*; N.L. Bert et al., unpub. data, https://doi.org/10.1101/2020.05.26.115832). Data on the earlier coronavirus SARS-CoV-1 indicated

that cellular immunity was detectable for >17 years after infection. Similar to our findings, studies from Sweden and France recently observed T cell responses against SARS-CoV-2 in seronegative persons (*6*; Gallais et al.), Sekine et al. reported that 4/31 (13%) patients who recovered from mild symptoms of COVID-19 were seronegative, which is very similar to 17% of seronegative results in our cohort. Assessment of T cell immunity by flow cytometry showed a greater difference of T-cell responses toward S1/S2 and M peptide pools between seronegative and seropositive patients than our study; this difference may be attributable to several differences between the studies; that is, we here used the ELISpot method instead of flow cytometry to measure specific T cells and our seronegative CP donors were all PCR positive, whereas none of the CP donors was tested positive by SARS-CoV-2 PCR (*6*).

ELISpot data on other coronaviruses have been reported since 2004. The authors of these early studies used either human leukocyte antigens (HLA)–A2 restricted peptides (*25*) or overlapping peptide pools spanning the whole SARS-CoV-1 proteome (*26*). ELISpot data in patients in China who recovered from SARS-CoV-1 infection 1 month earlier showed T-cell immunity in 100% of participants (*25*), and in 50% of patients recovered 12 months earlier (*26*). Our ELISpot data determined at a median of 2 months after the onset of symptoms indicate that 79% of participants had detectable T-cell immunity, which fits well with the previous data on the structurally related coronavirus SARS-CoV-1. A study on SARS-CoV-1 from 2008 (*26*) showed that T cell responses were mainly directed against the S protein and that CD8+ T-cell responses were more frequent and of a greater magnitude than CD4+ T-cell responses. Furthermore, a recent study indicated that on day 14 after injection of an adenovirus-vectored COVID-19 vaccine vigorous ELISpot responses against overlapping peptides of the S protein were induced (*27*). Compared with our data, responses at day 14 were higher. However, compared with a recent study using mosaic surface protein consisting of exposed extracellular domains of the SARS-CoV-2 spike, envelope, and membrane proteins (*28*), we observed slightly stronger T-cell responses in our convalescent patients, although the assays with mosaic surface protein were performed earlier after the onset of symptoms (day 6–32). This difference could be attributable to the use of various stimuli.

As of August 2020, we face the challenge of estimating how many persons are still susceptible to SARS-CoV-2 infection. The ELISpot assay we established may help to identify patients with adaptive immunity against SARS-CoV-2 infection. The assay has the following advantages: it is applicable for routine use, measures cellular immunity within 1 day on a single cell level, determines functional cells, and is independent from HLA restriction. However, it does not allow researchers to determine which T-cell population responds upon restimulation. According to our data in volunteers with confirmed SARS-CoV-2 infection, it could be speculated that the majority of persons with undetectable systemic IgG may presumably be protected by specific T-cell immunity, which would be good news for the control of the pandemic.

### Acknowledgments

We thank Babette Große-Rhode and Martina Filipovic for their excellent technical assistance. We thank all volunteers for their participation and the donation of blood samples.

This study was supported by the Stiftung Universitätsmedizin Essen (A.K.) and the Rudolf Ackermann Foundation (O.W.).

### About the Author

Ms. Schwarzkopf is a bachelor student in medical biology working in the group of M. Lindemann at the Institute for Transfusion Medicine, University Hospital Essen, Germany. The research focus of her group is antimicrobial immune responses in immunocompromised patients.

### References

1. Chen L, Xiong J, Bao L, Shi Y. Convalescent plasma as a potential therapy for COVID-19. Lancet Infect Dis. 2020;20:398–400. https://doi.org/10.1016/S1473-3099(20)30141-9
2. Shen C, Wang Z, Zhao F, Yang Y, Li J, Yuan J, et al. Treatment of 5 critically ill patients with COVID-19 with convalescent plasma. JAMA. 2020;323:1582–9. https://doi.org/10.1001/jama.2020.4783
3. Salazar E, Christensen PA, Graviss EA, Nguyen DT, Castillo B, Chen J, et al. Treatment of coronavirus disease 2019 patients with convalescent plasma reveals a signal of significantly decreased mortality. Am J Pathol. 2020 Aug 10 [Epub ahead of print]. https://doi.org/10.1016/j.ajpath.2020.08.001
4. Zhao J, Alshukairi AN, Baharoon SA, Ahmed WA, Bokhari AA, Nehdi AM, et al. Recovery from the Middle East respiratory syndrome is associated with antibody and T cell responses. Sci Immunol. 2017;2:eaan5393. https://doi.org/10.1126/sciimmunol.aan5393
5. Braun J, Loyal L, Frentsch M, Wendisch D, Georg P, Kurth F, et al. SARS-CoV-2-reactive T cells in healthy donors and patients with COVID-19. Nature. 2020. https://doi.org/10.1038/s41586-020-2598-9
6. Sekine T, Perez-Potti A, Rivera-Ballesteros O, Strålin K, Gorin J-B, Olsson A, et al.; Karolinska COVID-19 Study Group. Robust T cell immunity in convalescent individuals with asymptomatic or mild COVID-19. Cell. 2020

Aug 14 [Epub ahead of print]. https://doi.org/10.1016/j.cell.2020.08.017
7. Heilingloh CS, Aufderhorst UW, Schipper L, Dittmer U, Witzke O, Yang D, et al. Susceptibility of SARS-CoV-2 to UV irradiation. Am J Infect Control. 2020;S0196-6553(20)30756-2.
8. Liu Y, Yan LM, Wan L, Xiang TX, Le A, Liu JM, et al. Viral dynamics in mild and severe cases of COVID-19. Lancet Infect Dis. 2020;20:656–7. https://doi.org/10.1016/S1473-3099(20)30232-2
9. Zhou F, Yu T, Du R, Fan G, Liu Y, Liu Z, et al. Clinical course and risk factors for mortality of adult inpatients with COVID-19 in Wuhan, China: a retrospective cohort study. Lancet. 2020;395:1054–62. https://doi.org/10.1016/S0140-6736(20)30566-3
10. Tay MZ, Poh CM, Rénia L, MacAry PA, Ng LFP. The trinity of COVID-19: immunity, inflammation, and intervention. Nat Rev Immunol. 2020;20:363–74. https://doi.org/10.1038/s41577-020-0311-8
11. Ni L, Ye F, Cheng ML, Feng Y, Deng YQ, Zhao H, et al. Detection of SARS-CoV-2-specific humoral and cellular immunity in COVID-19 convalescent individuals. Immunity. 2020;52:971–7 e3.
12. To KK, Tsang OT, Leung WS, Tam AR, Wu TC, Lung DC, et al. Temporal profiles of viral load in posterior oropharyngeal saliva samples and serum antibody responses during infection by SARS-CoV-2: an observational cohort study. Lancet Infect Dis. 2020;20:565–74. https://doi.org/10.1016/S1473-3099(20)30196-1
13. Hoffmann M, Kleine-Weber H, Schroeder S, Kruger N, Herrler T, Erichsen S, et al. SARS-CoV-2 cell entry depends on ACE2 and TMPRSS2 and is blocked by a clinically proven protease inhibitor. Cell. 2020;181:271–80 e8. https://doi.org/10.1016/j.cell.2020.02.052
14. Zhou P, Yang XL, Wang XG, Hu B, Zhang L, Zhang W, et al. A pneumonia outbreak associated with a new coronavirus of probable bat origin. Nature. 2020;579:270–3. https://doi.org/10.1038/s41586-020-2012-7
15. Wrapp D, Wang N, Corbett KS, Goldsmith JA, Hsieh CL, Abiona O, et al. Cryo-EM structure of the 2019-nCoV spike in the prefusion conformation. Science. 2020;367:1260–3. https://doi.org/10.1126/science.abb2507
16. Wang C, Li W, Drabek D, Okba NMA, van Haperen R, Osterhaus ADME, et al. A human monoclonal antibody blocking SARS-CoV-2 infection. Nat Commun. 2020;11:2251. https://doi.org/10.1038/s41467-020-16256-y
17. Okba NMA, Müller MA, Li W, Wang C, GeurtsvanKessel CH, Corman VM, et al. Severe acute respiratory syndrome coronavirus 2–specific antibody responses in coronavirus disease patients. Emerg Infect Dis. 2020;26:1478–88. https://doi.org/10.3201/eid2607.200841
18. Jaimes JA, André NM, Chappie JS, Millet JK, Whittaker GR. Phylogenetic analysis and structural modeling of SARS-CoV-2 spike protein reveals an evolutionary distinct and proteolytically sensitive activation loop. J Mol Biol. 2020;432:3309–25. https://doi.org/10.1016/j.jmb.2020.04.009
19. Ahmed SF, Quadeer AA, McKay MR. Preliminary identification of potential vaccine targets for the COVID-19 coronavirus (SARS-CoV-2) based on SARS-CoV immunological studies. Viruses. 2020;12:254. https://doi.org/10.3390/v12030254
20. Neuman BW, Kiss G, Kunding AH, Bhella D, Baksh MF, Connelly S, et al. A structural analysis of M protein in coronavirus assembly and morphology. J Struct Biol. 2011;174:11–22. https://doi.org/10.1016/j.jsb.2010.11.021
21. Grifoni A, Weiskopf D, Ramirez SI, Mateus J, Dan JM, Moderbacher CR, et al. Targets of T cell responses to SARS-CoV-2 coronavirus in humans with COVID-19 disease and unexposed individuals. Cell. 2020;181:1489–501. https://doi.org/10.1016/j.cell.2020.05.015
22. Chandrashekar A, Liu J, Martinot AJ, McMahan K, Mercado NB, Peter L, et al. SARS-CoV-2 infection protects against rechallenge in rhesus macaques. Science. 2020;369:812–7. https://doi.org/10.1126/science.abc4776
23. Deng W, Bao L, Liu J, Xiao C, Liu J, Xue J, et al. Primary exposure to SARS-CoV-2 protects against reinfection in rhesus macaques. Science. 2020;369:818–23. https://doi.org/10.1126/science.abc5343
24. Kirkcaldy RD, King BA, Brooks JT. COVID-19 and postinfection immunity. JAMA. 2020;323:2245–6. https://doi.org/10.1001/jama.2020.7869
25. Wang YD, Sin WY, Xu GB, Yang HH, Wong TY, Pang XW, et al. T cell epitopes in severe acute respiratory syndrome (SARS) coronavirus spike protein elicit a specific T-cell immune response in patients who recover from SARS. J Virol. 2004;78:5612–8. https://doi.org/10.1128/JVI.78.11.5612-5618.2004
26. Li CK, Wu H, Yan H, Ma S, Wang L, Zhang M, et al. T cell responses to whole SARS coronavirus in humans. J Immunol. 2008;181:5490–500. https://doi.org/10.4049/jimmunol.181.8.5490
27. Zhu FC, Li YH, Guan XH, Hou LH, Wang WJ, Li JX, et al. Safety, tolerability, and immunogenicity of a recombinant adenovirus type-5 vectored COVID-19 vaccine: a dose-escalation, open-label, non-randomised, first-in-human trial. Lancet. 2020;395:1845–54. https://doi.org/10.1016/S0140-6736(20)31208-3
28. Thijsen S, Heron M, Gremmels H, van der Kieft R, Reusken C, Kremer K, et al. Elevated nucleoprotein-induced interferon-γ release in COVID-19 patients detected in a SARS-CoV-2 enzyme-linked immunosorbent spot assay. J Infect. 2020;81:452–82. https://doi.org/10.1016/j.jinf.2020.06.015

Address for correspondence: Monika Lindemann, Institute for Transfusion Medicine, Robert-Koch-Haus, Virchowstr 179, University Hospital Essen, 45147 Essen, Germany; email: monika.lindemann@uk-essen.de

# Estimating the Force of Infection for Dengue Virus Using Repeated Serosurveys, Ouagadougou, Burkina Faso

Jacqueline K. Lim, Mabel Carabali, Tansy Edwards, Ahmed Barro, Jung-Seok Lee, Desire Dahourou, Kang Sung Lee, Teguewende Nikiema, Mee Young Shin, Emmanuel Bonnet, Therese Kagone, Losseni Kaba, Suk Namkung, Paul-André Somé, Jae Seung Yang, Valéry Ridde, In-Kyu Yoon, Neal Alexander, Yaro Seydou

Because of limited data on dengue virus in Burkina Faso, we conducted 4 consecutive age-stratified longitudinal serologic surveys, ≈6 months apart, among persons 1–55 years of age, during June 2015–March 2017, which included a 2016 outbreak. The seroconversion rate before the serosurvey enrollment was estimated by binomial regression, taking age as the duration of exposure, and assuming constant force of infection (FOI) over age and calendar time. We calculated FOI between consecutive surveys and rate ratios for potentially associated characteristics based on seroconversion using the duration of intervals. Among 2,897 persons at enrollment, 66.3% were IgG-positive, and estimated annual FOI was 5.95%. Of 1,269 enrollees participating in all 4 serosurveys, 438 were IgG-negative at enrollment. The annualized FOI ranged from 10% to 20% (during the 2016 outbreak). Overall, we observed high FOI for dengue. These results could support decision-making about control and preventive measures for dengue.

Author affiliations: International Vaccine Institute, Seoul, South Korea (J.K. Lim, M. Carabali, J.-S. Lee, K.S. Lee, M.Y. Shin, S. Namkung, J.S. Yang); London School of Hygiene and Tropical Medicine, London, UK (J.K. Lim, T. Edwards, N. Alexander); Centre MURAZ, Bobo-Dioulasso, Burkina Faso (D. Dahourou, T. Nikiema, T. Kagone, Y. Seydou); McGill University, Montreal, Quebec, Canada (M. Carabali); Action, Gouvernance, Intégration, Renforcement Program Equité, Ouagadougou, Burkina Faso (A. Barro, P.-A. Somé); Institut de Recherché en Sciences de la Santé, Ouagadougou (D. Dahourou); Institute for Research on Sustainable Development, Université de Paris, Paris, France (E. Bonnet, V. Ridde); Centre National de Transfusion Sanguine, Ouagadougou (L. Kaba); Coalition for Epidemic Preparedness Innovations, Washington, DC, USA (I.-K. Yoon)

DOI: https://doi.org/10.3201/eid2701.191650

Dengue fever is a mosquitoborne disease caused by 4 related but antigenically distinct dengue viruses (DENVs), serotypes 1–4. Annually, ≈50–100 million cases of dengue are reported worldwide, with 20,000 deaths (*1*). *Aedes* mosquitoes and dengue cases were documented in Africa as early as 1823, and cases have since been reported in 34 countries in Africa (*2*). In Burkina Faso, since the first outbreak in 1925, there have been multiple others (*2*), including in 2013, 2016, and 2017 (*3*–*5*). The 2016 outbreak included 1,061 dengue rapid-diagnostic test (RDT) positive cases and 15 deaths in the capital, Ouagadougou, with a reported case-fatality rate (CFR) of 1.2% (*4*,*6*). The 2017 outbreak included 5,773 RDT-positive cases and 18 deaths throughout the country, for a CFR of 0.2% (*5*). These repeated outbreaks suggest a considerable dengue burden in the country.

Despite this burden, data on dengue seroprevalence and force of infection (FOI), the rate at which initial or heterotypic infections are acquired, are scarce in Burkina Faso and Africa (*7*). In terms of seroprevalence in Burkina Faso, 1 study found the dengue IgG seroprevalence among 683 pregnant women and blood donors to be 26.3% in rural and 36.5% in urban settings in 2003–2004 (*8*). To define DENV transmission in Burkina Faso, we conducted 4 serologic surveys in the same study participants in Ouagadougou during 2015–2017. The study targeted 3 objectives. First, we measured seroprevalence of DENV by IgG positivity at enrollment, serosurvey 1 (S1). Second, we estimated age-specific annual FOI, measured by seroconversion in the repeated follow-up surveys (S2–S4). Last, because a dengue outbreak occurred in 2016, between the third and fourth serosurveys, we identified and compared demographic and clinical characteristics associated with DENV seroconversion in the outbreak and nonoutbreak periods.

## Methods

### Study Area and Population

We selected the study area based on data, including seroprevalence and modeling results, available in the literature and existing research infrastructure (*9*–*11*). Ouagadougou is the capital of Burkina Faso in West Africa; most of the population resides in urban settings (*12*,*13*). The rainy season is May–October. The serosurveys were conducted in a defined catchment population of 100,000 residents. The resident population in Ouagadougou is stable, with an annual rate of migration of only 4.1% and >80% of residents owning their homes (*14*).

### Study Design

We conducted 4 serosurveys, each ≈6 months apart. The age-stratified sample of ≈3,000 residents 1–55 years of age, 80% <35 years of age, reflected the age distribution of the general population of Ouagadougou (*9*). In 6 preselected sectors, we randomly selected households on the basis of existing census data; all eligible household members were offered enrollment. To reach the needed sample size, if members of the initially invited household declined, we invited a neighboring household to enroll. We conducted a short interview and collected blood samples (*9*). Test results were shared with the participants and we followed the same procedures with the same participants for the 3 subsequent serosurveys.

### Laboratory Testing Algorithm

We tested samples using a Panbio Dengue IgG Indirect ELISA test (Abbott Diagnostics, https://www.abbott.com), as described elsewhere (*9*). Following the manufacturer's guidelines, we set the IgG threshold for positivity at an index value of 1.1, to detect levels resulting from past or recent infections of any serotype. An index value of 0.9–1.1 was classified equivocal (requiring repeated testing), and <0.9 was considered negative. We considered seroconversion of dengue IgG between the pretransmission and posttransmission surveys to result from dengue infection.

### Statistical Analysis

#### Characteristics by Dengue IgG Status at Enrollment

We present a descriptive summary by dengue IgG status at enrollment (seropositive vs. seronegative). We used $\chi^2$ or Fisher exact tests to make categorical pair-wise comparisons across dengue status. Continuous variables were compared using Student *t*-test or analysis of variance.

#### FOI Calculations

DENV infection can occur with any of the 4 serotypes and, assuming lifelong acquired homotypic immunity, we estimated the FOI based on IgG seropositivity status (*15*,*16*). However, because IgG ELISA tests cannot distinguish among the 4 serotypes, infection in this analysis refers to seroconversion to any DENV serotype (*15*). We used binomial regression with a complementary log-log link function (*17*–*20*). In part A of the FOI analysis, in which data from the enrollment serosurvey were analyzed, we estimated the average FOI over each participant's lifetime using age as the time at risk. In part B of the FOI analysis, using data from the subset of participants who contributed to all 4 serosurveys, we estimated the FOI between consecutive surveys. We considered participants who were initially seronegative to be at risk for seroconversion and used the interval between consecutive surveys as the time at risk. We provide details of FOI calculations in the Appendix (https://wwwnc.cdc.gov/EID/article/27/1/19-1650-App1.pdf).

#### Seroconversion Rate Ratios

For the between-survey analyses, we estimated seroconversion rate ratios (RRs) using binomial regression models with the log time of the actual duration of each participant's interval (i.e., time between consecutive surveys for that person) for potential risk factors, including age, sex, neighborhood, level of education, occupation, any known previous dengue infection, yellow fever (YF) vaccination history, and any self-reported signs and symptoms during the particular interval. As a sensitivity analysis, seroconversion RRs were estimated for consecutive paired results, irrespective of results from other surveys. For example, if a participant was IgG-negative at S2, then IgG-positive at S3, we considered this seroconversion between S2 and S3, even if the person had been IgG-positive at S1.

S1–S2 covered the nonoutbreak rainy season in 2015, S2–S3 covered the nonoutbreak nonrainy season in 2016, and S3–S4 covered the 2016 outbreak. To assess how demographic and clinical characteristics are associated with DENV seroconversion and the difference in patterns in the outbreak (S3–S4) compared with those in nonoutbreak periods (S1–S2 and S2–S3), we compiled a descriptive summary of demographic and clinical characteristics for participants at risk (IgG-negative) at each serosurvey, broken down between participants who had or had not seroconverted by the subsequent serosurvey. All analyses were performed using SAS version 9.4 (https://www.sas.com).

### Ethics Considerations

The study protocol received ethics approvals from the institutional review boards of the International Vaccine Institute, the London School of Hygiene and Tropical Medicine, the National Ethical Committee for Health Research of Burkina Faso, and the Ethics Committee of the Centre Hospitalier de l'Université de Montréal at University of Montreal. We obtained written consent forms from each participant ≥18 years old. For participants 8–17 years old, we obtained an assent form from the participant and an informed consent from ≥1 parent or legal guardian. For participants ≤7 years old, we obtained an informed consent from ≥1 parent or legal guardian.

## Results

We obtained complete demographic (age and neighborhood) and laboratory data for 2,897 of 3,026 participants (Figure 1). At enrollment (S1), in June 2015, 1,920 (66.3%) of 2,897 participants were IgG positive. At S2, in December 2015, 1,417 (67.2%) of 2,109 participants were IgG positive. At S3, in May 2016, 1,400 (66.5%) of 2,106 participants were IgG positive. At S4, in March 2017, 1,121 (67.9%) of 1,651 participants were IgG positive.

#### Characteristics by Dengue IgG Status at Enrollment

Based on data from the 2,897 participants with complete information, 82% of 1–4-year-olds and 65% of 5–9-year-olds were IgG negative and therefore at risk of infection at the start of the study (Table 1). IgG positivity increased with age, so that by age 26, IgG positivity reached 80% (Figure 2). The binomial regression based on IgG positivity by age at enrollment, assuming the FOI was constant over ages and calendar time (part A), resulted in an annual FOI of 5.95% (95% CI 5.66–6.24) (Figure 2).

#### Annual FOI in IgG-Negative Participants Who Contributed to All 4 Serosurveys

In part B, we calculated annualized FOI among participants who had been IgG negative at the preceding serosurvey using binomial regression with the inter-survey interval, calculated in years, as the time at risk. For the interval S1–S2, FOI per year was 14.0% (95% CI 9.5%–18.4%); for the interval S2–S3, 9.6% (95% CI 5.4%–13.8%); and for the interval S3–S4, 20.3% (95% CI 16.1%–24.5%) (Figure 1). The mean duration was 0.53 years (≈6 months) for interval S1–S2; 0.44 years for S2–S3; and 0.84 years for S3–S4. Age-specific annual FOIs were calculated and older age groups with <5 seronegative participants were merged. For intervals S1–S2 and S2–S3, FOI was higher for older participants (Figure 1). For interval S3–S4, high FOIs of 30% per year were found in participants 15–19 and 25–29 years of age.

#### Seroconversion RRs from Outbreak Versus Nonoutbreak Intervals

We analyzed data from each pair of surveys, not restricted to data from participants in all 4 surveys, to examine differences in dengue seroconversion

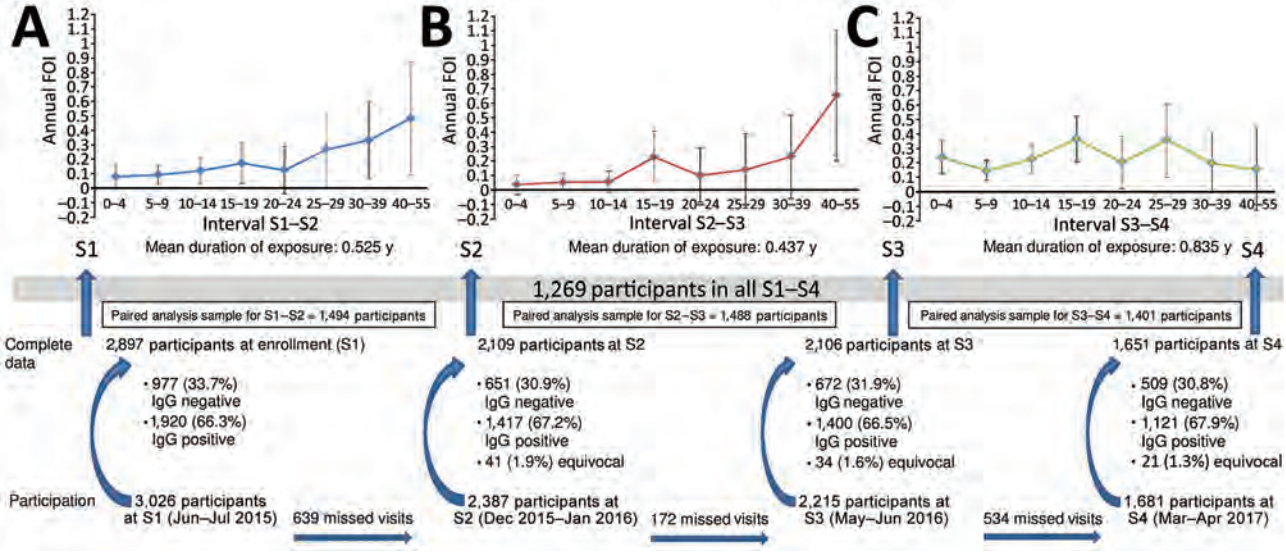


**Figure 1.** Flowchart of participant enrollment and graphs of annual force of infection rates during a rainy season (A), a nonrainy season (B), and the 2016 dengue outbreak (C) in study of force of infection for dengue virus, Ouagadougou, Burkina Faso, June–July 2015. Labels along x-axes (e.g., 0–4) indicate age ranges in years. Error bars indicate 95% CIs. To be considered complete, records had to contain lab results and basic demographic information. Seroconversion rates in the paired analyses were based solely on results from one survey to the next (e.g., S2–S3). Dengue serostatus in previous or subsequent surveys was not considered. S, serosurvey.

during outbreak versus nonoutbreak intervals. During nonoutbreak interval S1–S2 (analysis sample = 1,494), 33 (7.3%) of 455 participants at risk (i.e., IgG negative at S1), showed seroconversion. During nonoutbreak interval S2–S3 (analysis sample = 1,488), 23 (5.2%) of 443 participants at risk (i.e., IgG negative at S2), showed

**Table 1.** Demographic and clinical characteristics of participants in study of force of infection for dengue virus, by dengue IgG status at enrollment, Ouagadougou, Burkina Faso, June–July 2015*

| Characteristics | All participants,† N = 2,897 | Seropositive,‡ n = 1,920 | Seronegative,‡ n = 977 | p value§ |
|---|---|---|---|---|
| Mean age, SD | 22.32 (13.92) | 27.02 (13.36) | 13.08 (9.74) | <0.001 |
| Age group, y | | | | <0.001 |
| 1–4 | 208 (7.2) | 37 (1.9) | 171 (17.5) | |
| 5–9 | 410 (14.2) | 142 (7.4) | 268 (27.4) | |
| 10–14 | 384 (13.3) | 189 (9.8) | 195 (20.0) | |
| 15–19 | 379 (13.1) | 243 (12.7) | 136 (13.9) | |
| 20–29 | 694 (24.0) | 560 (29.2) | 134 (13.7) | |
| 30–39 | 410 (14.2) | 357 (18.6) | 53 (5.4) | |
| 40–49 | 264 (9.1) | 249 (13.0) | 15 (1.5) | |
| 50–55 | 148 (5.1) | 143 (7.5) | 5 (0.5) | |
| Sex¶ | | | | <0.001 |
| M | 1,154 (39.9) | 700 (36.5) | 454 (46.5) | |
| F | 1,741 (60.1) | 1,218 (63.5) | 523 (53.5) | |
| Ethnicity | | | | 0.712 |
| Burkinabé | 2,871 (99.6) | 1,906 (99.6) | 965 (99.5) | |
| Others | 13 (0.5) | 8 (0.4) | 5 (0.5) | |
| Neighborhood/sector | | | | <0.001 |
| Sector 22 | 447 (18.2) | 342 (20.5) | 105 (13.3) | |
| Sector 25 | 510 (20.7) | 395 (23.6) | 115 (14.6) | |
| Juvenat fille | 517 (21.0) | 353 (21.1) | 164 (20.8) | |
| Pazani | 433 (17.6) | 281 (16.8) | 152 (19.2) | |
| Zongo | 547 (22.2) | 297 (17.8) | 250 (31.7) | |
| Nioko | 8 (0.3) | 4 (0.2) | 4 (0.5) | |
| Occupation | | | | <0.001 |
| Student | 1,033 (35.8) | 586 (30.6) | 447 (46.0) | |
| Housewife | 885 (30.7) | 666 (34.8) | 219 (22.5) | |
| Small business owner | 163 (5.7) | 130 (6.8) | 33 (3.4) | |
| Unskilled worker | 153 (5.3) | 124 (6.5) | 29 (3.0) | |
| Government official | 92 (3.2) | 77 (4.0) | 15 (1.5) | |
| Private sector employee | 82 (2.8) | 66 (3.5) | 16 (1.7) | |
| Merchant | 55 (1.9) | 46 (2.4) | 9 (0.9) | |
| Retired | 53 (1.8) | 26 (1.4) | 27 (2.8) | |
| Farmer | 49 (1.7) | 35 (1.8) | 14 (1.4) | |
| Skilled worker | 43 (1.5) | 32 (1.7) | 11 (1.1) | |
| Service sector worker | 43 (1.5) | 34 (1.8) | 9 (0.9) | |
| Education level | | | | <0.001 |
| Illiterate | 887 (30.7) | 596 (31.1) | 291 (29.9) | |
| Literate, no education | 72 (2.5) | 58 (3.0) | 14 (1.4) | |
| 1–6 y of school | 803 (27,8) | 455 (23.8) | 348 (35.8) | |
| 7–10 y of school | 551 (19.1) | 388 (20.3) | 163 (16.8) | |
| 11–13 y of school | 274 (9.5) | 200 (10.4) | 74 (7.6) | |
| ≥University | 210 (7.5) | 171 (8.9) | 39 (3.0) | |
| Others# | 57 (2.0) | 39 (2.0) | 18 (1.9) | |
| Self-reported preexisting conditions | | | | |
| Cardiovascular | 113 (4.0) | 100 (5.3) | 13 (1.4) | <0.001 |
| Diabetes | 10 (0.4) | 7 (0.4) | 3 (0.3) | 0.817 |
| Lung disease | 19 (0.7) | 17 (0.9) | 2 (0.2) | 0.034 |
| Cerebrovascular | 27 (0.9) | 18 (0.9) | 9 (0.9) | 0.990 |
| Musculoskeletal | 101 (3.5) | 82 (4.3) | 19 (2.0) | 0.002 |
| Gastrointestinal | 193 (6.7) | 148 (7.8) | 45 (4.7) | 0.002 |
| Anemia | 10 (0.4) | 2 (0.1) | 8 (0.80) | 0.002 |
| Others | 108 (3.8) | 79 (4.1) | 29 (3.0) | 0.139 |
| Self-reported previous dengue | | | | <0.001 |
| Yes | 13 (0.5) | 13 (0.7) | 0 | |
| No | 2,421 (84.7) | 1,635 (86.0) | 786 (82.1) | |
| Unknown | 426 (14.9) | 254 (13.4) | 172 (18.0) | |

*Values are no. (%) except as indicated.
†Total participants enrolled at serosurvey 1.
‡Results of IgG indirect ELISA among participants at serosurvey 1.
§p values based on $\chi^2$ test.
¶2 individuals with missing information on sex.
#Religious and other informal education.

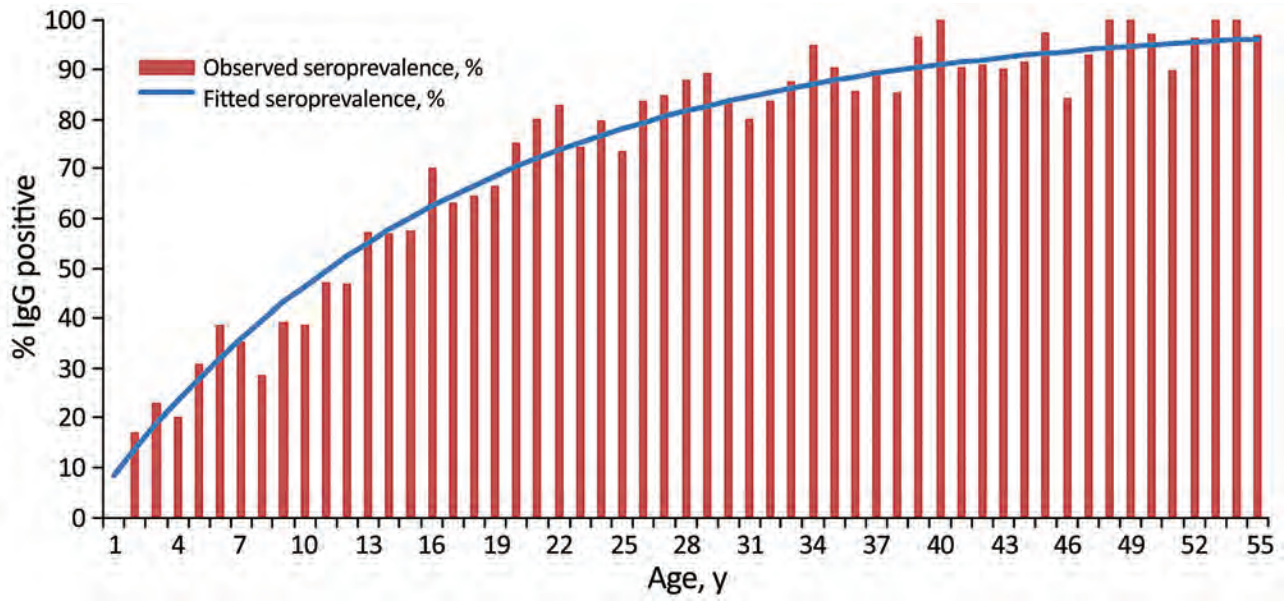


**Figure 2.** Seroprevalence, measured by IgG ELISA, of dengue IgG by age at enrollment and fitted prevalence using the FOI per year in study of force of infection for dengue virus, Ouagadougou, Burkina Faso, June–July 2015. Graph shows observed seroprevalence at enrollment among all 2,897 participants and fitted seroprevalence using FOI. In the FOI analysis part A, the FOI per year was 0.0595 (95% CI 0.0566–0.0624), estimated by binomial regression, with the assumption of constant risk across ages and calendar time prior to the enrollment serosurvey, and a complementary log-log link, with log(midpoint of age) as an offset. The intercept is interpreted as the logarithm of the FOI. FOI, force of infection.

seroconversion. During outbreak interval S3–S4 (analysis sample = 1,401) 78 (17.1%) of 455 participants at risk (i.e., IgG negative at S3), showed seroconversion. We compiled demographic and clinical characteristics of participants with IgG seroconversion compared with participants who remained IgG negative during each interval (Table 2, https://wwwnc.cdc.gov/EID/article/27/1/19-1650-T2.htm).

To assess how these variables might be associated with changes in rates of seroconversion, we estimated RRs of seroconversion during the intervals. We found that older age was positively associated with an increased rate of seroconversion. Compared with those 1–4 years of age, participants 25–55 years of age had higher seroconversion over S1–S2 [RR 4.1 (95% CI 1.4–15.0)]; both 15–24-year-old participants [RR 4.6 (95% CI 1.4–17.4)] and 25–55-year-old participants [RR 9.1 (95% CI 12.9–34.2)] had higher seroconversion over S2–S3 (Table 3).

## Discussion

Our study provides data on population-based seroprevalence and rates of DENV seroconversion that may help with assessing the largely undocumented burden of dengue fever in Africa. The dengue burden in Africa has been conjectured to be similar to that in the Americas but has been largely unrecognized and masked by other illnesses with similar symptoms (*21*,*22*). In particular, the major strength of this study was that we longitudinally followed the same participants using 4 repeated serosurveys to measure the FOI of dengue in Burkina Faso.

Although IgG ELISA test results might be influenced by cross-reactivity with different flaviviruses, our estimate of seroprevalence was comparable to prevalence estimates from other studies, all tested using IgG ELISA: 61% of participants 1–65 years of age in Colombia (*25*); 83.1% in participants 15–19 years of age in Tahiti (*26*); 74% in participants in a low socioeconomic area in Recife, Brazil (*27*); and 68.7% in participants in Salvador, Brazil (*28*). The overall proportion of IgG-positive participants remained similar across the surveys, although it was highest at S4 (68%). The small increase in seropositivity despite an outbreak between S3 and S4 may have resulted from different participants being lost to follow-up at each consecutive survey. Such losses were substantial during the S1–S2 and S3–S4 intervals. The mean age of participants lost during S1–S2 was 20.7 years (95% CI 19.3–22.0) and was 23.7 (95% CI: 22.5–24.9) during S3–S4. The mean age of the participants was 22.2 years (95% CI 21.6–22.9) during S1–S2 and 21.6 (95% CI 21.0–22.2) during S3–S4. For S1–S2, the mean age was not significantly different between nonparticipants

and remaining participants, but lost participants were significantly older for S3–S4; participants lost at follow-up might have tended to be IgG positive, plausibly resulting in underestimating IgG positivity at the follow-up survey. While decreasing representativeness is a limitation, we based FOI calculations on seroconversion meaning they likely would not have been substantially affected. We found apparent seroreversion from seropositive to seronegative in <3% of the paired samples: 29 during S1–S2, 14 during S2–S3; and 38 during S3–S4. However, we could not distinguish whether such cases were due to test errors or waning immunity.

Data from the baseline serosurvey in this study (part A) resulted in an annual FOI of 6.0%, although this assumes that it was constant over age and calendar time. This finding is comparable with estimates from other regions, such as Sri Lanka at 14% per year (*15*); Colombia at 8.7% (*22*); and a low socioeconomic area in Recife, Brazil, at 5.3% (*25*). Our model seems to capture the increase in baseline seroprevalence with age (Figure 1). However, any given age profile in a cross-sectional study can result from different combinations of incidence varying over age or over calendar time (*27*). Therefore, the estimated FOI from the baseline survey is subject to more limitations than FOIs estimated from the paired surveys. Nonetheless, our data support that dengue may be a bigger public health problem in Africa than is currently recognized.

From the repeat surveys (part B) for which we knew the exact duration of the intervals, we could measure the FOI more directly without assuming a constant value over age, providing a more accurate estimate of the magnitude of transmission. These estimates were higher than the 6% annual FOI based on the enrollment survey. Among 1,269 participants with IgG results from all 4 serosurveys, annual FOIs were 14% for S1–S2, 10% for S2–S3, and 20% for S3–S4. Testing of paired samples showed that 7.3% (33/455) seroconverted during S1–S2, 5.2% (23/443) during S2–S3, and 17.1% (78/455) during S3–S4. As we expected, the annualized estimates of rates were ≈2 times the simple proportions for the first 2 intervals. For the third interval (S3–S4), the annualized FOI was ≈1.5 times (12/8 months) the proportion seroconverting, because the conversion between proportions and rates is less linear for higher values.

The paired survey analyses did not require an assumption of constant FOI before the study and showed that FOI varied markedly across time within the study. In particular, a high annualized FOI (20%) was observed between S3–S4, coinciding with a major outbreak. However, even during nonoutbreak intervals, we found considerable dengue transmission; annualized FOIs ranged from 10% (in a nonrainy

**Table 3.** Univariable binomial regression showing ratio of rates of seroconversion in study of force of infection for dengue virus, based on results of IgG indirect ELISA assays, Ouagadougou, Burkina Faso, June–July 2015*

| | S1–S2,† N = 455, IgG-S (n = 33) vs. IgG-N (n = 422) | | S2–S3,† N = 443, IgG-S (n = 23) vs. IgG-N (n = 420) | | S3–S4,† N = 455, IgG-S (n = 78) vs. IgG-N (n = 377) | |
|---|---|---|---|---|---|---|
| Characteristics | IgG-S rate (95% CI) | p value‡ | IgG-S rate (95% CI) | p value‡ | IgG-S rate (95% CI) | p value‡ |
| Age range, y | | **0.006** | | **0.002** | | 0.038 |
| 1–4 | Referent | | Referent§ | | Referent | |
| 5–9 | 0.70 (0.19–2.84) | | | | 0.65 (0.31–1.37) | |
| 10–14 | 1.00 (0.27–4.05) | | 2.25 (0.53–9.52) | | 1.00 (0.48–2.12) | |
| 15–24 | 1.99 (0.65–7.35) | | **4.55 (1.37–17.38)** | | 1.77 (0.91–3.60) | |
| 25–55 | **4.11 (1.37–14.99)** | | **9.13 (2.87–34.20)** | | 1.29 (0.55–2.94) | |
| Sex | | 0.155 | | 0.166 | | 0.686 |
| M | Referent | | Referent | | Referent | |
| F | 1.67 (0.84–3.51) | | 1.83 (0.80–4.55) | | 1.10 (0.70–1.72) | |
| Preexisting conditions¶ | | **0.016** | | **0.017** | | 0.433 |
| None/unknown | Referent | | Referent | | Referent | |
| Yes | **2.67 (1.13–5.67)** | | **3.11 (1.12–7.48)** | | 1.29 (0.64–2.34) | |
| Occupation | | 0.935 | | **0.025** | | 0.177 |
| Student | Referent | | Referent | | Referent | |
| At home# | 1.11 (0.45–2.56) | | **3.81 (1.45–11.05)** | | 1.64 (0.96–2.75) | |
| Others** | 1.15 (0.50–2.54) | | 1.70 (0.53–5.45) | | 1.16 (0.66–2.01) | |
| Level of education | | 0.917 | | 0.191 | | 0.164 |
| Illiterate/no schooling | Referent | | Referent | | Referent | |
| Elementary | 1.19 (0.52–2.89) | | 0.39 (0.12–1.06) | | 0.80 (0.45–1.42) | |
| ≥Secondary | 1.15 (0.48–2.85) | | 0.61 (0.23–1.55) | | 1.33 (0.78–2.32) | |

*Bold indicates statistical significance. IgG-S, IgG seroconverted; IgG-N, IgG negative; S, serosurvey.
†Paired survey intervals. S1–S2: July–December 2015; S2–S3: January 2016–May 2016; S3–S4: June 2016–March 2017.
‡p values based on $\chi^2$ test.
§Age groups 1–4 and 5–9 merged due to data scarcity in seroconverted participants.
¶Based on self-report by participants.
#Housewife, retired, unemployed.
**Business owners, employees, workers, etc.

season, such as S2–S3) to 14% (in a rainy season, S1–S2) (*28*). Little comparable information from the region is available, but these rates are comparable to the 8.7% per year reported from Colombia (*23*).

These annual rates of infection, measured by seroconversion, may include both initial and subsequent heterotypic infection, because these are indistinguishable by IgG ELISA. However, in our analysis, the influence of past infection is minimal, because we focused on participants with IgG-negative status at enrollment for calculations of FOIs between surveys. This study was unable to distinguish participants with single or multiple infections during the study period. Furthermore, among those with multiple infections, cyclical dominance among DENV serotypes is observed in regions with better-documented dengue endemicity (*29*,*30*). However, cocirculation of multiple DENV serotypes in Burkina Faso has yet to be fully demonstrated. Thus, in our study, we calculated an overall FOI, for the totality of serotypes (*20*,*31*). Still, we recognize the need for more in-depth analyses using neutralization assays to understand serotype-specific transmission patterns in Africa.

In part B of the study, without having to assume that risk is constant over age, we found that FOI was higher in older than in younger participants, although these findings are based on small numbers, given that most people had already seroconverted at younger ages. FOI increased with age in the intervals of the nonoutbreak times (S1–S2 and S2–S3), which has also been found in Colombia (*23*). Our data are from IgG seroconversion rather than clinical dengue, but incidence of dengue fever in the 2016 outbreak in Burkina Faso was also higher among teenagers and young adults (*4*,*6*,*32*). In contrast, in the outbreak interval S3–S4, the FOI was similar across ages (13%–34%), possibly suggesting the emergence of a different serotype with little preexisting population immunity (*20*). Without much data on serotype-specific DENV incidence in Burkina Faso, previous studies and reports of ministry of health and World Health Organization investigations suggest that the 2016 outbreak was mainly caused by DENV-2 (*4*,*6*,*32*).

Myalgia during S1–S2, arthralgia during S2–S3, and fatigue during S3–S4 were positively associated with seroconversion with statistical significance. Whereas cases of seroconversion may have been associated with either mild or subclinical illnesses, participants were asked whether they had experienced these symptoms in the interval since the previous survey. These symptoms are common in dengue illness; myalgia and arthralgia were listed in the 1997 World Health Organization dengue case classifications, and fatigue or lethargy in 2009 classifications (*33*–*35*). However, because these self-reported symptoms were recorded at intervals of 6–8 months, without prompt investigation to identify a cause, we cannot conclude that any associations with seroconversion are causal.

This study is subject to several limitations. First, the generalizability of this study is limited by participants all being recruited from the urban population in the capital city. The magnitude and patterns of DENV transmission may differ in other regions of Burkina Faso, including rural areas, with different age profiles, ecologic settings, or socioeconomic conditions. Also, although a large number of participants (1,269) participated in all 4 serosurveys, a substantial number of original participants missed surveys. Those participants who missed ≥1 surveys were more likely to be older than those who participated in all surveys. This shortfall could have led us to underestimate prevalence.

Second, our results were based on serologic testing using IgG ELISA. Further analyses using neutralization assays are planned, but no confirmatory testing was applied to verify the IgG results. For estimating dengue FOI, serologic cross-reaction with other flaviviruses affecting the observed dengue IgG rates is a commonly reported limitation (*36*,*37*). Ultimately, this limitation could result in inaccurate seroprevalence and FOI estimates because antibodies against nondengue flaviviruses could have been detected (*15*,*38*). In particular, Zika virus has been reported in Burkina Faso (*39*,*40*), as have outbreaks of YF in 1998, 2003, and 2004 (*41*–*43*). Vaccine-induced YF antibodies could also result in interference with the specificity of IgG ELISA (*38*). In our data, at each of the serosurveys, <5% of participants answered that they had received YF vaccination; although subject to recall bias, this rate is much lower than the coverage rate of 85% reported by the Expanded Program on Immunization in 2007 (*42*). Using self-reported YF vaccination history as a proxy for YF virus seropositivity, we found no difference in IgG positivity between participants reporting and not reporting vaccination, a finding supported by others (*38*,*44*).

Despite the possible effect of cross-reactivity on dengue ELISAs, 2 studies reported a concordance level of 99% between the plaque reduction neutralization test (PRNT) and dengue IgG results (*37*,*45*). Also, when IgG ELISA results were verified by using serologic data among 13,661 participants from 13 countries to estimate dengue FOI, IgG ELISA results were confirmed by 50% PRNT in >97% of the IgG-positive samples (*20*). Samples from 277 healthy

adults in a rural district in Malaysia were tested with the same ELISA test used in our study, and PRNT was performed on a subset of IgG-positive samples (*46*). Evidence of past infection was found in 75.5% (209/277) of participants and, of 96 samples randomly selected to undergo PRNT testing, all 96 were dengue-confirmed with ≥50% plaque reduction for DENV and showed that the detected antibodies were specific to dengue virus (*46*).

The sensitivity of this commercial DENV IgG indirect ELISA was reported as 99.2% and the specificity as 96.2% when compared with the hemagglutination inhibition (HI) method (*47*). A study compared performance of IgG ELISA to that of HI testing in a serosurvey of 327 children in Tahiti and reported sensitivity and specificity, as well as agreement between the 2 tests, to be >83% for all DENV serotypes (*24*). Another study reported 90.9% sensitivity and 92.9% specificity of the IgG indirect ELISA when compared with HI, also with a high correlation between the tests (*48*). Whereas those data are from outside of Africa, where a different and unknown composition of flaviviruses may be circulating, the results indicate a high degree of agreement between IgG ELISA and more confirmatory and better validated tests, such as HI and PRNT.

If cross-reactivity across other flaviviruses were to result in misclassifications, leading to a high rate of false positives, our findings would be overestimates of the true disease prevalence and FOI. However, given the high concordance between IgG and PRNT or HI assay results based on available data and because we analyzed data from paired serosurveys of participants who were IgG negative at enrollment, we believe that our results were minimally affected by this issue.

In conclusion, our estimates of both seroprevalence and FOI were comparable with those from dengue-endemic countries in the Americas. Repeated outbreaks indicate a considerable level of DENV transmission in Ouagadougou, but the extent of transmission and hyperendemicity needs to be further verified. Specifically, additional longitudinal evaluation with confirmatory tests and linked clinical evaluation of dengue fever in the general population in the region would be necessary to further validate our findings. Seroprevalence and FOI are important factors to be considered when making evidence-based decisions to implement interventions for prevention and control, including vaccine introduction. In the absence of other reliable data, our findings on dengue seroprevalence and FOI based on consecutive serosurveys provide practical evidence that could be used to support policy decisions.

This study was supported by funding from the Bill and Melinda Gates Foundation (grant no. OPP 1053432), as well as funding from the governments of Sweden, India, and South Korea. This research project was part of the "Community Research Studies and Interventions for Health Equity in Burkina Faso" program, funded by the Canadian Institutes of Health Research (ROH-115213). N.A. and T.E. were supported by award MR/R010161/1, which is jointly funded by the UK Medical Research Council (MRC) and the UK Department for International Development (DFID) under the MRC/DFID Concordat agreement and is also part of the European and Developing Countries Clinical Trials Partnership (EDCTP) -2 program, supported by the European Union.

## About the Author

Dr. Lim is a research scientist in the Development and Delivery Unit of the International Vaccine Institute (IVI), Seoul, South Korea. She has been working as an epidemiologist in IVI for the Global Dengue and *Aedes*-Transmitted Diseases Consortium, previously the Dengue Vaccine Initiative, where she was in charge of field operations in Thailand, Colombia, Vietnam, Cambodia, Burkina Faso, Gabon, and Kenya.

## References

1. World Health Organization. Global strategy for dengue prevention and control 2012–2020. Geneva: World Health Organization; 2012. Report no.: WHO/HTM/NTD/VEM/2012.5 [cited 2018 Aug 18]. https://www.who.int/denguecontrol/9789241504034
2. Amarasinghe A, Kuritsky J, Letson G, Margolis H. Dengue virus infection in Africa. Emerg Infect Dis. 2011;17:1349–54. https://dx.doi.org/10.3201/eid1708.101515
3. Ministère de la Santé. Progress report on the investigation of suspected cases of dengue in the Central health region [in French]. Ouagadougou, Burkina Faso: Directorate of Disease Control; 2013.
4. World Health Organization. Dengue fever—Burkina Faso. Disease outbreak news: 2016 November 18 [cited 2018 Aug 18]. http://www.who.int/csr/don/18-november-2016-dengue-burkina-faso/en/
5. World Health Organization. Dengue fever—Burkina Faso. Disease outbreak news: 2017 November 6 [cited 2018 Aug 18]. http://www.who.int/csr/don/6-november-2017-dengue-burkina-faso/en/
6. Tarnagda Z, Cissé A, Bicaba B, Diagbouga S, Sagna T, Ilboudo A, et al. Dengue fever in Burkina Faso, 2016. Emerg Infect Dis 2018;24:170–2. https://dx.doi.org/10.3201/eid2401.170973
7. Ridde V, Agier I, Bonnet E, Carabali M, Dabiré K, Fournet F, et al. Presence of three dengue serotypes in Ouagadougou (Burkina Faso): research and public health implications. Infect Dis Poverty. 2016;5:23. https://10.1186/s40249-016-0120-2

8. Collenberg E, Ouedraogo T, Ganame J, Fickenscher H, Kynast-Wolf G, Becher H, et al. Seroprevalence of six different viruses among pregnant women and blood donors in rural and urban Burkina Faso: a comparative analysis. J Med Virol. 2006;78:683–92. https://doi.org/10.1002/jmv.20593
9. Lim J, Carabali M, Lee J-S, Lee K-S, Namkung S, Lim S-K, et al. Evaluating dengue burden in Africa in passive fever surveillance and seroprevalence studies: protocol of field studies of the Dengue Vaccine Initiative. BMJ Open. 2018;8:e017673. https://doi.org/10.1136/bmjopen-2017-017673
10. Messina J, Brady O, Scott T, Zou C, Pigott D, Duda K, et al. Global spread of dengue virus types: mapping the 70 year history. Trends Microbiol. 2014;22:138–46. https://doi.org/10.1016/j.tim.2013.12.011
11. Brady OJ, Gething PW, Bhatt S, Messina JP, Brownstein JS, Hoen AG, et al. Refining the global spatial limits of dengue virus transmission by evidence-based consensus. PLoS Negl Trop Dis. 2012;6:e1760. https://doi.org/10.1371/journal.pntd.0001760
12. Ministry of Health (Burkina Faso). Statistical yearbook 2016 [in French]. Ouagadougou, Burkina Faso: Ministry of Health, 2017 [cited 2019 Apr 1]. http://ghdx.healthdata.org/record/burkina-faso-health-statistical-yearbook-2016
13. World Population Review. Population of cities in Burkina Faso (2019) [cited 2019 October 3]. http://worldpopulationreview.com/countries/burkina-faso-population/cities/
14. Rossier C, Soura A, Baya B, Compaoré G, Dabiré B, Dos Santos S, et al. Profile: the Ouagadougou Health and Demographic Surveillance System. Int J Epidemiol. 2012;41:658–66. https://doi.org/10.1093/ije/dys090
15. Tam CC, Tissera H, de Silva AM, De Silva AD, Margolis HS, Amarasinge A. Estimates of dengue force of infection in children in Colombo, Sri Lanka. PLoS Negl Trop Dis. 2013;7:e2259. https://doi.org/10.1371/journal.pntd.0002259
16. Egger JR, Ooi EE, Kelly DW, Woolhouse ME, Davies CR, Coleman PG. Reconstructing historical changes in the force of infection of dengue fever in Singapore: implications for surveillance and control. Bull World Health Organ. 2008;86:161–240. https://doi.org/10.2471/blt.07.040170
17. Bhavsar D. Modelling binary data. London: Chapman and Hall; 1991.
18. Bhavsar A, Tam C, Garg S, Jammy G, Taurel A, Chong S, et al. Estimated dengue force of infection and burden of primary infections among Indian children. BMC Public Health. 2019;19:1116. https://doi.org/10.1186/s12889-019-7432-7
19. Prayitno A, Taurel A, Nealon J, Satari HI, Karyanti MR, Sekartini R, et al. . Dengue seroprevalence and force of primary infection in a representative population of urban dwelling Indonesian children. PLoS Negl Trop Dis. 2017;11:e0005621. [Erratum in: PLoS Negl Trop Dis. 2018;12:e0006467.] https://doi.org/10.1371/journal.pntd.0005621
20. Nealon J, Bouckenooghe A, Cortes M, Coudeville L, Frago C, Macina D, et al. Dengue endemicity, force of infection, and variation in transmission intensity in 13 endemic countries. J Infect Dis. 2020:jiaa132. [Erratum in: J Infect Dis. 2020;222:341–2.] https://doi.org/10.1093/infdis/jiaa132.
21. Bhatt S, Gething PW, Brady OJ, Messina JP, Farlow AW, Moyes CL, et al. The global distribution and burden of dengue. Nature. 2013;496:504–7. https://doi.org/10.1038/nature12060
22. Jaenisch T, Junghanss T, Wills B, Brady OJ, Eckerle I, Farlow A, et al. Dengue expansion in Africa—not recognized or not happening? Emerg Infect Dis. 2014;20:e140487. http://dx.doi.org/10.3201/eid2010.140487
23. Carabali M, Lim J, Velez D, Trujillo A, Egurrola J, Lee K, et al. Dengue virus serological prevalence and seroconversion rates in children and adults in Medellin, Colombia: implications for vaccine introduction. Int J Infect Dis. 2017;58:27–36. https://doi.org/10.1016/j.ijid.2017.02.016
24. Chungue E, Marché G, Plichart R, Boutin J, Roux J. Comparison of immunoglobulin g enzyme-linked immunosorbent assay (IgG-ELISA) and haemagglutination inhibition (HI) test for the detection of dengue antibodies, prevalence of dengue IgG-ELISA antibodies in Tahiti. Trans R Soc Trop Med Hyg. 1989;83:708–11. https://doi.org/10.1016/0035-9203(89)90404-5
25. Braga C, Luna CF, Martelli CM, de Souza WV, Cordeiro MT, Alexander N, et al. Seroprevalence and risk factors for dengue infection in socio-economically distinct areas of Recife, Brazil. Acta Tropica. 2010;113:234–40. https://doi.org/10.1016/j.actatropica.2009.10.021
26. Teixeira MG, Barreto ML, Costa MCN, Ferreira LDA, Vasconcelos PFC, Cairncross S. Dynamics of dengue virus circulation: a silent epidemic in a complex urban area. Trop Med Int Health. 2002;7:757–62. https://doi.org/10.1046/j.1365-3156.2002.00930.x
27. Boni M, Mølbak K, Krogfelt K. Inferring the time of infection from serological data. In: Held L, Hens N, O'Neill P, Wallinga, J, editors. Handbook of infectious disease data analysis. Boca Raton (FL): CRC Press; 2019. p. 287–303.
28. Wongkoon S, Jaroensutasinee M, Jaroensutasinee K. Distribution, seasonal variation and dengue transmission prediction in Sisaket, Thailand. Indian J Med Res. 2013;138:347–53.
29. Tan K-K, Zulkifle T-I, Abd-Jamil J, Sulaiman S, Yaacob CN, Azizan NS, et al. Disruption of predicted dengue virus type 3 major outbreak cycle coincided with switching of the dominant circulating virus genotype. Infect Genet Evol. 2017:271–5. https://doi.org/10.1016/j.meegid.2017.07.008
30. Gubler DJ. Dengue and dengue hemorrhagic fever. Clin Microbiol Rev 1998;11:480–96.
31. Imai N, Dorigatti I, Cauchemez S, Ferguson NM. Estimating dengue transmission intensity from sero-prevalence surveys in multiple countries. 2015;9(4):e0003719. https://doi.org/10.1371/journal.pntd.0003719
32. Lim JK, Seydou Y, Carabali M, Barro A, Dahourou DL, Lee KS, et al. Clinical and epidemiologic characteristics associated with dengue during and outside the 2016 outbreak identified in health facility-based surveillance in Ouagadougou, Burkina Faso. PLoS Negl Trop Dis. 2019;13:e0007882. https://doi.org/10.1371/journal.pntd.0007882
33. World Health Organization. Dengue guidelines for diagnosis, treatment, prevention, and control: new edition. Geneva: The Organization; 2009.
34. World Health Organization. Dengue and severe dengue. Fact sheets 2019 2 February [cited 2019 May 12]. http://www.who.int/news-room/fact-sheets/detail/dengue-and-severe-dengue
35. Hadinegoro SRS. The revised WHO dengue case classification: does the system need to be modified? Paediatr Int Child Health 2012;32 Suppl 1:33–8. https://doi.org/10.1179/2046904712Z.00000000052
36. Oliveira RA, de Oliveira-Filho EF, Fernandes AI, Brito CA, Marques ET, Tenório MC, et al. Previous dengue or Zika virus exposure can drive to infection enhancement or neutralisation of other flaviviruses. Mem Inst Oswaldo Cruz. 2019;114:e190098. https://doi.org/10.1590/0074-02760190098

37. Garg S, Chakravarti A, Singh R, Masthi NRR, Goyal RC, Jammy GR, et al. Dengue serotype–specific seroprevalence among 5- to 10-year-old children in India: a community-based cross-sectional study. Int J Infect Dis. 2017;54:25–30. https://doi.org/10.1016/j.ijid.2016.10.030
38. Santiago e Souza NC, Félix AC, de Paula AV, Levi JE, Pannuti CS, Romano CM. Evaluation of serological cross-reactivity between yellow fever and other flaviviruses. Int J Infect Dis. 2019;81:4–5. https://doi.org/10.1016/j.ijid.2019.01.023
39. World Health Organization. Zika virus (ZIKV) classification table. Geneva: The Organization; 2018 [cited 2019 June 1]. https://apps.who.int/iris/handle/10665/260419
40. Majumder MS, Hess R, Ross R, Piontkivska H. Seasonality of birth defects in West Africa: could congenital Zika syndrome be to blame? F1000 Res. 2018;2018:159. https://doi.org/10.12688/f1000research.13858.2
41. Collenberg E, Ouedraogo T, Ganamé J, Fickenscher H, Kynast-Wolf G, Becher H, et al. Seroprevalence of six different viruses among pregnant women and blood donors in rural and urban Burkina Faso: a comparative analysis. J Med Virol. 2006;78:683–92. https://doi.org/10.1002/jmv.20593
42. World Health Organization. Yellow fever in Burkina Faso. 2008 [cited 2019 May 29]. https://www.who.int/csr/don/2008_11_03
43. Mutebi J-P, Barrett ADT. The epidemiology of yellow fever in Africa. Microbes Infect. 2002;4:1459–68. https://doi.org/10.1016/s1286-4579(02)00028-x
44. da Silva-Nunes M, de Souza V, Pannuti C, Sperança M, Terzian A, Nogueira M, et al. Risk factors for dengue virus infection in rural Amazonia: population-based cross-sectional surveys. Am J Trop Med Hyg 2008;79:485–94.
45. Sasmono R, Taurel A, Prayitno A, Sitompul H, Yohan B, Hayati R, et al. Dengue virus serotype distribution based on serological evidence in pediatric urban population in Indonesia. PLoS Negl Trop Dis. 2018;12:e0006616. https://doi.org/10.1371/journal.pntd.0006616
46. Dhanoa A, Hassan S, Jahan N, Reidpath D, Fatt Q, Ahmad M, et al. Seroprevalence of dengue among healthy adults in a rural community in Southern Malaysia: a pilot study. Infect Dis Poverty. 2018;16:1. https://doi.org/10.1186/s40249-017-0384-1
47. McBride WJ, Mullner H, LaBrooy JT, Wronski I. The 1993 dengue 2 epidemic in North Queensland: a serosurvey and comparison of hemagglutination inhibition with an ELISA. Am J Trop Med Hyg. 1998;59:457–61. https://doi.org/10.4269/ajtmh.1998.59.457
48. Inoue S, Alonzo M, Kurosawa Y, Mapua C, Reyes J, Dimaano E, et al. Evaluation of a dengue IgG indirect enzyme-linked immunosorbent assay and a Japanese encephalitis IgG indirect enzyme-linked immunosorbent assay for diagnosis of secondary dengue virus infection. Vector Borne Zoonotic Dis. 2010;10:143–50.

Address for correspondence: Jacqueline K. Lim, Research Scientist, Global Dengue and *Aedes*-transmitted Diseases Consortium, International Vaccine Institute, SNU Research Park, Gwankak-ro 1, Gwanak-gu, Seoul 151-191, South Korea; email: kajlim@gmail.com

# Estimate of Burden and Direct Healthcare Cost of Infectious Waterborne Disease in the United States

Sarah A. Collier, Li Deng, Elizabeth A. Adam, Katharine M. Benedict, Elizabeth M. Beshearse, Anna J. Blackstock, Beau B. Bruce, Gordana Derado, Chris Edens, Kathleen E. Fullerton, Julia W. Gargano, Aimee L. Geissler, Aron J. Hall, Arie H. Havelaar, Vincent R. Hill, Robert M. Hoekstra, Sujan C. Reddy, Elaine Scallan, Erin K. Stokes, Jonathan S. Yoder, Michael J. Beach

Provision of safe drinking water in the United States is a great public health achievement. However, new waterborne disease challenges have emerged (e.g., aging infrastructure, chlorine-tolerant and biofilm-related pathogens, increased recreational water use). Comprehensive estimates of the health burden for all water exposure routes (ingestion, contact, inhalation) and sources (drinking, recreational, environmental) are needed. We estimated total illnesses, emergency department (ED) visits, hospitalizations, deaths, and direct healthcare costs for 17 waterborne infectious diseases. About 7.15 million waterborne illnesses occur annually (95% credible interval [CrI] 3.88 million–12.0 million), results in 601,000 ED visits (95% CrI 364,000–866,000), 118,000 hospitalizations (95% CrI 86,800–150,000), and 6,630 deaths (95% CrI 4,520–8,870) and incurring US $3.33 billion (95% CrI 1.37 billion–8.77 billion) in direct healthcare costs. Otitis externa and norovirus infection were the most common illnesses. Most hospitalizations and deaths were caused by biofilm-associated pathogens (nontuberculous mycobacteria, *Pseudomonas*, *Legionella*), costing US $2.39 billion annually.

At the beginning of the 20th century, diseases commonly transmitted by water, such as cholera and typhoid, were major causes of death in the United States (*1*). Reliable provision of treated, safe drinking water dramatically reduced the burden of these diseases and has been recognized as one of the greatest public health achievements of the 20th century (*2*). Despite this achievement, waterborne disease in the United States persists (*3*–*5*).

Author affiliation: Centers for Disease Control and Prevention, Atlanta, Georgia, USA

DOI: https://doi.org/10.3201/eid2701.190676

In the United States, outbreaks associated with large public drinking water systems have sharply declined in the past 40 years (*3*,*6*), likely the result of improvements in regulation and operation. However, transmission of disease via drinking water systems still occurs, often attributable to aging infrastructure, operational challenges, and the private or unregulated water systems (e.g., private wells) that serve an estimated 43 million persons (*7*). At the same time, the complexity and scope of water use has increased; drinking, sanitation, hygiene, cooling, and heating needs are supported by 6 million miles of plumbing inside US buildings (i.e., premise plumbing) (*8*,*9*). Premise plumbing water quality can be compromised by long water residency times, reduced disinfectant levels, and inadequate hot water temperatures, creating environments where pathogens (e.g., nontuberculous mycobacteria [NTM], *Pseudomonas*, and *Legionella*) can amplify in biofilms (*10*). People can be exposed to these pathogens through contact, ingestion, or inhalation of aerosols (e.g., from showerheads, building cooling towers, or decorative fountains).

As leisure time has increased, swimming pools, waterparks, water playgrounds, and hot tubs have proliferated (*5*). These venues rely largely on chlorination as the major barrier against disease transmission. *Cryptosporidium* has emerged as the major cause of outbreaks associated with treated aquatic venues because it is extremely chlorine resistant and has a low infectious dose (*5*,*11*,*12*). Warmer oceans have led to *Vibrio*-associated wound infections farther north than previously documented (*13*).

Estimates of the overall burden of foodborne disease in the United States, including both known and unknown agents, have been useful in directing prevention

activities and setting public health goals (*14*,*15*). Quantifying the burden of infectious waterborne disease in the United States would also be beneficial.

Previous studies have attempted to estimate the burden of gastrointestinal illness (*16*,*17*) or all illness associated with drinking water (*18*) and untreated recreational water (*19*) in the United States, but the burden of disease from all water sources (drinking, recreational, environmental) and exposure routes (ingestion, contact, inhalation) has not been estimated. We present an estimate of the burden of waterborne disease in the United States that includes gastrointestinal, respiratory, and systemic disease; accounts for underdiagnosis; and includes all water sources and exposure routes.

## Methods

We defined waterborne disease as disease in which water was the proximate vehicle for exposure to an infectious pathogen. Thus, diseases such as Legionnaires' disease (typically transmitted via inhaled water droplets containing *Legionella* bacteria) were considered waterborne. In contrast, arboviral diseases like malaria, for which standing water can increase the population of mosquitoes that transmit the parasite that causes malaria, were not considered waterborne. Algal toxins and chemical exposures were not considered. We determined the proportion of disease totals that were attributed to domestic waterborne exposure.

For this estimate, we chose diseases for which surveillance data, administrative data, or literature reports indicated that waterborne transmission for the disease in the United States was plausible, the disease was likely to cause substantial illness or death, and data were available to quantify associated health outcomes. Diseases included in this analysis were campylobacteriosis, cryptosporidiosis, giardiasis, Legionnaires' disease, NTM infection, norovirus infection, acute otitis externa, *Pseudomonas* pneumonia and septicemia, Shiga toxin–producing *Escherichia coli* (STEC) infection serotype O157, non-O157 serotype STEC infection, salmonellosis, shigellosis, and vibriosis (including infection by *Vibrio alginolyticus*, *V. parahaemolyticus*, *V. vulnificus*, and other species). To aid in quantifying the burden of respiratory diseases and enteric disease separately, we considered Legionnaires' disease, NTM infection, and *Pseudomonas* pneumonia primarily respiratory diseases, whereas we considered campylobacteriosis, cryptosporidiosis, giardiasis, norovirus infection, salmonellosis, and shigellosis primarily enteric diseases.

We employed methods similar to those of Scallan et al. (*14*,*15*) to estimate the number of illnesses, treat-and-release emergency department (ED) visits (i.e., visits in which the person was not admitted to the hospital), hospitalizations, and deaths attributed to waterborne transmission in the United States. We also quantified the direct healthcare costs of treat-and-release ED visits and hospitalizations, as measured by insurer and out-of-pocket payments. Our overall methods are described here; detailed methods are described in Appendices 1–3 (https://wwwnc.cdc.gov/EID/article/27/1/19-0676-App1.pdf; https://wwwnc.cdc.gov/EID/article/ 27/1/19-0676-App2.pdf; https://wwwnc.cdc.gov/EID/ article/27/1/19-0676-App3.pdf).

Data were for 2000–2015. All estimates were based on the 2014 US population (318.6 million persons); 2014 was the most recent year for which data were available for all surveillance sources. Estimates were derived from statistical models; each model input had uncertainty represented by a distribution of plausible values. Inputs are described in Appendix 1 and more details on the modeling process are described in Appendix 2. All estimates were rounded to 3 significant figures.

### Illnesses

The initial model input was the number of reported or documented cases of illness for each disease, selected hierarchically: data from active surveillance systems were preferred, passive surveillance data were used if active surveillance data were not available, and administrative data were used if no active or passive surveillance system for the disease existed (Table 1). Administrative data sources included the Health Care Utilization Project (HCUP) National Inpatient Sample (HCUP NIS) hospitalization database, the HCUP National Emergency Department Sample (HCUP NEDS) ED visit database, and, in the case of otitis externa, the National Ambulatory Medical Care Survey (NAMCS), which surveys visits to physicians' offices. These administrative data sources use complex sample survey weighting methods and are considered nationally representative. We multiplied the initial reported or documented number of cases for each disease by a series of multipliers that accounted for underreporting and underdiagnosis (including illness severity, medical care-seeking, likelihood of specimen submission, proportion of laboratories capable of performing a diagnostic test, and test sensitivity).

### Emergency Department Visits

The surveillance systems used do not tally treat-and-release ED visits but do capture the proportion of patients hospitalized with a given disease; we combined this proportion with the ratio of treat-and-release ED visits for each disease (reported in HCUP NEDS) to hospitalizations for that disease (in HCUP NIS) to calculate the estimated proportion of reported cases

**Table 1.** Data sources used to estimate the total number of illnesses for selected infectious diseases, United States*

| Active surveillance data (name of surveillance system) | Passive surveillance data | Administrative data |
|---|---|---|
| Campylobacteriosis (FoodNet) | Giardiasis (NNDSS) | NTM infection (HCUP NEDS/NIS) |
| Cryptosporidiosis (FoodNet) | Legionnaires' disease (NNDSS) | Otitis externa (NAMCS, HCUP NEDS/NIS) |
| Norovirus (*20*,*21*) | *Vibrio* spp. infection (COVIS) | *Pseudomonas* pneumonia (HCUP NEDS/NIS) |
| Salmonellosis, nontyphoidal (FoodNet) | *Vibrio alginolyticus* infection (COVIS) | *Pseudomonas* septicemia (HCUP NEDS/NIS) |
| STEC infection, O157 (FoodNet) | *Vibrio parahaemolyticus* infection (COVIS) | |
| STEC infection, non-O157 (FoodNet) | *Vibrio vulnificus* infection (COVIS) | |
| Shigellosis (FoodNet) | Other *Vibrio* infection (COVIS) | |

*COVIS, Cholera and Other Vibrio Illness Surveillance; FoodNet, Foodborne Diseases Active Surveillance Network; HCUP NEDS/NIS, Healthcare Cost and Utilization Project's National Emergency Department Sample and National Inpatient Sample; NAMCS, National Ambulatory Medical Care Survey; NNDSS, National Notifiable Diseases Surveillance System; NTM, nontuberculous mycobacterial; STEC, Shiga toxin–producing *Escherichia coli*.

with an ED visit. Although not all patients who visited the ED would have been reported or received a diagnosis, they were assumed to be more likely to receive a diagnosis than patients without an ED visit. Instead of applying the higher underdiagnosis factor used for illness, we used an underdiagnosis factor with a modal value of 2, consistent with previous estimates, and supported by a recent analysis comparing the incidence of bacterial gastroenteritis captured in surveillance and hospital discharge data (*14*,*22*,*23*).

### Hospitalizations

We applied the proportion of patients hospitalized according to surveillance data to the estimated number of reported cases to calculate the estimated number of reported hospitalized patients. If surveillance data were not available, the number of hospitalizations reported in HCUP NIS for a particular disease was used. Hospitalized case-patients were assumed to be more likely to have received a diagnosis than nonhospitalized case-patients. Instead of applying the higher underdiagnosis factor used for illness, we used an underdiagnosis factor with a modal value of 2, consistent with previous estimates, and, for some bacterial enteric diseases, supported by recent work (*14*,*22*,*23*).

### Deaths

We applied the proportion of case-patients who died, as reported by surveillance data, to the estimated number of reported cases to calculate the estimated number of reported deaths. If surveillance data were not available, we used the method of Gargano et al. (*24*). In brief, we combined the number of in-hospital deaths for each disease reported in HCUP NIS with the number of out-of-hospital deaths reported in death certificate records. We assumed that patients who died were more likely have received a diagnosis than patients who did not die. Instead of applying the higher underdiagnosis factor used for illness, we used an underdiagnosis factor with a modal value of 2, consistent with previous estimates (*14*,*22*).

### Domestically Acquired Waterborne Disease

We used surveillance data, when available, to determine the proportion of persons with a given disease who traveled outside the United States during the incubation period. The remaining proportion of cases was considered domestically acquired. When this information was not available, we used literature estimates and expert consultation. We used recent attribution estimates for each disease (*25*; E.M. Beshearse, unpub. data), derived through structured expert judgment (SEJ), a formal process that answers questions for which data are sparse using expert opinions (*26*,*27*), to determine the proportion of disease attributable to waterborne transmission.

### Uncertainty Estimates

For each input and multiplier in the model, we used a distribution that accounted for low, high, and midpoint estimates. This distribution accounted for the uncertainty in each input and multiplier and facilitated calculation of uncertainty intervals for final estimates. For diseases with surveillance data available, we used the methods of Scallan et al. to produce model inputs (*14*). For diseases with administrative data only (e.g., NTM infection and *Pseudomonas* pneumonia and septicemia), we used the mean hospitalization count from HCUP NIS and computed the illness count as the ratio of hospitalization count to hospitalization rate. We assumed the distribution of the hospitalization count to be normal, with the SD calculated from the reported 95% CI. As we did with surveillance data, we included the variation of hospitalization count over time in the model and assumed that the distribution for each multiplier followed the 4-parameter Program Evaluation and Review Technique (PERT) distribution (*28*), with disease-specific parameter values based on available publications.

Uncertainty in the final estimates is a cumulative effect of the uncertainty of each model input. Each multiplier was generated independently. Using 100,000 iterations, we obtained distributions of counts and used them to generate point estimates of means

and the corresponding 95% credible interval (CrI, the 2.5th percentile through the 97.5th percentile of the empirical distribution). We generated all-disease totals for each outcome by sampling from the distributions generated for each individual disease, using SAS 9.4 (https://www.sas.com) and R 3.5.1 (*29*).

### Direct Healthcare Cost per ED Visit and Hospitalization

We used methods described previously (*30*,*31*) to calculate the direct cost of healthcare for ED visits and hospitalizations, using the 2012–2013 MarketScan research databases (IBM Watson Health, https://www.ibm.com/watson-health). These databases contain deidentified insurance billing data for tens of millions of persons covered by private, Medicare (which covers primarily persons ≥65 years of age), and Medicaid (which covers primarily persons with low incomes or disabilities) health insurance plans and contain information on insurance and out-of-pocket payments for hospitalizations, ED visits, doctors' office visits, laboratory testing, and outpatient drug prescriptions. We used these data to calculate the sum of insurer and out-of-pocket payments per hospitalization or visit, by insurance source. We calculated a weighted cost per hospitalization or visit by multiplying the mean total payments for each insurance source by the proportion of cases with the insurance source in HCUP NIS or HCUP NEDS. We assumed that persons with other sources of health insurance (e.g., Tricare, the US military health insurance plan) or no health insurance have the same costs as persons with private insurance. For ED visit costs, we used the data described by Adam et al. (*30*), except for norovirus infection (not examined by Adam et al.) and STEC O157 and non-O157 (categorized differently by Adam et al.) (Appendix 1).

### Total Direct Health Care Costs of Domestically Acquired Waterborne Hospitalizations and ED Visits

We estimated the total direct healthcare cost of ED visits and hospitalizations attributed to waterborne transmission in the United States using the total number of ED visits and hospitalizations attributed to waterborne transmission in the United States. We multiplied these figures by the weighted average cost per ED visit or hospitalization, using 100,000 iterations, with uncertainty distributions as described (Appendix 1).

## Results

### Illnesses

We estimate that 33,600,000 (95% CrI 23,500,000–48,000,000) illnesses from the diseases in this analysis occurred in 2014, and of those, 7,150,000 (95% CrI 3,880,000–12,000,000; 21.3%) were attributed to waterborne transmission in the United States (Table 2). The diseases that caused the greatest number of domestically acquired waterborne illnesses were otitis externa (4,670,000 illnesses; 95% CrI 2,350,000–7,290,000) and norovirus infection (1,330,000 illnesses; 95% Cr 5,310–5,510,000), followed by giardiasis (415,000 illnesses; 95% CrI 140,000–816,000) and cryptosporidiosis (322,000 illnesses; 95% CrI 61,700–993,000). An estimated 96,000 domestically acquired waterborne respiratory illnesses occurred, and 2,330,000 domestically acquired waterborne enteric illnesses occurred.

### Emergency Department Visits

An estimated 601,000 (95% CrI 364,000–866,000) treat-and-release emergency department visits for the included diseases were attributed to waterborne transmission in the United States in 2014 (Table 3). Otitis externa caused the largest number of visits (567,000; 95% CrI 337,000–823,000).

### Hospitalizations

We estimate that these diseases were responsible for 118,000 (95% CrI 86,800–150,000) hospitalizations attributed to waterborne transmission in the United States (Table 3). The diseases with the largest number of hospitalizations were NTM infection (51,400 hospitalizations; 95% CrI 26,800–74,100), otitis externa (23,200 hospitalizations; 95% CrI 13,900–33,600), and *Pseudomonas* pneumonia (15,500 hospitalizations; 95% CrI 4,130–28,100). An estimated 77,700 respiratory hospitalizations were attributed to waterborne transmission, and 10,900 enteric hospitalizations were attributed to waterborne transmission.

### Deaths

The diseases examined in this analysis were responsible for 6,630 deaths (95% CrI 4,520–8,870) attributed to waterborne transmission in the United States in 2014 (Table 3). The diseases with the largest number of deaths attributed to waterborne transmission in the United States were NTM infection (3,800, 95% CrI 1,950–5,620), Legionnaires' disease (995, 95% CrI 655–1,310), and *Pseudomonas* pneumonia (730, 95% CrI 185–1,460). An estimated 5,530 deaths from respiratory disease were attributed to waterborne transmission (83% of all domestically acquired waterborne deaths), and 131 deaths from enteric diseases were attributed to waterborne transmission.

### Direct Healthcare Costs of ED Visits and Hospitalizations

*Pseudomonas* septicemia had the highest cost per hospital stay ($38,200; 95% CrI $6,340–$172,000), followed by Legionnaires' disease ($37,300, CrI $7,950–$149,000) (Table 4). Payments for ED visits and hospitalizations attributed to waterborne transmission in the United States totaled US $3.33 billion (95% CrI $1.37–$8.77 billion) in 2014 dollars (Table 5). This amount included $1.33 billion (95% CrI $361 million–$4.44 billion) in commercial insurer payments, $1.52 billion (95% CrI $338 million–$5.84 billion) in Medicare payments, and $284 million (95% CrI $62.7 million–$906 million) in Medicaid payments (Appendix 3 Tables 1–3). The costliest diseases were NTM infection ($1.53 billion; 95% CrI $272 million–$6.38 billion), otitis externa ($564 million; 95% CrI $187 million–$1.57 billion), and *Pseudomonas* pneumonia ($453 million; 95% CrI $49.9 million–$1.95 billion). An estimated $2.39 billion in direct healthcare costs from domestically acquired waterborne respiratory disease were incurred (72% of all costs from domestically acquired waterborne disease), as were $160 million in direct healthcare costs from domestically acquired waterborne enteric diseases.

**Table 2.** Estimated number of total cases of domestically acquired waterborne illness in 2014 for selected infectious diseases, United States*

| Disease or syndrome | Estimated confirmed cases | Multipliers: Under-reporting | Multipliers: Under-diagnosis | Estimated total cases (95% CrI) | International travel, % | Waterborne, % (95% CrI) | Domestically acquired waterborne, no. (95% CrI) |
|---|---|---|---|---|---|---|---|
| Campylobacteriosis | 54,000 | 1.0 | 28.3 | 1,540,000 (597,000–3,250,000) | 14.4 | 13 (1–31) | 171,000 (13,900–586,000) |
| Cryptosporidiosis | 8,450 | 1.0 | 97.3 | 823,000 (243,000–2,160,000) | 9.9 | 43 (17–73) | 322,000 (61,700–993,000) |
| Giardiasis | 17,900 | 1.30 | 45.9 | 1,070,000 (727,000–1,560,000) | 12.3 | 44 (16–78) | 415,000 (140,000–816,000) |
| Legionnaires' disease | 5,030 | 1.0 | 2.3 | 11,400 (8,920–13,600) | 1.0 | 97 (67–100) | 11,000 (7,430–13,300) |
| NTM infection | 25,700 | 1.0 | 3.8 | 97,000 (75,700–122,000) | 1.0 | 72 (39–94) | 68,900 (35,800–100,000) |
| Norovirus | NA | 1.0 | NA | 21,800,000 (12,100,000–36,000,000) | 1.1 | 6 (0–25) | 1,330,000 (5,310–5,510,000) |
| Otitis externa† | 1,720,000 | 1.0 | 3.4 | 5,980,000 (3,200,000–8,880,000) | 1.3 | 79 (67–95)† | 4,670,000 (2,350,000–7,290,000) |
| *Pseudomonas* pneumonia | 15,800 | 1.0 | 2.0 | 31,700 (19,300–46,000) | 1.0 | 51 (14–80) | 15,900 (4,240–29,000) |
| *Pseudomonas* septicemia | 13,000 | 1.0 | 2.0 | 26,100 (16,700–35,900) | 1.0 | 22 (3–53) | 5,760 (743–14,400) |
| Salmonellosis, nontyphoidal | 46,400 | 1.0 | 29.1 | 1,350,000 (733,000–2,450,000) | 9.7 | 6 (0–22) | 77,000 (5,640–277,000) |
| STEC infection, serotype O157 | 3,530 | 1.0 | 18.2 | 64,200 (13,000–188,000) | 4.0 | 5 (1–13) | 3,360 (336–12,900) |
| STEC infection, serotype non-O157 | 4,550 | 1.0 | 48.1 | 219,000 (80,000–493,000) | 15.3 | 6 (0–17) | 11,400 (0–43,900) |
| Shigellosis | 13,600 | 1.0 | 33.1 | 449,000 (97,800–1,350,000) | 7.8 | 4 (1–21) | 17,300 (1,080–77,500) |
| *Vibrio* spp. infection | 1,230 | NA | NA | 172,000 (126,000–231,000) | NA | NA | 34,600 (17,600–56,900) |
| *V. alginolyticus* | 234 | 1.1 | 142.8 | 36,700 (23,600–54,800) | 6.5 | 37 (13–71) | 12,700 (4,100–25,400) |
| *V. parahaemolyticus* | 593 | 1.1 | 141.6 | 92,400 (55,000–144,000) | 6.7 | 24 (7–38) | 20,800 (6,000–39,000) |
| *V. vulnificus* | 133 | 1.1 | 1.7 | 249 (178–340) | 1.5 | 77 (40–91) | 188 (93–277) |
| Other *Vibrio* | 271 | 1.1 | 142.8 | 42,600 (25,500–66,500) | 14.4 | 2 (0–23) | 879 (3–8,490) |
| Total illness | NA | NA | NA | 33,600,000 (23,500,000–48,000,000) | NA | NA | 7,150,000 (3,880,000–12,000,000) |

*Estimates rounded to 3 significant figures. CrI, credible interval; NA, not applicable; NTM, nontuberculous mycobacteria; STEC, Shiga toxin–producing *Escherichia coli*.
†Combines the waterborne source attribution (*25*) for *Pseudomonas* spp. otitis externa (81%) and *Staphylococcus aureus* (75%) in a ratio of 2:1. More details provided in Appendix 1 (https://wwwnc.cdc.gov/EID/article/27/1/19-0676-App1.pdf).

**Table 3.** Estimated number of treat-and-release emergency department visits, hospitalizations, and deaths from domestically acquired waterborne transmission in 2014 for selected infectious diseases, United States*

| | Treat-and-release ED visits† | | Hospitalizations | | | Deaths | | |
|---|---|---|---|---|---|---|---|---|
| Disease or syndrome | Total visits (95% CrI) | Domestic waterborne visits (95% CrI) | % Admitted to hospital | Total stays (95% CrI) | Domestic waterborne stays (95% CrI) | % Deaths | Total deaths (95% CrI) | Domestic waterborne deaths (95% CrI) |
| Campylobacteriosis | 2,900 (1,620–4,630) | 319 (31–966) | 19.5 | 19,300 (8,790–34,900) | 2,150 (192–6,900) | 0.2 | 242 (0–1,150) | 27 (0–146) |
| Cryptosporidiosis | 1,260 (742–1,880) | 492 (167–957) | 19.2 | 2,870 (439–8,060) | 1,120 (102–3,550) | 0.3 | 61 (0–320) | 24 (0–136) |
| Giardiasis | 1,460 (902–2,090) | 567 (185–1,120) | 7.9 | 2,830 (1,760–4,070) | 1,100 (364–2,180) | <0.1 | 4 (0–11) | 1 (0–5) |
| Legionnaires' disease | 691 (316–1,220) | 667 (289–1,200) | 98.1 | 11,200 (8,750–13,300) | 10,800 (7,280–13,100) | 9.0 | 1,030 (762–1,330) | 995 (655–1,310) |
| NTM infection | 7,150 (5,110–9,620) | 5,080 (2,560–7,750) | 74.8 | 72,400 (57,300–89,700) | 51,400 (26,800–74,100) | 5.5 | 5,350 (4,020–6,920) | 3,800 (1,950–5,620) |
| Norovirus | 429,000‡ (318,000–605,000) | 26,300‡ (105–106,000) | 0.4 | 78,100 (58,500–104,000) | 4,780 (19–19,300) | <0.1 | 885 (742–1,120) | 54 (0–219) |
| Otitis externa | 726,000 (466,000–994,000) | 567,000 (337,000–823,000) | 0.9 | 29,700 (19,200–40,600) | 23,200 (13,900–33,600) | <0.1 | 280 (144–452) | 219 (107–367) |
| *Pseudomonas* pneumonia | 580 (321–902) | 291 (75–552) | 97.2 | 30,800 (18,700–44,700) | 15,500 (4,130–28,100) | 4.6 | 1,450 (786–2,420) | 730 (185–1,460) |
| *Pseudomonas* septicemia | 164 (36–326) | 36 (2–106) | 97.2 | 25,300 (16,300–34,800) | 5,590 (722–14,000) | 12.1 | 3,140 (1,990–4,430) | 695 (89–1,740) |
| Salmonellosis, nontyphoidal | 3,410 (2,100–4,900) | 194 (15–671) | 28.4 | 26,600 (11,400–52,800) | 1,520 (100–5,660) | 0.5 | 421 (0–1,140) | 24 (0–103) |
| STEC infection, serotype O157 | 252 (92–465) | 12 (2–35) | 38.5 | 2,640 (487–7,630) | 138 (14–503) | 0.7 | 36 (0–314) | 2 (0–17) |
| STEC infection, serotype non-O157 | 75 (12–171) | 4 (0–16) | 16.0 | 1,420 (264–3,810) | 74 (0–308) | 0.2 | 16 (0–184) | 1 (0–12) |
| Shigellosis | 1,650 (540–2,870) | 64 (5–311) | 24.4 | 6,380 (929–20,300) | 245 (12–1,140) | 0.1 | 26 (0–218) | 1 (0–9) |
| *Vibrio* spp. infection | 366 (122–700) | 76 (14–166) | NA | 782 (567–1,030) | 251 (153–362) | NA | 113 (67–156) | 60 (27–92) |
| *V. alginolyticus* | NA§ | NA§ | 15.9 | 74 (38–141) | 26 (8–58) | 0.8 | 4 (0–11) | 1 (0–5) |
| *V. parahaemolyticus* | NA§ | NA§ | 22.3 | 264 (136–410) | 60 (16–112) | 1.4 | 16 (7–32) | 4 (1–9) |
| *V. vulnificus* | NA§ | NA‡ | 85.4 | 213 (147–297) | 161 (79–241) | 28.8 | 72 (38–104) | 54 (24–85) |
| Other *Vibrio* | NA§ | NA§ | 42.5 | 231 (134–350) | 5 (0–46) | 3.8 | 20 (11–33) | 0 (0–4) |
| Total | 1,180,000 (877,000–1,490,000) | 601,000 (364,000–866,000) | NA | 310,000 (263,000–360,000) | 118,000 (86,800–150,000) | NA | 13,100 (10,600–15,900) | 6,630 (4,520–8,870) |

*Estimates rounded to 3 significant figures. CrI, credible interval; ED, emergency department; NA, not applicable; NTM, nontuberculous mycobacterial; STEC, Shiga toxin–producing *Escherichia coli*.
†Treat-and-release ED visits were defined as visits in which the person was not admitted to the hospital.
‡For norovirus infection only, ED visits in which the person was admitted to the hospital were included, for consistency with previous published estimates.
§No International Classification of Diseases, 9th Revision, Clinical Modification, codes are available for *Vibrio* spp. infections, only a general code for "Vibriosis and cholera." ED visit estimates relied on administrative data that used these codes, and thus are presented only for *Vibrio* infection overall.

## Discussion

Domestic waterborne transmission of 17 diseases in the United States caused ≈7.15 million (95% CrI 3.88–12.0 million) waterborne illnesses to occur annually during the study period, including 601,000 ED visits (95% CrI 364,000–866,000), 118,000 hospitalizations (95% CrI 86,800–150,000), and 6,630 deaths (95% CrI 4,520–8,870), and incurred $3.33 billion (95% CrI $1.31–$8.71 billion) in hospitalization and ED visit costs. This estimate includes drinking,

recreational, and environmental water exposures. Although the risk of illness from enteric pathogens readily controlled by water treatment processes still exists, this analysis highlights the expanding role of environmental pathogens (e.g., mycobacteria, *Pseudomonas*, *Legionella*) that can grow in drinking water distribution systems; plumbing in hospitals, homes, and other buildings; recreational water venues; and industrial water systems (e.g., cooling towers). This snapshot of waterborne disease transmission in the United States circa 2014 contrasts with historical waterborne disease transmission before the implementation of drinking water treatment and sanitation systems (e.g., cholera, typhoid fever, and other enteric pathogens) (*1*).

Few comparable waterborne disease burden estimates exist for the United States or other high-income countries. The World Health Organization (WHO) has estimated water, sanitation, and hygiene-related disease and injury (i.e., diarrhea, drowning, malnutrition) (*32*). WHO's estimated 6,600 annual US deaths from nondiarrheal infectious diseases is within the range of our estimate, although the infectious diseases included were not specified, making direct comparison difficult. Work from Australia used the WHO estimates to calculate the waterborne burden of 5 enteric pathogens, whereas estimates from Canada assessed the burden of AGI from drinking water and the burden of 5 enteric pathogens from private wells and small water systems (*33*–*35*). Work in Europe estimated the proportion of 9 primarily enteric diseases attributable to water (*36*). Prior estimates of the burden of waterborne disease in the United States focused on the burden of gastrointestinal illness associated with drinking water and an estimated 4–32 million cases of illness each year (*16*–*18*). Our estimate differs from previous work because it focuses on specific pathogens, includes nongastrointestinal diseases, and considers all waterborne exposure routes.

A previous estimate of foodborne disease found fewer illness, hospitalizations, and deaths from foodborne disease due to known pathogens (*14*), although it found more illness when unspecified agents were considered (*15*). For pathogens included in both estimates, underdiagnosis multipliers did not differ substantially, except for decreases in STEC multipliers because of improved laboratory capacity. The higher totals in this analysis reflect the diseases selected for inclusion, some of which cause severe respiratory diseases more likely to result in hospitalization and death than the diseases with primarily enteric effects that were included in the foodborne estimate. When estimates for the enteric pathogens included in both analyses are compared, the waterborne burden is lower than the foodborne burden. This difference could be because drinking and treated recreational water systems were designed to prevent enteric illness, and the intervention (disinfection) is relatively simple compared with the manifold interventions needed to prevent foodborne illness.

This work is subject to several limitations. First, we used a series of multipliers to generate estimates of

**Table 4.** Cost per hospital stay for selected diseases that can be transmitted by water, 2012–2013 IBM MarketScan health insurance databases, United States*

| | Cost in 2014 US dollars (95% CrI) | | | |
|---|---|---|---|---|
| Disease/syndrome | Commercial insurance | Medicare | Medicaid | Overall |
| Campylobacteriosis | 15,200 (1,520–47,100) | 15,100 (1,630–55,300) | 5,900 (85–29,000) | 13,600 (3,850–35,800) |
| Cryptosporidiosis | 17,900 (1,560–82,700) | 17,300 (1,800–79,400) | 10,700 (22–64,200) | 16,100 (4,360–55,400) |
| Giardiasis | 25,300 (1,790–168,000) | 22,300 (1,890–96,900) | 14,300 (159–88,000) | 21,800 (6,160–99,200) |
| Legionnaires' disease | 45,900 (2,320–306,000) | 33,600 (4,210–183,000) | 18,700 (17–99,300) | 37,100 (7,950–149,000) |
| NTM infection | 44,100 (1,650–244,000) | 27,600 (1,720–152,000) | 14,800 (49–69,100) | 29,600 (6,350–120,000) |
| Norovirus infection† | | | | 6,080 |
| Otitis externa | 13,800 (1,480–56,500) | 14,400 (1,490–65,100) | 6,680 (43–36,900) | 12,200 (3,320–42,400) |
| *Pseudomonas* pneumonia | 45,100 (1,510–193,000) | 28,200 (1,890–146,000) | 11,600 (18–53,200) | 29,300 (5,910–114,000) |
| *Pseudomonas* septicemia | 63,600 (1,450–386,000) | 34,400 (2,200–181,000) | 19,800 (47–113,000) | 38,200 (6,340–172,000) |
| Salmonellosis, nontyphoidal | 17,200 (2,010–73,600) | 17,100 (1,400–62,700) | 6,940 (70–26,300) | 14,900 (4,300–46,900) |
| STEC infection, serotype O157 | 25,900 (2,410–150,000) | 17,200 (1,860–82,200) | 4,530 (3–30,200) | 19,000 (3,790–85,000) |
| STEC infection, serotype non-O157 | 23,600 (1,390–95,700) | 31,900 (2,620–250,000) | 5,020 (458–32,000) | 24,200 (4,780–138,000) |
| Shigellosis | 19,000 (2,910–85,300) | 13,500 (1,610–39,600) | 7,710 (37–51,300) | 14,200 (4,130–48,000) |
| *Vibrio* spp. infection | 17,400 (2,260–50,500) | 18,400 (0,977–78,700) | 4,600 (13–46,000) | 16,000 (3,780–39,900) |

*Estimates rounded to 3 significant figures. Overall cost calculated using the sum of insurer and out-of-pocket payments per stay for each payment source multiplied by the proportion of persons in the Health Care Utilization Project's Nationwide Inpatient Sample with each payment source, for the corresponding disease or syndrome. This produces a weighted average cost per stay that reflects the differing proportion of payment sources for each disease or syndrome. Persons who had a payment source other than commercial insurance, Medicare, or Medicaid (i.e., persons covered by Tricare (the healthcare plan for persons affiliated with the US armed services, who were uninsured, or who had an unknown source of insurance) were assumed to have a cost per stay equivalent to the commercial insurance cost per stay. NTM, nontuberculous mycobacterial; STEC, Shiga toxin–producing *Escherichia coli*.

†Norovirus costs were derived from previously published estimates that did not specify cost per insurance source or include uncertainty intervals.

disease, and accuracy of these estimates relies on the accuracy of the multipliers. Although we attempted to account for the uncertainty of each data point using uncertainty intervals, any systematic errors in multipliers will produce a biased estimate. For example, waterborne transmission is not the sole route of transmission for any of the diseases in this work; many of the included diseases can be transmitted through multiple pathways (e.g., cryptosporidiosis can be waterborne, foodborne, or transmitted directly from animals or humans). We also relied on structured expert judgment (SEJ) to estimate the proportions of diseases attributed to waterborne transmission. SEJ is an approach used when primary data are not available, and is subject to limitations including expert bias (*26*,*27*). For norovirus infection, the uncertainty interval for the waterborne attribution percentage was large, reflecting a lack of consensus among experts, and resulting in an estimate of illness with a wide credibility interval (1,330,000 [95% CrI 5,310–5,510,000] illnesses). Second, this analysis is limited to 17 infectious diseases with adequate surveillance or administrative data available and does not include all disease associated with waterborne transmission in the United States. Insufficient data were available

**Table 5.** Total direct healthcare cost of ED visits and hospitalizations from domestically acquired waterborne transmission of selected infectious diseases, United States, 2014*

| | Value (95% CrI) | | | | | | |
|---|---|---|---|---|---|---|---|
| | Treat-and-release ED visits† | | | Hospitalization | | | Direct healthcare cost, millions |
| Disease or syndrome | Cost per visit | Total no. visits | Total cost, millions | Cost per stay | Total no. hospital stays | Total cost, millions | |
| Campylobacteriosis | 1,710 (137–5,810) | 319 (31–966) | 0.545 (0.0177–2.61) | 13,600 (3,850–35,800) | 2,150 (192–6,900) | 30.0 (1.71–121) | 30.5 (2.10–121) |
| Cryptosporidiosis | 1,960 (238–6,270) | 492 (167–957) | 0.963 (0.0802–3.44) | 16,100 (4,360–55,400) | 1,120 (102–3,550) | 17.9 (1.10–79.5) | 18.9 (1.82–80.4) |
| Giardiasis | 1,620 (196–7,510) | 567 (185–1,120) | 0.917 (0.0861–3.78) | 21,800 (6,160–99,200) | 1,100 (364–2,180) | 23.9 (3.53–104) | 24.8 (4.21–105) |
| Legionnaires' disease | 691 (288–1,390) | 667 (289–1,200) | 0.460 (0.127–1.13) | 37,100 (7,950–149,000) | 10,800 (7,280–13,100) | 401 (79.0–1,690) | 402 (79.5–1,690) |
| NTM infection | 1,610 (129–6,430) | 5,080 (2,560–7,750) | 8.17 (0.584–34.0) | 29,600 (6,350–120,000) | 51,400 (26,800–74,100) | 1,520 (266–6,370) | 1,530 (272–6,380) |
| Norovirus‡ | 1,140 | 26,300 | 30.1 | 6,080 | 4,780 | 29 | 59.1 |
| Otitis externa | 494 (120–1,430) | 567,000 (337,000–823,000) | 280 (60.2–846) | 12,200 (3,320–42,400) | 23,200 (13,900–33,600) | 285 (67.8–1,040) | 564 (187–1,570) |
| *Pseudomonas* pneumonia | 856 (89–4,190) | 291 (75–552) | 0.249 (0.0162–1.27) | 29,300 (5,910–114,000) | 15,500 (4,130–28,100) | 452 (49.8–1,950) | 453 (49.9– 1,950) |
| *Pseudomonas* septicemia | 923 (95–3,190) | 36 (2–106) | 0.0334 (0.000716–0.186) | 38,200 (6,340–172,000) | 5,590 (722–14,000) | 214 (11.4–1,030) | 214 (11.4–1,030) |
| Salmonellosis, nontyphoidal | 1,230 (161–4,500) | 194 (15–671) | 0.240 (0.00734–1.24) | 14,900 (4,300–46,900) | 1,520 (100–5,660) | 22.6 (0.870–110) | 22.8 (1.08–110) |
| STEC infection, serotype O157 | 1,070 (109–2,350) | 12 (2–35) | 0.0130 (0.00734–0.051) | 19,000 (3,790–85,000) | 138 (14–503) | 2.67 (0.129–14.5) | 2.68 (0.141–14.5) |
| STEC infection, serotype non-O157 | 1,070 (109–2,350) | 4 (0–16) | 0.00440 (0–0.0223) | 24,200 (4,780–138,000) | 74 (0–308) | 1.76 (0–11.0) | 1.76 (0.00186–11.0) |
| Shigellosis | 952 (115–3,980) | 64 (5–311) | 0.0609 (0.00171–0.349) | 14,200 (4,130–48,000) | 245 (13–1,140) | 3.41 (0.106–18.9) | 3.47 (0.140–19.0) |
| *Vibrio* spp. infection | 1,030 (293–3,330) | 76 (14–166) | 0.0777 (0.00765–0.276) | 16,000 (3,780–39,900) | 251 (153–362) | 4.02 (0.811–10.7) | 4.10 (0.891–10.8) |
| Total cost | | | 322 (100–889) | | | 3,010 (1,120–8,410) | 3,330 (1,370–8,770) |

*Values are 2004 US dollars except as indicated. Estimates rounded to 3 significant figures. CrI, credible interval; ED, emergency department; NTM, nontuberculous mycobacterial; STEC, Shiga toxin-producing *E. coli*.
†Treat-and-release ED visits were defined as visits in which the person was not admitted to the hospital.
‡For norovirus only, costs were derived from previously published estimates that did not include uncertainty intervals. In addition, the number of ED visits includes visits in which the patient was admitted to the hospital.

to quantify the contribution of many viral diseases, including sapovirus, rotavirus, and astrovirus; or free-living ameba infections, which cause deaths in the United States each year (*5*). Noninfectious diseases (e.g., from exposure to harmful algal blooms, heavy metals, disinfection byproducts) were not considered. Third, these estimates used administrative data and relied on coding from the International Classification of Diseases, 9th Revision, Clinical Modification, which might not accurately capture the actual disease of the ill person. Fourth, the cost estimates consider only out-of-pocket and insurer payments and do not account for the total amount of time or wages lost to ill health, disability, early death, or other indirect costs. Physicians' office visits were not included, because data were not available. Payment totals might not reflect the actual cost incurred by healthcare providers. Fifth, this work did not make separate estimates for different age, demographic, or risk groups. Risks could differ by group (e.g., children swim more often and have higher rates of cryptosporidiosis), resulting in over- or underestimation of waterborne disease (*37*,*38*). Cost estimates did not consider the contribution of immunosuppressing conditions or other concurrent conditions to the healthcare costs incurred. Finally, some estimates used data from FoodNet. In 2007, Hispanic persons were underrepresented in FoodNet sites (*39*). Appendix 1 contains additional pathogen-specific limitations. Analytic strengths of these burden estimates include the use of active surveillance data when possible, estimates from a comprehensive structured expert judgment, and credible intervals to acknowledge the inherent uncertainty in the model inputs and outputs.

The data presented here reflect the changing picture of waterborne disease in the United States and underscore the role of environmental pathogens that grow in biofilms. An estimated 7.15 million (95% CrI 3.88 million–12.0 million) domestically acquired waterborne illnesses occur in the United States each year, highlighting the need to focus public health resources on the prevention and control of these diseases, including surveillance for the diseases in this estimate that do not have a dedicated national case surveillance system (e.g., NTM infections). These findings should serve as a foundation for improved disease surveillance, inform waterborne disease prevention priorities, and help measure progress in the prevention of waterborne disease in the United States.

### Acknowledgments

The authors thank Jennifer Cope, Michele Hlavsa, Jennifer Huang, Mary Patrick, Logan Ray, Danielle Tack, Patricia Griffin, Tina Nane, Shelly Gleason, John Person, and Aubrey Gilliland for their assistance.

### About the Author

Ms. Collier is an analytic epidemiologist in the National Center for Emerging and Zoonotic Infectious Diseases at the Centers for Disease Control and Prevention, Atlanta, Georgia, USA. Her research focuses on describing and quantifying the impact of waterborne disease in the United States and often incorporates data from large healthcare databases.

### References

1. Armstrong GL, Conn LA, Pinner RW. Trends in infectious disease mortality in the United States during the 20th century. JAMA. 1999;281:61–6. https://doi.org/10.1001/jama.281.1.61
2. Centers for Disease Control and Prevention. Achievements in public health, 1900–1999: control of infectious diseases. MMWR Morb Mortal Wkly Rep. 1999;48:621–9.
3. Benedict KM, Reses H, Vigar M, Roth DM, Roberts VA, Mattioli M, et al. Surveillance for waterborne disease outbreaks associated with drinking water—United States, 2013–2014. MMWR Morb Mortal Wkly Rep. 2017;66:1216–21. https://doi.org/10.15585/mmwr.mm6644a3
4. McClung RP, Roth DM, Vigar M, Roberts VA, Kahler AM, Cooley LA, et al. Waterborne disease outbreaks associated with environmental and undetermined exposures to water—United States, 2013–2014. MMWR Morb Mortal Wkly Rep. 2017;66:1222–5. https://doi.org/10.15585/mmwr.mm6644a4
5. Hlavsa MC, Cikesh BL, Roberts VA, Kahler AM, Vigar M, Hilborn ED, et al. Outbreaks associated with treated recreational water—United States, 2000–2014. MMWR Morb Mortal Wkly Rep. 2018;67:547–51. https://doi.org/10.15585/mmwr.mm6719a3
6. Craun GF, Brunkard JM, Yoder JS, Roberts VA, Carpenter J, Wade T, et al. Causes of outbreaks associated with drinking water in the United States from 1971 to 2006. Clin Microbiol Rev. 2010;23:507–28. https://doi.org/10.1128/CMR.00077-09
7. Dieter CA, Maupin MA, Caldwell RR, Harris MA, Ivahnenko TI. Estimated use of water in the United States in 2015. US Geological Survey; 2018 [cited 2020 Sep 24]. https://doi.org/10.3133/cir1441
8. US Environmental Protection Agency. Community water system survey 2000. Volume 1: overview. 2002 [cited 2020 Sep 24]. https://nepis.epa.gov/Exe/tiff2png.cgi/20001ZK5.PNG?-r+75+-g+7+D%3A%5CZYFILES%5CINDEX%20DATA%5C00THRU05%5CTIFF%5C00000455%5C20001ZK5.TIF
9. US National Research Council. Committee on Public Water Supply Distribution Systems: Water Science and Technology Board. Drinking water distribution systems: assessing and reducing risks. Washington (DC): National Academies Press; 2006.
10. Falkinham JO III, Hilborn ED, Arduino MJ, Pruden A, Edwards MA. Epidemiology and ecology of opportunistic premise plumbing pathogens: *Legionella pneumophila*, *Mycobacterium avium*, and *Pseudomonas aeruginosa.* Environ Health Perspect. 2015;123:749–58. https://doi.org/10.1289/ehp.1408692
11. Shields JM, Hill VR, Arrowood MJ, Beach MJ. Inactivation of *Cryptosporidium parvum* under chlorinated recreational water conditions. J Water Health. 2008;6:513–20. https://doi.org/10.2166/wh.2008.068
12. Chappell CL, Okhuysen PC, Langer-Curry R, Widmer G, Akiyoshi DE, Tanriverdi S, et al. *Cryptosporidium hominis*: experimental challenge of healthy adults. Am J Trop

Med Hyg. 2006;75:851–7. https://doi.org/10.4269/ajtmh.2006.75.851
13. Paranjpye RN, Nilsson WB, Liermann M, Hilborn ED, George BJ, Li Q, et al. Environmental influences on the seasonal distribution of *Vibrio parahaemolyticus* in the Pacific Northwest of the USA. FEMS Microbiol Ecol. 2015;91:fiv121. https://doi.org/10.1093/femsec/fiv121
14. Scallan E, Hoekstra RM, Angulo FJ, Tauxe RV, Widdowson MA, Roy SL, et al. Foodborne illness acquired in the United States—major pathogens. Emerg Infect Dis. 2011;17:7–15. https://doi.org/10.3201/eid1701.P11101
15. Scallan E, Griffin PM, Angulo FJ, Tauxe RV, Hoekstra RM. Foodborne illness acquired in the United States—unspecified agents. Emerg Infect Dis. 2011;17:16–22. https://doi.org/10.3201/eid1701.P21101
16. Colford JM Jr, Roy S, Beach MJ, Hightower A, Shaw SE, Wade TJ. A review of household drinking water intervention trials and an approach to the estimation of endemic waterborne gastroenteritis in the United States. J Water Health. 2006;4(Suppl 2):71–88. https://doi.org/10.2166/wh.2006.018
17. Messner M, Shaw S, Regli S, Rotert K, Blank V, Soller J. An approach for developing a national estimate of waterborne disease due to drinking water and a national estimate model application. J Water Health. 2006;4(Suppl 2):201–40. https://doi.org/10.2166/wh.2006.024
18. Reynolds KA, Mena KD, Gerba CP. Risk of waterborne illness via drinking water in the United States. Rev Environ Contam Toxicol. 2008;192:117–58. https://doi.org/10.1007/978-0-387-71724-1_4
19. DeFlorio-Barker S, Wade TJ, Jones RM, Friedman LS, Wing C, Dorevitch S. Estimated costs of sporadic gastrointestinal illness associated with surface water recreation: a combined analysis of data from NEEAR and CHEERS studies. Environ Health Perspect. 2017;125:215–22. https://doi.org/10.1289/EHP130
20. Grytdal SP, DeBess E, Lee LE, Blythe D, Ryan P, Biggs C, et al. Incidence of norovirus and other viral pathogens that cause acute gastroenteritis (AGE) among Kaiser Permanente member populations in the United States, 2012–2013. PLoS One. 2016;11:e0148395. https://doi.org/10.1371/journal.pone.0148395
21. Hall AJ, Rosenthal M, Gregoricus N, Greene SA, Ferguson J, Henao OL, et al. Incidence of acute gastroenteritis and role of norovirus, Georgia, USA, 2004–2005. Emerg Infect Dis. 2011;17:1381–8. https://doi.org/10.3201/eid1708.101533
22. Mead PS, Slutsker L, Dietz V, McCaig LF, Bresee JS, Shapiro C, et al. Food-related illness and death in the United States. Emerg Infect Dis. 1999;5:607–25. https://doi.org/10.3201/eid0505.990502
23. Scallan E, Griffin PM, McLean HQ, Mahon BE. Hospitalisations due to bacterial gastroenteritis: a comparison of surveillance and hospital discharge data. Epidemiol Infect. 2018;146:954–60. https://doi.org/10.1017/S0950268818000882
24. Gargano JW, Adam EA, Collier SA, Fullerton KE, Feinman SJ, Beach MJ. Mortality from selected diseases that can be transmitted by water—United States, 2003–2009. J Water Health. 2017;15:438–50. https://doi.org/10.2166/wh.2017.301
25. Beshearse E, Bruce BB, Nane GF, Cooke RM, Aspinall W, Hald T, et al. Using structured expert judgment for attribution of foodborne and waterborne illnesses to comprehensive transmission pathways, United States. Emerg Infect Dis. 2021 Jan [in press]. https://doi.org/10.3201/eid2701.200316
26. Aspinall WP, Cooke RM, Havelaar AH, Hoffmann S, Hald T. Evaluation of a performance-based expert elicitation: WHO global attribution of foodborne diseases. PLoS One. 2016;11:e0149817. https://doi.org/10.1371/journal.pone.0149817
27. Cooke RM, Goossens LHJ; European Commission Directorate-General for Research and Innovation. Procedures guide for structured expert judgement. Brussels: Directorate-General for Research; 2000.
28. Vose D. Risk analysis: a quantitative guide. 3rd ed. Hoboken (NJ): Wiley; 2008.
29. R Core Team. R: A language and environment for statistical computing. Vienna: R Foundation for Statistical Computing; 2018.
30. Adam EA, Collier SA, Fullerton KE, Gargano JW, Beach MJ. Prevalence and direct costs of emergency department visits and hospitalizations for selected diseases that can be transmitted by water, United States. J Water Health. 2017;15:673–83. https://doi.org/10.2166/wh.2017.083
31. Collier SA, Stockman LJ, Hicks LA, Garrison LE, Zhou FJ, Beach MJ. Direct healthcare costs of selected diseases primarily or partially transmitted by water. Epidemiol Infect. 2012;140:2003–13. https:/doi.org/10.1017/S0950268811002858
32. Prüss-Ustün A, Bos R, Gore F, Bartram J; World Health Organization. Safer water, better health: costs, benefits and sustainability of interventions to protect and promote health. Geneva: The Organization; 2008.
33. Gibney KB, O'Toole J, Sinclair M, Leder K. Burden of disease attributed to waterborne transmission of selected enteric pathogens, Australia, 2010. Am J Trop Med Hyg. 2017;96:1400–3. https://doi.org/10.4269/ajtmh.16-0907
34. Murphy HM, Thomas MK, Medeiros DT, McFadyen S, Pintar KD. Estimating the number of cases of acute gastrointestinal illness (AGI) associated with Canadian municipal drinking water systems. Epidemiol Infect. 2016;144:1371–85. https://doi.org/10.1017/S0950268815002083
35. Murphy HM, Thomas MK, Schmidt PJ, Medeiros DT, McFadyen S, Pintar KD. Estimating the burden of acute gastrointestinal illness due to *Giardia*, *Cryptosporidium*, *Campylobacter*, *E. coli* O157 and norovirus associated with private wells and small water systems in Canada. Epidemiol Infect. 2016;144:1355–70. https://doi.org/10.1017/S0950268815002071
36. Cassini A, Colzani E, Kramarz P, Kretzschmar ME, Takkinen J. Impact of food and water-borne diseases on European population health. Curr Opin Food Sci. 2016;12:21–9. https://doi.org/10.1016/j.cofs.2016.06.002
37. Collier SA, Wade TJ, Sams EA, Hlavsa MC, Dufour AP, Beach MJ. Swimming in the USA: beachgoer characteristics and health outcomes at US marine and freshwater beaches. J Water Health. 2015;13:531–43. https://doi.org/10.2166/wh.2014.095
38. Centers for Disease Control and Prevention. Cryptosporidiosis summary report—National Notifiable Diseases Surveillance System, United States, 2017; 2019 [cited 2020 Sep 24]. https://www.cdc.gov/healthywater/surveillance/pdf/2017-Cryptosporidiosis-NNDSS-Report-508.pdf
39. Angulo FJ, Scallan E. Activities, achievements, and lessons learned during the first 10 years of the Foodborne Diseases Active Surveillance Network: 1996–2005. Clin Infect Dis. 2007;44:718–25. https://doi.org/10.1086/511648

Address for correspondence: Sarah Collier, Centers for Disease Control and Prevention, 1600 Clifton Road NE, Mailstop H24-9, Atlanta, GA 30029-4027, USA; email: sau9@cdc.gov

# Post–13-Valent Pneumococcal Conjugate Vaccine Dynamics in Young Children of Serotypes Included in Candidate Extended-Spectrum Conjugate Vaccines

Shalom Ben-Shimol, Noga Givon-Lavi, Leore Kotler, Bart Adriaan van der Beek, David Greenberg, Ron Dagan

After worldwide implementation of 10-valent and 13-valent pneumococcal conjugate vaccines (PCV10/PCV13), a 20-valent PCV (PCV20) was developed. We assessed dynamics of non-PCV13 additional PCV20 serotypes (VT20–13), compared with all other non-VT20 serotypes, in children <2 years of age in late PCV13 (2015–2017) and early PCV (2009–2011) periods. Our prospective population-based multifaceted surveillance included isolates from carriage in healthy children, children requiring chest radiography for lower respiratory tract infections (LRTIs), and children with non-LRTI illness, as well as isolates from acute conjunctivitis, otitis media (OM), and invasive pneumococcal disease (IPD). After PCV13 implementation, VT20–13 increased disproportionally in OM, IPD, and carriage in LRTI. VT20–13/non-VT20 prevalence ratio range was 0.26–1.40. VT20–13 serotypes were more frequently antimicrobial-nonsusceptible than non-VT20 serotypes. The disproportionate increase of VT20–13 in respiratory infections and IPD points to their higher disease potential compared with all other non-VT20 as a group.

*Streptococcus pneumoniae* is a major cause of illness and death worldwide (*1*,*2*). It causes otitis media, sinusitis, pneumonia, and invasive pneumococcal diseases (IPD) (*1*).

Capsular polysaccharides are considered the most important virulence factor in *S. pneumoniae* (*3*). Currently, >95 capsular serotypes have been identified. Each serotype is distinguished by the chemical structure of its polysaccharides, serologic response, and other genetic characteristics (*4*). Pneumococcal capsule types are associated with pathogenic processes including complement deposition, inflammation, and binding to the C-type lectin of host phagocytes (*3*). Pneumococcal serotype appears to be important in determining colonization, disease development, and clinical phenotype. Indeed, in the time before pneumococcal conjugate vaccines (PCVs), a limited number of serotypes among the known >95 serotypes were responsible for >70% of all IPD in children worldwide (*5*).

The routine use of PCVs in children worldwide has led to a decline of vaccine serotype (VT) IPD, mucosal diseases, and nasopharyngeal carriage (*6*–*9*). However, after PCV implementation, in spite of a decrease in overall pneumococcal disease rates, carriage of and disease from non-PCV serotypes (NVT) increased (*5*). As of October 2020, licensed PCVs contain 7 to 13 serotypes (7-valent [PCV7], 10-valent [PCV10], and 13-valent [PCV13]). Efforts to develop extended-spectrum (higher valency) PCVs have led to the development of 15- and 20-valent PCVs (PCV15, PCV20), both currently in advanced stages of clinical studies. The experimental PCV20 includes, beyond the 13 serotypes of PCV13 (1, 3, 4, 5, 6A, 6B, 7F, 9V, 14, 19A, 19F, 18C, and 23F), the additional pneumococcal serotypes 8, 10A, 11A, 12F, 15B/C, 22F and 33F (*10*), of which 2 (serotypes 22F and 33F) are also contained in PCV15 (*11*). These additional PCV20 serotypes (VT20–13) have been increasingly observed in recent years as common IPD serotypes. However, data are scarce in regard to their relative role in other entities such as carriage and respiratory disease in young children.

We compared the proportion rate dynamics of the added PCV20 serotypes (VT20–13) with PCV13 (VT13) and remaining non-VT20 (NVT20) serotypes

Author affiliations: Ben-Gurion University of the Negev, Beer Sheva, Israel (S. Ben-Shimol, N. Givon-Lavi, L. Kotler, B.A. van der Beek, D. Greenberg, R. Dagan); Soroka University Medical Center, Beer Sheva (S. Ben-Shimol, N. Givon-Lavi, L. Kotler, D. Greenberg)

DOI: https://doi.org/10.3201/eid2701.201178

in nasopharyngeal carriage of healthy young children and in children with non–lower respiratory tract infections (LRTIs) (pediatric emergency room [PER] visits in which chest radiography was not done), lower respiratory diseases requiring chest radiography, IPD, and pneumococcal culture-positive acute conjunctivitis and otitis media (OM).

## Materials and Methods

### Study Design

Our data derive from several ongoing, population-based, active surveillance projects conducted by the Pediatric Infectious Disease Unit, Soroka University Medical Center (SUMC) during 2009–2017. We defined 2 periods: early PCV (2009–2011) and late PCV13 (2015–2017). SUMC is the only hospital in southern Israel providing healthcare to the entire region, which enables us to conduct population-based studies.

### Setting and Study Population

During the study period, the average total number of annual births in the Negev district in southern Israel was ≈15,000. Over 95% of the children in the district are born and receive medical services at the SUMC. In the Negev district, the Jewish and the Bedouin populations live side-by-side. The socioeconomic conditions and the lifestyles of the 2 groups differ, but both have access to the same medical services. The Jewish population, mainly urban, resembles developed populations, whereas the Bedouin population, formerly desert nomads in transition to a Western lifestyle, resembles developing populations, with a high occurrence of infectious diseases including pneumococcal disease and complex OM (*6*,*7*,*9*). Contact between the children of the 2 populations is rare. During the study period, ≈50% of children <2 years of age in southern Israel were Jews and 50% were Bedouins. Our data derived from 5 prospective active surveillance projects.

#### 1) Carriage in Healthy Children (Group 1; Community Setting, Southern Israel)

This study, initiated in 2011, included nasopharyngeal cultures obtained from healthy children <2 years of age who were brought to the maternal and child healthcare centers in southern Israel for vaccination. A nasopharyngeal swab specimen was obtained after parents gave written informed consent.

#### 2) Carriage during Illness (Groups 2 and 3; Hospital PER Setting, Southern Israel)

This study, initiated in 2009, included cultures obtained from the PER of SUMC. Each workday, healthcare workers obtained nasopharyngeal cultures from the first 4 Jewish and 4 Bedouin children who were <2 years of age, residents of the Negev, and brought to the PER for any reason (*9*). We defined 2 groups in that surveillance: carriage in non-LRTI (children seen at the PER for any disease except those necessitating chest radiography); and carriage in LRTI (children with LRTI from whom a chest radiography was obtained) (*6*).

#### 3) Conjunctivitis (Group 4; Both Community and Hospital Settings, Southern Israel)

The study population included children <24 months of age who were residents of the Negev region, received a diagnosis of acute conjunctivitis in a community clinic or at SUMC (either PER or hospitalized), and had a conjunctival culture sent to the Clinical and Microbiology Laboratory of the SUMC since 2009.

#### 4) Otitis Media (Group 5; Both Community and Hospital Settings, Southern Israel)

The study population included children <24 months of age who were residents of the Negev region and had OM judged to necessitate middle ear fluid (MEF) culture. Cultures were obtained by tympanocentesis or by swab of the external canal of children with acute (<7 days) spontaneous otorrhea. Most of the children had complex OM (nonresponsive, recurrent, spontaneous perforation, or chronic ear effusion) (*7*,*12*,*13*). Children found to have pneumococcal MEF isolates during 2009–2017 were included (*7*).

#### 5) IPD (Group 6; Both Community and Hospital Settings, Israel, Nationwide)

This nationwide study was conducted in all 27 medical centers routinely obtaining cerebrospinal fluid (CSF) and blood cultures from children <24 months old in Israel; sites included 26 hospitals and 1 outpatient health maintenance organization (*14*). This setting enabled us to cover all culture-confirmed IPD cases among the population of Israel and calculate national incidence. No CSF cultures and <1% of blood cultures were obtained outside these centers. Data in our study were for IPD episodes identified since 2009.

### PCV Introduction to the Israeli National Immunization Plan and Uptake

Israel implemented PCV7 and PCV13 vaccination during July 2009–November 2010 on a schedule of 2, 4, and 12 months; catch-up vaccines were also administered for PCV7 in children <2 years. Vaccine uptake evaluation methods were as previously described (*14*). By June 2011, ≈80% of children 7–11 months of age had

received ≥2 doses of PCV7, PCV13, or both, and ≈90% by December 2012; thereafter, ≈95% had received ≥2 PCV13 doses. By June 2011, a total of 36% of children 24–35 months of age had received ≥3 PCV7/PCV13 doses; that number increased to 87% by December 2012, and thereafter, >90% received ≥3 PCV13 doses.

### Bacteriology

#### Nasopharyngeal Cultures

Nasopharyngeal samples were obtained as previously described (*9*). In brief, we used a flexible Dacron-tipped swab, introduced through the nostrils. These swabs were inoculated into modified Stewart transport medium (Medical Wire and Equipment Co., Ltd, https://www.mwe.co.uk) and were processed within 16 hours at SUMC's clinical microbiology laboratory. Material from swabs was plated on Columbia agar with 5% sheep blood and 5.0 mg/mL gentamicin and incubated for 48 h.

We presumptively identified *S. pneumoniae* on the basis of the presence of α-hemolysis and inhibition by optochin; we confirmed the identity of the bacteria present by a positive slide agglutination test result (Phadebact; MKL Diagnostics AB, http://www.mkldiagnostics.com).

#### Conjunctivitis Cultures

We enrolled in the study all patients <24 months of age who received a diagnosis of conjunctivitis from pediatricians at SUMC or at the primary clinical service in southern Israel and whose conjunctival swabs were cultured at SUMC's clinical microbiology laboratory and grew *S. pneumoniae*. Swabbing methods were described previously (*15*). Specimen swabs were placed in transport medium and were processed in a similar manner to the nasopharyngeal swabs.

#### Otitis Media and Middle Ear Fluid Cultures

Specimen swabs were sent in transport medium. They were processed in a similar manner to the nasopharyngeal and conjunctival swabs.

#### IPD

Pneumococcal isolates from blood and CSF were initially identified by each center using local standard procedures as described previously (*14*,*16*).

### Serotypes

All strains were serotyped by Quellung reaction using the antisera of Statens Serum Institute, Copenhagen, Denmark. Methods of specimen transport were described previously (*7*,*9*,*14*).

### Antimicrobial Susceptibility Testing

We performed antimicrobial susceptibility testing by Etest (AB Biodisk, http://www.abbiodisk.com) and Kirby-Bauer disk diffusion in accordance with Clinical Laboratory Standards Institute recommendations (*17*). Antimicrobial nonsusceptibility among isolates was defined as MIC above or a zone diameter below the susceptibility breakpoint. For penicillin, we defined 2 nonsusceptibility cutoff values: MIC ≥0.1 mg/L and MIC ≥1.0 mg/L. We used 2 nonsusceptibility values because the low cutoff (MIC ≥0.1 mg/L) indicates nonsusceptibility to oral penicillin (used for mucosal infections) and parenteral penicillin for CNS infections, whereas the high MIC (MIC ≥1.0 mg/L) indicates the possibility of nonsusceptibility to parenteral penicillin for non-CNS infections. We used MIC ≥1.0 μg/mL for ceftriaxone. For all other antimicrobial drugs, we tested susceptibility by the Kirby-Bauer method: for erythromycin, a zone diameter of ≤21 mm; for trimethoprim/sulfamethoxazole, ≤19 mm; for tetracycline, ≤23 mm; for chloramphenicol, ≤20 mm; and for clindamycin, ≤19 mm. Isolates nonsusceptible to ≥3 of the antimicrobial categories were defined as multidrug resistant (MDR). In this study, we present antimicrobial susceptibility testing data for the late PCV13 period (2015–2017), for comparison of the current resistance patterns of VT20–13 versus the NVT20 serotype.

### Statistical Analysis

We conducted statistical analysis using SPSS Statistics 25.0 software for Windows (https://www.ibm.com/analytics/spss-statistics-software); $p<0.05$ was considered statistically significant. We analyzed data from active surveillance during 2009–2017 by epidemiologic years, July through June. We calculated prevalence rate ratios (RRs) with 95% CIs, comparing VT13, VT20–13, and NVT20 proportions in late PCV13 (2015–2017) versus early PCV (2009–2011) periods. Prevalence RRs were adjusted for age and ethnicity (Table 1, https://wwwnc.cdc.gov/EID/article/27/1/20-1178-T1.htm; Figure 2).

## Results

During the study period, a total of 9,089 isolates were analyzed: 2,638 from carriage in healthy children, 2,450 from carriage in non-LRTI, 1,819 from carriage in LRTI, 477 conjunctivitis, 756 OM, and 949 IPD isolates. Overall, throughout the study, 23.9% of all isolates were VT13, 23.3% were VT20–13, and 52.7% were NVT20 (Appendix Table 1, https://wwwnc.cdc.gov/EID/article/27/1/20-1178-App1.pdf).

### VT13, VT20–13 and NVT20 Proportions during the Early PCV Period

To enable better appreciation of disease potential of the 3 serotype groups (VT13, VT20–13 and NVT20) before PCV13 implementation, we analyzed the early PCV period separately. In the early PCV period, VT13 predominated in all groups. The proportions of VT13 of all isolates were 43.9% in carriage in non-LRTI, 52.1% carriage in LRTI, 45.1% conjunctivitis, 65% OM, and 71.8% IPD. Data for carriage in healthy children in this period were not available (Table 1; Figure 1).

For VT20–13, proportions were 17.8% for carriage in non-LRI, 13.4% in carriage in LRI, 20.5% conjunctivitis, 14.1% OM, and 14.8% IPD. For NVT20, proportions were 38.4% in carriage in non-LRI, 34.4% carriage in LRI, 34.4% for conjunctivitis, 20.9% OM, and 13.4% IPD.

### Proportion Dynamics of VT13, VT20–13, and NVT20 Comparing Late PCV13 Period with Early PCV Period

The proportions of VT13 of all isolates declined significantly by 73%–86% in all groups when comparing late-PCV13 period with early-PCV period. During the late-PCV13 period, VT13 were identified in only 9%–14% of all pneumococcal isolates in the various groups (Figures 1, 2).

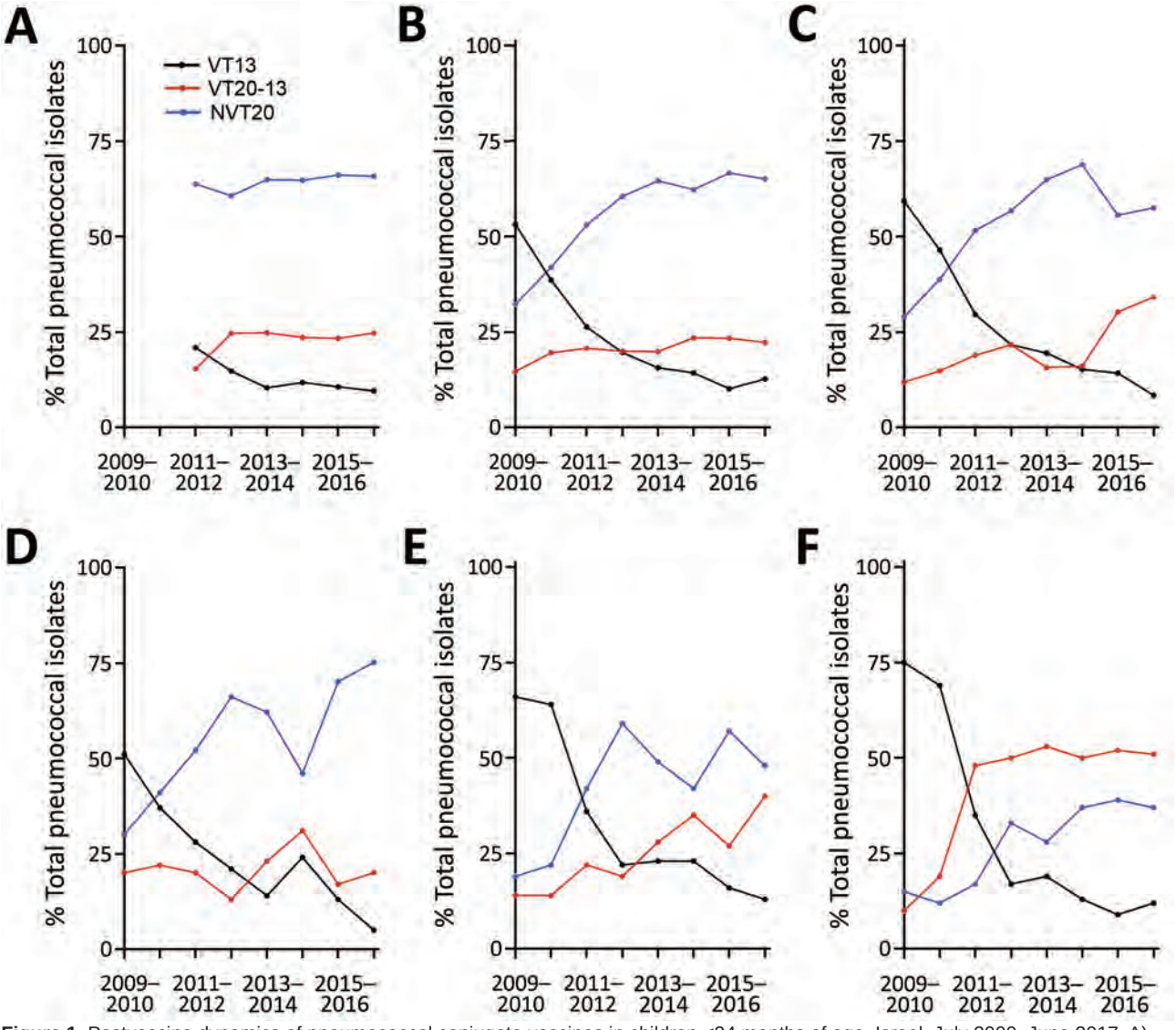


**Figure 1.** Postvaccine dynamics of pneumococcal conjugate vaccines in children <24 months of age, Israel, July 2009–June 2017. A) Healthy children; B) children with non–LRTIs; C) children with lower respiratory infections; D) children with conjunctivitis; E) children with otitis media (isolates from middle ear fluid were tested); and F) children with invasive pneumococcal disease (isolates from blood and cerebrospinal fluid were tested). Data show VT13, VT20–13, and NVT20 as the proportion of each serotype of all pneumococcal isolates. $p<0.05$ for all comparisons comparing 2015–2017 versus 2009–2011, except for VT20–13 in conjunctivitis. LRTI, lower respiratory tract infection; NVT, nonvaccine serotype; VT, vaccine serotype.

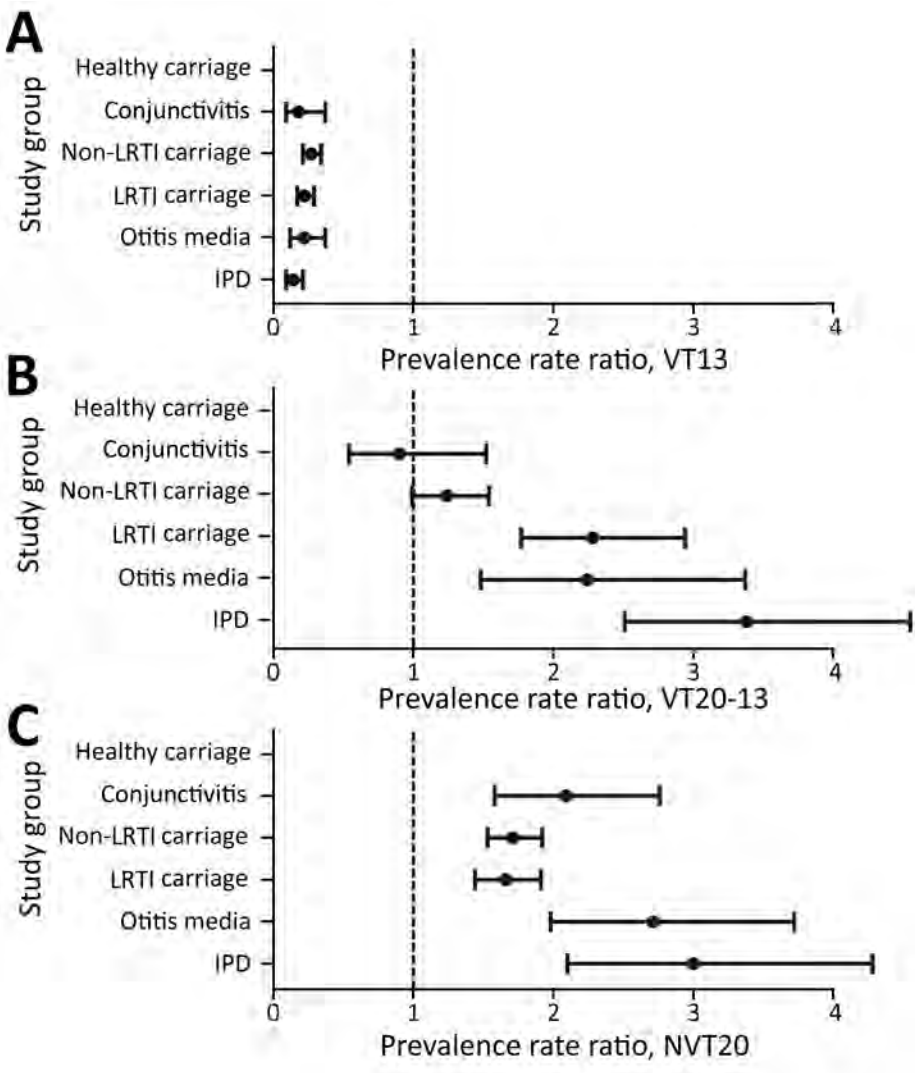


**Figure 2**. Prevalence rate ratios of pneumococcal VT13, VT20–13, and NVT20 of all pneumococcal isolates in carriage, conjunctivitis, OM, and IPD in children <24 months of age, Israel, comparing the late PCV13 period (2015–2017) to the early PCV period (2009–2011). The comparison could not be done for carriage in healthy children due to the nonavailability of data for the early PCV period. $p<0.05$ for all comparisons. Error bars indicate 95% CIs. IPD, invasive pneumococcal disease; LRTI, lower respiratory tract infection; NVT, nonvaccine serotype; OM, otitis media; PCV, pneumococcal conjugate vaccine; PCV13, 13-valent PCV; VT, vaccine serotype.

Proportions of VT20–13 did not increase significantly in conjunctivitis and carriage in non-LRI illness (Table 1; Figure 2). In contrast, we observed a significant increase of carriage in LRI, OM, and IPD ($p<0.05$ by test for trend in proportion for all groups). During the last study year, the proportions of VT20–13 of all identified pneumococcal isolates were 20%–25% in carriage in healthy children, carriage in non-LRTI, and conjunctivitis; 33% in carriage in LRTI; 40% in carriage in OM; and 51% in IPD. The fraction of VT20–13 became the leading one in IPD during the late-PCV13 period. The proportion rate ratios (2015–2017 vs. 2009–2011) for carriage in LRI, OM, and IPD were similar, whereas ratios for all 3 were significantly higher than those for conjunctivitis and carriage in non-LRTI disease.

Proportions of non-NVT20 increased in all groups, ranging from 66%–200% increase. The increase in IPD was significantly higher than in carriage in non-LRI and carriage in LRTI, but other increases did not differ significantly (Figure 2).

### VT20–13/NVT20 Ratio

To assess the relative role of VT20–13 among all NVT, we calculated the ratio between VT20–13 and NVT20. In the early PCV period, VT20–13/NVT20 ratio was the lowest for carriage in LRTI (0.39) followed by carriage in non-LRTI (0.46), conjunctivitis (0.60), OM (0.68), and IPD (1.19) (Table 2). In the late-PCV13 period (2015–2017), VT20–13/NVT20 ratio was the lowest in conjunctivitis (0.26), followed by carriage in healthy children (0.37) and carriage in non-LRTI diseases (0.35) (Figure 3). The ratios for OM and carriage in LRTI were significantly higher than for the conjunctivitis, carriage in non-LRTI, and carriage in healthy children groups. The highest ratio was observed for IPD (1.40), significantly higher than all other outcomes.

**Table 2**. Proportions of VT20–13/NVT20 ratios in children age <24 mo, Israel, 2009–2011 and 2015–2017*

| Clinical characteristic | 2009–2011 | | | 2015–2017 | | | 2015–2017 vs. 2009–2011 |
|---|---|---|---|---|---|---|---|
| | VT20–13, % | NVT20, % | VT20–13/NVT20 ratio (95% CI) | VT20–13, % | NVT20, % | VT20–13/NVT20 ratio (95% CI) | VT20–13/NVT20 ratio (95% CI) |
| Carriage in healthy children | NA | NA | NA | 24 | 66 | 0.37 (0.33–0.41) | NA |
| Carriage in non-LRTI | 18 | 38 | 0.46 (0.38–0.56) | 23 | 66 | 0.35 (0.30–0.40) | 0.80 (0.65–0.98) |
| Conjunctivitis | 20 | 34 | 0.60 (0.39–0.91) | 19 | 72 | 0.26 (0.17–0.40) | 0.57 (0.35–0.94) |
| Carriage in LRTI | 13 | 34 | 0.39 (0.30–0.50) | 32 | 57 | 0.56 (0.48–0.65) | 1.26 (1.00–1.60) |
| OM | 14 | 21 | 0.68 (0.49–0.94) | 34 | 52 | 0.60 (0.44–0.81) | 0.91 (0.66–1.25) |
| IPD | 15 | 13 | 1.19 (0.79–1.80) | 52 | 38 | 1.40 (1.12–1.73) | 1.05 (0.84–1.31) |

*No data were available for healthy children in 2009–2011. IPD, invasive pneumococcal disease; LRTI, lower respiratory tract infection; NA, not applicable; NVT20, serotypes not included in PCV20; OM, otitis media; PCV, pneumococcal conjugate vaccine; VT20–13, additional 20-valent PCV (PCV20) serotypes, not included in PCV13.

### Serotype-Specific VT20–13 Dynamics

Of all 2,126 VT20–13 isolates, serotype 15B/C was the most common (40.7%), followed by serotypes 11A (16.9%), 12F (12.8%), 33F (10.4%), 10A (9.6%), 22F (7.6%), and 8 (2.0%). (Figure 4; Appendix Table 2). Of note, serotype 15B/C was the most common VT20–13 serotype in all clinical syndromes; it constituted 37%–49% of all VT20–13 in each group, except for IPD, in which serotype 12F was the most common (50% of all VT20–13).

### Antimicrobial Nonsusceptibility Rates among VT20–13 and NVT20 during the Late PCV13 Period

Antibiotic nonsusceptibility was higher among VT20–13 as a group than NVT20 for erythromycin, tetracycline, trimethoprim-sulfamethoxazole, clindamycin, and for MDR (Table 3, https://wwwnc.cdc.gov/EID/article/27/1/20-1178-T3.htm; Figure 5). Similarly, in IPD, proportions of isolates with penicillin nonsusceptibility (MIC ≥0.1 μg/mL) were higher in VT20–13 compared with NVT20. In contrast, penicillin nonsusceptibility (MIC ≥0.1 μg/mL) was more prevalent in NVT20 than in VT20–13 in the all outcomes group; for penicillin nonsusceptibility with MIC ≥1.0 μg/mL, we observed these trends in carriage in healthy children, carriage in non-LRTI, and carriage in LRTI.

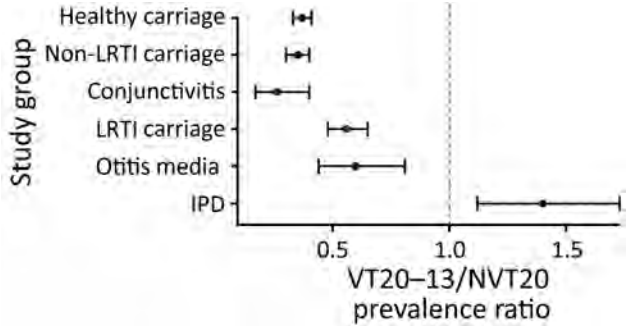


**Figure 3.** Ratio of prevalence of pneumococcal VT20–13/NVT20 ratio in children <24 months of age, Israel, during the late PCV13 period (2015–2017). Error bars represent 95% CI. IPD, invasive pneumococcal disease; LRTI, lower respiratory tract infection; NVT, nonvaccine serotype; PCV, pneumococcal conjugate vaccine; PCV13, 13-valent PCV; VT, vaccine serotype.

## Discussion

Widespread implementation of PCVs has universally resulted in complete or near-complete nasopharyngeal colonization replacement of VT by NVT (*9*,*18*,*19*). This, in turn, resulted in increased disease by NVT to a variable extent, depending mainly on the disease entity (i.e., mucosal or invasive diseases) and environmental and host factors (*3*,*4*). The currently licensed PCVs contain ≤13 serotypes, and the remaining >85 serotypes constitute potential replacing serotypes. However, not all serotypes are equally capable of progressing from colonization to disease, and not all are equally successful colonizers, resulting in selection of specific serotypes that will eventually be frequently associated with disease. Furthermore, the most successful colonizers will likely increasingly become nonsusceptible to the commonly used antimicrobial drugs (*20*–*22*). Therefore, although invasive and mucosal pneumococcal disease are invariably reduced in children after PCV implementation, the remaining potential disease may be related disproportionally to a relatively small fraction of the remaining serotypes. In this study, we have shown that as a group, the 7 serotypes selected to be included in PCV20 are indeed disproportionally associated with disease and were frequently more drug-nonsusceptible than the other remaining NVT20. Although VT20–13/NVT20 ratios declined throughout the study for carriage in non-LRTI and conjunctivitis, these ratios increased or remained stable for carriage in LRTI, OM, and IPD. These trends point to the high disease potential of VT20–13 compared with NVT20 for IPD (in which VT20–13 caused >50% of all episodes in the last study period), and possibly for certain pneumococcal mucosal diseases such as OM and LRTI (in which VT20–13/NVT20 ratio increased, but NVT20 caused >50% of all episodes). We believe that

these trends were driven by the vaccine-induced near-disappearance of the generally invasive PCV13 serotypes and the gradual differential replacement of those serotypes by NVT in different clinical syndromes, according to the specific NVT disease potential.

Several of the 7 additional PCV20 serotypes have been previously shown to have a high disease potential for IPD and other pneumococcal diseases (*4*,*5*,*23*–*26*). Nevertheless, all 7 serotypes were recognized as causing diseases and therefore were included in the 23-valent polysaccharide vaccine (PPV23), commonly used for the prevention of IPD in adults and in children ≥2 years of age with immunodeficiency and certain chronic medical conditions (*4*,*27*,*28*). Specifically, serotype 12F emerged as a major serotype in multiple countries, causing IPD and pneumonia (*5*,*10*,*22*–*24*,*29*,*30*). Its expansion was multiclonal, excluding a single hyperinvasive clone outbreak (*26*). This pattern bears similarities with the expansion of serotype 7F that occurred following PCV7 implementation; both serotypes were not expected to increase because they were frequently associated with low carriage. Serotype 8 was relatively

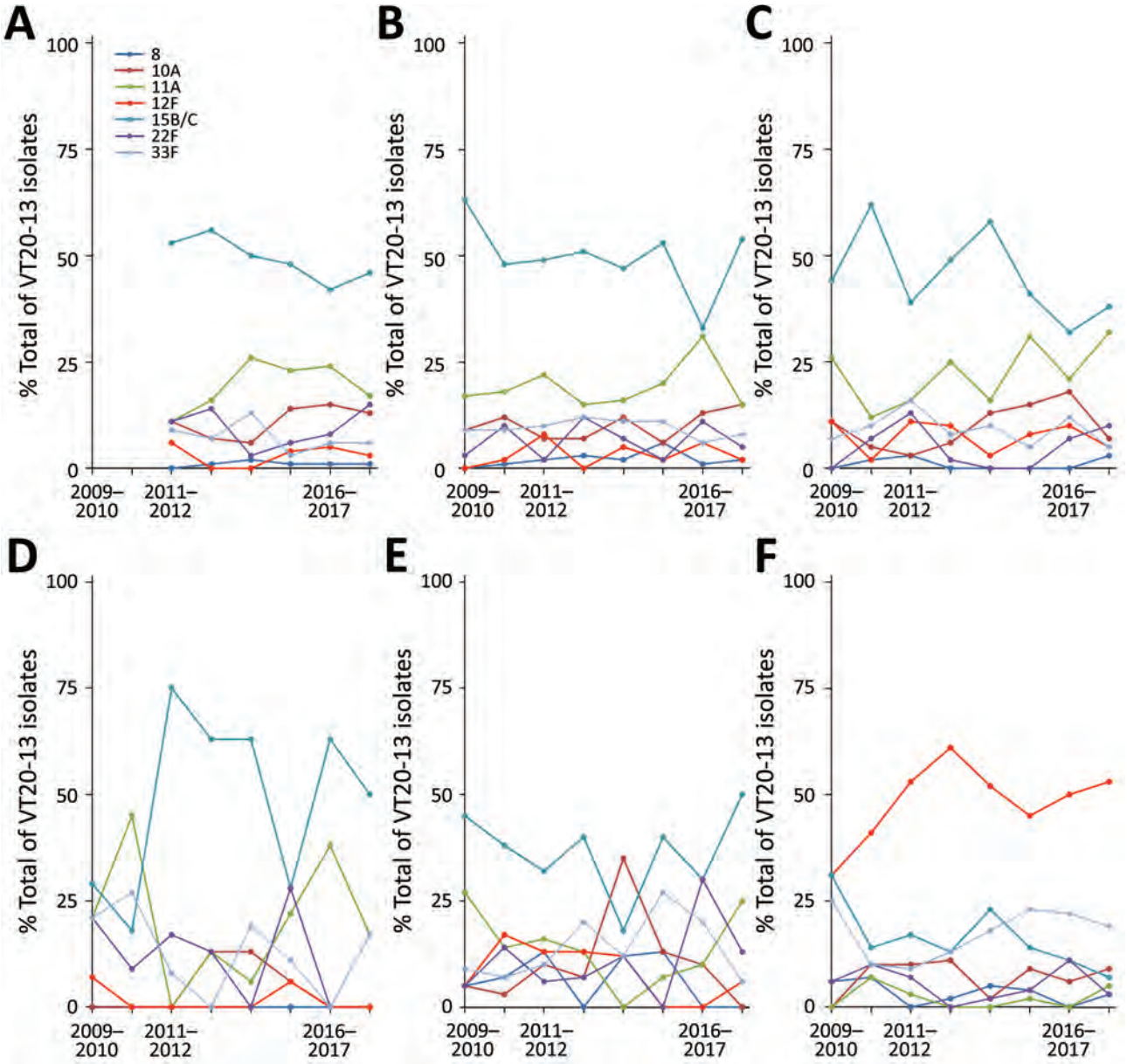


**Figure 4.** Serotype-specific VT20–13 pneumococcal isolates in children <24 months of age, Israel, 2009–2017. A) Healthy children; B) children with non–lower respiratory tract infections; C) children with lower respiratory tract infections; D) children with conjunctivitis; E) children with otitis media (isolates from middle ear fluid were tested); and F) children with invasive pneumococcal disease (isolates from blood and cerebrospinal fluid were tested). VT, vaccine serotype.

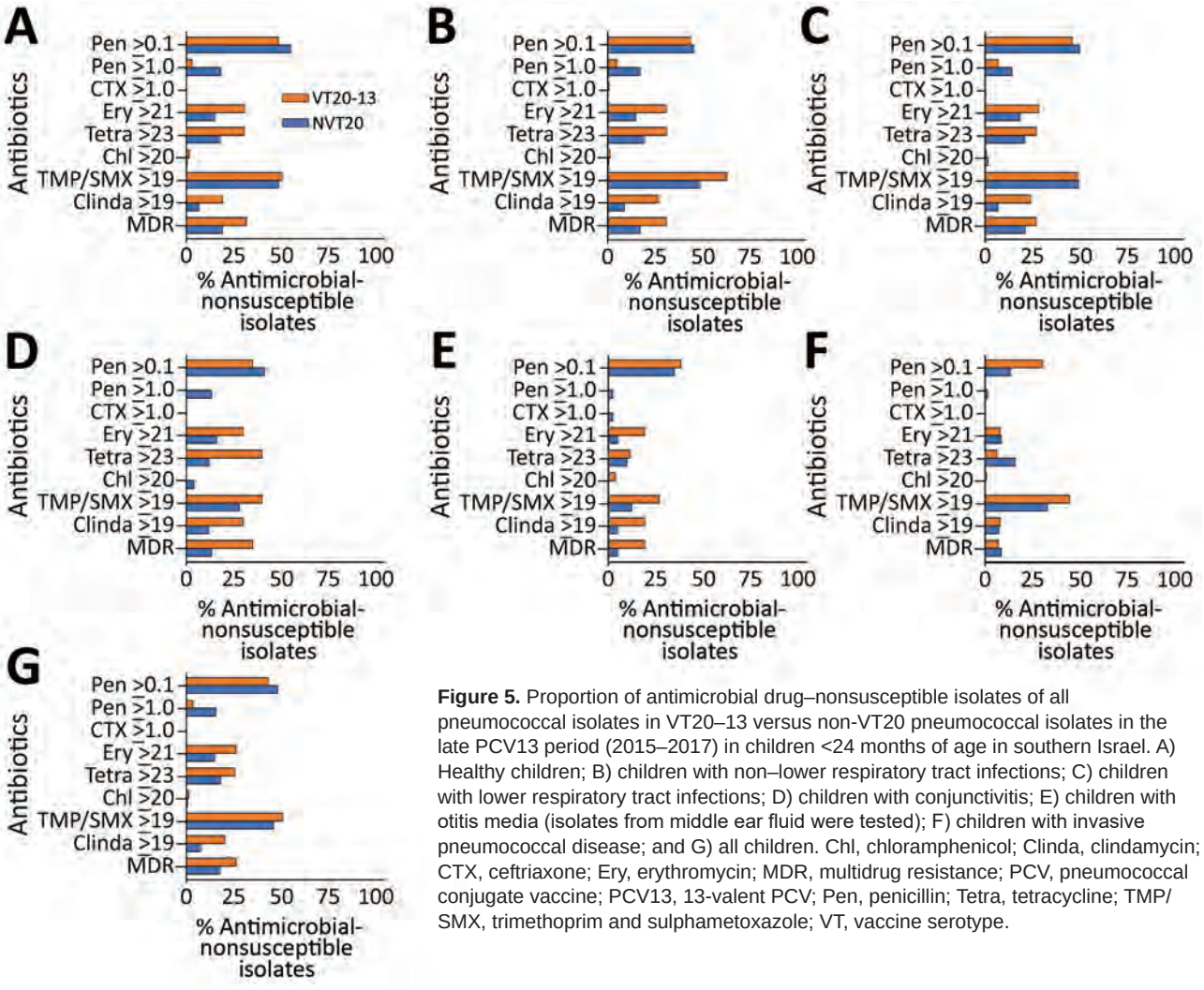


**Figure 5.** Proportion of antimicrobial drug–nonsusceptible isolates of all pneumococcal isolates in VT20–13 versus non-VT20 pneumococcal isolates in the late PCV13 period (2015–2017) in children <24 months of age in southern Israel. A) Healthy children; B) children with non–lower respiratory tract infections; C) children with lower respiratory tract infections; D) children with conjunctivitis; E) children with otitis media (isolates from middle ear fluid were tested); F) children with invasive pneumococcal disease; and G) all children. Chl, chloramphenicol; Clinda, clindamycin; CTX, ceftriaxone; Ery, erythromycin; MDR, multidrug resistance; PCV, pneumococcal conjugate vaccine; PCV13, 13-valent PCV; Pen, penicillin; Tetra, tetracycline; TMP/SMX, trimethoprim and sulphametoxazole; VT, vaccine serotype.

uncommon in the current study but has emerged as one of the most prominent replacing serotypes in IPD in adults after PCV implementation, including in Israel (*23*–*25*,*31*). However, reports of this serotype in children are also emerging (*26*). Serotypes 22F and 33F, which are also included in an experimental 15-valent PCV currently in an advanced stage of clinical studies (*11*,*32*,*33*), were recognized as important serotypes in IPD and pneumonia (*11*,*24*,*25*,*34*). In the United States, proportions of IPD caused by serotype 22F were 11% in children <5 years and 13% in adults ≥18 years, whereas serotype 33F caused 10% of residual IPD cases in children <5 years and 5% in adults ≥18 years (*11*,*32*). In addition, serotypes 10A, 11A, and 15B/C, considered to have lower disease potential than serotypes 12F, 8, 22F, and 33F, have been reported frequently following PCV implementation worldwide (*5*,*10*,*23*–*25*).

Despite the importance of VT20 as a group, several NVT20 have been shown to be able to have the potential to cause large outbreaks (i.e., pneumococcal serotype 2 responsible for large IPD outbreaks in Israel) (*35*) or reported as emerging IPD-causing serotypes (i.e., serotype 24F) (*5*,*6*,*22*). Others, considered less invasive NVT20 serotypes have been also reported in several sites (i.e., serotypes 15A and 16F) (*36*–*38*).

This study adds important information not only on the proportions of specific serotypes causing IPD in the PCV13 era, but also with regard to the proportions of specific serotypes in carriage in healthy children versus children with IPD and mucosal diseases. These data are relevant because carriage during disease probably reflects relative disease potential in the various clinical entities. We found that both the rates of incidence and the relative proportion of VT20–13 seen in IPD, OM, and carriage in LRTI requiring chest radiography were significantly higher than those in conjunctivitis and in carriage in non-LRTI not requiring chest radiography. Specifically, in IPD, serotype

12F emerged as the most common serotype causing IPD in children <2 years of age, with ≈25% of all IPD caused by this serotype in recent years. Thus, the addition of serotype 12F coverage in PCV20 is expected to further decrease overall IPD rates in this population. Similarly, serotype 15B/C was the most common serotype in pneumococcal carriage and mucosal diseases (≈10% of all pneumococcal isolates).

We found that antimicrobial nonsusceptibility was significantly more frequent among VT20–13 than among NVT20; other studies have also shown such increases among PCV20–13 serotypes (*21*,*22*,*39*,*40*). In the pre-PCV era, most nonsusceptible strains belonged to serotypes included in PCV7/PCV13. Although nonsusceptibility is still higher among those strains or even increasing, the overall nonsusceptibility has been reduced in countries which successfully implemented PCVs (*21*,*22*,*39*). However, high selective pressure continues to occur with excessive antibiotic consumption, especially in dominating carriage serotypes. The most successful replacing serotypes are now those frequently exposed to antimicrobial drugs during carriage, resulting in increased antimicrobial nonsusceptibility compared with the less successful colonizers often found among NVT20 (*21*,*22*,*39*,*40*). Of interest, isolates causing noninvasive disease tend to have higher rates of antimicrobial resistance than those causing IPD (*21*), similar to the observations in our study.

The main strengths of our study include relatively long-term surveillance duration, large number of episodes, and the ability to assess multiple clinical outcomes in the same populations. Nonetheless, our study has several limitations. First, we did not have data on the pre-PCV period. However, we still could follow the dynamics of the non-PCV7/PCV13 serotypes because the data from the first year of implementation are included. Second, with regard to carriage in healthy children, data are only available from 2011–2012. However, the similarity of the proportion rates for 2010–2011 when carriage in healthy children is compared with that of children with non-LRTI and children with conjunctivitis (the most superficial mucosal disease, potentially explaining the higher proportion of noninvasive serotypes in the disease compared with other diseases) lends support to the suggestion that there are similarities between these groups and healthy children during the entire study period. Third, our data derive from multiple studies in the setting of a single country. However, as discussed above, similarities with other reports from other countries suggest that our conclusion may be generalized, at least to some extent.

In conclusion, *S. pneumoniae* VT20–13 are disproportionally associated with IPD, OM, and carriage in LRTI, compared with the other remaining NVT20, suggesting higher disease potential for these diseases than NVT20. In addition, the VT20–13 serotypes were more often nonsusceptible to various antimicrobial drugs than the NVT20 group. These findings suggest that PCV20 introduction may result in substantial decrease in the rates of IPD, OM, and possibly LRTI, as well as antimicrobial nonsusceptibility in children.

This work was supported in part by a grant from Pfizer (grant no. 0887X1-4603). The funders had no role in study design, data collection and interpretation, or the decision to submit the work for publication.

S. B.-S. has received speakers' fees and a grant from Pfizer, has been a scientific consultant for Merck Sharp & Dohme, and has served as a speaker for GlaxoSmithKline and Merck Sharp & Dohme. D.G. has received grants from Merck Sharp & Dohme; has been a scientific consultant for GlaxoSmithKline, Merck Sharp & Dohme, and Pfizer; and has served as a speaker for GlaxoSmithKline, Merck Sharp & Dohme, and Pfizer. R.D. has received grants and research support from Pfizer, Merck Sharp & Dohme, and Medimmune; has been a scientific consultant for Pfizer, MeMed, Merck Sharp & Dohme, and Biondvax; had served on advisory boards of Pfizer, Merck Sharp & Dohme, and Biondvax; and has served as a speaker for Pfizer.

## About the Author

Dr. Ben-Shimol is a specialist in pediatric infectious diseases at the Pediatric Infectious Disease Unit of the Soroka University Medical Center and an associate professor at the Faculty of Health Sciences of the Ben-Gurion University of the Negev, Beer-Sheva, Israel. His research interests are pneumococcal infectious diseases, pneumococcal vaccines, zoonotic diseases, and parasitology.

## References

1. O'Brien KL, Wolfson LJ, Watt JP, Henkle E, Deloria-Knoll M, McCall N, et al.; Hib and Pneumococcal Global Burden of Disease Study Team. Burden of disease caused by *Streptococcus pneumoniae* in children younger than 5 years: global estimates. Lancet. 2009;374:893–902. https://doi.org/10.1016/S0140-6736(09)61204-6
2. Wahl B, O'Brien KL, Greenbaum A, Majumder A, Liu L, Chu Y, et al. Burden of *Streptococcus pneumoniae* and *Haemophilus influenzae* type b disease in children in the era of conjugate vaccines: global, regional, and national estimates for 2000-15. Lancet Glob Health. 2018;6:e744–57. https://doi.org/10.1016/S2214-109X(18)30247-X
3. Jedrzejas MJ. Pneumococcal virulence factors: structure and function. Microbiol Mol Biol Rev. 2001;65:187–207. https://doi.org/10.1128/MMBR.65.2.187-207.2001
4. Bogaert D, Hermans PWM, Adrian PV, Rümke HC, de Groot R. Pneumococcal vaccines: an update on current strategies. Vaccine. 2004;22:2209–20. https://doi.org/10.1016/j.vaccine.2003.11.038

5. Balsells E, Guillot L, Nair H, Kyaw MH. Serotype distribution of *Streptococcus pneumoniae* causing invasive disease in children in the post-PCV era: A systematic review and meta-analysis. PLoS One. 2017;12:e0177113. https://doi.org/10.1371/journal.pone.0177113
6. Ben-Shimol S, Dagan R, Givon-Lavi N, Avital D, Bar-Ziv J, Greenberg D. Use of chest radiography examination as a probe for pneumococcal conjugate vaccine impact on lower respiratory tract infections in young children. Clin Infect Dis. 2019;71:177–87. 10.1093/cid/ciz768 https://doi.org/10.1093/cid/ciz768
7. Ben-Shimol S, Givon-Lavi N, Leibovitz E, Raiz S, Greenberg D, Dagan R. Near-elimination of otitis media caused by 13-valent pneumococcal conjugate vaccine (PCV) serotypes in southern Israel shortly after sequential introduction of 7-valent/13-valent PCV. Clin Infect Dis. 2014;59:1724–32. https://doi.org/10.1093/cid/ciu683
8. de Oliveira LH, Camacho LAB, Coutinho ESF, Martinez-Silveira MS, Carvalho AF, Ruiz-Matus C, et al. Impact and effectiveness of 10 and 13-valent pneumococcal conjugate vaccines on hospitalization and mortality in children aged less than 5 years in Latin American countries: a systematic review. PLoS One. 2016;11:e0166736. https://doi.org/10.1371/journal.pone.0166736
9. Ben-Shimol S, Givon-Lavi N, Greenberg D, Dagan R. Pneumococcal nasopharyngeal carriage in children <5 years of age visiting the pediatric emergency room in relation to PCV7 and PCV13 introduction in southern Israel. Hum Vaccin Immunother. 2016;12:268–76. https://doi.org/10.1080/21645515.2015.1095414
10. Thompson A, Lamberth E, Severs J, Scully I, Tarabar S, Ginis J, et al. Phase 1 trial of a 20-valent pneumococcal conjugate vaccine in healthy adults. Vaccine. 2019;37:6201–7. https://doi.org/10.1016/j.vaccine.2019.08.048
11. Rupp R, Hurley D, Grayson S, Li J, Nolan K, McFetridge RD, et al. A dose ranging study of 2 different formulations of 15-valent pneumococcal conjugate vaccine (PCV15) in healthy infants. Hum Vaccin Immunother. 2019;15:549–59. https://doi.org/10.1080/21645515.2019.1568159
12. Ben-Shimol S, Givon-Lavi N, Leibovitz E, Greenberg D, Dagan R. Studying PCV impact on clinical presentation of otitis media helps to understand its pathogenesis. Vaccine. 2019;37:1–6. https://doi.org/10.1016/j.vaccine.2018.11.054
13. Ben-Shimol S, Givon-Lavi N, Leibovitz E, Raiz S, Greenberg D, Dagan R. Impact of widespread introduction of pneumococcal conjugate vaccines on pneumococcal and nonpneumococcal otitis media. Clin Infect Dis. 2016;63:611–8. https://doi.org/10.1093/cid/ciw347
14. Ben-Shimol S, Greenberg D, Givon-Lavi N, Schlesinger Y, Somekh E, Aviner S, et al. Early impact of sequential introduction of 7-valent and 13-valent pneumococcal conjugate vaccine on IPD in Israeli children <5 years: An active prospective nationwide surveillance. Vaccine. 2014;32:3452–9.10
15. Buznach N, Dagan R, Greenberg D. Clinical and bacterial characteristics of acute bacterial conjunctivitis in children in the antibiotic resistance era. Pediatr Infect Dis J. 2005;24:823–8. https://doi.org/10.1097/01.inf.0000178066.24569.98
16. Ben-Shimol S, Greenberg D, Givon-Lavi N, Elias N, Glikman D, Rubinstein U, et al.; Israeli Bacteremia and Meningitis Active Surveillance Group. Rapid reduction in invasive pneumococcal disease after introduction of PCV7 into the National Immunization Plan in Israel. Vaccine. 2012;30:6600–7. https://doi.org/10.1016/j.vaccine.2012.08.012
17. Clinical and Laboratory Standards Institute. Performance standards for antimicrobial susceptibility testing: 28th edition informational supplement (M100-S28). Wayne (PA): The Institute; 2018.
18. Weinberger DM, Malley R, Lipsitch M. Serotype replacement in disease after pneumococcal vaccination. Lancet. 2011;378:1962–73. https://doi.org/10.1016/S0140-6736 (10)62225-8
19. Usuf E, Bottomley C, Bojang E, Cox I, Bojang A, Gladstone R, et al. Persistence of nasopharyngeal pneumococcal vaccine serotypes and increase of nonvaccine serotypes among vaccinated infants and their mothers 5 years after introduction of pneumococcal conjugate vaccine 13 in The Gambia. Clin Infect Dis. 2019;68:1512–21. https://doi.org/10.1093/cid/ciy726
20. Danino D, Givon-Lavi N, Ben-Shimol S, Greenberg D, Dagan R. Understanding the evolution of antibiotic-nonsusceptible pneumococcal nasopharyngeal colonization following pneumococcal conjugate vaccine implementation in young children. Clin Infect Dis. 2019;69:648–56. https://doi.org/10.1093/cid/ciy926
21. Richter SS, Diekema DJ, Heilmann KP, Dohrn CL, Riahi F, Doern GV. Changes in pneumococcal serotypes and antimicrobial resistance after introduction of the 13-valent conjugate vaccine in the United States. Antimicrob Agents Chemother. 2014;58:6484–9. https://doi.org/10.1128/AAC.03344-14
22. Varon E, Cohen R, Béchet S, Doit C, Levy C. Invasive disease potential of pneumococci before and after the 13-valent pneumococcal conjugate vaccine implementation in children. Vaccine. 2015;33:6178–85. https://doi.org/10.1016/j.vaccine.2015.10.015
23. Amin-Chowdhury Z, Iyanger N, Ramsay ME, Ladhani SN. Outbreaks of severe pneumococcal disease in closed settings in the conjugate vaccines era, 2010-2018: A systematic review to inform national guidance in the UK. J Infect. 2019;79:495–502. https://doi.org/10.1016/j.jinf.2019.10.009
24. Pick H, Daniel P, Rodrigo C, Bewick T, Ashton D, Lawrence H, et al. Pneumococcal serotype trends, surveillance and risk factors in UK adult pneumonia, 2013-18. Thorax. 2020;75:38–49. https://doi.org/10.1136/thoraxjnl-2019-213725
25. Levy C, Ouldali N, Caeymaex L, Angoulvant F, Varon E, Cohen R. Diversity of serotype replacement after pneumococcal conjugate vaccine implementation in Europe. J Pediatr. 2019;213:252–253.e3. https://doi.org/10.1016/j.jpeds.2019.07.057
26. Lo SW, Gladstone RA, van Tonder AJ, Lees JA, du Plessis M, Benisty R, et al.; Global Pneumococcal Sequencing Consortium. Pneumococcal lineages associated with serotype replacement and antibiotic resistance in childhood invasive pneumococcal disease in the post-PCV13 era: an international whole-genome sequencing study. Lancet Infect Dis. 2019;19:759–69. https://doi.org/10.1016/S1473-3099(19)30297-X
27. Hausdorff WP, Feikin DR, Klugman KP. Epidemiological differences among pneumococcal serotypes. Lancet Infect Dis. 2005;5:83–93. https://doi.org/10.1016/S1473-3099(05)70083-9
28. Djennad A, Ramsay ME, Pebody R, Fry NK, Sheppard C, Ladhani SN, et al. Effectiveness of 23-valent polysaccharide pneumococcal vaccine and changes in invasive pneumococcal disease incidence from 2000 to 2017 in those aged 65 and over in England and Wales. EClinicalMedicine. 2018;6:42–50. https://doi.org/10.1016/j.eclinm.2018.12.007
29. Rokney A, Ben-Shimol S, Korenman Z, Porat N, Gorodnitzky Z, Givon-Lavi N, et al. Emergence of *Streptococcus pneumoniae* serotype 12F after sequential introduction of 7- and 13-valent vaccines, Israel. Emerg Infect Dis. 2018;24:453–61. https://doi.org/10.3201/eid2403.170769
30. Cohen R, Levy C, Bonnet E, Thollot F, Boucherat M, Fritzell B, et al. Risk factors for serotype 19A carriage after

introduction of 7-valent pneumococcal vaccination. BMC Infect Dis. 2011;11:95. https://doi.org/10.1186/1471-2334-11-95
31. Regev-Yochay G, Katzir M, Strahilevitz J, Rahav G, Finn T, Miron D, et al.; IAIPD group. The herd effects of infant PCV7/PCV13 sequential implementation on adult invasive pneumococcal disease, six years post implementation; a nationwide study in Israel. Vaccine. 2017; 35:2449–56. https://doi.org/10.1016/j.vaccine.2017.03.031
32. Moore MR, Link-Gelles R, Schaffner W, Lynfield R, Lexau C, Bennett NM, et al. Effect of use of 13-valent pneumococcal conjugate vaccine in children on invasive pneumococcal disease in children and adults in the USA: analysis of multisite, population-based surveillance. Lancet Infect Dis. 2015;15:301–9. https://doi.org/10.1016/S1473-3099(14)71081-3
33. Pilishvili T, Lexau C, Farley MM, Hadler J, Harrison LH, Bennett NM, et al.; Active Bacterial Core Surveillance/Emerging Infections Program Network. Sustained reductions in invasive pneumococcal disease in the era of conjugate vaccine. J Infect Dis. 2010;201:32–41. https://doi.org/10.1086/648593
34. van Hoek AJ, Andrews N, Waight PA, George R, Miller E. Effect of serotype on focus and mortality of invasive pneumococcal disease: coverage of different vaccines and insight into non-vaccine serotypes. PLoS One. 2012;7:e39150. https://doi.org/10.1371/journal.pone.0039150
35. Dagan R. Ben-Shimol S, Benisty R, Regev- Yochay G, Ron M, Givon-Lavi N, et al. A nationwide outbreak of invasive pneumococcal disease (IPD) caused by a novel *Streptococcus pneumoniae* serotype 2 (SP2) clone in the PCV13 era, in Israel. Abstract 1888. In: Abstracts of IDweek 2019; October 2–6, 2019; Washington, DC, USA. Alexandria (VA): Infectious Diseases Society of America; 2019.
36. Nakano S, Fujisawa T, Ito Y, Chang B, Matsumura Y, Yamamoto M, et al. Whole-genome sequencing analysis of multidrug-resistant serotype 15A *Streptococcus pneumoniae* in Japan and the emergence of a highly resistant serotype 15A-ST9084 clone. Antimicrob Agents Chemother. 2019;63:e02579–18. https://doi.org/10.1128/AAC.02579-18
37. Neves FPG, Cardoso NT, Cardoso CAA, Teixeira LM, Riley LW. Direct effect of the 13-valent pneumococcal conjugate vaccine use on pneumococcal colonization among children in Brazil. Vaccine. 2019;37:5265–9. https://doi.org/10.1016/j.vaccine.2019.07.056
38. Dayie NTKD, Tettey EY, Newman MJ, Bannerman E, Donkor ES, Labi A-K, et al. Pneumococcal carriage among children under five in Accra, Ghana, five years after the introduction of pneumococcal conjugate vaccine. BMC Pediatr. 2019;19:316. https://doi.org/10.1186/s12887-019-1690-5
39. Cohen R, Biscardi S, Levy C. The multifaceted impact of pneumococcal conjugate vaccine implementation in children in France between 2001 to 2014. Hum Vaccin Immunother. 2016;12:277–84. https://doi.org/10.1080/21645515.2015.1116654
40. Tomczyk S, Lynfield R, Schaffner W, Reingold A, Miller L, Petit S, et al. Prevention of antibiotic-nonsusceptible invasive pneumococcal disease with the 13-valent pneumococcal conjugate vaccine. Clin Infect Dis. 2016;62:1119–25. https://doi.org/10.1093/cid/ciw067

Address for correspondence: Ron Dagan, Pediatric Infectious Disease Unit, Soroka University Medical Center, Beer-Sheva, Israel; e-mail: rdagan@bgu.ac.il

# Precise Species Identification by Whole-Genome Sequencing of *Enterobacter* Bloodstream Infection, China

Wenjing Wu,[1] Li Wei,[1] Yu Feng, Yi Xie, Zhiyong Zong

The clinical importance of *Enterobacter* spp. remains unclear because phenotype-based *Enterobacter* species identification is unreliable. We performed a genomic study on 48 cases of *Enterobacter*-caused bloodstream infection by using in silico DNA–DNA hybridization to identify precise species. Strains belonged to 12 species; *Enterobacter xiangfangensis* (n = 21) and an unnamed species (taxon 1, n = 8) were dominant. Most (63.5%) *Enterobacter* strains (n = 349) with genomes in GenBank from human blood are *E. xiangfangensis*; taxon 1 (19.8%) was next most common. *E. xiangfangensis* and taxon 1 were associated with increased deaths (20.7% vs. 15.8%), lengthier hospitalizations (median 31 d vs. 19.5 d), and higher resistance to aztreonam, cefepime, ceftriaxone, piperacillin-tazobactam, and tobramycin. Strains belonged to 37 sequence types (STs); ST171 (*E. xiangfangensis*) was most common (n = 6). Four ST171 strains belonged to a defined clone. Precise species identification has greater implications for epidemiology and infection control than treatment.

*Enterobacter* spp. belongs to the family *Enterobacteriaceae* and is a common pathogen in a variety of infections, such as bloodstream and intraabdominal infections, most of which are healthcare associated (*1*). *Enterobacter* spp. is the third most common human pathogen, after *Escherichia coli* and *Klebsiella pneumoniae*, and is therefore of clinical importance (*1*). *Enterobacter* consists of several closely related species (*1*) that cannot typically be identified precisely by common phenotypic tests. The taxonomy of *Enterobacter* is complicated by the reassignment to other genera of some species that formerly belonged to the *Enterobacter* genus. For example, *E. aerogenes* has been moved to genus *Klebsiella* (*2*), *E. agglomerans* to genus *Pantoea* (*3*), and *E. sakazakii* to genus *Cronobacter* (*4*). Currently, 14 *Enterobacter* spp. with validly published names exist, and 3 additional *Enterobacter* spp. have tentative species designations awaiting validation under the rules of the International Code of Nomenclature of Bacteria (Bacteriological Code) (Appendix 1 Table 1, https://wwwnc.cdc.gov/EID/article/27/1/19-0154-App1.pdf).

Several *Enterobacter* spp., such as *E. asburiae, E. cloacae,* and *E. hormaechei*, cause infections in humans (*1*). *Enterobacter* strains extracted from clinical samples are usually reported as *E. cloacae,* and sometimes *E. asburiae*, *E. hormaechei,* or *E. kobei,* by automated microbial identification systems such as Vitek II (bioMérieux, https://www.biomerieux.com). However, such phenotype-based tests are unreliable for species identification of *Enterobacter* and can result in misidentification (*1*). For instance, all *Enterobacter* spp. have a positive reaction for β-galactosidase, arginine dihydrolase, citrate utilization, sucrose, amygdalin, arabinose, and D-glucose but are negative for lysine decarboxylase, $H_2S$ production, urease activity, indole production, deaminase, and gelatinase (*5*–*7*). Differentiating *Enterobacter* spp. by biochemical reactions commonly used in clinical microbiology laboratories is therefore difficult. The differences in clinical importance of each *Enterobacter* species remain largely unknown because they are regularly misidentified in clinical microbiology laboratories.

Because of the substantial reduction in cost of whole-genome sequencing for bacterial strains, we are entering the era of genomic microbiology (*8*). Newly created methods can determine the overall nucleotide identities between genome sequences and therefore enable more precise species identification (*9*). Calculation of average nucleotide identity (ANI) between genomes is widely used for species

Author affiliations: West China Hospital, Sichuan University, Chengdu, China (W. Wu, L. Wei, Y. Feng, Y. Zie, Z. Zong); State Key Laboratory of Biotherapy, Chengdu (W. Wu, Y. Feng, Z. Zong)

DOI: https://doi.org/10.3201/eid2701.190154

[1]These authors contributed equally to this article.

identification. It has been proposed that ANI >96% would guarantee species assignation, whereas ANI of <93% can be considered species differentiation (*10*). However, ANI values in the range of 93%–96% represent a vague zone in which the boundary of a species might fall (*10*). DNA–DNA hybridization (DDH) remains the standard for species identification, with a ≥70% cutoff recommended to define a species. However, DDH is cumbersome, prone to fluctuation, and requires the availability of type strains. To overcome the shortcomings of DDH, in silico DDH (isDDH) mimics DDH by comparing genome sequences and can be a reliable and convenient tool for species assignation. To provide insight into the potential clinical importance of different *Enterobacter* spp., we performed a genomic study using isDDH to identify bloodstream infection (BSI)–causing *Enterobacter* strains to the species level.

## Materials and Methods

### Strain and Susceptibility Tests

We collected nonduplicate *Enterobacter* strains recovered from blood cultures during January 2016–June 2018 at West China Hospital of Sichuan University (Appendix 2 Table 1, https://wwwnc.cdc.gov/EID/article/27/1/19-0154-App2.xlsx). West China Hospital is a 5,000-bed major referral hospital in western China. Initial species identification and in vitro susceptibility testing were performed by using Vitek II. We determined MICs of colistin by using the broth microdilution method of the Clinical and Laboratory Standards Institute (CLSI) and interpreted susceptibility following CLSI guidelines (*11*). For colistin and tigecycline, no CLSI breakpoints are available, so we used breakpoint standards defined by the European Committee on Antimicrobial Susceptibility Testing (https://www.eucast.org). Multidrug resistance was defined based on the criteria for *Enterobacteriaceae* (*12*).

### Patient Data

West China Hospital has a comprehensive hospital information system, which allowed us to retrieve patient data including age, sex, length of hospitalization, and clinical outcomes (death or discharge) from electronic medical records. One patient (with strain 090040) had an unusually long hospital stay (578 d) because of a medical dispute and was removed from our analysis of length of stay. According to social customs in China, dying at home is preferred over the hospital; it is likely many patients chose to stop treatment and return home if treatment was not working and patients felt death was imminent. We categorized patients who chose to be discharged but were likely to die in the hospital (judged by the consensus of 2 physicians reviewing blind data) as patients with predicted death. BSI, the type of BSI (primary or secondary to infection of other sites), central line–associated BSI (CLABSI), and healthcare-associated infection were determined by using criteria established by the Centers for Disease Control and Prevention's National Healthcare Safety Network (*13*,*14*). We conducted the study in accordance with the amended Declaration of Helsinki. The Ethics Committee of West China Hospital approved the study and waived informed consent.

### Short-Read Genome Sequencing, Analysis, and Precise Species Identification

All strains underwent whole-genome sequencing by using the HiSeq X10 platform (Illumina, https://www.illumina.com). Genomic DNA was prepared by using the QIAamp DNA mini kit (QIAGEN, https://www.qiagen.com). We used Unicycler version 0.4.3 (*15*), in the conservative mode for increased accuracy, to perform a de novo hybrid assembly. Precise species identification was established by determining the pairwise isDDH between the genome sequence of the query strain and those of type strains of *Enterobacter* spp., including the validly published species and the species awaiting validation (Appendix 1 Table 1). This process was performed by using the Genome-to-Genome Distance Calculator, formula 2 (*16*). A ≥70% cutoff was applied to define a species. In addition, we determined the pairwise ANI of the genome sequence of the query strain and those of type strains of *Enterobacter* spp. (Appendix 1 Table 1) by using JSpecies software (https://imedea.uib-csic.es/jspecies) with a >96% ANI cutoff to define a species (*10*). Sequence types (STs) were determined by using the genomic sequences to query the multilocus sequence typing database of *E. cloacae* (https://pubmlst.org/ecloacae). Antimicrobial resistance genes were identified from genome sequences by using the ABRicate program (https://github.com/tseemann/abricate) to query the ResFinder database (https://genomicepidemiology.org).

The genome sequences of all *Enterobacter* strains recovered from human blood (n = 349, Appendix 2 Table 2) were retrieved from GenBank (accessed 2018 Nov 1). These *Enterobacter* genomes were subjected to precise species identification by using the Genome-to-Genome Distance Calculator as described.

### Clonal Relatedness on the Basis of Single-Nucleotide Polymorphisms

We performed single-nucleotide polymorphism (SNP) calling for genome sequences to untangle the clonal relatedness of ST171 strains and to investigate whether the ST171 strains in this study are clonally related to strains recovered elsewhere. All genome sequences of ST171 *Enterobacter* strains (n = 102), regardless of types of the host source (human, nonhuman, or unknown) and source (blood, nonblood, or unknown), were retrieved from GenBank. We used the complete chromosome sequence of ST171 strain 34798 (GenBank accession no. CP012165), which was recovered from a bile sample in the United States in 2011, as our reference for mapping. Genome sequences of the strains were mapped against the reference genome by using Snippy version 4.3.6 (https://github.com/tseemann/snippy) at default settings. The resulting core SNPs (n = 1,918) were concatenated and used to infer a phylogenomic tree by using RAxML version 8.2.12 (*17*) under the general time-reversible plus gamma model with a 1,000-bootstrap test.

### Long-Read Genome Sequencing and Plasmid Analysis for ST171 Strains

We determined plasmid replicons of all ST171 strains in this study by using PlasmidFinder version 2.0 (https://cge.cbs.dtu.dk/services/PlasmidFinder). The first $bla_{NDM-5}$–harboring ST171 strain (090011) in this study and the only $bla_{NDM-1}$–harboring ST171 strain (045001) were selected for whole-genome sequencing by using the long-read MinION sequencer (Nanopore, https://nanoporetech.com) to obtain complete chromosomal and plasmid sequences. De novo hybrid assembly of short Illumina reads and long MinION reads was performed by using Unicycler version 0.4.3 (*15*) in conservative mode for increased accuracy. Complete circular contigs were then corrected by using Pilon version 1.22 (*18*) with Illumina reads for several rounds until no further improvements were reported. Short reads of the remaining four $bla_{NDM-5}$–harboring ST171 strains (090022, 090023, 090055, and 090059) were mapped against the $bla_{NDM-5}$-carrying plasmid (designated pNDM5_090011) of strain 090011 by using BWA version 0.7.17 (H. Ling, unpub. data, https://arxiv.org/abs/1303.3997) at default settings.

### Statistical Analysis

Continuous variables were presented as median and interquartile range and were compared by using rank-sum test. We used the Pearson $\chi^2$ test, Yates correction for continuity, or Fisher exact test to compare disparities between different groups for categorical variables. Pearson $\chi^2$ test was used when sample size (n) was $\geq$40 and theoretical frequency (T) $\geq$5, Yates correction for continuity when n$\geq$40 and 1$\leq$T<5, and Fisher exact test when n<40 or T<1. We used SPSS Statistics 21.0 (IBM Inc., https://www.ibm.com) to perform statistical analyses. All p values were 2-tailed, and p<0.05 was considered statistically significant. We used PASS version 11.0 (NCSS, https://www.ncss.com) to calculate statistical power after using the Wilcoxon test to conduct nonparametric adjustment.

Draft genome sequences of the strains in this study were deposited into GenBank (accession numbers in Appendix 2 Table 1). The complete genome sequence of strain 090011 was deposited into GenBank under accession nos. CP036310–2. and the sequence for strain 045001 was deposited under accession nos. CP043382–5.

## Results

### Precise Species Identification of *Enterobacter* Strains

A total of 48 nonduplicated *Enterobacter* strains were recovered from blood during our 2.5-year study period and were collected for study (Table 1; Appendix 2 Table 1). Whole-genome sequencing results, isDDH, and ANI values of these strains are summarized in Appendix 2 Table 1. The 48 strains were identified as *E. cloacae* (n = 42), *E. asburiae* (n = 3), and *E. kobei* (n = 3) by Vitek II. However, precise species identification on the basis of isDDH revealed that the most common species was actually *E. xiangfangensis* (n = 21) (Table 2); the next most common was an *Enterobacter* sp. (n = 8) that has no assigned species name but was previously known as *Enterobacter* cluster III, as defined by Hoffman et al. (*6*). This species is most closely related to *E. xiangfangensis* with a 66.6% isDDH value and is temporarily assigned taxon 1 here (Appendix 2 Table 2). The remaining strains were assigned to 10 *Enterobacter* species: *E. bugandensis* (n = 4), *E. cloacae* (n = 3), *E. asburiae* (n = 2), *E. hormaechei* (n = 2), *E. huaxiensis* (n = 2), *E. roggenkampii* (n = 2), *E. chuandaensis* (n = 1), *E. ludwigii* (n = 1), *E. sichuanensis* (n = 1), and an unnamed *Enterobacter* sp. (n = 1) (Table 2). The unnamed species is most closely related to *E. roggenkampii* with a 65.4% isDDH value (Appendix 1 Table 2) and is temporarily assigned taxon 2 here.

Of 349 *Enterobacter* strains in GenBank that were recovered from human blood, most (221, 63.3%) are also *E. xiangfangensis*; taxon 1 is the second most common species with 69 strains (19.8%) (Table 2). The remaining 59 strains (16.9%) belong to 14 species: *E. asburiae* (n = 14 [4.0%]), *E. kobei* (n = 10 [2.9%]), *E. bugandensis* (n = 7 [2.0%]), *E. roggenkampii* (n = 7 [2.0%]),

**Table 1.** *Enterobacter* strains in genomic study of *Enterobacter* bloodstream infection, China*

| Strain | Date | Species, by isDDH | ST† | Carbapenemase | BSI types | | | | Hospitalization, d | | Death |
|---|---|---|---|---|---|---|---|---|---|---|---|
| | | | | | P | S | CLA | HA | Before BSI | After BSI | |
| 090034 | 201706 | *Enterobacter asburiae* | N12 | | + | | | | 0 | 27 | |
| 090058 | 201805 | *E. asburiae* | 879 | | + | | + | + | 22 | 18 | |
| 090031 | 201711 | *E. bugandensis* | N10 | | + | | | | 1 | 0 | + |
| 090283 | 201610 | *E. bugandensis* | N16 | | | + | | + | 7 | 6 | |
| 090210 | 201607 | *E. bugandensis* | 499 | | | + | | | 1 | 16 | |
| 090029 | 201709 | *E. bugandensis* | 718 | NDM-5 | + | | | + | 71 | 16 | + |
| 090028 | 201708 | *E. chuandaensis* | N9 | | | + | | | 1 | 11 | |
| 090005 | 201706 | *E. cloacae* | 1 | NDM-1 | + | | + | + | 29 | 11 | |
| 090016 | 201703 | *E. cloacae* | 519 | | | + | | + | 17 | 24 | |
| 090014 | 201712 | *E. cloacae* | 922 | | | + | | + | 0 | 10 | |
| 090027 | 201704 | *E. hormaechei* | 528 | | | + | | + | 24 | 38 | |
| 090003 | 201705 | *E. hormaechei* | 696 | | + | | | + | 0 | 15 | |
| 045002 | 201609 | *E. huaxiensis* | N1 | | + | | | | 0 | 7 | |
| 090008 | 201709 | *E. huaxiensis* | N1 | | + | | | + | 3 | 23 | |
| 090017 | 201702 | *E. ludwigii* | 12 | | | + | | + | 6 | 8 | |
| 045158 | 201607 | *E. roggenkampii* | N2 | | + | | | + | 3 | 7 | |
| 090037 | 201608 | *E. roggenkampii* | 984 | | + | | + | + | 14 | 8 | |
| 090032 | 201712 | *E. sichuanensis* | N11 | | + | | + | + | 6 | 16 | + |
| 090004 | 201706 | *E. xiangfangensis* | N3 | | + | | | + | 6 | 13 | |
| 090006 | 201707 | *E. xiangfangensis* | N4 | | + | | | + | 12 | 8 | |
| 090007 | 201707 | *E. xiangfangensis* | N5 | | + | | | + | 24 | 19 | |
| 090012 | 201711 | *E. xiangfangensis* | N6 | | | + | | | 0 | 3 | |
| 090018 | 201705 | *E. xiangfangensis* | N7 | | + | | + | + | 12 | 14 | + |
| 090020 | 201712 | *E. xiangfangensis* | N8 | | + | | + | + | 4 | 60 | |
| 090057 | 201804 | *E. xiangfangensis* | N15 | NDM-1 | + | | + | + | 36 | 43 | |
| 090015 | 201712 | *E. xiangfangensis* | 50 | | + | | | | 0 | 2 | |
| 090026 | 201704 | *E. xiangfangensis* | 50 | | + | | | + | 11 | 52 | |
| 090035 | 201712 | *E. xiangfangensis* | 127 | | + | | | + | 13 | 20 | |
| 045001 | 201801 | *E. xiangfangensis* | 171 | NDM-1 | + | | + | + | 8 | 33 | |
| 090011 | 201710 | *E. xiangfangensis* | 171 | NDM-5 | + | | | + | 7 | 14 | + |
| 090022 | 201802 | *E. xiangfangensis* | 171 | NDM-5 | + | | | + | 40 | 20 | |
| 090023 | 201802 | *E. xiangfangensis* | 171 | NDM-5 | + | | + | + | 26 | 19 | |
| 090055 | 201806 | *E. xiangfangensis* | 171 | NDM-5 | | + | | + | 14 | 14 | |
| 090059 | 201805 | *E. xiangfangensis* | 171 | NDM-5 | + | | + | + | 17 | 31 | |
| 090043 | 201612 | *E. xiangfangensis* | 337 | | | + | | + | 11 | 4 | + |
| 090013 | 201711 | *E. xiangfangensis* | 418 | NDM-5 | + | | + | + | 28 | 10 | + |
| 090038 | 201609 | *E. xiangfangensis* | 418 | | + | | | + | 3 | 33 | |
| 090060 | 201806 | *E. xiangfangensis* | 550 | | + | | + | + | 20 | 8 | + |
| 090042 | 201611 | *E. xiangfangensis* | 828 | | + | | | + | 5 | 3 | |
| 090036 | 201605 | Taxon 1 | N13 | | + | | + | + | 13 | 22 | |
| 090019 | 201706 | Taxon 1 | 78 | | + | | | + | 16 | 62 | |
| 090030 | 201709 | Taxon 1 | 78 | | + | | + | + | 0 | 15 | |
| 090039 | 201610 | Taxon 1 | 78 | | | + | | + | 12 | 8 | + |
| 090021 | 201801 | Taxon 1 | 97 | | + | | + | + | 5 | 28 | |
| 090009 | 201709 | Taxon 1 | 104 | | | + | | + | 5 | 66 | |
| 090033 | 201704 | Taxon 1 | 316 | | + | | | + | 10 | 3 | |
| 090056 | 201803 | Taxon 1 | 568 | | + | | | + | 11 | 7 | |
| 090040 | 201611 | Taxon 2 | N14 | | + | | + | + | 208 | 370 | |

*BSI, bloodstream infection; CLA, central line–associated; HA, healthcare associated; isDDH, in silico DNA–DNA hybridization; P, primary; S, secondary; ST, sequence type.
†There are 16 new sequence types, which are temporarily assigned N1–N16 (Appendix 1 Table 3, https://wwwnc.cdc.gov/EID/article/27/1/19-0154-App1.pdf).

*E. ludwigii* (n = 6 [1.7%]), *E. cloacae* (n = 4 [1.1%]), taxon 1 (n = 2), *E. chengduensis* (n = 1), *E. mori* (n = 1), *E. sichuanensis* (n = 1), and 4 species without assigned species names (n = 1 or 2 for each species, 6 in total; Table 2). The 4 unnamed species were assigned taxon 3–6 (Table 2); the closest species of taxon 3–6 are listed in Appendix 1 Table 2 and are also shown in a phylogenomic tree in Appendix 1 Figure 1. *E. xiangfangensis* and taxon 1 are closely related as shown by their phylogenetic position in the phylogenomic tree of *Enterobacter* spp. and by their common 66.6% isDDH value (close to the 70% cutoff to define a species). We therefore combined the 2 species in the following analysis.

### BSI Types and Characteristics

Most of the 48 BSI cases (n = 36, 75%) were primary BSIs, including 16 cases of CLABSI. BSIs in the remaining 12 cases were secondary; original sources were intraabdominal infection (n = 5), cholangitis (n = 3), urinary tract infection (n = 2), wound infection

(n = 1), and gastrointestinal tract infection (n = 1). Most (n = 41, 85.4%) BSIs caused by *Enterobacter* spp. were healthcare-associated infections. *E. xiangfangensis* and taxon 1 were more likely to cause primary BSI (82.8% vs. 63.2%), CLABSI (27.9% vs. 17.2%), and healthcare-associated BSI (93.1% vs. 73.7%) than were other *Enterobacter* spp. However, the differences were not statistically significant (Table 3).

Two patients who had *Enterobacter* BSIs (1 *E. xiangfangensis* and 1 taxon 1) died in the hospital. In addition, 7 patients with *Enterobacter* BSIs (4 *E. xiangfangensis*, 2 *E. bugandensis,* and 1 *E. sichuanensis*) did not respond to treatment and were discharged in critical condition. These 7 case-patients were categorized as patients in whom death was predicted. The death rate for *Enterobacter* BSI was 18.8% (9/48); the death rate (20.7% [6/29]) of BSI caused by *E. xiangfangensis* or taxon 1 was not statistically different (15.8% [3/19] p>0.05) (Table 3) from that of BSI caused by other *Enterobacter* spp. Of note, 2 of the 4 patients with *E. bugandensis*–caused BSI had poor outcomes (predicted death) (Table 1). BSIs caused by *E. xiangfangensis* or taxon 1 were more common in younger patients and resulted in lengthier overall hospitalizations (median 33 vs. 19.5 d; p>0.05) (Table 3) than BSIs caused by other *Enterobacter* spp. This difference was largely because of the prolonged length of stay (median 11 d vs. 4.5 d; p>0.05) before the episode of BSI.

**Table 2.** Proportion of *Enterobacter* species recovered from blood in genomic study of *Enterobacter* bloodstream infection, China

| Species* | No. (%) Strains from blood in this study | No. (%) Strains from blood in GenBank |
|---|---|---|
| *Enterobacter xiangfangensis* | 21 (43.8) | 221 (63.3) |
| Taxon 1 | 8 (16.7) | 69 (19.8) |
| *E. bugandensis* | 4 (8.3) | 7 (2.0) |
| *E. cloacae* | 3 (6.3) | 4 (1.1) |
| *E. asburiae* | 2 (4.2) | 14 (4.0) |
| *E. roggenkampii* | 2 (4.2) | 7 (2.0) |
| *E. hormaechei* | 2 (4.2) | 0 |
| *E. huaxiensis* | 2 (4.2) | 0 |
| *E. ludwigii* | 1 (2.1) | 6 (1.7) |
| *E. sichuanensis* | 1 (2.1) | 1 (0.3) |
| *E. chuandaensis* | 1 (2.1) | 0 |
| Taxon 2 | 1 (2.1) | 2 (0.6) |
| *E. kobei* | 0 | 10 (2.9) |
| Taxon 3 | 0 | 2 (0.6) |
| Taxon 4 | 0 | 2 (0.6) |
| Taxon 5 | 0 | 1 (0.3) |
| Taxon 6 | 0 | 1 (0.3) |
| *E. chengduensis* | 0 | 1 (0.3) |
| *E. mori* | 0 | 1 (0.3) |
| Total | 48 (100.0) | 349 (100.0) |

*Taxons 1–6 represent 6 *Enterobacter* spp. without assigned names. Their most closely related *Enterobacter* spp. are listed in Appendix 1 Table 2 and shown in Appendix 1 Figure 1 (https://wwwnc.cdc.gov/EID/article/27/1/19-0154-App1.pdf).

### Antimicrobial Susceptibility and Antimicrobial Resistance Genes

The antimicrobial susceptibility and antimicrobial resistance gene repertoire of the 48 *Enterobacter* strains are shown in Appendix 2 Table 1. *E. xiangfangensis* and taxon 1 had substantially higher rates of resistance to aztreonam (48.3% vs. 10.5%), cefepime (41.4% vs. 10.5%), ceftriaxone (58.6% vs. 15.8%), piperacillin/tazobactam (41.4% vs. 10.5%), and tobramycin (44.8% vs. 5.3%) (Table 4) and were substantially more likely to be multidrug resistant (55.2% vs. 10.6%) (Table 3). There were 10 carbapenem-resistant strains (8 *E. xiangfangensis*, 1 *E. bugandensis,* and 1 *E. cloacae*), all of which carried a $bla_{NDM}$ gene ($bla_{NDM-5}$, n = 7; $bla_{NDM-1}$, n = 3) (Table 1; Appendix 2 Table 1), and they belonged to 5 STs (ST171 [n = 6], ST718 [n = 1], ST1 [n = 1], ST418 [n = 1], and a new ST [n = 1]). No carbapenemase genes were identified in carbapenem-susceptible strains.

### Sequence Types and Clonal Relatedness

The 48 *Enterobacter* strains belonged to 37 STs (Table 1; Appendix 1 Table 3) but only ST171 (*E. xiangfangensis*)

**Table 3.** Patient demographics, types of bloodstream infection, and outcomes in patients with bloodstream infection caused by *E. xiangfangensis* plus taxon 1 and other *Enterobacter* species, China*

| Characteristic | *E. xiangfangensis* and taxon 1, n = 29 | Other species, n = 19 | $\chi^2$ | p value | Power† |
|---|---|---|---|---|---|
| Age, y, median (IQR) | 15 (8–32) | 52 (16–71) | – | 0.958 | 0.085 |
| Male sex | 19 (65.5) | 14 (73.7) | 0.356 | 0.551 | 0.084 |
| MDR | **16 (55.2)** | **2 (10.6)** | **9.763** | **0.002** | – |
| Primary BSI | 24 (82.8) | 12 (63.2) | 1.423 | 0.233 | 0.317 |
| CLABSI | 11 (27.9) | 5 (17.2) | 0.697 | 0.404 | 0.115 |
| HA BSI | 27 (93.1) | 14 (73.7) | 2.091 | 0.148 | 0.430 |
| Deaths | 6 (20.7) | 3 (15.8) | 0.176 | 0.675 | 0.053 |
| Total time hospitalized, d, median (IQR)‡ | 33 (19–47) | 20 (2–40) | – | 0.098 | 0.265 |
| Time hospitalized before BSI onset, d, median (IQR)‡ | 11 (5–7) | 5 (1–18) | – | 0.154 | 0.070 |
| Time hospitalized after BSI onset, d, median (IQR) | 15 (8–32) | 13 (8–19) | – | 0.357 | 0.384 |

*Values are no. (%) except as indicated. Bold indicates significance. BSI, bloodstream infection; CLABSI, central line–associated bloodstream infection; HA BSI, healthcare-associated bloodstream infection; IQR, interquartile range; MDR, multidrug resistance; –, not calculated.
†Statistical power was calculated for parameters without statistical significance (p>0.05).
‡One patient belonging to the other species group had an unusually lengthy hospitalization (578 d) because of a medical dispute and was therefore removed from the analysis of hospitalization time.

and ST78 (taxon 1) contained ≥3 strains (6 for ST171 and 3 for ST78). We performed analysis of clonal relatedness based on SNPs for ST78 and ST171 strains. In the 3 ST78 strains, there were 306 to 1,052 SNPs difference, suggesting no recent shared origins (Appendix 1 Table 4). The 6 ST171 strains were all resistant to carbapenems and carried $bla_{NDM-5}$ (n = 5) or $bla_{NDM-1}$ (n = 1). Among the 6 ST171 strains, 4 (all carrying $bla_{NDM-5}$) had 0–2 SNPs difference (Table 5) and were recovered from patients in the same ward (cardiac surgery). One patient infected with strain 090011 died but the remaining 3 patients recovered.

The remaining 2 ST171 strains, 045001 (carrying $bla_{NDM-1}$) and 090055 (carrying $bla_{NDM-5}$), were 81–82 SNPs different from the 4 previously mentioned strains and were 38 SNPs different from each other. These 2 strains were recovered from patients in 2 different wards (medical and respiratory intensive care units). The 6 ST171 strains isolated in our study formed a phylogenetic cluster with strain CCBH10892, which was isolated from a rectal swab sample in Brazil in 2012 (GenBank accession no. JSBO00000000), and strain EC_849, which was isolated from a sputum sample in South Africa in 2012 (GenBank accession no. LRIZ00000000) (Appendix 1 Figure 2). The cluster contained 98 to 107 SNPs difference (Table 5; Appendix 1 Figure 2). Of note, both CCBH10892 and EC_849 carried $bla_{NDM-1}$. By contrast, the 6 strains were >300 SNPs different from other ST171 strains with genome sequences deposited in GenBank (Appendix 2 Table 3).

### Plasmid Analysis of ST171 Strains

The complete genome sequences of $bla_{NDM-5}$–harboring strain 090011 and the $bla_{NDM-1}$–harboring strain 045001 were obtained. Strain 090011 had a 4.64-Mb circular chromosome and 2 plasmids (a 102.5-kb plasmid containing IncFIA, IncFIB, and IncR replicons and a 46.1-kb plasmid containing an IncX3 replicon) (Appendix 1 Table 5). The $bla_{NDM-5}$ gene in strain 090011 was carried on the 46.1-kb IncX3 plasmid, designated pNDM5_090011. The short reads of the remaining 4 $bla_{NDM-5}$–harboring strains were then mapped against pNDM5_0900117. The 4 strains had contigs showing 100% coverage and 100% identity with pNDM5_090011, suggesting a common plasmid in all 5 $bla_{NDM-5}$–harboring ST171 strains in our study. Strain 045001 had a 4.70-Mb circular chromosome and 3 plasmids (an 85.7-kb IncFII plasmid, a 78.2-kb plasmid, and a 2.5-kb plasmid) (Appendix 1 Table 5). The replicon type of the latter 2 plasmids could not be determined by the current replicon-typing scheme. The $bla_{NDM-1}$ gene in strain 045001was carried on the 85.7-kb IncFII plasmid.

## Discussion

Although genome sequences deposited in GenBank might be biased in sampling, they can provide complementary information on the species distribution of *Enterobacter* in cases of BSI. Examination of our set of strains and those available in GenBank demonstrates that a variety of *Enterobacter* spp. can cause BSI, but most BSI-causing *Enterobacter* strains belong to either *E. xiangfangensis* or, less commonly, taxon 1. *E. xiangfangensis* and taxon 1 are closely related, with a 66.6% isDDH value (near the 70% cutoff to define a species). Why the 2 species account for most *Enterobacter* BSIs, however, remains unknown. Although the colonization of the human gastrointestinal tract by *Enterobacter* has not been investigated to the level of precise species identification, *E. xiangfangensis* and taxon 1 could be the most common *Enterobacter* species colonizing there, which warrants further study.

**Table 4.** Antimicrobial resistance rates in *E. xiangfangensis* plus taxon 1 and other *Enterobacter* spp. in genomic study of *Enterobacter* bloodstream infection, China*

| Antimicrobial agent | No. (%) *E. xiangfangensis* + taxon 1, n = 29 | No. (%) Other species, n = 19 | $\chi^2$ | p value | Power† |
|---|---|---|---|---|---|
| Amikacin | 2 (6.9) | 0 | – | 0.512 | ND |
| Gentamicin | 9 (31.0) | 1 (5.3) | 3.192 | 0.074 | 0.600 |
| Tobramycin | **13 (44.8)** | **1 (5.3)** | **8.698** | **0.003** | – |
| Aztreonam | **14 (48.3)** | **2 (10.5)** | **7.361** | **0.007** | **0.829** |
| Cefepime | **12 (41.4)** | **2 (10.5)** | **5.289** | **0.021** | – |
| Ceftriaxone | **17 (58.6)** | **3 (15.8)** | **8.664** | **0.003** | – |
| Imipenem | 8 (27.6) | 2 (10.5) | 1.123 | 0.289 | 0.258 |
| Piperacillin/tazobactam | **12 (41.4)** | **2 (10.5)** | **5.289** | **0.021** | – |
| Ciprofloxacin | **11 (37.9)** | **0** | **7.326** | **0.007** | ND |
| Levofloxacin | **11 (37.9)** | **0** | **7.326** | **0.007** | ND |
| Colistin | 10 (34.5) | 6 (31.6) | 0.044 | 0.835 | 0.052 |
| Tigecycline | 5 (17.2) | 0 | 2.043 | 0.153 | ND |
| Trimethoprim/sulfamethoxazole | **12 (41.4)** | **0** | **8.392** | **0.004** | ND |

*Bold indicates significance. ND, not determined; –, not calculated.
†Statistical power was calculated for parameters without statistical significance (p>0.05) but could not be calculated for any parameters being 0.

**Table 5.** Single-nucleotide polymorphisms between the 6 ST171 strains in genomic study of *Enterobacter* bloodstream infection, China, and strain EC_849 from South Africa and strain CCBH10892 from Brazil*

| Strain | 090011 | 090022 | 090023 | 090059 | 045001 | 090055 | EC_849 | CCBH10892 |
|---|---|---|---|---|---|---|---|---|
| 090011 | – | 1 | 0 | 1 | 81 | 81 | 106 | 102 |
| 090022 | 1 | – | 1 | 2 | 82 | 82 | 107 | 103 |
| 090023 | 0 | 1 | – | 1 | 81 | 81 | 106 | 102 |
| 090059 | 1 | 2 | 1 | – | 82 | 82 | 107 | 103 |
| 045001 | 81 | 82 | 81 | 82 | – | 38 | 103 | 99 |
| 090055 | 81 | 82 | 81 | 82 | 38 | – | 103 | 99 |
| EC_849 | 106 | 107 | 106 | 107 | 103 | 103 | – | 98 |
| CCBH10892 | 102 | 103 | 102 | 103 | 99 | 99 | 98 | – |

*–, not calculated.

Alternatively, *E. xiangfangensis* and taxon 1 could be more pathogenic than other *Enterobacter* spp., which also requires further study.

BSIs caused by *E. xiangfangensis* and taxon 1 were more likely to occur in younger patients and result in longer overall hospital stays, although the differences in length of hospitalization between the 2 groups were not statistically significant ($p>0.05$). This finding might be because of the relatively small sample size (power <0.8) (Table 3). Resistance rates to certain antimicrobial agents, including aztreonam, cefepime, ceftriaxone, piperacillin/tazobactam, and tobramycin and prevalence of multidrug resistance in *E. xiangfangensis* and taxon 1 were substantially higher than in other *Enterobacter* spp. This difference suggests that the identification of *Enterobacter* strains to precise species level also has implications in options of antimicrobial treatment. Although BSI caused by *E. xiangfangensis* and taxon 1 was not associated with higher death rates, 2 of the 4 patients with *E. bugandensis* had poor outcomes (predicted death). *E. bugandensis* has been reported to be a highly pathogenic species associated with life-threatening BSIs and sepsis (*19*). The virulence of this species warrants further study.

As previously noted, 4 $bla_{NDM-5}$–harboring ST171 strains had 0–2 SNPs difference (Table 5) and were taken from patients in the same ward (cardiac surgery). The first patient with BSI caused by a strain belonging to the clone (090011) had *Enterobacter* BSI before being transferred to West China Hospital from another facility. Although the particular *Enterobacter* strain from the first hospital was not available for analysis, it is very likely that 090011 was introduced to West China Hospital by transfer of this patient. The next 3 cases were acquired in West China Hospital, highlighting both interhospital and intrahospital transmission of a common strain. BSI in 2 of the 3 cases was CLABSI. These findings suggest that the 4 strains belong to a common clone that caused a cluster of BSI cases. In the hospital ward, central lines were commonly used for drawing blood but were not properly decontaminated after each use; in addition, healthcare workers were observed by anonymous interns to have low compliance (24.8%) with hand hygiene standards established by the World Health Organization. There have been no further *Enterobacter* BSIs after restricting access to central lines and promoting hand hygiene among healthcare workers, which resulted in the compliance rate increasing to 45.5%.

The remaining 2 ST171 strains, 045001 (harboring $bla_{NDM-1}$) and 090055 (harboring $bla_{NDM-5}$), belong to 2 clones (38 SNPs between each other) which differed from the aforementioned clone by 81–82 SNPs. The relatively low number of SNPs among the 3 ST171 clones also suggests recent divergence within the lineage. In addition, the 6 ST171 strains in this study were clustered together with 2 $bla_{NDM-1}$–harboring strains, strain CCBH10892 isolated from Brazil in 2012, and strain EC_849 from South Africa in 2012, with 98 to 107 SNPs, but had >300 SNPs with other ST171 strains that had genome sequences deposited in GenBank. This finding suggests that the 6 strains identified in this study, CCBH10892, and EC_849 represent a subclade of ST171, which carries $bla_{NDM}$, has an international distribution, and might have emerged within the past 10 years. In addition, although 090055 and the other 4 $bla_{NDM-5}$–harboring strains (090011, 090022, 090023, and 090059) belonged to 2 different clones, they had the same IncX3 plasmid carrying $bla_{NDM-5}$, which suggests that the spread of $bla_{NDM-5}$ in the hospital was both clonal (vertical) and plasmidborne (horizontal).

The association of ST171 *E. xiangfangensis* with outbreaks is not rare; repeated reports from different geographic locations have demonstrated the same association (*20*–*24*). This association suggests that ST171 is a lineage of *Enterobacter*, which might be well adapted to causing infections in healthcare settings. Previous reports have demonstrated that ST171 *E. xiangfangensis* is a high-risk clone mediating the spread of carbapenem resistance (*21*,*23*). Its emergence was initially documented in 2015 and 2016 by 2 studies in the United States (*24*,*25*). Subsequent

studies have revealed the international distribution of ST171 (*21*–*23*). Almost all carbapenem-resistant ST171 *E. xiangfangensis* strains have $bla_{KPC}$ (*21*), and only a small number of strains carry $bla_{NDM}$ instead (*21*,*26*). In this study, we identified in-hospital transmission of carbapenem-resistant ST171 strains, which carried $bla_{NDM-5}$ rather than $bla_{KPC}$ as seen in previous studies (*21*,*23*). The ability to acquire different carbapenemase genes and its adaptability to healthcare settings might be major drivers in the emergence of ST171, which warrants further study.

Our investigation demonstrates the value of whole-genome sequencing for precise species identification. However, this study has several limitations. First, because it is a single site study, the application of our findings could be limited. However, we analyzed genomes available in GenBank to provide the most comprehensive information possible. Second, the relatively small sample size in this study might not have adequate power to examine statistical significance in BSI type and patient outcomes. However, this study provided useful information on the clinical importance of *E. xiangfangensis* and its closely related taxon 1. Larger-scale studies are warranted.

In conclusion, most *Enterobacter* strains recovered from human blood in China were not *E. cloacae* but *E. xiangfangensis*. Most *Enterobacter* BSI cases in our study were healthcare-associated and primary infections. *E. xiangfangensis* ST171 is a major lineage of carbapenem-resistant *Enterobacter*, has an intercontinental distribution, is usually healthcare associated, and carries $bla_{NDM}$ rather than $bla_{KPC}$ in China. Precise species identification of *Enterobacter* has clinical importance in antimicrobial therapy and infection control.

**Addendum:** Since submission and acceptance of this manuscript, the taxonomy of *Enterobacter* has been substantially updated. The updated *Enterobacter* taxonomy is available at https://doi.org/10.1128/mSystems.00527-20. The update of new taxa identified in this study is shown in Appendix 3 Table (https://wwwnc.cdc.gov/EID/article/27/1/19-0154-App3.pdf).

### Acknowledgments

We are grateful for Alan McNally for his proofreading and helpful suggestions.

The work was supported by grants from the National Natural Science Foundation of China (project no. 81772233, 81661130159 and 81861138055), West China Hospital of Sichuan University (1.3.5 project for disciplines of excellence, project no. ZYYC08006) and the Newton Advanced Fellowship, Royal Society, UK (NA150363).

### About the Author

Dr. Wu is a scientist in the Department of Laboratory Medicine, West China Second Hospital, Sichuan University. Her major research interests are the epidemiology and clonal background of carbapenemase-producing *Enterobacter* spp.

### References

1. Mezzatesta ML, Gona F, Stefani S. *Enterobacter cloacae* complex: clinical impact and emerging antibiotic resistance. Future Microbiol. 2012;7:887–902. https://doi.org/10.2217/fmb.12.61
2. Tindall BJ, Sutton G, Garrity GM. *Enterobacter aerogenes* Hormaeche and Edwards 1960 (approved lists 1980) and *Klebsiella mobilis* Bascomb et al. 1971 (approved lists 1980) share the same nomenclatural type (ATCC 13048) on the approved lists and are homotypic synonyms, with consequences for the name *Klebsiella mobilis* Bascomb et al. 1971 (approved lists 1980). Int J Syst Evol Microbiol. 2017;67:502–4. https://doi.org/10.1099/ijsem.0.001572
3. Gavini R, Mergaert J, Beji A, Mielcarek C, Izard D, Kersters K, et al. Transfer of *Enterobacter agglomerans* (Beijerinck 1888) Ewing and Fife 1972 to *Pantoea* gen. nov. as *Pantoea agglomerans* comb. nov. and description of *Pantoea dispersa* sp. nov. Int J Syst Evol Microbiol. 1989;39:337–45.
4. Iversen C, Mullane N, McCardell B, Tall BD, Lehner A, Fanning S, et al. *Cronobacter* gen. nov., a new genus to accommodate the biogroups of *Enterobacter sakazakii*, and proposal of *Cronobacter sakazakii* gen. nov., comb. nov., *Cronobacter malonaticus* sp. nov., *Cronobacter turicensis* sp. nov., *Cronobacter muytjensii* sp. nov., *Cronobacter dublinensis* sp. nov., Cronobacter genomospecies 1, and of three subspecies, Cronobacter dublinensis subsp. *dublinensis* subsp. nov., *Cronobacter dublinensis* subsp. *lausannensis* subsp. nov. and *Cronobacter dublinensis* subsp. *lactaridi* subsp. nov. Int J Syst Evol Microbiol. 2008;58:1442–7. https://doi.org/10.1099/ijs.0.65577-0
5. Hoffmann H, Roggenkamp A. Population genetics of the nomenspecies *Enterobacter cloacae*. Appl Environ Microbiol. 2003;69:5306–18. https://doi.org/10.1128/AEM.69.9.5306-5318.2003
6. Hoffmann H, Stindl S, Stumpf A, Mehlen A, Monget D, Heesemann J, et al. Description of *Enterobacter ludwigii* sp. nov., a novel *Enterobacter* species of clinical relevance. Syst Appl Microbiol. 2005;28:206–12. https://doi.org/10.1016/j.syapm.2004.12.009
7. Wu W, Feng Y, Zong Z. *Enterobacter sichuanensis* sp. nov., recovered from human urine. Int J Syst Evol Microbiol. 2018;68:3922–7. https://doi.org/10.1099/ijsem.0.003089
8. Balloux F, Brønstad Brynildsrud O, van Dorp L, Shaw LP, Chen H, Harris KA, et al. From theory to practice: translating whole-genome sequencing (WGS) into the clinic. Trends Microbiol. 2018;26:1035–48. https://doi.org/10.1016/j.tim.2018.08.004
9. Besser J, Carleton HA, Gerner-Smidt P, Lindsey RL, Trees E. Next-generation sequencing technologies and their application to the study and control of bacterial infections. Clin Microbiol Infect. 2018;24:335–41. https://doi.org/10.1016/j.cmi.2017.10.013
10. Rosselló-Móra R, Amann R. Past and future species definitions for *Bacteria* and *Archaea*. Syst Appl Microbiol. 2015;38:209–16. https://doi.org/10.1016/j.syapm.2015.02.001

11. Clinical and Laboratory Standards Institute. Performance standards for antimicrobial susceptibility testing; twenty-seventh informational supplement. M100–S27. Wayne (PA): The Institute; 2017.
12. Magiorakos AP, Srinivasan A, Carey RB, Carmeli Y, Falagas ME, Giske CG, et al. Multidrug-resistant, extensively drug-resistant and pandrug-resistant bacteria: an international expert proposal for interim standard definitions for acquired resistance. Clin Microbiol Infect. 2012;18:268–81. https://doi.org/10.1111/j.1469-0691.2011.03570.x
13. Centers for Disease Control and Prevention. National Healthcare Safety Network FAQs: bloodstream infection (BSI) events. 2018 [cited 2018 Nov 1]. https://www.cdc.gov/nhsn/faqs/faq-bsi.html
14. Centers for Disease Control and Prevention. Identifying healthcare-associated infections (HAI) for NHSN surveillance. 2018 [cited 2018 Nov 1]. https://www.cdc.gov/nhsn/pdfs/pscmanual/2psc_identifyinghais_nhsncurrent.pdf
15. Wick RR, Judd LM, Gorrie CL, Holt KE. Unicycler: resolving bacterial genome assemblies from short and long sequencing reads. PLOS Comput Biol. 2017;13:e1005595. https://doi.org/10.1371/journal.pcbi.1005595
16. Meier-Kolthoff JP, Auch AF, Klenk HP, Göker M. Genome sequence-based species delimitation with confidence intervals and improved distance functions. BMC Bioinformatics. 2013;14:60. https://doi.org/10.1186/1471-2105-14-60
17. Stamatakis A. RAxML version 8: a tool for phylogenetic analysis and post-analysis of large phylogenies. Bioinformatics. 2014;30:1312–3. https://doi.org/10.1093/bioinformatics/btu033
18. Walker BJ, Abeel T, Shea T, Priest M, Abouelliel A, Sakthikumar S, et al. Pilon: an integrated tool for comprehensive microbial variant detection and genome assembly improvement. PLoS One. 2014;9:e112963. https://doi.org/10.1371/journal.pone.0112963
19. Pati NB, Doijad SP, Schultze T, Mannala GK, Yao Y, Jaiswal S, et al. *Enterobacter bugandensis*: a novel enterobacterial species associated with severe clinical infection. Sci Rep. 2018;8:5392. https://doi.org/10.1038/s41598-018-23069-z
20. Hawken SE, Washer LL, Williams CL, Newton DW, Snitkin ES. Genomic investigation of a putative endoscope-associated carbapenem-resistant *Enterobacter cloacae* outbreak reveals a wide diversity of circulating strains and resistance mutations. Clin Infect Dis. 2018;66:460–3. https://doi.org/10.1093/cid/cix934
21. Chavda KD, Chen L, Fouts DE, Sutton G, Brinkac L, Jenkins SG, et al. Comprehensive genome analysis of carbapenemase-producing *Enterobacter* spp.: new insights into phylogeny, population structure, and resistance mechanisms. MBio. 2016;7:02093–16. https://doi.org/10.1128/mBio.02093-16
22. Harada K, Shimizu T, Mukai Y, Kuwajima K, Sato T, Kajino A, et al. Phenotypic and molecular characterization of antimicrobial resistance in *Enterobacter* spp. isolates from companion animals in Japan. PLoS One. 2017;12:e0174178. https://doi.org/10.1371/journal.pone.0174178
23. Gomez-Simmonds A, Annavajhala MK, Wang Z, Macesic N, Hu Y, Giddins MJ, et al. Genomic and geographic context for the evolution of high-risk carbapenem-resistant *Enterobacter cloacae* complex clones ST171 and ST78. MBio. 2018;9:00542–18. https://doi.org/10.1128/mBio.00542-18
24. Hargreaves ML, Shaw KM, Dobbins G, Snippes Vagnone PM, Harper JE, Boxrud D, et al. Clonal dissemination of *Enterobacter cloacae* harboring $bla_{KPC-3}$ in the upper midwestern United States. Antimicrob Agents Chemother. 2015;59:7723–34. https://doi.org/10.1128/AAC.01291-15
25. Gomez-Simmonds A, Hu Y, Sullivan SB, Wang Z, Whittier S, Uhlemann AC. Evidence from a New York City hospital of rising incidence of genetically diverse carbapenem-resistant *Enterobacter cloacae* and dominance of ST171, 2007–14. J Antimicrob Chemother. 2016;71:2351–3. https://doi.org/10.1093/jac/dkw132
26. Peirano G, Matsumura Y, Adams MD, Bradford P, Motyl M, Chen L, et al. Genomic epidemiology of global carbapenemase-producing *Enterobacter* spp., 2008–2014. Emerg Infect Dis. 2018;24:1010–9. https://doi.org/10.3201/eid2406.171648


Address for correspondence: Zhiyong Zong, Center of Infectious Diseases, West China Hospital (Huaxi), Guoxuexiang 37, Chengdu 610041, China; email: zongzhiy@scu.edu.cn

# Delineating and Analyzing Locality-Level Determinants of Cholera, Haiti

Karolina Griffiths, Kenny Moise, Martine Piarroux, Jean Gaudart, Samuel Beaulieu, Greg Bulit, Jean-Petit Marseille, Paul Menahel Jasmin, Paul Christian Namphy, Jean-Hugues Henrys, Renaud Piarroux, Stanislas Rebaudet

Centre Department, Haiti, was the origin of a major cholera epidemic during 2010–2019. Although no fine-scale spatial delineation is officially available, we aimed to analyze determinants of cholera at the local level and identify priority localities in need of interventions. After estimating the likely boundaries of 1,730 localities by using Voronoi polygons, we mapped 5,322 suspected cholera cases reported during January 2015–September 2016 by locality alongside environmental and socioeconomic variables. A hierarchical clustering on principal components highlighted 2 classes with high cholera risk: localities close to rivers and unimproved water sources (standardized incidence ratio 1.71, 95% CI 1.02–2.87; p = 0.04) and urban localities with markets (standardized incidence ratio 1.69, 95% CI 1.25–2.29; p = 0.0006). Our analyses helped identify and characterize areas where efforts should be focused to reduce vulnerability to cholera and other waterborne diseases; these methods could be used in other contexts.

Haiti experienced a large and lasting cholera epidemic that began in October 2010. The epidemic originated in Centre Department in a hamlet hosting a camp of United Nations peacekeepers, then contaminated the Artibonite River and coastal plain (*1*,*2*). During 2010–2019, >820,000 suspected cholera cases and 9,792 deaths were reported (*3*). However, since February 2019 no suspected deaths have occurred, and no positive test results have been reported from >1,000 samples collected from patients with acute watery diarrhea.

Fecal contamination of water, food, or hands by toxigenic strains of the bacterium *Vibrio cholerae* O1 is the common mode of cholera transmission. The National Plan for the Elimination of Cholera, launched by the Ministry of Public Health and Population (Ministère de la Santé Publique et de la Population [MSPP]) in Haiti and co-authored by Haiti's National Drinking Water and Sanitation Directorate (La Direction Nationale de l'Eau Potable et de l'Assainissement [DINEPA]), is now in its third phase, focusing on reinforcing access to clean drinking water and sanitation (*4*,*5*). Reducing population vulnerability to cholera and other waterborne diseases at a community level is vital. However, with the constraints of limited resources, the most pertinent at-risk geographic zones must be prioritized for sustainable water sanitation and hygiene (WaSH) interventions.

Previous studies have performed spatial analyses at communal levels, but data at a finer scale are limited. High-resolution mapping is needed to understand the heterogeneous transmission patterns and to adapt specific intervention strategies at the community level (*6*–*9*). Although a previous study by Allan et al. (*6*) provided maps of the origin of cholera patients at a subcommunal level for the neighboring Artibonite Department, these maps are still at a relatively large scale, demonstrating communal sections hosting 10,000–30,000 persons. That study reported neighboring sections within the same commune with clear differences in relative risk for cholera in a mosaic pattern, highlighting the need for further locality-level investigation to guide WaSH

Author affiliations: Aix Marseille University, Marseille, France (K. Griffiths, J. Gaudart, S. Rebaudet); Université Quisqueya, Port-au-Prince, Haiti (K. Moise, J.-H. Henrys); Centre d'épidémiologie et de santé Publique des armées, Marseille (M. Piarroux); UNICEF, Kinshasa, Democratic Republic of the Congo (S. Beaulieu); UNICEF, New York, New York, USA (G. Built); Direction Nationale de l'Eau Potable et de l'Assainissement, Hinche, Haiti (J.-P. Marseille); Ministère de la Santé Publique et de la Population, Hinche (P.M. Jasmin); Direction Nationale de l'Eau Potable et de l'Assainissement, Petion-Ville, Haiti (P.C. Namphy); Sorbonne Université, Paris, France (R. Piarroux)

DOI: https://doi.org/10.3201/eid2701.191787

interventions. However, the mapping of rural localities in Haiti is sparse and no spatial delineation has been established, presenting a challenge in identifying microspots with recurrent cases and analyzing associated factors (*6*). A previous study collected fine-scale spatial data in Haiti by using spatial videos for cholera investigations; however, it was limited to intraurban areas and did not include case data (*10*).

Previous studies highlight the challenges in collecting fine-scale spatial data in Haiti, with limited official information on informal settlements (*10*–*12*). Our objective was to analyze the spatial determinants of cholera and to identify the priority localities in need of prevention interventions in the Centre Department in Haiti. We chose Centre Department because it was at the origin of the epidemic and had a high incidence of cholera that persisted for several years.

## Methods

### Study Design and Setting

We conducted an observational, ecologic study at the locality (hamlet) level in the Centre Department, Haiti (Figure 1), which covers an area of 3,487 km$^2$, is >80% rural, and in 2015 had a population of ≈746,236 (*13*). Centre is administratively subdivided into 12 civil townships, known as communes, each of which has an urban area (Figure 2, panel A). Each commune is further subdivided into communal sections, the smallest official administrative unit, which include several hundred localities. Localities are groups of residences and are the smallest spatial unit culturally used to define the place of residence for rural populations. However, the number, spelling, and delimitations of rural localities are not officially established, and only estimated geolocalization and populations are available (*14*).

The largest towns in Centre are Hinche and Mirebalais. Centre has a mean altitude of 447 m (range 84–1,820 m) and is situated northeast of the Montagnes Noires and Montagnes de Trou d'Eau mountain ranges and south of the Massif du Nord. Hundreds of rivers and streams provide natural water sources in the department.

### Materials

We obtained the deidentified case list of suspected cholera cases in Centre during January 2015–September 2016 from the MSPP. The case list provided the

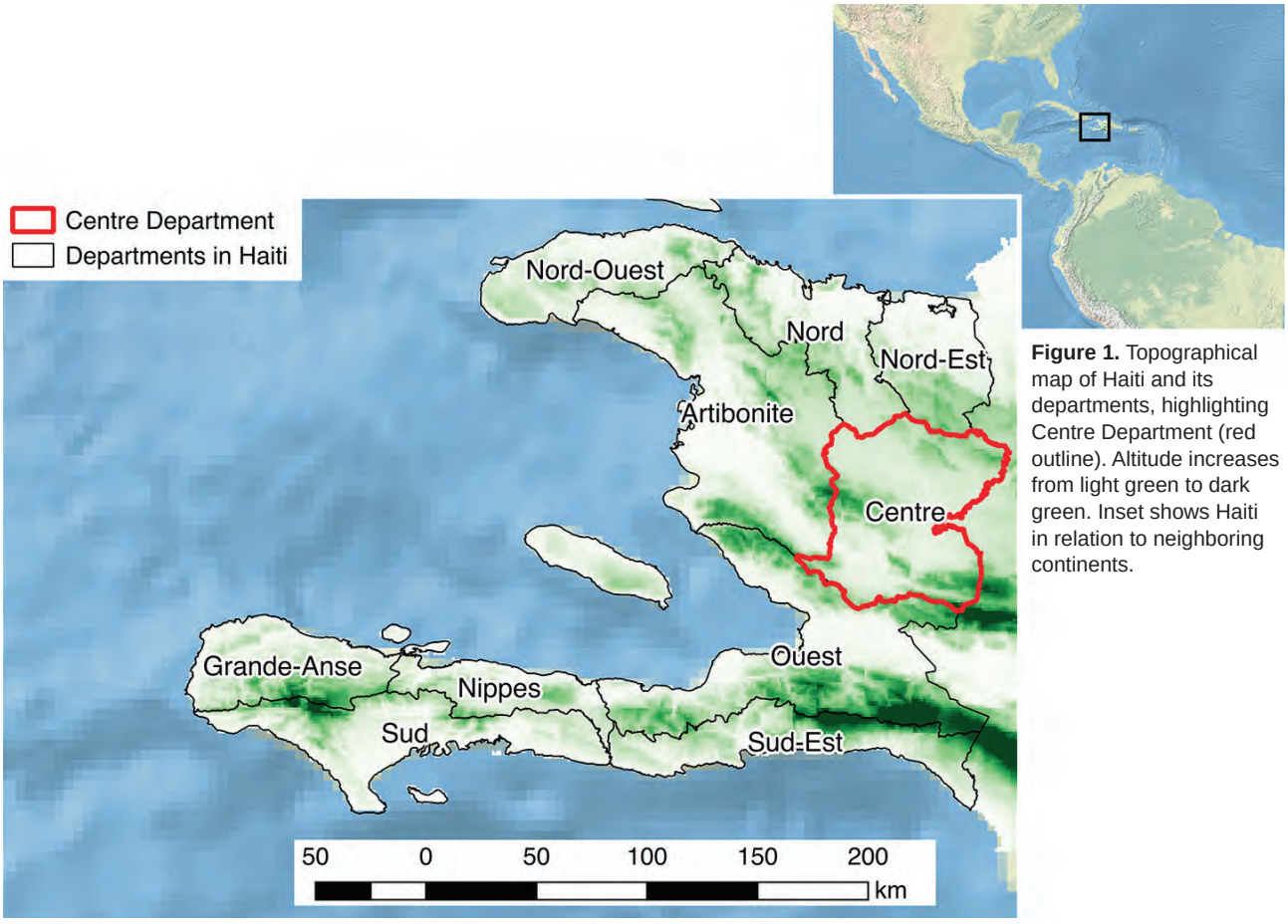


**Figure 1.** Topographical map of Haiti and its departments, highlighting Centre Department (red outline). Altitude increases from light green to dark green. Inset shows Haiti in relation to neighboring continents.

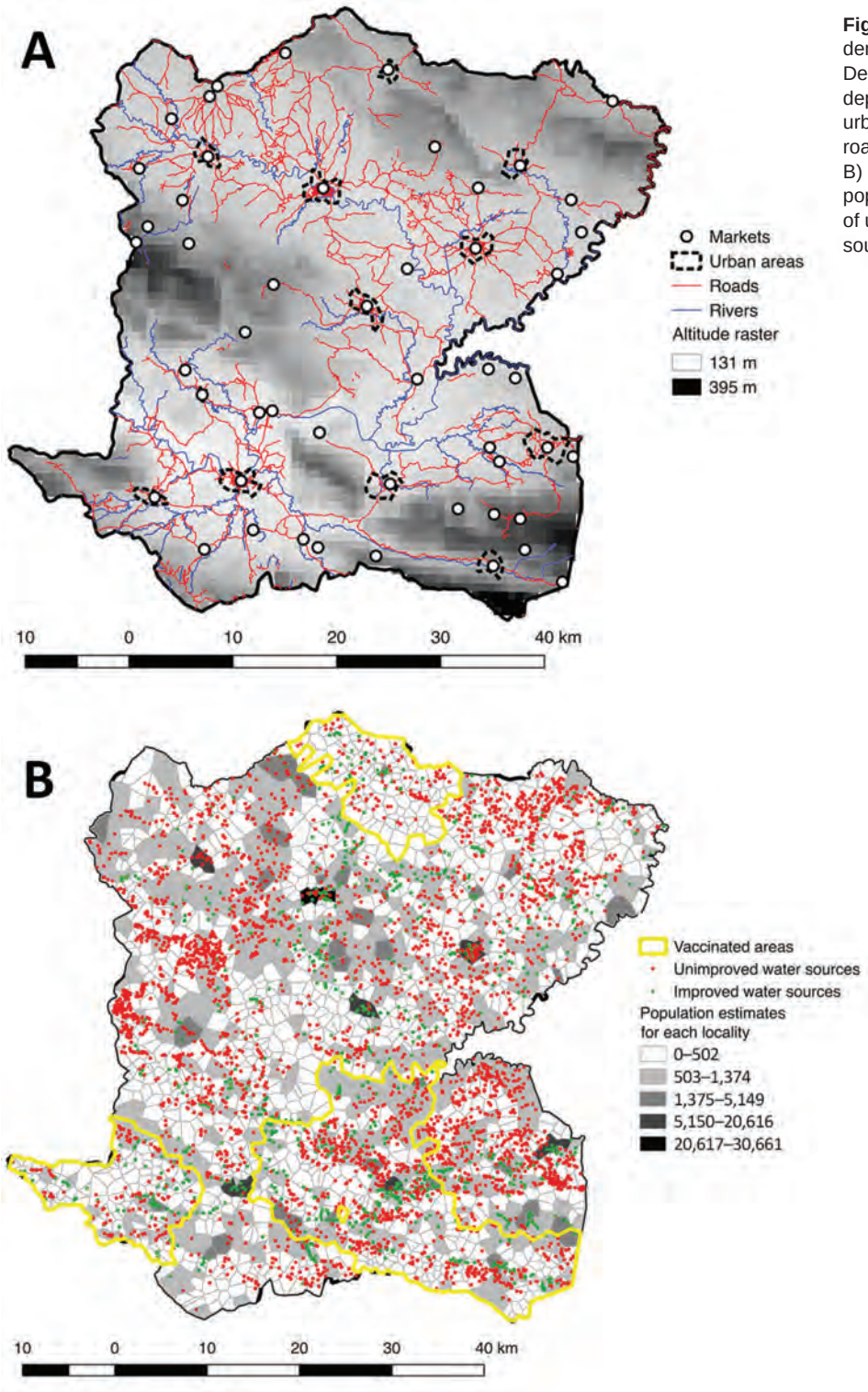


**Figure 2.** Geographic and demographic details of Centre Department, Haiti. A) Outline of the department's 12 communes, principal urban areas, altitude raster, rivers, roads, and position of markets. B) Polygon outline and estimated population for each locality, positions of unimproved and improved water sources, and vaccinated areas.

locality of residence for each patient and was collected by the Health Departmental Directorate of the MSPP to guide case-area targeted interventions conducted by rapid response teams (*15*). All patient identifiers were removed previously.

The mapping of rural localities in Haiti is incomplete (*6*). We collected point global positioning system (GPS) coordinates for each locality from field visits by mobile response teams, authors' field visits, or satellite photos and from geographic repositories,

including Haitian Institute of Statistics and Computer Science (http://ihsi.ht/publication_cd_atlas.htm), Index Mundi (https://www.indexmundi.com), OpenStreetMap (https://www.openstreetmap.org), Google Earth (https://earth.google.com), and Google Maps (https://www.google.fr/maps). We verified GPS coordinates against official data from Centre National d'Information Geospatiale (CNIGS), when available. Further data validation was performed by using computerized participatory mapping techniques to integrate spatial information from local community stakeholders in each commune, either individually or in small groups. These stakeholders included local healthcare professionals from mobile response teams, WaSH technicians, and local government personnel. We checked and unified locality names and used satellite imagery–assisted visual mapping techniques to validate the estimated GPS coordinates. This process ensured coherence with local knowledge of the terrain and identified inconsistencies, which was vital for rural areas without road access.

As part of a collaborative project financed by World Vision (https://www.worldvision.org), DINEPA and the nongovernmental partner organization Haiti Outreach (https://www.haitioutreach.org) collected an inventory of water sources and provided GPS coordinates by visiting each water point and validating data with local partners (*16*) (Figure 2, panel B). Water sources were classified as improved or unimproved according to the Joint Monitoring Program for Water Supply Sanitation and Hygiene (*17*,*18*).

We obtained the location of rivers, roads, and altitude for Centre from CNIGS (Figure 2, panel A). We obtained history of previous oral cholera vaccination campaigns by communal section from MSPP (Figure 2, panel B). We geolocated markets during field investigations in Centre.

We calculated Voronoi polygons from estimated point coordinates for each locality. These polygons, or proximity diagrams, consist of all locations closer to the locality point coordinate than any other point coordinate, providing estimated boundaries. We used Voronoi polygons as the basis for all variables to maintain spatial unit consistency and to reduce aggregation bias. We estimated the number of houses per polygon by using a satellite-based house detection shapefile from CNIGS and completed maps by using Google Earth and OpenStreetMap. We multiplied the number of houses by the mean number of household members in the area to estimate the population and incidence rates in each locality (*13*). The distances from each house to an unimproved water source, improved water source, river, and road were calculated and averaged for each polygon. The mean altitude was calculated for each polygon by using raster terrain analysis and rounded to the nearest meter.

### Statistical Analysis

We assessed variables for normal distribution by using histograms, quantile-quantile plots, and Shapiro-Wilk test. For continuous nonnormally distributed variables, we calculated the median and interquartile range (IQR); for categorical variables, we calculated counts and percentages. We categorized continuous variables, including altitude and distances to a road, to an improved water source, to an unimproved water source, and to a river, by using information from quartiles and histograms to form 4 classes. We performed univariate nonparametric statistical tests by using Kruskal-Wallis rank test and Spearman correlation coefficients on cholera incidence and environmental variables. We performed spatial analysis for hotspot detection by using SatScan (https://www.satscan.org).

We performed multistep nonsupervised analysis to classify the localities according to their environmental and spatial characteristics. Hierarchical clustering on the principal components of a multiple correspondence analysis (MCA) was detailed previously (*19*,*20*); we used these data to classify neighborhoods in towns in Haiti (*12*). The first step is an MCA, which is an exploratory method that considers the relationship between variables and reduces complex datasets into fewer dimensions (*21*). We performed MCA by using the original categorical variables and the categorized continuous variables. Active variables included the presence of a market, urban or rural location, vaccination status, and area averaged: altitude, distance to a road, distance to an improved water source, distance to an unimproved water source, and distance to a river. We retained quantitative information only as supplementary variables and did not use these in the determination of the principal components. To reduce basal noise and ensure a more stable classification, we retained the principal components that summarized 95% of the data. We performed hierarchical ascendant classification on the first 16 principal components' coordinates, which provided classes independent of the number of cholera cases. Then, we compared these classes to cholera cases in a general additive model (GAM) with quasi-Poisson distribution. For spatial autocorrelation, we performed Moran I tests on the number of cases and the GAM residuals. To model spatial dependence, we tested a trend-surface GAM, fitting the geographic location by

using 2 dimensional splines on latitude and longitude coordinates, as previously demonstrated (*22*–*24*). We accounted for the increasing population by using an offset of the log population and estimating standardized incidence ratios (SIRs) for each class. We considered p<0.05 statistically significant.

We used QGIS version 2.14.3 (QGIS Development Team, http://qgis.osgeo.org) as a geographic information system (GIS) for mapping. We performed all statistical analyses by using R version 3.3.0 (R Foundation for Statistical Computing, https://www.r-project.org). We used the FactoMineR package in R for classification analysis (*19*) and mgcv for GAMs, with generalized cross validation criteria for smoothing parameter estimations and the gam.check function to verify residual plots (*22*,*25*).

All data remained anonymous with no patient identifiers, in accordance with national and international ethics guidance (*26*). Ethics approval was obtained from the National Bioethics Committee in Haiti, MSPP (reference no. 1516-73).

## Results

A total of 5,322 suspected cholera cases were recorded in Centre during January 2015–September 2016, and 1,730 localities were identified and mapped. The median locality size was 1.77 km$^2$ (IQR 1.15–2.58 km$^2$) and median population 300 (IQR 153–530) persons. Among 1,730 localities, 689 (40%) had ≥1 suspected cholera case (Table 1). The median incidence ratio for all localities was 0 (IQR 0–61.9) per 10,000 persons. Incidence ranged from 0–6,050.9/10,000 persons; 25 localities had an incidence >1,000/10,000 persons (Figure 3). In univariate analysis, the categorical variables statistically significant for incidence were altitude, distance to an unimproved water source, distance to an improved water source, distance to road, distance to a river, presence of market, rural or urban location (p<0.0001), and cholera vaccination (p<0.0001 for all variables) (Table 1; Appendix, https://wwwnc.cdc.gov/EID/article/27/1/19-1787-App1.pdf).

### Hierarchical Clustering on Principal Components

Hierarchical clustering on MCA provided 4 different classes of localities (Table 2; Appendix Figure 1), demonstrating different environmental and spatial characteristics, which we mapped (Figures 4, 5). The categorical variables that best characterize the portioning into 4 classes were distance to a river, presence of a market, altitude, distance to an unimproved water source, urban or rural location, and distance to a road (p<0.0001 for all).

Class 1 (n = 621) was most strongly associated with being far from a river, at high altitude, and far from a road (Table 2). Class 1 localities also were remote and farther than average from both unimproved water sources (median 576 m) and improved water sources (median 1,213 m), had no markets, were rural, and had more vaccinated persons.

Class 2 (n = 941) was associated with being a medium distance to the river and at the lowest altitudes (Table 2). Class 2 localities also were associated with being a medium distance from a road, having no markets, being rural, and having more unvaccinated persons. These rural intermediary localities were slightly closer than the average distance to both improved water sources (median 712 m) and unimproved water sources (median 439 m) and lower than average distances to a road (median 390 m).

Class 3 (n = 61) was most notably associated with being closer to rivers (<200 m) and unimproved water sources (<150 m). Class 3 localities also had lower than average distances to a road (median 210 m).

Class 4 (n = 77) was most strongly associated with markets and urban localities. These localities were closer than average to unimproved water sources (median 347 m) and improved (median 338 m) sources and a lower than average distance to a road (median 135 m).

**Table 1.** Summary descriptive statistics for each locality and variables used for classification analysis used in delineating and analyzing locality-level determinants of cholera, Haiti

| Locality information | All localities, n = 1,730 | Association with incidence, p value |
|---|---|---|
| Median no. suspected cholera cases (IQR) | 0 (0–2) | – |
| Median no. houses (IQR) | 65 (33–115) | – |
| Median estimated population (IQR) | 300 (152–530) | – |
| Median estimated incidence/10,000 (IQR) | 0 (0–61.85) | – |
| Median altitude, m (IQR)*† | 360 (264–620) | <0.0001 |
| Median distance to nearest improved water source, m (IQR)*† | 842 (464–1,476) | <0.0001 |
| Median distance to nearest unimproved water source, m (IQR) *† | 451 (307–702) | <0.0001 |
| Median distance to nearest river, m (IQR)*† | 1,263 (554–2,706) | <0.0001 |
| Median distance to nearest road, m (IQR) | 638 (185–1,493) | <0.0001 |
| No. markets (%)* | 50 (2.9) | <0.0001 |
| No. rural locations (%)* | 1,686 (97.5) | <0.0001 |
| No. cholera vaccinations administered (%)* | 556 (32.1) | <0.0001 |

*Active variables used in classification analysis, statistically significant in nonparametric univariate analysis (p<0.05).
†Values transformed to categorical variables by using quartiles to form 4 classifications for analysis.

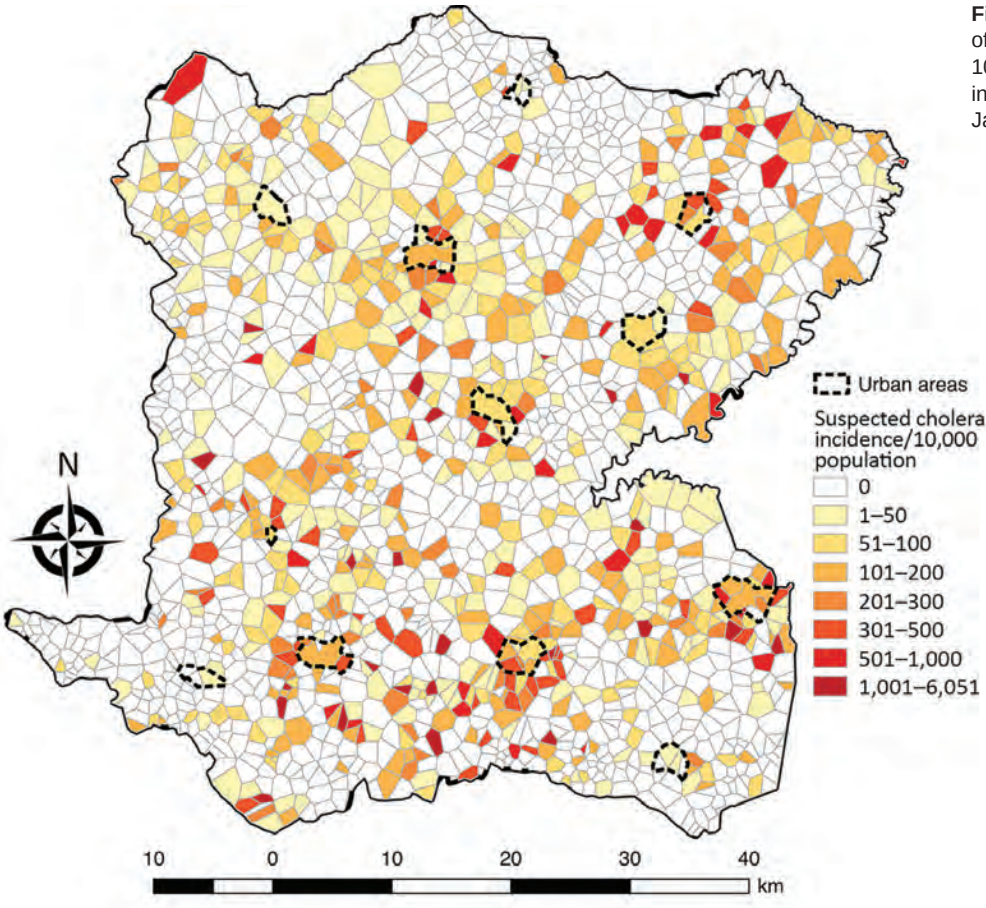


**Figure 3.** Estimated incidence of suspected cholera cases per 10,000 persons for each locality in Centre Department, Haiti, January 2015–September 2016.

Taking class 1 as the reference and taking geographic coordinates and population into consideration, we used a quasi-Poisson GAM to compare the classes and estimate SIRs (Table 2; Appendix). The model confirmed the statistically significantly higher cholera incidence in class 3 (SIR 1.71, 95% CI 1.02–2.87; p = 0.0425) and class 4 (SIR 1.69, 95% CI 1.25–2.29; p = 0.0006). We found class 2 had a slightly increased risk for cholera compared with class 1, with an SIR of 1.28 (95% CI 0.96–1.71), although this difference was not statistically significant at the 5% level (p = 0.0896) (Figure 6).

**Table 2.** Characteristics for each classification identified for analysis of locality-level determinants of cholera, Haiti*

| Information for each locality | Class 1, n = 651 | Class 2, n = 941 | Class 3, n = 61 | Class 4, n = 77 |
|---|---|---|---|---|
| Median no. suspected cholera cases (IQR) | 0 (0–1) | 0 (0–3) | 0 (0–3) | 6 (1–17) |
| Median no. houses (IQR) | 46 (23–86) | 79 (42–127) | 52 (26–79) | 146 (75–315) |
| Median estimated population (IQR) | 212 (106–396) | 364 (194–585) | 240 (120–364) | 673 (346–1,452) |
| Median estimated incidence, cases/10,000 population (IQR) | 0 (0–15.80) | 0 (0–72.31) | 0 (0–111) | 83.0 (8.6–197.2) |
| Median altitude, m (IQR)*† | 665 (520–816) | 287 (232–352) | 284 (227–414) | 339 (265–461) |
| Median distance to nearest improved water source, m (IQR)*† | 1,213 (665–1,819) | 712 (429–1,203) | 721 (263–1,357) | 338 (233–585) |
| Median distance to nearest unimproved water source, m (IQR)*† | 576 (331–1,080) | 439 (317–593) | 163 (136–183) | 347 (274–533) |
| Median distance to nearest river, m (IQR)†‡ | 2,932 (2,047–4,434) | 805 (447–1,346) | 177 (156–193) | 578 (353–1,407) |
| Median distance to nearest road, m (IQR)†‡ | 1,544 (882–2,462) | 390 (133–816) | 210 (70–594) | 135 (29–279) |
| No. (%) markets† | 0 | 0 | 2 (3) | 48 (62) |
| No. (%) rural locations† | 651 (100) | 941 (100) | 57 (93) | 40 (52) |
| Standardized incidence ratio (95% CI), p value | Referent | 1.28 (0.96–1.71), 0.0896 | 1.71 (1.02–2.87), <0.05 | 1.69 (1.25–2.29), <0.01 |

*Class 1 was the reference class, situated at high altitude, and furthest from river and sources. Class 2 was not much more at risk, characterized by a medium distance to roads. Classes 3 and 4 were much more at-risk. Class 3 localities were closer to a river or an unimproved water source and class 4 localities were more often urban with a market.
†Active variables used in classification analysis.
‡Transformed to categorical variables for analysis.

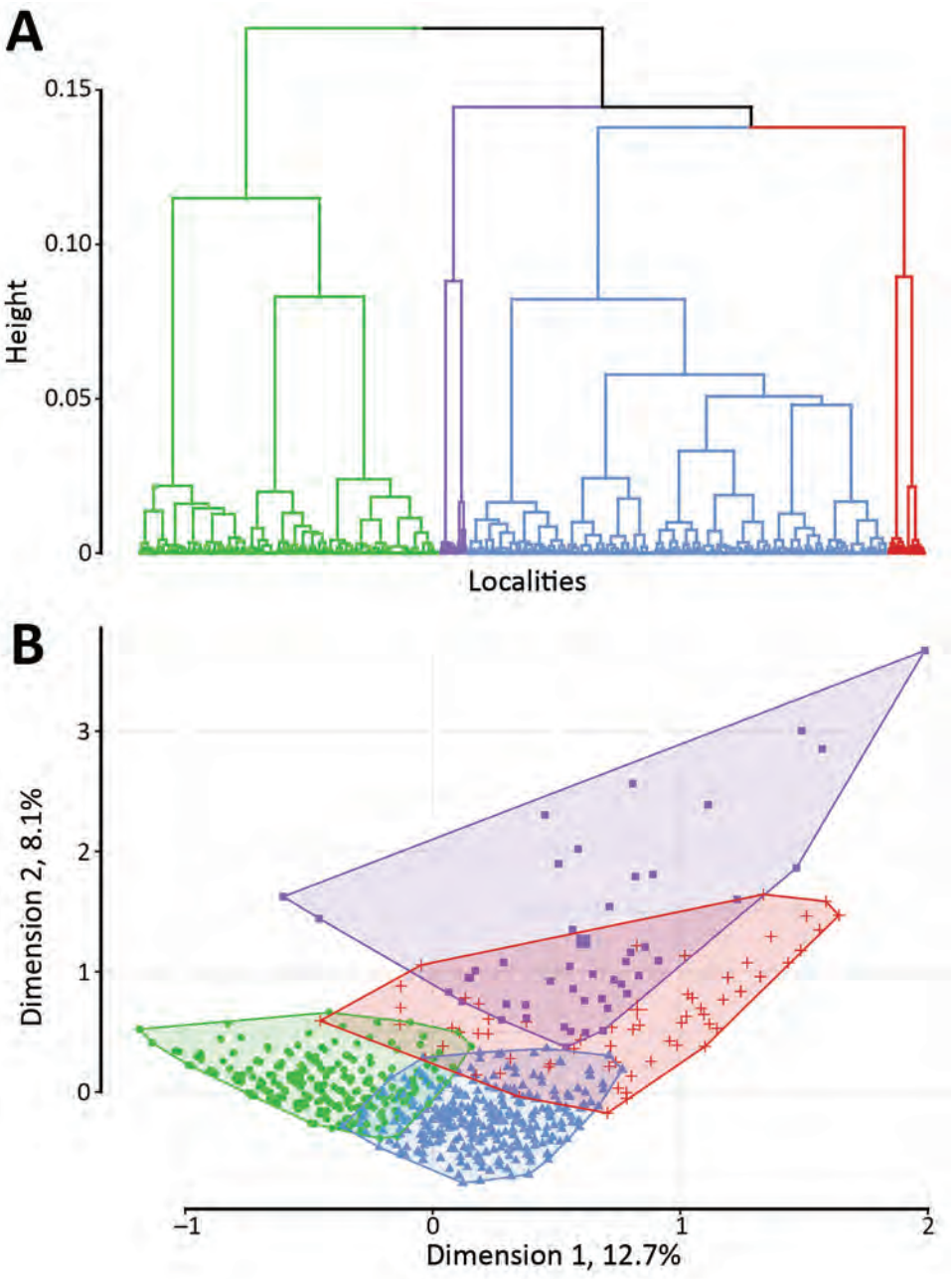


**Figure 4.** Classification analysis of localities regarding environmental variables based on hierarchical clustering on principal components of multiple correspondence analysis, Centre Department, Haiti. A) Cluster dendrogram demonstrating the division of localities into 4 classes: green, class 1; blue, class 2; purple, class 3; red, class 4. Height indicates the order at which the clusters were joined. B) Factor map demonstrating the 4 classes on the first 2 dimensions of the multiple correspondence analysis with the following variables: altitude, distance to an unimproved water source, distance to an improved water source, distance to road, distance to a river, presence of market, rural or urban, and cholera vaccination. The x and y axes represent the first 2 dimensions of the multiple correspondence analysis; the percentage of the total dataset inertia is represented by each dimension. Each point is a locality, with the shaded areas representing the 4 classes, as in panel A.

## Discussion

Our analysis identified 2 main classes of localities at higher risk for cholera: localities close to both rivers (<200 m) and unimproved water sources (<150 m) and urban localities with markets. These criteria are simple ways of identifying high-risk localities for source-based interventions within a large department like Centre. We identified total of 138 higher risk localities, accounting for 8% of all localities.

Reducing population vulnerability to diarrheal illnesses in a low-resource setting has complex challenges, which was confounded in Centre by the large geographic area and difficult terrain. Prioritizing strategies on an easily identifiable number of sources and localities might have implications for preventing cholera outbreaks in Haiti and elsewhere. Whereas previous research emphasized the importance of commune-level data focused on WaSH interventions (*27*), we highlight the importance of fine-scale mapping and using the spatial unit most logical at an operational level. Mapping of localities in Centre Department previously was unavailable, rendering the analysis of case lists impossible. Mapping performed in this study opens doors for further analysis related to

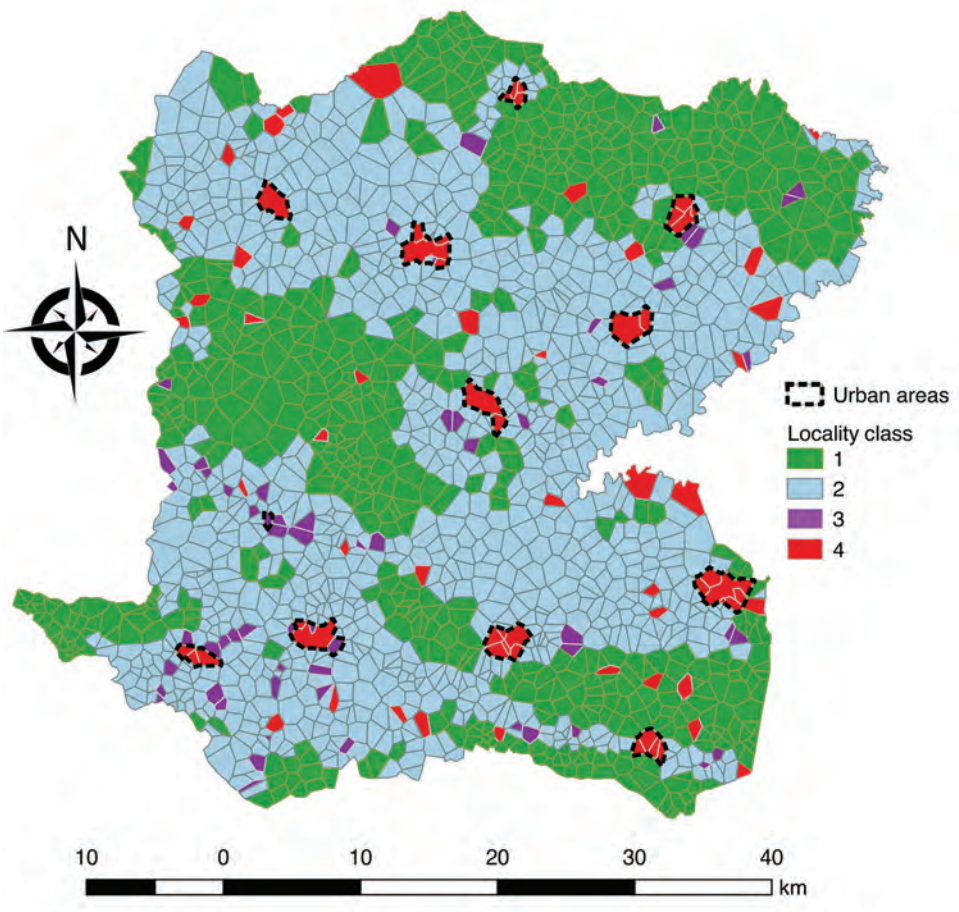


**Figure 5.** Localities of Centre Department, Haiti, mapped according to hierarchical clustering on principal components classification analysis. Classification analysis determined 2 large lower-risk classes: class 1 localities were remote and higher altitude, and class 2 localities were rural intermediary areas. Two high-risk classes were identified: class 3 localities are closer to rivers and unimproved water sources, and class 4 localities have markets and are in urban areas.

cholera and to other health conditions. Furthermore, cholera can be considered as a proxy for vulnerability to waterborne diseases, and targeting these high-risk localities can prevent other disease outbreaks.

Cholera case distribution seems to be linked to geographic patterns, specifically related to environmental hygiene and water source contamination (*28*). Previous studies have demonstrated a substantial association between cholera and populations living in proximity to water bodies (*29*–*32*), lakes (*28*,*33*,*34*), and rivers and to river density (*32*). Increasing elevation has been inversely linked to cholera distribution (*35*). However, due to geographic heterogeneity, the relationship between environmental factors does not fully explain cholera distribution in Haiti. Understanding environmental causation between water sources and cholera is confounded by the difficulties of sampling rivers and water sources and challenges in determining whether these sources are perennial reservoirs or temporary sources of pathogens (*36*,*37*). Other studies have highlighted the change in local populations' preferences and behaviors to type of water access (*38*,*39*). Furthermore, alongside the proximity to environmental factors, the role of population movement and social factors in the spatial determination of cholera must be considered (*28*,*40*).

Consistent with our results, previous cholera outbreak investigations have reported hotspots in proximity to busy markets (*9*,*12*) and main roads (*32*,*41*), presuming the role of population mobility in creating cholera transmission hubs through the fecal–oral route (*9*,*29*). These social and environmental characteristics must be considered when examining the spatial determinants of cholera in a region. This reinforces the notion that context matters. Our results demonstrate 2 different high-risk classes and highlight the heterogeneous factors across localities, even within the same communal section. We cannot point to a single clear high-risk variable but instead noted patterns of risk depending on the socioenvironmental context of each locality. Our study adds to the literature by using this adaptive contextualized approach at a fine scale across a department, not just limited to smaller urban areas, as seen previously (*9*,*12*).

Numerous reasons can explain an increased cholera risk in localities with markets (*9*). The regular large

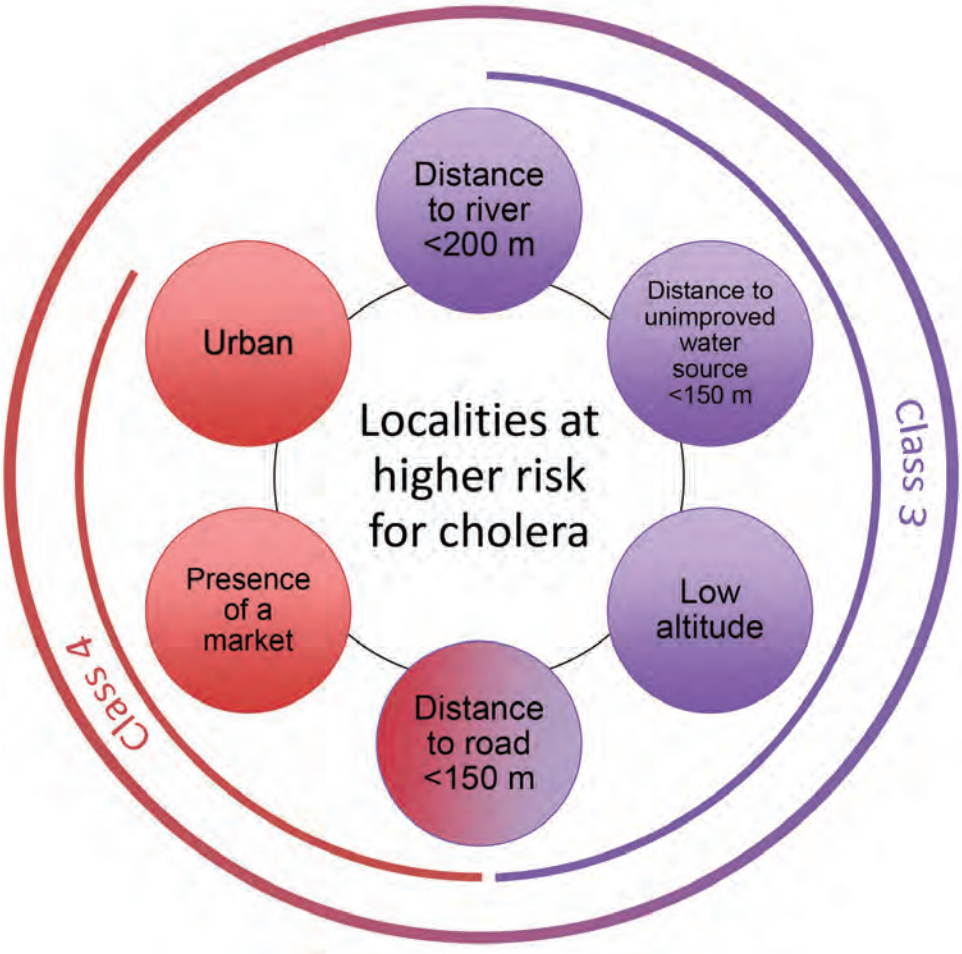


**Figure 6.** Comparison of the most strongly associated risk factors for cholera between 2 high-risk classes, Centre Department, Haiti. The most strongly associated risk factors for suspected cholera cases were distance <200 m to a river, distance <150 m to an unimproved water source, low altitude, distance to a road <150 m, presence of a market, and urban areas. Class 3 and class 4, both at higher risk for cholera, were close to a road but differed for the other identified risk factors.

flux of persons increases the risk for contact with cholera cases. In addition, the poor sanitary conditions of marketplaces increase risk because of inadequate waste disposal, lack of handwashing points, no or poor drainage systems, and the poor hygienic standards of food stalls and latrines, if available. Open defecation areas have been highlighted near Mirebalais market as a source of cholera (*42*). However, the association to markets might be confounded by the geographic proximity of treatment centers, which both often are located in urban areas where a concentration of ill patients aids cholera transmission via contamination of food and water.

Our results highlight the importance of distance to a road in both high-risk classes. Road distance <150 m was statistically significantly associated with class 3 ($p<0.0006$) and class 4 ($p<0.0001$). This finding can be interpreted in 2 ways. First, it confirms that cholera is propagated by population movement along main roads. However, main transport hubs also link localities and treatment centers; therefore, cases from localities with easier road access also are more likely to be notified. We used average estimated distances from a locality to a road as an accessible proxy for population mobility, but other information could be used, such as travel time to the nearest town (*43*). Information on actual population mobility by using mobile phone data could be a promising tool to examine spatial spread and improve outbreak preparedness strategies (*40*).

Of note, the association with distance to an improved water source was not a decisive factor in the classification. Increasing distance from an improved water source was associated more with the low-risk class 1, but unimproved water sources were also at a greater median distance. Furthermore, proximity to an improved water source was associated with the high-risk class 4. This finding suggests that the presence of improved water sources in a locality might not fully prevent diarrheal illnesses unless all other potential sources are considered for WaSH improvements. An improved water supply should be available within a 30-minute round trip, according to post-2015 Sustainable Development Goals

(*18*), but this availability cannot improve cholera incidence if an unimproved water source is still used for reasons of accessibility and affordability. Our study at the locality level did not consider individualized or household methods of drinking water collection or treatment because no piped water networks are available outside towns and those in towns do not function all the time. Instead, we studied the distance from a house to a water source, including rivers, averaged for the whole locality. However, this variable on geographic accessibility could be confounded by subsequent contamination during travel or storage.

Our study demonstrates the feasibility of fine-scale geographic analysis over a large, mainly rural area to study incidence and spatial epidemiology of cholera in relation to socioenvironmental characteristics and water sources. We used a grassroots approach incorporating expertise from local health and sanitation experts to define a list of localities and comprehensive documentation of water sources. Our approach has potential benefits for future studies by researchers in public health and other disciplines.

As can be common in resource-limited settings with multiple users, the case list required a lengthy data cleaning process. Limitations of the case list include possible missing data from patients who did not go to healthcare centers. However, we believe the case list provided the most comprehensive information available and impressive detail considering the setting constraints.

As demonstrated in previous studies, our field study corroborates that risk for cholera is associated with intertwined socioeconomic and environmental factors and highlights marketplaces located near water bodies and roads in high-density neighborhoods, such as Mirebalais (*29*), as risk factors. By analyzing a wide range of variables, without preceding presumptions on their relationship or correlation, we were able to conduct an exploratory analysis by using MCA. This analysis enabled inclusion of numerous variables despite collinearity and classification of the reduced dimensions in a multivariate model to outline the spatial determinants of cholera.

One limitation of our study was the lack of information regarding excrement management, a recognized predisposing risk factor (*29*,*44*). We attempted to retrieve this information by identifying the location of municipal latrines, but heterogeneous excrement disposal activities make this process futile because open defecation is a common practice (*45*). A recent survey of 13,405 households in Haiti reports only 31% of households have improved, nonshared toilets; in urban areas, 43% have such amenities, but half as many (23%) are found in rural areas (*45*). Another limitation is that trend-surface GAM does not fully address spatial autocorrelation by smoothing the spatial coordinates; however, it does account for trends in geographic data. Nonetheless, trend-surface GAM is a recognized method to model the spatial dependence in the systematic part of the model (*22*–*24*). Furthermore, we were unable to incorporate temporal analyses due to the relatively short timeframe (only 1 dry season). Therefore, we cannot account for all factors associated with cholera incidence, particularly the movement of cholera between localities. In addition, the geographic analysis could not incorporate meteorological information, which is unavailable at the locality level. However, our aim was not to model cholera incidence and dynamics of transmission, which previously has been studied (*46*–*50*). Instead of identifying individual patterns of risk, we used classification analysis to reduce the dimensions of numerous correlated variables to define local-scale risk profiles within a large area affected by cholera. Our study provides information to guide strategies to reduce vulnerability to diarrheal illnesses within a realistic setting, taking the social and environmental context into account.

With no confirmed cholera cases in Haiti since February 2019, the focus in this postepidemic period must be on reducing the vulnerability of the population of Haiti to cholera and other diarrheal illnesses. Our results highlight different typologies of risk at the locality level across a department, defining high risk by access to unimproved water sources and presence of markets in urban localities. Focusing hygiene awareness and prevention strategies in localities with known high-risk factors can help concentrate limited resources and improve efficiency in the fight against future cholera and other waterborne disease epidemics in Haiti and elsewhere.

#### Acknowledgments

We thank the staff from the department heath directorate, the technicians of La Direction Nationale de l'Eau Potable et de l'Assainissement, and the nongovernmental organizations Haiti Outreach, OXFAM-GB, and UNICEF for providing data and their invaluable support with field study organization.

### About the Author

Dr. Griffiths is an academic general practitioner at the Aix-Marseille University, France. Her research interests include medical statistics and epidemiology.

## References


1. Piarroux R, Barrais R, Faucher B, Haus R, Piarroux M, Gaudart J, et al. Understanding the cholera epidemic, Haiti. Emerg Infect Dis. 2011;17:1161–8. https://doi.org/10.3201/eid1707.110059
2. Gaudart J, Rebaudet S, Barrais R, Boncy J, Faucher B, Piarroux M, et al. Spatio-temporal dynamics of cholera during the first year of the epidemic in Haiti. PLoS Negl Trop Dis. 2013;7:e2145. https://doi.org/10.1371/journal.pntd.0002145
3. Ministère Santé Publique et de la Population (MSPP). Department of Epidemiology, Laboratories and Research (DELR). Report of the National Cholera Surveillance Network, 40th epidemiological week 2019 [in French] [cited 2019 Dec 1]. http://mspp.gouv.ht/site/downloads/Profil%20statistique%20Cholera%2040SE%202019.pdf
4. Republic of Haiti, Ministry of Public Health and Population, National Directorate for Water Supply and Sanitation. National plan for the elimination of cholera in Haiti 2013–2022 [in French] [cited 2019 Dec 1]. http://www.paho.org/hq/index.php?option=com_docman&task=doc_view&gid=20326&Itemid=270&lang=en
5. Republic of Haiti, Ministry of Public Health and Population, National Directorate for Water Supply and Sanitation. National plan for the elimination of cholera: development of the long term plan 2018–2022 [in French] [cited 2019 Dec 1]. http://mspp.gouv.ht/site/downloads/Plan%20a%20long%20terme%202018%202022%20pour%20l%20elimination%20du%20Cholera%20en%20Haiti.pdf
6. Allan M, Grandesso F, Pierre R, Magloire R, Coldiron M, Martinez-Pino I, et al. High-resolution spatial analysis of cholera patients reported in Artibonite Department, Haiti in 2010–2011. Epidemics. 2016;14:1–10. https://doi.org/10.1016/j.epidem.2015.08.001
7. Blackburn JK, Diamond U, Kracalik IT, Widmer J, Brown W, Morrissey BD, et al. Household-level spatiotemporal patterns of incidence of cholera, Haiti, 2011. Emerg Infect Dis. 2014;20:1516–9. https://doi.org/10.3201/eid2009.131882
8. Mukandavire Z, Smith DL, Morris JG Jr. Cholera in Haiti: reproductive numbers and vaccination coverage estimates. Sci Rep. 2013;3:997. https://doi.org/10.1038/srep00997
9. Luquero FJ, Banga CN, Remartínez D, Palma PP, Baron E, Grais RF. Cholera epidemic in Guinea-Bissau (2008): the importance of "place". PLoS One. 2011;6:e19005. https://doi.org/10.1371/journal.pone.0019005
10. Curtis A, Blackburn JK, Smiley SL, Yen M, Camilli A, Alam MT, et al. Mapping to support fine scale epidemiological cholera investigations: a case study of spatial video in Haiti. Int J Environ Res Public Health. 2016;13:187. https://doi.org/10.3390/ijerph13020187
11. Curtis A, Blackburn JK, Widmer JM, Morris JG Jr. A ubiquitous method for street scale spatial data collection and analysis in challenging urban environments: mapping health risks using spatial video in Haiti. Int J Health Geogr. 2013;12:21. https://doi.org/10.1186/1476-072X-12-21
12. Rebaudet S, Griffiths K, Trazillio M, Lebeau A-G, Abedi AA, Bulit G, et al. Cholera spatial-temporal patterns in Gonaives, Haiti: From contributing factors to targeted recommendations Adv Water Resour. 2017;108:377–85. https://doi.org/10.1016/j.advwatres.2016.12.012
13. Haitian Ministry of Economy and Finance and Haitian Institute of Statistics and Information. Total population, aged 18 and over, households and densities estimated in 2015 [in French] [cited 2019 Dec 1]. http://www.ihsi.ht/pdf/projection/Estimat_PopTotal_18ans_Menag2015.pdf
14. Milbin D. Geographical names of zones in Haiti. Ninth United Nations Conference on the standardization of geographical names [in French] [cited 2019 Dec 1]. https://unstats.un.org/unsd/geoinfo/UNGEGN/docs/9th-uncsgn-docs/crp/9th_UNCSGN_e-conf-98-crp-36.pdf
15. Rebaudet S, Bulit G, Gaudart J, Michel E, Gazin P, Evers C, et al. The case-area targeted rapid response strategy to control cholera in Haiti: a four-year implementation study. PLoS Negl Trop Dis. 2019;13:e0007263. https://doi.org/10.1371/journal.pntd.0007263
16. Haiti Outreach. FRAPE water infrastructure monitoring system [cited 2019 Dec 1]. https://frape.mwater.co/#/?locale=en
17. World Health, Organization (WHO) and the United Nations Children's Fund (UNICEF). Progress on Drinking Water, Sanitation and Hygiene: 2017 Update and SDG Baselines [cited 2019 Dec 1]. https://www.unicef.org/publications/files/Progress_on_Drinking_Water_Sanitation_and_Hygiene_2017.pdf
18. Water Supply and Sanitation Collaborative Council. WASH post-2015: proposed targets and indicators for drinking-water, sanitation and hygiene [cited 2019 Dec 1]. https://www.unicef.org/wash/files/2_WSSCC_JMP_Fact_Sheets_2_UK_LoRes.pdf
19. Lê S, Josse J, Husson F. FactoMineR: an R package for multivariate analysis. J Stat Softw. 2008;25:1–18. https://doi.org/10.18637/jss.v025.i01
20. Husson F, Josse J, Pagès J. Principal component methods—hierarchical clustering—partitional clustering: why would we need to choose for visualizing data? Technical Report—Agrocampus: Applied Mathematics Department, September 2010 [cited 2019 Dec 1]. http://factominer.free.fr/more/HCPC_husson_josse.pdf
21. Greenacre M. Correspondence analysis in medical research. Stat Methods Med Res. 1992;1:97–117. https://doi.org/10.1177/096228029200100106
22. Wood SN. Generalized additive models: an introduction with R. Boca Raton (FL): Chapman & Hall/CRC; 2006.
23. Hastie T, Tibshirani R. Generalized additive models. Boca Raton (FL): Chapman & Hall/CRC; 1999.
24. Cressie NAC. Statistics for spatial data. New York: John Wiley & Sons; 1993.
25. Wood S. mgcv: mixed GAM computation vehicle with automatic smoothness estimation 2019 [cited 2019 Dec 1]. https://CRAN.R-project.org/package=mgcv
26. World Health Organization. Ethical standards and procedures for research with human beings [cited 2016 Feb 15]. http://www.who.int/ethics/research
27. Barzilay EJ, Schaad N, Magloire R, Mung KS, Boncy J, Dahourou GA, et al. Cholera surveillance during the Haiti epidemic—the first 2 years. N Engl J Med. 2013;368:599–609. https://doi.org/10.1056/NEJMoa1204927
28. Rebaudet S, Sudre B, Faucher B, Piarroux R. Environmental determinants of cholera outbreaks in inland Africa: a systematic review of main transmission foci and propagation routes. J Infect Dis. 2013;208(Suppl 1):S46–54. https://doi.org/10.1093/infdis/jit195
29. Olanrewaju OE, Adepoju KA. Geospatial assessment of cholera in a rapidly urbanizing environment. J Environ Public Health. 2017;2017:6847376. https://doi.org/10.1155/2017/6847376
30. Mengel MA, Delrieu I, Heyerdahl L, Gessner BD. Cholera outbreaks in Africa. Curr Top Microbiol Immunol. 2014;379:117–44. https://doi.org/10.1007/82_2014_369
31. Birmingham ME, Lee LA, Ndayimirije N, Nkurikiye S, Hersh BS, Wells JG, et al. Epidemic cholera in Burundi:

patterns of transmission in the Great Rift Valley Lake region. Lancet. 1997;349:981–5. https://doi.org/10.1016/S0140-6736(96)08478-4
32. Bompangue Nkoko D, Giraudoux P, Plisnier P-D, Tinda AM, Piarroux M, Sudre B, et al. Dynamics of cholera outbreaks in Great Lakes region of Africa, 1978–2008. Emerg Infect Dis. 2011;17:2026–34.
33. Bompangue D, Giraudoux P, Piarroux M, Mutombo G, Shamavu R, Sudre B, et al. Cholera epidemics, war and disasters around Goma and Lake Kivu: an eight-year survey. PLoS Negl Trop Dis. 2009;3:e436. https://doi.org/10.1371/journal.pntd.0000436
34. Bompangue D, Giraudoux P, Handschumacher P, Piarroux M, Sudre B, Ekwanzala M, et al. Lakes as source of cholera outbreaks, Democratic Republic of Congo. Emerg Infect Dis. 2008;14:798–800. https://doi.org/10.3201/eid1405.071260
35. Luque Fernandez MA, Schomaker M, Mason PR, Fesselet JF, Baudot Y, Boulle A, et al. Elevation and cholera: an epidemiological spatial analysis of the cholera epidemic in Harare, Zimbabwe, 2008–2009. BMC Public Health. 2012;12:442. https://doi.org/10.1186/1471-2458-12-442
36. Alam MT, Weppelmann TA, Weber CD, Johnson JA, Rashid MH, Birch CS, et al. Monitoring water sources for environmental reservoirs of toxigenic *Vibrio cholerae* O1, Haiti. Emerg Infect Dis. 2014;20:356–63. https://doi.org/10.3201/eid2003.131293
37. Rebaudet S, Piarroux R. Monitoring water sources for environmental reservoirs of toxigenic *Vibrio cholerae* O1, Haiti. Emerg Infect Dis. 2015;21:169–70. https://doi.org/10.3201/eid2101.140627
38. MacRae D, Whittington D. Assessing preferences in cost-benefit analysis: reflections on rural water supply evaluation in Haiti. J Policy Anal Manage. 1988;7:246. https://doi.org/10.2307/3323827
39. Patrick M, Steenland M, Dismer A, Pierre-Louis J, Murphy JL, Kahler A, et al. Assessment of drinking water sold from private sector kiosks in post-earthquake Port-au-Prince, Haiti. Am J Trop Med Hyg. 2017;97(Suppl):84–91. https://doi.org/10.4269/ajtmh.16-0692
40. Bengtsson L, Gaudart J, Lu X, Moore S, Wetter E, Sallah K, et al. Using mobile phone data to predict the spatial spread of cholera. Sci Rep. 2015;5:8923. https://doi.org/10.1038/srep08923
41. Troeger C, Gaudart J, Truillet R, Sallah K, Chao DL, Piarroux R. Cholera outbreak in Grande Comore: 1998–1999. Am J Trop Med Hyg. 2016;94:76–81. https://doi.org/10.4269/ajtmh.15-0397
42. Maire de Mirebalais, Regional Office for Potable Water and Sanitation, ESA Consultance. Analysis of factors of persistence of cholera and the elaboration of an intervention plan for the town of Mirebalais [in French] [cited 2019 Dec 1]. https://en.calameo.com/read/005285856479e515bd3ba
43. Weiss DJ, Nelson A, Gibson HS, Temperley W, Peedell S, Lieber A, et al. A global map of travel time to cities to assess inequalities in accessibility in 2015. Nature. 2018;553:333–6.
44. Esrey SA, Potash JB, Roberts L, Shiff C. Effects of improved water supply and sanitation on ascariasis, diarrhoea, dracunculiasis, hookworm infection, schistosomiasis, and trachoma. Bull World Health Organ. 1991;69:609–21.
45. Haitian Institute for Children. ICF International. Mortality, morbidity and use of services survey 2016–2017 [in French] [cited 2019 Dec 1]. https://www.dhsprogram.com/pubs/pdf/FR326/FR326.pdf
46. DuBois AE, Sinkala M, Kalluri P, Makasa-Chikoya M, Quick RE. Epidemic cholera in urban Zambia: hand soap and dried fish as protective factors. Epidemiol Infect. 2006;134:1226–30. https://doi.org/10.1017/S0950268806006273
47. Dunkle SE, Mba-Jonas A, Loharikar A, Fouché B, Peck M, Ayers T, et al. Epidemic cholera in a crowded urban environment, Port-au-Prince, Haiti. Emerg Infect Dis. 2011;17:2143–6. https://doi.org/10.3201/eid1711.110772
48. Kanungo S, Sur D, Ali M, You YA, Pal D, Manna B, et al. Clinical, epidemiological, and spatial characteristics of *Vibrio parahaemolyticus* diarrhea and cholera in the urban slums of Kolkata, India. BMC Public Health. 2012;12:830. https://doi.org/10.1186/1471-2458-12-830
49. Morof D, Cookson ST, Laver S, Chirundu D, Desai S, Mathenge P, et al. Community mortality from cholera: urban and rural districts in Zimbabwe. Am J Trop Med Hyg. 2013;88:645–50. https://doi.org/10.4269/ajtmh.11-0696
50. Grandesso F, Allan M, Jean-Simon PSJ, Boncy J, Blake A, Pierre R, et al. Risk factors for cholera transmission in Haiti during inter-peak periods: insights to improve current control strategies from two case-control studies. Epidemiol Infect. 2014;142:1625–35. https://doi.org/10.1017/S0950268813002562

Address for correspondence: Karolina Griffiths, Montpellier University, 2 rue école de Médecine, 34000 Montpellier, France; email: karolina.griffiths@umontpellier.fr

# Attribution of Illnesses Transmitted by Food and Water to Comprehensive Transmission Pathways Using Structured Expert Judgment, United States

Elizabeth Beshearse, Beau B. Bruce, Gabriela F. Nane, Roger M. Cooke, Willy Aspinall, Tine Hald, Stacy M. Crim, Patricia M. Griffin, Kathleen E. Fullerton, Sarah A. Collier, Katharine M. Benedict, Michael J. Beach, Aron J. Hall, Arie H. Havelaar

Illnesses transmitted by food and water cause a major disease burden in the United States despite advancements in food safety, water treatment, and sanitation. We report estimates from a structured expert judgment study using 48 experts who applied Cooke's classical model of the proportion of disease attributable to 5 major transmission pathways (foodborne, waterborne, person-to-person, animal contact, and environmental) and 6 subpathways (food handler–related, under foodborne; recreational, drinking, and nonrecreational/nondrinking, under waterborne; and presumed person-to-person-associated and presumed animal contact-associated, under environmental). Estimates for 33 pathogens were elicited, including bacteria such as *Salmonella enterica, Campylobacter* spp., *Legionella* spp., and *Pseudomonas* spp.; protozoa such as *Acanthamoeba* spp., *Cyclospora cayetanensis*, and *Naegleria fowleri*; and viruses such as norovirus, rotavirus, and hepatitis A virus. The results highlight the importance of multiple pathways in the transmission of the included pathogens and can be used to guide prioritization of public health interventions.

Illnesses transmitted commonly by food and water result in a major disease burden on both a national and a global scale (*1*). Each year in the United States, ≈9.4 million illnesses, 56,000 hospitalizations, and 1,351 deaths are caused by 31 known pathogens transmitted through food (*2*). Previous estimates of the burden of waterborne disease in the United States have largely focused on the burden of gastrointestinal illness associated with drinking water; an estimated 4–32 million cases of illness occur each year (*3*,*4*).

Source attribution is a process of estimating the proportion of illnesses resulting from various exposures for specific pathogens. Attributing illnesses to sources can guide decisions about where to target prevention and control efforts by apportioning illnesses to specific sources, thus aiding in the development of specific interventions (*5*). Attributing to the comprehensive set of transmission pathways considered in this study (foodborne, waterborne, person-to-person, animal contact, and environmental) is challenging for many reasons, including limited data and difficulty combining existing data from multiple sources. For example, outbreak surveillance data, such as those collected through the National Outbreak Reporting System (NORS), can provide information on sources of illness but are subject to reporting biases and may not be representative of endemic disease (*6*). Other studies have also raised concerns of publication bias toward novel, unique, or large foodborne outbreaks, limiting the utility of systematic reviews of published outbreaks in assessing source attribution (*7*,*8*). One method to address these barriers is structured expert judgment (SEJ), a method to use and combine estimates produced by experts and quantify uncertainty for the purpose of risk analysis when the ability to gather data is hindered by high expense, data scarcity, or lack of reliable data. This method, when executed well, is formal, reproducible, and mathematically and scientifically rigorous (*9*–*11*).

Author affiliations: University of Florida, Gainesville, Florida, USA (E. Beshearse, A.H. Havelaar); Centers for Disease Control and Prevention, Atlanta, Georgia, USA (B.B. Bruce, S.M. Crim, P.M. Griffin, K.E. Fullerton, S.A. Collier, K.M. Benedict, M.J. Beach, A.J. Hall); Delft University of Technology, Delft, the Netherlands (G.F. Nane); Resources for the Future, Washington, DC, USA (R. Cooke); Aspinall & Associates, Tisbury, UK (W. Aspinall); University of Bristol, Bristol, UK (W. Aspinall); Technical University of Denmark, Lyngby, Denmark (T. Hald)

DOI: https://doi.org/10.3201/eid2701.200316

The Centers for Disease Control and Prevention (CDC) works to control and prevent illness caused by foodborne and waterborne pathogens in the United States. To accomplish this, CDC supports states and territories in tracking disease, detects and responds to outbreaks, and uses surveillance and sentinel site data to estimate the burden of these diseases in the United States. To inform this work, we implemented an SEJ study using Cooke's classical model to estimate the proportion of domestically acquired illnesses for 33 pathogens transmitted through food and water that can be attributed to each of 5 major transmission pathways and 6 subpathways (*12*).

## Methods

The process was divided into 3 stages: preparation, elicitation, and postelicitation (*11*). These stages are detailed in the following sections.

### Preparation

#### Selection of Pathogens

We included all pathogens transmitted commonly through food or water that were examined by Scallan et al. (2) and Collier et al. (*13*) except those for which the only syndrome of interest was considered to have >95% foodborne transmission (e.g., *Listeria monocytogenes*, *Clostridium botulinum*); we added 3 free-living amoebae (*2*,*13*). For some pathogens, subdivisions into categories by serotype, patient age, or clinical manifestations of interest were included because transmission pathways were assumed to be different. For example, for *Salmonella*, the 5 most common serotypes were included along with 2 groups of rarer serotypes based on a ranking of their coefficients of variation (CVs) calculated from the patients' ages, sexes, states of residence, and the year and month specimens were obtained (group 1, lowest CVs; group 2, highest CVs) as described by Boore et al. (*14*). This compilation resulted in a total of 33 pathogens and 47 target questions, or categories, for estimation. The 47 target questions were grouped into 15 panels on the basis of similarities between pathogen microbiology and ecology (Table 1).

#### Transmission Pathway Definitions

We used definitions for 5 major pathways that were mutually exclusive and comprehensive (i.e., covering

**Table 1.** Pathogen panels, target questions, and number of experts providing estimates, structured expert judgment, United States, 2017

| Panel | Pathogen and clinical manifestation target questions | No. experts who provided estimates in initial elicitation | No. experts who revised estimates | No. experts who provided re-elicitation estimates |
|---|---|---|---|---|
| Panel 1 | *Acanthamoeba* spp., *Balamuthia mandrillaris*, *Naegleria fowleri* | 14 | 4 | Not required |
| Panel 2 | Astrovirus, norovirus, rotavirus, sapovirus | 17 | 3 | Not required |
| Panel 3 | *Brucella* spp., *Mycobacterium bovis* | 16 | 5 | Not required |
| Panel 4 | *Campylobacter* spp., *Yersinia enterocolitica* | 19 | 5 | Not required |
| Panel 5 | *Cryptosporidium* spp.,*Giardia* spp. | 21 | 5 | Not required |
| Panel 6 | *Cyclospora cayetanensis* | 21 | 4 | Not required |
| Panel 7 | Enterotoxigenic *Escherichia coli*, other diarrheagenic *E. coli, Shigella* spp. | 21 | 3 | Not required |
| Panel 8 | Hepatitis A virus | 19 | 2 | Not required |
| Panel 9 | *Legionella* spp., nontuberculous *Mycobacterium* spp. | 9 | 1 | Not required |
| Panel 10 | *Pseudomonas* spp., otitis externa, pneumonia, septicemia | 16 | 7 | 7 |
| Panel 11 | *Salmonella enterica*, nontyphoidal: all serotypes and ages, <5 y of age; Enteritidis, Typhimurium, Newport, I 4,[5],12:i:-, Javiana; other serotypes group 1,* other serotypes group 2† | 14 | 3 | Not required |
| Panel 12 | Shiga toxin–producing *E. coli* O157 and non-O157 | 18 | 4 | Not required |
| Panel 13 | *Staphylococcus aureus*, group A *Streptococcus* | 19 | 4 | Not required |
| Panel 14 | *Toxoplasma gondii* | 16 | 3 | Not required |
| Panel 15 | *Vibrio alginolyticus*, AGI, non-AGI; *V. cholerae*, nontoxigenic, AGI, non-AGI; *V. parahaemolyticus*, AGI, non-AGI; *V. vulnificus*,‡ non-AGI; *Vibrio* spp., other, AGI, non-AGI | 15 | 6 | 9 |

*Group 1: serotypes such as Agona, Anatum, Braenderup, Hadar, Heidelberg, Infantis, Oranienburg, Saintpaul, Senftenberg, Thompson. AGI, acute gastrointestinal illness.
†Group 2: serotypes such as Bareilly, Gaminara, Give, Mississippi, Norwich, Pomona, Rubislaw, Tennessee, Urbana, Weltevreden.
‡Clinical manifestations of interest for initial elicitation were bacteremia and wound infections.

**Table 2.** Major transmission pathway definitions, structured expert judgment, United States, 2017

| Major transmission pathways | Description |
|---|---|
| Foodborne | Transmission occurs through eating food. Contamination can originate anywhere in the food production chain from primary production, to retail, and then to the home or restaurant. This pathway applies to all nonwater beverages and items ingested by humans as food (e.g., including raw milk and excluding items consumed for medicinal purposes). |
| Waterborne | Transmission occurs through the consumption of or direct contact with water or inhalation of aerosols originating from water. This includes drinking water, bottled water, recreational water (treated and untreated), and other water sources, such as water within buildings, used in medical devices, or for industry/manufacturing. |
| Person-to-person | Transmission occurs by direct contact with infected persons or their bodily fluids, or by contact with the local environment where an exposed person is simultaneously present with an infected person or visible excreta. |
| Animal contact | Transmission occurs through direct contact with an animal, its bodily fluids (excluding raw milk or other fluids consumed as food), fur, hair, feathers, scales, or skin, or by contact with the local environment where an infected animal, its visible excreta, fur, hair, feathers, scales, or skin was simultaneously present with the exposed person (e.g., barns, petting zoos, and pet stores). This pathway includes domestic animals, farm animals, wildlife, and pets. |
| Environmental | Transmission occurs through exposure to naturally occurring agents (e.g., free-living ameba or radon) or contact with contaminated air, mud, soil, or other outdoor or indoor surfaces or objects not attributable to foodborne, waterborne, person-to-person, or animal contact transmission, as defined for this project. |

100% of transmission modes) and that reflect those used by CDC for outbreak surveillance (*15*,*16*; Tables 2, 3). We defined 3 mutually exclusive waterborne subpathways (recreational water, drinking water, and nonrecreational nondrinking water) that were comprehensive (i.e., all waterborne pathway transmission fell into 1 of the 3 subpathways). We also defined and elicited 1 foodborne (food handler-related) and 2 environmental (presumed animal associated, presumed person-to-person) subpathways that accounted for only a portion of transmission within their main pathway. We calculated the unelicited proportion remaining of their respective main pathways during analysis and assigned it to the subpathways other foodborne and other environmental. For all transmission pathways, we defined the point of attribution as the point of exposure (i.e., the event during which a person ingested, or was otherwise exposed to, the pathogen).

#### Expert Identification and Selection

We identified 182 experts representing a range of scientific backgrounds (e.g., epidemiologists, laboratory scientists, and environmental engineers from government, academia, nongovernmental organizations,

**Table 3.** Transmission subpathway definitions, structured expert judgment, United States, 2017

| Subpathway | Description |
|---|---|
| Foodborne subpathway | |
| Food handler–related | When food processed or prepared for others is contaminated by an infected person. |
| Waterborne subpathways | |
| Recreational water, treated or untreated | Water that is used for recreational activities, such as in an aquatic facility or natural body of water. Can be treated or untreated. Treated water has undergone a systematic disinfection process (e.g., chlorination and filtration) with the goal of maintaining good microbiologic quality for recreation; untreated water has not undergone a disinfection or treatment process to maintain good microbiological quality for recreation (e.g., lakes, rivers, oceans, and reservoirs). |
| Drinking water | Water that is used primarily for drinking but including other domestic uses, such as washing or showering; can come from a public water system, a private well, or commercially bottled sources. |
| Nonrecreational, nondrinking water | Water that is used for purposes other than recreation or drinking (e.g., for agriculture, industry, medical treatment, backcountry streams or flood waters). Agricultural water includes water that is used to grow fresh produce and sustain livestock. Industrial water includes water used during manufacturing or in cooling equipment. Medical water includes any water used within medical devices or water used for washing surgical tools and equipment, and water used for hydrotherapy. This subcategory does not include transmission that can be accounted for by another major pathway, such as food or animals |
| Environmental subpathways | |
| Presumed animal contact associated | When a person becomes ill from exposure to soil, mud, or surfaces contaminated by an animal without direct contact or simultaneous presence with the animal, or when an infection is suspected to be animal associated because of previous knowledge about the pathogen. |
| Presumed person-to-person associated | When a person becomes ill from an exposure indirectly associated with an ill person. |

and industry) on the basis of publication records, experience, expertise, or previous participation in source attribution studies. We contacted the experts directly and invited them to apply for participation (Figure 1). Fifty-eight returned a curriculum vitae and publication record and completed a questionnaire about their professional interest, knowledge, and experience for each of the 33 pathogens using a 4-level Likert scale (high, medium, low, or none) by the requested deadline. We asked experts to suggest additional experts to be considered; the 3 who were suggested were also invited.

#### Assignment to Panels

We evaluated expert applications based on area of expertise, education, work history, professional interest, experience, and knowledge of the individual pathogens in this study. Publication record was not used to determine eligibility because it could have led to elimination of qualified experts who do not publish frequently. We used maximum bipartite matching in R version 3.3.1 with the igraph package version 1.0.1 to assign experts to panels based on their curricula vitae, publication records, and questionnaire responses (*17*,*18*). Final assignment ensured that experts were not on pathogen panels for which they reported none or low experience. Individual experts were on panels for ≤15 pathogens (Appendix 1, https://wwwnc.cdc.gov/EID/article/27/1/20-0316-App1.pdf).

#### Calibration Questions

The study administrators used unpublished data to develop calibration questions (Appendix 2, https://wwwnc.cdc.gov/EID/article/27/1/20-0316-App2.pdf). We developed 14 questions to evaluate the experts' statistical accuracy and informativeness by probing the experts' ability to provide reliable estimates under uncertainty. The subject domain of the questions aimed to represent expertise in public health surveillance of foodborne and waterborne diseases, food consumption patterns in the United States, and human exposure and occurrence data about pathogens in food, water, and the environment.

#### Target Questions

Target questions asked the proportion of illnesses transmitted through the 5 major pathways and 6 subpathways for all study pathogens. Study administrators blocked transmission pathways and subpathways for some pathogens based on their microbiology and ecology (Table 4). We created individualized Microsoft Excel version 14.7.7 (http://www.microsoft.com) files with separate sheets for calibration questions, target questions for each assigned pathogen, and additional instructions for each expert. We included verification aids in the worksheets to assist the experts (Appendix 3, https://wwwnc.cdc.gov/EID/article/27/1/20-0316-App3.xlsm).

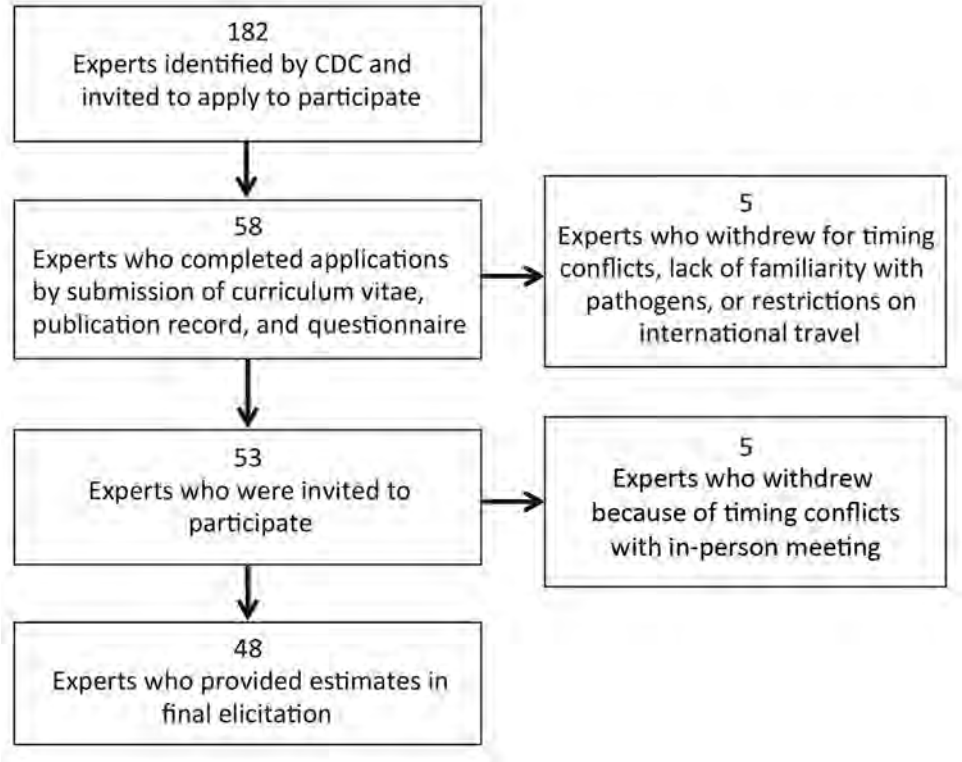


**Figure 1.** Expert selection process for study of attribution of illnesses transmitted by food and water to comprehensive transmission pathways using structured expert judgment, United States, 2017.

### Dry Run Exercise

We conducted a dry run exercise using video web conferencing to assess calibration questions, target question answer sheets, and expert training materials for completeness, clarity, and ease of use. Six persons from academia, state health departments, and CDC participated in this trial exercise, but not in the formal elicitation itself. We modified the elicitation materials based on feedback from this exercise.

### Expert Orientation

Before the formal elicitation, experts attended a training webinar to learn definitions of transmission pathways, subpathways, and point of attribution. To ensure common understanding of the definitions, experts completed a 20-question review of knowledge after the webinar (Appendix 4, https://wwwnc.cdc.gov/EID/article/27/1/20-0316-App4.pdf).

We provided a background document summarizing current surveillance data, when available, and

**Table 4.** Source attribution results for major transmission pathways, structured expert judgment, United States, 2017*

| Pathogen name | Mean % (95% uncertainty interval) | | | | |
|---|---|---|---|---|---|
| | Foodborne | Waterborne | Person-to-person | Animal contact | Environmental |
| Bacteria | | | | | |
| *Brucella* spp. | 45 (13–77) | 10 (0–42) | Blocked | 36 (10–73) | 9 (0–32) |
| *Campylobacter* spp. | 57 (30–80) | 13 (1–31) | 7 (0–23) | 16 (3–35) | 7 (0–30) |
| Enterotoxigenic *Escherichia coli* | 69 (37– 91) | 9 (0–38) | 7 (0–38) | Blocked | 15 (2–33) |
| STEC O157 | 60 (40–77) | 5 (1–13) | 16 (4–33) | 12 (3–25) | 7 (1–17) |
| STEC non-O157 | 50 (26–75) | 6 (0–17) | 15 (2–34) | 21 (2–46) | 8 (0–24) |
| *E. coli*, other diarrheagenic | 55 (27–80) | 9 (0–30) | 16 (2–39) | 9 (0–33) | 12 (0–33) |
| *Legionella* spp. | Blocked | 97 (67–100) | 0 (0–1) | Blocked | 2 (0–28) |
| *Mycobacterium bovis* | 75 (36–98) | 1 (0–9) | 9 (0–39) | 13 (0–50) | 2 (0–12) |
| Nontuberculous *Mycobacterium* spp. | Blocked | 72 (39–94) | 4 (0–21) | 2 (0–35) | 22 (0–49) |
| *Pseudomonas* spp., otitis externa | Blocked | 81 (67–95) | 3 (0–13) | 1 (0–4) | 15 (1–,25) |
| *Pseudomonas* spp., septicemia | Blocked | 22 (3–53) | 2 (0–19) | 2 (0–11) | 74 (41–94) |
| *Pseudomonas* spp., pneumonia | Blocked | 51 (14–80) | 4 (1–32) | 0 (0–2) | 45 (15–80) |
| *Salmonella enterica*, nontyphoidal | 66 (48–81) | 6 (0–22) | 7 (0–16) | 11 (3–24) | 9 (2–21) |
| *S. enterica*, nontyphoidal, age <5 y | 46 (20–66) | 7 (0–26) | 18 (6–35) | 13 (2–30) | 16 (2–36) |
| *S. enterica* serotype Enteritidis | 80 (63–92) | 4 (0–11) | 7 (1–16) | 5 (0–19) | 4 (1–14) |
| *S. enterica* serotype I 4,[5],12:i:- | 66 (40–82) | 6 (1–15) | 8 (1–17) | 12 (2–27) | 7 (0–20) |
| *S. enterica* serotype Javiana | 56 (29–76) | 7 (1–20) | 9 (2–22) | 14 (3–33) | 14 (2–29) |
| *S. enterica* serotype Newport | 74 (50–86) | 2 (0–9) | 7 (1–16) | 8 (1–19) | 8 (2–18) |
| *S. enterica* serotype Typhimurium | 59 (27–78) | 7 (1–18) | 8 (2–19) | 14 (3–29) | 13 (2–30) |
| *S. enterica*, all other serotypes group 1 | 60 (29–79) | 6 (1–18) | 9 (2–21) | 12 (2–29) | 12 (3–,29) |
| *S. enterica*, all other serotypes group 2 | 40 (10–65) | 7 (1–24) | 10 (2–26) | 17 (1–40) | 26 (6–51) |
| *Shigella* spp. | 8 (1–36) | 4 (1–21) | 81 (48–93) | Blocked | 6 (0–26) |
| *Staphylococcus aureus* | Blocked | 75 (23–98) | 18 (1–71) | 1 (0–5) | 5 (0–37) |
| *Streptococcus* spp., group A | 4 (0–33) | 1 (0–6) | 92 (55–99) | 1 (0–12) | 2 (0–19) |
| *Vibrio alginolyticus* | 60 (24–84) | 37 (13–71) | 0 (0–1) | 1 (0–4) | 2 (0–11) |
| *V. alginolyticus*, non-AGI | 2 (0–17) | 97 (79–100) | 0 (0–1) | 0 (0–2) | 0 (0–2) |
| *V. cholerae* nontoxigenic | 92 (61–100) | 6 (0–30) | 1 (0–3) | 0 (0–4) | 0 (0–3) |
| *V. cholerae* nontoxigenic, non-AGI | 33 (8–59) | 65 (39–90) | 0 (0–1) | 0 (0–1) | 2 (0–13) |
| *V. parahaemolyticus* | 74 (59–91) | 24 (7–38) | 0 (0–2) | 0 (0–2) | 1 (0 –5) |
| *V. parahaemolyticus*, non-AGI | 8 (2–39) | 90 (57–97) | 0 (0–1) | 0 (0–1) | 2 (0–8) |
| *V. vulnificus*† | 20 (7–54) | 77 (40–91) | 0 (0–3) | 1 (0–9) | 2 (0–12) |
| *V. vulnificus*, non-AGI | 20 (9–34) | 78 (58–89) | 0 (0–1) | 1 (0–16) | 2 (0–9) |
| *Vibrio* spp., other AGI | 96 (69–100) | 2 (0–23) | 0 (0–1) | 0 (0–2) | 1 (0–8) |
| *Vibrio* spp, other non-AGI | 95 (58–100) | 3 (0–27) | 0 (0–1) | 0 (0–2) | 2 (0–15) |
| *Yersinia enterocolitica* | 77 (44–100) | 9 (0–37) | 3 (0–17) | 4 (0–16) | 8 (0–33) |
| Protozoa | | | | | |
| *Acanthamoeba* spp. | Blocked | 82 (46–100) | Blocked | 0 (0–0) | 18 (0–54) |
| *Balamuthia mandrillaris* | Blocked | 54 (5–95) | Blocked | 0 (0–0) | 46 (5–95) |
| *Cryptosporidium* spp. | 7 (0–25) | 43 (17–73) | 20 (2–49) | 21 (4–48) | 8 (0–34) |
| *Cyclospora cayetanensis* | 83 (59–99) | 6 (0–25) | 3 (0–14) | 1 (0–9) | 7 (0–28) |
| *Giardia* spp. | 10 (0–35) | 44 (16–78) | 27 (3–59) | 10 (0–38) | 8 (0–37) |
| *Naegleria fowleri* | Blocked | 88 (61–100) | Blocked | Blocked | 12 (0–38) |
| *Toxoplasma gondii* | 28 (4–60) | 5 (0–27) | Blocked | 58 (24–86) | 9 (0–29) |
| Viruses | | | | | |
| Astrovirus | 15 (1–38) | 6 (0–25) | 73 (44–94) | Blocked | 6 (0–18) |
| Hepatitis A virus | 42 (9–78) | 8 (0–33) | 41 (8–77) | Blocked | 8 (0–34) |
| Norovirus | 19 (6–37) | 6 (0–25) | 70 (46–88) | Blocked | 5 (0–18) |
| Rotavirus | 5 (0–20) | 7 (0–28) | 81 (57–98) | Blocked | 5 (0–21) |
| Sapovirus | 13 (0–34) | 8 (0–30) | 75 (49–94) | Blocked | 4 (0–16) |

*Blocked indicates pathways blocked by study administrators. AGI, acute gastrointestinal disease; STEC, Shiga toxin–producing *Escherichia coli*.
†Clinical manifestations of interest for initial elicitation were bacteremia and wound infections.

relevant research findings for each pathogen. The document contained links to selected research articles. Experts were encouraged to use any data they felt were informative to make their estimates; they were not limited to only this document.

### Elicitation

For the formal elicitation, 48 experts representing a wide range of professional and scientific backgrounds participated at a 2-day, in-person workshop in May 2017. During the workshop, experts participated in a 2-hour information session on probabilistic methods and providing estimates under uncertainty.

#### Calibration Questions

Experts were not expected to know true values precisely and provided low (5th percentile), median (50th percentile), and high (95th percentile) estimates to represent their uncertainty on the answers provided to the calibration questions. Experts were not allowed access to any additional resources while answering the calibration questions and, after they had they had finished, they could not return to this section to change their responses.

#### Target Questions

After completion of the calibration questions, experts provided 5th, 50th, and 95th percentile estimates for the proportion of domestically acquired illnesses that are transmitted through each major pathway and subpathway annually for each pathogen and target question in each panel to which they were assigned. The experts were also asked to indicate if they did not agree with the pathways blocked by study administrators. One pathway, person-to-person transmission for *Legionella* spp., was unblocked based on this feedback, and experts provided this estimate with the others at the in-person elicitation. Experts could access resources and discuss them with colleagues, if desired. However, we emphasized that the final estimates should represent the expert's individual responses, not a group consensus.

### Postelicitation

#### Re-Elicitation

After the in-person elicitation was completed, we determined that re-elicitation for some pathogens was necessary. More granular detail was needed beyond the single estimate for *Pseudomonas*, so estimates were re-elicited for otitis externa, septicemia, and pneumonia. Based on feedback we received during the elicitation, we re-elicited estimates for non–acute gastrointestinal infections (non-AGI) for nontoxigenic *Vibrio cholerae*, *V. parahaemolyticus, V. vulnificus*, and *V. alginolyticus*. Experts were provided with feedback with updated surveillance data and given the opportunity to adjust their original estimates if new data led them to reconsider their previous estimates (Figure 1). The re-elicitations were completed through follow-up emails and web conferences.

#### Data Analysis

We analyzed data using EXCALIBUR (*19*). We combined all individual expert assessments by linear pooling into a single uncertainty assessment for each target question (*11*). For equal-based weighting, all experts' assessments contributed to the combined uncertainty assessment evenly. We computed performance-based weighting by combining the statistical accuracy and information scores of experts in each panel. The weighted combination of experts is referred to as the decision maker. We used the item weight decision maker because this calculates and applies weights per individual target question rather than for all questions an expert answered. We performed optimization to determine the threshold by which an expert's responses would be included in the final estimate or not. This was done separately per expert for each panel, based on each expert's statistical accuracy score (*12*).

We performed a subgroup analysis to determine whether separate schools of thought existed as a result of experts' self-identified background (categorized as mainly foodborne, mainly waterborne, or both). This analysis was completed by 2 independent reviewers who analyzed EXCALIBUR panel outputs for each target question to determine whether wide divergence existed among individual responses.

We normalized random samples from the weighted distributions for major transmission pathways and waterborne subpathways such that on each sample the values across pathways summed to 1. This process was done by resampling the cumulative distribution functions generated by EXCALIBUR 5,000 times in R version 3.4.3 for each pathogen, while dividing all sampled values by the sum of their values per iteration. Point estimates and 95% uncertainty intervals (UIs) for each target question and pathway were produced. We performed robustness analysis and out-of-sample validation to assess the performance of the method and to evaluate the effect of individual experts and individual calibration questions on the final distribution (Appendix 5, https://wwwnc.cdc.gov/EID/article/27/1/20-0316-App5.pdf) (*12*).

## Results

### Knowledge Review

The 20 questions were designed to be challenging, to emphasize application of the study definitions, and to represent scenarios at the boundaries among different transmission pathways. For 17 (85%) questions, >75% of participants answered with the correct major pathway, and of these questions, 13 (76%) were answered with the correct subpathway as well (Appendix 4).


**Figure 2.** Source attribution results for major transmission pathways of bacteria in study of attribution of illnesses transmitted by food and water to comprehensive transmission pathways using structured expert judgment, United States, 2017.

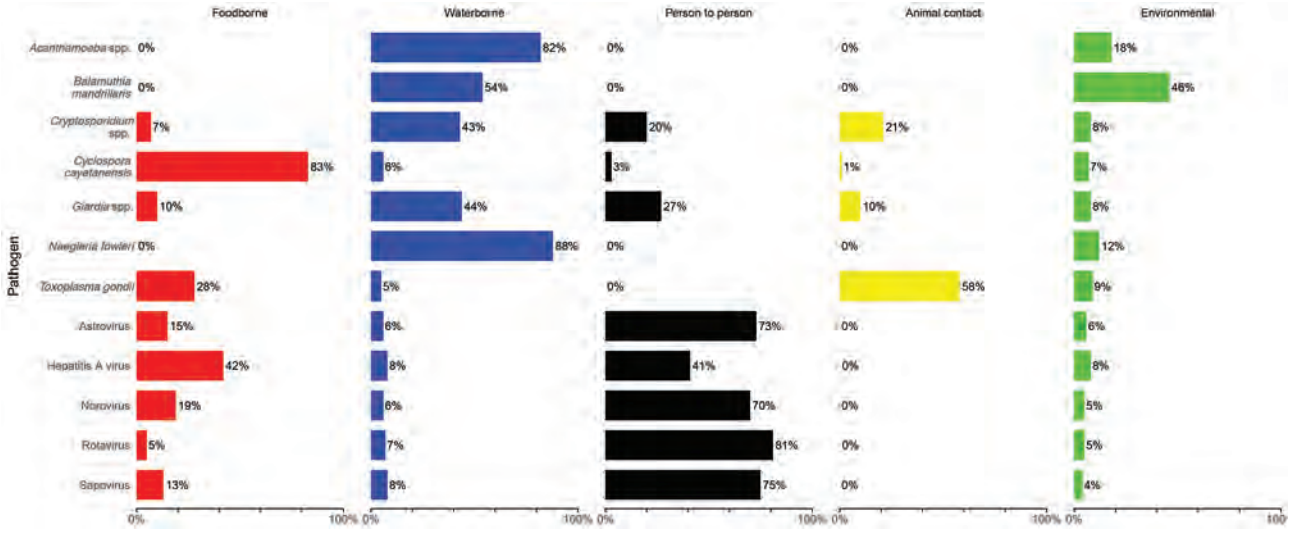


**Figure 3.** Source attribution results for major transmission pathways of protozoa and viruses for study of attribution of illnesses transmitted by food and water to comprehensive transmission pathways using structured expert judgment, United States, 2017.

## Major and Subpathway Results

Table 4 and Figures 2 and 3 show the proportion and UI of domestically acquired illnesses attributed to the 5 major transmission pathways; Tables 5 and 6 show the subpathway results. For all panels, a satisfactory number of accurate and informative experts were included. Differing schools of thought based on experts' backgrounds were not identified (Appendix 5).

### Bacteria

Most of the pathogens in this study were bacteria; they encompassed 35 of the 47 target questions. More than half of transmission (>50%) was attributed to the foodborne pathway for *Campylobacter* spp.; enterotoxigenic *Escherichia coli*; Shiga toxin-producing *Escherichia coli* (STEC) O157; other diarrheagenic *E. coli*; *Mycobacterium bovis*; nontyphoidal *Salmonella enterica* (all ages and serotypes); *S. enterica* serotypes Enteritidis, I 4,[5],12:i:-, Javiana, Newport, Typhimurium, and group 1 serotypes; *Vibrio alginolyticus*; *V. cholerae* nontoxigenic; *V. parahaemolyticus; Vibrio* spp., other AGI; *Vibrio* spp, other non-AGI; and *Yersinia enterocolitica*. In addition, *Legionella* spp.; nontuberculous *Mycobacterium* spp.; *Pseudomonas* spp., otitis externa; invasive *Staphylococcus aureus*; *V. alginolyticus*, non-AGI; *V. cholerae* nontoxigenic, non-AGI; *V. parahaemolyticus*, non-AGI; and *V. vulnificus* were all estimated to have majority transmission from the waterborne pathway. Most transmission for *Shigella* spp. and group A *Streptococcus* were estimated to be through person-to-person transmission. No bacterial pathogen had majority transmission through animal contact. *Pseudomonas* spp. septicemia was attributed primarily to the environmental pathway.

### Protozoa

*Cyclospora cayetanensis* was the only protozoan estimated to have majority transmission through the foodborne pathway. *Acanthamoeba* spp. and *Naegleria fowleri* both had >80% transmission attributed to the waterborne pathway, and 54% (UI 5%–95%) of *Balamuthia mandrillaris* infections were estimated to occur through waterborne transmission. No protozoa had majority person-to-person or environmental transmission. Waterborne transmission was estimated at 43% (UI 17%–73%) for *Cryptosporidium* spp. and 44% (UI 16%–78%) for *Giardia* spp. Among all pathogens, *Toxoplasma gondii* had the highest attribution to animal contact transmission, 58% (UI 24%–86%).

### Viruses

Most transmission for astrovirus, norovirus, rotavirus, and sapovirus was attributed to the person-to-person pathway. Hepatitis A virus was estimated to have the highest proportion of illness transmitted by the foodborne pathway at 42% (UI 9%–78%). Of this, 48% (UI 2%–93%) was considered food handler related. Of foodborne transmission, 50%–71% was estimated to be food handler related for astrovirus, norovirus, and sapovirus. For all viruses, 67%–88% of environmental transmission was attributed to the subpathway of presumed person-to-person transmission.

## Discussion

This study presents a novel method for estimating the proportion of illnesses from pathogens transmitted commonly by food and water in the United States

through comprehensive and mutually exclusive pathways. It includes estimates for food handler–related, recreational water, drinking water, nonrecreational nondrinking water, and various environmental subpathways. This method enabled estimates to be informed by multiple data sources, including outbreak surveillance data, studies of sporadic illnesses, case reports, and experts' professional knowledge. The use of calibration to weight expert responses is a distinguishing characteristic of the classical model and introduces mathematical rigor not found with other elicitation methods.

Similar SEJ studies have been conducted in numerous countries, including Australia, Canada, and

**Table 5.** Source attribution results for foodborne and environmental transmission subpathways, structured expert judgment, United States, 2017*

| | Mean % (95% uncertainty interval) | | | | |
|---|---|---|---|---|---|
| | Foodborne | | Environmental | | |
| Pathogen name | Food handler–related | Other foodborne | Presumed person-to-person | Presumed animal contact | Other environmental |
| Bacteria | | | | | |
| *Brucella* spp. | Blocked | 100 (100–100) | Blocked | 41 (2–96) | 59 (4–98) |
| *Campylobacter* spp. | 12 (0–58) | 88 (42–100) | 12 (0–46) | 62 (3–100) | 26 (0–89) |
| Enterotoxigenic *Escherichia coli* | 23 (1–71) | 77 (29–99) | 8 (0–43) | Blocked | 92 (54–100) |
| STEC O157 | 8 (0–55) | 92 (45–100) | 10 (0–46) | 76 (16–100) | 13 (0–73) |
| STEC non-O157 | 5 (0–29) | 95 (71–100) | 21(2–49) | 65(19–91) | 14 (0–55) |
| *E. coli*, other diarrheagenic | 7 (0–54) | 93 (46–100) | 59 (3–100) | 9 (0–39) | 31 (0–91) |
| *Legionella* spp. | Blocked | Blocked | 0 (0–6) | Blocked | 99 (91–100) |
| *Mycobacterium bovis* | 1 (0–13) | 99 (87–100) | 3 (0–34) | 45 (0–100) | 53 (0–100) |
| Nontuberculous *Mycobacterium* spp. | Blocked | Blocked | 3 (0–35) | 6 (0–87) | 91 (0–100) |
| *Pseudomonas* spp., otitis externa | Blocked | Blocked | 8 (0–51) | 2 (0–11) | 90 (16–100) |
| *Pseudomonas* spp., septicemia | Blocked | Blocked | 9 (0–59) | 1 (0–4) | 91 (39–100) |
| *Pseudomonas* spp., pneumonia | Blocked | Blocked | 10 (0–61) | 1 (0–6) | 88 (22–100) |
| *Salmonella enterica*, nontyphoidal | 10 (0–38) | 90 (62–100) | 20(2–52) | 45 (5–89) | 35 (0–83) |
| *S. enterica*, nontyphoidal, under 5 y | 10 (0–39) | 90 (61–100) | 35 (5–78) | 45 (6–84) | 20 (0–75) |
| *S. enterica* serotype Enteritidis | 11 (0–51) | 89 (49–100) | 22 (2–56) | 44 (3–88) | 34 (0–84) |
| *S. enterica* serotype I 4,[5],12:i:- | 10 (0–38) | 90 (62–100) | 21 (3–52) | 45 (3–89) | 34 (0–84) |
| *S. enterica* serotype Javiana | 11 (0–48) | 89 (52–100) | 36 (4–80) | 44 (5–84) | 20 (0–75) |
| *S. enterica* serotype Newport | 10 (0–39) | 90 (61–100) | 21 (3–53) | 48 (5–89) | 30 (0–82) |
| *S. enterica* serotype Typhimurium | 10 (0–39) | 90 (61–100) | 21 (2–50) | 49 (6–88) | 31 (0–81) |
| *S. enterica*, all other serotypes group 1 | 10 (0–38) | 90 (62–100) | 21 (2–52) | 48 (6–89) | 31 (0–81) |
| *S. enterica*, all other serotypes group 2 | 10 (0–39) | 90 (61–100) | 35 (5–79) | 44 (5–83) | 20 (0–74) |
| *Shigella* spp. | 71 (17–96) | 29 (4–83) | 90 (31–100) | Blocked | 10 (0–69) |
| *Staphylococcus aureus* | Blocked | Blocked | 76 (30–97) | 3 (0–43) | 21 (0–66) |
| *Streptococcus* spp., group A | 51 (0–100) | 49 (0–100) | 94 (29–100) | 2 (0–33) | 4 (0–70) |
| *Vibrio alginolyticus,* AGI | 5 (0–89) | 95 (11–100) | 2 (0–19) | 2 (0–36) | 96 (9–100) |
| *V. alginolyticus*, non-AGI | 0 (0–2) | 100 (98–100) | 1 (0–3) | 96 (45–100) | 3 (0–54) |
| *V. cholerae* nontoxigenic AGI | 1 (0–5) | 99 (95–100) | 6 (0–83) | 9 (0–97) | 85 (0–100) |
| *V. cholerae* nontoxigenic, non-AGI | 0 (0–1) | 100 (99–100) | 1(0–4) | 96 (26–100) | 3(0–73) |
| *V. parahaemolyticus* AGI | 5 (0–52) | 95 (48–100) | 2 (0–7) | 2(0–24) | 96 (18–100) |
| *V. parahaemolyticus*, non-AGI | 0 (0–2) | 100 (98–100) | 1 (0–3) | 96 (30–100) | 3 (0–69) |
| *V. vulnificus*† | 5 (0–72) | 95 (28–100) | 3 (0–48) | 3 (0–50) | 94 (0–100) |
| *V. vulnificus*, non-AGI | 0 (0–2) | 100 (98–100) | 1 (0–3) | 96 (29–100) | 3 (0–70) |
| *Vibrio* spp., other AGI | 3 (0–70) | 97 (30–100) | 1 (0–5) | 2 (0–27) | 96 (21–100) |
| *Vibrio* spp., other non-AGI | 3 (0–43) | 97 (57–100) | 1 (0–2) | 2 (0–31) | 97 (38–100) |
| *Yersinia enterocolitica* | 9 (0–55) | 91 (45–100) | 23 (0–67) | 56 (8–99) | 20 (0–82) |
| Protozoa | | | | | |
| *Acanthamoeba* spp. | Blocked | Blocked | Blocked | 1 (0–6) | 97 (45–100) |
| *Balamuthia mandrillaris* | Blocked | Blocked | Blocked | 2 (0–12) | 97 (37–100) |
| *Cryptosporidium* spp. | 24 (0–87) | 76 (13–100) | 18 (0–61) | 61 (7–99) | 21(0–81) |
| *Cyclospora cayetanensis* | 10 (0–68) | 90 (32–100) | 51 (0–100) | 6 (0–70) | 43 (0–100) |
| *Giardia* spp. | 19 (0–72) | 81 (28–100) | 26 (1–66) | 23 (0–86) | 51 (0–97) |
| *Naegleria fowleri* | Blocked | Blocked | Blocked | Blocked | 97 (47–100) |
| *Toxoplasma gondii* | Blocked | 100 (100–100) | Blocked | 80 (22–100) | 20 (0–78) |
| Viruses | | | | | |
| Astrovirus | 50 (0–100) | 50 (0–100) | 73 (1–100) | Blocked | 27 (0–99) |
| Hepatitis A virus | 48 (2–93) | 52 (7–98) | 86 (27–100) | Blocked | 12 (0–72) |
| Norovirus | 71 (29–99) | 29 (1–71) | 73 (2–100) | Blocked | 27 (0–98) |
| Rotavirus | 27 (0–98) | 73 (2–100) | 88 (35–100) | Blocked | 11 (0–65) |
| Sapovirus | 51 (0–99) | 49 (1–100) | 67 (0–100) | Blocked | 33 (0–100) |

*Blocked indicates pathways blocked by study administrators. AGI, acute gastrointestinal disease; STEC, Shiga toxin–producing *Escherichia coli*.
†Clinical manifestations of interest for initial elicitation were bacteremia and wound infections.

**Table 6.** Source attribution results for waterborne transmission subpathways (means and 95 uncertainty interval), structured expert judgment, United States, 2017*

| Pathogen name | Mean % (95% uncertainty interval) | | |
|---|---|---|---|
| | Recreational water | Drinking water | Nonrecreational, nondrinking water |
| Bacteria | | | |
| *Brucella* spp. | 45 (0–100) | 8 (0–97) | 47 (0–100) |
| *Campylobacter* spp. | 32 (0–97) | 44 (0–99) | 24 (0–99) |
| Enterotoxigenic *Escherichia coli* | 31 (3–85) | 57 (8–94) | 12 (0–58) |
| STEC O157 | 69 (33–94) | 26 (3–60) | 5 (0–28) |
| STEC non-O157 | 51 (18–77) | 12 (0–43) | 38 (12–69) |
| *E. coli*, other diarrheagenic | 20 (2–53) | 70 (34–92) | 10 (0–38) |
| *Legionella* spp. | 9 (2–35) | 52 (19–78) | 39 (13–69) |
| *Mycobacterium bovis* | 21 (0–100) | 14 (0–100) | 65 (0–100) |
| Nontuberculous *Mycobacterium* spp. | 13 (0–43) | 67 (33–93) | 20 (0–51) |
| *Pseudomonas* spp., otitis externa | 95 (75–100) | 3 (0–21) | 2 (0–11) |
| *Pseudomonas* spp., septicemia | 7 (2–37) | 16 (1–50) | 77 (37–94) |
| *Pseudomonas* spp., pneumonia | 48 (17–74) | 6 (1–33) | 46 (18–76) |
| *Salmonella enterica*, nontyphoidal | 18 (2–53) | 75 (37–93) | 7 (0–26) |
| *S. enterica*, nontyphoidal, <5 y | 19 (3–49) | 69 (38–91) | 12 (1–30) |
| *S. enterica* serotype Enteritidis | 20 (3–49) | 71 (38–92) | 9 (1–27) |
| *S. enterica* serotype I 4,[5],12:i:- | 18 (2–49) | 74 (38–93) | 9 (0–35) |
| *S. enterica* serotype Javiana | 21 (3–53) | 67 (29–90) | 12 (0–42) |
| *S. enterica* serotype Newport | 17 (2–48) | 74 (40–94) | 9 (0–39) |
| *S. enterica* serotype Typhimurium | 19 (3–51) | 73 (39–93) | 8 (1–29) |
| *S. enterica*, all other serotypes group 1 | 19 (3–51) | 72 (36–93) | 9 (0–39) |
| *S. enterica*, all other serotypes group 2 | 19 (2–50) | 69 (36–91) | 12 (1–40) |
| *Shigella* spp. | 77 (41–95) | 3 (0–25) | 20 (3–50) |
| *Staphylococcus aureus* | 91 (50–100) | 5 (0–29) | 4 (0–43) |
| *Streptococcus* spp., group A | 73 (0–100) | 10 (0–95) | 18 (0–100) |
| *Vibrio alginolyticus* AGI | 97 (66–100) | 1 (0–6) | 2 (0–21) |
| *V. alginolyticus*, non-AGI | 96 (49–100) | 2 (0–36) | 3 (0–47) |
| *V. cholerae* nontoxigenic AGI | 96 (56–100) | 2 (0–11) | 2 (0–22) |
| *V. cholerae* nontoxigenic, non-AGI | 96 (50–100) | 2 (0–14) | 3 (0–43) |
| *V. parahaemolyticus* | 98 (62–100) | 1 (0–10) | 1 (0–13) |
| *V. parahaemolyticus*, non-AGI | 97 (50–100) | 2 (0–35) | 2 (0–37) |
| *V. vulnificus*† | 98 (66–100) | 1 (0–9) | 2 (0–24) |
| *V. vulnificus*, non-AGI | 96 (49–100) | 2 (0–37) | 2 (0–43) |
| *Vibrio* spp., other AGI | 69 (0–100) | 4 (0–69) | 27 (0–100) |
| *Vibrio* spp, other non-AGI | 70 (0–100) | 4 (0–69) | 26 (0–100) |
| *Yersinia enterocolitica* | 51 (6–100) | 28 (0–83) | 21 (0–79) |
| Protozoa | | | |
| *Acanthamoeba* spp. | 52 (8–88) | 15 (0–51) | 33 (3–76) |
| *Balamuthia mandrillaris* | 48 (6–88) | 4 (0–26) | 48 (7–89) |
| *Cryptosporidium* spp. | 66 (21–96) | 24 (0–68) | 11 (0–41) |
| *Cyclospora cayetanensis* | 39 (0–99) | 32 (0–97) | 29 (0–100) |
| *Giardia* spp. | 49 (9–93) | 33 (2–82) | 18 (0–67) |
| *Naegleria fowleri* | 85 (51–98) | 3 (0–27) | 12 (1–45) |
| *Toxoplasma gondii* | 37 (0–100) | 27 (0–100) | 36 (0–100) |
| Viruses | | | |
| Astrovirus | 39 (0–99) | 47 (0–100) | 13 (0–92) |
| Hepatitis A virus | 35 (0–100) | 44 (0–100) | 21 (0–97) |
| Norovirus | 47 (8–90) | 45 (6–86) | 8 (0–42) |
| Rotavirus | 41 (7–84) | 50 (8–86) | 9 (0–41) |
| Sapovirus | 55 (11–97) | 37 (0–84) | 8 (0–41) |

*AGI, acute gastrointestinal disease; STEC, Shiga toxin–producing *Escherichia coli*.
†Clinical manifestations of interest for initial elicitation were bacteremia and wound infections.

the Netherlands, as well as for global subregions, by the World Health Organization. Each of these used different transmission pathway definitions, study designs, and elicitation methods (*20*–*23*). This and other variations in methods limit comparison of estimates across studies, but provide support for some of the differences between our study results and previous US pathway attribution estimates. Previous estimates of foodborne transmission for 33 pathogens and animal contact transmission for 6 pathogens included in our study are available (*2*,*24*). We compared published foodborne and waterborne attribution studies with this study (Tables 7, 8).

Differences from previously published work on foodborne transmission attribution proportions were noted, including for *Campylobacter* spp., STEC

non-O157, other diarrheagenic *E. coli*, nontyphoidal *S. enterica*, *M. bovis, Shigella* spp., *Y. enterocolitica, C. cayetanensis, T. gondii,* astrovirus, rotavirus, sapovirus, and hepatitis A virus. These differences could be the result of changes in data availability or analytic methods. For example, previous US foodborne illness estimates used data from surveillance, risk factor studies, and literature review (*2*). Based on available data for *S. enterica* (a case-control study of sporadic illness and unpublished outbreak data [*2*,*25*]), a study used an estimate of 94% foodborne transmission, notably higher than this study's estimate of 66% (UI 48%–81%). Estimates more similar to the current study were reported in SEJ studies in the Netherlands (55%), Canada (63%), and Australia (71%) (*21*,*22*); these studies examined attribution to similar major pathways to those included in this study versus foodborne transmission only. Our estimates of foodborne transmission of astrovirus (15%), rotavirus (5%), and sapovirus (13%) are much higher than the estimate of <1% for each in an earlier study (*2*); reports of foodborne outbreaks caused by these viruses in CDC's outbreak surveillance systems informed our estimates. Reporting of enteric disease outbreaks transmitted by nonfoodborne routes has improved, and experts probably used these new data to inform their estimates (*26*).

This study provides noteworthy estimates for the food handler–related subpathway. For hepatitis A, both the World Health Organization and this study estimate 42% foodborne transmission, of which this study estimated 48% (UI 2%–93%) to be food

**Table 7.** Comparison of proportion of illnesses attributed to foodborne transmission from this and earlier studies*

| | Study | | | | | |
|---|---|---|---|---|---|---|
| Details | Scallan et al. (*2*) | Hald et al. (*20*) | Havelaar et al. (*21*) | Butler et al. (22) | Vally et al. (*23*) | This study |
| Country | United States | AMR A (Canada, Cuba, USA) | Netherlands | Canada | Australia | United States |
| Type | Outbreak surveillance data or published studies | SEJ | SEJ | SEJ | SEJ | SEJ |
| Bacteria | | | | | | |
| *Brucella* spp. | 50 | 75 | NE | 34.6 | NE | 45 |
| *Campylobacter* spp. | 80 | 73 | 42 | 62.3 | 76 | 57 |
| STEC O157 | 68 | 59 | 40 | 61.4 | Combined as all STEC, 55 | 60 |
| STEC non-O157 | 82 | NE | 42 | 59.7 | Combined as all STEC, 55 | 50 |
| Enterotoxigenic *Escherichia coli* | 100 (only foodborne) | 36 | NE | 44.4 | Combined as other pathogenic *E. coli*, 24 | 69 |
| *E. coli*, other diarrheagenic | 30 | NE | NE | 41 | Combined as other pathogenic *E. coli*, 24 | 55 |
| *Mycobacterium bovis* | 95 | NE | NE | NE | NE | 75 |
| *Salmonella* spp. | 94 | 73 | 55 | 62.9 | 71 | 66 |
| *Shigella* spp. | 31 | 12 | NE | 25.9 | 11 | 8 |
| *Vibrio vulnificus* | 47 | NE | NE | 70.6 | NE | Non-AGI, 20 |
| *Vibrio parahaemolyticus* | 86 | NE | NE | 82.8 | NE | AGI, 74 |
| *Vibrio* spp. other | 57 | NE | NE | 88.9 | NE | Non-AGI, 8<br>AGI, 96<br>Non-AGI-95 |
| *Yersinia enterocolitica* | 90 | NE | NE | 82.8 | NE | 77 |
| Protozoa | | | | | | |
| *Cryptosporidium* spp. | 8 | 16 | 12 | 11.3 | NE | 7 |
| *Cyclospora cayetanensis* | 99 | NE | NE | 83.1 | NE | 83 |
| *Giardia* spp. | 7 | 11 | 13 | 7.2 | NE | 10 |
| *Toxoplasma gondii* | 50 | 60 | 56 | 51.4 | NE | 28 |
| Viruses | | | | | | |
| Astrovirus | <1 | NE | NE | 9.9 | NE | 15 |
| Hepatitis A virus | 7 | 42 | 11 | 29.5 | 12 | 42 |
| Norovirus | 26 | 23 | 17 | 18.4 | 17 | 19 |
| Rotavirus | <1 | NE | 13 | 7.3 | NE | 5 |
| Sapovirus | <1 | NE | NE | 16.9 | NE | 13 |

*NE, not estimated; SEJ, structured expert judgment; STEC, Shiga toxin–producing *Escherichia coli*.

**Table 8.** Comparison of proportion of illnesses attributed to waterborne transmission from this and earlier published studies*

| Details | Study | | | |
|---|---|---|---|---|
| | Hald et al. (*20*) | Butler et al. (*22*) | Vally et al. (*23*) | This study |
| Country | AMR A (Canada, Cuba, USA) | Canada | Australia | United States |
| Type | SEJ | SEJ | SEJ | SEJ |
| Bacteria | | | | |
| *Brucella* spp. | 1 | 4 | NE | 10 |
| *Campylobacter* spp. | 11 | 9.3 | 6 | 13 |
| STEC O157 | 7 | 13.3 | Combined as all STEC, 8 | 5 |
| STEC non-O157 | NE | 11.4 | Combined as all STEC, 8 | 6 |
| Enterotoxigenic *Escherichia coli* | 42 | 15.3 | Combined as other *E. coli*, 14 | 9 |
| *E. coli*, other diarrheagenic | NE | 15.6 | Combined as other *E. coli*, 14 | 9 |
| *Salmonella* spp. | 2 | 8 | 5 | 6 |
| *Shigella* spp. | 10 | 12.2 | 4 | 4 |
| *Vibrio vulnificus* | NE | 23.2 | NE | Non-AGI, 78 |
| *V. parahaemolyticus* | NE | 11 | NE | AGI, 24; non-AGI, 90 |
| *Vibrio* spp. other | NE | 7.6 | NE | AGI, 2; non-AGI, 3 |
| Protozoa | | | | |
| *Cryptosporidium* spp. | 37 | 36.8 | NE | 43 |
| *Cyclospora cayetanensis* | NE | 7.7 | NE | 6 |
| *Giardia* spp. | 42 | NE | NE | 44 |
| *Toxoplasma gondii* | 19 | 8.8 | NE | 5 |
| Viruses | | | | |
| Astrovirus | NE | 6.8 | NE | 6 |
| Hepatitis A virus | 1 | 6.2 | 4 | 8 |
| Norovirus | 22 | 7.4 | 3 | 6 |
| Rotavirus | NE | 5.9 | NE | 7 |
| Sapovirus | NE | 1.4 | NE | 8 |

*NE, not estimated; SEJ, structured expert judgment; STEC, Shiga toxin–producing *Escherichia coli*.

handler-related (*20*). However, this study was conducted before widespread awareness of a massive increase in person-to-person transmission in the United States (*27*). Previous estimates of foodborne transmission were 11% in the Netherlands and 7% in the United States (*2*,*21*). The use of different pathway definitions, points of attribution, and inclusion of travel-related illness in these other studies might have contributed to these differences (*21*,*28*). For norovirus, 71% (UI 29%–99%) of foodborne transmission in our study was attributed to the food handler subpathway, which is supported by studies of outbreaks in the United States (*29*,*30*).

For the waterborne transmission pathway, attribution in the context of the other pathways has not been done before in the United States. Furthermore, these estimates include subpathway estimates and non-gastroenteritis clinical outcomes. For bacterial pathogens, the estimates suggest that the proportion of illnesses linked to water is higher than previously appreciated. The estimates for waterborne bacterial pathogens were associated with high rates of illness and death, including nontuberculous *Mycobacterium* spp., *Pseudomonas* spp., and *Legionella* spp. Of note, neither *Giardia* spp. nor *Cryptosporidium* spp., parasites traditionally understood to be waterborne, were assessed as predominantly waterborne; instead, person-to-person and animal contact, particularly for *Cryptosporidium*, were key pathways. For the free-living amebae *Acanthamoeba* spp., *B. mandrillaris*, and *N. fowleri*, limited data are available on exact exposures associated with these rare illnesses (*31*,*32*). The proportion of viral pathogens transmitted by water was estimated to be relatively low (6%–8%), although for norovirus this represents a substantial proportion of estimated annual waterborne disease illnesses (*32*). This study also provides estimates for 3 waterborne disease subpathways. Of note is the proportion of otitis externa infections caused by *Pseudomonas* spp. that were attributed to recreational water exposure, and the combined contribution of drinking and nonrecreational, nondrinking water exposures to nongastroenteritis outcomes of *Pseudomonas* spp. (excluding otitis externa), nontuberculous *Mycobacterium* spp., and *Legionella* spp. CDC has used results from this SEJ to help estimate that 7.2 million waterborne illnesses occur from 17 pathogens annually, including 600,000 emergency department visits, 120,000 hospitalizations, and 7,000 deaths, incurring $3.2 billion (2014 US dollars) in direct healthcare costs (*33*).

Whereas the primary focus of this SEJ study was illnesses transmitted commonly by food and water, including person-to-person, animal contact, and environmental transmission was integral to the study and led to notable findings. For example, this study estimated animal contact transmission of STEC O157 at 12% (UI 3%–25%) and of STEC non-O157 at 21% (UI 2%–46%). Previous US animal contact estimates, which were based on a FoodNet case-control study and outbreak surveillance data, estimated STEC O157 at 6% and STEC non-O157 at 8% (*24*). This discrepancy may be the result of differences in pathway definitions and the inclusion of additional data.

As with other SEJ studies, this study is subject to limitations that can affect the interpretation of results. Estimates for many pathogens had wide UIs, highlighting areas in which data gaps remain and further investment into public health surveillance and research may be warranted. More detailed attribution, such as by food category, was beyond the scope of this study. This study considered attribution at a national level and does not represent the geographic variability that exists for some pathogens. Experts provided estimates considering data available during the elicitation session, but infectious disease epidemiology can change rapidly, so these results may not reflect current transmission patterns. New information should be considered when applying these estimates (e.g., for disease burden calculations). Expert fatigue may have been a factor for participants who were asked to provide estimates for a large number of pathogens. For intervention and policy-making purposes, these results should be considered in context with results from other data-driven approaches, such as those done by the Interagency Food Safety Analytics Collaboration and for the Model Aquatic Health Code (*34*,*35*).

In conclusion, our findings provide a balanced understanding of multiple routes of transmission for 33 pathogens. This information can be used to support appropriate targeting of resources to prevent infections transmitted by all pathways and to invest in research and surveillance.

### Acknowledgments

We thank all those who contributed their expertise and time to this study, especially our expert participants, dry run participants, subject matter experts at CDC, and other CDC and University of Florida staff who assisted.

### About the Author

Dr. Beshearse is an Epidemic Intelligence Service officer in the National Center for Emerging and Zoonotic Infectious Diseases at the Centers for Disease Control and Prevention, Atlanta, Georgia, USA. Her primary research interests include public health and foodborne and waterborne diseases.

### References

1. Havelaar AH, Kirk MD, Torgerson PR, Gibb HJ, Hald T, Lake RJ, et al.; World Health Organization Foodborne Disease Burden Epidemiology Reference Group. World Health Organization global estimates and regional comparisons of the burden of foodborne disease in 2010. PLoS Med. 2015;12:e1001923. https://doi.org/10.1371/journal.pmed.1001923
2. Scallan E, Hoekstra RM, Angulo FJ, Tauxe RV, Widdowson MA, Roy SL, et al. Foodborne illness acquired in the United States—major pathogens. Emerg Infect Dis. 2011;17:7–15. https://doi.org/10.3201/eid1701.P11101
3. Colford JM Jr, Roy S, Beach MJ, Hightower A, Shaw SE, Wade TJ. A review of household drinking water intervention trials and an approach to the estimation of endemic waterborne gastroenteritis in the United States. J Water Health. 2006;4(Suppl 2):71–88. https://doi.org/10.2166/wh.2006.018
4. Messner M, Shaw S, Regli S, Rotert K, Blank V, Soller J. An approach for developing a national estimate of waterborne disease due to drinking water and a national estimate model application. J Water Health. 2006;4(Suppl 2):201–40. https://doi.org/10.2166/wh.2006.024
5. Painter JA, Hoekstra RM, Ayers T, Tauxe RV, Braden CR, Angulo FJ, et al. Attribution of foodborne illnesses, hospitalizations, and deaths to food commodities by using outbreak data, United States, 1998–2008. Emerg Infect Dis. 2013;19:407–15. https://doi.org/10.3201/eid1903.111866
6. Hall AJ, Wikswo ME, Manikonda K, Roberts VA, Yoder JS, Gould LH. Acute gastroenteritis surveillance through the National Outbreak Reporting System, United States. Emerg Infect Dis. 2013;19:1305–9. https://doi.org/10.3201/eid1908.130482
7. O'Brien SJ, Gillespie IA, Sivanesan MA, Elson R, Hughes C, Adak GK. Publication bias in foodborne outbreaks of infectious intestinal disease and its implications for evidence-based food policy. England and Wales 1992–2003. Epidemiol Infect. 2006;134:667–74. https://doi.org/10.1017/S0950268805005765
8. Verhoef L, Hewitt J, Barclay L, Ahmed SM, Lake R, Hall AJ, et al. Norovirus genotype profiles associated with foodborne transmission, 1999–2012. Emerg Infect Dis. 2015;21:592–9. https://doi.org/10.3201/eid2104.141073
9. Hoffmann S, Fischbeck P, Krupnick A, McWilliams M. Informing risk-mitigation priorities using uncertainty measures derived from heterogeneous expert panels: a demonstration using foodborne pathogens. Reliab Eng Syst Saf. 2008;93:687–98. https://doi.org/10.1016/j.ress.2007.03.010
10. Colson AR, Cooke RM. Expert elicitation: using the classical model to validate experts' judgments. Rev Environ Econ Policy. 2018;12:113–32. https://doi.org/10.1093/reep/rex022
11. Cooke RM, Goossens LHJ. Procedures guide for structured expert judgment. Delft (the Netherlands): Delft University of Technology; 1999.
12. Cooke RM. Experts in uncertainty: opinion and subjective probability in science. New York: Oxford University Press; 1991.
13. Collier SA, Stockman LJ, Hicks LA, Garrison LE, Zhou FJ, Beach MJ. Direct healthcare costs of selected diseases

primarily or partially transmitted by water. Epidemiol Infect. 2012;140:2003–13. https://doi.org/10.1017/S0950268811002858
14. Boore AL, Hoekstra RM, Iwamoto M, Fields PI, Bishop RD, Swerdlow DL. *Salmonella enterica* infections in the United States and assessment of coefficients of variation: a novel approach to identify epidemiologic characteristics of individual serotypes, 1996–2011. PLoS One. 2015;10:e0145416. https://doi.org/10.1371/journal.pone.0145416
15. Centers for Disease Control and Prevention. National Outbreak Reporting System (NORS) user guidance—waterborne disease outbreaks. 2017 [cited 2019 Jan 18]. https://www.cdc.gov/nors/pdf/CDC_5212_guidance.pdf
16. Centers for Disease Control and Prevention. National Outbreak Reporting System (NORS) guidance. 2017 [cited 2019 Jan 18]. https://www.cdc.gov/nors/downloads/guidance.pdf
17. Sedgewick R, Wayne K. Algorithms, 4th ed. Upper Saddle River (NJ): Addison-Wesley; 2011.
18. R Core Team. R: a language and environment for statistical computing. Vienna: R Foundation for Statistical Computing; 2017.
19. EXCALIBUR [computer software]. Version 1.0. Delft (the Netherlands): TU Delft; 1989.
20. Hald T, Aspinall W, Devleesschauwer B, Cooke R, Corrigan T, Havelaar AH, et al. World Health Organization estimates of the relative contributions of food to the burden of disease due to selected foodborne hazards: a structured expert elicitation. PLoS One. 2016;11:e0145839. https://doi.org/10.1371/journal.pone.0145839
21. Havelaar AH, Galindo AV, Kurowicka D, Cooke RM. Attribution of foodborne pathogens using structured expert elicitation. Foodborne Pathog Dis. 2008;5:649–59. https://dx.doi.org/10.1089/fpd.2008.0115
22. Butler AJ, Thomas MK, Pintar KD. Expert elicitation as a means to attribute 28 enteric pathogens to foodborne, waterborne, animal contact, and person-to-person transmission routes in Canada. Foodborne Pathog Dis. 2015;12:335–44. https://doi.org/10.1089/fpd.2014.1856
23. Vally H, Glass K, Ford L, Hall G, Kirk MD, Shadbolt C, et al. Proportion of illness acquired by foodborne transmission for nine enteric pathogens in Australia: an expert elicitation. Foodborne Pathog Dis. 2014;11:727–33. https://doi.org/10.1089/fpd.2014.1746
24. Hale CR, Scallan E, Cronquist AB, Dunn J, Smith K, Robinson T, et al. Estimates of enteric illness attributable to contact with animals and their environments in the United States. Clin Infect Dis. 2012;54(Suppl 5):S472–9. https://doi.org/10.1093/cid/cis051
25. Mermin J, Hutwagner L, Vugia D, Shallow S, Daily P, Bender J, et al.; Emerging Infections Program FoodNet Working Group. Reptiles, amphibians, and human *Salmonella* infection: a population-based, case-control study. Clin Infect Dis. 2004;38(Suppl 3):S253–61. https://doi.org/10.1086/381594
26. Centers for Disease Control and Prevention. National Outbreak Reporting System (NORS) [cited 2019 Jan 18]. https://www.cdc.gov/nors/about.html
27. Foster MA, Hofmeister MG, Kupronis BA, Lin Y, Xia GL, Yin S, et al. Increase in hepatitis A virus infections—United States, 2013–2018. MMWR Morb Mortal Wkly Rep. 2019;68:413–5. https://doi.org/10.15585/mmwr.mm6818a2
28. Centers for Disease Control and Prevention. Surveillance for viral hepatitis—United States, 2015 [cited 2019 Oct 15]. https://www.cdc.gov/hepatitis/statistics/2015surveillance/index.htm
29. Hall AJ, Wikswo ME, Pringle K, Gould LH, Parashar UD; Division of Viral Diseases, National Center for Immunization and Respiratory Diseases, CDC. Vital signs: foodborne norovirus outbreaks—United States, 2009–2012. MMWR Morb Mortal Wkly Rep. 2014;63:491–5.
30. Hall AJ, Eisenbart VG, Etingüe AL, Gould LH, Lopman BA, Parashar UD. Epidemiology of foodborne norovirus outbreaks, United States, 2001–2008. Emerg Infect Dis. 2012;18:1566–73. https://doi.org/10.3201/eid1810.120833
31. Centers for Disease Control and Prevention. Balamuthia amebic encephalitis—California, 1999–2007. MMWR Morb Mortal Wkly Rep. 2008;57:768–71.
32. Cope JR, Murphy J, Kahler A, Gorbett DG, Ali I, Taylor B, et al. Primary amebic meningoencephalitis associated with rafting on an artificial whitewater river: case report and environmental investigation. Clin Infect Dis. 2018;66:548–53. https://doi.org/10.1093/cid/cix810
33. Collier SA, Deng L, Adam EA, Benedict KM, Beshearse EM, Blackstock A, et al. Estimate of burden and direct healthcare cost of infectious waterborne disease in the United States. Emerg Infect Dis. 2020 Dec XX [Epub ahead of print]. https://doi.org/10.3201/eid2701.190676
34. Blake R, Peters J. Model Aquatic Health Code (MAHC) and International Swimming Pool and Spa Code (ISPSC). J Environ Health. 2012;74:36–9.
35. Centers for Disease Control and Prevention. Model Aquatic Health Code; 2018 [cited 2019 Feb 13]. https://www.cdc.gov/mahc/index.html

Address for correspondence: Elizabeth Beshearse, Centers for Disease Control and Prevention, 1600 Clifton Rd, Mailstop H16-3, Atlanta, GA 30329-4027, USA; email: pgz1@cdc.gov

# Territorywide Study of Early Coronavirus Disease Outbreak, Hong Kong, China

Kenneth Siu-Sing Leung, Timothy Ting-Leung Ng, Alan Ka-Lun Wu, Miranda Chong-Yee Yau, Hiu-Yin Lao, Ming-Pan Choi, Kingsley King-Gee Tam, Lam-Kwong Lee, Barry Kin-Chung Wong, Alex Yat-Man Ho, Kam-Tong Yip, Kwok-Cheung Lung, Raymond Wai-To Liu, Eugene Yuk-Keung Tso, Wai-Shing Leung, Man-Chun Chan, Yuk-Yung Ng, Kit-Man Sin, Kitty Sau-Chun Fung, Sandy Ka-Yee Chau, Wing-Kin To, Tak-Lun Que, David Ho-Keung Shum, Shea Ping Yip, Wing Cheong Yam, Gilman Kit-Hang Siu

Initial cases of coronavirus disease in Hong Kong were imported from mainland China. A dramatic increase in case numbers was seen in February 2020. Most case-patients had no recent travel history, suggesting the presence of transmission chains in the local community. We collected demographic, clinical, and epidemiologic data from 50 patients, who accounted for 53.8% of total reported case-patients as of February 28, 2020. We performed whole-genome sequencing to determine phylogenetic relationship and transmission dynamics of severe acute respiratory syndrome coronavirus 2 infections. By using phylogenetic analysis, we attributed the community outbreak to 2 lineages; 1 harbored a common mutation, *Orf3a*-G251V, and accounted for 88.0% of the cases in our study. The estimated time to the most recent common ancestor of local coronavirus disease outbreak was December 24, 2019, with an evolutionary rate of $3.04 \times 10^{-3}$ substitutions/site/year. The reproduction number was 1.84, indicating ongoing community spread.

Coronavirus disease (COVID-19) refers to a cluster of viral pneumonia cases that first occurred in Wuhan, a city in Hubei Province, China, beginning in December 2019. Etiology was unknown during the early stage of the outbreak until a novel coronavirus, severe acute respiratory syndrome coronavirus 2 (SARS-CoV-2), was isolated on January 7, 2020, and the genome was sequenced (*1*).

During the initial outbreak, fever was the main symptom of COVID-19, and about one third of patients experienced acute respiratory distress syndrome. Approximately 16% of patients were in severe condition at admission, and the estimated mortality rate was 1.4% (*2*). Sustained human-to-human transmission was confirmed upon identification of cases clustering among families and transmission from patients to healthcare workers (*3*,*4*), which triggered China's urgent public health actions and international concern.

As of February 28, 2020, a total of 78,824 COVID-19 cases had been diagnosed in mainland China and 2,788 persons had died. The disease had also spread to 50 other countries (*5*). The World Health Organization declared COVID-19 a pandemic in March 2020.

In Hong Kong, the first imported case was identified on January 23, 2020; the case-patient was a resident of mainland China who traveled to Hong Kong from Wuhan through Shenzhen by high-speed rail. The first local case with unknown source (i.e., patient who had no travel record during the 14-day incubation period) was reported on February 4, 2020 (*6*).

By February 28, 2020, a total of 93 COVID-19 cases had been recorded in Hong Kong; ≥70 (75.3%) of those were local cases and those case-patients' close contacts (*6*,*7*). Secondary and tertiary transmissions were observed in some case clusters. Because source of infection is unknown in most index cases in these clusters, hidden transmission chains were believed to be present in the community.

Author affiliations: The University of Hong Kong, Hong Kong, China (K.S.-S. Leung, K.K.-G. Tam, W.C. Yam); The Hong Kong Polytechnic University, Hong Kong (T.T.-L. Ng, H.-Y. Lao, M.-P. Choi, L.-K. Lee, D.H.-K. Shum, S.P. Yip, G.K.-H. Siu); Pamela Youde Nethersole Eastern Hospital, Hong Kong (A.K.-L. Wu, M.C.-Y. Yau, K.-C. Lung); United Christian Hospital, Hong Kong (B.K.-C. Wong, E.Y.-K. Tso, K.S.-C. Fung, S.K.-Y. Chau); Princess Margaret Hospital, Hong Kong (A.Y.-M. Ho, W.-S. Leung, M.-C. Chan, W.-K. To); Tuen Mun Hospital, Hong Kong (K.-T. Yip, Y.-Y. Ng, K.-M. Sin, T.-L. Que); Ruttonjee Hospital, Hong Kong (R.W.-T. Liu)

DOI: https://doi.org/10.3201/eid2701.201543

We report the demographic, clinical, and epidemiologic data of 50 hospitalized patients who accounted for 53.8% of COVID-19 cases in Hong Kong at the data cutoff point (February 28, 2020), including 3 imported cases and 6 transmission clusters of local infections. We characterized viral genomes in all these cases by using nanopore and Illumina sequencing. Phylogenetic and molecular evolutionary analyses were performed to determine the transmission link and the evolutionary rate of COVID-19 cases in the community.

## Methods

### Cases

For this retrospective, multicenter study, we enrolled case-patients with laboratory-confirmed COVID-19 from 4 public hospital clusters managed under the Hospital Authority of Hong Kong, namely Hong Kong East Cluster, Kowloon East Cluster, Kowloon West Cluster, and New Territories West Cluster, during January 26–February 28, 2020. Sputum specimens and throat swab specimens pooled with nasopharyngeal aspirates were collected from patients who fulfilled the reporting or enhanced surveillance criteria at hospital admission (*8*). Laboratory-confirmed infection was defined as the detection of SARS-CoV-2 by real-time reverse transcription PCR, which amplified the envelope (*E*) gene and RNA-dependent RNA polymerase (*RdRp*) gene (*9*).

We obtained demographic, clinical, and microbiologic data from patients' medical records. Epidemiologic information was retrieved from the Centre for Health Protection of the Department of Health (*6*) and the website https://wars.vote4.hk (*7*). The definitions of clinical symptoms and complications are based on World Health Organization guidance (*10*). We adopted the Centre for Health Protection case numbering system, which is based on the date of case confirmation. This study was approved by the Institutional Review Boards of The Hong Kong Polytechnic University (approval no. RSA20021) and the public hospitals involved (HKECREC-20200014; KCC/KEC-20200070; KWC-20200040; NTWC-20200038).

### Specimen Preparation

The respiratory specimens were centrifuged at 16,000 × *g* for 2 minutes. Total nucleic acid was extracted from supernatant using MagNA Pure 96 System (Roche, https://lifescience.roche.com) or NucliSENS easyMAG (bioMérieux, https://www.biomerieux-nordic.com) according to the manufacturers' instructions. DNase treatment was done by using TURBO DNA-free Kit (ThermoFisher Scientific, https://www.thermofisher.com) to remove residual host DNA.

### Reverse Transcription and Viral Genome Amplification Using Multiplex PCR

DNase-treated RNA was reverse-transcribed using random hexamers and SuperScript IV Reverse Transcriptase (ThermoFisher Scientific) as previously described (*11*). Viral cDNA was then amplified by using 2 PCRs containing tiled, multiplexed primers (Appendix 1 Table 1, https://wwwnc.cdc.gov/EID/article/27/1/20-1543-App1.xlsx) described in the ARTIC protocol (https://artic.network/ncov-2019) (*12*). Details of the multiplex PCR are provided in Appendix 2 (https://wwwnc.cdc.gov/EID/article/27/1/20-1543-App2.pdf).

### Nanopore MinION Sequencing

Ligation-based 1D sequencing was carried out by using Litigation Sequencing Kit SQK-LSK109 (Oxford Nanopore Technologies, https://nanoporetech.com) according to manufacturer's instructions. Multiplex PCR amplicons of each sample were normalized to 1 ng/μL before end-repair and native barcode ligation by using EXP-NBD104/114 (Oxford Nanopore Technologies). Barcoded samples were pooled and ligated to AMII sequencing adaptor. Sequencing was performed with Nanopore MinION device (Oxford Nanopore Technologies) by using R9.4.1 flow cell for 48 hours.

### Illumina MiSeq Sequencing

Multiplex PCR amplicons were subjected to library preparation and dual-indexing by using KAPA HyperPrep Kit and Unique Dual-Indexed Adaptor Kit (Roche) according to manufacturer's instructions. Ligated libraries were enriched by 6-cycle PCR amplification and purification and size selection by using AMPure XP beads (Beckman Coulter, https://www.beckmancoulter.com/). The pooled library was sequenced with the MiSeq Reagent Kit V2 Nano on an Illumina MiSeq System (Illumina, https://www.illumina.com).

### Bioinformatic Analysis

We analyzed nanopore sequencing data using modified Artic Network nCoV-2019 novel coronavirus bioinformatics protocol (Appendix 2) (*13*). Illumina sequencing reads were mapped with reference to respective consensus genome of each sample constructed from nanopore data. Variants were called by using freebayes version 1.0.0 (https://github.com/freebayes/

freebayes) with haploid decoding and minimum base quality set at Q30. Consensus genomes were constructed by GATK 4.1.4.1 based on the VCF file (*14*). SPAdes genome assembler 3.14.0 (https://cab.spbu.ru/software/spades) and minimap2 version 2.17 (https://anaconda.org/bioconda/minimap2) were used to combine nanopore and Illumina sequencing results for de novo assembly and to identify the sequence of the unmapped gap regions. The sequences have been submitted to GenBank (accession nos. MT232662711).

### Genomic and Phylogenetic Analysis

To identify the amino acid change caused by each single-nucleotide polymorphism, we BLAST-searched the consensus genome of each specimen against the reference NC_045512.2 using BLASTX (https://blast.ncbi.nlm.nih.gov/Blast.cgi). Nonsynonymous mutations were identified using custom Python script (https://github.com/kenssl/Blast_mismatch_search).

Consensus genomes were aligned by Clustal Omega 1.2.4 (https://www.ebi.ac.uk/Tools/msa/clustalo). Phylogenetic tree was constructed with PhyML 3.0 (http://www.atgc-montpellier.fr/phyml/) using the maximum-likelihood algorithm. Best-fitting substitution model was selected by Akaike information criteria, in which we selected the general time-reversible model with fixed proportion of invariable sites (*15*). Bootstrap replicates were set at 1,000×, and maximum-likelihood phylogenetic tree was rooted on the earliest published genome (accession no. NC_045512.2). Transmission clusters were defined by clear epidemiologic and onset-time relationship. Meanwhile, we downloaded an additional 478 SARS-CoV-2 genomes from the GISAID (https://www.gisaid.org) SARS-CoV-2 data hub (*16*) and analyzed the phylogenetic relationships by using maximum-likelihood with bootstrap value set at 500× and rooted on SARS-CoV-2 genome NC_045512.2.

### Estimation of Evolutionary Rate and Divergence Time of Transmission

To reconstruct the evolutionary model of COVID-19 cases using the viral genomes obtained in Hong Kong, we implemented Bayesian inference through Markov Chain Monte Carlo (MCMC) framework in BEAST version 2.6.2 (*17*). Death rate δ (which refers to the time needed for a case-patient to become noncontagious) was determined as the lag time between date of symptom onset and date of hospital admission, because the transmission link in Hong Kong was practically stopped once the patient was hospitalized. Bayesian phylodynamic analysis was performed using strict clock and relaxed clock models with coalescent exponential growth tree priors. We ran MCMC chains for $10^9$ generations and sampled every 500 steps. Bayesian output was analyzed after the results were visualized by Tracer version 1.7.1 (*18*). All parameters had an effective sample size of >200, indicating sufficient sampling.

## Results

Our investigation included 50 COVID-19 patients; 54.0% were women, and the mean age was 55.2 (range 22–96) years (Table 1). Of the case-patients, we categorized 3 cases as imported because the patients stayed in Wuhan before traveling to Hong Kong in mid-January. Four patients traveled to Japan and other provinces of China in mid-January and were hospitalized after they returned to Hong Kong, but active community transmission of COVID-19 was not officially reported in these areas during the study period, so these cases were considered possible local infections. The other 43 patients' cases were categorized as local infection because of no recent travel history.

Eighteen (36.0%) patients had chronic illnesses, of which cardiovascular and cerebrovascular diseases were the most common (Table 1). In total, 74.0% of the patients were experiecncing cough at admission. Fever occurred in 58.0% of patients at time of admission, but that rate gradually increased to 64.0% during the course of hospitalization. Other less common symptoms were muscle aches (25.0%), sore throat

**Table 1.** Demographics, travel record, and baseline medical history of 50 coronavirus disease patients, Hong Kong, February 2020*

| Characteristic | Case-patients, n = 50 |
|---|---|
| Age group, y | |
| Mean (SD) | 55.2 (19.5) |
| Range | 22–96 |
| ≤30 | 8 (16.0) |
| 31–40 | 5 (10.0) |
| 41–50 | 6 (12.0) |
| 51–60 | 11 (22.0) |
| 61–70 | 10 (20.0) |
| ≥71 | 10 (20.0) |
| Sex | |
| F | 27 (54.0) |
| M | 23 (46.0) |
| Travel record ≤14 d before symptom onset | 7 (14.0) |
| Wuhan, Hubei Province, China | 3 (6.0) |
| Other regions in mainland China | 1 (2.0) |
| Regions outside mainland China | 3 (6.0) |
| No travel record | 43 (86.0) |
| Chronic medical illnesses | 18 (36.0) |
| Cardiovascular and cerebrovascular diseases | 14 (28.0) |
| Endocrine system diseases | 11 (22.0) |
| Nervous system diseases | 5 (10.0) |
| Digestive system diseases | 4 (8.0) |
| Malignant tumor | 1 (2.0) |

*Values are no. (%) except as indicated.

(24.0%), shortness of breath (24.0%), and diarrhea (14.3%) (Table 2). Two persons (4.0%) were asymptomatic throughout the study period. On radiologic examination, 27 (54.0%) had bilateral pneumonia, 11 (22.0%) had unilateral pneumonia, and 17 (34.7%) showed multiple areas of mottling and ground-glass opacity. None of the patients were co-infected with other respiratory viruses or fungi.

Intensive care unit admission was relatively uncommon (3/50, 6.0%) in our cohort compared with admission rates in previous studies (*19*–*22*). This difference could be attributed to underdiagnosis of milder cases during the initial COVID-19 outbreak in China. One patient's sputum specimen was culture-positive for *Klebsiella aerogenes* bacteria; a second patient's specimen was culture-positive for *Ralstonia pickettii* bacteria. Both had acute respiratory distress syndrome and acute respiratory injury accompanied by septic shock or acute renal injury and required admission to the intensive care unit.

Of the 50 case-patients, 42 (84.0%) could be clustered based on their epidemiologic links (Figure 1, https://wwwnc.cdc.gov/EID/article/27/1/20-1543-F1.htm). We identified 6 transmission clusters (clusters 1–6). Cluster 1 involved a 4-member family. The father, who traveled to Guangdong, China, in late January 2020, was believed to have infected his wife and subsequently their daughter and son-in-law at a family gathering. Clusters 2 and 3 were family clusters of local infection and unknown source. Both clusters involved 3 household members with no recent travel history. Cluster 4 was attributed to a superspreading event (SSE): a barbecue and hotpot party involving 19 family members in late January. Symptom onset in these patients occurred during days 2–13 after the party. A colleague of 1 infected person, who did not attend the party, also tested positive for SARS-CoV-2. Cluster 5 initiated from a resident of a public housing estate, in whom COVID-19 was diagnosed on January 30. Eleven days later, diagnoses were made in 3 members of a household that resided in the same building (10 stories below) the index case-patient. Two household members subsequently attended a family gathering of 29 persons at a Chinese restaurant during the incubation period. COVID-19 was diagnosed consecutively in 3 persons ≈2 weeks after the gathering. In addition, a Filipino domestic aide of 1 infected family member, who did not attend the family gathering, also tested positive. For cluster 6, the first reported case was in a 70-year-old woman who visited a Buddhist worship hall during the Chinese New Year. A further 8 persons who visited the same Buddhist worship hall during this period later tested positive for SARS-CoV-2. At the data cutoff point, ≥4 other household members who had never been to the worship hall also tested positive. Details of the demographic and epidemiologic information on the cases and clusters are provided in Appendix 1 Tables 2–8.

**Table 2.** Clinical characteristics and outcomes of 50 coronavirus disease patients, Hong Kong, February 2020*

| Characteristic | Case-patients, n = 50* |
|---|---|
| Signs and symptoms | |
| Fever at admission | 29 (58.0) |
| Fever during hospitalization | 32 (64.0) |
| Cough | 37 (74.0) |
| Sore throat | 12 (24.0) |
| Shortness of breath | 12 (24.0) |
| Muscle ache | 12 (25.0)† |
| Diarrhea | 7 (14.3)‡ |
| Rhinorrhea | 4 (8.0) |
| Nausea and vomiting | 4 (8.2)‡ |
| Confusion | 1 (2.0) |
| >1 sign or symptom | 41 (82.0) |
| Asymptomatic | 2 (4.0) |
| Complications§ | |
| Acute respiratory distress syndrome | 2 (4.0) |
| Acute respiratory injury | 1 (2.0) |
| Acute renal injury | 5 (10.0) |
| Septic shock | 1 (2.0) |
| >1 complication | 2 (4.0) |
| No complications | 45 (90.0) |
| Radiological findings | |
| Unilateral pneumonia | 11 (22.0) |
| Bilateral pneumonia | 27 (54.0) |
| Multiple areas of mottling and ground-glass opacity | 17 (34.7)‡ |
| No abnormality | 4 (8.0) |
| Coinfection | |
| Other viruses | 0 |
| Bacteria | 2 (4.0)¶ |
| Fungi | 0 |
| Clinical outcome# | |
| In serious condition, ICU admission | 3 (6.0) |
| Hospitalized, in stable condition | 27 (54.0) |
| Discharged | 20 (40.0) |
| Interval from symptom onset to hospital admission, d** | |
| Average (SD) | 8.5 (3.9) |
| Range | 1–26 |
| Length of hospital stay, d†† | |
| Average (SD) | 17.7 (7.7) |
| Range | 8–35 |

*Values are no. (%) except as indicated. ICU, intensive care unit.
†Data were missing for 2 patients.
‡Data were missing for 1 patient.
§Definitions of complications are provided in Appendix 2 (https://wwwnc.cdc.gov/EID/article/27/1/20-1543-App2.pdf).
¶Moderate growth of *Klebsiella aerogenes* and *Ralstonia pickettii* bacteria were obtained from sputum specimens collected from case 38 and 70.
#Data cutoff of the clinical outcome of patients was February 28, 2020.
**Data from symptomatic patients were excluded.
††Calculated based on the 18 patients who had been discharged as of February 28, 2020.

Consensus genomes of all 50 cases were constructed based on nanopore sequencing and refined by Illumina sequencing. On average, 62,387 reads/genome were obtained with 550× coverage for nanopore, and 18,747 reads/genome were obtained with 132× coverage for Illumina platform. The consensus genome size was ≈29.9

kbp with GC content ≈38%. The genomes were highly conserved with the first SARS-CoV-2 genome and had an average sequence identity of 99.98% (range 99.94%–100.0%). We identified 64 nonsynonymous substitutions from all 50 genomes (Appendix 1 Table 9). *Orf3a*-G251V was the most frequent amino acid substitution; 44/50 (88.0%) of the samples harbored this mutation, after which *Orf1ab*-H3233Y (30/50, 60.0%) and *S*-L8V (27/50, 54.0%) were most common.

Genomewide single-nucleotide polymorphisms were used to contextualize phylogenetic placement of Hong Kong strains in SARS-CoV-2 global phylogeny (Appendix 2 Figure 1). However, because the samples were taken at the early stage of global outbreak, the genetic variability between strains was limited, resulting in several unresolved branches and marginal supporting bootstrap values. Nevertheless, when compared with SARS-CoV-2 strains isolated from other regions, Hong Kong strains tended to aggregate mainly in 2 lineages. Lineage 1 consisted of 4 Hong Kong strains that clustered with most isolates from China (n = 32). Lineage 2, which consisted of 44 Hong Kong strains, was more closely related to strains seen in South Korea (n = 7) and France (n = 5).

In examining the phylogeny of the COVID-19 outbreak in Hong Kong, we identified 2 distinctive groups (Figure 2). The first group consisted of 2 imported cases and the cases in cluster 1. The second group originated with a single robust node with bootstrap value of 94% and a common mutation *Orf3a*-G251V. The second group could be further separated into 3 subgroups. The first subgroup mainly consisted of the cases in cluster 5, the public housing estate–related SSE. The second subgroup included cases in cluster 4 associated with the family hotpot party, cluster 3, and 2 isolated cases (case 23 and case 43). These samples shared the same missense mutations at *S*-L8V and *Orf1ab*-H3233Y. Finally, the third subgroup included the cases from cluster 6, an SSE originating from a Buddhist worship hall, in which *Orf1ab*-G295V were identified.

According to Bayesian time-scaled phylodynamic analysis, strict clock and relaxed clock models estimated the time of most recent common ancestor of COVID-19 outbreak in Hong Kong as December 24, 2019 (95% Bayesian credible interval [BCI] December 11, 2019–January 5, 2020). The evolutionary rate was $3.04 \times 10^{-3}$ substitutions/site/year (95% BCI 2.04–4.09 $\times 10^{-3}$ substitutions/site/year) (Appendix 2 Figure 2). Based on demographic data, the average time from symptom onset to hospital admission was ≈8.5 days. The estimated reproduction number was calculated at 1.84 (95% BCI 1.37–2.35).

## Discussion

This study provides a territorywide overview of the early COVID-19 outbreak in Hong Kong, an international city with borders connecting to mainland China, by integrating demographic, clinical, epidemiologic, phylogenomic, and phylodynamic data. In Hong Kong, most cases recorded in January 2020 were imported cases. After February 1, most were local cases and close contacts of those case-patients, indicating local community transmissions. Transmission in closed settings, especially during family and religious gatherings, is a hallmark of recent cases recorded in Hong Kong. Among 6 clusters identified on the basis of epidemiologic links, 3 (clusters 4–6; Figure 1) were considered SSEs because of the larger number of persons involved (n = 8–13). We performed whole-genome sequencing on all 50 cases to investigate phylogenetic relationship and transmission link.

The SARS-CoV-2 samples in Hong Kong had 99.98% identity to the reference genome (GenBank accession no. NC_045512.2) and demonstrated no apparent major genome modification since the initial COVID-19 outbreak in Wuhan. As shown in global phylogeny, SARS-CoV-2 genomes isolated in Hong Kong could be segregated into 2 lineages. Lineage 1 was phylogenetically related to the strains isolated from China and was the cause of the cases in Cluster 1. Lineage 2 was more closely related to strains from France and South Korea. It also harbored a common mutation at *Orf3a*-G251V, which accounted for 88.0% of cases in this study.

Regarding the local phylogenetic analysis, clustering of samples was highly concordant to the epidemiologic link, despite the marginally supportive bootstrap value of the nodes because of the limited genetic variability. Cluster 1 demonstrated the closest genetic distance to the reference genome among all cases reported in Hong Kong (Figures 1, 2). The index case of cluster 1 (case 66) was initially defined as possible local infection because the patient traveled to Guangdong Province, which was not considered to have active community transmission at that time. However, our sequencing result demonstrated that the genome of case 66 was 100% identical to the first published SARS-CoV-2 genome, and all cases in cluster 1 did not harbor *Orf3a*-G251V, which was recognized as a hallmark of local cases with unknown source in our community. Therefore, instead of possible local infections, cluster 1 was more likely imported from mainland china through index case-patient 66.

Cluster 5 originated within a public housing estate, in which a family of 3 members (cases 42, 48, and

49) were suspected to have been infected through a confirmed case-patient (case 12) who lived 10 stories above them in the same building, through a potentially faulty sewage pipe setup or other environmental exposure. Based on phylogenetic analysis, viral genomes in cluster 5 shared a similar genetic distance from the reference genome and were assigned to the same branch of the tree. This finding supports a potential transmission link among these cases.

Cluster 4 was a family gathering–associated SSE during Chinese New Year. In concert with epidemiologic information, all 11 cases from cluster 4 shared 3 common missense mutations, namely *S*-L8V, *Orf1ab*-H3233Y, and *Orf3a*-G251V; 7 cases shared identical

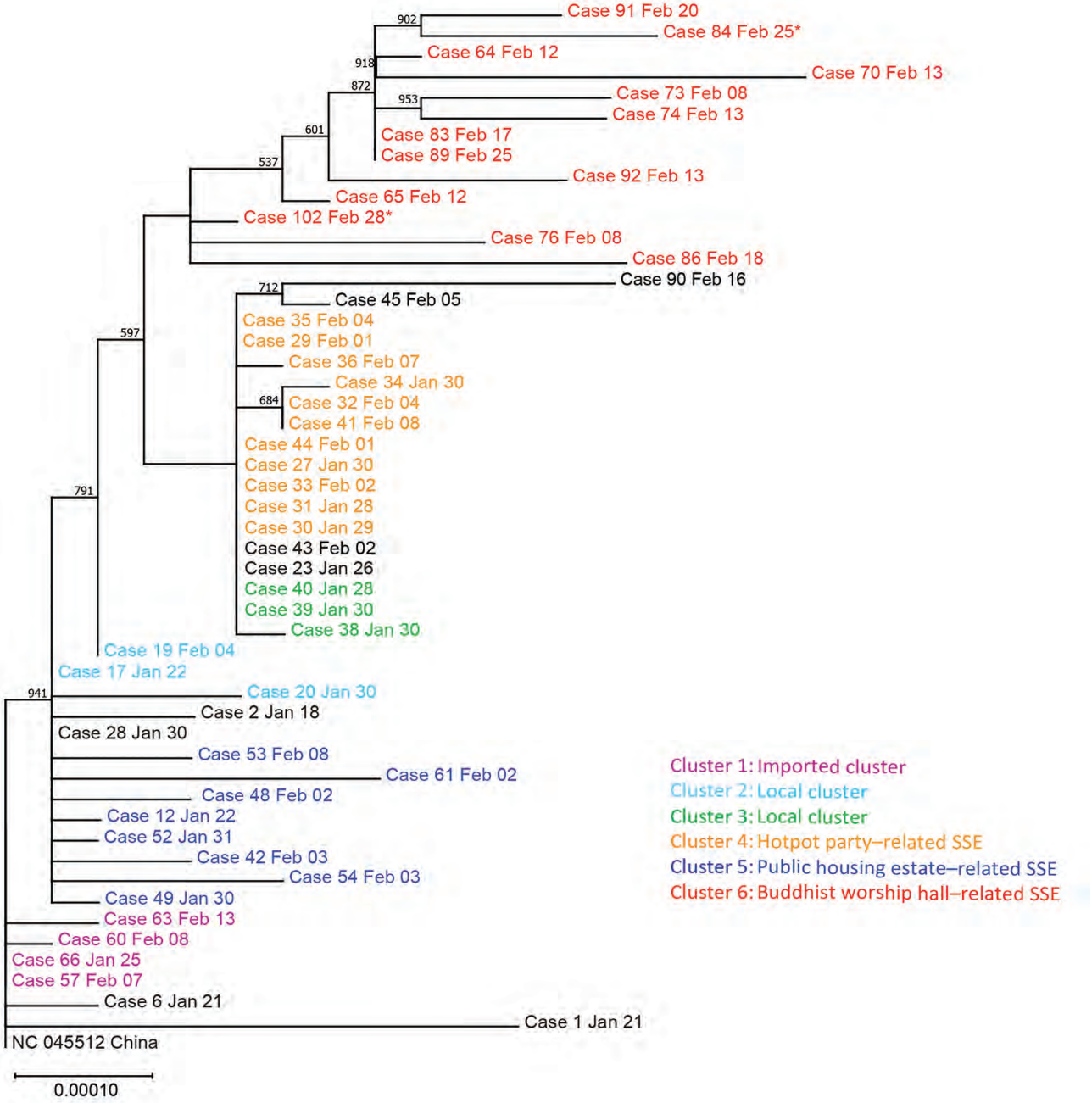


**Figure 2.** Maximum-likelihood phylogenetic tree of 50 coronavirus disease cases, Hong Kong, February 2020. The tree was rooted on the earliest published genome of severe acute respiratory syndrome coronavirus 2 (GenBank accession no. NC_045512.2). Bootstrap value was set at 1,000× and nodes with bootstrap value >50% were shown. Branch lengths were measured in number of substitutions per site. Samples are color-coded by epidemiologic link. Cases 84 and 102 were asymptomatic at the time of sample collection and are marked with asterisks. Each case is identified by case number used by the Centre of Health Protection, Department of Health, Hong Kong, and date of symptom onset. SSE, superspreading event.

genomes. Considering the fast-evolving property of RNA viruses, the presence of identical genetic sequences among the strains implies that transmission occurred over a short period or even in a single event. Meanwhile, 2 isolated cases (case 23 and case 43) and 3 cases from another local cluster (case 38, case 39, and case 40) shared highly similar genomes to those of cluster 4 (Figures 1, 2). Although no apparent epidemiologic links were observed, the high degree of genomic similarity suggests that these cases might have originated in a single source. That speculation was further supported by the geographic distribution of case-patients who lived near one another and whose social circles might have overlapped (Figure 3). Our results demonstrate that the integration of epidemiologic and phylogenetic data is critical for providing more accurate information about transmission patterns.

Cluster 6 was an SSE occurring in a Buddhist worship hall. Two missense mutations, *Orf1ab*-G295V and *Orf1ab*-L3606F, were unique to this cluster. Epidemiologic investigation identified a 43-year-old monk (case 102; Figure 1), who was the abbot of the worship hall and had traveled to mainland China in early January. He was sent to a quarantine center in late February after being linked to a series of confirmed cases connected to the worship hall. He was asymptomatic throughout the study period. Phylogenetic analysis showed that this case was closest to the root of the cluster (Figure 2), suggesting that case 102 could be the index patient of cluster 6. By the time of data cutoff, the cluster involved 13 patients and spread was ongoing. This pattern demonstrates the possibility of a hidden spreader as a source of COVID-19 community outbreak. That likelihood also highlights the importance of rapid quarantine of close contacts of confirmed case-patients, regardless of the presence of symptoms, to halt community spread.

In the evolutionary clock study, the reproduction number of COVID-19 within Hong Kong as of February 28, 2020, was estimated at 1.84 (95% BCI 1.37–2.35). That value strongly indicated that the

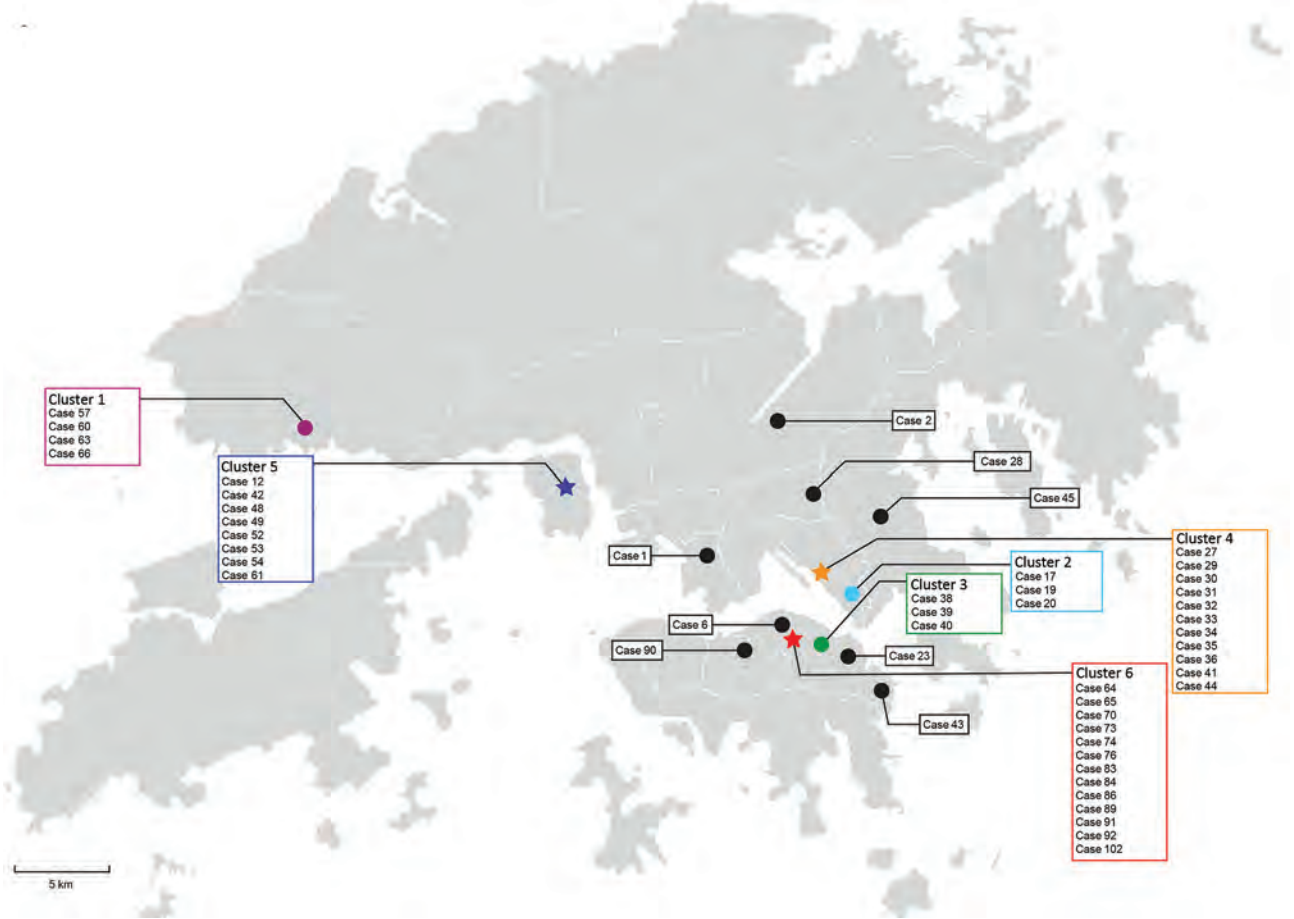


**Figure 3.** Geographic distribution of 50 coronavirus disease cases, Hong Kong, February 2020**.** Geographic information is marked according to the residence of the index case-patient in each cluster. Clusters known to be caused by superspreading events are marked by asterisks; other clusters are marked by dots.

outbreak in Hong Kong was ongoing, but it was smaller than the estimated reproduction number of 2.6 in Wuhan (*23*,*24*). The smaller value is a combined outcome of reduced growth rate and increased δ. The reduced growth rate is attributed to strong public health awareness among the general public, which resulted in greatly reduced social activities and strong compliance with mask-wearing during this period (*25*,*26*). The increased δ can be attributed to robust laboratory surveillance and fast quarantine time. In addition, time of most recent common ancestor for the cases in Hong Kong was determined to be December 24, 2019, ≈25 days before the first patient in our cohort (Case 2) demonstrated symptoms on January 18, 2020 (Figure 1).

Our study has several limitations. Although we included 53.8% of the cases reported in Hong Kong as of February 28, another 43 cases, including 2 fatal cases, were not analyzed in this study. Moreover, incubation periods of cases in which the source of infection is unknown might vary widely. Studies have demonstrated that incubation periods can vary from 4.5 to 15.8 days (*24*) and can be longer for patients experiencing mild symptoms. However, because patients might already be infectious during the incubation period, the reproductive number in this study could be underestimated. Furthermore, our calculations were based solely on phylodynamic analysis, which could differ from calculations on the basis of epidemiologic models. Finally, ambiguous bases were observed in some of our consensus genomes. This ambiguity is mainly because whole-genome sequencing was performed on respiratory specimens instead of viral culture, in which viral load plays a critical role in the subsequent genome quality as reflected by the cycle threshold of each specimen. The paucity of viral load in specimens could affect the yield of sequencing libraries. In our study, specimens with cycle threshold <28 were usually free of ambiguous bases. Nevertheless, the uncovered area only accounted for ≈1–3% of the entire viral genome, although the remaining mapped regions had an average coverage of >100×, which should provide sufficient and accurate information for subsequent analyses (Appendix 1).

In conclusion, phylogenomic data were consistent with epidemiologic findings that transmission in closed settings, especially during family and religious gatherings, is a hallmark of COVID-19 outbreak in Hong Kong. Social distancing and vigilant infection control measures, such as rapid isolation of suspected or confirmed case-patients and their close contacts, are crucial for containing COVID-19 in the community.

### Acknowledgments

We appreciate Oxford Nanopore Technologies Limited, especially Hai Wang and Eva Yu, for their supportive service in the delivery of sequencing flow cells and reagents, and the provision of technical advices.

This study was supported by the Faculty of Health and Social Science and the Department of Health Technology and Informatics of The Hong Kong Polytechnic University. It was also supported by the Health and Medical Research Fund Commissioned Research on COVID-19 (COVID190204) and the Innovation and Technology Fund Innovation and Technology Support Programme's Public Sector Trial Scheme (SST/050/20GP).

K.S.-S.L. and G.K.-H.S. designed the study, collected, analyzed, and interpreted the data, conducted literature search, and drafted and critically reviewed the manuscript; and G.K.-H. S. was also responsible for securing funding for this study. T.T.-L.N., H.-Y.L., M.-P.C., K.K.-G.T., and L.-K.L. conducted experiments and analyzed the data. A.K.-L.W., M.C.-Y.Y., B.K.-C.W., A.Y.-M.H., K.-T.Y., K.-C.L., R.W.-T.L., E.Y.-K.T., W.-S.L., M.-C.C., Y.-Y.N., K.-M.S., K.S.-C.F., S.K.-Y.C., W.-K.T., and T.-L.Q. were responsible for collecting and analyzing the data and finalizing the manuscript. D.H.-K.S. and S.P.Y. analyzed the data and wrote and critically reviewed the manuscript. W.C.Y. was involved in data analysis, data interpretation, and writing of the manuscript. All authors reviewed and approved the final version of the manuscript.

### About the Author

Dr. Leung obtained his PhD in Microbiology at the University of Hong Kong in 2019 and received bioinformatic and phylogenetic analysis training under HKU Pasteur institute. His research interests are molecular diagnosis and epidemiology of emerging infectious disease such as *Mycobacterium tuberculosis* and HIV.

### References

1. Zhu N, Zhang D, Wang W, Li X, Yang B, Song J, et al.; China Novel Coronavirus Investigating and Research Team. A novel coronavirus from patients with pneumonia in China, 2019. N Engl J Med. 2020;382:727–33. https://doi.org/10.1056/NEJMoa2001017
2. Guan WJ, Ni ZY, Hu Y, Liang WH, Ou CQ, He JX, et al.; China Medical Treatment Expert Group for Covid-19. Clinical characteristics of coronavirus disease 2019 in China. N Engl J Med. 2020;382:1708–20. https://doi.org/10.1056/NEJMoa2002032
3. Chan JF, Yuan S, Kok KH, To KK, Chu H, Yang J, et al. A familial cluster of pneumonia associated with the 2019 novel coronavirus indicating person-to-person transmission: a study of a family cluster. Lancet. 2020;395:514–23. https://doi.org/10.1016/S0140-6736(20)30154-9

4. Li Q, Guan X, Wu P, Wang X, Zhou L, Tong Y, et al. Early transmission dynamics in Wuhan, China, of novel coronavirus-infected pneumonia. N Engl J Med. 2020;382:1199–207. https://doi.org/10.1056/NEJMoa2001316
5. Dong E, Du H, Gardner L. An interactive web-based dashboard to track COVID-19 in real time. Lancet Infect Dis. 2020;20:533–4. https://doi.org/10.1016/S1473-3099(20)30120-1
6. Centre for Health Protection. Latest local situation of severe respiratory disease associated with a novel infectious agent. 2020 [cited 2020 Feb 24]. https://chp-dashboard.geodata.gov.hk/covid-19/en.html
7. Leung YF, Wong HB, Shing Y, Wong HW, Wong WK. COVID-19 in HK. 2020 [cited 2020 Feb 25]. https://wars.vote4.hk
8. Centre for Health Protection. Severe respiratory disease associated with a novel infectious agent—letters to doctors. 2020 [cited 2020 Feb 6]. https://www.chp.gov.hk/files/pdf/letters_to_doctors_20200107.pdf
9. Corman VM, Landt O, Kaiser M, Molenkamp R, Meijer A, Chu DK, et al. Detection of 2019 novel coronavirus (2019-nCoV) by real-time RT-PCR. Euro Surveill. 2020;25. https://doi.org/10.2807/1560-7917.ES.2020.25.3.2000045
10. World Health Organization. Clinical management of severe acute respiratory infection when novel coronavirus (nCoV) infection is suspected: interim guidance. 2020 [cited 2020 Jan 11]. https://www.who.int/publications/i/item/clinical-management-of-covid-19
11. Peiris JS, Lai ST, Poon LL, Guan Y, Yam LY, Lim W, et al.; SARS study group. Coronavirus as a possible cause of severe acute respiratory syndrome. Lancet. 2003;361:1319–25. https://doi.org/10.1016/S0140-6736(03)13077-2
12. Quick J. Artic Network-nCoV 2019 sequencing protocol. 2020 [cited 2020 Feb 24]. https://artic.network/ncov-2019
13. Loman N, Rambaut A. nCoV-2019 novel coronavirus bioinformatics protocol. [cited 2020 Mar 10]. https://artic.network/ncov-2019/ncov2019-bioinformatics-sop.html
14. DePristo MA, Banks E, Poplin R, Garimella KV, Maguire JR, Hartl C, et al. A framework for variation discovery and genotyping using next-generation DNA sequencing data. Nat Genet. 2011;43:491–8. https://doi.org/10.1038/ng.806
15. Guindon S, Dufayard JF, Lefort V, Anisimova M, Hordijk W, Gascuel O. New algorithms and methods to estimate maximum-likelihood phylogenies: assessing the performance of PhyML 3.0. Syst Biol. 2010;59:307–21. https://doi.org/10.1093/sysbio/syq010
16. Elbe S, Buckland-Merrett G. Data, disease and diplomacy: GISAID's innovative contribution to global health. Glob Chall. 2017;1:33–46. https://doi.org/10.1002/gch2.1018
17. Bouckaert R, Heled J, Kühnert D, Vaughan T, Wu CH, Xie D, et al. BEAST 2: a software platform for Bayesian evolutionary analysis. PLOS Comput Biol. 2014;10:e1003537. https://doi.org/10.1371/journal.pcbi.1003537
18. Rambaut A, Drummond AJ, Xie D, Baele G, Suchard MA. Posterior summarization in Bayesian phylogenetics ssing Tracer 1.7. Syst Biol. 2018;67:901–4. https://doi.org/10.1093/sysbio/syy032
19. Chen N, Zhou M, Dong X, Qu J, Gong F, Han Y, et al. Epidemiological and clinical characteristics of 99 cases of 2019 novel coronavirus pneumonia in Wuhan, China: a descriptive study. Lancet. 2020;395:507–13. https://doi.org/10.1016/S0140-6736(20)30211-7
20. Huang C, Wang Y, Li X, Ren L, Zhao J, Hu Y, et al. Clinical features of patients infected with 2019 novel coronavirus in Wuhan, China. Lancet. 2020;395:497–506. https://doi.org/10.1016/S0140-6736(20)30183-5
21. Wang D, Hu B, Hu C, Zhu F, Liu X, Zhang J, et al. Clinical characteristics of 138 hospitalized patients with 2019 novel coronavirus-infected pneumonia in Wuhan, China. JAMA. 2020;323:1061–9. PMID 32031570
22. Wu J, Liu J, Zhao X, Liu C, Wang W, Wang D, et al. Clinical characteristics of imported cases of COVID-19 in Jiangsu Province: a multicenter descriptive study. Clin Infect Dis. 2020;71:706–12.
23. Boskova V, Stadler T, Magnus C. The influence of phylodynamic model specifications on parameter estimates of the Zika virus epidemic. Virus Evol. 2018;4:vex044. https://doi.org/10.1093/ve/vex044
24. Lai A, Bergna A, Acciarri C, Galli M, Zehender G. Early phylogenetic estimate of the effective reproduction number of SARS-CoV-2. J Med Virol. 2020;92:675–9. https://doi.org/10.1002/jmv.25723
25. Sung AD, Sung JAM, Thomas S, Hyslop T, Gasparetto C, Long G, et al. Universal mask usage for reduction of respiratory viral infections after stem cell transplant: a prospective trial. Clin Infect Dis. 2016;63:999–1006. https://doi.org/10.1093/cid/ciw451
26. Seto WH, Tsang D, Yung RW, Ching TY, Ng TK, Ho M, et al.; Advisors of Expert SARS group of Hospital Authority. Effectiveness of precautions against droplets and contact in prevention of nosocomial transmission of severe acute respiratory syndrome (SARS). Lancet. 2003;361:1519–20. https://doi.org/10.1016/S0140-6736(03)13168-6

Address for correspondence: Gilman Siu, Room Y928, 9/F, Block Y, The Hong Kong Polytechnic University, Hung Hom, Kowloon, Hong Kong; email: gilman.siu@polyu.edu.hk

# Viral Metagenomic Analysis of Cerebrospinal Fluid from Patients with Acute Central Nervous System Infections of Unknown Origin, Vietnam

Nguyen To Anh, Le Nguyen Truc Nhu, Nguyen Thi Thu Hong, Tran My Phuc, Pham Thi Thanh Tam, Dang Thao Huong, Tran Tuan Anh, Xutao Deng, Ho Dang Trung Nghia, Tran Thua Nguyen, Nguyen Van Hung, Nguyen Dac Thuan, Pham Thi Hong Phuong, Nguyen Van Vinh Chau, Stephen Baker, Eric Delwart, Guy Thwaites, Le Van Tan, for the VIZIONS Consortium[1]

Central nervous system (CNS) infection is a serious neurologic condition, although the etiology remains unknown in >50% of patients. We used metagenomic next-generation sequencing to detect viruses in 204 cerebrospinal fluid (CSF) samples from patients with acute CNS infection who were enrolled from Vietnam hospitals during 2012–2016. We detected 8 viral species in 107/204 (52.4%) of CSF samples. After virus-specific PCR confirmation, the detection rate was lowered to 30/204 (14.7%). Enteroviruses were the most common viruses detected (n = 23), followed by hepatitis B virus (3), HIV (2), molluscum contagiosum virus (1), and gemycircularvirus (1). Analysis of enterovirus sequences revealed the predominance of echovirus 30 (9). Phylogenetically, the echovirus 30 strains belonged to genogroup V and VIIb. Our results expanded knowledge about the clinical burden of enterovirus in Vietnam and underscore the challenges of identifying a plausible viral pathogen in CSF of patients with CNS infections.

Worldwide, the annual incidence of acute encephalitis in nonoutbreak settings during 1983–2000 ranged from 0.07 to 12.6 cases/100,000 population (*1*). According to the World Health Organization, meningitis caused 379,000 deaths and encephalitis caused 150,000 deaths globally in 2015 (*2*). As a consequence, central nervous system (CNS) infection is a leading cause of years lived with disability in low-income countries (*3*).

More than 100 known pathogens can cause CNS infections (*1*). However, the distribution of CNS infection pathogens is geographically dependent and has been shaped by the emergence of novel viruses. In Asia, Nipah virus and enterovirus A71 have been recognized as emerging neurotropic pathogens over the past few decades. In 1999, West Nile virus arrived in the United States and since then has established endemic circulation (*4*).

Despite recent advances in molecular diagnostics, especially sensitive virus-specific PCR, encephalitis cases of unknown origin remain a substantial problem. Worldwide, ≈50% of patients with CNS infections have no etiology identified (*1*,*5*,*6*).

Over the past decade, metagenomic next-generation sequencing (mNGS) has emerged as a sensitive hypothesis-free approach for detection of pathogens (especially viruses) in clinical samples (*7*). However, in resource-limited settings like Southeast Asia and Vietnam, a limited number of mNGS studies

Author affiliations: Oxford University Clinical Research Unit, Ho Chi Minh City, Vietnam (N.T. Anh, L.N.T. Nhu, N.T.T. Hong, T.M. Phuc, P.T.T. Tam, D.T. Huong, T.T. Anh, H.D.T. Nghia, G. Thwaites, L.V. Tan); Hue Central Hospital, Hue City, Vietnam (T.T. Nguyen); Dak Lak General Hospital, Ban Me Thuot City, Vietnam (N.V. Hung); Khanh Hoa General Hospital, Nha Trang City, Vietnam (N.D. Thuan); Dong Thap General Hospital, Dong Thap, Vietnam (P.T.H. Phuong); Vitalant Research Institute, San Francisco, California, USA (X. Deng, E. Delwart); University of California Department of Laboratory Medicine, San Francisco (X. Deng, E. Delwart); Pham Ngoc Thach University, Ho Chi Minh City (H.D.T. Nghia); Hospital for Tropical Diseases, Ho Chi Minh City (N.V.V. Chau); University of Cambridge Institute of Therapeutic Immunology and Infectious Disease, Cambridge, UK (S. Baker); Centre for Tropical Medicine, Nuffield Department of Medicine, University of Oxford, Oxford, UK (S. Baker, G. Thwaites)

DOI: https://doi.org/10.3201/eid2701.202723

[1]Members are listed at the end of this article.

examining known and unknown viruses in cerebrospinal fluid (CSF) samples from patients with CNS infections have been conducted, even though in this tropical region of the world, novel viruses are likely to emerge (P. Zhou et al., unpub. data, https://doi.org/10.1101/2020.01.22.914952), and diverse CNS infection pathogens have been documented. Collectively, improving our knowledge about viral causes of CNS infections is essential for clinical management and development of intervention strategies. In this study, by using a mNGS approach, we set out to search for known and unknown viruses in CSF samples collected from patients in Vietnam with CNS infections of unknown causes who were enrolled in a hospital-based surveillance study conducted during 2012–2016.

## Materials and Methods

### Clinical Study and Selection of CSF Samples for mNGS Analysis

The study used CSF samples collected from patients with suspected CNS infection enrolled in a hospital-based surveillance program conducted in Vietnam during December 2012–October 2016 (*5*). The study was conducted as part of the Vietnam Initiative on Zoonotic Infections (VIZIONS) project (*5*), and patient recruitment was carried out at 7 provincial hospitals across Vietnam. After collection, as per the study protocol, all CSF samples were tested for a range of pathogens by using the diagnostic work-up of the clinical study (Appendix Table 1, https://wwwnc.cdc.gov/EID/article/27/1/20-2723-App1.pdf). The remaining volume of the CSF samples were stored at −80°C for further testing.

We focused our metagenomic analysis on patients of unknown origin from 4 provincial hospitals in central (Hue and KhanhHoa), highland (DakLak), and southern (DongThap) Vietnam (Figure 1), representing 3 distinct geographic areas in Vietnam. To increase the chance of detecting a virus in the CSF samples, we only selected patients with CSF leukocyte counts ≥5 cells/mm$^3$ and an illness duration ≤5 days.

### mNGS Assay

mNGS assay was carried out as previously described (*8*). Before viral nucleic acid (NA) isolation, 100 µL of each CSF sample was treated with Turbo DNase (Ambion, Life Technology, ThermoFisher, https://www.thermofisher.com) and RNase I enzyme (Ambion). Then viral NA was isolated using a QIAamp viral RNA kit (QIAGEN GmbH, https://www.qiagen.com), and recovered in 50 µL of elution buffer provided with the extraction kit. Double-stranded DNA was synthesized from the isolated viral NA by using a set of 96 nonribosomal primers (FR26RV–Endoh primers) and then was randomly amplified by using the FR20RV primer (5′-GCCGGAGCTCTGCAGATATC-3′). Finally, the amplified product was subjected to a library preparation step by using Nextera XT sample preparation kit (Illumina, https://www.illumina.com), following the manufacturer's instructions, and sequenced by using a MiSeq reagent kit, version 3 (600 cycles) (Illumina) in a MiSeq platform (Illumina).

### mNGS Data Analysis

Potential viral reads were identified by using an in-house viral metagenomic pipeline running on a 36-node Linux cluster as described previously (*9*). In

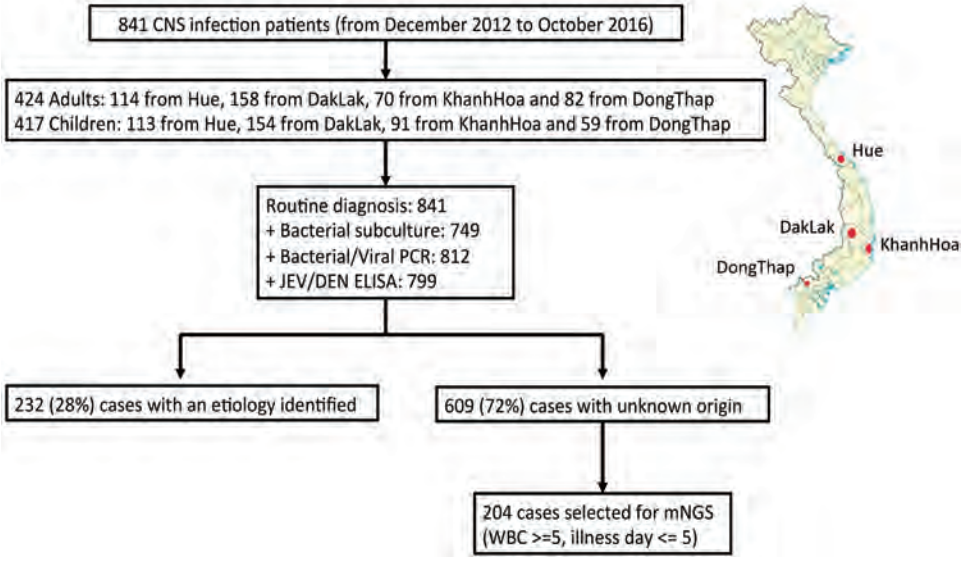


**Figure 1.** Flowchart overview of diagnostic results for study of patients with suspected central nervous system infections admitted to 4 of 7 provincial hospitals, Vietnam, December 2012–October 2016. Inset map indicates places where samples were collected (red dots).

brief, after duplicate reads and reads belonging to human or bacterial genomes were filtered out, the remaining reads were assembled de novo. The resulting contigs and singlet reads were then aligned against a customized viral proteome database by using an approach based on BLAST (https://blast.ncbi.nlm.nih.gov/Blast.cgi). Next, the candidate viral reads were aligned against a nonredundant nonvirus protein database to remove any false-positive reads (i.e., reads with expected values higher than those against viral protein databases). Any virus-like sequence with an expected value ≤0.00001 was considered a significant hit. Finally, a reference-based mapping approach (Genious 8.1.5; Biomatters, https://www.geneious.com) was used to assess the levels of identity and genome coverage of the corresponding viruses.

### PCR Confirmatory Testing of mNGS Results

PCR assays were conducted to confirm mNGS hits for each specific virus identified from the viral metagenomic pipeline. Depending on availability of CSF, the PCR confirmations were performed either on leftover NA or newly extracted NA. A viral mNGS result was considered positive only if it was subsequently confirmed by PCR analysis of the original NA samples. The nucleotide sequences of primers and probes used for PCR confirmatory testing are shown in Appendix Table 2 (*8*).

### Serotype Identification and Phylogenetic Analysis

For enterovirus serotype determination based on the obtained sequences generated by viral mNGS, we used a publicly available genotyping tool (*10*). To determine the relationship between enterovirus strains we sequenced and global strains, we first performed pairwise alignment by using the ClustalW tool in Geneious 8.1.5, and then reconstructed a maximum-likelihood phylogenetic tree by using IQ Tree 1.4.3 (*11*). A similar phylogenetic approach was used for other viruses. The generated sequences of this study were submitted to GenBank (accession no. PRJNA561465).

### Ethics

The study was approved by the corresponding institutional review broad of local hospitals in Vietnam, where the patients were enrolled, and the Oxford Tropical Ethics Committee. Informed consent was obtained from each study participant or a legal guardian.

## Results

### CSF Samples Available for mNGS Analysis

From the clinical study described previously, a total of 841 patients were enrolled from Hue, Khanh Hoa, Dak Lak, or Dong Thap provincial hospitals. Of these, 609/841 (72%) patients had no etiology identified. The etiologic profiles of the patients in

**Table.** Baseline characteristics and clinical data of patients with acute central nervous system infections enrolled for mNGS analysis of CSF samples, Vietnam, December 2012–October 2016*

| Characteristic | Patients with unknown cause enrolled for mNGS, n = 204 | Patients with mNGS negative, n = 174 | Patients with enterovirus detected, n = 23 | p value† |
|---|---|---|---|---|
| Sex | | | | |
| M | 135 (66) | 114 (65.5) | 15 (65) | |
| F | 69 (34) | 60 (34.5) | 8 (35) | |
| Age, y, median (range) | 20.5 (0–92) | 24 (0–92) | 13 (2–27) | 0.005 |
| Location | | | | |
| Hue | 37 (18) | 28 (16) | 9 (39) | |
| Dak lak | 98 (48) | 87 (50) | 10 (43.5) | |
| Khanh Hoa | 28 (14) | 22 (13) | 4 (17.5) | |
| Dong Thap | 41 (20) | 37 (21) | 0 | |
| 3-d fever (at enrollment or preceding 3 d) | | | | |
| Fever | 148 (72.5) | 126 (72.4) | 17 (74) | 0.054 |
| Temperature, C°, median (range) | 39 (37.5–42.0) | 39 (37.5–42.0) | 38.5 (38.0–40.5) | |
| Fever with unknown temperature | 29 (14.2) | 22 (12.6) | 6 (26) | |
| No fever | 20 (9.8) | 19 (11) | 0 | |
| Unknown | 7 (3.5) | 7 (4) | 0 | |
| Outcome | | | | |
| Death or discharge to die | 22 (11) | 22 (12.6) | 0 | |
| Discharge with complete recovery | 108 (53) | 86 (49.4) | 18 (78.3) | |
| Discharge with incomplete recovery | 35 (17) | 31 (17.8) | 2 (8.7) | |
| Transfer to another hospital | 34 (16.5) | 30 (17.2) | 3 (13) | |
| Other (patient request) | 3 (1.5) | 3 (1.7) | 0 | |
| Unknown | 2 (1) | 2 (1.3) | 0 | |
| CSF white cells, cells/mm$^3$ median (min–max) | 88.5 (5–40,000) | 71.5 (5–40,000) | 110 (8–1200) | 0.343 |

*Values are no. (%) except as indicated, CSF, cerebrospinal fluid; mNGS, metagenomic next-generation sequencing.
†Statistical comparisons were performed for groups of patients with mNGS-negative results and enterovirus detected, by Mann-Whiney test.

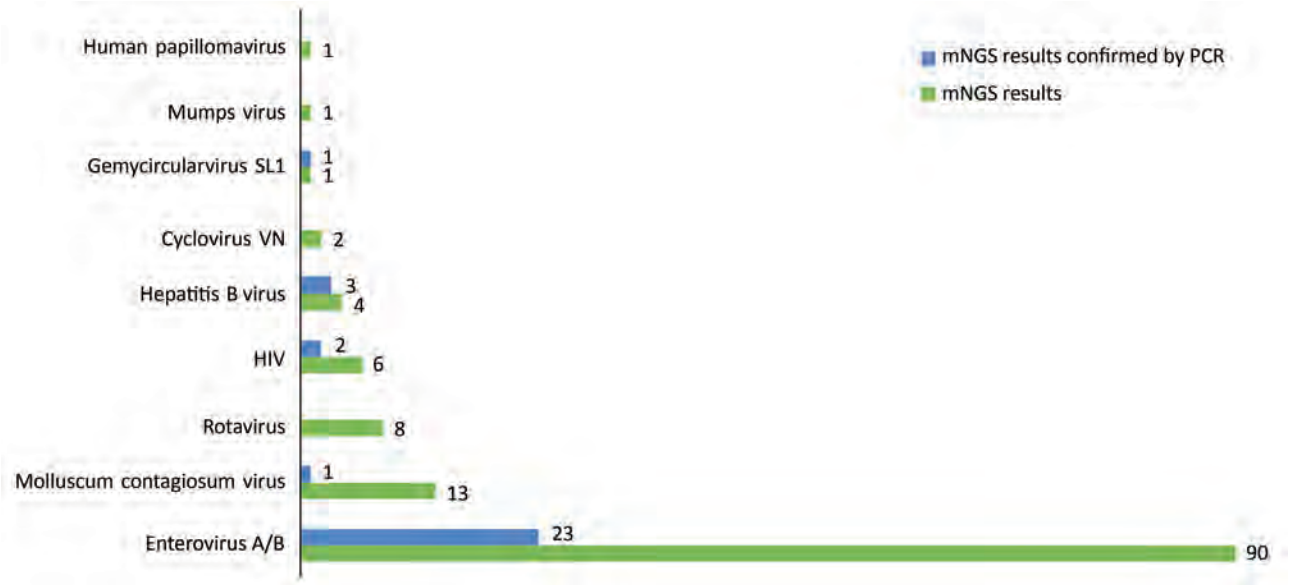


**Figure 2.** Number of cerebrospinal fluid samples with detected viruses by metagenomic next-generation sequencing and then confirmed by virus-specific PCR or reverse-transcription PCR, Vietnam, December 2012–October 2016. Samples were collected from patients with suspected central nervous system infection. For human papillomavirus, confirmatory testing was not performed because of the unavailability of a PCR assay.

whom a pathogen was detected will be reported separately. Of the patients in whom a pathogen was not identified, 204 met our selection criteria, and their CSF samples were included for viral mNGS analysis (Figure 1).

### Baseline Characteristics of the Included Patients

The baseline characteristics and outcome of the 204 study patients are described in Table 1. Male patients were predominant. A substantial proportion of the patients were seriously ill; fatal outcome was recorded in 22 (11%), whereas incomplete recovery was recorded in 17% (n = 35) and deterioration (reflected by being transferred to other hospitals) in 16.5% (n = 34).

### General Description of mNGS Results

A total of 204 CSF samples were subjected to 3 NGS runs, and 108 million reads were obtained (median number of reads per sample 445,412 [range 430–908,890]). Of these, viral reads accounted for 0.64% (n = 692,731; median number of reads per sample 2,001 [range 4–268,933]). Excluding common contaminants and commensal viruses such as torque teno virus, which are not reported in this article, sequences related to a total of 8 distinct viral species were identified in 107/204 (52.4%) patients. These viruses are either known to be infectious to humans (e.g., enteroviruses, rotavirus, molluscum contagiosum virus [MCV], human papillomavirus, HIV, and hepatitis B virus [HBV]) or are without evidence of human infections besides previous detection in sterile human samples (e.g., cyclovirus-VN and gemycircularvirus) (Figure 2).

### mNGS Result Assessment by Specific PCR Analysis

After virus-specific PCR confirmatory testing, the proportion of patients in whom a virus was found by mNGS was reduced from 53% (108/204) to 14.7% (30/204). Accordingly, the number of virus species was reduced from 8 to 5 (Figure 2); enteroviruses were the most common virus detected, accounting for 11.3% (23/204) of the included patients, followed by HBV (n = 3), HIV (n = 2), gemycircularvirus, and MCV (1 each) (Figure 2). Because of the focus of our study and the unavailability of the PCR assays, confirmatory testing for human papillomavirus was not performed.

### Characteristics of the 23 Enterovirus-Infected Patients

All 23 enterovirus-infected patients were admitted to hospitals from the central or highland areas (Table), and none were from Dong Thap Province. Male patients were slightly predominant, accounting for

56%. Notably, the enterovirus-infected patients were younger than those who were mNGS-negative (Table). At discharge, incomplete recovery or transfer to other hospitals because of disease deterioration were recorded in 21.7% (Table).

Enterovirus cases were not detected during January 2015–December 2016. During 2013 and 2014, two main peaks were observed during March–July and September–December (Figure 3, panel A); cases from Dak Lak and Khanh Hoa contributed to the first peak (Figure 3, panels B and C), and cases from Khanh Hoa and Hue contributed to the second (Figure 3, panels C and D). The general baseline characteristics of patients with HBV, HIV, gemycircularvirus, and MCV are shown in Appendix Table 3.

### Genetic Characterization of Enteroviruses and Gemycircularvirus

mNGS generated sufficient sequence information for an enterovirus serotyping assessment in 11/23 cases. Subsequently, results of serotyping analysis based on the NGS sequences showed that echovirus 30 (E30)

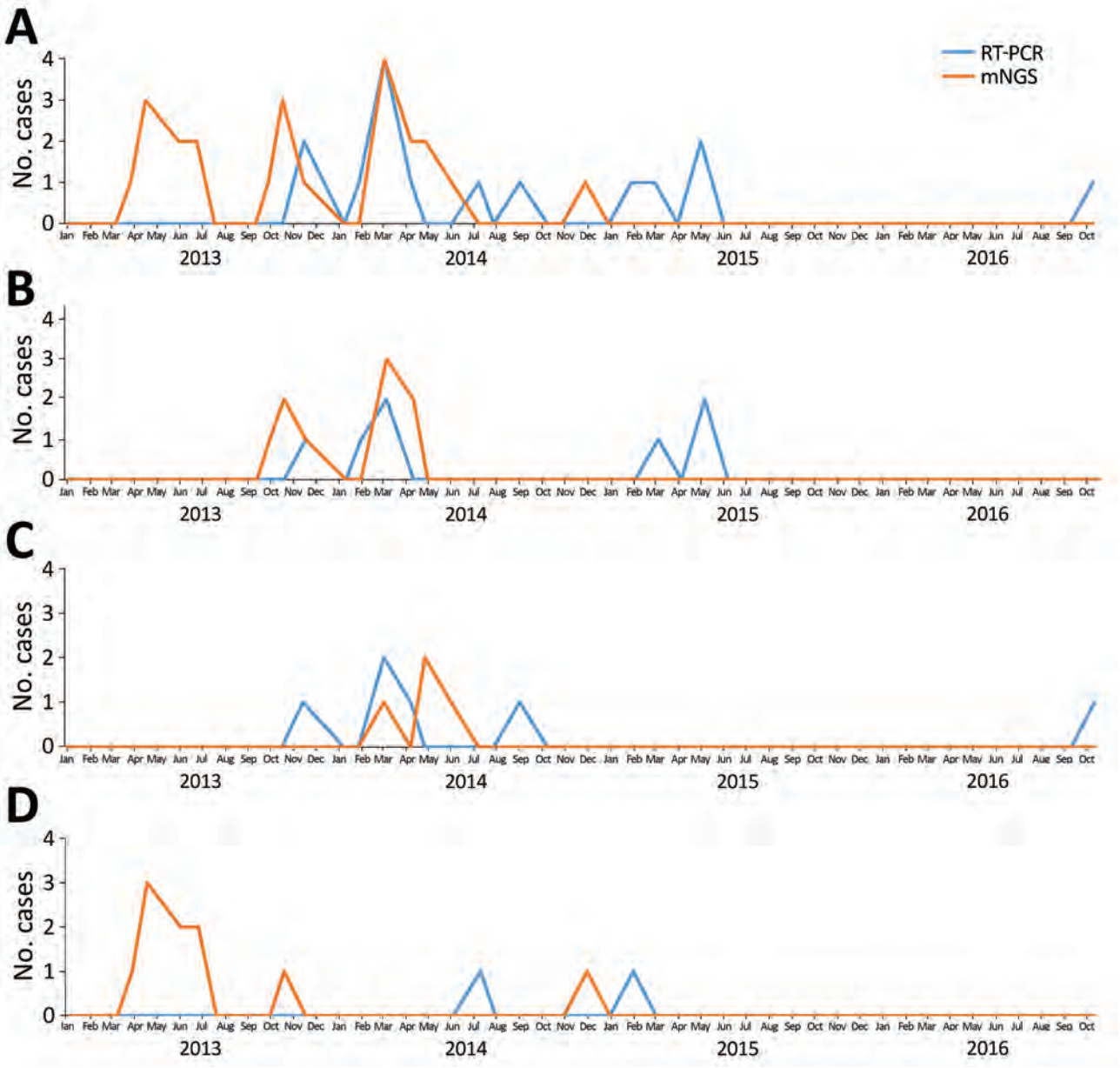


**Figure 3.** Temporal distribution of enterovirus cases detected from cerebrospinal fluid samples of patients with suspected central nervous system infection by metagenomic next-generation sequencing and RT-PCR, Vietnam, December 2012–October 2016. Enterovirus RT-PCR results were obtained from the original study. RT-PCR, reverse transcription PCR. A) Combined data from 3 provinces; B) data from Hue province; C) data from Khanh Hoa province; D) data from Dak Lak province.

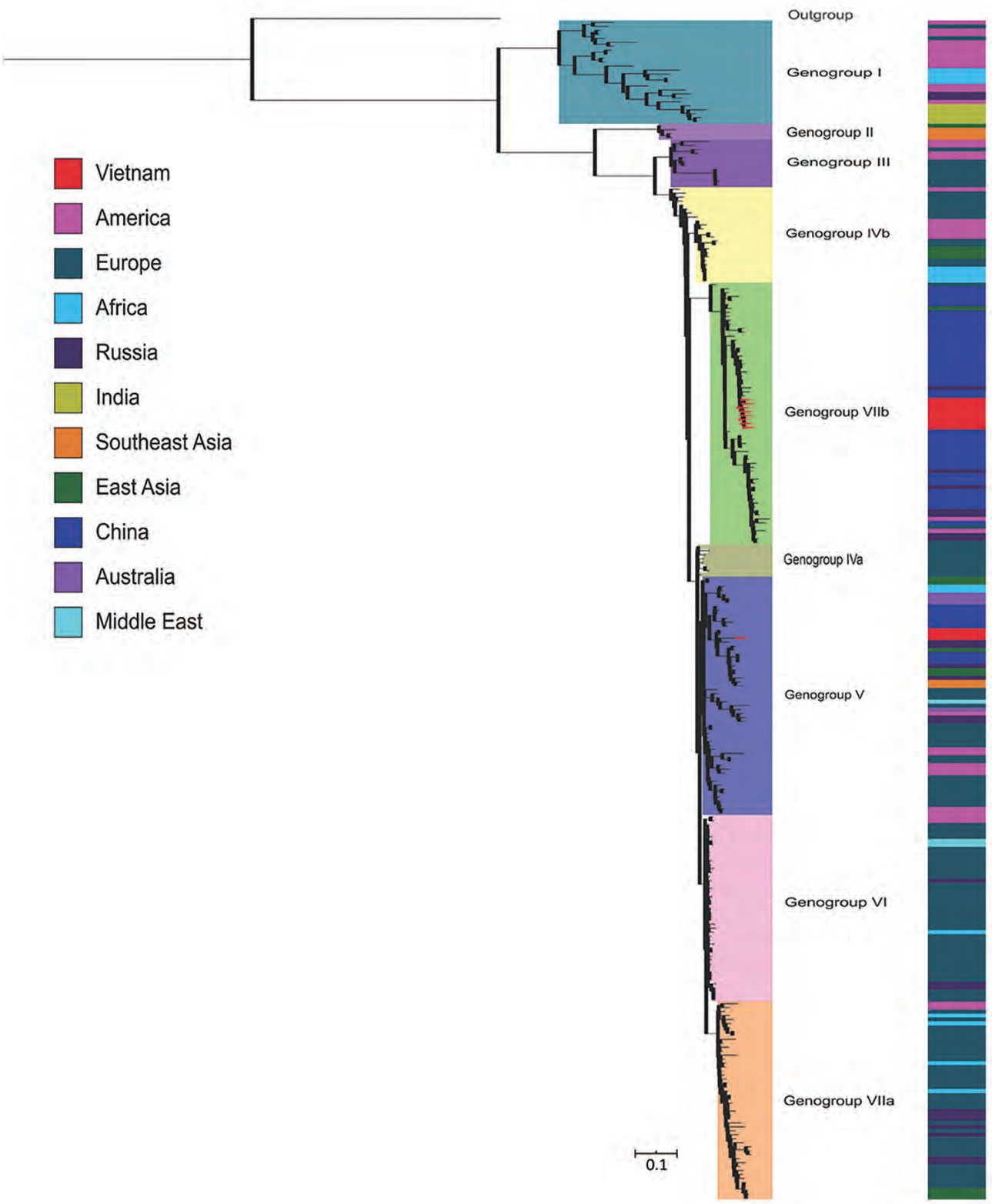


**Figure 4.** Phylogenetic tree of 298 complete viral protein 1 sequences of echovirus 30 (876 nt) isolated from cerebrospinal fluid samples of patients with suspected central nervous system infection, Vietnam, December 2012–October 2016. The inner color strip indicates 7 genogroups. The outer color strip indicates different countries of echovirus 30 isolates included in the tree. The outgroup is echovirus 21 Farina. The E30 sequences generated by metagenomic next-generation sequencing ae highlighted in red.

was the most common serotype detected (n = 9, 39% of enteroviruses), followed by enterovirus A71 and enterovirus B80 (1 each, 4.3%). Phylogenetically, the 9 E30 strains sequenced in our study belonged to 2 distinct genogroups, V and VIIb, and showed close relationship with E30 strains circulating in Russia and elsewhere in Asia, including China (Figure 4).

In additional to enterovirus sequences, a gemycircularvirus genome was obtained from a 12-year-old boy. Phylogenetic analysis revealed that this gemycircularvirus strain was closely related to a gemycircularvirus species previously found in CSF sample from a patient with a CNS infection of unknown origin in Sri Lanka (*12*); the level of amino acid identities between the 2 strains were 98.79% for replication-coding sequences and 99.3% for capsid protein–coding sequences.

## Discussion

We describe a viral mNGS investigation characterizing the human virome in CSF of 204 patients in Vietnam with suspected CNS infection of unknown origin. We successfully detected 4 human viral pathogens (enteroviruses, HIV, HBV, and MCV) and 1 virus species (gemycircularvirus) of unknown tropism and pathogenicity in a total of 30 (14.7%) patients. Most patients therefore remained without a known etiology, underscoring the ongoing challenge in identifying a plausible viral pathogen in CSF of patients with CNS infections.

Enteroviruses were the most common viruses, found in 11.3% (23/204) of all analyzed patients (Figure 2), most of whom were children and young adults. This age distribution of enterovirus-infected patients is consistent with observational data from a previous report from Vietnam (*6*), although the median age was slightly higher compared with data from other countries (*13*,*14*). Geographically, all the enterovirus-infected patients were admitted to hospitals from central and highland Vietnam, and none was from southern Vietnam. The underlying mechanism determining this observed spatial pattern of enterovirus-positive cases in this study remains unknown. Our sampling timescale perhaps was not long enough to capture the circulation of enteroviruses in Dong Thap Province. Enteroviruses were previously reported as a leading cause of CNS infection across central and southern Vietnam (*6*,*15*,*16*). Collectively, our findings suggest that reverse transcription PCR (RT-PCR) testing for enteroviruses should be considered in children and young adults with CNS infections.

Of the detected enteroviruses, E30 was the most common serotype. E30 is a well-known pathogen of pediatric aseptic meningitis worldwide (*17*). Phylogenetically, at global scale, E30 belongs to 2 different lineages with distinct patterns of circulation and spread, 1 with a global distribution and the other with geographic restriction within Asia (*17*). The cocirculation of 2 E30 lineages in Vietnam suggests that E30 was imported into Vietnam on at least 2 occasions. Our analyses thus also contribute to the body of knowledge about the genetic diversity of E30 strains circulating in Vietnam.

The detection of bloodborne viruses such as HBV and HIV is unlikely to have a direct link with patients' neurologic symptoms, although HBV has previously been reported in CSF of patients with CNS infections of unknown origin (*18*). The detection of HIV in CSF might have been a consequence of traumatic tap occurring during the lumbar puncture, as reflected by the high number of red blood cells in 1 of 2 HIV-positive CSF samples (data not shown). However, neuroinvasion of HIV has also been reported (*19*). Likewise, the pathogenic potential of a gemycircularvirus genome requires further investigation, although the detection of the gemycircularvirus genome in CSF has been reported in several papers (*12*,*18*,*20*). The detection of MCV and papillomavirus in CSF might result from contamination of viral skin flora during lumbar puncture.

Similar to previous reports about discrepancy between mNGS and conventional diagnostic testing (*8*,*18*,*21*), our observations found that most mNGS-positive results were not confirmed by subsequent viral RT-PCR assays, especially the sensitive enterovirus-specific RT-PCR with a limit of detection of ≈9 copies/reaction (*22*). Such results could be attributable to bleedover (also called index hopping) of indices from reads of 1 sample into reads of another sample co-sequenced on the same Illumina run (R. Sinha et al., unpub. data, https://doi.org/10.1101/125724). Applying double indexes, which was not used in our study, has been shown to substantially reduce, but not eliminate, the cross-contamination phenomenon between samples in the same run.

Our study has some limitations. First, as outlined previously, we did not employ a double unique index combination strategy per sample as part of the sequencing procedure. The well-known index hopping phenomenon possibly explains the high discrepancy between confirmatory PCR and mNGS results (*21*,*23*,*24*) and emphasizes the usefulness of dual indexing and including no template controls. As such, we pragmatically chose to verify our mNGS by performing specific PCR on original materials. Second, the DNase treatment step in our assay meant to reduce cellular DNA concentration in CSF

might reduce the sensitivity of mNGS for the detection of DNA viruses such as herpes simplex virus (*25*,*26*). Third, some of the non–PCR-confirmed viral sequences likely originated from contamination of reagents, which is a lingering problem for mNGS (*27*,*28*).

In summary, our results emphasize that mNGS could detect a broad range of viral nucleic acids in CSF. In spite of extensive investigation, establishing the etiology in many patients with CNS infections remains a challenge. However, our findings indicate that enteroviruses are important causes of viral CNS infections in Vietnam and thus should be considered in the differential diagnosis among young patients with CNS infections.

VIZIONS Consortium members: from the Oxford University Clinical Research Unit, Bach Tuan Kiet, Stephen Baker, Alessandra Berto, Maciej F. Boni, Juliet E. Bryant, Bui Duc Phu, James I. Campbell, Juan Carrique-Mas, Dang Manh Hung, Dang Thao Huong, Dang Tram Oanh, Jeremy N. Day, Dinh Van Tan, H. Rogier van Doorn, Duong An Han, Jeremy J. Farrar, Hau Thi Thu Trang, Ho Dang Trung Nghia, Hoang Bao Long, Hoang Van Duong, Huynh Thi Kim Thu, Lam Chi Cuong, Le Manh Hung, Le Thanh Phuong, Le Thi Phuc, Le Thi Phuong, Le Xuan Luat, Luu Thi Thu Ha, Ly Van Chuong, Mai Thi Phuoc Loan, Behzad Nadjm, Ngo Thanh Bao, Ngo Thi Hoa, Ngo Tri Tue, Nguyen Canh Tu, Nguyen Dac Thuan, Nguyen Dong, Nguyen Khac Chuyen, Nguyen Ngoc An, Nguyen Ngoc Vinh, Nguyen Quoc Hung, Nguyen Thanh Dung, Nguyen Thanh Minh, Nguyen Thi Binh, Nguyen Thi Hong Tham, Nguyen Thi Hong Tien, Nguyen Thi Kim Chuc, Nguyen Thi Le Ngoc, Nguyen Thi Lien Ha, Nguyen Thi Nam Lien, Nguyen Thi Ngoc Diep, Nguyen Thi Nhung, Nguyen Thi Song Chau, Nguyen Thi Yen Chi, Nguyen Thieu Trinh, Nguyen Thu Van, Nguyen Van Cuong, Nguyen Van Hung, Nguyen Van Kinh, Nguyen Van Minh Hoang, Nguyen Van My, Nguyen Van Thang, Nguyen Van Thanh, Nguyen Van Vinh Chau, Nguyen Van Xang, Pham Ha My, Pham Hong Anh, Pham Thi Minh Khoa, Pham Thi Thanh Tam, Pham Van Lao, Pham Van Minh, Phan Van Be Bay, Maia A. Rabaa, Motiur Rahman, Corinne Thompson, Guy Thwaites, Ta Thi Dieu Ngan, Tran Do Hoang Nhu, Tran Hoang Minh Chau, Tran Khanh Toan, Tran My Phuc, Tran Thi Kim Hong, Tran Thi Ngoc Dung, Tran Thi Thanh Thanh, Tran Thi Thuy Minh, Tran Thua Nguyen, Tran Tinh Hien, Trinh Quang Tri, Vo Be Hien, Vo Nhut Tai, Vo Quoc Cuong, Voong Vinh Phat, Vu Thi Lan Huong, Vu Thi Ty Hang, and Heiman Wertheim; from the Centre for Immunity, Infection, and Evolution, University Of Edinburgh, Edinburgh, Scotland, UK, Carlijn Bogaardt, Margo Chase-Topping, Al Ivens, Lu Lu, Dung Nyugen, Andrew Rambaut, Peter Simmonds, and Mark Woolhouse; from The Wellcome Trust Sanger Institute, Hinxton, UK, Matthew Cotten, Bas B. Oude Munnink, Paul Kellam, and My Vu Tra Phan; from the Laboratory of Experimental Virology, Department of Medical Microbiology, Center for Infection and Immunity Amsterdam (CINIMA), Academic Medical Center of the University of Amsterdam, Amsterdam, the Netherlands, Martin Deijs, Lia van der Hoek, Maarten F. Jebbink, and Seyed Mohammad Jazaeri Farsani; and from Metabiota, California, USA, Karen Saylors and Nathan Wolfe.

### Acknowledgments

We would like to thank Le Thi Kim Thanh for her logistic support and the patients for their participation in this study.

The study was funded by the Wellcome Trust of Great Britain (awards nos. WT/093724 and 106680/B/14/Z [to the Oxford University Clinical Research Unit in Vietnam], 100087/Z/12/Z [to S.B.] and 204904/Z/16/Z [to L.V.T.]), and the Royal Society (grant no. 098511/Z/12/Z [to S.B.]). X.D. and E.D. were supported by the Blood Systems Research Institute and the National Heart, Lung, and Blood Institute (grant no. R01 HL105770).

## About the Author

Ms. Nguyen is a PhD student in life science at Open University, Milton Keynes, UK. Her research interests are virus discovery and evolution of emerging pathogens such as enteroviruses.

### References

1. Granerod J, Tam CC, Crowcroft NS, Davies NWS, Borchert M, Thomas SL. Challenge of the unknown. A systematic review of acute encephalitis in non-outbreak situations. Neurology. 2010;75:924–32. https://doi.org/10.1212/WNL.0b013e3181f11d65
2. Feigin VL, Krishnamurthi RV, Theadom AM, Abajobir AA, Mishra SR, Ahmed MB, et al.; GBD 2015 Neurological Disorders Collaborator Group. Global, regional, and national burden of neurological disorders during 1990-2015: a systematic analysis for the Global Burden of Disease Study 2015. Lancet Neurol. 2017;16:877–97. https://doi.org/10.1016/S1474-4422(17)30299-5
3. World Health Organization. Neurological disorders: public health challenges. 2006 [cited 2017 Nov 11]. https://www.who.int/mental_health/publications/neurological_disorders_ph_challenges
4. Sejvar JJ. West nile virus: an historical overview. Ochsner J. 2003;5:6–10.
5. Rabaa MA, Tue NT, Phuc TM, Carrique-Mas J, Saylors K, Cotten M, et al. The Vietnam Initiative on Zoonotic Infections (VIZIONS): a strategic approach to studying emerging zoonotic infectious diseases. EcoHealth. 2015;12:726–35. https://doi.org/10.1007/s10393-015-1061-0

6. Ho Dang Trung N, Le Thi Phuong T, Wolbers M, Nguyen Van Minh H, Nguyen Thanh V, Van MP, et al.; VIZIONS CNS Infection Network. Aetiologies of central nervous system infection in Viet Nam: a prospective provincial hospital-based descriptive surveillance study. PLoS One. 2012;7:e37825. https://doi.org/10.1371/journal.pone.0037825
7. Brown JR, Bharucha T, Breuer J. Encephalitis diagnosis using metagenomics: application of next generation sequencing for undiagnosed cases. J Infect. 2018;76:225–40. https://doi.org/10.1016/j.jinf.2017.12.014
8. Anh NT, Hong NTT, Nhu LNT, Thanh TT, Lau C-Y, Limmathurotsakul D, et al. Viruses in Vietnamese patients presenting with community-acquired sepsis of unknown cause. J Clin Microbiol. 2019;57:e00386–19. https://doi.org/10.1128/JCM.00386-19
9. Aiemjoy K, Altan E, Aragie S, Fry DM, Phan TG, Deng X, et al. Viral species richness and composition in young children with loose or watery stool in Ethiopia. BMC Infect Dis. 2019;19:53. https://doi.org/10.1186/s12879-019-3674-3
10. Kroneman A, Vennema H, Deforche K, v d Avoort H, Peñaranda S, Oberste MS, et al. An automated genotyping tool for enteroviruses and noroviruses. J Clin Virol. 2011;51:121–5. https://doi.org/10.1016/j.jcv.2011.03.006
11. Nguyen LT, Schmidt HA, von Haeseler A, Minh BQ. IQ-TREE: a fast and effective stochastic algorithm for estimating maximum-likelihood phylogenies. Mol Biol Evol. 2015;32:268–74. https://doi.org/10.1093/molbev/msu300
12. Phan TG, Mori D, Deng X, Rajidrajith S, Ranawaka U, Fan Ng TF, et al. Small viral genomes in unexplained cases of human encephalitis, diarrhea, and in untreated sewage. Virology. 2015;482:98–104. https://doi.org/10.1016/j.virol.2015.03.011
13. Sun Y, Miao Z, Yan J, Gong L, Chen Y, Chen Y, et al. Sero-molecular epidemiology of enterovirus-associated encephalitis in Zhejiang Province, China, from 2014 to 2017. Int J Infect Dis. 2019;79:58–64. https://doi.org/10.1016/j.ijid.2018.11.002
14. Richter J, Tryfonos C, Christodoulou C. Molecular epidemiology of enteroviruses in Cyprus 2008–2017. PLoS One. 2019;14:e0220938. https://doi.org/10.1371/journal.pone.0220938
15. Taylor WR, Nguyen K, Nguyen D, Nguyen H, Horby P, Nguyen HL, et al. The spectrum of central nervous system infections in an adult referral hospital in Hanoi, Vietnam. PLoS One. 2012;7:e42099. https://doi.org/10.1371/journal.pone.0042099
16. Tan V, Thai H, Phu NH, Nghia HDT, Chuong LV, Sinh DX, et al. Viral aetiology of central nervous system infections in adults admitted to a tertiary referral hospital in southern Vietnam over 12 years. PLoS Negl Trop Dis. 2014;8:e3127. https://doi.org/10.1371/journal.pntd.0003127
17. Lema C, Torres C, Van der Sanden S, Cisterna D, Freire MC, Gómez RM. Global phylodynamics of Echovirus 30 revealed differential behavior among viral lineages. Virology. 2019;531:79–92. https://doi.org/10.1016/j.virol.2019.02.012
18. Schibler M, Brito F, Zanella MC, Zdobnov EM, Laubscher F, L'Huillier AG, et al. Viral sequences detection by high-throughput sequencing in cerebrospinal fluid of individuals with and without central nervous system disease. Genes (Basel). 2019;10:1–12. https://doi.org/10.3390/genes10080625
19. Zayyad Z, Spudich S. Neuropathogenesis of HIV: from initial neuroinvasion to HIV-associated neurocognitive disorder (HAND). Curr HIV/AIDS Rep. 2015;12:16–24. https://doi.org/10.1007/s11904-014-0255-3
20. Zhou C, Zhang S, Gong Q, Hao A. A novel gemycircular-virus in an unexplained case of child encephalitis. Virol J. 2015;12:197. https://doi.org/10.1186/s12985-015-0431-0
21. Wilson MR, Sample HA, Zorn KC, Arevalo S, Yu G, Neuhaus J, et al. Clinical metagenomic sequencing for diagnosis of meningitis and encephalitis. N Engl J Med. 2019;380:2327–40. https://doi.org/10.1056/NEJMoa1803396
22. Thanh TT, Anh NT, Tham NT, Van HM, Sabanathan S, Qui PT, et al. Validation and utilization of an internally controlled multiplex Real-time RT-PCR assay for simultaneous detection of enteroviruses and enterovirus A71 associated with hand foot and mouth disease. Virol J. 2015;12:85. https://doi.org/10.1186/s12985-015-0316-2
23. Wilson MR, Fedewa G, Stenglein MD, Olejnik J, Rennick LJ, Nambulli S, et al. Multiplexed metagenomic deep sequencing to analyze the composition of high-priority pathogen reagents. mSystems. 2016;1:1–9. https://doi.org/10.1128/mSystems.00058-16
24. Yang J, Yang F, Ren L, Xiong Z, Wu Z, Dong J, et al. Unbiased parallel detection of viral pathogens in clinical samples by use of a metagenomic approach. J Clin Microbiol. 2011;49:3463–9. https://doi.org/10.1128/JCM.00273-11
25. Nguyen TTH, Nguyen TA, Nguyen Thi Hoang M, Ho DTN, Le NNT. Tran tan T, et al. Performance of metagenomic next-generation sequencing for the diagnosis of viral meningoencephalitis in a resource limited setting. Open Forum Infect Dis. 2020;7:ofaa046. https://doi.org/10.1093/ofid/ofaa046
26. Perlejewski K, Popiel M, Laskus T, Nakamura S, Motooka D, Stokowy T, et al. Next-generation sequencing (NGS) in the identification of encephalitis-causing viruses: Unexpected detection of human herpesvirus 1 while searching for RNA pathogens. J Virol Methods. 2015;226:1–6. https://doi.org/10.1016/j.jviromet.2015.09.010
27. Asplund M, Kjartansdóttir KR, Mollerup S, Vinner L, Fridholm H, Herrera JAR, et al. Contaminating viral sequences in high-throughput sequencing viromics: a linkage study of 700 sequencing libraries. Clin Microbiol Infect. 2019;25:1277–85. https://doi.org/10.1016/j.cmi.2019.04.028
28. Holmes EC. Reagent contamination in viromics: all that glitters is not gold. Clin Microbiol Infect. 2019;25:1167–8. https://doi.org/10.1016/j.cmi.2019.06.019


Address for correspondence: Nguyen To Anh or Le Van Tan, Oxford University Clinical Research Unit, 764 VoVan Kiet, District 5, Ho Chi Minh City, Vietnam; email: anhnt@oucru.org or email: tanlv@oucru.org

# Recency-Weighted Statistical Modeling Approach to Attribute Illnesses Caused by 4 Pathogens to Food Sources Using Outbreak Data, United States

Michael B. Batz, LaTonia C. Richardson, Michael C. Bazaco, Cary Chen Parker, Stuart J. Chirtel, Dana Cole,[1] Neal J. Golden, Patricia M. Griffin, Weidong Gu,[2] Susan K. Schmitt,[3] Beverly J. Wolpert, Joanna S. Zablotsky Kufel, R. Michael Hoekstra[4]

Foodborne illness source attribution is foundational to a risk-based food safety system. We describe a method for attributing US foodborne illnesses caused by nontyphoidal *Salmonella enterica*, *Escherichia coli* O157, *Listeria monocytogenes,* and *Campylobacter* to 17 food categories using statistical modeling of outbreak data. This method adjusts for epidemiologic factors associated with outbreak size, down-weights older outbreaks, and estimates credibility intervals. On the basis of 952 reported outbreaks and 32,802 illnesses during 1998–2012, we attribute 77% of foodborne *Salmonella* illnesses to 7 food categories (seeded vegetables, eggs, chicken, other produce, pork, beef, and fruits), 82% of *E. coli* O157 illnesses to beef and vegetable row crops, 81% of *L. monocytogenes* illnesses to fruits and dairy, and 74% of *Campylobacter* illnesses to dairy and chicken. However, because *Campylobacter* outbreaks probably overrepresent dairy as a source of nonoutbreak campylobacteriosis, we caution against using these *Campylobacter* attribution estimates without further adjustment.

Each year in the United States, nontyphoidal *Salmonella*, *Escherichia coli* O157, *Listeria monocytogenes,* and *Campylobacter* cause >2 million estimated foodborne illnesses, 31,000 hospitalizations, and 700 deaths (*1*), representing an estimated $9–$11 billion in impacts to human health (*2*,*3*). Estimating the percentage of these illnesses attributable to the consumption of specific foods (i.e., foodborne illness source attribution) is foundational to a risk-based national food safety system (*4*). Such estimates can inform strategic planning, priority setting, risk assessments, economic analyses, and evaluations of the impacts of regulations and interventions (*5*).

Numerous studies in the United States and worldwide have estimated source attribution on the basis of aggregated foodborne outbreak data (*6*–*12*). For the United States, the Centers for Disease Control and Prevention (CDC) previously estimated the number of domestically acquired foodborne illnesses, hospitalizations, and deaths attributable to food categories based on analysis of outbreaks during 1998–2008 (*13*).

Through the Interagency Food Safety Analytics Collaboration (IFSAC), CDC, the US Food and Drug Administration, and the US Department of Agriculture Food Safety and Inspection Service work in partnership to develop improved source attribution estimates through multiple interconnected projects (*14*,*15*). This study reflects a tri-agency effort to update and harmonize estimates for the United States for nontyphoidal *Salmonella*, *E. coli* O157, *L. monocytogenes,* and *Campylobacter* using data from outbreaks that occurred during 1998–2012.

Author affiliations: US Food and Drug Administration, College Park, Maryland, USA (M.B. Batz, M.C. Bazaco, C. Chen Parker, S.J. Chirtel, B.J. Wolpert); Centers for Disease Control and Prevention, Atlanta, Georgia, USA (L.C. Richardson, D. Cole, P.M. Griffin, W. Gu, R.M. Hoekstra); US Department of Agriculture, Washington, DC, USA (N.J. Golden, S.K. Schmitt, J.S. Zablotsky Kufel)

DOI: https://doi.org/10.3201/eid2701.203832

[1]Current affiliation: US Department of Agriculture, Fort Collins, Colorado, USA.

[2]Current affiliation: US Department of Defense, Bethesda, Maryland, USA.

[3]Current affiliation: US Department of Veterans Affairs, Palo Alto, California, USA.

[4]Retired.

IFSAC's approach addresses some of the limitations of prior studies. We describe this method here. We use statistical modeling to mitigate the influence of large outbreaks that might bias estimates, and we incorporate epidemiologic factors relevant to outbreak size. We weight recent outbreaks more heavily than older ones and quantify uncertainty by estimating credibility intervals around estimates. We also use an updated food categorization scheme that better meets the needs of the regulatory agencies.

## Methods

### Data Sources

CDC's Foodborne Disease Outbreak Surveillance System (FDOSS) collects standardized reports submitted by state, local, and territorial health departments on foodborne disease outbreaks. In FDOSS, outbreaks are defined as the occurrence of ≥2 cases of a similar illness resulting from the ingestion of a common food (*16*). We extracted data from FDOSS on reported foodborne outbreaks caused by nontyphoidal *Salmonella enterica*, *E. coli* O157 (*E. coli* O157:H7 and *E. coli* O157:NM), *L. monocytogenes,* and *Campylobacter* spp., in which the first illness occurred in a US state or the District of Columbia during 1998–2012. We extracted data on December 18, 2013. Analysis was conducted by using SAS 9.3, JMP Pro (SAS Institute, https://www.sas.com), and R (R Foundation for Statistical Computing, https://www.r-project.org).

We included only outbreaks with a single causal pathogen and for which implicated foods could be assigned to a single food category because those outbreaks have the clearest information. We excluded outbreaks caused by multiple pathogens or for which no food or ingredient was implicated, including outbreaks with a complex food vehicle (i.e., consisting of ingredients belonging to >1 food category) for which the implicated ingredient was not determined. A previously published method (*13*) for assigning the food category for complex food outbreaks could not be applied to more recent data without substantial revision.

We excluded outbreaks for which implicated foods came from >1 food category (i.e., multiple foods). For example, an outbreak for which apples and cantaloupe were both implicated would be included because both fall into the fruits category, but an outbreak for which apples and cheese were both implicated would be excluded.

By using a hierarchical scheme of 22 food categories, we assigned outbreaks to a single category on the basis of implicated foods or ingredients (*17*). Because of sparse data, outbreaks in 8 food categories were aggregated into 3 combined categories: other meat and poultry (other meat, other poultry); other seafood (shellfish, other aquatic animals); and other produce (fungi, herbs, root-underground, nuts-seeds), resulting in 17 food categories for our analysis (Appendix Figure 1, https://wwwnc.cdc.gov/EID/article/27/1/20-3832-App1.pdf).

In FDOSS, an outbreak must have ≥2 ill persons (*16*). For *Salmonella*, *E. coli* O157, and *Campylobacter*, outbreaks with confirmed etiology are defined as those in which the outbreak strain was isolated from ≥2 patients or from epidemiologically implicated food; confirmed outbreaks of *L. monocytogenes* infections must have 1 person with the outbreak strain isolated from a normally sterile site (*18*). (Cases of listeriosis can also be diagnosed based on symptoms and culture of pregnancy-associated products of conception, which are not sterile.) The etiology of an outbreak not meeting these conditions is considered to be suspected. We found no statistically significant differences in outbreak size or foods implicated between outbreaks with confirmed and those with suspected status, and therefore included outbreaks with suspected etiology in the analysis (Appendix). The final dataset used for exploratory analysis and estimates of sources included 952 outbreaks assigned to 17 food categories (Table 1).

### Exploratory Analysis

We focused exploratory analysis on factors influencing outbreak size. We used the total number of reported illnesses as the measure of outbreak size. Whereas most outbreaks are small, some are very large. For example, of the 4,732 reported *Campylobacter* outbreak illnesses during the entire 15-year period, more than one third (1,644) were from a single outbreak. Large outbreaks might not be representative of the sources of sporadic illnesses and might overly influence estimates of food sources (*13*).

Untransformed outbreak size is skewed and varies across pathogens (Figure 1). Log transformation of outbreak size results in distributions that are more symmetric and normally distributed, although considerable variation remains within and across pathogens (Figure 1). We therefore used log-transformed outbreak size in statistical modeling.

FDOSS data include epidemiologic factors that might relate to the size and scope of an outbreak, including pathogen, number of states in which outbreak exposures occurred, implicated foods and ingredients, and the type of location in which food was prepared (e.g., restaurant or private home). We explored the relationships between outbreak size and these variables.

**Table 1.** Number of outbreaks and outbreak illnesses caused by a single pathogen and due to a single food category for *Salmonella, Escherichia coli* O157, *Listeria monocytogenes,* and *Campylobacter*, Foodborne Disease Outbreak Surveillance System, United States, 1998–2012*

| Food category | Nontyphoidal *Salmonella* spp. | *E. coli* O157 | *Listeria monocytegenes* | *Campylobacter* spp. | Total |
|---|---|---|---|---|---|
| Beef | 47 (1,473) | 97 (1,813) | 1 (4) | 2 (5) | 147 (3,295) |
| Pork | 51 (1,098) | 0 | 2 (11) | 1 (27) | 54 (1,136) |
| Chicken | 114 (2,648) | 1 (36) | 1 (3) | 24 (230) | 140 (2,917) |
| Turkey | 49 (1,308) | 1 (2) | 4 (124) | 5 (44) | 59 (1,478) |
| Other meat or poultry | 6 (84) | 2 (9) | 0 | 2 (6) | 10 (99) |
| Game | 2 (8) | 4 (18) | 0 | 1 (2) | 7 (28) |
| Dairy | 24 (793) | 18 (399) | 12 (124) | 106 (3,395) | 160 (4,711) |
| Eggs | 140 (5,245) | 0 | 0 | 0 | 140 (5,245) |
| Fish | 12 (286) | 0 | 0 | 1 (3) | 13 (289) |
| Other seafood | 4 (36) | 0 | 0 | 5 (344) | 9 (380) |
| Grains, beans | 7 (268) | 0 | 0 | 0 | 7 (268) |
| Oils, sugars | 0 | 0 | 0 | 1 (3) | 1 (3) |
| Fruits | 46 (2,510) | 11 (893) | 1 (147) | 2 (29) | 60 (3,579) |
| Seeded vegetables | 34 (4,001) | 0 | 0 | 3 (136) | 37 (4,137) |
| Sprouts | 33 (1,266) | 6 (55) | 2 (26) | 0 | 41 (1,347) |
| Vegetable row crops | 10 (412) | 29 (1,029) | 1 (10) | 7 (372) | 47 (1,823) |
| Other produce | 18 (1,923) | 1 (8) | 0 | 1 (136) | 20 (2,067) |
| Total | 597 (23,359) | 170 (4,262) | 24 (449) | 161 (4,732) | 952 (32,802) |

*Number of outbreak-associated illnesses in parentheses. Nontyphoidal *Salmonella* is divided into *S. enterica* serovar Enteritidis and other serovars (Appendix Table 2, https://wwwnc.cdc.gov/EID/article/27/1/20-3832-App1.pdf).

Distinct differences in distributions of outbreak size can be observed by pathogen and 3 categorical variables: food category, type of food preparation location, and whether exposures occurred in multiple states or a single state (Figure 2). For example, the mean size of multistate outbreaks is larger than single-state outbreaks for *Salmonella*, *E. coli* O157, and *L. monocytogenes*. Differences in grouped means can be observed for all 3 categorical variables for *L. monocytogenes* despite the small number of outbreaks.

### Statistical Modeling

Whereas prior studies calculated attribution proportions on the basis of observed counts of reported outbreak events or outbreak illnesses (*6*,*13*), in this study we developed a model-based approach to estimate the number of outbreak illnesses for attribution. This approach mitigates the impact of large outbreaks and enables the incorporation of epidemiologic factors beyond pathogen and food category.

After considering several approaches, we chose analysis of variance (ANOVA) of log-transformed outbreak sizes as the modeling framework, partly based on simplicity and interpretability (Appendix). For each pathogen, we developed a model to estimate the log-transformed number of illnesses based on the 3 factors shown to be associated with outbreak size: food category, type of food preparation location, and whether exposures occurred in multiple states or a single state. Each of these factors was found through

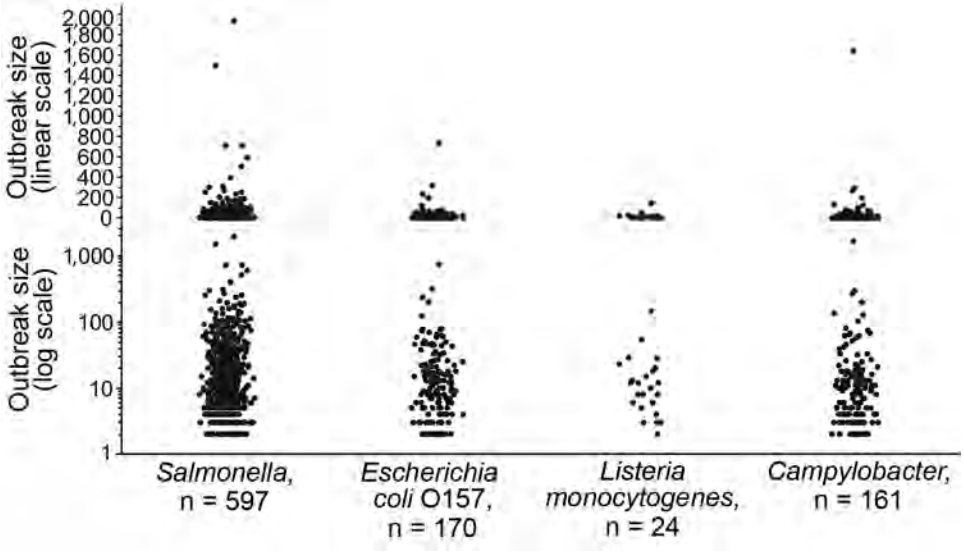


**Figure 1.** Number of reported illnesses for foodborne disease outbreaks caused by a single pathogen and attributable to a single food category, using linear and log scales, for *Salmonella*, *Escherichia coli* O157, *Listeria monocytogenes*, and *Campylobacter*, Foodborne Disease Outbreak Surveillance System, United States, 1998–2012.

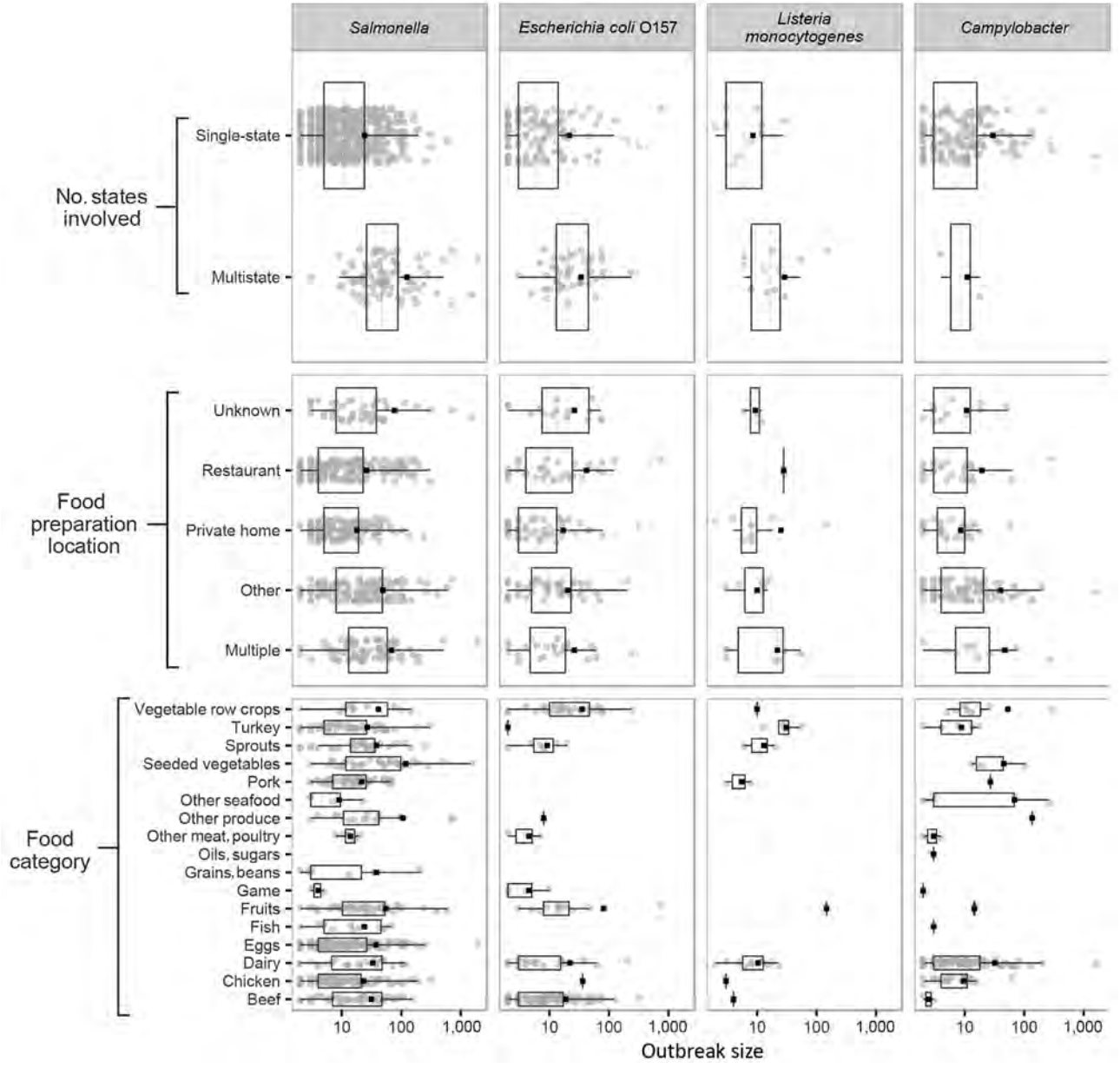


**Figure 2.** Number of reported illnesses (log scale) for foodborne disease outbreaks caused by a single pathogen and attributable to a single food category, for 3 outbreak characteristics, for *Salmonella, Escherichia coli O157, Listeria monocytogenes, and Campylobacter*, Foodborne Disease Outbreak Surveillance System, United States, 1998–2012. Each panel displays outbreak size for a given pathogen, grouped by 1 of 3 categorical variables. Each includes a scatterplot of individual outbreaks (indicated by solid circles), the mean (indicated by solid squares), and a boxplot showing median, interquartile range, and minimum and maximum values inside the inner and outer fences (1.5 interquartile range).

1-way ANOVA to be a statistically significant ($p<0.05$) predictor of outbreak size for ≥1 pathogens. Although not all 3 factors were significant for all pathogens, we included them to maintain uniformity across the analysis. We explored serotype-specific ANOVA models for *Salmonella*, but for most serotypes these models did not find different distributions of outbreaks across food categories or meaningful differences in outbreak size across the other factors. The exception was serotype Enteritidis, outbreaks of which did display differences from other serotypes. Therefore, we developed 2 distinct *Salmonella* ANOVA models: 1 for Enteritidis and 1 for all other serotypes.

Each of the 5 pathogen-specific models estimates the log-transformed number of illnesses for each reported outbreak on the basis of that outbreak's characteristics as defined by the categorical variables. We then back-transformed the model-estimated numbers of illnesses

(*e* raised to the transformed values) and summed the 2 sets of *Salmonella* estimates. Additional information on model selection and fit is presented in the Appendix.

As expected, ANOVA models reduce variation in outbreak size and the influence of very large outbreaks. This effect is shown in Appendix Figure 3, which compares the number of reported illnesses with the number of model-estimated illnesses. The figure also shows the wide variation in the number of outbreaks for different pathogen–food category pairs.

### Recency Weighting

Because of changes over time in food consumption patterns, food production and processing practices, food safety activities, regulatory interventions, and other factors, recent outbreaks are probably more representative of current foodborne illness attribution than older outbreaks. We explored estimating attribution on the basis of only 3, 5, or 7 years of the most recent outbreaks, but data sparseness and high year-to-year variability, particularly in food categories for which outbreaks were not reported every year, led to instability and more statistical uncertainty in attribution estimates when older outbreaks were excluded (Appendix). Therefore, we included older outbreaks but down-weighted them on the basis of recency. Outbreaks older than 5 years were multiplied by an exponential decay function, an approach long used in many fields to down-weight older data in forecasting and time-series models, including public health surveillance (*19*,*20*). This approach is flexible to inclusion of additional years of data; as the number of years of data increases, the earliest years have less and less weight.

The multiplicative recency-weighting factor $w$ for an outbreak in year $y$ is defined as a function of decay parameter $a$ and the most recent year of data $Y$:

$$w_y = \begin{cases} a^{(Y-5)-y}, y < Y-5 \\ 1, y \geq Y-5 \end{cases}$$

We used a decay parameter $a$ of 5/7 (0.7142). This factor resulted in outbreaks occurring during 2008–2012 providing 67% of the overall information, with 28% from outbreaks occurring during 2003–2007, and 5% outbreaks occurring during 1998–2002 (Appendix Table 4).

### Calculating Attribution Percentages

For pathogen $p$ and food category $c$, the attribution percentage $AP_{pc}$ is calculated by dividing the sum of recency-weighted model-estimated illnesses of that pathogen–food category pair across all years by the sum of recency-weighted model-estimated illnesses for all food categories associated with that pathogen for all years. The estimated attribution percentage $AP_{pc}$ is defined as:

$$AP_{pc} = \frac{\sum_y \sum_i w_y \times MEI\,(o_{pcyi})}{\sum_y \sum_c \sum_i w_y \times MEI\,(o_{pcyi})} \times 100$$

where $MEI\,(o_{pcyi})$ is the number of model-estimated illnesses for a specific outbreak $o_i$ and $i$ is the instance in the set of outbreaks associated with a pathogen–food pair occurring in a given year. To estimate 90% credibility intervals for each $AP_{pc}$, Bayesian bootstrap resampling (10,000 per pathogen–food category pair) was performed on the weighted model estimates (*21*,*22*). The 5th and 95th percentiles of the bootstrap distributions were used as the lower and upper bounds for the credibility intervals.

We conducted sensitivity analyses to examine the impacts of data selection and modeling choices on estimates. These analyses included comparing our attribution estimates to those based on reported outbreak illnesses and log-transformed illnesses, evaluating the impact of alternate ANOVA model specifications, examining the impact of recency-weighting choices and approaches, and evaluating the impact of particularly large and influential outbreaks.

## Results

We extracted data on 2,732 US outbreaks caused by nontyphoidal *Salmonella*, *E. coli* O157, *L. monocytogenes*, and *Campylobacter* that occurred during 1998–2012. We excluded 77 outbreaks because they were caused by multiple pathogens, excluded an additional 1,014 because they did not have an identified food vehicle, and excluded an additional 689 that could not be assigned to a single food category (Appendix Figure 2). These exclusions resulted in a dataset with 952 outbreaks (35% of 2,732), each caused by a single pathogen and assignable to 1 of 17 food categories (Table 1).

The final estimates (Table 2; Figure 3) attributed *Salmonella* illnesses more broadly than other pathogens, with nonzero estimates for 16 categories; of those, 4 food categories had estimated percentages >10%: seeded vegetables (e.g., tomatoes), eggs, fruits, and chicken. Cumulatively, the top 7 food categories accounted for 77% of illnesses. Credibility intervals for *Salmonella* were largely overlapping but comparatively narrow, attributable in part to the high number of *Salmonella* outbreaks in the analysis. In contrast, 82% of illnesses caused by *E. coli* O157 were attributed to only 2 food categories, beef and vegetable row crops (e.g., leafy greens). Only 2 other food categories, dairy and fruits, had estimated attribution percentages >1%. Similarly, 81% of illnesses caused by *L. monocytogenes* were attributed to 2 food categories, dairy and fruits.

**Table 2.** Estimated percentages of foodborne illnesses attributed to 17 food categories and 90% credibility intervals for *Salmonella*, *Escherichia coli* O157, *Listeria monocytogenes*, and *Campylobacter*, based on analysis of single pathogen, single food category outbreaks, Foodborne Disease Outbreak Surveillance System, 1998–2012*

| Food category | % (90% credibility interval) | | | |
|---|---|---|---|---|
| | *Salmonella* | *E. coli* O157 | *L. monocytogenes* | *Campylobacter* |
| Land animals | | | | |
| Beef | 9 (6–13) | 46 (36–55) | 0 (0–1) | 1 (<1–1) |
| Pork | 8 (6–10) | – | 2 (<1–8) | 3 (<1–8) |
| Chicken | 10 (7–13) | 0 (0–1) | 0 (0–2) | 8 (5–12) |
| Turkey | 7 (5–10) | 0 (0–<1) | 6 (2–16) | 2 (1–4) |
| Other meat or poultry | 0 (<1–1) | 0 (0–1) | – | 1 (<1–1) |
| Game | 0 (0–<1) | 1 (<1–3) | – | 0 (0–<1) |
| Dairy | 3 (1–5) | 9 (5–14) | 31 (12–64) | 66 (57–74) |
| Eggs | 12 (9–17) | – | – | – |
| Aquatic animals | | | | |
| Fish | 2 (1–3) | – | – | 0 (0–<1) |
| Other seafood | 0 (0–<1) | – | – | 6 (2–11) |
| Plants | | | | |
| Grains, beans | 1 (<1–2) | – | – | – |
| Oils, sugars | – | – | – | 0 (0–1) |
| Fruits | 12 (8–16) | 7 (3–12) | 50 (5–77) | 1 (<1–2) |
| Seeded vegetables | 18 (13–25) | – | – | 6 (1–13) |
| Sprouts | 8 (5–12) | 1 (<1–1) | 8 (1–22) | – |
| Vegetable row crops | 3 (1–6) | 36 (26–46) | 3 (<1–13) | 6 (2–11) |
| Other produce | 7 (3–11) | 1 (0–2) | – | 2 (<1–6) |

*Estimates calculated by using analysis of variance model–estimated outbreak illnesses for single pathogen, single food category outbreaks occurring during 1998–2012, with down-weighting of outbreaks that occurred during 1998–2007. Because of rounding, 0 indicates nonzero estimates <0.5. Dashes indicate pathogen–food category pairs for which we did not estimate attribution percentages because of a lack of outbreaks.

Only 4 other food categories (sprouts, turkey, vegetable row crops, and pork) had estimated attribution percentages >1%. The wide and overlapping credibility intervals reflect the very small number of *L. monocytogenes* outbreaks in the analysis (n = 24).

An estimated 66% of *Campylobacter* outbreak illnesses were attributed to the dairy category. This percentage was substantially higher than for any other food category. About 8% of illnesses are attributed to chicken; 6% were attributed respectively to vegetable row crops, seeded vegetables, and other seafood.

We found estimates to be robust across a wide variety of scenarios. We assessed the sensitivity of estimates to particularly influential outbreaks and to modeling decisions, such as choices in statistical modeling, down-weighting of older outbreaks, and consideration of etiology status (Appendix).

## Discussion

Although only a small proportion of foodborne illnesses are part of recognized outbreaks, outbreak investigations can provide insights into the causes and contributing factors leading to infection. Because linking an illness to a particular food is rarely possible except during an outbreak, aggregated data from foodborne outbreaks have been used to estimate the food sources of all illnesses caused by specific pathogens in numerous countries (*6*–*12*).

Whereas our approach addresses numerous challenges with estimating attribution percentages on the basis of outbreak data, some issues must be considered when using these estimates to inform food safety decision-making. Our analysis does not indicate the point of contamination, because outbreak investigations implicate only the food vehicle that was consumed. Moreover, the outbreaks included in this analysis include only 35% of the reported foodborne disease outbreaks caused by these pathogens during the study period, and they might not be representative of all foodborne outbreaks caused by these pathogens. The exclusion of outbreaks attributable to complex foods for which the contaminated ingredient was not determined could result in underrepresentation of food categories containing foods often eaten as part of complex dishes (e.g., leafy greens and eggs) (*23*). However, because the published method for assigning food categories to these complex food outbreaks is somewhat subjective and relies on internet searches for recipes (*24*), excluding these outbreaks provides results based on the most accurate available data. A method to incorporate data from these outbreaks is being developed.

Foods are implicated in outbreaks through epidemiologic analyses, by isolation of the causal pathogen from implicated food, through examination of supply chain records or environmental assessments, or by other information. The strength of evidence implicating foods varies widely across outbreaks.

For some pathogens and pathogen–food pairs, the number of outbreaks available for analyses was

quite low. For example, our data include only 24 outbreaks caused by *L. monocytogenes*, so 1 fruits-linked outbreak (a very large outbreak that occurred in 2011 and was associated with contaminated cantaloupe) had a profound influence on attribution estimates for this pathogen. However, our approach reflects the uncertainties associated with sparse data in wider credibility intervals.

Although we weighted recent outbreaks more heavily than older ones because recent outbreaks are probably more representative of current attribution, we did not formally account for possible changes in underlying factors over time in the main effects model. Examples of such factors could include changes in pathogen-specific disease incidence, outbreak investigation practices, or outbreak reporting by states. Generalizing outbreak-based attribution to overall foodborne disease assumes, implicitly, that the foods implicated in outbreaks reflect the food sources of illness in the general population. However, these assumptions might not always hold. For example, ≈10% of outbreaks occurred among institutionalized populations, such as those in correctional facilities, hospitals, and nursing homes. In these populations, case-ascertainment rates, food options, and sources of food contamination might not be representative of the general population. However, such outbreaks might elucidate setting- or subpopulation-specific contamination problems that are difficult to identify among the general population.

*Campylobacter* attribution presents a specific challenge. Our outbreak-based model attributes 66% (90% credibility interval 57%–74%) of foodborne campylobacteriosis to dairy, which is in line with other outbreak-based estimates for the United States (*6*,*13*). However, most foodborne *Campylobacter* outbreaks in this study were associated with unpasteurized fluid milk, which is not widely consumed by the general population. For example, in a Foodborne Active Surveillance Network population survey of food exposures, only 3% reported consuming unpasteurized milk in the preceding week (*25*). Moreover, outbreak-based estimates are not consistent with other lines of evidence. An analysis of 38 case–control studies of sporadic campylobacteriosis found a much smaller percentage of illnesses attributable to consumption of raw milk than chicken (*12*). For example, 1 of these studies, a Foodborne Active Surveillance Network

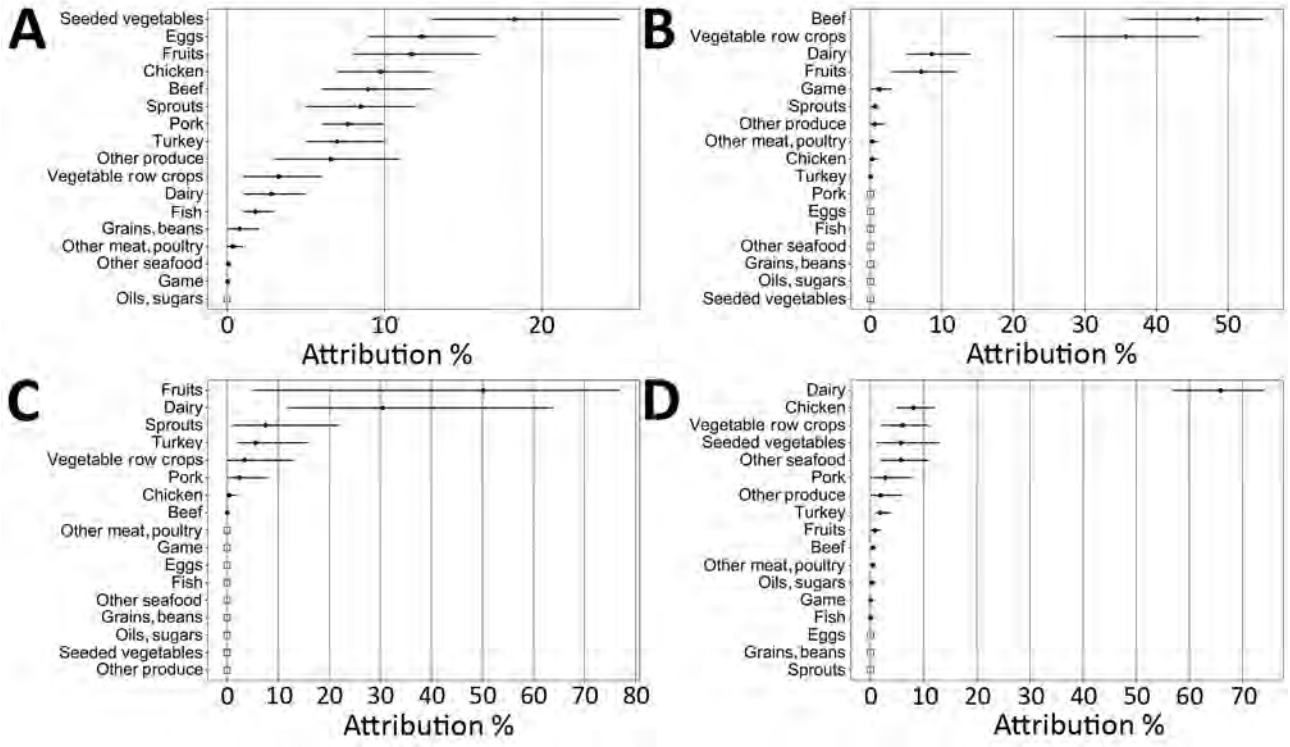


**Figure 3.** Estimated percentages of foodborne illnesses attributed to food categories and 90% credibility intervals (error bars) for *Salmonella* (A), *Escherichia coli* O157 (B), *Listeria monocytogenes* (C), *and Campylobacter* (D), based on analysis of single-pathogen, single-food category outbreaks, Foodborne Disease Outbreak Surveillance System, United States, 1998–2012. Percentages are presented in descending order. Open squares indicate that no illnesses were attributed to that food category because no outbreaks were reported for that pathogen in that food category during the study period. Estimates calculated by using analysis of variance model–estimated outbreak illnesses for single pathogen, single food category outbreaks occurring during 1998–2012, with down-weighting of outbreaks that occurred during 1998–2007.

case–control study, attributed 1.5% of campylobacteriosis cases to consumption of unpasteurized milk, compared with 24% to consumption of chicken prepared in a restaurant (*26*). Structured expert judgment studies conducted in the United States and in other countries estimate 8%–10% of foodborne campylobacteriosis to be attributable to dairy products (principally, raw milk), compared with 33%–72% to chicken (*27*–*30*).

Because *Campylobacter* outbreaks appear to overrepresent dairy as a source of sporadic *Campylobacter* illness, we do not advise using these attribution percentages without further adjustment or without considering additional information. Removing the dairy category entirely might be an appropriate adjustment, given that the resulting distribution of *Campylobacter* attribution estimates across other food categories is more consistent with the published literature (*31*). When the dairy category is excluded from this analysis, 29% of *Campylobacter* illnesses are attributed to poultry (23.5% to chicken and 5.5% to turkey), 18% to vegetable row crops, 17% to seeded vegetables, 17% to other seafood, 8% to pork, 6% to other produce, and 6% to other food categories.

Our estimates reflect data on outbreaks that occurred during 1998–2012 because those were the most recent data available at the outset of this effort. We do not include more recent outbreaks in this analysis because substantial preparation of the data was needed, and because the primary purpose of this report is to describe our methods and explain modeling decisions. IFSAC has published reports based on more recent outbreaks using the methodology described in this article (*32*).

To address some of the challenges with using outbreak data to estimate the food categories responsible for foodborne illnesses, we developed an approach that reduces the influence of large outbreaks, adjusts for important epidemiologic characteristics, and weights recent data more heavily than older data. We also incorporate an updated food categorization scheme better aligned to the needs of regulatory agencies and provide statistical uncertainty around the estimates. This approach can be used for routine updating of estimates by incorporating additional years of data.

The resulting estimates of attribution percentages for *Salmonella*, *E. coli* O157, *L. monocytogenes*, and *Campylobacter* can play an important role in science- and risk-based decision-making because they can be used alongside other data to inform regulatory decisions, to prioritize food safety efforts, and to evaluate the effectiveness of prevention measures. Further, federal agency consensus on a single set of outbreak-based attribution estimates improves the transparency of governmental efforts to inform and engage stakeholders, such as industry and consumers, about food safety strategies.

### Acknowledgments

The authors are indebted to Christopher Alvares, Christopher Aston, Marc Boyer, Chris Braden, Beau Bruce, Eric Ebel, David Goldman, Chuanfa Guo, Kristin Holt, Shacara Johnson, Sherri McGarry, Kara Morgan, Debra Street, Robert Tauxe, Curtis Travis, Iris Valentin-Bon, Antonio Vieira, Katherine Vierk, Christopher Waldrop, Michael Williams, and others within Centers for Disease Control and Prevention (CDC), the Food and Drug Administration, and the US Department of Agriculture's Food Safety and Inspection Service who provided input on this work. We also thank the many other persons from outside these agencies who shared feedback. Special thanks also go to the CDC National Outbreak Reporting System Team for access and guidance in using outbreak data, and to the state, local, tribal, and territorial health departments who report these outbreaks to CDC.

### About the Author

Mr. Batz is a senior policy advisor in the Office of Analytics and Outreach, Center for Food Safety and Applied Nutrition, US Food and Drug Administration. His research focus is on improving public health decision-making by quantifying foodborne disease risks.

### References

1. Scallan E, Hoekstra RM, Angulo FJ, Tauxe RV, Widdowson MA, Roy SL, et al. Foodborne illness acquired in the United States—major pathogens. Emerg Infect Dis. 2011;17:7–15. https://doi.org/10.3201/eid1701.P11101
2. Hoffmann S, Maculloch B, Batz MB. Economic burden of major foodborne illnesses acquired in the United States. Washington: US Department of Agriculture Economic Research Service; 2015. Economic Information Bulletin No. (EIB-140) [cited 2018 Jun 6]. https://www.ers.usda.gov/publications/pub-details/?pubid=43987
3. Minor T, Lasher A, Klontz K, Brown B, Nardinelli C, Zorn D. The per case and total annual costs of foodborne illness in the United States. Risk Anal. 2015;35:1125–39. https://doi.org/10.1111/risa.12316
4. Institute of Medicine and National Research Council Committee on the Review of Food and Drug Administration's Role in Ensuring Safe Food. Enhancing food safety: the role of the Food and Drug Administration. Wallace RB, Oria M, editors. Washington: National Academies Press; 2010.
5. Mangen MJ, Batz MB, Käsbohrer A, Hald T, Morris JG Jr, Taylor M, et al. Integrated approaches for the public health prioritization of foodborne and zoonotic pathogens. Risk Anal. 2010;30:782–97. https://doi.org/10.1111/j.1539-6924.2009.01291.x

6. Batz MB, Hoffmann S, Morris JG Jr. Ranking the disease burden of 14 pathogens in food sources in the United States using attribution data from outbreak investigations and expert elicitation. J Food Prot. 2012;75:1278–91. https://doi.org/10.4315/0362-028X.JFP-11-418
7. Greig JD, Ravel A. Analysis of foodborne outbreak data reported internationally for source attribution. Int J Food Microbiol. 2009;130:77–87. https://doi.org/10.1016/j.ijfoodmicro.2008.12.031
8. Jackson BR, Griffin PM, Cole D, Walsh KA, Chai SJ. Outbreak-associated *Salmonella enterica* serotypes and food commodities, United States, 1998–2008. Emerg Infect Dis. 2013;19:1239–44. https://doi.org/10.3201/eid1908.121511
9. King N, Lake R, Campbell D. Source attribution of nontyphoid salmonellosis in New Zealand using outbreak surveillance data. J Food Prot. 2011;74:438–45. https://doi.org/10.4315/0362-028X.JFP-10-323
10. Pires SM, Vigre H, Makela P, Hald T. Using outbreak data for source attribution of human salmonellosis and campylobacteriosis in Europe. Foodborne Pathog Dis. 2010;7:1351–61. https://doi.org/10.1089/fpd.2010.0564
11. Ravel A, Greig J, Tinga C, Todd E, Campbell G, Cassidy M, et al. Exploring historical Canadian foodborne outbreak data sets for human illness attribution. J Food Prot. 2009;72:1963–76. https://doi.org/10.4315/0362-028X-72.9.1963
12. Domingues AR, Pires SM, Halasa T, Hald T. Source attribution of human campylobacteriosis using a meta-analysis of case-control studies of sporadic infections. Epidemiol Infect. 2012;140:970–81. https://doi.org/10.1017/S0950268811002676
13. Painter JA, Hoekstra RM, Ayers T, Tauxe RV, Braden CR, Angulo FJ, et al. Attribution of foodborne illnesses, hospitalizations, and deaths to food commodities by using outbreak data, United States, 1998–2008. Emerg Infect Dis. 2013;19:407–15. https://doi.org/10.3201/eid1903.111866
14. Interagency Food Safety Analytics Collaboration. About IFSAC. 2017 [cited 2017 Aug 7]. https://www.cdc.gov/foodsafety/ifsac/overview/index.html
15. Ebel ED, Williams MS, Cole D, Travis CC, Klontz KC, Golden NJ, et al. Comparing characteristics of sporadic and outbreak-associated foodborne illnesses, United States, 2004–2011. Emerg Infect Dis. 2016;22:1193–200. https://doi.org/10.3201/eid2207.150833
16. Gould LH, Walsh KA, Vieira AR, Herman K, Williams IT, Hall AJ, et al.; Centers for Disease Control and Prevention. Surveillance for foodborne disease outbreaks—United States, 1998–2008. MMWR Surveill Summ. 2013;62:1–34.
17. Richardson LC, Bazaco MC, Parker CC, Dewey-Mattia D, Golden N, Jones K, et al. An updated scheme for categorizing foods implicated in foodborne disease outbreaks: a tri-agency collaboration. Foodborne Pathog Dis. 2017;14:701–10. https://doi.org/10.1089/fpd.2017.2324
18. Centers for Disease Control and Prevention. Guide to confirming an etiology in foodborne disease outbreak. 2015 [cited 2018 Jul 12]. https://www.cdc.gov/foodsafety/outbreaks/investigating-outbreaks/confirming_diagnosis.html
19. Brown RG. Smoothing, forecasting and prediction of discrete time series. Englewood Cliffs (NJ): Prentice-Hall; 1963.
20. Ngo L, Tager IB, Hadley D. Application of exponential smoothing for nosocomial infection surveillance. Am J Epidemiol. 1996;143:637–47. https://doi.org/10.1093/oxfordjournals.aje.a008794
21. Rubin DB. The Bayesian bootstrap. Ann Stat. 1981;9:130–4. https://doi.org/10.1214/aos/1176345338
22. Davison AC, Hinkley DV. Bootstrap methods and their application. Cambridge and New York: Cambridge University Press; 1997.
23. St Louis ME, Morse DL, Potter ME, DeMelfi TM, Guzewich JJ, Tauxe RV, et al. The emergence of grade A eggs as a major source of *Salmonella enteritidis* infections. New implications for the control of salmonellosis. JAMA. 1988;259:2103–7. https://doi.org/10.1001/jama.1988.03720140023028
24. Painter JA, Ayers T, Woodruff R, Blanton E, Perez N, Hoekstra RM, et al. Recipes for foodborne outbreaks: a scheme for categorizing and grouping implicated foods. Foodborne Pathog Dis. 2009;6:1259–64. https://doi.org/10.1089/fpd.2009.0350
25. Centers for Disease Control and Prevention. Foodborne Active Surveillance Network (FoodNet) population survey atlas of exposure, 2006–2007. Atlanta: US Department of Health and Human Services, Centers for Disease Control and Prevention; 2011 [cited 2019 Dec 12]. https://www.cdc.gov/foodnet/surveys/foodnetexposureatlas0607_508.pdf
26. Friedman CR, Hoekstra RM, Samuel M, Marcus R, Bender J, Shiferaw B, et al.; Emerging Infections Program FoodNet Working Group. Risk factors for sporadic *Campylobacter infection* in the United States: a case-control study in FoodNet sites. Clin Infect Dis. 2004;38(Suppl 3):S285–96. https://doi.org/10.1086/381598
27. Hoffmann S, Fischbeck P, Krupnick A, McWilliams M. Using expert elicitation to link foodborne illnesses in the United States to foods. J Food Prot. 2007;70:1220–9. https://doi.org/10.4315/0362-028X-70.5.1220
28. Havelaar AH, Galindo AV, Kurowicka D, Cooke RM. Attribution of foodborne pathogens using structured expert elicitation. Foodborne Pathog Dis. 2008;5:649–59. https://doi.org/10.1089/fpd.2008.0115
29. Tam CC, Larose T, O'Brien SJ. Costed extension to the Second Study of Infectious Intestinal Disease in the Community: identifying the proportion of foodborne disease in the UK and attributing foodborne disease by food commodity. Liverpool (UK): University of Liverpool; 2014. Project B18021 (FS231043) [cited 2019 Dec 12]. https://livrepository.liverpool.ac.uk/3014609
30. Butler AJ, Pintar KD, Thomas MK. Estimating the relative role of various subcategories of food, water, and animal contact transmission of 28 enteric diseases in Canada. Foodborne Pathog Dis. 2016;13:57–64. https://doi.org/10.1089/fpd.2015.1957
31. Interagency Food Safety Analytics Collaboration. Foodborne illness source attribution estimates for 2013 for *Salmonella, Escherichia coli* O157, *Listeria monocytogenes*, and *Campylobacter* using multi-year outbreak surveillance data, United States. Atlanta and Washington: Centers for Disease Control and Prevention, US Food and Drug Administration, US Department of Agriculture Food Safety and Inspection Service; 2017 [cited 2020 May 4]. https://www.cdc.gov/foodsafety/ifsac/annual-reports.html
32. Interagency Food Safety Analytics Collaboration. Foodborne illness source attribution estimates for 2017 for *Salmonella, Escherichia coli* O157, *Listeria monocytogenes*, and *Campylobacter* using multi-year outbreak surveillance data, United States. Atlanta and Washington: Centers for Disease Control and Prevention, US Food and Drug Administration, US Department of Agriculture Food Safety and Inspection Service; 2019 [cited 2020 May 4]. https://www.cdc.gov/foodsafety/ifsac/annual-reports.html


Address for correspondence: Michael B. Batz, Center for Food Safety and Applied Nutrition, Food and Drug Administration, 5001 Campus Dr, College Park, MD, 20740, USA; email: michael.batz@fda.hhs.gov

# Hannibal's Ophthalmia—A New Answer to An Ancient Question

Justin T. Denholm, Patrick N. Hunt

In the spring of 217 BCE, shortly after Hannibal's famous elephantborne crossing of the Alps, the general was afflicted by an acute, painful eye condition that has never been adequately explained and that led to permanent unilateral loss of vision in 1 eye. In modern times, scant attention has been given to understanding this condition. We review the historical and geographic evidence and considers possible infective explanations for Hannibal's condition, including elephant-associated zoonoses. Ultimately, we suggest that a keratitis from waterborne organisms, such as *Pseudomonas* spp. or *Acanthamoeba* spp., might provide the best answer to this ancient enigma.

In the spring of 217 BCE, shortly after Hannibal's famous elephant-borne crossing of the Alps, the general was afflicted by an acute, painful eye condition that has never been adequately explained. The Roman historian Polybius' account in Greek of Hannibal's affliction is brief, stating, "Hannibal himself on the sole remaining elephant got across with much difficulty and suffering, being in great pain from a severe attack of ophthalmia (Greek ʼοφθαλμια), which finally led to the loss of one eye as he had no time to stop and apply any treatment to it, the circumstances rendering that impossible" (*1*). Earlier passages set the scene of a grueling 3-day march through the marshes of the Arno River, as Hannibal once again attempted to take his Roman opponents by surprise by arriving just west of Arezzo (ancient Arretium; "the back way"). Although his bold movement was militarily successful, the illness he acquired led to the permanent loss of vision in 1 eye. This affliction became a defining characteristic of Hannibal's portrayal in history, as seen by how his visual loss is referenced as influencing his actions on campaign, and in later artistic depictions of the general (*2*).

Author affiliations: Royal Melbourne Hospital, Parkville, Victoria, Australia (J.T. Denholm); University of Melbourne, Parkville (J.T. Denholm); Stanford University, Palo Alto, California USA (P.N. Hunt)

DOI: https://doi.org/10.3201/eid2701.191696

## Historical Arno Valley Swamps

Hannibal's marsh crossing most likely took place in the middle Arno River Valley in upper Tuscany in northern central Italy, just east of modern Florence. Late Quaternary sedimentology of the mountain-rimmed Arno River watershed has documented long-term drainage problems with marshlands both coastal and inland, and peat deposits in the Arno Valley also attest to old bog contexts (*3*,*4*). Although land reclamation in the late 1800s finally reduced the perennial flooding in the Florentine floodplain region, the middle Arno valley was once a series of ancient lakes with a pervasive semipermanent swamp area called le padule and many small bogs still exist (*5*). Occasional flooding of the region still occurs, with the most recent catastrophic instances in 1966 and 1987, which damaged or threatened many notable works of art.

## Ophthalmia in the Ancient World

A diverse range of eye diseases were recognized and described in antiquity (*6*). The ocular process that caused Hannibal's blindness has been generally referred to as ophthalmia, following the term used by Polybius. Elsewhere in the ancient world, this term seems mainly to describe inflammatory eye disease, whether acute or chronic, without evidence that a particular disease process is implied. Ophthalmia was described by Hippocrates, including treatment regimens, and by the time of the Roman Empire, specialist eye doctors (medicus ocularius) were recognized (*7*). Hippocrates also tells us that ophthalmia was more common in the spring, at the time Hannibal went through the marshes, and that there is an association with stagnant and muddy conditions (*7*,*8*). Herodotus reported that 2 Spartans were afflicted with ophthalmia before the battle of Thermopylae, also in the context of nearby marshlands (*9*). Neither, however, provides further insight into the likely cause of this disease.

In instances in which further clarification has been offered, later historians have sometimes labeled

Hannibal's ophthalmia as a form of conjunctivitis, perhaps contracted, as Polybius noted, after "long periods without sleep weakened [Hannibal's] resistance" (*10*). However, there are various reasons why this diagnosis might be questioned. Viral conjunctivitis most commonly progresses to become bilateral, and although bacterial infections might remain unilateral, it is uncommon for pain to be a severe manifestation of this disease (*11*). Regardless of the etiologic pathogen, conjunctivitis is more common in childhood and normally resolves without sequelae. Hannibal's illness, then, as an adult manifestation with severe unilateral pain and ultimate permanent loss of vision, is not strongly suggestive of a simple conjunctivitis.

## Diagnosis

If history has been hasty in arriving at such a conclusion, does the contemporary historical record permit a more likely diagnosis to be reached? The list of potential etiologies for acute, spontaneous inflammatory conditions leading to unilateral blindness is lengthy, although predominantly infectious in nature. Polybius stated that the process was painful, but gave no indication of a systemic illness, suggesting that septic conditions, such as bacterial or fungal endophthalmitis, are unlikely to have been involved. No mention in the account is made of a rash or skin lesions, weighing against conditions such as smallpox or herpes zoster ophthalmicus.

Today, syphilitic keratitis would be considered as a differential diagnosis of this manifestation, but it can be excluded because the condition does not appear in Europe until far later than Hannibal's march (*12*). A variety of other infections are well known to cause blindness, particularly in developing nations today. These infections include Whipple's disease, leishmaniasis, leprosy, and onchocerciasis. However, they can be reasonably excluded in this instance because the chronic nature of these conditions is inconsistent with rapid onset described in this historical account.

## Pachydermal Zoonosis

Given Hannibal's well-documented close contact with elephants (as mentioned, he was riding the sole remaining elephant at the time of his illness), zoonotic infections must be considered (*13*). One intriguing possibility would be leptospirosis. Elephants are known to frequently harbor the bacteria that causes this disease, which might be transmitted to humans through urine contact (*14*). However, leptospirosis rarely causes uveitis, and invariably causes bilateral disease when present, making this an unlikely cause.

Among possible alternatives, tuberculosis and brucellosis are both recognized to have potential for ocular involvement, including choroiditis and uveitis. Both *Mycobacterium tuberculosis* and *M. bovis* are known to infect elephants, and human-to-elephant transmission has been described (*15*). No systemic illness suggestive of disseminated tuberculosis was indicated by the historical account; however, ocular tuberculosis might rarely be manifested in isolation (*16*). Because tuberculosis was present in Europe during Hannibal's era, this diagnosis cannot be excluded, although would be considered a particularly rare manifestation of disease and is probably less likely.

## Possible Solution

Perhaps the diagnosis most consistent with Polybius' account is a form of keratitis. Keratitis might be caused by a range of pathogens, with or without preceding trauma, and is manifested typically with unilateral pain and visual disturbance (*17*). Untreated, it might result in permanent visual loss, as ultimately occurred in Hannibal's case. The most common pathogens to cause keratitis are bacterial, including *Staphylococcus* spp. and *Streptococcus pneumoniae* (*18*). However, the timing of Hannibal's illness arising in the context of a 3-day forced march through swamp and marshland, cannot be ignored (*19*). Although coincidental onset of an unrelated condition remains a possibility, the setting of illness strongly suggests a waterborne pathogen as the most likely etiologic agent. In particular, either *Pseudomonas aeruginosa* or *Acanthamoeba* keratitis would be consistent with the setting and clinical description of Hannibal's illness.

Of the 2 forms of keratinitis, pseudomonal keratitis is more common and acute and perhaps the more likely. However, although *Acanthamoeba* keratitis in industrialized world settings today is most commonly associated with contact lens use, globally, it has been reported in the setting of either minor trauma or environmental exposure to contaminated water and so remains plausible as a cause of Hannibal's condition given the environmental settings in which it originated (*20*,*21*). Seasonal variation in *Acanthamoeba* keratitis has also been reported from a variety of settings, although this appears to predominate in summer months and might in part be related to modern patterns of contact lens use (*21*,*22*).

In conclusion, although no definitive diagnosis can ever be established, we would argue that the historical record most strongly suggests keratitis caused by a waterborne pathogen, particularly *P. aeruginosa or Acanthamoeba*, as the cause of Hannibal's ophthalmia. This diagnosis provides a more adequate account of his visual

loss than traditional explanations have offered and, we hope, sheds a small additional light on the life of one of the greatest military leaders in world history.

## About the Authors

Dr. Denholm is an infectious diseases physician at the Royal Melbourne Hospital, Parkville, Victoria, Australia. His research interests are clinical and public health management of tuberculosis and ethical issues related to infectious diseases.

Dr. Hunt is an archaeologist at Stanford University, Palo Alto, CA. His research interests are archaeological science applied to historical persons such as Hannibal or Otzi the Iceman and prehistoric understanding of medicine.

## References

1. Polybius, History III.79.12; also preceding sections in III.78.6–79.11 [cited 2020 Oct 19]. http://penelope.uchicago.edu/Thayer/E/Roman/Texts/Polybius/3*.html
2. Miles R. Hannibal and propaganda. In: Hoyos D, editor. A companion to the Punic Wars. Oxford (UK): Blackwell; 2011. p. 273–4.
3. Aguzzi M, Amorosi A, Colalongo ML, Lucchi MR, Rossi V, Sarti G, et al. Lay Quaternary climatic evolution of the Arno coastal plain (Western Tuscany, Italy) from subsurface data. Sediment Geol. 2007;202:211–29. https://doi.org/10.1016/j.sedgeo.2007.03.004
4. Falini F. On the formation of coal deposits of lacustrine origin. Geological Society of America Bulletin. 1965;76:1317–46. https://doi.org/10.1130/0016-7606(1965)76[1317b:OTFOCD]2.0.CO;2
5. Saul AJ, editor. Flood and flood management. London: Springer; 1992.
6. Zipser B. Deleted text in a manuscript. Galen on the eye and the Marc. Gr. 276. Galenos. 2009;3:107–12.
7. Papadopoulos G, Liarmakopoulou A, Zisoulis E, Tzimas P, Lena A, Kitsos G. Treatment of eye diseases in the Hippocratic era. Hellenic J Surg. 2018;90:143–5. https://doi.org/10.1007/s13126-018-0459-x
8. Herodotus, History VII. 229 [cited 2020 Oct 19]. http://www.perseus.tufts.edu/hopper/text?doc=Perseus%3Atext%3A1999.01.0126%3Abook%3D7%3Achapter%3D229
9. Lancel S. Hannibal. Nevill A, translator. Oxford (UK) Blackwell; 1999.
10. Kanski JJ. Clinical ophthalmology, 6th ed. Edinburgh: Elsevier Butterworth Heinemann; 2007.
11. Harper KN, Ocampo PS, Steiner BM, George RW, Silverman MS, Bolotin S, et al. On the origin of the treponematoses: a phylogenetic approach. PLoS Negl Trop Dis. 2008;2:e148. https://doi.org/10.1371/journal.pntd.0000148
12. Hunt P, Seicean A. Alpine archaeology and paleopathology: was Hannibal's army also decimated by epidemic while crossing the Alps? Archaeology; 2007 [cited 2020 Dec 10]. https://web.stanford.edu/group/archaeolog/cgi-bin/archaeolog/2007/05/20/alpine-archaeology-and-paleopathology-was-hannibals-army-also-decimated-by-epidemic-while-crossing-the-alps
13. Srivastava SK, Kumar AA. Seroprevalence of leptospirosis in animals and human beings in various regions of the country. Indian Journal of Comparative Microbiology, Immunology and Infectious Diseases. 2003;24:155–9.
14. Michalak K, Austin C, Diesel S, Bacon MJ, Zimmerman P, Maslow JN. Mycobacterium tuberculosis infection as a zoonotic disease: transmission between humans and elephants. Emerg Infect Dis. 1998;4:283–7. https://doi.org/10.3201/eid0402.980217
15. Sarvananthan N, Wiselka M, Bibby K. Intraocular tuberculosis without detectable systemic infection. Arch Ophthalmol. 1998;116:1386–8.
16. Schaefer F, Bruttin O, Zografos L, Guex-Crosier Y. Bacterial keratitis: a prospective clinical and microbiological study. Br J Ophthalmol. 2001;85:842–7. https://doi.org/10.1136/bjo.85.7.842
17. Bourcier T, Thomas F, Borderie V, Chaumeil C, Laroche L. Bacterial keratitis: predisposing factors, clinical and microbiological review of 300 cases. Br J Ophthalmol. 2003;87:834–8. https://doi.org/10.1136/bjo.87.7.834
18. Leck AK, Matheson MM, Hagan M, Ackuaku E. Acanthamoeba keratitis in Ghana. Br J Ophthalmol. 2002;86:1187–8. https://doi.org/10.1136/bjo.86.10.1187-a
19. Hunt PN. Hannibal. New York: Simon and Schuster; 2017.
20. Roshni Prithiviraj S, Rajapandian SG, Gnanam H, Gunasekaran R, Mariappan P, Sankalp Singh S, et al. Clinical presentations, genotypic diversity and phylogenetic analysis of Acanthamoeba species causing keratitis. J Med Microbiol. 2020;69:87–95. https://doi.org/10.1099/jmm.0.001121
21. McAllum P, Bahar I, Kaiserman I, Srinivasan S, Slomovic A, Rootman D. Temporal and seasonal trends in Acanthamoeba keratitis. Cornea. 2009;28:7–10. https://doi.org/10.1097/ICO.0b013e318181a863
22. Kao PM, Hsu BM, Hsu TK, Liu JH, Chang HY, Ji WT, et al. Seasonal distribution of potentially pathogenic Acanthamoeba species from drinking water reservoirs in Taiwan. Environ Sci Pollut Res Int. 2015;22:3766–73. https://doi.org/10.1007/s11356-014-3651-8

Address for correspondence: Justin T. Denholm, Victorian Infectious Diseases Service, Royal Melbourne Hospital, Parkville, VIC 3050, Australia; email: justin.denholm@mh.org.au

# Severe Human Bocavirus–Associated Pneumonia in Adults at a Referral Hospital, Seoul, South Korea

Sang-Ho Choi,[1] Jin Won Huh,[1] Sang-Bum Hong, Jiwon Jung, Min Jae Kim, Yong Pil Chong, Sung-Han Kim, Heungsup Sung, Eun Jin Chae, Kyung-Hyun Do, Sang-Oh Lee, Chae-Man Lim, Yang Soo Kim, Jun Hee Woo, Younsuck Koh

We report a case series of severe human bocavirus–associated pneumonia in adults in Seoul, South Korea. The virus accounted for 0.5% of all severe pneumonia cases. Structural lung disease and hematologic malignancy were common underlying diseases. Overall death rate was 54.5%. Higher death rates were associated with co-infection (83.3%) and immunocompromise (80.0%).

Human bocavirus (HBoV), a DNA virus in the *Parvoviridae* family, was first identified in 2005 (*1*). HBoV is distributed worldwide and has been found in 2%–33% of respiratory specimens, primarily from children with acute respiratory tract infection (*2*,*3*). In adults, HBoV is an uncommon cause of upper respiratory tract infection and pneumonia (*4*–*6*). It can also be associated with the acute exacerbation of chronic obstructive pulmonary disease (*7*). Recently, a few case reports have shown that HBoV can be associated with life-threatening pneumonia (*8*–*12*). However, severe HBoV-associated pneumonia has not been reported in a case series, and little is known about the characteristics of HBoV-associated pneumonia in critically ill adult patients. We investigated the incidence, clinical characteristics, and outcomes of severe HBoV-associated pneumonia in adults in Seoul, South Korea.

## The Study

We conducted a prospective observational cohort study of severe pneumonia in adult patients admitted to the medical intensive-care unit (ICU) at a 2,700-bed referral hospital in Seoul, South Korea, during March 2010–February 2019 (*13*,*14*). We initially included all adult patients admitted to the ICU with a diagnosis of pneumonia but later excluded patients with non-severe pneumonia. We collected data on demographics, underlying diseases or conditions, immune status, seasonality, clinical manifestations, laboratory findings, pathogens, complications, treatment, and outcomes. This data collection was a routine part of the management and care of these patients at our hospital. Definitions and microbial evaluations are summarized in the Appendix (https://wwwnc.cdc.gov/EID/article/27/1/20-2061-App1.pdf). The Institutional Review Board of Asan Medical Center approved this study (approval no. 2010-0079) and waived informed-consent requirements.

During the study, 2,519 adult patients were admitted to the ICU with the diagnosis of severe pneumonia. After excluding 298 patients (83 community-acquired pneumonia [CAP] cases and 215 hospital-acquired pneumonia [HAP] cases) for whom multiplex respiratory virus PCR was not performed, 2,221 severe pneumonia patients (1,482 CAP cases and 739 HAP cases) were included. Among these 2,221 severe pneumonia patients, septic shock occurred in 1,306 (58.8%), and 2,141 (96.4%) required mechanical ventilation. Septic shock occurred in 80 patients (3.6%) who did not require mechanical ventilation.

Mean patient age was 65.8 years (range 16–97 years). Structural lung disease (26.9%) was the most common underlying disease in patients with CAP, and hematologic malignancy (25.4%) was the most common in patients with HAP (Appendix Table 1). One or more respiratory pathogens were identified in 1,510 patients (68.0%) (Appendix Table 2). Overall,

Author affiliation: Asan Medical Center, University of Ulsan College of Medicine, Seoul, South Korea

DOI: https://doi.org/10.3201/eid2701.202061

[1]These authors contributed equally to this article.

888 (40.0%) patients had bacterial infections, 711 (32.0%) had viral infections, and 230 (10.4%) patients had bacterial–viral co-infection. A total of 787 viruses were identified in 711 patients. Two viruses were identified in 60 patients and 3 viruses in 8 patients. Influenza virus (8.6%) and rhinovirus (8.4%) were the most common viral pathogens for severe CAP, whereas parainfluenza virus and respiratory syncytial virus were the most common viral pathogens for severe HAP.

Eleven HBoV-associated severe pneumonia cases (0.5% [11/2,221]) were reported. Of those, HBoV accounted for 0.4% (6/1,482) of CAP cases and 0.7% (5/739) of HAP cases. Of the 711 virus-associated severe pneumonia cases, HBoV accounted for 1.2% (6/501) of CAP cases and 2.4% (5/210) of HAP cases. Appendix Table 3 summarizes the characteristics and outcomes of the 11 patients with HBoV-associated severe pneumonia, which included 6 patients with CAP and 5 patients with HAP. HBoV occurred in all 4 seasons but was more common during September–February (8 cases). Nine patients were men (81.8%); the median age was 69.0 years (range 36–81 years). All patients had ≥1 severe underlying diseases. Structural lung disease (5 patients) and hematologic malignancy (4 patients) were the most common underlying illnesses. Five patients (45.5%) were immunocompromised.

Viruses were detected by using nasopharyngeal aspirate or swab specimens. In 1 patient, the virus was detected in bronchoalveolar lavage fluid and nasopharyngeal samples. Co-infection was observed in 6 patients (54.5%). Eight patients underwent chest computed tomography. The most common radiologic findings were bilateral and multifocal consolidation and ground-glass opacity.

The median length of ICU stay was 9.0 days (range 1–74 days). Overall death rate was 54.5% (6/11). The death rate was 80.0% (4/5) for immunocompromised patients and 33.3% (2/6) for immunocompetent patients. Higher death rates were observed in cases of co-infection (83.3%, 5/6) than in cases of sole HBoV infection (20.0% [1/5]) ($p = 0.08$). All immunocompromised patients with co-infection died (3/3), whereas no immunocompetent patients without co-infection died (0/3).

## Conclusions

Our study demonstrated that HBoV is an uncommon pathogen for adult patients with severe pneumonia requiring ICU admission. All episodes we investigated occurred in patients with serious underlying diseases, and co-infection was frequent. Overall death rates were high and closely associated with immunocompromised state and presence of co-infection.

Information on severe HBoV-associated pneumonia in adults is limited. Five cases of severe HBoV-associated pneumonia have been reported to date (*8*–*12*), which included 3 cases from the same facility in Germany (*9*,*10*,*12*). Of the 5 patients, 3 had hematologic malignancy and 1 had cystic fibrosis. One of the patients was a 74-year-old immunocompetent man (*10*). He had an acute head injury and rib fracture, probably because of weakness from HBoV pneumonia, necessitating mechanical ventilation. In our study, patients with structural lung diseases, including chronic obstructive pulmonary disease and bronchiectasis, were predisposed to severe HBoV-associated pneumonia. Most of these patients were not immunocompromised and had CAP. Therefore, clinicians should consider HBoV as an uncommon pathogen of severe pneumonia in adults with structural lung disease.

Consistent with previous reports (*4*,*5*), we found a high rate of co-infection with other pathogens in patients with HBoV infection. HBoV has shown a prolonged persistence in the mucosa of the respiratory tract. Viral persistence contributes to the high frequency of coinfections with proper respiratory pathogens (*15*). This phenomenon might be associated with the underlying severe diseases. Of note, co-infection was closely related to higher overall death rates in our patients. Our series included 5 cases of sole HBoV infection, which was more common in CAP patients and associated with lower death rates. These findings indicated that HBoV itself has a lower virulence potential and rarely causes severe pneumonia, which is predominant in immunocompromised patients or patients with underlying structural lung disease. The higher incidence of severe HBoV-associated pneumonia in HAP patients compared with CAP patients (0.7% vs. 0.4%) might be explained by the higher proportion of immunocompromised patients in the HAP population.

Our study has some limitations. First, we excluded 298 patients (83 of 1,565 CAP patients [5.8%] and 215 of 954 HAP patients [22.5%]) for whom multiplex respiratory virus PCR was not performed. Because our study was observational, microbial evaluations and patient-management decisions were made by attending physicians, and multiplex respiratory virus PCR test was not used for all patients. Therefore, selection bias might have occurred, especially for HAP. Second, HBoV was mostly identified through nasopharyngeal specimens only and was frequently accompanied by copathogens. Therefore, we could

not evaluate in detail the virulence potential of sole HBoV infection. Finally, we did not conduct a genotypic study of HBoV, and the viral load therefore was not tested.

In summary, in this study, HBoV accounted for 0.5% of severe pneumonia cases in adults. HBoV-associated severe pneumonia could lead to high death rates. Underlying severe diseases and frequent coinfection seem to be responsible for poor outcomes.

This work was supported by Asan Institute of Life Sciences (grant 2010-0079) and generous gifts from Sam Won Song.

## About the Author

Dr. Choi is an infectious disease specialist and professor at Asan Medical Center, Ulsan University College of Medicine, in Seoul, South Korea. His main research interest is the epidemiology of severe pneumonia caused by respiratory viruses. Dr. Huh is an intensivist and professor at Asan Medical Center. Her main research interest is the pathogenesis and management of acute respiratory distress syndrome.

## References

1. Allander T, Tammi MT, Eriksson M, Bjerkner A, Tiveljung-Lindell A, Andersson B. Cloning of a human parvovirus by molecular screening of respiratory tract samples. Proc Natl Acad Sci U S A. 2005;102:12891–6. https://doi.org/10.1073/pnas.0504666102
2. Jartti T, Hedman K, Jartti L, Ruuskanen O, Allander T, Söderlund-Venermo M. Human bocavirus—the first 5 years. Rev Med Virol. 2012;22:46–64. https://doi.org/10.1002/rmv.720
3. Choi EH, Lee HJ, Kim SJ, Eun BW, Kim NH, Lee JA, et al. The association of newly identified respiratory viruses with lower respiratory tract infections in Korean children, 2000–2005. Clin Infect Dis. 2006;43:585–92. https://doi.org/10.1086/506350
4. Liu WK, Chen DH, Liu Q, Liang HX, Yang ZF, Qin S, et al. Detection of human bocavirus from children and adults with acute respiratory tract illness in Guangzhou, southern China. BMC Infect Dis. 2011;11:345. https://doi.org/10.1186/1471-2334-11-345
5. Lee HN, Koo HJ, Kim SH, Choi SH, Sung H, Do KH. Human bocavirus infection in adults: clinical features and radiological findings. Korean J Radiol. 2019;20:1226–35. https://doi.org/10.3348/kjr.2018.0634
6. Gu K, Van Caeseele P, Dust K, Ho J. Atypical pneumonia due to human bocavirus in an immunocompromised patient. CMAJ. 2017;189:E697–9. https://doi.org/10.1503/cmaj.161134
7. Longtin J, Bastien M, Gilca R, Leblanc E, de Serres G, Bergeron MG, et al. Human bocavirus infections in hospitalized children and adults. Emerg Infect Dis. 2008;14:217–21. https://doi.org/10.3201/eid1402.070851
8. Kupfer B, Vehreschild J, Cornely O, Kaiser R, Plum G, Viazov S, et al. Severe pneumonia and human bocavirus in adult. Emerg Infect Dis. 2006;12:1614–6. https://doi.org/10.3201/eid1210.060520
9. Krakau M, Brockmann M, Titius B, Limmroth C, Khalfaoui S, Schildgen V, et al. Acute human bocavirus infection in MDS patient, Cologne, Germany. J Clin Virol. 2015;69:44–7. https://doi.org/10.1016/j.jcv.2015.05.029
10. Krakau M, Gerbershagen K, Frost U, Hinzke M, Brockmann M, Schildgen V, et al. Case report: human bocavirus associated pneumonia as cause of acute injury, Cologne, Germany. Medicine (Baltimore). 2015;94:e1587. https://doi.org/10.1097/MD.0000000000001587
11. Sadeghi M, Kantola K, Finnegan DP, McCaughey C, Hedman L, Söderlund-Venermo M, et al. Possible involvement of human bocavirus 1 in the death of a middle-aged immunosuppressed patient. J Clin Microbiol. 2013;51:3461–3. https://doi.org/10.1128/JCM.01157-13
12. Dieninghoff D, Karagiannidis C, Straßmann S, Pieper M, Dammaschek S, Zabner J, et al. Fatal HBoV-1 infection in adult female cystic fibrosis patient. Hum Pathol (N Y). 2017;7:51–2. https://doi.org/10.1016/j.ehpc.2016.07.001
13. Choi SH, Hong SB, Ko GB, Lee Y, Park HJ, Park SY, et al. Viral infection in patients with severe pneumonia requiring intensive care unit admission. Am J Respir Crit Care Med. 2012;186:325–32. https://doi.org/10.1164/rccm.201112-2240OC
14. Hong HL, Hong SB, Ko GB, Huh JW, Sung H, Do KH, et al. Viral infection is not uncommon in adult patients with severe hospital-acquired pneumonia. PLoS One. 2014;9:e95865. https://doi.org/10.1371/journal.pone.0095865
15. Broccolo F, Falcone V, Esposito S, Toniolo A. Human bocaviruses: possible etiologic role in respiratory infection. J Clin Virol. 2015;72:75–81. https://doi.org/10.1016/j.jcv.2015.09.008

Address for correspondence: Younsuck Koh, Department of Pulmonary and Critical Care Medicine, Asan Medical Center, University of Ulsan College of Medicine, 88, Olympic-ro 43-gil, Songpa-gu, Seoul, 138-736, South Korea; email: yskoh@amc.seoul.kr

# Prevalence of SARS-CoV-2, Verona, Italy, April–May 2020

Massimo Guerriero,[1] Zeno Bisoffi,[1] Albino Poli, Claudio Micheletto, Antonio Conti, Carlo Pomari

We used random sampling to estimate the prevalence of severe acute respiratory syndrome coronavirus 2 infection in Verona, Italy. Of 1,515 participants, 2.6% tested positive by serologic assay and 0.7% by reverse transcription PCR. We used latent class analysis to estimate a 3.0% probability of infection and 2.0% death rate.

On May 25, 2020, Italy had the third highest number of cases and the second highest number of deaths in Europe caused by the novel betacoronavirus severe acute respiratory syndrome coronavirus 2 (SARS-CoV-2) (*1*) as part of the ongoing pandemic of coronavirus disease (COVID-19). The continuing spread of infection and the resulting strain on healthcare systems has made the identification of asymptomatic persons crucial to limiting transmission (*2*–*6*). We conducted a cross-sectional study on a representative sample of the general population to estimate the prevalence and death rate of SARS-CoV-2 infection in Verona, Italy.

## The Study

We estimated the prevalence of active or past SARS-CoV-2 infection among the population of Verona among randomly selected participants ≥10 years of age. This investigation was an observational, cross-sectional study approved by the Ethics Committee of Verona and Rovigo provinces on April 15, 2020 (internal protocol no. 2641CESC), in compliance with the Strengthening the Reporting of Observational Studies in Epidemiology guidelines (*7*).

According to Verona's municipal register, 235,034 persons ≥10 years of age lived in Verona on January 1, 2020 (*8*). We used systematic random sampling to compile a list of potential participants. Because the prevalence of asymptomatic SARS-CoV-2 infection in Italy had previously been estimated at 10.0% (*9*,*10*), we decided to randomly sample 1,527 participants, resulting in a standard error of ≤1.5%. We predicted a dropout rate of 35% and accordingly mailed invitations to 2,061 potential participants. We selected the first sample using a random starting point; for subsequent samples, we used a sampling interval calculated by dividing the population size by the desired sample size (235,034/2,061 = 114).

We collected data from April 24 through May 8, 2020. We required a parent's or guardian's consent for participants <18 years of age. All participants gave their informed consent. Participants first completed a phone interview about COVID-19 symptoms within the previous 15 days. Specialized staff at Istituto di Ricovero e Cura a Carattere Scientifico then collected blood and nasopharyngeal swab samples from each participant. These staff extracted total RNA from nasopharyngeal swab samples using a MagnaPure LC.2 instrument and MagNA Pure LC RNA Isolation Kit (Roche Molecular Systems Inc., https://lifescience.roche.com), according to the manufacturer's instructions. We analyzed the eluted RNA by reverse transcription PCR (RT-PCR) to detect the presence of active infections (*11*). We analyzed serum samples for IgG against SARS-CoV-2 by serologic assay (Abbott, https://www.abbott.com) to detect previous infections. Experienced laboratory personnel conducted each test independently and blindly.

Because neither assay has perfect sensitivity, we used latent class analysis (LCA) to estimate the prevalence of SARS-CoV-2 infection. LCA models were based on SARS-CoV-2 test results and selected clinical variables (*12*). We interpreted the outcomes as the probability that a given person was (or had been) infected (*13*). We reported all parameters and estimations with 95% CIs. We adjusted statistical models and estimations for covariates.

A total of 1,515 persons participated in the study (Figure). We found no significant difference in sex proportions between the general population (53%

Author affiliations: Istituto di Ricovero e Cura a Carattere Scientifico Ospedale Sacro Cuore Don Calabria, Negrar, Italy (M. Guerriero, Z. Bisoffi, A. Conti, C. Pomari); Università di Verona, Verona, Italy (Z. Bisoffi, A. Poli); Azienda Ospedaliera Universitaria di Verona, Verona (C. Micheletto)

DOI: https://doi.org/10.3201/eid2701.202740

[1]These authors contributed equally to this article.

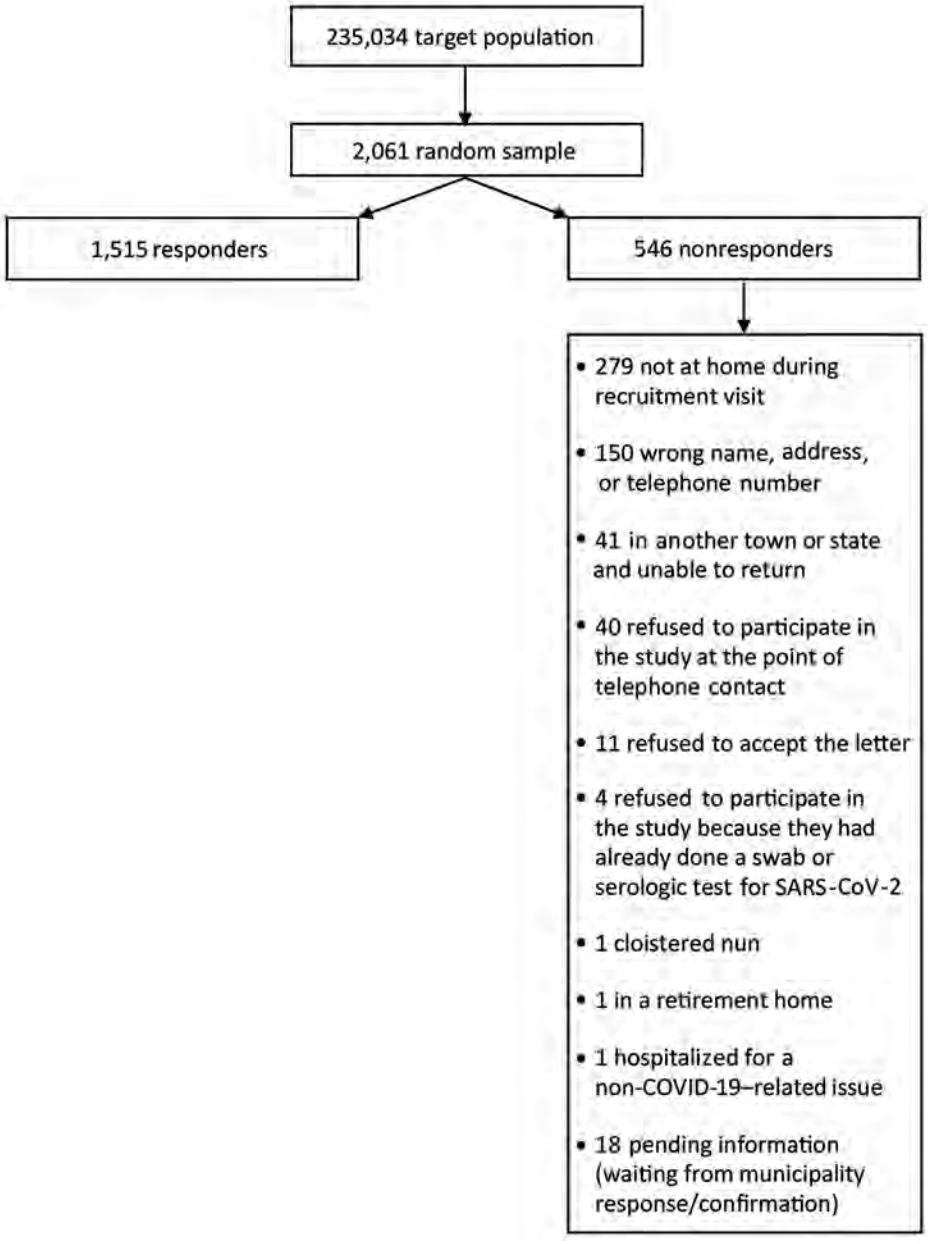


**Figure.** Flowchart of participant testing for SARS-CoV-2 infection, Verona, Italy, 2020. COVID-19, coronavirus disease; SARS-CoV-2, severe acute respiratory syndrome coronavirus 2.

female) and the study sample (54% female). The mean age of all participants was 52.1 (SD = 20.0) years in the general population and 49.1 (SD = 22.2) years in the study sample. We summarized demographic and clinical data using descriptive statistics and measures of variability and precision (Table 1). Of 1,515 participants, 9 (0.6%) tested positive for SARS-CoV-2 RNA but negative for IgG against SARS-CoV-2, 40 (2.6%) tested negative for viral RNA but positive for IgG, and 1,465 (96.7%) tested negative for both indicators. Only 1 participant tested positive for RNA and IgG. Participants who tested negative for viral RNA but positive for IgG reported symptoms such as anosmia (39.5%), temperature ≥37.5°C (30.8%), fatigue (35.9%), and persistent cough (28.2%). Less than 2% of participants who tested negative by both tests reported symptoms.

We used a backward stepwise multinomial multivariate logistic regression model to compare selected COVID-19 symptoms (i.e., anosmia, dyspnea, diarrhea, and fever) in the RNA-positive and RNA-negative/IgG-positive groups with the RNA-negative/IgG-negative group. Fever and anosmia were each significantly associated with belonging to the RNA-negative/IgG-positive group ($p<0.01$) but not the RNA-positive group.

**Table 1.** Demographic and clinical characteristics of participants tested for SARS-CoV-2, Verona, Italy, 2020*

| Characteristic | Total | RNA-positive | RNA-negative/IgG-positive | RNA-negative/IgG-negative | p value† | Missing values |
|---|---|---|---|---|---|---|
| Total, no (%) | 1,515 (100.0) | 10 (0.7) | 40 (2.6) | 1465 (96.7) | NA | 0 |
| Mean age, y (SD) | 52.1 (20.0) | 53.4 (15.5) | 47.3 (17.6) | 52.2 (20.1) | 0.31 | 0 |
| Sex, no. | | | | | | |
| M | 699 | 3 | 17 | 679 | 0.57 | 0 |
| F | 816 | 7 | 23 | 786 | | 0 |
| SARS-CoV-2 symptoms, % | | | | | | |
| Anosmia | 2.4 | 10.0 | 39.5 | 1.4 | <0.01 | 3.9 |
| Conjunctivitis | 8.0 | 0 | 12.8 | 7.9 | 0.38 | 3.1 |
| Temperature >37.5°C | 2.7 | 10.0 | 30.8 | 1.8 | <0.01 | 3.1 |
| Dry cough or phlegm | 9.3 | 0 | 28.2 | 8.9 | <0.01 | 3.0 |
| General muscle pain | 5.4 | 10.0 | 23.1 | 4.9 | <0.01 | 3.2 |
| Fatigue | 8.3 | 10.0 | 35.9 | 7.5 | <0.01 | 3.1 |
| Headache | 10.4 | 10.0 | 15.4 | 10.2 | 0.48 | 3.0 |
| Sore throat | 7.6 | 0 | 7.7 | 7.6 | 1.00 | 3.2 |
| Chills | 4.4 | 10.0 | 10.5 | 3.9 | <0.01 | 3.0 |
| Diarrhea | 7.9 | 20.0 | 13.2 | 7.7 | 0.09 | 3.2 |
| Dyspnea | 3.5 | 10.0 | 18.0 | 3.0 | <0.01 | 3.2 |
| Nausea/vomiting | 2.6 | 10.0 | 10.5 | 2.3 | <0.01 | 3.1 |

*NA, not applicable; SARS-CoV-2, severe acute respiratory syndrome coronavirus 2.
†Mean difference in age tested with analysis of variance. All other p values calculated by Fisher's exact test.

We used LCA to estimate the prevalence of infection considering the results of RT-PCR, the serologic assay, and the symptoms selected by stepwise regression. The estimated probability of belonging to class 1 (uninfected) was 0.97 and class 2 (infected) was 0.03 (Table 2).

As of May 25, 2020, Verona had 1,528 cumulative patients in whom SARS-CoV-2 infection was diagnosed, including 144 who had died, indicating a 9.4% death rate (*14*). Verona was the province in Veneto with the most cases and deaths caused by SARS-CoV-2 (15). Our LCA estimated a prevalence of 3.0%, suggesting 7,051 cumulative cases (4.6 times higher than the official count). These estimates suggest that 144 reported deaths would indicate a 2.0% death rate. According to the crude rates, the 50 SARS-CoV-2–positive participants in our study would account for 3.3% of the total study population. Applying this percentage to the whole population of Verona would indicate 7,756 cases and a 1.9% death rate.

Of the 10 RNA-positive participants, only 1 tested positive by serologic assay. This finding raises concerns about the current screening policy of 2-step testing, which comprises a serologic assay and, if the assay results are positive, PCR. Given the economic costs associated with testing, officials should carefully advise the public on all testing options.

Our study has a few limitations. Because participation was voluntary, our study might have been influenced by selection bias (Figure). Also, LCA might have underestimated the accuracy of both diagnostic tests. For example, considering past and active infections together might have reduced test sensitivity. Furthermore, the PCR assay did not have 100% specificity, as is usually assumed (A.N. Cohen, unpub. data, https://www.medrxiv.org/content/10.1101/2020.04.26.20080911v4). The model might have also underestimated the specificity of the serologic assay. However, the crude rates estimate a prevalence only slightly higher, and the death rate only slightly lower, than predicted by our model.

## Conclusions

Our study estimated the prevalence of SARS-CoV-2 infection in Verona using a random sample of its population. Similar studies are currently underway

**Table 2.** Latent class analysis of SARS-CoV-2 infection, Verona, Italy, 2020

| Factor | Probability % (95% CI) | | % (95% CI) | | | |
|---|---|---|---|---|---|---|
| | Class 1 (SARS-CoV-2–negative) | Class 2 (SARS-CoV-2–positive) | Sensitivity | Specificity | Positive predictive value | Negative predictive value |
| SARS-CoV-2 IgG | 1.1 (0.6–2.0) | 53.5 (30.8–74.8) | 53.5 (51.0–53.0) | 98.9 (98.4–99.4) | 60.1 (57.6–62.5) | 98.6 (98.0–99.2) |
| SARS-CoV-2 RNA | 0.5 (0.2–1.1) | 6.1 (1.6–20.9) | 6.1 (4.9–5.7) | 99.5 (99.1–99.9) | 27.4 (25.1–29.6) | 97.2 (96.3–98.0) |
| Anosmia* | 0.8 (0.03–1.8) | 54.5 (33.2–74.2) | 54.5 (52.0–54.1) | 99.2 (98.8–99.6) | 67.8 (65.5–70.2) | 98.6 (98.0–99.2) |
| Diarrhea* | 7.0 (5.7–8.6) | 37.2 (21.6–55.9) | 37.2 (34.8–35.9) | 93.0 (91.7–94.3) | 14.1 (12.4–15.9) | 98.0 (97.2–98.7) |
| Fever* | 1.3 (0.8–2.2) | 45.8 (26.3–66.7) | 45.8 (43.3–45.2) | 98.7 (98.1–99.3) | 52.1 (49.6–54.7) | 98.3 (97.7–99.0) |
| Dyspnea* | 2.6 (1.8–3.6) | 32.3 (17.9–51.0) | 32.3 (29.9–31.5) | 97.4 (96.6–98.2) | 27.8 (25.5–30.0) | 97.9 (97.2–98.6) |

*The clinical variables used in the latent class analysis were selected by backward stepwise multinomial logistic regression with a significance level for removal of 0.2.

on a larger scale. The results will estimate the true circulation of SARS-CoV-2, better approximate the death rate, and inform infection containment and management. Our study provides a clear picture of the circulation of SARS-CoV-2 infection in the general population of a city and an estimation of the true death rate caused by the infection. The results also suggest that 2-step testing might not detect all active infections. We are currently organizing phase 2 of our study, during which we will conduct follow-up serologic testing on all PCR-positive and PCR-negative/IgG-positive participants, enabling the evaluation of any antibody seroconversion, negativization, or change in titer.

### Acknowledgments

We thank Nicoletta De Santis for editing, Elinor Julie Rae Anderson for language editing and Luciano Marchiori and Luca Heller for helping with data collection. We are also grateful to the laboratory team of the Microbiology Unit of Istituto di Ricovero e Cura a Carattere Scientifico Sacro Cuore Don Calabria Hospital for performing the tests and helping with the database.

This work was partially supported by the Italian Ministry of Health under "Fondi Ricerca Corrente - Linea 1" and "Progetto COVID Ricerca Finalizzata 2020 12371675" to Istituto di Ricovero e Cura a Carattere Scientifico Sacro Cuore Don Calabria Hospital.

## About the Author

Dr. Guerriero is a senior epidemiologist and biostatistician at the Clinical Research Unit, Istituto di Ricovero e Cura a Carattere Scientifico Sacro Cuore Don Calabria Hospital. His primary research interests are prevalence cross-sectional studies and advanced models in medicine statistics.

### References

1. World Health Organization. Coronavirus disease (COVID-19) situation report—126. 2020 May 25 [cited 2020 May 25]. https://www.who.int/docs/default-source/coronaviruse/situation-reports/20200525-covid-19-sitrep-126.pdf
2. Chan JF, Yuan S, Kok KH, To KK, Chu H, Yang J, et al. A familial cluster of pneumonia associated with the 2019 novel coronavirus indicating person-to-person transmission: a study of a family cluster. Lancet. 2020;395:514–23. https://doi.org/10.1016/S0140-6736(20)30154-9
3. Liu YC, Liao CH, Chang CF, Chou CC, Lin YR. A locally transmitted case of SARS-CoV-2 infection in Taiwan. N Engl J Med. 2020;382:1070–2. https://doi.org/10.1056/NEJMc2001573
4. Rocklöv J, Sjödin H, Wilder-Smith A. COVID-19 outbreak on the Diamond Princess cruise ship: estimating the epidemic potential and effectiveness of public health countermeasures. J Travel Med. 2020;27:taaa030. https://doi.org/10.1093/jtm/taaa030
5. Nishiura H, Kobayashi T, Miyama T, Suzuki A, Jung S, Hayashi K, et al. Estimation of the asymptomatic ratio of novel coronavirus infections (COVID-19). Int J Infect Dis. 2020;94:154–5.
6. Arons M, Hatfield KM, Reddy Sc, Kimball A et al. Presymptomatic SARS-CoV-2 infections and transmission in a skilled nursing facility. N Engl J Med 2020;382:2081–90.
7. STROBE statement: strengthening the reporting of observational studies in epidemiology. 2014 Jan 9 [cited 2020 May 31]. https://www.strobe-statement.org/index.php?id=strobe-home
8. Istituto Nazionale di Statistica. Demografia in cifre. 2020 Oct 1 [cited 2020 May 31]. demo.istat.it/index.html
9. Università degli Studi di Milano. Doxa: potrebbero essere oltre 5 milioni gli italiani infettati da COVID-19 a marzo 2020. 2020 Apr 2 [cited 2020 May 31]. https://lastatalenews.unimi.it/doxa-potrebbero-essere-oltre-5-milioni-italiani-infettati-covid-19-marzo-2020
10. De Natale G, Ricciardi V, De Luca G, De Natale D, Di Meglio G, Ferragamo A, et al. The COVID-19 infection in Italy: a statistical study of an abnormally severe disease. J Clin Med. 2020;9:1564. https://doi.org/10.3390/jcm9051564
11. Corman VM, Landt O, Kaiser M, Molenkamp R, Meijer A, Chu DK, et al. Detection of 2019 novel coronavirus (2019-nCoV) by real-time RT-PCR. Euro Surveill. 2020;25:2000045. https://doi.org/10.2807/1560-7917.ES.2020.25.3.2000045
12. Goodman LA. Latent class analysis: the empirical study of latent types, latent variables, and latent structures. In: Hagenaars JA, McCutcheon AL, editors. Applied Latent Class Analysis. Cambridge (UK): Cambridge University Press; 2002. p. 3–55.
13. Goetghebeur E, Liinev J, Boelaert M, Van der Stuyft P. Diagnostic test analyses in search of their gold standard: latent class analyses with random effects. Stat Methods Med Res. 2000;9:231–48. https://doi.org/10.1177/096228020000900304
14. Azienda Zero–Regione del Veneto. SARS-CoV-2 in Veneto. 2020 [cited 2020 May 25]. https://www.azero.veneto.it/-/emergenza-coronavirus
15. Bollettino Regione Veneto. Report del 31.05 ore 17.00. 2020 [cited 2020 June 1]. https://www.larena.it/filedelivery/policy:7.2807808:1590944213/aggiornamentotrentuno.pdf

Address for correspondence: Zeno Bisoffi, Dipartimento di Malattie Infettive Tropicali e Microbiologia (DITM), IRCCS Ospedale Sacro Cuore Don Calabria, Via Sempreboni 5, 37024 Negrar (Verona), Italy; email: zeno.bisoffi@sacrocuore.it

# Limited Specificity of Serologic Tests for SARS-CoV-2 Antibody Detection, Benin

Anges Yadouleton,[1] Anna-Lena Sander,[1] Andres Moreira-Soto,[1] Carine Tchibozo, Gildas Hounkanrin, Yvette Badou, Carlo Fischer, Nina Krause, Petas Akogbeto, Edmilson F. de Oliveira Filho, Anges Dossou, Sebastian Brünink, Melchior A. Joël Aïssi, Mamoudou Harouna Djingarey, Benjamin Hounkpatin, Michael Nagel,[2] Jan Felix Drexler[2]

We used commercially available ELISAs to test 68 samples from coronavirus disease cases and prepandemic controls from Benin. We noted ≤25% false-positive results among controls, likely due to unspecific immune responses elicited by acute malaria. Serologic tests must be carefully evaluated to assess coronavirus disease spread and immunity in tropical regions.

Since its emergence in China late 2019, coronavirus disease (COVID-19) had caused >41 million cases and >1.1 million deaths globally by October 2020, according to the World Health Organization (https://www.who.int/publications/m/item/weekly-operational-update--30-october-2020). Diagnosis of the causative pathogen, severe acute respiratory syndrome coronavirus 2 (SARS-CoV-2), is based on reverse transcription-PCR (RT-PCR) to detect viral nucleic acid or serologic assays to detect SARS-CoV-2 antigens in early stages of disease (*1*,*2*). In later stages of disease, antibody-based serologic testing can complement diagnosis of SARS-CoV-2 infection. In addition, antibody-based serologic testing is a valuable epidemiologic tool to assess COVID-19 spread and potential immunity to SARS-CoV-2. Serologic studies in Europe and Asia indicate high sensitivity and specificity of widely used SARS-CoV-2 antibody ELISAs (*3*,*4*). However, many serologic tests have not been validated in resource-limited settings (*5*). We conducted a SARS-CoV-2 serologic assessment in Benin by using samples from patients with RT-PCR–confirmed SARS-CoV-2 infection and controls sampled before the first SARS-CoV-2 detection in March 2020.

Author affiliations: Université Nationale des Sciences, Technologies, Ingénierie et Mathématiques, Cotonou, Benin (A. Yadouleton); Laboratoire des Fièvres Hémorragiques Virales du Benin, Cotonou (A. Yadouleton, C. Tchibozo, G. Hounkanrin, Y. Badou); Charité-Universitätsmedizin Berlin, corporate member of Freie Universität Berlin, Humboldt-Universität zu Berlin, and Berlin Institute of Health, Berlin, Germany (A.-L. Sander, A. Moreira-Soto, C. Fischer, N. Krause, E.F. de Oliveira Filho, S. Brünink, J.F. Drexler); Ministry of Health, Cotonou (P. Akogbeto, A. Dossou, B. Hounkpatin); Conseil National de Lutte contre le VIH-Sida, la Tuberculose, le Paludisme, les IST et les Epidémies, Cotonou (M.A. Joël Aïssi); World Health Organization Regional Office for Africa, Health Emergencies Programme, Brazzaville, Congo (M.H. Djingarey); Deutsche Gesellschaft für Internationale Zusammenarbeit, Bonn, Germany (M. Nagel); German Centre for Infection Research, associated partner Charité-Universitätsmedizin, Berlin, Germany (J.F. Drexler)

DOI: https://doi.org/10.3201/eid2701.203281

## The Study

We obtained convalescent serum samples from 8 patients in Benin with RT-PCR–confirmed COVID-19 during March–April 2020. The average sampling time was 8 (range 1–10) days after RT-PCR confirmation of SARS-CoV-2 infection (Table 1). We also included 60 serum samples from patients with acute febrile illness tested as part of hemorrhagic fever surveillance during October–November 2019 as prepandemic controls (Table 2). Sampling was approved by the ethics committee of the Benin Ministry of Health (approval no. 030/MS/DC/SGM/DNSP/CJ/SA/027SGG2020).

We tested all 68 serum samples by using commercially available ELISAs from EUROIMMUN (https://www.euroimmun.com) that rely on different antigens and antibody classes: SARS-CoV-2 nucleocapsid (N) antigen (IgG), spike 1 (S1) subunit (IgG and IgA), and Middle East respiratory syndrome coronavirus (MERS-CoV) S1 (IgG). We also used the SCoV-2 Detect IgG ELISA (InBios, https://inbios.com), an IgG-only S1 antigen-based test authorized for emergency use by the US Food and Drug Administration. Serum samples also were tested by using commercially available ELISA kits (EUROIMMUN) against the Zika virus (ZIKV)

[1]These first authors contributed equally to this article.

[2]These senior authors contributed equally to this article.

**Table 1.** Characteristics of patients with RT-PCR–confirmed SARS-CoV-2 infection from whom serum samples were collected during March–April 2020 in Benin*

| Sample ID | Age, y/sex | Sampling month | Location | Travel history | Symptoms | Day serum sample taken after RT-PCR–confirmed SARS-CoV-2 infection |
|---|---|---|---|---|---|---|
| 1 | 36/M | March | Cotonou | France | Fever | 8 |
| 2 | 43/M | March | Cotonou | Niger | Fever | 1 |
| 3 | 34/F | March | Cotonou | France | Fever | 8 |
| 4 | 29/M | March | Cotonou | France | Fever | 10 |
| 5 | 44/M | April | Cotonou | Germany | Fever | 10 |
| 6 | 39/F | April | Cotonou | France | Fever | 9 |
| 7 | 41/F | April | Cotonou | France | Fever | 8 |
| 8 | 37/M | April | Cotonou | Germany | Fever | 8 |

*ID, identification; RT-PCR, reverse transcription PCR; SARS-CoV-2, severe acute respiratory syndrome coronavirus 2.

nonstructural protein 1 (NS1) antigen (IgG), the Epstein-Barr virus (EBV) nuclear antigen 1 (EBNA1) (IgG), and the EBV viral capsid (CA) antigen (IgM and IgG), as well as real-time PCR tests (TIB MOLBIOL, https://www.tib-molbiol.com) for all human pathogenic *Plasmodium* species, EBV, and cytomegalovirus (CMV). Plaque-reduction neutralization tests (PRNTs) were performed by using similar methods for SARS-CoV-2 and ZIKV as described (*4*,*6*). We used previously described recombinant S-based immunofluorescence assays (*7*) to test for specific antibodies to common cold betacoronavirus human coronavirus (HCoV) OC43 and HCoV-HKU1.

Among the 8 patients with RT-PCR–confirmed SARS-CoV-2 infection, seroconversion ranged from 62.5%–100% (95% CI 30.8%–100.0%), depending on the ELISA used (Figure 1, panel A), suggesting differential sensitivity of ELISAs on the basis of immunoglobulin detected and the commercial kit used. Indeed, early after infection, IgA-based tests had a higher sensitivity than most IgG-based SARS-CoV-2 ELISAs; only the InBios IgG-based kit was positive for all RT-PCR–confirmed patients (Figure 1, panel A). A total of 87.5% (7/8) of ELISA results were confirmed by a highly specific SARS-CoV-2 PRNT (Figure 1, panel B).

When summarizing all antibody classes, antigens, and kits among the 60 prepandemic controls, we observed 25.0% (15/60; 95% CI 15.7%–37.3%) positive or borderline ELISA results (*8*). Different from RT-PCR–confirmed cases, ELISA reactivity in those samples contrasted with the complete lack of SARS-CoV-2–specific neutralizing antibodies, suggesting unspecific ELISA reactivity (Figure 1, panel B).

Unspecific SARS-CoV-2 ELISA reactivity might be consistent with, but not limited to, 3 scenarios. First, antibodies elicited by common infections with endemic human coronaviruses might cross-react with SARS-CoV-2 antigens (*1*). However, a Fisher exact test showed no statistically significant difference in the frequency of antibody reactivity with common cold coronavirus antigens between SARS-CoV-2 ELISA-positive serum samples compared with SARS-CoV-2 ELISA-negative samples. In detail, reactivity with HCoV-OC43 was 63.6% in SARS-CoV-2 ELISA-positive samples and 70.4% in SARS-CoV-2 ELISA-negative samples (p = 0.7); reactivity with HCoV-HKU-1 was 45.7% in SARS-CoV-2 ELISA-positive samples and 74.0% in SARS-CoV-2 ELISA-negative samples (p = 0.1) (Appendix Figure 1, panel A, http://wwwnc.cdc.gov/EID/article/27/1/20-3281-App1.pdf). Similarly, a Student *t*-test revealed no statistically significant difference in the magnitude of antibody titers against common cold coronaviruses between SARS-CoV-2 ELISA-positive or ELISA-negative samples (p = 0.09 for HCoV OC-43 and p = 0.8 for HCoV HKU-1) (Appendix Figure 1, panel B). Of note, no serum reacted with MERS-CoV antigens, suggesting that unspecific reactivity might not apply to all coronavirus antigens and tests (Appendix Figure 2). Second, polyclonal B-cell activation can occur in infections with or reactivations of herpesviruses, such as CMV and EBV, and elicit false-positive results in serologic tests (*9*). However, only 2 patients had a positive CMV PCR and only 1 patient had a positive EBV PCR (Figure 2). In addition, persons with SARS-CoV-2 ELISA-positive versus ELISA-negative results did not differ in their past exposure to EBV, according to detailed serologic analyses (Figure 2; Appendix Figure 3). Finally, polyclonal B cell activation also can be caused by acute malaria, which is widespread in Africa (*10*). More (71.4%) persons with SARS-CoV-2–positive ELISAs than those with negative ELISAs (54.3%) were positive for *Plasmodium* in a highly sensitive PCR test, but the difference was not statistically significant by Fisher exact test (p = 0.35; Figure 1, panel C). However, parasite loads were statistically significantly higher among SARS-CoV-2 ELISA-positive than ELISA-negative persons by Student *t*-test (p = 0.035; Figure 1, panel C). In malaria, higher parasite loads are detected at early stages of infection and decrease over time, suggesting a higher proportion of acute malaria in SARS-CoV-2 ELISA–positive patients compared with likely subacute or chronic malaria in SARS-CoV-2 ELISA–negative patients (*11*). Thus, acute malaria is the most plausible explanation for unspecific SARS-CoV-2 ELISA reactivity in prepandemic controls. To assess the breadth of

**Table 2.** Characteristics of prepandemic controls with febrile illnesses of unknown origin from whom samples were collected during October–November 2019 in Benin*

| Sample ID | Age, y/sex | Health center | Sampling month | Symptoms |
|---|---|---|---|---|
| 215 | 28/M | CNHU | October | Fever |
| 311 | 15/F | CB | October | Fever |
| 312 | 34/F | CB | October | Fever |
| 313 | 27/M | CB | October | Fever |
| 314 | 18/M | CB | October | Fever |
| 315 | 21/M | CB | October | Fever |
| 316 | 31/M | CB | October | Fever |
| 317 | 25/F | CB | October | Fever |
| 318 | 23/F | CB | October | Fever |
| 319 | 18/M | CB | October | Fever |
| 320 | 22/F | CB | October | Fever |
| 321 | 19/F | CB | October | Fever |
| 322 | 23/M | CB | October | Fever |
| 323 | 21/M | CB | October | Fever |
| 324 | 34/F | CB | October | Fever |
| 325 | 47/M | CB | October | Fever |
| 326 | 29/M | CB | October | Fever |
| 327 | 42/F | CB | October | Fever |
| 328 | 21/M | CB | October | Fever |
| 329 | 12/M | CB | October | Fever |
| 330 | 19/F | CB | October | Fever |
| 331 | 46/M | CB | October | Fever |
| 332 | 44/F | CB | October | Fever |
| 333 | 59/M | CB | October | Fever |
| 334 | 37/M | CB | October | Fever |
| 335 | 65/M | CB | October | Fever |
| 336 | 39/F | CB | October | Fever |
| 337 | 56/M | CB | October | Fever |
| 338 | 19/M | CB | October | Fever |
| 339 | 29/M | CB | October | Fever |
| 201 | 42/M | CB | November | Fever |
| 202 | 23/M | CB | November | Fever |
| 203 | 29/M | CB | November | Fever |
| 204 | 18/M | CB | November | Fever |
| 205 | 30/F | AHC | November | Fever |
| 206 | 26/F | AHC | November | Fever |
| 207 | 19/M | AHC | November | Fever |
| 208 | 25/F | AHC | November | Fever |
| 209 | 34/F | AHC | November | Fever |
| 210 | 61/F | AHC | November | Fever |
| 211 | 18/F | AHC | November | Fever |
| 212 | 32/M | AHC | November | Fever |
| 213 | 63/F | AHC | November | Fever |
| 214 | 40/M | AHC | November | Fever |
| 216 | 50/F | CNHU | November | Fever |
| 217 | 38/M | CNHU | November | Fever |
| 218 | 55/M | CNHU | November | Fever |
| 219 | 13/F | CNHU | November | Fever |
| 220 | 12/F | CNHU | November | Fever |
| 221 | 29/F | CNHU | November | Fever |
| 222 | 35/M | CNHU | November | Fever |
| 223 | 22/M | CNHU | November | Fever |
| 224 | 15/M | CNHU | November | Fever |
| 225 | 19/M | CNHU | November | Fever |
| 226 | 33/F | CNHU | November | Fever |
| 227 | 16/F | CNHU | November | Fever |
| 228 | 26/M | CNHU | November | Fever |
| 229 | 31/F | CNHU | November | Fever |
| 230 | 26/F | CNHU | November | Fever |
| 291 | 29/F | AHC | November | Fever |

*AHC, Akkasato Health Center; CB, Clinique Boni; CNHU, Centre National Hospitalier Universitaire Hubert Koutoukou; ID, identification.

unspecific reactivity, we tested the serum samples from prepandemic controls by using a ZIKV IgG ELISA, for which unspecific reactivity has been reported in cases of acute malaria (*10*). We found that 57.1% of samples that elicited potentially unspecific SARS-CoV-2 ELISA results also showed ZIKV ELISA–positive results, whereas only 23.9% of samples that were SARS-CoV-2 ELISA–negative were ZIKV ELISA–positive. This difference was statistically significant by Fisher exact test ($p = 0.019$) (Figure 1, panel D; Appendix Figure 4).

From the prepandemic controls that were SARS-CoV-2 ELISA positive, no ZIKV ELISA–positive serum samples showed ZIKV-specific neutralizing antibodies, suggesting unspecific reactivity of those samples in the ZIKV ELISA, similar to the discrepant results of SARS-CoV-2 ELISA and PRNT observed in those serum samples (Figure 1, panel E; Figure 2).

## Conclusion

We assessed SARS-CoV-2 antibody-based serologic diagnostics in Benin and noted unspecific reactivity in up to 25% of febrile patients, possibly due to acute malaria. Limitations of our study include the small sample size and limited patient metadata. Testing of serum samples for CMV and EBV by PCR might not have been sensitive due to lack of cell-associated viral nucleic acid; therefore, we cannot exclude potential herpesvirus reactivation affecting serologic testing. Nevertheless, our analyses point to acute malaria as the likely cause of the unspecific serologic reactivity, although we cannot exclude other coexisting conditions in the tropics, such as dengue virus, which also can affect testing (*12*).

Unspecific reactivity in serologic tests might affect public health interventions in tropical regions, leading to overestimates of SARS-CoV-2 circulation in regions where malaria is endemic and to misidentification of SARS-CoV-2 hotspots. In addition, due to false-positive SARS-CoV-2 results, target populations for vaccine campaigns might be missed when vaccines become available, and coexistent diseases, such as malaria, might be overlooked, leading to higher mortality rates from endemic diseases (*13*,*14*). The robustness of current and future SARS-CoV-2 serologic tests should be further assessed by multicentric seroepidemiologic studies from different tropical regions (*15*).

This article was preprinted at https://www.medrxiv.org/content/10.1101/2020.06.29.20140749v1.

### Acknowledgments

We thank Arne Kühne, Wendy Jo-lei, and Patricia Tscheak from the Institute of Virology, Charité, Berlin, Germany for laboratory assistance and Olfert Landt from TIB MOLBIOL GmbH, Germany for providing diagnostic reagents.

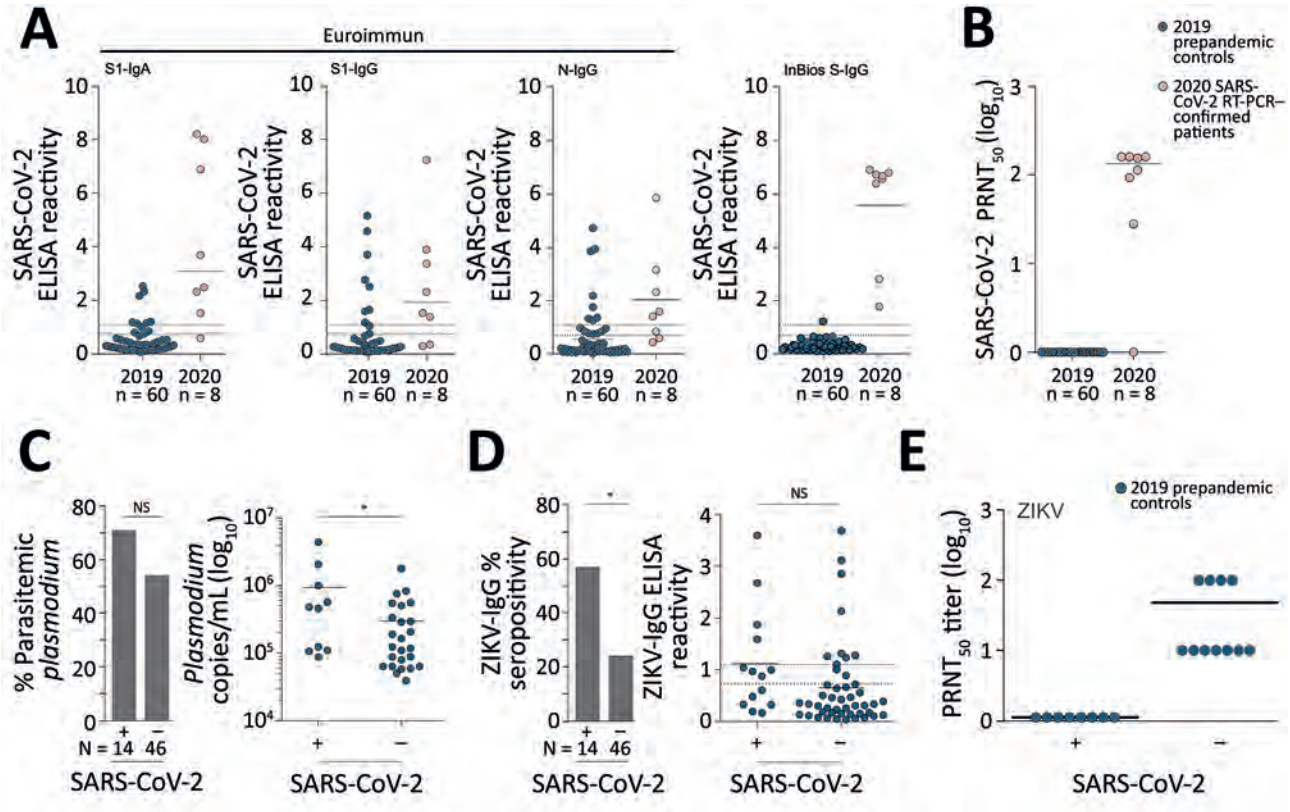


**Figure 1.** Serologic diagnostics and co-existing pathogens in Benin. A) SARS-CoV-2 ELISA reactivity by using different commercially available assays in prepandemic controls from 2019 and SARS-CoV-2 RT-PCR-confirmed patients from 2020. Dashed lines denote the ratio thresholds of ≥1.1 (positive) and ≤0.9 (negative); results between these values are considered borderline, as defined by the manufacturers, EUROIMMUN (https://www.euroimmun.com) and InBios (https://inbios.com). Solid line denotes mean ELISA reactivity. B) SARS-CoV-2 $PRNT_{50}$ in prepandemic controls from 2019 and SARS-CoV-2 RT-PCR–confirmed patients from 2020, shown in $log_{10}$ scale for clarity. Solid line denotes mean PRNT $log_{10}$ titer. C) Percentage of prepandemic controls with *Plasmodium* parasitemia who were SARS-CoV-2 ELISA–positive versus those who were SARS-CoV-2 ELISA-negative, shown in $log_{10}$ scale for clarity. Solid line denotes the mean copies/mL. Asterisk denotes p<0.05. D) ZIKV ELISA IgG ELISA percent seropositivity and ZIKV ELISA reactivity within SARS-CoV-2–positive and SARS-CoV-2–negative prepandemic controls. Continuous line denotes the mean ELISA reactivity. Asterisk denotes p<0.05. E) ZIKV $PRNT_{50}$ results. Continuous line denotes the mean $PRNT_{50}$ $log_{10}$ reactivity. NS, not statistically significant; $PRNT_{50}$, 50% plaque reduction neutralization test; SARS-CoV-2, severe acute respiratory syndrome coronavirus 2; ZIKV, Zika virus.

This work was supported by the Deutsche Gesellschaft für Internationale Zusammenarbeit (GIZ) GmbH.

## About the Author

Dr. Yadouleton is a medical entomologist in the Centre de Recherche Entomologique de Cotonou, Benin, head of the Laboratoire des Fièvres Hémorragiques in Cotonou, and a teacher at the University of Natitingou, Benin. His research interests include mosquito control and the diagnosis of viral hemorrhagic fevers.

## References

1. Meyer B, Drosten C, Müller MA. Serological assays for emerging coronaviruses: challenges and pitfalls. Virus Res. 2014;194:175–83. https://doi.org/10.1016/j.virusres.2014.03.018
2. He X, Lau EHY, Wu P, Deng X, Wang J, Hao X, et al. Temporal dynamics in viral shedding and transmissibility of COVID-19. Nat Med. 2020;26:672–5. https://doi.org/10.1038/s41591-020-0869-5
3. Zhao R, Li M, Song H, Chen J, Ren W, Feng Y, et al. Early detection of SARS-CoV-2 antibodies in COVID-19 patients as a serologic marker of infection. Clin Infect Dis. 2020;ciaa523. https://doi.org/10.1093/cid/ciaa523
4. Okba NMA, Müller MA, Li W, Wang C, GeurtsvanKessel CH, Corman VM, et al. Severe acute respiratory syndrome coronavirus 2-specific antibody responses in coronavirus disease 2019 patients. Emerg Infect Dis. 2020;26:1478–88. https://doi.org/10.3201/eid2607.200841
5. Fischer C, Drosten C, Drexler JF. The difficulties in obtaining reliable Zika virus diagnostics. Lancet Infect Dis. 2019;19:240–1. https://doi.org/10.1016/S1473-3099(19)30049-0
6. Netto EM, Moreira-Soto A, Pedroso C, Höser C, Funk S, Kucharski AJ, et al. High Zika virus seroprevalence in Salvador, northeastern Brazil limits the potential for further outbreaks. MBio. 2017;8:e01390-17. https://doi.org/10.1128/mBio.01390-17

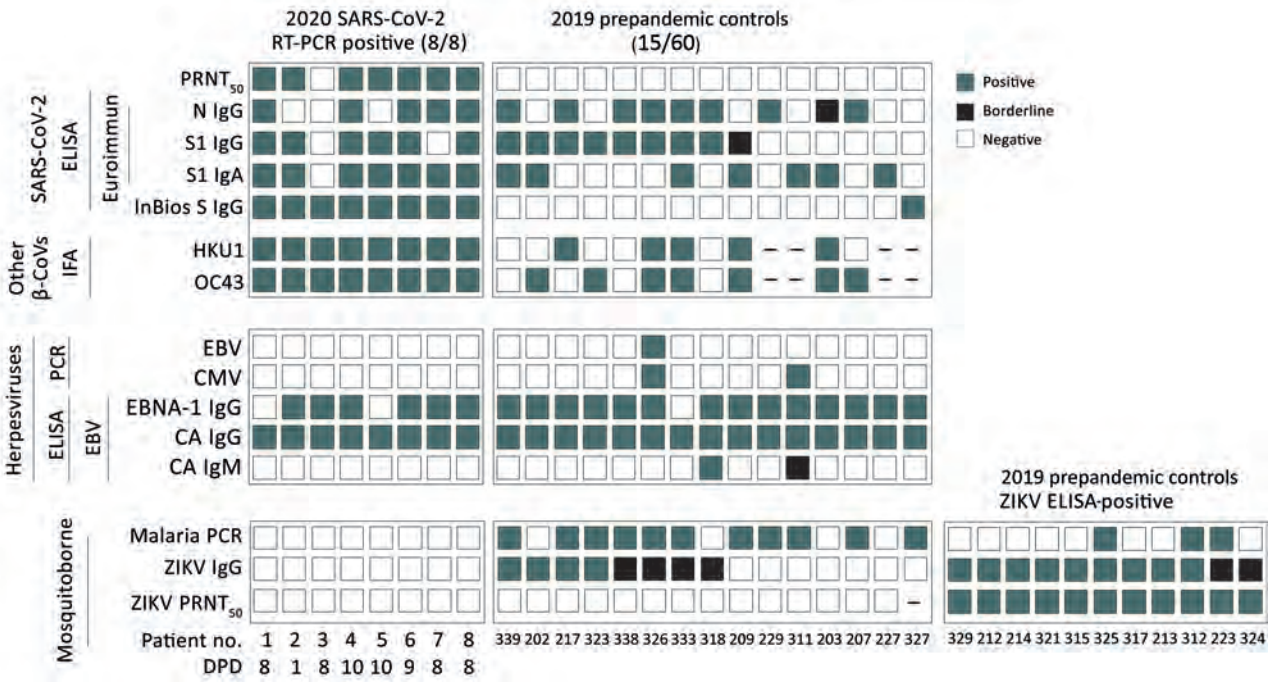


**Figure 2**. Molecular and serologic test results for betacoronaviruses and co-existing pathogens in Benin. Individual results are shown for reactivity of different commercially available SARS-CoV-2 ELISAs, SARS-CoV-2 PRNT, and IFA reactivity to common cold human coronaviruses OC43 and HKU1 in prepandemic controls from 2019 and SARS-CoV-2 RT-PCR confirmed patients from 2020; EBV PCR, CMV PCR, and 3 EBV ELISAs (EBV-CA IgM, EBV-CA IgG, and EBV-EBNA IgG) from the same groups; and ZIKV-IgG ELISA, ZIKV-PRNT, and malaria PCR from the same groups. Gray squares denote positive results; black squares denote inconclusive results; and white squares denote negative results. Dash (–) denotes samples in which the assay was not performed due to low sample volume. β-CoVs, betacoronaviruses; CA, viral capsid; CMV, cytomegalovirus; DPD, days the serum sample was taken after positive RT-PCR SARS-CoV-2 diagnosis; EBNA, nuclear antigen 1; EBV, Epstein-Barr virus; IFA, immunofluorescence; $PRNT_{50}$, 50% plaque reduction neutralization test; RT-PCR, reverse transcription PCR; SARS-CoV-2, severe acute respiratory syndrome coronavirus 2; ZIKV, Zika virus.


7. Corman VM, Müller MA, Costabel U, Timm J, Binger T, Meyer B, et al. Assays for laboratory confirmation of novel human coronavirus (hCoV-EMC) infections. Euro Surveill. 2012;17:20334. https://doi.org/10.2807/ese.17.49. 20334-en
8. Harvey R, Mattiuzzo G, Hassall M, Sieberg A, Müller MA, Drosten C, et al.; study participants. Comparison of serologic assays for Middle East respiratory syndrome coronavirus. Emerg Infect Dis. 2019;25:1878–83. https://doi.org/10.3201/eid2510.190497
9. Sangster MY, Topham DJ, D'Costa S, Cardin RD, Marion TN, Myers LK, et al. Analysis of the virus-specific and nonspecific B cell response to a persistent B-lymphotropic gammaherpesvirus. J Immunol. 2000;164:1820–8. https://doi.org/10.4049/jimmunol.164.4.1820
10. Van Esbroeck M, Meersman K, Michiels J, Arien KK, Van den Bossche D. Letter to the editor: Specificity of Zika virus ELISA: interference with malaria. Euro Surveill. 2016;21(21). https://doi.org/10.2807/1560-7917.ES.2016.21.21.30237
11. Dormond L, Jaton-Ogay K, de Vallière S, Genton B, Bille J, Greub G. Multiplex real-time PCR for the diagnosis of malaria: correlation with microscopy. Clin Microbiol Infect. 2011;17:469–75. https://doi.org/10.1111/j.1469-0691.2010.03218.x
12. Lustig Y, Keler S, Kolodny R, Ben-Tal N, Atias-Varon D, Shlush E, et al. Potential antigenic cross-reactivity between SARS-CoV-2 and dengue viruses. Clin Infect Dis. 2020 Aug 14 [Epub ahead of print]. https://doi.org/10.1093/cid/ciaa1207
13. Fischer C, de Oliveira-Filho EF, Drexler JF. Viral emergence and immune interplay in flavivirus vaccines. Lancet Infect Dis. 2020;20:15–7. https://doi.org/10.1016/S1473-3099(19)30697-8
14. Plucinski MM, Guilavogui T, Sidikiba S, Diakité N, Diakité S, Dioubaté M, et al. Effect of the Ebola-virus-disease epidemic on malaria case management in Guinea, 2014: a cross-sectional survey of health facilities. Lancet Infect Dis. 2015;15:1017–23. https://doi.org/10.1016/S1473-3099(15)00061-4
15. Elm J, Desowitz R, Diwan A. Serological cross-reactivities between the retroviruses HIV and HTLV-1 and the malaria parasite *Plasmodium falciparum*. P N G Med J. 1998;41:15–22.


Address for correspondence: Jan Felix Drexler, Helmut-Ruska-Haus, Institute of Virology, Campus Charité Mitte, Charitéplatz 1, Berlin 10117, Germany; email: felix.drexler@charite.de

# Fatal Case of Chronic Jamestown Canyon Virus Encephalitis Diagnosed by Metagenomic Sequencing in Patient Receiving Rituximab

Isaac H. Solomon,[1] Vijay S. Ganesh,[1] Guixia Yu, Xian Ding Deng, Michael R. Wilson, Steve Miller, Tracey A. Milligan, Shibani S. Mukerji, Abigail Mathewson, Justin Linxweiler, Darlene Morse, Jana M. Ritter, J. Erin Staples, Holly Hughes, Carolyn V. Gould, Pardis C. Sabeti,[2] Charles Y. Chiu,[2] Anne Piantadosi[2,3]

A 56-year-old man receiving rituximab who had months of neurologic symptoms was found to have Jamestown Canyon virus in cerebrospinal fluid by clinical metagenomic sequencing. The patient died, and postmortem examination revealed extensive neuropathologic abnormalities. Deep sequencing enabled detailed characterization of viral genomes from the cerebrospinal fluid, cerebellum, and cerebral cortex.

Jamestown Canyon orthobunyavirus (JCV) is a negative-sense RNA virus in the California serogroup. Its tripartite genome comprises small (nucleocapsid), medium (glycoprotein), and large (polymerase) segments. JCV is distributed throughout the United States and Canada and has been isolated from multiple mammals and mosquitoes (*1*,*2*). Most infections occur in adults, during the summer, and are asymptomatic, but manifestations can include fever and acute meningoencephalitis (*2*). Cerebrospinal fluid (CSF) typically shows a lymphocytic pleocytosis with elevated protein and normal glucose. Diagnosis is made by detection of JCV IgM in serum or CSF and confirmed by plaque-reduction neutralization testing to rule out cross-reactivity with other California serogroup viruses (*3*). Detection of viral RNA in human CSF has rarely been described, with viremia presumed to be of short duration, so reverse transcription PCR (RT-PCR) is not routinely used for diagnosis (*3*–*5*). No specific treatments are available, although intravenous ribavirin has been reported to improve seizures (*6*). Because of the limited number of cases described, the full range of findings associated with JCV infection is unknown. No fatal cases were reported to the Centers for Disease Control and Prevention (CDC) before 2017, and no autopsy reports have been published (*7*).

## The Case-Patient

A 56-year-old man from New England with a history of mantle cell lymphoma in remission, receiving maintenance rituximab since 2014, had fatigue, arthralgias, and weight loss in summer 2017. He was empirically treated for Lyme disease without improvement, had progressive insomnia and inattention, and was eventually admitted for workup of rapidly progressive dementia in April 2018. On examination, he had impaired arousal and attention (Montreal Cognitive Assessment score 6 of 30). Cranial nerve, tone, strength, sensory, and reflex

Author affiliations: Brigham and Women's Hospital, Boston, Massachusetts, USA (I.H. Solomon, V.S. Ganesh, T.A. Milligan); Harvard Medical School, Boston (I.H. Solomon, V.S. Ganesh, T.A. Milligan, S.S. Mukerji, A. Piantadosi); Broad Institute, Cambridge, Massachusetts, USA (V.S. Ganesh, P.C. Sabeti, A. Piantadosi); University of California–San Francisco, San Francisco, California, USA (G. Yu, X.D. Deng, M.R. Wilson, S. Miller, C.Y. Chiu); Massachusetts General Hospital, Boston (S.S. Mukerji, A. Piantadosi); New Hampshire Division of Public Health Services, Concord, New Hampshire, USA (A. Mathewson, J. Linxweiler, D. Morse); Centers for Disease Control and Prevention, Atlanta, Georgia, USA (J.M. Ritter); Centers for Disease Control and Prevention, Fort Collins, Colorado, USA (J.E. Staples, H. Hughes, C.V. Gould); Harvard University, Cambridge (P.C. Sabeti); Harvard T.H. Chan School of Public Health, Boston (P.C. Sabeti); Howard Hughes Medical Institute, Chevy Chase, Maryland, USA (P.C. Sabeti)

DOI: https://doi.org/10.3201/eid2701.203448

[1]These authors contributed equally to this article.

[2]These senior authors contributed equally to this article.

[3]Current affiliation: Emory University, Atlanta, Georgia, USA.

examinations were normal. Gait was wide-based and slow without ataxia or parkinsonism. Magnetic resonance imaging of the brain showed mild ventriculomegaly attributed to atrophy but was otherwise unremarkable, without contrast enhancement, cortical diffusion restriction, mass lesions, hemorrhage, or infarction (Figure 1). Electroencephalography showed moderate bihemispheric slowing without epileptiform features. CSF from multiple lumbar punctures showed mild lymphocytic pleocytosis (0–22 leukocytes/μL, 83%–98% lymphocytes), elevated total protein (40–116 mg/dL; reference 10–44 mg/dL), and unremarkable glucose (65–78 mg/dL; reference 40–80 mg/dL) (Appendix Table 1, https://wwwnc.cdc.gov/EID/article/27/1/20-3448-App1.pdf). An extensive infectious, autoimmune, and neurodegenerative disease workup was normal (Appendix Table 2).

A CSF sample collected in April 2018 underwent clinical metagenomic next-generation sequencing (mNGS) testing at the University of California–San Francisco (*8*) and was positive for California encephalitis virus most closely matching JCV, with reads mapping to 2 of the 3 viral genome segments (Appendix Figure 1). Another CSF sample, obtained approximately 3 weeks later in May, was negative for JCV by RT-PCR performed by CDC's Arboviral Diseases Branch (Division of Vector-Borne Diseases, National Center for Emerging and Zoonotic Infectious Diseases; Fort Collins, CO, USA); however, concurrent serum JCV RT-PCR was positive. Results of JCV IgM and neutralizing antibody testing were negative for CSF and blood from the samples obtained in May. Concurrent samples had 0% CD20+ circulating lymphocytes (reference 3%–20% lymphocytes), attributed to rituximab treatment, last administered in December 2017.

The patient was treated with intravenous immunoglobulin (total 2 g/kg), followed by a 2-week course of favipiravir, an experimental inhibitor of viral RNA polymerase, without improvement. His mental status deteriorated to a comatose state. He was transitioned to comfort care and died in June 2018, ≈1 year after suspected symptom onset.

At autopsy, the unfixed brain weighed 1,240 g and appeared grossly normal, with no masses, hemorrhage, infarctions, or herniation. Histologic abnormalities were most prominent in the cerebral cortex (particularly frontal and temporal lobes), cerebellum, and hippocampus; milder changes in basal ganglia, thalamus, and brainstem were observed, including severe loss of neurons, diffuse microgliosis with microglial nodules and neuronophagia, and perivascular and

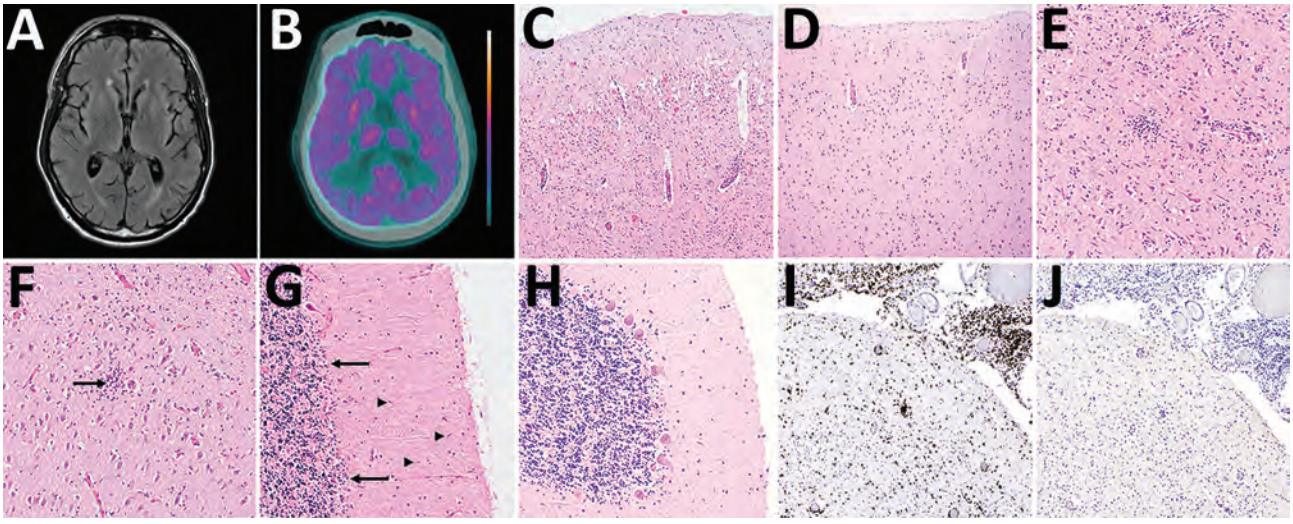


**Figure 1.** Brain imaging and autopsy findings in a case of chronic Jamestown Canyon virus (JCV) meningoencephalitis in a patient receiving rituximab, Boston, Massachusetts, USA. A) Brain magnetic resonance imaging T2-weighted fluid-attenuated inversion recovery showed mild atrophy with secondary ventriculomegaly but was otherwise unremarkable. B) Brain positron emission tomography with 2-deoxy-2-[fluorine-18] fluoro-D-glucose integrated with computed tomography showed global hypometabolism. Color scale ranges from blue-green (hypometabolic) to orange-white (hypermetabolic). C, D) Hematoxylin and eosin stained section of cerebral cortex at low magnification shows loss of neurons and perivascular chronic inflammation (C), compared with a JCV-negative control with a normal complement of cortical neurons (D). E, F) Higher-power magnification of cerebral cortex (E) and hippocampus (F) show microgliosis, microglial nodules, and neuronophagia (arrow). G, H) Severe Purkinje cell loss, Bergmann gliois (arrows), and microgliosis (arrowheads) of the molecular layer are present in the cerebellum (G), compared with a JCV-negative control with normal complement of Purkinje cells (H). I, J) Immunohistochemistry shows abundant perivascular, parenchymal, and leptomeningeal CD3+ T cells (I) and is negative for B-cell lineage–specific activator protein positive B cells (J). Panels C, D, I, and J, original magnification ×100; panels E, F, G, and H, original magnification ×200.

parenchymal chronic inflammation (Figure 1). Leptomeninges showed numerous chronic inflammatory cells. No viral inclusions were identified. There was no evidence of lymphoma. Immunohistochemical staining highlighted abundant perivascular, parenchymal, and leptomeningeal T cells with a complete lack of B cells. Formalin-fixed paraffin-embedded brain tissue was positive for JCV by RT-PCR (performed by CDC's Arboviral Diagnostic and Reference Laboratory); results were negative for immunohistochemistry for flaviviruses and enteroviruses (performed by CDC's Infectious Diseases Pathology Branch [Division of High-Consequence Pathogens and Pathology, National Center for Emerging and Zoonotic Infectious Diseases; Atlanta, GA, USA]).

Complete or near-complete JCV genomes were recovered from premortem CSF and postmortem cerebellum and cortex tissue (both frozen and formalin-fixed paraffin-embedded) (Table; Appendix Supplementary Methods, Figure 2). Phylogenetic analysis of the small (nucleocapsid) segment showed that sequences from this patient were most closely related to JCV from mosquitoes in Connecticut (Figure 2, panel A) (*9*). Comparison of JCV genomes between this patient's CSF, cerebellum, and cortex revealed 27 high-confidence within-patient single-nucleotide polymorphisms (SNPs) (Figure 2, panel B; Appendix Tables 3, 4). For 13 SNPs, the variant present in CSF was different from that in cerebellum and cortex, suggesting evolution over time. For another 4 SNPs, the variant present in cerebellum was different from that in cortex, suggesting compartmentalization. The remaining 10 SNPs could represent either compartmentalization or evolution over time, because only 1 brain tissue (cerebellum or cortex) was sequenced to sufficient depth. Variability was greater in the small segment (nucleocapsid) and medium segment (glycoprotein) than the large segment (polymerase).

## Conclusions

We describe an unusual fatal case of chronic JCV encephalitis in a patient who was being treated with rituximab. In contrast to this case, previously described patients with JCV have had acute illness, and JCV infection is rarely fatal (*7*,*10*). The neuropathologic findings in this patient, although nonspecific, are similar to those of a cerebellar biopsy from a patient with JCV encephalitis that showed severe loss of Purkinje and granule cells, diffuse microgliosis of the molecular layer, and leptomeningeal inflammation (*5*).

The lack of distinguishing clinical, radiographic, and pathologic features of JCV underscores the diagnostic utility of clinical mNGS (*8*). Attributable in part to low incidence and lack of commercially available targeted testing, JCV is often not considered a priori, especially in the setting of chronic progressive neurologic illness. As a further complication, standard clinical testing by serology can be negative in the setting of B-cell–depleting therapy; our patient had negative JCV serologic tests and lack of B lymphocytes by immunohistochemical staining. Similar phenomena have been reported in rituximab-treated patients with other arboviral infections (e.g., Cache Valley orthobunyavirus, Powassan virus, and West Nile virus) who lack detectable antibodies but remain viremic longer than immunocompetent patients, highlighting the importance of nucleic acid–based testing methods (*11*–*13*).

In addition to diagnosis, mNGS also provides valuable information about pathogen genomics. We report the unique assembly of a JCV genome from human clinical samples, an important advance in the study of JVC pathogenesis, virus evolution, and differences between the enzootic transmission cycle and human infection (*14*). The functional importance of the identified SNPs could not be evaluated from the genomic data alone; however, none

**Table.** Results of JCV sequencing across samples from an immunocompromised patient with encephalitis, Boston, Massachusetts, USA*

| Specimen | Method | Total reads† | Unique JCV reads‡ | % Genome assembled, by segment§ | | | Mean depth, by genome segment§ | | |
|---|---|---|---|---|---|---|---|---|---|
| | | | | Small | Medium | Large | Small | Medium | Large |
| CSF | mNGS, MSSPE | 1,917,836,676 | 894 | 100 | 80 | 90 | 14.3 | 3.7 | 5.3 |
| Cerebellum, frozen | mNGS, MSSPE | 1,031,252,808 | 558 | 98 | 66 | 100 | 9.4 | 1.3 | 6.1 |
| Cerebellum, FFPE | mNGS, hybrid capture | 38,974,996 | 294 | 70 | 56 | 90 | 7.1 | 1.2 | 3.1 |
| Cortex, frozen | mNGS, MSSPE | 729,867,496 | 3,652 | 100 | 100 | 100 | 61.6 | 15.2 | 40.2 |
| Cortex, FFPE | mNGS, hybrid capture | 101,331,284 | 518 | 100 | 72 | 91 | 20.1 | 2.1 | 4.5 |

*Methods detailed in Appendix (https://wwwnc.cdc.gov/EID/article/27/1/20-3448-App1.pdf). CSF, cerebrospinal fluid; FFPE, formalin-fixed, paraffin-embedded; JCV, Jamestown Canyon virus; mNGS, metagenomic next-generation sequencing; MSSPE, metagenomic sequencing with spiked primer enrichment.
†Total reads reflect the number of raw reads that were generated from each sample.
‡Unique JCV reads reflects removal of PCR duplicates and mapping to JCV reference sequences.
§Small, 989 nt; Medium, 4,509 nt; Large, 6,960 nt.

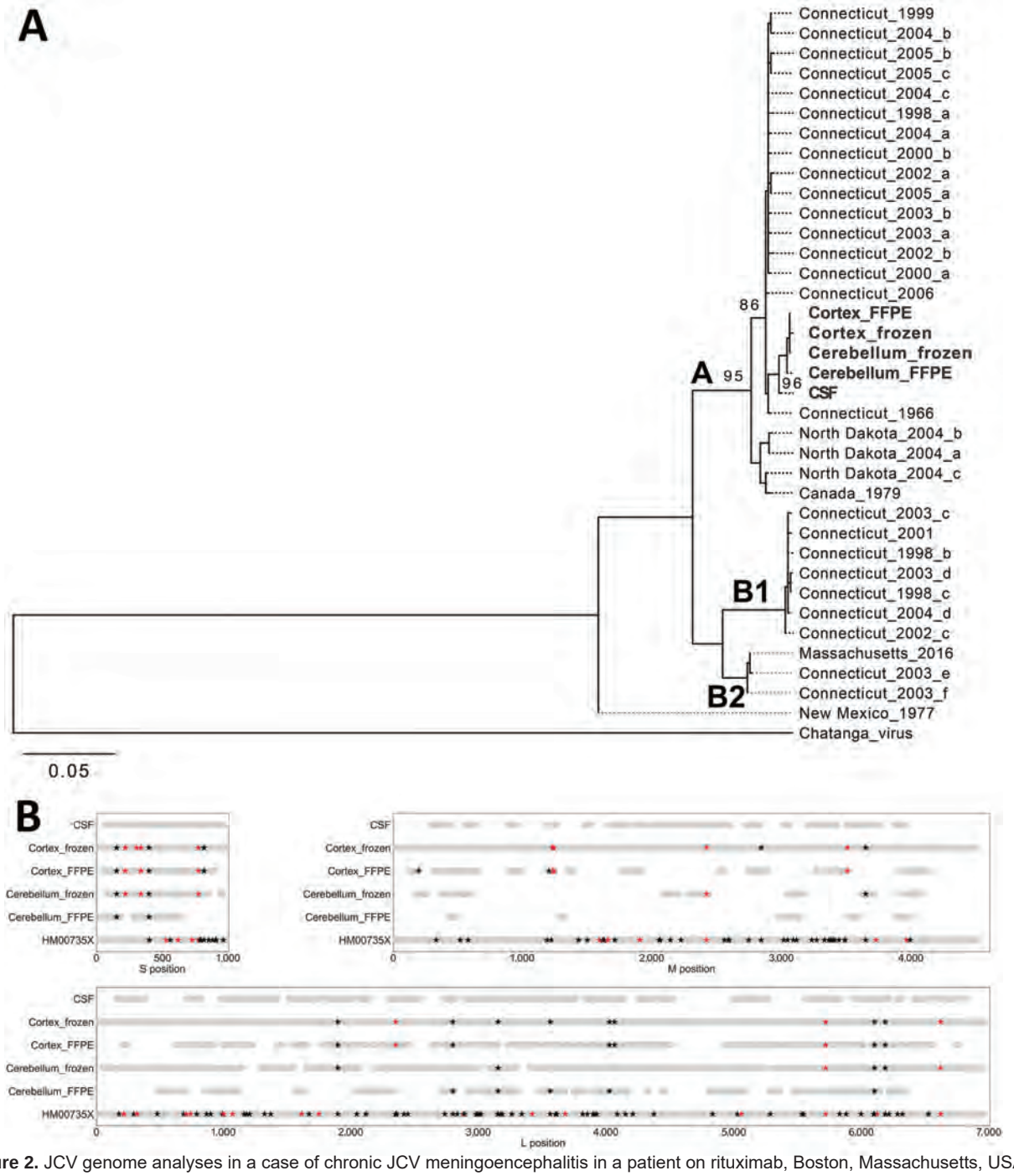


**Figure 2.** JCV genome analyses in a case of chronic JCV meningoencephalitis in a patient on rituximab, Boston, Massachusetts, USA. A) Maximum-likelihood phylogenetic tree of the coding region of the JCV small segment (nucleocapsid). Sequences from the patient (bold) were most closely related to a JCV strain isolated from Simsbury, Connecticut, USA (GenBank accession no. EF681842), with ≈70% bootstrap support. Clades A, B1, and B2 are as previously reported (*9*). B) Single-nucleotide polymorphisms (SNPs) observed between samples from patient in this study. The consensus genome derived from each sample was aligned to a mosquito-derived JCV sequence (GenBank accession nos. HM007356 [S segment], HM007357 [M segment], and HM007358 [L segment], all represented in the figure as HM00735X). For each sample in this study, the light gray bar indicates positions for which there was coverage of ≥3 reads. Using the sequence derived from CSF as the reference, positions with a SNP are marked with a star; black indicates a synonymous change, and red indicates a nonsynonymous change. Only high-confidence (confirmed) SNPs are shown in this figure; all SNPs observed are shown in Appendix Tables 3, 4 (https://wwwnc.cdc.gov/EID/article/27/1/20-3448-App1.pdf). Sequence data is available under National Center for Biotechnology Information BioProject no. PRJNA662969 (GenBank accession nos. MW072986–MW073000). CSF, cerebrospinal fluid; FFPE, formalin-fixed, paraffin-embedded; JCV, Jamestown Canyon virus; L, large; M, medium; S, small.

were associated with alterations of potential N-linked glycosylation sites, cysteine bonds, or the conserved fusion domain (*15*). One SNP that arose between CSF and brain (small segment gA397G; aT109A) also varied between JCV strains with different neurovirulence in mice, although the functional importance is unknown (*4*).

Although treatment options for JCV infection are largely unexplored, response to antiviral drugs probably depends on initiating treatment early in the disease course and reaching therapeutic levels in the CSF before extensive neuronal loss. Thus, broad-spectrum molecular assays such as mNGS could potentially lead to earlier treatment with improved outcomes (*8*).

### Acknowledgments

We thank the patient's family for granting permission to publish this information. We also wish to acknowledge contributions by Asmeeta Achari, Sarah Reagan-Steiner, and the molecular pathology and immunohistochemistry teams at CDC's Infectious Disease Pathology Branch.

This study was supported by the National Institutes of Health (grant no. U19AI110818 awarded to P.C.S, grant no. KL2 TR001100 awarded to A.P., and grant no. R33AI129455 awarded to C.Y.C.), the Charles and Helen Schwab Foundation (grant awarded to C.Y.C.), and a Broad*next*10 gift from the Broad Institute (awarded to P.C.S.).

## About the Author

Dr. Solomon is a neuropathologist at Brigham and Women's Hospital and Harvard Medical School, in Boston, Massachusetts. His primary research interests include viral infections of the central nervous system.

### References

1. Matkovic E, Hoang Johnson DK, Staples JE, Mora-Pinzon MC, Elbadawi LI, Osborn RA, et al. Enhanced arboviral surveillance to increase detection of Jamestown Canyon virus infections, Wisconsin, 2011–2016. Am J Trop Med Hyg. 2019;100:445–51. https://doi.org/10.4269/ajtmh.18-0575
2. Patriquin G, Drebot M, Cole T, Lindsay R, Schleihauf E, Johnston BL, et al. High seroprevalence of Jamestown Canyon virus among deer and humans, Nova Scotia, Canada. Emerg Infect Dis. 2018;24:118–21. https://doi.org/10.3201/eid2401.170484
3. Pastula DM, Hoang Johnson DK, White JL, Dupuis AP II, Fischer M, Staples JE. Jamestown Canyon virus disease in the United States—2000–2013. Am J Trop Med Hyg. 2015;93:384–9. https://doi.org/10.4269/ajtmh.15-0196
4. Bennett RS, Nelson JT, Gresko AK, Murphy BR, Whitehead SS. The full genome sequence of three strains of Jamestown Canyon virus and their pathogenesis in mice or monkeys. Virol J. 2011;8:136. https://doi.org/10.1186/1743-422X-8-136
5. Huang C, Campbell W, Grady L, Kirouac I, LaForce FM. Diagnosis of Jamestown Canyon encephalitis by polymerase chain reaction. Clin Infect Dis. 1999;28:1294–7. https://doi.org/10.1086/514789
6. Savard M, Paradis A, Francoeur CL. Jamestown Canyon encephalitis with NORSE and electrographic response to ribavirin: a case report. Epilepsia Open. 2018;3:286–9. https://doi.org/10.1002/epi4.12113
7. Curren EJ, Lehman J, Kolsin J, Walker WL, Martin SW, Staples JE, et al. West Nile virus and other nationally notifiable arboviral diseases—United States, 2017. MMWR Morb Mortal Wkly Rep. 2018;67:1137–42. https://doi.org/10.15585/mmwr.mm6741a1
8. Wilson MR, Sample HA, Zorn KC, Arevalo S, Yu G, Neuhaus J, et al. Clinical metagenomic sequencing for diagnosis of meningitis and encephalitis. N Engl J Med. 2019;380:2327–40. https://doi.org/10.1056/NEJMoa1803396
9. Armstrong PM, Andreadis TG. Genetic relationships of Jamestown Canyon virus strains infecting mosquitoes collected in Connecticut. Am J Trop Med Hyg. 2007;77:1157–62. https://doi.org/10.4269/ajtmh.2007.77.1157
10. Kinsella CM, Paras ML, Smole S, Mehta S, Ganesh V, Chen LH, et al. Jamestown Canyon virus in Massachusetts: clinical case series and vector screening. Emerg Microbes Infect. 2020;9:903–12. https://doi.org/10.1080/22221751.2020.1756697
11. Solomon IH, Spera KM, Ryan SL, Helgager J, Andrici J, Zaki SR, et al. Fatal Powassan encephalitis (deer tick virus, lineage II) in a patient with fever and orchitis receiving rituximab. JAMA Neurol. 2018;75:746–50. https://doi.org/10.1001/jamaneurol.2018.0132
12. Levi ME, Quan D, Ho JT, Kleinschmidt-Demasters BK, Tyler KL, Grazia TJ. Impact of rituximab-associated B-cell defects on West Nile virus meningoencephalitis in solid organ transplant recipients. Clin Transplant. 2010;24:223–8. https://doi.org/10.1111/j.1399-0012.2009.01044.x
13. Yang Y, Qiu J, Snyder-Keller A, Wu Y, Sun S, Sui H, et al. Fatal Cache Valley virus meningoencephalitis associated with rituximab maintenance therapy. Am J Hematol. 2018;93:590–4. https://doi.org/10.1002/ajh.25024
14. Elliott RM. Orthobunyaviruses: recent genetic and structural insights. Nat Rev Microbiol. 2014;12:673–85. https://doi.org/10.1038/nrmicro3332
15. Garry CE, Garry RF. Proteomics computational analyses suggest that the antennavirus glycoprotein complex includes a class I viral fusion protein (α-penetrene) with an internal zinc-binding domain and a stable signal peptide. Viruses. 2019;11:E750. https://doi.org/10.3390/v11080750

Address for correspondence: Isaac H. Solomon, Department of Pathology, Brigham and Women's Hospital, 75 Francis St, Boston, MA 02115, USA; email: ihsolomon@bwh.harvard.edu

# Coronavirus Disease among Workers in Food Processing, Food Manufacturing, and Agriculture Workplaces

Michelle A. Waltenburg, Charles E. Rose, Tristan Victoroff, Marilee Butterfield, Jennifer A. Dillaha, Amy Heinzerling, Meagan Chuey, Maria Fierro, Rachel H. Jervis, Kristen M. Fedak, Andrea Leapley, Julie A. Gabel, Amanda Feldpausch, Eileen M. Dunne, Connie Austin, Caitlin S. Pedati, Farah S. Ahmed, Sheri Tubach, Charles Rhea, Julius Tonzel, Anna Krueger, David A. Crum, Johanna Vostok, Michael J. Moore, Hannah Kempher, Joni Scheftel, George Turabelidze, Derry Stover, Matthew Donahue, Deepam Thomas, Karen Edge, Bernadette Gutierrez, Erica Berl, Meagan McLafferty, Kelly E. Kline, Nichole Martz, James C. Rajotte, Ernest Julian, Abdoulaye Diedhiou, Rachel Radcliffe, Joshua L. Clayton, Dustin Ortbahn, Jason Cummins, Bree Barbeau, Stacy Carpenter, Julia C. Pringle, Julia Murphy, Brandy Darby, Nicholas R. Graff, Tia K.H. Dostal, Ian W. Pray, Courtney Tillman, Dale A. Rose, Margaret A. Honein; CDC COVID-19 Emergency Response Team

Author affiliations: Centers for Disease Control and Prevention, Atlanta, Georgia, USA (M.A. Waltenburg, C.E. Rose, T. Victoroff, M. Chuey, E.M. Dunne, M. Donahue, J.C. Pringle, I.W. Pray, D.A. Rose, M.A. Honein); Arizona Department of Health Services, Phoenix, Arizona, USA (M. Butterfield); Arkansas Department of Health, Little Rock, Arkansas, USA (J.A. Dillaha); California Department of Public Health, Richmond, California, USA (A. Heinzerling); County of San Diego Health and Human Services Agency, San Diego, California, USA (M. Chuey); Imperial County Public Health Department, El Centro, California, USA (M. Fierro); Colorado Department of Public Health and Environment, Denver, Colorado, USA (R.H. Jervis, K.M. Fedak); Florida Department of Health, Tallahassee, Florida, USA (A. Leapley); Georgia Department of Public Health, Atlanta (J.A. Gabel, A. Feldpausch); Idaho Department of Health and Welfare, Boise, Idaho, USA (E.M. Dunne); Illinois Department of Public Health, Springfield, Illinois, USA (C. Austin); Iowa Department of Public Health, Des Moines, Iowa, USA (C.S. Pedati); Kansas Department of Health and Environment, Topeka, Kansas, USA (F.S. Ahmed, S. Tubach); Kentucky Department for Public Health, Frankfort, Kentucky, USA (C. Rhea); Louisiana Department of Health, New Orleans, Louisiana, USA (J. Tonzel); Maine Center for Disease Control and Prevention, Augusta, Maine, USA (A. Krueger); Maryland Department of Health, Baltimore, Maryland, USA (D.A. Crum); Massachusetts Department of Public Health, Boston, Massachusetts, USA (J. Vostok, M.J. Moore); Minnesota Department of Health, St. Paul, Minnesota, USA (H. Kempher, J. Scheftel); Missouri Department of Health and Senior Services, Jefferson City, Missouri, USA (G. Turabelidze); Nebraska Department of Health and Human Services, Lincoln, Nebraska, USA (D. Stover, M. Donahue); New Jersey Department of Health, Trenton, New Jersey, USA (D. Thomas); New Mexico Department of Health, Santa Fe, New Mexico, USA (K. Edge, B. Gutierrez); North Carolina Department of Health and Human Services, Raleigh, North Carolina, USA (E. Berl); Oregon Health Authority, Portland, Oregon, USA (M. McLafferty); Pennsylvania Department of Health, Harrisburg, Pennsylvania, USA (K.E. Kline); Pennsylvania Department of Agriculture, Harrisburg (N. Martz); Rhode Island Department of Health, Providence, Rhode Island, USA (J.C. Rajotte, E. Julian); South Carolina Department of Health and Environmental Control, Columbia, South Carolina, USA (A. Diedhiou, R. Radcliffe); South Dakota Department of Health, Pierre, South Dakota, USA (J.L. Clayton, D. Ortbahn); Tennessee Department of Health, Nashville, Tennessee, USA (J. Cummins); Utah Department of Health, Salt Lake City, Utah, USA (B. Barbeau); Vermont Department of Public Health, Burlington, Vermont, USA (S. Carpenter, J.C. Pringle); Virginia Department of Health, Richmond, Virginia, USA (J. Murphy, B. Darby); Washington State Department of Health, Shoreline, Washington, USA (N.R. Graff, T.K.H. Dostal); Wisconsin Department of Health Services, Madison, Wisconsin, USA (I.W. Pray); Wyoming Department of Health, Cheyenne, Wyoming, USA (C. Tillman)

DOI: https://doi.org/10.3201/eid2701.203821

We describe coronavirus disease (COVID-19) among US food manufacturing and agriculture workers and provide updated information on meat and poultry processing workers. Among 742 food and agriculture workplaces in 30 states, 8,978 workers had confirmed COVID-19; 55 workers died. Racial and ethnic minority workers could be disproportionately affected by COVID-19.

High-density workplaces can cause high risk for transmission of severe acute respiratory syndrome coronavirus 2 (SARS-CoV-2), the virus that causes coronavirus disease (COVID-19) (*1*–*3*). US food processing, food manufacturing, and agriculture workplaces employ >3.6 million persons (*4*). Several factors contribute to workplace and community transmission, including prolonged close contact with coworkers, congregate housing, shared transportation, and frequent community contact among workers (*1*,*2*). Prior reports have characterized COVID-19 among meat and poultry processing workers (*1*,*2*).

**Table 1.** Laboratory-confirmed COVID-19 among workers in food manufacturing and agriculture workplaces in 30 US states, March 1–May 31, 2020*

| State† | Type of food manufactured or farmed | No. workplaces affected | No. workers in affected workplaces | Confirmed COVID-19 cases among workers, no. (%) | COVID-19–related deaths, no. (%) ‡ |
|---|---|---|---|---|---|
| Arkansas | Various | 14 | NA | 68 (–) | 1 (1.5) |
| California§ | Fruits, vegetables, dairy, packaged foods, frozen foods, seafood, other | 30 | NA | 518 (–) | 2 (0.4) |
| Colorado | Vegetables, dairy, baked goods, packaged foods, other | 19 | 5,773 | 443 (7.7) | 3 (0.7) |
| Florida | Vegetables, fruits, spices, other | 10 | NA | 280 (–) | 2 (0.7) |
| Georgia | Blueberry, seasonal fruits, other | 6 | 728 | 268 (36.8) | 0 |
| Idaho | Vegetables | 3 | 559 | 100 (17.9) | 0 |
| Illinois | Fruits, dairy, pizza, packaged foods, other | 61 | NA | 987 (–) | 6 (0.6) |
| Iowa | Eggs, dairy, other | 9 | 1870 | 391 (20.9) | 2 (0.5) |
| Kansas | Baked goods, fruits, dairy, seasonings, other | 13 | NA | 140 (–) | 0 |
| Kentucky | Baked goods, jelly, salad dressing, other | 8 | NA | 53 (–) | 1 (1.9) |
| Louisiana | Seafood, dairy | 5 | 607 | 264 (43.5) | 0 |
| Maine | Seafood | 1 | 65 | 15 (23.1) | 0 |
| Massachusetts | Seafood, baked goods, other | 173 | NA | 859 (–) | 4 (0.5) |
| Minnesota | Fruits, vegetables, baked goods, packaged foods, frozen foods, other | 36 | 9,829 | 434 (4.4) | 4 (0.9) |
| Missouri | Prepared foods, cereal, corn | 4 | 2,180 | 144 (6.6) | 1 (0.7) |
| Nebraska | Eggs, milk products, baked goods, frozen foods, other | 14 | 3,348 | 123 (3.7) | 0 |
| New Jersey | Produce | 3 | 515 | 93 (18.1) | 2 (2.2) |
| North Carolina¶ | Fruits, vegetables, packaged foods | 16 | NA | 302 (–) | 2 (0.7) |
| Oregon | Vegetables, fruits, frozen foods, packaged foods, other | 22 | 4,579 | 211 (4.6) | 3 (1.4) |
| Pennsylvania | Seafood, mushrooms, apples, cheese, eggs, other | 91 | NA | 968 (–) | 6 (0.6) |
| Rhode Island | Seafood, apples, cheese, eggs, other | 75 | NA | 346 (–) | 13 (3.8) |
| South Carolina | Vegetables, fruits, pasta, canned foods, frozen foods, other | 11 | NA | 22 (–) | 0 |
| South Dakota | Cheese | 1 | 200 | 7 (3.5) | 0 |
| Tennessee | Vegetables, fruits, other | 6 | NA | 323 (–) | 1 (0.3) |
| Utah | Cherries, dairy, baked goods, candy, other | 19 | NA | 186 (–) | 0 |
| Vermont | Cheese | 1 | 300 | 6 (2.0) | 0 |
| Virginia | Eggs | 1 | 50 | 4 (8.0) | 0 |
| Washington | Seafood, mushrooms, vegetables, fruits, pasta, frozen foods | 37 | NA | 755 (–) | 1 (0.1) |
| Wisconsin | Vegetables, dairy, pizza, baked goods, other | 52 | NA | 667 (–) | 1 (0.1) |
| Wyoming | Other | 1 | 6 | 1 (16.7) | 0 |
| Total | Various | 742 | 30,609# | 8,978 | 55 |

*COVID-19, coronavirus disease; NA, not available; –, percentage not calculated due to missing data.
†Arizona, Maryland, Montana, New Hampshire, New Mexico, and North Dakota reported no cases of COVID-19 among workers in food manufacturing and agriculture workplaces.
‡Percentage of deaths among cases.
§Data from 7 California counties.
¶Reported cases are among workers and close contacts of workers.
#Among 15 of 30 states that reported the number of workers in affected workplaces, 8.2% of 30,609 workers received COVID-19 diagnoses.

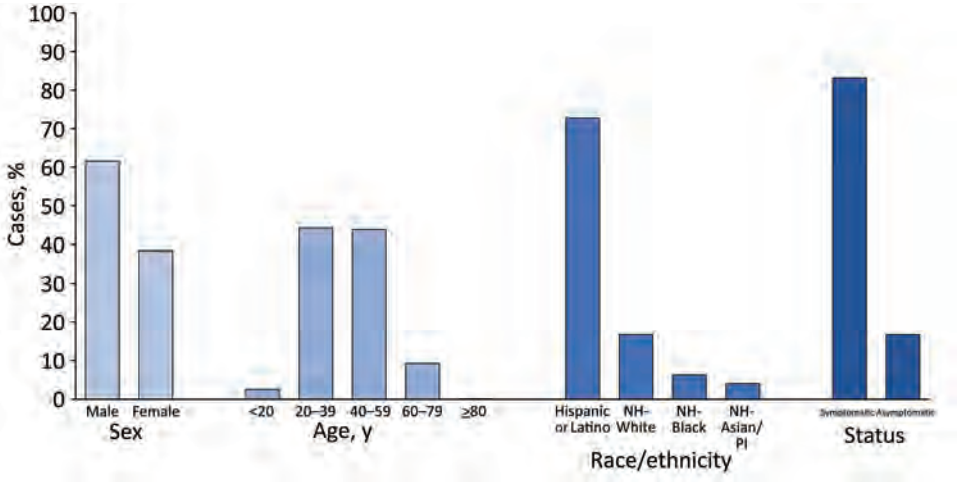


**Figure 1.** Characteristics of laboratory-confirmed COVID-19 cases among workers in food manufacturing and agriculture workplaces in 28 US states, March 1–May 31, 2020. The analytic dataset includes Arkansas, California, Florida, Georgia, Idaho, Illinois, Iowa, Kansas, Kentucky, Louisiana, Maine, Massachusetts, Minnesota, Missouri, Nebraska, New Jersey, Oregon, Pennsylvania, Rhode Island, South Carolina, South Dakota, Tennessee, Utah, Vermont, Virginia, Washington, Wisconsin, and Wyoming. Characteristics of workers with COVID-19 were not available for 2 states, Colorado and North Carolina. Arizona, Maryland, Montana, New Hampshire, New Mexico, and North Dakota reported no cases of COVID-19 among workers in food manufacturing and agriculture workplaces. The dataset excludes cases among workers for whom information was missing on sex (n = 1,331), age (n = 1,207), race/ethnicity (n = 3,257), and symptom status (n = 3,021). White, Black, and Asian/Pacific Islander workers were non-Hispanic; Hispanic or Latino workers could be of any race. Testing strategies and symptom categorization varied by facility. Symptom status was available for a single timepoint, either the time of testing or the time of interview. Column percentages might not equal 100% due to rounding. COVID-19, coronavirus disease; NH, non-Hispanic; PI, Pacific Islander.

We describe COVID-19 among workers in other US food manufacturing and agriculture workplaces and update information on COVID-19 among meat and poultry processing workers.

## The Study

The Centers for Disease Control and Prevention (CDC) collected cumulative aggregate data from state health departments on workers in US food processing, food manufacturing, and agriculture workplaces who had laboratory-confirmed COVID-19 (*5*). Requested data elements included the number and type of workplaces that reported ≥1 COVID-19 case among workers during March 1–May 31, 2020; the number of workers in affected workplaces; the number, demographics, and symptom status of workers with COVID-19; and the number of COVID-19–related deaths among workers. CDC requested the same information for meat and poultry processing workers and published preliminary data (*1*). Symptom data collection varied by workplace; clinical signs and symptom severity were not requested. None of these data had personal identifying information.

Workplaces were defined by the North American Industry Classification System codes 111 (Crop Production) and 311 (Food Manufacturing) (*6*). Demographic and symptom status proportions were calculated after excluding missing and unknown values. Data on sex were missing for 14.8% of food manufacturing and agriculture workers with COVID-19; on age for 13.4%; on symptom status for 33.6%; and on race and ethnicity for 36.3%. Because characteristics of total worker populations in affected workplaces were not available, we compared the racial and ethnic distribution of workers with COVID-19 to the distribution of all workers in the animal slaughtering and processing industry. CDC determined the investigation to be nonresearch as defined in 45 CFR 46.102(l); Paperwork Reduction Act was waived with respect to voluntary collection of information during a public health emergency (*7*).

Among 50 US states, 36 (72.0%) responded to the CDC inquiry; 33 (91.7%) reported ≥1 laboratory-confirmed COVID-19 case among food processing, food manufacturing, or agriculture workers during March 1–May 31, 2020. States reported 8,978 cases and 55 (0.6%) deaths among workers in 742 food manufacturing and agriculture workplaces in 30 states (Table 1). Among the 30 states reporting cases, the median number of affected facilities per state was 12 (interquartile range [IQR] 4–30 facilities); among 15 states that reported worker populations in affected workplaces, 8.2% of 30,609 workers received COVID-19 diagnoses. The percentage of workers with COVID-19 ranged from 2.0%–43.5% per state.

Of cases among food manufacturing and agriculture workers with information on sex (n = 7,647) and age (n = 7,771), 4,713 (61.6%) workers were male, 2,934 (38.4%) were female, and 3,439 (44.3%) workers were 20–39 years of age (Figure 1). Among 5,721 workers

**Table 2.** Laboratory-confirmed COVID-19 among workers in meat and poultry processing facilities in 31 US states, March 1–May 31, 2020*

| State† | Type of meat or poultry | No. workplaces affected | No. workers in affected workplaces | Confirmed COVID-19 cases among workers, no. (%) | COVID-19–related deaths, no. (%)‡ |
|---|---|---|---|---|---|
| Arizona | Beef | 1 | 1,750 | 162 (9.3) | 0 |
| Arkansas | Poultry | 49 | NA | 779 (–) | 10 (1.3) |
| California§ | Beef, lamb, pork, poultry, other | 11 | NA | 466 (–) | 2 (0.4) |
| Colorado | Beef, bison, lamb, poultry | 7 | 7,711 | 422 (5.5) | 9 (2.1) |
| Georgia | Poultry | 14 | 16,500 | 509 (3.1) | 1 (0.2) |
| Idaho | Beef | 2 | 797 | 72 (9.0) | 0 |
| Illinois | Beef, pork, poultry | 26 | NA | 1,029 (–) | 10 (1.0) |
| Iowa | Beef, pork, poultry | 26 | 22,170 | 6,131 (27.7) | 19 (0.3) |
| Kansas | Beef, pork, poultry | 10 | NA | 2,670 (–) | 8 (0.3) |
| Kentucky | Pork, poultry | 7 | 7,633 | 559 (7.3) | 4 (0.7) |
| Louisiana | Poultry | 2 | 1,430 | 51 (3.6) | 0 |
| Maine | Poultry | 1 | 411 | 50 (12.2) | 1 (2.0) |
| Maryland | Poultry | 2 | 2,036 | 208 (10.2) | 5 (2.4) |
| Massachusetts | Poultry, other | 33 | NA | 263 (–) | 0 |
| Minnesota | Beef, pork, poultry, other | 19 | 15,025 | 2,120 (14.1) | 2 (0.1) |
| Missouri | Beef, pork, poultry | 9 | 8,469 | 745 (8.8) | 2 (0.3) |
| Nebraska | Beef, pork, poultry | 23 | 26,134 | 3,438 (13.2) | 14 (0.4) |
| New Jersey | Beef | 1 | 500 | 33 (6.6) | 0 |
| New Mexico | Beef, pork, poultry | 2 | 550 | 24 (4.4) | 0 |
| North Carolina¶ | Pork, poultry | 28 | 32,325 | 2,491 (7.7) | 13 (0.5) |
| Oregon | Beef, pork, poultry, other | 7 | 1,945 | 60 (3.1) | 0 |
| Pennsylvania | Beef, pork, poultry, other | 30 | 15,548 | 1,169 (7.5) | 8 (0.7) |
| Rhode Island | Beef, pork, poultry, other | 6 | NA | 78 (–) | 0 |
| South Carolina | Beef, pork, poultry, other | 16 | NA | 97 (–) | 0 |
| South Dakota | Beef, pork, poultry | 4 | 6,500 | 1,593 (24.5) | 3 (0.2) |
| Tennessee | Pork, poultry, other | 7 | NA | 640 (–) | 2 (0.3) |
| Utah | Beef, pork, poultry | 4 | NA | 67 (–) | 1 (1.5) |
| Virginia | Pork, poultry, other | 14 | NA | 1,109 (–) | 10 (0.9) |
| Washington | Beef, poultry | 7 | 4,452 | 468 (10.5) | 4 (0.9) |
| Wisconsin | Beef, pork, veal | 14 | 14,125 | 860 (6.1) | 4 (0.5) |
| Wyoming# | Beef | 0 | NA | 1 (–) | 0 |
| Total | Beef, bison, lamb, pork, poultry, veal, other | 382 | 186,011** | 28,364 | 132 |

*Preliminary data published in Morbidity and Mortality Weekly Report (*1*); 8 additional states, Arkansas, California, Iowa, Louisiana, Minnesota, New Jersey, North Carolina, and Oregon, provided data that was not included in the prior assessment. COVID-19, coronavirus disease; NA, not available; –, percent not calculated due to missing data.
†Florida, Montana, New Hampshire, North Dakota, and Vermont reported no cases of COVID-19 among workers in meat and poultry processing facilities.
‡Percentage of deaths among cases.
§Data from 7 California counties.
¶Reported cases are among workers and close contacts of workers.
#One worker with COVID-19 worked at a meat processing facility in another state.
**Among 20 of 31 states reporting the number of workers in affected workplaces, 11.4% of 186,011 workers received COVID-19 diagnoses.

with race and ethnicity reported, 4,164 (72.8%) workers were Hispanic or Latino, 963 (16.8%) were non-Hispanic White, 362 (6.3%) were non-Hispanic Black, and 232 (4.1%) were non-Hispanic Asian/Pacific Islander. Overall, 83.2% of cases occurred among racial and ethnic minority workers. Symptom status was reported for 5,957 workers; 4,957 (83.2%) workers were symptomatic and 1,000 (16.8%) were asymptomatic or presymptomatic.

States reported 28,364 cases and 132 (0.5%) deaths among workers in 382 meat and poultry processing facilities in 31 states (Table 2). Demographic characteristics and symptom status of workers with COVID-19 indicated most were symptomatic and members of racial and ethnic minority groups (Figure 2).

## Conclusions

We describe COVID-19 among workers in US food processing, food manufacturing, and agriculture workplaces during March 1–May 31, 2020. Among all food manufacturing and agriculture workers in 28 states reporting race and ethnicity data, 36.5% of workers are Hispanic or Latino, 52.6% are non-Hispanic White, 5.9% are non-Hispanic Black, 3.5% are non-Hispanic Asian/Pacific Islander, and 1.5% are of other non-Hispanic race or ethnicity groups (*4*). However, among workers with COVID-19 for whom race or ethnicity data were reported, 72.8% were Hispanic or Latino, 6.3% were non-Hispanic Black, and 4.1% were non-Hispanic Asian/Pacific Islander, suggesting that Hispanic or Latino, non-Hispanic Black, and non-Hispanic Asian/Pacific Islander workers in these

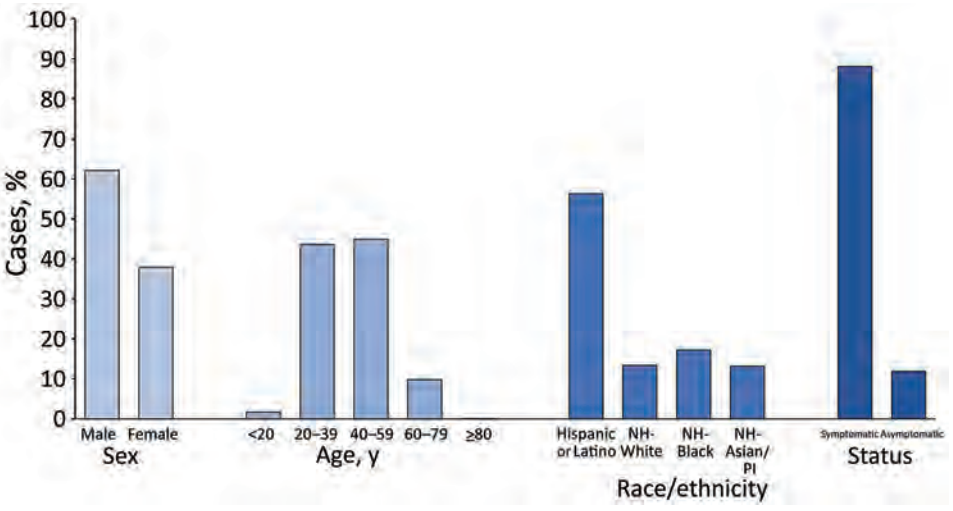


**Figure 2.** Characteristics of laboratory-confirmed COVID-19 cases among workers in meat and poultry processing facilities in 29 US states, March 1–May 31, 2020. Preliminary data were published in Morbidity and Mortality Weekly Report (*1*); 8 additional states, Arkansas, California, Iowa, Louisiana, Kansas, Minnesota, New Jersey, and Oregon provided data that was not included in the prior assessment. Characteristics of workers with COVID-19 were not available for 2 states, Colorado and North Carolina. Florida, Montana, New Hampshire, North Dakota, and Vermont reported no cases of COVID-19 among workers in meat and poultry processing facilities. The analytic dataset excludes cases among workers for whom information was missing on sex (n = 4,475), age (n = 6,695), race/ethnicity (n = 8,553), and symptom status (n = 8,437). White, Black, and Asian/Pacific Islander workers were non-Hispanic; Hispanic or Latino workers could be of any race. Testing strategies and symptom categorization varied by facility. Symptom status was available for a single timepoint, at the time of testing or at the time of interview. Column percentages might not equal 100% due to rounding. COVID-19, coronavirus disease; NH, non-Hispanic; PI, Pacific Islander.

workplaces might be disproportionately affected by COVID-19.

The sex, age, and symptom distribution of meat and poultry processing workers with COVID-19 was similar to that observed for food manufacturing and agriculture workers. The racial and ethnic distribution of meat and poultry processing workers with COVID-19 differed slightly; a higher percentage of cases were reported among non-Hispanic Black and non-Hispanic Asian/Pacific Islander workers.

Our study supports findings from prior reports that part of the disproportionate burden of COVID-19 among some racial and ethnic minority groups is likely related to occupational risk (*8*,*9*). These findings should be considered when implementing workplace interventions to ensure communication and training are culturally and linguistically tailored for each workforce.

Reports on mass testing in US meat and poultry processing facilities revealed widespread COVID-19 outbreaks and identified high proportions of asymptomatic or presymptomatic infections (*10*,*11*). Although most food manufacturing and agriculture workers (83.2%) and meat and poultry processing workers (88.1%) in our study reported symptoms, not all workplaces performed mass testing; therefore, workers with asymptomatic or presymptomatic infections might have been missed. These findings support the need for comprehensive testing strategies, coupled with contact tracing and symptom screening, for high-density critical infrastructure workplaces to aid in identifying infections and reducing transmission within the workplace (*12*).

Reducing workplace exposures is critical for protecting workers in US food processing, food manufacturing, and agriculture workplaces and might help reduce health disparities among disproportionately affected populations. Adherence to workplace-specific intervention and prevention efforts, including engineered controls, such as physical distancing; administrative controls, such as proper sanitation, cleaning, and disinfection; and providing personal protective equipment likely would protect both workers and surrounding communities (*13*,*14*).

This study has several limitations. First, only 36 states reported data; these results might not be representative of all US food processing, food manufacturing, and agriculture workers and workplaces. Second, testing strategies varied by workplace, influencing the number of cases detected and reported among workers. Workers might have been hesitant to report illness or seek healthcare, which could have led to underestimating cases among workers. Delays in linking cases and deaths to workplace outbreaks likely also contributed to an underestimation. Third, demographic characteristics of total worker populations in all affected workplaces were not available, limiting the ability to quantify the degree to which some racial and ethnic minority groups might be disproportionately affected by COVID-19. Fourth, preferred language,

English proficiency, and migration and immigration status of workers were not captured; culturally and linguistically appropriate public health monitoring and interventions are crucial considerations for this workforce. Finally, workers are members of their local communities; transmission of SARS-CoV-2 could have occurred both at the workplace and in the surrounding community and thus could be affected by levels of community transmission.

Comprehensive evaluations in food processing, food manufacturing, and agriculture workplaces and communities are needed to clarify and address risk factors for SARS-CoV-2 transmission among workers. The extent of control measures and timing of implementations should be evaluated to assess effectiveness of workplace interventions. Several factors at the individual-, household-, community-, and occupational-level, including long-standing health and social disparities, likely contribute to disproportionate disease incidence among racial and ethnic minority workers.

### Acknowledgments

We thank Logan Hudson, Ellie Morgan, Michelle Holshue, Alison Stargel, Alyssa Carlson, Laina Mitchell, Renee Canady, Tim Roth, Lea Hamner, Betsy Bertelsen, Anna Halloran, Sarah Murray, Zachary Doobovsky, Shawn Magee, Melissa Sixberry, Stephanie Kellner, Meredith Davis, Jonathan Richardson, Katrina Saphrey, Lisa Sollot, Julia Banks, Amal Patel, Betsy Schroeder, Alexander Neifert, Keith Amoroso, Lynn Bahta, Brooke Wiedinmyer, Mateo Frumholtz, Margaret Roddy, Paula Kriner, Jeff Lamoure, Linda Martinez, Karen Haught, Jessica Morales, Marifi Pulido, Lana O'Son, Alex U. Cox, and Jennifer Fuld for collating and collating epidemiologic data; Elyse Bevers and Jennifer Lam for data management support; Chas DeBolt and Laura Newman for conceptualization and consultation for Washington state; and Kristin Labar and Kate Fowlie for administrative support. We also thank the members of the CDC COVID-19 Emergency Response Team for their collaboration, including Michelle M. Dittrich, Gail Burns-Grant, Sooji Lee, Alisa Spieckerman, Kashif Iqbal, Sean M. Griffing, Alicia Lawson, Hugh M. Mainzer, Andreea E. Bealle, Erika Edding, Kathryn E. Arnold, Tomas Rodriquez, Sarah Merkle, Kristen Pettrone, Karen Schlanger, Alba E. Phippard, Kate Hendricks, Arielle Lasry, Vikram Krishnasamy, and Henry T. Walke.

T.K.H. Dostal is supported by the Applied Epidemiology Fellowship Program administered by the Council of State and Territorial Epidemiologists (CDC cooperative agreement no. 1NU38OT000297-01-00).

### About the Author

Dr. Waltenburg is an Epidemic Intelligence Service Officer in the Division of Foodborne, Waterborne, and Environmental Diseases, National Center for Emerging and Zoonotic Infectious Diseases, CDC. Her primary research interests include epidemiology of and outbreak response for zoonotic diseases of public health importance.

### References

1. Waltenburg MA, Victoroff T, Rose CE, Butterfield M, Jervis RH, Fedak KM, et al. COVID-19 Response Team. Update: COVID-19 among workers in meat and poultry processing facilities—United States, April–May 2020. MMWR Morb Mortal Wkly Rep. 2020;69:887–92. https://doi.org/10.15585/mmwr.mm6927e2
2. Dyal JW, Grant MP, Broadwater K, Bjork A, Waltenburg MA, Gibbins JD, et al. COVID-19 among workers in meat and poultry processing facilities—19 States, April 2020. MMWR MMWR Morb Mortal Wkly Rep. 2020;69:557–61. https://doi.org/10.15585/mmwr.mm6918e3
3. Baker MG, Peckham TK, Seixas NS. Estimating the burden of United States workers exposed to infection or disease: a key factor in containing risk of COVID-19 infection. PLoS One. 2020;15:e0232452. https://doi.org/10.1371/journal.pone.0232452
4. United States Census Bureau. 2014–2018 American community survey 5-year public use microdata samples (PUMS). 2018 [cited 2020 Jul 31]. https://www.census.gov/acs/www/data/data-tables-and-tools/data-profiles/2018
5. Council of State and Territorial Epidemiologists. Coronavirus Disease 2019 (COVID-19) 2020 interim case definition. 2020 Apr 5 [cited 2020 May 26]. https://wwwn.cdc.gov/nndss/conditions/coronavirus-disease-2019-covid-19/case-definition/2020
6. United States Census Bureau. North American industry classification system. 2017 [cited 2020 Jul 31]. https://www.census.gov/eos/www/naics
7. United States Department of Health and Human Services, Office of the Assistant Secretary for Planning and Evaluation. Notice of Paperwork Reduction Act waiver – coronavirus disease 2019 (COVID-19). 2020 Apr 28 [cited 2020 May 24]. https://aspe.hhs.gov/system/files/pdf/258866/CDC-PHE-PRA-Waiver-Notice-COVID-19-04-28-20.pdf
8. Hawkins D. Differential occupational risk for COVID-19 and other infection exposure according to race and ethnicity. Am J Ind Med. 2020;63:817–20. https://doi.org/10.1002/ajim.23145
9. Artiga S, Rae M. The COVID-19 outbreak and food production workers: who is at risk? 2020 Jun 3 Kaiser Family Foundation [cited 2020 Jul 31]. https://www.kff.org/coronavirus-covid-19/issue-brief/the-covid-19-outbreak-and-food-production-workers-who-is-at-risk
10. Crews J. Tyson confirms hundreds of COVID-19 cases at Missouri chicken plant. Meat + Poultry. 2020 Jun 29 [cited 2020 Jul 31]. https://www.meatpoultry.com/articles/23379-tyson-confirms-hundreds-of-covid-19-cases-at-missouri-chicken-plant
11. McCarthy R. Tyson announces more COVID-19 test results from Arkansas counties. Meat + Poultry. 2020 Jun 23 [cited 2020 Jul 31]. https://www.meatpoultry.com/articles/23340-tyson-announces-more-covid-19-test-results-from-arkansas-counties

12. Centers for Disease Control and Prevention. Testing strategy for coronavirus (COVID-19) in high-density critical infrastructure workplaces after a COVID-19 case is identified. 2020 Jun 13 [cited 2020 Jul 31]. https://www.cdc.gov/coronavirus/2019-ncov/community/worker-safety-support/hd-testing.html
13. Centers for Disease Control and Prevention. Meat and poultry processing workers and employers—interim guidance from CDC and the Occupational Safety and Health Administration (OSHA). 2020 Jul 9 [cited 2020 Aug 10]. https://www.cdc.gov/coronavirus/2019-ncov/community/organizations/meat-poultry-processing-workers-employers.html
14. Centers for Disease Control and Prevention. Agriculture workers and employers—interim guidance from CDC and the U.S. Department of Labor. 2020 Jun 11 [cited 2020 Aug 10]. https://www.cdc.gov/coronavirus/2019-ncov/community/guidance-agricultural-workers.html

Address for correspondence: Michelle Waltenburg, Centers for Disease Control and Prevention, 1600 Clifton Rd NE, Mailstop H24-10, Atlanta, GA 30329-4027, USA; email: nvr6@cdc.gov

# etymologia

## Petri Dish [pe′tre ′dish]

Monika Mahajan

The Petri dish is named after the German inventor and bacteriologist Julius Richard Petri (1852–1921). In 1887, as an assistant to fellow German physician and pioneering microbiologist Robert Koch (1843–1910), Petri published a paper titled "A minor modification of the plating technique of Koch." This seemingly modest improvement (a slightly larger glass lid), Petri explained, reduced contamination from airborne germs in comparison with Koch's bell jar.

Similar alterations had been suggested earlier by Slavonian researcher Emanuel Klein (1844–1925), who was working in England and described a nearly identical dish in his 1885 book Micro-organisms. An 1886 research paper published by Percy Frankland (1858–1946) in the Proceedings of the Royal Society portrayed a comparable shallow, circular, and covered dish. Available historical complications accord credit of discovery of the Petri dish to other bacteriologists.

Top left: Julius Richard Petri, inventor of the Petri dish, ≈1888. Unknown photographer, from file Gruppenaufnahme von Bakteriologischen Kursen im RKI um 1888-A.jpg, Public Domain, https://commons.wikimedia.org/w/index.php?curid=31684326. Top right: Robert Koch, unknown photographer, from the National Institutes of Health, US Department of Health and Human Services. Bottom: Petri dish showing *Bacillus anthracis* bacterial colonies grown on sheep's blood agar for 24 hours. Photograph Centers for Disease Control and Prevention/ Megan Mathias and J. Todd Parker, 2009.

### Sources

1. Central Sheet for Bacteriology and Parasite Science [in German]. Biodiversity Heritage Library. Volume 1, 1887 [cited 2020 Aug 25]. https://www.biodiversitylibrary.org/item/210666#page/313/mode/1up
2. Petri JR. A minor modification of the plating technique of Koch [in German]. Cent für Bacteriol und Parasitenkd. 1887;1:279–80.
3. Shama G. The "Petri" dish: a case of simultaneous invention in bacteriology. Endeavour. 2019;43:11–6. https://doi.org/10.1016/j.endeavour.2019.04.001
4. The big story: the Petri dish. The Biomedical Scientist. Institute of Biomedical Science [cited 2020 Aug 25]. https://thebiomedicalscientist.net/science/big-story-petri-dish

Author affiliation: Post Graduate Institute of Medical Education and Research, Chandigarh, India

Address for correspondence: Monika Mahajan, Department of Medical Microbiology, Post Graduate Institute of Medical Education and Research, Research Block A, Sector 12, Chandigarh 160012, India; email: monideepmj@yahoo.com

DOI: https://doi.org/10.3201/eid2701.ET2701

# Large-Scale Testing of Asymptomatic Healthcare Personnel for Severe Acute Respiratory Syndrome Coronavirus 2

Catherine A. Hogan, Saurabh Gombar, Hannah Wang, Katharina Röltgen, Run-Zhang Shi, Marisa Holubar, Sang-ick Chang, Grace M. Lee, Scott D. Boyd, James Zehnder, Benjamin A. Pinsky

Large-scale, 1-time testing of >12,000 asymptomatic healthcare personnel in California, USA, during April–June 2020 showed that prevalence of severe acute respiratory syndrome coronavirus 2 was low (<1%). Testing might identify asymptomatic and presymptomatic persons, including some with high viral burden, enabling prompt implementation of measures to limit nosocomial spread.

Healthcare personnel (HCP) represent a unique group of concern for transmission of severe acute respiratory syndrome coronavirus 2 (SARS-CoV-2), the causative agent of coronavirus disease (COVID-19), because of their increased exposure risk from infected patients under their care and risk for onward transmission to patients and coworkers. The current evidence on the large-scale testing of HCP has focused on symptomatic persons (*1*). However, the potential for asymptomatic transmission of SARS-CoV-2 is well-recognized (*2*–*4*), and presymptomatic HCP might contribute to nosocomial outbreaks (*5*).

Testing HCP before symptom onset represents an opportunity for early detection of infectious persons. In this study, we assessed the prevalence of SARS-CoV-2 infection through mass real-time reverse transcription PCR (rRT-PCR) and IgG testing of asymptomatic HCP and describe the clinical and laboratory characteristics of infected persons.

Author affiliations: Stanford University School of Medicine, Stanford, California, USA (C.A. Hogan, S. Gombar, H. Wang, K. Röltgen, R.-Z. Shi, M. Holubar, S.-i. Chang, G.M. Lee, S.D. Boyd, J. Zehnder, B.A. Pinsky); Stanford Health Care, Stanford (C.A. Hogan, B.A. Pinsky)

DOI: https://doi.org/10.3201/eid2701.203892

## The Study

This study was approved by the Stanford Privacy Office, and individual consent was waived. Stanford Medicine, which comprises Stanford Health Care (SHC), Stanford Children's Health, and Stanford School of Medicine, is located in the San Francisco Bay area, California, USA, and is staffed by >26,000 HCP. We performed a SARS-CoV-2 testing study of asymptomatic HCP during April 20–June 8, 2020. Both patient-facing and non–patient-facing SHC HCP were invited for testing on a voluntary basis through messaging across all hospital departments to encourage a safe working environment. All HCP were eligible for testing, and risk-based eligibility criteria were not enforced.

rRT-PCR of nasopharyngeal swab samples was performed by using the SHC envelope gene laboratory-developed test and a commercial assay (Panther Fusion SARS-CoV-2; Hologic Inc., https://www.hologic.com), as described (*6*). The distribution of cycle threshold ($C_t$) values of positive results with these assays ranged from 10 to 45. Plasma IgG testing was also performed by using a SHC laboratory-developed ELISA specific for the spike glycoprotein receptor-binding domain antigen (Appendix, https://wwwnc.cdc.gov/EID/article/27/1/20-3892-App1.pdf).

Demographic data were extracted from an institutional database for the entire cohort, and chart review for persons with positive SARS-CoV-2 rRT-PCR results was performed by using electronic medical records. We excluded from the study persons with a positive rRT-PCR result and an illness consistent with COVID-19 in the preceding 6 weeks. Only the first rRT-PCR result per person was included for the main analysis. Repeat rRT-PCR or IgG serologic

analysis within 2 weeks was recommended to each HCP who had an initial positive rRT-PCR result. HCP were classified as asymptomatic or presymptomatic on the basis of symptoms developing consistent with COVID-19 within 2 weeks after testing.

Statistical analysis was performed by using Stata version 15.1 (https://www.stata.com) and the $\chi^2$ test or Fisher exact test for categorical variables with ≤5 datapoints/cell and the Mann-Whitney U test for continuous variables. Results were interpreted as significant according to a p value <0.05.

After excluding 12 persons who had a positive rRT-PCR result and earlier illness consistent with COVID-19, we included 12,418 asymptomatic HCP in the study (Figure 1). Of these persons, 8,775 (70.7%) were female, and median age was 39.5 years (interquartile range [IQR] 32.4–50.3 years). The SARS-CoV-2 rRT-PCR positivity rate was 26/12,418 (0.2%; 95% CI 0.1%–0.3%), and IgG seropositivity rate was 111/12,373 (0.9%; 95% CI 0.7–1.1). IgG serologic results were not available for 45 persons from the part of the study population for whom only nasopharyngeal rRT-PCR was performed.

Of the 26 persons who had positive rRT-PCR results, 20 remained asymptomatic; for the

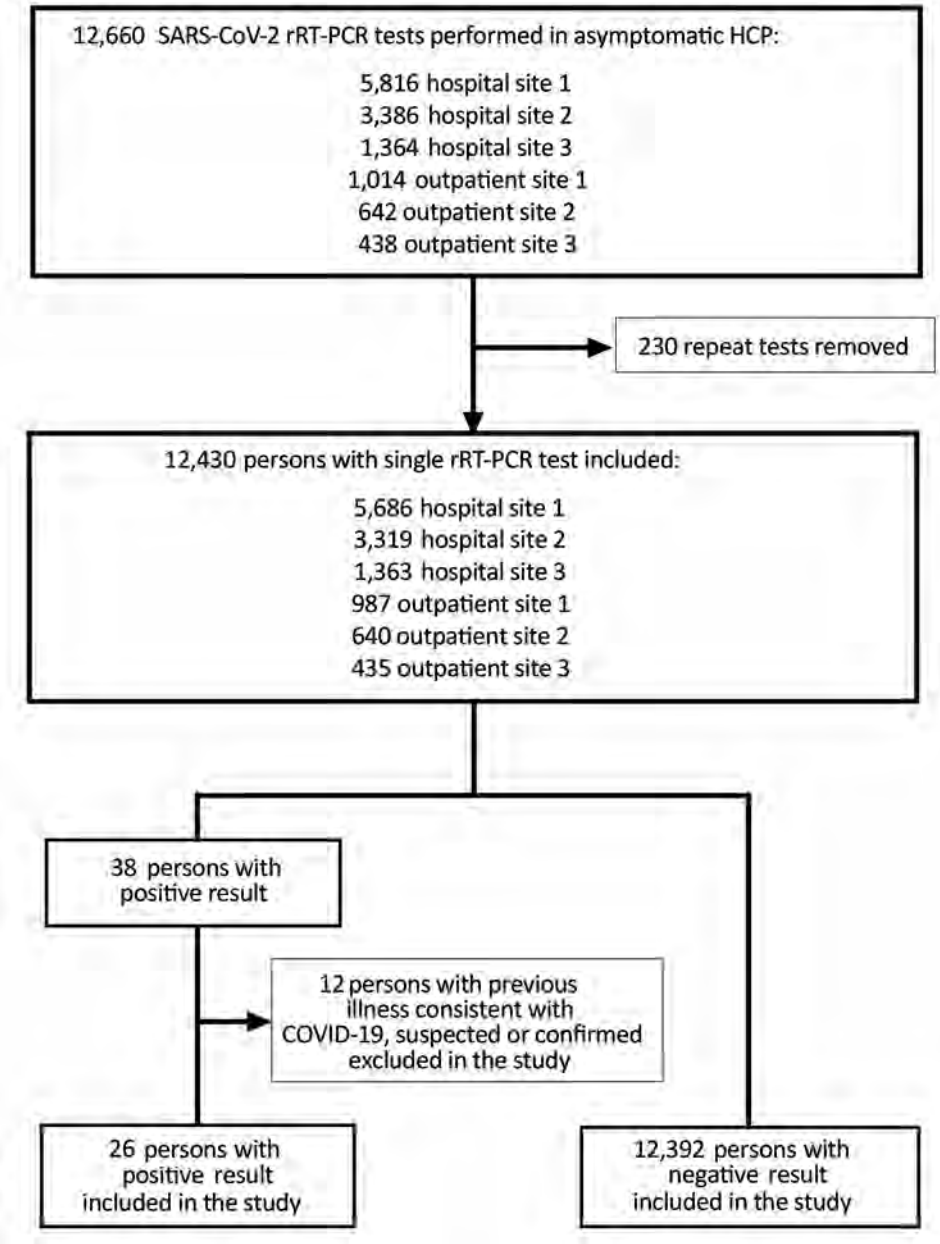


**Figure 1.** Flowchart for study of large-scale testing of asymptomatic healthcare personnel for SARS-CoV-2, California, USA, April–June 2020. COVID-19, coronavirus disease; HCP, healthcare personnel; rRT-PCR, real-time reverse transcription PCR; SARS-CoV-2, severe acute respiratory syndrome coronavirus 2.

**Table.** Clinical and laboratory characteristics for 26 healthcare personnel who had positive initial results by rRT-PCR for severe acute respiratory syndrome coronavirus 2, California, USA, April–June 2020*

| Characteristic | Overall, n = 26 | Asymptomatic, n = 20 | Presymptomatic, n = 6 | Unadjusted p-value† |
|---|---|---|---|---|
| Median age, y (IQR) | 39.5 (31–46) | 41 (32.5–47) | 32.5 (30–40) | 0.3 |
| Sex | | | | |
| M | 7 (26.9) | 7 (35.0) | 0 | 0.1 |
| F | 19 (73.1) | 13 (65.0) | 6 (100) | |
| Occupation | | | | |
| Nurse | 8 (30.8) | 6 (30.0) | 2 (33.3) | 1 |
| Physician | 4 (15.4) | 2 (10.0) | 2 (33.3) | 0.3 |
| Other, direct patient facing | 6 (23.1) | 5 (25.0) | 1 (16.7) | 1 |
| Other, nondirect patient facing | 6 (23.1) | 5 (25.0) | 1 (16.7) | 1 |
| Unknown | 2 (7.7) | 2 (10.0) | 0 | NT |
| Suspected exposure‡ | | | | |
| Yes | 4 (15.4) | 2 (10.0) | 2 (33.3) | 0.2 |
| No | 17 (65.4) | 13 (65.0) | 4 (66.7) | |
| Unknown | 5 (19.2) | 5 (25.0) | 0 | |
| Concurrent conditions | | | | |
| Yes | 7 (26.9) | 5 (25.0) | 2 (33.3) | 1 |
| No | 18 (69.2) | 14 (70.0) | 4 (66.7) | |
| Unknown | 1 (3.9) | 1 (5.0) | 0 | |
| Median days from NP testing to symptom onset (IQR) | NA | NA | 3 (1–9) | NT |
| Signs/symptoms | | | | |
| Fever (self-reported or objective) | NA | NA | 1 (16.7) | NT |
| Sweats | NA | NA | 1 (16.7) | |
| Cough | NA | NA | 5 (83.3) | |
| Shortness of breath | NA | NA | 1 (16.7) | |
| Sore throat | NA | NA | 3 (50.0) | |
| Rhinorrhea | NA | NA | 2 (33.3) | |
| Malaise/fatigue | NA | NA | 4 (66.7) | |
| Myalgia | NA | NA | 1 (16.7) | |
| Headache | NA | NA | 2 (33.3) | |
| Gastrointestinal | NA | NA | 2 (33.3) | |
| Unknown | 2 (7.4) | 2 (9.5) | 0 | |
| NP $C_t$ | | | | |
| 20–25 | 1 (3.9) | 1 (5.0) | 0 | 0.2 |
| >25–35 | 3 (11.5) | 1 (5.0) | 2 (33.3) | |
| >35–45 | 22 (84.6) | 18 (90.0) | 4 (66.7) | |
| Median NP $C_t$ (IQR) | 38.1 (37.8–38.4) | 38.1 (37.9–38.4) | 38.1 (29.5–38.3) | 0.8 |
| Plasma IgG | | | | |
| Positive | 6 (23.1) | 6 (30.0) | 0 | 0.3 |
| Negative | 20 (76.9) | 14 (70.0) | 6 (100) | |
| Repeat rRT-PCR within 30 d, first test result | | | | |
| Positive | 4 (15.4) | 2 (10.0) | 2 (33.3) | 0.3 |
| Negative | 19 (73.1) | 15 (75.0) | 4 (66.7) | |
| Not performed | 3 (11.5) | 3 (15.0) | 0 | |
| Repeat IgG within 30 d, first test result | | | | |
| Positive | 2 (7.7) | 2 (10.0) | 0 | 1 |
| Negative | 16 (61.5) | 12 (60.0) | 4 (66.7) | |
| Not performed | 8 (30.8) | 6 (30.0) | 2 (33.3) | |

*Values are no. (%) unless indicated otherwise. $C_t$, cycle threshold; IQR, interquartile range; NA, not applicable; NP, nasopharyngeal; NT, not tested; rRT-PCR, real-time reverse transcription PCR.
†By $\chi^2$ test, Fisher exact test, or Mann-Whitney U test.
‡Exposure known or suspected occurring in the community or hospital setting.

remaining 6, COVID-19 subsequently developed within a median of 3 days (IQR 1–9 days) (Table; Figure 2). None of the persons who had positive rRT-PCR results were hospitalized. Of the 20 persons who remained asymptomatic, 6 were IgG positive at the time of their positive rRT-PCR result (median $C_t$ 38.1 [IQR 36.7–38.1]), and 2 of the 15 persons retested with the IgG test seroconverted 12 days later ($C_t$ 20.8 and 38.0).

On the basis of the assumption that these 14 persons (6 presymptomatic and 8 asymptomatic who had early or delayed positive IgG results) had true positive results, the clinical specificity of the test was estimated to be 12,392 (99.9%) of 12,404 (Appendix Table). The overall median $C_t$ was 38.1 (IQR 37.8–38.4) and overlapped between asymptomatic and presymptomatic persons (Appendix Figure). One asymptomatic HCP had a $C_t$ value of 20.8, consistent with high viral load.

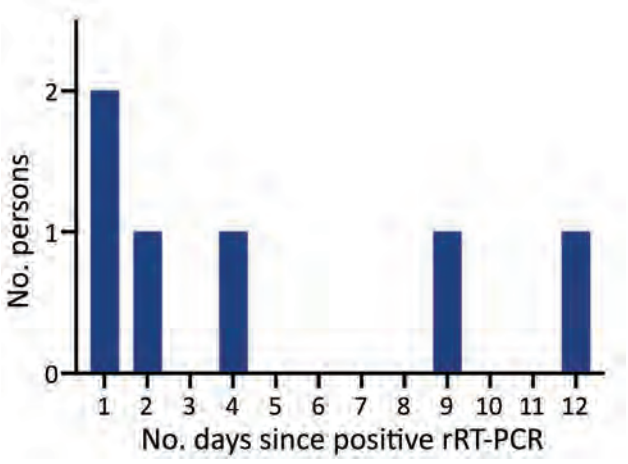


**Figure 2.** Timing of symptom onset in presymptomatic persons for study of large-scale testing of asymptomatic healthcare personnel for severe acute respiratory syndrome coronavirus 2, California, USA, April–June 2020. rRT-PCR, real-time reverse transcription PCR.

## Conclusions

In this cohort of >12,000 asymptomatic HCP from an area that had low COVID-19 in-hospital and community burden at the time of the study, the prevalence of SARS-CoV-2 was low (<1%) by rRT-PCR and IgG serologic analysis. The combined rRT-PCR positivity rate for symptomatic and asymptomatic persons tested during the same period in Santa Clara County was 3.2%, and the county-level proportion of hospitalizations due to COVID-19 was also 3.2% (*7*). Other smaller asymptomatic HCP studies have demonstrated positive rRT-PCR prevalence ranging from 1% to 7% (*3*; E.S. Barrett et al., unpub. data). In addition, point-of-care IgG positivity estimates for asymptomatic persons in studies from Santa Clara and Los Angeles Counties ranged from 1% to 5% (*8*; E. Bendavid et al., unpub. data).

There are limitations in comparability given that rRT-PCR positivity indicates active infection and potentially contagious persons, whereas IgG positivity might indicate past or active infection. However, the findings in the current study suggest that, in low-prevalence settings, HCP SARS-CoV-2 transmission risk might be driven mostly by community exposure, given the limited evidence of nosocomial transmission. In this study, there was no apparent cluster of transmission events from HCP with positive rRT-PCR results. Nonetheless, given that most persons infected with SARS-CoV-2 in this cohort were involved in direct patient care, mass testing that focuses on these persons, as well as implementation in settings lacking personal protective equipment or with a high burden of infection, might show a higher yield (E.S. Barrett et al., unpub. data).

In this study, 1 asymptomatic person was identified who showed high nasopharyngeal viral load, and 6 persons were given a diagnosis before the onset of symptoms. Despite their low frequency, these persons are examples of key groups to identify given the higher likelihood of onward transmission with high viral loads. This study confirmed the overlap in SARS-CoV-2 RNA levels between asymptomatic and presymptomatic HCP, supporting the need for testing both groups to prevent transmission (*9*).

There is increasing evidence from congregate settings that relying on the presence of symptoms to initiate testing is insufficient (*2*,*4*). As laboratory capacity increases, asymptomatic mass testing programs might facilitate earlier and more accurate case detection and help maintain workforce readiness, especially in high-prevalence settings (*10*). This testing approach was strengthened by its large scale and comprehensiveness, including tests for viral RNA and SARS-CoV-2 antibodies. Such HCP testing might help build public confidence in the safety of the hospital environment and thus limit delays in care for persons who have non–COVID-19 illnesses.

However, there are limitations to this approach. Previous symptoms were assessed by self-report, which might result in bias. In addition, although the rRT-PCR–positive results in this study could not all be confirmed as true positive results, the estimated clinical specificity of rRT-PCR was 99.9%. Finally, this approach necessitates adequate infrastructure to support intensive clinical triaging, testing, and follow-up. Sample pooling might increase testing throughput, lower cost, and enable SARS-CoV-2 detection in persons who have high viral load and represent a priority group to prevent transmission.

In summary, large-scale testing of HCP might identify asymptomatic and presymptomatic persons, including some with high viral burden. Early detection might enable prompt implementation of infection control measures to limit nosocomial spread.

### Acknowledgments

We thank the members of the Stanford Clinical Virology and Special Chemistry Laboratories for their contributions to testing, and members of the Stanford Occupational Health Center for their work in planning and coordinating this testing effort.

## About the Author

Dr. Hogan is an infectious diseases physician and medical microbiologist at Stanford University School, Palo Alto, CA, and currently a visiting instructor in the Department

of Pathology at Stanford University. Her research interests include novel and point-of-care diagnostics, clinical impact of diagnostic methods, and global health.

## References


1. Kluytmans-van den Bergh MF, Buiting AG, Pas SD, Bentvelsen RG, van den Bijllaardt W, van Oudheusden AJ, et al. Prevalence and clinical presentation of health care workers with symptoms of coronavirus disease 2019 in 2 Dutch hospitals during an early phase of the pandemic. JAMA Netw Open. 2020;3:e209673. https://doi.org/10.1001/jamanetworkopen.2020.9673
2. Arons MM, Hatfield KM, Reddy SC, Kimball A, James A, Jacobs JR, et al.; Public Health–Seattle and King County and CDC COVID-19 Investigation Team. Presymptomatic SARS-CoV-2 infections and transmission in a skilled nursing facility. N Engl J Med. 2020;382:2081–90. https://doi.org/10.1056/NEJMoa2008457
3. Treibel TA, Manisty C, Burton M, McKnight Á, Lambourne J, Augusto JB, et al. COVID-19: PCR screening of asymptomatic health-care workers at London hospital. Lancet. 2020;395:1608–10. https://doi.org/10.1016/S0140-6736(20)31100-4
4. Rivett L, Sridhar S, Sparkes D, Routledge M, Jones NK, Forrest S, et al.; CITIID-NIHR COVID-19 BioResource Collaboration. Screening of healthcare workers for SARS-CoV-2 highlights the role of asymptomatic carriage in COVID-19 transmission. eLife. 2020;9:9. https://doi.org/10.7554/eLife.58728
5. Kimball A, Hatfield KM, Arons M, James A, Taylor J, Spicer K, et al.; Public Health—Seattle & King County; CDC COVID-19 Investigation Team. Asymptomatic and presymptomatic SARS-CoV-2 infections in residents of a long-term care skilled nursing facility—King County, Washington, March 2020. MMWR Morb Mortal Wkly Rep. 2020;69:377–81. https://doi.org/10.15585/mmwr.mm6913e1
6. Hogan CA, Sahoo MK, Huang C, Garamani N, Stevens B, Zehnder J, et al. Comparison of the panther fusion and a laboratory-developed test targeting the envelope gene for detection of SARS-CoV-2. J Clin Virol. 2020;127:104383. https://doi.org/10.1016/j.jcv.2020.104383
7. County of Santa Clara. Open data portal; COVID-19. 2020 [cited 2020 Aug 23] https://data.sccgov.org/browse?category=COVID-19
8. Sood N, Simon P, Ebner P, Eichner D, Reynolds J, Bendavid E, et al. Seroprevalence of SARS-CoV-2-specific antibodies among adults in Los Angeles County, California, April 10–11, 2020. JAMA. 2020;323:2425–7. https://doi.org/10.1001/jama.2020.8279
9. Lee S, Kim T, Lee E, Lee C, Kim H, Rhee H, et al. Clinical course and molecular viral shedding among asymptomatic and symptomatic patients with SARS-CoV-2 infection in a community treatment center in the Republic of Korea. JAMA Intern Med. 2020 Aug 6 [Epub ahead of print]. https://doi.org/10.1001/jamainternmed.2020.3862
10. Black JR, Bailey C, Przewrocka J, Dijkstra KK, Swanton C. COVID-19: the case for health-care worker screening to prevent hospital transmission. Lancet. 2020;395:1418–20. https://doi.org/10.1016/S0140-6736(20)30917-X


Address for correspondence: Benjamin A. Pinsky, Stanford University School of Medicine, 3375 Hillview, Rm 2913, Palo Alto, CA 94304, USA; email: bpinsky@stanford.edu

# Economic Burden of Legionnaires' Disease, United States, 2014

Madeleine Baker-Goering, Kakoli Roy, Chris Edens, Sarah Collier

Through the use of published estimates of medical costs and new calculations of productivity losses, we estimate the lifetime economic burden of 2014 Legionnaires' disease cases in the United States at ≈$835 million. This total includes $21 million in productivity losses caused by absenteeism and $412 million in productivity losses caused by premature deaths.

Legionnaires' disease is a severe form of pneumonia that often results in hospitalization (*1*). The disease is caused by the *Legionella* bacteria, which can grow and spread in poorly maintained manmade water systems and can then be inhaled in aerosolized water droplets. In the United States, reported cases of Legionnaires' disease have been increasing since 2000, yet evidence suggests that many outbreaks are related to failures in building water system maintenance and might be preventable (*2*). Estimates of costs associated with Legionnaires' disease could help inform prevention efforts.

A recent estimate of the direct medical costs imposed by domestically acquired Legionnaires' disease in 2014 included $402 million in costs incurred as a result of hospitalizations and emergency department (ED) visits (*1*). Previous studies have not estimated productivity losses caused by Legionnaires' disease.

We estimate productivity losses caused by absenteeism and premature deaths. These amounts, when combined with existing estimates of medical costs, provide a more comprehensive estimate of the lifetime economic impact of Legionnaires' disease in the United States for 2014.

## The Study

The analysis estimates the lifetime cost of illness of 2014 Legionnaires' disease cases in the United States by including direct medical costs and indirect costs, measured in terms of productivity losses caused by absenteeism and premature deaths. Intangible costs (e.g., pain and suffering) are not included. The estimate draws on secondary data from published, peer-reviewed literature and surveillance data (Table 1). All costs are reported in 2014 US dollars.

The estimates (and range) of the incidence, healthcare utilization, and medical costs of Legionnaires' disease for 2014 were drawn from published sources (*1*). We used estimates of waterborne and domestically acquired cases, hospitalizations, and deaths. We assumed all Legionnaires' disease deaths occurred in hospitalized patients and estimated the associated costs, which comprise medical expenses and productivity losses caused by premature death. The costs associated with nonfatal hospitalized patients included medical expenses and productivity losses caused by workdays lost because of hospitalization and the subsequent recovery period.

The human capital approach, frequently used in cost-of-illness analysis, was used to value productivity losses (i.e., costs of time lost from productive activities) caused by illness and premature death (*7*). Productivity loss for nonfatal cases requiring hospitalization was estimated as the product of workdays lost per case and the average daily wage rate, among the cases occurring in the working-age population (Table 1). We valued lost workdays by using an average hourly wage rate of $22.71 for 2014 and doubled that rate to account for benefits and overhead (*4*). We assumed that 60% of nonfatal cases requiring hospitalization occurred among working-age persons, on the basis of the age distribution of case-patients from the Centers for Disease Control and Prevention's Active Bacterial Core surveillance program (ABCs) during 2011–2015 (*3*). We calculated the range by using the 5th and 95th credible interval of cases (*1*) and the low and high range for workdays lost.

Productivity losses caused by premature death were calculated by using age-specific estimates of future lifetime earnings, which included market earnings and the value of household services (*5*). Estimates of earnings were discounted at 3% to account for losses

Author affiliation: Centers for Disease Control and Prevention, Atlanta, Georgia, USA

DOI: https://doi.org/10.3201/eid2701.191198

**Table 1.** Inputs used to estimate economic burden of Legionnaires' disease, United States, 2014*

| Input | Value (range) | Source |
|---|---|---|
| Cases of Legionnaires' diseases, no. | 11,000 (7,430–13,300) | Collier et al. (*1*), Table 1, domestically acquired waterborne cases |
| Hospitalizations, no. | 10,800 (7,280–13,100) | Collier et al. (*1*), Table 2, domestically acquired waterborne cases requiring hospitalization |
| Workdays lost per hospitalization. no. | 10 (8–12) | ABCs 2011–2015 (*3*), length of stay (6 d), plus assumed additional prior to hospitalization and for recovery (4 d), minus weekend (2 d). Range assumed. |
| Proportion of hospitalized cases occurring among working-age patients, % | 60 | ABCs 2011–2015 (*3*) |
| Loss per day because of absenteeism, USD | $363 | National Occupational Employment and Wage Estimates, Bureau of Labor Statistics hourly earnings for all occupations, 2014 (*4*) |
| Deaths, no. | 995 (655–1,310) | Collier et al. (*1*), Table 2, fatal, domestically acquired, waterborne cases |
| Value per premature death (weighed average), USD | $413,727 | Grosse et al. (*5*),† updated to 2014 USD by using employment cost index (*6*) |

*ABCs, Active Bacterial Core surveillance; USD, 2014 US dollars.
†We used the estimates of the present value of lifetime production, which were discounted at 3%.

incurred in future years. Earnings were updated to 2014 dollars according to the Bureau of Labor Statistics' employment cost index (*6*). We calculated the proportion of deaths by age category on the basis of data from ABCs during 2011–2015 (*3*). Deaths with no age reported were valued at the lowest estimates (i.e., equivalent to a death of a person ≥80 years of age). We calculated the range by using the 5th and 95th credible interval of deaths (*1*).

Table 2 shows the lifetime costs associated with Legionnaires' disease. An estimated 5,183/8,639 nonfatal cases in hospitalized working-age patients resulted in ≈59,540 workdays lost and $21.3 million in productivity losses. In addition, the 995 premature deaths caused by Legionnaires' disease resulted in an estimated $412 million in productivity losses. Collier et al. (*1*) estimated approximately $402 million in medical expenses incurred as a result of hospitalizations ($401.0 million) and ED visits ($0.5 million). The estimated total lifetime cost of illness associated with an estimated 11,000 domestically acquired cases of Legionnaires' disease in 2014 is $835 million (range $362 million–$2.263 billion).

These estimates depend directly on the rate and age distribution of fatalities. Although half of fatal cases occurred in persons ≥65 years of age, 74% of the total productivity losses caused by premature deaths were for patients <65 years of age, because future lifetime earnings decrease with age. Also, age was not reported in ABCs for 13% of fatal cases, and productivity losses for estimated fatal cases were valued conservatively (i.e., equivalent to a death occurring in a person ≥80 years of age). Productivity losses caused by premature deaths might be greater if these deaths occurred among younger persons.

## Conclusions

Productivity losses caused by Legionnaires' disease account for just more than half of its lifetime economic burden, almost all of which (95%) is caused by productivity losses from premature deaths. The human capital approach used in this analysis provides a conservative estimate of the disease's indirect costs because it only accounts for productivity losses in its cost estimate of lost workdays and premature deaths. An alternative approach is to estimate the indirect costs of illness and death in terms of societal value or willingness to pay for averting them. This approach would also include such intangible costs as pain and suffering. For illustration, calculated at a constant value of $9.3 million/death, the economic value of the 995 deaths from Legionnaires' disease cases in 2014 would be $9.3 billion (*8*). This approach is most commonly used in cost-benefit analyses to consider tradeoffs between the societal benefits of a policy,

**Table 2.** Economic burden of Legionnaires' disease, United States, 2014

| Type of cost | Estimate (range) |
|---|---|
| Medical costs (1) for estimate and range | $402 million ($80–$1,690 million) |
| Productivity losses from workdays lost* | $21,634,454 ($11–$31 million) |
| Productivity losses from premature deaths | $411,658,786 ($271–$542 million) |
| Total economic burden | $835,035,255 ($362–$2,263 million) |

*Productivity losses from workdays lost were calculated among nonfatal cases requiring hospitalization (10,800 patients – 995 deaths = 9,805 nonfatal cases requiring hospitalization), of which 60% are assumed to be among working-age persons (5,883). Each hospitalized patient is assumed to lose 10 workdays because of hospitalization (5883 × 10 = 58,830 workdays lost); each workday is valued at $363.36.

including the value society places on fewer deaths, and the costs of implementing a policy.

Our analysis is subject to several limitations. Key limitations that apply to the case-number estimate (*1*) will also apply here, such as reliance on a series of multipliers, including some generated by structured expert judgment, and lack of information on sensitivity of the urinary antigen test for all *Legionella* species and serogroups. We excluded some costs because of lack of available data. However, because estimates suggest that >90% of persons with Legionnaires' disease are hospitalized or treated in the ED (*1*), these excluded costs (e.g., outpatient non-ED medical expenses and workdays lost for persons who are not hospitalized) are likely small. In addition, we estimated the economic value of workdays lost for all nonfatal cases occurring among working-age persons; however, whether all persons who contracted Legionnaires' disease were employed is unknown, so the financial costs incurred might be lower.

In conclusion, our analysis indicates that the economic burden of Legionnaires' disease more than doubles when lifetime productivity losses are added to medical costs. Our estimate can help demonstrate the value of investments in preventing Legionnaires' disease, such as water management programs and outbreak investigations.

## About the Author

Dr. Baker-Goering is an economist in the Division of Global HIV and TB in the Center for Global Health at the Centers for Disease Control and Prevention, Atlanta. Her research interests include public health economics, behavioral economics, environmental economics, and impact evaluation.

## References

1. Collier SA, Deng L, Adam EA, Benedict KM, Beshearse EM, Blackstock AJ, et al. Estimate of burden and direct healthcare cost of infectious waterborne disease in the United States. Emerg Infect Dis. 2021;27:140-9.
2. Garrison LE, Kunz JM, Cooley LA, Moore MR, Lucas C, Schrag S, et al. Vital signs: deficiencies in environmental control identified in outbreaks of Legionnaires' disease—North America, 2000–2014. MMWR Morb Mortal Wkly Rep. 2016;65:576–84. https://doi.org/10.15585/mmwr.mm6522e1
3. Dooling KL, Toews KA, Hicks LA, Garrison LE, Bachaus B, Zansky S, et al. Active Bacterial Core surveillance for legionellosis—United States, 2011–2013. MMWR Morb Mortal Wkly Rep. 2015;64:1190–3. https://doi.org/10.15585/mmwr.mm6442a2
4. Bureau of Labor Statistics. May 2014 National Occupational Employment and Wage Estimates United States. Washington: US Department of Labor; March 2015 [cited 2018 Apr 12]. https://www.bls.gov/oes/2014/may/oes_nat.htm#00-0000<
5. Grosse SD, Krueger KV, Mvundura M. Economic productivity by age and sex: 2007 estimates for the United States. Med Care. 2009;47(Suppl 1):S94–103. https://doi.org/10.1097/MLR.0b013e31819c9571
6. Bureau of Labor Statistics. Employment cost index historical listing V3. Current dollar, March 2001–September 2017. Table 4: employment cost index for total compensation, for civilian workers, by occupation and industry. Washington: US Department of Labor; April 2018 [cited 2018 Apr 12]. https://www.bls.gov/web/eci/echistrynaics.pdf
7. Zhang W, Bansback N, Anis AH. Measuring and valuing productivity loss due to poor health: a critical review. Soc Sci Med. 2011;72:185–92. https://doi.org/10.1016/j.socscimed.2010.10.026
8. Office of the Assistant Secretary for Planning and Evaluation. Guidelines for regulatory impact analysis. Washington: US Department of Health and Human Services; 2016 [cited 2018 Apr 12]. https://aspe.hhs.gov/system/files/pdf/242926/HHS_RIAGuidance.pdf

Address for correspondence: Madeleine M. Baker-Goering, 1600 Clifton Rd NE, Mailstop D-28, Atlanta, GA 30329-4027, USA; email: wqf3@cdc.gov

# Optimization of Notification Criteria for Shiga Toxin–Producing *Escherichia coli* Surveillance, the Netherlands

Ingrid H.M. Friesema, Sjoerd Kuiling, Zsofia Igloi, Eelco Franz

We describe the consequences of 2 major changes in notification criteria for Shiga toxin–producing *Escherichia coli* surveillance in the Netherlands. The change to reporting acute, more severe infections appears to be a good compromise between workload, redundancy, and public health relevance, provided isolates remain available for typing and sequencing.

Shiga toxin–producing *Escherichia coli* (STEC) is a zoonotic pathogen that causes illnesses ranging from mild diarrhea to hemolytic uremic syndrome (HUS) and death (*1*,*2*). Infection mainly occurs through consumption of contaminated food or contact with animals or manure. In most countries in Europe, STEC infections are notifiable at a national level. In 2017, the mean notification rate in Europe was 1.8 cases/100,000 population (*3*). Because STEC can cause severe disease and outbreaks, its notification is essential (*4*).

By combining epidemiologic case data with pathogen typing information, which has become increasingly genome-based in recent years, the Netherlands implemented STEC surveillance to follow trends in incidence and circulating types and detect and define outbreaks. STEC surveillance also provides data to inform public health actions to prevent and control further spread of the pathogen.

The Netherlands started surveillance for STEC O157 in 1999. The introduction of PCR, especially PCR targeting the Shiga toxin–producing genes, facilitated diagnosis of all STEC and PCR was faster and more sensitive than the standard culture (*5*–*8*). A pilot study in the Netherlands during 2005–2006 showed the common presence of non-O157 STEC infections (*9*); subsequently, STEC O157 surveillance was extended to all STEC in July 2007. The extension caused an overload of reports at the regional public health service, with the result that case-level information about the disease and its course was missed. Furthermore, available information suggested that most reports were from cases with mild long-term symptoms. In July 2016, the notification criteria were narrowed to target acute, more severe STEC infections. We reviewed the effects of changes in notification criteria on STEC surveillance in the Netherlands.

Author affiliations: National Institute for Public Health and the Environment, Bilthoven, the Netherlands (I.H.M. Friesema, S. Kuiling, Z. Igloi, E. Franz); European Program for Public Health Microbiology Training, Stockholm, Sweden (Z. Igloi)

DOI: https://doi.org/10.3201/eid2701.200339

## The Study

In the Netherlands, laboratories and medical doctors must report laboratory confirmed STEC cases to the regional public health service. The public health service subsequently reports cases to the National Institute for Public Health and the Environment (RIVM). Information gathered includes sex, birth year, date of illness onset, symptoms, hospitalization, and death. From its inception in January 1999, STEC surveillance in the Netherlands has been enhanced by laboratory surveillance in which laboratories are requested to voluntarily send STEC isolates to RIVM for further typing.

When STEC notification began in 1999, there were 2 criteria: 1) notification for every person with diarrhea, stomachache, or both; STEC O157 confirmed via a culture; or demonstration of Shiga toxin (Stx) or Shiga toxin genes (stx) in feces or bowel contents; and 2) notification for every person with HUS or with STEC O157 confirmed via a specific antibody response for STEC O157, a culture, or demonstration of Stx or *stx1* or *stx2* genes in feces or bowel contents. In July 2007, notification criteria shifted from notification for STEC O157 to notification of all STEC serotypes, using the

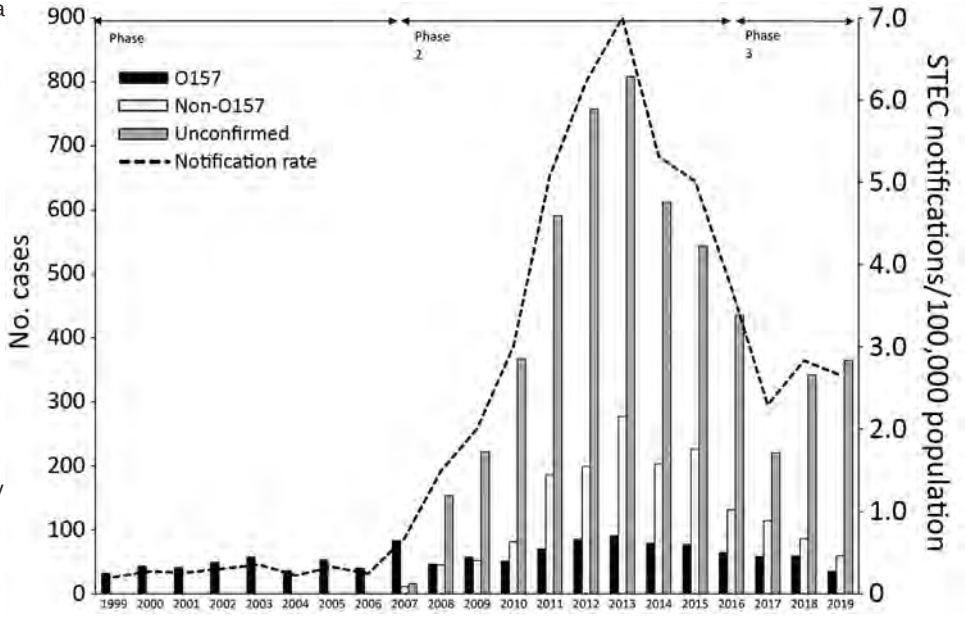


**Figure.** Number of reported Shiga toxin–producing *Escherichia coli* (STEC) infections per STEC group, the Netherlands, 1999–2019. In total, 8,307 infections were reported. For unconfirmed cases, no isolate was sent in for typing or isolates sent to the National Institute for Health and the Environment could not be confirmed or typed. During phase 1, 1999–June 2007, notification criteria were 1) notification for every person with diarrhea, stomachache, or both; STEC O157 confirmed via a culture; or demonstration of Shiga toxin (Stx) or Shiga toxin genes (*stx*) in feces; and 2) notification for every person with HUS; STEC O157 confirmed via a specific antibody response for STEC O157, a culture, or demonstration of Stx or *stx1* or *stx2* genes in feces. During phase 2, July 2007–June 2016, notification criteria shifted from notification for STEC O157 to notification of all STEC serotypes using the same 2 criteria. During phase 3, July 2016–December 2019, the first criterium was changed to notification of every person with diarrhea, blood in stool, vomiting or any combination, and <21 days between date of symptom onset and date of fecal sample taken in combination with STEC confirmation via a culture, demonstration of the combination of *stx1* gene with the *eae* or *escV* gene, or demonstration of *stx2* gene.

same 2 criteria. Then, in July 2016, the first criterium was changed to notification of every person with diarrhea, blood in stool, vomiting or any combination, and <21 days between date of symptom onset and date of fecal sample taken in combination with STEC confirmation via a culture, demonstration of the combination of *stx1* gene with the *eae* or *escV* gene, or demonstration of *stx2* gene.

During 1999–2019, a total of 8,307 STEC infections, including 230 HUS cases, were reported (Figure). After the change in notification criteria in 2007, we noted a 20-fold increase in reported STEC cases (Figure). Comparable increases were seen in the United States and other countries in Europe after introduction of methods for detecting all STEC serotypes (*10*–*13*). The 2016 criteria change for notification halved the number of reported cases. Introduction of molecular diagnostics also led to omission of culturing strains for further typing for most cases, which is especially apparent since 2018.

STEC O157 is the only serotype for which the Netherlands has 21 years of available data on infections. The number of cases per year varied from 32 in 1999 to 90 in 2013. The highest annual numbers were seen in 2007 (83 cases, 41 of which were part of a national outbreak) and during 2011–2015 (70–90 cases/year). In other years, 32–64 cases were notified. The proportion of HUS cases was highest (12%–26%) during the early years of surveillance, 1999–2004; since 2005, HUS incidence varies from 2%–11% per year. The median number of HUS cases were 12.5 (range 5–23) cases during 2008–2015 and 21 (range 12–22) cases during 2017–2019. During July 2016–December 2019, median age among HUS cases was 29 years compared with median age of 18 years during 1999–2007 and 22 years during July 2007–June 2016.

**Table 1.** Most prevalent serotypes in non-O157 Shiga toxin–producing *Escherichia coli*, the Netherlands, July 2007–June 2016 and July 2016–December 2019*

| | July 2007–June 2016, n = 1,370 | | July 2016–December 2019, n = 299 | |
|---|---|---|---|---|
| Most prevalent | Serotype | No. (%) | Serotype | No. (%) |
| 1 | O26 | 171 (12) | O26 | 80 (27) |
| 2 | O91 | 137 (10) | O103 | 31 (10) |
| 3 | O146 | 89 (6) | O63 | 18 (6) |
| 4 | O103 | 87 (6) | O146 | 16 (5) |
| 5 | O63 | 54 (6) | O145 | 13 (4) |

*Non-O157 includes O nontypeable serotypes. Because O nontypeable is a diffuse group, we left it out of the list of most prevalent serotypes. However, during July 2007–June 2016, 118/1,370 (9%) serotypes were O nontypeable; during July 2016–December 2019, 11/299 (4%) were O nontypeable.

**Table 2.** Most prevalent genes in non-O157 Shiga toxin–producing *Escherichia coli*, the Netherlands, July 2007–June 2016 and July 2016–December 2019*

| Most prevalent genes, | July 2007–June 2016, n = 1,366 | | | | July 2016–December 2019, n = 292 | | | |
|---|---|---|---|---|---|---|---|---|
| no. (%) | *eae* | *hly* | *eae + hly* | None | *eae* | *hly* | *eae + hly* | None |
| *stx1* | 18 (1) | 170 (12) | 287 (21) | 130 (10) | 3 (1) | 7 (2) | 95 (33) | 10 (3) |
| *stx2* | 4 (0.3) | 99 (7) | 82 (6) | 173 (13) | 3 (1) | 18 (6) | 53 (18) | 35 (12) |
| *stx1 + stx2* | 0 | 158 (12) | 52 (4) | 30 (2) | 1 (0.3) | 12 (4) | 21 (7) | 6 (2) |
| *stx2f* | 160 (12) | 0 | 0 | 3 (0.2) | 26 (9) | 0 | 1 (0.3) | 1 (0.3) |

**eae*, attaching and effacing gene; *hly*, hemolysin gene; *stx1*, Shiga toxin type 1 gene; *stx2*, Shiga toxin type 2 gene.

Hospitalization rates for STEC remained stable, fluctuating from 29% to 54% per year.

In the Netherlands, STEC O26 is the most prevalent and severe non-O157 STEC serotype. Among 37 HUS cases reported to be caused by a non-O157 STEC, 20 (54%) were diagnosed STEC O26 infections. In addition, STEC O26 prevalence increased from 12% during July 2007–June 2016 to 27% during July 2016–December 2019 (Table 1). STEC O103 also moved from fourth most prevalent to second most prevalent after the last change in notification criteria; whereas STEC O91 dropped out of the top 5 most prevalent serotypes. Since July 2016, gene profiles *stx1* + *hly* and *stx1* + *stx2* + *hly* were seen less often in non-O157 STEC, but profiles *stx1* + *eae* + *hly* and *stx2* + *eae* + *hly* became more common (Table 2).

## Conclusions

The introduction of PCR facilitated detection of all STEC in the Netherlands. However, STEC is a heterogeneous group and some serotypes are more prone to cause severe disease than others. Expanding surveillance to all STEC caused a 20-fold increase of reported cases, some of which were from cases with mild and long-term symptoms. Because PCR is faster, cheaper, and easier than culture, it might be requested more for rapid results in cases of less severe disease. Furthermore, many laboratories implemented reverse transcription PCR multiplex assays in which a specimen is tested for several diseases in a single run, instead of testing for 1 disease at a time. A study in Norway showed that in laboratories introducing a multiplex assay as standard detection method, the number of STEC reports, especially of low-virulence STEC, increased substantially compared with laboratories without this method (*13*). Introduction of a multiplex assay also lead to an increase in detection of concomitant infections.

Surveillance of STEC serotypes and virulence gene profiles remains vital and relevant. The confinement of the notification criteria to acute disease onset with ≥1 of 3 predefined symptoms increased the public health relevance of surveillance. The data did not show large effects of the criteria changes on STEC O157, which implies no noticeable effects on notifications of relatively severe disease within the surveillance. However, a new challenge emerged. Isolates are needed to provide information on confirmed STEC cases and circulating serotypes and are used for nationwide outbreak detection using whole-genome sequencing. In an era of increased molecular diagnostics, less culturing is performed by the regional laboratories, especially as serotype information is not relevant for treating patients. The current notification criteria in the Netherlands appear to be a good compromise between medical laboratory workload, redundancy of less public health-relevant cases, and the ability to carry out public health actions. However, we stress that national surveillance is threatened by reduced culturing and urge public health institutes and laboratories to coordinate to safeguard against loss of cultures in the future.

### Acknowledgments

The authors thank the public health services for interviewing STEC patients and the laboratories for submitting STEC isolates for additional typing.

### About the Author

Dr. Friesema is an epidemiologist at the Centre for Infectious Disease Control of the National Institute of Public Health and the Environment, the Netherlands. Her research interests involve the epidemiology and public health surveillance of pathogens causing gastroenteritis and of foodborne diseases.

### References

1. Karmali MA, Gannon V, Sargeant JM. Verocytotoxin-producing *Escherichia coli* (VTEC). Vet Microbiol. 2010;140:360–70. https://doi.org/10.1016/j.vetmic.2009.04.011
2. Page AV, Liles WC. Enterohemorrhagic *Escherichia coli* infections and the hemolytic-uremic syndrome. Med Clin North Am. 2013;97:681–95, xi. https://doi.org/10.1016/j.mcna.2013.04.001
3. European Centre for Disease Prevention and Control. Shiga-toxin/verocytotoxin–producing *Escherichia coli* (STEC/VTEC) infections. In: European Centre for Disease Prevention and Control, editor. Annual epidemiological report for 2017. Stockholm: The Centre; 2019 [cited 2020 Feb 17]. https://www.ecdc.europa.eu/en/publications-data/shiga-toxinverocytotoxin-producing-escherichia-coli-stecvtec-infection-annual-0

4. Caprioli A, Morabito S, Brugère H, Oswald E. Enterohaemorrhagic *Escherichia coli*: emerging issues on virulence and modes of transmission. Vet Res. 2005;36:289–311. https://doi.org/10.1051/vetres:2005002
5. Grys TE, Sloan LM, Rosenblatt JE, Patel R. Rapid and sensitive detection of Shiga toxin–producing *Escherichia coli* from nonenriched stool specimens by real-time PCR in comparison to enzyme immunoassay and culture. J Clin Microbiol. 2009;47:2008–12. https://doi.org/10.1128/JCM.02013-08
6. de Boer RF, Ott A, Kesztyüs B, Kooistra-Smid AM. Improved detection of five major gastrointestinal pathogens by use of a molecular screening approach. J Clin Microbiol. 2010;48:4140–6. https://doi.org/10.1128/JCM.01124-10
7. Newell DG, La Ragione RM. Enterohaemorrhagic and other Shiga toxin–producing *Escherichia coli* (STEC): where are we now regarding diagnostics and control strategies? Transbound Emerg Dis. 2018;65(Suppl 1):49–71. 10.1111/tbed.12789 https://doi.org/10.1111/tbed.12789
8. Pedersen RM, Nielsen MTK, Möller S, Ethelberg S, Skov MN, Kolmos HJ, et al. Shiga toxin–producing *Escherichia coli*: incidence and clinical features in a setting with complete screening of patients with suspected infective diarrhoea. Clin Microbiol Infect. 2018;24:635–9. https://doi.org/10.1016/j.cmi.2017.10.002
9. van Duynhoven YTHP, Friesema IHM, Schuurman T, Roovers A, van Zwet AA, Sabbe LJM, et al. Prevalence, characterization and clinical profiles of Shiga toxin–producing *Escherichia coli* in the Netherlands. Clin Microbiol Infect. 2008;14:437–45. https://doi.org/10.1111/j.1469-0691.2008.01963.x
10. Carroll KJ, Harvey-Vince L, Jenkins C, Mohan K, Balasegaram S. The epidemiology of Shiga toxin–producing *Escherichia coli* infections in the South East of England: November 2013–March 2017 and significance for clinical and public health. J Med Microbiol. 2019;68:930–9. https://doi.org/10.1099/jmm.0.000970
11. Rice T, Quinn N, Sleator RD, Lucey B. Changing diagnostic methods and increased detection of verotoxigenic *Escherichia coli*, Ireland. Emerg Infect Dis. 2016;22:1656–7. https://doi.org/10.3201/eid2209.160477
12. Stigi KA, Macdonald JK, Tellez-Marfin AA, Lofy KH. Laboratory practices and incidence of non-O157 Shiga toxin–producing *Escherichia coli* infections. Emerg Infect Dis. 2012;18:477–9. https://doi.org/10.3201/eid1803.111358
13. Jenssen GR, Veneti L, Lange H, Vold L, Naseer U, Brandal LT. Implementation of multiplex PCR diagnostics for gastrointestinal pathogens linked to increase of notified Shiga toxin–producing *Escherichia coli* cases in Norway, 2007–2017. Eur J Clin Microbiol Infect Dis. 2019;38:801–9. https://doi.org/10.1007/s10096-019-03475-5

Address for correspondence: Ingrid Friesema, RIVM-EPI, Centre for Infectious Disease Control, National Institute of Public Health and the Environment (RIVM), Box 1, 3720 BA Bilthoven, the Netherlands; email: ingrid.friesema@rivm.nl

# Seventh Pandemic *Vibrio cholerae* O1 Sublineages, Central African Republic

Sebastien Breurec,[1] Thierry Franck,[1,2] Elisabeth Njamkepo, Jean-Robert Mbecko, Jean Rauzier, Hugues Sanke-Waïgana, Guyguy Kamwiziku, Renaud Piarroux, Marie-Laure Quilici,[3] François-Xavier Weill[3]

Four cholera outbreaks were reported in the Central African Republic during 1997–2016. We show that the outbreak isolates were *Vibrio cholerae* O1 serotype Inaba from 3 seventh pandemic El Tor sublineages originating from West Africa (sublineages T7 and T9) or the African Great Lakes Region (T10).

Cholera is a life-threatening diarrheal disease caused by the bacterium *Vibrio cholerae*, which produces cholera toxin. The seventh cholera pandemic, caused by *V. cholerae* O1 biotype El Tor, began in Indonesia in 1961 and reached Africa in 1970 (*1*). Fifty years later, >100,000 cases of cholera are reported annually in sub-Saharan Africa (*2*).

The Central African Republic (CAR) is a landlocked and resource-limited country in central Africa; it was ranked 188/189 on the United Nations Human Development Index in 2018 (http://hdr.undp.org). CAR is relatively large but has a low population density; 2019 data estimate ≈4.75 million inhabitants, or 7.75 persons/km$^2$ (Macrotrends LLC, https://www.macrotrends.net). CAR largely has been spared by the cholera epidemic; only 4 outbreaks had been reported by 2020 (Table 1; Figure 1). The first 2 cholera outbreaks occurred during the same month in 1997 (*4*). In the first, 443 cases and 88 deaths were reported in southern CAR, along the Oubangui River, close to the border with the Democratic Republic of the Congo (DRC). In the second, 113 cases and 19 deaths were reported in northern CAR, close to the borders with Cameroon and Chad, after which cholera cases continued to be detected in southern CAR, along the Oubangui River. According to reports from the International Federation of Red Cross and Red Crescent Societies, 172 cholera cases and 16 deaths were reported in the region in 2011 (https://reliefweb.int/sites/reliefweb.int/files/resources/MDRCF009finrep.pdf) and 265 cases and 20 deaths were reported in 2016 (https://reliefweb.int/report/central-african-republic/central-africa-republic-cholera-epidemic-outbreak-dref-operation).

The Institut Pasteur de Bangui in CAR performed microbial analyses to confirm the causal agent of these outbreaks and identified 30 *V. cholerae* O1 serotype Inaba isolates collected during 1997–2016 (Appendix 1 Table 1, https://wwwnc.cdc.gov/EID/article/27/1/20-0375-App1.x1sx). We used whole-genome sequencing to fully characterize all 30 *V. cholerae* O1 isolates in terms of virulence and antimicrobial resistance determinants. We also placed these genomes within a broader phylogenetic context to elucidate their origins and evolutionary history.

## The Study

The 30 *V. cholerae* O1 isolates were received at the Institut Pasteur, Paris, France. We performed antimicrobial susceptibility testing, whole-genome sequencing, comparative genomics, and phylogenetic analyses by using methods previously described (*3*,*5*–*11*) (Appendix 2, https://wwwnc.cdc.gov/EID/

Author affiliations: Institut Pasteur de la Guadeloupe, Les Abymes, France (S. Breurec); INSERM Centre d'Investigation Clinique 1424, Pointe-à-Pitre/Les Abymes, France (S. Breurec); Université des Antilles, Pointe-à-Pitre, France (S. Breurec); Institut Pasteur de Bangui, Bangui, Central African Republic (S. Breurec, T. Franck, J.-R. Mbecko); Institut Pasteur, Paris, France (E. Njamkepo, J. Rauzier, M.-L. Quilici, F.-X. Weill); Université de Kinshasa, Kinshasa, Democratic Republic of the Congo (G. Kamwiziku); Assistance Publique-Hôpitaux de Paris, Paris (R. Piarroux)

DOI: https://doi.org/10.3201/eid2701.200375

[1]These first authors contributed equally to this article.

[2]Deceased.

[3]These authors were joint principal investigators.

**Table 1.** Characteristics of the *Vibrio cholerae* O1 isolates associated with outbreaks of cholera, Central African Republic*

| Characteristics | Outbreak no. 1, 1997 Jun–Oct | Outbreak no. 2, 1997 Jun–Aug | Outbreak no. 3, 2011 Sept–Oct | Outbreak no. 4, 2016 Jul–Dec |
|---|---|---|---|---|
| No. deaths/no. cases† | 88/443 | 19/113 | 16/172 | 20/265 |
| No. isolates | 9 | 6 | 7 | 8 |
| 7PET sublineage | T7 | T9 | T10 | T10 |
| Sequence type | 69 | 69 | 515 | 515 |
| *ctxB* | B3 | B1 | B1 | B1 |
| *wbeT*‡ | A03 | C19 | B01 | B01 |
| AMR phenotypes (no. isolates)§ | R1 (8), R2 (1) | R3 (6) | R3 (7) | R3 (8) |
| AMR determinants | | | | |
| Plasmid | IncA/C¶ | NT | NT | NT |
| VC_0715 | WT | R169C | R169C | R169C |
| VC_A0637 | WT | Q5Stop | Q5Stop | Q5Stop |
| SXT/R391 element | NT | ICE*Vch*Ind5 | ICE*Vch*Ind5 | ICE*Vch*Ind5 |
| *gyrA* | WT | WT | S83I | S83I |

*7PET, seventh pandemic *Vibrio cholerae* O1 El Tor; AMR, antimicrobial resistance; NT, not detected; WT, wild type.
†Data from the International Federation of Red Cross and Red Crescent Societies 2011 (https://reliefweb.int/sites/reliefweb.int/files/resources/MDRCF009finrep.pdf) and 2016 (https://reliefweb.int/report/central-african-republic/central-africa-republic-cholera-epidemic-outbreak-dref-operation).
‡Nomenclature according to Weill et al. (*3*) (Table 2).
§R1, resistance to polymyxin B and colistin; R2, resistance to polymyxin B, colistin, ampicillin, streptomycin, sulfonamides, vibriostatic agent, trimethoprim/sulfamethoxazole, chloramphenicol; R3, resistance to polymyxin B, colistin, streptomycin, sulfonamides, vibriostatic agent, trimethoprim/sulfamethoxazole, furazolidone, and resistance or intermediate resistance to chloramphenicol.
¶Isolate (CNRVC970079) with the R2 AMR type.

article/27/1/20-0375-App2.pdf). We then contextualized these 30 *V. cholerae* O1 isolates within a global collection of 1,185 seventh pandemic *V. cholerae* El Tor (7PET) genomic sequences and constructed a maximum-likelihood phylogeny of 1,215 genomes by using 9,964 single-nucleotide variants (SNVs) evenly distributed over the nonrepetitive, nonrecombinant core genome (Figure 2, panel A). Our phylogenomic analysis (Appendix 1 Tables 2–4) showed that all CAR isolates belonged to the 7PET lineage (*12*,*13*).

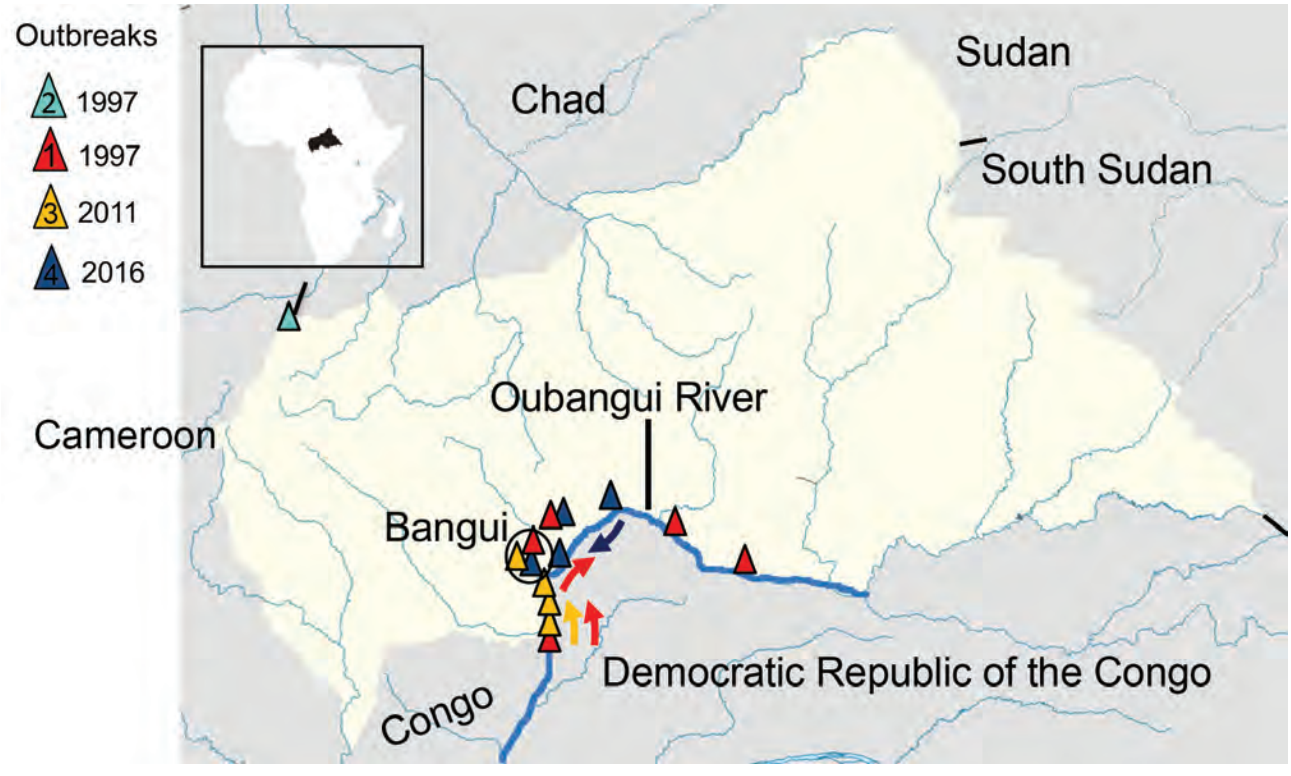


**Figure 1.** Geographic location of cholera cases during the 4 outbreaks reported in the Central African Republic, 1997–2016. Inset shows the location of Central African Republic in the continent of Africa. Numbers correspond to outbreaks during 1) June–October 1997; 2) June–August 1997; 3) September–October 2011; and 4) July–December 2016. Arrows show movement of outbreaks corresponding to colors for each outbreak.

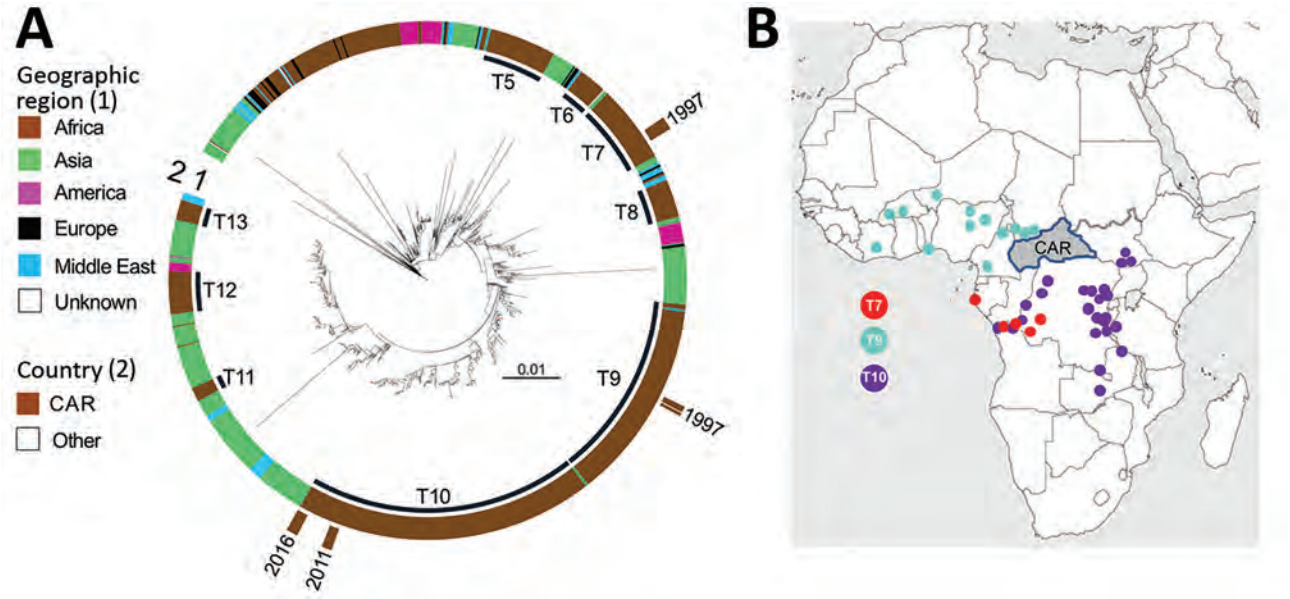


**Figure 2.** Phylogenomics of the *Vibrio cholerae* O1 El Tor isolates from CAR, 1997–2016. A) Maximum-likelihood phylogeny for 1,215 7PET genomic sequences. A6 was used as an outgroup. The last 9 sublineages introduced into Africa (T5–T13) are indicated. On inner ring, color scale denotes geographic locations of the *V. cholerae* isolates. On outer ring, brown denotes isolates from CAR. Tree branches containing isolates from CAR are shown in red. Scale bar indicates substitutions per variable site. B) Locations on the African continent in which T7, T9, and T10 *V. cholerae* O1 serotype Inaba isolates were detected before their identification in CAR. CAR, Central African Republic.

Previous genomic studies described 12 introductions of the 7PET lineage from Southern Asia into Africa during 1970–2016 (*3*,*6*). The introduced sublineages were called T1 and T3–T13. The 2 cholera outbreaks in CAR in 1997 were caused by sublineage T7, which had been introduced into West Africa during the early 1980s, and T9, which was introduced in the late 1980s, according to Weill et al. (*3*). T9 isolates were identified in neighboring countries such as Chad and Cameroon (particularly northern Cameroon) before they were detected in northwest CAR, but T7 isolates were identified in Gabon and the western part of DRC, along the Congo River in Kinshasa, before being identified in CAR along the Oubangui River, a tributary of the Congo River (Figure 2, panel B; Appendix 2 Figures 1, 2).

The 2011 and 2016 outbreaks were caused by closely related bacterial populations from the same sublineage, T10, introduced into East Africa during the 1990s and later detected in the African Great Lakes Region (AGLR) (*3*) (Figure 2, panel B; Appendix 2 Figure 3). The prevalent T10 sublineage has several clades, and the 2011 and 2016 CAR isolates are characterized by multilocus sequence type (ST) 515, a single-locus variant of ST69; ST69 is the predominant ST among 7PET isolates. In addition, these isolates have an alteration to the *wbeT* gene, a 4-nucleotide deletion called B01 (Tables 1, 2), that underly the Inaba serotype. Phylogenetic data showed that the 7PET strains causing the 2011 and 2016 cholera outbreaks in CAR spread from AGLR to the western part of the DRC and CAR (Figure 2, panel B; Appendix 2 Figure 3). These genomic data are consistent with results from a recent epidemiologic study showing the spatiotemporal distribution of cholera cases during the 2011–2012 and 2015–2017 outbreaks in DRC, suggesting a spread from cholera hotspots in AGLR to major cities in the upstream section of the Congo River, followed by a downstream spread toward the densely populated CAR capital, Kinshasa, and then to the mouth of the Congo River, which opens into the Gulf of Guinea (*14*).

**Table 2.** Alterations of the *wbeT* (formerly *rfbT*) gene in *Vibrio cholerae* El Tor isolates from the Central African Republic*

| Alteration no. | Alteration type | Genetic alteration | Protein consequence† | 7PET sublineage |
|---|---|---|---|---|
| A03 | Premature stop codon | G133T | G45-to-STOP | T7 |
| B01 | Premature stop codon | Deletion TGTAC (nt 24–28) | Frameshift after N7; then STOP | T10 |
| C19 | Amino acid substitution | G674A | C225Y | T9 |

*7PET, seventh pandemic *Vibrio cholerae* O1 El Tor.
†The codon number and single-letter amino acid abbreviation are shown (STOP corresponds to a stop codon).

Except during the outbreak in northwest CAR in 1997, all cholera cases were reported along or close to the Oubangui River, suggesting that 7PET strains probably moved from area to area along the river and with the displacement of human populations. The risk factors in these remote areas are unknown, but the prevailing conditions, such as poor hygiene and sanitary conditions, overcrowding, lack of latrines, and drinking water from the Oubangui River, likely would increase the risk for transmission via the fecal–oral route, as evidenced by the high attack rates observed at several sites when the 2011 outbreak began (*15*). Nevertheless, since the declaration of the first case in 1997, the small number (≤1,000) of cholera cases in CAR contrasts with the much larger numbers in central Africa (*2*). The low population density of CAR, its poor transport infrastructure, and poor trading links are probably key factors limiting disease spread (*15*). Phylogenetic analyses showed no other isolates from Africa were derived from CAR isolates in the aftermath of the 4 outbreaks, which also suggests that the transmission of cholera is impeded in this country. Of note, all 4 outbreaks were caused by serotype Inaba 7PET strains. This serotype has a nonmethylated form of lipopolysaccharide caused by an alteration to the *wbeT* gene (*3*) (Table 2). The implication of this serotype in all 4 outbreaks suggests that these 7PET sublineages circulated regionally for some time, long enough to acquire this alteration to the *wbeT* gene, before reaching CAR (Appendix 2 Figures 1–3).

All CAR isolates in this study displayed resistance to polymyxin B, consistent with the susceptibility pattern reported for the El Tor biotype until recently (*6*). All but 1 of the isolates collected along the Oubangui River in 1997 were susceptible to all other antimicrobial drugs tested; the outlying isolate contained the extended-spectrum β-lactamase $bla_{\text{SHV-2a}}$ gene on an IncA/C2 plasmid (Table 1; Appendix 1 Table 3). No susceptible isolates have been collected in CAR since. All the other isolates display mutations of the *VC_0715* and *VC_A0637* genes, conferring nitrofuran resistance, and carry an SXT/R391 genomic element called ICE*Vch*Ind5, encoding resistance to streptomycin (*strAB*), sulfonamides (*sul2*), trimethoprim, the O/129 vibriostatic agent (*dfrA1*), and trimethoprim-sulfamethoxazole (*sul2* and *dfrA1*). The 2011 and 2016 CAR isolates also recently acquired *gyrA* mutations (Table 1), resulting in resistance to nalidixic acid (Appendix 1 Table 3).

## Conclusions

Strains from 3 7PET sublineages caused 4 cholera outbreaks identified in CAR during 1997–2016. The southern and southeastern parts of CAR are higher risk areas for cholera outbreaks, particularly when cases are reported in the western part of DRC. These findings highlight the need for an effective surveillance system, and for coordinated communication actions on cholera that target healthcare professionals and the populations living along the Oubangui River, to prevent and control cholera outbreaks in CAR.

This work was supported by the Institut Pasteur, Santé Publique France and the French Government's Investissement d'Avenir program, Laboratoire d'Excellence Integrative Biology of Emerging Infectious Diseases (grant no. ANR-10-LABX-62-IBEID).

## About the Author

Dr. Breurec is a medical microbiologist on the faculty of medicine and the University Medical Center of Pointe-à-Pitre, Guadeloupe, and at the Institut Pasteur International Network. His research interests include genomic epidemiology, resistance, and the virulence determinants of bacterial pathogens.

## References

1. Barua DWBG, editor. Cholera. New York: Plenum; 1992.
2. Lessler J, Moore SM, Luquero FJ, McKay HS, Grais R, Henkens M, et al. Mapping the burden of cholera in sub-Saharan Africa and implications for control: an analysis of data across geographical scales. Lancet. 2018;391:1908–15. https://doi.org/10.1016/S0140-6736(17)33050-7
3. Weill FX, Domman D, Njamkepo E, Tarr C, Rauzier J, Fawal N, et al. Genomic history of the seventh pandemic of cholera in Africa. Science. 2017;358:785–9. https://doi.org/10.1126/science.aad5901
4. Germani Y, Quilici ML, Glaziou P, Mattera D, Morvan J, Fournier JM. Emergence of cholera in the Central African Republic. Eur J Clin Microbiol Infect Dis. 1998;17:888–90. https://doi.org/10.1007/s100960050217
5. Abubakar A, Bwire G, Azman AS, Bouhenia M, Deng LL, Wamala JF, et al. Cholera epidemic in south Sudan and Uganda and need for international collaboration in cholera control. Emerg Infect Dis. 2018;24:883–7. https://doi.org/10.3201/eid2405.171651
6. Weill FX, Domman D, Njamkepo E, Almesbahi AA, Naji M, Nasher SS, et al. Genomic insights into the 2016–2017 cholera epidemic in Yemen. Nature. 2019;565:230–3. https://doi.org/10.1038/s41586-018-0818-3
7. Irenge LM, Ambroise J, Mitangala PN, Bearzatto B, Kabangwa RKS, Durant JF, et al. Genomic analysis of pathogenic isolates of *Vibrio cholerae* from eastern Democratic Republic of the Congo (2014–2017). PLoS Negl Trop Dis. 2020;14:e0007642. https://doi.org/10.1371/journal.pntd.0007642
8. Bankevich A, Nurk S, Antipov D, Gurevich AA, Dvorkin M, Kulikov AS, et al. SPAdes: a new genome assembly algorithm and its applications to single-cell sequencing. J Comput Biol. 2012;19:455–77. https://doi.org/10.1089/cmb.2012.0021

9. Larsen MV, Cosentino S, Rasmussen S, Friis C, Hasman H, Marvig RL, et al. Multilocus sequence typing of total-genome-sequenced bacteria. J Clin Microbiol. 2012;50:1355–61. https://doi.org/10.1128/JCM.06094-11
10. Croucher NJ, Page AJ, Connor TR, Delaney AJ, Keane JA, Bentley SD, et al. Rapid phylogenetic analysis of large samples of recombinant bacterial whole genome sequences using Gubbins. Nucleic Acids Res. 2015;43:e15. https://doi.org/10.1093/nar/gku1196
11. Stamatakis A. RAxML-VI-HPC: maximum likelihood-based phylogenetic analyses with thousands of taxa and mixed models. Bioinformatics. 2006;22:2688–90. https://doi.org/10.1093/bioinformatics/btl446
12. Domman D, Quilici ML, Dorman MJ, Njamkepo E, Mutreja A, Mather AE, et al. Integrated view of *Vibrio cholerae* in the Americas. Science. 2017;358:789–93. https://doi.org/10.1126/science.aao2136
13. Mutreja A, Kim DW, Thomson NR, Connor TR, Lee JH, Kariuki S, et al. Evidence for several waves of global transmission in the seventh cholera pandemic. Nature. 2011;477:462–5. https://doi.org/10.1038/nature10392
14. Ingelbeen B, Hendrickx D, Miwanda B, van der Sande MAB, Mossoko M, Vochten H, et al. Recurrent cholera outbreaks, Democratic Republic of the Congo, 2008–2017. Emerg Infect Dis. 2019;25:856–64. https://doi.org/10.3201/eid2505.181141
15. Penguele A, Djeintote M, Balekouzou A, Tembeti J, Feilema P, Kazambu D, et al. Cholera outbreak investigation in the Central African Republic, October–November 2011 [cited 2020 Feb 23]. https://www.cdcfoundation.org/sites/default/files/upload/pdf/2011CholeraOutbreakReport.pdf

Address for correspondence: François-Xavier Weill, Unité des Bactéries pathogènes Entériques, Institut Pasteur, 28 rue du docteur Roux, 75724 Paris CEDEX 15, France; email: francois-xavier.weill@pasteur.fr

# Impact of a Nationwide Lockdown on SARS-CoV-2 Transmissibility, Italy

Giorgio Guzzetta,[1] Flavia Riccardo,[1] Valentina Marziano, Piero Poletti, Filippo Trentini, Antonino Bella, Xanthi Andrianou, Martina Del Manso, Massimo Fabiani, Stefania Bellino, Stefano Boros, Alberto Mateo Urdiales, Maria Fenicia Vescio, Andrea Piccioli, COVID-19 Working Group,[2] Silvio Brusaferro, Giovanni Rezza, Patrizio Pezzotti,[3] Marco Ajelli,[3] Stefano Merler[3]

On March 11, 2020, Italy imposed a national lockdown to curtail the spread of severe acute respiratory syndrome coronavirus 2. We estimate that, 14 days after lockdown, the net reproduction number had dropped below 1 and remained stable at ≈0.76 (95% CI 0.67–0.85) in all regions for ≥3 of the following weeks.

On February 21, 2020, the earliest known case of locally transmitted severe acute respiratory syndrome coronavirus 2 (SARS-COV-2) infection was reported in Italy (*1*; D. Cereda et al., unpub. data, https://arxiv.org/abs/2003.09320). Since then, several interventions have been deployed to control disease spread in regions with sustained transmission, including quarantine of most-affected municipalities, ban of mass gatherings, and local school closures. School closure at the national level was mandated on March 5, and a national lockdown (stay-home mandate and closure of all nonessential productive activities) was issued on March 11 (*2*,*3*), then eased after May 4, 2020 (Appendix, https://wwwnc.cdc.gov/EID/article/27/1/20-2114-App1.pdf). The aim of this study is to evaluate the impact of these interventions on SARS-CoV-2 transmissibility in Italy.

Author affiliations: Fondazione Bruno Kessler, Trento, Italy (G. Guzzetta, V. Marziano, P. Poletti, F. Trentini, S. Merler); Istituto Superiore di Sanità, Rome, Italy (F. Riccardo, A. Bella, X. Andrianou, M. Del Manso, M. Fabiani, S. Bellino, S. Boros, A. Mateo. Urdiales, M.F. Vescio, A. Piccioli, S. Brusaferro, G. Rezza, P. Pezzotti); Cyprus University of Technology, Limassol, Cyprus (X. Andrianou); European Centre for Disease Prevention and Control, Stockholm, Sweden (M. Del Manso, A. Mateo Urdiales); Indiana University School of Public Health, Bloomington, Indiana, USA (M. Ajelli); Northeastern University, Boston, Massachusetts, USA (M. Ajelli)

DOI: https://doi.org/10.3201/eid2701.202114

## The Study

We measured SARS-CoV-2 transmissibility in terms of the basic ($R_0$) and net ($R_t$) reproduction numbers. These quantities represent the mean number of secondary infections generated by 1 primary infector in a fully susceptible population ($R_0$) and in the presence of control interventions and human behavioral adaptations ($R_t$). When $R_t$ decreases below the threshold of 1, the number of new infections begins to decline. Estimates were obtained through a Bayesian approach applied to case-based surveillance data collected by regional health authorities (Appendix).

To account for the geographic heterogeneity in contacts, healthcare organization, and timelines of interventions, $R_t$ was estimated separately for different provinces and regions. We considered all 19 regions in Italy plus the 2 autonomous provinces of Trento and Bolzano. Moreover, we considered 100 of the remaining 105 provinces for which the data were sufficiently complete. The selected provinces covered 99.1% of the population of Italy and, as of May 3, 2020, accounted for 153,558 symptomatic cases (97.9% of the total recorded in the surveillance database). To evaluate the progressive decrease of transmission, we computed $R_t$ at 3 dates: the day before lockdown (March 10) and 1 and 2 weeks after lockdown (March 18 and 25). In addition, we considered the average value of $R_t$ over the successive 3 weeks (March 26–April 15). These choices were suggested by the trend of the national $R_t$ (Appendix).

The $R_0$ range was 2.83–3.10 (Figure 1) in the 8 regions for which the estimate was possible

[1]These authors contributed equally to the article.

[2]Members of the COVID-19 working group are listed at the end of this article.

[3]These authors are joint senior authors.

(Appendix). On March 10, $R_t$ range was 1.79–3.36 across regions; Basilicata and Molise had an insufficient number of symptomatic cases (Figure 1). One week into lockdown, on March 18, $R_t$ had decreased consistently, but no region or autonomous province was yet below the epidemic threshold (Figure 1). As of March 25, $R_t$ was <1 in most regions and autonomous provinces (12/21) and <1 in the successive 3 weeks for all regions except Molise and Piedmont

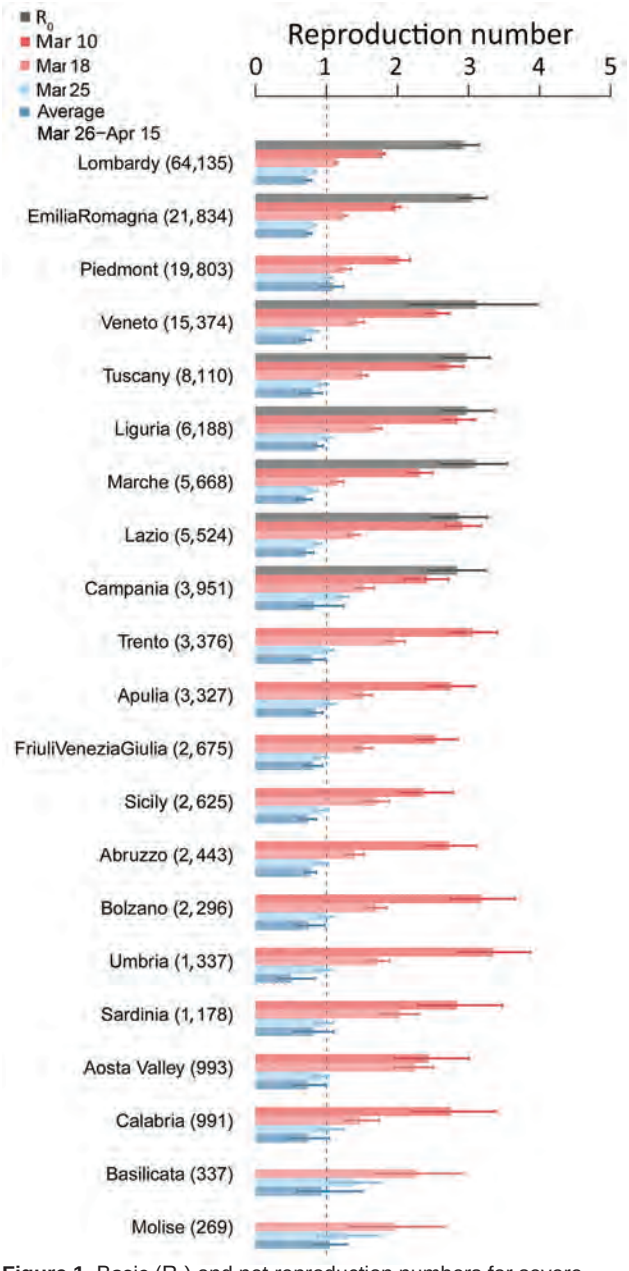


**Figure 1.** Basic ($R_0$) and net reproduction numbers for severe acute respiratory syndrome coronavirus 2 for all regions and autonomous provinces in Italy. Regions are sorted by decreasing number of cases (numbers in parentheses) on April 17. Bars indicate mean numbers; error bars indicate 95% CIs.

(Figure 1). The mean value of $R_t$ across the regions and autonomous provinces, weighted by the number of reported cases at the corresponding date, fell from an average of 2.03 (95% CI 1.94–2.13) on March 10 to 1.28 (95% CI 1.23–1.33) on March 18, to 0.88 (95% CI 0.84–0.91) on March 25, corresponding to an overall 62.6% reduction (range across regions 45.6%–85.0%). In the 3 weeks of March 26–April 15, $R_t$ remained stable in all regions, showing a further slight reduction at an average value of 0.76 (95% CI 0.67–0.85).

Results were consistent when analyzing estimates from the 100 selected provinces (Figure 2). As of March 10, no province had a mean estimated value of $R_t$ <1 (n = 75; the number of symptomatic cases was insufficient for the estimate in 25 provinces). One week after lockdown, on March 18, 5/93 provinces (5.4%) had an average $R_t$ <1, whereas on March 25 this figure increased to 49/96 provinces (51.0%). The fraction of provinces with $R_t$ below 1 rose to 84/100 (84.0%) when considering the average over the following 3 weeks. The mean value of the reproduction number across the provinces, weighted by the province's number of reported cases at the corresponding date, was 2.01 (95% CI 1.83–2.22) on March 10, 1.26 (95%CI 1.15–1.38) on March 18, 0.88 (95% CI 0.79–0.97) on March 25, and 0.77 (95% CI 0.63–0.95) for the period March 26–April 15.

## Conclusions

Our results suggest that the national lockdown put in place as of March 11 to limit the spread of SARS-CoV-2 in Italy brought $R_t$ below 1 in most regions and provinces within 2 weeks. Although $R_t$ had been declining steeply even before the national lockdown (*3*) in regions with intense interventions, we estimated that the epidemic was brought under control only after the implementation of the lockdown. Lockdown was fundamental to prevent an explosion in the number of cases in other regions in which transmission had started weeks later compared with the outbreak epicenter (Lombardy, Veneto, Emilia Romagna). The range of estimates of $R_0$ in 8 regions was 2.8–3.1, within the range of estimates obtained for other countries (*4*–*6*).

A massive and sustained scale-up of testing capacity was set up in all regions of Italy during the course of the epidemic (*7*); it was not accompanied by a corresponding increase of confirmed incident cases in the weeks following March 25, as indicated by the declining proportion of positive tests (Appendix). This finding suggests an increase of notification rates and thus a possible overestimation of $R_t$ (*8*). To compensate for possible biases, we supplemented our results by computing alternative estimates based on the

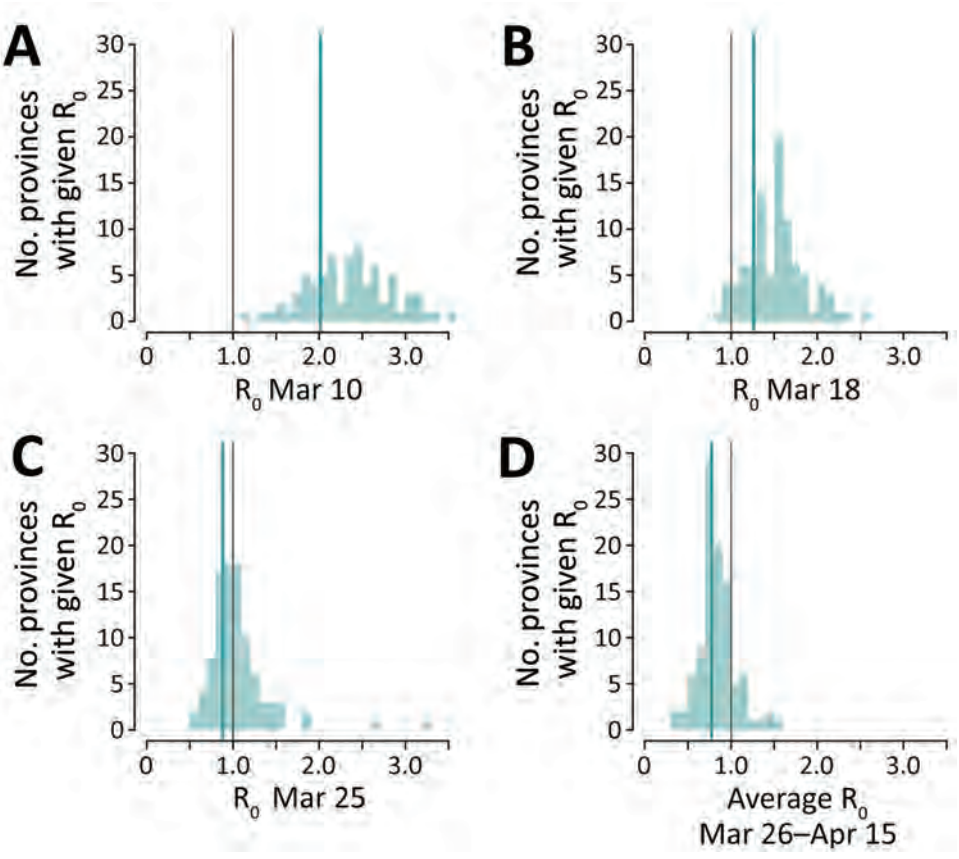


**Figure 2.** Distribution of the mean net reproduction numbers for severe acute respiratory syndrome coronavirus 2 in 100 selected provinces in Italy. Green lines indicate average value of $R_t$, weighted by the number of reported cases by each province. Gray line indicates epidemic threshold.

time series of hospitalized cases. Criteria for hospitalization are more homogeneous across local health systems and over time than testing criteria because they are grounded in the patient's need for medical assistance. Furthermore, the hospitalization date is an easier piece of information to collect with respect to the symptom onset date, which requires an epidemiologic investigation and may be subject to recall bias. Results obtained with this additional method were consistent with our conclusions (Appendix).

We did not consider asymptomatic cases in our analysis. The adopted methodology is robust even in the presence of large underdetection rates, provided that these rates are constant over time or even slightly fluctuating (*8*,*9*). We did not consider imported cases either, due to the lack of data; imported cases are potential infectors, but do not contribute to the number of transmitted cases, thereby lowering estimates of reproduction numbers. In Italy, most cases were probably locally transmitted. After March 11, the ban of movement across provinces imposed by the lockdown made the role of imported cases negligible. Reproduction numbers were computed using the distribution of serial interval for Italy (*10*; D. Cereda et al.), which is an acceptable approximation of the generation interval (*11*; S. Hu et al., unpub. data, https://10.1101/2020.07.23.20160317). Both distributions are strongly influenced by country-dependent variables, such as behavior of infected persons and the adopted interventions. Estimates of the generation interval distribution are still unavailable for Italy as of October 2020.

Italy was the first country outside of Asia to impose a nationwide lockdown, rapidly followed by many countries worldwide. The effectiveness of lockdown had been proven in China, where the reproduction number was estimated to fall to ≈0.3 in Wuhan (*12*) and 0.5 in other provinces (*8*); Western countries had enforced a comparatively softer version of restrictions. We have shown that these measures enabled rapid reversal of the epidemic trend within 2 weeks, although probably at higher values of the reproduction number.

Members of the COVID-19 working group: Maria Rita Castrucci, Alessandra Ciervo, Fortunato (Paolo) D'Ancona, Corrado Di Benedetto, Antonietta Filia, Stefania Giannitelli, Ornella Punzo, Maria Cristina Rota, Andrea Siddu, Paola Stefanelli, Marco Tallon, and Roberta Urciuoli (Istituto Superiore di Sanità); regional representatives: Antonia Petrucci (Abruzzo), Michele Labianca (Basilicata), Anna

Domenica Mignuoli (Calabria), Angelo D'Argenzio (Campania), Erika Massimiliani (Emilia-Romagna), Tolinda Gallo (Friuli Venezia Giulia), Paola Scognamiglio (Lazio), Camilla Sticchi (Liguria), Danilo Cereda (Lombardia), Daniel Fiacchini (Marche), Francesco Sforza (Molise), Maria Grazia Zuccaro (P.A. Bolzano), Pier Paolo Benetollo (P.A. Trento), Donatella Tiberti (Piemonte), Maria Chironna (Puglia), Maria Antonietta Palmas (Sardegna), Salvatore Scondotto (Sicilia), Emanuela Balocchini (Toscana), Anna Tosti (Umbria), Mauro Ruffier (Valle D'Aosta), and Filippo Da Re (Veneto).

G.G., V.M., P. Po., F.T., and S.M. acknowledge funding from the European Commission H2020 project MOOD and from the VRT Foundation Trento project "Epidemiologia e transmissione di COVID-19 in Trentino." M.A. has received research funding unrelated to COVID-19 from Seqirus.

## About the Author

Dr. Guzzetta is a researcher at the Bruno Kessler Foundation in Trento, Italy. His primary research interests are mathematical models of infectious disease transmission dynamics with a focus on public health applications, assessments of potential risks, and evaluation of effectiveness of interventions.

## References

1. Guzzetta G, Poletti P, Ajelli M, Trentini F, Marziano V, Cereda D, et al. Potential short-term outcome of an uncontrolled COVID-19 epidemic in Lombardy, Italy, February to March 2020. Euro Surveill. 2020;25:2000293. https://doi.org/10.2807/1560-7917.ES.2020.25.12.2000293
2. Decree of the Prime Minister. Further implementing provisions of the Decree-Law 23 February 2020, No. 6, with urgent measures in relation to containment and management of the epidemiological emergency from COVID-19, applicable throughout the country. (20A01605) G.U. General Series, no. 64 [in Italian]. 2020 Mar 11 [cited 2020 Oct 6]. http://www.trovanorme.salute.gov.it/norme/dettaglioAtto?id=73643
3. Riccardo F, Ajelli M, Andrianou X, Bella A, Del Manso M, Fabiani M, et al. Epidemiological characteristics of COVID-19 cases in Italy and estimates of the reproductive numbers one month into the epidemic. Euro Surveill. In press 2020.
4. Munayco CV, Tariq A, Rothenberg R, Soto-Cabezas GG, Reyes MF, Valle A, et al. Early transmission dynamics of COVID-19 in a southern hemisphere setting: Lima, Peru: February 29–March 30, 2020. Infect Dis Model. 2020;5:338–45. https://10.1016/j.idm.2020.05.001
5. Muniz-Rodriguez K, Fung IC-H, Ferdosi SR, Ofori SK, Lee Y, Tariq A, et al. Severe acute respiratory syndrome coronavirus 2 transmission potential, Iran, 2020. Emerg Infect Dis. 2020;26:1915–7. https://doi.org/10.3201/eid2608.200536
6. Park M, Cook AR, Lim JT, Sun Y, Dickens BL. A systematic review of COVID-19 epidemiology based on current evidence. J Clin Med. 2020;9:967. https://doi.org/10.3390/jcm9040967
7. Dipartimento di Protezione Civile. COVID-19 Italy—situation monitoring. Github [cited 2020 Oct 6]. https://github.com/pcm-dpc/COVID-19
8. Cori A, Ferguson NM, Fraser C, Cauchemez S. A new framework and software to estimate time-varying reproduction numbers during epidemics. Am J Epidemiol. 2013;178:1505–12. https://doi.org/10.1093/aje/kwt133
9. Zhang J, Litvinova M, Wang W, Wang Y, Deng X, Chen X, et al. Evolving epidemiology and transmission dynamics of coronavirus disease 2019 outside Hubei province, China: a descriptive and modelling study. Lancet Infect Dis. 2020;20:793–802. https://doi.org/10.1016/S1473-3099(20)30230-9
10. Lavezzo E, Franchin E, Ciavarella C, Cuomo-Dannenburg G, Barzon L, Del Vecchio C, et al.; Imperial College COVID-19 Response Team. Suppression of a SARS-CoV-2 outbreak in the Italian municipality of Vo'. Nature. 2020;584:425–9. https://doi.org/10.1038/s41586-020-2488-1
11. Ganyani T, Kremer C, Chen D, Torneri A, Faes C, Wallinga J et al. Estimating the generation interval for coronavirus disease (COVID-19) based on symptom onset data, March 2020. Euro Surveill 2020;25:2000257. https://doi.org/10.2807/1560-7917.ES.2020.25.17.2000257
12. Pan A, Liu L, Wang C, Guo H, Hao X, Wang Q, et al. Association of public health interventions with the epidemiology of the COVID-19 outbreak in Wuhan, China. JAMA. 2020.;323:1919–23. https://doi.org/10.1001/jama.2020.6130

Address for correspondence: Marco Ajelli, Department of Epidemiology and Biostatistics, Indiana University School of Public Health, 1025 E 7th St, Bloomington, IN 47405, USA; email: marco.ajelli@gmail.com

# Geographic Range of Recreational Water–Associated Primary Amebic Meningoencephalitis, United States, 1978–2018

Radhika Gharpure, Michelle Gleason, Zainab Salah, Anna J. Blackstock, David Hess-Homeier, Jonathan S. Yoder, Ibne Karim M. Ali, Sarah A. Collier,[1] Jennifer R. Cope[1]

*Naegleria fowleri* is a free-living ameba that causes primary amebic meningoencephalitis (PAM), a rare but usually fatal disease. We analyzed trends in recreational water exposures associated with PAM cases reported during 1978–2018 in the United States. Although PAM incidence remained stable, the geographic range of exposure locations expanded northward.

Primary amebic meningoencephalitis (PAM) is a rare but usually fatal brain infection caused by *Naegleria fowleri,* a free-living ameba found in soil and warm freshwater (*1*,*2*). The ameba enters the brain via the nasal passages, causing an acute brain infection that usually results in death within 3–7 days of symptom onset. *N. fowleri* is frequently detected in warm freshwater (*3*–*6*); however, ≤8 cases of PAM are reported each year in the United States (*2*). Generally, US PAM cases occur after recreational exposure to warm, untreated freshwater in US southern states during the summer (*2*).

*N. fowleri* is thermophilic, preferring high temperatures of up to 45°C (*7*). However, the ameba tolerates a range of conditions by changing its morphology in response to the environment: it feeds and reproduces in the trophozoite form; assumes a more mobile, flagellated form in low nutrient environments; and forms a resistant cyst in adverse conditions, such as cold temperatures (*1*,*8*). The thermophilic nature of *N. fowleri* suggests it might be sensitive to global changes in surface temperature (*9*–*12*). Analysis of recreational water exposures resulting in PAM could aid risk prediction, prevention, and public communication efforts.

Author affiliation: Centers for Disease Control and Prevention, Atlanta, Georgia, USA

DOI: https://doi.org/10.3201/eid2701.202119

The US Centers for Disease Control and Prevention (CDC) maintains a database of reported PAM cases in the United States since 1962, cataloging information about dates, locations, and suspected exposures (*2*). In 1978, CDC established its Free-living Ameba Laboratory, which increased the national capacity for clinical testing and contributed to an increase in the number of reported PAM cases in the United States. We analyzed to PAM cases reported in the USA during 1978–2018 with known or suspected recreational water exposure in a lake, pond, reservoir, river, stream, or outdoor aquatic venue.

## The Study

For this study, we included cases with a single known exposure site or multiple sites within an 80 km radius. We conducted negative binomial regression to assess trends in annual PAM incidence. We mapped exposure locations according to regions defined by the United States Census Bureau using ArcMap version 10.5 GIS software (Esri, https://www.arcgis.com). We categorized the exposures into quartiles by case year and evaluated the latitudes of exposure locations using Kruskal-Wallis tests for overall comparisons and Dwass-Steel-Critchlow-Fligner tests for pairwise comparisons. We used linear regression to examine trends in annual maximum (i.e., northernmost) and minimum (i.e., southernmost) latitudes of the exposures. We conducted sensitivity analyses to determine the effect of excluding years with single cases and excluding outliers on the basis of leverage, Cook's distance, and studentized residual values.

In the temperature analysis, we included patients with a known or imputed date of exposure

[1]These senior authors contributed equally to this article.

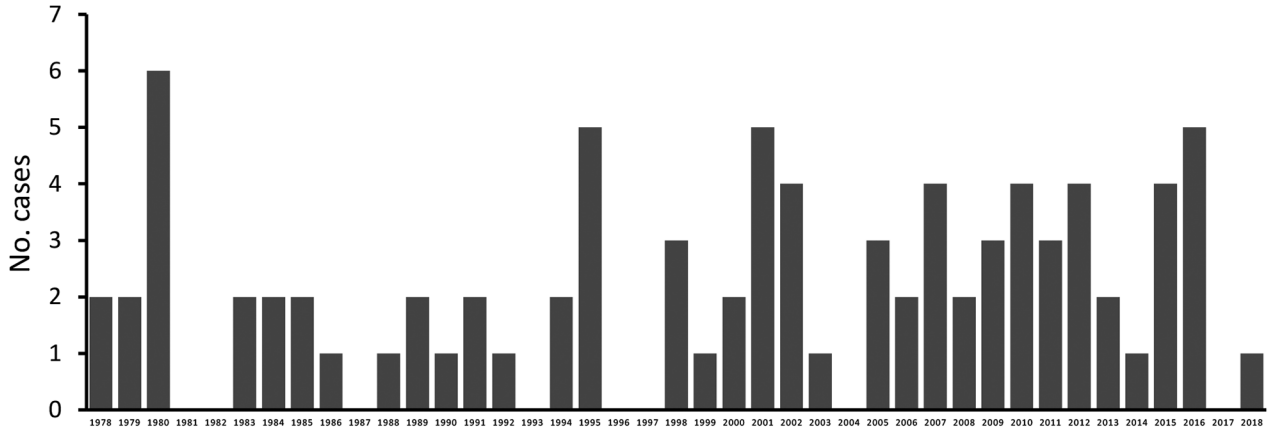


Figure 1. Annual incidence of primary amebic meningoencephalitis cases associated with recreational water exposures, United States, 1978–2018. Negative binomial regression did not detect a trend in the annual incidence of cases (relative risk = 1.015; p = 0.16).

(Appendix, https://wwwnc.cdc.gov/EID/article/27/1/20-2119-App1.pdf). We obtained temperature records from the National Oceanic and Atmospheric Administration's National Climatic Data Center (http://www.ncdc.noaa.gov/cdo-web) from the weather station closest to each exposure location (maximum distance of 50 km). We used generalized estimating equation models to compare daily temperatures from the 2 weeks before exposure with average temperatures from the same location and calendar dates from the 20 years before exposure. We selected an autoregressive correlation structure using quasi-likelihood under the independence model criterion. We analyzed data with SAS 9.4 (SAS Institute, https://www.sas.com).

Among 120 PAM cases reported to CDC's free-living ameba database during 1978–2018, a total of 85 patients had an eligible known or suspected recreational water exposure: 69 patients at a lake, pond, or reservoir; 14 patients at a river or stream; and 2 patients at an outdoor aquatic venue. We excluded 35 patients who were exposed at canals, puddles, or ditches; to geothermally heated water or tap water; at unknown locations; or at multiple locations >80 km apart.

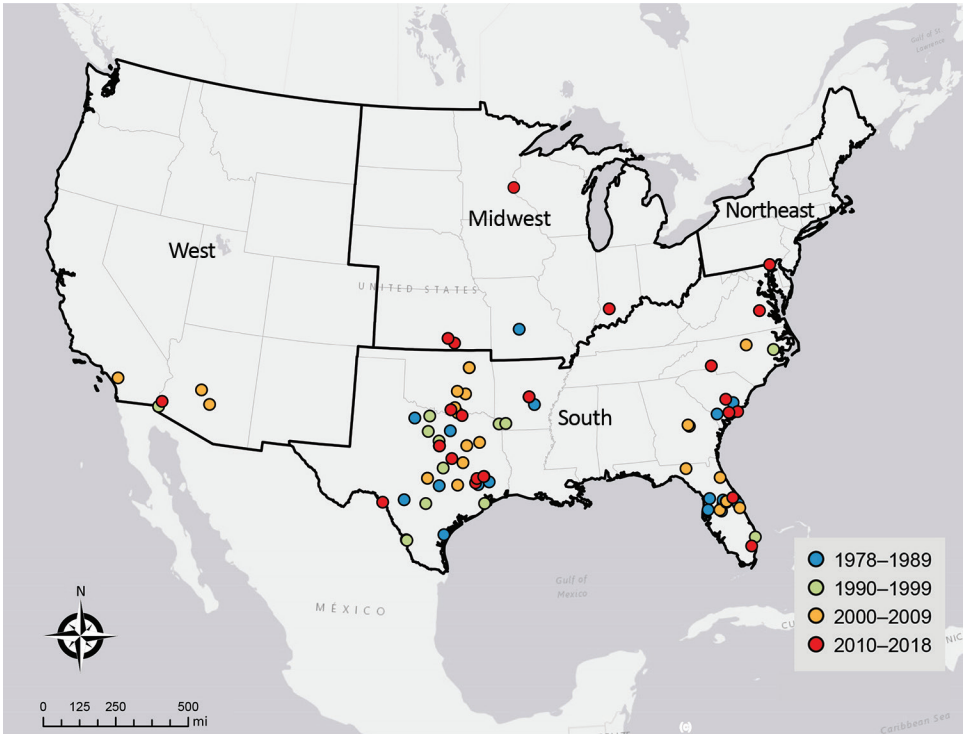


**Figure 2.** Locations of recreational water exposures associated with cases of primary amebic meningoencephalitis, United States, 1978–2018. Labels indicate US Census Bureau regions.

**Table.** Recreational water–associated primary amebic meningoencephalitis, United States, 1978–2018

| Years | No. cases | Median latitude, decimal degrees (range) | p value* |
|---|---|---|---|
| 1978–1989 | 20 | 30.3 (27.8–38.0) | Referent |
| 1990–1999 | 15 | 32.5 (26.5–35.5) | 0.90 |
| 2000–2009 | 26 | 32.3 (28.1–36.1) | 0.47 |
| 2010–2018 | 24 | 33.6 (26.1–45.0) | 0.02 |

*Pairwise comparison to reference group using Dwass-Steel-Critchlow-Fligner test.

The incidence of PAM associated with recreational water exposures ranged from 0–6 cases per year during 1978–2018 in the United States (Figure 1). Negative binomial regression did not detect a trend in annual incidence (relative risk [RR] = 1.015; p = 0.16). Among case exposures, 74 occurred in the South and 5 in the West (Figure 2). Six case exposures occurred in the Midwest, 5 of which occurred after 2010 (Minnesota [2010], Kansas [2011], Minnesota [2012], Indiana [2012], and Kansas [2014]).

PAM cases occurred in 33 of the 41 study years. We categorized the case exposures into quartiles by case year: 1978–1989, 1990–1999, 2000–2009, and 2010–2018. The median latitudes of case exposures in the 4 quartiles differed by Kruskal-Wallis analysis (p = 0.02); pairwise comparisons showed an increase in the median latitude of the final quartile, 2010–2018, in comparison to the first quartile, 1978–1989 (p = 0.02) (Table). We modeled the maximum latitude and observed an annual increase of 0.12 decimal degrees (95% CI 0.01–0.20; p = 0.04), equivalent to a shift of ≈13.3 km northward per year. We did not observe a change in the minimum latitude (0.04 decimal degrees, 95% CI -0.04 to 0.10; p = 0.30). We used sensitivity analyses to confirm a northward trend in maximum latitude (Appendix).

Among 85 cases, 81 (95%) had a known or imputed exposure date. Air temperatures varied widely in the 2 weeks before exposure (Appendix Figure). On average, daily temperatures were higher in the 2 weeks before exposure than the 20-year average for that date and location: high temperatures were 0.77°C greater (p<0.01), and low temperatures were 0.76°C greater (p<0.01) than the 20-year average.

## Conclusions

The rise in cases in the Midwest region after 2010 and increases in maximum and median latitudes of PAM case exposures suggest a northward expansion of *N. fowleri* exposures associated with lakes, ponds, reservoirs, rivers, streams, and outdoor aquatic venues in the United States. We observed an increase in air temperatures in the 2 weeks before exposures compared with 20-year historic averages. It is possible that rising temperatures and consequent increases in recreational water use, such as swimming and water sports, could contribute to the changing epidemiology of PAM. Although reported incidence of PAM has increased worldwide (*12*,*13*), the incidence of reported cases of PAM in the United States remained stable during 1978–2018. The worldwide trends might reflect changes in international diagnostic capacity (*13*).

This study is subject to limitations. First, PAM is probably underrecognized and underreported in the United States (*14*), so these data might not fully capture trends in incidence and exposure characteristics. Second, temperature data were not collected simultaneously with exposure, and thus might differ from actual exposure conditions. Our analysis used air temperatures because water temperature records were unavailable for most exposure sites. However, prior studies have indicated that air temperature is the main driver for lake surface temperatures (*15*) and thus is an appropriate proxy. Third, our analysis included years with single cases, which could bias the results of the regression analyses of latitude. However, our sensitivity analysis indicated that these years did not change our findings.

In summary, our results show a suggested northward expansion of PAM and its potential association with higher temperatures warrants further investigation. Characterizing recreational water exposures could improve risk prediction and prevention strategies, helping to prevent cases, aid natural resource custodians, and reduce burden on state and local health departments.

### Acknowledgments

We thank Vincent R. Hill, Michael J. Beach, and Govinda S. Visvesvara for contributions to analysis conception and Andrew K. Hennenfent for collation of environmental data.

## About the Author

Dr. Gharpure is an Epidemic Intelligence Service officer in the Waterborne Disease Prevention Branch, Division of Foodborne, Waterborne, and Environmental Diseases, National Center for Emerging and Zoonotic Infectious Diseases, Centers for Disease Control and Prevention, Atlanta, Georgia, USA. Her research interests include infectious diseases at the intersection of human, animal, and environmental health.

## References

1. Visvesvara GS, Moura H, Schuster FL. Pathogenic and opportunistic free-living amoebae: *Acanthamoeba* spp., *Balamuthia mandrillaris, Naegleria fowleri*, and *Sappinia diploidea*. FEMS Immunol Med Microbiol. 2007;50:1–26. https://doi.org/10.1111/j.1574-695X.2007.00232.x
2. Yoder JS, Eddy BA, Visvesvara GS, Capewell L, Beach MJ. The epidemiology of primary amoebic meningoencephalitis in the USA, 1962–2008. Epidemiol Infect. 2010;138:968–75. https://doi.org/10.1017/S0950268809991014
3. Wellings FM, Amuso PT, Chang SL, Lewis AL. Isolation and identification of pathogenic *Naegleria* from Florida lakes. Appl Environ Microbiol. 1977;34:661–7. https://doi.org/10.1128/AEM.34.6.661-667.1977
4. John DT, Howard MJ. Seasonal distribution of pathogenic free-living amebae in Oklahoma waters. Parasitol Res. 1995;81:193–201.
5. Ettinger MR, Webb SR, Harris SA, McIninch SP, C Garman G, Brown BL. Distribution of free-living amoebae in James River, Virginia, USA. Parasitol Res. 2003;89:6–15. https://doi.org/10.1007/s00436-002-0707-3
6. Maclean RC, Richardson DJ, LePardo R, Marciano-Cabral F. The identification of *Naegleria fowleri* from water and soil samples by nested PCR. Parasitol Res. 2004;93:211–7. https://doi.org/10.1007/s00436-004-1104-x
7. de Jonckheere J, Voorde H. The distribution of *Naegleria fowleri* in man-made thermal waters. Am J Trop Med Hyg. 1977;26:10–5. https://doi.org/10.4269/ajtmh.1977.26.10
8. Chang S-L. Resistance of pathogenic *Naegleria* to some common physical and chemical agents. Appl Environ Microbiol. 1978;35:368–75. https://doi.org/10.1128/AEM.35.2.368-375.1978
9. Kemble SK, Lynfield R, DeVries AS, Drehner DM, Pomputius WF III, Beach MJ, et al. Fatal *Naegleria fowleri* infection acquired in Minnesota: possible expanded range of a deadly thermophilic organism. Clin Infect Dis. 2012;54:805–9. https://doi.org/10.1093/cid/cir961
10. Yoder JS, Straif-Bourgeois S, Roy SL, Moore TA, Visvesvara GS, Ratard RC, et al. Primary amebic meningoencephalitis deaths associated with sinus irrigation using contaminated tap water. Clin Infect Dis. 2012;55:e79–85. https://doi.org/10.1093/cid/cis626
11. Gompf SG, Garcia C. Lethal encounters: the evolving spectrum of amoebic meningoencephalitis. IDCases. 2019;15:e00524. https://doi.org/10.1016/j.idcr.2019.e00524
12. Maciver SK, Piñero JE, Lorenzo-Morales J. Is *Naegleria fowleri* an emerging parasite? Trends Parasitol. 2020;36:19–28. https://doi.org/10.1016/j.pt.2019.10.008
13. Gharpure R, Bliton J, Goodman A, Ali IKM, Yoder J, Cope JR. Epidemiology and clinical characteristics of primary amebic meningoencephalitis caused by *Naegleria fowleri*: a global review. Clin Infect Dis. 2020;ciaa520. https://doi.org/10.1093/cid/ciaa520
14. Matanock A, Mehal JM, Liu L, Blau DM, Cope JR. Estimation of undiagnosed *Naegleria fowleri* primary amebic meningoencephalitis, United States. Emerg Infect Dis. 2018;24:162–4. https://doi.org/10.3201/eid2401.170545
15. Schmid M, Hunziker S, Wüest A. Lake surface temperatures in a changing climate: a global sensitivity analysis. Clim Change. 2014;124:301–15. https://doi.org/10.1007/s10584-014-1087-2


Address for correspondence: Radhika Gharpure, Centers for Disease Control and Prevention, 1600 Clifton Rd NE, Mailstop H24-10, Atlanta, GA 30329-4027, USA; email: krr4@cdc.gov

# Emerging Human Metapneumovirus Gene Duplication Variants in Patients with Severe Acute Respiratory Infection, China, 2017–2019

Zhibo Xie, Jin Xu, Yunhui Ren, Aili Cui, Huiling Wang, Jinhua Song, Qiang Zhang, Manli Hu, Wenbo Xu, Yan Zhang

We detected human metapneumovirus (HMPV) in 72 (7.1%) of 1,021 patients hospitalized with severe acute respiratory infection in Luohe, China, during 2017–2019. We detected HMPV most frequently in young children and less often in adults. HMPV genotype A2c variants 111 nt and 180 nt duplications predominated, demonstrating their continuing geographic spread.

Human metapneumovirus (HMPV; family *Pneumoviridae*, genus *Metapneumovirus*) is a major cause of acute respiratory tract infections, especially in children and elderly persons (*1*,*2*). Its genome is ≈13.2 kb, containing 8 genes encoding 9 proteins. The G gene, around 654–867 nt acids sequence length, is the most variable nucleotide sequence in the whole genome of HMPV and has been widely used to study HMPV genetic variation (*3*–*5*). HMPV has 1 serotype with 2 subgroups A and B, further divided into 5 genotypes, including A1, A2a, A2b, B1, and B2, based mainly on variations in the G gene (*4*,*6*,*7*). Recently, unique HMPV variants possessing a 180 nt duplication (nt-dup) in the G gene, first reported in Spain, and a 111 nt-dup in the G gene, first reported Japan (*5*,*8*,*9*), followed by Croatia and Guangdong, China (*10*,*11*). These variants were clustered in the A2c lineage of the phylogenetic tree (*11*). In this study, we investigated the prevalence of HMPV associated with patients with severe acute respiratory infection (SARI) and identified genetic variations in the G gene of HMPV in Luohe, in Henan Province, China, during 2017–2019.

Author affiliations: National Institute for Viral Disease Control and Prevention, Beijing, China (Z. Xie, A. Cui, H. Wang, J. Song, Q. Zhang, M. Hu, W. Xu, Y. Zhang); Henan Provincial Center for Disease Control and Prevention, Zhengzhou, China (J. Xu); Luohe Prefectural Center for Disease Control and Prevention, Luohe, China (Y. Ren)

DOI: https://doi.org/10.3201/eid2701.201043

## The Study

Luohe is a city of 2.8 million people in Henan Province, northern China. In this study, we collected throat swab specimens and clinical data from 1,021 patients with SARI admitted to Luohe Central Hospital during October 2017–June 2019. Patients were 1 month–95 (median 3) years of age; most (76.7%) of the SARI cases involved children <5 years old. All swab specimens were tested by multiplex real-time reverse transcription PCR assay using a nucleic acid diagnostic kit (Kinghawk, http://www.kinghawk828.com), which identifies HMPV, influenza types A and B, human respiratory syncytial virus (RSV), human coronaviruses, human rhinovirus and enterovirus, human adenovirus, human parainfluenza viruses, and human bocavirus.

Overall, 83.2% (849/1021) of SARI patients were positive for ≥1 respiratory viruses; human adenovirus was the predominant virus identified, at 22% (225/1021). HMPV was identified in 7.1% (72/1021) of SARI patients, consistent with other studies that identified HMPV in 6%–12% of SARI cases (*12*,*13*). The proportion of HMPV-positive patients with co-detected respiratory viruses was 63.9% (46/72). The rates of HMPV positivity decreased gradually with age, from 9.1% in those <2 years old to 0.9% in adults (Table 1). The epidemic season for HMPV lasted from November through May or June, with the peak number of cases occurring in March and May in 2018 and March in 2019 (Figure 1). Most (98.5%) HMPV-positive

**Table 1.** Age composition of the 1,021 SARI patients with HMPV-positive samples from patients with SARI admitted to Luohe Central Hospital, Luohe, China, during October 2017–June 2019*

| Age, y | SARI | HMPV-positive | HMPV-positive, by age, total, % |
|---|---|---|---|
| <2 | 385 | 35 (9.1) | 48.6 |
| 2–4 | 351 | 26 (7.4) | 36.1 |
| 5–17 | 171 | 10 (5.9) | 13.9 |
| 18–95 | 113 | 1 (0.9) | 1.4 |
| Total | 1,021 | 72 (7.1) | 100.0 |

*HMPV, human metapneumovirus; SARI, severe acute respiratory infection.

patients in this study exhibited cough or dyspnea and were diagnosed with bronchopneumonia (74.6%). No clear differences in clinical signs and symptoms were apparent among the patients infected with duplication variants compared with other HMPV viruses.

Forty-three entire coding-region sequences of the G gene were obtained from 72 HMPV-positive samples, as described elsewhere (*3*,*5*,*6*) (Table 2). The nucleotide sequences generated in this study were submitted to GenBank (accession nos. MN944056–97). We selected 86 subgroup A sequences (54 from GenBank and 32 from this study) and 23 subgroup B sequences (12 from GenBank and 11 from this study) to construct the phylogenetic tree by maximum-likelihood method (Figure 2, https://wwwnc.cdc.gov/EID/article/27/1/20-1043-F2.htm). The HMPV sequences obtained in this study were clustered into 4 genotypes, including A2c, A2b, B1, and B2 (Table 2; Figure 2). Twenty-eight out of 31 A2c sequences were grouped together in 1 distinct cluster with the duplication variants, mainly detected in Spain, Japan, Croatia, and Guangzhou, China. In the sequence alignment comparison analysis, we identified 22 viruses containing 111 nt-dup variants and 6 viruses contained 180 nt-dup variants in the G gene. The 111 nt-dup variants were detected in Luohe in 2018 and continued to spread in 2019, while 180 nt-dup variants were detected during 2017 and 2018 (Table 2). The 111 nt-dup variants were separated from the 180 nt-dup variants in the phylogenetic tree, which indicates that the 2 duplication variants evolved by independent patterns in different evolutionary lineages (Figure 2, panel A).

The twenty-two 111 nt-dup variants circulating in Luohe during 2018–2019 were closely related to the duplication-variant viruses identified in Japan, Croatia, and Guangdong, China, in 2017, with nucleotide identity of 95.7% to 100%. Six 180 nt-dup variants circulating in Luohe during 2017–2018 were clustered in 1 small cluster with high nucleotide identity at 99.1% and 100% and closely related to the duplication viruses identified in Japan, Croatia, Spain, and Beijing, China, during 2014–2017 (Figure 2A). This finding indicates that the 111 nt-dup and 180 nt-dup variants have already spread and might spread extensively throughout the world.

## Discussion

Our findings show that 7.1% of SARI patients in the Luohe study tested positive for HMPV during 2017–2019. The rate of HMPV-positivity decreased gradually with patient age. Among the HMPV patients, 63.9% were co-infected with other respiratory viruses. Four different genotypes were cocirculating, including A2b, A2c, B1, and B2. We identified most of

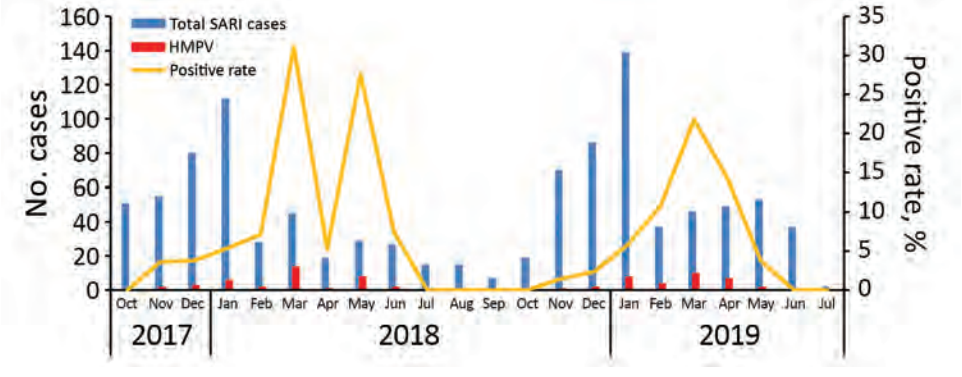


**Figure 1.** Distribution by month of SARI cases and HMPV-positive rates in Luohe, China, 2017–2019. HMPV, human metapneumovirus; SARI, severe acute respiratory infection.

**Table 2**. Distribution of HMPV positive samples and genotypes by year among patients with SARI admitted to Luohe Central Hospital, Luohe, China, during October 2017–June 2019*

| Year (months) | HMPV-positive samples | Total sequences obtained | A2b | A2c | | | B1 | B2 |
|---|---|---|---|---|---|---|---|---|
| | | | | Non-dup | 111 nt-dup | 180 nt-dup | | |
| 2017 (Oct–Dec) | 5 | 1 | 0 | 0 | 0 | 1 | 0 | 0 |
| 2018 (Jan–Dec) | 36 | 21 | 0 | 3 | 9 | 5 | 3 | 1 |
| 2019 (Jan–Jun) | 31 | 21 | 1 | 0 | 13 | 0 | 2 | 5 |
| Total | 72 | 43 | 1 | 3 | 22 | 6 | 5 | 6 |

*dup, duplication; HMPV, human metapneumovirus; SARI, severe acute respiratory infection.

the A2c viruses as duplication variants, including the 111 nt-dup and 180 nt-dup variants, and found that these 2 variants were the predominant viruses circulating in Luohe during 2017–2019.

The 111 nt-dup and 180 nt-dup variants have also been detected in different regions of the world, including in Spain, Japan, Croatia, and Guangzhou, China, in recent years (*5*,*8*–*11*). Similar duplications in the G gene have been reported in HRSV, another member of the family *Pneumoviridae*. The HRSV duplication variants of both BA9 and ON1 have rapidly spread globally, becoming the predominant viruses in many countries for many years (*14*,*15*). These findings suggest that the emerging HMPV 111 nt-dup and 180 nt-dup variants might also become predominant viruses throughout the world.

There were some limitations in this study. The epidemic seasons were not covered for the entire 3 years, and only 1 hospital was involved in this study. Continuous surveillance will be required to determine whether these novel HMPV 111 nt-dup and 180 nt-dup variants will persist as predominant viruses and have a wider geographic distribution in the future.

Although no difference in clinical symptoms was observed between the patients infected with HMPV duplication variants and those with non–duplication-variant viruses in this study, the increased transmission frequency of the duplication variants suggests a role for duplication in the G gene in potentially expanding its transmission. Therefore, further study is needed to clarify if and how the duplications result in an evolutionary advantage for HMPV.

This work was supported by the National Natural Science Foundation of China (project no. 81772195), and the Key Technologies R&D Program of the National Ministry of Science (2018ZX10713002, 2018ZX10711001, 2017ZX10104001-002, and 2018ZX10713001-003).

## About the Author

Dr. Xie is a master degree student at the China CDC. Her research focuses on the epidemiology and genetic variations of human metapneumovirus and human respiratory syncytial virus.

## References

1. Esposito S, Mastrolia MV. Metapneumovirus infections and respiratory complications. Semin Respir Crit Care Med. 2016;37:512–21. https://doi.org/10.1055/s-0036-1584800
2. Rima B, Collins P, Easton A, Fouchier R, Kurath G, Lamb R, et al. ICTV virus taxonomy profile: Pneumoviridae. J Gen Virol. 2017;98:2912–3. https://doi.org/10.1099/jgv.0.000959
3. van den Hoogan BG, Herfst S, Sprong L, Cane PA, Forleo-Neto E, de Swart RL, et al. Antigenic and genetic variability of human metapneumoviruses. Emerg Infect Dis. 2004;10:658–66. https://doi.org/10.3201/eid1004.030393
4. Knipe DM, Howley PM, editors. Fields Virology. 6th ed. Philadelphia: Lippincott Williams & Wilkins; 2013.
5. Saikusa M, Kawakami C, Nao N, Takeda M, Usuku S, Sasao T, et al. 180-nucleotide duplication in the G gene of Human metapneumovirus A2b subgroup strains circulating in Yokohama City, Japan, since 2014. Front Microbiol. 2017;8:402. https://doi.org/10.3389/fmicb.2017.00402
6. Huck B, Scharf G, Neumann-Haefelin D, Puppe W, Weigl J, Falcone V. Novel human metapneumovirus sublineage. Emerg Infect Dis. 2006;12:147–50. https://doi.org/10.3201/eid1201.050772
7. Kim HR, Cho AR, Lee M, Yun SW, Kim T. Genotype variability and clinical features of human metapneumovirus isolated from Korean children, 2007 to 2010. J Mol Diagn. 2012;14:61–4. https://doi.org/10.1016/j.jmoldx.2011.09.004
8. Piñana M, Vila J, Gimferrer L, Valls M, Andrés C, Codina MG, et al. Novel human metapneumovirus with a 180-nucleotide duplication in the G gene. Future Microbiol. 2017;12:565–71. https://doi.org/10.2217/fmb-2016-0211
9. Saikusa M, Nao N, Kawakami C, Usuku S, Tanaka N, Tahara M, et al. Predominant detection of the subgroup A2b human metapneumovirus strain with a 111-nucleotide duplication in the G gene in Yokohama City, Japan in 2018. Jpn J Infect Dis. 2019;72:350–2. https://doi.org/10.7883/yoken.JJID.2019.124
10. Jagusic M, Slovic A, Ivancic-Jelecki J, Ljubin-Sternak S, Vilibić-Čavlek T, Tabain I, et al. Molecular epidemiology of human respiratory syncytial virus and human metapneumovirus in hospitalized children with acute respiratory infections in Croatia, 2014–2017. Infect Genet Evol. 2019;76:104039. https://doi.org/10.1016/j.meegid.2019.104039
11. Yi L, Zou L, Peng J, Yu J, Song Y, Liang L, et al. Epidemiology, evolution and transmission of human metapneumovirus in Guangzhou China, 2013–2017. Sci Rep. 2019;9:14022. https://doi.org/10.1038/s41598-019-50340-8
12. Al Amad MA, Al Mahaqri AA, Al Serouri AA, Khader YS. Severe acute respiratory infections with influenza and noninfluenza respiratory viruses: Yemen, 2011–2016. Inquiry. 2019;56:46958019850731. https://doi.org/10.1177/0046958019850731
13. Breiman RF, Cosmas L, Njenga MK, Williamson J, Mott JA, Katz MA, et al. Severe acute respiratory infection in children in a densely populated urban slum in Kenya, 2007–2011. BMC Infect Dis. 2015;15:95. https://doi.org/10.1186/s12879-015-0827-x
14. Song J, Wang H, Shi J, Cui A, Huang Y, Sun L, et al. Emergence of BA9 genotype of human respiratory syncytial virus subgroup B in China from 2006 to 2014. Sci Rep. 2017;7:16765. https://doi.org/10.1038/s41598-017-17055-0
15. Song J, Zhang Y, Wang H, Shi J, Sun L, Zhang X, et al. Emergence of ON1 genotype of human respiratory syncytial virus subgroup A in China between 2011 and 2015. Sci Rep. 2017;7:5501. https://doi.org/10.1038/s41598-017-04824-0

Address for correspondence: Yan Zhang and Wenbo Xu, National Institute for Viral Disease Control and Prevention, China Center for Disease Control and Prevention, No. 155, Changbai Road, Changping District, Beijing 102206, China; email: zhangyan9876543@163.com and wenbo_xu1@aliyun.com.

# Fatal 3-Nitropropionic Acid Poisoning after Consuming Coconut Water

Thomas Birkelund, Rakel F. Johansen, Dorte G. Illum, Stig Eric Dyrskog, Jakob A. Østergaard, Travis M. Falconer, Chris Andersen, Helena Fridholm, Søren Overballe-Petersen, Jørgen S. Jensen

We describe the fatal course of a patient with initial symptoms of vomiting and nausea who developed symptoms of dystonia, encephalopathy, and coma. The cause of death was poisoning with 3-nitropropionic acid from coconut water spoiled with the fungus *Arthrinium saccharicola*. We present the clinical findings and forensic analysis.

A 69-year old Caucasian man was admitted to Aarhus University Hospital, Aarhus, Denmark, in a state of reduced consciousness and Glasgow Coma Scale (GCS) score of 13–14. Approximately 4.5 hours before admission, the patient had consumed coconut water directly from a coconut using a straw. Because the water had a foul taste, he swallowed only a small amount. Afterward, he opened the nut and described to his wife that the interior was slimy and looked rotten.

The coconut was preshaved, with visible endosperm (coconut meat) at the top for easy access to the carpels (holes) and the coconut water. A straw was included and used for puncturing the coconut at the time of consumption (Figure). Recommended storage was at 4°C–5°C in the refrigerator, but the coconut had been kept on the kitchen table for 1 month after purchase.

Approximately 3 hours after drinking the coconut water, the patient developed sweating, nausea, and vomiting. Ambulance attendants found the patient in distress with pale and clammy skin, reduced mental state with confusion, dystonia, and poor balance but normal strength in the extremities. The patient was able to answer questions with delay and had no local neurologic deficits.

At the emergency department, the patient's consciousness level descended to GCS 3. A computed tomography angiography of the cerebrum, thorax, abdomen, and pelvis was performed and showed no abnormalities. Blood pressure was 200/110 mm Hg; pupils were small and reactive to light. The physical exam, including the abdomen, was unremarkable. An electrocardiogram showed sinus tachycardia of 130 beats/min with new right bundle branch block, which had not been present on an electrocardiogram 7 months earlier. Body temperature was 37.5°C.

Arterial blood gas analysis revealed metabolic acidosis with a pH of 7.29, $PaCO_2$ of 2.1 kPa (reference 9.6–13.7 kPa), base excess -18.3 mmol/L (reference -1.5 to –3.0 mmol/L), lactate level of 10.9 mmol/L (reference 0.5–2.5 mmol/L), and unremarkable strong ion difference. Elevated 3-hydroxybutyrate level of 2.2 mmol/L (reference <0.3 mmol/L) and slightly elevated blood glucose of 9.5 mmol/L (reference 4.2–7.8 mmol/L) were found. Other initial blood samples were unremarkable. Carbon monoxide was not detected.

The patient was brought to the intensive care unit 2 hours after his arrival at the hospital. At this point he had pronation and jerks of the forearms and calves and his body temperature had increased to 39.7°C. The patient was intubated and actively cooled to 37.5°C. Treatment for meningitis and encephalitis (penicillin, ceftriaxone, and acyclovir) was initiated and insulin was administered, keeping blood glucose at 5–10 mmol/L. Pinpoint pupils were noted; to rule out opioid intoxication, naloxone was administered, with no response. The patient had stable hemodynamics at the intensive care unit. High diuresis of ≤450 mL/hour was noticed. Interviews with the family provided no reason to suspect intake of acetaminophen, salicylic acid, methanol, glycols, or other acids

Author affiliations: Prehospital Emergency Medical Services, Central Denmark Region, Denmark (T. Birkelund); Aarhus University Hospital, Aarhus, Denmark (T. Birkelund, R.F. Johansen, D.G. Illum, S.E. Dyrskog, J.A. Østergaard); US Food and Drug Administration, Cincinnati, Ohio, USA (T.M. Falconer); Aarhus University, Aarhus (C. Andersen); Statens Serum Institut, Copenhagen, Denmark (H. Fridholm, S. Overballe-Petersen, J.S. Jensen)

DOI: https://doi.org/10.3201/eid2701.202222

or drugs or a suicide attempt. A urine drug screen was negative except for opioids, which had been administered to facilitate intubation.

Lumbar puncture was performed 11 and 22 hours after admission. No blood, leukocytes, or protein were detected. PCR examination for bacteria and herpes encephalitis, including cultures, was negative. EEG showed nonspecific abnormalities without seizure activity or reactivity on stimulation.

Fourteen hours after admission, magnetic resonance imaging of the cerebrum demonstrated global diffusion restrictions in the white matter. T2-weighted fluid-attenuated inversion recovery signal showed edema in the putamen, hippocampi, and cerebellum. Judging by the magnetic resonance imaging findings, severe toxic/metabolic encephalopathy was suspected. Sixteen hours after admission, new blood samples revealed levels of ammonia 100 μmol/L (reference <50 μmol/L), myoglobin 1,635 μg/L (reference <75 μg/L) and creatine kinase 905 U/L (reference 50–200 U/L). Approximately 24 hours after admission, a new computed tomography scan of the cerebrum showed severe edema, especially in the infratentorial region, with impending signs of brain herniation. The pupils were dilated, brainstem reflexes were absent, and the patient had no spontaneous respiration. The patient was not sedated at any point during treatment. Twenty-six hours after admission to the hospital, the clinical appearance and imaging indicated clinical brain death, and treatment was discontinued.

Medicolegal autopsy of the cerebrum showed sporadic microscopic bleedings in the basal ganglia. Analysis of tracheal aspirate revealed growth of the fungus *Rhizopus arrhizus*. Because the patient developed symptoms after intake of a coconut product, intoxication with bongkrekic acid was suspected. This mitochondrial toxin is produced by the bacterium *Burkholderia gladioli* pathovar cocovenenans (*B. cocovenenans*) and has been implicated in outbreaks of foodborne illness involving coconut products in Asia (*1*). We therefore analyzed a part of the coconut. Culture revealed growth of *Pseudomonas* species and *R. arrhizus*. Because some *Rhizopus* spp. carry *Burkholderia* spp. as symbionts (*2*), we subjected DNA from the fungal isolate to PCR with primers targeting universal bacterial 16S rRNA gene sequences, but no amplification of bacterial DNA was seen.

We subjected DNA extracted from the coconut to microbiota characterization with Illumina sequencing (https://www.illumina.com) of 16S and 18S rRNA gene products amplified with universal primers (*3*); among eukaryotic 18S sequences, most were identified as *Arthrinium* spp. and *R. arrhizus*, which were isolated from the coconut. Most bacterial 16S sequences were mapped to *Pseudomonas fragi*, a common spoilage bacterium. No sequences were mapped to *Burkholderia* spp.

**Figure.** The type of ecologically grown coconut involved in the case of a 69-year old Caucasian man in Aarhus, Denmark, who died of poisoning with 3-nitropropionic acid from coconut water spoiled with the fungus *Arthrinium saccharicola*. The coconut was commercially prepared, including removal of the husk, and was sold as ready-to-drink, with an included punch and straw for easy access to the carpels (holes) and the coconut water.

Because of the strong suspicion of bongkrekic acid, we tested extracted DNA with 3 *Burkholderia*-specific PCR assays (developed for differentiation of *B. cocovenenans* from other species [*4*]); all results were negative. We sent pieces of the coconut endosperm for detection of bongkrekic acid to the US FDA Forensic Chemistry Center (Cincinnati, Ohio, USA), which has developed a method for the detection of bongkrekic acid (*5*,*6*). However, neither bongkrekic acid nor the isomer isobongkrekic acid could be detected at a level of ≥4 μg/g.

We instilled homogenized coconut via gastric tube in a set of 3 mice, but no toxicity was observed, even after prolonged observation. Metagenomic sequencing using MinION sequencing (Oxford Nanopore Technologies, https://nanoporetech.com) initially revealed only *Pseudomonas* species using Oxford Nanopore's online tools. However, upon further analysis with the tool K-Mer Aligner (*7*), *Arthrinium saccharicola* was mapped at 145× coverage, *Arthrinium* mitochondria at 180×, and *Pseudomonas* sp. at 290×.

## Conclusions

Fungi of the *Arthrinium* genus produce the lipophilic and highly toxic 3-nitropropionic acid (3-NPA), which is involved in the etiology of moldy sugar cane poisoning (*8*) with severe encephalopathy (*9*). 3-NPA irreversibly binds to and inhibits succinate dehydrogenase in the mitochondria, thereby blocking the citric acid cycle and ATP generation in cells, which would explain the observed severe lactate acidosis. Other proposed mechanisms include increased generation of reactive oxygen species and release of apoptogenic factors in the cytosol of the basal ganglia, resembling the pathological findings and clinical symptoms related to Huntington's disease (*10*,*11*).

We reexamined the coconut endosperm and a blood sample from the patient for 3-NPA, which was detected at level of ≈120 mcg/g in the coconut sample and 0.36 mcg/g in blood from the patient. The oral lethal dose for mice is 68 mcg/g (Sigma safety data sheet, https://pubchem.ncbi.nlm.nih.gov/compound/1678), but the toxic dose for humans is not known, and rodents are likely to be more resistant to toxicity, in agreement with the lack of symptoms in the mouse experiment. The symptoms of 3-NPA toxicity in humans are similar to those for bongkrekic acid, as described regarding sugar cane poisoning in humans in China and Africa, including initial gastrointestinal symptoms with vomiting and diarrhea and progressing encephalopathy leading to coma and death (*8*,*11*,*12*). These symptoms are similar to those of the patient. The collaboration between several national and international authorities contributed to resolve this challenging case, providing an understanding of the rapid disease progression and sudden death of the patient.

### About the Author

Dr. Birkelund is a senior consultant in the intensive care unit at Aarhus University Hospital, Aarhus, Denmark, and works as prehospital critical care physician on the prehospital critical care team. His primary research interest is cardiac arrest management and critical care.

### References

1. Anwar M, Kasper A, Steck AR, Schier JG. Bongkrekic acid—a review of a lesser-known mitochondrial toxin. J Med Toxicol. 2017;13:173–9. https://doi.org/10.1007/s13181-016-0577-1
2. Ibrahim AS, Gebremariam T, Liu M, Chamilos G, Kontoyiannis D, Mink R, et al. Bacterial endosymbiosis is widely present among zygomycetes but does not contribute to the pathogenesis of mucormycosis. J Infect Dis. 2008;198:1083–90. https://doi.org/10.1086/591461
3. Krogsgaard LR, Andersen LO, Johannesen TB, Engsbro AL, Stensvold CR, Nielsen HV, et al. Characteristics of the bacterial microbiome in association with common intestinal parasites in irritable bowel syndrome. Clin Transl Gastroenterol. 2018;9:e161. https://doi.org/10.1038/s41424-018-0027-2
4. Clode FE, Kaufmann ME, Malnick H, Pitt TL. Evaluation of three oligonucleotide primer sets in PCR for the identification of *Burkholderia cepacia* and their differentiation from *Burkholderia gladioli*. J Clin Pathol. 1999;52:173–6. https://doi.org/10.1136/jcp.52.3.173
5. Falconer TM, Kern SE, Brzezinski JL, Turner JA, Boyd BL, Litzau JJ. Identification of the potent toxin bongkrekic acid in a traditional African beverage linked to a fatal outbreak. Forensic Sci Int. 2017;270:e5–11. https://doi.org/10.1016/j.forsciint.2016.10.015
6. Gudo ES, Cook K, Kasper AM, Vergara A, Salomao C, Oliveira F, et al. Description of a mass poisoning in a rural district in Mozambique: the first documented bongkrekic acid poisoning in Africa. Clin Infect Dis. 2018;66:1400–6. https://doi.org/10.1093/cid/cix1005
7. Clausen PTLC, Aarestrup FM, Lund O. Rapid and precise alignment of raw reads against redundant databases with KMA. BMC Bioinformatics. 2018;19:307. https://doi.org/10.1186/s12859-018-2336-6
8. Liu X, Luo X, Hu W. Studies on the epidemiology and etiology of moldy sugarcane poisoning in China. Biomed Environ Sci. 1992;5:161–77.
9. Ludolph AC, He F, Spencer PS, Hammerstad J, Sabri M. 3-Nitropropionic acid—exogenous animal neurotoxin and possible human striatal toxin. Can J Neurol Sci. 1991;18:492–8. https://doi.org/10.1017/S0317167100032212
10. Su D, Gadda G. 3-Nitropropionate. In: Liu D, editor. Handbook of foodborne diseases. Boca Raton (FL): Taylor & Francis; 2019. p. 945–50.
11. Francis K, Smitherman C, Nishino SF, Spain JC, Gadda G. The biochemistry of the metabolic poison propionate 3-nitronate and its conjugate acid, 3-nitropropionate. IUBMB Life. 2013;65:759–68. https://doi.org/10.1002/iub.1195
12. He F, Zhang S, Qian F, Zhang C. Delayed dystonia with striatal CT lucencies induced by a mycotoxin (3-nitropropionic acid). Neurology. 1995;45:2178–83. https://doi.org/10.1212/WNL.45.12.2178

Address for correspondence: Thomas Birkelund, Department of Intensive Care, Aarhus University Hospital, Palle Juul-Jensens Boulevard 99, 8200 Aarhus N, Aarhus, Denmark; e-mail: thomas.birkelund@dadlnet.dk

# In Vivo Observation of Cutaneous Larva Migrans by Fluorescence-Advanced Videodermatoscopy

Alice Ramondetta,[1] Simone Ribero,[1] Pietro Quaglino,[2] Paolo Broganelli[2]

Fluorescence-advanced videodermatoscopy is not a widespread diagnostic technique. Its application in dermatology can facilitate the diagnosis of diseases such as cutaneous larva migrans by enabling us to recognize the precise position of larva in vivo on the skin. Using this noninvasive technique, we detected a case of cutaneous larva migrans in a patient.

Dermoscopy alone is not useful for identifying cases of cutaneous larva migrans. Therefore, we conducted a study to introduce a simple and useful noninvasive method for clinical practice. Although still relatively unknown, this method provides more information than clinical procedures and simple dermatoscopy.

## The Study

We report the case of a 34-year-old man who came to our attention at the Dermatological Clinic of the University of Turin (Turin, Italy) after the appearance of an intensely itchy, erythematous-papular serpiginous lesion that was gradually increasing in size. It was located near the right groin. Our suspicion that it was cutaneous larva migrans was validated because the patient had returned from Thailand, a country to which this infestation is endemic, where he had gone for a seaside holiday.

Dermoscopy alone was not useful for identifying the cause in this case. Although the diagnosis of larva migrans is usually clinical, to obtain a diagnosis of certainty by using a biopsy specimen of suspected larva, we used fluorescence-advanced videodermatoscopy to identify its precise position (*1*).

Fluorescence-advanced videodermatoscopy is an optical electronic system that uses a monochromatic light-emitting source with an a mean ± SD λ of 405 ± 5 nm and a field of view of 340 μm to examine the skin. This system uses the ability of endogenous molecules to absorb specific wavelengths and emit fluorescence. The examination is conducted in vivo, and the optical device is directly applied to the skin by using liquid paraffin oil as an interface. The images are visualized in real time by using greyscale to indicate the levels of light absorption (i.e., black indicates no fluorescence and white indicates the highest fluorescence) (*2*).

In this instance, by positioning the probe on the surrounding skin downstream of the distal end of the serpiginous path, within an area of 0.5 cm, we were able to recognize an oval-shaped figure with a rounded tip, a darker gray color than the adjacent tissue (undamaged skin), and a white linear outline of the larva. (Figure, panel A). Once the actual position of the larva was recognized, a 4-mm punch biopsy specimen was obtained and analyzed microscopically; we obtained subsequent histologic confirmation. (Figure, panel B).

We prescribed a 7-day therapy regimen with topical ivermectin, under occlusion. Complete resolution of the cutaneous lesion was obtained (*3*). It was not essential to perform a biopsy for successful treatment; however, although oral ivermectin is the most recommended treatment, because of its side effects and the difficulty in obtaining this drug, the topical formulation is preferable and is equally effective as other localized forms of this drug.

## Conclusions

Cutaneous larva migrans (creeping eruption) is a cutaneous disease that manifests as an erythematous migrating linear or serpiginous tract because of penetration of a hookworm larva into the epidermis. The hookworms most frequently responsible for cutaneous larva migrans are the dog

Author affiliation: Università degli Studi di Torino, Turin, Italy

DOI: https://doi.org/10.3201/eid2701.203137

[1]These authors contributed equally to this article.

[2]These senior authors contributed equally to this article.

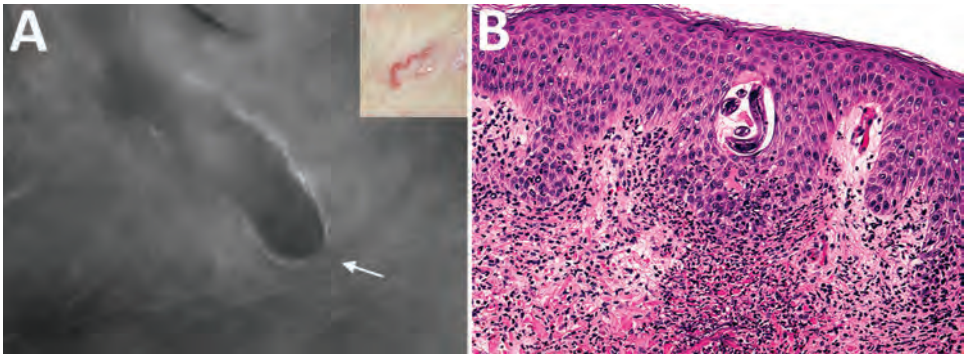


**Figure.** Imaging and biopsy results for patient with cutaneous larva migrans, Turin, Italy. A) Fluorescence-advanced videodermatoscopy showed larva with a diameter of 70–80 μm, located intraepidermally, ≈0.5 cm to the right of the distal end of the serpentine path (indicated in the inset) caused by its passage in the skin. White arrow indicates head of the larva (original magnification ×500). B) Hematoxylin and eosin–stained longitudinal skin section obtained from a 4-mm biopsy specimen, showing the cavity at the epidermal level in which it is possible to observe the larva inside (original magnification ×20). Once the biopsy specimen was obtained, confirmation of a larva by morphologic details or molecular techniques was necessary to differentiate animal nematodes from other larvae, particularly *Strongyloides stercoralis*, because treatment and follow-up would be different.

hookworms *Ancylostoma braziliense* or *An. caninum*. These hookworms are found worldwide, predominantly in tropical and subtropical countries, such as those in Southeast Asia, Africa, South America, the Caribbean, Australia, and southeastern parts of the United States. A similar condition known as larva currens is caused by *Strongyloides stercoralis* roundworms and should be considered in the differential diagnosis.

The life cycle of these nematodes includes male and female adult stages in the intestines of dogs and cats; eggs are passed in the feces of the host and are deposited in the soil (sandy beaches, sand boxes, under dwellings). Under favorable conditions, these eggs hatch and give rise to the infective larval phase. Humans, defined as dead-end hosts, might become infected when infective filariform larvae in soil penetrate the skin. Within a few days, an increased erythematous or vesiculobullous serpiginous track will appear, accompanied by intense pruritis at the site of larval penetration. Larvae migrate at a rate of several millimeters per day (*4*), and lesions are ≈3 mm wide and might be up to 15–20 mm in length. The larva is usually located 1–2 cm ahead of the eruption (*5*). Vesiculobullous lesions develop in ≈10% of cases (*6*). In comparison, the rash of larva currens is typically pink, evanescent, and urticarial and might be linear, serpiginous, annular, arcuate, or plaquelike (*7*). This rash usually appears on the buttocks and abdomen during the chronic autoinfective stage of strongyloidiasis.

The diagnosis of cutaneous larva migrans is based on clinical history and physical findings. Infected patients typically have a history of exposure to contaminated soil or sand (walking barefoot or lying on sand) and the characteristic serpiginous lesion on the skin. Nevertheless, a definitive diagnosis by biopsy specimen sampling is difficult to obtain because the precise position of the larva is unpredictable. To overcome this problem, flight theory was applied by identification of an uncertainty circle in which the possible position of the larva would be obtained by means of a mathematical formula. The distance D between the last observation point and the possible actual point would be obtained by multiplying 3 parameters: $D = V \times T \times R$, in which V is the speed of the larva (mm/d), T is the time elapsed between the last and possible actual observations, and R is a multiplying factor that takes into account the characteristics of the path (*8*).

It would be useful to have a procedure or instrument that can identify in vivo the precise position of the larva to enable accurate biopsy sampling. Methods to identify the position of the larva downstream from the distal end of the serpiginous tract have used dermoscopy; features identified, including translucent, brown, structureless areas corresponding to larval bodies and red-dotted vessels corresponding to an empty burrow, have been reported (*9*).

In conclusion, fluorescence-advanced videodermatoscopy, a simple-to-use method of noninvasive diagnosis, is not a widely used procedure. However, our results show that it appears useful for examinng skin that is apparently healthy or does not have specific clinical–dermoscopic parameters, especially in the context of parasitology, which enables immediate recognition of the etiologic agent (*10*).

## About the Author

Dr. Ramondetta is a fourth-year resident in dermatology at the Dermatology Clinic, University of Turin, Turin, Italy. Her primary research interests are pediatric dermatology and digital dermoscopy.

## References


1. Cinotti E, Adamo A, Broganelli P. Fluorescence videodermoscopy. In: Fimiani M, Rubegni P, Cinotti E, editors. Technology in practical dermatology: non-invasive imaging, lasers and ulcer management. New York: Springer; 2020. p. 111–9.
2. Sanlorenzo M, Vujic I, De Giorgi V, Tomasini C, Deboli T, Quaglino P, et al. Fluorescence-advanced videodermatoscopy: a new method for in vivo skin evaluation. Br J Dermatol. 2017;177:e209–10. https://doi.org/10.1111/bjd.15594
3. Gerbig AW, Kempf W. Topical treatment of cutaneous larva migrans with ivermectin 1. Int J Dermatol. 2019; Oct 24. doi: 10.1111/ijd.14673 [Online ahead of print].
4. Caumes E, Danis M. From creeping eruption to hookworm-related cutaneous larva migrans. Lancet Infect Dis. 2004; 4:659–60. https://doi.org/10.1016/S1473-3099(04)01178-8
5. Hochedez P, Caumes E. Common skin infections in travelers. J Travel Med. 2008;15:252–62. https://doi.org/10.1111/j.1708-8305.2008.00206.x
6. Veraldi S, Çuka E, Pontini P, Vaira F. Bullous cutaneous larva migrans: case series and review of atypical clinical presentations. G Ital Dermatol Venereol. 2017;152:516–9.
7. Pichard DC, Hensley JR, Williams E, Apolo AB, Klion AD, DiGiovanna JJ. Rapid development of migratory, linear, and serpiginous lesions in association with immunosuppression. J Am Acad Dermatol. 2014;70:1130–4. https://doi.org/10.1016/j.jaad.2013.11.036
8. Tomasini C, Gamarra M, Pippione M. Playfulness leavens seriousness: the theory of flight navigation applied to capturing a larva of cutaneous larva migrans. Dermatology Practical and Conceptual. 2000;6:356–8.
9. Zalaudek I, Giacomel J, Cabo H, Di Stefani A, Ferrara G, Hofmann-Wellenhof R, et al. Entodermoscopy: a new tool for diagnosing skin infections and infestations. Dermatology. 2008;216:14–23. https://doi.org/10.1159/000109353
10. Ramondetta A, Ribero S, Peano A, Quaglino P, Broganelli P. In vivo observation of trombiculosis with fluorescence-advanced videodermatoscopy. Emerg Infect Dis. 2020;26:1904–5. https://doi.org/10.3201/eid2608.200077


Address for correspondence: Alice Ramondetta, Dermatology Clinic, Department of Medical Sciences, University of Turin, Via Cherasco 23, Turin, Italy; email: ramondetta.alice@gmail.com

# Listeriosis Caused by Persistence of *Listeria monocytogenes* Serotype 4b Sequence Type 6 in Cheese Production Environment

Magdalena Nüesch-Inderbinen, Guido V. Bloemberg, Andrea Müller, Marc J.A. Stevens, Nicole Cernela, Beat Kollöffel, Roger Stephan

A nationwide outbreak of human listeriosis in Switzerland was traced to persisting environmental contamination of a cheese dairy with *Listeria monocytogenes* serotype 4b, sequence type 6, cluster type 7488. Whole-genome sequencing was used to match clinical isolates to a cheese sample and to samples from numerous sites within the production environment.

Listeriosis is a potentially lethal infection, and the elderly population, pregnant women, and immunocompromised persons at particular risk (*1*). Foods, in particular ready-to-eat foodstuffs, including meat, fish, dairy products, fruits, and vegetables, represent the major vehicle for sporadic cases and outbreaks of listeriosis (*2*). *Listeria monocytogenes* serotype 4b sequence type 6 (ST6) has emerged since 1990 as a hypervirulent clone that is associated with particularly worse outcome for case-patients who have *Listeria* meningitis and therefore poses a particular threat to consumer health (*3*,*4*).

*L. monocytogenes* ST6 is increasingly associated with outbreaks, including an outbreak linked to frozen vegetables in 5 countries in Europe during 2015–2018 (*5*), an outbreak associated with contaminated meat pâté in Switzerland during 2016 (*6*), and the largest listeriosis outbreak globally, which occurred in South Africa during 2017–2018 (*7*,*8*). More recently, the largest outbreak of listeriosis in Europe in the past 25 years was reported in Germany and was traced back to blood sausages contaminated with *L. monocytogenes* ST6 belonging to a particular clone referred to as Epsilon1a (*9*).

Human listeriosis is a reportable disease in Switzerland. All cases of culture- or PCR-confirmed human listeriosis are reported to the Swiss Federal Office of Public Health (SFOPH). Diagnostic laboratories and regional (cantonal) laboratories forward isolates to the Swiss National Reference Centre for Enteropathogenic Bacteria and *Listeria* for strain characterization, ensuring early recognition of *Listeria* clusters among food isolates or human cases. We report an outbreak of listeriosis associated with cheese contaminated with *L. monocytogenes* 4b ST6 in Switzerland.

## The Study

In 2018, the SFOPH recorded 52 human cases of listeriosis, corresponding to a normal annual incidence rate of 0.6 cases/100,000 inhabitants (*10*). However, during March 6, 2018–July 31, 2018, an increase of *L. monocytogenes* serotype 4b from 13 human cases was recorded. Whole-genome sequencing (WGS) was performed on these strains by using MiSeq next generation sequencing technology (Illumina, https://www.illumina.com). Sequencing reads were mapped against an mutlilocus sequencing typing (MLST) scheme based on 7 housekeeping genes and a 1,701-locus core genome MLST (cgMLST) scheme by using Ridom SeqSphere+ software version 5.1.0 (*11*). STs and cluster types (CTs) were determined upon submission to the *L. monocytogenes* cgMLST Ridom SeqSphere+ server (http://www.cgmlst.org/ncs/schema/690488/).

A cluster was defined as a group of isolates with ≤10 different alleles between neighboring isolates (*9*,*11*). Twelve of 13 isolates were assigned to ST6 CT7448, a unique profile in the database, showed

Author affiliations: Institute for Food Safety and Hygiene, Zurich, Switzerland (M. Nüesch-Inderbinen, M.J.A. Stevens, N. Cernela, R. Stephan); National Reference Centre for Enteropathogenic Bacteria and *Listeria*, Zurich (G.V. Bloemberg, A. Müller); Kantonales Laboratorium der Urkantone, Brunnen, Switzerland (B. Kollöffel)

DOI: https://doi.org/10.3201/eid2701.203266

by cluster detection to be closely related. Accordingly, we defined an outbreak case-patient as a patient who had listeriosis and *L. monocytogenes* ST6 CT7448. An outbreak investigation was initiated by the SFOPH, and patients were contacted to assess food exposures by using a standardized questionnaire. Diagnostic and cantonal laboratories were notified nationwide to ensure rapid submission of *L. monocytogenes* isolates to the National Reference Centre for Enteropathogenic Bacteria and *Listeria* for laboratory typing, including WGS. However, the questionnaire-based outbreak investigation did not lead to a suspect food, and the vehicle of infection remained unknown.

In a second wave, onset dates ranged from January 22 to May 26, 2020 (Figure 1). Another 27 cases of infection with *L. monocytogenes* serotype 4b were recorded; 4 cases were in hospital patients who had underlying conditions. During this period, questionnaire-based data were not available to support a food hypothesis.

A total of 22 strains grouped on the basis of WGS in a tight cluster, with the exception of N20–2045, which differed by ≥8 alleles (Figure 2). This strain was within the cluster definition. However, in absence of supportive epidemiologic data, we were not able to verify whether N20–0245 was truly involved in the outbreak.

Median age of the patients was 81 years (range <1–99 years). More than half of the patients were female (18/34, 53%). Of the 34 human isolates, 30 were from blood samples and 1 each from an abscess, ascites, maternal placenta tissue, or stool sample (Table). One case of perinatal transmission and 10 deaths (29%) were reported.

On April 30, 2020, a cheese manufacturer reported to the cantonal laboratory detection of *L. monocytogenes* from a sample of soft (brie) cheese made from pasteurized milk. Analysis had been conducted as part of the manufacturer's routine quality control practices, which are mandatory in Switzerland (Swiss Foodstuffs Act, Article 23). The cheese isolate N20–639 matched the outbreak strain CT by WGS (Table; Figure 2). The cantonal authorities started the tracing of the distribution chain of the dairy. The cheese producer supplied several buyers who provide cheese to retailers throughout Switzerland. The buyers were requested to immediately stop the delivery of the products of this specific producer.

These findings prompted extensive environmental sampling on the production site of the manufacturer. A total of 50 swab specimens from locations, such as vats, cheese harps, skimming devices, sink drains, brushes, scrub sponges, trays, door handles, ripening cellar floors, and walls were obtained. Swabs were incubated in Half Frazer Broth (Bio-Rad, https://www.bio-rad.com) at 30°C for 48 h. *L. monocytogenes* was detected by real-time PCR with the Assurance Genetic Detection System (Endotell, https://www.endotell.ch) according to the manufacturer's instructions. To obtain strains for WGS, 5 enriched Half Frazer Broth cultures were streaked on chromogenic *Listeria* agar plates (Oxoid, Pratteln, Switzerland) and incubated at 37°C for 24 h.

*L. monocytogenes* was identified in 11 (22%) of 50 environmental samples, and all 5 sequenced isolates

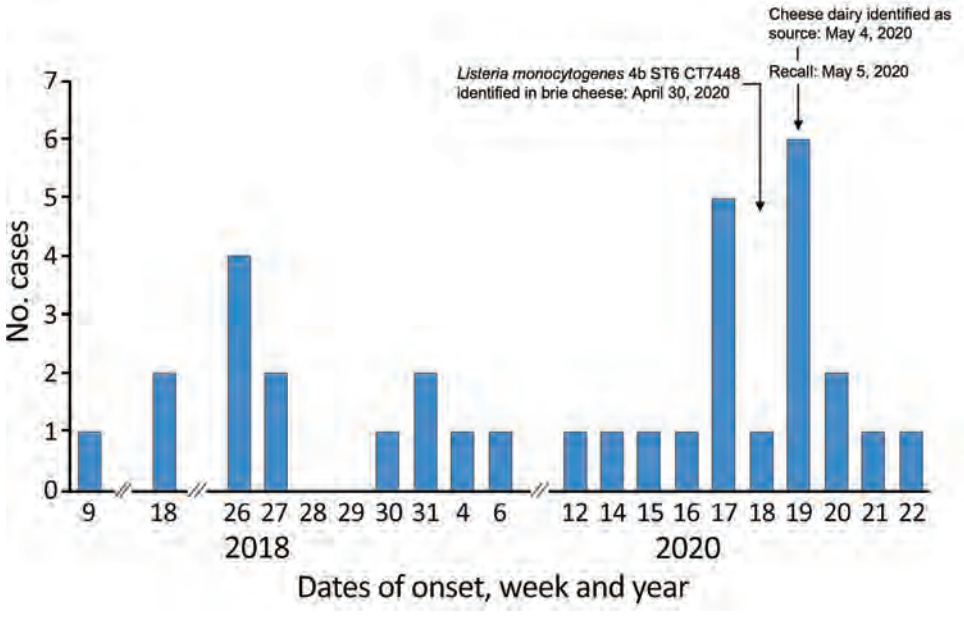


**Figure 1.** Cases of human listeriosis caused by *Listeria monocytogenes* ST6 CT7488, by week and year, Switzerland, 2018 and 2020. CT, cluster type; ST, sequence type.

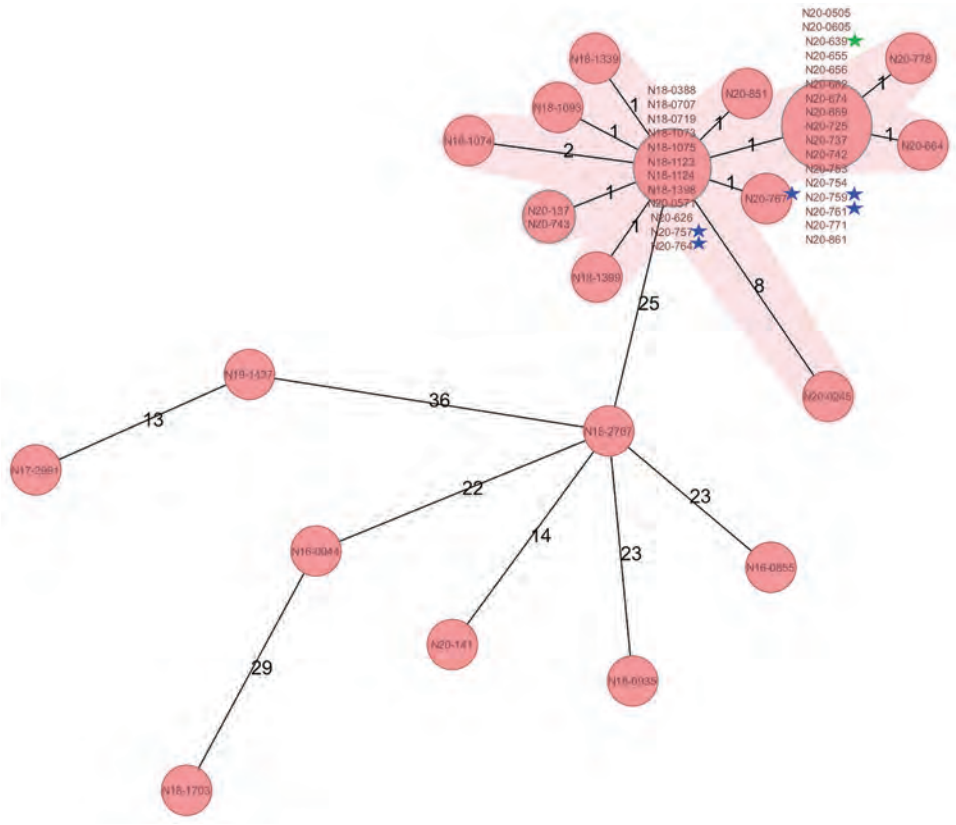


**Figure 2.** Minimum-spanning tree based on cgMLST allelic profiles of 34 human *Listeria monocytogenes* isolates, 1 food isolate, and 5 environmental isolates, Switzerland. Each circle represents an allelic profile based on sequence analysis of 1,701 cgMLST target genes. Values on connecting lines indicate number of allelic differences between 2 strains. Each circle contains the strain identification(s). The food isolate is indicated by a green star, and environmental strains are indicated by blue stars. Outbreak strains are shaded in pink and are shown in comparison with other *L. monocytogenes* sequence type 6 isolates from Switzerland collected during 2016–2020. cgMLST, core genome multilocus sequence typing.

matched the outbreak strain CT (Table; Figure 2). These results lead to a recall on May 5, 2020, of 26 items, including brie, sheep and goat cheese, and organic cheeses; production was stopped immediately. The findings were reported to the Epidemic Intelligence Information System for Food and Waterborne Diseases and Zoonoses. After the recall of the implicated products and a public warning issued by the Federal Food Safety and Veterinary Office, 7 cases of listeriosis caused by the outbreak strain were recorded (Figure 1). The last known case caused by this outbreak strain was sampled on May 20, 2020, and reported to SFOPH on May 25, 2020. Sequence data have been deposited in the National Center for Biotechnology Information (Bethesda, MD, USA) BioSample database under project no. PRJNA640586. We provide accession numbers (Table).

## Conclusions

This prolonged outbreak of *L. monocytogenes* 4b ST6 CT7448 caused 34 laboratory-confirmed listeriosis cases and 10 deaths. The outbreak investigation is an example of successful collaboration between laboratories and food safety and public health authorities to determine sources of contamination and reconstruct outbreak development. The results of the investigation implicated a cheese dairy with sanitation shortcomings and persisting environmental contamination throughout the production site. Isolation and WGS typing of *L. monocytogene*s from a quality-control cheese sample provided crucial information that enabled identification of the origin of contamination. WGS played a key role in showing close relatedness between the isolates from the cheese item and from the environment, and in linking the listeriosis cases from 2018 to the 2020 outbreak.

This outbreak highlights the risk for recontamination of pasteurized cheese products during manufacturing and emphasizes the need for routine sampling of products, manufacturing equipment, and the production environment. Routine quality controls should include WGS typing of environmental *L. monocytogenes* isolates to enable early recognition of potential food contamination and to ultimately mitigate the risk for listeriosis.

### Acknowledgments

We thank the Swiss Federal Office of Public Health and the Federal Food Safety and Veterinary Office for critically reviewing the manuscript.

This study was partly supported by the Swiss Federal Office of Public Health, Division Communicable Diseases.

**Table.** *Listeria monocytogenes* 4b sequence type 6 cluster type 7448 isolates associated with listeriosis outbreak, Switzerland, 2018–2020*

| Isolate ID | Date of isolation | Origin | Source | Patient age, y/sex | BioSample accession no. |
|---|---|---|---|---|---|
| N18–0388 | 2018 Mar 6 | Human | Blood | 82/F | SAMN15325567 |
| N18–0707 | 2018 Apr 30 | Human | Ascitic fluid | 79/F | SAMN15325568 |
| N18–0719 | 2018 May 2 | Human | Blood | 59/F | SAMN15325569 |
| N18–1073 | 2018 Jun 26 | Human | Blood | <1/F | SAMN15325570 |
| N18–1074 | 2018 Jun 26 | Human | Blood | 88/F | SAMN15325571 |
| N18–1075 | 2018 Jun 26 | Human | Maternal placenta tissue | 38/F | SAMN15325572 |
| N18–1093 | 2018 Jun 27 | Human | Blood | 82/M | SAMN15325573 |
| N18–1123 | 2018 Jul 3 | Human | Blood | 81/M | SAMN15325574 |
| N18–1124 | 2018 Jul 3 | Human | Blood | 99/M | SAMN15325575 |
| N18–1339 | 2018 Jul 24 | Human | Blood | 82/F | SAMN15325576 |
| N18–1398 | 2018 Jul 31 | Human | Blood | 48/M | SAMN15325577 |
| N18–1399 | 2018 Jul 31 | Human | Blood | 14/M | SAMN15325578 |
| N20–0137 | 2020 Jan 22 | Human | Blood | 77/M | SAMN15325579 |
| N20–0245 | 2020 Feb 7 | Human | Blood | 73/M | SAMN15325580 |
| N20–0505 | 2020 Mar 17 | Human | Blood | 73/M | SAMN15325581 |
| N20–0571 | 2020 Mar 30 | Human | Blood | 85/M | SAMN15325582 |
| N20–0605 | 2020 Apr 6 | Human | Blood | 73/M | SAMN15325583 |
| N20–0626 | 2020 Apr 15 | Human | Blood | 85/M | SAMN15325584 |
| N20–0655 | 2020 Apr 20 | Human | Blood | 66/F | SAMN15325585 |
| N20–0656 | 2020 Apr 20 | Human | Blood | 81/F | SAMN15325586 |
| N20–0662 | 2020 Apr 22 | Human | Blood | 86/F | SAMN15325587 |
| N20–0664 | 2020 Apr 22 | Human | Blood | 69/F | SAMN15325588 |
| N20–0674 | 2020 Apr 23 | Human | Blood | 84/F | SAMN15325589 |
| N20–689 | 2020 Apr 29 | Human | Blood | 63/F | SAMN15325590 |
| N20–725 | 2020 May 4 | Human | Blood | 81/M | SAMN15325592 |
| N20–737 | 2020 May 5 | Human | Blood | 86/M | SAMN15325593 |
| N20–742 | 2020 May 6 | Human | Blood | 78/F | SAMN15325594 |
| N20–743 | 2020 May 6 | Human | Blood | 37/M | SAMN15325595 |
| N20–753 | 2020 May 8 | Human | Blood | 75/M | SAMN15325596 |
| N20–754 | 2020 May 8 | Human | Blood | 85/F | SAMN15325597 |
| N20–771 | 2020 May 11 | Human | Blood | 95/F | SAMN15325598 |
| N20–778 | 2020 May 12 | Human | Blood | 95/F | SAMN15325599 |
| N20–851 | 2020 May 22 | Human | Perianal abscess | 85/M | SAMN15325600 |
| N20–861 | 2020 May 26 | Human | Blood | 83/F | SAMN15325601 |
| N20–639 | 2020 Apr 30 | Food | Cheese sample | NA/NA | SAMN15325591 |
| N20–757 | 2020 May 3 | Environment | Scrub sponge | NA/NA | SAMN15375881 |
| N20–759 | 2020 May 3 | Environment | Drainage channel | NA/NA | SAMN15375882 |
| N20–761 | 2020 May 3 | Environment | Door handle | NA/NA | SAMN15375884 |
| N20–764 | 2020 May 3 | Environment | Cellar floor | NA/NA | SAMN15375885 |
| N20–767 | 2020 May 3 | Environment | Ripening cellar floor | NA/NA | SAMN15375883 |

*ID, identification; NA, not applicable.

## About the Author

Dr. Nüesch-Inderbinen is a research associate at the Institute for Food Safety and Hygiene, University of Zurich, Zurich, Switzerland. Her primary research interest is pathogenic and antimicrobial-resistant bacteria in humans, animals, and the food chain.

## References

1. Allerberger F, Wagner M. Listeriosis: a resurgent foodborne infection. Clin Microbiol Infect. 2010;16:16–23. https://doi.org/10.1111/j.1469-0691.2009.03109.x
2. Buchanan RL, Gorris LG, Hayman MM, Jackson TC, Whiting RC. A review of Listeria monocytogenes: an update on outbreaks, virulence, dose-response, ecology, and risk assessments. Food Control. 2017;75:1–13. https://doi.org/10.1016/j.foodcont.2016.12.016
3. Maury MM, Tsai YH, Charlier C, Touchon M, Chenal-Francisque V, Leclercq A, et al. Uncovering Listeria monocytogenes hypervirulence by harnessing its biodiversity. Nat Genet. 2016;48:308–13. https://doi.org/10.1038/ng.3501
4. Koopmans MM, Brouwer MC, Bijlsma MW, Bovenkerk S, Keijzers W, van der Ende A, et al. Listeria monocytogenes sequence type 6 and increased rate of unfavorable outcome in meningitis: epidemiologic cohort study. Clin Infect Dis. 2013;57:247–53. https://doi.org/10.1093/cid/cit250
5. European Centre for Disease Prevention and Control. Multi-country outbreak of Listeria monocytogenes PCR serogroup IVb MLST ST6, 2017 [cited 2020 Jun 6]. https://www.ecdc.europa.eu/en/publications-data/rapid-risk-assessment-multi-country-outbreak-listeria-monocytogenes-pcr-serogroup
6. Althaus D, Jermini M, Giannini P, Martinetti G, Reinholz D, Nüesch-Inderbinen M, et al. Local outbreak of Listeria monocytogenes serotype 4b sequence type 6 due to contaminated meat pâté. Foodborne Pathog Dis. 2017;14:219–22. https://doi.org/10.1089/fpd.2016.2232
7. Thomas J, Govender N, McCarthy KM, Erasmus LK, Doyle TJ, Allam M, et al. Outbreak of listeriosis in South

Africa associated with processed meat. N Engl J Med. 2020;382:632–43. https://doi.org/10.1056/NEJMoa1907462
8. Smith AM, Tau NP, Smouse SL, Allam M, Ismail A, Ramalwa NR, et al. Outbreak of Listeria monocytogenes in South Africa, 2017–2018: laboratory activities and experiences associated with whole-genome sequencing analysis of isolates. Foodborne Pathog Dis. 2019;16:524–30. https://doi.org/10.1089/fpd.2018.2586
9. Halbedel S, Wilking H, Holzer A, Kleta S, Fischer MA, Lüth S, et al. Large nationwide outbreak of invasive listeriosis associated with blood sausage, Germany, 2018–2019. Emerg Infect Dis. 2020;26:1456–64. https://doi.org/10.3201/eid2607.200225
10. European Food Safety Authority. Trends and sources of zoonoses and zoonotic agents in foodstuffs, animals and feedingstuffs including information on foodborne outbreaks, antimicrobial resistance in zoonotic and indicator bacteria and some pathogenic microbiological agents in 2018 [cited 2020 Jun 6]. http://www.efsa.europa.eu/sites/default/files/zoocountryreport18ch.pdf
11. Ruppitsch W, Pietzka A, Prior K, Bletz S, Fernandez HL, Allerberger F, et al. Defining and evaluating a core genome multilocus sequence typing scheme for whole-genome sequence-based typing of Listeria monocytogenes. J Clin Microbiol. 2015;53:2869–76. https://doi.org/10.1128/JCM.01193-15

Address for correspondence: Magdalena Nüesch-Inderbinen, Institute for Food Safety and Hygiene, Vetsuisse Faculty, Winterthurerstrasse 272, University of Zurich, 8057 Zürich, Switzerland; e-mail: magdalena.nueesch-inderbinen@uzh.ch

# Detection of Norovirus Variant GII.4 Hong Kong in Asia and Europe, 2017–2019

Martin Chi-Wai Chan,[1] Sunando Roy, Joseph Bonifacio, Lin-Yao Zhang, Preeti Chhabra, Jenny C.M. Chan, Cristina Celma, Mary Ann Igoy, Sin-Leung Lau, Kirran N. Mohammad, Jan Vinjé, Harry Vennema, Judith Breuer, Marion Koopmans, Miranda de Graaf, for NOROPATROL[2]

We report a new norovirus GII.4 variant, GII.4 Hong Kong, with low-level circulation in 4 Eurasia countries since mid-2017. Amino acid substitutions in key residues on the virus capsid associated with the emergence of pandemic noroviruses suggest that GII.4 Hong Kong has the potential to become the next pandemic variant.

Noroviruses are a genetically diverse group of RNA viruses found in a plethora of terrestrial, aerial, and aquatic mammalian species, including humans, pigs, cows, sheep, rats, bats, sea lions, and harbor porpoises (*1*). These viruses are classified into 48 genotypes, including the pandemic GII.4 genotype. In humans, norovirus is the cause of almost one fifth of all cases of acute gastroenteritis globally and the leading cause in all age groups (*2*,*3*). The highest disease burden has been documented in young children (*4*,*5*), whereas, in developed countries, infections have been associated with increased deaths in the elderly (*6*).

Norovirus GII.4 viruses have caused most gastroenteric infections for >2 decades, and new variants have emerged every 2–4 years since 2002 (*7*). Six pandemic GII.4 variants have been named after the place of first reported sequence and year of predominance: US 95–96, Farmington Hills 2002, Hunter 2004, Den Haag 2006, New Orleans 2009, and Sydney 2012. Several norovirus vaccine candidates are in preclinical studies and clinical trials (*8*); however, it is currently unclear if these vaccine formulations could protect against newly emerging GII.4 viruses that are often associated with more norovirus outbreaks and hospitalizations.

Norovirus surveillance networks, such as NoroNet, CaliciNet U.S. and CaliciNet China, are tracking norovirus genotypes (*9*–*11*). Surveillance data from NoroNet has shown that GII.4 variants can be detected at low levels years before they cause a new pandemic (*9*). We report the detection of a new norovirus variant called GII.4 Hong Kong that was circulating sporadically in communities of 2 countries in Asia and 2 in Europe during 2017–2019. This new variant has sequence features of a potential pandemic GII.4 variant.

## The Study

We recently reported the full genome of a new norovirus GII.4 variant called GII.4 Hong Kong, discovered from the local molecular surveillance of norovirus gastroenteritis in hospitalized patients in Hong Kong, China (*12*). The strain Hu/HK/2019/GII.4 Hong Kong[P31]/CUHK-NS-2200 was collected in August 2019. Preliminary analysis indicated that the full genome had 91.1% nucleotide identity to that of the prototype of the most recent pandemic GII.4 Sydney variant, Hu/GII.4/Sydney/NSW0514/2012/AU, which had predominated worldwide since 2012. The major capsid protein of GII.4 Hong Kong had 89.6% amino acid identity with GII.4 Sydney 2012; phylogenetic distance within this new variant had no overlap with distance between other known GII.4 variants, suggesting a new GII.4 variant (Appendix Figure,

Author affiliations: The Chinese University of Hong Kong, Hong Kong, China (M.C.-W. Chan, L.-Y. Zhang, J.C.M. Chan, S.-L. Lau, K.N. Mohammad); University College London, London, UK (S. Roy, J. Breuer); Research Institute for Tropical Medicine, Muntinlupa City, the Philippines (J. Bonifacio, M.A. Igoy); Centers for Disease Control and Prevention, Atlanta, Georgia, USA (P. Chhabra, J. Vinjé); Public Health England, London (C. Celma); National Institute for Public Health and the Environment, Bilthoven, the Netherlands (H. Vennema); Erasmus Medical Center, Rotterdam, the Netherlands (M. Koopmans, M. de Graaf)

DOI: https://doi.org/10.3201/eid2701.203351

[1]Current affiliation: Research Office, Food and Health Bureau, Hong Kong, China.

[2]Members who contributed data are listed at the end of this article.

**Table 1.** Norovirus GII.4 Hong Kong strains detected during 2017–2019

| Collection date | Strain designation | City and country of origin | Settings | Patient age/sex | Sequence availability | GenBank accession no. |
|---|---|---|---|---|---|---|
| 2017 May | RS17–1713 | Pangasinan, Philippines | Inpatient* | 11 mo/M | Complete capsid | MT774555 |
| 2017 Nov | Zandvoort/0471 | Zandvoort, the Netherlands | Sporadic† | 23 mo/F | Full genome | MT735394 |
| 2018 Mar | CUHK-NS-1772 | Hong Kong, China | Inpatient‡ | 15 y/M | Partial polymerase/capsid | MT577843 |
| 2019 Mar | WT_NORO_0887 | Manchester, UK | Nursing home§ | 90 y/F | Full genome | MT742777 |
| 2019 Aug | CUHK-NS-2200 | Hong Kong, China | Inpatient¶ | 42 y/F | Full genome | MN400355# |

*Eight (12.1%) of 66 genotyped norovirus samples tested positive for GII.4 Hong Kong in 2017 in Philippines.
†One (0.2%) of 482 genotyped norovirus samples tested positive for GII.4 Hong Kong in the 2017–18 season in the Netherlands.
‡One (0.3%) of 307 genotyped norovirus samples tested positive for GII.4 Hong Kong in 2018 in Hong Kong.
§One (1.0%) of 105 genotyped norovirus samples tested positive for GII.4 Hong Kong in the 2018–19 season in the United Kingdom.
¶One (0.3%) of 368 genotyped norovirus samples tested positive for GII.4 Hong Kong in 2019 in Hong Kong.
#Prototype sequence of the GII.4 Hong Kong variant.

https://wwwnc.cdc.gov/EID/article/27/1/20-3351-App1.pdf). Coordinated through the international norovirus classification working group (*1*), the 2 most widely used norovirus and calicivirus typing tools hosted by the National Institute for Public Health (RIVM) of the Netherlands (https://www.rivm.nl/mpf/typingtool/norovirus) and the US Centers for Disease Control and Prevention (https://norovirus.ng.philab.cdc.gov) have been updated and synchronized to include the new norovirus to enable retrospective identification and prospective monitoring of GII.4 Hong Kong.

We subsequently identified and sequenced 4 additional GII.4 Hong Kong strains from archived stool samples from Hong Kong, the Philippines, the Netherlands, and the United Kingdom (Table 1); these strains were collected during May 2017–March 2019 (2 in 2017, 1 in 2018, and 1 in 2019).

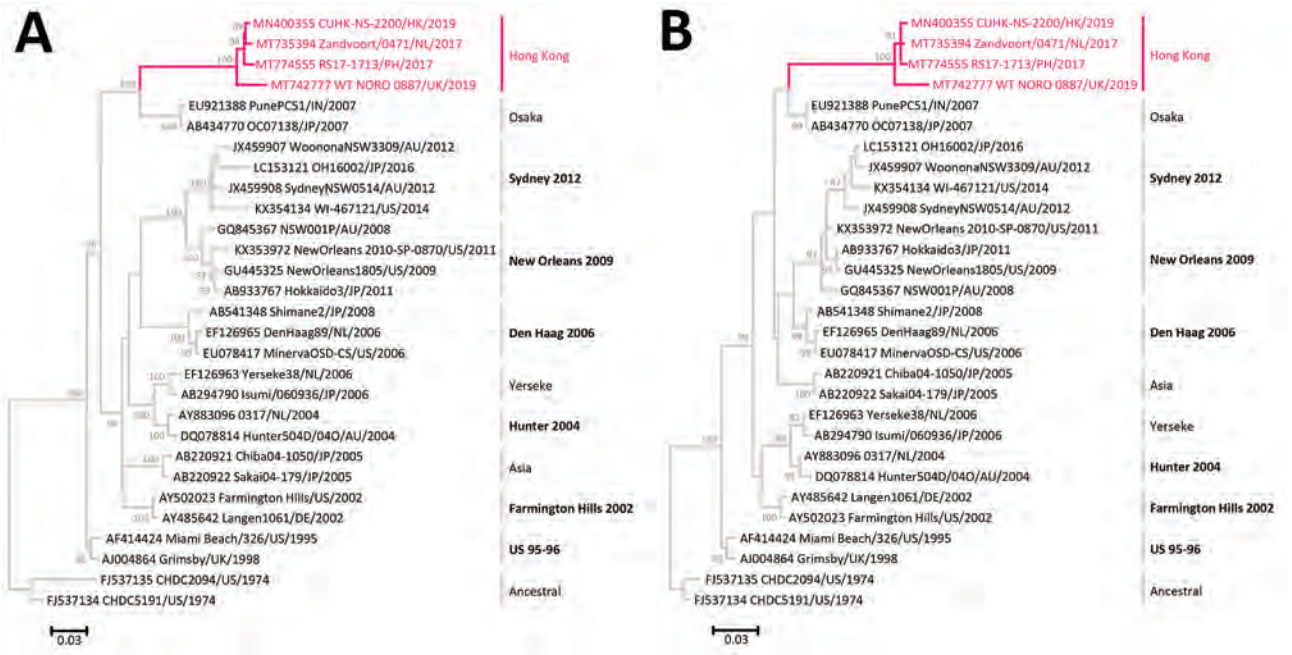


**Figure 1.** Maximum-likelihood phylogeny of complete sequences of the major capsid protein of norovirus GII.4 variants. A) Nucleotide phylogenetic inference was computed using the Tamura-Nei model with gamma distribution of evolutionary rates among sites. A total of 1,617 positions were included in the final dataset. B) Amino acid phylogenetic inference was computed using the Jones-Taylor-Thornton model with gamma distribution of evolutionary rates among sites. A total of 536 positions were included in the final dataset. Best substitution models were selected using the lowest Bayesian Information Criterion scores. Magenta text indicates the 4 GII.4 Hong Kong sequences. Other GII.4 sequences used as references in the human calicivirus typing tool (https://norovirus.ng.philab.cdc.gov) were downloaded from GenBank. Sequence names are in the following format: GenBank accession no., virus strain name, 2-letter code of country/city of collection, year of collection. Bootstrap values ≥70% (of 100 iterations) are shown at nodes. Tree branches are drawn to scale; scale bars indicate number of substitutions per site. Trees are rooted to the oldest sequences collected from 1970s. GII.4 variants with pandemic spread are shown in bold text and annotated with the year of predominance (e.g., Sydney 2012); those without pandemic spread are labeled with variant names only (e.g., Osaka). AU, Australia; DE, Germany; HK, Hong Kong; IN, India; JP, Japan; NL, the Netherlands; PH, Philippines; UK, United Kingdom; US, United States.

Prevalence of the new variant was <1% in each country, except the Philippines (Table 1). The youngest patient was an 11-month-old hospitalized infant and the oldest patient was a 90-year-old woman living in a nursing home.

We obtained full genomes from 2 patients using next-generation sequencing and a complete major capsid protein sequence from 1 patient using Sanger sequencing. We sequenced part of the polymerase-capsid junction region in another case but could not sequence the complete capsid because of low viral load. All consensus virus sequences have been deposited into GenBank (Table 1). The new GII.4 variant was not found in norovirus outbreaks in the United States.

We performed sequence analysis on the 4 available complete major capsid protein sequences of GII.4 Hong Kong. Sequence alignment showed that they shared a pairwise identity of 96.4%–99.3% at nucleotide level and 97.2%–99.4% at amino acid level. We performed maximum-likelihood phylogenetic inference using MEGA version 6.06 (http://megasoftware.net). The 4 GII.4 Hong Kong strains formed a monophyletic cluster that was distant from other pandemic GII.4 variants but was closest to GII.4 Osaka, which had no pandemic spread (Figure 1). We calculated root-to-tip distance that reflected phylogenetic relatedness using TempEst version 1.5.3 (http://tree.bio.ed.ac.uk/software/tempest). Sequences of GII.4 Hong Kong had the longest distance from the root at both nucleotide and amino acid levels (Figure 2), indicating the virus had evolved farthest from ancestral GII.4. Inclusion of the new variant preserved and extended the strong linear clock–like relationship of evolutionary distance with time (nucleotide $R^2 = 0.9691$; amino acid $R^2 = 0.9362$). $R^2$ values of ≈1 indicate a nearly constant rate of accumulation of virus mutations over time, which has been characteristic in the molecular evolution of the major capsid protein of GII.4 variants since the 1970s (*7*). Of note, amino acid sequences of GII.4 Hong Kong occupied a distinct

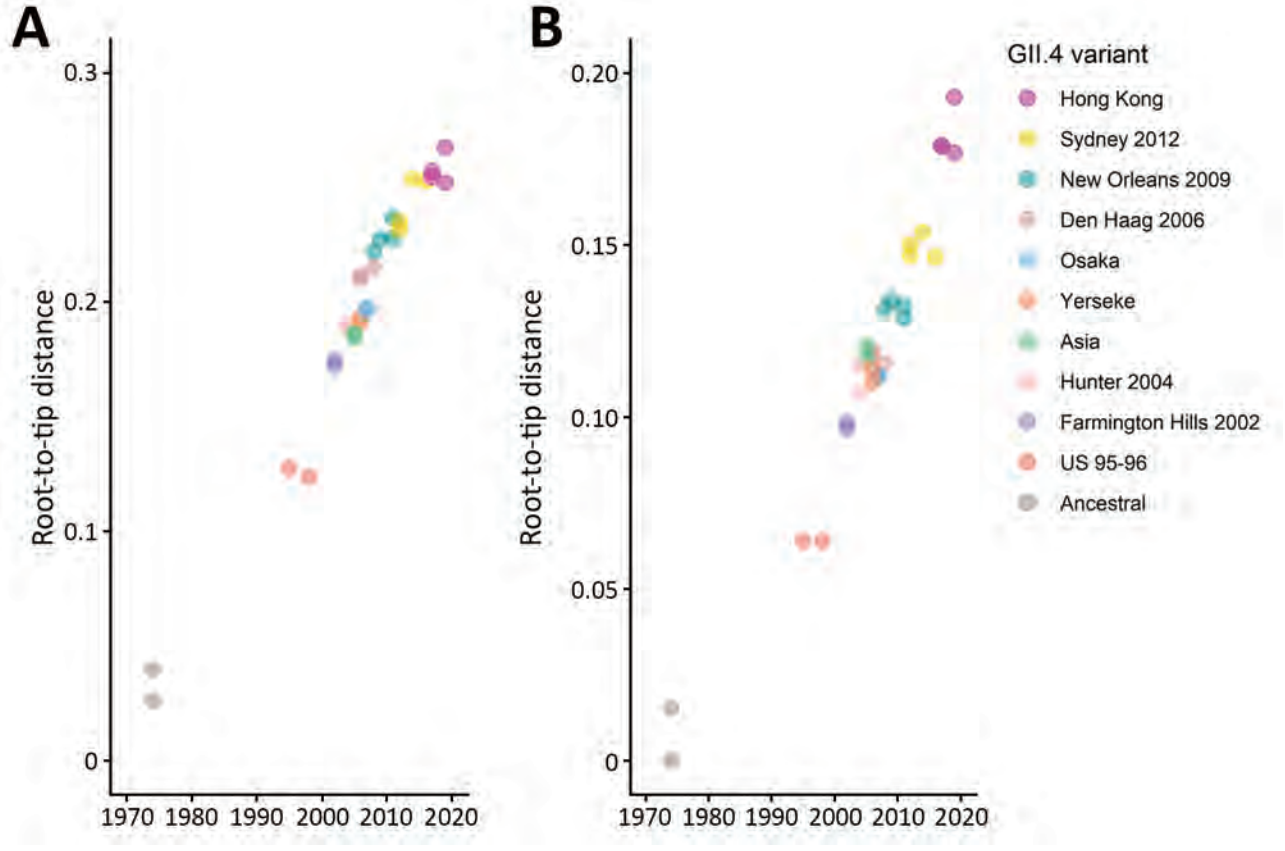


**Figure 2.** Root-to-tip distance plots of the major capsid protein nucleotide (A) and amino acid (B) sequences of norovirus GII.4 variants. Distance from best-fitting root was calculated using the corresponding maximum-likelihood phylogenetic tree shown in Figure 1. Each circle represents 1 strain color-coded by GII.4 variant; darker shades of color indicate ≥2 strains of the same variant. $R^2$ values indicate the linearity of the accumulation of virus mutations over time; for nucleotide sequences, $R^2 = 0.9691$, and for amino acid sequences, $R^2 = 0.9362$. An identical set of sequences were used in phylogenetic inference and root-to-tip distance estimation.

**Table 2.** Amino acids on the major capsid protein at 5 positions proposed to be influential in the emergence and replacement of pandemic norovirus GII.4 variants since 1995*

| GII.4 variant | Amino acid position | | | | |
|---|---|---|---|---|---|
| | 352 | 355 | 357 | 368 | 378 |
| Hong Kong | S | A | D | G | G |
| Osaka | L | S | D | A | G |
| Sydney 2012 | Y | S | D | E | N |
| New Orleans 2009 | Y | S | D | A | N |
| Den Haag 2006 | Y | S | P | S | H |
| Hunter 2004 | S | S | H | S | G |
| Farmington Hills 2002 | S | D | H | N | G |
| US 1995–96 | S | S | H | T | G |

*GII.4 variants with pandemic spread are annotated with the year of predominance (e.g., Sydney 2012). Amino acids are shown by 1-letter codes and color-coded to show variations. Source: (*7*).

spatial-temporal area on the plot with no overlap with other GII.4 variants (Figure 2, panel B). A recent large-scale sequence analysis and antibody blockage confirmation study proposed a set of 5 residues on the major capsid protein that are influential in the emergence and replacement of pandemic GII.4 variants since 1995 (*7*). We observed that residues on 4 of these 5 positions on GII.4 Hong Kong have changed compared with the consensus of GII.4 Sydney 2012 and that 3 residues have changed compared with the consensus of GII.4 Osaka (Table 2).

## Conclusions

The last GII.4 variant, GII.4 Sydney, which has been circulating since 2012, had only a few substitutions when a new recombinant, GII.4 Sydney[P16], emerged in 2015 (*10*). Our findings in 4 countries of low-level circulation (but probably not unique cases) of a new GII.4 variant over a 2-year period clearly indicates that the evolution of GII.4 has been ongoing, if mostly underreported. Phylogeny indicates that the major capsid protein of GII.4 Hong Kong may have evolved from the older GII.4 Osaka variant that was epidemic in 2007, rather than from the newer GII.4 Sydney 2012 variant. The cause of this finding and its implications into GII.4 evolution remain elusive. Although substitutions were found in most of key antigenic residues that have been suggested to be influential in the emergence of new pandemic GII.4 variants, GII.4 Hong Kong has yet to cause outbreaks. Previously, GII.4 variants have been detected at low levels for as long as 18 years before they became pandemic (*13*). GII.4 Hong Kong viruses may still need to further explore the antigenicity landscape to evade herd immunity in humans or to wait for waning of cross-reacting host immunity against GII.4 variants, ultimately allowing pandemic spread of the new variant (*14*). The mechanism for GII.4 viruses to become pandemic remains poorly understood; viral RNA polymerase may also contribute to virus fitness by influencing replication and shedding amount (*15*). Not all GII.4 variants have resulted in pandemics; those of GII.4 Asia, GII.4 Yerseke, and GII.4 Osaka did not.

In conclusion, we report a new norovirus GII.4 variant called GII.4 Hong Kong that has been circulating sporadically in Eurasia since mid-2017. Because some GII.4 variants do not become predominant pandemic strains, continued surveillance of both outbreaks and sporadic cases is important for monitoring emergent norovirus strains.

Members of NOROPATROL who contributed: Sunando Roy, Florencia Tettamanti Boshier, Helena Tutill, Ellen Fragaszy, Rachel Williams, Richard Goldstein, Judith Breuer, Andrew Hayward (University College London, UK); Shilpi Sheth, Daniel Kelly, Kathleen O'Reilly, David Allen, John Edmunds (London School of Hygiene and Tropical Medicine, UK); Sarah O'Brien (University of Liverpool, UK); Lisa Lindesmith, Ralph Baric (University of North Carolina, USA); Cristina Celma, Karen Fuentes, Stuart Beard (Public Health England, UK).

## Acknowledgments

We thank Amy Douglas for her support in collecting the metadata for the UK case and Gabriel Parra for his helpful advice and comments on the manuscript.

This work was supported in part by the commissioned Health and Medical Research Fund of the HKSAR Government (CU-15-C2 to M.C.-W.C.) and the Wellcome Trust (203268/Z/16/Z to J.B.). M.d.G was funded through METASTAVA (grant no. 773830).

Author contributions: M.C.-W.C. and M.d.G. conceived the study. M.C.-W.C., S.R., J.B., L.-Y.Z., J.C.M.C., C.C., M.A.I., S.-L.L., K.N.M., H.V., J.B., M.K. and M.d.G. coordinated data collection. P.C. prepared the Appendix Figure. J.V. and H.V. implemented data integration into virus typing tools. M.C.-W.C. performed initial data analysis and drafted the manuscript. All authors contributed to data analysis and interpretation and critically reviewed and commented on the manuscript before submission.

## About the Author

Dr. Chan is a senior scientific reviewer at the Research Office of the Food and Health Bureau of Hong Kong. At the time of this study, he was an assistant professor in the Department of Microbiology and Stanley Ho Centre for Emerging Infectious Diseases and a principal investigator in the Li Ka Shing Institute of Health Sciences of the Chinese University of Hong Kong. His research interest is intestinal and respiratory viral infections, especially those caused by noroviruses and influenza viruses.

## References


1. Chhabra P, de Graaf M, Parra GI, Chan MC, Green K, Martella V, et al. Updated classification of norovirus genogroups and genotypes. J Gen Virol. 2019;100:1393–406. https://doi.org/10.1099/jgv.0.001318
2. Havelaar AH, Kirk MD, Torgerson PR, Gibb HJ, Hald T, Lake RJ, et al.; World Health Organization Foodborne Disease Burden Epidemiology Reference Group. World Health Organization global estimates and regional comparisons of the burden of foodborne disease in 2010. PLoS Med. 2015;12:e1001923. https://doi.org/10.1371/journal.pmed.1001923
3. Ahmed SM, Hall AJ, Robinson AE, Verhoef L, Premkumar P, Parashar UD, et al. Global prevalence of norovirus in cases of gastroenteritis: a systematic review and meta-analysis. Lancet Infect Dis. 2014;14:725–30. https://doi.org/10.1016/S1473-3099(14)70767-4
4. Kowalzik F, Riera-Montes M, Verstraeten T, Zepp F. The burden of norovirus disease in children in the European Union. Pediatr Infect Dis J. 2015;34:229–34. https://doi.org/10.1097/INF.0000000000000546
5. Zhou H, Wang S, von Seidlein L, Wang X. The epidemiology of norovirus gastroenteritis in China: disease burden and distribution of genotypes. Front Med. 2020;14:1–7. https://doi.org/10.1007/s11684-019-0733-5
6. Trivedi TK, Desai R, Hall AJ, Patel M, Parashar UD, Lopman BA. Clinical characteristics of norovirus-associated deaths: a systematic literature review. Am J Infect Control. 2013;41:654–7. https://doi.org/10.1016/j.ajic.2012.08.002
7. Tohma K, Lepore CJ, Gao Y, Ford-Siltz LA, Parra GI. Population genomics of GII.4 noroviruses reveal complex diversification and new antigenic sites involved in the emergence of pandemic strains. MBio. 2019;10:e02202-19. https://doi.org/10.1128/mBio.02202-19
8. Cates JE, Vinjé J, Parashar U, Hall AJ. Recent advances in human norovirus research and implications for candidate vaccines. Expert Rev Vaccines. 2020;19:539–48. https://doi.org/10.1080/14760584.2020.1777860
9. van Beek J, de Graaf M, Al-Hello H, Allen DJ, Ambert-Balay K, Botteldoorn N, et al.; NoroNet. Molecular surveillance of norovirus, 2005–16: an epidemiological analysis of data collected from the NoroNet network. Lancet Infect Dis. 2018;18:545–53. https://doi.org/10.1016/S1473-3099(18)30059-8
10. Cannon JL, Barclay L, Collins NR, Wikswo ME, Castro CJ, Magaña LC, et al. Genetic and epidemiologic trends of norovirus outbreaks in the United States from 2013 to 2016 demonstrated emergence of novel GII.4 recombinant viruses. J Clin Microbiol. 2017;55:2208–21. https://doi.org/10.1128/JCM.00455-17
11. Jin M, Wu S, Kong X, Xie H, Fu J, He Y, et al. Norovirus outbreak surveillance, China, 2016–2018. Emerg Infect Dis. 2020;26:437–45. https://doi.org/10.3201/eid2603.191183
12. Tse EHY, Zhang LY, Lau SL, Chan MC. Genome sequence of a human norovirus GII.4 Hong Kong[P31] variant in Hong Kong, China. Microbiol Resour Announc. 2020;9:e01391-19. https://doi.org/10.1128/MRA.01391-19
13. Allen DJ, Trainor E, Callaghan A, O'Brien SJ, Cunliffe NA, Iturriza-Gómara M. Early detection of epidemic GII-4 norovirus strains in UK and Malawi: role of surveillance of sporadic acute gastroenteritis in anticipating global epidemics. PLoS One. 2016;11:e0146972. https://doi.org/10.1371/journal.pone.0146972
14. Ruis C, Lindesmith LC, Mallory ML, Brewer-Jensen PD, Bryant JM, Costantini V, et al. Preadaptation of pandemic GII.4 noroviruses in unsampled virus reservoirs years before emergence. Virus Evol. 2020 Nov 21 [Epub ahead of print]. https://doi.org/10.1093/ve/veaa067
15. Parra GI. Emergence of norovirus strains: a tale of two genes. Virus Evol. 2019;5:vez048. https://doi.org/10.1093/ve/vez048


Address for correspondence: Martin Chan, Department of Microbiology, 1/F, Lui Che Woo Clinical Sciences Building, Prince of Wales Hospital, Shatin, Hong Kong; email: martin.chan@link.cuhk.edu.hk, or Miranda de Graaf, Erasmus Medical Center–Viroscience, Wytemaweg 80, Rotterdam 3015CN, Netherlands; email: m.degraaf@erasmusmc.nl

# Increase in Kelch 13 Polymorphisms in *Plasmodium falciparum*, Southern Rwanda

Clara Bergmann, Welmoed van Loon, Felix Habarugira, Costanza Tacoli, Julia C. Jäger, Darius Savelsberg, Fabian Nshimiyimana, Elias Rwamugema, Djibril Mbarushimana, Jules Ndoli, Augustin Sendegeya, Claude Bayingana, Frank P. Mockenhaupt

Artemisinin resistance in *Plasmodium falciparum* is associated with nonsynonymous mutations in the *Kelch 13* (*K13*) propeller domain. We found that 12.1% (8/66) of clinical *P. falciparum* isolates from Huye district, Rwanda, exhibited *K13* mutations, including R561H, a validated resistance marker. *K13* mutations appear to be increasing in this region.

Emerging artemisinin resistance to *Plasmodium falciparum* endangers malaria control worldwide. Currently, the resistance epicenter is the greater Mekong subregion in Southeast Asia (*1*). In sub-Saharan Africa, where illnesses and deaths from *P. falciparum* malaria are highest, such resistance may result in disastrous consequences (*2*). Early detection and close monitoring are therefore crucial.

Artemisinin resistance in *P. falciparum* is associated with *pfkelch13* polymorphisms encoding the parasite's *Kelch 13* (*K13*) propeller domain, which consequently serve as a molecular marker in surveillance (*3*). More than 200 nonsynonymous *K13* single-nucleotide polymorphisms have been reported, including 11 candidate resistance mutations (i.e., associated with delayed parasite clearance) and 9 validated mutations (i.e., also reduced in vitro sensitivity) (*4*). Compared with those from Asia, isolates from sub-Saharan Africa show pronounced heterogeneity of nonsynonymous *K13* polymorphisms, most of them rare, possibly reflecting lower drug pressure (*5*).

Author affiliations: Charité–Universitätsmedizin Berlin, Berlin, Germany (C. Bergmann, W. van Loon, C. Tacoli, J.C. Jäger, D. Savelsberg, F.P. Mockenhaupt); University Teaching Hospital of Butare, Butare, Rwanda (F. Habarugira, E. Rwamugema, D. Mbarushimana, J. Ndoli, A. Sendegeya); Kabutare District Hospital, Butare (F. Nshimiyimana); University of Rwanda, Kigali, Rwanda (C. Bayingana)

DOI: https://doi.org/10.3201/eid2701.203527

Rwanda achieved substantial reductions in malaria during 2006–2011, partly due to home-based management using artemether/lumefantrine (*6*). In 2010, at our study site in Huye district, southern Rwanda, we observed a pattern in the *P. falciparum* multidrug resistance: 1 gene suggestive of intense artemether/lumefantrine drug pressure, whereas *K13* mutations were absent. However, among *P. falciparum* isolates, 2.5% in 2014 and 4.5% in 2015 harbored *K13* variants, including 2 candidate mutations (*7*,*8*). A recent report showed the presence of a validated *pfkelch13* mutation, R561H, at 2 sites in Rwanda (*9*). We conducted a cross-sectional molecular surveillance study to update records of the prevalence of *K13* variants in Huye among isolates collected in 2019.

## The Study

During September–December 2019, we recruited study patients with uncomplicated malaria seeking treatment at the Sovu Health Centre and Kabutare District Hospital, Huye district, Rwanda. Huye district (population ≈390,000) is located on the central plateau of Rwanda (average altitude 1,700 m, yearly rainfall 1,200 mm, mean temperature 19°C). Malaria transmission peaks in October–November and March–May. In 2010, a total of 11.7% of children had microscopically confirmed *Plasmodium* infection (*8*).

We obtained written informed consent from all participants or from the caregivers for children; we also obtained written assent from participants 7–18 years of age. The study was approved by the Rwanda National Ethics Committee. Eligibility criteria for participants included age >1 year; a positive result on a rapid diagnostic test, SD Bioline Malaria Ag Pf/Pan (Abbott Global Point of Care, https://www.globalpointofcare.abbott); and a fever (axillary temperature ≥37.5°C) at the time they sought treatment or within 48 hours beforehand (self-reported). We collected whole blood in S-Monovette EDTA (ethylenediaminetetraacetic

acid; Sarstedt, https://www.sarstedt.com) tubes and confirmed malaria diagnosis by microscopy of Giemsa-stained thick blood smears; patients were also seen by a physician. We provided a 3-day regimen of artemether/lumefantrine for treatment, the first dose given under observation. All patients were asked to return after 3 days to evaluate residual parasitemia on Giemsa-stained thick blood smears.

Definite parasite density was counted per 200 leukocytes on Giemsa-stained thick blood smears by 2 independent microscopists, assuming a mean leukocyte count of 8,000/μL. We extracted DNA using a QIAamp DNA Blood Mini kit (QIAGEN, https://www.qiagen.com). *Plasmodium* species were typed by real-time PCRs with commercially available primers and probes for *P. falciparum*, *P. vivax*, *P. ovale*, *P. malariae*, and *P. knowlesi* (TIB MolBiol, https://www.tib-molbiol.com) on a Roche LightCycler 480 device (https://lifescience.roche.com). *K13* was amplified (codons ≥441≤688) by using nested PCR (*3*) and sequenced by a commercial provider (Eurofins Genomics, https://www.eurofinsgenomics.com). Sequences were aligned to reference *K13* 3D7–1343700 (PlasmoDB, https://plasmodb.org) by using Geneious Prime version 2020.1 (https://www.geneious.com). We used R version 3.6.3 (https://cran.r-project.org) for statistical analysis and a binomial logistic regression model to estimate the time-trend of nonsynonymous mutations ($p<0.05$).

Of 90 patients included in the study, 74 tested positive by microscopy and PCR and 2 by PCR only. Among these patients, 51.3% (39/76) were female and 4 were pregnant; the median age was 18 years (range 2–69 years). *P. falciparum* was found in 88.2% (67/76), *P. vivax* in 7.9% (6/76), *P. ovale* in 7.9% (6/76) and *P. malariae* in 1.3% (1/76). The geometric mean parasite density, based on microscopy results, was 8,926 parasites/μL (95% CI 5,911–13,478 parasites/μL); mean temperature was 37.4°C (SD ±1.3°C). After 3 days of treatment, 61 malaria patients had a negative blood smear, 1 patient (1.6%, 1/62) had asymptomatic parasitemia (31,520 parasites/μL), and 14 patients did not return for the day 3 checkup.

None of the patients infected with *K13* variant parasites tested positive after 3 days of treatment. One pregnant patient sought treatment again. Initially, she had *K13* wild-type parasites and was given artemether/lumefantrine; her day 3 microscopy result was negative. Three weeks later, we detected *K13* R561H parasites, possibly due to reinfection, and administered quinine.

Samples from 98% (66/67) of *P. falciparum* isolates were successfully sequenced for the *K13* propeller domain. We found 5 different nonsynonymous polymorphisms in 8 isolates (Table); 3 harbored R561H, a validated resistance mutation, and the 2 candidate polymorphisms C469F and A675V (*4*). This finding suggests that the number of isolates with nonsynonymous *K13* mutations had increased significantly over the previous decade (OR 1.4, 95% CI 1.1–1.8; $p = 0.003$).

## Conclusions

Of *P. falciparum* isolates from symptomatic patients in southern Rwanda, 12% exhibited nonsynonymous *K13* mutations, a significant increase (OR 1.4, 95% CI 1.1–1.8; $p = 0.003$) over the previous decade compared with their absence in 2010 and 4.5% prevalence in 2015 (*7*). Of note, the validated marker R561H alone occurred in 4.5% of the isolates collected in 2019. Recent studies report 1%–3.5% of nonsynonymous *K13* polymorphisms in parasite isolates from East Africa (*10*), whereas during 2013–2015 in Rwanda, this figure was 6.9% (*9*).

The R561H artemisinin resistance mutation is regularly observed across Asia (*10*). A recent study that reported R561H in 7.4% of isolates collected during 2013–2015 in central Rwanda and 0.7% of isolates in south-central Rwanda (*9*) suggested that this mutation emerged indigenously and independently from Asia 561H strains. We do not have data in our study to support this. None of the *K13* variant parasites showed delayed clearance in our study, which may be due to the partner drug lumefantrine still being effective, similar to observations in Southeast Asia (*11*). In addition, the absence of delayed parasite clearance despite *K13* mutations may reflect partial immunity contributing to parasite elimination (*12*).

We found other nonsynonymous polymorphisms only once among the isolates tested. C469F and A675V are considered artemisinin resistance candidate

**Table.** Nonsynonymous single nucleotide polymorphisms in the *Kelch 13* propeller domain of clinical *Plasmodium falciparum* isolates collected in the Huye District, Rwanda, 2010–2019*

| Year | No. sequenced isolates | No. (%) isolates with nonsynonymous mutations | Amino acid changes and nucleotide changes |
|---|---|---|---|
| 2010 | 75 | 0 | Not applicable |
| 2014 | 81 | 2 (2.5) | V555A, A626S |
| 2015 | 66 | 3 (4.5) | P574L,† D648H, A675V† |
| 2019 | 66 | 8 (12.1) | C469F,† G533A, V555A, R561H‡ (3×), A578S, A675V† |

*Data during 2010–2015 derived from Tacoli et al. (*7*).
†Candidate mutations for artemisinin resistance.
‡Validated mutation for artemisinin resistance (*4*).

mutations (*4*) and have previously been seen in East Africa (*7*,*13*,*14*). G533A and V555A have also been previously reported in Africa but have not yet been evaluated for resistance (*7*,*13*). A578S is a common *K13* polymorphism across Africa but is not linked to artemisinin resistance (*1*).

Our study has clear limitations. Data from only 2 healthcare facilities, with limited catchment areas, were included. Adherence to treatment was assessed by patient self-report, and drug susceptibility testing was not performed. Future research should include ring-stage susceptibility assays to contribute to understanding the role of *K13* mutations in Africa. Separate testing for each drug in a combination for efficacy and continued surveillance for antimicrobial resistance are needed.

Our results show that *K13* mutations are present in Rwanda and that their prevalence in *P. falciparum* malaria patients in the Huye District increased from 0% in 2010 to >12% in 2019. The validated artemisinin resistance mutation R561H occurs in 4.5% of *P. falciparum* isolates being transmitted in this area. The emergence of artemisinin resistance–related mutations in Rwanda is alarming because it might indicate developing resistance against commonly used antimalarials in this region. Countermeasures need to be considered early, potentially including 3-drug antimalarial combinations (*2*).

### Acknowledgments

We are grateful to the staff of Sovu Health Centre and Kabutare District Hospital for their collaboration and help for over 10 years.

This study was financially supported by grant GRK2046 from the German Research Foundation (DFG), which also supported W.L.C. Bergmann was supported by DFG grant GRK2290. The funding bodies had no role in designing the study, collecting, analyzing, or interpreting data, or writing the manuscript.

## About the Author

Ms. Bergmann is a medical student at Charité–Universitaetsmedizin Berlin, interested in infectious disease epidemiology and tropical diseases. This manuscript forms part of her medical doctoral thesis.

### References

1. Ménard D, Khim N, Beghain J, Adegnika AA, Shafiul-Alam M, Amodu O, et al. A worldwide map of *Plasmodium falciparum* K13-propeller polymorphisms. N Engl J Med. 2016;374:2453–64. https://doi.org/10.1056/NEJMoa1513137
2. Hanboonkunupakarn B, White NJ. The threat of antimalarial drug resistance. Trop Dis Travel Med Vaccines. 2015;2:10. https://doi.org/10.1186/s40794-016-0027-8
3. Ariey F, Witkowski B, Amaratunga C, Beghain J, Langlois AC, Khim N, et al. A molecular marker of artemisinin-resistant *Plasmodium falciparum* malaria. Nature. 2014;505:50–5. https://doi.org/10.1038/nature12876
4. World Health Organisation Global Malaria Programme. Status report on artemisinin resistance and artemisinin-based combination therapy efficacy. Geneva: The Organisation; 2018 Aug [cited 10 May 2020]. https://apps.who.int/iris/bitstream/handle/10665/274362/WHO-CDS-GMP-2018.18-eng.pdf
5. Amato R, Miotto O, Woodrow CJ, Almagro-Garcia J, Sinha I, Campino S, et al. Genomic epidemiology of artemisinin resistant malaria. Elife. 2016;5:e08714. https://doi.org/10.7554/eLife.08714</unknown>
6. Uwimana A, Penkunas MJ, Nisingizwe MP, Uyizeye D, Hakizimana D, Musanabaganwa C, et al. Expanding home-based management of malaria to all age groups in Rwanda: analysis of acceptability and facility-level time-series data. Trans R Soc Trop Med Hyg. 2018;112:513–21. https://doi.org/10.1093/trstmh/try093
7. Tacoli C, Gai PP, Bayingana C, Sifft K, Geus D, Ndoli J, et al. Artemisinin resistance-associated K13 polymorphisms of *Plasmodium falciparum* in southern Rwanda, 2010–2015. Am J Trop Med Hyg. 2016;95:1090–3. https://doi.org/10.4269/ajtmh.16-0483
8. Gahutu JB, Steininger C, Shyirambere C, Zeile I, Cwinya-Ay N, Danquah I, et al. Prevalence and risk factors of malaria among children in southern highland Rwanda. Malar J. 2011;10:134. https://doi.org/10.1186/1475-2875-10-134
9. Uwimana A, Legrand E, Stokes BH, Ndikumana JLM, Warsame M, Umulisa N, et al. Emergence and clonal expansion of in vitro artemisinin-resistant *Plasmodium falciparum kelch13* R561H mutant parasites in Rwanda. Nat Med. 2020;26:1602–8. https://doi.org/10.1038/s41591-020-1005-2
10. Ocan M, Akena D, Nsobya S, Kamya MR, Senono R, Kinengyere AA, et al. K13-propeller gene polymorphisms in *Plasmodium falciparum* parasite population in malaria affected countries: a systematic review of prevalence and risk factors. Malar J. 2019;18:60. https://doi.org/10.1186/s12936-019-2701-6
11. Ashley EA, Dhorda M, Fairhurst RM, Amaratunga C, Lim P, Suon S, et al. Spread of artemisinin resistance in *Plasmodium falciparum* malaria. N Engl J Med. 2014;371:411–23. https://doi.org/10.1056/NEJMoa1314981
12. Ataide R, Ashley EA, Powell R, Chan JA, Malloy MJ, O'Flaherty K, et al. Host immunity to *Plasmodium falciparum* and the assessment of emerging artemisinin resistance in a multinational cohort. Proc Natl Acad Sci U S A. 2017;114:3515–20. https://doi.org/10.1073/pnas.1615875114
13. Conrad MD, Nsobya SL, Rosenthal PJ. The diversity of the *Plasmodium falciparum* K13 propeller domain did not increase after implementation of artemisinin-based combination therapy in Uganda. Antimicrob Agents Chemother. 2019;63:e01234-19. https://doi.org/10.1128/AAC.01234-19
14. Ikeda M, Kaneko M, Tachibana SI, Balikagala B, Sakurai-Yatsushiro M, Yatsushiro S, et al. Artemisinin-resistant *Plasmodium falciparum* with high survival rates, Uganda, 2014–2016. Emerg Infect Dis. 2018;24:718–26. https://doi.org/10.3201/eid2404.170141

Address for correspondence: Welmoed van Loon, Institute of Tropical Medicine and International Health, Charité-Universitätsmedizin Berlin, Campus Virchow-Klinikum, Augustenburger Platz 1, 13353 Berlin, Germany; email: welmoed.vanloon@gmail.com.

# Ocular Filariasis in Human Caused by *Breinlia* (*Johnstonema*) *annulipapillata* Nematode, Australia

Anson V. Koehler, Jennifer M.B. Robson, David M. Spratt, Joshua Hann, Ian Beveridge, Michael Walsh, Rodney McDougall, Mark Bromley, Anna Hume, Harsha Sheorey, Robin B. Gasser

We report a human case of ocular filariasis, caused by a species of *Breinlia* nematode, from Queensland, Australia. Morphological and molecular evidence indicated that the nematode *Breinlia* (*Johnstonema*) *annulipapillata*, or a closely related taxon, likely transmitted from a macropodid marsupial host was involved, which might represent an accidental finding or an emerging zoonosis.

Filariasis of the eye is commonly caused by adults or larvae of the filarioid nematodes *Onchocerca volvulus, Loa loa*, and *Dirofilaria immitis* (*1*), although sporadic cases involving *Acanthocheilonema*, *Loaina* (*1*,*2*), or *Pelecitus* (*3*) nematodes have been reported. Filarioids in eyes are challenging to identify morphologically to genus or species, because often only single, immature worms of 1 sex are present, the worms are degraded, or both (*2*). Molecular tools can generally improve the identification of worms of the eyes (e.g., *Dirofilaria hongkongensis* [*4*]), even if only to genus (e.g., *Pelecitus* sp. [*3*]). In Australia, *D. immitis* nematodes have typically been the causative agent of ocular filariasis infection in humans; the prevalence of dirofilariasis in dogs was historically quite high (up to 64%) in the subtropical and tropical climes, such as around Brisbane (*5*). We report a human case of an ocular infection by a *Breinlia* sp. nematode commonly found in Australian marsupials and rodents.

Author affiliations: The University of Melbourne, Parkville, Victoria, Australia (A.V. Koehler, I. Beveridge, R.B. Gasser); Sullivan Nicolaides Pathology, Brisbane, Queensland, Australia (J.M.B. Robson, M. Walsh, R. McDougall, M. Bromley, A. Hume); Australian National Wildlife Collection, Commonwealth Scientific and Industrial Research Organisation, Canberra, Australian Capital Territory, Australia (D.M. Spratt); Eastside Eye Specialist Care, Carindale, Queensland, Australia (J. Hann); St. Vincent's Hospital, Melbourne, Victoria, Australia (H. Sheorey)

DOI: https://doi.org/10.3201/eid2701.203585

## The Study

In May 2019, a 73-year-old man in Brisbane, Queensland, Australia came to his optometrist with an irritated right eye and eyelid. Entropion was suspected, although the patient was unable to tolerate a thorough examination because of extreme irritation of the involved eye. He was referred to an ophthalmologist 3 weeks later; the eye was still irritated, but not grossly inflamed or red. Slit lamp examination revealed a motile nematode in the subconjunctiva (Figure 1; Video, https://wwwnc.cdc.gov/EID/article/27/1/20-3585-V1.htm), which was extracted and fixed in neutral-buffered formalin. Initial morphological examination of the specimen revealed a male filarioid (17–20 mm long) with short, heavily sclerotized spicules; the right spicule had a bifid distal extremity, highly suggestive of *Breinlia* (*Johnstonema*) *annulipapillata* (Figure 1).

The patient was born in Poland and immigrated to Melbourne in 1969, where he spent his working life before retiring to Brisbane in 2005. He had no pets or close contact with animals. His only recent travel was to the Gold Coast and to an island in Moreton Bay, both near Brisbane. The patient had no noteworthy medical history apart from hyperthyroidism, which was well controlled. C-reactive protein (CRP) and full blood count (FBC) test results were within reference ranges, with no eosinophilia, and results of filarial serologic testing (IgG enzyme immunoassay using antigen Bm14) were negative. After the nematode was removed from the patient's eye, symptoms resolved. No anthelmintic medication was prescribed.

We extracted genomic DNA from the formalin-fixed paraffin-embedded worm using a GeneRead DNA FFPE kit (QIAGEN, https://www.qiagen.com) and then subjected it to PCR, targeting the small subunit of nuclear ribosomal RNA gene

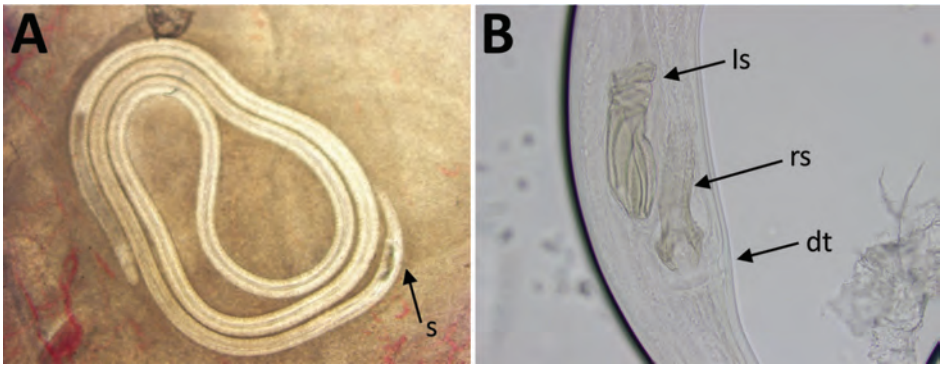


**Figure 1.** Identification of *Breinlia* sp. nematodes from a patient with ocular filariasis, Brisbane, Queensland, Australia, 2019. A) Photograph (in situ) of male *B.* (*Johnstonema*) *annulipapillata* nematode from the subconjunctiva, illustrating thick heavily sclerotized spicules (s). B) Right lateral view of male tail of *B.* (*J.*) *annulipapillata* nematode, illustrating left (ls) and right (rs) spicules; right spicules showed a bifurcated distal extremity (dt), a diagnostic character of the species.

(SSU), and a nested PCR, targeting the mitochondrial cytochrome c oxidase subunit 1 gene (*cox*-1) (Table; *6*). Known positive (*Onchocerca volvulus* DNA) and no-template controls were included. Amplicons were sequenced using an established protocol (*8*).

We assessed the sequences (GenBank accession nos. MT752937 [*SSU,* 724 bp] and MT754705 [*cox*-1, 660 bp]) for quality and compared them with those available publicly. Because sequence data for *SSU*, *cox*-1, or both were publicly available for only 3 taxa of 24 known species of *Breinlia*—*B. mundayi* from the swamp wallaby (*Wallabia bicolor*); *Breinlia* sp. from a Leadbeater's possum (*Gymnobelideus leadbeateri*); and *B. jittapalapongi* from an Asian house rat (*Rattus tanezumi*) —molecular identification was limited to these taxa. The *SSU* sequence (724 bp) obtained for the worm under investigation was 99% similar to those of *B. mundayi* (GenBank accession no. JF934735; 708/710 bp), *Breinlia* sp. from an opossum (GenBank accession no. MT731343; 711/712 bp), and *B. jittapalapongi* (GenBank accession no. KP760119; 656/665 bp). The *cox*-1 sequence (660 bp) obtained was 92% similar to that of *B. jittapalapongi* (GenBank accession no. KP760170; 553/604 bp) and 91% similar to that of *Breinlia* sp. from the opossum (GenBank accession no. MT724666; 601/659 bp); no *cox*-1 sequence was publicly available for *B. mundayi*.

The sequences obtained were aligned to those accessible publicly for 34 (*SSU*) or 29 (*cox*-1) species of filarioid and of *Mastophorus muris* (outgroup) (Figure 2). Aligned *SSU* and *cox*-1 sequence data were subjected to separate phylogenetic analyses using the Bayesian inference method (*8*), with nodal support values given as posterior probabilities. The resultant trees (Figure 2) revealed that the nematode under study is a member of the genus *Breinlia*, as it grouped with *Breinlia* from the opossum, *B. mundayi* (*SSU* only), and *B. jittapalapongi* with strong statistical support. Thus, this worm could be identified molecularly as a *Breinlia* sp.; it could not be identified to species because of the lack of sequence data for *Breinlia* spp. in public databases.

There are 5 reports of human intraocular filariasis from Australia: 4 suspected *D. immitis* cases from New South Wales, Queensland, and Victoria (*9*–*12*); and 1 *Dipetalonema* (*Acanthocheilonema*) *reconditum* case from Victoria (*13*). The short, heavily sclerotized spicules of this specimen, with a bifid distal extremity on the right spicule (Figure 1), indicated that it was neither of these taxa, but rather *B.* (*J.*) *annulipapillata*. This species occurs in a range of macropodid species, predominantly in northern Australia, although it is also found in swamp wallabies in the south. The nematodes of only other known species of the subgenus *Johnstonema*, *B.* (*J.*) *woerlei,* has much

**Table.** Primer sequences used in PCR of the amplification regions of the SSU or *cox*-1 genes of *Breinlia* sp. nematodes from a patient with ocular filariasis, Brisbane, Queensland, Australia, 2019*

| Designation | Primer pair | Oligonucleotide sequence, 5′ → 3′ | Annealing temperature, °C (time)† | Expected size, bp | Reference |
|---|---|---|---|---|---|
| SSU | | | | | |
| 1° PCR | F18ScF1 | ACCGCCCTAGTTCTGACCGTAAA | 58 (45 s) | 830 | (*6*) |
| | F18ScR1 | GGTTCAAGCCACTGCGATTAAAGC | | | |
| *cox*-1 | | | | | |
| 1° PCR | FCo1extdF1 | TATAATTCTGTTYTDACTA | 52 (45 s) | 970 | (*6*) |
| | FCo1extdR1 | ATGAAAATGAGCYACWACATAA | | | |
| 2° PCR | COIintF | TGATTGGTGGTTTTGGTAA | 52 (45 s) | 650 | (*7*) |
| | COIintR | ATAAGTACGAGTATCAATATC | | | |

* *cox*-1, cytochrome *c* oxidase subunit 1; SSU small subunit of nuclear ribosomal RNA.
†All PCRs used 35 cycles with an initial denaturation at 94°C for 5 min, all subsequent denaturation cycles were 30 s, and all extensions were 1 min.

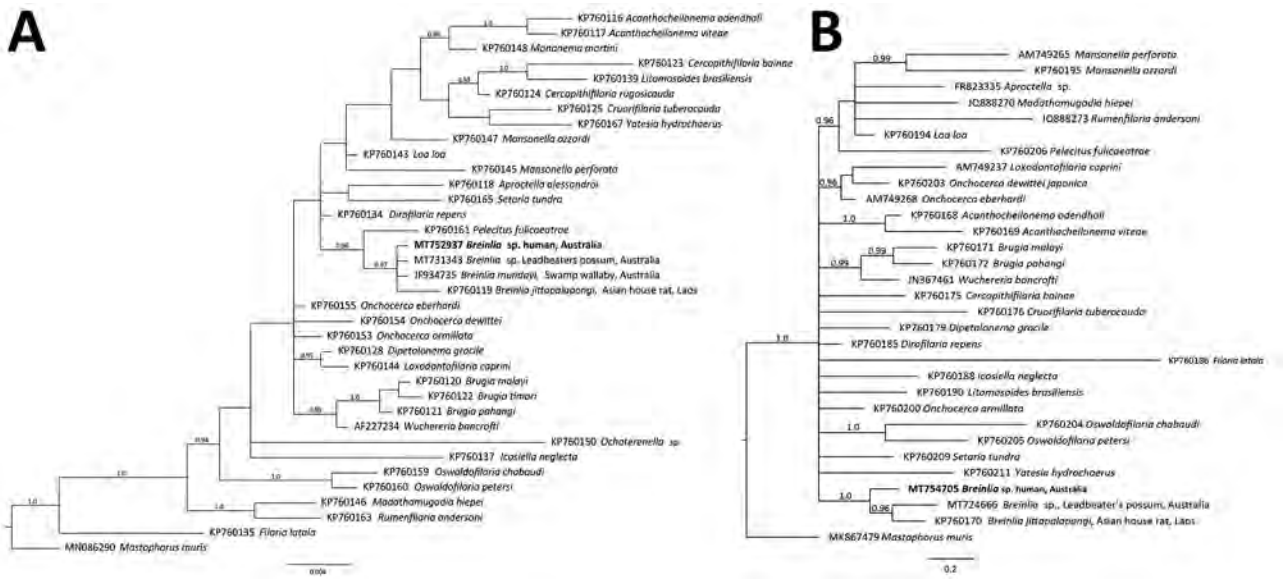


**Figure 2.** Relationship of the novel *Breinlia* sp. taxon (bold type), the nematode species recovered from the eye of a human patient with ocular filariasis, Brisbane, Queensland, Australia, 2019, with representative sequences from members of the family Onchocercidae based on phylogenetic analysis. A) Small subunit of nuclear ribosomal RNA gene; B) cytochrome oxidase 1 gene. Data were compiled using the Bayesian inference method. Branch support given in posterior probability. Respective sequences for *Mastophorus muris* (outgroup) were included in the analyses. GenBank accession numbers are provided. Scale bars represent expected substitutions per site.

larger, heavily sclerotized spicules, but without a bifid extremity on the right spicule, and occurs in the short-eared rock wallaby (*Petrogale brachyotis*) in the Northern Territory (*14*).

Although no life cycles of subgenus *Johnstonema* nematodes are known, those of 4 species of the subgenus *Breinlia* are known and involve *Aedes* mosquitoes as intermediate hosts (*14*). The patient was probably been bitten by the intermediate host of this filarioid, possibly a mosquito, that had previously taken a blood meal from a macropodid and was carrying infective larval stages (L3s). Once in the patient, the L3s would have undergone 2 additional molts and established themselves in the eye and perhaps in other tissues throughout the body (although there was no evidence of infection elsewhere). Adult *Breinlia* nematodes are found predominantly in the peritoneal and pleural cavities of mammalian definitive hosts (*14*). However, other filarial nematodes have a tropism for the eye, and several cases have been reported of zoonotic filariasis of the eye relating to *Dirofilaria* sp. nematodes (*1*). *Breinlia* nematodes had not been found previously in humans, but *B. sergenti* nematodes has been recorded in the slow loris (*Nycticebus coucang*) in Southeast Asia (*14*). It is possible that ocular *Breinlia* infections may go undetected in humans, particularly in less conspicuous places than the eye, and may be more common than expected in areas where *Breinlia*-infected marsupials are prevalent.

## Conclusions

This human case of ocular filariasis caused by *Breinlia* sp. nematodes is highly unusual and was likely transmitted from a kangaroo or wallaby via a blood-feeding intermediate host, possibly a mosquito, to the patient. Microscopic identification of filarioids can be challenging, depending on their stage of development and sex, but fortuitously that was not the case here. Nevertheless, the use of the current molecular approach can be advantageous for generic or specific identification, provided that sufficient sequence data are available in public databases. We recommend that both morphological and molecular tools be used to attempt to achieve a specific diagnosis in cases of human ocular filariasis.

This study was partially supported through a grant from the Australian Research Council (grant no. LP160101299 to R.B.G. and A.V.K.).

### About the Author

Dr. Koehler is a molecular parasitologist in the Gasser Lab in the Department of Veterinary Biosciences at The University of Melbourne, Australia. His research interests include the phylogenetics and biology of parasites.

## References


1. Otranto D, Eberhard ML. Zoonotic helminths affecting the human eye. Parasit Vectors. 2011;4:41. https://doi.org/10.1186/1756-3305-4-41
2. Beaver PC. Intraocular filariasis: a brief review. Am J Trop Med Hyg. 1989;40:40–5. https://doi.org/10.4269/ajtmh.1989.40.40
3. Bain O, Otranto D, Diniz DG, Nascimento dos Santos J, Pinto de Oliveira N, Frota de Almeida IN, et al. Human intraocular filariasis caused by *Pelecitus* sp. nematode, Brazil. Emerg Infect Dis. 2011;17:867–9. https://doi.org/10.3201/eid1705.101309
4. Winkler S, Pollreisz A, Georgopoulos M, Bagò-Horvath Z, Auer H, To KK-W, et al. Candidatus *Dirofilaria hongkongensis* as causative agent of human ocular filariosis after travel to India. Emerg Infect Dis. 2017;23:1428–31. https://doi.org/10.3201/eid2308.170423
5. Orr B, Ma G, Koh WL, Malik R, Norris JM, Westman ME, et al. Pig-hunting dogs are an at-risk population for canine heartworm (*Dirofilaria immitis*) infection in eastern Australia. Parasit Vectors. 2020;13:69. https://doi.org/10.1186/s13071-020-3943-4
6. Lefoulon E, Bain O, Bourret J, Junker K, Guerrero R, Cañizales I, et al. Shaking the tree: multi-locus sequence typing usurps current onchocercid (filarial nematode) phylogeny. PLoS Negl Trop Dis. 2015;9:e0004233. https://doi.org/10.1371/journal.pntd.0004233
7. Casiraghi M, Anderson TJ, Bandi C, Bazzocchi C, Genchi C. A phylogenetic analysis of filarial nematodes: comparison with the phylogeny of *Wolbachia* endosymbionts. Parasitology. 2001;122:93–103. https://doi.org/10.1017/S0031182000007149
8. Koehler AV, Haydon SR, Jex AR, Gasser RB. *Cryptosporidium* and *Giardia* taxa in faecal samples from animals in catchments supplying the city of Melbourne with drinking water (2011 to 2015). Parasit Vectors. 2016;9:315. https://doi.org/10.1186/s13071-016-1607-1
9. Kerkenezov N. Intra-ocular filariasis in Australia. Br J Ophthalmol. 1962;46:607–15. https://doi.org/10.1136/bjo.46.10.607
10. Moorhouse DE. *Dirofilaria immitis*: a cause of human intra-ocular infection. Infection. 1978;6:192–3. https://doi.org/10.1007/BF01641909
11. Boreham RE, Cooney PT, Stewart PA. Dirofilariasis with conjunctival inflammation. Med J Aust. 1997;167:51. https://doi.org/10.5694/j.1326-5377.1997.tb138768.x
12. Chong EW, Sheorey H, Lo CH, Spratt DM, Graue-Hernández E. Subconjunctival dog heartworm. Med J Aust. 2010;193:184. https://doi.org/10.5694/j.1326-5377.2010.tb03845.x
13. Huynh T, Thean J, Maini R. *Dipetalonema reconditum* in the human eye. Br J Ophthalmol. 2001;85:1391–2. https://doi.org/10.1136/bjo.85.11.1384i
14. Spratt DM. New records of filarioid nematodes (Nematoda: Filarioidea) parasitic in Australasian monotremes, marsupials and murids, with descriptions of nine new species. Zootaxa. 2011;2860:1–61 https://doi.org/10.11646/zootaxa.2860.1.1


Address for correspondence: Anson Koehler, Department of Veterinary Biosciences, Melbourne Veterinary School, Faculty of Veterinary and Agricultural Sciences, The University of Melbourne, Corner of Park Drive and Flemington Road, Parkville, VIC 3010, Australia; email: anson.koehler@unimelb.edu.au

# Attitudes about COVID-19 Lockdown among General Population, France, March 2020

Patrick Peretti-Watel, Valérie Seror, Sébastien Cortaredona, Odile Launay, Jocelyn Raude, Pierre Verger, François Beck, Stéphane Legleye, Olivier L'Haridon, Jeremy Ward, for the Coronavirus and Confinement: Enquête Longitudinale (COCONEL) Study Group

Author affiliations: VITROME (Vecteurs–Infections Tropicales et Méditerranéennes), Institut Méditerranée Infection, Aix Marseille Université, Marseille, France (P. Peretti-Watel, V. Seror, S. Cortaredona, J. Ward); Observatoire Régional de la Santé Provence-Alpes-Côte d'Azur, Marseille (P. Peretti-Watel, P. Verger); Centre d'Investigation Clinique Cochin-Pasteur, Paris, France (O. Launay); École des Hautes Études en Santé Publique, Rennes (J. Raude); Centre de Recherche en Épidémiologie et Santé des Populations, Villejuif, France (F. Beck, S. Legleye); Université de Rennes, Rennes (O. L'Haridon); Groupe d'Étude des Méthodes de l'Analyse Sociologique de la Sorbonne, Paris (J. Ward)

DOI: https://doi.org/10.3201/eid2701.201377

Because the effectiveness of a coronavirus disease lockdown in curbing coronavirus disease spread depends on public support, acquiring real-time information about the way populations reacted to the lockdown is crucial. In France, such public support remained fragile among low-income persons, probably because the lockdown exacerbated preexisting social inequalities and conflicts.

During the spring of 2020, because of the coronavirus disease (COVID-19) pandemic, >3 billion persons worldwide lived under lockdown, and many of them were probably angry, uncertain, and distrustful of their national leaders (*1*). Thus, acquiring real-time information about the way populations react and comply to such stringent measures across different socio-economic groups and sociocultural contexts is crucial (*2*). Social acceptability is especially important in the case of France, because the general population did not adhere to governmental recommendations against the previous 2009 influenza A(H1N1) pandemic, during which only 8% of adults complied with the mass vaccination campaign promoted by health authorities (*3*,*4*).

To investigate attitudes toward the lockdown among the general population in France, we conducted a cross-sectional online survey among a nationally representative sample (N = 1,012) of residents ≥18 years of age (Table). The survey was administered during March 27–29, about 10 days after the nationwide lockdown was introduced. To limit selection bias, categories of persons who are less prone to participate in internet surveys (e.g., workers and older persons) were oversampled, and the invitational email did not mention the theme of the survey. In terms of response bias, self-administered questionnaires tend to yield fewer reports in the socially desirable direction than do interviewer-administered questionnaires, and online surveys might have the lowest levels of social-desirability bias (*5*). We computed participants' equivalized household income per month, taking into account household size and composition. Low income refers to the bottom quartile, medium income to the second and third quartiles, and high income to the top quartile. Participants were asked to express their level of agreement toward 12 statements related to lockdown. We asked them whether they were experiencing financial difficulties because of the lockdown. We also asked for household size and housing surface area to identify participants confined in an overcrowded household.

Most participants supported the current lockdown as the only effective way to fight the epidemic and the need to maintain it for several more weeks; however, this support was significantly lower ($p<0.001$ by $\chi^2$ test) among low-income respondents (Table). Strong support was observed across all income groups in favor of strengthening controls to making the lockdown more effective. Only a few respondents (more frequently low-income respondents) expressed open criticisms, including statements indicating that the lockdown is "disproportionate considering the real gravity of the epidemic" (35% among low-income respondents vs. 10% among high-income respondents) and that it should be less coercive to be more acceptable (33% among low-income respondents vs. 13% among high-income respondents).

However, the consensus for the lockdown was based on the fact that it appeared a stopgap measure implemented because of a lack of alternatives: 66% of respondents agreed that the lockdown was the consequence of the lack of hospital resources, 65% agreed that mass testing could replace the lockdown, and 50% considered that the lockdown could have been "avoided by the widespread wearing of masks." Once again, such statements were more frequent among low-income respondents. Similarly,

**Table.** Opinion about the coronavirus disease lockdown among 1,012 respondents to the Coronavirus and Confinement: Enquête Longitudinale (COCONEL) survey, France, March 27–29, 2020*

| Statement or condition | % Respondents who agreed with statement, by income level (± MoE) | | | | p value |
|---|---|---|---|---|---|
| | Overall | Lower income, n = 216 | Medium income, n = 566 | Higher income, n = 230 | |
| The lockdown: | | | | | |
| Is the only effective way to fight the epidemic | 88 (±2) | 81 (±5) | 90 (±2) | 93 (±3) | <0.001 |
| Should last several more weeks to be effective | 93 (±1) | 89 (±4) | 94 (±2) | 98 (±2) | <0.01 |
| Should be strengthened to be effective | 80 (±2) | 75 (±6) | 82 (±3) | 81 (±5) | NS |
| Is disproportionate considering the real gravity of the epidemic | 20 (±2) | 35 (±6) | 18 (±3) | 10 (±4) | <0.001 |
| Should be less coercive to be more acceptable | 22 (±3) | 33 (±6) | 21 (±3) | 13 (±4) | <0.001 |
| Is the consequence of the lack of hospital resources | 66 (±3) | 72 (±6) | 68 (±4) | 54 (±6) | <0.001 |
| Could have been avoided by the widespread wearing of masks | 50 (±3) | 61 (±7) | 51 (±4) | 40 (±6) | <0.001 |
| Could be replaced by mass screening tests | 65 (±3) | 74 (±6) | 65 (±4) | 60 (±6) | <0.01 |
| Has already disastrous economic consequences | 93 (±2) | 93 (±3) | 91 (±2) | 96 (±2) | NS |
| Will cause family tragedies | 76 (±3) | 78 (±6) | 76 (±4) | 75 (±6) | NS |
| Causes too much restriction on civil liberties | 41 (±3) | 58 (±7) | 40 (±4) | 28 (±6) | <0.001 |
| Is an opportunity to develop local solidarity | 91 (±2) | 92 (±4) | 90 (±2) | 91 (±4) | NS |
| Experiencing financial difficulties because of the lockdown | 19 (±2) | 40 (±7) | 16 (±3) | 6 (±3) | <0.001 |
| Confined in an overcrowded household† | 9 (±2) | 23 (±6) | 7 (±2) | 1 (±1) | <0.001 |

*Sample was randomly drawn from online research panel of >750,000 nationally representative households of the general population in France, developed and maintained by the Institut Français d'Opinion Publique, a survey research firm (https://www.ifop.com). Collected data were weighted to match official national census statistics for sex, age, occupation, size of population in the area of residence, and region. The study design was approved by the Ethics Committee of the University Hospital Institute Méditerranée Infection (approval no. 2020-018). MoE, margin of error at 95% confidence level; NS, not statistically significant.
†Defined as <194 square feet per capita.

although all socioeconomic groups acknowledged some major drawbacks (including disastrous economic consequences and family tragedies), low-income respondents were more likely than high-income respondents to state that the lockdown was causing "too much restriction on civil liberties" (58% vs. 28%).

Social differences in attitudes toward the lockdown are probably related to practical differences in persons' living conditions during the lockdown. After 10 days of confinement, 40% of respondents in the low-income group were already reporting financial difficulties because of the lockdown (compared with 6% among high-income respondents). In terms of housing conditions, 9% of participants were confined in an overcrowded household, but that was the case for 23% of low-income respondents (compared with 1% of high-income respondents). Overcrowded housing can impair mental health, and the lockdown made crowded situations even more unbearable because engaging in outdoor activities typically is the easiest way to cope with such situations (*6*,*7*).

In France, as in most other countries, the COVID-19 pandemic fueled contradictory information and intense controversies in traditional and social media. Our survey suggests that a social consensus has been maintained in France in favor of the national lockdown and that excessive politicization of public health has been avoided so far (*8*). However, this consensus remained fragile. First, opinion might have changed if the public got the impression that authorities did not promote alternatives fast enough to end the confinement period. Second, as exemplified by the lower support observed in the poorest groups, the pandemic and the lockdown both exacerbated existing social inequalities and conflicts; besides social inequalities in terms of income and housing conditions, hospital workers in France had been on strike for months during the previous year demanding more resources, and many opponents accused the government of impinging on civil liberties during the so-called "yellow vests" protest movement.

In summary, in late March, most persons in France did support the lockdown; however, such consensus remained fragile because of existing social inequalities and conflicts. Continuous monitoring of population's attitudes and practices during the pandemic will remain key for guiding the public health response (*9*) and communication strategy (*10*).

The COCONEL survey was funded by France's National Agency for Research (grant no. ANR-20-COVI-0035-01), la Fondation de France, and France's National Research Institute for Sustainable Development.

## About the Author

Dr. Peretti-Watel is research director at the French National Institute for Medical Research. His primary research interests include perceptions, attitudes, and behaviors toward infectious diseases.

## References

1. The Lancet. COVID-19: learning from experience [editorial]. Lancet. 2020;395:1011. https://doi.org/10.1016/S0140-6736(20)30686-3
2. Betsch C. How behavioural science data helps mitigate the COVID-19 crisis. Nat Hum Behav. 2020;4:438. https://doi.org/10.1038/s41562-020-0866-1
3. Schwarzinger M, Flicoteaux R, Cortarenoda S, Obadia Y, Moatti JP. Low acceptability of A/H1N1 pandemic vaccination in French adult population: did public health policy fuel public dissonance? PLoS One. 2010;5:e10199. https://doi.org/10.1371/journal.pone.0010199
4. Sherlaw W, Raude J. Why the French did not choose to panic: a dynamic analysis of the public response to the influenza pandemic. Sociol Health Illn. 2013;35:332–44. https://doi.org/10.1111/j.1467-9566.2012.01525.x
5. Kreuter F, Presser S, Tourangeau R. Social desirability bias in CATI, IVR, and web surveys. The effects of mode and question sensitivity. Public Opin Q. 2008;72:847–65. https://doi.org/10.1093/poq/nfn063
6. National Housing Federation. Housing issues during lockdown: health, space and overcrowding [cited 2020 Sep 1]. https://www.housing.org.uk/globalassets/files/homes-at-the-heart/housing-issues-during-lockdown—health-space-and-overcrowding.pdf
7. Peretti-Watel P, Alleaume C, Léger D, Beck F, Verger P; COCONEL Group. Anxiety, depression and sleep problems: a second wave of COVID-19. Gen Psych. 2020;33:e100299. https://doi.org/10.1136/gpsych-2020-100299
8. Gostin LO. Language, science, and politics: the politicization of public health. JAMA. 2018;319:541–2. https://doi.org/10.1001/jama.2017.21763
9. Anderson RM, Heesterbeek H, Klinkenberg D, Hollingsworth TD. How will country-based mitigation measures influence the course of the COVID-19 epidemic? Lancet. 2020;395:931–4. https://doi.org/10.1016/S0140-6736(20)30567-5
10. Cowper A. Covid-19: are we getting the communications right? BMJ. 2020;368:m919. https://doi.org/10.1136/bmj.m919


Address for correspondence: Patrick Peretti-Watel, VITROME, IHU Méditerranée Infection, 19-21 bd Jean Moulin, 13005 Marseille, France; email: patrick.peretti-watel@inserm.fr

# Risk for SARS-CoV-2 Infection in Healthcare Workers, Turin, Italy

Andrea Calcagno, Valeria Ghisetti, Teresa Emanuele, Mattia Trunfio, Silvia Faraoni, Lucio Boglione, Elisa Burdino, Sabrina Audagnotto, Filippo Lipani, Marco Nigra, Antonio D'Avolio, Stefano Bonora, Giovanni Di Perri

Author affiliations: University of Torino, Torino, Italy (A. Calcagno, M. Trunfio, S. Audagnotto, F. Lipani, A. D'Avolio, S. Bonora, G. Di Perri); Azienda Sanitaria Locale Città di Torino, Torino (V. Ghisetti, T. Emanuele, S. Faraoni, E. Burdino, M. Nigra); University of Eastern Piedmont, Novara, Italy (L. Boglione)

DOI: https://doi.org/10.3201/eid2701.203027

We measured severe acute respiratory syndrome coronavirus 2 spike protein subunits S1/S2 antibodies by using capillary electrophoresis and a chemiluminescence immunoassay for 5,444 active healthcare workers in Italy. Seroprevalence was 6.9% and higher among participants having contact with patients. Seroconversion was not observed in 37/213 previously infected participants.

The ongoing coronavirus disease (COVID-19) pandemic is having an unprecedented impact on the worldwide population. Seroconversion for severe acute respiratory syndrome coronavirus 2 (SARS-CoV-2) was described to occur 7–14 days after onset of symptoms, 100% within 19 days after clinical onset (*1*). Recent serologic data suggest that, in affected areas, SARS-CoV-2 infection had been acquired by more persons than what could be extrapolated by PCR analysis of nasopharyngeal swab specimens (*1*–*3*).

Large studies reported seroprevalences of 1%–6.9% (*2*). In February 2020, seroprevalence for 12 blood donors in Lodi, Italy, a heavily affected zone, was as high as 23% (*3*). Studying high-risk persons, such as healthcare workers, could be relevant for implementing preemptive and protective strategies. In Italy, 30,383 healthcare workers (of 253,619 confirmed cases; 12.0%) have been reported to be infected since the beginning of the pandemic (*4*).

Active healthcare workers (n = 7,457) from Azienda Sanitaria Locale Città di Torino public hospitals and outpatient services (Turin, Italy) were invited by email and printed leaflets to participate in our study. During April 17–May 20, 2020, they underwent blood withdrawal. SARS-CoV-2 antibodies were measured by using capillary electrophoresis and chemiluminescence immunoassay

targeting IgGs against S1/S2 regions of spike protein (LIAISON; DiaSorin, https://www.diasorin.com). This assay has a sensitivity of 97.9% and a specificity of 98.5% and a 94.4% positive agreement with the plaque reduction neutralization test (*5*). SARS-CoV-2 IgG concentrations were expressed in arbitrary units/mL (AU/mL) and deemed negative if <12 AU/mL. Persons who had equivocal (12–15 AU/mL) or positive (>15 AU/mL) results provided nasopharyngeal swab specimens for SARS-CoV-2 RNA detection by using an in-house real-time reverse transcription PCR, according to Corman et al. (*6*).

Ethics approval was obtained, and all participants signed an informed consent form. Anonymous data were collected and analyzed by using SPSS Statistics version 26 (IBM, https://www.ibm.com) and described as number (%) or mean ± SD. Disease severity information was not collected.

We tested 5,444 (73.0%) of 7,457 healthcare workers; 4,068 (74.7%) were women. Participants had a mean ± SD age of 49.4 ± 10.6 years. S1/S2 SARS-CoV-2 antibodies were found in 377 (6.9%) participants; 176 (46.7%) had cured COVID-19, 146 (38.7%) had contacts with COVID-19 patients, and 55 (14.6%) had no known epidemiologic link. Seroprevalence was not significantly higher in men than in women (7.9% vs. 6.5%; p = 0.097 by $\chi^2$ test), and no differences were observed among age groups. Mean ± SD IgG titer was 49.2 ± 39.5 AU/mL. IgG titers were higher in older participants (Pearson r = 0.227, p<0.001 and p = 0.001 by analysis of variance; Appendix Figure, https://wwwnc.cdc.gov/EID/article/27/1/20-3027-App1.pdf) and in those previously given a diagnosis of COVID-19 (57.9 AU/mL vs. 41.6 AU/mL in those without a previous diagnosis; p<0.001 by *t*-test).

Detailed task information was available for 4,630 participants. Seroprevalence was highest in laboratory personnel (18/175, 10.3%), although numbers were small, followed by nurse assistants (44/520, 8.5%), nurses (150/1983, 7.6%), and doctors (55/755, 7.3%). A significantly higher seroprevalence was observed in healthcare workers working in close contact with patients versus those with limited/indirect contacts (7.5% vs. 5.2%; p = 0.013 by $\chi^2$ test; odds ratio 1.464, 95% CI 1.077–1.992) (Figure).

Among persons who had a previously diagnosed SARS-CoV-2 infection, 176 (82.6%) had S1/S2 SARS-CoV-2 antibodies. Participants without S1/S2 SARS-CoV-2 antibodies were younger (41.4 vs. 49.1 years; p<0.001) and had a shorter time since diagnosis (36 vs. 44 days; p = 0.008). When we excluded persons who previously had COVID-19, all serology-positive participants (n = 201) provided a nasopharyngeal swab specimen for detection of SARS-CoV-2 RNA; 7 (3.5%) were positive.

We found that SARS-CoV-2 infection had been acquired by 6.9% of healthcare workers in Torino, Italy. Variable seroprevalence has been described among healthcare workers in Belgium (*7*), Spain (*8*), and Germany (*9*) (1.6%–9.3%): no major difference in IgG prevalence was found according to job types. In our study, the highest prevalence was observed for healthcare workers in direct contact with patients and the lowest for administrative staff members. S1/S2 IgG titers were higher in older participants and in those who had a previous diagnosis of COVID-19. In an assay validation study in Boise, Idaho, USA, a seroprevalence of 1.79% was reported; older participants had the highest rates (4%, >80 years of age).

Higher titers in symptomatic patients (we presume were healthcare workers given a diagnosis

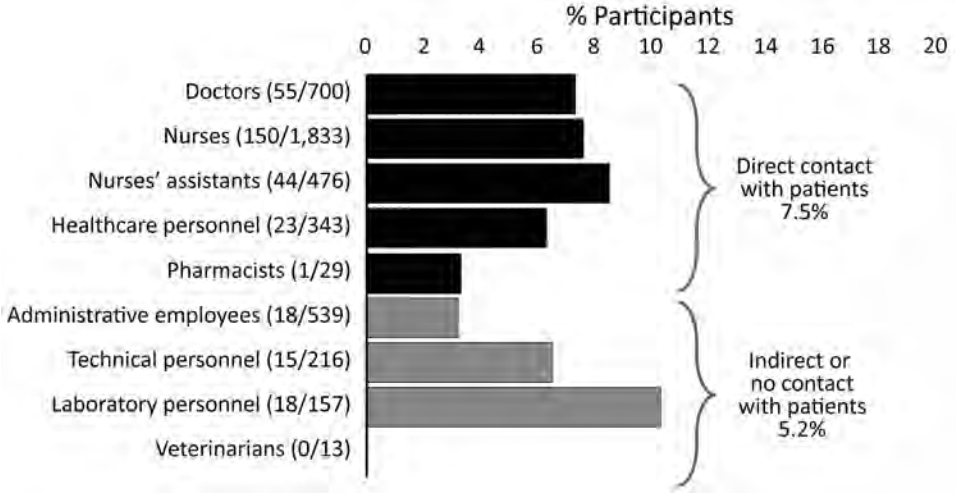


**Figure.** Seroprevalence of severe acute respiratory syndrome coronavirus 2 antibodies in healthcare workers according to tasks of participants, Turin, Italy. Participants are grouped according to direct (black bars) or indirect/no contact (gray bars) with patients. The difference between these 2 groups (7.5% vs. 5.2%) is significant (p = 0.013 by $\chi^2$ test). The healthcare personnel category includes psychologists, nutritionists, welfare workers, religious assistants, physical therapists, and orthoptists.

of COVID-19 according to the local testing policy) have been described (https://www.cdc.gov/coronavirus/2019-ncov/lab/resources/antibody-tests-guidelines.html; https://www.who.int/docs/default-source/coronaviruse/whoin-houseassays.pdf?sfvrsn=de3a76aa_2). Although a shorter time from disease onset might explain the lack of antibodies, a lower seroprevalence in younger, previously infected healthcare workers was unexpected. A total of 3.5% of seropositive participants with no previous diagnosis of COVID-19 had positive PCR results for nasopharyngeal swab specimens; this finding might represent late-stage infections with low/no infectivity.

Our study has limitations, including incomplete coverage of healthcare workers (27% did not respond) and lack of complete job description and disease severity for all participants. Some persons did not show development of IgG after having COVID-19; thus, our study could have missed a subset of previously infected persons (*10*). Despite limitations, our study provides noteworthy estimates about the differential risk for acquiring SARS-CoV-2 infection by healthcare workers according to their specific job setting in a large occupational survey.

### Acknowledgments

We thank all healthcare workers who worked during the COVID-19 epidemic for their passionate hard work despite the risk for their lives and those of their family members. We also want to remember those persons who died from SARS-CoV-2 infection: their names are listed on the website of the National Federation of Medical Doctors and Dentists (https://portale.fnomceo.it/elenco-dei-medici-caduti-nel-corso-dellepidemia-di-covid-19/).

A.C. was supported by VIIV Healthcare Limited, GILEAD Sciences, JANSSEN-CILAG Pharmaceutica, Insmed Inc., and Merck Sharp & Dohme; A.D. was supported by Correvio, CoQua Lab, and GILEAD Sciences; and S.B. and G.D.P. were supported by Healthcare Limited, GILEAD Sciences, JANSSEN-CILAG Pharmaceutica, and Merck Sharp & Dohme.

T.E., V.G., A.C., and G.D.P. planned the study; TE, M.T., S.A., and F.L. collected samples; V.G., M.N., S.F., E.B., and A.D. analyzed samples; A.C. analyzed data; A.C. and L.B. prepared the figures; A.C., M.T., and L.B. performed the literature search; A.C., G.D.P., A.D., and S.B. prepared the first draft of the manuscript. All authors read and participated in preparing the final version of the manuscript.

### About the Author

Dr. Calcagno is an associate professor at the University of Torino, Italy. His primary research interests are clinical pharmacology and pharmacogenetics of antiinfective agents (antiretroviral, antibiotic, antifungal) and central nervous system complications of HIV infection.

### References

1. Long Q-X, Liu BZ, Deng HJ, Wu GC, Deng K, Chen YK, et al. Antibody responses to SARS-CoV-2 in patients with COVID-19. Nat Med. 2020;26:845–8. https://doi.org/10.1038/s41591-020-0897-1
2. Havers FP, Reed C, Lim T, Montgomery JM, Klena JD, Hall AJ, et al. Seroprevalence of antibodies to SARS-CoV-2 in 10 sites in the United States, March 23–May 12, 2020. JAMA Intern Med. 2020 Jul 21 [Epub ahead of print]. https://doi.org/10.1001/jamainternmed.2020.4130
3. Percivalle E, Cambiè G, Cassaniti I, Nepita EV, Maserati R, Ferrari A, et al. Prevalence of SARS-CoV-2 specific neutralising antibodies in blood donors from the Lodi Red Zone in Lombardy, Italy, as at 06 April 2020. Euro Surveill. 2020;25:25. https://doi.org/10.2807/1560-7917.ES.2020.25.24.2001031
4. Istituto Superiore di Sanità, Italian Ministry of Health. Integrated surveillance of COVID-19 in Italy [cited 2020 Sep 12]. https://www.epicentro.iss.it/coronavirus/bollettino/Infografica_19marzo%20ENG.pdf
5. Bonelli F, Sarasini A, Zierold C, Calleri M, Bonetti A, Vismara C, et al. Clinical and analytical performance of an automated serological test that identifies S1/S2-neutralizing IgG in COVID-19 patients semiquantitatively. J Clin Microbiol. 2020;58:e01224-20. https://doi.org/10.1128/JCM.01224-20
6. Corman VM, Landt O, Kaiser M, Molenkamp R, Meijer A, Chu DK, et al. Detection of 2019 novel coronavirus (2019-nCoV) by real-time RT-PCR. Euro Surveill. 2020;25:25. https://doi.org/10.2807/1560-7917.ES.2020.25.3.2000045
7. Steensels D, Oris E, Coninx L, Nuyens D, Delforge ML, Vermeersch P, et al. Hospital-wide SARS-CoV-2 antibody screening in 3,056 staff in a tertiary center in Belgium. JAMA. 2020;324:195–7. https://doi.org/10.1001/jama.2020.11160
8. Garcia-Basteiro AL, Moncunill G, Tortajada M, Vidal M, Guinovart C, Jiménez A, et al. Seroprevalence of antibodies against SARS-CoV-2 among health care workers in a large Spanish reference hospital. Nat Commun. 2020;11:3500. https://doi.org/10.1038/s41467-020-17318-x
9. Korth J, Wilde B, Dolff S, Anastasiou OE, Krawczyk A, Jahn M, et al. SARS-CoV-2-specific antibody detection in healthcare workers in Germany with direct contact to COVID-19 patients. J Clin Virol. 2020;128:104437. https://doi.org/10.1016/j.jcv.2020.104437
10. Yongchen Z, Shen H, Wang X, Shi X, Li Y, Yan J, et al. Different longitudinal patterns of nucleic acid and serology testing results based on disease severity of COVID-19 patients. Emerg Microbes Infect. 2020;9:833–6. https://doi.org/10.1080/22221751.2020.1756699

Address for correspondence: Andrea Calcagno, Unit of Infectious Diseases, Department of Medical Sciences, University of Torino, c/o Amedeo di Savoia Hospital, C.so Svizzera 164, 10149 Torino, Italy; email: andrea.calcagno@unito.it

# Nonpolio Enterovirus Activity during the COVID-19 Pandemic, Taiwan, 2020

Shu-Chen Kuo,[1] Hsiao-Hui Tsou,[1] Hsiao-Yu Wu, Ya-Ting Hsu, Fang-Jing Lee, Shu-Man Shih, Chao A. Hsiung, Wei J. Chen[1]

Author affiliations: National Health Research Institutes, Zhunan, Taiwan

DOI: https://doi.org/10.3201/eid2701.203394

In Taiwan, lower nonpolio enterovirus activity during the coronavirus disease pandemic in 2020 compared with 2014–2019 might be attributable to adherence to nonpharmaceutical interventions. The preventable fraction among unexposed persons indicated that 90% of nonpolio enterovirus activity might have been prevented during 2014–2019 by adopting the same measures enforced in 2020.

Nonpharmaceutical interventions have been shown to be effective in preventing the spread of infectious diseases. The strict compliance with nonpharmaceutical interventions implemented during the coronavirus disease (COVID-19) pandemic has been associated with a decline in influenza activity in many countries, including Taiwan (*1*–*4*). Handwashing, disinfecting frequently touched surfaces, and closure of schools might also be effective against nonpolio enteroviruses (NPEV), which commonly cause a spectrum of illnesses in young populations in Asia (*5*). We observed lower NPEV activity during the 2019–20 season in Taiwan compared with the average of the 5 previous seasons, which might be attributable to strict compliance with nonpharmaceutical interventions. We further estimated the protective effect that could have been achieved if the population strictly adhered to the same nonpharmaceutical interventions during those previous seasons.

We collected nationwide data on weekly outpatient and emergency department (ED) visits during November 2014–June 2020 from the Taiwan National Infectious Disease Statistics System (https://nidss.cdc.gov.tw) (*6*). Patients ≥15 years of age were excluded because of their milder symptoms and low number of cases. The original data were transferred from the National Health Insurance program of Taiwan, which covers >99% of Taiwan residents (Appendix, https://wwwnc.cdc.gov/EID/article/27/1/20-3394-App1.pdf). The Institutional Review Board of the National Health Research Institutes approved this study (approval no. EC1051207-R4).

[1]These authors contributed equally to this article.

NPEV activity was measured by using the number of visits that yielded diagnoses of hand, foot, and mouth disease (International Classification of Diseases [ICD], 9th Revision, Clinical Modification, code 074.3 or ICD, 10th Revision, Clinical Modification, code B08.4) or herpangina (ICD, 9th Revision, Clinical Modification, code 074.0 or ICD, 10th Revision, code B08.5). The period from week 47 of 1 year and week 23 of the following year was defined as 1 season. We estimated the change in NPEV activity after the first imported COVID-19 case in Taiwan, when nonpharmaceutical interventions were introduced and enforced, by using a difference-in-difference model used in a previous influenza study (Appendix) (*4*). The total number of outpatient and ED visits for NPEV at baseline was adjusted to eliminate the preintervention differences in NPEV activity between groups (2019–20 season vs. 2014–2019 seasons). The total number of outpatient and ED visits for all disease in different weeks and different years was used for normalization because their numbers decreased after the COVID-19 pandemic. We estimated the preventable fraction among the unexposed ($PF_u$) to measure the reduction of NPEV that would have been possible in each week of the 2014–2019 seasons, had the same nonpharmaceutical interventions been strictly followed, and adjusted $PF_u$ to control for potential confounder (Appendix).

The number of NPEV visits during the 2019–20 season was 81,942, compared with the average of 205,979 during the 2014–2019 seasons (Appendix Table 1). NPEV activity increased after week 16 across the past 6 seasons except 2019–20, when the earlier low level of weekly activity continued (Figure; Appendix Figure 1). The difference-in-difference analysis revealed that after normalization by visits for NPEV at baseline and for all diseases, NPEV activity during weeks 16–23 in the 2019–20 season was significantly lower than during the same calendar weeks of the 2014–2019 seasons (Appendix Table 2). The lower activity during weeks 16–23 in 2019–20 remained significant across all age groups and hospital settings (Appendix Table 3, 4). The weekly $PF_u$ increased from 73% to 90% (from 17% to 71% for adjusted $PF_u$) during weeks 16–23 (Table; Appendix Table 5). Similar benefits of the nonpharmaceutical interventions were observed across different age groups of patients and hospital settings (Table; Appendix Table 6).

We observed a significant and persistent decrease of NPEV during the 2019–20 season, which might be attributable to strict compliance with the nonpharmaceutical interventions. Up to 90% (71% adjusted) of NPEV activity might have been prevented during the 2014–2019 seasons by adopting the same nonpharmaceutical interventions enforced in 2020. Many

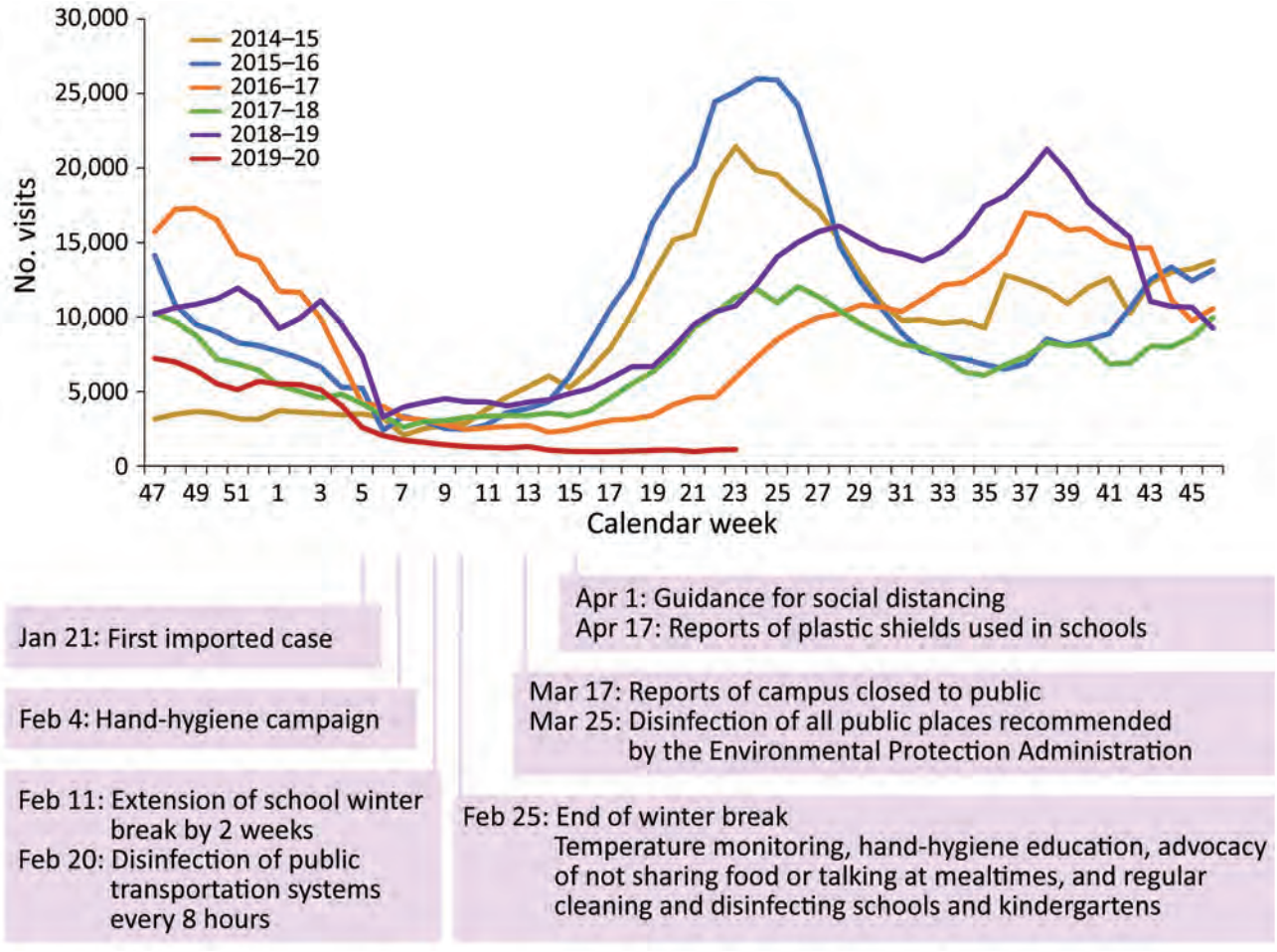


**Figure.** Nonpolio enterovirus activity during 2019–20 season compared with the same weeks in the previous 5 seasons in patients <15 years of age, Taiwan. The y-axis represents the number of outpatient department and emergency department visits in which a diagnosis of hand, foot and mouth disease or herpangina was made for patients <15 years of age.

factors, such as detection bias and healthcare avoidance, might confound our analyses. However, the detection of NPEV is based on symptoms and was less likely to be affected by the COVID-19 pandemic. In addition, COVID-19 had little impact on the surveillance system in Taiwan because <450 total COVID-19 cases had been reported as of June 17 and no local cases have been reported since April 12.

Our study is limited by the healthcare avoidance caused by the COVID-19 pandemic (4). The normalization procedure using the number of visits for all diseases in our study and subgroup analyses on ED patients (Appendix Table 4, 6) are insufficient to eliminate the impact of healthcare avoidance; active surveillance is required. The effect of individual nonpharmaceutical intervention is difficult to assess. The

**Table.** Weekly estimated $PF_u$ during calendar weeks 16–23 in 2020 compared with the same weeks in the previous 5 seasons in patients <15 years of age, by age group, Taiwan*

| Calendar week | Estimated $PF_u$ (95% CI) | | | | |
|---|---|---|---|---|---|
| | Overall | 0–2 y | 3–4 y | 5–9 y | 10–14 y |
| 16 | 0.73 (0.67–0.78) | 0.55 (0.46–0.63) | 0.76 (0.70–0.81) | 0.78 (0.73–0.83) | 0.74 (0.68–0.79) |
| 17 | 0.76 (0.72–0.80) | 0.61 (0.54–0.67) | 0.79 (0.75–0.82) | 0.81 (0.77–0.85) | 0.78 (0.73–0.81) |
| 18 | 0.79 (0.76–0.82) | 0.66 (0.61–0.70) | 0.82 (0.79–0.84) | 0.84 (0.81–0.86) | 0.81 (0.78–0.83) |
| 19 | 0.82 (0.80–0.84) | 0.70 (0.67–0.73) | 0.84 (0.82–0.86) | 0.86 (0.84–0.88) | 0.83 (0.81–0.85) |
| 20 | 0.84 (0.82–0.86) | 0.74 (0.71–0.76) | 0.86 (0.84–0.88) | 0.88 (0.86–0.89) | 0.86 (0.84–0.87) |
| 21 | 0.86 (0.84–0.88) | 0.77 (0.74–0.80) | 0.88 (0.86–0.89) | 0.89 (0.88–0.91) | 0.87 (0.86–0.89) |
| 22 | 0.88 (0.86–0.90) | 0.80 (0.77–0.83) | 0.89 (0.87–0.91) | 0.91 (0.89–0.92) | 0.89 (0.87–0.91) |
| 23 | 0.90 (0.87–0.91) | 0.82 (0.79–0.85) | 0.91 (0.89–0.93) | 0.92 (0.90–0.94) | 0.91 (0.88–0.92) |

*All values are statistically significant. $PF_u$, estimated preventable fraction among the unexposed.

prolonged winter break might have played a major role in reducing NPEV activity. However, considering the high contagiousness of NPEV, their activity was expected to peak after school reopening if no other interventions were implemented. The persistent low NPEV activity throughout the semester, which began in March 2020, indicated the effectiveness of other interventions.

### Acknowledgments

We thank the Taiwan CDC for making their data publicly available. We also thank Kung-Yee Liang, Huey-Kang Sytwu, Shiow-Ing Wu, and Yu-Chieh Cheng for their valuable comments and support.

This project was supported by intramural grants from the National Health Research Institutes (grant nos. IV-109-PP-01, PH-109-PP-02, and PH-109-GP-02).

### About the Author

Dr. Kuo is an attending physician and associate investigator at the National Institute of Infectious Diseases and Vaccinology, National Health Research Institutes, Taiwan. His primary research interest involves infectious diseases and clinical microbiology.

### References

1. Kuo SC, Shih SM, Chien LH, Hsiung CA. Collateral benefit of COVID-19 control measures on influenza activity, Taiwan. Emerg Infect Dis. 2020;26:1928–30. https://doi.org/10.3201/eid2608.201192
2. Galvin CJ, Li YJ, Malwade S, Syed-Abdul S. COVID-19 preventive measures showing an unintended decline in infectious diseases in Taiwan. Int J Infect Dis. 2020;98:18–20. https://doi.org/10.1016/j.ijid.2020.06.062
3. Choe YJ, Lee JK. The impact of social distancing on the transmission of influenza virus, South Korea, 2020. Osong Public Health Res Perspect. 2020;11:91–2. https://doi.org/10.24171/j.phrp.2020.11.3.07
4. Sakamoto H, Ishikane M, Ueda P. Seasonal influenza activity during the SARS-CoV-2 outbreak in Japan. JAMA. 2020;323:1969–71. https://doi.org/10.1001/jama.2020.6173
5. Owino CO, Chu JJH. Recent advances on the role of host factors during non-poliovirus enteroviral infections. J Biomed Sci. 2019;26:47. https://doi.org/10.1186/s12929-019-0540-y
6. Jian SW, Chen CM, Lee CY, Liu DP. Real-time surveillance of infectious diseases: Taiwan's experience. Health Secur. 2017;15:144–53. https://doi.org/10.1089/hs.2016.0107

Address for correspondence: Wei J. Chen, Center for Neuropsychiatric Research, National Health Research Institutes, No. 35 Keyan Rd, Zhunan, Miaoli 350, Taiwan; email: wjchen@nhri.edu.tw; or Shu-Chen Kuo, National Institute of Infectious Diseases and Vaccinology, National Health Research Institutes, No. 35 Keyan Rd, Zhunan, Miaoli 350, Taiwan; email: sckuo@nhri.edu.tw

# Absence of SARS-CoV-2 Transmission from Children in Isolation to Guardians, South Korea

Eun Joo Lee, Dong Hyun Kim, Sung Hee Chang, Sun Bok Suh, Jina Lee, Hyunju Lee, Mi Seon Han

Author affiliations: Seongnam Citizens Medical Center, Seongnam, South Korea (E.J. Lee); Inha University Hospital, Incheon, South Korea (D.H. Kim); Seoul Medical Center, Seoul, South Korea (S.H. Chang); Busan Medical Center, Busan, South Korea (S.B. Suh); Asan Medical Center, University of Ulsan College of Medicine, Seoul (J. Lee); Seoul National University Bundang Hospital, Seoul National University College of Medicine, Seongnam (H. Lee); Seoul Metropolitan Government-Seoul National University Boramae Medical Center, Seoul (M.S. Han)

DOI: https://doi.org/10.3201/eid2701.203450

We explored transmission of severe acute respiratory syndrome coronavirus 2 among 12 children and their uninfected guardians in hospital isolation rooms in South Korea. We found that, even with close frequent contact, guardians who used appropriate personal protective equipment were not infected by children with diagnosed coronavirus disease.

Coronavirus disease (COVID-19) in children is known to occur mainly from family clusters (*1*). However, children can be the only infected members in a household, especially when COVID-19 is contracted from relatives or teachers. Such situations raise concerns about isolation because little information is available on transmission of severe acute respiratory syndrome coronavirus 2 (SARS-CoV-2), which causes COVID-19, during colocation of young children with their uninfected guardians. Although children generally are asymptomatic or have mild symptoms, they could be infective (*1*,*2*). We explored whether SARS-CoV-2 was transmitted from children to their uninfected guardians in a hospital isolation setting.

During February 18–June 7, 2020, we analyzed all children <19 years of age with COVID-19 and their uninfected guardians who were isolated together in 7 hospitals in South Korea. The infected children were encouraged to wear face masks. The guardians were advised to wear personal protective equipment (PPE), but the degree of PPE varied among hospitals. Adherence to PPE was monitored by the medical staff; compliance was judged as good when PPE was worn most of the time, fair for frequent adherence,

and poor when PPE was worn for less than half of the observed time. Children's isolation was lifted when 2 consecutive negative respiratory samples were obtained ≥24 hours apart. To ascertain secondary transmission, guardians' respiratory samples were tested for SARS-CoV-2 if symptoms developed, before their child's isolation was lifted, and 2 weeks after the end of isolation. This study was approved by the institutional review board of each hospital and written informed consent was waived.

Among 94 children with COVID-19 isolated in 7 hospitals, 12 children were isolated with a single uninfected guardian (Table). The median age of the patients was 6 years (range 2 months–11 years), and children were isolated for a median of 17 days (range 7–37 days). Most (7/12) children were asymptomatic, 4 had fever or respiratory symptoms, and 1 had pneumonia. Only 4 children cooperated well with wearing face masks.

The guardians included 10 mothers, 1 father, and 1 uncle; all complied with wearing PPE (Table). Most (10/12) guardians wore gloves and masks, either KF94 masks, which filter ≈94% of particles of 0.4 μm in size, or N95 masks which filter ≈95% of particles of 0.3 μm in size; 7 also wore gowns or coveralls. One guardian used a surgical mask and 1 guardian wore a KF80 mask, which filters ≈80% of particles of 0.6 μm, and gloves. Most (10/12) guardians had frequent close contact, but 2 children kept a distance of ≥1 m from their guardians during isolation. None of the guardians were SARS-CoV-2–positive during the study.

For comparison, we also analyzed 2 cases in which adults with COVID-19 were isolated with their uninfected children because no other caregivers were available (Appendix Table, https://wwwnc.cdc.gov/EID/article/27/1/20-3450-App1.pdf). The adult patients always wore face masks, but the 2 children never wore PPE and always had physical contact with their parents. However, the children did not become infected. The infected parents' adherence to the use of masks likely aided in curbing SARS-CoV-2 transmission to their uninfected children by reducing virus particles in respiratory droplets (*3*).

Appropriate use of PPE, especially face masks, might have protected uninfected guardians in our study. Previous reports have emphasized the use of face masks to prevent SARS-CoV-2 transmission in healthcare and community settings (*4*). Considering the decreased risk for virus transmission noted with PPE, guardians should be counseled on the proper use of PPE when in isolation with infected children.

We did not observe SARS-CoV-2 transmission from children to guardians in isolation settings in which close proximity would seem to increase transmission risk. Recent studies have suggested that children are not the main drivers of the COVID-19 pandemic, although the reasons remain unclear (*5*). A large study on contacts of COVID-19 case-patients in South Korea observed that household transmission was lowest when the index case-patient was 0–9 years of age (*6*). Among pediatric cases, the secondary

**Table.** Clinical characteristics and infection control measures of 12 children with COVID-19 and their uninfected guardians sharing hospital isolation rooms, South Korea, February 18–June 7, 2020*

| | Patient no. | | | | | | | | | | | |
|---|---|---|---|---|---|---|---|---|---|---|---|---|
| Characteristics | 1 | 2 | 3 | 4 | 5 | 6 | 7 | 8 | 9 | 10 | 11 | 12 |
| Patient sex | F | F | M | F | M | M | M | M | F | M | M | M |
| Patient age, y | 6 | 9 | 8 | 9 | 11 | 8 | 0 | 6 | 6 | 5 | 4 | 4 |
| Days of isolation | 7 | 37 | 17 | 9 | 15 | 21 | 19 | 12 | 16 | 31 | 30 | 17 |
| Symptoms | None | None | Mild FV, C | None | None | None | FV, C, S | None | None | FV, ST | FV, V | C, S |
| Pneumonia | N | N | Y | N | N | N | N | N | N | N | N | N |
| Face mask† | KF94 | Surgical | Surgical | Surgical | Surgical | Surgical | None | KF94 | KF94 | KF80 | None | KF94 |
| Compliance | Good | Good | Poor | Good | Good | Poor | NA | Fair | Fair | Fair | NA | Poor |
| Guardian | Mother | Mother | Mother | Mother | Mother | Mother | Father | Mother | Uncle | Mother | Mother | Mother |
| Symptoms‡ | None | None | None | None | None | None | None | None | None | None | None | C, S, H |
| Face mask | KF94 | KF94 | N95 | N95 | N95 | N95 | KF94 | KF94 | KF94 | KF80 | Surgical | KF94 |
| Goggles | N | Y | Y | Y | Y | Y | Y | N | N | N | N | N |
| Gloves | Y | Y | Y | Y | Y | Y | Y | Y | Y | Y | N | Y |
| Gown/coverall | Y/N | Y/N | N/Y | N/Y | N/Y | N/Y | N/Y | N/N | N/N | N/N | N/N | Y/N |
| Contact with patient§ | ≥1 m | Close | Close | Close | Close | Close | Close | Close | ≥1 m | Close | Close | Close |

*Guardians were with the children for the duration of their isolation. COVID-19, coronavirus disease; C, cough; FV, fever; H, headache; NA, not applicable; S, sputum; ST, sore throat; V, vomiting.
†Compliance was deemed good when masks were worn most of the time, fair for frequent adherence, and poor when worn <50% of observed time. A KF94 mask filters ≈94% of particles of 0.4 μm in size, an N95 mask filters ≈95% of particles of 0.3 μm in size, and a KF80 mask filters ≈80% of particles of 0.6 μm.
‡None of the guardians tested positive for COVID-19.
§Guardians for patients 1 and 9 maintained ≥1-meter distance from patients, but other guardians had frequent close contact with patients.

attack rate from children to household members was estimated to be only 0.5% (*7*). Reduced transmission from children in households was also reported in Switzerland and China and in educational settings in Australia (*8*–*10*).

This study is limited by its small sample size, which limits the ability to generalize its results. Moreover, we did not assess the patients' viral load, which could indirectly reflect the infectivity of the children, nor did we assess patient serology, which could further ascertain their infection status. Despite these limitations, our study provides information on SARS-CoV-2 transmission from children to guardians in isolation rooms. Additional assessments of the transmissibility of SARS-CoV-2 by children and the role of PPE in preventing infection could provide guidance during the ongoing pandemic. Nonetheless, our study adds to growing evidence that young children are less likely to contribute to the spread of COVID-19 among their adult guardians.

### About the Author

Dr. E.J. Lee is a pediatrician at the Seongnam Citizens Medical Center, Seongnam, Korea. Her clinical expertise is in the field of pediatric gastroenterology, and her primary research focuses on gut microbiome in children.

### References


1. Han MS, Choi EH, Chang SH, Jin B-L, Lee EJ, Kim BN, et al. Clinical characteristics and viral RNA detection in children with COVID-19 in the Republic of Korea. JAMA Pediatr. 2020 Aug 28 [Epub ahead of print]. https://doi.org/10.1001/jamapediatrics.2020.3988
2. Furukawa NW, Brooks JT, Sobel J. Evidence supporting transmission of severe acute respiratory syndrome coronavirus 2 while presymptomatic or asymptomatic. Emerg Infect Dis. 2020 May 4 [Epub ahead of print]. https://doi.org/10.3201/eid2607.201595
3. Leung NHL, Chu DKW, Shiu EYC, Chan KH, McDevitt JJ, Hau BJP, et al. Respiratory virus shedding in exhaled breath and efficacy of face masks. Nat Med. 2020;26:676–80. https://doi.org/10.1038/s41591-020-0843-2
4. Chu DK, Akl EA, Duda S, Solo K, Yaacoub S, Schünemann HJ, et al.; COVID-19 Systematic Urgent Review Group Effort (SURGE) study authors. Physical distancing, face masks, and eye protection to prevent person-to-person transmission of SARS-CoV-2 and COVID-19: a systematic review and meta-analysis. Lancet. 2020;395:1973–87. https://doi.org/10.1016/S0140-6736(20)31142-9
5. Lee B, Raszka WV Jr. COVID-19 transmission and children: the child is not to blame. Pediatrics. 2020;146:e2020004879. https://doi.org/10.1542/peds.2020-004879
6. Park YJ, Choe YJ, Park O, Park SY, Kim YM, Kim J, et al.; COVID-19 National Emergency Response Center, Epidemiology and Case Management Team. Contact tracing during coronavirus disease outbreak, South Korea, 2020. Emerg Infect Dis. 2020;26:2465–8. https://doi.org/10.3201/eid2610.201315
7. Kim J, Choe YJ, Lee J, Park YJ, Park O, Han MS, et al. Role of children in household transmission of COVID-19. Arch Dis Child. 2020 [Epub ahead of print]. https://doi.org/10.1136/archdischild-2020-319910
8. Posfay-Barbe KM, Wagner N, Gauthey M, Moussaoui D, Loevy N, Diana A, et al. COVID-19 in children and the dynamics of infection in families. Pediatrics. 2020;146:e20201576. https://doi.org/10.1542/peds.2020-1576
9. Jiehao C, Jin X, Daojiong L, Zhi Y, Lei X, Zhenghai Q, et al. A case series of children with 2019 novel coronavirus infection: clinical and epidemiological features. Clin Infect Dis. 2020;71:1547–51. https://doi.org/10.1093/cid/ciaa198
10. Macartney K, Quinn HE, Pillsbury AJ, Koirala A, Deng L, Winkler N, et al.; NSW COVID-19 Schools Study Team. Transmission of SARS-CoV-2 in Australian educational settings: a prospective cohort study. Lancet Child Adolesc Health. 2020;4:807–16. https://doi.org/10.1016/S2352-4642(20)30251-0


Address for correspondence: Mi Seon Han, Department of Pediatrics, Seoul Metropolitan Government-Seoul National University Boramae Medical Center, 20 Boramae-ro 5-gil, Dongjak-gu, Seoul 07061, South Korea; email: msh0827@snu.ac.kr

## Superspreading Event of SARS-CoV-2 Infection at a Bar, Ho Chi Minh City, Vietnam

Nguyen Van Vinh Chau, Nguyen Thi Thu Hong, Nghiem My Ngoc, Tran Tan Thanh, Phan Nguyen Quoc Khanh, Lam Anh Nguyet, Le Nguyen Truc Nhu, Nguyen Thi Han Ny, Dinh Nguyen Huy Man, Vu Thi Ty Hang, Nguyen Thanh Phong, Nguyen Thi Hong Que, Pham Thi Tuyen, Tran Nguyen Hoang Tu, Tran Tinh Hien, Ngo Ngoc Quang Minh, Le Manh Hung, Nguyen Thanh Truong, Lam Minh Yen, H. Rogier van Doorn, Nguyen Thanh Dung, Guy Thwaites, Nguyen Tri Dung, Le Van Tan, for the OUCRU COVID-19 research group[1]

[1]Members of the group are listed in the Appendix (https://wwwnc.cdc.gov/EID/article/27/1/20-3480-App1.pdf).

Author affiliations: Hospital for Tropical Diseases, Ho Chi Minh City, Vietnam (N.V.V. Chau, N.M. Ngoc, D.N.H. Man, N.T. Phong, N.T.H. Que, P.T. Tuyen, T.N.H. Tu, L.M. Hung, N.T. Truong, N.T. Dung); Oxford University Clinical Research Unit, Ho Chi Minh City (N.T.T. Hong, T.T. Thanh, P.N.Q. Khanh, L.A. Nguyet, L.N.T. Nhu, N.T.H. Ny, V.T.T. Hang, T.T. Hien, L.M. Yen, H.R. van Doorn, G. Thwaites, L.V. Tan); Children's Hospital 1, Ho Chi Minh City (N.N.Q. Minh); Centre for Tropical Medicine and Global Health, Oxford, UK (H.R. van Doorn, G. Thwaites); Ho Chi Minh City Centre for Disease Control and Prevention Ho Chi Minh City (N.T. Dung)

DOI: https://doi.org/10.3201/eid2701.203480

We report a superspreading event of severe acute respiratory syndrome coronavirus 2 infection initiated at a bar in Vietnam with evidence of symptomatic and asymptomatic transmission, based on ministry of health reports, patient interviews, and whole-genome sequence analysis. Crowds in enclosed indoor settings with poor ventilation may be considered at high risk for transmission.

Superspreading events occur when a few persons infect a larger number of secondary persons with whom they have contact (*1*,*2*). For severe acute respiratory syndrome coronavirus 2 (SARS-CoV-2), an $R_0$ of 2–3 with 6–8 secondary cases has been suggested to constitute a superspreading event (*3*).

Although SARS-CoV-2 is known to be transmitted through droplets and fomites, there has been growing evidence of airborne transmission (*4*,*5*). Better understanding of specific settings in which superspreading events are facilitated remains critical to inform the development and implementation of control measures to avoid future waves of the pandemic (*5*).

On March 18, 2020, a 43-year old man, patient 1, sought treatment at the Hospital for Tropical Diseases in Ho Chi Minh City, Vietnam, for fever, cough, muscle aches, fatigue, and headache. A sample from a nasopharyngeal throat swab specimen taken at admission tested positive for SARS-CoV-2 by reverse transcription PCR.

During the 14 days before the onset of his symptoms on March 17, he had traveled to Thailand and within Vietnam, between Hanoi and Ho Chi Minh City. From 10:00 PM on March 14 until 2:30 AM of the next day, he participated in a St. Patrick's Day celebration at bar X in Ho Chi Minh City. The bar had 2 indoor areas for clients, an ≈300-$m^2$ area downstairs and an ≈50-$m^2$ area upstairs, with no mechanical ventilation. During open hours, the left and right entrances were typically kept closed to facilitate cooling with air conditioners that recycle indoor air; the middle entrance was kept open. The bar also has naturally ventilated outdoor spaces (Appendix, https://wwwnc.cdc.gov/EID/article/27/1/20-3480-App1.pdf). Patient 1 was inside the bar during the party.

After the confirmed diagnosis of COVID-19 in patient 1, we used contact tracing and testing to

**Table.** History of travel and patients and contacts of patients positive for severe acute respiratory syndrome coronavirus 2 in cluster associated with bar, Ho Chi Minh City, Vietnam, 2020*

| Patient no. | Contact history and epidemiologic factors | Inside bar? | Travel history† | Occupation | Symptom onset | Diagnosed |
|---|---|---|---|---|---|---|
| Patients present at bar X for celebration on March 14–15, 2020 | | | | | | |
| 1 | Attended with patients 2, 3, and 4 | Y | Y | Pilot | 03/17 | Mar 18 |
| 2 | Attended with patients 1, 3, and 4; roommate of patient 3 | UNK | Y | Teacher | Unavail.‡ | Mar 22 |
| 3 | Attended with patients 1, 2, and 4; roommate of patient 2 | UNK | Y | Teacher | Unavail. | Mar 22 |
| 4 | Attended with patients 1, 2, and 3 | UNK | N | Teacher | Mar 21 | Mar 22 |
| 5 | Attendee; works at shoe company Y | UNK | N | Unavail. | Asympt. | Mar 23 |
| 6 | Waiter at bar X; in close contact with patient 1 | Y | N | Bar X waiter | Mar 16 | Mar 23 |
| 7 | Attendee | UNK | N | Unavail. | Unavail. | Mar 24 |
| 8 | Attendee; friend of patient 7 | UNK | N | Teacher | Unavail. | Mar 24 |
| 9 | Attendee | UNK | N | Teacher | Mar 25 | Mar 26 |
| 10 | Attendee | UNK | N | Technician | Asympt. | Mar 26 |
| 11 | Attended with patient 5 | UNK | N | Unavail. | Unavail. | Mar 28 |
| 12 | Attendee | UNK | N | Unavail. | Asympt. | 04/02 |
| 13 | Attended with patient 12 | UNK | N | Unavail. | Mar 26 | 04/03 |
| Contacts of patients present at bar X for celebration on March 14–15, 2020 | | | | | | |
| 14 | Contact of patients 5 and 19 as coworkers at shoe company Y | NA | N | Unavail. | Asympt. | Mar 25 |
| 15 | Household contact of patient 10 | NA | N | Unavail. | Asympt. | Apr 1 |
| 16 | Household contact of patient 6 | NA | N | Unavail. | Unavail. | Mar 27 |
| 17 | Contact (driver) of patients 5 and 14 | NA | N | Driver | Mar 27 | Mar 30 |
| 18 | Household contact of patient 14; also contact of patient 5 as a coworker at shoe company Y | NA | N | Unavail. | Asympt. | Mar 30 |
| 19 | Contact of patients 5 and 14 as coworkers at shoe company Y | NA | N | Unavail. | Unavail. | Apr 6 |

*Asympt., asymptomatic; NA, Not applicable; unavail., unavailable; UNK, unknown.
†Traveled to an area with known local transmission in previous 14 d.
‡Because patient did not enroll in the clinical study, but asymptomatic at time of diagnosis.

detect 18 additional PCR-confirmed cases. Of these, 12 (patients 2–13) were at bar X during the evening of March 14; the other 6 (patients 14–19) were contacts (Table; Appendix Figure). Of the patients with confirmed cases attending the celebration, 4 were in close contact with patient 1: patients 2–4 went to the celebration with patient 1 and patient 6 worked as a waiter in the bar. Patients 2 and 3, who were roommates, had traveled to Malaysia and returned to Vietnam, patient 2 on March 13 and patient 3 on

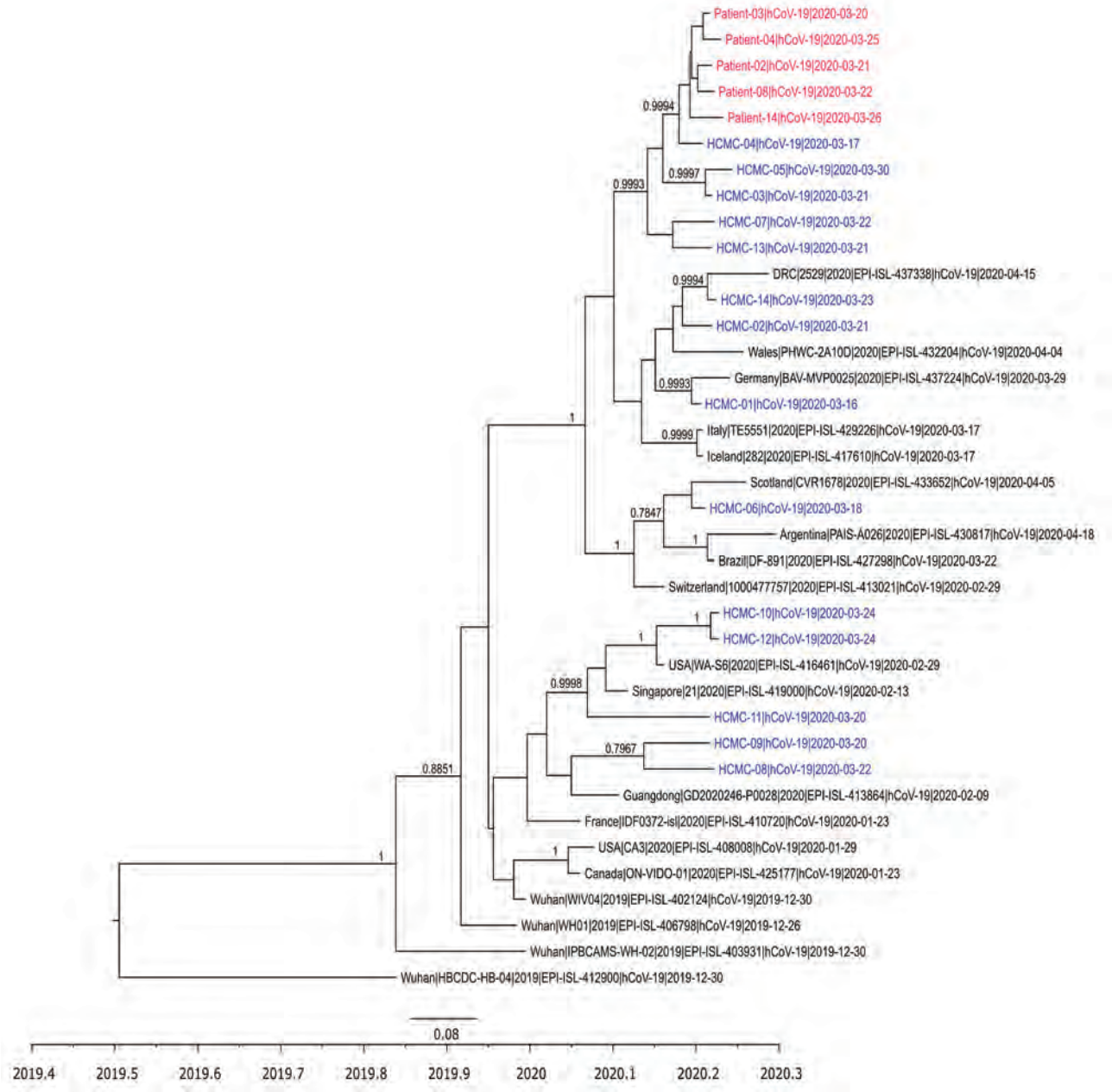


**Figure.** Time-scale phylogenetic tree illustrating the relatedness between whole-genome sequences of severe acute respiratory syndrome coronavirus 2 obtained from patients with confirmed cases of the cluster associated with a bar in Ho Chi Minh City, Vietnam, 2020, and reference sequences. Sequences from the cluster patients are in red; sequences from coronavirus disease patients in Ho Chi Minh City, not related to the cluster, are in blue. For those sequences, we obtained 21 genomes from the remaining 35 patients reported in Ho Chi Minh City as of April 24, 2020, for the purpose of the analysis; subsequently, we used 14 nonidentical sequences for the analysis. Representative sequences from patients not in Vietnam are in black. Posterior probabilities ≥75% are indicated at all nodes. The analysis was carried out using BEAST version 1.8.3 (https://beast.community). For time-scale analysis, only 1 representative of sequences that were 100% identical to each other was included. Whole-genome sequences were generated using ARTIC primers version 3 (ARTIC Network, https://artic.network/ncov-2019).

March 6. The other patients, except for patient 1, had no recent history of travel outside of HCMC (Table).

By exploring the epidemiologic links discovered from in-depth interviews, we identified 3 possible transmission chains involving patients who attended the March 14 celebration (Table; Figure; Appendix Figure). Of these, 2 or 3 patients (patients 5, 10, and possibly 14) were asymptomatic but transmitted SARS-CoV-2 to their contacts (Table; Figure). None of the 19 patients with confirmed cases reported that they had respiratory signs or symptoms on March 14–15. However, in addition to patient 1, a total of 5 others developed mild respiratory symptoms (patient 4 on March 16, patient 6 on March 21, patient 9 on March 25, patient 13 on March 26, and patient 17 on March 27), suggesting an incubation period of 2–12 days. Follow-up data were available for 12 patients who participated in our clinical study (Appendix). Six remained asymptomatic during follow-up (Appendix Table 1).

A total of 11 whole-genome sequences of SARS-CoV-2 were obtained from the patients in the cluster. The obtained sequences were either 100% identical or different from each other by only 1–2 nt (Appendix Table 2). Phylogenetically, they clustered together tightly but were different from sequences obtained from other cases in Ho Chi Minh City during the same period.

As of September 15, 2020, only 30 cases of locally acquired infection had been reported in Ho Chi Minh City (*6*), but this cluster represents the only documented superspreading event (*6*,*7*). Together with data from previous reports (*3*,*8*,*9*), these data suggest that closed settings are facilitators of community transmission of SARS-CoV-2. The mechanism by which infected people without symptoms spread SARS-CoV-2 to others, especially in closed settings, warrants further research, including on transmission through aerosols, which has been suggested (*4*,*10*).

The high level of genome sequence similarity between the SARS-CoV-2 genomes obtained from the patients and the tight clustering on the phylogenetic tree strengthen the epidemiologic link between the PCR-confirmed cases from this cluster. Together with contact history, these data also support transmission chains involving asymptomatic carriers (patients 5 and 14) as the sources of the ongoing infection. However, the identity of the patient in the index case from the bar could not be confirmed, in part because in-depth interview data were available from only 8 of 13 patients with confirmed cases who consented to participate in the study. In conclusion, our results emphasize that persons in crowded indoor settings with poor ventilation may be considered to be at high risk for SARS-CoV-2 transmission.

### Acknowledgments

We are indebted to Nguyen Thanh Ngoc, Le Kim Thanh, and the OUCRU IT/CTU/Lab management departments, especially Ho Van Hien, Dang Minh Hoang, and Nguyen Than Ha Quyen, for their support. We thank Maia Rabaa at OUCRU for her initial discussion about the analysis, and Leigh Jones at OUCRU for her input with some of the epidemiological data. Finally, we thank the patients for their participation in this study and the doctors and nurses of the Hospital for Tropical Diseases, who cared for the patients and provided the logistic support with the study.

This study was funded by the Wellcome Trust of Great Britain (106680/B/14/Z and 204904/Z/16/Z).

## About the Author

Dr. Chau is the director of the Hospital for Tropical Diseases in Ho Chi Minh City, Vietnam. He is a frontline healthcare worker in the COVID-19 pandemic.

### References

1. Wang SX, Li YM, Sun BC, Zhang SW, Zhao WH, Wei MT, et al. The SARS outbreak in a general hospital in Tianjin, China—the case of super-spreader. Epidemiol Infect. 2006;134:786–91. https://doi.org/10.1017/S095026880500556X
2. Cho SY, Kang J-M, Ha YE, Park GE, Lee JY, Ko J-H, et al. MERS-CoV outbreak following a single patient exposure in an emergency room in South Korea: an epidemiological outbreak study. Lancet. 2016;388:994–1001. https://doi.org/10.1016/S0140-6736(16)30623-7
3. Adam DC, Wu P, Wong JY, Lau EHY, Tsang TK, Cauchemez S, et al. Clustering and superspreading potential of SARS-CoV-2 infections in Hong Kong. Nat Med. 2020 Sep 17 [Epub ahead of print].
4. Morawska L, Milton DK. It is time to address airborne transmission of COVID-19. Clin Infect Dis. 2020;ciaa939. https://doi.org/10.1093/cid/ciaa939
5. World Health Organization. Transmission of SARS-CoV-2: implications for infection prevention precautions. 2020. [cited on 2020 Jul 24] https://www.who.int/news-room/commentaries/detail/transmission-of-sars-cov-2-implications-for-infection-prevention-precautions
6. Ministry of Health of Vietnam. Updated information about COVID-19 pandemic. Official page on acute respiratory infections COVID-19 [cited 2020 Sep 5]. http://ncov.moh.gov.vn
7. Thanh HN, Van TN, Thu HNT, Van BN, Thanh BD, Thu HPT, et al. Outbreak investigation for COVID-19 in northern Vietnam. Lancet Infect Dis. 2020;20:535–6. https://doi.org/10.1016/S1473-3099(20)30159-6
8. Pung R, Chiew CJ, Young BE, Chin S, Chen MIC, Clapham HE, et al.; Singapore 2019 Novel Coronavirus Outbreak Research Team. Investigation of three clusters of COVID-19 in Singapore: implications for surveillance and response measures. Lancet. 2020;395:1039–46. https://doi.org/10.1016/S0140-6736(20)30528-6

9. Ghinai I, Woods S, Ritger KA, McPherson TD, Black SR, Sparrow L, et al. Community Transmission of SARS-CoV-2 at Two Family Gatherings—Chicago, Illinois, February–March 2020. MMWR Morb Mortal Wkly Rep. 2020;69:446–50. https://doi.org/10.15585/mmwr.mm6915e1
10. Somsen GA, van Rijn C, Kooij S, Bem RA, Bonn D. Small droplet aerosols in poorly ventilated spaces and SARS-CoV-2 transmission. Lancet Respir Med. 2020;8:658–9. https://doi.org/10.1016/S2213-2600(20)30245-9

Address for correspondence: Le Van Tan, Oxford University Clinical Research Unit, Vo Van Kiet, District 5, Ho Chi Minh City, Vietnam; email: tanlv@oucru.org

# Racial and Workplace Disparities in Seroprevalence of SARS-CoV-2, Baton Rouge, Louisiana, USA

Amy K. Feehan, Cruz Velasco, Daniel Fort, Jeffrey H. Burton, Eboni G. Price-Haywood, Peter T. Katzmarzyk, Julia Garcia-Diaz, Leonardo Seoane

Author affiliations: Ochsner Clinic Foundation, New Orleans, Louisiana, USA (A.K. Feehan, C. Velasco, D. Fort, J.H. Burton, E.G. Price-Haywood, J. Garcia-Diaz, L. Seoane); The University of Queensland Faculty of Medicine, Ochsner Clinical School, New Orleans (A.K. Feehan, E.G. Price-Haywood, J. Garcia-Diaz, L. Seoane); Pennington Louisiana State University, Baton Rouge, Louisiana, USA (P.T. Katzmarzyk); Louisiana State University Health Sciences Center-Shreveport, Shreveport, Louisiana, USA (L. Seoane)

DOI: https://doi.org/10.3201/eid2701.203808

By using paired molecular and antibody testing for severe acute respiratory syndrome coronavirus 2 infection, we determined point prevalence and seroprevalence in Louisiana, USA, during the second phase of reopening. Infections were highly variable by race and ethnicity, work environment, and ZIP code. Census-weighted seroprevalence was 3.6%, and point prevalence was 3.0%.

We previously reported results from a seroprevalence study conducted in New Orleans, Louisiana, USA, which was hit hard early in the coronavirus disease (COVID-19) pandemic (*1*). Baton Rouge is a large metropolitan area roughly 80 miles northwest of New Orleans; at the time of this study, it was in the second phase of reopening after a stay-at-home order. Although the seroprevalence in New Orleans (6.9%) (*1*) was similar to prevalence recorded in Spain (5%), São Paulo, Brazil (4.7%), and New York, USA (6.9%) (*2*,*3*; B.H. Tess, unpub. data, https://doi.org/10.1101/2020.06.29.20142331), Baton Rouge had only 3,427 more cases as of August 2, 2020 (17,093 cases), than New Orleans did by May 16, 2020 (13,666 cases) (*4*). This latest study estimated severe acute respiratory syndrome coronavirus 2 (SARS-CoV-2) infections in the greater Baton Rouge area (Ascension, East Baton Rouge, Livingston, and West Baton Rouge Parishes), with additional information on potential workplace exposures.

The protocol was approved by the Ochsner institutional review board and was designed to enroll and test ≤2,500 participants at 13 sites throughout Baton Rouge during July 15–31. Recruitment targeted a representative sample by using a method developed by Public Democracy (https://www.publicdemocracy.io) and described elsewhere (*1*,*5*). In contrast to the New Orleans study, in which persons tested were under a stay-at-home order, Baton Rouge was in phase 2 of reopening. A randomized subset of 500,000 Baton Rouge residents were targeted with digital ads for recruitment. Of those, 3,687 volunteers were recruited and restratified according to census designations; 2,309 were invited to participate, 2,179 enrolled and completed testing, and 2,138 were included in our final analysis. A total of 38 persons were excluded because they lived in ineligible ZIP codes, and 3 withdrew consent (Appendix Figure 1, https://wwwnc.cdc.gov/EID/article/27/1/20-3808-App1.pdf). All study materials were provided in English, Spanish, and Vietnamese. Participants were offered free transportation. Research staff verbally obtained consent from participants and electronically documented consent and survey responses. We then procured blood samples and nasopharyngeal swab specimens from participants.

We used US Food and Drug Administration Emergency Use Authorization–approved tests. Real-time reverse transcription PCR of nasopharyngeal swab specimens was performed by using the Abbott m2000 RealTime system (Abbott, https://www.molecular.abbott). Qualitative IgG blood tests were performed by using the ARCHITECT i2000SR (Abbott). The IgG test meets criteria established by the Centers for Disease Control and Prevention to yield high positive predictive value, which was validated by Ochsner Health laboratory and others (*6*,*7*). Study participants who tested positive on either or both tests were

**Table.** Prevalence of past and present severe acute respiratory syndrome coronavirus 2 infections by race and ethnicity across Baton Rouge, Louisiana, after phased reopening, July 2020*

| Race or ethnicity | Positive no./total no. (% of sample) | Residents >18 y, no. (% of population)* | Any infection, raw,† % (95% CI) | Any infection, weighted,‡ % (95% CI) | Weighted point prevalence,§ % (95% CI) | Weighted seroprevalence,¶ % (95% CI) |
|---|---|---|---|---|---|---|
| Total | 128/2138 (100) | 551,185 (100) | 6.0 (5.0–7.1) | 6.6 (5.7–7.7) | 3.0 (2.3–3.7) | 3.6 (2.8–4.4) |
| White alone | 54/1431 (66.9) | 332,445 (60.3) | 3.8 (2.9–4.9) | 4.2 (3.2–5.2) | 2.4 (1.6–3.2) | 1.8 (1.1–2.5) |
| Black or African American alone | 57/516 (24.1) | 177,950 (32.3) | 11.0 (8.5–14.1) | 11.0 (8.5–14.1) | 3.5 (1.9–5.1) | 7.5 (5.2–9.8) |
| Asian alone | 2/59 (3.4) | 13,630 (2.5) | 3.4 (0.4–11.7) | 3.5 (0.0–8.2) | 1.7 (0.0–9.1) | 1.7 (0.0–9.1) |
| Other# | 1/28 (1.3) | 7,025 (1.3) | 3.6 (0.1–18.4) | 2.7 (0.0–8.7) | 0.0 | 2.7 (0.0–8.7) |
| Hispanic or Latino, any race | 14/104 (4.9) | 20,125 (3.7) | 13.5 (7.6–21.6) | 11.8 (5.6–18.0) | 10.1 (4.3–15.9) | 1.6 (0.0–4.0) |

*Census 2018 population estimates. By August 2, 2020, a total of 17,093 state-aggregated, confirmed cases had been reported in Ascension, East Baton Rouge, Livingston, and West Baton Rouge parishes (*4*).
†Percentage of sample with a PCR-positive test, an IgG-positive test, or both.
‡Census-weighted percentage of PCR-positive test, IgG-positive test, or both calculated to match 2018 racial demographics by parish and combined.
§Census-weighted percentage of PCR-positive and IgG-negative tests calculated to match 2018 racial demographics by parish and combined.
¶Census-weighted percentage of IgG–positive tests calculated to match 2018 racial demographics by parish and combined.
#Other includes American Indian or Alaska Native, Pacific Islander, and multiracial persons.

assessed as having been infected with SARS-CoV-2. Point estimates and corresponding 95% CIs for proportions of SARS-CoV-2 exposure (PCR+ or IgG+ tests), point prevalence (PCR+, IgG–), and seroprevalence (IgG+ tests regardless of PCR test result) were estimated for the Baton Rouge area by using raw and census-weighted counts. Unadjusted odds ratios with Firth correction were calculated for all variables.

The sample was 63.6% female and 66.9% white; average age was 48.7 years (range 18–91) and average household size 2.84 persons. The census-weighted estimate of SARS-CoV-2 infections in the sample is 6.6% (6.0%, raw), with 3.0% positive for active viral shedding without detectable antibody, which translates to 16,536 contagious persons. By race and ethnicity, seroprevalence was highest (7.5%) in Black participants, compared with White non-Hispanic (1.8%), Asian non-Hispanic (1.7%), Hispanic of any race (1.6%), and other (2.7%) participants (Table).

The point prevalence and any SARS-CoV-2 infection were mapped by ZIP codes across the greater Baton Rouge area (Appendix Figure 2). Point prevalence and all infections were highly variable by ZIP code.

Marital status was associated with prevalence ($p = 0.0005$ by $\chi^2$ test). Single persons had the highest rate of infection (9.3%), compared with rates for married or cohabitating participants (5.0%), and were 1.9 times more likely to test positive (Figure). Work environment also affected prevalence ($p = 0.01$ by $\chi^2$ test); the lowest prevalence was in participants who worked from home part-time and went to a workplace part-time (3.7%). Those who worked primarily outside the home had the highest prevalence (8.2%) and were 2.3 times more likely to test positive than those who worked from home at least part-time. Infection rates varied by occupation ($p = 0.01$ by $\chi^2$ test); the lowest positivity was in office workers (3.0%) and increased odds of testing positive occurred in delivery, healthcare, and other public-facing jobs. However, based on seroprevalence, which also varied substantially by occupation ($p = 0.03$ by $\chi^2$ test), healthcare workers and public-facing workers bore the brunt of early infections, as demonstrated by higher odds of testing positive for antibodies (Figure).

We found the prevalence of SARS-CoV-2 infection in Baton Rouge to be 6.6% but with a heavy concentration of new, contagious infections (3.0%). Persons who were infected early possibly no longer had antibodies. This finding differed from our New Orleans study, which was performed after extensive lockdowns and estimated new infections at 0.9% (*1*). Some populations had higher rates of infection than others, including Black and Hispanic communities and public-facing workers or those who do not work from home.

### Acknowledgments

The authors would like to especially thank the laboratories at the Ochsner Medical Center Jefferson Highway Campus for testing and keeping track of research samples; Christy Reeves for liaising with public leaders and sites; Eric Sapp and Dan Nichols for their recruitment effort; Susan Green, Charlene Ho, Lena Hooper, Patty Kline, and Candace Melancon for clinical site management; Johanna Veal, Lyndsey Buckner-Baiamonte, Ansley Hammons, and Ashley LaRoche for research site management; and countless research coordinators, clinical staff, marketing personnel, medical students, and Epic and IT staff for making site testing possible. The Ochsner Health Market Planning and Analysis team designed the maps in Appendix Figure 1. The authors thank Kathleen McFadden for her thorough editing. We would like to thank the Ochsner Language Services Department for helping to increase inclusivity and to acknowledge the East Baton

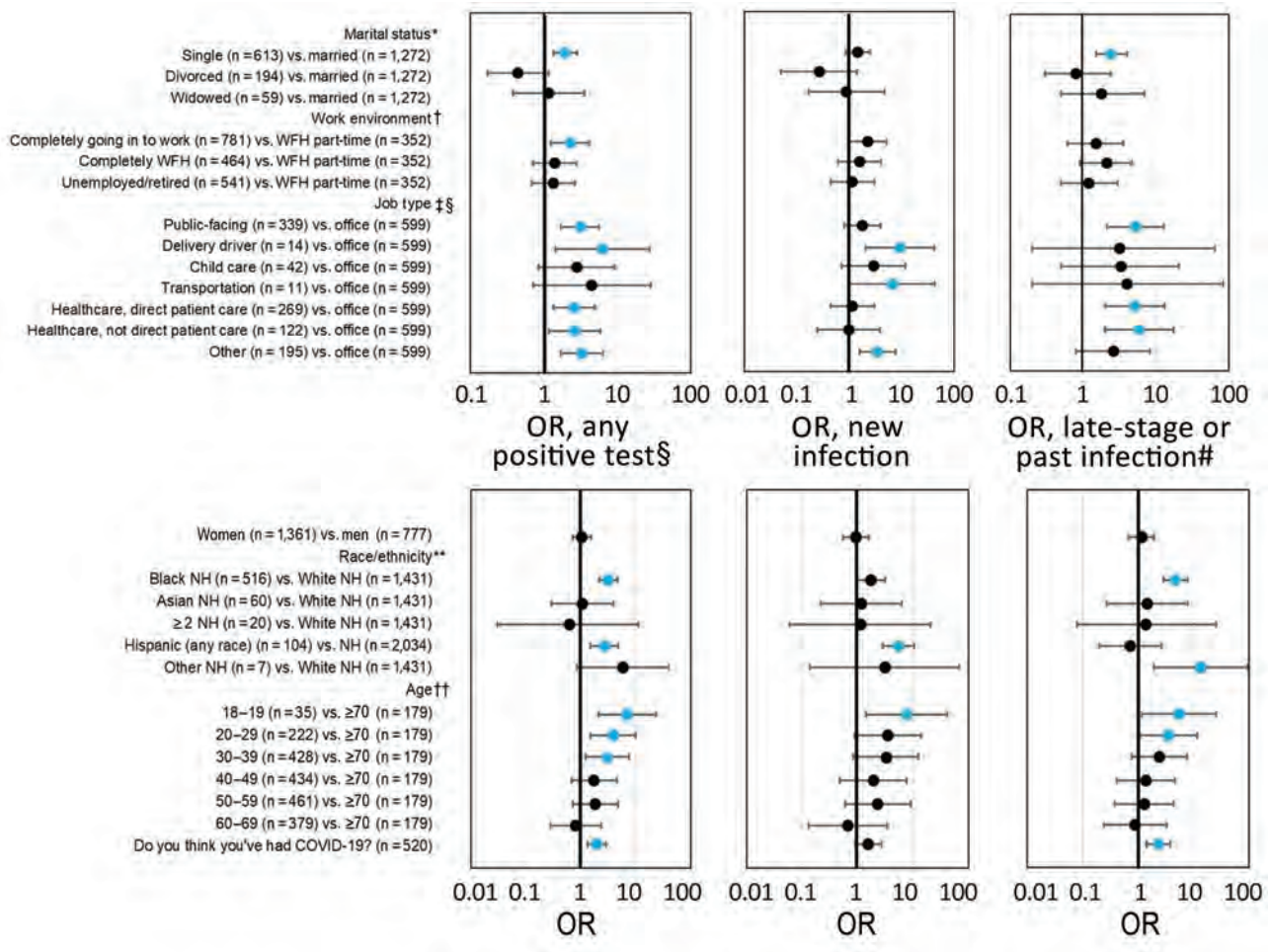


**Figure.** Odds ratios of severe acute respiratory syndrome coronavirus 2 infections by marital status, work environment, and job type after phased reopening in Baton Rouge, Louisiana, USA, July 2020. OR from unweighted logistic regression without covariates with Firth correction are shown with 95% CIs. Reference categories' percent positivity are married (5.0% any infection, 2.3% seroprevalence), WFH part-time (3.7% any infection, 2.0% seroprevalence), and office workers (3.0% any infection, 1.0% seroprevalence). WFH, work from home; NH, non-Hispanic; OR, odds ratio. *Odds of any infection (p = 0.0005) and seroprevalence (p = 0.03) differ by marital status. †Odds of any infection (p = 0.01) differ by work environment. ‡Odds of any infection (p = 0.01) and seroprevalence (p = 0.03) differ by job type. §Six people did not give an answer for job type; none tested positive on any test. Unemployed/retired people (n = 541) are not included in this category. ¶Percentage and OR of any positive test (PCR+ or IgG+). #Percentage and OR of late-stage or past infections (IgG+, regardless of PCR status). **Odds of any infection (p<0.0001) and seroprevalence (p<0.0001) differ by race and ethnicity. ††Odds of any infection (p<0.0001) and seroprevalence (p = 0.0074) differ by age.

Rouge Mayor–President Sharon Weston Broome and Pennington Biomedical Research Center for their collaboration and support of this project.

The study was funded by the Baton Rouge Area Foundation, Louisiana COVID-19 Health Equity Task Force, and the Humana Foundation, with additional support from the Blue Cross and Blue Shield of Louisiana Foundation, Healthy Blue, the Huey and Angelina Wilson Foundation, and the Irene W. and C.B. Pennington Foundation. The funders had no role in study design, data collection and analysis, decision to publish, or preparation of the manuscript.

## About the Author

Dr. Feehan is a research scientist at the Ochsner Clinic Foundation's Infectious Disease Clinical Research Department. Her research focuses on the gut microbiome as a treatment modality for neurologic disease, but more immediately on the COVID-19 pandemic.

## References

1. Feehan AK, Fort D, Garcia-Diaz J, Price-Haywood EG, Velasco C, Sapp E, et al. Seroprevalence of SARS-CoV-2 and infection fatality ratio, Orleans and Jefferson parishes, Louisiana, USA, May 2020. Emerg Infect Dis. 2020;26:2766–9. https://doi.org/10.3201/eid2611.203029

2. Pollán M, Pérez-Gómez B, Pastor-Barriuso R, Oteo J, Hernán MA, Pérez-Olmeda M, et al.; ENE-COVID Study Group. Prevalence of SARS-CoV-2 in Spain (ENE-COVID): a nationwide, population-based seroepidemiological study. Lancet. 2020;396:535–44. https://doi.org/10.1016/S0140-6736(20)31483-5
3. Havers FP, Reed C, Lim T, et al. Seroprevalence of Antibodies to SARS-CoV-2 in 10 sites in the United States, March 23–May 12, 2020. JAMA Intern Med. 2020 Jul 21 [Epub ahead of print].
4. Louisiana Department of Public Health. Louisiana coronavirus COVID-19 information [cited 2020 Sep 20]. http://ldh.la.gov/Coronavirus
5. Feehan A, Fort D, Garcia-Diaz J, Price-Haywood E, Velasco C, Sapp E, et al. Frequency of symptoms and asymptomatic SARS-CoV-2 infection in New Orleans, Louisiana after 7 weeks of a stay-at-home order [cited 2020 Sep 8]. https://ssrn.com/abstract=3633166 https://doi.org/10.2139/ssrn.3633166
6. US Centers for Disease Control and Prevention. Interim guidelines for COVID-19 antibody testing [cited 2020 Aug 10]. https://www.cdc.gov/coronavirus/2019-ncov/lab/resources/antibody-tests-guidelines.html
7. Bryan A, Pepper G, Wener MH, Fink SL, Morishima C, Chaudhary A, et al. Performance characteristics of the Abbott Architect SARS-CoV-2 IgG assay and seroprevalence in Boise, Idaho. J Clin Microbiol. 2020;58:e00941-20. https://doi.org/10.1128/JCM.00941-20

Address for correspondence: Amy Feehan, Clinical Infectious Diseases Research, 1st Fl AT, 1514 Jefferson Hwy, Jefferson, LA 70121, USA; email: amy.feehan@ochsner.org

# SARS-CoV-2 Cluster in Nursery, Poland

Magdalena Okarska-Napierała, Joanna Mańdziuk, Ernest Kuchar

Author affiliation: Medical University of Warsaw, Warsaw, Poland

DOI: https://doi.org/10.3201/eid2701.203849

We report a cluster of surprisingly high spread of severe acute respiratory syndrome coronavirus 2 (SARS-CoV-2) associated with a single nursery in Poland. Our findings contrast with the presumed negligible role of children in driving the SARS-CoV-2 pandemic. Children 1–2 years of age might be effective SARS-CoV-2 spreaders.

Despite robust research, knowledge about coronavirus disease (COVID-19) spread and effective control measures is still limited. Until recently, research has indicated that children rarely spread the infection to adults and are not the primary drivers of severe acute respiratory syndrome coronavirus 2 (SARS-CoV-2) transmission (*1*).

We describe characteristics of the cluster of SARS-CoV-2 cases that emerged in a single nursery in Poland within 2 weeks of its reopening. We anonymized all data and collected no sensitive data. The Bioethics Committee of the Medical University of Warsaw approved the study protocol.

The nursery at issue was reopened after a nationwide lockdown on May 18, 2020. On May 31, a nursery worker reported family contact with a symptomatic SARS-CoV-2–infected person, and the nursery was closed. During the 14 days the nursery was open, a mean of 25 children attended the nursery daily. Children spent ≈8 hours there, divided into 3 groups, each cared for by 2 caregivers (Appendix, https://wwwnc.cdc.gov/EID/article/27/1/20-3849-App1.pdf). Neither children nor caregivers moved across multiple classes. Caregivers wore facemasks when in contact with children. Parents did not enter the building when dropping off and picking up children. Contacts between parents and nursery workers lasted <15 minutes, with facemasks on. Family members of different children did not mix.

The index case of SARS-CoV-2 infection (in a nursery worker with family contact) was confirmed on June 4. Subsequent PCR testing of nursery staff, children attending the facility, and family members (2 initial case-patients plus 104 other persons) (Appendix) revealed positive results in an additional 4 nursery workers (of whom 1 was also a parent of a child attending the facility), 3 children of the nursery workers, 8 children attending the facility, 3 siblings of those children, 8 parents, and 1 grandparent. The cluster involved a total of 29 persons; 8 were children attending the nursery, and 12 were children's family members who did not enter the facility (Table). One child with a negative result had 2 parents with positive results. One child's parent tested negative in this cluster but had tested positive within the previous 2 weeks, involved in another cluster.

The overall positivity rate in our cluster was 27%. COVID-19 prevalence in Poland is low. The number of tests conducted in the voivodeship was 124,194 in June, whereas the number of positive cases was 1,374, which corresponded to a positivity rate of 1% (2). Thus, local SARS-CoV-2 circulation in society is not sufficient to explain the positivity rate in our cluster.

**Table.** Severe acute respiratory syndrome coronavirus 2 testing outcomes of potentially infected persons in a nursery setting, Poland, 2020

| Person | No. tested | No. positive by PCR | % Positive |
|---|---|---|---|
| Children attending the nursery | 28 | 8 | 29 |
| Parents of children attending nursery* | 31 | 8 | 26 |
| Siblings of children attending nursery | 16 | 3 | 19 |
| Grandparent of children attending nursery | 1 | 1 | 100 |
| Nursery workers | 25 | 5 | 20 |
| Spouses of nursery workers | 2 | 1 | 50 |
| Children of nursery workers | 3 | 3 | 100 |
| Total | 106 | 29 | 27 |

*One of the parents of children attending the nursery was also a nursery worker; she is counted as a worker in this table.

The case of the COVID-19–negative child with positive parents could have been a false-negative result or a negative result after being infected. The result might also have been a true negative, and the parents were infected from another source. However, other potential exposures could not explain infections in all parents involved in our cluster.

We depict probable chains of transmission in the Figure. Of note, physical contact between nursery workers and children's family members who were infected was strictly limited, and the only close contacts for these groups of adults were children. Given that most COVID-19–positive persons were asymptomatic and tested on the same day, determining with certainty whether children transmitted the virus to their parents or the workers is not possible. Nevertheless, children seemed to be effective mediators of infection between adults.

Several reports concerning clusters of COVID-19 in childcare settings imply little to no SARS-CoV-2 transmission among children and from children to adults (1,4,5; A. Fontanet, unpub. data, https://doi.org/10.1101/2020.06.25.20140178; R.M. Viner, unpub. data, https://doi.org/10.1101/2020.05.20.20108126). However, such estimations are open to bias, given that most published data were obtained at the time of lockdown, when children's social contacts were limited to family members. Another limitation of those publications is that they applied mostly to school-age children.

The high infection attack rate among children in our cluster could be explained by prolonged close contact between very young children, who are less able to adjust to control measures. Similarly, specific intimate contact between toddlers and their family members could have led to effective spread within families. This observation might be particularly important in light of novel findings that nasopharyngeal SARS-CoV-2 levels are the highest in the youngest children (6). Moreover, the airborne transmission route in the nursery rooms' confined environment could have played an important role (7).

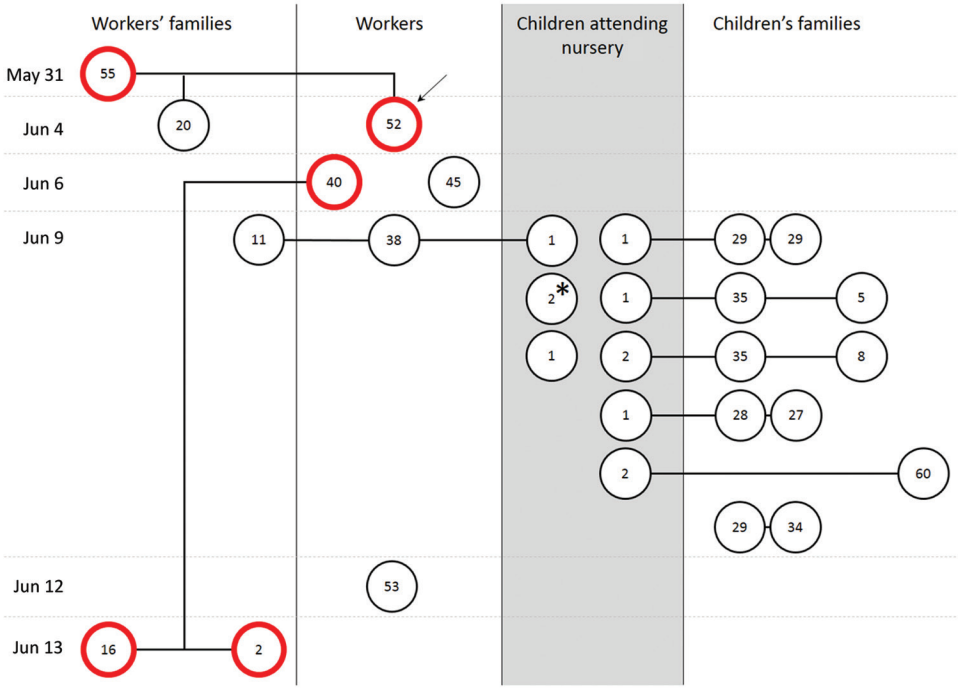


**Figure.** All persons testing positive for severe acute respiratory syndrome coronavirus 2 infection in a cluster associated with a nursery, Poland 2020. Dates to left indicate first positive results in consecutive case-patients. Circles indicate infected case-patients; numbers in circles indicate age in years. Red circles indicate infected case-patients with symptoms. Circles connected by lines indicate case-patients who are members of the same household. Arrow indicates the probable index case-patient. Asterisk indicates child whose parent tested negative in this cluster but tested positive within the previous 2 weeks.

Our study has some potential limitations. We could not determine whether the infection in the nursery worker was the real index case because one of the children's parents had tested positive within the previous 2 weeks and that child could also have been the primary case. Moreover, we could not verify the information we obtained from the nursery about the facility's prevention methods.

Our report questions the role of young children in driving the COVID-19 pandemic. Of note, most children in our study were asymptomatic, and this cluster would likely not have been detected without subsequent testing of persons who had direct contact with the index case-patient. We believe further studies are needed to clarify young children's role in the transmission of SARS-CoV-2.

### Acknowledgments

We thank Lucyna Wiśniewska, who provided anonymized characteristics of persons in the cluster.

### About the Author

Dr. Okarska-Napierała works as an attending physician and professor in the Department of Pediatrics with the Clinical Assessment Unit, Medical University of Warsaw. Her research is focused on Kawasaki disease.

### References

1. Ludvigsson JF. Children are unlikely to be the main drivers of the COVID-19 pandemic—a systematic review. Acta Paediatr. 2020;109:1525–30. https://doi.org/10.1111/apa.15371
2. Rogalski M. COVID-19 w Polsce. Database based on Polish Ministry of Health reports [cited 2020 Aug 26]. http://bit.ly/covid19-polska
3. Li X, Xu W, Dozier M, He Y, Kirolos A, Theodoratou E; UNCOVER. The role of children in transmission of SARS-CoV-2: a rapid review. J Glob Health. 2020;10:011101. https://doi.org/10.7189/jogh.10.011101
4. Yung CF, Kam KQ, Nadua KD, Chong CY, Tan NWH, Li J, et al. Novel coronavirus 2019 transmission risk in educational settings. Clin Infect Dis. 2020;ciaa794. https://doi.org/10.1093/cid/ciaa794
5. Somekh E, Gleyzer A, Heller E, Lopian M, Kashani-Ligumski L, Czeiger S, et al. The role of children in the dynamics of intra family coronavirus 2019 spread in densely populated area. Pediatr Infect Dis J. 2020;39:e202–4. https://doi.org/10.1097/INF.0000000000002783
6. Heald-Sargent T, Muller WJ, Zheng X, Rippe J, Patel AB, Kociolek LK. Age-related differences in nasopharyngeal severe acute respiratory syndrome coronavirus 2 (SARS-CoV-2) levels in patients with mild to moderate coronavirus disease 2019 (COVID-19). JAMA Pediatr. 2020;174:902–3. https://doi.org.10.1001/jamapediatrics.2020.3651
7. Morawska L, Cao J. Airborne transmission of SARS-CoV-2: the world should face the reality. Environ Int. 2020;139:105730. https://doi.org/10.1016/j.envint.2020.105730

Address for correspondence: Joanna Mańdziuk, Department of Pediatrics with Clinical Assessment Unit, Medical University of Warsaw, 61 Żwirki i Wigury St, 02-091 Warsaw, Poland; email: joanna.mandziuk@uckwum.pl

# Developing Endemicity of Schistosomiasis, Corsica, France

Camilla Rothe, Thorbjörn Zimmer, Mirjam Schunk, Claudia Wallrauch, Kerstin Helfrich, Fatih Gültekin, Gisela Bretzel, Jean-François Allienne, Jérôme Boissier

Author affiliations: University Hospital, LMU Munich, Munich, Germany (C. Rothe, T. Zimmer, M. Schunk, C. Wallrauch, K. Helfrich, F. Gültekin, G. Bretzel); Université de Perpignan Via Domitia, Université de Montpellier, Perpignan, France (J.-F. Allienne, J. Boissier)

DOI: https://doi.org/10.3201/eid2701.204391

Urogenital schistosomiasis was diagnosed in a man from Germany who had never traveled outside Europe. He likely acquired the infection in Corsica, France, but did not swim in the Cavu River, which was linked to a previous outbreak. This case highlights that transmission of schistosomiasis in Corsica is ongoing.

A 49-year-old man from Germany experienced macrohematuria in June 2020 and underwent cystoscopy in August 2020. Histologic analysis of a bladder biopsy specimen showed ova of *Schistosoma* spp. He was referred to the outpatient department for tropical medicine at LMU Hospital Munich.

The patient had never traveled outside Europe. He had, however, traveled twice to Corsica, France, in 2013 and 2019. He never swam in the Cavu River, which has been associated with cases of schistosomiasis in recent years (*1*–*3*).

The patient visited Corsica during August 22–September 4, 2019. By using GPS data from his smartphone and camera, he reconstructed his bathing sites precisely. During August 22–24, he swam

several times in the Solenzara River in the southeastern part of the island, near a busy campsite (Figure). Further minor water contacts might have occurred at the Gravona River in western Corsica near Ajaccio, at a turtle park and near a campsite, and at the Tavignano River (Figure). He did not bathe in either of Corsica's other rivers but could not rule out contact with water for cooling purposes. The patient reported swimming in the Restonica River in 2013 (Figure), but he did not recall any itchy rash suggestive of cercarial dermatitis.


**Figure.** Locations of rivers referenced in investigation of developing endemicity of schistosomiasis, Corsica, France. Map adapted by using UBehrje (https://www.demis.nl); in public domain (https://upload.wikimedia.org/wikipedia/commons/3/3e/Corsica_Map.png).

Physical examination was unremarkable. Full blood count did not show any eosinophilia. Urine sediment microscopy showed terminal-spined ova resembling those of *S. hematobium* parasites. Urine tested in-house by quantitative PCR for *S. hematobium* parasites was positive. A schistosoma serologic test was positive by enzyme immunoassay (64 U/L; reference <10 U/L); results of a blood immunochromatographic rapid diagnostic test were positive, but Western blot results were negative. Results of a urine circulating cathodic antigen point-of-care test was weakly positive. His son, who traveled with him in 2013, and his wife, who had joined him on both trips, had negative serologic test results and were negative for urine schistosoma by PCR.

DNA extracted from 7 ova was successfully amplified on nuclear internal transcribed spacer and mitochondrial cytochrome oxidase I markers. For the nuclear marker, DNA (995 bp) of all eggs showed a typical signature of *S. hematobium* parasite. The mitochondrial marker (873 bp) of all eggs had a typical signature of *S. bovis* parasite and displayed the same haplotype. In summary, all eggs were identified as hybrids of *S. hematobium* and *S. bovis* (ShxSb) parasites. This type of hybrid (nuclear Sh and mitochondrial Sb) was the most frequently observed type during the 2013 outbreak (*4*). The mitochondrial cytochrome oxidase I sequences of all eggs had 100% homology with haplotype Sb2, the most frequent haplotype observed during the 2013 outbreak (*4*). Presence of this haplotype was also documented in subsequent reports on the first outbreak in Corsica (*2*,*3*).

Transmission of schistosomiasis in Corsica has been documented since 2013 (*3*,*5*). Cases have been detected in residents and in tourists (*5*,*6*). In spring 2014, after the first outbreak, intense screening and public health efforts led to the identification of 106 cases linked to the Cavu River (*7*). During 2015–2018, sporadic cases were detected and linked to the Cavu (*8*). The cases reported in 2018 involved 2 patients who had bathed in the Cavu and Solenzara Rivers (*3*).

The patient we describe reported having no contact with the Cavu River. Instead, the infection was most likely acquired in the Solenzara River, near a busy campsite. The Solenzara neighbors the Cavu, but their waters do not intermingle. No confirmed cases acquired in the Solenzara River have been documented, but *Bulinus truncatus* snails or their DNA have been found along the river during environmental surveys (*1*,*9*). Snail density close to the main bathing site of our patient appears to be high (*9*). Neither of the other rivers mentioned was ever proven to be a source of schistosomiasis; in addition, they are all relatively far away from the Cavu region.

Genotyping revealed the *S. hematobium–S.bovis* hybrid parasite described in previous outbreaks, suggesting ongoing transmission rather than reintroduction. The parasite's emergence in another river cannot be explained by the persistence of infected snails (*9*) but could be explained by reseeding of the river by a mammalian host.

Animal reservoirs have been discussed as a possible explanation for ongoing transmission; however, evidence of a major role is lacking. No infection has been detected in livestock in the region, and the only infected animals found were 2 rats (*10*). Even if we cannot rule out the influence of an undetected animal reservoir (e.g., *Ovis aries musimon,* wild sheep native to Corsica, have never been tested), the most likely explanation is that 1 or several infected persons continue to infest the water.

In summary, this case highlights that transmission of schistosomiasis in Corsica is ongoing and is no longer restricted to the Cavu River. The parasite appears to be of the same strain detected previously on the island. The infection was acquired at a frequented tourist site, suggesting that more persons might have been infected. Further screening of residents and tourists is urgently needed.

### About the Author

Dr. Rothe is deputy head of the division of tropical medicine at the LMU Hospital Munich. Her main areas of interest are clinical tropical medicine, neglected tropical diseases, emerging infections, travel medicine, and migrant medicine.

### References


1. Berry A, Moné H, Iriart X, Mouahid G, Aboo O, Boissier J, et al. Schistosomiasis haematobium, Corsica, France. Emerg Infect Dis. 2014;20:1595–7. https://doi.org/10.3201/eid2009.140928
2. Moné H, Holtfreter MC, Allienne JF, Mintsa-Nguéma R, Ibikounlé M, Boissier J, et al. Introgressive hybridizations of *Schistosoma haematobium* by *Schistosoma bovis* at the origin of the first case report of schistosomiasis in Corsica (France, Europe). Parasitol Res. 2015;114:4127–33. https://doi.org/10.1007/s00436-015-4643-4
3. Ramalli L, Mulero S, Noël H, Chiappini JD, Vincent J, Barré-Cardi H, et al. Persistence of schistosomal transmission linked to the Cavu River in southern Corsica since 2013. Euro Surveill. 2018;23. https://doi.org/10.2807/1560-7917.ES.2018.23.4.18-00017
4. Boissier J, Grech-Angelini S, Webster BL, Allienne JF, Huyse T, Mas-Coma S, et al. Outbreak of urogenital schistosomiasis in Corsica (France): an epidemiological case study. Lancet Infect Dis. 2016;16:971–9. https://doi.org/10.1016/S1473-3099(16)00175-4
5. Holtfreter MC, Moné H, Müller-Stöver I, Mouahid G, Richter J. *Schistosoma haematobium* infections acquired in Corsica, France, August 2013. Euro Surveill. 2014;19:20821. https://doi.org/10.2807/1560-7917.ES2014.19.22.20821
6. Berry A, Paris L, Boissier J, Caumes E. Schistosomiasis screening of travelers to Corsica, France. Emerg Infect Dis. 2016;22:159. https://doi.org/10.3201/eid2201.151290
7. Noël H, Ruello M, Maccary A, Pelat C, Sommen C, Boissier J, et al. Large outbreak of urogenital schistosomiasis acquired in Southern Corsica, France: monitoring early signs of endemicization? Clin Microbiol Infect. 2018;24:295–300. https://doi.org/10.1016/j.cmi.2017.06.026
8. Ramalli L, Noel H, Mulero S, Vincent J, Malfait P, Alliene JF, et al. Persistence of urogenital schistosomiasis in Southern Corsica since 2013 [in French]. Med Mal Infect. 2018;48:S126.
9. Mulero S, Rey O, Arancibia N, Mas-Coma S, Boissier J. Persistent establishment of a tropical disease in Europe: the preadaptation of schistosomes to overwinter. Parasit Vectors. 2019;12:379. https://doi.org/10.1186/s13071-019-3635-0
10. Oleaga A, Rey O, Polack B, Grech-Angelini S, Quilichini Y, Pérez-Sánchez R, et al. Epidemiological surveillance of schistosomiasis outbreak in Corsica (France): are animal reservoir hosts implicated in local transmission? PLoS Negl Trop Dis. 2019;13:e0007543. https://doi.org/10.1371/journal.pntd.0007543


Address for correspondence: Camilla Rothe, LMU University Hospital Munich, 4th Medical Department, Division of Infectious Diseases and Tropical Medicine, Leopoldstr. 5, D-80802 Munich, Germany; email: rothe@lrz.uni-muenchen.de

# Relapsing Fever Group Borreliae in Human-Biting Soft Ticks, Brazil

Sebastián Muñoz-Leal,[1] Álvaro A. Faccini-Martínez, Bruno M. Teixeira, Maria Marlene Martins, Maria Carolina A. Serpa, Glauber M.B. Oliveira, Felipe R. Jorge, Richard C. Pacheco, Francisco B. Costa, Hermes R. Luz, Marcelo B. Labruna

Author affiliations: Universidade de São Paulo, São Paulo, Brazil (S. Muñoz-Leal, M.C.A. Serpa, G.M.B. Oliveira, M.B. Labruna); Asociación Colombiana de Infectología, Bogotá, Colombia (Á.A. Faccini-Martínez); Centro Universitario INTA–UNINTA, Sobral, Brazil (B.M. Teixeira, F.R. Jorge); Universidade Federal de

[1]Current affiliation: Universidad de Concepción, Chillán, Ñuble, Chile.

Uberlândia, Uberlândia, Brazil (M.M. Martins); Universidade Federal de Mato Grosso, Cuiabá, Brazil (R.C. Pacheco); Universidade Estadual do Maranhão, São Luís, Brazil (F.B. Costa); Universidade Federal do Maranhão, São Luís (H.R. Luz)

DOI: https://doi.org/10.3201/eid2701.200349

We conducted a molecular survey for *Borrelia* spp. in *Ornithodoros* ticks previously reported as biting humans. We collected specimens in natural ecosystems and inside human dwellings in 6 states in Brazil. Phylogenetic analyses unveiled the occurrence of 4 putatively new species of relapsing fever group borreliae.

Tick-borne relapsing fever (TBRF) is a vectorborne disease caused by spirochetes of the genus *Borrelia* that thrive in enzootic cycles and are transmitted mainly by soft ticks of the genus *Ornithodoros* (*1*). Humans bitten by infected ticks can become ill and present a typical recurrent febrile syndrome (*1*). In the New World, research on TBRF persists mainly in North America, where *Borrelia turicatae*, *B. parkeri*, and *B. hermsii* infect humans (*1*). Meanwhile, the knowledge on relapsing fever spirochetes in South America has remained comparatively incomplete. In Brazil, *Ornithodoros brasiliensis*, *O. fonsecai, O. mimon*, *O. rietcorreai*, and *O. rostratus* ticks have been reported to parasitize humans (*2*,*3*), yet their role as vectors of *Borrelia* spp. is unknown. Recently, in Brazil, *B. venezuelensis*, the agent of South American TBRF during the first half of the 20th century, was isolated from the anthropophilic tick *O. rudis* (*4*). This finding highlighted the occurrence of pathogenic relapsing fever group borreliae (RFGB) and called attention to study human-biting *Ornithodoros* ticks as possible vectors of these microorganisms.

During December 2018–October 2019, we conducted collections of soft ticks in the Brazilian states of Ceará (CE), Goiás (GO), Mato Grosso (MT), Mato Grosso do Sul (MS), Maranhão (MA), and Rondônia (RO) (Appendix Figure, https://wwwnc.cdc.gov/EID/article/27/1/20-0349-App1.pdf). Collections in MS were implemented using dry ice as an attractor; in CE, GO, MA, and RO, we collected soft ticks inside caves, abandoned nests or between rocks in rural areas. In MT, specimens were collected on the walls of an inhabited house in an urban area. Collections of ticks were authorized by Instituto Chico Mendes de Conservação da Biodiversidade (ICMBio permits 65137-1 and 36413-1).

A total of 665 specimens (236 males, 145 females, 284 nymphs) belonging to 8 species of the genus *Ornithodoros* were submitted to individual or pooled DNA extractions (Appendix Table 1). We screened extractions with a *Borrelia*-specific real-time PCR with primers Bor16S3F and Bor16S3R and probe Bor16S3P, using 2 μL of genomic DNA, to amplify a fragment of the 16S rRNA gene (*5*). Samples with cycle threshold values <32 were tested with a battery of PCRs targeting the 16S rRNA and the *flab* and *glpQ* borrelial genes.

Four species of ticks were positive by *Borrelia*-specific real-time PCR. We generated sequences of *Borrelia* 16S rRNA, *flaB*, and *glpQ* genes for these specimens (Appendix Table 1). Two haplotypes of 16S rRNA gene were sequenced from each of the 2 positive *O. mimon* ticks, and the obtained sequences of *flaB* and *glpQ* were identical for both specimens. One haplotype for each gene was obtained for *O. hasei* and the *Ornithodoros* sp. ticks from CE, and only a 16S rDNA sequence was obtained from *O. rietcorreai* ticks (Appendix Table 2). With high support values, Bayesian phylogenetic analyses showed that the *Borrelia* spp. characterized from *O. mimon*, *O. rietcorreai*, and the *Ornithodoros* sp. ticks from CE form a monophyletic clade related to RFGB occurring in the Old World. In turn, the *Borrelia* sp. harbored by *O. hasei* ticks clustered within New World RFGB (Figure). These results add further evidence that Old and New World RFGB do not necessarily have defined geographic distributions but rather correspond to arbitrary groups.

Five species of *Ornithodoros* ticks have been reported to parasitize humans in Brazil (*2*,*3*). We have added 2 more species to this list, as *O. hasei* and the *Ornithodoros* sp. ticks from CE avidly bit us during collections in the field (data not shown). Although with low prevalence, these 2 species, together with *O. mimon* and *O. rietocorreai*, harbored DNA of putatively new *Borrelia* spp. phylogenetically related to the relapsing fever group. The implications of these new spirochetes as human pathogens are still unknown. *O. mimon* and *O. rietcorreai* ticks are associated with human parasitism in urban and rural dwellings in Brazil (*2*,*3*), so vector roles of both species should not be overlooked.

TBRF courses with febrile episodes and should be considered as a differential diagnosis within the spectrum of diseases that cause an undifferentiated febrile syndrome (UFS) (*6*). Although specific data are vague for the states where tick collections were performed in this study, UFS is common in Brazil; mosquitoborne viruses and malaria are the main etiologic agents (*7*,*8*). Nevertheless, febrile illnesses still remain underdiagnosed in a substantial proportion of the cases in the country (*7*,*8*). The results of this study are a contribution to the knowledge of RFGB in human-biting *Ornithodoros* ticks, and stress the

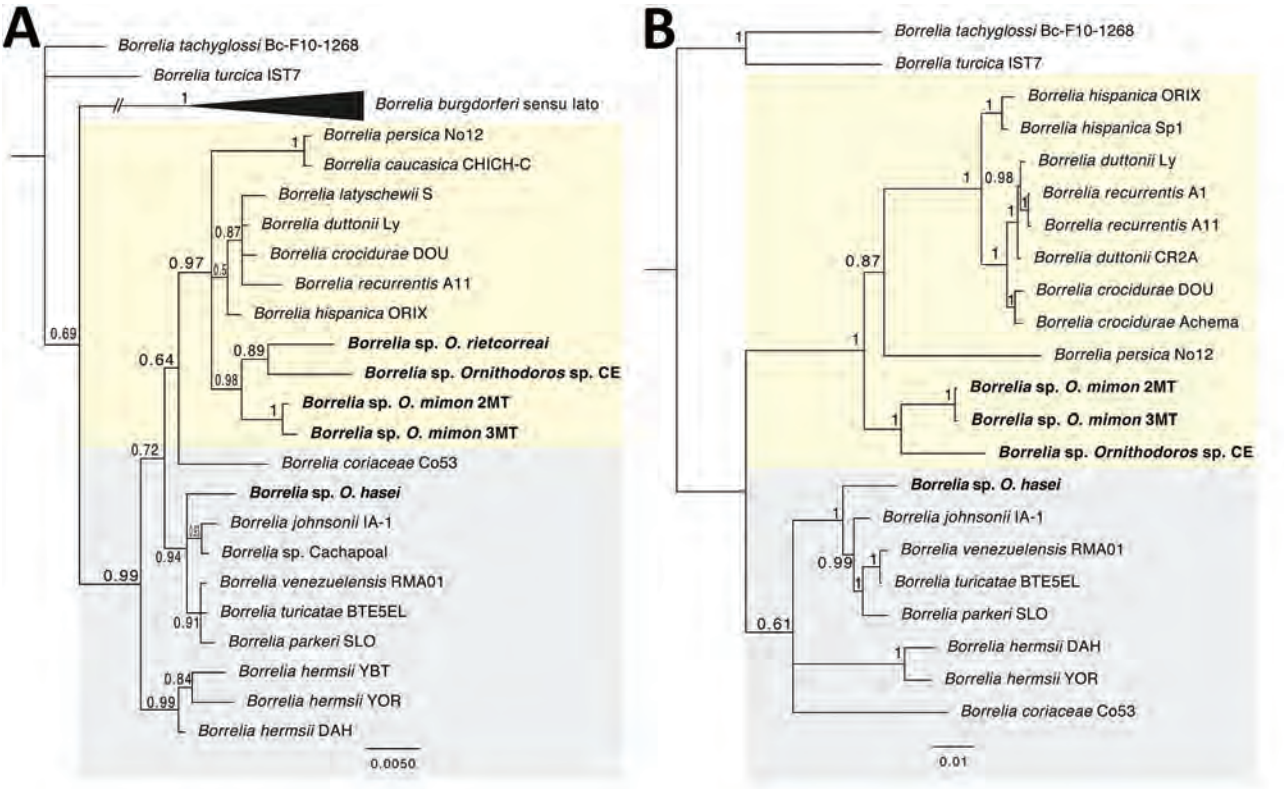


**Figure.** Bayesian phylogenetic trees inferred for the *Borrelia* spp. characterized in study of relapsing fever group borreliae in human-biting soft ticks, Brazil. A) Ambiguous alignments of single 16S rRNA gene (1,274 bp); B) concatenated 16S rRNA-*flaB-glpQ* genes (2,435 bp). Bold indicates borreliae from this study. Trees are drawn to scale. Four independent Markov chain runs for 1,000,000 metropolis-coupled MCMC generations were implemented for the analyses, sampling a tree every 100th generation. The first 25% of the trees represented burn-in, and the remaining trees were used to calculate Bayesian posterior probability values. Both trees were inferred using the Hasegawa-Kishino-Yano model with gamma distribution. Numbers above or below tree branches represent Bayesian posterior probabilities. Light yellow and gray backgrounds denote Old World and New World relapsing fever group *Borrelia* spp., respectively. Scale bar indicates nucleotide substitutions per site.

investigation of TBRF as a possible cause of UFS in Brazil. It is known that antibodies of patients exposed to RFGB infection cross-react in serologic tests for the diagnosis of Lyme borreliosis (*9*). This cross-reactivity is particularly relevant in Brazil because serologic evidence for an alleged Lyme-like disease in humans has been reiteratively published, yet refuted (*10*), and TBRF has not yet been considered as a possible cause of such disease.


## Acknowledgments

We thank Gilson Miranda from Serra das Almas Natural Reserve for his assistance during our visit to this location; Jerônimo Carvalho Martins from Jericoacoara National Park for gently allowing us the use of their facilities at Jericoacoara village; and Adriane Suzin, Ana Carolina Souza, Flavio A. Terassini, Ivaneide N. Costa, Luís Marcelo A. Camargo, Romilson S. Lopes Jr., Simone D. Tojal, and Vinicius S. Rodrigues for their valuable assistance in field work.

Laboratory work was funded by Fundação de Amparo à Pesquisa do Estado de São Paulo (FAPESP), and Conselho Nacional de Desenvolvimento Científico e Tecnológico (CNPq, grant no. 09262/2018-8). S.M.L. was funded by FAPESP (grant nos. 2018/02521-1 and 2019/17960-3).



## About the Author

Dr. Muñoz-Leal is a veterinarian affiliated with Universidad de Concepción, Chillán, Chile, who specializes in tickborne diseases. His research is focused on soft ticks and tickborne relapsing fever in South America.


## References


1. Lopez J, Krishnavahjala A, Garcia M, Bermudez S. Tick-borne relapsing fever spirochetes in the Americas. Vet Sci. 2016;3:16. https://doi.org/10.3390/vetsci3030016
2. de Oliveira SV, Bitencourth K, Borsoi ABP, de Freitas FSS, Coelho GCB, Amorim M, et al. Human parasitism and toxicosis by *Ornithodoros rietcorreai* (Acari: Argasidae) in

an urban area of Northeastern Brazil. Ticks Tick Borne Dis. 2018;9:1494–8. https://doi.org/10.1016/j.ttbdis.2018.07.011
3. Labruna MB, Marcili A, Ogrzewalska M, Barros-Battesti DM, Dantas-Torres F, Fernandes AA, et al. New records and human parasitism by *Ornithodoros mimon* (Acari: Argasidae) in Brazil. J Med Entomol. 2014;51:283–7. https://doi.org/10.1603/ME13062
4. Muñoz-Leal S, Faccini-Martínez ÁA, Costa FB, Marcili A, Mesquita ETKC, Marques EP, et al. Isolation and molecular characterization of a relapsing fever *Borrelia* recovered from *Ornithodoros rudis* in Brazil. Ticks Tick Borne Dis. 2018;9:864–71. https://doi.org/10.1016/j.ttbdis.2018.03.008
5. Parola P, Diatta G, Socolovschi C, Mediannikov O, Tall A, Bassene H, et al. Tick-borne relapsing fever borreliosis, rural Senegal. Emerg Infect Dis. 2011;17:883–5. https://doi.org/10.3201/eid1705.100573
6. Chikeka I, Dumler JS. Neglected bacterial zoonoses. Clin Microbiol Infect. 2015;21:404–15. https://doi.org/10.1016/j.cmi.2015.04.022
7. Doltario AB, Menon LJB, Bollela VR, Martinez R, de Almeida E Araújo DC, da Fonseca BAL, et al. Malaria and other febrile diseases among travellers: the experience of a reference centre located outside the Brazilian Amazon Region. Malar J. 2016;15:294. https://doi.org/10.1186/s12936-016-1347-x
8. Moreira J, Bressan CS, Brasil P, Siqueira AM. Epidemiology of acute febrile illness in Latin America. Clin Microbiol Infect. 2018;24:827–35. https://doi.org/10.1016/j.cmi.2018.05.001
9. Rath PM, Fehrenbach FJ, Rögler G, Pohle HD, Schönberg A. Relapsing fever and its serological discrimination from Lyme borreliosis. Infection. 1992;20:283–6. https://doi.org/10.1007/BF01710797
10. de Oliveira SV, Faccini-Martínez ÁA, Cerutti Junior C. Lack of serological evidence for Lyme-like borreliosis in Brazil. Travel Med Infect Dis. 2018;26:62–3. https://doi.org/10.1016/j.tmaid.2018.04.005

Address for correspondence: Sebastián Muñoz-Leal, Departamento de Patología y Medicina Preventiva, Facultad de Ciencias Veterinarias, Universidad de Concepción, Av. Vicente Méndez 595–Casilla 537, Chillán–Región de Ñuble, Chile; email: sebamunoz@udec.cl

# Etiology of Severe Acute Respiratory Infections, Bangladesh, 2017

Md R. Rahaman, Karen A. Alroy, Chris A. Van Beneden, Michael S. Friedman, Erin D. Kennedy, Mahmudur Rahman, Arunmozhi Balajee, A.K.M. Muraduzzaman, Tahmina Shirin, Meerjady S. Flora, Eduardo Azziz-Baumgartner

Author affiliations: The University of Adelaide, Adelaide, South Australia, Australia (M.R. Rahaman); Institute of Epidemiology, Disease Control, and Research, Dhaka (M.R. Rahaman, A.K.M. Muraduzzaman, T. Shirin, M.S. Flora); Centers for Disease Control and Prevention, Atlanta, Georgia, USA (K.A. Alroy, C.A. Van Beneden, M.S. Friedman, E.D. Kennedy, A. Balajee, E. Azziz-Baumgartner) icddr,b, Dhaka, Bangladesh (M.R. Rahman);

DOI: https://doi.org/10.3201/eid2701.201347

In April 2017, surveillance detected a surge in severe acute respiratory infections (SARI) in Bangladesh. We collected specimens from SARI patients and asymptomatic controls for analysis with multipathogen diagnostic tests. Influenza A(H1N1)pdm09 was associated with the SARI epidemic, suggesting that introducing vaccines and empiric antiviral drugs could be beneficial.

In April 2017, the Institute of Epidemiology Disease Control and Research (IEDCR) in Bangladesh noted an 89% increase in severe acute respiratory infections (SARI) compared with April 2016 through the National Influenza Surveillance Bangladesh (NISB) at 10 tertiary-care hospitals. During April 10–June 21, 2017, we conducted a case–control study to ascertain the cause of the outbreak and its associated risk factors.

We defined a SARI case as acute respiratory illness in a patient within 10 days of onset, with history of fever and cough, and requiring hospitalization (*1*). We sought to enroll all adults ≥18 years of age who were admitted to NISB hospitals with SARI. Staff screened patients for eligibility, obtained written informed consent, surveyed participants about demographics, and took combined nasal and throat swab samples. Patients who died in hospital wards before enrollment were ineligible. Within 2 days of case-patient enrollment, staff enrolled 2 asymptomatic controls, identified by convenience from the same hospitals' outpatient clinics, surveyed them, and took combined nasal and throat swab samples. Patients who had fever or respiratory symptoms in the previous 14 days were ineligible to serve as controls. Swab

specimens from case-patients and controls were tested for viral, bacterial, and fungal nucleic acids using FTD Respiratory pathogens 33 real-time reverse transcription PCR (Fast Track Diagnostics, http://www.fast-trackdiagnostics.com)(*2*).

We examined the association between SARI case-status and sociodemographic characteristics, preexisting conditions, and pathogens detected through multivariate logistic regressions. The investigation was judged to be public health action by the institutional review boards of the IEDCR and US Centers for Disease Control and Prevention (approval no. IEDCR/IRB/2016/17).

We identified 79 eligible SARI case-patients and 158 eligible controls from 5 NISB hospitals (Figure). Of these, 73 (92%) eligible patients and 146 (92%) eligible controls consented to participate (Table). Case-patients were more likely than controls to be male (89% vs. 77%; p = 0.041 by Fisher exact test) and have preexisting underlying chronic conditions (47% vs. 25%; p = 0.001), including asthma (36% vs. 12%; p = 0.000) and allergies (27% vs. 10%; p = 0.003) (Table). Although 34 (47%) of case-patients were treated with antibiotics, none were treated with antiviral drugs.

Fifty-three (73%) case-patients and 92 (63%) controls tested positive for ≥1 pathogens (Table). Among 53 test-positive case-patients, 18 (25%) tested positive for influenza viruses (Figure), including 12 (67%) for influenza A(H1N1)pdm09, 5 (28%) for unsubtyped influenza A, and 1 (6%) for influenza C. Among 92 test-positive controls, 8 (5%) tested positive for influenza viruses (Figure), including 3 (38%) for influenza A(H1N1), 4 (50%) for unsubtyped influenza A, and 2 (25%) for influenza C, 1 of whom had a codetection of an unsubtyped influenza A virus.

Male sex (odds ratio [OR] 2.4, 95% CI 1.0–5.4), ≥1 preexisting conditions (OR 2.7, 95% CI 1.5–4.8), asthma (OR 4.2, 95% CI 2.1–8.4), and history of allergies (OR 3.1, 95% CI 1.5–6.6) were more common among SARI case-patients than controls (Table). Any influenza virus (OR 5.7, 95% CI 2.3–13.7; p = 0.000), and influenza A(H1N1) specifically (OR 9.4, 95% CI 2.6–34.4; p = 0.001), was significantly associated with SARI status. Only influenza A(H1N1) (OR 11.4, 95% CI 2.7–47.4) remained associated with case status.

The surge in SARI during April 2017 was attributable to influenza viruses. Although influenza epidemics in Bangladesh typically occur during May–September (*6*), our investigation suggests the 2017 season started a month early. The government of Bangladesh has purchased Northern Hemisphere formulation influenza vaccines for Hajjis (i.e., for persons entering Mecca) (*7*,*8*) but does not otherwise have a vaccination policy because its possible benefit has not been shown in Bangladesh. Influenza vaccines are sporadically available in Bangladesh's private market but rarely used. Our findings suggest the potential utility of estimating the cost-benefit ratio of influenza vaccination among persons at high risk for SARI using Southern Hemisphere formulations, which incorporate the most current vaccine strains recommended by the World Health Organization (*7*) before the April–May start of the Bangladesh influenza season.

Patients with SARI were frequently prescribed antibiotics but not antiviral drugs. Whether antibiotics benefit SARI patients or solely drive antibiotic resistance is unclear; however, observational data suggest the benefit of empiric antiviral drugs to prevent influenza complications during epidemics (*9*). IEDCR recommended empiric treatment of

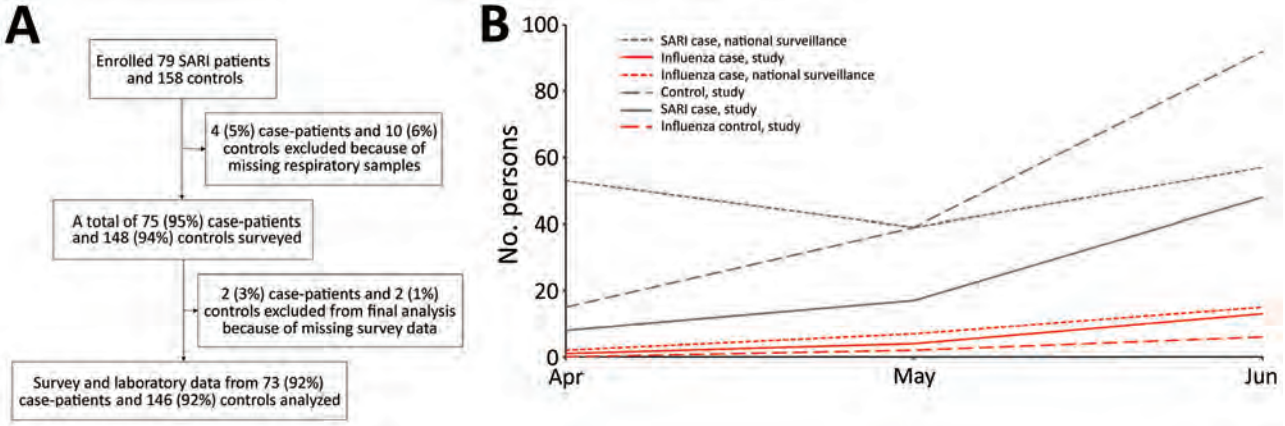


**Figure.** Participant enrollment in study of etiology of severe acute respiratory infections and influenza activities in Bangladesh, April–June, 2017. A) Enrollment of adults with severe acute respiratory infections (SARI) and their corresponding controls. B) Influenza activities, study (April 10–June 21) and national surveillance (April–June). Percentages might not sum to 100 because of rounding.

patients with SARI with antiviral drugs during the 2009 pandemic but does not currently (*10*). Quantifiying the cost-effectiveness of empiric antiviral treatment for SARI patients during influenza epidemics could be valuable, particularly when used within 48 hours of symptom onset, when antivirals are most effective (*6*,*9*).

This investigation had limitations. Controls were not randomly selected, and age and sex were not matched with case-patients. We limited our sample collection to the upper respiratory tract, did not have wells to identify influenza A(H3N2) RNA, and did not collect blood or other samples that would have more accurately detected bacterial infections.

Our investigation of a surge in SARI cases during April 2017 in Bangladesh suggests the value of surveillance and rapid response in identifying the etiology of outbreaks. Our findings also suggest the potential value of estimating the cost-effectiveness of influenza vaccination campaigns among groups at high risk for SARI administered as early as late March to early April and of empiric antivirals during Bangladesh's influenza epidemics.

### Acknowledgments

We are grateful to all NISB surveillance staff including the IEDCR virology laboratory staff for their support in respiratory sample testing. We thank Mirza Mohammad Omer Farrque, and Jimmy Breen for their statistical input. We also thank Kaniz Fatema for help training NISB surveillance staff. We acknowledge the technical and editorial support provided by Lindsay Kim and Mary Ann Hall. Multipathogen diagnostic tests were provided by CDC's Division of Viral Diseases with support from the Global Health Security Agenda.

## About the Author

Dr. Rahaman, a current PhD candidate at the University of Adelaide, is a medical doctor with specialist training in field epidemiology, international public health, and health management. His research interests include infectious disease epidemiology, particularly influenza; zoonoses, such as Q fever prevention; environmental epidemiology; and a One Health approach.

### References

1. World Health Organization. A manual for estimating disease burden associated with seasonal influenza. Geneva: World Health Organization; 2015 [cited 2018 Oct 21]. https://www.who.int/influenza/resources/publications/manual_burden_of_disease
2. Salez N, Vabret A, Leruez-Ville M, Andreoletti L, Carrat F, Renois F, et al. Evaluation of four commercial multiplex molecular tests for the diagnosis of acute respiratory infections. PLoS One. 2015;10:e0130378. https://doi.org/10.1371/journal.pone.0130378
3. Staff correspondent. Bangladesh's per capita income rises to $1,314. bdnews24.com. 2015 May 14 [cited 2019 Jan 13]. https://bdnews24.com/economy/2015/05/14/bangladeshs-per-capita-income-rises-to-1314
4. Centers for Disease Control and Prevention. About adult BMI: how is BMI interpreted for adults? 2017 Aug 29 [cited 2017 Sep 20]. https://www.cdc.gov/healthyweight/assessing/bmi/adult_bmi/index.html
5. Huque R, Zaman MM, Huq SM, Sinha DN. Smokeless tobacco and public health in Bangladesh. Indian J Public Health. 2017;61(Suppl 1):S18–24. https://doi.org/10.4103/ijph.IJPH_233_17
6. Zaman RU, Alamgir AS, Rahman M, Azziz-Baumgartner E, Gurley ES, Sharker MAY, et al. Influenza in outpatient ILI case-patients in national hospital-based surveillance, Bangladesh, 2007–2008. PLoS One. 2009;4:e8452. https://doi.org/10.1371/journal.pone.0008452
7. Hirve S, Newman LP, Paget J, Azziz-Baumgartner E, Fitzner J, Bhat N, et al. Influenza seasonality in the tropics and subtropics—when to vaccinate? PLoS One. 2016;11:e0153003. https://doi.org/10.1371/journal.pone.0153003
8. Saha S, Chadha M, Al Mamun A, Rahman M, Sturm-Ramirez K, Chittaganpitch M, et al. Influenza seasonality and vaccination timing in tropical and subtropical areas of southern and south-eastern Asia. Bull World Health Organ. 2014;92:318–30. https://doi.org/10.2471/BLT.13.124412
9. Muthuri SG, Venkatesan S, Myles PR, Leonardi-Bee J, Al Khuwaitir TSA, Al Mamun A, et al.; PRIDE Consortium Investigators. Effectiveness of neuraminidase inhibitors in reducing mortality in patients admitted to hospital with influenza A H1N1pdm09 virus infection: a meta-analysis of individual participant data. Lancet Respir Med. 2014;2:395–404. https://doi.org/10.1016/S2213-2600(14)70041-4
10. Chowdhury F, Sturm-Ramirez K, Mamun AA, Iuliano AD, Bhuiyan MU, Chisti MJ, et al. Factors driving customers to seek health care from pharmacies for acute respiratory illness and treatment recommendations from drug sellers in Dhaka city, Bangladesh. Patient Prefer Adherence. 2017;11:479–86. https://doi.org/10.2147/PPA.S121800

Address for correspondence: Md Rezanur Rahaman, School of Public Health, The University of Adelaide, AHMS Building, 4 North Terrace, Adelaide, South Australia 5000, Australia; email: mdrezanur.rahaman@adelaide.edu.au

# Waning Antibody Responses in Asymptomatic and Symptomatic SARS-CoV-2 Infection

Pyoeng Gyun Choe,[1] Chang Kyung Kang,[1] Hyeon Jeong Suh, Jongtak Jung, Kyoung-Ho Song, Ji Hwan Bang, Eu Suk Kim, Hong Bin Kim, Sang Won Park, Nam Joong Kim, Wan Beom Park, Myoung-don Oh

Author affiliation: Seoul National University College of Medicine, Seoul, South Korea

DOI: https://doi.org/10.3201/eid2701.203515

We investigated the kinetics of severe acute respiratory syndrome coronavirus 2 neutralizing antibodies in 7 asymptomatic persons and 11 patients with pneumonia. The geometric mean titer of neutralizing antibodies declined from 219.4 at 2 months to 143.7 at 5 months after infection, indicating a waning antibody response.

Neutralizing antibodies develop in asymptomatic persons with severe acute respiratory syndrome coronavirus 2 (SARS-CoV-2) infection; however, the initial immune response is not as strong as in patients with more severe disease (*1*,*2*). We investigated the kinetics of SARS-CoV-2 neutralizing antibodies during the 5 months after infection in asymptomatic persons and patients with pneumonia caused by SARS-CoV-2.

We studied 7 persons infected with SARS-CoV-2 who were isolated in a community treatment center operated by Seoul National University (SNU) Hospital in Daegu, South Korea (*3*). Comprehensive monitoring confirmed that these 7 patients were asymptomatic (*4*). We also evaluated 11 SARS-CoV-2–positive patients with pneumonia at the Biocontainment Unit in the SNU Hospital and SNU Bundang Hospital. We classified each case of pneumonia as subtle (i.e., infiltrations observed only on computed tomography) or apparent (i.e., infiltrations observed on plain chest radiograph) (Appendix Table, https://wwwnc.cdc.gov/EID/article/27/1/20-3515-App1.pdf). All patients provided informed consent.

We evaluated the antibody responses at 2 and 5 months after infection, as reported (*1*). We semiquantitatively measured IgG against SARS-CoV-2 using ELISA (Euroimmun, https://www.euroimmun.com) with the recombinant S1 domain of the SARS-CoV-2 spike protein as the antigen. We interpreted the optical density ratio (sample/calibrator) as negative (<0.8), borderline (≥0.8 to <1.1), or positive (≥1.1), according to the manufacturer's recommendations. We also conducted neutralization assays as previously described (*5*) using BetaCoV/Korea/SNU01/2020 virus (*6*) and 2-fold serially diluted plasma samples (2–4,096-fold). We recorded the highest dilution of plasma that showed inhibition activity of SARS-CoV-2 as the neutralizing antibody titer. We considered a ≥4-fold reduction in antibody titer to be a waning response. The Institutional Review Boards of Seoul National University Hospital approved the study (IRB no. H-2004-158-1118).

Two months after infection, 11 (100%) patients with pneumonia and 5 (71%) with asymptomatic infection had positive ELISA results. Five months after infection, 5 (100.0%) patients with apparent pneumonia, 5 (83.3%) with subtle pneumonia, and 4 (57.1%) with asymptomatic infection had positive ELISA results. The mean ELISA optical density decreased significantly from 2 to 5 months after infection (4.93 at 2 months vs. 4.09 at 5 months; p = 0.01).

Two months after infection, all patients had neutralizing antibodies. Antibody titers correlated with disease severity; the geometric mean titer was 105 among symptomatic persons, 161 among patients with subtle pneumonia, and 891 among patients with apparent pneumonia. Five months after infection, all patients still had neutralizing antibodies, but the geometric mean titer decreased significantly (219.4 at 2 months vs. 143.7 at 5 months; p = 0.03). In the linear regression model, the decline was significantly associated with the antibody levels at 2 months as measured by ELISA (r = 0.536, p = 0.02) and the neutralization assay (r = 0.563, p = 0.02) (Appendix Figure). The waning neutralizing antibody response occurred in 2 (40%) of 5 patients with apparent pneumonia and 2 (33%) of 6 with subtle pneumonia, but none of the asymptomatic persons (Figure).

Determining the longevity of humoral immunity to SARS-CoV-2 is essential to predicting herd immunity to coronavirus disease. Among patients with severe acute respiratory syndrome coronavirus, which is closely related to SARS-CoV-2, a total of 90% maintained IgG for 2 years and 50% for 3 years (*7*). However, humoral immunity to common human coronavirus is short-lived; antibodies against seasonal coronaviruses return to baseline levels by 52 weeks after infection, enabling homologous reinfections (*8*). A recent study showed that the antibody titers of patients with mild coronavirus disease declined more quickly than did those of patients with severe acute respiratory syndrome (*9*).

[1]These first authors equally contributed to this article.

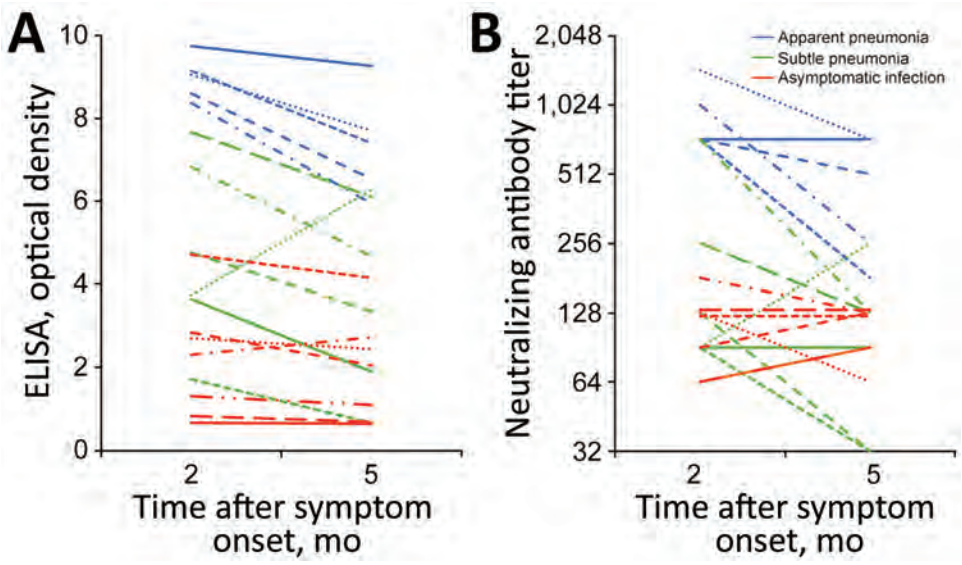


**Figure.** Waning antibody response against severe acute respiratory virus coronavirus 2, South Korea, 2020. Responses measured by A) ELISA optical density measurements (p = 0.01); B) neutralizing antibody titers (p = 0.03). Each line indicates data from a single patient.

Our findings demonstrate waning humoral immunity in patients with SARS-CoV-2 infection. We documented the decline of neutralizing antibody titers in asymptomatic and symptomatic patients. In this study, the initial neutralizing antibody reaction appeared to correlate with the severity of the disease. However, patients with pneumonia were considerably older than asymptomatic persons, and increasing age is associated with a stronger neutralizing antibody response (*10*). In this study, neutralizing antibody titer decreased more in symptomatic than asymptomatic patients. Our study reinforces the concern that naturally acquired humoral immunity against SARS-CoV-2 might not be long-lasting.

### Acknowledgments

We thank Kyung Sook Ahn for administrative support. We thank Areum Jo and Su Jin Choi for technical support.

This project was supported by the research fund of Seoul National University Hospital (grant no. 04-2020-0030). The funding agencies had no role in the design and conduct of the study; collection, management, analysis, and interpretation of the data; preparation, review, or approval of the manuscript; and decision to submit the manuscript for publication.

### About the Author

Dr. Choe is a clinical scientist at Seoul National University Hospital. His research interests focus on preventing healthcare-associated infection and responding to emerging infectious diseases.

### References

1. Choe PG, Kang CK, Suh HJ, Jung J, Kang E, Lee SY, et al. Antibody responses to SARS-CoV-2 at 8 weeks postinfection in asymptomatic patients. Emerg Infect Dis. 2020;26:2484–7. https://doi.org/10.3201/eid2610.202211
2. Long QX, Tang XJ, Shi QL, Li Q, Deng HJ, Yuan J, et al. Clinical and immunological assessment of asymptomatic SARS-CoV-2 infections. Nat Med. 2020;26:1200–4. https://doi.org/10.1038/s41591-020-0965-6
3. Kang E, Lee SY, Jung H, Kim MS, Cho B, Kim YS. Operating protocols of a community treatment center for isolation of patients with coronavirus disease, South Korea. Emerg Infect Dis. 2020;26:2329–37. https://doi.org/10.3201/eid2610.201460
4. Choe PG, Kang EK, Lee SY, Oh B, Im D, Lee HY, et al. Selecting coronavirus disease 2019 patients with negligible risk of progression: early experience from non-hospital isolation facility in Korea. Korean J Intern Med. 2020;35:765–70. https://doi.org/10.3904/kjim.2020.159
5. Shen C, Wang Z, Zhao F, Yang Y, Li J, Yuan J, et al. Treatment of 5 critically ill patients with COVID-19 with convalescent plasma. JAMA. 2020;323:1582–9. https://doi.org/10.1001/jama.2020.4783
6. Park WB, Kwon NJ, Choi SJ, Kang CK, Choe PG, Kim JY, et al. Virus isolation from the first patient with SARS-CoV-2 in Korea. J Korean Med Sci. 2020;35:e84. https://doi.org/10.3346/jkms.2020.35.e84
7. Wu LP, Wang NC, Chang YH, Tian XY, Na DY, Zhang LY, et al. Duration of antibody responses after severe acute respiratory syndrome. Emerg Infect Dis. 2007;13:1562–4. https://doi.org/10.3201/eid1310.070576
8. Callow KA, Parry HF, Sergeant M, Tyrrell DA. The time course of the immune response to experimental coronavirus infection of man. Epidemiol Infect. 1990;105:435–46. https://doi.org/10.1017/S0950268800048019
9. Ibarrondo FJ, Fulcher JA, Goodman-Meza D, Elliott J, Hofmann C, Hausner MA, et al. Rapid decay of anti-SARS-CoV-2 antibodies in persons with mild Covid-19. N Engl J Med. 2020;383:1085–7. https://doi.org/10.1056/NEJMc2025179

10. Wang X, Guo X, Xin Q, Pan Y, Hu Y, Li J, et al. Neutralizing antibodies responses to SARS-CoV-2 in COVID-19 inpatients and convalescent patients. Clin Infect Dis. 2020;ciaa721. https://doi.org/10.1093/cid/ciaa721

Address for correspondence: Wan Beom Park or Myoung-don Oh, Department of Internal Medicine, Seoul National University College of Medicine, 103 Daehak-ro, Jongno-gu, Seoul 03080, South Korea; email: wbpakr1@snu.ac.kr or mdohmd@snu.ac.kr

# Postmortem Stability of SARS-CoV-2 in Nasopharyngeal Mucosa

Fabian Heinrich, Kira Meißner, Felicia Langenwalder, Klaus Püschel, Dominik Nörz, Armin Hoffmann, Marc Lütgehetmann, Martin Aepfelbacher, Eric Bibiza-Freiwald, Susanne Pfefferle, Axel Heinemann

Author affiliation: University Medical Center Hamburg-Eppendorf, Hamburg, Germany

DOI: https://doi.org/10.3201/eid2701.203112

Analyses of infection chains have demonstrated that severe acute respiratory syndrome coronavirus 2 is highly transmissive. However, data on postmortem stability and infectivity are lacking. Our finding of nasopharyngeal viral RNA stability in 79 corpses showed no time-dependent decrease. Maintained infectivity is supported by virus isolation up to 35 hours postmortem.

Detailed analyses of severe acute respiratory syndrome coronavirus 2 (SARS-CoV-2) transmission have shown the virus to be highly transmissible through droplet and contact-transmitted viral spreading; reproduction indices were 2.2–3.6 (*1*). Amid the coronavirus disease (COVID-19) pandemic, case-fatality rates of up to 9.26% occur in areas hard-struck by SARS-CoV-2 (*2*). The likelihood of virus transmission through deceased persons remains unclear. However, in recent pandemics of influenza, high and sustainable virus stability and infectivity within corpses were demonstrated (*3*,*4*), necessitating careful and conscious handling. To determine the possibility of SARS-CoV-2 transmission through deceased persons, we conducted a study of postmortem viral RNA stability.

The federal state of Hamburg, Germany, has mandated autopsies since March 2020 in accordance with the German Infection Protection Act for all patients with reverse transcription PCR (RT-PCR)–confirmed SARS-CoV-2 infection. Data and sample acquisition for the study were performed during March 22–May 1, 2020. To confirm the initial diagnosis and quantify the viral load in the corpses, nasopharyngeal swab samples (ESwab; Copan, https://products.copangroup.com) were taken at patient admission to the Department of Legal Medicine (University Medical Center Hamburg-Eppendorf). Corpses were stored at 4°C in the refrigerator. Antemortem and postmortem nasopharyngeal swab samples were taken according to recent standards (*5*) by trained, medically qualified personnel to ensure maximum reliability and consistent quality. Samples were analyzed for SARS-CoV-2 RNA as described previously (*6*).

The Ethics Committee of the Hamburg Chamber of Physicians approved the study (no. PV7311). The local clinical institutional review board, complying with the Declaration of Helsinki, also approved the study.

Antemortem nasopharyngeal swab samples (Appendix Figure, https://wwwnc.cdc.gov/EID/article/27/1/20-3112-App1.pdf) were collected by medical staff at the intensive care unit of the University Medical Center Hamburg and by general practitioners from on-call duty at a median of 6 days (range 2–14 [interquartile range (IQR) 6.3]) before death (n = 10). Using a Wilcoxon test for paired data, we did not detect any effect of the event of death on the SARS-CoV-2 RNA load (U= −5; p = 0.85). We found no correlation between the postmortem interval (time of death until cooling at 4°C; median 17.8 [range 2.7–482.6]) hours and the viral RNA loads of corpses, as indicated by Spearman correlation of 79 matched datasets (Figure, panel A).

To analyze postmortem stability of SARS-CoV-2 RNA, we selected 11 corpses with short postmortem intervals for a detailed observation over 7 days (168 hours) (Table). The median postmortem interval was 5.7 (range 2.9–32.0 [IQR 6.9]) hours. The median cycle threshold ($C_t$) of SARS-CoV-2 RNA in swab samples taken at admission was 29.52 (range 15.2–50.0 [IQR 22.5]) (Figure, panel A). We determined viral load in a series of 9 sequential pharyngeal swab samples (time points 0, 12, 24, 36, 48, 60, 72, 96, and 168 hours after admission). We consistently detected SARS-CoV-2 RNA at constant levels at all time points analyzed (Figure, panel B), except for patient 7 at 0, 12, and 24 hours after admission and patient 8 at admission. Because subsequent samples were positive for all corpses, we attributed those

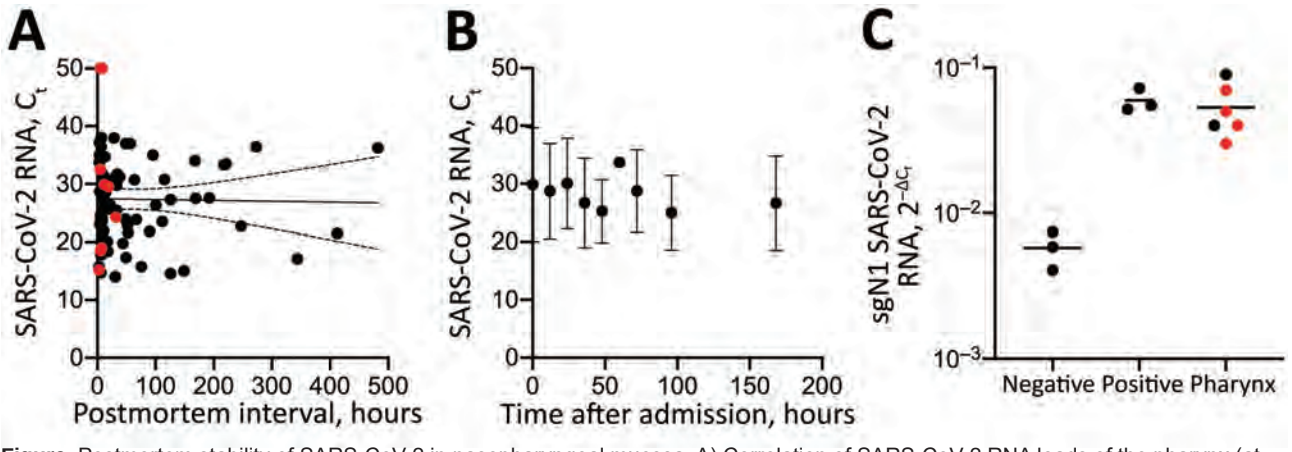


**Figure.** Postmortem stability of SARS-CoV-2 in nasopharyngeal mucosa. A) Correlation of SARS-CoV-2 RNA loads of the pharynx (at corpse admission to the Department of Legal Medicine) with the postmortem interval (time of death until cooling at 4°C) in 79 matched datasets. Red indicates patients in the longitudinal cohort. Spearman R = –0.07; 2-tailed p = 0.5. B) Median SARS-CoV-2 RNA loads with 95% CIs (error bars) in a series of 9 sequential pharyngeal swab samples (time points 0, 12, 24, 36, 48, 60, 72, 96, and 168 hours after admission) for 11 corpses. C) sgN1 RNA loads of SARS-CoV-2 in pharyngeal tissue of 6 corpses. Negative and positive controls from SARS-CoV-2 cell cultures. Red indicates samples with successful virus isolation from pharyngeal tissue (S. Pfefferle, unpub. data, https://doi.org/10.1101/2020.10.10.334458). Negative results are reflected by $C_t$ 50. Ct, cycle threshold; SARS-CoV-2, severe acute respiratory syndrome coronavirus 2; sgN1 RNA, subgenomic RNA loads of the N1-gene.

discrepancies to deviations in the sample collection. A general mixed model found no time-dependent effect on SARS-CoV-2 RNA loads (estimate −0.06, SE 0.01; p = 0.58) (*7*). Because of impaired interval-scaling of metric variables, we excluded negative $C_t$ values from the statistical analysis. Intriguingly, the estimate suggests an increase of the viral load without revealing significant results (0.6%/hour).

Six patients in this study (patients 11–16) previously were part of a study in which virus growth from different tissues (including pharynx) of patients dying of RT-PCR–confirmed SARS-CoV-2 infection was investigated (S. Pfefferle, unpub. data, https://doi.org/10.1101/2020.10.10.334458) (Table). That study showed that replicating virus was detected in the throat of patients up to 35.8 hours after death. Both the

**Table.** Basic clinical information about and autopsy findings of patients in a longitudinal follow-up cohort and for virus isolation, Department of Legal Medicine, Hamburg, Germany, 2020*

| Patient no. | Age, y/sex | BMI, kg/m$^2$ | Main autopsy finding | Disease duration, d | Postmortem interval, h† | Postmortem SARS-CoV-2 RNA load at admission, $C_t$‡ |
|---|---|---|---|---|---|---|
| 1§ | 54/F | 29.6 | Pneumonia | 5 | 11.92 | 29.86 |
| 2§ | 66/M | 25.3 | Pneumonia | ND | 32.03 | 24.22 |
| 3§ | 63/M | 37.3 | Pulmonary embolism, pneumonia | 6 | 5.03 | 32.55 |
| 4§ | 70/M | 22.2 | Pneumonia, bronchitis, respiratory failure | 6 | 7.48 | 18.97 |
| 5§ | 52/M | 38.8 | Pulmonary embolism | 10 | 5.32 | ND |
| 6§ | 90/F | 24.9 | Pneumonia, aspiration | 13 | 19.35 | 29.52 |
| 7§ | 71/M | ND | Pneumonia, MODS | ND | 7.87 | 50 |
| 8§ | 77/M | 33.2 | Pneumonia | 18 | 5.08 | 50 |
| 9§ | 61/M | 32.3 | Intracerebral hemorrhage, pneumonia | ND | 4.37 | ND |
| 10§ | 76/M | 37.7 | Pneumonia, MODS, endocarditis, leukemia | ND | 2.85 | 15.22 |
| 11§,¶ | 59/F | 22.2 | Pneumonia, multiple myeloma | 18 | 5.67 | 18.55 |
| 12¶ | 83/F | 26.0 | Pneumonia, non-Hodgkin lymphoma | 25 | 6.83 | ND |
| 13¶ | 80/M | 28.5 | Pulmonary embolism, pneumonia, myelofibrosis | 12 | 6.5 | ND |
| 14¶ | 71/F | 29.0 | Pneumonia, myelofibrosis | 25 | 12.1 | ND |
| 15¶ | 84/F | 21.4 | Pneumonia | ND | 35.75 | ND |
| 16¶ | 31/M | 20.6 | Pneumonia, germ cell tumor | ND | 9.08 | ND |

*$C_t$, cycle threshold; MODS, multiple organ dysfunction syndrome; ND, not determined; SARS-CoV-2, severe acute respiratory syndrome coronavirus 2.
†Time of death until cooling at 4°C.
‡Negative results are reflected by $C_t$ 50.
§Longitudinal cohort.
¶Virus isolation cohort (S. Pfefferle, unpub. data, https://doi.org/10.1101/2020.10.10.334458).

detection of subgenomic RNA (sgRNA) by next-generation sequencing and virus growth could be shown in those throat samples. We also detected sgRNA by RT-PCR in throat tissue samples of these 6 previously published patients (*8*–*10*) (Figure, panel C); samples in which virus could be cultivated (S. Pfefferle, unpub. data, https://doi.org/10.1101/2020.10.10.334458) are highlighted in red.

We demonstrated maintained infectivity of SARS-CoV-2 in tissues of deceased patients. SARS-CoV-2 RNA persisted over time at constantly high titers. Taken together, our data indicate potentially high infectivity of human corpses, requiring hazard assessments in professional fields concerned and careful and conscious handling.

Our infectivity study relies on a limited number of cases and patients with severe immunosuppression. Further research should investigate viral persistence in corpses with longer postmortem intervals (>1 week) and corpses exhibiting lower initial viral loads. We recommend all work on corpses be conducted according to guidelines recently published by the World Health Organization, especially in the framework of widespread death in pandemics (https://apps.who.int/iris/rest/bitstreams/1300088/retrieve).

### Acknowledgments

We offer condolences to the families and friends of all the patients whose deaths were attributable to COVID-19.

This work was funded by a grant given to M.A. and A.H., within the research consortium DEFEAT PANDEMics, funded by the Netzwerk Universitätsmedizin (NUM). The funders had no role in study design, data collection, and analysis, decision to publish, or preparation of the manuscript.

## About the Author

Mr. Heinrich is a medical student employed at the Institute of Legal Medicine, University Medical Center Hamburg-Eppendorf. His primary research interests include infectiologic and immunologic research.

### References

1. Lipsitch M, Cohen T, Cooper B, Robins JM, Ma S, James L, et al. Transmission dynamics and control of severe acute respiratory syndrome. Science. 2003;300:1966–70. https://doi.org/10.1126/science.1086616
2. Khafaie MA, Rahim F. Cross-country comparison of case fatality rates of COVID-19/SARS-COV-2. Osong Public Health Res Perspect. 2020;11:74–80. https://doi.org/10.24171/j.phrp.2020.11.2.03
3. Sheng ZM, Chertow DS, Ambroggio X, McCall S, Przygodzki RM, Cunningham RE, et al. Autopsy series of 68 cases dying before and during the 1918 influenza pandemic peak. Proc Natl Acad Sci U S A. 2011;108:16416–21. https://doi.org/10.1073/pnas.1111179108
4. Franková V, Jirásek A, Tůmová B. Type A influenza: postmortem virus isolations from different organs in human lethal cases. Arch Virol. 1977;53:265–8. https://doi.org/10.1007/BF01314671
5. Marty FM, Chen K, Verrill KA. How to obtain a nasopharyngeal swab specimen. N Engl J Med. 2020;382:e76. https://doi.org/10.1056/NEJMvcm2010260
6. Pfefferle S, Reucher S, Nörz D, Lütgehetmann M. Evaluation of a quantitative RT-PCR assay for the detection of the emerging coronavirus SARS-CoV-2 using a high throughput system. Euro Surveill. 2020;25. https://doi.org/10.2807/1560-7917.ES.2020.25.9.2000152
7. University of California, Los Angeles, Statistical Consulting Group. Introduction to linear mixed models [cited 2020 Jul 9]. https://stats.idre.ucla.edu/other/mult-pkg/introduction-to-linear-mixed-models/
8. Wichmann D, Sperhake JP, Lütgehetmann M, Steurer S, Edler C, Heinemann A, et al. Autopsy findings and venous thromboembolism in patients with COVID-19: a prospective cohort study. Ann Intern Med. 2020;173:268–77. https://doi.org/10.7326/M20-2003
9. Wölfel R, Corman VM, Guggemos W, Seilmaier M, Zange S, Müller MA, et al. Virological assessment of hospitalized patients with COVID-2019. Nature. 2020;581:465–9. https://doi.org/10.1038/s41586-020-2196-x
10. Centers for Disease Control and Prevention. Research use only 2019-novel coronavirus (2019-nCoV) real-time RT-PCR primer and probe information [cited 2020 Oct 9]. https://www.cdc.gov/coronavirus/2019-ncov/lab/rt-pcr-panel-primer-probes.html

Address for correspondence: Fabian Heinrich, Institute of Legal Medicine, University Medical Center Hamburg Eppendorf, Butenfeld 34, 20259 Hamburg, Germany; email: fa.heinrich@uke.de

# Novel 6-Month Treatment for Drug-Resistant Tuberculosis, United States

Connie A. Haley, Patricia Macias, Supriya Jasuja, Betsy A. Jones, Marie-Claire Rowlinson, Roshni Jaimon, Pennelyn Onderko, Elaine Darnall, Maria E. Gomez, Charles Peloquin, David Ashkin, Neela D. Goswami

Author affiliations: University of Florida, Gainesville, Florida, USA (C.A. Haley, M.E. Gomez, D. Ashkin); Cook County Department of Public Health, Chicago, Illinois, USA (P. Macias, S. Jasuja, R. Jaimon, P. Onderko); Florida Department of Health, Jacksonville, Florida, USA (B.A. Jones, M.-C. Rowlinson, D. Ashkin) Illinois Department of Public Health, Springfield, Illinois, USA (E. Darnall); University of Florida College of Pharmacy, Gainesville (C. Peloquin); Centers for Disease Control and Prevention, Atlanta, Georgia, USA (N.D. Goswami)

DOI: https://doi.org/10.3201/eid2701.203766

The US Food and Drug Administration approved a 6-month regimen of pretomanid, bedaquiline, and linezolid for extensively drug-resistant or multidrug-intolerant tuberculosis after a trial in South Africa demonstrated 90% effectiveness 6 months posttreatment. We report on a patient who completed the regimen using a lower linezolid dose.

A woman from eastern Europe in her late 40s undergoing treatment for stage III cervical adenocarcinoma was found to have a right upper lobe pulmonary nodule. Pathology from tissue biopsy demonstrated necrotizing granulomas and numerous acid-fast bacilli (AFB); the sample was PCR positive for *Mycobacterium tuberculosis*. Adjuvant chemotherapy was held, and the patient was referred to the local public health department. The patient provided informed written consent for publication of her case study.

On evaluation, the patient was asymptomatic without physical findings and reported no previous diagnosis or treatment of tuberculosis (TB) disease or latent TB infection. Results of serologic testing for HIV and viral hepatitis B and C were negative. She had a mild chronic anemia and transient transaminitis during chemotherapy (peak alanine aminotransferase 215 IU/L; aspartate aminotransferase 185 IU/L). Three sputum samples were negative by AFB smear and culture; 1 was tested by PCR and was *M. tuberculosis* negative.

Treatment with rifampin, isoniazid, pyrazinamide, ethambutol and pyridoxine was initiated. Lung biopsy cultures grew *M. tuberculosis,* and GeneXpert MTB/RIF assay (Cepheid, https://www.cepheid.com) detected an *rpoB* mutation indicating likely rifampin resistance. Rapid molecular detection of drug resistance and growth-based drug susceptibility testing performed by the Centers for Disease Control and Prevention (CDC) and Florida Bureau of Public Health Laboratories yielded concordant results. We detected resistance to isoniazid, rifampin, the fluoroquinolones (levofloxacin and moxifloxacin), and an injectable (kanamycin), confirming a diagnosis of extensively drug-resistant TB (XDR TB). Resistance was also detected for pyrazinamide but not for ethambutol, bedaquiline, or linezolid. The patient and her medical providers, in consultation with a CDC-funded TB Center of Excellence (COE, https://www.cdc.gov/tb/education/tb_coe), determined that her best treatment option was a 6-month all-oral regimen of bedaquiline, pretomanid, and linezolid (BPaL).

BPaL was approved by the US Food and Drug Administration (FDA) on August 14, 2019, based in part on results from the Nix-TB trial in South Africa, which included patients with XDR TB or multidrug-resistant (MDR) TB who failed or were intolerant of prior therapy (*1*). Pretomanid, the novel agent in the regimen, is a nitroimidazooxazine that blocks cell-wall production in actively replicating MTB organisms and acts as a respiratory poison and protein synthesis inhibitor to kill nonreplicating persister organisms (*2*). Bedaquiline is a diarylquinoline that inhibits mycobacterial adenosine triphosphate synthase in replicating and persister organisms, and linezolid is an oxazolidinone that also inhibits protein synthesis (*3*,*4*). The combined activity of BPaL enables cure in a far shorter period compared with currently recommended 18- to 24-month MDR TB regimens (*5*). In the Nix-TB trial, BPaL produced favorable outcomes in 98/109 (90%) patients at 6 months posttreatment (*1*); in addition, little preexisting resistance to bedaquiline, pretomanid, or linezolid has been reported (*4*,*6*).

Because pretomanid was not yet commercially available in the United States, the TB Alliance required an FDA-approved single-patient investigational new drug application and provided 6 months of pretomanid acquired internationally. A bridging regimen of bedaquiline, linezolid, moxifloxacin, cycloserine, clofazimine, and ethambutol was initiated for 2 weeks, then was narrowed to BPaL when pretomanid arrived.

For this patient, we initiated linezolid at 600 mg/d, given the toxicity of the Nix-TB dose of 1,200 mg/d, the patient's paucibacillary disease, and TB COE's

**Table 1.** Molecular susceptibility sequencing results and therapeutic drug monitoring data from treatment of XDR TB, Florida, USA*

| Drug (dose) | Sequencing result | Date drug level drawn | Trough, μg/mL | 2h postdose level, μg/mL | 6h postdose level, μg/mL | Typical peak serum concentration, μg/mL |
|---|---|---|---|---|---|---|
| Bedaquiline (200 mg MWF) | No *atpE* (ORF) mutation detected; no Rv0678/mmpR (ORF) mutation detected | 2019 Nov 13 | 0.51 (42.25 h postdose) | 1.40 | 1.42 | 1.2–1.8 (5–6 h postdose, maintenance phase) |
| N-monodesmethyl bedaquiline (metabolite) | NT | 2019 Nov 13 | 0.22 (42.25 h postdose) | 0.24 | 0.27 | NT |
| Pretomanid (200 mg/d) | NT | 2019 Nov 13 | 2.07 (18.25 h postdose) | 3.43 | 2.98 | 2.3–4.3 (5–6 h postdose, at steady state) |
| Linezolid (600 mg/d) | No rplC (ORF aa 84–217) mutation detected; no rrl (nt 2191–2929) mutation detected | 2019 Nov 13 | 7.62 (18.25 h postdose) | 24.15 | 17.88 | 12–26 |
| Linezolid (600 mg MWF) | NT | 2020 Mar 12 | <2.00† | 19.04 | 13.6 | 12–26 |

*MWF, Monday/Wednesday/Friday; NT, not tested; ORF, open reading frame; XDR, extensively drug-resistant tuberculosis.
†Trough sample was not collected; based on the apparent elimination half-life, the linezolid concentration at 48 h was calculated to be <2 μg/mL, a value associated with minimal toxicity.

experience with linezolid dosing (*1,4,7,8*). Therapeutic drug monitoring performed at the University of Florida Infectious Diseases Pharmacokinetic Laboratory (https://idpl.pharmacy.ufl.edu) was used to maintain a linezolid peak of 12–26 μg/mL and trough <2 μg/mL to reduce drug-induced toxicity (*4,9*).

The patient received outpatient BPaL treatment 7 days a week by directly observed therapy. We assessed liver, renal, hematologic, and neurologic function plus QTc intervals at baseline and every 2–4 weeks during treatment (Table 1). A few weeks into therapy, the patient's linezolid level 18 hours postdose was measured at 7.62 μg/mL (serum trough level at 24 hours was likely lower but was still higher than expected) (Table 2, https://wwwnc.cdc.gov/EID/article/27/1/20-3766-T2.htm). To reduce the trough while maintaining a peak serum level 4–16 times over her *M. tuberculosis* isolate's linezolid MIC of 0.12 μg/mL, we extended the linezolid dosing interval to 600 mg every Monday, Wednesday, and Friday. A subsequent linezolid trough at 48 hours was calculated at <2 μg/mL. The patient completed 182 doses of BPaL over 26 weeks without treatment interruptions. Other than mild nausea that responded to pantoprazole, she had no adverse events or notable changes in laboratory values or electrocardiographs. Nine months after completion, the patient remained well; the state health department expects to closely monitor her for recurrent TB for 24 months after BPaL completion.

The patient, physicians, and public health staff involved reported high satisfaction with BPaL. Providers and TB programs in the United States considering this regimen for TB patients can seek guidance from CDC Division of Tuberculosis Elimination or their TB COE. Current trials using BPaL, such as ZeNix (https://www.tballiance.org/portfolio/trial/11883), are evaluating lower doses and shorter duration of linezolid compared with those of the Nix-TB trial. The 6-month, all oral, highly effective BPaL regimen is a notable advancement toward reducing global TB deaths (*10*).

## About the Author

Dr. Haley is a medical consultant for the Southeast National TB Center and an adjunct clinical professor in the Department of Medicine, Division of Infectious Diseases and Global Medicine, University of Florida.

## References

1. Conradie F, Diacon AH, Ngubane N, Howell P, Everitt D, Crook AM, et al.; Nix-TB Trial Team. Treatment of highly drug-resistant pulmonary tuberculosis. N Engl J Med. 2020;382:893–902. https://doi.org/10.1056/NEJMoa1901814
2. Keam SJ. Pretomanid: first approval. Drugs. 2019;79:1797–803. https://doi.org/10.1007/s40265-019-01207-9
3. Lee M, Lee J, Carroll MW, Choi H, Min S, Song T, et al. Linezolid for treatment of chronic extensively drug-resistant tuberculosis. N Engl J Med. 2012;367:1508–18. https://doi.org/10.1056/NEJMoa1201964
4. Brown AN, Drusano GL, Adams JR, Rodriquez JL, Jambunathan K, Baluya DL, et al. Preclinical evaluations to identify optimal linezolid regimens for tuberculosis therapy. MBio. 2015;6:e01741-15. https://doi.org/10.1128/mBio.01741-15
5. Nahid P, Mase SR, Migliori GB, Sotgiu G, Bothamley GH, Brozek JL, et al. Treatment of drug-resistant tuberculosis. An official ATS/CDC/ERS/IDSA clinical practice guideline. Am J Respir Crit Care Med. 2019;200:e93–142. https://doi.org/10.1164/rccm.201909-1874ST
6. Xu J, Wang B, Hu M, Huo F, Guo S, Jing W, et al. Primary clofazimine and bedaquiline resistance among isolates from patients with multidrug-resistant tuberculosis. Antimicrob Agents Chemother. 2017;61:e00239-17.

https://doi.org/10.1128/AAC.00239-17
7. Peloquin C. The role of therapeutic drug monitoring in mycobacterial infections. Microbiol Spectr. 2017;5. https://doi.org/10.1128/microbiolspec.TNMI7-0029-2016
8. Heinrichs MT, Drusano GL, Brown DL, Maynard MS, Sy SKB, Rand KH, et al. Dose optimization of moxifloxacin and linezolid against tuberculosis using mathematical modeling and simulation. Int J Antimicrob Agents. 2019;53:275–83. https://doi.org/10.1016/j.ijantimicag.2018.10.012
9. Song T, Lee M, Jeon HS, Park Y, Dodd LE, Dartois V, et al. Linezolid trough concentrations correlate with mitochondrial toxicity-related adverse events in the treatment of chronic extensively drug-resistant tuberculosis. EBioMedicine. 2015;2:1627–33. https://doi.org/10.1016/j.ebiom.2015.09.051
10. Harding E. WHO global progress report on tuberculosis elimination. Lancet Respir Med. 2020;8:19. https://doi.org/10.1016/S2213-2600(19)30418-7

Address for correspondence: Connie A. Haley, Southeastern National Tuberculosis Center, Box 103600, Gainesville, FL 32610-3600, USA; email: connie.haley@medicine.ufl.edu

# COMMENT LETTERS

## Large-Scale Isolation Facilities and Potential for Secondary Infectious Disease Outbreak

Shi Yu Derek Lim,[1] Hong Liang Tey[1]

Author affiliations: National Skin Centre, Singapore (S.Y.D. Lim, H.L. Tey); Woodlands Health Campus, Singapore (S.Y.D. Lim, H.L. Tey); National University of Singapore (H.L. Tey); Nanyang Technological University, Singapore (H.L. Tey)

DOI: https://doi.org/10.3201/eid2701.203127

**To the Editor:** Singapore has instituted large-scale isolation facilities similar to those detailed by Choi et al. (*1*) for patients with mild coronavirus disease. We highlight the risk for transmission of secondary infectious diseases by sharing our experience with a varicella outbreak.

Three patients, all migrant workers housed in the same isolation hall, were seen for vesicular eruptions, later laboratory confirmed as varicella, within the span of 9 days. The first patient's symptoms were truncal erythematous-based vesicles and erosions after a prodrome of fever and headache. He was promptly transferred for further hospital isolation. As part of a ring vaccination strategy, we offered 200 close contacts postexposure vaccination. However, 2 other patients, not close contacts of the first, had similar eruptions; for the second patient, 7 days later with a rash duration of 2 days, and for the third, 8 days after, with a rash duration of 6 days (Figure). After these additional cases, vaccination was offered to all remaining patients in the isolation facility.

All 3 patients probably contracted varicella from unidentified persons with varicella or zoster infection, given that illness onset fell short of the usual 10–21-day incubation period (*2*). Although varicella seroprevalence among adults in Singapore is high (88%), data on seroprevalence among migrant workers remain limited (*3*).

Although isolation facilities obviate the capacity constraints of hospital isolation, our experience highlights the potential for secondary outbreaks, which are disruptive and costly to investigate and control. To mitigate this risk, preentry screening inquiring about previous chickenpox infection or vaccination should be considered. Serologic screening is ideal but challenging to implement. Among patients, social distancing and face coverings should be enforced. We also recommend active surveillance for vesicular rash and fever, prompt isolation of patients with suspected cases, and vaccination of identified close contacts without previous infection, vaccination, or contraindications to vaccination, as

**Figure.** Vesicle on an erythematous base (arrow), commonly described as "dewdrop on rose petal", over the forehead of a patient with varicella, Singapore, 2020.

[1]These authors contributed equally to this article.

well as temporarily halting patient flow while these measures are implemented.

The initial patient described in this article has given his consent for his image and other clinical information to be reported. The patient understands that his name and initials will not be published, and due efforts will be made to conceal his identity, but anonymity cannot be guaranteed.

### References


1. Choi WS, Kim HS, Kim B, Nam S, Sohn JW. Community treatment centers for isolation of asymptomatic and mildly symptomatic patients with coronavirus disease, South Korea. Emerg Infect Dis. 2020;26:2338–45. https://doi.org/10.3201/eid2610.201539
2. Czumbel I, Quinten C, Lopalco P, Semenza JC; ECDC expert panel working group. Management and control of communicable diseases in schools and other child care settings: systematic review on the incubation period and period of infectiousness. BMC Infect Dis. 2018;18:199. https://doi.org/10.1186/s12879-018-3095-8
3. Fatha N, Ang LW, Goh KT. Changing seroprevalence of varicella zoster virus infection in a tropical city state, Singapore. Int J Infect Dis. 2014;22:73–7. https://doi.org/10.1016/j.ijid.2013.10.003


Address for correspondence: Shi Yu Derek Lim, National Skin Centre, Singapore, 1 Mandalay Rd 308205, Singapore; email: derek.lim@mohh.com.sg

## Relative Bradycardia in Patients with Mild-to-Moderate Coronavirus Disease, Japan

Gabriel Yan,[1] Alicia Ang, Sai Meng Tham, Alvin Ng, Ka Lip Chew[1]

Author affiliation: National University Health System, Singapore

DOI: https://doi.org/10.3201/eid2701.203312

**To the Editors:** Ikeuchi et al. (*1*) described the phenomenon of relative bradycardia in patients as an adjunct to the clinical diagnosis of mild-to-moderate coronavirus disease (COVID-19). Relative bradycardia is defined as an increase in pulse rate of <18 bpm for each 1°C rise in body temperature or a body temperature >38.9°C and pulse rate <120 bpm (*2*). We performed a retrospective study comparing COVID-19 and influenza patients in a tertiary hospital in Singapore. Our study was reviewed and approved by the National Healthcare Group Domain Specific Review Board (reference no. 2020/00324)

We reviewed medical records of patients with COVID-19 or influenza, confirmed by reverse transcription PCR, who were treated during October 2019–April 2020. Patients on β-blockers were excluded (14 COVID-19 patients and 25 influenza patients). Eighty-six patients with COVID-19 and 74 patients with influenza were included; 73 influenza cases were influenza A and 1 influenza B. For COVID-19 patients, median age was 40.6 (range 18–72) years and 49/86 (57%) were male; for influenza patients, median age was 54 (range 22–85) years and 34/74 (45.9%) were male. Fourteen (16.3%) COVID-19 patients and 29 (39.2%) influenza patients had fever >38.9°C; only 4 (13.8%) influenza patients and 0 COVID-19 patients had pulse rates >120 bpm. Median pulse rate was 98.5 (interquartile range 94–101) bpm for COVID-19 patients and 99 (interquartile range 97–116) bpm for influenza patients. Linear regression of the peak temperature and the associated pulse rate of the patient predicted an increase in pulse rate of 11.12 (95% CI 7.65–14.60) bpm for COVID-19 patients and 9.5 (95% CI 5.86–13.14) bpm for influenza patients for each 1°C increase in body temperature.

Our data support the observations by Ikeuchi et al. (*1*) of relative bradycardia in COVID-19 patients. However, results from our cohort demonstrate relative bradycardia in patients with both viral illnesses, indicating that this phenomenon cannot be used to reliably distinguish COVID-19 from influenza and has limited clinical utility in patients who have acute respiratory illnesses.

### References


1. Ikeuchi K, Saito M, Yamamoto S, Nagai H, Adachi E. Relative bradycardia in patients with mild-to-moderate coronavirus disease, Japan. Emerg Infect Dis. 2020;26:2504–6. https://doi.org/10.3201/eid2610.202648
2. Cunha BA. The diagnostic significance of relative bradycardia in infectious disease. Clin Microbiol Infect. 2000;6:633–4. https://doi.org/10.1046/j.1469-0691.2000.0194f.x


Address for correspondence: Gabriel Yan, Division of Infectious Diseases, Department of Medicine, National University Health System, NUHS Tower Block, 1E Kent Ridge Rd, Singapore 119228; email: gabriel_zherong_yan@nuhs.edu.sg

[1]These authors contributed equally to this article.

**Joseph Mallord William Turner (1775–1851). *The Fighting Temeraire* (*Tugged to Her Last Berth to Be Broken Up*), *1838* (1838)** (detail). Oil on canvas, 36 in × 48 in / 91cm × 122 cm. National Gallery, London, UK. Public Domain.

# A Final Voyage Framed by Balance and Contrast

Byron Breedlove

Considered among Britain's greatest artists, Joseph Mallord William Turner (known better as J.M.W. Turner) was compelled by a lifelong need to create, and he is known to have completed more than 550 oil paintings, 2,000 watercolors, and 30,000 works on paper. The National Gallery in London calls Turner "the painter of light" because of his prominent use of brilliant colors in landscapes and seascapes. Water, both turbulent and tranquil, appears in many of his better-known works, and a measure of irony is that he later died from an illness caused by contaminated water.

Art critic Jonathan Jones ventures the opinion that "One measure is the fascination an artist holds, not just for the general public, but for other artists. If an artist of the past is still haunting, provoking and inspiring modern artists, that has to suggest some deep vitality. To this day, Turner haunts art in that way. It is not yet done with the grandiose after-echoes of his smoky light."

Before admission to the Royal Academy of Arts when he was 14 years old, Turner had received little formal education. Soon acknowledged as a prodigy, Turner became the youngest painter to have works featured in the Academy's annual exhibition, and at age 26, was the youngest student to be designated Royal Academician, the Academy's highest rank. He also gained experience working with architects and draughtsmen and painting theatre sets.

According to art historian Elizabeth Barker, Turner was "an innovator who has been hailed as a forerunner of modernist abstraction." She explains how he honed his method on a series of small topographical watercolors: "To create details, Turner scraped, blotted, and wiped the paint while it was still wet, and scratched into or drew on dry surfaces." Turner also applied that technique to oil painting. Barker notes, "He built up from foundations of color to create uniquely evocative shapes and glowing forms."

In the final phase of his career, "Turner's painting became more vigorous, intense and liberated than ever before," states art critic Alastair Sooke. Turner is remembered not only for those colorful, luminous works but also for the range of subjects portrayed in his art. Some works depicted tragic and horrific events such as wars, fires, and shipwrecks; others offered insightful commentaries on the contemporary world's transformation as the industrial revolution gained traction.

Turner completed The Fighting Temeraire, this month's cover image, in 1838, at the zenith of his career, and the painting was displayed at the Royal Academy in 1839. Launched in 1798, the UK Navy ship HMS *Temeraire* saw naval action in 1805 during the Battle of Trafalgar, when it rescued Admiral Horatio Nelson's

Author affiliation: Centers for Disease Control and Prevention, Atlanta, Georgia, USA

DOI: https://doi.org/10.3201/eid2701.AC2701

besieged flagship HMS *Victory* and captured two French warships. After being repaired, the *Temeraire* blockaded French fleets and supported British military operations off the coast of Spain. Historical records indicate that in 1811 an outbreak of yellow fever swept through the *Temeraire,* killing nearly 100 of the ship's crew members, double the number who died at Trafalgar.

Later moored at the Sheerness Dockyard, UK, the warship served as a floating prison, barracks for new recruits, depot ship, and stationary guard ship. Per standard orders, the ship's cannons, masts, and rigging would have then been removed for reuse.

For much of his life, Turner lived close to the Thames, though no evidence suggests he saw the man-of-war's final voyage in 1838, and he took substantial artistic license in his romanticized depiction. Turner restored the masts and sails to the pallid titan as a nod to its glory days. He framed the *Temeraire* with a triangle of blue sky, the massive vessel drifting high in the water toward the center of the painting, so that the heroic ship looms over the squat tug dragging it to its destruction.

Turner expertly draws on balance and contrast in the painting. Behind the ghostly lit *Temeraire*, a square-rigged sailing vessel and other faintly visible ships head down the river toward the setting sun. Lit by the sun, the stout tug, rendered in bold colors, churns upstream and bellows smoke across the derelict's spar where a flag would have waved. Vivid warm colors play across the low clouds and reflect on the water's surface, calling attention to the low sun. A faint crescent moon wreathed in cool blues and grays hangs near the upper left of the canvas and contrasts with the brilliant sunset.

Turner's choice of colors and positioning the tug in front of the *Temeraire* serve both as an elegiac farewell to the waning dominance of wooden sailing vessels and an acknowledgment the growing reliance on steam-powered ships. The quiet steadiness of wind power is yielding to the loud urgency of steam engines.

Turner was an eccentric, reclusive character, especially in his later years. A cholera epidemic in 1831–32 had terrified him, and some 20 years later, when he was already in declining health, a severe case of this waterborne disease led to his death.

Today, diarrheal diseases, including cholera, kill more children than AIDS, malaria, and measles combined. According to the Centers for Disease Control and Prevention, 780 million people lack access to safe water and 2.5 billion people lack access to adequate sanitation. Such conditions also contribute to the spread of other waterborne diseases such as schistosomiasis, Guinea worm disease, giardiasis, and dysentery.

Access to piped water does not guarantee freedom from the threat of waterborne illness. Legionnaires' disease is caused by *Legionella* bacteria that can grow and spread in poorly maintained plumbing, especially in buildings. Collier et al. found that during 2000–2015, a total of 7.15 million waterborne illnesses occurred each year, resulting in 601,000 visits to emergency departments, 118,000 hospitalizations, and 6,630 deaths annually. The challenges of providing access to safe water and addressing pathogens that live in manufactured water systems underscore the need for more public health resources to address waterborne infections.

## Bibliography


1. Barker EE. Heilbrunn timeline of art history. New York: Metropolitan Museum of Art. Joseph Mallord William Turner (1775–1851) [cited 2020 Dec 1]. https://www.metmuseum.org/toah/hd/trnr/hd_trnr.htm
2. Centers for Disease Control and Prevention. Safe water system. Diseases and SWS impact [cited 2020 Dec 4]. https://www.cdc.gov/safewater/disease.html
3. Collier SA, Deng L, Adam EA, Benedict KM, Beshearse EM, Blackstock AJ, et al. Estimate of burden and direct healthcare cost of infectious waterborne disease in the United States. Emerg Infect Dis. 2021;27:140–9.
4. Costello LJ. Turner and the subject of history. Milton Park (UK): Taylor and Francis, 2017.
5. Jones J. The Guardian, 2014. Is JMW Turner Britain's greatest artist? [cited 2020 Dec 1]. https://www.theguardian.com/artanddesign/jonathanjonesblog/2014/jul/28/jmw-turner-britains-greatest-artist
6. National Gallery. Heroine of Trafalgar: The fighting Temeraire. [cited 2020 Nov 22]. https://www.nationalgallery.org.uk/paintings/learn-about-art/paintings-in-depth/heroine-of-trafalgar-the-fighting-temeraire
7. National Gallery. Joseph Mallord William Turner. 1775−1851 [cited 2020 Nov 22]. https://www.nationalgallery.org.uk/artists/joseph-mallord-william-turner
8. Shanes E. The life and masterworks of J.M.W. Turner. New York: Parkstone International, 2012. .
9. Shank I. What you need to know about J.M.W. Turner, Britain's great painter of tempestuous seas [2020 Dec 1]. https://www.artsy.net/article/artsy-editorial-jmw-turner-britains-great-painter-tempestuous-seas
10. Sooke A, How JM. Turner set painting free. Culture [cited 2020 Dec 1]. https://www.bbc.com/culture/article/20140915-how-turner-set-painting-free
11. Tate Museum. Joseph Mallord William Turner 1775–1851 [cited 2020 Nov 25]. https://www.tate.org.uk/art/artists/joseph-mallord-william-turner-558
12. Wainwright SP, Williams C. Biography and vulnerability: loss, dying and death in the romantic paintings of J.M.W. Turner (1775–1851). Auto/Biography. 2005;13:16–32 . https://doi.org/10.1191/0967550705ab015oa
13 Willis S. The fighting Temeraire: the Battle of Trafalgar and the ship that inspired J.M.W. Turner's most beloved painting. New York: Pegasus Books, 2012.


Address for correspondence: Byron Breedlove, EID Journal, Centers for Disease Control and Prevention, 1600 Clifton Rd NE, Mailstop H16-2, Atlanta, GA 30329-4027, USA; email: wbb1@cdc.gov

# EMERGING INFECTIOUS DISEASES®

## Upcoming Issue

- Childcare Exposure to Severe Acute Respiratory Syndrome Coronavirus 2 for 4-Year-Old Presymptomatic Child, South Korea
- Symptom Onset and Progression in Hospitalized and Nonhospitalized Patients with Coronavirus Disease, Colorado, USA
- Characteristics and Timing of Initial Virus Shedding in Severe Acute Respiratory Syndrome Coronavirus 2, Utah, USA
- Clinical Characteristics of Patients Co-infected with Severe Acute Respiratory Syndrome Coronavirus 2 and Dengue Virus, Buenos Aires, Argentina, March–June 2020
- Zika Virus–Associated Birth Defects, Costa Rica, 2016–2018
- Addressing COVID-19 Misinformation on Social Media Preemptively and Responsively
- Rapid Transmission of Severe Acute Respiratory Syndrome Coronavirus 2 in Detention Facility, Louisiana, USA, May–June, 2020
- Nationwide Outbreak of Severe Vomiting in Dogs Associated with a Canine Enteric Coronavirus, United Kingdom
- Excess Deaths during Influenza and Coronavirus Disease and Infection-Fatality Rate for Severe Acute Respiratory Syndrome Coronavirus 2, the Netherlands
- Universal Admission Screening for SARS-CoV-2 Infections among Hospitalized Patients, Switzerland, 2020
- Highly Pathogenic Avian Influenza A(H5N8) Virus Spread by Short- and Long-Range Transmission, France, 2016–17
- Increasing Incidence of Invasive Group A Streptococcal Disease in First Nations Population, Alberta, Canada, 2003–2017
- Transmission Clusters of Hepatitis C Virus in Public Health and Correctional Settings, Wisconsin, USA, 2016–2017
- Spread of Multidrug-Resistant *Rhodococcus equi*, United States
- Plasma MicroRNA Profiling of *Plasmodium falciparum* Biomass and Association with Severity of Malaria Disease
- Prolonged Maternal Zika Viremia as a Marker of Adverse Perinatal Outcomes
- Use of Commercial Claims Data for Evaluating Trends in Lyme Disease Diagnosis, United States
- Role of *Burkholderia pseudomallei*–Specific IgG2 Antibodies in Adults with Acute Melioidosis, Thailand
- Effects of Social Distancing Measures during the First Epidemic Wave of Severe Acute Respiratory Syndrome Coronavirus 2, Greece
- Murine Typhus in Canary Islands, Spain, 1999–2015
- *Salmonella enterica* Serovar Typhi AcrB-R717Q/L Azithromycin-Resistant Isolates, Singapore
- Evidence of Zika Virus Infection in Pigs and Mosquitoes, Mexico
- Prevalence of SARS-CoV-2–Specific Antibodies, Japan, June 2020
- Novel Arterivirus Associated with Outbreak of Fatal Encephalitis in European Hedgehogs, England
- Early Transmission Dynamics, Spread, and Genomic Characterization of SARS-CoV-2 in Panama
- *Plasmodium cynomolgi* Coinfections among Symptomatic Malaria Patients, Thailand
- SARS-CoV-2 Transmission between Mink (*Neovison vison*) and Humans, Denmark

**Complete list of articles in the February issue at http://www.cdc.gov/eid/upcoming.htm**

## Earning CME Credit

To obtain credit, you should first read the journal article. After reading the article, you should be able to answer the following, related, multiple-choice questions. To complete the questions (with a minimum 75% passing score) and earn continuing medical education (CME) credit, please go to http://www.medscape.org/journal/eid. Credit cannot be obtained for tests completed on paper, although you may use the worksheet below to keep a record of your answers.

You must be a registered user on http://www.medscape.org. If you are not registered on http://www.medscape.org, please click on the "Register" link on the right hand side of the website.

Only one answer is correct for each question. Once you successfully answer all post-test questions, you will be able to view and/or print your certificate. For questions regarding this activity, contact the accredited provider, CME@medscape.net. For technical assistance, contact CME@medscape.net. American Medical Association's Physician's Recognition Award (AMA PRA) credits are accepted in the US as evidence of participation in CME activities. For further information on this award, please go to https://www.ama-assn.org. The AMA has determined that physicians not licensed in the US who participate in this CME activity are eligible for AMA PRA Category 1 Credits™. Through agreements that the AMA has made with agencies in some countries, AMA PRA credit may be acceptable as evidence of participation in CME activities. If you are not licensed in the US, please complete the questions online, print the AMA PRA CME credit certificate, and present it to your national medical association for review.

## Article Title

# Invasive Fusariosis in Nonneutropenic Patients, Spain, 2000–2015

## CME Questions

**1. Your patient is a 67-year-old man with chronic heart disease suspected of having Invasive fusariosis (IF). According to the retrospective observational study by Pérez-Nadales and colleagues, which of the following statements about the incidence of IF and fungal isolates from patients with IF in 18 Spanish hospitals during the 15-year period from 2000 to 2015 is correct?**

A. Global incidence density of IF (all cases of IF/100,000 admissions) remained stable over the study period
B. IF incidence in nonneutropenic patients increased by 50% from 2000 to 2015
C. Reasons for increased IF in nonneutropenic patients may include increased population at risk, environmental exposure to *Fusarium conidia*, and/or use of antimold prophylaxis
D. *F. brachygibbosum* was the most frequently isolated *Fusarium* species

**2. According to the retrospective observational study by Pérez-Nadales and colleagues, which of the following statements about the clinical features of patients with IF in 18 Spanish hospitals during the 15-year period from 2000 to 2015 is correct?**

A. IF in nonneutropenic patients was always accompanied by hematologic conditions
B. Lungs, bloodstream, and skin were the most frequent organs involved
C. Previous treatment with corticosteroids or antifungal agents was uncommon
D. Nonneutropenic patients were more likely to have skin lesions than neutropenic patients

**3. According to the retrospective observational study by Pérez-Nadales and colleagues, which of the following statements about the treatment and outcomes of patients with IF in 18 Spanish hospitals during the 15-year period from 2000 to 2015 is correct?**

A. 90-day mortality was 28.6% in nonneutropenic patients, 38.1% in neutropenic patients with resolved neutropenia ($p = 0.72$), and 91.3% in patients with persistent neutropenia ($p<0.001$)
B. Prior treatment with corticosteroids was the only mortality risk factor in a multivariate Cox-regression analysis
C. Use of amphotericin B was significantly more frequent in nonneutropenic than in neutropenic patients
D. Combination therapy was associated with significantly better outcomes

# Earning CME Credit

To obtain credit, you should first read the journal article. After reading the article, you should be able to answer the following, related, multiple-choice questions. To complete the questions (with a minimum 75% passing score) and earn continuing medical education (CME) credit, please go to http://www.medscape.org/journal/eid. Credit cannot be obtained for tests completed on paper, although you may use the worksheet below to keep a record of your answers.

You must be a registered user on http://www.medscape.org. If you are not registered on http://www.medscape.org, please click on the "Register" link on the right hand side of the website.

Only one answer is correct for each question. Once you successfully answer all post-test questions, you will be able to view and/or print your certificate. For questions regarding this activity, contact the accredited provider, CME@medscape.net. For technical assistance, contact CME@medscape.net. American Medical Association's Physician's Recognition Award (AMA PRA) credits are accepted in the US as evidence of participation in CME activities. For further information on this award, please go to https://www.ama-assn.org. The AMA has determined that physicians not licensed in the US who participate in this CME activity are eligible for AMA PRA Category 1 Credits™. Through agreements that the AMA has made with agencies in some countries, AMA PRA credit may be acceptable as evidence of participation in CME activities. If you are not licensed in the US, please complete the questions online, print the AMA PRA CME credit certificate, and present it to your national medical association for review.

## Article Title

## Incidence of Acute Rheumatic Fever and Rheumatic Heart Disease among Ethnic Groups, New Zealand, 2000–2018

## CME Questions

**1. Which of the following statements regarding acute rheumatic fever (ARF) and rheumatic heart disease (RHD) is most accurate?**

A. It occurs in approximately 12% of patients with untreated group A streptococcal pharyngitis
B. ≈34 million people worldwide have RHD
C. The highest prevalence of RHD is found in South America
D. Group A streptococcal skin infections now account for the majority of cases of ARF

**2. Which of the following variables was most associated with a higher risk for ARF in the current study?**

A. Asian race
B. Socioeconomic deprivation
C. Age <5 years
D. Male sex

**3. Which of the following trends was noted in hospitalizations for ARF in the current study?**

A. Most cases were between the ages of 10 and 14 years
B. There was a sharp increase in the rate of hospitalization because of ARF between 2000 and 2018
C. Approximately half of ARF cases occurred among adults aged >30 years
D. Hospitalization rates for patients aged <30 years declined during the study period

**4. Which of the following trends was noted in hospitalizations for RHD in the current study?**

A. The average age of patients admitted with RHD was 40 years
B. RHD hospitalization rates increased during the study period
C. Ethnicity was not a risk factor for hospitalization with RHD
D. Female sex was associated with a higher risk for hospitalization with RHD

DEPARTMENT OF
HEALTH & HUMAN SERVICES
Public Health Service
Centers for Disease Control and Prevention (CDC)
Mailstop D61, Atlanta, GA 30329-4027





**Joseph Mallord William Turner (1775–1851). *The Fighting Temeraire (Tugged to Her Last Berth to Be Broken Up), 1838* (1838).** Oil on canvas, 36 in × 48 in /91cm × 122 cm. National Gallery, London, UK. Public Domain.